frontiers | Research Topics

Advances in natural polysaccharides and oligosaccharides: Purification techniques, analysis methods, and physiochemical properties

Edited by
Xiaolong Ji, Qiu Li and Xin Wang

Published in
Frontiers in Nutrition

FRONTIERS EBOOK COPYRIGHT STATEMENT

The copyright in the text of individual articles in this ebook is the property of their respective authors or their respective institutions or funders. The copyright in graphics and images within each article may be subject to copyright of other parties. In both cases this is subject to a license granted to Frontiers.

The compilation of articles constituting this ebook is the property of Frontiers.

Each article within this ebook, and the ebook itself, are published under the most recent version of the Creative Commons CC-BY licence. The version current at the date of publication of this ebook is CC-BY 4.0. If the CC-BY licence is updated, the licence granted by Frontiers is automatically updated to the new version.

When exercising any right under the CC-BY licence, Frontiers must be attributed as the original publisher of the article or ebook, as applicable.

Authors have the responsibility of ensuring that any graphics or other materials which are the property of others may be included in the CC-BY licence, but this should be checked before relying on the CC-BY licence to reproduce those materials. Any copyright notices relating to those materials must be complied with.

Copyright and source acknowledgement notices may not be removed and must be displayed in any copy, derivative work or partial copy which includes the elements in question.

All copyright, and all rights therein, are protected by national and international copyright laws. The above represents a summary only. For further information please read Frontiers' Conditions for Website Use and Copyright Statement, and the applicable CC-BY licence.

ISSN 1664-8714
ISBN 978-2-83251-672-0
DOI 10.3389/978-2-83251-672-0

About Frontiers

Frontiers is more than just an open access publisher of scholarly articles: it is a pioneering approach to the world of academia, radically improving the way scholarly research is managed. The grand vision of Frontiers is a world where all people have an equal opportunity to seek, share and generate knowledge. Frontiers provides immediate and permanent online open access to all its publications, but this alone is not enough to realize our grand goals.

Frontiers journal series

The Frontiers journal series is a multi-tier and interdisciplinary set of open-access, online journals, promising a paradigm shift from the current review, selection and dissemination processes in academic publishing. All Frontiers journals are driven by researchers for researchers; therefore, they constitute a service to the scholarly community. At the same time, the *Frontiers journal series* operates on a revolutionary invention, the tiered publishing system, initially addressing specific communities of scholars, and gradually climbing up to broader public understanding, thus serving the interests of the lay society, too.

Dedication to quality

Each Frontiers article is a landmark of the highest quality, thanks to genuinely collaborative interactions between authors and review editors, who include some of the world's best academicians. Research must be certified by peers before entering a stream of knowledge that may eventually reach the public - and shape society; therefore, Frontiers only applies the most rigorous and unbiased reviews. Frontiers revolutionizes research publishing by freely delivering the most outstanding research, evaluated with no bias from both the academic and social point of view. By applying the most advanced information technologies, Frontiers is catapulting scholarly publishing into a new generation.

What are Frontiers Research Topics?

Frontiers Research Topics are very popular trademarks of the *Frontiers journals series*: they are collections of at least ten articles, all centered on a particular subject. With their unique mix of varied contributions from Original Research to Review Articles, Frontiers Research Topics unify the most influential researchers, the latest key findings and historical advances in a hot research area.

Find out more on how to host your own Frontiers Research Topic or contribute to one as an author by contacting the Frontiers editorial office: frontiersin.org/about/contact

Advances in natural polysaccharides amnd oligosaccharides: Purification techniques, analysis methods, and physiochemical properties

Topic editors

Xiaolong Ji — Zhengzhou University of Light Industry, China
Qiu Li — Qingdao Agricultural University, China
Xin Wang — Northwest A&F University, China

Citation

Ji, X., Li, Q., Wang, X., eds. (2023). *Advances in natural polysaccharides and oligosaccharides: Purification techniques, analysis methods, and physiochemical properties*. Lausanne: Frontiers Media SA. doi: 10.3389/978-2-83251-672-0

Table of contents

08 Structural Characterization and Anti-breast Cancer Activity *in vitro* of a Novel Polysaccharide From *Cymbopogon citratus*
Yi Chen, Saifeng Qiao, Huiping Liu, Huizhen Xing and Pei Chen

22 Structural Elucidation, Modification, and Structure-Activity Relationship of Polysaccharides in Chinese Herbs: A Review
Bei Wang, Lingling Yan, Shuchen Guo, Ling Wen, Mengli Yu, Liang Feng and Xiaobin Jia

40 Effect of Polysaccharide Extracted From *Gynostemma Pentaphyllum* on the Body Weight and Gut Microbiota of Mice
Shiwei Li, Yingna Wang, Weipeng Dun, Wanqing Han, Tao Ning, Qi Sun and Zichao Wang

48 Structural Characterization, Antioxidant and Antibacterial Activities of a Novel Polysaccharide From *Zingiber officinale* and Its Application in Synthesis of Silver Nanoparticles
Yongshuai Jing, Wenjing Cheng, Yunfeng Ma, Yameng Zhang, Mingsong Li, Yuguang Zheng, Danshen Zhang and Lanfang Wu

60 Quality Markers of *Dendrobium officinale* by "Oligosaccharide-Spectrum-Effect" Relationships
Ruimin Liu, Songshan Shi, Si Xiong, Juan Su, Xiaona Gan, Jianjun Wu, Huijun Wang and Shunchun Wang

74 Structural Characterization and Anti-inflammatory Activity of a Galactorhamnan Polysaccharide From *Citrus medica* L. var. *sarcodactylis*
Bi Luo, Jia Lv, Kejie Li, Peiran Liao and Peng Chen

84 Ultrasound-Assisted Deep Eutectic Solvents Extraction of Polysaccharides From *Morchella importuna*: Optimization, Physicochemical Properties, and Bioactivities
Xu Pan, Lijing Xu, Junlong Meng, Mingchang Chang, Yanfen Cheng, Xueran Geng, Dongdong Guo and Rongzhu Liu

95 Structural Characterization of Polysaccharides in Waste Liquor Produced by Wet Decortication of Sesame Seeds
Yao-Ran Li, Shuai Xu, Run-Yang Zhang, Ming-Xuan Yang, Hua-Min Liu and Xue-De Wang

106 Hemicellulosic Polysaccharides From Bamboo Leaves Promoted by Phosphotungstic Acids and Its Attenuation of Oxidative Stress in HepG2 Cells
Zhuqian Xiao, Jiajie Li, Hongpeng Wang, Qiang Zhang, Qing Ge, Jianwei Mao and Ruyi Sha

122 Characterization and Antibacterial Activity of a Polysaccharide Produced From Sugarcane Molasses by *Chaetomium globosum* CGMCC 6882
Li Ma, Xueliang Guo, Jiaoyang Yang, Xiangru Zeng, Kaili Ma, Lu Wang, Qi Sun and Zichao Wang

131 Characterization of Structure and Antioxidant Activity of Polysaccharides From Sesame Seed Hull
Run-Yang Zhang, Jing-Hao Gao, Yi-Lin Shi, Yi-Fei Lan, Hua-Min Liu, Wen-Xue Zhu and Xue-De Wang

144 Corrigendum: Characterization of structure and antioxidant activity of polysaccharides from sesame seed hull
Run-Yang Zhang, Jing-Hao Gao, Yi-Lin Shi, Yi-Fei Lan, Hua-Min Liu, Wen-Xue Zhu and Xue-De Wang

146 Chemical Structure and Immune Activation of a Glucan From *Rhizoma Acori Tatarinowii*
Wuxia Zhang, Jiaqi He, Yihua Hu, Jingwu Lu, Jinzhong Zhao and Peng Li

156 Two Novel Polysaccharides From *Clitocybe squamulosa*: Their Isolation, Structures, and Bioactivities
Dongdong Guo, Jiayu Lei, Lijing Xu, Yanfen Cheng, Cuiping Feng, Junlong Meng, Mingchang Chang and Xueran Geng

171 Hypoglycemic Effects of *Lycium barbarum* Polysaccharide in Type 2 Diabetes Mellitus Mice *via* Modulating Gut Microbiota
Qingyu Ma, Ruohan Zhai, Xiaoqing Xie, Tao Chen, Ziqi Zhang, Huicui Liu, Chenxi Nie, Xiaojin Yuan, Aobai Tu, Baoming Tian, Min Zhang, Zhifei Chen and Juxiu Li

190 Determining Methyl-Esterification Patterns in Plant-Derived Homogalacturonan Pectins
Yang Yu, Liangnan Cui, Xianbin Liu, Yuwen Wang, Chenchen Song, UnHak Pak, Kevin H. Mayo, Lin Sun and Yifa Zhou

205 Anti-cancer Potential of Polysaccharide Extracted From *Polygonatum sibiricum* on HepG2 Cells via Cell Cycle Arrest and Apoptosis
Mo Li, Yumeng Liu, Henan Zhang, Yanfeng Liu, Weiming Wang, Shengbo You, Xinyu Hu, Meijun Song, Rina Wu and Junrui Wu

217 Preparation and Structure Characterization of High-Value *Laminaria digitata* Oligosaccharides
Kit-Leong Cheong, Jia-Kang Li and Saiyi Zhong

227 Antitumor Potential and Structure Characterization of Polysaccharides From *Lagotis brevituba* Maxim in the Tibetan Plateau
Ruixue Gong, Weiguo Cao, Haijun Huang, Bao Yu, Huan Chen, Wei Tao, Quji Luorong, Juan Luo and Dan Zhang

238 Pectin Stabilized Fish Gelatin Emulsions: Physical Stability, Rheological, and Interaction Properties
Sheng Huang, Hui Wang, Shu Wang, Xiaomei Sha, Ning Chen, Yueming Hu and Zongcai Tu

250 Research progress on extraction, purification, structure and biological activity of *Dendrobium officinale* polysaccharides
Yuan He, Lin Li, Hao Chang, Bin Cai, Huajun Gao, Guoyu Chen, Wen Hou, Zubaydan Jappar and Yizhe Yan

265 Effect of ultrasonic degradation on the physicochemical property and bioactivity of polysaccharide produced by *Chaetomium globosum* CGMCC 6882
Shiwei Li, Yingna Wang, Weipeng Dun, Wanqing Han, Chunping Xu, Qi Sun and Zichao Wang

275 Polysaccharide immunization and colorectal cancer: A systematic review and network meta-analysis
Yuefeng Chen, Xinnan Pan, Baoming Tian and Yajun Hu

285 Extraction, purification, structural features and biological activities of longan fruit pulp (Longyan) polysaccharides: A review
Xuan Yue, Zhejie Chen, Jinming Zhang, Chi Huang, Shiyi Zhao, Xuebo Li, Yan Qu and Chen Zhang

313 Structural characterization and bioactivity evaluation of water-extractable polysaccharides from chickpeas (*Cicer arietinum* L.) seeds
Yingying Zhu, Baoqing Dun, Zhenxing Shi, Yuanji Wang, Li Wu and Yang Yao

324 Effects of monosaccharide composition on quantitative analysis of total sugar content by phenol-sulfuric acid method
Fangfang Yue, Jinrui Zhang, Jiaxin Xu, Tengfei Niu, Xin Lü and Manshun Liu

334 Comparison of structural characteristics and bioactivity of *Tricholoma mongolicum* Imai polysaccharides from five extraction methods
Nan Zhang, Bing Yang, Kemin Mao, Yuwei Liu, Bimal Chitrakar, Xianghong Wang and Yaxin Sang

346 Physicochemical and functional properties of *Lycium ruthenicum* pectin by different extraction methods
Ziyang Wu, Dan Qin, Hehe Li, Dongqi Guo, Huan Cheng, Jinyuan Sun, Mingquan Huang, Xingqian Ye and Baoguo Sun

358 Polysaccharide from *Hemerocallis citrina* Borani by subcritical water with different temperatures and investigation of its physicochemical properties and antioxidant activity
Yongrui Ti, Yanli Zhang, Yüqian Ban, Xiaoxiao Wang, Yüqing Hou and Zihan Song

371 Characterization and macrophages immunomodulatory activity of two water-soluble polysaccharides from *Abrus cantoniensis*
Dongshuai Qu, Shuaitao Lian, Hongjie Hu, Wenjing Sun and Hongbin Si

388 Structural characterization, antioxidant activity and anti-inflammatory of the phosphorylated polysaccharide from *Pholiota nameko*
Xu Zhang, Tingting Liu, Xi Wang, Lanying Zhou, Ji Qi and Siyu An

404 Extraction and characterization of a pectin from sea buckthorn peel
Yulian Zhu, Keshan Liu, Michael Yuen, Tina Yuen, Hywel Yuen and Qiang Peng

419 Extraction, purification, structure, modification, and biological activity of traditional Chinese medicine polysaccharides: A review
Hongkun Xue, Pengcheng Li, Jiayue Bian, Yuchao Gao, Yumei Sang and Jiaqi Tan

443 A novel acidic polysaccharide from blackened jujube: Structural features and antitumor activity *in vitro*
Guifeng Zhang, Chuang Liu and Rentang Zhang

455 Immunomodulatory activity of glycoproteins isolated from chickpea (*Cicer arietinum* L.)
Zhenxing Shi, Shiyu Li, Zuchen Wei, Yuanji Wang, Nong Zhou, Qiang Ma and Yang Yao

466 Benefits of neutral polysaccharide from rhizomes of *Polygonatum sibiricum* to intestinal function of aged mice
Li-Xia Li, Xin Feng, Meng-Ting Tao, Berit Smestad Paulsen, Chao Huang, Bin Feng, Wei Liu, Zhong-Qiong Yin, Xu Song, Xinghong Zhao, Xiao-Xia Liang, Li-Zi Yin, Hua-Qiao Tang and Yuan-Feng Zou

481 Systematic evaluation on the physicochemical characteristics of a series polysaccharides extracted from different edible lilies by ultrasound and subcritical water
Zihan Song, Yanli Zhang, Yulin Luo, Yongrui Ti, Weizhen Wang, Yuqian Ban, Yuchao Tang, Yuqing Hou, Leifeng Xu, Jun Ming and Panpan Yang

492 Structural characterization and anti-oxidation activity evaluation of pectin from *Lonicera japonica* Thunb.
Xiaodan Qi, Yang Yu, Xinyi Wang, Jialei Xu, Xiang Wang, Zhangkai Feng, Yifa Zhou, Hongxing Xiao and Lin Sun

506 Acetyl-glucomannan from *Dendrobium officinale*: Structural modification and immunomodulatory activities
Xiaoyu Guo, Mingguan Yang, Changlu Wang, Shaoping Nie, Steve W. Cui and Qingbin Guo

520 Effects of molecular weight on intestinal anti-inflammatory activities of β-D-glucan from *Ganoderma lucidum*
Yanfang Liu, Qingjiu Tang, Jie Feng, Jing Liu, Chuanhong Tang, Mengqiu Yan, Shuai Zhou, Liping Liu, Jing Zhou and Jingsong Zhang

534 A review of extraction, purification, structural properties and biological activities of legumes polysaccharides
Yingying Zhu, Xuewei Feng, Jianhang Guo, Li Wang, Xudan Guo and Xiangzhen Zhu

544 The synergism of lytic polysaccharide monooxygenases with lichenase and their co-immobilization on silica nanospheres for green conversion of lichen biomass
Lixi Ca, Ying Zheng, Yunmeng Chu, Yuanqing Lin, Lixing Liu and Guangya Zhang

556 Effects of various degrees of esterification on antioxidant and immunostimulatory activities of okra pectic-polysaccharides
Wei Li, Jie Li, Jin Wang, Yuan He, Yi-Chen Hu, Ding-Tao Wu and Liang Zou

569 Extraction, purification, structural characterization, and antioxidant activity of a novel polysaccharide from *Lonicera japonica* Thunb.
Feiyu An, Guangyu Ren, Junrui Wu, Kaixin Cao, Mo Li, Yumeng Liu, Yanfeng Liu, Xinyu Hu, Meijun Song and Rina Wu

frontiers | Frontiers in Nutrition

ORIGINAL RESEARCH
published: 11 May 2022
doi: 10.3389/fnut.2022.911838

Structural Characterization and Anti-breast Cancer Activity *in vitro* of a Novel Polysaccharide From *Cymbopogon citratus*

Yi Chen, Saifeng Qiao, Huiping Liu, Huizhen Xing and Pei Chen*

State Key Laboratory of Food Nutrition and Safety, College of Food Science and Engineering, Tianjin University of Science and Technology, Tianjin, China

Cymbopogon citratus is an important functional food, widely used for flavoring in Africa and South America. In this study, a novel high-molecular-weight polysaccharide (CCP) from *C. citratus* was extracted, and its structural characteristics and anti-breast cancer activity *in vitro* were investigated. CCP contained both α and β configurations and mainly composed of galactose (36.89%), arabinose (23.97%), glucose (18.35%) and rhamnose (9.36%) with an average molecular weight of 1.98×10^6 Da. The main glycosyl residues of CCP detected by methylation analysis were 1,3,6-linked Gal*p*, 1,3-linked Glc*p*, 1,5-linked Ara*f*, T-Ara*f*, and T-Rha*p*. *In vitro* experiments suggested that CCP significantly inhibited the proliferation of MDA-MB-231 cells, decreased the expressions of cyclin D1 and CDK4 and stocked cells at G_0/G_1 phase. Meanwhile, the typical morphological features of apoptotic cells were also observed. Combining with the consequences of Annexin V-FITC/PI staining, Hoechst 33258 staining and western blot analysis, CCP induced apoptosis of MDA-MB-231 cells by triggering the Fas/FasL-mediated death receptor pathway. Overall, these results provide a theoretical basis for the application of *C. citratus* polysaccharide as a potential anti-breast cancer agent in functional food and medicine.

Keywords: ***Cymbopogon citratus*, polysaccharide, structural characteristics, anti-breast cancer activity, Fas/FasL signaling pathway**

OPEN ACCESS

Edited by:
Xiaolong Ji,
Zhengzhou University of Light Industry, China

Reviewed by:
Kit Leong Cheong,
Shantou University, China
Yun peng Fan,
Northwest A&F University, China

****Correspondence:***
Huiping Liu
liuhuiping111@163.com

Specialty section:
This article was submitted to Food Chemistry, a section of the journal Frontiers in Nutrition

Received: *03 April 2022*
Accepted: *19 April 2022*
Published: *11 May 2022*

Citation:
Chen Y, Qiao S, Liu H, Xing H and Chen P (2022) Structural Characterization and Anti-breast Cancer Activity in vitro of a Novel Polysaccharide From Cymbopogon citratus. Front. Nutr. 9:911838. doi: 10.3389/fnut.2022.911838

INTRODUCTION

Malignant tumors are considered to be a key threat to human health worldwide due to their high recurrence rate and high mortality (1). Among cancer subtypes, breast cancer (BC), which accounts for almost 30% of all female cancers worldwide, is the second most prevalent cancer and the fifth leading cause of death from cancer in women (2–4). Nowadays, chemotherapy is regarded as the most commonly used in the clinical treatment of BC, improving the survival rate of patients (5). However, the clinical use of chemotherapy agents such as anthracyclines is frequently associated with severe adverse reactions, like acute and chronic dose-dependent cardiotoxicity (6, 7). Accumulating evidence indicates that natural products extracted from plants possess strong antitumor activity and had no significant adverse effects compared with synthetic compounds (8, 9). Hence, it is necessary to seek natural products with high efficacy and low toxicity for BC treatment.

Polysaccharides are widely existing in animals, plants and microorganisms, and have various physiological activities such as antioxidant, antiviral, hypoglycemic, anti-tumor and immunomodulatory (10–12). *Cymbopogon citratus* (lemongrass), belonging to the genus *Cymbopogon*, is widely cultivated in tropical countries, especially in Southeast Asia (13). *Cymbopogon citratus* has been used in the food, perfume, soap, cosmetics, pharmaceutical and pesticide industries (14). For many years, the biological properties of *C. citratus* have been reported, including but not limited to anti-inflammatory, antibacterial, antiprotozoal, antitussive, antioxidant, anticancer, cardioprotective and antirheumatic activities (15–17). Studies have shown that *C. citratus* contains polyphenols, terpenes, alcohols, ketones, citral and polysaccharides (18, 19). Recently, the research of *C. citratus* polysaccharide has attracted the attention of scholars. It has been researched that polysaccharide is one of the main active ingredients of *C. citratus* and possesses a variety of bioactivities, such as preventing neurodegenerative diseases, immuno-stimulating activity, anti-oxidant and anti-tumor activity (20–22).

Cymbopogon citratus extract has been shown to have anti-breast cancer effect (23, 24). However, there are few reports on the efficacy of *C. citratus* polysaccharide in breast cancer cell lines, and the mechanism of its anti-breast cancer cells has not been reported. Therefore, a novel water-soluble polysaccharide (CCP) from *C. citratus* was prepared and the mechanism of its action on MDA-MB-231 cells was studied. This study highlights the potential of CCP in functional foods for breast cancer therapy, and provide new ideas for the development and utilization of *C. citratus* in the food and pharmaceutical industry.

MATERIALS AND METHODS

Materials and Reagents

The leaves of *C. citratus* was purchased from Chinese herbal medicine market in Anguo (Anguo, China). Human breast cancer MDA-MB-231 cells were obtained from Shanghai Cell Bank of Chinese Academy of Sciences (Shanghai, China). The 0.25% trypsin and fetal bovine serum (FBS) were bought from GIBCO (Carlsbad, USA). The 3-(4,5-Dimethyl-2-thiazolyl)-2,5-diphenyl-2-H-tetrazolium bromide (MTT), Hoechst 33258, Propidium Iodide (PI), Annexin V-FITC/PI apoptosis detection kit and Reactive Oxygen Species assay kit were purchased from Solarbio Science & Technology Co. Ltd (Beijing, China). Bradford protein assay (BCA) kit and enhanced chemiluminescence (ECL) detection kit were provided by Beyotime Biotechnology (Shanghai, China). All antibodies were obtained from Wuhan Sanying Biotechnology (Wuhan, China). All of other chemicals and reagents were analytical grade.

Isolation and Purification of the *Cymbopogon citratus* Polysaccharide

The dried *C. citratus* leaves were pulverized to obtain the powder. And the powder was extracted with ultrapure water (solid-liquid ratio of 1:20, w/v) at 80°C for three times (each time for 2 h). The aqueous extracts were concentrated with a rotary evaporator to 1/3 of the original volume, and precipitated *via* adding absolute ethanol (final concentration 60%) at 4°C for 24 h. The precipitate was collected and dissolved in water, then added with Sevag solution to remove the protein. Subsequently, the polysaccharide solution was dialyzed to remove small molecular substances, and lyophilized to obtain the crude polysaccharide. Finally, we further purified the crude polysaccharide through Sephadex G-200 column, and then reserved after freeze-drying, named as CCP.

HPGPC Assays

The molecular weight of CCP was calculated according to the standards T-series dextrans (T-10, T-40, T-70, T-500 and T-2000), which using a high-performance gel permeation chromatograph (HPGPC; Agilent-1200, USA) equipped with a Tsk-gel G4000PWxl column (7.8 × 300 mm, column temperature 30°C) and refractive index detector (RID, detecting temperature 35°C; Schambeck SFD GmbH, Bad Honnef, German). Twenty microliter CCP solution (1 mg/ml) was injected by using ultrapure water as the mobile phase at flow rate of 0.6 ml/min.

UV–Visible Spectra and FT-IR Spectrum Assays

Using distilled water as a reference, 1 mg/ml CCP solution was scanned at the range of 200–400 nm by UV-vis spectrophotometer (spectrum-2102UV, USA). The FT-IR spectrum was scanned by KBr tablet method using Fourier-transform infrared spectrophotometer (Bruker VECTOR-22, Germany) in the range from 4,000 to 400 cm^{-1}.

Monosaccharide Composition and NMR Analysis

Ion chromatography (IC; Dionex ICS2500, USA) was used to investigate the monosaccharide composition of CCP. CCP was degraded for 3 h at 110°C after dissolved by using trifluoroacetic acid (TFA). After hydrolysis, the excess TFA was removed by the addition of methanol and blow-dried three times with nitrogen (N_2). Then we dissolved the hydrolysis with ultrapure water completely and diluted to 200 ppm. Meanwhile, L-fucose (Fuc), L-rhamnose (Rha), L-arabinose (Ara), D-galactose (Gal), D-glucose (Glc), D-xylose (Xyl), D-mannose (Man), D-ribose (Rib), D-glucuronic acid (GlcA) and D-galacturonic acid (GalA) were prepared as references. The CCP was dissolved in D_2O, and detected with the Bruker Advance DPX-500 spectrometer to obtain the ^1H NMR and ^{13}C NMR spectra.

Methylation Analysis

CCP was methylated according to the reported method with some modifications (25, 26). Ten milligram of dry CCP powder was weighed and dissolved in dimethyl sulfoxide (DMSO). After adding NaOH, the reaction was carried out under ultrasonic and dark conditions. Then the solution was mixed with iodomethane and kept at the same condition. After the reaction, water and dichloromethane were added, and the dichloromethane phase was collected and dried. The methylated products were analyzed by FT-IR. The methylation sample was hydrolyzed with trifluoroacetic acid (TFA) at 121°C, and subsequently was dried. The ammonium hydroxide and $NaBD_4$ were added and allowed

to react at room temperature. The reaction was stopped by adding the acetic acid and drying them under nitrogen flow. The reaction product was then gently washed with methanol and subsequently acetylated using acetic anhydride at 100°C. After adding water and dichloromethane, the water phase was discarded and the dichloromethane phase was collected and analyzed using GC-MS (7890A-5977B, Agilent Technologies Inc., CA, USA). The split ratio was 10:1 and Helium was used as carrier gas. The temperature programed was set at 140°C for 2 min initially with gradually increasing at 3°C/min to 230°C, finally kept at 230°C for 3 min.

Cell Culture

DMEM with 10% FBS was used to culture MDA-MB-231 cells. These cells were kept in an incubator (Thermo, USA) with 95% humidity and 5% CO_2 at 37°C.

MTT Assay

The viability of MDA-MB-231 cells was determined by MTT assay. 5×10^4 cells per well were seeded in 96 well plates. After 48 h of treatment with CCP, MTT (5 mg/ml, 20 μl) was added to each well incubated for 4 h. Then, 150 μl of DMSO was added to each well with vibration until the insoluble purple crystal product was dissolved. The absorbance values of each well were recorded at 570 nm by Microplate Reader (Bio-Rad, USA). The growth inhibitory rate formula is as follows:

$$\text{Inhibitory rate (\%)} = \left(1 - \frac{\text{B}}{\text{A}}\right) \times 100$$

where A is the absorbance value of control group, B is absorbance value of CCP treatment group.

Cell Morphological Observation

The MDA-MB-231 cells, with a density of 2×10^5 cells/ml, were incubated in six well plates. The morphological changes were observed under inverted light microscope (Nikon, Japan) after the cells were treated with distinct levels of CCP for 48 h. The nuclear morphological changes were evaluated by Hoechst 33258 staining. Cells cultured with CCP were washed three times with phosphate buffered saline (PBS). Then 1 ml of Hoechst 33258 was added to cells followed by washing with PBS. The changes of nuclear morphology in untreated and treated groups were observed by fluorescence microscope (Nikon, Japan).

Cell Apoptosis Assay

The apoptosis rate of MDA-MB-231 cells was detect using Annexin V-FITC/PI staining. The treated cells were digested with trypsin and collected in centrifuge tube. Then, the precipitate was washed three times with PBS. According to the instructions of the apoptosis detection kit, the Annexin V-FITC and PI were added to suspension cells and incubated for 10 min at the room temperature without light. After that, the flow cytometry (Becton Dicknson, USA) was used to measure the stained cells.

Measurement of Intracellular ROS

The 2,7-Dichlorodihydrofluorescein diacetate (DCFH-DA) staining was applied to measure the production of intracellular ROS. Cells treated with CCP (0, 400, 600 and 800 μg/ml) for 48 h were collected, and centrifuged to remove the supernatant. Then the precipitate was incubated with 20 μl DCFH-DA at 37°C for 20 min. After incubation, ROS was immediately analyzed with a flow cytometry (Becton Dicknson, USA).

Cell Cycle Assay

Propidium Iodide staining was performed to measure dose-response effects of CCP on cell cycle progression. MDA-MB-231 cells treated with distinct levels of CCP were harvested and fixed with precooled 70% ethanol solution at 4°C for 18 h, respectively. After that, the fixed cells were incubated with 0.1 mg/ml RNase A and stained with 50 μg/ml PI for 10 min at 37°C. Finally, the stained cells were analyzed by a flow cytometry (Becton Dicknson, USA).

Western Blot Assay

The apoptosis-related proteins expression was detected by Western blot assay. Cell lysates were prepared at 4°C by adding phenylmethylsulfonyl fluoride (PMSF) inhibitor into RIPA lysis buffer. 12% sodium salt (SDS)-Polyacrylamide gel electrophoresis (SDS-PAGE) was used to separate the protein samples, and then it was imprinted on PVDF membranes. TBST buffer containing 5% bovine serum albumin was used to block the membrane for 2 h. The membrane was incubated with primary antibody overnight at 4°C, which contained β-actin, cyclin D1, CDK4, FasL, Fas, FADD, caspase-3, caspase-8. Subsequently, the horseradish peroxidase conjugated antibodies were incubated with the washed membranes for 2 h at room temperature. Ultimately, the protein bands were detected using ECL reagent in a dark room. Then, the densitometric quantification was carried out using ImageJ Software.

Statistical Analysis

All data were expressed as mean ± standard deviation (SD) and the analysis was evaluated using GraphPad Prism version 6. Student's *t*-test was used to evaluate the significant differences between two groups. $^*P < 0.05$ compared to control group was considered as significant. $^{**}P < 0.01$ compared to control group was considered as very significant. $^{***}P < 0.001$ compared to control group was considered as extremely significant.

RESULTS

Molecular Weight and UV Analysis of CCP

CCP was isolated from *C. citratus* through hot-water extraction, ethanol precipitation, deproteinization by Sevage, dialysis against water and Sephadex G-200 gel column purification. The yield of CCP was 3.42 ± 0.31%. Determination of the molecular weight of CCP using HPGPC. A single narrow symmetrical peak with a retention time of 8.713 min was observed (**Figure 1A**), indicating that CCP was a homogeneous high-molecular-weight polysaccharide. According to the regression equation ($y = -0.3967x + 9.7523$, $R^2 = 0.9985$), the molecular weight of CCP is 1.98×10^6 Da. CCP had no obvious absorption peak at 260∼280 nm (**Figure 1B**), which indicated that it contains almost no protein or nucleic acid (27).

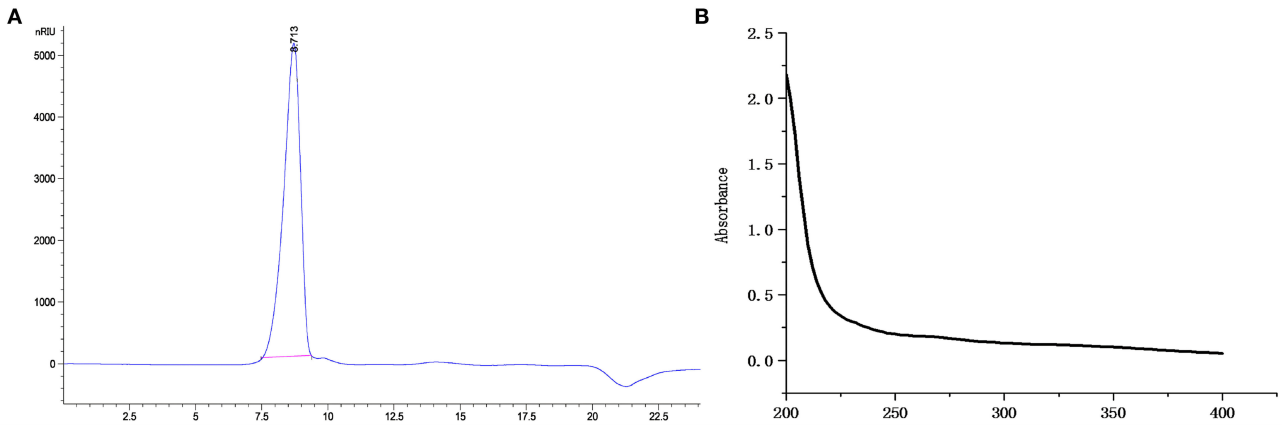

FIGURE 1 | The HPGPC chromatograms **(A)** and UV-vis spectra **(B)** of CCP.

FT-IR Analysis and Monosaccharide Composition of CCP

FT-IR spectra of CCP was displayed in **Figure 2A**. The characteristic absorption peaks of polysaccharide appeared at 3,417.57, 2,923.43, 1,381.43 and 1,268.29 cm^{-1}, respectively, due to the stretching vibration of –OH, the stretching, the variable angle and the bending vibrations of C–H (28). The absorption peak at 1,622.57 cm^{-1} was obtained, which derived from C=O stretching vibration (29). There was a weak absorption peak at 1,714.57 cm^{-1} showed the presence of lesser amounts of uronic acid in CCP. And the bands ranging from 1,000 to 1,200 cm^{-1} were attributed to the vibration of C–O–C glycoside ring, which suggested the presence of pyranose (30). Additionally, the peaks at 810.14 and 878.54 cm^{-1} confirmed that CCP contained α- and β- glycosidic bonds (31). The IC results (**Figure 2B**) showed that CCP was mainly composed of Rha, Ara, Gal and Glc, but also contained a small amount of Xyl, Man, Glca and GalA. Moreover, the molar ratio of Rha, Ara, Gal, Glc, Xyl, Man, Glca and GalA was 1:2.56:3.94:1.96:0.41:0.42:0.29:0.10.

NMR Analysis of CCP

^{1}H NMR and ^{13}C NMR spectra of CCP were showed in **Figure 3**. Usually, the chemical shift of the α-form was observed at δ5.0–6.0 ppm, whereas the chemical shift of the β-form was δ4.5–5.0 ppm (32). It can be seen that CCP had the chemical shifts in both segments, which determined that α- and β-configurations were present. In ^{1}H NMR spectrum, the peak overlap of spectrum signal was serious and it was not suitable for attribution. There were multiple signal peaks in the 13C NMR spectrum from 90 to 110 ppm, indicating that CCP contained both α-glycosidic and β-glycosidic bonds, which was consistent with the ^{1}H NMR conclusion. The signal at 16.53 ppm was assigned to α-L-Rha. The peaks in the region of δ110–100.38 ppm indicated the presence of α-L-Ara, β-D-Gal, β-D-Glc, α-D-Man, α-D-Gal, and β-D-Xyl (33, 34). The ^{13}C chemical shifts of CCP between 170 and 180 ppm were attributed to the presence of a small amount of uronic acid. The results of NMR analysis were consistent with those of monosaccharide composition analysis and FT-IR analysis.

Methylation Analysis of CCP

The glycosidic linkages of the CCP were determined by methylation analysis. On the basis of the monosaccharide composition of CCP, the glycosyl linkages of the monosaccharides are presented and summarized in **Table 1** according to the retention times and mass fragments in GC-MS. As summarized in **Table 1**, CCP was composed of nine glycosidic residues assigned to be 1,3,6-linked Gal*p* (24.36%), 1,3-linked Glc*p* (18.33%), 1,5-linked Ara*f* (15.26%), T-Rha*p* (10.67%), T-Ara*f* (9.76%), 1,6-linked Gal*p* (8.03%), 1,6-linked Man*p* (4.62%), 1,3-linked Gal*p* (4.51%), and 1,4-linked Xyl*p* (4.49%). The proportions of Gal, Ara, Glc, Rha, Man and Xyl (36.90:25.02:18.33:10.67:4.62:4.49) was basically close to the result of monosaccharide composition, which indicate the reliability of methylation analysis.

CCP Inhibited the Cells Proliferation

The cell growth inhibitory rate was assessed by MTT assay to determine the cancer suppressive potential of CCP *in vitro*. The experimental data (**Figure 4A**) suggested that CCP remarkably suppressed MDA-MB-231 cell proliferation in the dose-dependent manner. The inhibition rate of MDA-MB-231 cells treated with CCP (600 μg/ml) for 48 h was approximately 50%. Therefore, MDA-MB-231 cells were treated with 400, 600, and 800 μg/ml CCP for 48 h in subsequent experiments, respectively. The results demonstrated that CCP could act as a potential anticancer drug.

CCP Induced Cells Morphological Changes

The morphological changes in MDA-MB-231 cells on treatment with CCP were presented in **Figure 4B**. The normal MDA-MB-231 cells displayed well growth, typical spindle shapes and clear edge. However, after treated with CCP in different concentrations for 48 h, the cells exhibited apparent morphological alterations including cells volume reduction, cells surface curl and cytoplasmic vacuoles appearance. Especially, most of the cell membranes seriously contracted, the number of exfoliated cells

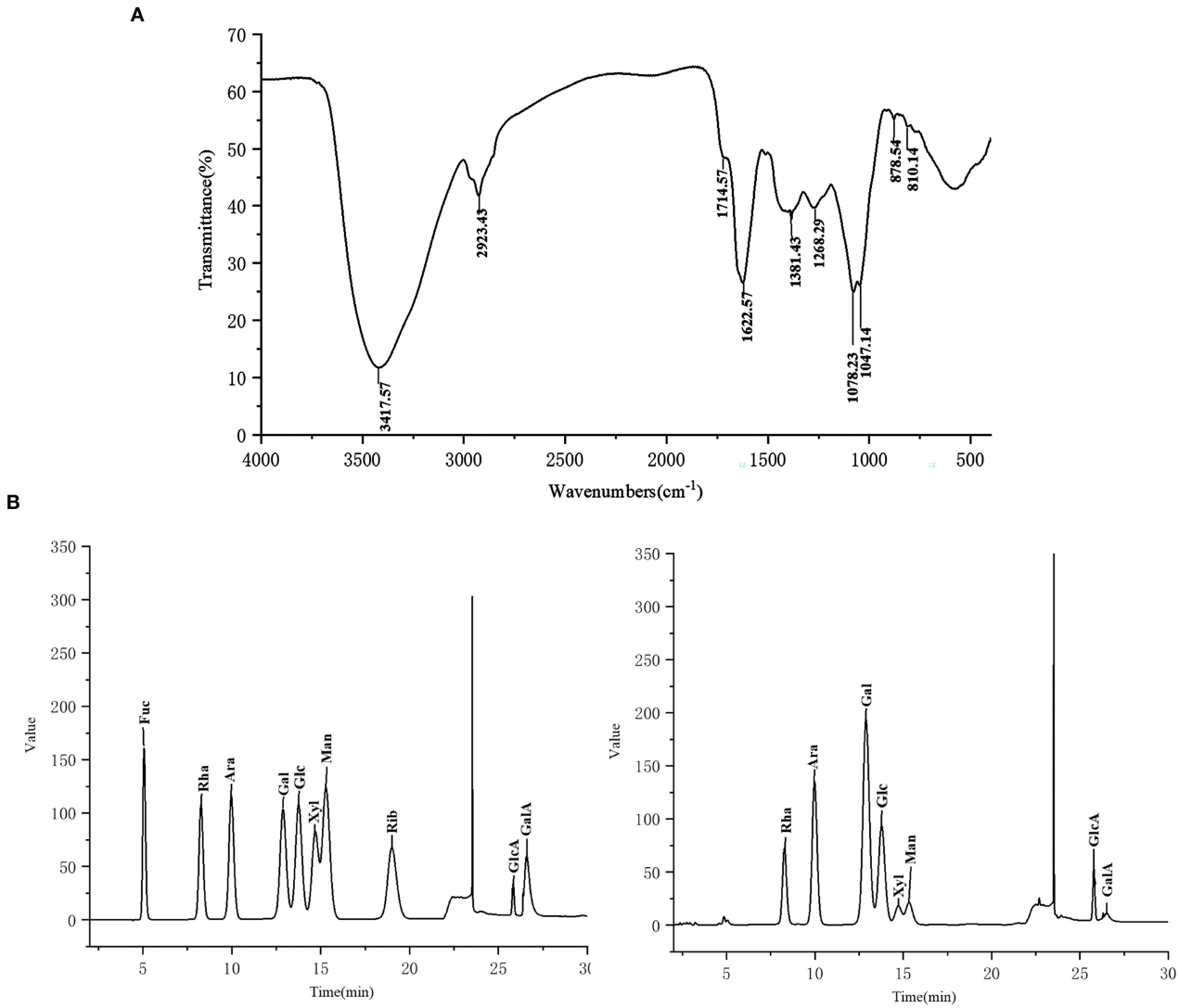

FIGURE 2 | The FT-IR spectra **(A)** and monosaccharide composition **(B)** of CCP.

gradually increased, apoptotic bodies gradually appeared and some cells were broken into particles of different sizes.

The morphological characteristics changes of nucleus of apoptotic cells were further investigated by Hoechst 33258 staining (**Figure 4C**). In the untreated group, the nucleus was light blue, indicating a stable distribution of chromatin in the nucleolus. As chromatin aggregates and nucleoli contract, the treated cell glows bright blue fluorescence and the intensity of bright blue fluorescence also increased with the increase of CCP concentration. The staining results were consistent with the results of morphological observation. These phenomena indicated that CCP induces apoptosis in MDA-MB-231 cells.

CCP Induced Cells Apoptosis

Apoptosis cells induced by different concentrations of CCP were further confirmed by Annexin V-FITC/PI double staining (**Figure 5A**). The viable cells decreased gradually and apoptotic cells increased significantly in the experimental group in a dose-dependent manner. With the increase of CCP concentration, the early apoptotic cells up-regulated from 1.02 to 38.31% and the late apoptotic cells elevated from 2.42 to 33.07%, while the percentage of alive cells was reduced from 94.20 to 28.46% (**Figutre 5B**). These results con-firmed that CCP had the significant effect on regulating MDA-MB-231 cells apoptosis.

Apoptosis has been increasingly proved to be closely associated to oxidative stress (35). The effect of CCP on production of intracellular ROS was analyzed by flow cytometry. Compared with the untreated group (**Figure 5C**), the fluorescence intensity of CCP-treated cells was significantly enhanced in a dose-dependent manner. The level of ROS increased from 1.18 to 25.10%, 51.34 and 74.47%, respectively.

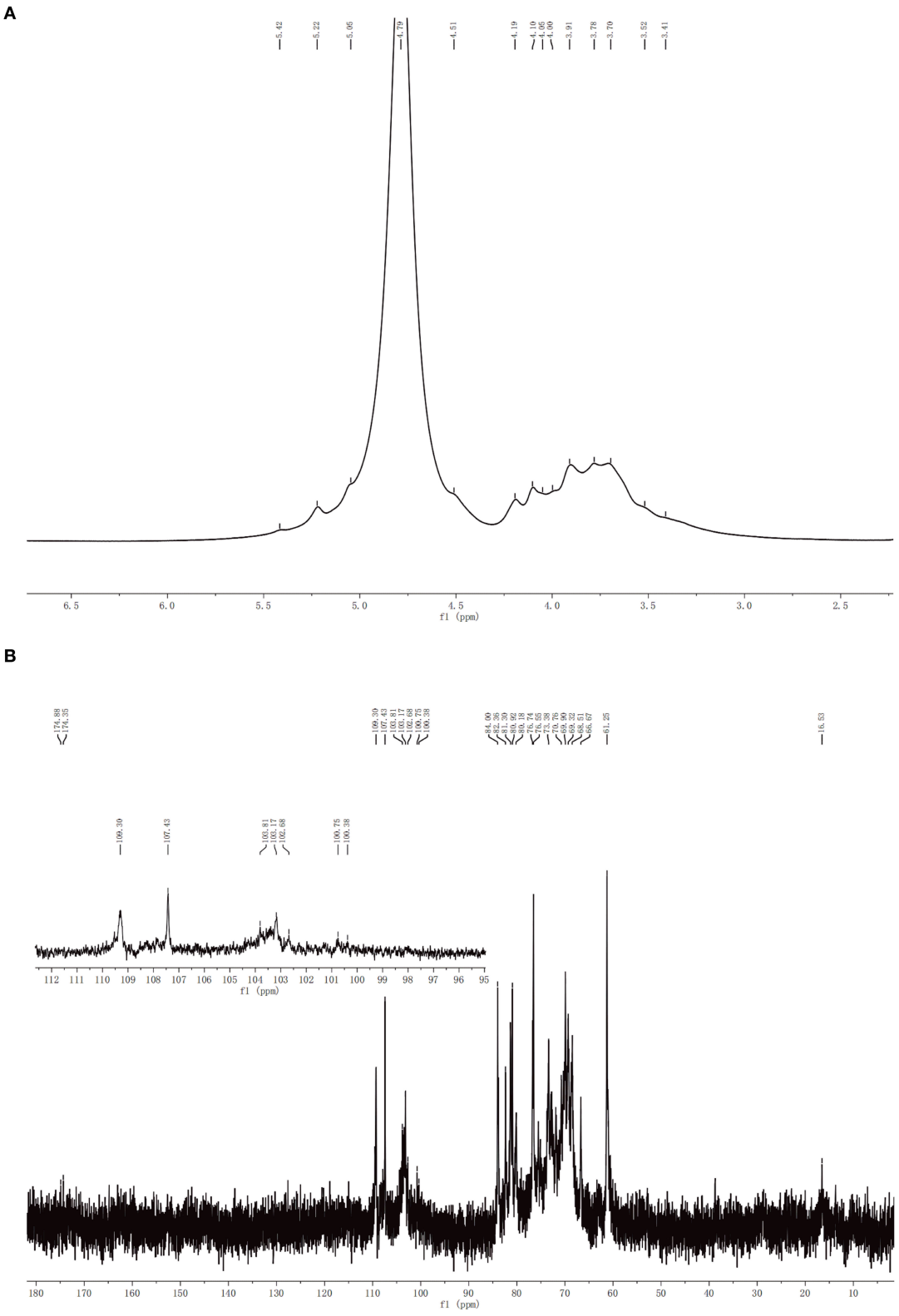

FIGURE 3 | ^{1}H **(A)** and ^{13}C **(B)** NMR spectra of CCP.

TABLE 1 | Methylation analysis of CCP.

Retention time	Linkage type	Methylated sugars	Molar ratio (%)	Mass fragments (*m/z*)
5.976	T-Rha*p*	1,5-di-O-acetyl-6-deoxy-2,3,4-tri-O-methyl rhamnitol	10.67	59, 72, 89, 102, 118, 131, 145, 162, 175, 211
6.243	T-Ara*f*	1,4-di-O-acetyl-2,3,5-tri-O-methyl arabinitol	15.26	71, 87, 102, 118, 129, 145, 161
10.965	5-Ara*f*	1,4,5-tri-O-acetyl-2,3-di-O-methyl arabinitol	9.76	59, 87, 102, 118, 129, 162, 189, 232
11.806	4-Xyl*p*	1,4,5-tri-O-acetyl-2,3-di-O-methyl xylitol	4.49	71, 87, 103, 118, 129, 149, 162, 189, 205
12.573	3-Glc*p*	1,3,5-tri-O-acetyl-2,4,6-tri-O-methyl glucitol	18.33	59, 87, 101, 118, 129, 161, 202, 234
13.264	3-Gal*p*	1,3,5-tri-O-acetyl-2,4,6-tri-O-methyl galactitol	4.51	59, 87, 101, 118, 129, 161,174, 243
14.154	6-Man*p*	1,5,6-tri-O-acetyl-2,3,4-tri-O-methyl mannitol	4.62	71, 87, 99, 102, 118, 129, 162, 189, 233
15.906	6-Gal*p*	1,5,6-tri-O-acetyl-2,3,4-tri-O-methyl galactitol	8.03	71, 87, 99, 102, 118, 129, 162, 189, 233
19.389	3, 6-Gal*p*	1,3,5,6-tetra-O-acetyl-2,4-di-O-methyl galactitol	24.36	59, 87, 101, 118, 129, 160, 189, 234

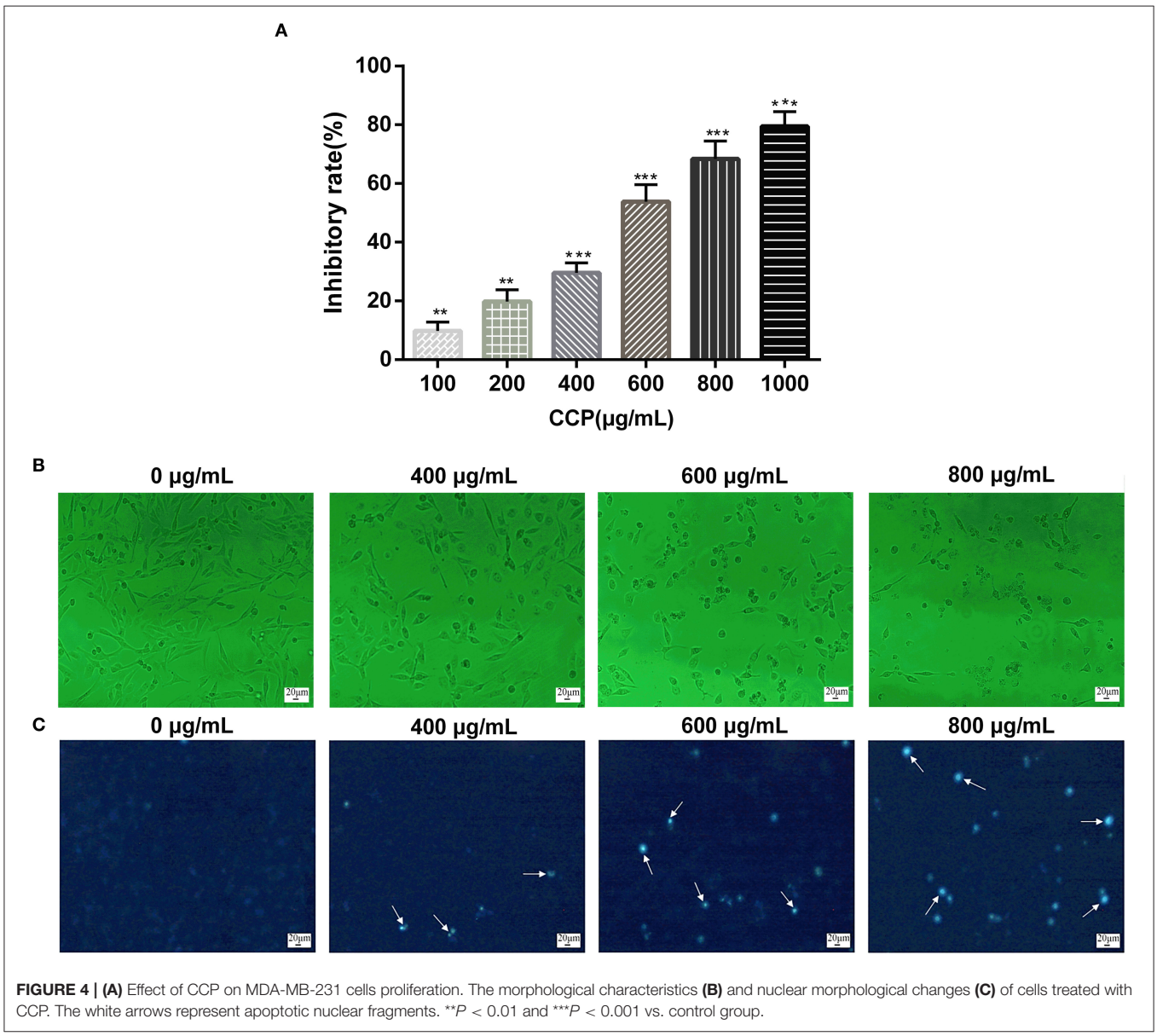

FIGURE 4 | (A) Effect of CCP on MDA-MB-231 cells proliferation. The morphological characteristics **(B)** and nuclear morphological changes **(C)** of cells treated with CCP. The white arrows represent apoptotic nuclear fragments. $^{**}P < 0.01$ and $^{***}P < 0.001$ vs. control group.

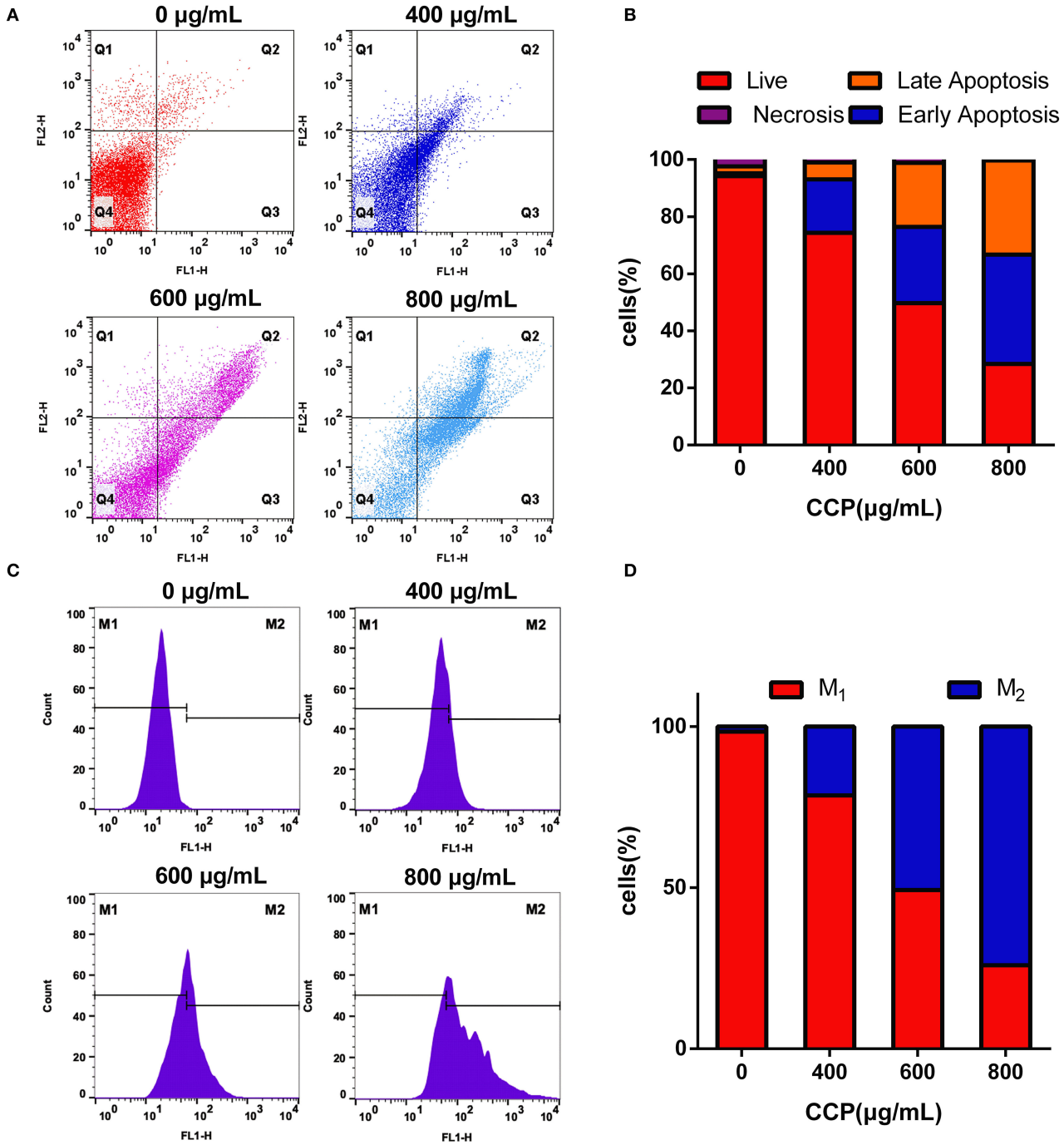

FIGURE 5 | The scatter **(A)** and column **(B)** showed the Annexin V-FITC/PI staining results. The DCFH-DA staining results **(C)** and quantitative analysis **(D)** of the intracellular ROS.

It is verified that CCP may induce MDA-MB-231 cells apoptosis *via* triggering ROS generation.

CCP Induced Cells Cycle Arrest

Changes in DNA content were detected by flow cytometry to assess the proportional distribution of cells throughout the cell cycle. Results (**Figures 6A,B**) showed that after treatment with different CCP concentrations (0, 400, 600, 800 μg/ml), the G_0/G_1 phase of MDA-MB-231 cells increased from 35.73 to 44.10%, 55.21 and 60.43%, respectively. Meanwhile, the significant reduction in the percentage of cells in the G_2/M phase and S phase were found. As the proteins associated with the

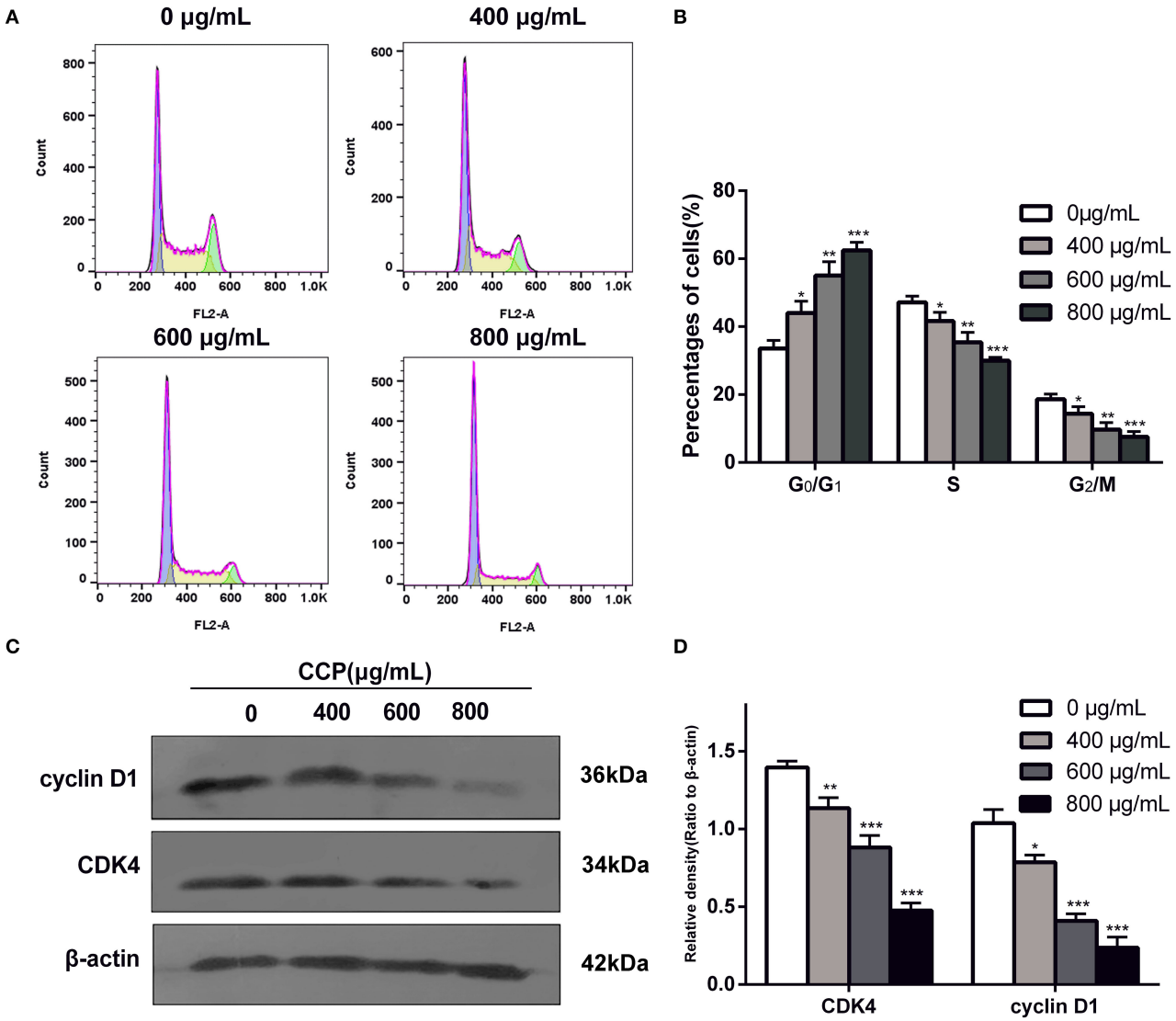

FIGURE 6 | Distribution **(A)** and proportions **(B)** of treated cell in various phases of the cell cycle. The expressions levels **(C)** and quantitative analysis **(D)** of cyclin D1 and CDK4. $^{*}P < 0.05$, $^{**}P < 0.01$ and $^{***}P < 0.001$ vs. control group.

G_0/G_1 phase, cyclin D1 and CDK4 were detected using western blot analysis to further investigate the G_0/G_1 phase arrest. The experimental data suggested that cyclin D1 and CDK4 levels were significantly decreased as the concentration of the CCP increased (**Figures 6C,D**). These data suggested that CCP induced G_0/G_1 phase cycle arrest in MDA-MB-231 cells.

CCP Regulated the Expression of Apoptosis-Associated Proteins

To confirm the role of the Fas/FasL death pathway in CCP-induced apoptosis of MDA-MB-231 cells, we determined the protein expressions of Fas, FasL, FADD, Caspase-3 and Caspase-8. The results (**Figure 7**) showed that CCP treatment resulted in a dose-dependent increased in the level of FADD, Fas and FasL. And the expression of pro-caspase-8 was decreased in CCP-treated MDA-MB-231 cells, while the expression of cleaved-caspase-8 was increased. These indicated that caspase-8 was activated. Subsequently, the cleaved-caspase-3 level in treated cells significantly increased, which confirmed that caspase-3 was activated downstream of caspase-8. These results suggest that CCP played its pro-apoptotic role in MDA-MB-231cells by regulating the Fas/FasL pathway.

DISCUSSION

In this study, a novel water-soluble polysaccharide (CCP) was extracted from *C. citratus*. The molecular weight of CCP (1.98×10^6 Da) was much larger than those reported in

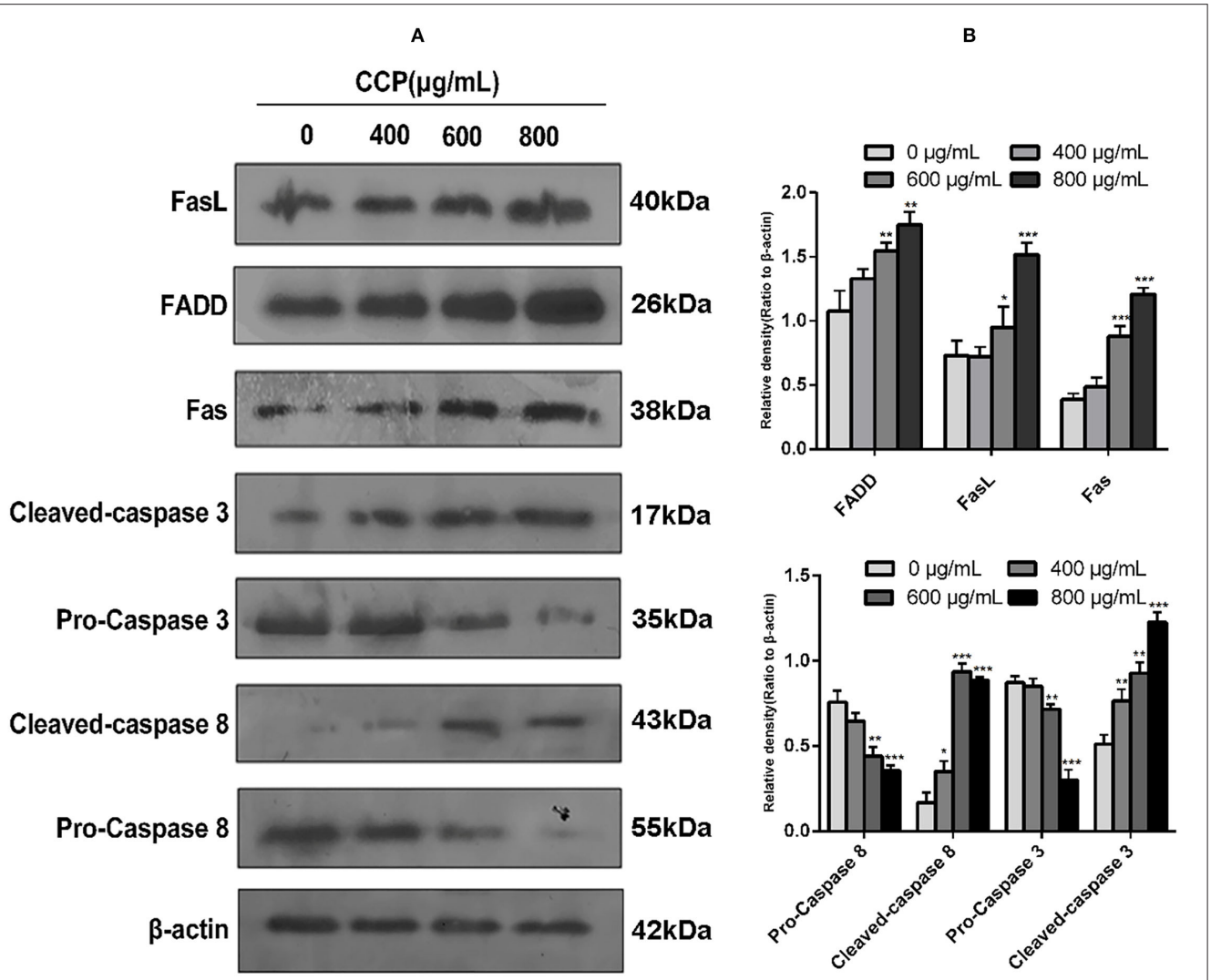

FIGURE 7 | (A) Western blot assay for FasL, FADD, Fas, caspase-3, cleaved-caspase-3, caspase-8 and cleaved-caspase-8 protein expression levels. **(B)** Columns represent the expression of the FasL, FADD, Fas, caspase-3, cleaved-caspase-3, caspase-8 and cleaved-caspase-8 relative to β-actin. $^{*}P < 0.05$, $^{**}P < 0.01$ and $^{***}P < 0.001$ vs. control group.

previous studies, which are hinge on extraction and purification conditions (36). It has been suggested that the high-molecular-weight polysaccharides shown superior antitumor activity (37). Although we suspect that the antitumor activity of CCP may be related to the ability of high-molecular-weight polysaccharides to form higher-order structures, this will need further research. It is worth noting that the monosaccharide composition of *C. citratus* polysaccharides shows a diversity distribution, some are mainly composed of Glc, and some consists mainly of Xyl, which is different from the monosaccharide composition of CCP mentioned in this experiment (36, 38). The content of galactose in CCP was higher than the other monosaccharides such as Glc, Xyl, Ara, Rha and Man. Most of the present studies on the antitumor efficiency of *C. citratus* polysaccharide are limited to crude polysaccharides and low-molecular-weight polysaccharides, and little information about the anti-breast cancer activity of polysaccharides from this plant is available. Therefore, this study examined structural characteristics and the anticancer effect of extracted polysaccharide with high molecule weight on MDA-MB-231 cells and further investigated the action mechanism. To the best of our knowledge, this is first time that high-molecular-weight polysaccharide from *C. citratus* induced G_0/G_1 arrest and apoptosis of MDA-MB-231 cells *via* Fas/FasL-mediated death receptor pathway is reported.

Inhibition of cancer cell proliferation is an effective way to promote cancer cell death. In this experiment, MTT assay revealed that CCP had a dose-dependent inhibitory effect on the proliferation of MDA-MB-231 cells. Apoptosis is considered to be the programmed physiological death of cells, which is related to homeostasis, physiology and pathology (39). Cell death caused by apoptosis involved multiple particular morphological changes, such as cell volume reduction, chromatin condensation,

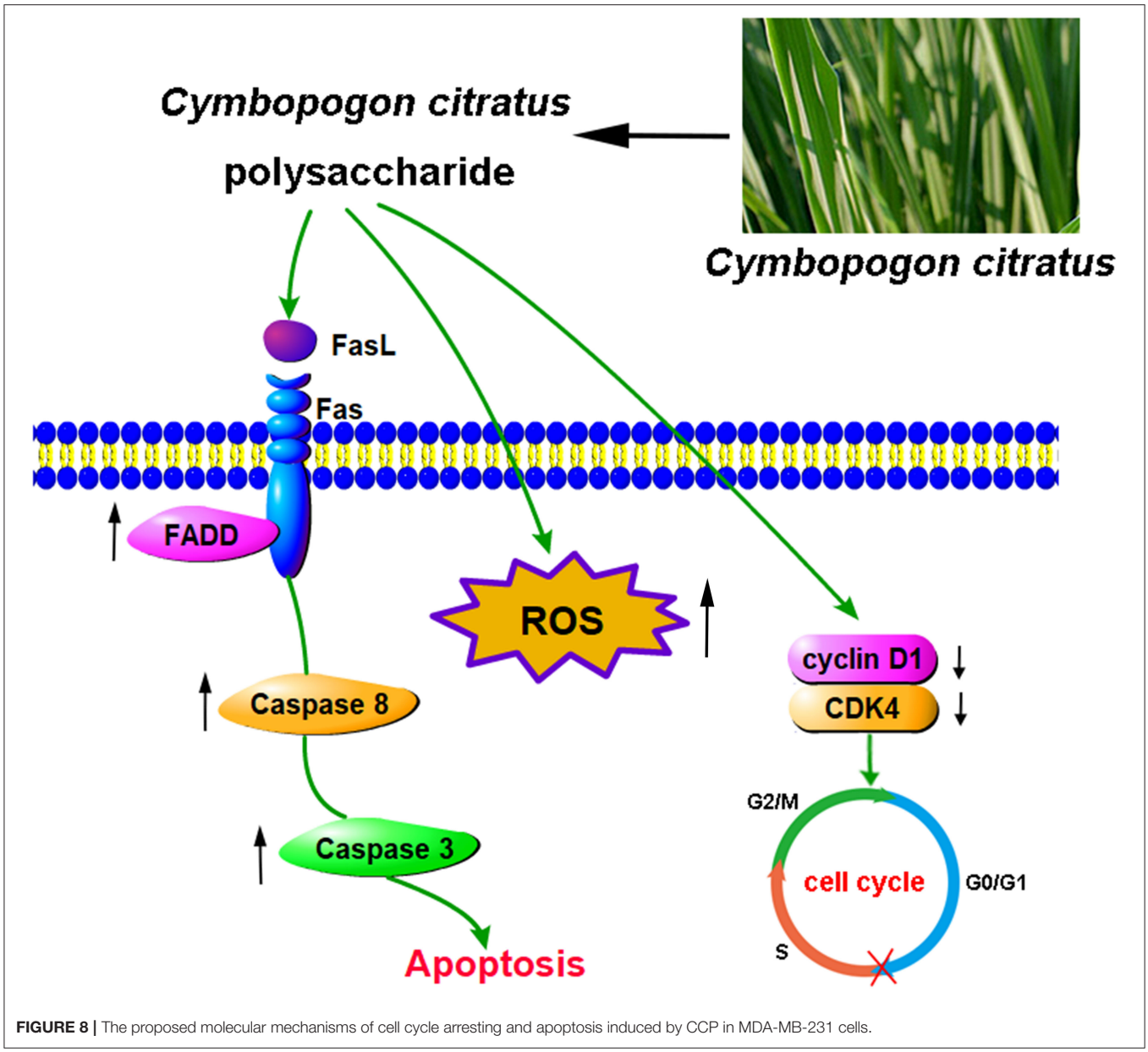

FIGURE 8 | The proposed molecular mechanisms of cell cycle arresting and apoptosis induced by CCP in MDA-MB-231 cells.

cytoplasmic vacuolation, nucleolus fragmentation of the nuclear membrane, formation of apoptotic bodies, and extravagation of phosphatidylserine (PS) inside the membrane to the membrane surface (40). Annexin-V, a phospholipid binding protein, has higher affinity for PS and can combine with the nucleic acid dye PI to distinguish viable cells from apoptotic and necrotic cells (40, 41). The characteristic morphological changes of the MDA-MB-231 cells were obviously observed in this study when they were treated with CCP for 48 h. In addition, CCP had been further demonstrated to induce apoptosis of MDA-MB-231 cells according to the Annexin V-FITC/PI double staining results. Reactive oxygen species (ROS), containing hydroxyl radicals and singlet oxygen, are closely as-sociated with oxidative stress. According to Parvaiz, ROS was involved in the process of protein fraction from *Withania somnifera* induced apoptosis of MDA-MB-231 cells (42). Our findings indicated that different concentrations of CCP significantly induced ROS production in MDA-MB-231 cells, which may induce cell apoptosis.

Since cell cycle can regulate cell proliferation, differentiation and apoptosis, interfering with cell cycle is recognized as a potent approach for cancer treatment (43). The realization of cell cycle progression depends on the precise and rigorous regulation of cell cycle by various levels of regulatory factors, such as cyclin-dependent kinases (CDK) and cyclins (44). It is known that many substances could modulate regulators at specific cell cycle checkpoints to provoke cell cycle arrest (45–47). Cyclin D1/D3 and Cyclin E were closely related to CDK4/6 and CDK2, which played a pivotal role in controlling the progression of G_1 cell cycle

(48). Li et al. (49) found that a heptamethine cyanine dye (IR-783) decreased the levels of cyclin D1, cyclin E, CDK2 which led to cycle G_0/G_1 arrest in breast cancer cells. Likewise, Gao et al. (50) pointed out that β-Cryptoxanthin mediated the downregulation of cyclin E, cyclin D1, and CDK4, CDK6 to induce G_0/G_1 arrest in SGC-7901 cells and AGS cells. In this study, flow cytometry detected that cell cycle was strongly arrested at G_0/G_1 phase. Consistent with this, we observed significant de-creased levels of cyclin D1 and CDK4 in MDA-MB-231 cells treated with CCP. These results indicated that cell cycle of MDA-MB-231 cells was arrested at G_0/G_1 phase in the case of CCP.

The death receptor pathways, including TNFR, TRAIL and Fas/FasL signaling pathways, are one of the most important pathways of cell apoptosis (51). The Fas/FasL system played an important role in maintaining cell colonies, clearing malignant transformed cells and regulating the immune system (52). Fas, a type I cell surface glycoprotein, belongs to the cytokine receptor family, which is similar to tumor necrosis factor (TNF) receptors (53). FasL is a type II across a membrane protein on the surface of the cell, belonging to the tumor necrosis factor (TNF) family (54). When the ligand FasL binds to the Fas receptor, it attracts FADD with the same death domain in the cytoplasm. Subsequently, FADD can recruit procaspase-8 through its death effector domain (DED). Once caspase-8 is activated, it cleaves and activates the key downstream apoptotic executive factor caspases-3 to induce apoptosis (55). According to the results of this study, CCP treatment significantly increased the level of activated Caspase-8/-3. Furthermore, the expression of Fas, FasL, FADD in MDA-MB-231 cells were significantly increased, suggesting that CCP-induced apoptosis could be triggered through Fas/FasL-mediated death receptor pathway in MDA-MB-231 cells (**Figure 8**). In consistent with our results, the antitumor activities of *Gracilariopsis lemaneiformis* Polysaccharide was associated with apoptosis-related Fas/FasL signaling pathway in the human lung cancer cell line A549, the gastric cancer cell line MKN28, and the mouse melanoma cell line B16 (56).

CONCLUSIONS

Collectively, CCP was a high molecular weight polysaccharide extracted from *C. citratus*. According to the results of HPGPC, IC, FT-IR, methylation and NMR, CCP was a 1.98×10^6 Da acidic polysaccharide with a complex structure mainly composed of Gal, Ara, Glc and Rha. In MDA-MB-231 cells, the proliferation was significantly inhibited after CCP treatment. Moreover, we found that the G_0/G_1 arrest was induced by CCP in a dose-dependent manner, and Fas/FasL-mediated death receptor pathway was thought to participate in the process of CCP-induced apoptosis. These experimental results demonstrated that *C. citratus* polysaccharide could potentially be used as an easily available natural source for breast cancer therapy, which can be widely used in the food industry in the future.

DATA AVAILABILITY STATEMENT

The raw data supporting the conclusions of this article will be made available by the authors, without undue reservation.

AUTHOR CONTRIBUTIONS

YC and HL designed the whole study. YC and SQ carried out all experiments. SQ, YC, and HX acquired and interpreted data. YC wrote the original version of the manuscript. HL and PC revised and edited the manuscript. All authors contributed to the article and approved the submitted version.

FUNDING

This research work was funded by the Key Research and Development Project of Shanxi Province (Grant No. 201903D211008), the Natural Science Foundation of Jiangsu Province (Grant No. BE2019351), and the Natural Science Foundation of Tianjin City of China (Grant No. 21YDTPJC00060).

REFERENCES

1. Sengar P, Juárez P, Verdugo MA, Arellano DL, Jain A, Chauhan K, et al. Development of a functionalized UV-emitting nanocomposite for the treatment of cancer using indirect photodynamic therapy. *J Nanobiotechnology.* (2018) 16:19. doi: 10.1186/s12951-018-0344-3
2. Lei Q, Xiong L, Xia Y, Feng Z, Gao T, Wei W, et al. YLT-11, a novel PLK4 inhibitor, inhibits human breast cancer growth *via* inducing maladjusted centriole duplication and mitotic defect. *Cell Death Dis.* (2018) 9:1066. doi: 10.1038/s41419-018-1071-2
3. Dou D, Ren X, Han M, Xu X, Ge X, Gu Y, et al. Cancer-associated fibroblasts-derived exosomes suppress immune cell function in breast cancer *via* the miR-92/PD-L1 pathway. *Front Immunol.* (2020) 11:2026. doi: 10.3389/fimmu.2020.02026
4. Kaverina N, Borovjagin AV, Kadagidze Z, Baryshnikov A, Baryshnikova M, Malin D, et al. Astrocytes promote progression of breast cancer metastases to the brain *via* a KISS1-mediated autophagy. *Autophagy.* (2017) 13:1905–23. doi: 10.1080/15548627.2017.1360466
5. Ge C, Cao B, Feng D, Zhou F, Zhang J, Yang N, et al. The down-regulation of SLC7A11 enhances ROS induced P-gp over-expression and drug resistance in MCF-7 breast cancer cells. *Sci Rep.* (2017) 7:3791. doi: 10.1038/s41598-017-03881-9
6. Giordano SH, Lin YL, Kuo YF, Hortobagyi GN, Goodwin JS. Decline in the use of anthracyclines for breast cancer. *J Clin Oncol.* (2012) 30:2232–9. doi: 10.1200/JCO.2011.40.1273
7. Guenancia C, Lefebvre A, Cardinale D, Yu AF, Ladoire S, Ghiringhelli F, et al. Obesity as a risk factor for anthracyclines and trastuzumab cardiotoxicity in breast cancer: a systematic review and meta-analysis. *J Clin Oncol.* (2016) 34:3157–65. doi: 10.1200/JCO.2016.67.4846
8. Tong R, Wu X, Liu Y, Liu Y, Zhou J, Jiang X, et al. Curcumin-induced DNA demethylation in human gastric cancer cells is mediated by the DNA-damage response pathway. *Oxid Med Cell Longev.* (2020) 2020:2543504. doi: 10.1155/2020/2543504
9. Chen L, Gong MW, Peng ZF, Zhou T, Ying MG, Zheng QH, et al. The marine fungal metabolite, dicitrinone B, induces A375 cell apoptosis through the ROS-related caspase pathway. *Mar Drugs.* (2014) 12:1939–58. doi: 10.3390/md12041939
10. Tian WT, Zhang XW, Liu HP, Wen YH Li HR, Gao J. Structural characterization of an acid polysaccharide from *Pinellia ternata* and its induction effect on apoptosis of HepG2 cells. *Int J*

Biol Macromol. (2020) 153:451–60. doi: 10.1016/j.ijbiomac.2020.02.219
11. Chen F, Huang G. Preparation and immunological activity of polysaccharides and their derivatives. *Int J Biol Macromol.* (2018) 112:211–6. doi: 10.1016/j.ijbiomac.2018.01.169
12. Ferreira ICFR, Heleno SA, Reis FS, Stojkovic D, Queiroz MJRP, Vasconcelos MH, et al. Chemical features of Ganoderma polysaccharides with antioxidant, anti-tumor and anti-microbial activities. *Phytochemistry.* (2015) 114:38–55. doi: 10.1016/j.phytochem.2014.10.011
13. Shah G, Shri R, Panchal V, Sharma N, Singh B, Mann AS. Scientific basis for the therapeutic use of *Cymbopogon citratus*, Stapf (Lemongrass). *J Adv Pharm Technol Res.* (2011) 2:3–8. doi: 10.4103/2231-4040.79796
14. Haque A, Remadevi R, Naebe M. Lemongrass (Cymbopogon): a review on its structure, properties, applications and recent developments. *Cellulose.* (2018) 25:5455–77. doi: 10.1007/s10570-018-1965-2
15. Ekpenyong CE, Akpan E. Nyoh A. Ethnopharmacology, phytochemistry, and biological activities of *Cymbopogon citratus* (DC) Stapf extracts. *Chin J Nat Med.* (2015) 13:321–37. doi: 10.1016/S1875-5364(15)30023-6
16. Francisco V, Figueirinha A, Neves BM, García-Rodríguez C, Lopes MC, Cruz MT, et al. *Cymbopogon citratus* as source of new and safe anti-inflammatory drugs: bio-guided assay using lipopolysaccharide-stimulated macrophages. *J Ethnopharmacol.* (2011) 133:818–27. doi: 10.1016/j.jep.2010.11.018
17. Trang DT, Hoang TKV, Nguyen TTM, Van Cuong P, Dang NH, Dang HD, et al. Essential oils of lemongrass (*Cymbopogon citratus* Stapf) induces apoptosis and cell cycle arrest in A549 lung cancer cells. *Biomed Res Int.* (2020) 2020:5924856. doi: 10.1155/2020/5924856
18. Ruvinov I, Nguyen C, Scaria B, Vegh C, Zaitoon O, Baskaran K, et al. Lemongrass extract possesses potent anti-cancer activity against human colon cancers, inhibits tumorigenesis, enhances efficacy of Folfox, and reduces its adverse effects. *Integr Cancer Ther.* (2019) 18:1534735419889150. doi: 10.1177/1534735419889150
19. Figueirinha A, Paranhos A, Pérez-Alonso J, Santos-Buelga C, Batista MT. *Cymbopogon citratus* leaves: characterization of flavonoids by HPLC–PDA–ESI/MS/MS and an approach to their potential as a source of bioactive polyphenols. *Food Chem.* (2008) 110:718–28. doi: 10.1016/j.foodchem.2008.02.045
20. Mediesse FK, Boudjeko T, Hasitha A, Gangadhar M, Mbacham WF. Yogeeswari P. Inhibition of lipopolysaccharide (LPS)-induced neuroinflammatory response by polysaccharide fractions of *Khaya grandifoliola* (CDC) stem bark, *Cryptolepis sanguinolenta* (Lindl) Schltr and *Cymbopogon citratus* Stapf leaves in raw 2647 macrophages and U87 glioblastoma cells. *BMC Complement Altern Med.* (2018) 18:86. doi: 10.1186/s12906-018-2156-2
21. Burana-Osot J, Pattanapanyasat K, Soonthornchareonnon N, Sukapirom K, Toida T. Characterisation and immuno-stimulating activity of polysaccharides from Thai medicinal plants. *Nat Prod Res.* (2010) 24:1403–12. doi: 10.1080/14786410902940974
22. Thangam R, Suresh V, Kannan S. Optimized extraction of polysaccharides from *Cymbopogon citratus* and its biological activities. *Int J Biol Macromol.* (2014) 65:415–23. doi: 10.1016/j.ijbiomac.2014.01.033
23. Nigjeh SE, Yeap SK, Nordin N, Rahman H, Rosli R. *In vivo* anti-tumor effects of citral on 4T1 breast cancer cells *via* induction of apoptosis and downregulation of aldehyde dehydrogenase activity. *Molecules.* (2019) 24:3241. doi: 10.3390/molecules24183241
24. Chaouki W, Leger DY, Liagre B, Beneytout JL, Hmamouchi M. Citral inhibits cell proliferation and induces apoptosis and cell cycle arrest in MCF-7 cells. *Fundam Clin Pharmacol.* (2009) 23:549–56. doi: 10.1111/j.1472-8206.2009.00738.x
25. Chen G, Bai Y, Zeng Z, Peng Y, Zhou W, Shen W, et al. Structural characterization and immunostimulatory activity of heteropolysaccharides from Fuzhuan brick tea. *J Agric Food Chem.* (2021) 69:1368–78. doi: 10.1021/acs.jafc.0c06913
26. Pan LC, Zhu YM, Zhu ZY, Xue W, Liu CY, Sun HQ, et al. Chemical structure and effects of anti-oxidation and against α-glucosidase of natural polysaccharide from *Glycyrrhiza inflata* Batalin. *Int J Biol Macromol.* (2020) 155:560–71. doi: 10.1016/j.ijbiomac.2020.03.192
27. Ji X, Guo J, Ding D, Gao J, Hao L, Guo X, et al. Structural characterization and anti-oxidant activity of a novel high-molecular-weight polysaccharide from *Ziziphus Jujuba* cv. Muzao. *J Food Meas Charact.* (2022). doi: 10.1007/s11694-022-01288-3. [Epub ahead of print].
28. Zhang Q, Xu Y, Zou S, Zhang X, Cao K, Fan Q. Novel functional polysaccharides from Radix Polygoni Multiflori water extracted residue: preliminary characterization and immunomodulatory activity. *Carbohydr Polym.* (2016) 137:625–31. doi: 10.1016/j.carbpol.2015.11.023
29. Feng YY Ji HY, Dong XD, Liu AJ. An alcohol-soluble polysaccharide from *Atractylodes macrocephala* Koidz induces apoptosis of Eca-109 cells. *Carbohydr Polym.* (2019) 226:115–36. doi: 10.1016/j.carbpol.2019.115136
30. Yu J, Ji HY, Liu C, Liu AJ. The structural characteristics of an acid-soluble polysaccharide from *Grifola frondosa* and its anti-tumor effects on H22-bearing mice. *Int J Biol Macromol.* (2020) 158:1288–98. doi: 10.1016/j.ijbiomac.2020.05.054
31. Dong XD, Feng YY, Liu YN, Ji HY, Yu SS, Liu A, et al. A novel polysaccharide from *Castanea mollissima* Blume: preparation, characteristics and anti-tumor activities *in vitro* and *in vivo*. *Carbohydr Polym.* (2020) 240:116323. doi: 10.1016/j.carbpol.2020.116323
32. Su Y, Li L. Structural characterization and anti-oxidant activity of polysaccharide from four auriculariales. *Carbohydr Polym.* (2020) 229:115407. doi: 10.1016/j.carbpol.2019.115407
33. Ren Y, Zhu Z, Sun H, Chen L. Structural characterization and inhibition on α-glucosidase activity of acidic polysaccharide from *Annona squamosa*. *Carbohydr Polym.* (2017) 174:1–12. doi: 10.1016/j.carbpol.2017.05.092
34. Agrawal PK, NMR. Spectroscopy in the structural elucidation of oligosaccharides and glycosides. *Phytochemistry.* (1992) 31:3307–30. doi: 10.1016/0031-9422(92)83678-R
35. Wang R, Wang L, He J, Li S, Yang X, Sun P, et al. Specific inhibition of CYP4A alleviates myocardial oxidative stress and apoptosis induced by advanced glycation end-products. *Front Pharmacol.* (2019) 10:876. doi: 10.3389/fphar.2019.00876
36. Thangam R, Sathuvan M, Poongodi A, Suresh V, Pazhanichamy K, Sivasubramanian S, et al. Activation of intrinsic apoptotic signaling pathway in cancer cells by *Cymbopogon citratus* polysaccharide fractions. *Carbohydr Polym.* (2014) 107:138–50. doi: 10.1016/j.carbpol.2014.02.039
37. Chen P, Liu HP Ji HH, Sun NX, Feng YY, A cold-water soluble polysaccharide isolated from *Grifola frondosa* induces the apoptosis of HepG2 cells through mitochondrial passway. *Int J Biol Macromol.* (2019) 125:1232–41. doi: 10.1016/j.ijbiomac.2018.09.098
38. Bao XL, Yuan HH, Wang CZ, Fan W, Lan MB. Polysaccharides from *Cymbopogon citratus* with anti-tumor and immunomodulatory activity. *Pharm Biol.* (2015) 53:1–8. doi: 10.3109/13880209.2014.911921
39. Eisenberg-Lerner A, Bialik S, Simon HU, Kimchi A. Life and death partners: apoptosis, autophagy and the cross-talk between them. *Cell Death Differ.* (2009) 16:966–75. doi: 10.1038/cdd.2009.33
40. Doonan F, Cotter TG. Morphological assessment of apoptosis. *Methods.* (2008) 44:200–4. doi: 10.1016/j.ymeth.2007.11.006
41. Yu J, Ji H, Dong X, Feng Y, Liu A. Apoptosis of human gastric carcinoma MGC-803 cells induced by a novel *Astragalus membranaceus* polysaccharide *via* intrinsic mitochondrial pathways. *Int J Biol Macromol.* (2019) 126:811–9. doi: 10.1016/j.ijbiomac.2018.12.268
42. Dar PA, Mir SA, Bhat JA, Hamid A, Singh LR, Malik F, et al. An anti-cancerous protein fraction from *Withania somnifera* induces ROS-dependent mitochondria-mediated apoptosis in human MDA-MB-231 breast cancer cells. *Int J Biol Macromol.* (2019) 135:77–87. doi: 10.1016/j.ijbiomac.2019.05.120
43. Yu S, Ji H, Dong X, Liu A, Yu J. FAS/FAS-L-mediated apoptosis and autophagy of SPC-A-1 cells induced by water-soluble polysaccharide from *Polygala tenuifolia*. *Int J Biol Macromol.* (2020) 150:449–58. doi: 10.1016/j.ijbiomac.2020.02.010
44. Zhang X, Feng H, Du J, Sun J, Li D, Hasegawa T, et al. Aspirin promotes apoptosis and inhibits proliferation by blocking G_0G_1 into S phase in rheumatoid arthritis fibroblast-like synoviocytes *via* downregulation of JAK/STAT3 and NF-κB signaling pathway. *Int J Mol Med.* (2018) 42:3135–48. doi: 10.3892/ijmm.2018.3883
45. Wang Z, Wang Y, Wang S, Meng X, Song F, Huo W, et al. Coxsackievirus A6 induces cell cycle arrest in G_0G_1 phase for viral production. *Front Cell Infect Microbiol.* (2018) 8:279. doi: 10.3389/fcimb.2018.00279

46. Mantso T, Anestopoulos I, Lamprianidou E, Kotsianidis I, Pappa A, Panayiotidis MI. Isothiocyanate-induced cell cycle arrest in a novel *in vitro* exposure protocol of human malignant melanoma (A375) cells. *Anticancer Res.* (2019) 34:591–6. doi: 10.21873/anticanres.13152
47. Zhang HT, Yang J, Liang GH, Gao XJ, Sang Y, Gui T, et al. Andrographolide induces cell cycle arrest and apoptosis of chondrosarcoma by targeting TCF-1/SOX9 axis. *J Cell Biochem.* (2017) 118:4575–86. doi: 10.1002/jcb.26122
48. Malumbres M, Barbacid M. Cell cycle, CDKs and cancer: a changing paradigm. *Nat Rev Cancer.* (2009) 9:153–66. doi: 10.1038/nrc2602
49. Li P, Liu Y, Liu W, Li G, Tang Q, Zhang Q, et al. IR-783 inhibits breast cancer cell proliferation and migration by inducing mitochondrial fission. *Int J Oncol.* (2019) 55:415–24. doi: 10.3892/ijo.2019.4821
50. Gao M, Dang F, Deng C. β-Cryptoxanthin induced anti-proliferation and apoptosis by G_0G_1 arrest and AMPK signal inactivation in gastric cancer. *Eur J Pharmacol.* (2019) 859:172528. doi: 10.1016/j.ejphar.2019.172528
51. He X, Wu J, Yuan L, Lin F, Yi J, Li J, et al. Lead induces apoptosis in mouse TM3 Leydig cells through the Fas/FasL death receptor pathway. *Environ Toxicol Phar.* (2017) 56:99–105. doi: 10.1016/j.etap.2017.08.034
52. Zhao T, Xu Y, Ren S, Liang C, Zhou X, Wu J. The siRNA silencing of DcR3 expression induces Fas ligand-mediated apoptosis in HepG2 cells. *Exp Ther Med.* (2018) 15:4370–8. doi: 10.3892/etm.2018.5964
53. Gao J, Zhao Y, Wang C, Ji H, Yu J, Liu C, et al. A novel synthetic *chitosan selenate* (CS) induces apoptosis in A549 lung cancer cells *via* the Fas/FasL pathway. *Int J Biol Macromol.* (2020) 158:689–97. doi: 10.1016/j.ijbiomac.2020.05.016
54. Pinti M, Troiano L, Nasi M, Moretti L, Monterastelli E, Mazzacani A, et al. Genetic polymorphisms of Fas (CD95) and FasL (CD178) in human longevity: studies on centenarians. *Cell Death Differ.* (2002) 9:431–8. doi: 10.1038/sj.cdd.4400964
55. Wu P, Yu SS, Liu C, Liu AJ. Seleno-Chitosan induces apoptosis of lung cancer cell line SPC-A-1 *via* Fas/FasL pathway. *Bioorg Chem.* (2020) 97:103701. doi: 10.1016/j.bioorg.2020.103701
56. Kang Y, Wang ZJ, Xie D, Sun X, Yang W, Zhao X, et al. Characterization and potential anti-tumor activity of polysaccharide from *Gracilariopsis lemaneiformis*. *Mar Drugs*. (2017) 15:100. doi: 10.3390/md15040100

Conflict of Interest: The authors declare that the research was conducted in the absence of any commercial or financial relationships that could be construed as a potential conflict of interest.

Publisher's Note: All claims expressed in this article are solely those of the authors and do not necessarily represent those of their affiliated organizations, or those of the publisher, the editors and the reviewers. Any product that may be evaluated in this article, or claim that may be made by its manufacturer, is not guaranteed or endorsed by the publisher.

Copyright © 2022 Chen, Qiao, Liu, Xing and Chen. This is an open-access article distributed under the terms of the Creative Commons Attribution License (CC BY). The use, distribution or reproduction in other forums is permitted, provided the original author(s) and the copyright owner(s) are credited and that the original publication in this journal is cited, in accordance with accepted academic practice. No use, distribution or reproduction is permitted which does not comply with these terms.

frontiers | Frontiers in Nutrition

REVIEW
published: 20 May 2022
doi: 10.3389/fnut.2022.908175

Structural Elucidation, Modification, and Structure-Activity Relationship of Polysaccharides in Chinese Herbs: A Review

Bei Wang†, Lingling Yan†, Shuchen Guo, Ling Wen, Mengli Yu, Liang Feng and Xiaobin Jia**

State Key Laboratory of Natural Medicines, School of Traditional Chinese Pharmacy, China Pharmaceutical University, Nanjing, China

OPEN ACCESS

Edited by:
Xiaolong Ji, Zhengzhou University of Light Industry, China

Reviewed by:
Qiang Peng, Northwest A & F University, China
Liuqing Yang, Jiangsu University, China

***Correspondence:**
Liang Feng
wenmoxiushi@163.com
Xiaobin Jia
jiaxiaobin2015@163.com

†These authors have contributed equally to this work and share first authorship

Specialty section:
This article was submitted to Food Chemistry, a section of the journal Frontiers in Nutrition

Received: *30 March 2022*
Accepted: *22 April 2022*
Published: *20 May 2022*

Citation:
Wang B, Yan L, Guo S, Wen L, Yu M, Feng L and Jia X (2022) Structural Elucidation, Modification, and Structure-Activity Relationship of Polysaccharides in Chinese Herbs: A Review. Front. Nutr. 9:908175. doi: 10.3389/fnut.2022.908175

Chinese herbal polysaccharides (CHPs) are natural polymers composed of monosaccharides, which are widely found in Chinese herbs and work as one of the important active ingredients. Its biological activity is attributed to its complex chemical structure with diverse spatial conformations. However, the structural elucidation is the foundation but a bottleneck problem because the majority of CHPs are heteropolysaccharides with more complex structures. Similarly, the studies on the relationship between structure and function of CHPs are even more scarce. Therefore, this review summarizes the structure-activity relationship of CHPs. Meanwhile, we reviewed the structural elucidation strategies and some new progress especially in the advanced structural analysis methods. The characteristics and applicable scopes of various methods are compared to provide reference for selecting the most efficient method and developing new hyphenated techniques. Additionally, the principle structural modification methods of CHPs and their effects on activity are summarized. The shortcomings, potential breakthroughs, and developing directions of the study of CHPs are discussed. We hope to provide a reference for further research and promote the application of CHPs.

Keywords: Chinese herbal polysaccharides, structure-activity relationship, structural elucidation, modification, bioactivity

INTRODUCTION

The polysaccharides derived from Chinese herbs are mostly heteropolysaccharides which consist of different kinds of monosaccharides. Modern pharmacological studies reported that CHPs had functions such as anti-tumor (1), immunologic enhancement (2), intestinal microenvironment regulation (3), and anti-oxidation (4). As a drug, it is related to the occurrence and treatment of a variety of diseases and is favored on clinical settings. CHP preparations such as *Astragalus* polysaccharide injection, *Ginseng* polysaccharide injection, and *Poria cocos* polysaccharide oral liquid have been widely applied for clinical use.

Previous research focused on small molecules in Chinese herbs, while ignoring the research on macromolecular polysaccharides, resulting in a waste of resources. The complexity and instability

of polysaccharides' structure make the process of revealing its mechanism and the development of products or drugs more complicated. As a result, it will impede the development of new polysaccharide drugs and reduce the application scope of polysaccharides. To play the better role of CHPs, the structure-activity relationship of polysaccharides must be clarified.

The primary structure and chain conformation of polysaccharides are closely related to the construction of various functions. However, due to the intricate structure and imperfection of technical support, current methods cannot fully clarify the exact structure of CHPs, especially the three-dimensional structure. There are fewer reports on the structure-activity relationship. In addition, some studies have shown that not all polysaccharides can express their ideal bio-activities (5). Nevertheless, the above problem is effectively solved by modifying its structure. Biological activity of polysaccharides after modification can be enhanced greatly and even new biological activity can be produced (6, 7). Structural modification can improve the physicochemical properties and activities of polysaccharides, which promotes the exploration of the structure-activity relationship of polysaccharides. Therefore, we summarized the structural elucidation, modification, and structure-activity relationship of CHPs, so as to provide theoretical reference and technical support for the development and utilization of CHPs.

STRUCTURE-ACTIVITY RELATIONSHIP

Various polysaccharides show certain chemical structures. Wherein their biological activities depend on events that occur at the molecular structure level (8). Therefore, exploring the structure-activity relationship of polysaccharides in CHPs is of great significance for the development of new-carbohydrate drugs or pharmaceutical excipients. For example, different structural parts of Marine algae polysaccharides can directly or indirectly interact with the immune system and trigger several signal pathways, which lead to immune system activation (**Figure 1**) (9).

Relationship Between Molecular Weight and Activity

The molecular weight of polysaccharides only represents the average distribution within a certain range of relative molecular mass, which is mainly expressed by the mass average molar mass (M_w) and number-average molecular weight (M_n). Polydispersity (α) is generally used to describe the molecular weight distribution of polysaccharides, that is, $\alpha = M_w/M_n$.

Firstly, molecular weight is an important feature affecting the therapeutic action of polysaccharides. The functional feature of molecular weight is related to amounts of active groups, and molecular weight indirectly affects the physicochemical properties such as solubility and viscosity, thereby affecting the absorption of polysaccharides *in vivo*. Secondly, the higher or lower molecular weight might reduce the activity of CHPs. It should be noted that a high molecular weight of polysaccharide normally has a large excluded volume that promotes intermolecular interaction of polysaccharide and impedes its uptake. On the contrary, if the relative molecular weight is too low, polysaccharides cannot form active-polymer structures such as triple-helical conformation (10). For example, the polysaccharide with moderate molecular weight from *Dendrobium officinale* showed the strongest inhibitory effect on the cells (11). Polysaccharides with less than 5 kDa or more than 400 kDa showed marginal immunomodulatory activity or lost the activity directly (12). Therefore, the dimension of molecular weight is closely related to biological activities in polysaccharides including antioxidation, lipid-lowering, antiviral, and so on.

Thirdly, the molecular weight shows a certain tendency of efficacy in an appropriate range. The low molecular weight of polysaccharides can play better exerting their antioxidant activity with containing more free hydroxyl groups to accept and eliminate more hydrogen radicals (13). It was found that a polysaccharide with the lower molecular weight obtained from corn whiskers showed the stronger antioxidant activity (14). It is worth noting that CHPs with intestinal barrier protection have higher molecular weight (15), which may be because high molecular weight polysaccharides can maintain the integrity of intestinal barrier structure by forming something similar to the sticky gel (16).

Taken together, polysaccharides in CHPs perform the best only on specific biological activities within the optimal range of relative molecular weight.

Relationship Between Monosaccharide Composition and Activity

The monosaccharide composition is divided into the type and proportion of monosaccharide, which is closely associated with biological activity. As an illustration, *Angelica sinensis* polysaccharides with radio-protective activity tended to be richer in galacturonic acid, galactose, and arabinose (17). It is generally considered that the monosaccharide composition with more complex shows the better biological activity (18). Two kinds of polysaccharides, RLP-1 and RLP-2, from *Rosa Laevigata* Fructus, had different monosaccharide compositions and activities. RLP-1 consisted of xylose, mannose, and galactose reducing hyperlipidemia of model rats, while RLP-2 only contained glucose having no such activity (19). Some studies demonstrated the monosaccharide composition in polysaccharide with intestinal barrier protection function is galactose, mannose, arabinose, xylose, and rhamnose (16, 20). In addition, the high content of uronic acid showed good antioxidant activity of polysaccharide (21). The mechanism may be the breakage of uronic acid chain caused by free radicals (22). Similarly, polysaccharides with amounts of uronic acid were beneficial to its hepatoprotective activity (18). In addition, the polysaccharides containing mannose and rhamnose were proved to have tumor-inhibitory and antioxidant activities, individually (23, 24). However, the specific rules and mechanisms have not been clearly set forth and need further exploration.

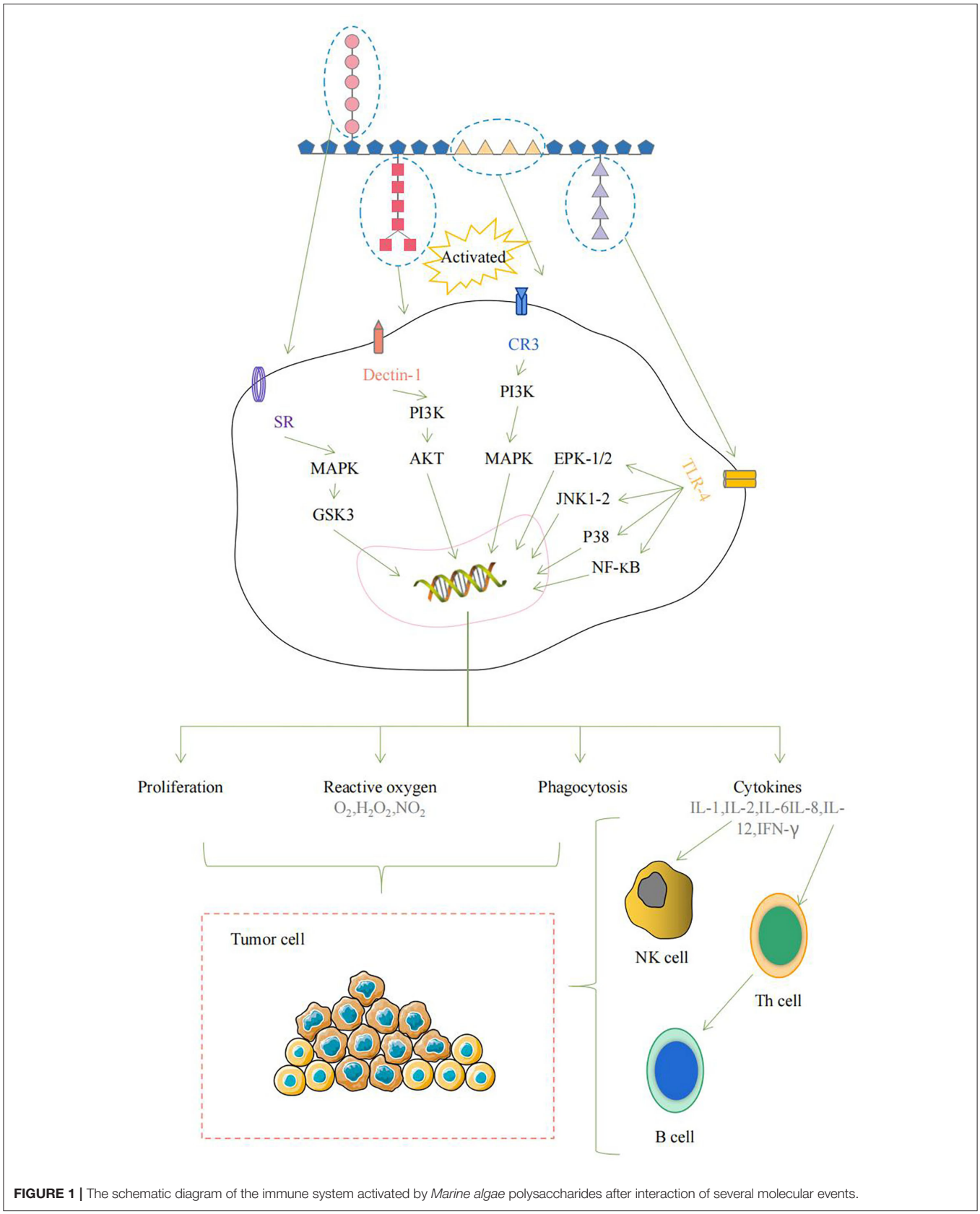

FIGURE 1 | The schematic diagram of the immune system activated by *Marine algae* polysaccharides after interaction of several molecular events.

Relationship Between Glycosidic-Bond Type and Activity

The flexible connection between monosaccharides causes the complex structure of polysaccharides. The glycosidic bond is divided into α-type or β-type because the configuration of the glycosidic bond is determined by the configuration of the hemiacetal (ketone) hydroxyl group. It is generally considered that polysaccharides with β configuration have the higher activity, while most of polysaccharides with α configurations have no biological activity (25, 26). This is due to the existence of α-glucoamylase in the human body, which can hydrolyze α-glycosidic bonds under certain conditions. However, with the depth of research, it was found that α-glucan as vaccine adjuvants had good biocompatibility and biodegradability to maintain the homeostasis of the intestinal environment (27, 28). In addition, α-(1 $\rightarrow$ 4)-GalpA and α-(1 $\rightarrow$ 4)-Galp in the main chain of *Ginseng* polysaccharides were essential to biological activities such as anti-tumor (29).

The main glycosidic bond types of polysaccharides with different activities are also different. Most of the glucans with anti-tumor are mainly composed of the β- (1 $\rightarrow$ 3)-*D*-glucan as the main chain, with the β-(1 $\rightarrow$ 6)-*D*-glucan randomly as the branched chain (30), while the antitumor effect of glucans composed of the β-(1 $\rightarrow$ 6)-*D*-glucan as the main chain is much weaker. Some CHPs regulating intestinal flora activity are mostly connected by (1 $\rightarrow$ 3) glycosidic bond (31). Additionally, CHPs with hypoglycemic effect mostly have (1 $\rightarrow$ 3), (1 $\rightarrow$ 4), (1 $\rightarrow$ 6) glycosidic bonds (32–34).

Relationship Between Branching Degree and Activity

The degree of branching (DB) of CHPs influences the biological activity by affecting the molecular weight and conformation (35). Generally speaking, the higher the complexity of the branch, the stronger the activity of CHPs (36, 37). Three kinds of polysaccharides with different DBs were obtained from *Ganoderma atrum*. Their antioxidant activity and anti-tumor cell proliferation were positively correlated with DB (38). This may be related to the effect of DB on the binding ability of polysaccharides to specific receptors (39, 40). In recent years, the hyperbranched polysaccharides with highly branched structure have received extensive attention due to their diverse biological activities and applications, which may be because the hyperbranched structure has good water solubility, low viscosity, and high chain end density (41). A hyperbranched polysaccharide from *Cordyceps sinensis* with DB of 43% could stimulate macrophage function, which was thought to attribute to its hyperbranched structure (42). However, it was found that polysaccharide from ginseng with small branching degrees showed better immune-enhancing activity (43). Accordingly, the activity of CHPs is related to DB, and there may be an optimal DB value (44). This may be because too high DB value would lead to the decrease of water solubility, while the DB value is too low, resulting in fewer binding sites (45).

Relationship Between Chain Conformation and Activity

Compared with the primary structure, advanced structure of polysaccharides is more likely to affect their functions (46, 47). Three-dimensional network structures of polysaccharide molecules are easily formed *via* van der Waals forces, hydrogen bonds, and covalent bonds. Moreover, the inter-chain association of structures is common because of the large degree of freedom and flexibility. Polysaccharides have multiple conformational forms in solutions, including single random coil (48, 49), helix (50), double helix (51), triple helix (52), rod-like structures (53), worm-like (54), semiflexible chains (55), and sphere-like structures (56). At present, the triple-helical structure of polysaccharides is one of the most studied chain conformations with some specific biological activities, especially anti-tumor (57). If triple-helical structure is destroyed, the anti-tumor activity would be decreased. The lentinan had a good antitumor activity with triple-helical stereo-configuration, but when the stereo-configuration was destroyed, the anti-tumor activity disappeared as consequence (58). The antiviral activity could be affected by the change of triple-helical structure of pollen polysaccharides in *Pinus massoniana* (59), which might be related to the chain rigidity and exposure sites of the triple-helical structure. Furthermore, the polysaccharide chain with triple-helical conformation is more rigid and easier to be recognized by the receptor (60). When the polysaccharide with triple-helical structure is linearly distributed, more exposure sites were utilized to strengthen the activity. The research substantiated that the polysaccharide having extended linear conformation showed the better good hypolipidemic activity on four sulfated polysaccharides in sea cucumber (61).

At present, there are few studies about the relationship between the chain conformation and biological activity in polysaccharides, which is one of the key breakthroughs for the advancement of polysaccharides in CHPs.

PRIMARY STRUCTURE IDENTIFICATION

Determination of Molecular Weight

In recent years, gel permeation chromatography (GPC) has been widely used in laboratories to calculate the molecular weight of the polysaccharide as well as detect the homogeneity of the polysaccharide (**Figure 2**) (62, 63). Most of the current studies employ high-performance GPC (HPGPC) or high-performance exclusion chromatography (HPSEC) (64), which is based on the characteristic that polysaccharide with certain molecular weight has a corelated elution retention time (t_R) on a gel column. Polysaccharides with known molecular weight are used to make a standard curve, and then the molecular weight of the sample can be calculated according to the t_R and the standard curve. In this method, if a single and symmetrical peak appears, the component is usually considered to be a homogeneous polysaccharide (65). Differential refraction index detector (RID) in HPGPC was applied to determine the molecular weight of polysaccharides. As long as the refractive index of the detected compound is different from the liquid solvent system, it can be detected. The universal

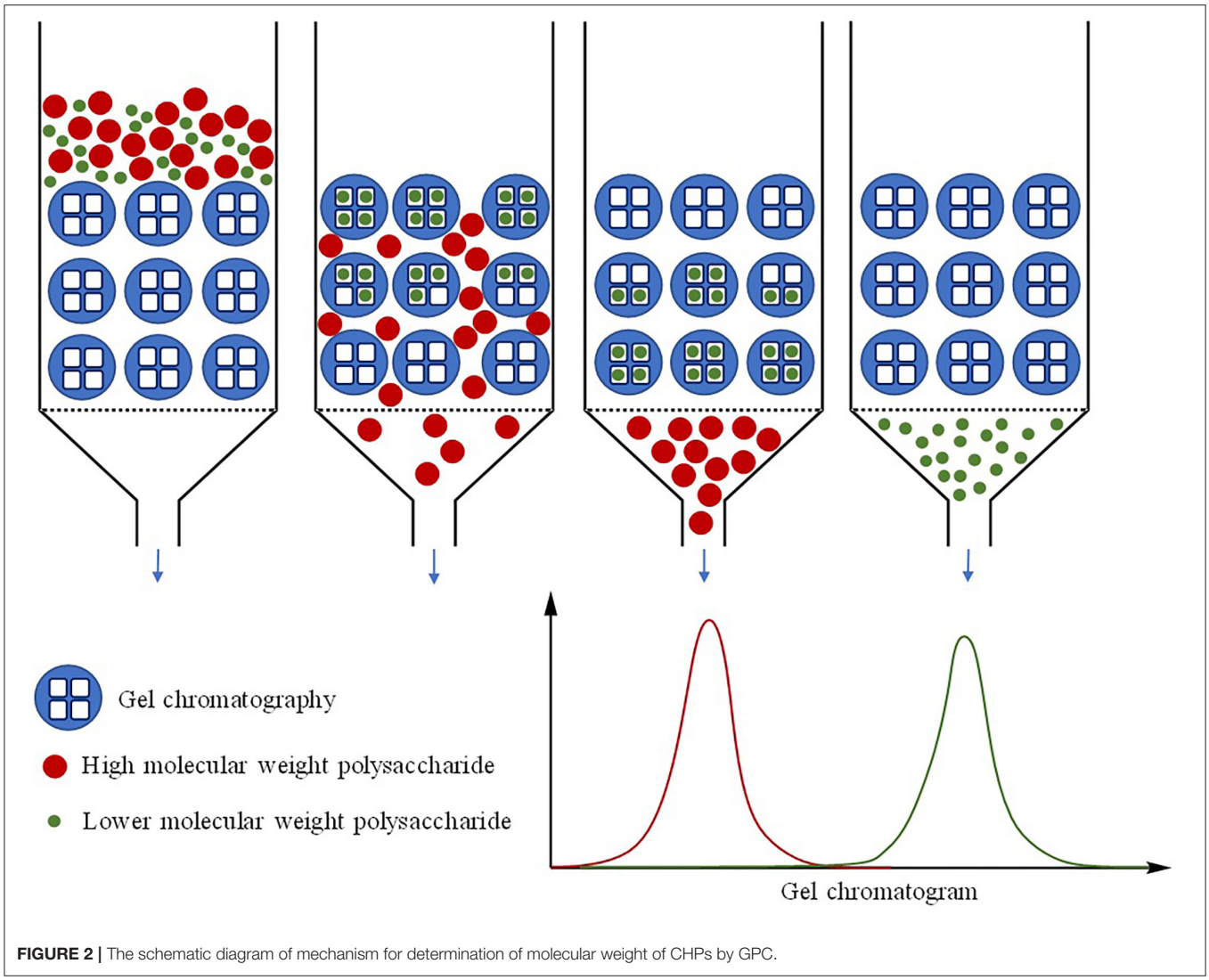

FIGURE 2 | The schematic diagram of mechanism for determination of molecular weight of CHPs by GPC.

detector evaporative light scattering detector (ELSD) can also be used to determine the molecular weight of polysaccharides (66).

In addition, some hyphenated techniques have been developed to determine the molecular weight of polysaccharides, such as size exclusion chromatography (SEC)/GPC combined with a multi-angle laser light scattering (MALLS) detector (67, 68). A small-angle laser scattering device can be used to determine the molecular weight of macromolecular compounds quickly and accurately, without extrapolating the angle and concentration. The comparison of popular methods on determination molecular weight is shown in **Table 1**.

Determination of Monosaccharide Composition

The combination of gas chromatography (GC) and mass spectrometry (MS) or flame ionization detection (FID) is usually used as a conventional analysis method for monosaccharide composition (72, 73). The first step in determining the composition of monosaccharides is to degrade polysaccharides into monosaccharides. The acid hydrolysis method is the most widely used, and its process varies depending on the type of polysaccharide. Next, due to the lack of volatility of carbohydrates, it is necessary to use sugar alcohol acetate, sugar acetonitrile acetate derivatives, methyl ether, trimethylsilyl oxime, trimethylsilyl ether, and other reagents to derivatize the hydrolysate, making it suitable for GC.

High performance liquid chromatography (HPLC) with ultraviolet detector (UVD) is becoming more commonly used for quantifying monosaccharides (74). Separation rate of monosaccharides can be accelerated accordingly in reversed-phase liquid chromatography with stationary phase of C18 (75). Polysaccharides are not retained on the C18 chromatographic column and do not contain chromophoric groups. Monosaccharides need to be derivatized so that the separation efficiency of chromatography and sensitivity of UVD can be improved to observable level. 1-phenyl-3-methyl-5-pyrazolone (PMP) is usually used as a probe molecule for its characteristic of quantitative reaction with carbohydrates under

TABLE 1 | Comparison of determination methods of molecular weight.

	Method	Characteristic	Application	References
Traditional techniques	Osmotic pressure method, Viscosimetry, Vapor pressure osmometry, Terminal method, Sugar Electrophoresis, Ultrafiltration	Complicated to operate, inaccurate	Tea polysaccharide (TPS) Mw 2.287 × 10^5-2.762 × 10^5 g/mol	(69)
GPC	HPSEC/HPGPC-RID	Fast, convenient for detection, high resolution and good reproducibility, homogeneity and molecular weight can be detected simultaneously	*Bletilla striata* polysaccharide (pFSP) Mw 9.1 × 10^4 Da	(4)
	HPSEC/HPGPC-ELSD		*Lepidium meyenii* polysaccharide (MP1) Mw 4.67 × 10^5 Da	(70)
Combined techniques	HPSEC/HPGPC-MALLS	Less affected by sample structure or relative molecular weight, not necessary to use reference materials for calibration, high accuracy, can provide samples conformational information in solution	*Ligusticum chuanxiong hort* polysaccharide (LCP70-2A) Mw 6.46 × 10^4	(71)

TABLE 2 | Comparison of determination methods of monosaccharide composition.

Method	Characteristics	Application	References
GC/MS	High sensitivity and accuracy, tedious derivatization process, lead to sample loss, cannot deal with acidic polysaccharides containing uronic acid, generate isomers	*Lycium barbarum* polysaccharide (LBP1) mannose: glucose: galactose: xylose: arabinose=6.52:78.12:8.85:1.81:4.69.	(83)
HPLC-PMP derivatization	Easy to operate, no isomers peaks, high specificity and accuracy, less sensitive than GC, low specificity of UVD, long analysis time, not suitable for ketose	*Dendrobium nobile Lindl* polysaccharide (DOP) D-glc$_p$: D-man$_p$=1.00:4.41.	(84)
Detecting directly by HPLC	Non-derivative, simplicity of operation, low sensitivity Sugar analysis columns: suitable for separating monosaccharides, separation conditions, convenient sample preparation, and a wide pH range of 1–14; Amino column: suitable for separating samples oligosaccharides, cheap, lifespan is short, with many precautions for use.		
HPCE	High sensitivity, unique effect in separating charged sugars, high requirements for instruments, complicated to operate, low reproducibility	*Acanthopanax senticosus* leaves polysaccharide (ASLP) Rhamnose: xylose: glucose: mannose: arabinose: galactose: glucuronic acid= 7.45:18.63:25.15:0.93:8.35:2.79:5.69	(85)
HPAEC-PAD	Not necessary for derivatization, high sensitivity, columns bearable for NaOH are needed.	The fibrous roots and tuber of *Bletilla striata* polysaccharide (pFSP) D-glucose: D-galactose: D-mannose=1:2.03: 3.45	(4)

mild conditions (76). Besides, the monosaccharide composition of polysaccharides can be determined without derivatization by using sugar analysis column or amino column and equipped with RID or ELSD or pulsed amperometric detector (PAD).

High performance anion exchange chromatography-pulsed amperometric detector (HPAEC-PAD) is a technology used to analyze polysaccharide currently (77–79), as it can analyze the hydrolytic products without sample derivation (80). The mechanism of HPAEC-PAD method is to use the dissociation of mono or oligosaccharides by elution in medium with pH above 12. Then the anions are fully exchanged on an agglomerated shell type anion exchange resin column. The separated components go into PAD for detection. The composition of monosaccharides can be determined referring to standard samples (81).

Capillary electrophoresis can also be used to determine the monosaccharide composition of CHPs. Samples are labeled by reagents with acidic groups, and then assayed by high performance capillary electrophoresis (HPCE) and detected by laser induced fluorescence detector (LIFD) (82). The advantages and disadvantages of various methods are listed in **Table 2**. The general process of determining the composition of monosaccharides is shown in **Figure 3**.

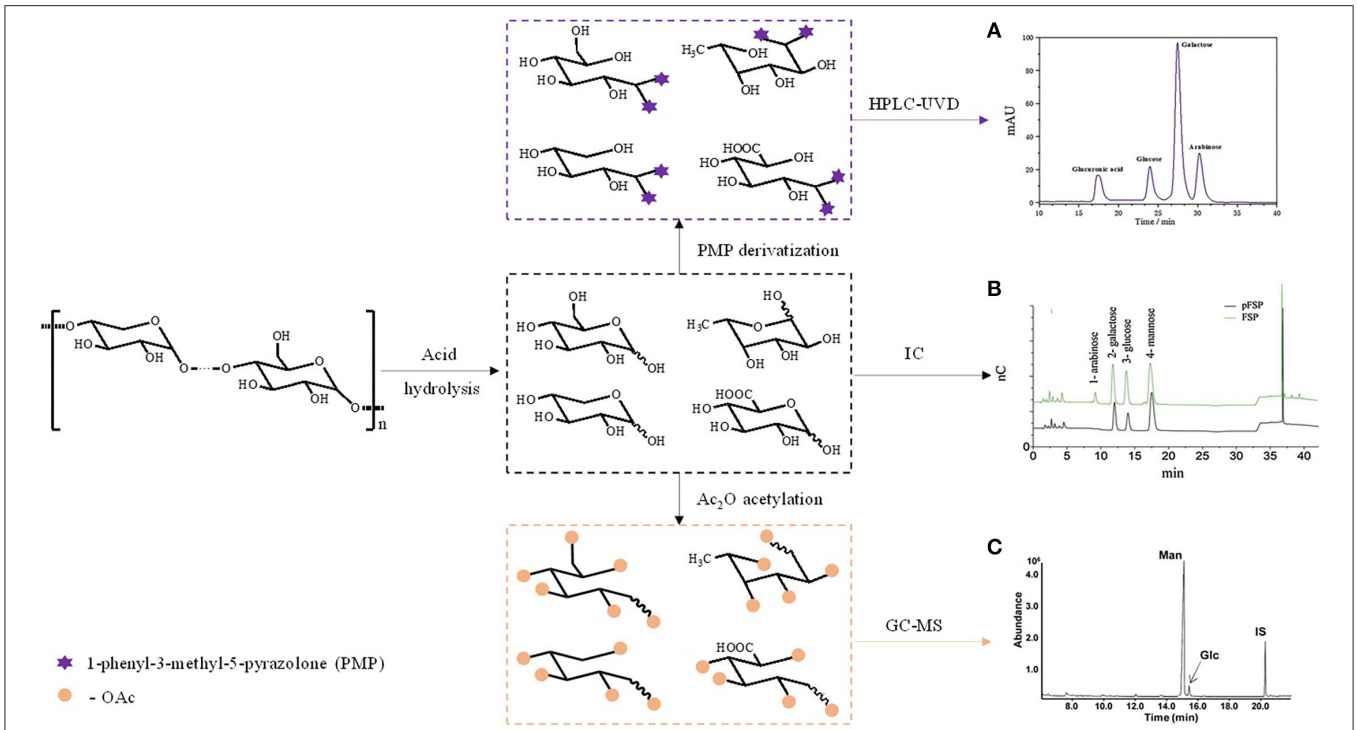

FIGURE 3 | The general process of determining the composition of monosaccharides. **(A)** Monosaccharide composition of *Angelica sinensis* polysaccharide by HPLC-UVD; **(B)** Monosaccharide composition of polysaccharide from the fibrous roots and tuber of *Bletilla striata* by IC; **(C)** Monosaccharide composition of polysaccharide from *Dendrobium devonianum* by GC-MS.

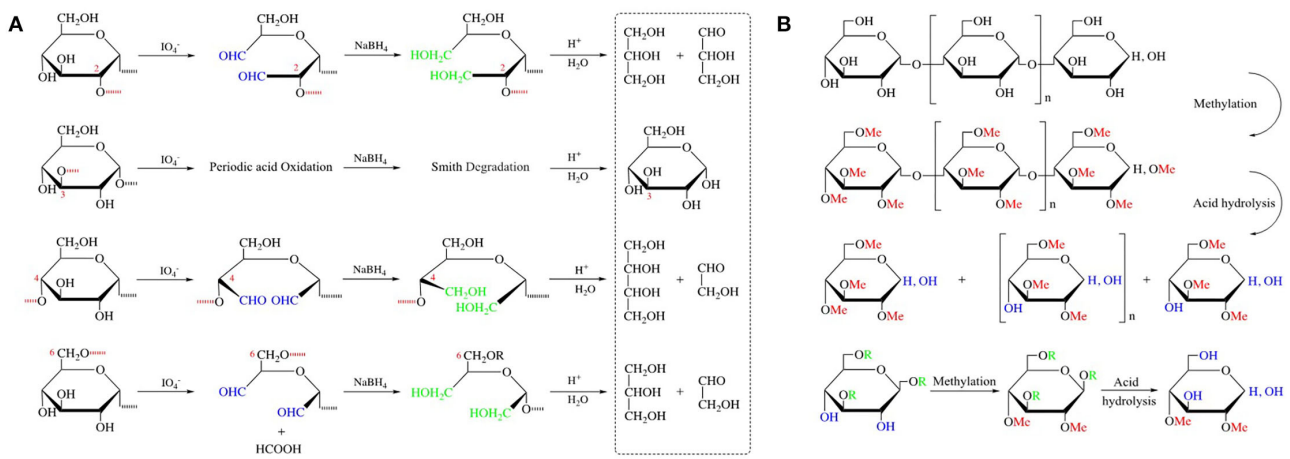

FIGURE 4 | Chemical reactions related to the determination of glycosidic bonds. **(A)** Different polysaccharides are oxidized by HIO_4, reduced by $NaBH_4$, and then hydrolyzed with dilute acid to obtain different products; **(B)** Products obtained by methylation and acid hydrolysis of linear glucans and branched polysaccharides.

Glycosidic Bonds Identification

Chemical reaction is an important step in glycosidic bond identification methods, including acid hydrolysis, periodic acid oxidation, Smith cleavage, and methylation reactions (**Figure 4**). Partial acid hydrolysis is currently the most commonly used method (86), which can be used to detect the sequence of glycosidic linkages breaks and preliminarily infer the possible glycosidic bond types. By measuring the usage of periodic acid and the release of formic acid, the position of glycosidic bonds, the degree of polymerization of linear polysaccharides and the number of branches of branched polysaccharides can be judged. The characteristic of Smith's degradation is that only glycosidic bonds are broken by periodic acid, while the sugar residues that are not oxidized are still attached to the sugar chain. The key

TABLE 3 | Common determination methods of glycosidic bonds of polysaccharides.

Method	Information	Characteristic	References
Partial acid hydrolysis	Ranking of stability of various sugar: the pyran sugar residue>the furan sugar residue, the hexose sugar>the pentose sugar, the sugar residues in main chain>the branched sugar residues	Poor selectivity, requires precise reaction conditions, not suitable for the complex mixed polysaccharides or heterogeneous structure products	(88–90)
Periodic acid oxidation	The position of glycosidic bonds; the degree of polymerization of linear polysaccharides; the number of branches of branched polysaccharides.	Carried out in the dark in an aqueous solution with pH 3–5, less polysaccharide samples are required	(4)
Smith degradation	Degradation product erythrose: 1 → 4 combined glycosidic bonds; glycerol:1 → 6, 1 → 2 glycosidic bonds or a reducing terminal glucose residue; monosaccharides such as glucose, galactose, mannose: 1 → 3 glycosidic bonds.	Combined with periodic acid oxidation	(91)
Methylation reaction	GC/MS spectral library; the standard PMAA spectrum; the ionization law of PMAA.	α/β stereochemical information cannot be obtained	(92, 93)
Enzymatic digestion	α-glucosidase hydrolysis α-glycosidic bond; β-glucosidase hydrolysis β-glycosidic bond.	Specific, few by-products, little digestive enzymes for polysaccharide	(94, 95)

point to the methylation reaction is whether the methylation is complete (87). For polysaccharides containing uronic acid and aminohexose, whether methylated acid hydrolysis will cause side reactions. It is necessary to reduce the polysaccharide before methylation, if the samples contain uronic acid.

The common determination methods of glycosidic bonds in polysaccharides are shown in **Table 3**. And there are some new methods to identify the glycosidic bonds of polysaccharides. Amicucci described the development and application of a chemical method for producing oligosaccharides from polysaccharides. The released oligosaccharides are characterized by the advanced LC-MS methods with high sensitivity, accuracy, and throughput. The technique is first used to identify polysaccharides by oligosaccharide fingerprinting. The Fenton's initiation toward defined oligosaccharide groups (FITDOG) process was developed to produce oligosaccharides from polysaccharides. The process was initiated by a reaction between a metal catalyst, Fe^{3+}, and an oxidizing agent, hydrogen peroxide, to produce reactive radical species that cleave glycosidic bonds. The radicals induce oxidative cleavage of the polysaccharide backbone to produce oligosaccharides that are representative of the parent polysaccharide structure (96).

Spectroscopy Techniques

IR is mainly used to identify various functional groups, determine the α/β configuration of glycosidic bonds, distinguish five-carbon and six-carbon sugars, and identify different monosaccharides in polysaccharides (**Table 4**) (97, 98). The characteristic absorption peaks of polysaccharides are at 3,600–3,200, 3,000–2,800, and 1,200–1,000 cm^{-1} (99). Among them, polysaccharides contain lots of hydroxyl groups, which usually has a distinct broad stretching vibration absorption peak at the wavelength of 3,500–3,000 cm^{-1}. The C-H stretching vibration can form a weak peak near 2,935 cm^{-1} (100). The absorption peak of sugar ring C-O-H, C-O-C is 1,000–1,100 cm^{-1}. In addition, according to the absorption peak in the 1,170–700 cm^{-1} interval of the infrared spectrum, the size of sugar ring and the configuration of the glycosidic bond can be judged. Pyrannoside has 3 strong absorption peaks in the interval of 1,100–1,010 cm^{-1}, while furanoside only has 2 absorption peaks in the corresponding region. The vibrations of the pyranose ring

TABLE 4 | The IR wavenumbers of functional groups in polysaccharides.

Functional group	Vibration mode	Wavenumbers/cm^{-1}
-OH	O-H, ν (stretching vibration)	3,700–3,100
	O-H, δ (scissoring vibration)	1,075–1,010; 1,120–1,105
-COOH	C=O	1,740–1,680
	C-O	1,440–1,395
	O-H	1,320–1,210
-O-COR	C=O	1,749–1,725
	C-O	1,245
$-NH_2$	N-H, ν	3,450–3,380
	N-H, δ	1,650–1,500
=NH	N-H, ν	3,460–3,420
-NH+ 3	N=H	3,350–3,150
	N-H	1,650–1,550
-C-O-C	C-O (fatty ether)	1,150–1,060
	C-O (cyclic ether)	1,150–1,080
$-CH_2$	C-H, ν	2,926–2,853
	C-H, δ	1,465
$-CH_3$	C-H, ν	2,962; 2,872
-C=O-CHO	C=O	1,780–1,540
	C=O	1,740, 1,650
α-D-Glc$_p$	C-H	855–833
β-D-Glc$_p$		905–876
α-D-Gal$_p$		839–810
β-D-Gal$_p$		914–886
α-D-Man$_p$		843–818
β-D-Man$_p$		898–888
α-D-Xyl$_p$		760–740
β-D-Arb$_p$		855–830

are at 917 and 770 cm^{-1}, while the furanose ring is at 924 and 799 cm^{-1}. Generally, 890 cm^{-1} is the characteristic peak of β-pyranoside bonds, and 840 cm^{-1} is the characteristic peak of α-pyranoside bonds.

Nuclear magnetic resonance spectroscopy (NMR) provides information about the structure of polysaccharides, which involves the identification of monosaccharides, α or β anomeric confirmation, glycosidic bonds type, and the sequence of repeating units in the polysaccharide chain. In the ^{1}H-NMR spectrum, the chemical shifts of the polysaccharide signal are mainly distributed in δ 3.5–4.4 and δ 4.4–5.8 (anomeric proton region). Among them, the anomeric proton region plays a significant part of the structure analysis of polysaccharide, such as providing information on the configuration of polysaccharide residues. Generally, the chemical shift δ of the anomeric hydrogen of the pyranose residue with α configuration is larger than 5.0. For β configuration, the δ is less than 5.0. The configuration of the anomeric hydrogen can also be judged by combining the coupling constant $J_{1,2}$ of the anomeric hydrogen and the vicinal hydrogen. For the β configuration, $J_{1,2}$ = 7–9 Hz, and for the α configuration, $J_{1,2}$ = 2–4 Hz. Unsaturated double bond in non-reducing end H4 falls in 5.9–6.0 ppm, H1 in 4.8–5.5 ppm and H2–H6 in 4.0–4.8 ppm. There are also some special proton signals that are helpful to determine the type of monosaccharide residues, such as δ 1.1–1.3, which may be the hydrogen at C6 position of fucose. When methyl (around 1.0 ppm), acetyl (around 2.0 ppm), sulfate and phosphate groups were substituted, the ^{1}H chemical shift often shifted downward by about 0.2–0.5 ppm.

The ^{13}C-NMR spectrum can confirm various carbon nuclei and distinguish the configuration and conformation of molecules in polysaccharide structure analysis. It can also be used to determine the substitution position and branch point of polysaccharide residues. In the ^{13}C-NMR spectrum, the characteristic peaks of polysaccharides fall in 60–110 ppm. Among them, monosaccharide composition and sugar ring configuration can be determined by the isomeric carbon signal of 95–105 ppm. Allocarbons above 101 ppm can be distinguished as β-configuration, and between 95 to 103 as α-configuration. For C2–C5, 78–85 ppm is the carbon signal at the substituted position and 65–80 ppm is the one at unsubstituted position. Signals around 61 ppm belong to unsubstituted C6, and the substituted C6 signal moves to lower around 69 ppm. The signals in 96–110 ppm are the peaks of terminal carbons of sugar, and the other signals are the peaks of non-terminal carbons. The signals of unsubstituted C2, C3, C4, and C5 are at 78–70 ppm, while the unsubstituted C6 signals are at 64–60 ppm. The chemical shift of methyl carbon is about 35–40 ppm (100). Chemical shift of polysaccharide 13C substituted by methyl, acetyl, sulfate, or phosphate group shifts downward 6–7 ppm. Two-dimensional NMR (2D NMR) plays an indispensable role in the full attribution of ^{13}C-NMR spectra of polysaccharides (101). Currently, NMR is a tool that can be used to analyze molecular structure completely independently, but it also has the problems of low sensitivity. Additionally, the severe overlap of the peaks makes the elucidation extremely complex, especially for Chinese herbal heteropolysaccharides.

The LC-MS methods have been developed and have brought remarkable advances in terms of sensitivity and specificity to the general analysis of polysaccharides, which can provide reliable molecular weights, and the information of fragments (102, 103). Xu et al. have developed a comprehensive method for quantitation of both neutral and acidic monosaccharides using ultra-high performance liquid chromatography triple quadrupole mass spectrometry (UHPLC/QqQ-MS) in dynamic multiple reaction monitoring (dMRM) mode. This method can achieve the separation, detection, and quantification of 14 PMP-derived monosaccharides (including fructose) and two sialic acids with label-free within 10 min, which has high sensitivity and wide linear range (104). Amicucci et al. presented a general LC-MS-based workflow for the *de novo* characterization of structurally diverse polysaccharides. This report presented the characterization of the maize polysaccharide by employing new analytical strategies, which is quantifying monosaccharide and glycosidic linkages by combining chemical depolymerization and UHPLC/QqQ-MS analysis. Partial acid hydrolysis paired with nano-HPLC/QTOF MS was used to analyze oligosaccharides sequencing. The elucidation of this complicated structure illustrates the high sensitivity, good reproducibility and fast speed of the analytical methods, which may serve as a general platform for polysaccharide analysis in the future (105).

ADVANCED STRUCTURE ANALYSIS

The traditional methods of studying the high-level structure of polysaccharides have limitations in application. A new technique as X-ray diffraction (XRD) method can obtain various information such as bond angle, bond length, configuration angle at the same time (106). But this technology requires that the polysaccharide sample must have high purity and crystallization. In other words, amorphous polysaccharides are not applicable. Except for polymers with triple helical structure, there is no other report using XRD to study chain conformation (57). Additionally, the Congo red experiment does not require special equipment and is easy to popularize. However, this method can only be used to determine whether the sample has a triple helix structure. It cannot elucidate the precise structure and has low sensitivity.

Analytical Methods Based on the Theory of Polymer Dilute Solution

At present, the most commonly used analysis methods of advanced structure are HPLC combined with dynamic light scattering (DLS), static light scattering (SLS) or viscosity determination based on the theory of polymer dilute solution (107, 108). Normally, four main characteristics are considered when identifying polymer conformations, which concludes persistence length (q), molar mass per unit contour length (M_L), diameter of chain (d), and contour length of chain (L). These four key parameters can be calculated by thermodynamic and hydrodynamic properties parameters including molecular weight (M_w), radius of gyration (R_g), intrinsic viscosity (η), diffusion coefficient (D), and hydrodynamic radius (R_h), which can be

TABLE 5 | The parameters, calculation formulas, and the chain conformation information reflected by them.

Formula	Diameter	Range	Conformation	References
(1) $\frac{K_c}{R_\theta} = \frac{1}{M_w}[1 + \frac{16\pi^2 n^2}{3\lambda^2} R_g^2 \sin^2(\frac{\theta}{2})] + 2A_2 c$	v	0.2–0.4	A tightly coiled conformation with high branches	(116, 117)
		0.5–0.6	A compliant molecule	
(2) $R_g = KM_w^v$		0.6–1.0	A rigid or semi-rigid rod	
(3) $d_f = 1/v$	d_f	1.0	A rigid rod-like structure	(116, 118)
(4) $I_s(\omega) = I_0(\omega_0)\frac{C\Gamma}{(\omega-\omega_0^2)+\Gamma^2}$		5/3–2	A linear polymer with a Gaussian coil shape	
		2.5	A branched structure	
(5) $G^{(2)}(q,\tau) = A[1 + \beta\lvert g^{(1)}(q,\tau)^2\rvert]$		3	A compact and uniform spherical structure	
(6) $\lvert g^{(1)}(q,\tau)\rvert = \int_0^\infty G(\Gamma)\, d\Gamma$	ρ	0.77	A hard sphere conformation	(119)
(7) $\Gamma = Dq^2$		1.0–1.1	A highly branched conformation	
(8) $R_h = \frac{k_B T}{6\pi\eta_0 D}$		1.5–1.8	A compliant molecule	
		> 2	A worm-like or rigid structure	
(9) $[\eta] = KM_w^\alpha$	α	0.5	A spherical structure	(120, 121)
(10) $\eta_{sp}/C = [\eta] + K'[\eta]^2 C$		0.6–0.8	A elastic random curl conformation	
(11) $(ln\eta_r)/C = [\eta] + K''[\eta]^2 C$		>0.8/> 1.0	A rigid chain conformation	

obtained through the Kratky-Porod model, helical worm-like chain model, or models derived from them (109).

The HPLC-SLS technology is a simple but effective analysis method for advanced structure of polysaccharides (110). It is based on the light scattering properties of polymer solutions and the related characteristics of molecular mass, size and concentration. Various structural information such as M_w, molecular mass distribution (MWD), and R_g can be obtained through formula *(1)* (111). Majority of studies still use Zimm mapping for data processing (112), while the Debye method can not only ensure accuracy but also shorten the experimental period (113). The exponent v of formula *(2)* is the slope of the linear regression of R_g to M_w, which is one of the parameters that characterize the conformation of the polymer. Similar to v, the fractal dimension d_f is also a parameter that characterizes the tightness of the internal structure of the polymer, and it is calculated with formula *(3)*.

Because of the molecular thermal motion or Brownian motion in polymer solution, the phase of scattered particles in solution changes with time. The basic principle of DLS is that the frequency and the intensity of scattered light change and fluctuate with time. The values of R_h and D can be determined by DLS. R_h is an important parameter describing the size of a polymer in solution, and R_g is the root mean square value of the distance between the center of mass of the polymer and the axis of rotation. The form and rigidity of the polymer in a dilute solution can also be described by ρ (R_g/R_h) (114).

Viscometry is another simple method for measuring. The exponent α is a characteristic parameter of the high-level structure of polymers, which can be calculated according to formula *(9)*. And then the intrinsic viscosity η can be obtained by extrapolation using a viscometer according to Huggins equation *(10)* and Kraemer equation *(11)*. A large number of studies have combined these three methods for the analysis of the advanced structure of polysaccharides. Li S. et al. established an analytical method combining HPLC with multiple detectors to realize the analysis of β-Online separation and real-time detection of dextran aggregates and non-aggregates (115). The parameters, calculation formulas and the chain conformation information reflected by them are listed in **Table 5**.

Microscope Observation Methods

High resolution and large depth of field are two main features of scanning electron microscope (SEM). The rough surface with certain fluctuations of polysaccharides can be directly observed by it (122). The surface morphology of polysaccharides significantly differs from each other due to various sources of polysaccharides. Spherical, flake and branched structures have been observed before, among which, spherical or flake morphology are most common (123, 124). And the extraction, purification, and preparation conditions could also influence on the surface morphology of polysaccharides (125). For example, three polysaccharides from *Sagittaria sagittifolia* L. separately obtained with hot water, ultrasound-assisted, and subcritical water extraction presented different SEM images (21). The different surface morphology of polysaccharides acquired by SEM can preliminarily infer the force between molecules. Polysaccharides usually have honeycomb-like structures, rough surfaces, and porous structures, indicating that the interaction among molecules is weak (126). A flake layer with unregular curls was observed indicating the strong attractions between functional groups on the surface to create the polysaccharide chains aggregation (127). The variation on morphology and shape mainly contributed to the changes of intramolecular hydrogen bonds (127). And the morphology and shape will affect the physical and chemical properties of polysaccharides. For instance, the smooth surface of polysaccharide probably had negative effect on the rehydration performance to reduce the solubility of polysaccharide itself (4).

Atomic force microscopy (AFM) is an analytical instrument that can study the three-dimensional (3D) surface morphology of polymers on the nanoscale in air and liquid (128). In AFM, when the probe scans the surface of the sample with a constant force between the probe and the sample, its motion trajectory can

be recorded and converted into an integral 3D image. AFM does not require any special treatment on the sample, such as copper or carbon plating, which will cause irreversible damage to the sample. The disadvantage of AFM is that the imaging range is too small, the speed is slow, and it is too much affected by the probe. In early research, AFM was usually used to calculate the shape of the chain, including the diameter of the chain, the length of the chain, and the chain distribution of the polymer (129, 130). Zhao et al. used an AFM to observe the aggregation state, morphology and size of *Schisandra* polysaccharide particles in pure water. The heights of the particle were in the range of 1–5 nm and found that the polysaccharide particles had agglomeration phenomenon at 100 °C (131). The agglomerations suggest polysaccharide molecules have gathered and that their structures were branched and entangled (132).

Other Methods

According to the different characteristics of the sample's absorption of left-handed and right-handed circularly polarized light, circular dichroism (CD) can be used to observe the structure of polysaccharides (133, 134). Zhang et al. analyzed the CD spectra of the *Cistanche deserticola* polysaccharide in the range of 190–300 nm. They found that some fragments of the *Cistanche deserticola* polysaccharide mainly exist in an ordered structure, and locally form a spiral structure (135). The results of CD analysis of the *Artemisia sphaeroides* polysaccharide before and after the sulfonation showed that the shielding effect of the charged components promoted the transformation of the polysaccharide chain to a more rigid conformation (136).

The differential scanning calorimetry (DSC) can not only describe the change about temperature between the sample and the reference but also record the change law between the heat difference and the temperature in real time. Liu et al. used this method to study the conformational transition process of *Ganoderma lucidum* polysaccharide 20 (GLP20). As a result, in the DSC heating curve, the endothermic peak indicated that the intermolecular hydrogen bond was broken, and GLP20 changed from a triple helical structure to a single-stranded random coil (137).

Polysaccharide macromolecules are usually in a dynamic equilibrium state of multiple spatial conformations, and the structural information provided by NMR is the average information of these dynamic conformations. A series of spatial structures that meet the NMR data and truly reflect the dynamic equilibrium of the sugar chain are obtained through the method of molecular calculation. Usually, molecular dynamics simulation (MDS) can depict the chain conformation of macromolecules with more than 10 repeating units. Based on the lowest energy state, the optimal conformation of the polysaccharide could be confirmed after simulated annealing (57). For instance, the complex 3D conformation of lentinan that can retain its triple-helix through hydrogen network was revealed using MDS and rigid macromolecule docking, as well as spectral methods (40).

STRUCTURAL MODIFICATION

The common methods of structural modification in CHPs are mainly divided into three categories, namely chemical modification, physical modification, and biological modification (**Figure 5**).

Chemical Modification

Chemical modification is the most common approach to tailor polysaccharide structure by inletting the required groups and thereby changing its original activity as well as producing new bioactivities (138). For instance, it was reported the anti-tumor activity of *Poria cocos* polysaccharide after modifications exhibit the stronger than the former (139). The modification was performed to achieve good water solubility, high chain rigidity and moderate molecular weight, which may be the reason for the improvement of its anti-tumor activity.

The branched chains of the polysaccharide can be modified by sulfation, phosphorylation, carboxymethylation, acetylation, etc., to enhance the bio-activity.

In sulfated modification, sulfuric acid groups are used to replace the hydroxyl, carboxyl, and amino ending on the sugar chain to exert activities. The degree of sulfation is positively related to anti-HIV and anticoagulant activity of CHPs. Firstly, sulfate groups are considered to be one of the determinants of anti-HIV activity of CHPs (8, 140). Then, sulfate groups can enhance the anticoagulant activity of CHPs by generating the high level of negative charge density. The sulfated polysaccharides obtained from *Zingiber officinale* with the higher degree of sulfation and suitable molecular weight showed better anticoagulant activities (141). In addition, CHPs exert their antioxidant activity by providing hydrogen atoms from polysaccharide chain and the presence of sulfated groups could increase the ability to provide hydrogen atoms (142, 143). In summary, sulfated polysaccharide are increasingly causing more attention, as they have been proved to improve structural properties and promote a variety of bioactivity.

The water solubility of polysaccharide can be improved by carboxymethylation with introduction of carboxymethyl into polysaccharide chain and thereby enhancing the biological activities of unmodified polysaccharides. After carboxymethylation, the molecular weight of polysaccharide from *Cyclocarya paliurus* decreased and correspondingly the molar ratio of monosaccharide composition changed (144). Among carboxymethylated polysaccharides, the antioxidant activity aims to terminate free radicals against oxidation reactions from occurring by increasing the ability of chelating transition metal ions and providing single electron or hydrogen atoms with the increased content of -COOH (145). It is worth mentioning that there is a positive correlation between antioxidant activity and the degree of carboxymethylation within a certain range (146). In addition, carboxymethylation can also enhance other biological activities of CHPs, such as anti-tumor and immune regulation activity (147). However, the mechanisms of action of carboxymethylated polysaccharides are still unclear and need to be explored forward.

On top of carboxymethylation, acetylation with the hydroxyl oxygen or amino nitrogen as the acetyl substitution sites can also enhance the water solubility of CHPs, mainly due to the exposure of hydroxyl groups from polysaccharide caused by the extension of polysaccharide chains (148). After the exposure of hydroxyl, the supply of hydrogen could be raised up, thereby

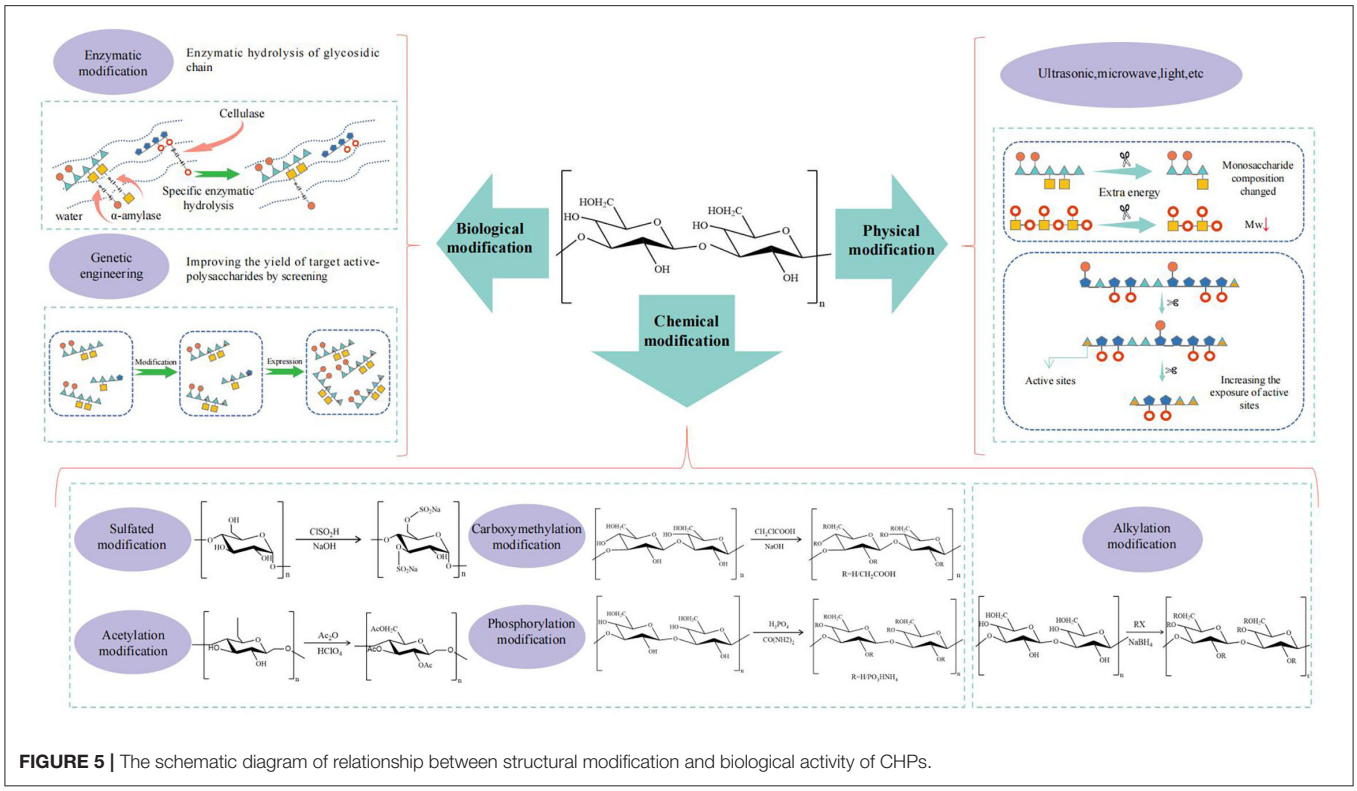

FIGURE 5 | The schematic diagram of relationship between structural modification and biological activity of CHPs.

enhancing the antioxidant activity of CHPs (149). It was found that the acetylated pumpkin polysaccharides with high degree of substitution had better antioxidant activity than those with low degree of substitution, and all of them perform better than those without modification (150). In addition, the potential application of acetylated CHPs is a feasible strategy to be an immunotherapeutic adjuvant (151).

A specific method used to modify the main chain of polysaccharides is the alkylation reaction by alkyl and long-chain aromatic alcohol for improving water solubility, reducing the viscosity of the solution, and thus improving the bioavailability. A good example was that *Ganoderma lucidum* polysaccharide was hydroxypropylated to improve the aqueous solubility and its antioxidant activity was significantly enhanced (152). An acceptable reason is that the hydroxyl groups in the molecules are more easily exposed to the reactive oxygen species (ROS), including free radicals and oxidants.

However, it should be noted that the appropriated degree of substitution is crucial to the activity. The crude polysaccharides of *Cordyceps militaris* were successfully modified by carboxymethylation and acetylation, but the expressed α-glucosidase inhibitory activity did not change significantly (153). To sum up, the change of the structure in polysaccharides has certain impacts on the biological activity with the degree of substitution and the substituent position as important factors affecting the result.

Physical Modification

In the physical modification, the degradation products with low molecular weight were obtained by serials of ultrasound, high energy radiation, microwave, and light to cut off some chemical bonds in the main chain due to high molecular weight of polysaccharides showing characteristics of high viscosity and poor solubility against absorption and utilization *in vivo* (154).

Ultrasonic treatment is the most commonly used method in physical modification. The ultrasonic treatment in the process of polysaccharide can break glycosidic bond to reduce the molecular weight, the viscosity, and enhance the solubility (155). It has been reported that the decreased molecular weight is positively correlated with ultrasonic intensity (154). In the process of ultrasonic, monosaccharide composition and uronic acid content would be also monitored as important indexes (156). The molecular weight of corn whisker polysaccharides after ultrasonic degradation decreased significantly, but the monosaccharide composition did not change. Interestingly, the molar ratio of mannose to galactose decreased significantly, suggesting that mannose and galactose residues may be the main active sites in the process of ultrasonic degradation. In the process, ultrasonic treatment also exposed more groups such as uronic acid, and thus provided more binding sites for increasing of α-glucosidase inhibitory activity (157).

Biological Modification

The biological modification for polysaccharides mainly involves enzymatic modification and genetic engineering. In enzymatic modification, specific biological enzymes are often used to degrade polysaccharides, and in which the non-reducing ends are cleaved resulting in double bonds forming. The molecular weight and solution viscosity of polysaccharides are decreased after side-chain detachment occurring by enzyme-modified

treatment beyond the change of monosaccharide composition and biological activities enhancing (125, 158). It was found that the antioxidant activity of *Morus alba* L. polysaccharides hydrolyzed by cellulase was higher than original polysaccharides, which may be attributed to the exposure of more active groups of polysaccharides (159). After enzymatic hydrolysis, the primary structure of polysaccharide from *Hericium erinaceus* with the shorter branched chains did not change, which led to the decrease of molecular weight, the increase of glucose content and the enhancement of immunomodulatory activity of the polysaccharide (160). At present, it should be noted that most of the enzymes can be used in enzymatic modification as degradable enzymes, and the applicable types are limited, which blocks the usage of this method.

To promote the industrial production of polysaccharides, genetic engineering is employed to control the biosynthesis pathway of polysaccharides by manipulating the gene expression of microorganisms or introducing exogenous genes in microorganisms for obtaining target active-polysaccharides (161). The proportion of galactose and mannose in polysaccharides and the antioxidant activity of polysaccharides were greatly boosted by efficient expression of the Vitreoscilla hemoglobin gene in Ganoderma lucidum (162). However, genetic engineering is difficult to be operated and foreign genes are not easy to obtain, which still needs to be further developed.

CONCLUSIONS AND PROSPECTS

Up to now, researches on CHPs are still in the initial stage with many shortcomings. It can be concluded that there has been a conventional structure analysis procedure and common structure-modified approach, but no unified conclusion on the structure-activity relationship of CHPs.

The biological activities of CHPs are closely related to its structure. Firstly, according to the facts we consolidated, the activity of polysaccharide performs the best only in the relative optimum molecular weight range while the determination of the specific range still needs more work. Secondly, the type and proportion of monosaccharide composition has a certain influence on the activity of polysaccharides. Nevertheless, the rules reflected different polysaccharides on activities are multifarious. Thirdly, as for the effect of glycosidic bonds on the activity of CHPs, CHPs with anti-tumor effect composed of the β-(1 $\rightarrow$ 3)-*D*-glucan as the main chain and the β-(1 $\rightarrow$ 6)-*D*-glucan randomly as the branched chain were in-depth studied. However, the studies on the glycosidic bonds of CHPs with other activities are not systematic enough, and most of them are in a state of scattered research. Fourthly, the DB of CHPs affects biological activity by changing molecular weight and conformation, and an ideal DB value may exist. This might be due to the fact that a high DB value reduces water solubility, whereas a low DB value results in fewer binding sites. The attention should be paid to the study of the type and length of branches, so as to reveal the mechanism of their influence on biological activity. Finally, the polysaccharides of triple helix conformation show excellent activities. On the one hand, the study of mechanism between triple helix conformation and activities should be strengthened. On the other hand, the research of CHPs with other conformations should not be ignored.

With regard to molecular modification, chemical modifications are much more focused due to obviously enhancing the activity of CHPs by inletting the required groups, wherein degree of substitution and position of substituent play the important role. In addition, physical and biological modification could affect the activity of polysaccharides by changing their molecular weight, monosaccharide composition, and physicochemical properties. Physical modification can degrade the main chain of polysaccharides, which is relatively friendly to the acquisition for small molecule-weight of polysaccharides, but the method is too unstable. In addition, enzymes are widely used in biological modification with high efficiency and controllability, but the categories and amounts of available enzymes are finite. Finally, genetic engineering technology can achieve a large number of targeted polysaccharides, but this method is difficult to operate and exogenous genes are not easy to obtain.

In light of the aforementioned issues, some modern equipment also promoted the development of structural analysis techniques for polysaccharide. Besides, multidisciplinary approaches can help researchers think outside the box. MDS and other calculation techniques can better examine the three-dimensional structure of polysaccharides. Through the combined use of multiple technologies, interdisciplinary methods are applicable to the structural characterization, especially the analysis of chain conformation of CHPs. Meanwhile, combined with the structural modification, the desired biological activity could be obtained by degrading or introducing the target groups. Then, in wake of structural elucidation, some rules are deduced among structure-activity relationship of polysaccharide, which may speed up the application of CHPs.

AUTHOR CONTRIBUTIONS

BW and LY: investigation and writing original draft. SG, LW, and MY: writing. LF and XJ: reviewing. All authors contributed to the article and approved the submitted version.

FUNDING

This work was financially supported by the National Key research and development program of China (2018YFC1706906), Double First-Class University project of China Pharmaceutical University (CPU2018GF07 and CPU2018PZQ19), National Natural Science Foundation Committee of P.R. China (Nos. 81703775 and 81973536), and the Special Fund for Transformation of Scientific and Technological Achievements in Jiangsu Province (BA2020077) and the Project Program of State Key Laboratory of Natural Medicines, China Pharmaceutical University (SKLNMZZ202025).

REFERENCES

1. Bian Y, Zeng H, Tao H, Huang L, Du Z, Wang J, et al. A pectin-like polysaccharide from *polygala tenuifolia* inhibits pancreatic cancer cell growth in vitro and in vivo by inducing apoptosis and suppressing autophagy. *Int J Biol Macromol.* (2020) 162:107–15. doi: 10.1016/j.ijbiomac.2020.06.054
2. Cui L, Chen L, Yang G, Li Y, Qiao Z, Liu Y, et al. Structural characterization and immunomodulatory activity of a heterogalactan from *panax ginseng* flowers. *Food Res Int.* (2021) 140:109859. doi: 10.1016/j.foodres.2020.109859
3. Guo C, Wang Y, Zhang S, Zhang X, Du Z, Li M, et al. *Crataegus pinnatifida* polysaccharide alleviates colitis via modulation of gut microbiota and scfas metabolism. *Int J Biol Macromol.* (2021) 181:357–68. doi: 10.1016/j.ijbiomac.2021.03.137
4. Chen Z, Zhao Y, Zhang M, Yang X, Yue P, Tang D, et al. Structural characterization and antioxidant activity of a new polysaccharide from *bletilla striata* fibrous roots. *Carbohydr Polym.* (2020) 227:115362. doi: 10.1016/j.carbpol.2019.115362
5. Xie L, Shen M, Hong Y, Ye H, Huang L, Xie J. Chemical modifications of polysaccharides and their anti-tumor activities. *Carbohydr Polym.* (2020) 229:115436. doi: 10.1016/j.carbpol.2019.115436
6. Chen F, Huang G. Preparation and immunological activity of polysaccharides and their derivatives. *Int J Biol Macromol.* (2018) 112:211–6. doi: 10.1016/j.ijbiomac.2018.01.169
7. Cao Y-Y, Ji Y-H, Liao A-M, Huang J-H, Thakur K, Li X-L, et al. Effects of sulfated, phosphorylated and carboxymethylated modifications on the antioxidant activities in-vitro of polysaccharides sequentially extracted from *amana edulis*. *Int J Biol Macromol.* (2020) 146:887–96. doi: 10.1016/j.ijbiomac.2019.09.211
8. Li S, Xiong Q, Lai X, Li X, Wan M, Zhang J, et al. Molecular modification of polysaccharides and resulting bioactivities. *Compr Rev Food Sci Food Saf.* (2016) 15:237–50. doi: 10.1111/1541-4337.12161
9. Xu S-Y, Huang X, Cheong K-L. Recent advances in marine algae polysaccharides: isolation, structure, and activities. *Mar. Drugs.* (2017) 15. doi: 10.3390/md15120388
10. Wang C, Li W, Chen Z, Gao X, Yuan G, Pan Y, et al. Effects of simulated gastrointestinal digestion in vitro on the chemical properties, antioxidant activity, α-amylase and α-glucosidase inhibitory activity of polysaccharides from *inonotus obliquus*. *Food Res Int.* (2018) 103:280–8. doi: 10.1016/j.foodres.2017.10.058
11. Zhang X, Duan S, Tao S, Huang J, Liu C, Xing S, et al. Polysaccharides from *dendrobium officinale* inhibit proliferation of osteosarcoma cells and enhance cisplatin-induced apoptosis. *J Funct Foods.* (2020) 73:104143. doi: 10.1016/j.jff.2020.104143
12. Im SA, Oh ST, Song S, Kim MR, Kim DS, Woo SS, et al. Identification of optimal molecular size of modified *aloe* polysaccharides with maximum immunomodulatory activity. *Int Immunopharmacol.* (2005) 5:271–9. doi: 10.1016/j.intimp.2004.09.031
13. Jia Y, Xue Z, Wang Y, Lu Y, Li R, Li N, et al. Chemical structure and inhibition on α-glucosidase of polysaccharides from corn silk by fractional precipitation. *Carbohydr Polym.* (2021) 252:117185. doi: 10.1016/j.carbpol.2020.117185
14. Jia Y, Gao X, Xue Z, Wang Y, Lu Y, Zhang M, et al. Characterization, antioxidant activities, and inhibition on α-glucosidase activity of corn silk polysaccharides obtained by different extraction methods. *Int J Biol Macromol.* (2020) 163:1640–8. doi: 10.1016/j.ijbiomac.2020.09.068
15. Błaszczyk K, Wilczak J, Harasym J, Gudej S, Suchecka D, Królikowski T, et al. Impact of low and high molecular weight oat beta-glucan on oxidative stress and antioxidant defense in spleen of rats with lps induced enteritis. *Food Hydrocoll.* (2015) 51:272–80. doi: 10.1016/j.foodhyd.2015.05.025
16. Huo J, Wu Z, Sun W, Wang Z, Wu J, Huang M, et al. Protective effects of natural polysaccharides on intestinal barrier injury: a review. *J Agric Food Chem.* (2022) 70:711–35. doi: 10.1021/acs.jafc.1c05966
17. Hou C, Yin M, Lan P, Wang H, Nie H. Ji X. Recent progress in the research of angelica sinensis (oliv) diels polysaccharides: extraction, purification, structure and bioactivities. *Chem Biol Technol Agric.* (2021) 8:13. doi: 10.1186/s40538-021-00214-x
18. Qu J, Huang P, Zhang L, Qiu Y, Qi H, Leng A, et al. Hepatoprotective effect of plant polysaccharides from natural resources: a review of the mechanisms and structure-activity relationship. *Int J Biol Macromol.* (2020) 161:24–34. doi: 10.1016/j.ijbiomac.2020.05.196
19. Yu CH Dai XY, Chen Q, Zang JN, Deng LL, Liu YH, et al. Hypolipidemic and antioxidant activities of polysaccharides from *rosae laevigatae* fructus in rats. *Carbohydr Polym.* (2013) 94:56–62. doi: 10.1016/j.carbpol.2013.01.006
20. Li F, Du P, Yang W, Huang D, Nie S, Xie M. Polysaccharide from the seeds of *plantago asiatica* l. alleviates nonylphenol induced intestinal barrier injury by regulating tight junctions in human caco-2 cell line. *Int J Biol Macromol.* (2020) 164:2134–40. doi: 10.1016/j.ijbiomac.2020.07.259
21. Gu J, Zhang H, Yao H, Zhou J, Duan Y, Ma H. Comparison of characterization, antioxidant and immunological activities of three polysaccharides from *Sagittaria Sagittifolia* L. *Carbohydr Polym.* (2020) 235:115939. doi: 10.1016/j.carbpol.2020.115939
22. Zheng L, Ma Y, Zhang Y, Meng Q, Yang J, Wang B, et al. Increased antioxidant activity and improved structural characterization of sulfuric acid-treated stepwise degraded polysaccharides from *pholiota nameko* Pn-01. *Int J Biol Macromol.* (2021) 166:1220–9. doi: 10.1016/j.ijbiomac.2020.11.004
23. Saito Y, Kinoshita M, Yamada A, Kawano S, Liu HS, Kamimura S, et al. Mannose and phosphomannose isomerase regulate energy metabolism under glucose starvation in leukemia. *Cancer Sci.* (2021) 112:4944–56. doi: 10.1111/cas.15138
24. Sorourian R, Khajehrahimi AE, Tadayoni M, Azizi MH, Hojjati M. Ultrasound-assisted extraction of polysaccharides from *typha domingensis*: structural characterization and functional properties. *Int J Biol Macromol.* (2020) 160:758–68. doi: 10.1016/j.ijbiomac.2020.05.226
25. Du B, Meenu M, Liu H, Xu B. A concise review on the molecular structure and function relationship of β-glucan. *Int J Mol Sci.* (2019) 20. doi: 10.3390/ijms20164032
26. Jin Y, Li P, Wang F. B-Glucans as potential immunoadjuvants: a review on the adjuvanticity, structure-activity relationship and receptor recognition properties. *Vaccine.* (2018) 36:5235–44. doi: 10.1016/j.vaccine.2018.07.038
27. Mutaillifu P, Bobakulov K, Abuduwaili A, Huojiaaihemaiti H, Nuerxiati R, Aisa HA, et al. Structural characterization and antioxidant activities of a water soluble polysaccharide isolated from *Glycyrrhiza Glabra*. *Int J Biol Macromol.* (2020) 144:751–9. doi: 10.1016/j.ijbiomac.2019.11.245
28. Moreno-Mendieta S, Guillén D, Hernández-Pando R, Sánchez S, Rodríguez-Sanoja R. Potential of glucans as vaccine adjuvants: a review of the α-glucans case. *Carbohydr Polym.* (2017) 165:103–14. doi: 10.1016/j.carbpol.2017.02.030
29. Ji X, Hou C, Shi M, Yan Y, Liu Y. An insight into the research concerning panax ginseng C. A. meyer polysaccharides: a Review. *Food Rev Int.* (2020) 1–17. doi: 10.1080/87559129.2020.1771363
30. Wasser SP. Medicinal mushrooms as a source of antitumor and immunomodulating polysaccharides. *Appl Microbiol Biotechnol.* (2002) 60:258–74. doi: 10.1007/s00253-002-1076-7
31. Zhao D, Dai W, Tao H, Zhuang W, Qu M. Chang YN. Polysaccharide isolated from auricularia auricular-judae (bull) prevents dextran sulfate sodium-induced colitis in mice through modulating the composition of the gut microbiota. *J Food Sci.* (2020) 85:2943–51. doi: 10.1111/1750-3841.15319
32. Ai J, Bao B, Battino M, Giampieri F, Chen C, You L, et al. Recent advances on bioactive polysaccharides from mulberry. *Food Funct.* (2021) 12:5219–35. doi: 10.1039/D1FO00682G
33. Wang J, Jia J, Song L, Gong X, Xu J, Yang M, et al. Extraction, structure, and pharmacological activities of *astragalus* polysaccharides. *Appl Sci.* (2019) 9. doi: 10.3390/app9010122
34. Ji X, Peng B, Ding H, Cui B, Nie H, Yan Y. Purification, structure and biological activity of pumpkin polysaccharides: a review. *Food Rev Int.* (2021) 1–13. doi: 10.1080/87559129.2021.1904973
35. Ye J, Zhang C, Lyu X, Hua X, Zhao W, Zhang W, et al. Structure and physicochemical properties of arabinan-rich acidic polysaccharide from the by-product of peanut oil processing. *Food Hydrocoll.* (2021) 117:106743. doi: 10.1016/j.foodhyd.2021.106743
36. Gan T, Feng C, Lan H, Yang R, Zhang J, Li C, et al. Comparison of the structure and immunomodulatory activity of polysaccharides from fresh and dried longan. *J Funct Foods.* (2021) 76:104323. doi: 10.1016/j.jff.2020.104323

37. Li M, Li T, Hu X, Ren G, Zhang H, Wang Z, et al. Structural, rheological properties and antioxidant activities of polysaccharides from mulberry fruits (murus alba l) based on different extraction techniques with superfine grinding pretreatment. *Int J Biol Macromol.* (2021) 183:1774–83. doi: 10.1016/j.ijbiomac.2021.05.108
38. Zhang H, Wang J-Q, Nie S-P, Wang Y-X, Cui SW, Xie M-Y. Sulfated modification, characterization and property of a water-insoluble polysaccharide from *Ganoderma Atrum*. *Int J Biol Macromol.* (2015) 79:248–55. doi: 10.1016/j.ijbiomac.2015.04.070
39. Zheng Z, Pan X, Luo L, Zhang Q, Huang X, Liu Y, et al. Advances in oral absorption of polysaccharides: mechanism, affecting factors, and improvement strategies. *Carbohydr Polym.* (2022) 282:119110. doi: 10.1016/j.carbpol.2022.119110
40. Wu X, Zheng Z, Guo T, Wang K, Zhang Y. Molecular dynamics simulation of lentinan and its interaction with the innate receptor dectin-1. *Int J Biol Macromol.* (2021) 171:527–38. doi: 10.1016/j.ijbiomac.2021.01.032
41. Chen L, Ge MD, Zhu YJ, Song Y, Cheung PCK, Zhang BB, et al. Structure, bioactivity and applications of natural hyperbranched polysaccharides. *Carbohydr Polym.* (2019) 223:115076. doi: 10.1016/j.carbpol.2019.115076
42. Wu D-T, Meng L-Z, Wang L-Y, Lv G-P, Cheong K-L, Hu D-J, et al. Chain conformation and immunomodulatory activity of a hyperbranched polysaccharide from *cordyceps sinensis*. *Carbohydr Polym.* (2014) 110:405–14. doi: 10.1016/j.carbpol.2014.04.044
43. Li B, Zhang N, Feng Q, Li H, Wang D, Ma L, et al. The core structure characterization and of *ginseng* neutral polysaccharide with the immune-enhancing activity. *Int J Biol Macromol.* (2019) 123:713–22. doi: 10.1016/j.ijbiomac.2018.11.140
44. Bae IY, Kim HW, Yoo HJ, Kim ES, Lee S, Park DY, et al. Correlation of branching structure of mushroom β-glucan with its physiological activities. *Food Res Int.* (2013) 51:195–200. doi: 10.1016/j.foodres.2012.12.008
45. Li N, Wang C, Georgiev MI, Bajpai VK, Tundis R, Simal-Gandara J, et al. Advances in dietary polysaccharides as anticancer agents: structure-activity relationship. *Trends Food Sci Technol.* (2021) 111:360–77. doi: 10.1016/j.tifs.2021.03.008
46. Patel BK, Campanella OH, Janaswamy S. Impact of urea on the three-dimensional structure, viscoelastic and thermal behavior of iota-carrageenan. *Carbohydr Polym.* (2013) 92:1873–9. doi: 10.1016/j.carbpol.2012.11.026
47. Tao Y, Zhang R, Yang W, Liu H, Yang H, Zhao Q. Carboxymethylated hyperbranched polysaccharide: synthesis, solution properties, and fabrication of hydrogel. *Carbohydr Polym.* (2015) 128:179–87. doi: 10.1016/j.carbpol.2015.04.012
48. Chen X, Xu X, Zhang L, Kennedy JF. Flexible chain conformation of (1 → 3)-B-D-Glucan from *poria cocos* sclerotium in naoh/urea aqueous solution. *Carbohydr Polym.* (2009) 75:586–91. doi: 10.1016/j.carbpol.2008.08.027
49. Morris ER, Cutler AN, Ross-Murphy SB, Rees DA, Price J. Concentration and shear rate dependence of viscosity in random coil polysaccharide solutions. *Carbohydr Polym.* (1981) 1:5–21. doi: 10.1016/0144-8617(81)90011-4
50. Kido S, Nakanishi T, Norisuye T, Kaneda I, Yanaki T. Ordered conformation of succinoglycan in aqueous sodium chloride. *Biomacromolecules.* (2001) 2:952–7. doi: 10.1021/bm010064h
51. Anderson NS, Campbell JW, Harding MM, Rees DA, Samuel JW. X-Ray diffraction studies of polysaccharide sulphates: double helix models for K- and L-carrageenans. *J Mol Biol.* (1969) 45:85–99. doi: 10.1016/0022-2836(69)90211-3
52. Meng Y, Shi X, Cai L, Zhang S, Ding K, Nie S, et al. Triple-Helix conformation of a polysaccharide determined with light scattering, afm, and molecular dynamics simulation. *Macromolecules.* (2018) 51:10150–9. doi: 10.1021/acs.macromol.8b02017
53. Jana NR, Gearheart L, Murphy CJ. Seed-mediated growth approach for shape-controlled synthesis of spheroidal and rod-like gold nanoparticles using a surfactant template. *Adv Mater.* (2001) 13:1389–93. doi: 10.1002/1521-4095(200109)13:18<1389::AID-ADMA1389>3.0.CO;2-F.3.0.CO;2-F
54. Fang Y, Duan B, Lu A, Liu M, Liu H, Xu X, et al. Intermolecular interaction and the extended wormlike chain conformation of chitin in naoh/urea aqueous solution. *Biomacromolecules.* (2015) 16:1410–7. doi: 10.1021/acs.biomac.5b00195
55. Kök MS, Abdelhameed AS, Ang S, Morris GA, Harding SE. A novel global hydrodynamic analysis of the molecular flexibility of the dietary fibre polysaccharide konjac glucomannan. *Food Hydrocoll.* (2009) 23:1910–7. doi: 10.1016/j.foodhyd.2009.02.002
56. Gu J, Catchmark JM. Impact of hemicelluloses and pectin on sphere-like bacterial cellulose assembly. *Carbohydr Polym.* (2012) 88:547–57. doi: 10.1016/j.carbpol.2011.12.040
57. Meng Y, Lyu F, Xu X, Zhang L. Recent advances in chain conformation and bioactivities of triple-helix polysaccharides. *Biomacromolecules.* (2020) 21:1653–77. doi: 10.1021/acs.biomac.9b01644
58. Maeda YY, Watanabe ST, Chihara C, Rokutanda M. Denaturation and renaturation of a beta-1,6;1,3-glucan, lentinan, associated with expression of t-cell-mediated responses. *Cancer Res.* (1988) 48:671–5. doi: 10.1016/0192-0561(88)90374-8
59. Cui W, Huang J, Niu X, Shang H, Sha Z, Miao Y, et al. Screening active fractions from *pinus massoniana* pollen for inhibiting alv-j replication and their structure activity relationship investigation. *Vet Microbiol.* (2021) 252:108908. doi: 10.1016/j.vetmic.2020.108908
60. Yuan H, Lan P, He Y, Li C, Ma X. Effect of the modifications on the physicochemical and biological properties of B-Glucan-a critical review. *Molecules.* (2019) 25. doi: 10.3390/molecules25010057
61. Li S, Li J, Zhi Z, Wei C, Wang W, Ding T, et al. Macromolecular properties and hypolipidemic effects of four sulfated polysaccharides from sea cucumbers. *Carbohydr Polym.* (2017) 173:330–7. doi: 10.1016/j.carbpol.2017.05.063
62. Lv X, Wang C, Cheng Y, Huang L, Wang Z. Isolation and structural characterization of a polysaccharide Lrp4-a from *Lycium Ruthenicum* Murr. *Carbohydr Res.* (2013) 365:20–5. doi: 10.1016/j.carres.2012.10.013
63. Mirhosseini H, Amid BT, Cheong KW. Effect of Different drying methods on chemical and molecular structure of heteropolysaccharide–protein gum from durian seed. *Food Hydrocoll.* (2013) 31:210–9. doi: 10.1016/j.foodhyd.2012.11.005
64. Zhang X, Liu L, Lin C. Isolation, structural characterization and antioxidant activity of a neutral polysaccharide from sisal waste. *Food Hydrocoll.* (2014) 39:10–8. doi: 10.1016/j.foodhyd.2013.12.012
65. Zeng H, Miao S, Zhang Y, Lin S, Jian Y, Tian Y. et al. Isolation, preliminary structural characterization and hypolipidemic effect of polysaccharide fractions from fortunella margarita (Lour) swingle. *Food Hydrocoll.* (2016) 52:126–36. doi: 10.1016/j.foodhyd.2015.05.028
66. Chen F, Ran L, Mi J, Yan Y, Lu L, Jin B, et al. Isolation, characterization and antitumor effect on Du145 cells of a main polysaccharide in pollen of chinese wolfberry. *Molecules.* (2018) 23. doi: 10.3390/molecules23102430
67. Yang C, Gou Y, Chen J, An J, Chen W, Hu F. Structural characterization and antitumor activity of a pectic polysaccharide from *Codonopsis Pilosula*. *Carbohydr Polym.* (2013) 98:886–95. doi: 10.1016/j.carbpol.2013.06.079
68. Zhou S, Rahman A, Li J, Wei C, Chen J, Linhardt RJ, et al. Extraction methods affect the structure of goji (*Lycium Barbarum*) polysaccharides. *Molecules.* (2020) 25. doi: 10.3390/molecules25040936
69. Guo L, Du X, Lan J, Liang Q. Study on molecular structural characteristics of tea polysaccharide. *Int J Biol Macromol.* (2010) 47:244–9. doi: 10.1016/j.ijbiomac.2010.03.026
70. Wang W, Zhang F, Li Q, Chen H, Zhang W, Yu P, et al. Structure characterization of one polysaccharide from *lepidium meyenii* walp., and its antioxidant activity and protective effect against H[[sb]]2[[/s]]O[[sb]]2[[/s]]-Induced Injury Raw264.7 Cells. *Int J Biol Macromol.* (2018) 118:816–33. doi: 10.1016/j.ijbiomac.2018.06.117
71. Zhang S, An L, Li Z, Wang X, Wang H, Shi L, et al. Structural elucidation of an immunological arabinan from the rhizomes of ligusticum chuanxiong, a traditional Chinese medicine. *Int J Biol Macromol.* (2021) 170:42–52. doi: 10.1016/j.ijbiomac.2020.12.069
72. Medeiros PM, Simoneit BR. Analysis of sugars in environmental samples by gas chromatography-mass spectrometry. *J Chromatogr A.* (2007) 1141:271–8. doi: 10.1016/j.chroma.2006.12.017
73. Ma J, Adler L, Srzednicki G, Arcot J. Quantitative determination of non-starch polysaccharides in foods using gas chromatography with flame ionization detection. *Food Chem.* (2017) 220:100–7. doi: 10.1016/j.foodchem.2016.09.206

74. Li H, Long C, Zhou J, Liu J, Wu X, Long M. Rapid analysis of monosaccharides and oligo-saccharides in hydrolysates of lignocellulosic biomass by Hplc. *Biotechnol Lett.* (2013) 35:1405–9. doi: 10.1007/s10529-013-1224-4
75. Saba JA, Shen X, Jamieson JC, Perreault H. Investigation of different combinations of derivatization, separation methods and electrospray ionization mass spectrometry for standard oligosaccharides and glycans from ovalbumin. *J Mass Spectrom.* (2001) 36:563–74. doi: 10.1002/jms.158
76. Honda S, Akao E, Suzuki S, Okuda M, Kakehi K, Nakamura J. High-performance liquid chromatography of reducing carbohydrates as strongly ultraviolet-absorbing and electrochemically sensitive 1-Phenyl-3-Methyl-5-Pyrazolone derivatives. *Anal Biochem.* (1989) 180:351–7. doi: 10.1016/0003-2697(89)90444-2
77. Zhang Z, Khan NM, Nunez KM, Chess EK, Szabo CM. Complete monosaccharide analysis by high-performance anion-exchange chromatography with pulsed amperometric detection. *Anal Chem.* (2012) 84:4104–10. doi: 10.1021/ac300176z
78. Hentati F, Delattre C, Ursu AV, Desbrières J, Le Cerf D, Gardarin C, et al. Structural characterization and antioxidant activity of water-soluble polysaccharides from the tunisian brown seaweed *Cystoseira Compressa*. *Carbohydr Polym.* (2018) 198:589–600. doi: 10.1016/j.carbpol.2018.06.098
79. Du X, Zhang Y, Mu H, Lv Z, Yang Y, Zhang J. Structural elucidation and antioxidant activity of a novel polysaccharide (Tapb1) from *Tremella Aurantialba*. *Food Hydrocoll.* (2015) 43:459–64. doi: 10.1016/j.foodhyd.2014.07.004
80. Ren Y, Bai Y, Zhang Z, Cai W, Del Rio Flores A. The preparation and structure analysis methods of natural polysaccharides of plants and fungi: a review of recent development. *Molecules.* (2019) 24. doi: 10.3390/molecules24173122
81. Miao M, Bai A, Jiang B, Song Y, Cui SW, Zhang T. Characterisation of a novel water-soluble polysaccharide from leuconostoc citreum Sk24002. *Food Hydrocoll.* (2014) 36:265–72. doi: 10.1016/j.foodhyd.2013.10.014
82. Xiao-Li M, Feng Feng S, Hui Z, Xie H, Song Ya L. Compositional monosaccharide analysis of *morus nigra* linn by hplc and HPCE quantitative determination and comparison of polysaccharide from *Morus Nigra* Linn by Hpce and Hplc. *Curr Pharm Anal.* (2017) 13:433–7. doi: 10.2174/1573412913666170330150807
83. Zhou Y, Duan Y, Huang S, Zhou X, Zhou L, Hu T, et al. Polysaccharides from *Lycium Barbarum* ameliorate amyloid pathology and cognitive functions in App/Ps1 transgenic mice. *Int J Biol Macromol.* (2020) 144:1004–12. doi: 10.1016/j.ijbiomac.2019.09.177
84. Liu Y, Yang L, Zhang Y, Liu X, Wu Z, Gilbert RG, et al. *Dendrobium officinale* polysaccharide ameliorates diabetic hepatic glucose metabolism via glucagon-mediated signaling pathways and modifying liverglycogen structure. *J Ethnopharmacol.* (2020) 248:112308. doi: 10.1016/j.jep.2019.112308
85. Chen R, Liu Z, Zhao J, Chen R, Meng F, Zhang M, et al. Antioxidant and immunobiological activity of water-soluble polysaccharide fractions purified from *Acanthopanax Senticosu*. *Food Chem.* (2011) 127:434–40. doi: 10.1016/j.foodchem.2010.12.143
86. Amicucci MJ, Galermo AG, Nandita E, Vo T-TT, Liu Y, Lee M, et al. A rapid-throughput adaptable method for determining the monosaccharide composition of polysaccharides. *Int J Mass Spectrom.* (2019) 438:22–8. doi: 10.1016/j.ijms.2018.12.009
87. Ciucanu I, Caprita R. Per-O-Methylation of neutral carbohydrates directly from aqueous samples for gas chromatography and mass spectrometry analysis. *Anal Chim Acta.* (2007) 585:81–5. doi: 10.1016/j.aca.2006.12.015
88. Guan J, Li SP. Discrimination of polysaccharides from traditional chinese medicines using saccharide mapping—enzymatic digestion followed by chromatographic analysis. *J Pharm Biomed Anal.* (2010) 51:590–8. doi: 10.1016/j.jpba.2009.09.026
89. Neeser JR, Schweizer TF. A quantitative determination by capillary gas-liquid chromatography of neutral and amino sugars (as O-Methyloxime Acetates), and a study on hydrolytic conditions for glycoproteins and polysaccharides in order to increase sugar recoveries. *Anal Biochem.* (1984) 142:58–67. doi: 10.1016/0003-2697(84)90516-5
90. Ip CC, Manam V, Hepler R, Hennessey JP. Carbohydrate composition analysis of bacterial polysaccharides: optimized acid hydrolysis conditions for hpaec-pad analysis. *Anal Biochem.* (1992) 201:343–9. doi: 10.1016/0003-2697(92)90349-C
91. Tang Y, Zhu ZY, Pan LC, Sun H, Song QY, Zhang Y. Structure analysis and anti-fatigue activity of a polysaccharide from *lepidium meyenii* walp. *Nat Prod Res.* (2019) 33:2480–9. doi: 10.1080/14786419.2018.1452017
92. Ciucanu I, Kerek F. A Simple and rapid method for the permethylation of carbohydrates. *Carbohydr Res.* (1984) 131:209–17. doi: 10.1016/0008-6215(84)85242-8
93. Hakomori S-I. A rapid permethylation of glycolipid, and polysaccharide catalyzed by methylsulfinyl carbanion in dimethyl sulfoxide. *J Biol Chem.* (1964) 55:205–8.
94. Shao P, Chen X, Sun P. Improvement of antioxidant and moisture-preserving activities of *sargassum horneri* polysaccharide enzymatic hydrolyzates. *Int J Biol Macromol.* (2015) 74:420–7. doi: 10.1016/j.ijbiomac.2014.12.021
95. Xia YG, Wang TL, Sun LM, Liang J, Yang BY, Kuang HX, et al. New Uplc-Ms/Ms method for the characterization and discrimination of polysaccharides from genus *ephedra* based on enzymatic digestions. *Molecules.* (2017) 22:12. doi: 10.3390/molecules22111992
96. Amicucci MJ, Nandita E, Galermo AG, Castillo JJ, Chen S, Park D, et al. A nonenzymatic method for cleaving polysaccharides to yield oligosaccharides for structural analysis. *Nat Commun.* (2020) 11:3963. doi: 10.1038/s41467-020-17778-1
97. Niu L-L, Wu Y-R, Liu H-P, Wang Q, Li M-Y, Jia Q. Optimization of extraction process, characterization and antioxidant activities of polysaccharide from *Leucopaxillus Giganteus*. *J Food Meas Charact.* (2021) 15:2842–53. doi: 10.1007/s11694-021-00865-2
98. Zhang X, Kong X, Hao Y, Zhang X, Zhu Z. Chemical Structure and Inhibition on Alpha-Glucosidase of Polysaccharide with Alkaline-Extracted from *Glycyrrhiza Inflata* Residue. *Int J Biol Macromol.* (2019) 147:1125–35. doi: 10.1016/j.ijbiomac.2019.10.081
99. Zhang G, Yin Q, Han T, Zhao Y, Su J, Li M, et al. Purification and antioxidant effect of novel fungal polysaccharides from the stroma of *cordyceps kyushuensis*. *Ind Crops Prod.* (2015) 69:485–91. doi: 10.1016/j.indcrop.2015.03.006
100. Huang H, Huang G. Extraction, separation, modification, structural characterization, and antioxidant activity of plant polysaccharides. *Chem Biol Drug Des.* (2020) 96:1209–22. doi: 10.1111/cbdd.13794
101. Zhang H, Zou P, Zhao H, Qiu J, Regenstein JM, Yang X. Isolation, purification, structure and antioxidant activity of polysaccharide from pinecones of *pinus koraiensis*. *Carbohydr Polym.* (2021) 251:117078. doi: 10.1016/j.carbpol.2020.117078
102. Wu X, Jiang W, Lu J, Yu Y, Wu B. Analysis of the monosaccharide composition of water-soluble polysaccharides from *sargassum fusiforme* by high performance liquid chromatography/electrospray ionisation mass spectrometry. *Food Chem.* (2014) 145:976–83. doi: 10.1016/j.foodchem.2013.09.019
103. Rühmann B, Schmid J, Sieber V. Fast carbohydrate analysis via liquid chromatography coupled with ultra violet and electrospray ionization ion trap detection in 96-well format. *J Chromatogr A.* (2014) 1350:44–50. doi: 10.1016/j.chroma.2014.05.014
104. Xu G, Amicucci MJ, Cheng Z, Galermo AG, Lebrilla CB. Revisiting monosaccharide analysis - quantitation of a comprehensive set of monosaccharides using dynamic multiple reaction monitoring. *Analyst.* (2017) 143:200–7. doi: 10.1039/C7AN01530E
105. Amicucci MJ, Galermo AG, Guerrero A, Treves G, Nandita E, Kailemia MJ, et al. Strategy for structural elucidation of polysaccharides: elucidation of a maize mucilage that harbors diazotrophic bacteria. *Anal Chem.* (2019) 91:7254–65. doi: 10.1021/acs.analchem.9b00789
106. Chuang L, Panyoyai N, Shanks R, Kasapis S. Effect of sodium chloride on the glass transition of condensed starch systems. *Food Chem.* (2015) 184:65–71. doi: 10.1016/j.foodchem.2015.03.031
107. Guérin G, Raez J, Manners I, Winnik MA. Light scattering study of rigid, rodlike organometallic block copolymer micelles in dilute solution. *Macromolecules.* (2005) 38:7819–27. doi: 10.1021/ma0498870
108. Ioan CE, Aberle T, Burchard W. Light scattering and viscosity behavior of dextran in semidilute solution. *Macromolecules.* (2001) 34:326–36. doi: 10.1021/ma992060z

109. Kratky O, Porod G. Röntgenuntersuchung gelöster fadenmoleküle. *Recl Trav Chim Pays-Bas.* (1949) 68:1106–22. doi: 10.1002/recl.19490681203
110. Jayme M, Ames F, Bersani-Amado C, Machado M, Mangolin C, Gonçalves R, et al. Primary characterization and evaluation of anti ulcerogenic activity of an aqueous extract from callus culture of cereus peruvianus mill. (Cactaceae). *Curr Pharm Biotechnol.* (2015) 16. doi: 10.2174/1389201016666150303154342
111. Xu S, Xu X, Zhang L. Effect of heating on chain conformation of branched β-glucan in Water. *J Phys Chem B.* (2013) 117:8370–7. doi: 10.1021/jp403202u
112. Tao Y, Yan Y, Xu W. Shrinking factors of hyperbranched polysaccharide from fungus. *Carbohydr Res.* (2009) 344:1311–8. doi: 10.1016/j.carres.2009.05.004
113. Renard D, Lepvrier E, Garnier C, Roblin P, Nigen M, Sanchez C. Structure of glycoproteins from acacia gum: an assembly of ring-like glycoproteins modules. *Carbohydr Polym.* (2014) 99:736–47. doi: 10.1016/j.carbpol.2013.08.090
114. Shao L, Wu Z, Tian F, Zhang H, Liu Z, Chen W, et al. Molecular characteristics of an exopolysaccharide from lactobacillus rhamnosus Kf5 in Solution. *Int. J. Biol. Macromol.* (2015) 72:1429–34. doi: 10.1016/j.ijbiomac.2014.10.015
115. Li S, Huang Y, Wang S, Xu X, Zhang L. Determination of the triple helical chain conformation of β-glucan by facile and reliable triple-detector size exclusion chromatography. *J Phys Chem B.* (2014) 118:668–75. doi: 10.1021/jp4087199
116. Shakun M, Maier H, Heinze T, Kilz P, Radke W. Molar Mass Characterization of Sodium Carboxymethyl Cellulose by Sec-Malls. *Carbohydr Polym.* (2013) 95:550–9. doi: 10.1016/j.carbpol.2013.03.028
117. Deng Y, Li M, Chen L-X, Chen X-Q, Lu J-H, Zhao J, et al. Chemical Characterization and Immunomodulatory Activity of Acetylated Polysaccharides from *Dendrobium Devonianum*. *Carbohydr Polym.* (2018) 180:238–45. doi: 10.1016/j.carbpol.2017.10.026
118. Sillrén P, Swenson J, Mattsson J, Bowron D, Matic A. The temperature dependent structure of liquid 1-propanol as studied by neutron diffraction and epsr simulations. *J Chem Phys.* (2013) 138:214501. doi: 10.1063/1.4807863
119. Feng L, Yin J, Nie S, Wan Y, Xie M. Structure and conformation characterization of galactomannan from seeds of *Cassia Obtusifolia*. *Food Hydrocoll.* (2018) 76:67–77. doi: 10.1016/j.foodhyd.2017.06.008
120. Arinaitwe E, Pawlik M. Dilute solution properties of carboxymethyl celluloses of various molecular weights and degrees of substitution. *Carbohydr Polym.* (2014) 99:423–31. doi: 10.1016/j.carbpol.2013.08.030
121. Zhang Z, Guo L, Yan A, Feng L, Wan Y. Fractionation, structure and conformation characterization of polysaccharides from *Anoectochilus Roxburghii*. *Carbohydr Polym.* (2020) 231:115688. doi: 10.1016/j.carbpol.2019.115688
122. Wang Y, Li Y, Ma X, Ren H, Fan W, Leng F, et al. Extraction, purification, and bioactivities analyses of polysaccharides from *Glycyrrhiza Uralensis*. *Ind Crops Prod.* (2018) 122:596–608. doi: 10.1016/j.indcrop.2018.06.011
123. Zhao S, Han Z, Yang L, Hong B, Zhu H. Extraction, characterization and antioxidant activity evaluation of polysaccharides from *Smilacina Japonica*. *Int J Biol Macromol.* (2020) 151:576–83. doi: 10.1016/j.ijbiomac.2020.02.015
124. Hu J-L, Nie S-P, Li C, Wang S, Xie M-Y. Ultrasonic irradiation induces degradation and improves prebiotic properties of polysaccharide from seeds of *plantago asiatica* l. during in vitro fermentation by human fecal microbiota. *Food Hydrocoll.* (2018) 76:60–6. doi: 10.1016/j.foodhyd.2017.06.009
125. Ma F, Wang D, Zhang Y, Li M, Qing W, Tikkanen-Kaukanen C, et al. Characterisation of the mucilage polysaccharides from *dioscorea opposita* thunb. *With Enzymatic Hydrolysis Food Chem.* (2018) 245:13–21. doi: 10.1016/j.foodchem.2017.10.080
126. Rozi P, Abuduwaili A, Mutailifu P, Gao Y, Rakhmanberdieva R, Aisa HA, et al. Sequential extraction, characterization and antioxidant activity of polysaccharides from *fritillaria pallidiflora* schrenk. *Int J Biol Macromol.* (2019) 131:97–106. doi: 10.1016/j.ijbiomac.2019.03.029
127. Li Q, Wang W, Zhu Y, Chen Y, Zhang W, Yu P, et al. Structural elucidation and antioxidant activity a novel se-polysaccharide from se-enriched *Grifola Frondosa*. *Carbohydr Polym.* (2017) 161:42–52. doi: 10.1016/j.carbpol.2016.12.041
128. Kong L, Yu L, Feng T, Yin X, Liu T, Dong L. Physicochemical characterization of the polysaccharide from *bletilla striata*: effect of drying method. *Carbohydr Polym.* (2015) 125:1–8. doi: 10.1016/j.carbpol.2015.02.042
129. McIntire TM, Brant DA. Observations of the (1 → 3)-B-D-Glucan linear triple helix to macrocycle interconversion using noncontact atomic force microscopy. *J Am Chem Soc.* (1998) 120:6909–19. doi: 10.1021/ja981203e
130. Schefer L, Adamcik J, Mezzenga R. Unravelling secondary structure changes on individual anionic polysaccharide chains by atomic force microscopy. *Angew Chem Int Ed.* (2014) 53:5376–9. doi: 10.1002/anie.201402855
131. Zhao T, Mao G, Zhang M, Feng W, Mao R, Zhu Y. et al. Structure analysis of a bioactive heteropolysaccharide from schisandra chinensis (Turcz) Baill. *Carbohydr Polym.* (2014) 103:488–95. doi: 10.1016/j.carbpol.2013.12.058
132. Gao Y, Zhou Y, Zhang Q, Zhang K, Peng P, Chen L, et al. Hydrothermal extraction, structural characterization, and inhibition hela cells proliferation of functional polysaccharides from chinese tea zhongcha 108. *J Funct Foods.* (2017) 39:1–8. doi: 10.1016/j.jff.2017.09.057
133. Duan B, Zou S, Sun Y, Xu X. Nanoplatform constructed from a β-glucan and polydeoxyadenylic acid for cancer chemotherapy and imaging. *Biomacromolecules.* (2019) 20:1567–77. doi: 10.1021/acs.biomac.8b01780
134. Liu Q, Xu X, Zhang L. Variable chain conformations of renatured β-glucan in dimethylsulfoxide/water mixture. *Biopolymers.* (2012) 97:988–97. doi: 10.1002/bip.22115
135. Zhang W, Huang J, Wang W, Li Q, Chen Y, Feng W, et al. Extraction, Purification, Characterization and Antioxidant Activities of Polysaccharides from *Cistanche Tubulosa*. *Int J Biol Macromol.* (2016) 93:448–58. doi: 10.1016/j.ijbiomac.2016.08.079
136. Wang J, Niu S, Zhao B, Luo T, Liu D, Zhang J. Catalytic synthesis of sulfated polysaccharides. ii: comparative studies of solution conformation and antioxidant activities. *Carbohydr Polym.* (2014) 107:221–31. doi: 10.1016/j.carbpol.2014.02.074
137. Liu Y, Zhang J, Tang Q, Yang Y, Guo Q, Wang Q, et al. Physicochemical characterization of a high molecular weight bioactive β-d-glucan from the fruiting bodies of *Ganoderma Lucidum*. *Carbohydr Polym.* (2014) 101:968–74. doi: 10.1016/j.carbpol.2013.10.024
138. Wang B, Wang X, Xiong Z, Lu G, Ma W, Lv Q, et al. A review on the applications of traditional chinese medicine polysaccharides in drug delivery systems. *Chinese Med.* (2022) 17:12. doi: 10.1186/s13020-021-00567-3
139. Wang Y, Zhang L, Li Y, Hou X, Zeng F. Correlation of structure to antitumor activities of five derivatives of a beta-glucan from *poria cocos* sclerotium. *Carbohydr Res.* (2004) 339:2567–74. doi: 10.1016/j.carres.2004.08.003
140. Zhao Y, Tian N, Wang H, Yan H. Chemically sulfated polysaccharides from *agaricus blazei* murill: synthesis, characterization and anti-hiv activity. *Chem Biodiversity.* (2021) 18:e2100338. doi: 10.1002/cbdv.202100338
141. Wang C, He Y, Tang X, Li N. Sulfation, structural analysis, and anticoagulant bioactivity of ginger polysaccharides. *J Food Sci.* (2020) 85:2427–34. doi: 10.1111/1750-3841.15338
142. Wang X, Zhang Z, Yao Q, Zhao M, Qi H. Phosphorylation of low-molecular-weight polysaccharide from *enteromorpha linza* with antioxidant activity. *Carbohydr Polym.* (2013) 96:371–5. doi: 10.1016/j.carbpol.2013.04.029
143. Abuduwaili A, Nuerxiati R, Mutailifu P, Gao Y, Lu C, Yili A. Isolation, structural modification, characterization, and bioactivity of polysaccharides from *folium isatidis*. *Ind Crops Prod.* (2022) 176:114319. doi: 10.1016/j.indcrop.2021.114319
144. Wang Z-J, Xie J-H, Shen M-Y, Tang W, Wang H, Nie S-P, et al. Carboxymethylation of polysaccharide from *cyclocarya paliurus* and their characterization and antioxidant properties evaluation. *Carbohydr Polym.* (2016) 136:988–94. doi: 10.1016/j.carbpol.2015.10.017
145. Li CY, Liu L, Zhao YW, Chen JY, Sun XY, Ouyang JM. Inhibition of calcium oxalate formation and antioxidant activity of carboxymethylated *Poria Cocos* Polysaccharides. *Oxid Med Cell Longevity.* (2021) 2021:6653593. doi: 10.1155/2021/6653593
146. Wang Y, Mo Q, Li Z, Lai H, Lou J, Liu S, et al. Effects of degree of carboxymethylation on physicochemical and biological properties of pachyman. *Int J Biol Macromol.* (2012) 51:1052–6. doi: 10.1016/j.ijbiomac.2012.08.022
147. Liu X, Wang X, Xu X, Zhang X. Purification, antitumor and anti-inflammation activities of an alkali-soluble and carboxymethyl

polysaccharide cmp33 from *Poria Cocos*. *Int J Biol Macromol.* (2019) 127:39–47. doi: 10.1016/j.ijbiomac.2019.01.029
148. Chen F, Huang G. Extraction, derivatization and antioxidant activity of bitter gourd polysaccharide. *Int J Biol Macromol.* (2019) 141:14–20. doi: 10.1016/j.ijbiomac.2019.08.239
149. Chen Y, Zhang H, Wang Y, Nie S, Li C, Xie M. Acetylation and carboxymethylation of the polysaccharide from *ganoderma atrum* and their antioxidant and immunomodulating activities. *Food Chem.* (2014) 156:279–88. doi: 10.1016/j.foodchem.2014.01.111
150. Song Y, Yang Y, Zhang Y, Duan L, Zhou C, Ni Y, et al. Effect of acetylation on antioxidant and cytoprotective activity of polysaccharides isolated from pumpkin (*Cucurbita Pepo*, Lady Godiva). *Carbohydr Polym.* (2013) 98:686–91. doi: 10.1016/j.carbpol.2013.06.049
151. Liu X, Xie J, Jia S, Huang L, Wang Z, Li C, et al. Immunomodulatory Effects of an Acetylated Cyclocarya Paliurus Polysaccharide on Murine Macrophages Raw2647. *Int J Biol Macromol.* (2017) 98:576–81. doi: 10.1016/j.ijbiomac.2017.02.028
152. Liu W, Xu J, Jing P, Yao W, Gao X, Yu L. Preparation of a Hydroxypropyl *Ganoderma Lucidum* Polysaccharide and Its Physicochemical Properties. *Food Chem.* (2010) 122:965–71. doi: 10.1016/j.foodchem.2009.11.087
153. Ren YY, Sun PP Ji YP, Wang XT Dai SH, Zhu ZY. Carboxymethylation and acetylation of the polysaccharide from *cordyceps militaris* and their α-glucosidase inhibitory activities. *Nat Prod Res.* (2020) 34:369–77. doi: 10.1080/14786419.2018.1533830
154. Yuan D, Li C, Huang Q, Fu X. Ultrasonic degradation effects on the physicochemical, rheological and antioxidant properties of polysaccharide from *sargassum pallidum*. *Carbohydr Polym.* (2020) 239:116230. doi: 10.1016/j.carbpol.2020.116230
155. Yan J-K, Wang Y-Y, Ma H-L, Wang Z-B. Ultrasonic effects on the degradation kinetics, preliminary characterization and antioxidant activities of polysaccharides from *phellinus linteus* mycelia. *Ultrason Sonochem.* (2016) 29:251–7. doi: 10.1016/j.ultsonch.2015.10.005
156. Xiao J, Chen X, Zhan Q, Zhong L, Hu Q, Zhao L. Effects of ultrasound on the degradation kinetics, physicochemical properties and prebiotic activity of *flammulina velutipes* polysaccharide. *Ultrason Sonochem.* (2022) 82:105901. doi: 10.1016/j.ultsonch.2021.105901
157. Jia Y, Lu Y, Wang Y, Zhang M, He C, Chen H. Spheroidization of ultrasonic degraded corn silk polysaccharide to enhance bioactivity by the anti-solvent precipitation method. *J Sci Food Agric.* (2022) 102:53–61. doi: 10.1002/jsfa.11329
158. Wu Q, Qin D, Cao H, Bai Y. Enzymatic hydrolysis of polysaccharide from *auricularia auricula* and characterization of the degradation product. *Int J Bio. Macromol.* (2020) 162:127–35. doi: 10.1016/j.ijbiomac.2020.06.098
159. Hu TG, Zou YX Li EN, Liao ST, Wu H, Wen P. Effects of enzymatic hydrolysis on the structural, rheological, and functional properties of mulberry leaf polysaccharide. *Food Chem.* (2021) 355:129608. doi: 10.1016/j.foodchem.2021.129608
160. Liu X, Ren Z, Yu R, Chen S, Zhang J, Xu Y, et al. Structural characterization of enzymatic modification of *hericium erinaceus* polysaccharide and its immune-enhancement activity. *Int J Biol Macromol.* (2021) 166:1396–408. doi: 10.1016/j.ijbiomac.2020.11.019
161. Huang S, Chen F, Cheng H, Huang G. Modification and application of polysaccharide from traditional chinese medicine such as *dendrobium officinale*. *Int J Biol Macromol.* (2020) 157:385–93. doi: 10.1016/j.ijbiomac.2020.04.141
162. Wang ZX, Li N, Xu JW. Effects of efficient expression of vitreoscilla hemoglobin on production, monosaccharide composition, and antioxidant activity of exopolysaccharides in ganoderma lucidum. *Microorganisms.* (2021) 9. doi: 10.3390/microorganisms9081551

Conflict of Interest: The authors declare that the research was conducted in the absence of any commercial or financial relationships that could be construed as a potential conflict of interest.

Publisher's Note: All claims expressed in this article are solely those of the authors and do not necessarily represent those of their affiliated organizations, or those of the publisher, the editors and the reviewers. Any product that may be evaluated in this article, or claim that may be made by its manufacturer, is not guaranteed or endorsed by the publisher.

Copyright © 2022 Wang, Yan, Guo, Wen, Yu, Feng and Jia. This is an open-access article distributed under the terms of the Creative Commons Attribution License (CC BY). The use, distribution or reproduction in other forums is permitted, provided the original author(s) and the copyright owner(s) are credited and that the original publication in this journal is cited, in accordance with accepted academic practice. No use, distribution or reproduction is permitted which does not comply with these terms.

frontiers | Frontiers in Nutrition

ORIGINAL RESEARCH
published: 26 May 2022
doi: 10.3389/fnut.2022.916425

Effect of Polysaccharide Extracted From *Gynostemma Pentaphyllum* on the Body Weight and Gut Microbiota of Mice

Shiwei Li[1,2], *Yingna Wang*[1], *Weipeng Dun*[1], *Wanqing Han*[1], *Tao Ning*[3], *Qi Sun*[4]* and *Zichao Wang*[3]*

[1] College of Life Sciences and Agronomy, Zhoukou Normal University, Zhoukou, China, [2] College of Food Science and Technology, Henan University of Technology, Zhengzhou, China, [3] School of Biological Engineering, Henan University of Technology, Zhengzhou, China, [4] College of Life Sciences, Chongqing Normal University, Chongqing, China

Researchers have investigated the role of polysaccharides in disease treatment *via* gut microbiota regulation but ignore their function in disease prevention and physique enhancement. In this work, a *Gynostemma pentaphyllum* polysaccharide (GPP) was tested by methyl thiazolyl tetrazolium (MTT) assay and proved to be safe to Caco-2 cells. Animal experiments showed that the administration of GPP for 3 weeks decreased the body weight gain of mice from 15.4 ± 1.7 to 12.2 ± 1.8 g in a concentration-dependent manner. Analysis of short-chain fatty acids (SCFAs) indicated that GPP increased the levels of acetate, propionate, butyrate, and total SCFAs in the cecum contents of normal mice. Furthermore, GPP improved the species richness and abundance in the gut microbiota but reduced the Firmicutes/Bacteroidetes ratio from 0.8021 to 0.3873. This work provides a basis for incorporating GPP into diet to prevent or mitigate the occurrence of obesity *via* gut microbiota regulation.

Keywords: ***Gynostemma pentaphyllum*, polysaccharide, mice, body weight, gut microbiota**

OPEN ACCESS

Edited by:
Xin Wang,
Northwest A&F University, China

Reviewed by:
Lin Peng,
Taizhou University, China
Baoming Tian,
Zhejiang University of Technology, China

***Correspondence:**
Qi Sun
sunqi2017@cqnu.edu.cn
Zichao Wang
zcwang@haut.edu.cn

Specialty section:
This article was submitted to Food Chemistry, a section of the journal Frontiers in Nutrition

Received: *09 April 2022*
Accepted: *05 May 2022*
Published: *26 May 2022*

Citation:
Li S, Wang Y, Dun W, Han W, Ning T, Sun Q and Wang Z (2022) Effect of Polysaccharide Extracted From Gynostemma Pentaphyllum on the Body Weight and Gut Microbiota of Mice. Front. Nutr. 9:916425. doi: 10.3389/fnut.2022.916425

INTRODUCTION

With lifestyle changes and living standard improvement, unreasonable diet has become an important factor that directly influences human health. Three high-metabolic syndromes, namely, hyperglycemia, hyperlipidemia, and hypertension caused by high sugar and high fat diet, have become a serious threat to physical health, quality of life, and national economy development. Therefore, the irreplaceable diet in people's daily life could be used as an entry point by modifying functional properties to improve health and prevent the occurrence and development of diseases. A daily intake of dietary fiber could reduce the harmful effects of stroke, coronary disease, type 2 diabetes, and colon cancer (1). Active substances in diet have good prevention and treatment effects against nutritional diseases and may include functional polysaccharides from natural medicinal and edible plants (2). Functional polysaccharides derived from edible plants can be used as food supplements that can improve people's diet by scavenging oxygen free radicals and inhibiting lipid peroxidation, α-glucosidase activity, α-amylase activity, promoting insulin secretion, and regulating the metabolism of glucose and lipids (3).

Gut microbiota, a community of microorganisms in the gut, plays an important role as a bridge among food nutrition and health. The gut microbiota not only participates in nutrition, metabolism, and immune regulation but also in the occurrence and development of nutritional, metabolic, and immune diseases. Cani (4) found that depending on the source of amino acids, gut microbiota can mitigate metabolic diseases *via* improving or altering metabolism of body and the corresponding metabolites. Zhao et al. (5) suggested that dietary fibers could promote gut microbiota to produce diversity and abundance of short-chain fatty acids (SCFAs) and diminish production of metabolically detrimental compounds such as indole and hydrogen sulfide, thus alleviating type 2 diabetes *via* improving hemoglobin A1c levels and increasing glucagon-like peptide-1 production. Mardinoglu et al. (6) reported that low-carbohydrate diet alleviated non-alcoholic fatty liver might *via* increasing the folate-producing *Streptococcus* in gut microbiota and serum folate concentrations, thus down-regulating of the fatty acid synthesis pathway and up-regulating of folate-mediated one-carbon metabolism and fatty acid oxidation pathways. Furthermore, certain effects have been achieved by gut microbiota transplantation, in which the feces of a healthy donor are transplanted into patients to reconstruct a new gut microbiota and regulate health (7). Gut microbiota has gradually developed into a biomarker of human health, disease prevention, and immune regulation.

Polysaccharides can affect nutrition and health by regulating the gut microbiota. For instance, Sun et al. (8) demonstrated that polysaccharides extracted from plants could alleviate circadian rhythm disorders and related psychiatric disorders by regulating the gut microbiota. Liu et al. (9) verified that mannan-oligosaccharide could alleviate the cognitive and behavioral disorders of mice with 5xFAD Alzheimer's disease by regulating the gut microbiota–brain axis. Mo et al. (10) found that insoluble yeast β-glucan could alleviate the high-fat diet-induced obesity of mice by regulating the gut microbiota and its metabolites. Li et al. (11) suggested that alginate oligosaccharides can protect against fumonisin B1-induced intestinal damage by promoting gut microbiota homeostasis. In our previous work, we found that a *Gynostemma pentaphyllum* polysaccharide (GPP) could adjust the high blood sugar level of diabetic mice to the normal level (12). When the absorption mechanisms of a *Ganoderma lucidum* polysaccharide (GLP) were investigated *in vivo* and *in vitro*, we found that GLP entered the body and reached the posterior part of the intestinal tract to participate in gut microbiota metabolism (13). However, the role of GPP is improving body health through gut microbiota regulation remains unclear. Therefore, the toxicity of GPP was first investigated; after which, the effect of GPP on body weight and short-chain fatty acids (SCFAs) in the intestine and gut microbiota of mice was analyzed.

MATERIALS AND METHODS

Materials

Gynostemma pentaphyllum (Thumb) Makino herb was bought from a local drugstore of Zhengzhou (China). Caco-2 cells (HTB037) were acquired from the American Type Culture Collection and stored in our laboratory (13). Specific pathogen-free Kunming male mice (SCXK 2017-0002, 18–22 g) were bought from the Experimental Animal Center of Henan province (China). Dimethyl sulfoximine (DMSO), Dulbecco's modified Eagle's medium (DMEM), and 3-(4,5-Dimethylthiazol-2-yl)-2,5-bromo diphenyltetrazolium were purchased from Sigma-Aldrich (Shanghai, China). Fetal bovine serum, penicillin, and streptomycin were bought from Beyotime Biotechnology Co., Ltd., (Shanghai, China). Ethyl alcohol, sodium chloride, ethyl ether, sulfuricacid, calcium chloride, acetate, propionate, butyrate, and other chemical reagents were bought from Sinopharm Chemical Reagent Co., Ltd., (Beijing, China).

Preparation of GPP

Extraction, collection, and purification of the *Gynostemma pentaphyllum* polysaccharide (GPP) were conducted based on previous methods (12), no protein or nucleic acid were detected in the obtained GPP. Then, the freeze-dried GPP powder was used in following experiments.

Toxicity Analysis of GPP

Toxicity of GPP was determined using methyl thiazolyl tetrazolium (MTT) method against Caco-2 cells by using a previously reported method with some modifications (14). The freeze-dried GPP powder was dissolved and stirred in DMEM to concentrations of 50, 100, 200, 400, and 800 μg/ml, respectively. Meanwhile, DMEM solution without dissolving GPP was used as blank control. Caco-2 cells were cultured in DMEM with fetal bovine serum (10%, v/v), penicillin (100 U/ml), and streptomycin (100 μg/ml) in a humidified 5% CO_2 incubator (Series 8000 WJ, Thermo Fisher Scientific, Waltham, MA, United States) at 37°C. During cultivation, Caco-2 cells were digested and counted intermittently. Upon reaching 2×10^4 cells/ml, Caco-2 cells were transferred into 96-well plates and incubated in the CO_2 incubator for 24 h at 37°C. Each well was added with 100 μl of GPP solution with different concentrations by using a pipette (Eppendorf, Germany) and cultured for another 24 h. The solution was then added with 20 μl of 3-(4,5-dimethylthiazol-2-yl)-2,5-bromo diphenyltetrazolium (5 mg/ml) and incubated for 4 h. The cell supernatant was discarded, and the insoluble crystals in Caco-2 cells were dissolved by adding 150 μl of DMSO. Absorbance was recorded using a microplate reader (BIO-RAD, Hercules, CA, United States) at 490 nm.

Experimental Design and Sample Collection

Thirty mice (20 ± 1.0 g) were acquired from the Experimental Animal Center of Henan province (China) and fed in a specific-free pathogen environment, with temperature of 22–26°C, humidity of 60 ± 5%, and light: dark cycle of 12: 12 h. All animal procedures were performed in accordance with the guidelines for care and use of laboratory animals of Henan University of Technology. Experiments were approved by the Animal Ethics Committee of Henan University of Technology. Mice were fed according to routine feeding procedure and given food and drink freely for the first 7 days to acclimatize. After which, the mice ate (components of mice food are as follows: water 95 g/kg, crude

protein 195.5 g/kg, crude fat 47.3 g/kg, coarse fiber 21.4 g/kg, crude ash 54.6 g/kg, calcium 13.6 g/kg, and total phosphorus 8.09 g/kg) and drank (tap water is boiled and cooled for use) freely throughout the whole experiment except for administration process. Then, twenty-four robust mice were selected and randomly divided into four groups, with six mice each (n = 6): control group (NC), administered with 0.4 ml of distilled water orally once a day; based on the preliminary experiment, experimental groups, orally administered with 100 μg/ml (2 g/kg) GPP (low-dose group, LOW), 400 μg/ml (8 g/kg) GPP (middle-dose group, MID), and 800 μg/ml (16 g/kg) GPP (high-dose group, HIG). If a single administration of 0.4 ml was difficult, then two consecutive doses of 0.2 ml were given. The night before administration, mice were fasted but drank freely. Mouse experiments lasted for 21 days, and the mice weight was measured weekly. The experimental mice were then fasted for 12 h and sacrificed by cervical dislocation. The contents in cecum were collected and stored at −80°C for further analysis.

Detection of Short-Chain Fatty Acids

In brief, 0.2 g of cecum contents were dissolved in 1 ml of deionized water, vibrated for 3 min, and processed with ultrasonic wave for 30 min. The solution was added with 0.2 ml of 50% H_2SO_4 and 2 ml of diethyl ether and mixed acutely for 30 min. The mixture was placed in a water bath shaker at room temperature at 250 r/min for 30 min and centrifuged at 8,000 × g and 4°C for 10 min. The organic supernatant was collected and mixed with 1.0 g of anhydrous calciumchloride for 10 min to remove water. The supernatant was filtered against a 0.22 μm organic-based filter membrane, and SCFAs in organic layer were analyzed according to previously reported methods (14).

Gut Microbiota Analysis

Gut microbiota was extracted and detected according to method reported previously with some modifications (14). Briefly, the total microbial DNA in the bacteria of collected cecum contents was extracted by using DNA extraction kit. V3-V4 hypervariable region of 16S rRNA was used as primer, and the primer sequences were 338F (5′-ACTCC TACGG GAGGC AGCAG-3′) and 806R (5′-GGACT ACHVG GGTWT CTAAT-3′). The amplification process was repeated three times for each sample, and the PCR products were recovered by using 2% (w/v) agarose gel electrophoresis. Meanwhile, AxyPrep DNA Gel Extraction Kit was used to purify the PCR products. After which, the PCR products were sent to Majorbio Co., Ltd., China (Shanghai, China) for gut microbiota analysis using Illumina MiSeq platforms according to the operation manual.

Statistical Analysis

All data were expressed as mean of three parallel experiments. Analysis of variance (ANOVA) was performed using Origin software (Origin Pro 8.5).

RESULTS AND DISCUSSION

Toxicity Analysis of GPP

Previously, a polysaccharide of GPP was successfully extracted from *Gynostemma pentaphyllum* herb, the monosaccharide composition of which was rhamnose, arabinose, galactose, glucose, xylose, mannose, galacturonic acid and glucuronic acid with molar ratio of 4.11: 7.34: 13.31: 20.99: 1.07: 0.91: 4.75: 0.36. Meanwhile, weight-average molecular weight (Mw) and number-average molecular weight (Mn) of GPP were 4.070 × 10^4 and 3.924× 10^4 Da, and its polydispersity (Mw/Mn) was 1.037 (12). However, due to geography and climate difference, monosaccharide composition and molecular weight of GPP were different from polysaccharides extracted from different *G. pentaphyllum* herbs reported by other researchers (15, 16).

Meanwhile, GPP could reduce the blood sugar level of diabetic mice to normal *via* α-glucosidase inhibition and anti-inflammatory effects (3, 12), but the safety of GPP has been neglected. The toxicity of GPP to Caco-2 cells was detected by MTT assay. **Figure 1** shows that none of the detected GPP

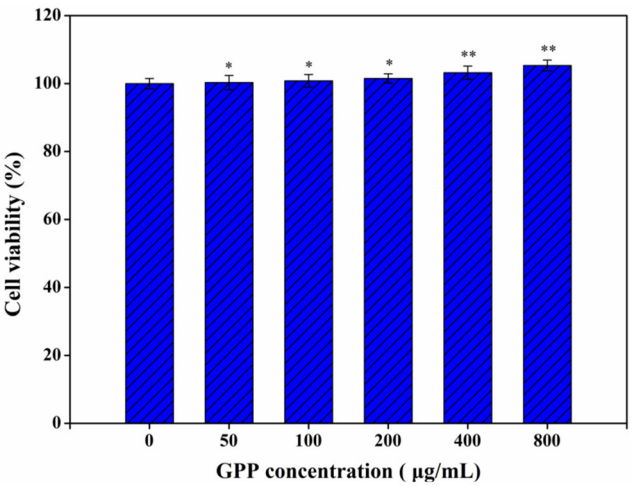

FIGURE 1 | Toxicity of GPP to Caco-2 cells by MTT assay. Data are expressed as mean ± SD (n = 3). Significance was determined through ANOVA, *P < 0.05, **P < 0.01.

TABLE 1 | Influence of GPP on body weight of mice.

Mice weight	CON	LOW	MID	HIG
0 day (g)	19.3 ± 1.3^a	19.8 ± 1.2^a	20.1 ± 1.8^a	19.5 ± 2.2^a
7 day (g)	24.0 ± 2.1^b	24.5 ± 1.9^b	25.2 ± 1.6^b	24.4 ± 2.1^b
14 day (g)	28.2 ± 1.9^c	28.1 ± 1.8^c	28.5 ± 1.5^c	27.6 ± 1.7^c
21 day (g)	31.7 ± 2.0^d	31.3 ± 1.6^d	31.2 ± 1.8^d	30.1 ± 1.5^d
28 day (g)	34.7 ± 1.8^e	34.1 ± 2.1^e	33.8 ± 2.0^e	31.7 ± 1.9^d
Weight gain (g)	15.4 ± 1.7^a	14.3 ± 1.9^b	13.7 ± 1.6^b	12.2 ± 1.8^c

CON, control group; LOW, 100 μg/ml GPP; MID, 400 μg/ml GPP; HIG, 800 μg/ml GPP. Data are expressed as mean ± SD (n = 6). Different letters represent significant differences, P < 0.05.

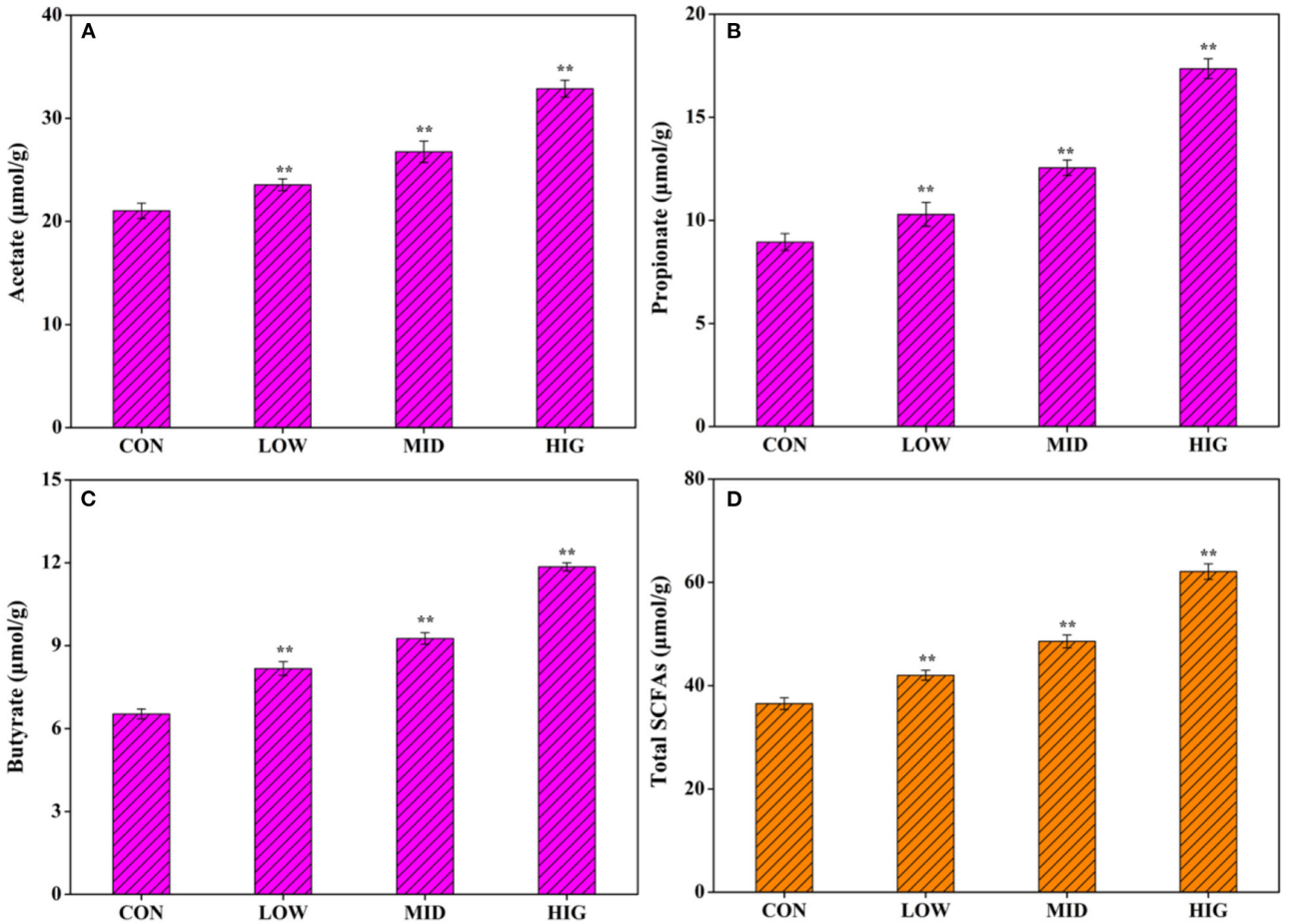

FIGURE 2 | Influence of GPP on acetate, propionate, butyrate, and total SCFAs. **(A)** Acetate, **(B)** propionate, **(C)** butyrate, and **(D)** total SCFAs. CON: control group, LOW: 100 μg/ml GPP, MID: 400 μg/ml GPP, HIG: 800 μg/ml GPP. Data are expressed as mean ± SD ($n = 6$). Significance was determined through ANOVA, $^{*}P < 0.05$, $^{**}P < 0.01$.

concentration affected the viability of Caco-2 cells, indicating that GPP was safe to Caco-2 cells. Similarly, Li et al. (17) reported that *G. pentaphyllum* polysaccharide had no specific cytotoxicity to Hs-68 cells. Li et al. (18) also found that *Eucommia ulmoides* polysaccharide was non-toxic to Raw 264.7 macrophages. In our previous works, we found that *Ganoderma lucidum* polysaccharide and *Chaetomium globosum* CGMCC 6882 exo-polysaccharide were not toxic to Caco-2 cells (13, 14). In the present work, experimental mice showed no symptoms of death or disease, suggesting the safety of GPP to mice, which was in consistent with the safe result of GPP to Caco-2 cells. Furthermore, He et al. (19) reported that polysaccharide produced by *Streptomyces Virginia* H03 was non-toxic and did not kill mice even at 500 mg/kg/day.

Influence of GPP on Mouse Body Weight

With improvement of living standards, changes in lifestyle, and reduction in physical activity, an increasing number of people suffer from obesity. Except for proper exercise and diet control, reasonable diet structure is an effective means to prevent and alleviate obesity (20). As shown in **Table 1**, the weights of mice in the control and experimental groups increased gradually with extension of feeding time. However, the body weight gain of experimental mice was negatively correlated with GPP concentration, that is, it decreased from 15.4 ± 1.7 g (CON) to 14.3 ± 1.9 g (LOW), 13.7 ± 1.6 g (MID), and 12.2 ± 1.8 g (HIG). Hence, GPP could be added in food or diet to prevent and mitigate obesity. Similarly, Chen et al. (21) reported that *Pueraria lobata* polysaccharide had similar body weight regulation effects. In contrast to the present study, Zhao et al. (22) found that *Auricularia auricular* polysaccharide did not affect the body weight. Furthermore, Yin et al. (23) found that non-polysaccharide substance of resveratrol could regulate the loss of body weight. GPP regulates body weight possibly by three mechanisms: inhibiting enzyme activity and nutrient absorption rate (24); adjusting the composition and proportion of gut microbiota, especially Firmicutes/Bacteroidetes (F/B) ratio (25); and degradation and conversion of GPP into SCFAs (26). The exact mechanism of GPP in regulating body weight is still being investigated.

TABLE 2 | Influence of GPP on the α-diversity of gut microbiota.

Groups	Species richness		Species diversity	
	Chao1	Ace	Shannon	Simpson
CON	1,970 ± 163[a]	2,018 ± 174[a]	6.58 ± 0.42[a]	0.98 ± 0.005[a]
LOW	2,116 ± 203[b]	2,209 ± 195[b]	7.39 ± 0.35[b]	0.97 ± 0.003[a]
MID	2,289 ± 314[c]	2,278 ± 269[b]	7.54 ± 0.51[b]	0.97 ± 0.003[a]
HIG	2,536 ± 295[d]	2,641 ± 357[c]	8.26 ± 0.48[c]	0.95 ± 0.002[a]

CON, control group; LOW, 100 μg/ml GPP; MID, 400 μg/ml GPP; HIG, 800 μg/ml GPP. Data are expressed as mean ± SD (n = 6). Different letters represent significant differences, P < 0.05.

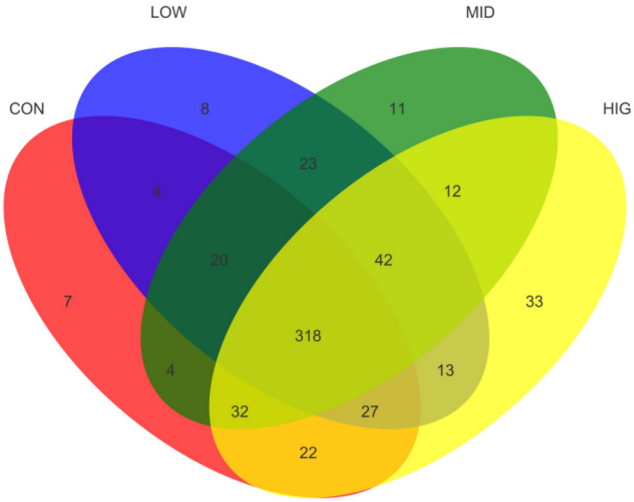

FIGURE 3 | Venn diagram of the gut microbiota among different groups.

Effect of GPP on SCFAs

Non-starch polysaccharides are resistant to saliva, succus gastricus, and succus entericus, which will be digested by the gut microbiota into SCFAs to exert biological activities (26). As shown in **Figure 2A**, after administration of different concentrations of GPP for 3 weeks, the acetate concentration in the cecum contents increased from 21.03 ± 0.75 μmol/g (CON) to 23.55 ± 0.58 μmol/g (LOW), 26.75 ± 1.03 μmol/g (MID), and 32.88 ± 0.82 μmol/g (HIG). **Figure 2B** shows that the propionate concentration increased from 8.95 ± 0.41 μmol/g (CON) to 10.29 ± 0.53 μmol/g (LOW), 12.55 ± 0.37 μmol/g (MID), and 17.36 ± 0.48 μmol/g (HIG). **Figure 2C** indicates that the butyrate concentration increased from 6.53 ± 18 μmol/g (CON) to 8.17 ± 0.25 μmol/g (LOW), 9.26 ± 0.21 μmol/g (MID), and 11.85 ± 0.15 μmol/g (HIG). **Figure 2D** illustrates that the level of total SCFAs increased from 36.51 ± 1.15 μmol/g (CON) to 42.01 ± 96 μmol/g (LOW), 48.56 ± 1.24 μmol/g (MID), and 62.09 ± 1.53 μmol/g (HIG). Furthermore, the increase in SCFAs was positively correlated with GPP concentration, with acetate having the highest increment.

Previously, Gao et al. (27) verified that when gellan gum was degraded to gellan oligosaccharide with molecular weight of 72,903 Da, the production of acetic acid and propionic acid by gellan oligosaccharide was increased in a bionic intestinal reactor *in vitro*, indicating that relatively low molecular weight is a key factor for polysaccharide to regulate gut microbiota for SCFAs production. Molecular weight of GPP used in present work was 40,700 Da (12), which might be a factor affecting its probiotic activity on increasing SCFAs production. SCFAs not only are important in energy supply and gut microbiota health but also might affect the metabolism or function of peripheral tissues *via* entering systemic circulation (28), such as body weight regulation. For instance, Canfora et al. (29) found that SCFAs could prevent and counteract obesity by promoting satiety. Other researchers reported that acetate in SCFAs plays an important role in body weight regulation (30). GPP reduced body weight possibly *via* increasing the level of SCFAs, especially acetate.

Effect of GPP on Gut Microbiota

Influence of Gut Microbiota Diversity by GPP

Many statistical indices are used to assess the abundance and diversity of microbial communities. Ace and Chao1 indices are used to assess the number of operational taxonomic units (OTUs) in the gut microbiota; Simpson and Shannon indices reflect the species diversity of the gut microbiota (31). As shown in **Table 2**, the Ace and Chao1 indices of the gut microbiota in the experimental group increased compared with that in the control group in a concentration-dependent manner. Hence, the intake of GPP increased the species richness of the gut microbiota. The Shannon index of the gut microbiota showed an increasing trend, whereas the Simpson index had a downward trend. This finding suggested that the increase of species diversity of the gut microbiota was induced by administration of GPP (22). When Deng et al. (32) studied different molecular weights konjac glucomannans (KGM) on the hypoglycemic effects of type 2 diabetic rats, they found that medium molecular weights KGMs could increase gut microbiota diversity. Therefore, molecular weight (40,700 Da) might be one of the factors affecting gut microbiota diversity by GPP (12).

The effect of GPP on the species richness of the gut microbiota was detected by number of OTUs, and the results are shown as Venn diagram in **Figure 3**. The total numbers of OTUs in CON, LOW, MID, and HIG were 434, 455, 462, and 499, respectively. Among all OTUs, 318 were shared by four groups and 42 were only shared by three experimental groups. Meanwhile, the numbers of OTUs separately shared between control group and experimental groups were 369 (CON and LOW), 374 (CON and MID), and 399 (CON and HIG). In addition, each group had its own unique OTUs: 7 for CON, 8 for LOW, 11 for MID, and 33 for HIG. Hence, GPP improved the species richness and diversity of the gut microbiota.

Gut Microbiota Analysis at Phylum Level

The regulatory effect of GPP on the gut microbiota is shown in **Figure 4**. Among the four groups, the main bacteria (relative abundance > 1%) at the phylum level are Bacteroidetes, Firmicutes, Spirochaete, Proteobacteria, Verrucomicrobia, and Cyanobacteria, accounting for more than 95% of the sequences.

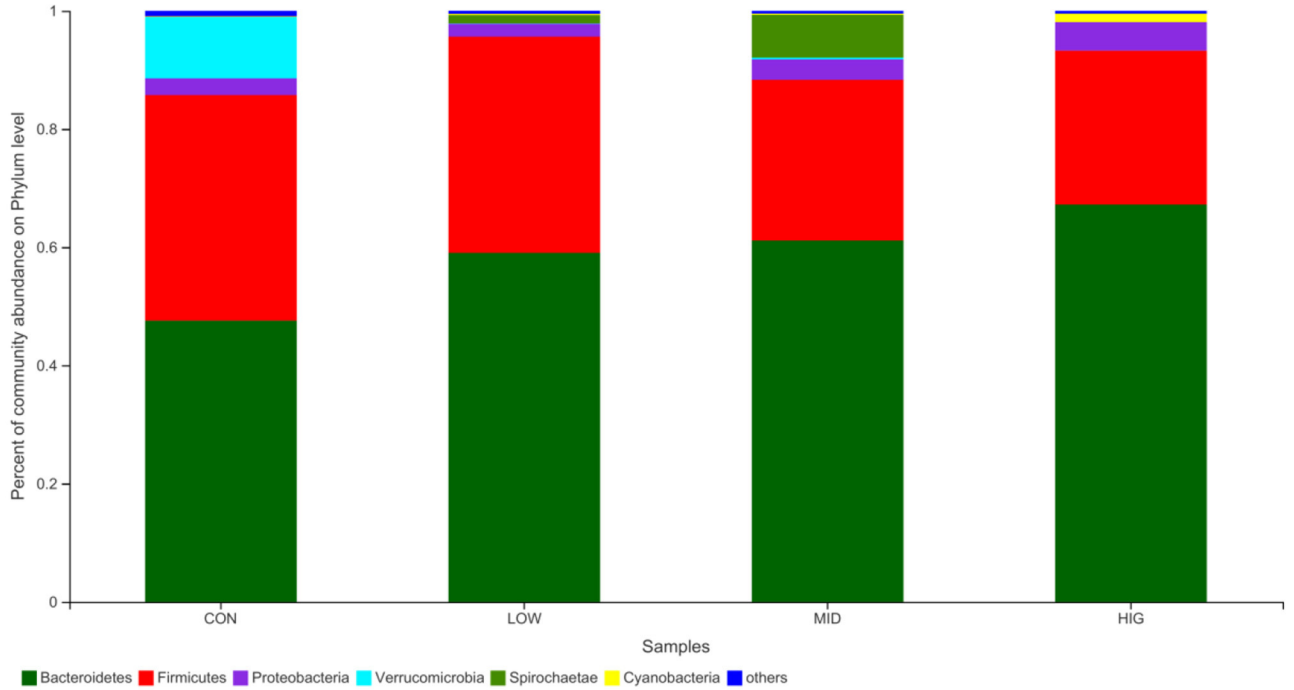

FIGURE 4 | Relative abundance of the gut microbiota at phylum level.

Bacteroidetes and Firmicutes are the main bacteria that utilize undigested non-starch polysaccharides (33) and are involved in maintaining the balance of energy metabolism (25). In experimental mice, the relative abundance levels of Bacteroidetes were 47.58% (CON), 59.04% (LOW), 61.13% (MID) and 67.21% (HIG), and those of Firmicutes were 38.16, 36.58, 27.20, and 26.03%, respectively. The F/B ratios in the four groups were 0.8021, 0.6196, 0.4450, and 0.3873, indicating a decreasing trend. Bacteroidetes possess genes for encoding succinate pathway and are the primary polysaccharide-degrading and propionate-producing bacteria in gut (34), this might be the reason of SCFAs increase in gut induced by F/B ratio decrease and Bacteroidetes increase.

Many structural characteristics could affect the probiotic activity of polysaccharides. For instance, Yu et al. (34) reported that the monosaccharide order of sugar beet pulp polysaccharide used by gut microbiota might arabinose, glucose, fucose and galacturonic acid. Zhao et al. (35) found that glycosidic bond type could not only affect the body weight of mice, but also the composition and proportion of mice gut microbiota. Deng et al. (32) suggested that molecular weight of konjac glucomannan might affect its effect on gut microbiota diversity. Gong et al. (36) demonstrated that uronic acid could affect the biological activity of polysaccharides. GPP was composed of rhamnose, arabinose, galactose, glucose, xylose, mannose, galacturonic acid and glucuronic acid in a molar ratio of 4.11: 7.34: 13.31: 20.99: 1.07: 0.91: 4.75: 0.36, and its weight-average molecular weight was 4.070 × 104 Da (12). Arabinose, glucose and uronic acid in its monosaccharide composition and moderate molecular weight (4.070 × 104 Da) might be the reason for probiotic activity of GPP.

Although Gao et al. (37) found that there was no direct relationship between F/B ratio and body weight regulation, many researchers suggested that an increase in the F/B ratio induced obesity and prevented body weight loss. Zhao et al. (22) reported that the body weight reduction effect of *Auricularia auricular* polysaccharide might be related to decrease in the F/B ratio. Ley et al. (33) demonstrated that an increase in Firmicutes and a decrease in Bacteroidetes are likely to induce obesity. Chang et al. (38) and Koliada et al. (39) suggested that the reduction in the F/B ratio could lead to weight loss and improved body health. Therefore, the decreased F/B ratio may lead to decrease in body weight gain caused by GPP.

CONCLUSION

In present work, a polysaccharide fraction of GPP extracted from *Gynostemma pentaphyllum* was used to detect its effect on the body weight and gut microbiota of normal mice. With administration of GPP once a day for 3 weeks, body weight gain of normal mice reduced but SCFAs levels in gut increased. Meanwhile, GPP increased gut microbiota diversity but decreased Firmicutes/Bacteroidetes ratio in the gut of normal mice. However, the mechanism through which the polysaccharide affects the gut microbiota and the type of

bacteria that participate in the degradation of polysaccharides remain unclear.

DATA AVAILABILITY STATEMENT

The original contributions presented in the study are included in the article/supplementary material, further inquiries can be directed to the corresponding author/s.

ETHICS STATEMENT

The animal study was reviewed and approved by the Animal Ethics Committee of Henan University of Technology.

AUTHOR CONTRIBUTIONS

SL contributed to conception, design, and funding of the study. YW, WD, and WH organized the database. TN wrote the first draft of the manuscript. QS and ZW contributed to writing—review and editing. All authors contributed to the article and approved the submitted version.

FUNDING

This work was supported by the Science and Technology Research Project of Henan Province (182102310687), Henan Provincial Education Department Project (19B550010), the Natural Science Foundation of Henan Province (212300410131), and the Natural Science Foundation of Chongqing (cstc2019jcyj-msxmX0459).

REFERENCES

1. Reynolds A, Mann J, Cummings J, Winter N, Mete E, Te Morenga L. Carbohydrate quality and human health: a series of systematic reviews and meta-analyses. *Lancet.* (2019) 393:434–45. doi: 10.1016/S0140-6736(18)31809-9
2. Ji X, Hou C, Shi M, Yan Y, Liu Y. An insight into the research concerning *Panax ginseng* C. A. meyer polysaccharides: a review. *Food Rev Int.* (2020) 1–17. doi: 10.1080/87559129.2020.1771363
3. Wang Z, Wang Z, Huang W, Suo J, Chen X, Ding K, et al. Antioxidant and anti-inflammatory activities of an anti-diabetic polysaccharide extracted from *Gynostemma pentaphyllum* herb. *Int J Biol Macromol.* (2020) 145:484–91. doi: 10.1016/j.ijbiomac.2019.12.213
4. Cani PD. Microbiota and metabolites in metabolic diseases. *Nat Rev Endocrinol.* (2019) 15:69–70. doi: 10.1038/s41574-018-0143-9
5. Zhao L, Zhang F, Ding X, Wu G, Lam YY, Wang X, et al. Gut bacteria selectively promoted by dietary fibers alleviate type 2 diabetes. *Science.* (2018) 359:1151–6. doi: 10.1126/science.aao5774
6. Mardinoglu A, Wu H, Bjornson E, Zhang C, Hakkarainen A, Räsänen SM, et al. An integrated understanding of the rapid metabolic benefits of a carbohydrate-restricted diet on hepatic steatosis in humans. *Cell Metab.* (2018) 27:559–71.e555. doi: 10.1016/j.cmet.2018.01.005
7. Wu Z, Huang S, Li T, Li N, Han D, Zhang B, et al. Gut microbiota from green tea polyphenol-dosed mice improves intestinal epithelial homeostasis and ameliorates experimental colitis. *Microbiome.* (2021) 9:184. doi: 10.1186/s40168-021-01115-9
8. Sun Q, Ho CT, Zhang X, Liu Y, Zhang R, Wu Z. Strategies for circadian rhythm disturbances and related psychiatric disorders: a new cue based on plant polysaccharides and intestinal microbiota. *Food Funct.* (2022) 13:1048–61. doi: 10.1039/D1FO02716F
9. Liu Q, Xi Y, Wang Q, Liu J, Li P, Meng X, et al. Mannan oligosaccharide attenuates cognitive and behavioral disorders in the 5xFAD Alzheimer's disease mouse model *via* regulating the gut microbiota-brain axis. *Brain Behav Immun.* (2021) 95:330–43. doi: 10.1016/j.bbi.2021.04.005
10. Mo X, Sun Y, Liang X, Li L, Hu S, Xu Z, et al. Insoluble yeast β-glucan attenuates high-fat diet-induced obesity by regulating gut microbiota and its metabolites. *Carbohydr Polym.* (2022) 281:119046. doi: 10.1016/j.carbpol.2021.119046
11. Li T, Huang S, Wang J, Yin P, Liu H, Sun C. Alginate oligosaccharides protect against fumonisin B1-induced intestinal damage *via* promoting gut microbiota homeostasis. *Food Res Int.* (2022) 152:110927. doi: 10.1016/j.foodres.2021.110927
12. Wang Z, Zhao X, Liu X, Lu W, Jia S, Hong T, et al. Anti-diabetic activity evaluation of a polysaccharide extracted from *Gynostemma pentaphyllum*. *Int J Biol Macromol.* (2019) 126:209–14. doi: 10.1016/j.ijbiomac.2018.12.231
13. Wang Z, Zhang H, Shen Y, Zhao X, Wang X, Wang J, et al. Characterization of a novel polysaccharide from *Ganoderma lucidum* and its absorption mechanism in Caco-2 cells and mice model. *Int J Biol Macromol.* (2018) 118:320–6. doi: 10.1016/j.ijbiomac.2018.06.078
14. Sun X, Wang Z, Hu X, Zhao C, Zhang X, Zhang H. Effect of an antibacterial polysaccharide produced by *Chaetomium globosum* CGMCC 6882 on the gut microbiota of mice. *Foods.* (2021) 10:1084. doi: 10.3390/foods10051084
15. Li B, Zhang X, Wang M. Jiao L. Characterization and antioxidant activities of acidic polysaccharides from *Gynostemma pentaphyllum* (Thunb) Markino. *Carbohydr Polym.* (2015) 127:209–14. doi: 10.1016/j.carbpol.2015.03.069
16. Liu J, Zhang L, Ren Y, Gao Y, Kang L, Qiao Q. Anticancer and immunoregulatory activity of *Gynostemma pentaphyllum* polysaccharides in H22 tumor-bearing mice. *Int J Biol Macromol.* (2014) 69:1–4. doi: 10.1016/j.ijbiomac.2014.05.014
17. Li XL, Wang ZH, Zhao YX, Luo SJ, Zhang DW, Xiao SX, et al. Purification of a polysaccharide from *Gynostemma pentaphyllum* Makino and its therapeutic advantages for psoriasis. *Carbohydr Polym.* (2012) 89:1232–7. doi: 10.1016/j.carbpol.2012.04.001
18. Li Q, Feng Y, He W, Wang L, Wang R, Dong L, et al. Post-screening characterisation and *in vivo* evaluation of an anti-inflammatory polysaccharide fraction from *Eucommia ulmoides*. *Carbohydr Polym.* (2017) 169:304–14. doi: 10.1016/j.carbpol.2017.04.034
19. He F, Yang Y, Yang G, Yu L. Studies on antibacterial activity and antibacterial mechanism of a novel polysaccharide from *Streptomyces virginia* H03. *Food Control.* (2010) 21:1257–62. doi: 10.1016/j.foodcont.2010.02.013
20. Cao SY, Zhao CN, Xu XY, Tang GY, Corke H, Gan RY, et al. Dietary plants, gut microbiota, and obesity: effects and mechanisms. *Trends Food Sci Tech.* (2019) 92:194–204. doi: 10.1016/j.tifs.2019.08.004
21. Chen R, Liu B, Wang X, Chen K, Zhang K, Zhang L, et al. Effects of polysaccharide from *Pueraria lobata* on gut microbiota in mice. *Int J Biol Macromol.* (2020) 158:740–9. doi: 10.1016/j.ijbiomac.2020.04.201
22. Zhao R, Cheng N, Nakata PA, Zhao L, Hu Q. Consumption of polysaccharides from *Auricularia auricular* modulates the intestinal microbiota in mice. *Food Res Int.* (2019) 123:383–92. doi: 10.1016/j.foodres.2019.04.070
23. Yin X, Liao W, Li Q, Zhang H, Liu Z, Zheng X, et al. Interactions between resveratrol and gut microbiota affect the development of hepatic steatosis: a fecal microbiota transplantation study in high-fat diet mice. *J Funct Foods.* (2020) 67:103883. doi: 10.1016/j.jff.2020.103883
24. Yuan Q, He Y, Xiang PY, Wang SP, Cao ZW, Gou T, et al. Effects of simulated saliva-gastrointestinal digestion on the physicochemical properties and bioactivities of okra polysaccharides. *Carbohydr Polym.* (2020) 238:116183. doi: 10.1016/j.carbpol.2020.116183
25. Goodrich Julia K, Waters Jillian L, Poole Angela C, Sutter Jessica L, Koren O, Blekhman R, et al. Human genetics shape the gut microbiome. *Cell.* (2014) 159:789–99. doi: 10.1016/j.cell.2014.09.053
26. Chen G, Xie M, Wan P, Chen D, Ye H, Chen L, et al. Digestion under saliva, simulated gastric and small intestinal conditions and fermentation *in vitro* by human intestinal microbiota of polysaccharides from Fuzhuan brick tea. *Food Chem.* (2018) 244:331–9. doi: 10.1016/j.foodchem.2017.10.074

27. Gao M, Li H, Yang T, Li Z, Hu X, Wang Z, et al. Production of prebiotic gellan oligosaccharides based on the irradiation treatment and acid hydrolysis of gellan gum. *Carbohydr Polym.* (2022) 279:119007. doi: 10.1016/j.carbpol.2021.119007
28. Liu L, Li M, Yu M, Shen M, Wang Q, Yu Y, et al. Natural polysaccharides exhibit anti-tumor activity by targeting gut microbiota. *Int J Biol Macromol.* (2019) 121:743–51. doi: 10.1016/j.ijbiomac.2018.10.083
29. Canfora EE, Jocken JW, Blaak EE. Short-chain fatty acids in control of body weight and insulin sensitivity. *Nat Rev Endocrinol.* (2015) 11:577–91. doi: 10.1038/nrendo.2015.128
30. Tian B, Zhao J, An W, Zhang J, Cao X, Mi J, et al. *Lycium ruthenicum* diet alters the gut microbiota and partially enhances gut barrier function in male C57BL/6 mice. *J Funct Foods.* (2019) 52:516–28. doi: 10.1016/j.jff.2018.11.034
31. Wu T, Shen M, Guo X, Huang L, Yang J, Yu Q, et al. *Cyclocarya paliurus* polysaccharide alleviates liver inflammation in mice *via* beneficial regulation of gut microbiota and TLR4/MAPK signaling pathways. *Int J Biol Macromol.* (2020) 160:164–74. doi: 10.1016/j.ijbiomac.2020.05.187
32. Deng J, Zhong J, Long J, Zou X, Wang D, Song Y, et al. Hypoglycemic effects and mechanism of different molecular weights of konjac glucomannans in type 2 diabetic rats. *Int J Biol Macromol.* (2020) 165:2231–43. doi: 10.1016/j.ijbiomac.2020.10.021
33. Ley RE, Bäckhed F, Turnbaugh P, Lozupone CA, Knight RD, Gordon JI. Obesity alters gut microbial ecology. *P Nat A Sci.* (2005) 102:11070–5. doi: 10.1073/pnas.0504978102
34. Yu C, Ahmadi S, Shen S, Wu D, Xiao H, Ding T, et al. Structure and fermentation characteristics of five polysaccharides sequentially extracted from sugar beet pulp by different methods. *Food Hydrocolloid.* (2022) 126:107462. doi: 10.1016/j.foodhyd.2021.107462
35. Zhao D, Dai W, Tao H, Zhuang W, Qu M. Chang YN. Polysaccharide isolated from *Auricularia auricular-judae* (Bull) prevents dextran sulfate sodium-induced colitis in mice through modulating the composition of the gut microbiota. *J Food Sci.* (2020) 85:2943–51. doi: 10.1111/1750-3841.15319
36. Gong Y, Zhang J, Gao F, Zhou J, Xiang Z, Zhou C, et al. Structure features and *in vitro* hypoglycemic activities of polysaccharides from different species of *Maidong*. *Carbohydr Polym.* (2017) 173:215–22. doi: 10.1016/j.carbpol.2017.05.076
37. Gao R, Zhu C, Li H, Yin M, Pan C, Huang L, et al. Dysbiosis signatures of gut microbiota along the sequence from healthy, young patients to those with overweight and obesity. *Obesity.* (2018) 26:351–61. doi: 10.1002/oby.22088
38. Chang CJ, Lin CS, Lu CC, Martel J, Ko YF, Ojcius DM, et al. *Ganoderma lucidum* reduces obesity in mice by modulating the composition of the gut microbiota. *Nat Commun.* (2015) 6:7489. doi: 10.1038/ncomms8489
39. Koliada A, Syzenko G, Moseiko V, Budovska L, Puchkov K, Perederiy V, et al. Association between body mass index and Firmicutes/Bacteroidetes ratio in an adult Ukrainian population. *BMC Microbiol.* (2017) 17:120. doi: 10.1186/s12866-017-1027-1

Conflict of Interest: The authors declare that the research was conducted in the absence of any commercial or financial relationships that could be construed as a potential conflict of interest.

Publisher's Note: All claims expressed in this article are solely those of the authors and do not necessarily represent those of their affiliated organizations, or those of the publisher, the editors and the reviewers. Any product that may be evaluated in this article, or claim that may be made by its manufacturer, is not guaranteed or endorsed by the publisher.

Copyright © 2022 Li, Wang, Dun, Han, Ning, Sun and Wang. This is an open-access article distributed under the terms of the Creative Commons Attribution License (CC BY). The use, distribution or reproduction in other forums is permitted, provided the original author(s) and the copyright owner(s) are credited and that the original publication in this journal is cited, in accordance with accepted academic practice. No use, distribution or reproduction is permitted which does not comply with these terms.

frontiers | Frontiers in Nutrition

ORIGINAL RESEARCH
published: 03 June 2022
doi: 10.3389/fnut.2022.917094

Structural Characterization, Antioxidant and Antibacterial Activities of a Novel Polysaccharide From *Zingiber officinale* and Its Application in Synthesis of Silver Nanoparticles

Yongshuai Jing[1], *Wenjing Cheng*[1], *Yunfeng Ma*[1], *Yameng Zhang*[1], *Mingsong Li*[1], *Yuguang Zheng*[2], *Danshen Zhang*[1] *and Lanfang Wu*[2]*

[1] College of Chemistry and Pharmaceutical Engineering, Hebei University of Science and Technology, Shijiazhuang, China, [2] College of Pharmacy, Hebei University of Chinese Medicine, Shijiazhuang, China

OPEN ACCESS

Edited by:
Qiu Li,
Qingdao Agricultural University, China

Reviewed by:
Shengyuan Zhang,
Jiaying University, China
Ran Xu,
Guizhou Medical University, China
Junwei He,
Jiangxi University of Traditional Chinese Medicine, China

***Correspondence:**
Lanfang Wu
wulanfang757@163.com

Specialty section:
This article was submitted to Food Chemistry, a section of the journal Frontiers in Nutrition

Received: 10 April 2022
Accepted: 13 May 2022
Published: 03 June 2022

Citation:
Jing Y, Cheng W, Ma Y, Zhang Y, Li M, Zheng Y, Zhang D and Wu L (2022) Structural Characterization, Antioxidant and Antibacterial Activities of a Novel Polysaccharide From Zingiber officinale and Its Application in Synthesis of Silver Nanoparticles. Front. Nutr. 9:917094. doi: 10.3389/fnut.2022.917094

A novel polysaccharide (ZOP) was extracted from *Zingiber officinale* with ultrasonic assisted extraction method. ZOP monosaccharide composition and mole ratio is GlcA: GalA: Glc: Gal: Ara = 1.97:1.15:94.33:1.48:1.07. Then, the particle size of ZOP-NPs prepared by nano-precipitation method was 230.5 nm, and the polydispersity index (PDI) was 0.260. Using ZOP and ZOP-NPs as reductants and stabilizers, ZOP-AgNPs and ZOP-NPs-AgNPs were prepared. They were characterized by ultraviolet-visible spectrophotometer (UV-Vis), fourier transform infrared spectroscopy (FT-IR), scanning electron microscope (SEM), transmission electron microscope (TEM), and X-ray diffraction (XRD). The silver chelation rate of polysaccharide silver nanoparticles (AgNPs) ranged from 68.70 to 82.12%. ZOP-AgNPs (0.5%, w/v; 1%, w/v) and ZOP-NPs-AgNPs (0.5%, w/v; 1%, w/v) exhibited a narrow particle size distribution of 31.1, 34.6, 25.1 and 27.6 nm, respectively. And the zeta potential values of them were −19.4, −21.6, −19.7 and −23.8 mV, respectively. The antioxidant and antibacterial activities of ZOP-NPs-AgNPs were superior to those of ZOP, ZOP-NPs and ZOP-AgNPs.

Keywords: *Zingiber officinale* (ginger), polysaccharides, nanoparticles, nano-silver, antioxidant activity, antibacterial activity

INTRODUCTION

In this millennium, nanotechnology, as an advanced material science, has gradually entered the field of medicine. Nanoparticles are said to be raw materials used in nanotechnology (1). These raw materials are found in different types, e.g., gold, copper, iron, nickel, and silver nanoparticles (2). Polysaccharide nano-silver (AgNPs) has attracted wide attention due to its high antibacterial, anti-inflammatory and anticancer activities, and is widely used in personal care products, textiles, food packaging, building materials and medical devices (3). The preparation methods of nano-silver include physical method, chemical reduction method and biological reduction method (4).

Because most of the physical and chemical reduction methods are high energy consumption, high cost, toxic, non-environmental protection and low productivity, today's nanotechnology needs to adopt various green biological reduction methods to synthesize nanoparticles (5). Polysaccharides can be used as natural reducing agents because of their excellent biocompatibility, wide sources, biodegradability and non-toxicity. At the same time, no toxic substances are produced in the synthesis process, and the whole synthesis process is very green and environmentally friendly. The nano-silver particles generated by polysaccharide have the advantages of high stability and difficult agglomeration, and the addition of polysaccharide gives the nano-silver some other biological activities (6).

Zingiber officinale is a plant belonging to the Zingiber aceae family, contains polyphenols, terpenes, polysaccharides, gingerol and its derivatives and other active ingredients. It has certain therapeutic effects on inflammation, high cholesterol, tumor, atherosclerosis, ulcers, dyspepsia, diabetes, cardiovascular diseases and so on (7, 8). With the increase of *Z. officinale* production, it can be processed into many other foods, such as condiments, syrups, candy, dry powder and so on (9). At the same time, there will be more and more by-products, namely *Z. officinale* pomace. *Z. officinale* pomace is also rich in bioactive components, especially polysaccharides. A lot of data suggested that *Z. officinale* polysaccharide has broad application prospect in disease prevention and health care product development, and has the advantages of anti-tumor, anti-oxidation, hypoglycemic, antitussive, anti-fatigue, high safety and low toxic and side effects (10, 11).

Considering the ideal properties of ZOP and silver nanoparticles, polysaccharides from *Z. officinale* pomace were extracted, nanoparticles and silver nanoparticles with different concentrations or different UV irradiation time were prepared. Their physical and chemical properties such as UV-Vis, FT-IR, SEM, TEM, and XRD were studied, and their antioxidant and antibacterial activities were compared. This study provides a green method for preparing nano-silver. At the same time, it is hoped that the pomace of traditional Chinese medicine can be better utilized in the future.

MATERIALS AND METHODS

Experimental Materials and Reagents

Z. officinale (No. 2019031401) was purchased from AnguoYaoyuan Trading Co., LTD. The sample was identified as the rhizome of *Zingiber officinale* Roscoe by associate professor Lanfang Wu (Department of Pharmacy, Hebei University of Chinese Medicine). A voucher specimen was deposited at the College of Chemistry and Pharmaceutical Engineering, Hebei University of Science and Technology, China. Standard monosaccharides, T-series dextrans, dimethyl sulfoxide (DMSO), 1-phenyl-3-methyl-5-pyrazolone (PMP), 1,1-diphenyl-2-picrylhydrazyl (DPPH), NaCl, $NH_3{\cdot}H_2O$ and $AgNO_3$ were purchased from Shanghai Aladdin Biochemical Technology Co., Ltd. *Escherichia coli* (*E. coli*, ATCC 8739) was used in this experiment. All reagents were analytical grade.

Extraction of ZOP

The rhizome of *Z. officinale* was crushed, and its powder (100 g) was extracted with 1:13 ethanol reflux for twice in 2 h to remove pigment and lipid, and remove supernatant. The dried ginger residue after fat removal and distilled water (1:30 w/v) were placed in a round-bottom flask, and ginger polysaccharide was extracted by ultrasonic assisted extraction. The specific conditions were as follows: ultrasonic extraction for 20 min, then boiling water extraction (90°C), twice in 2 h. The supernatant was concentrated with 80% ethanol, precipitated at 4°C for 12 h, centrifuged (3,000 ×g, 10 min, 4°C), and lyophilized to obtain the precipitate (named ZOP).

Physicochemical Properties of ZOP

Determination of Total Soluble Sugar Content

The total soluble sugar content in ZOP was determined by phenol-sulfuric acid method (12).

Determination of Average Molecular Weight

The molecular weight of ZOP was determined by high performance gel permeation chromatography (HPGPC) (13). It was equipped with TSK-GEL G5000PW_{XL} (300 mm × 7.8 mm, i.d.) and G3000PW_{XL} (300 mm × 7.8 mm, i.d.) gel columns in series (Tosoh Biosep, Japan) and a Waters 2414 refractive index detector (Massachusetts, USA). The samples were eluted at 0.6 mL/min flow rate with monopotassium phosphate solution as mobile phase. The T-series dextran was used as standard.

Determination of Monosaccharide Composition

The monosaccharide composition of ZOP was analyzed by HPLC with pre-column derivatization (14). In simple terms, 2 mol/L trifluoroacetic acid and ZOP were hydrolyzed in a sealed tube at 110°C for 4 h, followed by PMP derivatization. The monosaccharide composition analysis was performed on an ODS C18 column (4.6 mm × 250 mm) connected to an Agilent 1260 HPLC system. The standard monosaccharides were determined under the same conditions described above (15).

Preparation of Silver Nanoparticles From Polysaccharides

The green methods for silver nanoparticles synthesis using ZOP and ZOP-NPs were as **Figure 1**.

Preparation of ZOP-NPs

0.5 g and 1 g ZOP were dissolved in 100 mL deionized water to prepare 0.5% (w/v) and 1% (w/v) polysaccharide solutions, respectively. The polysaccharide solution was then added to methanol in a ratio of 1:10 and stirred magnetically. All polysaccharide solutions were dropped into methanol and stirred mechanically for 2 h to obtain nano-polysaccharide solutions. ZOP-NPs was then obtained by freeze-drying (16).

Preparation of AgNPs

ZOP-AgNPs and ZOP-NPs-AgNPs were prepared under the condition that the solution volume ratio of polysaccharide (0.5%, w/v; 1%, w/v), $AgNO_3$ (0.05 mol/L) and NaCl (1 mg/L) was 1: 2: 1.5. Adjust the mixture to pH = 8.7 with $NH_3{\cdot}H_2O$. Subsequently, the mixture was placed in a magnetic agitator and

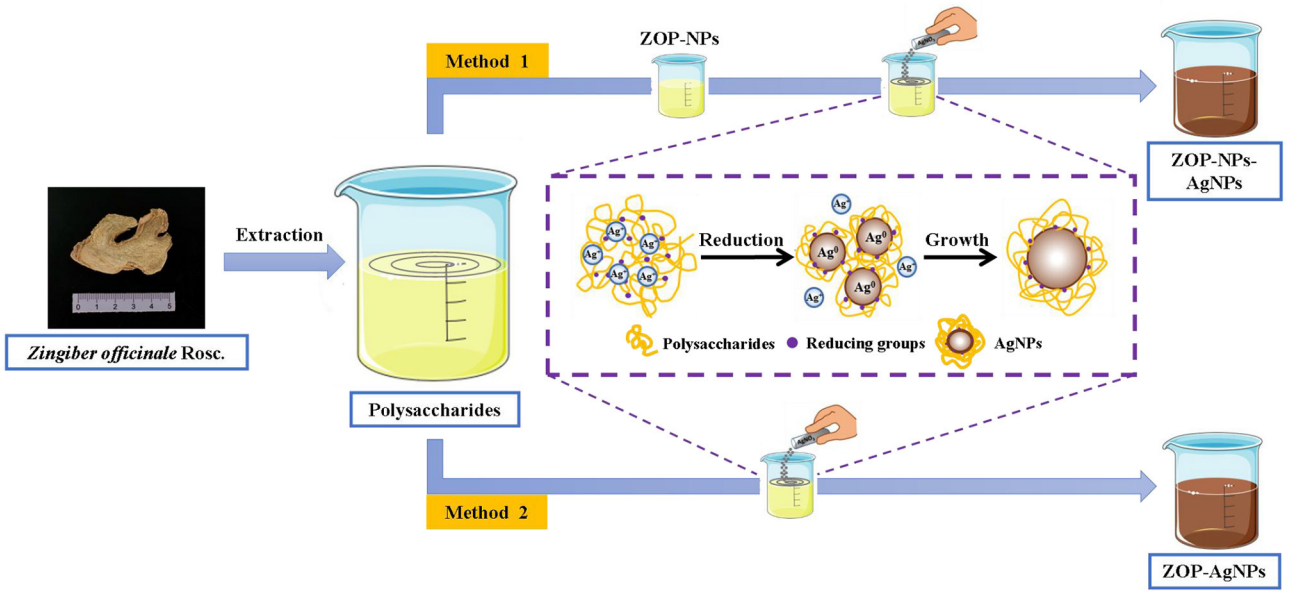

FIGURE 1 | Schematic representation of ZOP-NPs, ZOP-AgNPs, ZOP-NPs-AgNPs synthesis.

reacted for 4 h at room temperature with 365 nm UV irradiation and continuous agitation to form a brown AgNPs solution. After the reaction, the precipitate was collected by repeated centrifugation (9,000 × g ; 15 min) and lyophilized (17).

Volhard method was used to determine the chelation rate of silver ions in polysaccharide nanoparticles. In this method, ferric ammonium alum is used as a tracer agent and ammonium thiocyanate as a standard solution to titrate silver ions in solution.

$$A(\%) = \frac{C_0 - C}{C_0} \times 100\%$$

where, A, C_0 and C were the chelation rate (%), the concentration of silver ion in the solution before the reaction (mg/mL) and the concentration of silver ion in the solution after the reaction (mg/mL).

Size and Polydispersity Indexanalysis

Appropriate amount of AgNPs prepared above was diluted with ultra-pure water (0.1%). The particle size, polydispersity index (PDI) and Zeta potential were determined by using Zetasizer Nano dynamic light scattering (DLS) technique.

Characterization of AgNPs

Thermal Analysis

The thermal stability of the samples was determined by TGA-DSC (TA Instruments Ltd., Q600, America). N_2 was used as a protective gas to heat the sample from room temperature to 800°C at a temperature of 10°C/min.

UV-Vis Spectroscopy Analysis

The AgNPs obtained by the reaction was scanned in the range of 200–800 nm with UV-vis Spectrophotometer (18).

FT-IR Spectroscopy Analysis

Infrared absorption spectra of ZOP, ZOP-NPs, ZOP-AgNPs, and ZOP-NPs-AgNPs were recorder by S-100 FT-IR Spectrometer (PerkinElmer, America) at the frequency of 4,000–400 cm^{-1} range.

SEM Analysis

ZOP, ZOP-NPs, ZOP-AgNPs, and ZOP-NPs-AgNPs after gold spraying were analyzed by SEM (JSM 7610F, JEOL Ltd. Japan). The acceleration voltage was 3.0 kV and the resolution was 7.1 mm. The micro solid morphology of ZOP, ZOP-NPs, ZOP-AgNPs, and ZOP-NPs-AgNPs were photographed and recorded at different magnification and the element distributions of them were determined by SEM-EDS-mapping.

TEM Analysis

The synthesized nano silver sol sample was directly used for TEM testing. The carbon supporting film carrying the sample was placed on a clean filter paper, a small amount of sample liquid was absorbed with a pipette gun, a drop of sample liquid was dropped on the carbon supporting film, and then placed in a 40°C oven to dry or air dry at room temperature. The preparation of samples to be tested was completed. Then the samples were analyzed by TEM JM-2100.

XRD Analysis

The crystal structure of the samples was analyzed by X-ray diffractometer model (XRD-6000, Shimadzu, Japan). Cu-Kα ray (λ = 0.15406 nm) was used as the target, the tube voltage was 40 kV, the tube current was 30 mA, the scanning rate was 5 °/min, and the diffraction Angle was 2θ = 10–90° (19).

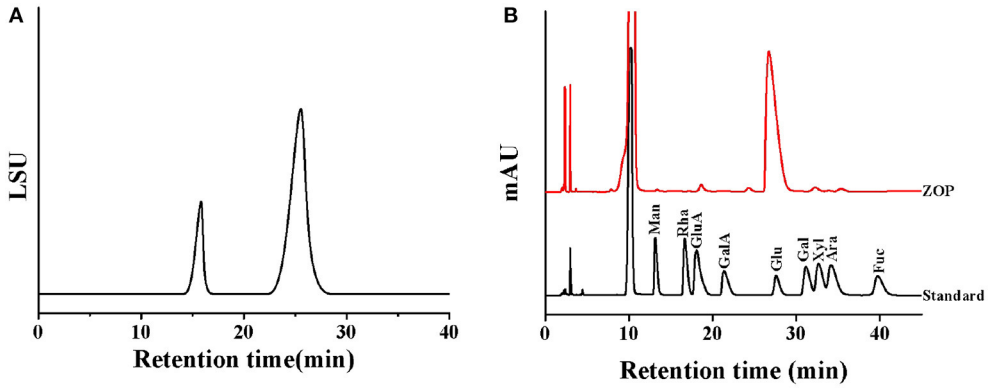

FIGURE 2 | The physical and chemical properties analysis of ZOP. Molecular weight distribution of ZOP **(A)**, HPLC of standard monosaccharides and ZOP **(B)**.

Antioxidant Activities

The scavenging activities of ZOP, ZOP-NPs, ZOP-AgNPs, and ZOP-NPs-AgNPs against DPPH· and OH· were determined at different concentrations (20).

Antibacterial Activity

The antibacterial activity of the samples against *E. coli* was investigated by oxford cup method. The agar medium was prepared by inverted dish method, sterilized, cured and inoculated with bacterial suspension. Different concentrations of Ag nanoparticles, nano-polysaccharide solutions and ZOP solutions were placed in precultured agar mediums. The mediums were incubated at 37°C for 24 h. Then the diameter was measured (21).

Data Statistics and Analysis

Microsoft Excel 2019 and SPSS 26.0 were used to process and analyze the data, and Origin 2019 was used for drawing.

RESULTS AND DISCUSSION

Physicochemical Properties of ZOP

Determination of Total Soluble Sugar Content

The crude polysaccharide of *Z. officinale* was 6.77 g by ultrasonic assisted boiling water extraction and ethanol precipitation. The glucose standard curve equation for determination of *Z. officinale* polysaccharide content by phenol-sulfuric acid method was: $y = 15.673x\text{-}0.0153$ ($R^2 = 0.9996$), and the linear range was 0–0.1 mg/mL. Therefore, the total soluble sugar content of ZOP was (78.6 ± 0.6)%.

Determination of Average Molecular Weight

The high performance gel permeation chromatogram of ZOP was shown in **Figure 2A**. The regression equation of the standard curve of dextran molecular weight was $y = -0.3108x+11.749$ ($R^2 = 0.9911$), and the molecular weight of two different components of ZOP were 6.04×10^6 Da (7.17%) and 5.42×10^3 Da (92.83%), respectively.

Determination of Monosaccharide Composition

After HPLC analysis, the monosaccharide composition of ZOP was determined by comparing the retention time with that of standard monosaccharide (**Figure 2B**). The results showed that the monosaccharide composition and molar ratio of ZOP were GlcA: GalA: Glc: Gal: Ara = 1.97:1.15:94.33:1.48:1.07.

AgNPs Characterization

Silver Chelation Rate and Elemental Analysis

Polysaccharide, as a reducing agent and stabilizer, plays an important role in the synthesis of polysaccharide silver nanoparticles (22). The silver chelating rates of 0.5% (w/v)-ZOP-AgNPs, 0.5% (w/v)-ZOP-NPs-AgNPs, 1% (w/v)-ZOP-AgNPs, and 1% (w/v)-ZOP-NPs-AgNPs were 68.70, 72.28, 79.88, and 82.12%, respectively. In addition, when the reaction time, solution volume ratio and $AgNO_3$ concentration were the same, the chelating rate of AgNPs increased with the increase of polysaccharide concentration. After comparison, it was found that the ZOP-NPs-AgNPs prepared by ZOP-NPs had a higher silver chelation rate. Moreover, according to the analysis of the Mapping spectrum (**Figure 3**), the silver content in the AgNPs was positively correlated with the polysaccharide concentration, and the silver content in the AgNPs after the polysaccharide nanocrystallization was higher, which was consistent with the results of the determination of silver chelation rate.

Particle Size and Zeta Potential Analysis

The results were as follows: the particle size of ZOP-NPs was 230.5 nm, and the PDI value was 0.260, the ZOP-AgNPs (0.5%, w/v; 1%, w/v) and ZOP-NPs-AgNPs (0.5%, w/v; 1%, w/v) exhibited a narrow particle size distribution of 31.1, 34.6, 25.1 and 27.6 nm, respectively. In addition, their PDI values were 0.394, 0.431, 0.368, 0.387, respectively.

The larger the PDI, the wider the molecular weight distribution; The smaller the PDI, the more uniform the molecular weight distribution (23). After comparison, it was found that ZOP-AgNPs and ZOP-NPs-AgNPs particle size and PDI were positively correlated with polysaccharide concentration. Under the condition of the same polysaccharide

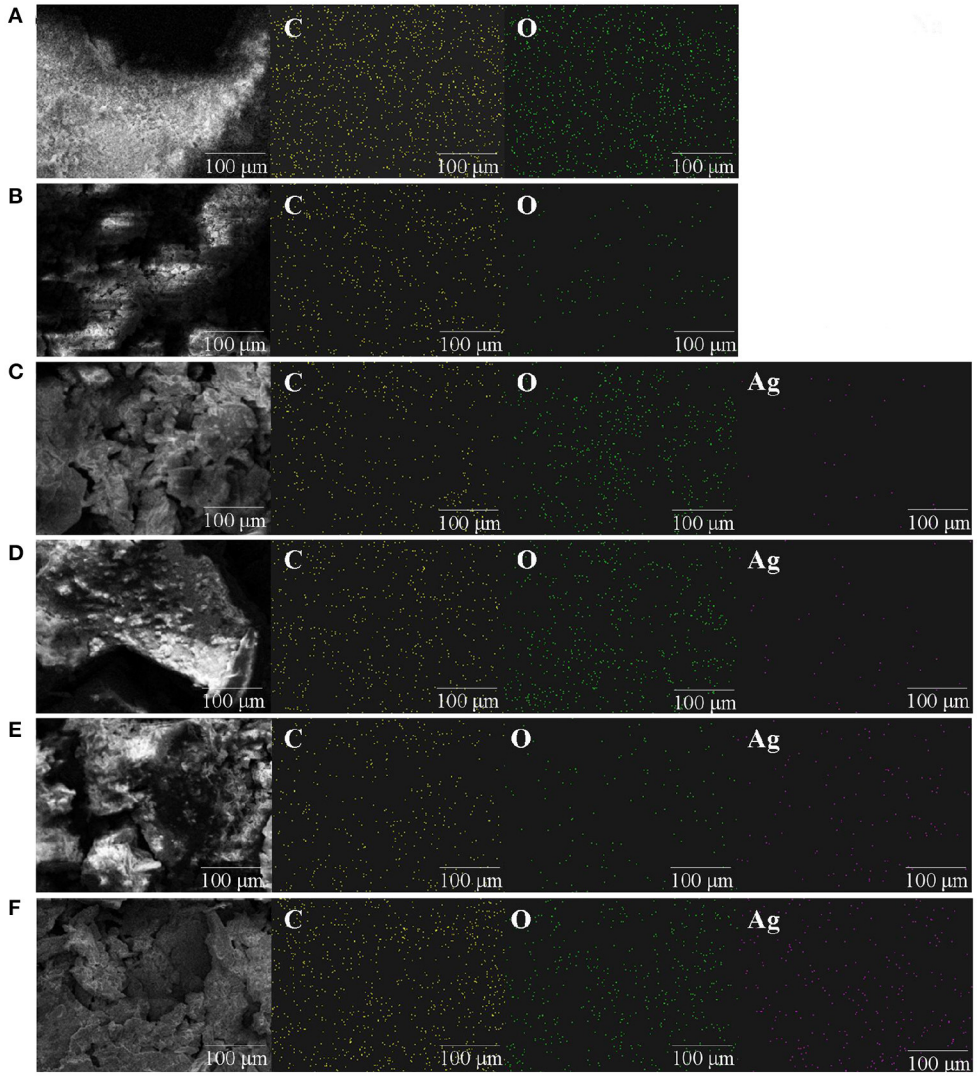

FIGURE 3 | Mapping images of ZOP **(A)**, ZOP-NPs **(B)**, 0.5% (w/v)-ZOP-AgNPs **(C)**, 0.5% (w/v)-ZOP-NPs-AgNPs **(D)**, 1% (w/v)-ZOP-AgNPs **(E)**, 1% (w/v)-ZOP-NPs-AgNPs **(F)** (×30,000).

concentration, the particle size and PDI of ZOP-NPs-AgNPs was smaller, and 0.5%-ZOP-NPs-AgNPs had the smallest particle size and PDI, and the best dispersion. The colloidal solution of nanoparticles had a larger negative potential, so it had a higher electrostatic stability. The zeta potential values of ZOP-AgNPs (0.5%, w/v; 1%, w/v) and ZOP-NPs-AgNPs (0.5%, w/v; 1%, w/v) were −19.4, −21.6, −19.7, −23.8 mV, respectively (**Table 1**). Their zeta potential values were larger, which confirms that the nano-silver synthesized by ZOP in this experiment had good stability. After comparison, it was found that 1%-ZOP-NPs-AgNPs had higher stability.

TABLE 1 | Zeta potential, particle size and distribution of ZOP, ZOP-NPs, ZOP-AgNPs, and ZOP-NPs-AgNPs.

Name	Size/nm	PDI	Zeta potential/mV
ZOP	345.2	0.520	−10.9
ZOP-NPs	230.5	0.260	−27.1
0.5% (w/v)-ZOP-AgNPs	31.1	0.394	−19.4
0.5% (w/v)-ZOP-NPs-AgNPs	25.1	0.368	−19.7
1% (w/v)-ZOP-AgNPs	34.6	0.431	−21.6
1% (w/v)-ZOP-NPs-AgNPs	27.6	0.387	−23.8

TGA-DSC Analysis

The changes of ZOP, ZOP-NPs, ZOP-AgNPs, and ZOP-NPs-AgNPs with temperature were shown in **Figure 4**. Due to loose binding water in the polysaccharide, the mass of ZOP decreased slightly between 0 and 210°C, and the weight loss rate of ZOP was 16.8%. When the temperature was about 220°C, the thermal decomposition of polysaccharide itself occurred, leading to the

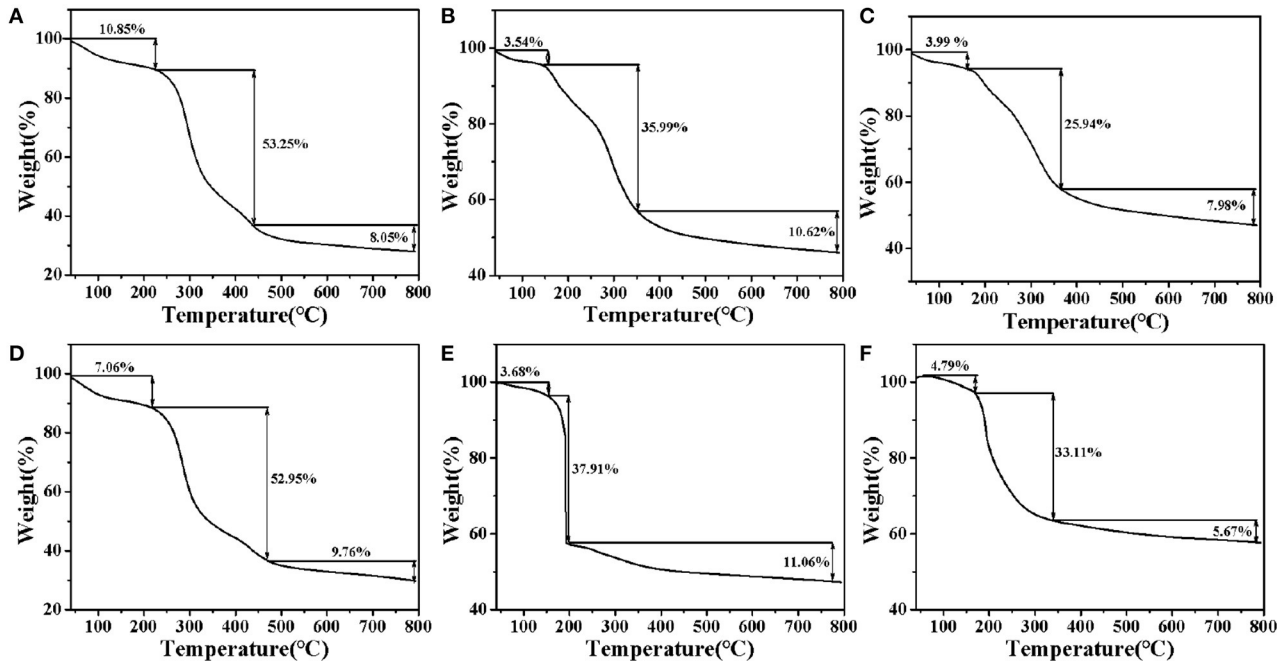

FIGURE 4 | DSC-TGA analysis of ZOP **(A)**, 0.5% (w/v)-ZOP-AgNPs **(B)**, 1% (w/v)-ZOP-AgNPs **(C)**, ZOP-NPs **(D)**, 0.5% (w/v)-ZOP-NPs-AgNPs **(E)**, and 1% (w/v)-ZOP-NPs-AgNPs **(F)**.

breaking of glycosidic bonds and ring-opening reaction. The weight of ZOP decreased sharply by 63.25% between 220 and 800°C (24).

It can be seen from **Figure 4D** that the thermal degradation process of ZOP-NPs did not changed. From the initial degradation temperature, it can be seen that the thermal stability of ZOP and ZOP-AgNPs were similar. Thermal decomposition curve of ZOP-AgNPs (0.5%, w/v; 1%, w/v), as shown in **Figures 4B,C**. ZOP-AgNPs (0.5%, w/v; 1%, w/v) weightlessness in the process of 25–170°C was mainly caused by water loss. Their weight loss rates are 3.54 and 3.99%, respectively. The second and third stages were 170–370°C and 370–800°C, respectively. In these two stages, the weight loss rates of 0.5%-ZOP-AgNPs and 1%-ZOP-AgNPs were 46.61 and 33.92%, respectively. **Figures 4E,F** illustrates the thermogravimetric analysis of ZOP-NPs-AgNPs (0.5%, w/v; 1%, w/v). ZOP-NPs-AgNPs (0.5%, w/v; 1%, w/v) of the first stage of weightlessness rate were 3.68 and 4.79%, respectively. The second stage and third stage of 0.5%-ZOP-NPs-AgNPs were 160–190°C and 190–800°C, respectively. And the weight loss rate of these two stages was 48.97%. The second and third stages of 1%-ZOP-NPs-AgNPs were 160–340°C and 340–800°C, respectively, and the weight loss rate of these two stages was 38.78%. After comparison, it was found that the weight loss rate of ZOP-NPs-AgNPs was slightly higher than that of ZOP-AgNPs, which might because of the lesser particle size of ZOP-NP-AgNPs and easier to decompose. It can be seen that water loss and thermal decomposition of polysaccharide itself are the main causes of thermal weight loss of nano-silver polysaccharide. In addition, the weight loss rate of the modified silver nanoparticles decreased significantly, and with the increase of silver concentration in the AgNPs, the weight loss rate of the AgNPs also decreased significantly, indicating that the AgNPs could protect and stabilize the silver nanoparticles in the synthesis process (25).

UV-Vis Spectroscopy Analysis

UV-Vis spectroscopy was an important technique to determine the structure of polysaccharides and the formation of metal nanoparticles. It could be seen from **Figures 5A,B** that there were no absorbances peak at 280 and 260 nm in UV-Vis, indicating that ZOP and ZOP-NPs does not contain protein and nucleic acid. With the increase of UV-irradiation time, the color of the prepared ZOP-AgNPs and ZOP-NPs-AgNPs solutions changed from light yellow to yellowish brown. This was due to silver nanoparticles absorbed the radiation in the visible region of electromagnetic spectrum, resulting in the reaction mixture becoming a dark brown solution (26). In the UV absorption spectrum, the wider absorption peak at 430 nm was typical surface plasmon resonance absorption of silver nanoparticles, which also indicated the formation of spherical silver nanoparticles. As can be seen from **Figure 5C**, ZOP-NPs-AgNPs showed stronger absorption peaks than ZOP-AgNPs. Moreover, the absorption peak was positively correlated with the polysaccharide concentration. This indicated that when the polysaccharide concentration sincreased, more polysaccharides participate in the reduction of silver, and more AgNPs was generated. At the same time, there were no other peaks in the

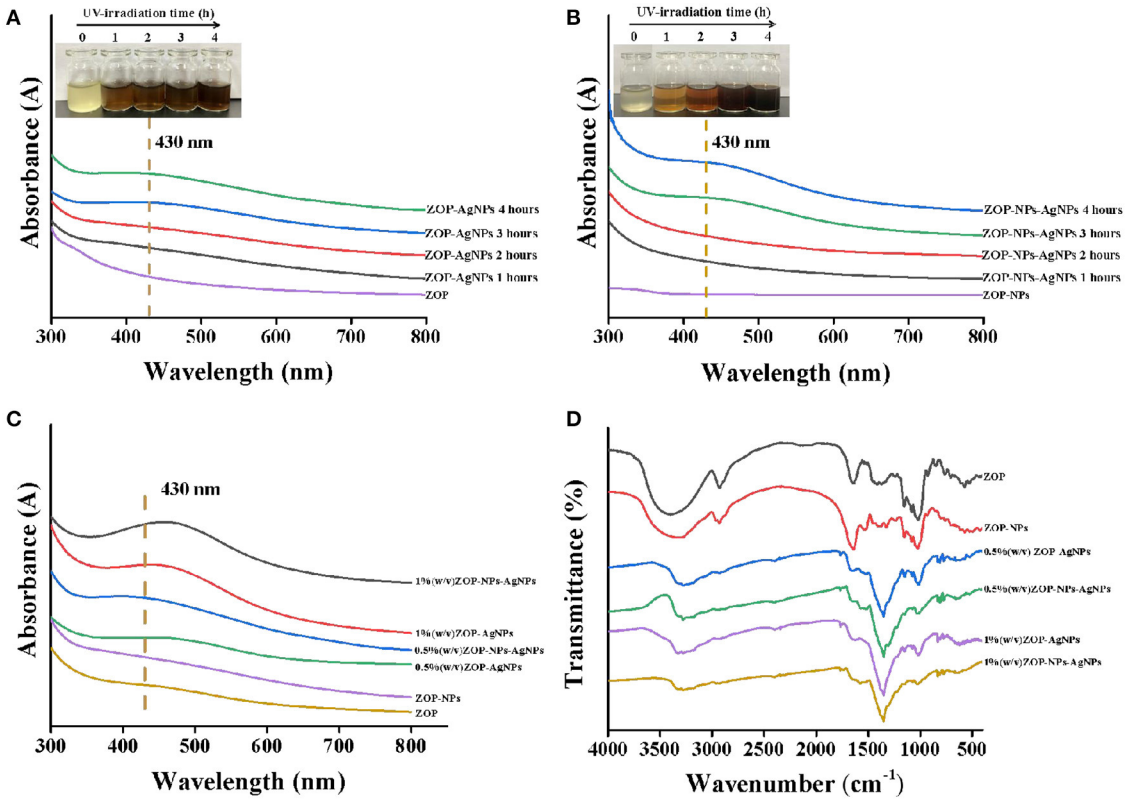

FIGURE 5 | UV-vis of ZOP-AgNPs **(A)** and ZOP-NPs-AgNPs **(B)**under different time conditions; UV-Vis **(C)** and FT-IR **(D)** analysis of ZOP, ZOP-NPs, ZOP-AgNPs, and ZOP-NPs-AgNPs.

range of 300–600 nm, indicating that there was no aggregation or cluster formation of silver particles (27).

FT-IR Analysis

ZOP, ZOP-NPs, ZOP-AgNPs, and ZOP-NPs-AgNPs were characterized by FT-IR spectra, and the results were shown in **Figure 5D**. In the FT-IR spectrum of ZOP (**Figure 5D**), a broad peak around 3,400 cm^{-1} is the characteristic of O-H stretching frequency which shifts to 3,250 cm^{-1} and becomes narrower for ZOP-AgNPs. The absorption peak at 2,929 cm^{-1} was due to -CH_2 stretching vibration. A band at 1,642 cm^{-1} was attributed to stretching vibration of C=O group of ester group. The absorption peak at 1,416 and 1,370 cm^{-1} were observed due to the C-H bending vibrations. The absorption peak at 1,155, 1,081, and 1,021 cm^{-1} were due to the stretching variation of C-O-C group (28). In case of AgNPs the peaks corresponding to the above functionalities appeared at 2,931, 1,644, 1,350, and 1,151 cm^{-1}, respectively. The abundant hydroxyl, carboxyl and macromolecular matrix structures on the surface of natural polysaccharides endows polysaccharides with the ability to stabilize AgNPs (29). It can be seen from **Figure 5D** that compared with ZOP and ZOP-NPs, the band shift in O-H and the increased band intensities for C=O in the FT-IR spectra of AgNPs prepared by polysaccharides increased, which can be inferred that both hydroxyl and carbonyl groups of ZOP and ZOP-NPs are involved in the synthesis of silver nanoparticles. **Figure 5D** also shown that the infrared visible spectrum of 1% (w/v)-ZOP-NPs and 1% (w/v)-ZOP-NPs-AgNPs were almost the same as that of 0.5% (w/v)-ZOP-NPs and 0.5% (w/v)-ZOP-NPs-AgNPs, except that 1% (w/v)-ZOP-NPs and 1% (w/v)-ZOP-NPs-AgNPs had a slight red shift (30).

SEM Analysis

SEM of ZOP (**Figure 6**) shown that ZOP was a compact and stable sheet structure with smooth surface and irregular folds. Most of the shapes of the synthesized AgNPs were similar to spherical, while a few are lumpy, which might be caused by the fact that the synthesized AgNPs were frozen together in the freeze-drying process. Moreover, the particle size of AgNPs prepared by ZOP-NPs is smaller and the shape is more uniform.

TEM Analysis

It could be observed from **Figures 7A–D**, ZOP-AgNPs and ZOP-NP-AgNPs were spherical with uniform distribution and few signs of aggregation, with particle sizes ranging from 2.89 to 8.14 nm. Further high resolution images confirmed that the ZOP-AgNPs and ZOP-NPs-AgNPs were highly crystalline in nature (**Figure 7E**). The lattice fringes of AgNPs could be observed in **Figure 7E**, and the distance was 2.11 Å, which supported the XRD data of AgNPs (the lattice plane is 111) (31). The crystal

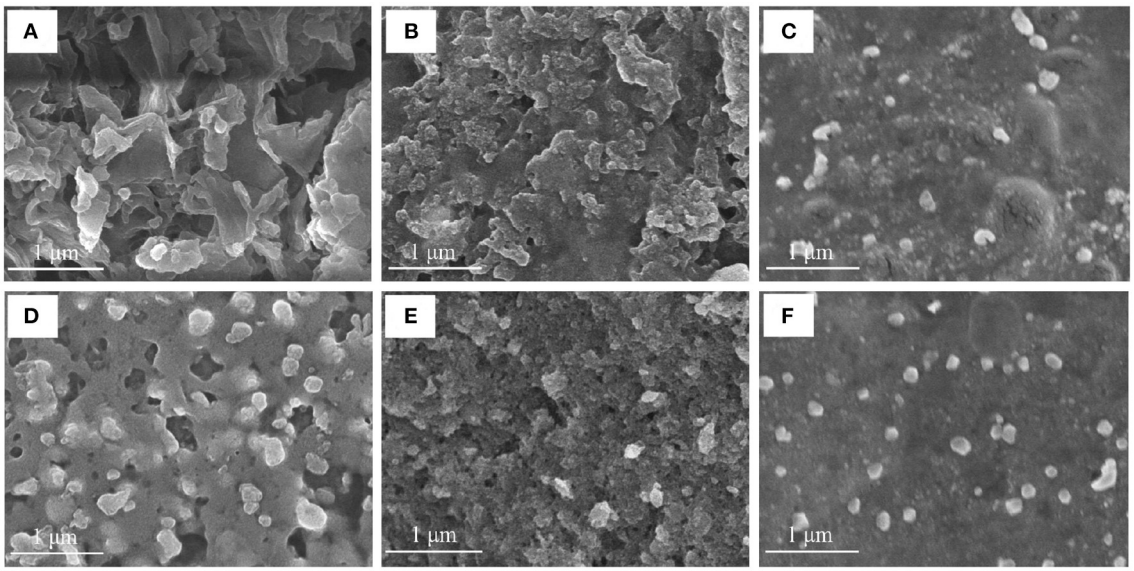

FIGURE 6 | The SEM images of ZOP **(A)**, 0.5% (w/v)-ZOP-AgNPs **(B)**, 0.5% (w/v)-ZOP-NPs-AgNPs **(C)**, ZOP-NPs **(D)**, 1% (w/v)-ZOP-AgNPs **(E)** and 1% (w/v)-ZOP-NPs-AgNPs **(F)** (×30,000).

structure of AgNPs is also demonstrated by the selected area electron diffraction (SAED) mode (**Figure 7F**).

XRD Analysis

As shown in **Figure 8**, the XRD patterns of ZOP and ZOP-NPs show a low diffraction maximum at 10 ∼ 30°, indicating that the internal structure of ZOP and ZOP-NPs was amorphous or semi-crystalline. XRD patterns of ZOP-AgNPs and ZOP-NPs-AgNPs showed four obvious diffraction peaks, which were located at (2θ) 38.28, 47.56, 64.56, and 77.52°, respectively, corresponding to the four planes of (111), (200), (220), and (311) of face-centered cube (FCC), which further confirmed the successful preparation of silver particles (30).

Antioxidant Activities

Antioxidants are a class of substances that can help capture and neutralize free radicals, thereby reducing the risk of other degenerative diseases caused by reactive oxygen species (32). In this study, the ability of vitamin C (Vc), ZOP, ZOP-NPs, ZOP-AgNPs (0.5%, w/v; 1%, w/v), and ZOP-NPs-AgNPs (0.5%, w/v; 1%, w/v) to scavenge DPPH· and hydroxyl radicals were determined (**Figures 9A,B**). The half maximal inhibitory concentration (IC_{50}) of ZOP, ZOP-NPs, 0.5% (w/v)-ZOP-AgNPs, 0.5% (w/v)-ZOP-NPs-AgNPs, 1% (w/v)-ZOP-AgNPs, 1% (w/v)-ZOP-NPs-AgNPs and Vc against DPPH· were 226.8, 164.3, 370.2, 376.9, 192.2, 141.6, and 37.0 μg/mL, respectively. The lower IC_{50} value of the free radical scavenging compound, the stronger the antioxidant capacity. At their concentration of 1,600 mg/mL, the scavenging order of DPPH· was V_C > 1% (w/v)-ZOP-NPs-AgNPs > ZOP-NPs > 1% (w/v)-ZOP-AgNPs > ZOP > 0.5% (w/v)-ZOP-NPs-AgNPs > 0.5% (w/v)-ZOP-AgNPs. It could be seen that 1%-ZOP-NPs-AgNPs had high DPPH· radical scavenging ability. The IC_{50} values of 0.5% (w/v)-ZOP-AgNPs, 0.5% (w/v)-ZOP-NPs-AgNPs, 1% (w/v)-ZOP-AgNPs, 1% (w/v)-ZOP-NPs-AgNPs and Vc against OH· were 102.7, 74.8, 210.6, 243.5, and 16.8 μg/mL, respectively. Similarly, 0.5%-ZOP-NPs-AgNPs showed better OH· scavenging ability. However, as the concentration increases, when the concentration reaches 1,600 mg/mL, the scavenging order of OH· radical was VC > 1% (w/v)-ZOP-NPs-AgNPs > 1% (w/v)-ZOP-AgNPs > 0.5% (w/v)-ZOP-NPs-AgNPs > 0.5% (w/v)-ZOP-AgNPs > ZOP-NPs > ZOP. Thus, the ability of several compounds to scavenge free radicals showed concentration dependence, which was consistent with the results of Cameron et al. (33).

In conclusion, ZOP mediated metal nanoparticles ZOP-NPs-AgNPs had a higher antioxidant activity on the formation of free radicals into the life system. Firstly, polysaccharides and their derivatives may play an antioxidant role through the interaction between electron transfer and hydrogen ions and free radicals (34). Second, ZOP-NPs-AgNPs had the characteristics of smaller particle size and larger specific surface area than other polysaccharide nanoparticles, which can integrate with more free radical scavenger and had a better antioxidant activity. Last but not least, the intermediate compounds formed by polysaccharide and metal ions during the formation of silver nanoparticles may also play a role in scavenging free radicals (35).

Antimicrobial Activity

The antibacterial activities of ZOP-AgNPs and ZOP-NPs-AgNPs were studied in this paper, and the results are shown in **Figures 9C,D**. There was no inhibition zone around ZOP and ZOP-NPs, indicating that ZOP and ZOP-NPs had no antibacterial activity against *E. coli*. ZOP-AgNPs (0.5%, w/v; 1%, w/v) and ZOP-NPs-AgNPs (0.5%, w/v; 1%, w/v) had significant

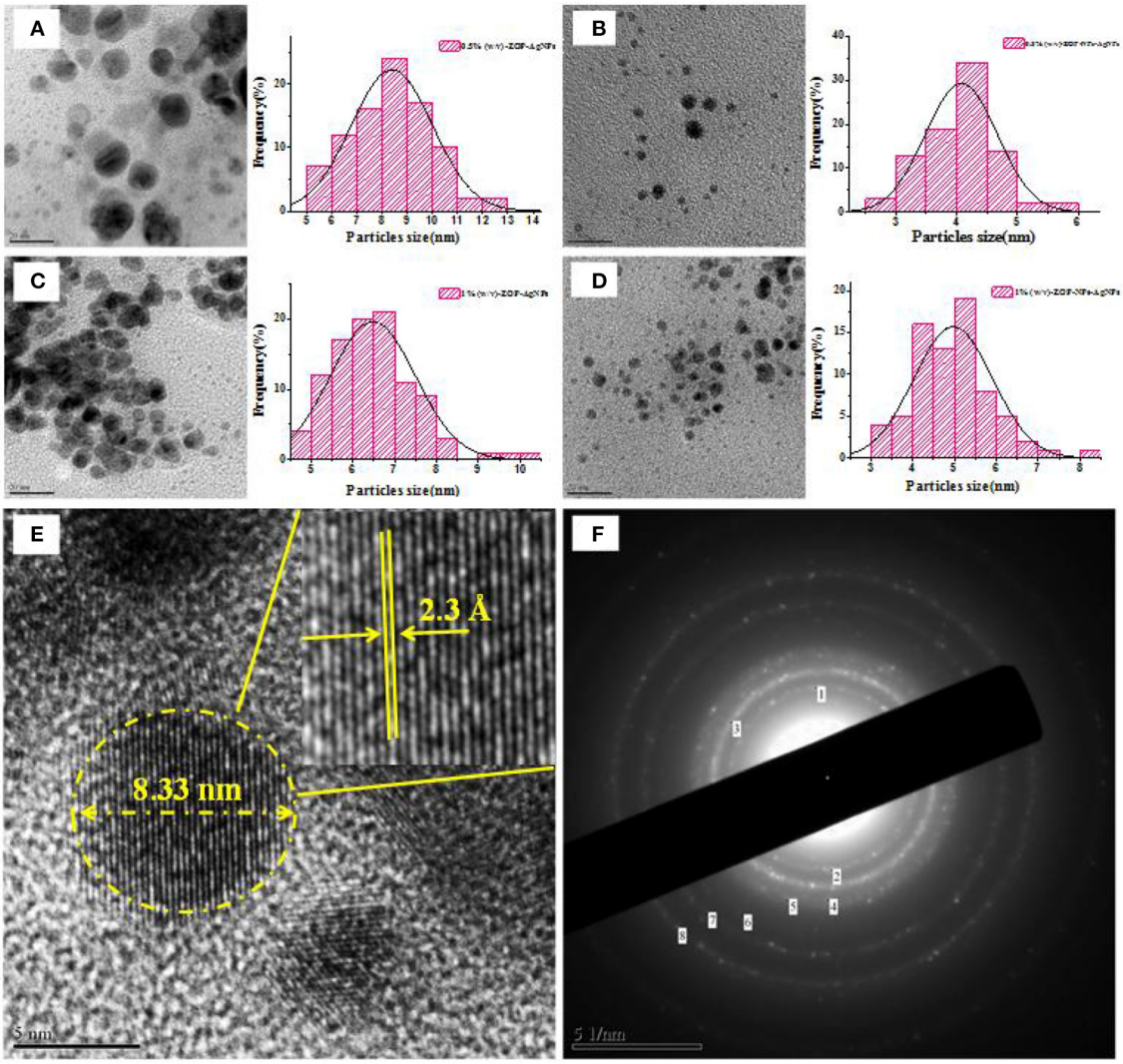

FIGURE 7 | The TEM images of AgNPs and corresponding size distribution curve of AgNPs [**(A)** 0.5% (w/v)-ZOP-AgNPs; **(B)** 0.5% (w/v)-ZOP-NPs-AgNPs; **(C)** 1% (w/v)-ZOP-AgNPs; **(D)** 1% (w/v)-ZOP-NPs-AgNPs]; The TEM images of ultra-magnified image showing lattice fringe **(E)** and electron diffractogram of AgNPs **(F)**.

inhibitory effect on E. coli., and the size of inhibition zone of them were positively correlated with polysaccharide concentrations.

The diameters of their inhibition zones were 13.32, 13.67, 14.02, and 15.70 mm, respectively. Wang et al. (36) showed that active silver nanoparticles may first destroy the cell membrane of bacteria, leading to the leakage of cell materials. The silver nanoparticles then enter the inner membrane of the cell and inactivate the respiratory chain dehydrogenase, thereby inhibiting the cell's respiration and growth. At the same time, silver particles can also affect the biological activity of some proteins and phosphates, causing the collapse of cell membranes, and ultimately leading to the decomposition and death of cells. For the silver nanoparticles, the larger the surface area, the more silver atoms attached to the solid surface, the stronger the antibacterial activity. Therefore, the antibacterial activity of silver nanoparticles is stronger than that of bulk silver (37). It could be seen from **Figures 9C,D**, with the increase of the concentration of ZOP-AgNPs and ZOP-NPs-AgNPs, their antibacterial activity also increased. In addition, ZOP-NPs-AgNPs had better antibacterial activity than ZOP-AgNPs at the same concentration. At different concentrations, with the increase of the concentration of AgNPs, that is, the number of polysaccharide nanoparticles in the same volume increases, more AgNPs can attack bacterial cells, resulting in the death of more bacterial cells, thus showing better antibacterial effect. In addition, ZOP-NPs-AgNPs had better antibacterial activity than ZOP-AgNPs at the same concentration. In other words, ZOP-NPs-AgNPs with small particle size showed higher antimicrobial activity.

In conclusion, under different concentrations, the antibacterial activity of AgNPs in a certain concentration range will increase with the increase of its concentration; Under the condition of the same concentration, the nanoparticles with smaller particle size, and larger specific surface area had better antibacterial performance.

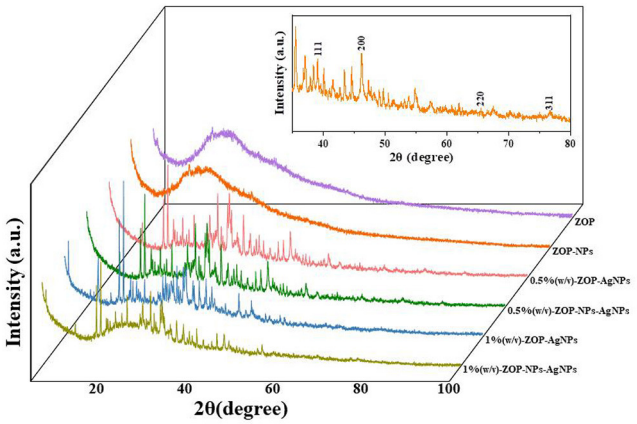

FIGURE 8 | XRD analysis of ZOP, ZOP-NPs, 0.5% (w/v)-ZOP-AgNPs, 0.5% (w/v)-ZOP-NPs-AgNPs, 1% (w/v)-ZOP-AgNPs, 1% (w/v)-ZOP-NPs-AgNPs.

CONCLUSION

In this study, ZOP was used as raw material to prepare AgNPs. In this method, ZOP was used as a green reducing agent and stabilizer, overcoming the toxicity and pollution caused by chemical reducing agent in conventional methods. In conclusion, ZOP had the advantages of good reducibility and environmental protection, and provided a new method and approach for the green reduction of nano-silver. In addition, ZOP can also be used as a green reducing agent and stabilizer to further study its reducing and stability of other metals. Polysaccharide mediated generation of nano-silver, due to its good antibacterial activity, can be used in pharmaceutical, medical, food hygiene, preservation and other fields, to reduce microbial infection, and due to its high antioxidant activity, AgNPs will also be increasingly used in beauty products and the development of new antioxidants.

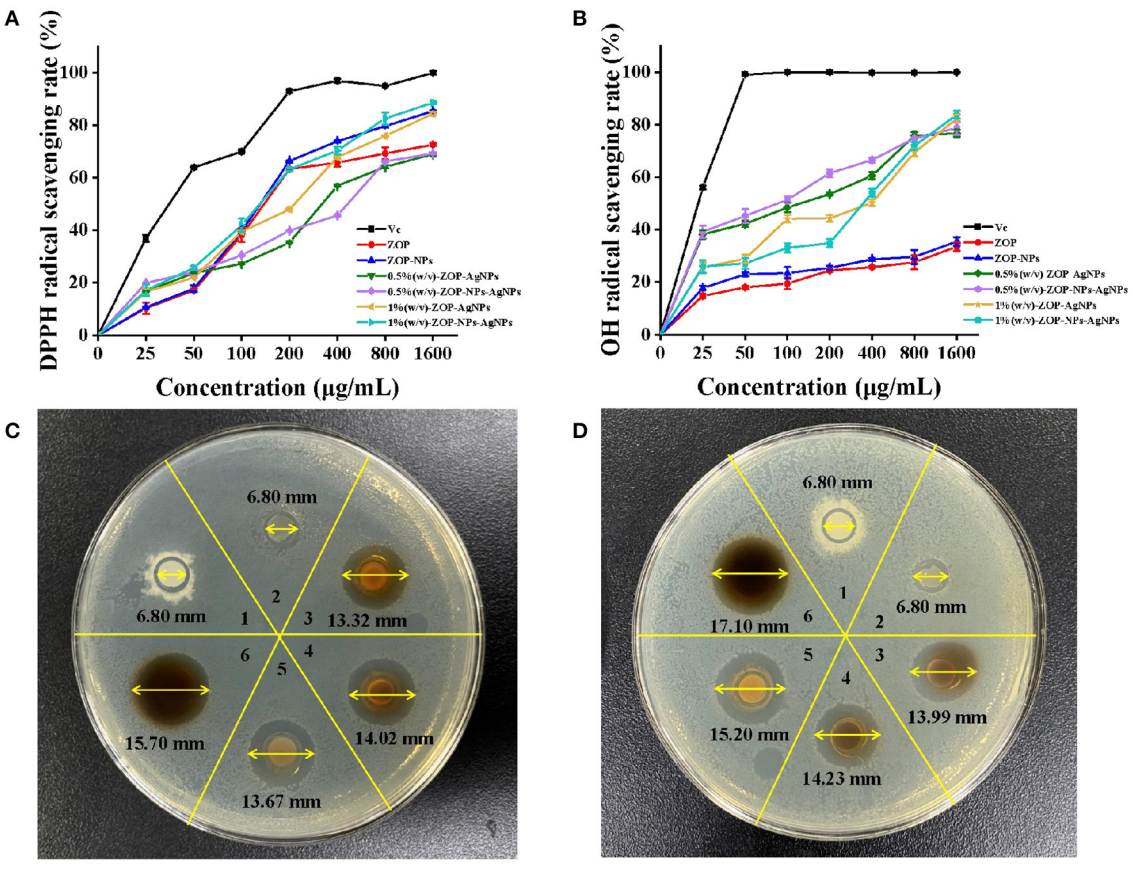

FIGURE 9 | Antioxidant activities of ZOP, ZOP-NPs, ZOP-AgNPs, ZOP-NPs-AgNPs [**(A)** DPPH· radical; **(B)** OH· radical]; Antibacterial activity of ZOP, ZOP-NPs, ZOP-AgNPs, ZOP-NPs-AgNPs [1: ZOP; 2: ZOP-NPs; 3: 0.5% (w/v)-ZOP-AgNPs; 4: 0.5% (w/v)-ZOP-NPs-AgNPs; 5: 1% (w/v)-ZOP-AgNPs; 6: 1% (w/v)-ZOP-NPs-AgNPs; **(C)** 20 mg/mL; **(D)** 40 mg/mL].

DATA AVAILABILITY STATEMENT

The original contributions presented in the study are included in the article/supplementary material, further inquiries can be directed to the corresponding author/s.

AUTHOR CONTRIBUTIONS

YJ and LW designed and conceived the study. YJ, WC, and YM performed the experiments. WC and YZ analyzed the data and drafted the manuscript. ML, YZ, and DZ contributed to the writing of the manuscript. YJ and DZ provided the funding and resources. All authors revised and approved the submitted version of the manuscript.

FUNDING

This work was supported by the S & T Program of Hebei (No. H2021208007), the Key Research and Development Program of Hebei Province (No. 20370509D) and the Science and Technology Project of the Hebei Education Department (No. ZD2022021).

REFERENCES

1. Magaye R, Zhao J. Recent progress in studies of metallic nickel and nickel-based nanoparticles' genotoxicity and carcinogenicity. *Environ Toxicol Pharmacol.* (2012) 34:644–50. doi: 10.1016/j.etap.2012.08.012
2. Geng YC, Khodadadi H, Karimipour A, Safaei MR, Nguyen TK. A comprehensive presentation on nanoparticles electrical conductivity of nanofluids: statistical study concerned effects of temperature, nanoparticles type and solid volume concentration. *Phys A Stat Mech Its Appl.* (2020) 542:123432. doi: 10.1016/j.physa.2019.123432
3. Wang X, Yuan L, Deng H, Zhang Z. Structural characterization and stability study of green synthesized starch stabilized silver nanoparticles loaded with isoorientin. *Food Chem.* (2021) 338:127807. doi: 10.1016/j.foodchem.2020.127807
4. Veeraraghavan VP, Periadurai ND, Karunakaran T, Hussain S, Surapaneni KM, Jiao S, et al. Green synthesis of silver nanoparticles from aqueous extract of *Scutellaria barbata* and coating on the cotton fabric for antimicrobial applications and wound healing activity in fibroblast cells (L929). *Saudi J Biol Sci.* (2021) 28:3633–40. doi: 10.1016/j.sjbs.2021.05.007
5. El-Rafie HM, El-Rafie MH, Zahran MK. Green synthesis of silver nanoparticles using polysaccharides extracted from marine macro algae. *Carbohyd Polym.* (2013) 96:403–10. doi: 10.1016/j.carbpol.2013.03.071
6. Ji XL, Hou CY, Shi MM, Yan YZ, Liu YQ. An insight into the research concerning *Panax ginseng* C. A Meyer polysaccharides: a review. *Food Rev Int.* (2020) 36:1771363. doi: 10.1080/87559129.2020.1771363
7. Hsiang CY, Cheng HM, Lo HY, Li CC, Chou PC, Lee YC, et al. Ginger and zingerone ameliorate lipopolysaccharide-induced acute systemic inflammation in mice, assessed by nuclear factor-κB bioluminescent imaging. *J Agric Food Chem.* (2015) 63:6051–8. doi: 10.1021/acs.jafc.5b01801
8. Shanmugam KR, Mallikarjuna K, Kesireddy N, Reddy KS. Neuroprotective effect of ginger on anti-oxidant enzymes in streptozotocin-induced diabetic rats. *Food Chem Toxicol.* (2011) 49:893–7. doi: 10.1016/j.fct.2010.12.013
9. Chen GT, Yuan B, Wang HX, Qi GH, Cheng SJ. Characterization and antioxidant activity of polysaccharides obtained from ginger pomace using two different extraction processes. *Int J Biol Macrimol.* (2019) 139:801–9. doi: 10.1016/j.ijbiomac.2019.08.048
10. Yang XL, Wei SQ, Lu XM, Qiao XG, Simal-Gandara J, Capanoglu E, et al. A neutral polysaccharide with a triple helix structure from ginger: characterization and immunomodulatory activity. *Food Chem.* (2021) 350:129261. doi: 10.1016/j.foodchem.2021.129261
11. Chen XH, Chen GJ, Wang ZR, Kan JQ. A comparison of a polysaccharide extracted from ginger (*Zingiber officinale*) stems and leaves using different methods: preparation, structure characteristics, and biological activities. *Int J Biol Macromol.* (2020) 151:635–49. doi: 10.1016/j.ijbiomac.2020.02.222
12. Liao DW, Cheng C, Liu JP, Zhao LY, Huang DC, Chen GT. Characterization and antitumor activities of polysaccharides obtained from ginger (*Zingiber officinale*) by different extraction methods. *Int J Biol Macromol.* (2020) 152:894–903. doi: 10.1016/j.ijbiomac.2020.02.325
13. Bi SX, Jing YS, Zhou QQ, Hu XJ, Zhu JH, Guo ZY, et al. Structural elucidation and immunostimulatory activity of a new polysaccharide from *Cordyceps militaris*. *Food Funct.* (2017) 9:279–93. doi: 10.1039/C7FO01147D
14. Ma LP, Jiao KP, Luo L, Xiang JL, Fan JL, Zhang XY, et al. Characterization and macrophage immunomodulatory activity of two polysaccharides from the flowers of *Paeonia suffruticosa* Andr. *Int J Biol Macrimol.* (2019) 124:955–62. doi: 10.1016/j.ijbiomac.2018.12.035
15. Ji XL, Cheng YQ, Tian JY, Zhang SQ, Jing YS, Shi MM. Structural characterization of polysaccharide from jujube (*Ziziphus jujube* Mill.) fruit. *Chem Biol Technol Ag.* (2021) 54:1–7. doi: 10.1186/s40538-021-00255-2
16. Wang L, Zhang Y. Heat-induced self-assembly of zein nanoparticles: fabrication, stabilization and potential application as oral drug delivery. *Food Hydrocolloid.* (2018) 90:403–12. doi: 10.1016/j.foodhyd.2018.12.040
17. Liao ZP, Wang F, Wang WT, Liu JY, Ma XR, Wu SH, et al. Optimization of preparation process for emblic polysaccharide-silver nanoparticles by response surface methodology. *Nat Prod Res Dev.* (2017) 29:1409–14. doi: 10.16333/j.1001-6880.2017.8.025
18. Ghetas HA, Abdel-Razek N, Shakweer MS, Abotaleb MM, Paray BA, Ali S, et al. Antimicrobial activity of chemically and biologically synthesized silver nanoparticles against some fish pathogens. *Saudi J Biol Sci.* (2021) 29:1298–305. doi: 10.1016/j.sjbs.2021.11.015
19. Jing YS, Zhang RJ, Li L, Zhang DS, Liu Y, Wu LF, et al. Optimization of ultrasonic-assisted extraction, characterization, and antioxidant activities of polysaccharides from Sojae Semen Praeparatum. *Nat Prod Commun.* (2021) 16:1–10. doi: 10.1177/1934578X211020622
20. Kakakhel MA, Sajjad W, Wu F, Bibi N, Shah K, Zhang YL, et al. Green synthesis of silver nanoparticles and their shortcomings, animal blood a potential source for silver nanoparticles: a review. *J Hazard Mater Adv.* (2021) 1:100005. doi: 10.1016/j.hazadv.2021.100005
21. Shetta A, Kegere J, Mamdouh W. Comparative study of encapsulated peppermint and green tea essential oils in chitosan nanoparticles: encapsulation, thermal stability, *in-vitro* release, antioxidant and antibacterial activities. *Int J Biol Macrimol.* (2019) 126:731–42. doi: 10.1016/j.ijbiomac.2018.12.161
22. Dalvi SV, Dave RN. Controlling particle size of a poorly water-soluble drug using ultrasound and stabilizers in antisolvent precipitation. *Ind Eng Chem Res.* (2009) 48:7581–93. doi: 10.1021/ie900248f
23. Vasquez RD, Apostol JG, Leon JD. Polysaccharide-mediated green synthesis of silver nanoparticles from *Sargassum siliquosum* J.G. Agardh: assessment of toxicity and hepatoprotective activity. *Open Nano.* (2016) 1:16–24. doi: 10.1016/j.onano.2016.03.001
24. Liu JX, Wang YX, Wu JZ, Georgiev MLI, Xu BJ, Wong KH, et al. Isolation, structural properties, and bioactivities of polysaccharides from Mushrooms Termitomyces: a review. *J Agric Food Chem.* (2022) 70:21–33. doi: 10.1021/acs.jafc.1c06443
25. Liu JH, Guo QQ, Hua HY, Yuan B, Zhao YX, Huang YZ. Study on the improvement of nano-silver penetration activity by membrane-penetrating peptide. *Chin J Mod Appl Pharm.* (2012) 29:865–8. doi: 10.13748/j.cnki.issn1007-7693.2012.10.002
26. Manivasagana P, Kanga KH, Kim DG, Kim SK. Production of polysaccharide-based bioflflocculant for the synthesis of silver nanoparticles by *Streptomyces* sp. *Int J Biol Macromol.* (2015) 77:159–67. doi: 10.1016/j.ijbiomac.2015.03.022
27. Ghosal K, Ghosh S, Ghosh D, Sarkar K. Natural polysaccharide derived carbon dot based *in situ* facile green synthesis of silver nanoparticles:

synergistic effect on breast cancer. *Int J Biol Macromol.* (2020) 162:1605–15. doi: 10.1016/j.ijbiomac.2020.07.315
28. Ma ZX, Liu J, Liu YC, Zheng XJ, Tang KY. Green synthesis of silver nanoparticles using soluble soybean polysaccharide and their application in antibacterial coatings. *Int J Biol Macromol.* (2020) 166:567–77. doi: 10.1016/j.ijbiomac.2020.10.214
29. Ran LX, Zou YN, Cheng JW, Lu F. Silver nanoparticles *in situ* synthesized by polysaccharides from *Sanghuangporus sanghuang* and composites with chitosan to prepare scaffolds for the regeneration of infected full-thickness skin defects. *Int J Biol Macromol.* (2018) 125:392–403. doi: 10.1016/j.ijbiomac.2018.12.052
30. Padinjarathil H, Joseph MM, Unnikrishnan BS, Preethi GU, Shiji R, Archana MG, et al. Galactomannan endowed biogenic silver nanoparticles exposed enhanced cancer cytotoxicity with excellent biocompatibility. *Int J Biol Macrimol.* (2018) 118:1174–82. doi: 10.1016/j.ijbiomac.2018.06.194
31. Wang LM, Zhang TL, Li PY, Huang WX, Tang JL, Wang PY, et al. Use of synchrotron, radiation-analytical techniques to reveal chemical origin of silver-nanoparticle cytotoxicity. *ACS Nano.* (2015) 9:6532–47. doi: 10.1021/acsnano.5b02483
32. Chakraborty B, Kumar RS, Almansour AI, Kotresha D, Rudrappa M, Pallavi SS, et al. Evaluation of antioxidant, antimicrobial and antiproliferative activity of silver nanoparticles derived from *Galphimia glauca* leaf extract. *J King Saud Univ Sci.* (2021) 33:101660. doi: 10.1016/j.jksus.2021.101660
33. Cameron S, Farah Hosseinian F, Willmore W. A current overview of the biological and cellular effects of nanosilver. *Int J Mol Sci.* (2018) 19:2030–70. doi: 10.3390/ijms19072030
34. Chavan RR, Bhinge SD, Bhutkar MA, Randive DS, Wadkar GH, Todkar SS, et al. Characterization, antioxidant, antimicrobial and cytotoxic activities of green synthesized silver and iron nanoparticles using alcoholic *Blumea eriantha* DC plant extract. *Mater Today Commun.* (2020) 24:101320. doi: 10.1016/j.mtcomm.2020.101320
35. Jing YS, Li JY, Zhang YW, Zhang RJ, Zheng YG, Hu BB, et al. Structural characterization and biological activities of a novel polysaccharide from *Glehnia littoralis* and its application in preparation of nano-silver. *Int J Biol Macrimol.* (2021) 183:1317–26. doi: 10.1016/j.ijbiomac.2021.04.178
36. Wang L, Xie J, Huang T, Ma Y, Wu Z. Characterization of silver nanoparticles biosynthesized using crude polysaccharides of *Psidium guajava* L. leaf and their bioactivities. *Mater Lett.* (2017) 208:126–9. doi: 10.1016/j.matlet.2017.05.014
37. Singh J, Kaur N, Rawat M. Eco-friendly approach for synthesis of silver nanoparticles and their catalytic application towards 4-nitrophenol to 4-aminophenol reduction. *Micro Nano Lett.* (2018) 13:1600–3. doi: 10.1049/mnl.2018.5139

Conflict of Interest: The authors declare that the research was conducted in the absence of any commercial or financial relationships that could be construed as a potential conflict of interest.

Publisher's Note: All claims expressed in this article are solely those of the authors and do not necessarily represent those of their affiliated organizations, or those of the publisher, the editors and the reviewers. Any product that may be evaluated in this article, or claim that may be made by its manufacturer, is not guaranteed or endorsed by the publisher.

Copyright © 2022 Jing, Cheng, Ma, Zhang, Li, Zheng, Zhang and Wu. This is an open-access article distributed under the terms of the Creative Commons Attribution License (CC BY). The use, distribution or reproduction in other forums is permitted, provided the original author(s) and the copyright owner(s) are credited and that the original publication in this journal is cited, in accordance with accepted academic practice. No use, distribution or reproduction is permitted which does not comply with these terms.

frontiers | Frontiers in Nutrition

ORIGINAL RESEARCH
published: 06 June 2022
doi: 10.3389/fnut.2022.914380

Quality Markers of *Dendrobium officinale* by "Oligosaccharide-Spectrum-Effect" Relationships

Ruimin Liu[1], Songshan Shi[1], Si Xiong[1], Juan Su[1], Xiaona Gan[2], Jianjun Wu[1], Huijun Wang[1] and Shunchun Wang[1]**

[1] *The MOE Key Laboratory for Standardization of Chinese Medicines and the SATCM Key Laboratory for New Resources and Quality Evaluation of Chinese Medicines, Institute of Chinese Materia Medica, Shanghai University of Traditional Chinese Medicine, Shanghai, China,* [2] *Nutrilite Health Institute, Amway (China) Co., Ltd., R&D Center, Shanghai, China*

Dendrobium officinale Kimura et Migo has been used as a traditional Chinese medicine (TCM) and a functional food for thousands of years. Carbohydrate is one of the most important effective substances and indicative components in *D. officinale*. However, since the qualitative and quantitative analysis of polysaccharides in *D. officinale* remains a challenge and limitation, herein, an oligosaccharide-quality marker approach was newly developed for quality assessment of *D. officinale* by spectrum–effect relationships between high performance liquid chromatographic (HPLC) fingerprints and anti-inflammatory effects. The HPLC fingerprints of 48 batches of oligosaccharides from *D. officinale* (DOOS) were developed and analyzed with similarity analysis (SA) and hierarchical cluster analysis (HCA), and eight common peaks were identified. *In vitro* screening experiment indicated that DOOS potentially inhibited nitric oxide (NO) production and effectively reduced the release of inflammatory cytokines, such as TNF-α, IL-6, and IL-1β in RAW 264.7 cells, thereby reducing the inflammatory response of cells. Finally, the HPLC fingerprint of different batches of DOOS was combined with *in vitro* anti-inflammatory activity to assess the spectrum–effect relationships of DOOS by gray correlation analysis (GCA), in addition, the purified oligosaccharide components were identified and validated for NO inhibitory activity. Our results showed four DOOS (maltotetraose, maltopentaose, maltohexaose, and mannohexaose) were relevant to anti-inflammatory effects and could be as quality markers for the quality control of *D. officinale*. It suggests that the "oligosaccharide-spectrum-effect" relationships approach is a simple and reliable method for the quality control of herb medicines or nutritious foods.

Keywords: ***Dendrobium officinale*, oligosaccharides, anti-inflammatory, spectrum-effect relationships, quality markers (Q-markers)**

OPEN ACCESS

Edited by:
Xin Wang,
Northwest A&F University, China

Reviewed by:
Xue Zhang,
Yangzhou University, China
Quanbin Zhang,
Institute of Oceanology (CAS), China

****Correspondence:***
Huijun Wang
huijun.wang@outlook.com
orcid.org/0000-0001-6319-498X
Shunchun Wang
shunchunwang@126.com
orcid.org/0000-0003-0384-1350

Specialty section:
This article was submitted to Food Chemistry, a section of the journal Frontiers in Nutrition

Received: *06 April 2022*
Accepted: *05 May 2022*
Published: *06 June 2022*

Citation:
Liu R, Shi S, Xiong S, Su J, Gan X, Wu J, Wang H and Wang S (2022) Quality Markers of Dendrobium officinale by "Oligosaccharide-Spectrum-Effect" Relationships. Front. Nutr. 9:914380. doi: 10.3389/fnut.2022.914380

INTRODUCTION

Dendrobium is one of the largest genera of orchids. More than 1,100 species of *Dendrobium* have been identified worldwide. A total of 74 species are found in China, of which more than 50 species can be used as China's precious *Dendrobium* Tea. *Dendrobium officinale* Kimura et Migo, Chinese name Tiepi Shihu, is a perennial herb in the biological classification of Orchidaceae

recorded in the Chinese Pharmacopeia (1–3). It is derived from the dried stems of *D. officinale*, traditionally considered to be the best tonic. *D. officinale* is a kind of a rare, endangered, and precious folk medicine and food, mainly distributed in Zhejiang, Anhui, and Yunnan provinces in China (4). *D. officinale* is removed from impurities and some fibrous roots are cut off, twisted into a spiral or spring shape while heating, and dried to obtain "Tiepi Fengdou." Nowadays, due to the extreme scarcity of wild resources and the increasing demand, Tiepi Fengdou has become one of the most expensive tea ingredients in the world. *Dendrobium* genus has high species diversity, inconspicuous macroscopic identification features, and a high price of Tiepi Fengdou, resulting in adulteration, confusion of varieties, and counterfeiting from time to time. *D. officinale* is valued for its medicinal uses and has a history of thousands of years in traditional Chinese medicine (TCM) (5). Medication history shows that *D. officinale* has the effects of clearing internal heat, nourishing Yin, benefiting the stomach, and generating body fluid (6). *D. officinale* possesses hepatoprotective, anti-tumor, hypoglycemic, gastro-protective, anti-inflammatory, immunomodulatory, and vasodilating effects. Anti-inflammatory is one of the most important biological effects of *D. officinale*, which is an essential causative factor in many diseases such as Alzheimer's disease (AD), type 2 diabetes, and so on (7, 8).

Recently, many components from *D. officinale*, such as alkaloids, flavonoids, amino acids, and polysaccharides have been reported to have important bioactivities, including anti-inflammatory activity (9–12), especially the reports on *D. officinale* polysaccharides (DOPS). DOPS is the indicator component identified under the item of *D. officinale* in the Chinese Pharmacopeia, and many reports confirmed that DOPS exhibited anti-inflammatory activity (13). Previous research mentioned that glucomannans (GMs) from different plants including *D. officinale* played an important role in their anti-inflammatory properties. Furthermore, the high molecular weight may negatively affect their beneficial effect (14). It has also been noted that for some polysaccharides, molecular degradation modification is required to enhance their activity by reducing their molecular weight to improve their solubility in the water phase, and the quality control for DOPS is very difficult and limited (15). It is suggested that the natural oligosaccharides present in the plant itself have a lower molecular weight and greater solubility, foreshadowing that oligosaccharides may exhibit similar or even greater activity. Moreover, there was a lack of studies for the determination of the anti-inflammatory activity of oligosaccharides from *D. officinale* (DOOS), and also the investigation of anti-inflammatory DOOS was insufficient. Therefore, it is hypothesized to establish a fast and effective method to identify and improve the true and false quality of *D. officinale* by exploring anti-inflammatory DOOS markers.

The quality standard of most TCM is the determination of single or multiple active ingredients or characteristic ingredients that are not related to their efficacy. To establish a quality control and quality traceability system of TCM, a new concept of quality marking (Q-marker) has been proposed in recent years. Q-markers refer to the inherent chemical components of TCM or compounds produced during the preparation process. Their biological activities are closely related to the functional properties of TCM, and their chemical structures have been clarified. Q-markers can be closely linked to the material basis, effectiveness, and quality control of TCM. High performance liquid chromatographic (HPLC) fingerprint is a useful tool to identify the authenticity of TCM, evaluate the quality, and distinguish the components of TCM (16). The spectrum–effect relationship that determines the correlations between fingerprints and biological activity is a scientific method for elucidating the pharmacodynamic basis and establishing a method for controlling the quality of TCM. Determining the spectral–effect relationship between fingerprints and biological activity is a scientific method to clarify the basis of pharmacodynamics and establish quality control methods for TCM. It has been used to explore the biologically active components of TCM, combined with various statistical methods such as regression analysis (RA), hierarchical cluster analysis (HCA), principal component analysis (PCA), orthogonal partial least squares discriminant analysis (OPLS-DA), and gray correlation analysis (GCA). Among them, GCA is a simple and effective method to evaluate the relationship of spectrum effects by judging the correlation grade between factors based on the similarity of the geometry of the change curve of each factor (17, 18), although the China State Food and Drug Administration recommends that all chromatographic fingerprints should be evaluated by similarity analysis (SA).

In this study, the HPLC- charged aerosol detector (CAD) fingerprints combined with the inhibition of nitric oxide (NO) secretion of RAW264.7 cells by different batches of DOOS were evaluated by GCA to determine the spectrum–effect relationships of DOOS active components. Meanwhile, the purified oligosaccharide components were characterized and validated for NO inhibition activity *in vitro*. Due to the singularity of the Chinese Pharmacopeia in the selection of quality control index components of *D. officinale*, the opportunity for adulteration and substandard is made available. As a result, DOOS may potentially become a powerful quality marker for the identification and quality control of *D. officinale*.

MATERIALS AND METHODS

Materials

Forty-seven batches of *D. officinale* raw material samples (S1–S47) were collected from Zhejiang, Fujian, Yunnan, and other regions at diverse periods. The various sources of the samples are shown in **Supplementary Table 4** and were authenticated by *Prof*. L.H. Wu from the Institute of Chinese Materia Medica, Shanghai University of Traditional Chinese Medicine, and the reference batch (S48) was purchased from China National Institute for Food and Drug Control.

Chemicals and Reagents

Deionized water was obtained through a Milli-Q water purification system (Millipore, Bedford, MA, United States). HPLC grade acetonitrile was purchased from Aladdin Chemistry Co., Ltd (Shanghai, China). Formic acid for chromatographic

analysis was obtained from J.T. Baker (Phillipsburg, PA, United States). Ammonium formate was provided by Sigma Aldrich (Sigma Aldrich, St. Louis, MO, United States). The standards of sucrose, maltotriose, maltotetraose, maltopentaose, maltohexaose, maltoheptaose, maltooctaose, mannobiose, mannotriose, mannotetraose, mannopentaose, and mannohexaose were purchased from Aladdin (Shanghai, China). Monosaccharides D-glucose (Glc), D-galactose (Gal), L-arabinose (Ara), L-rhamnose (Rha), D-mannose (Man), D-xylose (Xyl), and L-fucose (Fuc), as well as trifluoroacetic acid (TFA) were obtained from Sigma Aldrich (St Louis, MO, United States). Molecular weight 6100 standard was purchased from Shodex Co. (Tokyo, Japan). CNWBOND Carbon-GCB Cartridge (500 mg, 6 mL) was from Shanghai Ampel Scientific Instrument (China) and D_2O (99.8 Atom% Deuterium) was from Schweres Wasser, United States). Fetal bovine serum (FBS), Dulbecco's modified Eagle medium (DEME medium), PBS, trypsin, and penicillin/streptomycin were obtained from Gibco (Grand Island, NY, United States). LPS (lipopolysaccharide) was obtained from Sigma Aldrich (St Louis, MO, United States). CCK-8 was purchased from Yeasen Biotech Co., Ltd. (Shanghai, China). NO assay kit was purchased from Nanjing Jiancheng Bioengineering Institute (Nanjing, China). Commercial ELISA kits were bought from Sigma Aldrich (Sigma Aldrich, St. Louis, MO, United States). RAW264.7 cells were obtained from the American Type of Culture Collection (ATCC, Manassas, VA). All chemicals used were of analytical-reagent grade unless stated otherwise.

High Performance Liquid Chromatographic-Charged Aerosol Detector Fingerprint Assessment

High Performance Liquid Chromatographic-Charged Aerosol Detector Sample Preparation

Extraction conditions were designed to maximize DOOS preparation yield. The three-dimensional response surface and two-dimensional contours drawn by Design Expert software showed the optimized extraction parameters of the DOOS as follows: extraction temperature 70°C, extraction time 2 h, extraction times twice, and the ratio of solution to material 60 mL/g by Design Expert software (Supporting information, Part I).

All batches of samples were dried at 60°C using hot air to a constant weight and then ground to a fine powder that could pass through a 50-mesh sieve. Each batch of sample powder was extracted with 0.5 g under the same conditions. The extraction conditions were controlled as follows: extraction temperature 70°C, extraction time 2 h, extraction times twice, and the ratio of solution to material 60 mL/g. The extraction solution was prepared by weight-relief method to compensate for the weight lost during the two extractions. The aqueous extracts were combined and centrifuged at 10,000 × g for 10 min, then 30 mL of supernatant was precisely removed, and 120 mL of anhydrous ethanol was added to the supernatant to ensure that the final concentration of ethanol in the mixture was 80% (v/v) and kept at 4°C for 12 h. After centrifuging at 10,000 × g for 10 min, the supernatant was concentrated to dryness and dissolved with 1 mL of deionized water.

Previous extraction studies have shown that oligosaccharides can be largely retained by graphitized carbon (19). In this context, Carbon–GCB SPE Cartridge (CNW, Shanghai) was used to obtain oligosaccharides from solutions. Prior to use, the packing should be washed with 6 mL deionized water, methanol, and deionized water, respectively. A total of 1 mL of the extract obtained by the above method was added and centrifuged (10,000 × g for 10 min), and the supernatant was applied to the activated Carbon-GCB SPE Cartridge. Salts and monosaccharides were washed off with 6 mL of deionized water, while the oligosaccharides were adsorbed to Carbon-GCB SPE Cartridge, then eluted with 6 mL 50% concentration of methanol in deionized water and dried. The samples were dissolved in 0.5 mL of deionized water and kept at 4°C for HPLC-CAD analysis.

The Fingerprint Analysis

The HPLC chromatographic fingerprint analysis was performed by HPLC U3000 with a Corona® CAD (Thermo Scientific, Idstein, Germany). A Prevail Carbohydrate ES column (250 mm × 4.6 mm, 5 μm, Grace) was used to separate the samples at 45°C. The mobile phase was composed of acetonitrile as the phase A and 30 mM ammonium formate with 0.3% formic acid in deionized water as the phase B. The gradient elution program was set as follows: 0-60 min, 20–50% B; 60-80 min, 50% B. The injection volume was 10 μL and the flow rate was set to 1 mL/min. The settings for the CAD were as follows: data collection rate, 20 Hz; filter, 5.0; and evaporation temperature, 35°C. Data acquisition and analysis were performed using Thermo ScientificTM Dionex Chromeleon 7.2 SR4 software.

Validation of High Performance Liquid Chromatographic-Charged Aerosol Detector Method

To ensure the reliability of the method, precision, repeatability, and stability of the method were verified in this study. The precision of the analysis was determined by injecting the same sample solution six times in succession. The stability of DOOS solution was verified by analyzing at 0, 2, 4, 8, 16 and 24 h, respectively. The repeatability of the method was assessed by analyzing six independently prepared sample solutions from the same batch of *D. officinale*. Finally, the method was evaluated by RSD. The method was evaluated by determining the RSD of relative retention time (RRT) and the relative peak area (RPA) of compounds to assess the precision, stability, and repeatability.

Similarity of High Performance Liquid Chromatographic-Charged Aerosol Detector Analysis

Similarity analysis was analyzed by the software Similarity Evaluation System for Chromatographic Fingerprint of Traditional Chinese Medicine software (Version 2004A). The spectrum of sample S48 was used as the reference spectrum, which was obtained from China National Institute for Food and Drug Control; the fingerprints were automatically matched and established. Subsequently, the median method was used to compare the fingerprints of each batch, and the

similarity between the reference fingerprint and each batch chromatogram was calculated.

Hierarchical Clustering Analysis

Hierarchical clustering analysis (HCA) is a multivariate analysis method that classifies samples into clusters (20). In the present study, HCA of 48 batches DOOS was performed using by SPSS 22 (SPSS Inc., United States) software.

Identification of Common Peaks

Isolation and Purification of DOOS

Dendrobium officinale powder (500 g) was extracted with the response surface optimized extraction method and the extracts were mixed and concentrated in a rotary evaporator at 60°C under reduced pressure. The concentrated solution was centrifuged at 4,000 × *g* for 20 min to remove insoluble contaminants. To ensure that the final concentration of ethanol in the mixture is 80% (v/v), anhydrous ethanol was added to the supernatant. The supernatant was kept at room temperature for 12 h and collected after centrifugation at 4,000 × g for 20 min. Then the supernatant was concentrated at 60°C under reduced pressure and then lyophilized to obtain crude oligosaccharides.

The crude oligosaccharides were dissolved sufficiently with distilled water and then centrifuged at 10,000 × g for 10 min. The supernatant was loaded on a graphitized carbon–diatomite column which was mixed in a ratio of 1:1. Then it was eluted with distilled water (DOOS-W), 20% ethanol solution (DOOS-20), and 50% ethanol solution (DOOS-50), respectively. DOOS-20 was further purified using a CAPCELL PAK C18-AQ (10 mm × 250 mm, 5 μm) preparative column at a flow rate of 2 mL/min and collected separately according to the chromatographic results. Each purified portion of DOOS-20 (10 mg/mL) was analyzed by the established HPLC-CAD fingerprint method and compared with the behavior of the standards (10 mg/mL), respectively.

Monosaccharide Composition Analysis

DOOS-20 of each purified oligosaccharide was weighed at 1 mg and then hydrolyzed with 2 M TFA for 2 h at 100°C. After neutralization with 2 M NaOH, the oligosaccharides were reduced with $NaBH_4$ in a water bath at 40°C for 90 min according to the method of Lehrfeld (21) and acetylated with Ac_2O for 10 min at 40°C. The resulting alditol acetates were subjected to GC-Mass Spectrum analysis. Data were analyzed with Agilent MassHunter Workstation.

High-Performance Liquid Chromatography Quadrupole Time-of-Flight Spectroscopy Analysis

The HPLC-Quadrupole Time of Flight (QTOF)-Mass Spectrum (MS) analysis was performed on an Agilent 1290 Infinity system coupled to an Agilent 6546 Quadrupole Time of Flight mass spectrometer (Santa Clara, CA, United States) equipped with an electrospray ionization (ESI) interface. The Mass Spectrum system was run in negative ionization mode and the Mass Spectrum conditions were as follows: gas temperature 320°C, drying gas flow 8 L/min, nebulizer 35 psi, sheath gas temperature 350°C, sheath gas flow 11 L/min, capillary voltage 3500 V, skimmer voltage 65 V, octupole RF voltage 750 V, fragmentor voltage 175 V. The full-scan mass range was 50–1,700 Da. Accurate mass measurements were obtained by using a calibration solution which contains the internal reference masses at *m/z* 112.9855 and 1033.9881 in negative mode. Data were analyzed with Agilent MassHunter Workstation.

Nuclear Magnetic Resonance Analysis

DOOS-20 of each purified oligosaccharide (5–20 mg) was dissolved in 0.4 mL D_2O (99.8 Atom% Deuterium; Schweres Wasser, United States), separately. Nuclear magnetic resonance (NMR) spectra were recorded using the Bruker Avance III 600 Spectrometer (Bruker Instruments, Inc., Billerica, MA, United States) at 25°C. All the experiments were recorded, and data were processed using standard Bruker software and MestReNova.

Anti-inflammatory Activity of DOOS *in vitro*

Cell Culture and Cytotoxicity

RAW264.7 cells were cultured at 37°C in Dulbecco's modified eagle's medium (DMEM) containing 1% PS (Penicillin–Streptomycin) solution and 10% FBS in a 5% CO_2 atmosphere. RAW267.4 cells were inoculated overnight in 96-well plates at a density of 4×10^4 cells/well and then pretreated with different concentrations of DOOS (40, 20, 10, 5, 2.5 mg/mL, the concentration of the drug is calculated by the mass of the corresponding raw herb) for 1 h, followed by stimulation with 1 μg/mL of LPS for 24 h. Then 20 μL of CCK-8 solution was added to each well. Absorbance was measured at 450 nm using a microplate reader (Biotek, United States) after 30 min incubation. All experiments were performed in triplicate and repeated at least three times. Data are expressed as a percentage relative to untreated control cells.

Nitrite Determination

RAW267.4 cells were inoculated overnight in 96-well plates at a density of 4×10^4 cells/well and then pretreated with different concentrations of DOOS (20, 10, 5, 2.5, 1.25, 0.625 mg/mL, the concentration of the drug is calculated by the mass of the corresponding raw herb) for 1 h. In addition, aminoguanidine hydrochloride (50 μg/mL) was used as a positive control (22). After incubation for 1 h, LPS was added at a concentration of 1 μg/mL and incubated for 24 h. The concentration of nitrite accumulated in the culture solution was measured according to the Griess reaction as an indicator of NO production (23). The absorbance was monitored at 540 nm with a microplate reader. All experiments were performed in triplicate and repeated at least three times.

Measurements of Cytokines by Enzyme-Linked Immunosorbent Assay

RAW267.4 cells were inoculated overnight in 24-well plates at a density of 2×10^5 cells/well and then pretreated with different concentrations of DOOS (20, 10, 5, 2.5, 1.25, 0.625 mg/mL, the concentration of the drug is calculated by the mass of the corresponding raw herb) for 1 h. In addition, dexamethasone (40 μM) was used as a positive control (24). After 1 h of incubation, LPS was added at a concentration of 1 μg/mL for

24 h. Culture medium was collected for the determination of inflammatory cytokines. The levels of TNF-α, IL-6, and IL-1β were tested using the commercially available ELISA kits according to the manufacturer's instruction. All experiments were performed in triplicate and repeated at least three times.

Nitrite Determination for Different Batches

In this paper, different batches of DOOS were incubated at the same concentration (5 mg/mL, the concentration of the drug is calculated by the mass of the corresponding raw herb) in a model of LPS-induced inflammation in RAW264.7 macrophages, aminoguanidine hydrochloride (50 μg/mL) was used as a positive control, and the nitrite accumulated in culture medium was detected with Griess reagent. The inhibition rate of NO was calculated to evaluate the anti-inflammatory activity of different batches of DOOS.

Nitrite Determination for Each Purified Oligosaccharide of DOOS-20

In the present study, each purified oligosaccharide of DOOS-20 was incubated in the LPS-induced inflammation in RAW264.7 macrophages at the same concentration gradients (400, 200, 100, 50, 25 μg/mL) with aminoguanidine hydrochloride (50 μg/mL) as the positive control. The release of nitrite accumulated in the culture medium was detected with Griess reagent.

Spectrum-Effect Relationships Analysis

In this study, GCA was used to evaluate the spectrum-effect relationships between common peaks in HPLC-CAD fingerprints and anti-inflammatory activity with SPSS 22. Before data analysis, all raw data should be normalized by equation (1) to eliminate the differences caused by different dimensions, where Xmax and Xmin refer to the maximum and minimum values in the sequence, respectively.

$$\mathrm{X} = \frac{\text{X-Xmin}}{\text{Xmax} - \text{Xmin}} \tag{1}$$

The inhibition rate of LPS-induced NO secretion from RAW264.7 cells by different batches of DOOS was used as the reference sequence and recorded as X_0 (k), and the peak area of the common peaks shared by the fingerprints of each batch of DOOS was used as the comparison sequence and recorded as Xi (k). The correlation coefficient (ξ_i (k)) and the gray correlation grade (γ_i) were calculated as follows:

$$\xi_i(\mathrm{k}) = \frac{\min_{\mathrm{i}} \min_{\mathrm{k}} \left|X_0(k) - X_i(k)\right| + \rho \max_i \max_k \left|X_0(k) - X_i(k)\right|}{\left|X_0(k) - X_i(k)\right| + \rho \max_i \max_k \left|X_0(k) - X_i(k)\right|} \tag{2}$$

$$\gamma_i = \frac{1}{N} \sum_{k\ 1}^{n} \xi_i(\mathrm{k}) \tag{3}$$

where k is different batches of DOOS, ρ is the distinctive coefficient lying between $0 < \rho < 1$ and it is generally set as 0.5, and $\max_i \max_k \left|X_0(k) - X_i(k)\right|$ and $\min_{\mathrm{i}} \min_{\mathrm{k}} \left|X_0(k) - X_i(k)\right|$ represent the maximum and the minimum difference between the two levels, respectively.

Data Analysis

The experimental data are expressed as the means ± SD and analyzed with Graphpad Prism 7. One-way ANOVA was used to examine differences among groups. The value of $P < 0.05$ was considered statistically significant.

RESULTS AND DISCUSSION

Validation of High Performance Liquid Chromatographic-Charged Aerosol Detector Method

The HPLC-CAD method was established for the fingerprinting of DOOS, as well as the precision, stability, and reproducibility of the method were evaluated. According to the results shown in the **Supplementary Table 5**, peak 1 was used as the reference peak, the RSD values of RRT and RPA for precision, stability, and repeatability did not exceed 3%, indicating that the apparatus precision was satisfactory, the method repeatability was adequate, and the sample solutions were stable within 24 h.

Fingerprint Analysis and Similarity Evaluation

Graphitized carbon can be used as a solid-phase extraction cartridge to purify oligosaccharides from the solution (25). In this context, Carbon-GCB SPE Cartridge was used to purify the oligosaccharides from the extracts, and different batches of DOOS were analyzed by HPLC-CAD. A total of 48 batches of DOOS samples were analyzed by using the software Chinese Medicine Fingerprint Similarity Evaluation (2004A Version). The HPLC chromatogram was recorded and the results are shown in **Figure 1A**, and ten common characteristic peaks were observed. The spectrum of standard sample S48 was selected as the reference spectrum, and the software automatically matched the peaks by multi-point calibration. A reference fingerprint was generated by the selected median method, as shown in **Figure 1B**. The similarity values between the chromatogram for each batch were calculated, and the results are shown in **Supplementary Table 6**. According to the result listed in **Supplementary Table 6**, the similarity index was in a range of 0.222–0.995, indicating that there was a large difference between batches of different origins, thus it is reasonable to suspect that it may be due to differences in climate and growth environment of different origins.

Results of Hierarchical Clustering Analysis

To validate the results of the SA and further elucidate the similarity relationships among these samples, HCA analysis was performed and the results are shown in **Figure 2**. HCA in this study showed that the specimens could be divided into two clusters, where S4, S9, S10, S11, S12, S13, S14, S27, S45, and S47

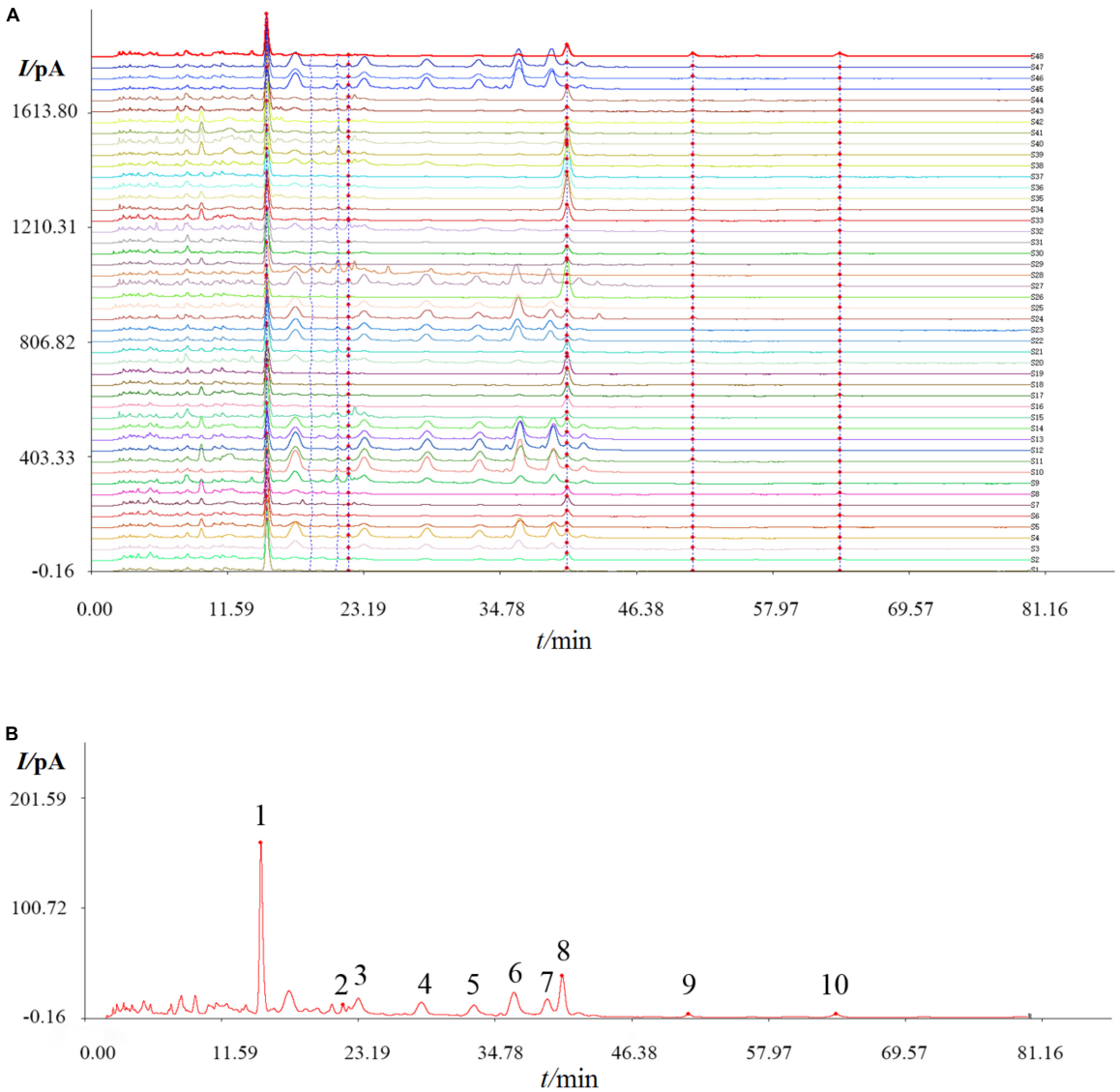

FIGURE 1 | High performance liquid chromatographic (HPLC) fingerprint of 48 batches of DOOS **(A)**, and the reference chromatogram **(B)** that was obtained by using the software Chinese Medicine Fingerprint Similarity Evaluation (2004A Version). Common peaks were marked with 1–10 in the chromatogram.

were classified in group 1 and the rest were in group 2, which was divided into two subgroups again. S45 and S47 were in group 1–2 and the others were in group 1–1, while S18, S19, S26, S33, S34, S35, S36, S37, S38, and S39 were in group 2-1 and the others were in group 2-2. Compared with the results of SA, group 1 had higher similarity with the reference crude drug, while group 2 was less similar compared with other batches, suggesting that origins and harvesting season had a greater influence on the quality of *D. officinale*.

Identification of Common Peaks

Isolation and Purification of DOOS

The crude oligosaccharides were extracted from the stems of *D. officinale* by response surface optimization method and fractionated by graphitized carbon-diatomite column chromatography to obtain 20% ethanol solution (DOOS-20), which were further purified by CAPCELL PAK C18-AQ preparative column (**Figure 3A**). The purified samples were lyophilized and analyzed by HPLC-CAD at a concentration of 10 mg/mL and checked against mixed standards of glucose, sucrose, malto-oligosaccharide (DP3–DP8), and mannan-oligosaccharide (DP2–DP6) mixed standards (**Figure 3B**). As shown in **Figure 3B**, DOOS-20-1 was a monosaccharide and would not be considered for subsequent studies of oligosaccharide components. DOOS-20-2, DOOS-20-3, DOOS-20-4, DOOS-20-5, DOOS-20-6, DOOS-20-7, and DOOS-20-8 may be DP2-DP8, respectively. However, peak 9 and peak 10 in **Figure 1** cannot be obtained due to low yield rates.

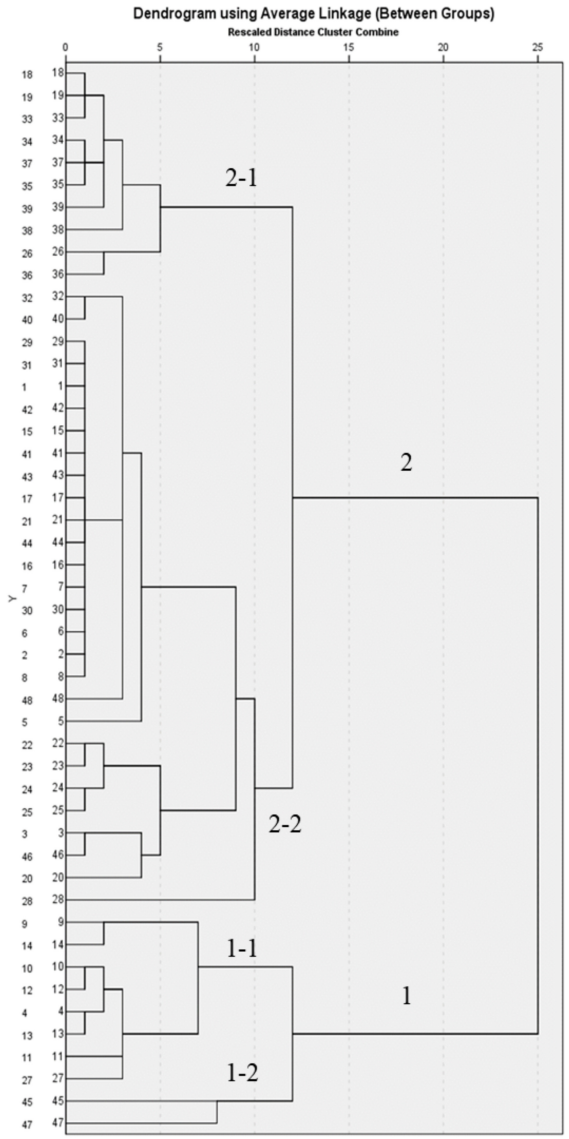

FIGURE 2 | Dendrograms of 48 batches of DOOS resulting from hierarchical clustering analysis.

Monosaccharide Composition Analysis

The results of monosaccharide composition are shown in **Figure 3C**. Compared with the monosaccharide standards, the monosaccharide peaks of DOOS-20-3, DOOS-20-4, DOOS-20-5, DOOS-20-6, and DOOS-20-8 were glucose and the monosaccharide peak of DOOS-20-7 was mannose. The monosaccharide composition of DOOS-20-2 was mannose and glucose.

High Performance Liquid Chromatographic-Quadrupole Time of Flight-Mass Spectrum Analysis

In the present study, HPLC-Quadrupole Time of Flight-Mass Spectrum was applied in negative ion mode to determine the quasi-molecular ions $[M–H]^-$ of each purified section of DOOS-20. The information was presented in **Table 1** and **Supplementary Figure 5**, including quasi-molecular ions $[M–H]^-$, molecular formula, and degree of polymerization (DP).

Nuclear Magnetic Resonance Analysis

To further confirm the oligosaccharide structure of each purified section of DOOS-20, Nuclear magnetic resonance analysis was performed. According to the characteristic signals, the ^1H, ^{13}C, and DEPT 135 Nuclear magnetic resonance spectra are shown in **Supplementary Figure 6**. Integrating the monosaccharide composition, molecular weight, and Nuclear magnetic resonance spectra, the following is known: DOOS-20-2 (peak 1) is sucrose (26). In the monosaccharide composition analysis, the reduction of fructose produces a mixture of sorbitol and mannitol, resulting in the appearance of a glucose peak together with a mannose peak. In accordance with the Nuclear magnetic resonance spectra as well as the monosaccharide composition, it is known that DOOS-20-3 (peak 3), DOOS-20-4 (peak 4), DOOS-20-5 (peak 5), DOOS-20-6 (peak 6), and DOOS-20-8 (peak 8) were maltotriose, maltotetraose, maltopentaose, maltohexaose, and maltoheptaose (27), respectively. DOOS-20-7 (peak 7) was mannohexaose (28).

Anti-inflammatory Activity of DOOS *in vitro*

Effect of DOOS on Cell Viability

Before assessing the potential anti-inflammatory activity of DOOS, the effect of DOOS on RAW 264.7 cell viability was first assayed and the results are shown in **Figure 4A**. The results of the CCK-8 assay showed that DOOS at concentrations of 40, 20, 10, 5, 2.5 mg/mL (concentration of the drug is calculated by the mass of the corresponding raw herb) had no cytotoxic effect on RAW 264.7 cells. It was confirmed that the effect of DOOS on RAW 264.7 cells was not caused by the reduction of cell viability.

Nitrite Determination

Macrophage cells play an essential role in the inflammatory process, and lipopolysaccharide (LPS) is one of the most widely used pro-inflammatory stimulators that can activate macrophages and trigger the inflammatory response (29). Recognition and binding of LPS by Toll-like receptor 4 (TLR4) or CD14 specific receptors on the cell membrane leads to the activation of macrophages and increased secretion of inflammatory mediators such as NO (30). The accumulation of the stable metabolite nitrite in the culture supernatant was measured with Griess reagent to evaluate the effect of DOOS on NO production by RAW 264.7 cells. According to the results shown in **Figure 4B**, compared with the control group, LPS significantly ($p < 0.001$) promoted NO production in macrophages. Furthermore, compared with the group that was treated with LPS, pretreatment with DOOS resulted in an inhibition of the NO production in RAW 264.7 cells, and a clear concentration-dependent manner has been shown between different concentrations, which indicated that DOOS had a strong anti-inflammatory activity.

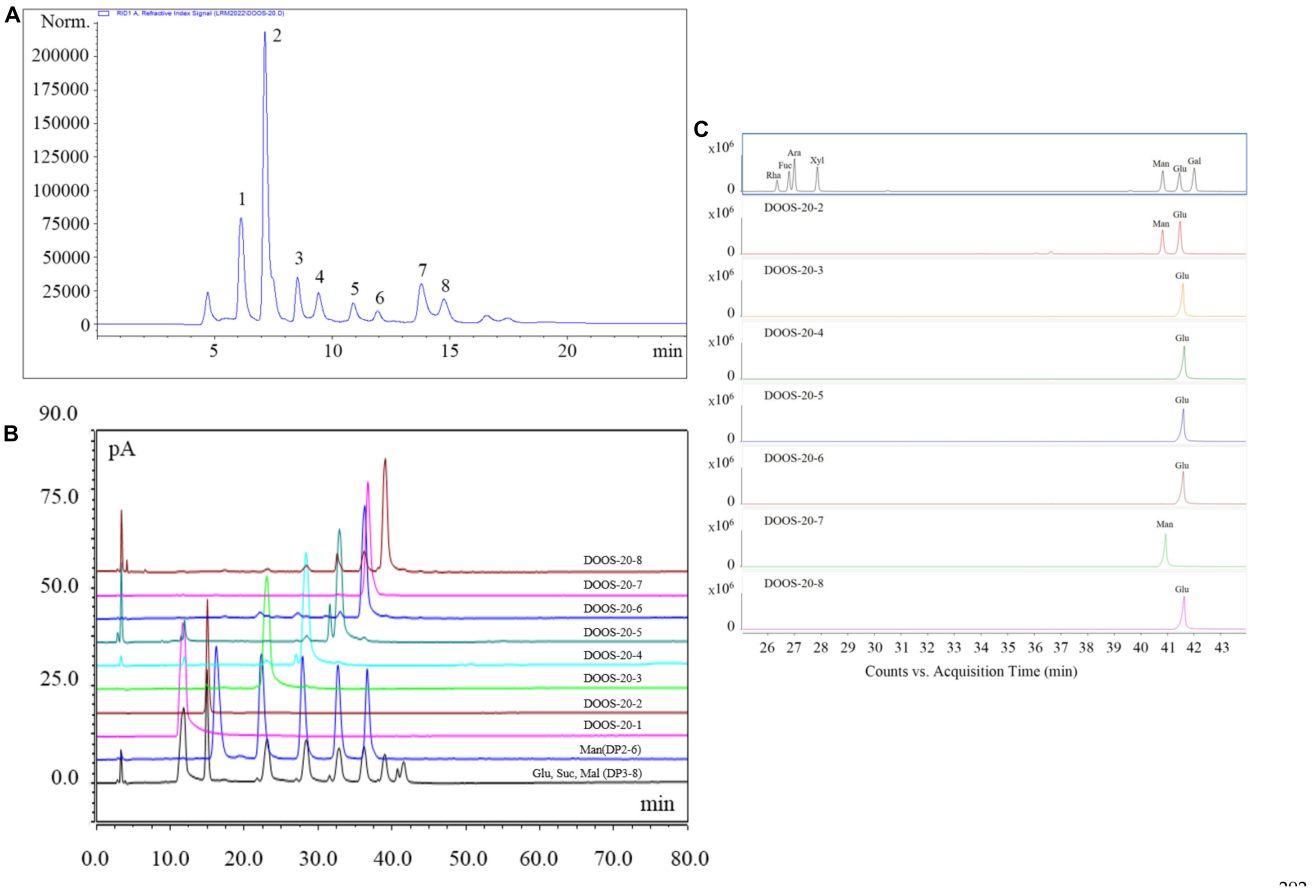

FIGURE 3 | (A) CAPCELL PAK C18-AQ preparative column chromatography elution curve of DOOS-20; **(B)** HPLC-CAD chromatography results of DOOS-20 purified sections and mixed standards of glucose, sucrose, malto-oligosaccharide standard (DP3-8), and mannan-oligosaccharide standard (DP2-6) control; **(C)** Monosaccharide composition analysis of DOOS-20 purified sections.

TABLE 1 | Structure identification of each purified section of DOOS-20.

Sample	$[M–H]^-$ (*m/z*)	Δ ppm	Molecular Formula	monosaccharide composition	DP	Structure
DOOS-20-2	341.1092	0.59	$C_{12}H_{22}O_{11}$	Man, Glu*	2	
DOOS-20-3	503.1617	−0.17	$C_{18}H_{32}O_{16}$	Glu	3	
DOOS-20-4	665.2150	0.46	$C_{24}H_{42}O_{21}$	Glu	4	
DOOS-20-5	827.2676	0.17	$C_{30}H_{52}O_{26}$	Glu	5	
DOOS-20-6	989.3204	0.09	$C_{36}H_{62}O_{31}$	Glu	6	
DOOS-20-7	989.3204	0.09	$C_{36}H_{62}O_{31}$	Man	6	
DOOS-20-8	1151.3730	−0.08	$C_{42}H_{72}O_{36}$	Glu	7	

: Glucose; : Mannose; : Fructose. DP: Degree of Polymerization.

**The reduction of fructose produces a mixture of sorbitol and mannitol, resulting in the appearance of a glucose peak together with a mannose peak.*

Measurements of Cytokines by Enzyme-Linked Immunosorbent Assay

Macrophages play an essential role in the inflammatory response through the release of a variety of factors, and in addition to NO, inflammatory cytokines such as TNF-α, IL-6, and IL-1β were used as representative cytokines in response to an activating stimulus (e.g., LPS) (31, 32). The concentrations of TNF-α, IL-6, and IL-1β in the culture medium were measured using commercial ELISA kits and the results are shown in **Figure 4C**. In comparison with the control group, LPS significantly ($p < 0.001$) increased the release of TNF-α (C1), IL-6 (C2), and IL-1β (C3). Furthermore, incubation with different concentrations of DOOS could effectively reduce the release of inflammatory cytokines and had a significant concentration-dependent manner, suggesting that DOOS had an inhibitory effect on the release of inflammatory cytokines.

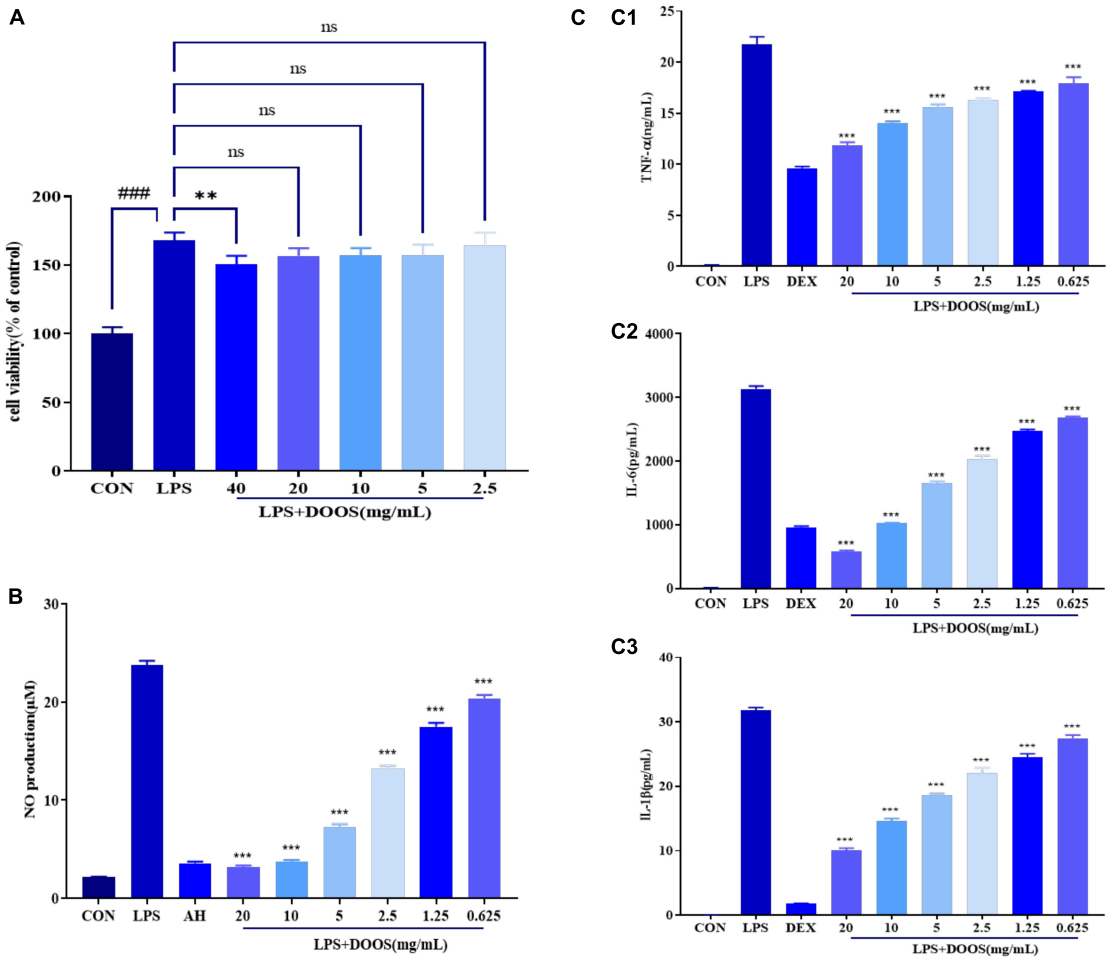

FIGURE 4 | (A) Effect of DOOS on the viability of RAW 264.7 cells. RAW 264.7 cells were incubated with different concentrations of DOOS and LPS (1 μg/mL) for 24 h. Cell viability was determined by CCK-8 assay. **(B)** Effects of DOOS on the production of NO in LPS-induced RAW 264.7 cells. The cells were treated with different concentrations of DOOS for 1 h prior to stimulation and LPS (1 μg/mL) for 24 h. **(C)** Effects of DOOS on TNF-α **(C1)**, IL-6 **(C2)**, and IL-1β **(C3)** secretion. The cells were treated with different concentrations of DOOS for 1 h prior to stimulation and LPS (1 μg/mL) for 24 h. Then the supernatant was collected to test cytokines production by ELISA. Values show the means and standard deviations of different concentrations performed in triplicate. $^{***}p < 0.001$ and $^{**}p < 0.01$ vs. LPS group; ns, no significance; $^{###}p < 0.001$ vs. control group.

Nitrite Determination for Different Batches

The DOOS could differentially inhibit the secretion of NO and inflammatory factors such as TNF-α, IL-6, and IL-1β, and it has a clear concentration-dependent manner between different concentrations, especially, the potential for inhibiting NO secretion is remarkable. Therefore, NO inhibition rate was selected to evaluate the anti-inflammatory activity of different batches of DOOS in this study. According to the results shown in **Figure 5A**, it indicated that different batches of DOOS exhibited a significant difference in the rate of inhibition of LPS-induced NO secretion from RAW 264.7 macrophages under the same dose conditions, in which S8 (Wuyi, Zhejiang), S13 (Yandang Mountain, Zhejiang), and S37 (Gengma, Yunnan) showed the strongest inhibition of NO secretion. It suggested that the differences in the NO secretion inhibitory activity of DOOS from different batches may be related to the differences in the content of anti-inflammatory components in different batches.

Established and Verified Spectrum–Effect Relationships Based on Oligosaccharides

Established Spectrum–Effect Relationships Between High Performance Liquid Chromatographic -Charged Aerosol Detector Fingerprints and Anti-inflammatory Activities

Gray correlation analysis was performed with SPSS 22 software to evaluate the spectrum–effect relationships between the 10 common peak areas in the HPLC-CAD fingerprints and anti-inflammatory activities, and the results of the correlation coefficients were expressed as a heat map shown in **Figure 6**. The gray correlation grade was calculated and ranked according to the gray correlation coefficient, which was shown in **Table 2**. Based on correlation coefficients, the contribution of each peak to the anti-inflammatory activity was in the order of

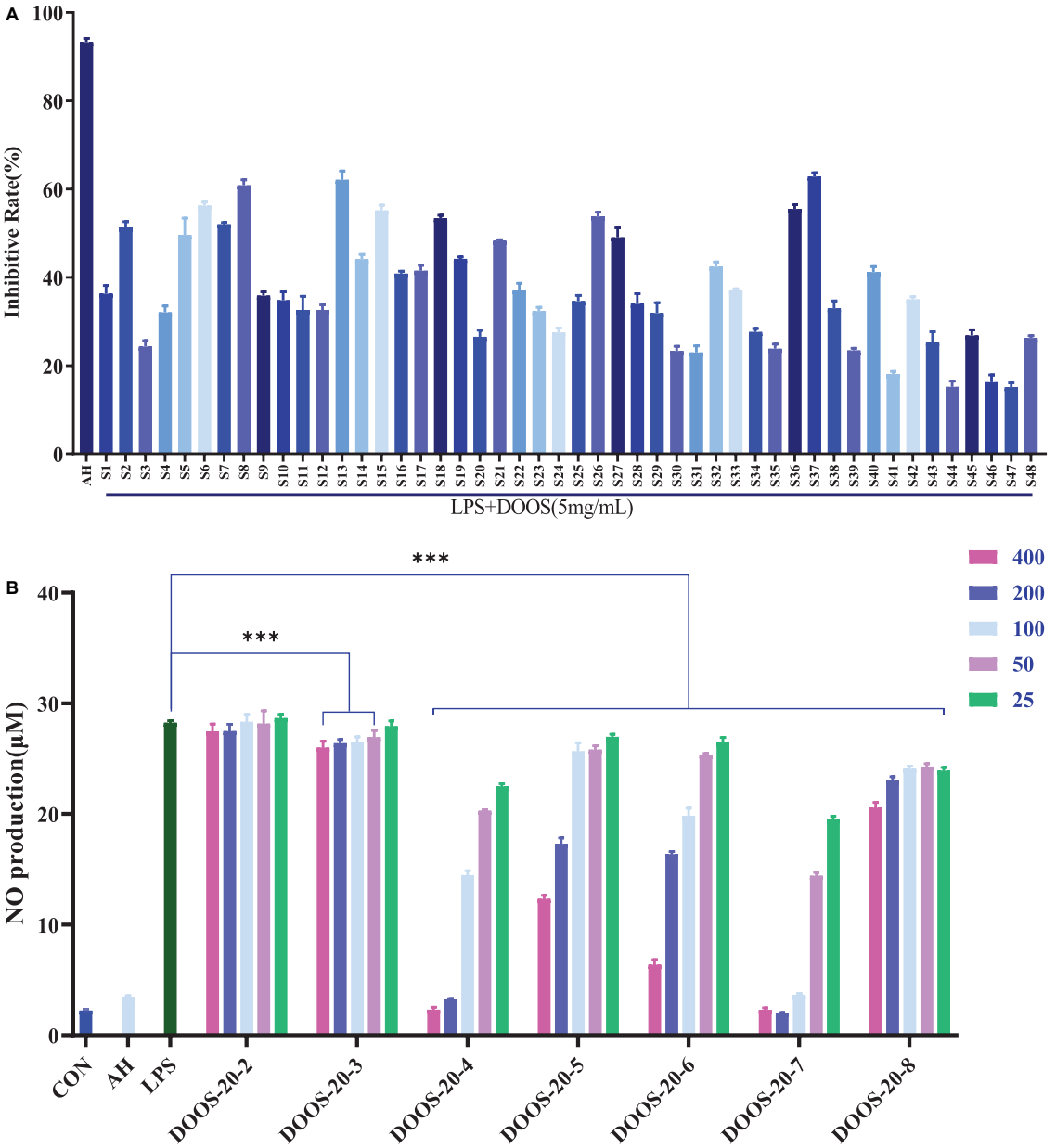

FIGURE 5 | (A) Nitric oxide (NO) inhibition rate of LPS induced RAW 264.7 cells with different batches of DOOS. The cells were treated with different batches of DOOS (5 mg/mL, the concentration of the drug is calculated by the mass of the corresponding raw herb) for 1 h prior to stimulation and LPS (1 μg/mL) for 24 h. Values show the means and standard deviations of different concentrations performed in triplicate. **(B)** Effects of DOOS-20 at different concentration gradients (400, 200, 100, 50, 25 μg/mL) in each purified section on production of NO in LPS induced RAW 264.7 cells. The cells were treated with different concentration sof DOOS-20 each purified section for 1 h prior to stimulation and LPS (1 μg/mL) for 24 h. Values show the means and standard deviations of different concentrations performed in triplicate. ***$p < 0.001$ significantly different from the LPS group; ns, no significance.

P7 > P4 > P2 > P9 > P5 > P10 > P6 > P3 > P8 > P1, where the correlation coefficient of peak 1 was below 0.5, indicating that peak 1 had little correlation with the anti-inflammatory activity. Except for peak 3 and peak 8, the correlation coefficient of the rest chromatographic peaks was above 0.9, indicating that these peaks (P7, P4, P2, P9, P5, P10, P6) correlate well with anti-inflammatory activity, and could as the quality makers of DOOS. Based on the results of inhibition of LPS-induced NO secretion by RAW264.7 macrophages *in vitro* in **Figure 5A**, GCA can be used to assess the correlation between the efficacy index and the chromatographic peaks and provide a possible prediction of the active components.

Verified the Spectrum-Effect Relationships Based on Purified Oligosaccharides

To examine the anti-inflammatory activity of each purified oligosaccharide (P2–P8) from DOOS-20 at different

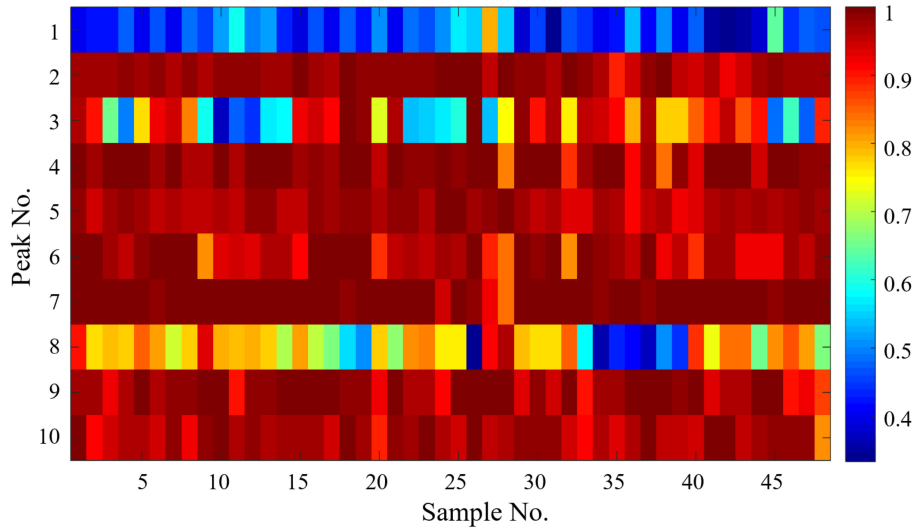

FIGURE 6 | Spectrum-effect relationships between HPLC-CAD fingerprints and anti-inflammatory activities.

concentration gradients (400, 200, 100, 50, 25 μg/mL), the secretion of NO was measured with Griess reagent. As shown in **Figure 5B**, the differences between different concentration gradients of P-2 (sucrose) on the secretion of NO from RAW264.7 macrophages compared with the LPS group were not statistically significant. The rest of DOOS-20 purification sections had a certain inhibitory effect on NO secretion from macrophages, among which P-4 (maltotetraose), P-5 (maltopentaose), P-6 (maltohexaose), and P-7 (mannohexaose) had a more significant NO inhibitory effect. It indicated that P-4 (maltotetraose), P-5 (maltopentaose), P-6 (maltohexaose), and P-7 (mannohexaose) could be the quality markers for quality control of *D. officinale*.

DISCUSSION

Dendrobium officinale, Chinese name Tiepi Shihu, is derived from the dried stems of *Dendrobium Kimura*, traditionally considered to be the best tonic for nourishing the stomach, nourishing body fluid, and strengthening the immunity (33). Polysaccharide is the indicator component identified under the item of *D. officinale* in the Chinese Pharmacopeia (Part I). However, only the total sugar content and monosaccharide composition ratio of polysaccharide from *D. officinale* are generally limited, which provides an opportunity for the existence of *D. officinale* fake products. Therefore, it is urgent to establish a fast and effective method to identify and improve the true and false quality of *D. officinale*.

TABLE 2 | Gray correlation grade for the common peak areas and their order.

Peak No.		Correlation Coefficient	Order
P1	Monosaccharide	0.460 ± 0.082	10
P2	Sucrose	0.974 ± 0.020	3
P3	Maltotriose	0.773 ± 0.189	8
P4	Maltotetraose	0.975 ± 0.038	2
P5	Maltopentaose	0.966 ± 0.019	5
P6	Maltohexaose	0.955 ± 0.046	7
P7	Mannohexaose	0.988 ± 0.025	1
P8	Maltoheptaose	0.720 ± 0.160	9
P9	–	0.969 ± 0.033	4
P10	–	0.962 ± 0.032	6

Carbohydrates are the most abundant natural products and can be classified according to their DP, initially divided into three main groups, namely monosaccharides (DP 1), oligosaccharides (DP 2–10), and polysaccharides (DP > 10). Functional oligosaccharides are indigestible and insensitive to human digestive enzymes, resulting in various pharmacological effects, for example, anti-inflammatory effect (34). *D. officinale* has the effects of clearing internal heat, nourishing Yin, benefiting the stomach and generating body fluid. Polysaccharides of *D. officinale* has good anti-inflammatory effects, consistent with TCM efficacy (13). GM is the main component of *Dendrobium* polysaccharide that exerts anti-inflammatory effect and higher molecular weight may have a negative impact on the anti-inflammatory effect (14), while compared with polysaccharide, oligosaccharide has lower molecular weight and better water solubility and are easily absorbed through the intestine (35). In our study, the HPLC-CAD fingerprints combined with the inhibition of NO secretion of RAW264.7 cells by different batches of DOOS were evaluated by GCA to determine the spectrum-effect relationships of DOOS active components. Meanwhile, the purified oligosaccharide components were characterized and validated for NO inhibition activity *in vitro*, and the results indicated that P-4 (maltotetraose), P-5 (maltopentaose), P-6 (maltohexaose), and P-7 (mannohexaose) could be the quality markers for quality control of *D. officinale*. As far as we know this is the first time that the anti-inflammatory effects of

maltotetraose, maltopentaose, maltohexaose, and mannohexaose in *D. officinale* were reported.

In 1990, Alpert first proposed the separation mode of hydrophilic interaction liquid chromatography (HILIC) (36), which solved the problem that compounds with high polarity could not be well retained in reversed-phase liquid chromatography (RP-LC) (37), and HILIC was widely used for the analysis of oligosaccharides (38, 39). HPLC with CAD, refractive index detection (RID), or evaporative light-scattering detection (ELSD) is often used for oligosaccharide analysis. RID, a traditional detector, has good linearity and stability and has a strong quantitative ability, but CAD detector could obtain a better quantitative limit, sensitive, reproducibility, and linearity than RID. HPLC with CAD is a new detection method that is developed on the basis of ELSD. Similar to ELSD, the response of CAD does not depend on the strong chromophore of the analyte structure, and CAD provides higher sensitivity in comparison to ELSD, making it a powerful tool for the determination of oligosaccharides (40–42). In our study, the fingerprints of DOOS were established by HPLC with HILIC model and CAD detector. Chromatographic fingerprinting is an effective method to evaluate the quality of herbal medicines, but it is difficult to reflect the active ingredient groups in herbal medicines (16). Therefore, it is imperative to establish spectrum–effect relationships between DOOS fingerprints and anti-inflammatory activity. GCA is an essential method of gray system theory, which is a simple and effective method to evaluate the relationship of spectrum-effect by judging the correlation grade between factors based on the similarity of the geometry of the change curve of each factor (17, 18). Many reports about the spectrum–effect relationship study by GCA, for example, reverse tracing anti-thrombotic active ingredients from dried *Rehmannia Radix* was studied based on multidimensional spectrum–effects relationship analysis of steaming and drying for nine cycles (43). Spectrum–effect relationship between constituents absorbed into blood and bioactivities of Baizhu Shaoyao San before and after processing on ulcerative colitis rats by GCA method (44). The spectrum–effect relationships between chemical fingerprints, and the analgesic and anti-inflammatory effects of *Rubia cordifolia L.* extract were established by the GCA method (20). Four chemometrics named PCA, GCA, partial least squares regression (PLSR), and the bivariate correlations analysis (BCA) were applied to construct spectrum–effect relationship between the UPLC fingerprints and biological activities of *Rosa rugosa*. The spectrum–effect relationship study revealed that di-O-galloyl-HHDP-glucoside, galloyl-HHDP-glucoside, and avicularin were more relevant to the antidiabetic activity. Di-O-galloyl-HHDP-glucoside, galloyl-HHDP-glucoside, and ellagic acid were the main antioxidant components of *R. rugosa* (45). In this study, the GCA method was used to evaluate the spectrum–effect relationships between the 10 common peak areas in the HPLC-CAD fingerprints and anti-inflammatory activities, and purified oligosaccharides were used to confirm the GCA results, and the results indicated that maltotetraose, maltopentaose, maltohexaose, and mannohexaose were relevant to anti-inflammatory effects and could be as the quality markers for quality control of *D. officinale*.

Polysaccharide, as one of the main bioactive components in *D. officinale*, was mainly composed of glucose and mannose (Manp: Glcp = 2.01:1.00–8.82:1.00), along with galactose, xylose, arabinose, and rhamnose in different molar ratios and types of glycosidic bonds. The basic skeleton of purified *D. officinale* polysaccharides has been elucidated. The backbone skeleton of *D. officinale* polysaccharides consists of 1,4-β-D-Man*p*, 1,4-β-D-Glc*p*, 1,3,6-β-D-Man*p*, 1,3-β-D- Man*p*, 1,2-β-D-Glc*p*, 1,4-α-D-Man*p*, and 1,6-α-D-Glc*p* (46). An oligosaccharide-marker approach was developed for quality assessment of polysaccharides in *D. officinale* by UPLC-Q-TOF/Mass Spectrum spectrometry previously. The method involved partial acid hydrolysis of *D. officinale* polysaccharide (DOPS) followed by p-aminobenzoic ethyl ester (ABEE) derivatization. Two ABEE-labeled oligosaccharides namely, Te-Man-ABEE and Pen-Man-ABEE, were selected as chemical markers due to their high specificity in herb formula. The linear relationship between the content of these two markers and the content of DOPS was then successfully established, respectively. The linear relationship was further transformed to that between the peak area of chemical markers and DOPS content so that chemical makers were not necessary to be isolated for analysis (47). The original oligosaccharides (no ABBE derivatization) were mannotetraose and mannopentaose, respectively. The structures of mannotetraose and mannoproteins are 1,4-β-D-Man*p*. It is obvious that the partial acid hydrolysis of polysaccharide and ABEE derivatization have the limitation of structural modification and complex procedures. In our study, the proposed Q-markers for quality control of *D. officinale* are maltotetraose, maltopentaose, maltohexaose, and mannohexaose, and among them maltotetraose, maltopentaose, maltohexaose have 1,4-α-D-Glc*p*, and mannohexaose has 1,4-β-D-Man*p*; the four oligosaccharides kept the original structure from *D. officinale*. It suggests that the oligosaccharide-marker approach is a simple, stable, and a reliable method for the quality control of herb medicines or nutritious foods.

CONCLUSION

In the present study, HPLC fingerprints were firstly combined with anti-inflammatory activity to evaluate DOOS spectrum–effect relationship by GCA, which provides the possibility to evaluate potential active ingredients and explore the quality markers. The HPLC fingerprints of 48 batches of DOOS were developed and analyzed with SA, and the results showed that the similarity index was in a range of 0.222–0.995, indicating that there was a large difference between batches of different origins. *In vitro* screening experiment indicated that DOOS potentially inhibited NO production and effectively reduced the release of inflammatory cytokines such as TNF-α, IL-6, and IL-1β in RAW 264.7 cells, thereby reducing the inflammatory response of cells. Furthermore, the anti-inflammatory activity of different batches of DOOS was evaluated by NO inhibition as an indicator, and the spectrum–effect relationships were analyzed with HPLC fingerprints by GCA. The oligosaccharides

isolated and purified from *D. officinale* were analyzed by monosaccharide composition, HPLC-Quadrupole Time of Flight-Mass Spectrum, and Nuclear magnetic resonance analysis to identify the common peaks as follows: DOOS-20-2 (peak 2) is sucrose, DOOS-20-3 (peak 3), DOOS-20-4 (peak 4), DOOS-20-5 (peak 5), DOOS-20-6 (peak 6), and DOOS-20-8 (peak 8) were maltotriose, maltotetraose, maltopentaose, maltohexaose, and maltoheptaose, respectively, and DOOS-20-7 (peak 7) was mannohexaose. Results of the inhibition of LPS-induced NO secretion by RAW264.7 cells *in vitro* showed that sucrose was not statistically significant compared with the LPS group, and on the other hand, maltotetraose, maltopentaose, maltohexaose, and mannohexaose had a more significant NO inhibitory effect, which was consistent with the correlation coefficient predicted by GCA. Our results showed four DOOS (maltotetraose, maltopentaose, maltohexaose, and mannohexaose) were relevant to anti-inflammatory effects, and could be the quality markers for quality control of *D. officinale*. In conclusion, the strategy of combining chemical fingerprints with pharmacodynamic analysis can provide useful references for the quality evaluation of herbal medicines or nutritious foods.

DATA AVAILABILITY STATEMENT

The original contributions presented in the study are included in the article/**Supplementary Material**, further inquiries can be directed to the corresponding authors.

AUTHOR CONTRIBUTIONS

RL: methodology, software, validation, formal analysis, investigation, and writing – original draft. SS: methodology, validation, analysis, and interpretation of data. SX: methodology, investigation, and resources. JS: investigation and conceptualization. XG and JW: investigation and resources. HW and SW: funding acquisition, conceptualization, supervision, and writing – review and editing. All authors contributed to the article and approved the submitted version.

FUNDING

This study was supported by the Key New Drug Creation and Manufacturing Program in China (2019ZX09735001-004), Shanghai Rising-Star Program (19QB1406500), Xinglin Young Scholars Program of Shanghai University of Traditional Chinese Medicine to HW, and the Budgetary Program of Shanghai University of Traditional Chinese Medicine (2019LK082).

SUPPLEMENTARY MATERIAL

The Supplementary Material for this article can be found online at: https://www.frontiersin.org/articles/10.3389/fnut.2022.914380/full#supplementary-material

REFERENCES

1. Chinese Pharmacopoeia Commission [CPC]. *Pharmacopoeia of the People's Republic of China*. Beijing: People's Medical Publishing House (2020).
2. Zheng S, Zhu Y, Jiao C, Shi M, Wei L, Zhou Y, et al. Extraction and analysis of gigantol from *Dendrobium officinale* with response surface methodology. *Molecules.* (2018) 23:818. doi: 10.3390/molecules23040818
3. Zhang X, Zhang S, Gao B, Qian Z, Liu J, Wu S, et al. Identification and quantitative analysis of phenolic glycosides with antioxidant activity in methanolic extract of *Dendrobium catenatum* flowers and selection of quality control herb-markers. *Food Res Int.* (2019) 123:732–45. doi: 10.1016/j.foodres.2019.05.040
4. Yue H, Liu Y, Qu H, Ding K. Structure analysis of a novel heteroxylan from the stem of *Dendrobium officinale* and anti-angiogenesis activities of its sulfated derivative. *Int J Biol Macromol.* (2017) 103:533–42. doi: 10.1016/j.ijbiomac.2017.05.097
5. Wei Y, Wang L, Wang D, Wang D, Wen C, Han B, et al. Characterization and anti-tumor activity of a polysaccharide isolated from *Dendrobium officinale* grown in the Huoshan County. *Chin Med.* (2018) 13:47. doi: 10.1186/s13020-018-0205-x
6. Luo QL, Tang ZH, Zhang XF, Zhong YH, Yao SZ, Wang LS, et al. Chemical properties and antioxidant activity of a water-soluble polysaccharide from *Dendrobium officinale*. *Int J Biol Macromol.* (2016) 89:219–27. doi: 10.1016/j.ijbiomac.2016.04.067
7. Yang S, Gong Q, Wu Q, Li F, Lu Y, Shi J. Alkaloids enriched extract from *Dendrobium nobile Lindl.* attenuates tau protein hyperphosphorylation and apoptosis induced by lipopolysaccharide in rat brain. *Phytomedicine.* (2014) 21:712–6. doi: 10.1016/j.phymed.2013.10.026
8. Verma S, Mathew V, Farkouh ME. Targeting inflammation in the prevention and treatment of type 2 diabetes: insights from CANTOS. *J Am Coll Cardiol.* (2018) 71:2402–4. doi: 10.1016/j.jacc.2018.03.480
9. Zhang Y, Zhang L, Liu J, Liang J, Si J, Wu S. *Dendrobium officinale* leaves as a new antioxidant source. *J Funct Foods.* (2017) 37:400–15. doi: 10.1016/j.jff.2017.08.006
10. Feng CZ, Cao L, Luo D, Ju LS, Yang JJ, Xu XY, et al. Dendrobium polysaccharides attenuate cognitive impairment in senescence-accelerated mouse prone 8 mice via modulation of microglial activation. *Brain Res.* (2019) 1704:1–10. doi: 10.1016/j.brainres.2018.09.030
11. Zhu Y, Zhang A, He B, Zhang X, Yu Q, Si J. Quantitative variation of total alkaloids contents in *Dendrobium officinale*. *Zhongguo Zhong Yao Za Zhi.* (2010) 35:2388–91.
12. Zhang A, Wei T, Si J, Jin L, Mo Y. Study on basic amino acid contents in *Dendrobium officinale*. *Zhongguo Zhong Yao Za Zhi.* (2011) 36:2632–5.
13. Liang J, Chen S, Chen J, Lin J, Xiong Q, Yang Y, et al. Therapeutic roles of polysaccharides from *Dendrobium officinaleon* colitis and its underlying mechanisms. *Carbohydr Polym.* (2018) 185:159–68. doi: 10.1016/j.carbpol.2018.01.013
14. Zhang LJ, Huang XJ, Shi XD, Chen HH, Cui SW, Nie SP. Protective effect of three glucomannans from different plants against DSS induced colitis in female BALB/c mice. *Food Funct.* (2019) 10:1928–39. doi: 10.1039/c8fo02305k
15. Huang S, Chen F, Cheng H, Huang G. Modification and application of polysaccharide from traditional Chinese medicine such as *Dendrobium officinale*. *Int J Biol Macromol.* (2020) 157:385–93. doi: 10.1016/j.ijbiomac.2020.04.141
16. Yang L, Jiang H, Wang S, Hou A, Man W, Zhang J, et al. Discovering the major antitussive, expectorant, and anti-inflammatory bioactive constituents in *Tussilago farfara* L. Based on the spectrum-effect relationship combined with chemometrics. *Molecules.* (2020) 25:620. doi: 10.3390/molecules25030620
17. Li K, Li J, Su J, Xiao X, Peng X, Liu F, et al. Identification of quality markers of Yuanhu Zhitong tablets based on integrative pharmacology and data mining. *Phytomedicine.* (2018) 44:212–9. doi: 10.1016/j.phymed.2018.03.002

18. Gao S, Chen H, Zhou X. Study on the spectrum-effect relationship of the xanthine oxidase inhibitory activity of *Ligustrum lucidum*. *J Sep Sci.* (2019) 42:3281–92. doi: 10.1002/jssc.201900531
19. Robinson RC, Colet E, Tian T, Poulsen NA, Barile D. An improved method for the purification of milk oligosaccharides by graphitised carbon-solid phase extraction. *Int Dairy J.* (2018) 80:62–8. doi: 10.1016/j.idairyj.2017.12.009
20. Shen CH, Liu CT, Song XJ, Zeng WY, Lu XY, Zheng ZL, et al. Evaluation of analgesic and anti-inflammatory activities of *Rubia cordifolia L.* by spectrum-effect relationships. *J Chromatogr B Analyt Technol Biomed Life Sci.* (2018) 1090:73–80. doi: 10.1016/j.jchromb.2018.05.021
21. Taylor RL, Conrad HE. Stoichiometric depolymerization of polyuronides and glycosaminoglycuronans to monosaccharides following reduction of their carbodiimide-activated carboxyl groups. *Biochemistry.* (1972) 11:1383–8. doi: 10.1021/bi00758a009
22. Boer R, Ulrich WR, Klein T, Mirau B, Haas S, Baur I. The inhibitory potency and selectivity of arginine substrate site nitric-oxide synthase inhibitors is solely determined by their affinity toward the different isoenzymes. *Mol Pharmacol.* (2000) 58:1026–34.
23. Green LC, Wagner DA, Glogowski J, Skipper PL, Wishnok JS, Tannenbaum SR. Analysis of nitrate, nitrite, and [^{15}N]nitrate in biological fluids. *Anal Biochem.* (1982) 126:131–8. doi: 10.1016/0003-2697(82)90118-x
24. Liu D, Yin Q, Zhang QH, Xiang J, Ruan CL, Liu HL, et al. New NO production inhibitors from Hyssopus cuspidatus in LPS-induced RAW264.7 cells. *Phytochem Lett.* (2019) 34:91–5. doi: 10.1016/j.phytol.2019.09.012
25. Packer NH, Lawson MA, Jardine DR, Redmond JW. A general approach to desalting oligosaccharides released from glycoproteins. *Glycoconj J.* (1998) 15:737–47. doi: 10.1023/a:1006983125913
26. Li Y, Wang C, Wang F, Dong H, Guo S, Yang J, et al. Chemical constituents of *Dendrobium candidum*. *Zhongguo Zhong Yao Za Zhi.* (2010) 35:1715–9.
27. Heyraud A, Rinaudo M, Vignon M, Vincendon M. ^{13}C-Nuclear magnetic resonance spectroscopic investigation of α- and β-1,4-D-glucose homooligomers. *Biopolymers.* (1979) 18:167–85. doi: 10.1002/bip.1979.360180113
28. Jiang RW, Du XG, Zhang X, Wang X, Hu DY, Meng T, et al. Synthesis and bioassay of β-(1,4)-D-mannans as potential agents against Alzheimer's disease. *Acta Pharmacol Sin.* (2013) 34:1585–91. doi: 10.1038/aps.2013.104
29. Vasarri M, Leri M, Barletta E, Ramazzotti M, Marzocchini R, Degl'Innocenti D. Anti-inflammatory properties of the marine plant *Posidonia oceanica* (L.) Delile. *J Ethnopharmacol.* (2020) 247:112252. doi: 10.1016/j.jep.2019.112252
30. Liu S, Yang T, Ming TW, Gaun TKW, Zhou T, Wang S, et al. Isosteroid alkaloids with different chemical structures from *Fritillariae cirrhosae* bulbus alleviate LPS-induced inflammatory response in RAW 264.7 cells by MAPK signaling pathway. *Int Immunopharmacol.* (2020) 78:106047. doi: 10.1016/j.intimp.2019.106047
31. Moro C, Palacios I, Lozano M, D'Arrigo M, Guillamon E, Villares A, et al. Anti-inflammatory activity of methanolic extracts from edible mushrooms in LPS activated RAW 264.7 macrophages. *Food Chem.* (2012) 130:350–5. doi: 10.1016/j.foodchem.2011.07.049
32. Zeng Q, Ko CH, Siu WS, Li KK, Wong CW, Han XQ, et al. Inhibitory effect of different Dendrobium species on LPS-induced inflammation in macrophages via suppression of MAPK pathways. *Chin J Nat Med.* (2018) 16:481–9. doi: 10.1016/s1875-5364(18)30083-9
33. Cao H, Ji Y, Li S, Lu L, Tian M, Yang W, et al. Extensive metabolic profiles of leaves and stems from the medicinal plant *Dendrobium officinale* Kimura et Migo. *Metabolites.* (2019) 9:215. doi: 10.3390/metabo9100215
34. Zhu D, Yan Q, Liu J, Wu X, Jiang Z. Can functional oligosaccharides reduce the risk of diabetes mellitus? *FASEB J.* (2019) 33:11655–67. doi: 10.1096/fj.201802802RRR
35. Yang Z, Pan Y, Chen J, Zhang H, Wei H, Wu Z, et al. Anti-inflammatory, anti-oxidative stress effect of Phascolosoma esculenta oligosaccharides on *Escherichia coli*-induced sepsis mice. *Food Sci Biotechnol.* (2019) 28:1871–9. doi: 10.1007/s10068-019-00620-w
36. Alpert AJ. Hydrophilic-interaction chromatography for the separation of peptides, nucleic acids and other polar compounds. *J Chromatogr.* (1990) 499:177–96. doi: 10.1016/s0021-9673(00)96972-3
37. Buszewski B, Noga S. Hydrophilic interaction liquid chromatography (HILIC)-a powerful separation technique. *Anal Bioanal Chem.* (2012) 402:231–47. doi: 10.1007/s00216-011-5308-5
38. Ghfar AA, Wabaidur SM, Ahmed AY, Alothman ZA, Khan MR, Al-Shaalan NH. Simultaneous determination of monosaccharides and oligosaccharides in dates using liquid chromatography-electrospray ionization mass spectrometry. *Food Chem.* (2015) 176:487–92. doi: 10.1016/j.foodchem.2014.12.035
39. Remoroza CA, Mak TD, De Leoz MLA, Mirokhin YA, Stein SE. Creating a mass spectral reference library for oligosaccharides in human milk. *Anal Chem.* (2018) 90:8977–88. doi: 10.1021/acs.analchem.8b01176
40. Inagaki S, Min JZ, Toyo'oka T. Direct detection method of oligosaccharides by high-performance liquid chromatography with charged aerosol detection. *Biomed Chromatogr.* (2007) 21:338–42. doi: 10.1002/bmc.751
41. Chen L, Hu D, Liang X, Zhao J, Li S. Preparation and identification of oligosaccharides in lotus seeds and determination of their distribution in different parts of lotus. *Electrophoresis.* (2018) 39:2020–8. doi: 10.1002/elps.201700490
42. Li J, Hu D, Zong W, Lv G, Zhao J, Li S. Determination of inulin-type fructooligosaccharides in edible plants by high-performance liquid chromatography with charged aerosol detector. *J Agric Food Chem.* (2014) 62:7707–13. doi: 10.1021/jf502329n
43. Gong PY, Guo YJ, Tian YS, Gu LF, Qi J, Yu BY. Reverse tracing anti-thrombotic active ingredients from dried Rehmannia Radix based on multidimensional spectrum-effect relationship analysis of steaming and drying for nine cycles. *J Ethnopharmacol.* (2021) 276:114177. doi: 10.1016/j.jep.2021.114177
44. Cai H, Xu Y, Xie L, Duan Y, Zhou J, Liu J, et al. Investigation on spectrum-effect correlation between constituents absorbed into blood and bioactivities of Baizhu Shaoyao San before and after processing on ulcerative colitis rats by UHPLC/Q-TOF-MS/MS coupled with gray correlation analysis. *Molecules.* (2019) 24:940. doi: 10.3390/molecules24050940
45. Nijat D, Lu CF, Lu JJ, Abdulla R, Hasan A, Aidarhan N, et al. Spectrum-effect relationship between UPLC fingerprints and antidiabetic and antioxidant activities of Rosa rugosa. *J Chromatogr B Anal Technol Biomed Life Sci.* (2021) 1179:122843. doi: 10.1016/j.jchromb.2021.122843
46. Chen WH, Wu JJ, Li XF, Lu JM, Wu W, Sun YQ, et al. Isolation, structural properties, bioactivities of polysaccharides from *Dendrobium officinale* Kimura et. Migo: a review. *Int J Biol Macromol.* (2021) 184:1000–13. doi: 10.1016/j.ijbiomac.2021.06.156
47. Wong TL, Li LF, Zhang JX, Bai SP, Zhou LS, Fung HY, et al. Oligosaccharide-marker approach for qualitative and quantitative analysis of specific polysaccharide in herb formula by ultra-high-performance liquid chromatography-quadrupole-time-of-flight mass spectrometry: *Dendrobium officinale*, a case study. *J Chromatogr A.* (2019) 1607:460388. doi: 10.1016/j.chroma.2019.460388

Conflict of Interest: XG was employed by Amway (China) Co., Ltd.

The remaining authors declare that the research was conducted in the absence of any commercial or financial relationships that could be construed as a potential conflict of interest.

Publisher's Note: All claims expressed in this article are solely those of the authors and do not necessarily represent those of their affiliated organizations, or those of the publisher, the editors and the reviewers. Any product that may be evaluated in this article, or claim that may be made by its manufacturer, is not guaranteed or endorsed by the publisher.

Copyright © 2022 Liu, Shi, Xiong, Su, Gan, Wu, Wang and Wang. This is an open-access article distributed under the terms of the Creative Commons Attribution License (CC BY). The use, distribution or reproduction in other forums is permitted, provided the original author(s) and the copyright owner(s) are credited and that the original publication in this journal is cited, in accordance with accepted academic practice. No use, distribution or reproduction is permitted which does not comply with these terms.

frontiers | Frontiers in Nutrition

ORIGINAL RESEARCH
published: 09 June 2022
doi: 10.3389/fnut.2022.916976

Structural Characterization and Anti-inflammatory Activity of a Galactorhamnan Polysaccharide From *Citrus medica* L. var. *sarcodactylis*

Bi Luo[1,2,3], *Jia Lv*[1,2,3], *Kejie Li*[1,2,3], *Peiran Liao*[1,2,3]* *and Peng Chen*[4]*

[1] School of Traditional Chinese Medicine, Guangdong Pharmaceutical University, Guangzhou, China, [2] Key Laboratory of State Administration of Traditional Chinese Medicine for Production & Development of Cantonese Medicinal Materials, Guangzhou, China, [3] Comprehensive Experimental Station of Guangzhou, Chinese Materia Medica, China Agriculture Research System, Guangzhou, China, [4] School of Pharmaceutical Sciences, Guangzhou University of Chinese Medicine, Guangzhou, China

OPEN ACCESS

Edited by:
Xiaolong Ji,
Zhengzhou University of Light Industry, China

Reviewed by:
Hongshun Yang,
National University of Singapore, Singapore
Wuxia Zhang,
Shanxi Agricultural University, China
Yuanhao Qiu,
Pingdingshan University, China

***Correspondence:**
Peiran Liao
westpp@126.com
Peng Chen
15292394251@163.com

Specialty section:
This article was submitted to Food Chemistry, a section of the journal Frontiers in Nutrition

Received: 10 April 2022
Accepted: 09 May 2022
Published: 09 June 2022

Citation:
Luo B, Lv J, Li K, Liao P and Chen P (2022) Structural Characterization and Anti-inflammatory Activity of a Galactorhamnan Polysaccharide From Citrus medica L. var. sarcodactylis. Front. Nutr. 9:916976. doi: 10.3389/fnut.2022.916976

This study aimed to extract polysaccharides from *Citrus medica* L. var. *sarcodactylis* (finger citron fruits) and analyze their structures and potential bioactivities. A new polysaccharide named K-CMLP was isolated and purified by Diethylaminoethylcellulose (DEAE)-Sepharose Fast Flow and DEAE-52 cellulose column chromatography with an average molecular weight of 3.76×10^3 kDa. Monosaccharide composition analysis revealed that K-CLMP consisted of rhamnose, galactose, and glucose, with a molar ratio of 6.75:5.87:1.00. Co-resolved by methylation and two-dimensional nuclear magnetic resonance (NMR), K-CLMP was alternately connected with 1, 2-Rha and 1, 4-Gal to form the backbone, and a small number of glucose residues was connected to O-4 of rhamnose. The results of *DPPH*· and $ABTS^{+}$· radical scavenging assays indicated that both crude polysaccharide Citrus medica L. var. polysaccharide (CMLP) and K-CLMP exhibited strong free-radical-scavenging properties in a dose-dependent manner. In addition, K-CMLP significantly inhibited the production of pro-inflammatory cytokines (IL-6 and TNF-α) and reactive oxygen species (ROS) in RAW 264.7 cells treated with LPS. These results provide a basis for further use as one of the potential functions of food or natural medicine.

Keywords: *Citrus medica* L. var. *sarcodactylis*, galactorhamnan polysaccharide, anti-inflammatory activity, antioxidant activity, structure characterization

INTRODUCTION

Citrus medica L. var. *sarcodactylis* (Noot) Swingle (Finger citron), also known as Buddha's hand, is a variation of *Citrus medica* L. and belongs to the genus *Citrus*, Rutaceae family. The main producing areas are in the south of China, especially in Guangdong, Fujian, Sichuan, and Zhejiang provinces (1). The fruit of *C. medica* L. var. *sarcodactylis* is widely used as a precious traditional Chinese medicine, perfume raw materials, decorative bonsai, and different types of processed foods such as preserved fruit "laoxianghuang." As a traditional Chinese medicinal food, it has the functions of depressed liver, harmonizing stomach, and expelling phlegm (2), and it was used as an

adjuvant herbal medicine to treat multiple chronic diseases like hypertension, tracheitis, respiratory tract infections, angiocardiopathy, and asthma (3). In recent years, the chemical constituents isolated from the fruits of finger citron include polysaccharides (3, 4), neolignans (2), flavonoids (5), coumarins (6), terpenoids (7), glycosides (2), and other bioactive substances (8), which have revealed a wide variety of biological activities, including antidepressants (9), antibacterial (10), anticancer (11), antiaging (12), antibiofilm (13), antioxidants (14), and anti-inflammatory activities (15).

Especially, as both an edible and a medicinal fruit, it has been confirmed that its many healing properties are attributed to the polysaccharides, one of the major active ingredients of finger citron (16). According to the functional and practical applications of finger citron in folk medicine, the most promising biological properties of these polysaccharides are anti-inflammatory and immunomodulatory activities.

Finger citron, naturally used in China as a medicine with anti-inflammatory and anti-oxidative activity, is widely used because of its edible and medicinal properties. It has been generally confirmed that its health benefits are closely related to the essential oils and flavonoids. Besides essential oils and flavonoids, polysaccharides in finger citron are also important bioactive ingredients. It has been reported to possess antioxidant and immunoregulatory activity (15). As finger citron is usually extracted by hot water when serving as medicine, the water-soluble components, especially polysaccharides, should be responsible for the pharmacological effects (17). However, the structure of polysaccharides is closely related to their pharmacological effects. Few reports are available on the anti-inflammatory activity of polysaccharides derived from finger citron. It is required to reveal which bioactive homogeneous component responsible for the anti-inflammatory and anti-oxidative activity is highly accumulated in finger citron.

This work presents a new galactorhamnan polysaccharide, K-CMLP, isolated and further purified from the crude polysaccharide *via* Diethylaminoethylcellulose (DEAE) sepharose fast flow and DEAE-52 column chromatography. The structure of polysaccharide K-CMLP was elucidated by monosaccharide composition and methylation analysis combined with 1 D and 2D nuclear magnetic resonance (NMR) spectroscopies. We also investigated polysaccharide K-CMLP as an antioxidant against *DPPH*· and $ABTS^{+}$·radicals, the anti-inflammatory activities effect on the production of pro-inflammatory cytokines (TNF-α, IL-6), as well as cell count and reactive oxygen species' (ROS) scavenging activity in LPS-induced RAW 264.7 cells.

MATERIALS AND METHODS

Plant Materials and Chemicals

The fruit of *Citrus medica* L. var. *sarcodactylis* was harvested in October 2018 from the planting base of Nanling Parmaceutica Co. Ltd., Tongyou village, Pingtang town, Yunfu city (22°46' N, 111°45' E), Guangdong, China. The material was identified by associate professor Jinzhu Liu at the School of traditional Chinese medicine, Guangdong Pharmaceutical University, China. Galacturonic acid, D-glucose, trifluoroacetic acid (TFA), T-series Dextran, lipopolysaccharide (LPS), and DEAE-cellulose were purchased from Aladdin Reagent Int. (Shanghai, China). Other chemicals used in this work were analytical grade. Macrophages from the macrophage cell line RAW 264.7 were purchased from Nanjing Kebai Biotechnology Co., Ltd.

Extraction of Crude Polysaccharide

Fresh fruits were cut into 0.5–1.0 cm palm-shaped slices and dried at 50°C till the moisture content was less than 15%. The dried slices were ground to a powder. The powder (1.00 kg) was depigmented, defatted, and alcohol-soluble ingredients were removed by pretreating with 75% ethanol (1:15, w/v) using the Ultrasound method triple for 1 h. The dried residues were extracted with distilled water (1:10, w/v) at 100°C triple for 2 h and then filtered (18). The combined filtrates were concentrated to dryness under pressure at 55°C. The residue was resolved with deionized water and then was centrifuged. The supernatant was precipitated by adding four times the volume of ethanol and left overnight at 4°C. After centrifugation, the precipitate was re-dissolved in distilled water. The solution was deproteinized by Sevage reagent (chloroform/*n*-butanol 4:1, v/v) according to the published method (19). The deproteinized solution was intensively dialyzed against tap water for 72 h (Mw cut off 1000 Da). Finally, the resulting portion was collected and freeze-dried, and a light brown crude polysaccharide Citrus medica L. var. polysaccharide (CMLP, 132.7 g) of finger citron was obtained. High-performance gel-permeation chromatography (HPGPC) was used to detect the purity of polysaccharide.

Separation and Purification of Citrus medica L. var. polysaccharide

CMLP was dissolved in deionized water and the mixture was centrifuged. The supernatant was loaded on a DEAE Sepharose Fast Flow column (2.5 cm × 40.0 cm) and eluted with distilled water and different concentrations of gradient NaCl solution (0.1 M, 0.2 M, 0.3 M NaCl) at a constant flow rate consecutively. Each fraction was detected by using phenol–sulfuric acid method and then the peak was merged independently. The water elute was further purified by DEAE-52 cellulose column (5 × 50 cm, OH^{-1} form) and eluted with distilled water at a flow rate of 0.8 mL/min, and the main polysaccharides fraction was collected, dialyzed, and lyophilized. Consequently, a white fluffy pure polysaccharide namely K-CMLP (7.71 g) was obtained. The K-CMLP solution was filtered through 0.22-μm membrane and analyzed by HPGPC.

Molecular Weight Analysis of K-CMLP

The molecular weight of K-CMLP was determined by HPGPC with three columns (Waters Ultra hydrogel 250, 1000, and 2000; 30 cm × 7.8 mm; 6 μm particles) in series. T-series Dextran standards with defined molecular masses were used to calibrate the HPGPC system (20).

Analysis of Chemical Compositions

Total carbohydrate content was determined by the phenol–sulfuric acid method with D-glucose as the standard (21). Uronic acid content was determined according to the *m*-hydroxydiphenyl-sulfuric acid method and galacturonic acid as the standard (22). Protein content was estimated by Bradford's with bovine serum albumin (BSA) as the standard (23). The monosaccharide compositions of K-CMLP were detected by high-performance liquid chromatography (HPLC), with 1-phenyl-3-methyl-5-pyrazolone (PMP) pre-column derivatization. Briefly, polysaccharide (10.0 mg) samples were hydrolyzed with 3 ml of 4 M TFA at 110°C for 4 h. Then, the residue was washed with methanol and lyophilized several times until TFA was removed completely after the solution was concentrated under vacuum. The sugar residues after hydrolysis were dissolved in distilled water, and PMP methanol solution and NaOH solution were added to the hydrolyzed samples for derivatization. The mixture was neutralized with HCl. Subsequently, chloroform was added and extracted in triplicate and the organic phase was discarded. Finally, the solution was analyzed using an HPLC system equipped with a COSMOSIL 5C18-PAQ column (4.6 × 150 mm, 5 μm), which was eluted with the mobile phase of a 0.05 M KH_2PO_4 (pH = 6.9) and acetonitrile in the volume ratio of 80:20 at 1.0 mL min^{-1}.

Methylation Analysis

To define the glycosyl linkages, K-CMLP was methylated according to the method of Hakomori (24) with slight modifications. KMCP (10.0 mg) was added to a suspension of NaH (1.2 equiv) in dry DMSO (5.0 mL/mmol) stirred under a nitrogen atmosphere, and the reaction mixture was stirred at room temperature overnight. Then 1.5 mL of methyl iodide was slowly added dropwise into the mixed solution in an ice bath with the ultrasonic method. The disappearance of the OH band in the FT-IR spectrum (3000–3400 cm^{-1}) was used to confirm complete methylation. Fully methylated polysaccharide was dissolved and hydrolyzed in 5 mL 2 M TFA at 110°C for 2 h. After cooling at r.t., methanol was added and evaporated to dryness to remove extra TFA. The residue was dissolved in 3 mL distilled water, and 30 mg $NaBH_4$ was added for reduction, 25%HOAc was used to neutralize until gas formation ceased. Subsequently, the spin-dried sample was acetylated with acetic anhydride at 110°C for 1 h. After the solution was extracted with the chloroform–water system three times and the chloromethane phases were collected, the methylated alditol acetate was obtained and detected by gas chromatography-mass spectrometry (GC-MS).

Nuclear Magnetic Resonance Analysis

The nuclear magnetic resonance of polysaccharide K-CMLP was performed with the method reported in Refs. (25, 26). Polysaccharide K-CMLP (30.0 mg) was dissolved in D_2O and freeze-dried several times to exchange H protons into deuterium completely. Subsequently, polysaccharide K-CMLP was dissolved in D_2O overnight before NMR analysis with TSP as the calibration standard. ^1H NMR, ^{13}C NMR, ^1H-^1H correlation spectroscopy (COSY), hetero-nuclear singular quantum correlation (HSQC), hetero-nuclear multiple bond correlation (HMBC) spectra were recorded with a Bruker Avance-600 NMR spectrometer (Bruker Instrumental Inc., Bremen, Germany), with a probe temperature of 25°C. The acquisition times were set to 64 times for ^1H NMR spectra, 5,120 times for ^{13}C NMR spectra, 64 times for ^1H-^1H COSY, 64 times for HSQC, and 128 times for HMBCspectra. The ^1H was recorded in the F2 channel with a 10.0 ppm spectrum width and ^{13}C was tested in the F1 channel with a 180.0 ppm spectrum width. The spectra were processed using MestReNova v14.0.0-23239 (Mestrelab Research, Santiago de Compostela, Spain) software. For correct peak integration, the spectra were previously baseline-corrected with the default option.

Antioxidant Activity of Citrus medica L. var. polysaccharide and K-CMLP

DPPH·Free Radical Scavenger

DPPH·radical-scavenging activity was evaluated with a method reported in Huang and Huang (27). In brief, 20 μL of CMLP and K-CMLP solutions (0–10.0 mg/mL) were mixed with 180 μL of *DPPH*· of ethanol solution (0.1 mM). Ascorbic acid (Vc) was used as the positive control. The mixtures have been shaken immediately and incubated in darkness for 30 min, and a value of A_{517} nm was detected using a microplate reader against a control containing 20 μL distilled water and 180 μL *DPPH*· solution.

ABTS+· Free Radical Scavenger

Assessment of $ABTS^+$· radical-scavenging activity was done according to a previously published method (28). A total of 7 mmol/L $ABTS^+$·and 2.45 mmol/L $K_2S_2O_8$ at the volume ratio of 1:1 was mixed and incubated in a dark place for 16 h at room temperature. The mixture was diluted with PBS at pH 7.4 to give an absorbance of 0.7 ± 0.02 at 734 nm. Then $ABTS^+$·solution (160 μL) was added to CMLP or K-CMLP solution at different concentrations. The reaction mixture was kept at room temperature for 6 min before measuring the absorbance at 734 nm.

Anti-inflammatory Activity of K-CMLP

Measurement of Cytotoxicity and Cytokines

RAW 264.7 macrophages were cultured in DMEM supplemented with 10% FBS and 100 U/mL of penicillin–streptomycin (double antibody) at 37°C in an atmosphere of 5% CO_2. RAW 264.7 macrophages (1×10^6 cells/well) were pretreated with K-CMLP whose final concentration was 50 μg/mL and stimulated with or without LPS (0.1 μg/mL) for 24 h at 37°C. The cell cytotoxicity of K-CMLP was tested by the MTT test. Levels of TNF-α and IL-6 were quantified using ELISA kits (Solarbio, Beijing, China) according to the manufacturer's instructions and a standard curve to calculate it. Briefly, samples were added in a captured antibody-coated 96-well plate for 60 min at 37°C. After washing, the detected antibody was incubated for 30 min at 37°C and HRP was reacted for 30 min at 37°C. The wells were filled with 100 μL substrate solution for 15 min in the dark and then a stop solution was added to terminate the reaction. The absorbance was measured at 450 nm using a microplate reader.

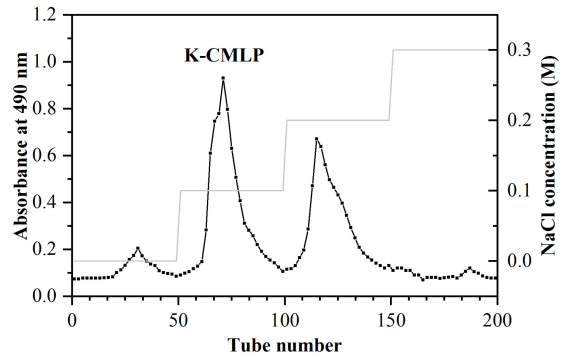

FIGURE 1 | DEAE cellulose-52 fractionation profile of polysaccharide K-CMLP.

Analysis of Intracellular Reactive Oxygen Species Production

The level of cellular ROS formation was assessed with the ROS assay kit. After treatment, the RAW 264.7 cells were collected and washed with PBS. 2′,7′-Dichlorodihydrofluorescein diacetate (DCFH-DA) is a cell-permeable probe (Ex/Em = 488/530 nm) for detecting intracellular ROS. The cell culture medium was removed and the cells were incubated with 10 μM DCFH-DA at 37°C for 20 min. After washing three times with serum-free cell culture medium, fluorescence emission (525 nm) was measured using a 488 nm laser and 530/30 filter on a BD LSRFortessa flow cytometer.

Statistical Analysis

Data for quantification were acquired from individual experiments repeated at least three times and were expressed as the means ± SD. Statistical significance was calculated by GraphPad Prism 7.00 software (GraphPad Software, Inc., San Diego, CA, United States) with unpaired two-tailed t-tests and accepted by $p < 0.05$ (*), $p < 0.01$ (**), $p < 0.001$ (***), $p < 0.0001$ (****). The IC_{50} was calculated using the GraphPad Prism 7.00 software according to the inhibition rates or reduction rates (y) plotted against the sample concentrations (x).

TABLE 1 | Composition analysis of bergamot polysaccharide.

Item	CMLP	K-CMLP
Carbohydrate (%)	96.35 ± 4.23	98.36 ± 2.35
Protein (%)	–	0.14 ± 0.06
Uronic acid (%)	3.03 ± 0.35	1.57 ± 0.45
Monosaccharide composition (%)		
Glc	15.64	7.39
Rha	27.54	43.38
Ara	8.3	–
Gal	39.73	49.88
Gal A	8.79	–

RESULTS AND DISCUSSION

Characterization of Citrus medica L. var. polysaccharide and K-CMLP

The crude polysaccharide was extracted from the fruit of bergamot with a yield of 13.27%. After alcohol precipitation, dialysis, DEAE Sepharose Fast Flow column, and DEAE-52 column chromatography, the elution curve is shown in **Figure 1**, a homogeneous polysaccharide of bergamot was obtained, named K-CMLP, and the yield was 5.81%. Measured by HPGPC, the chromatographic peak of K-CMLP was a single symmetrical peak, indicating that the purity of K-CMLP was very high (**Figure 2**). According to the dextran standard, the molecular weight-retention time standard curve was log(Mw) = −0.1841T + 12.1568, R^2 = 0.9843, and the calculated molecular weight of K-CMLP was 3.76×10^3 kDa.

As shown in **Table 1**, the results of the chemical composition of polysaccharide show that K-CMLP was mainly composed of neutral sugars, and the content of protein and uronic acid was less than 2%. The monosaccharide composition of K-CMLP was measured using pre-column PMP derivatization by HPLC. The results showed that K-CMLP was identified as an galactorhamnan which was mainly composed of rhamnose

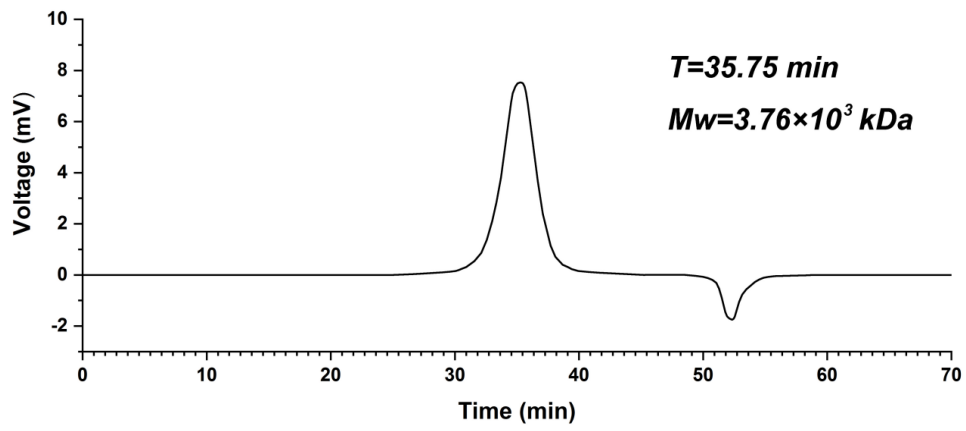

FIGURE 2 | High-performance gel-permeation chromatography chromatogram of polysaccharide K-CMLP.

and galactose with a relative molar ratio of 49.88 and 43.38% and also contained a small amount of glucose in a molar ratio of 7.39%.

Monosaccharide Composition of K-CMLP

The monosaccharide composition of K-CMLP was determined by HPLC-PAD (**Figure 3**). The presence of rhamnose, galactose, and glucose in K-CMLP were at the molar ratio of 6.75:5.87:1.00, indicating that K-CMLP was a type of heteropolysaccharide.

Methylation and Gas Chromatography-Mass Spectrometry Analysis of K-CMLP

Methylation analysis is an indispensable experimental method to study the types of glycosidic bonds in polysaccharides.

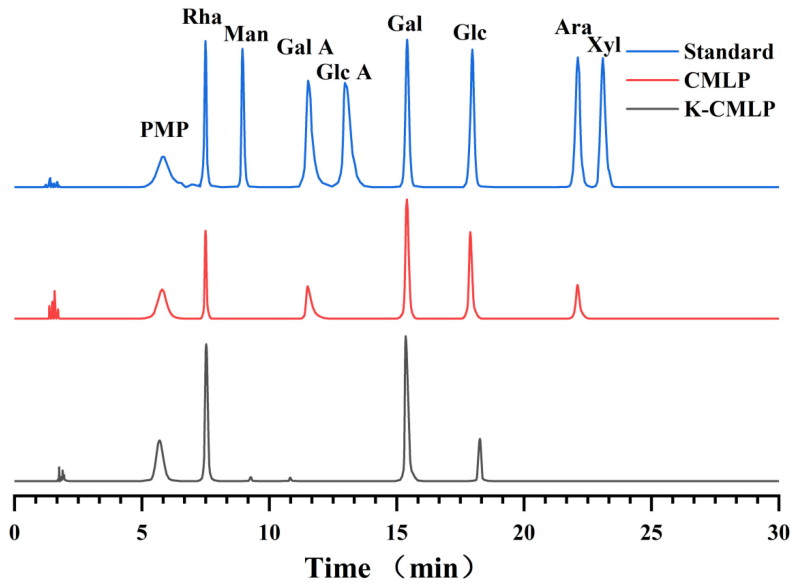

FIGURE 3 | High-performance liquid chromatography pre-column PMP derivative chromatogram of mixed monosaccharide standard, CMLP, and K-CMLP.

TABLE 2 | Methylation analysis of restored K-CMLP.

Methylation sugar	Ratio	Linkage type	Mass fragments (m/z)
3, 4-Me_2-Rha	3.9	1, 2-Rha	43,57,59,72,88,89,100,115,130,131,160,174,190
3-Me-Rha	1.0	1, 2,4-Rha	43,59,69,74,88,101,130,143,160,171,190,203
2, 3, 6-Me_3-Gal	4.8	1, 4-Gal	43,59,71,87,99,102,113,118,129,131,142,162,173,188,203,233
2, 3, 4, 6-Me_4-Glc	1.1	T-Glc	43,59,71,75,87,88,101,102,113,118,129,145,161,162,175,205

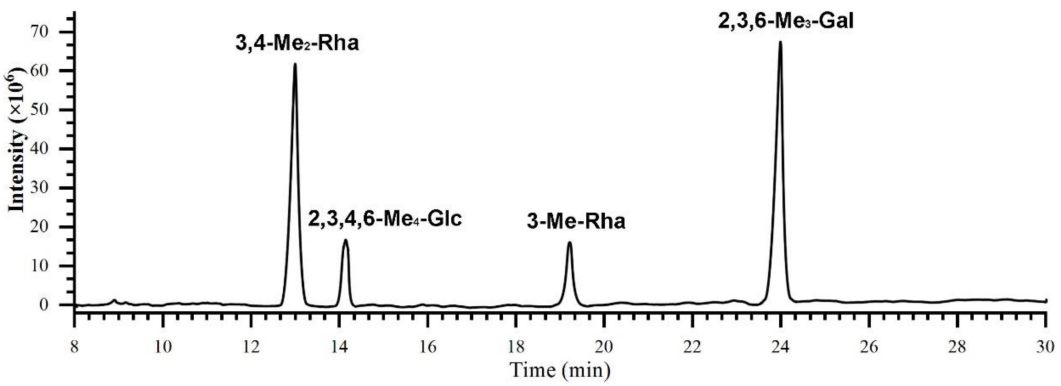

FIGURE 4 | The total ion chromatogram of K-CMLP by GC-MS.

In this study, polysaccharide K-CMLP structural analysis was performed using methylation analysis in combination with one-dimensional and two-dimensional nuclear magnetic resonance spectroscopy. After methylation, the fully methylated K-CMLP was hydrolyzed with acid, converted into alditol acetates, and analyzed by GC-MS. As shown in **Table 2** and **Figure 4**, the presence of four major alditol acetate compounds, 3, 4-Me_2-Rha, 3-Me-Rha, 2, 3, 6 -Me_3-Gal, and 2, 3, 4, 6-Me_4-Glc, which indicate the presence of 1, 2-Rha, 1, 2,4-Rha, 1, 4-Gal, and T-Glc in a ratio of 3.9:1.0:4.8:1.1. The contents of 1, 2,4-Rha and T-Glc were basically the same, indicating that the methylation results were reliable.

Nuclear Magnetic Resonance Spectroscopy Analysis

According to the ^{1}H NMR and ^{13}C NMR nuclear magnetic resonance spectra (**Figure 5A**), it was shown that K-CMLP had 3 signal peaks in the anomeric hydrogen region (4.3–5.5 ppm), and the chemical shifts were δ4.38, δ5.32, and δ5.21 ppm,

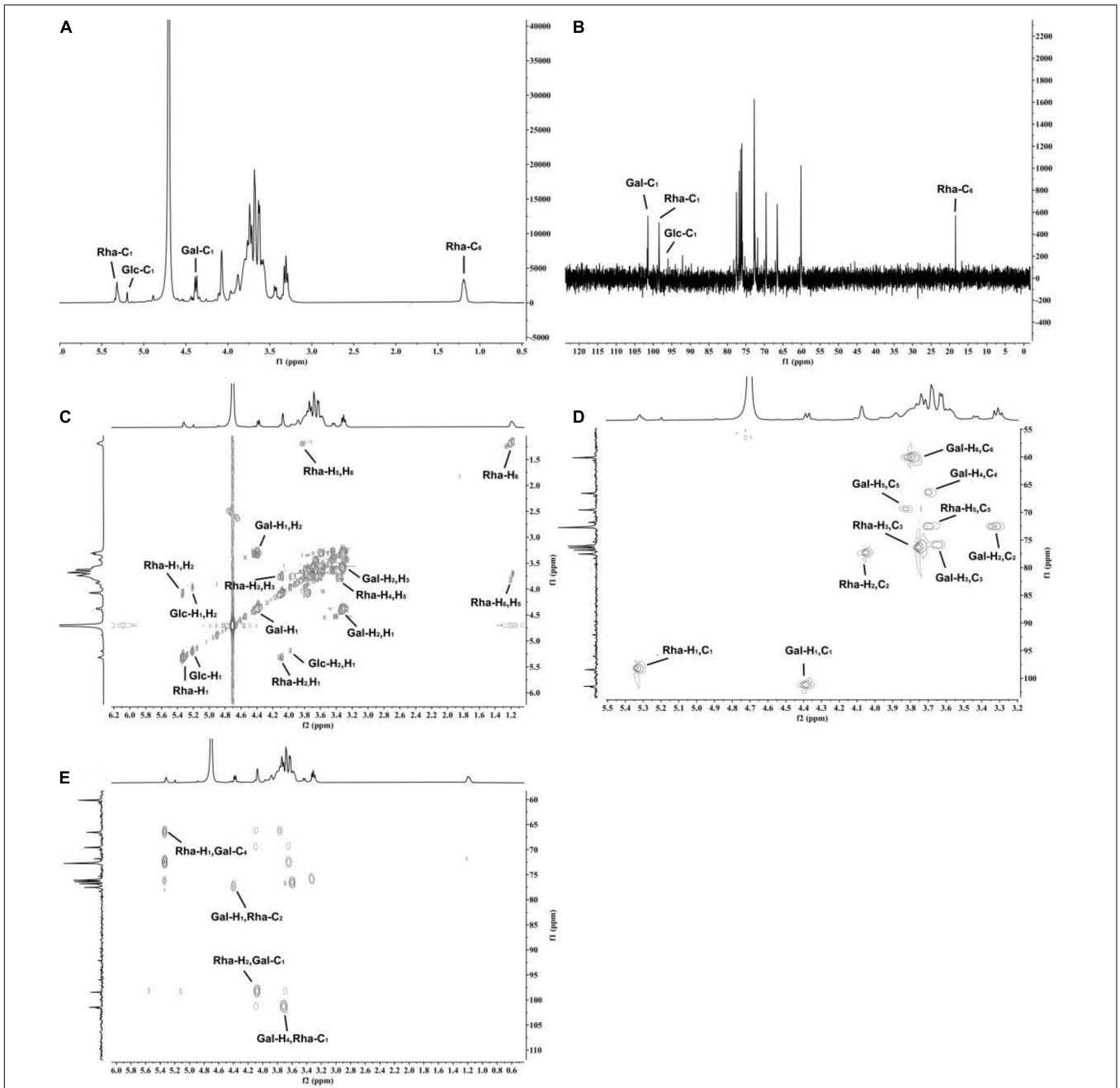

FIGURE 5 | The NMR spectroscopy of polysaccharide K-CMLP. ^{1}H NMR **(A)**, ^{13}C NMR **(B)**, ^{1}H- ^{1}H COSY **(C)**, ^{1}H-^{13}C HSQC **(D)**, and ^{1}H-^{13}C HMBC **(E)**.

TABLE 3 | Chemical shift assignment of K-CMLP.

Code	$^{1}H/^{13}C$ NMR δ [ppm]					
	1	2	3	4	5	6
Gal	4.38	3.30	3.58	3.62	3.75	3.73
	101.1	72.5	75.8	66.4	69.3	60.1
Rha	5.32	4.07	3.68	–	3.63	1.18
	98.5	77.6	76.5	–	72.4	18.4
Glc	5.21	3.97	–	–	–	–
	96.1	–	–	–	–	–

(–) Polysaccharide resonances were not assigned due to low intensity and overlap with other resonances.

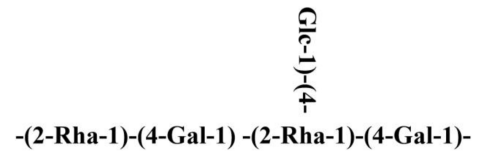

FIGURE 6 | Schematic diagram of polysaccharide K-CMLP.

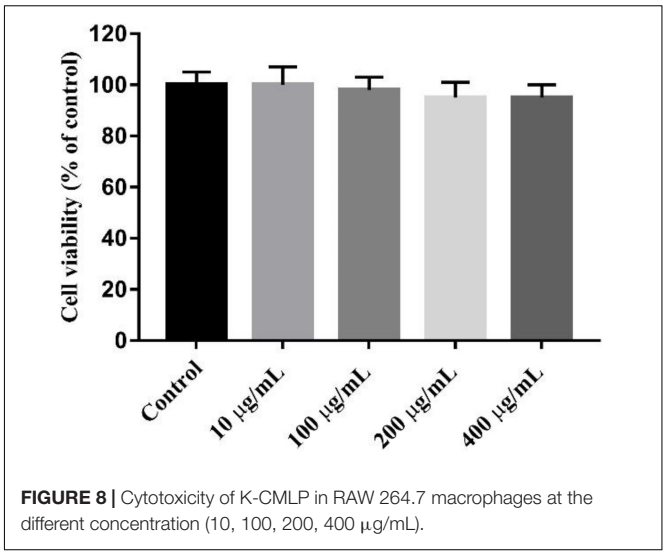

FIGURE 8 | Cytotoxicity of K-CMLP in RAW 264.7 macrophages at the different concentration (10, 100, 200, 400 μg/mL).

respectively. Combining with the results of monosaccharide composition (**Figure 5B**), it was concluded that these three anomeric hydrogens belong to β-Gal*p*, α-Rha*p*, and α-Glc*p*, respectively, and the chemical shifts of β-Gal*p*, α-Rha*p*, and α-Glc*p* of ^{13}C NMR were δ101.1, δ98.5, and δ96.1 ppm, respectively. The absorption peak at 18.41 ppm was the typical methyl signal peak of rhamnose. The chemical shifts of carbon and hydrogen on K-CMLP were assigned by ^{1}H-^{1}H COSY (**Figure 5C**) and HSQC (**Figure 5D**), and the results are summarized in **Table 3**. In the HMBC spectrum (**Figure 5E**), the (Gal-H4, Rha-C1) and (Rha-H1, Gal-C4) cross-peaks indicated that the rhamnose residue was connected to O-4 of galactose. The cross-peaks (Gal-H1,

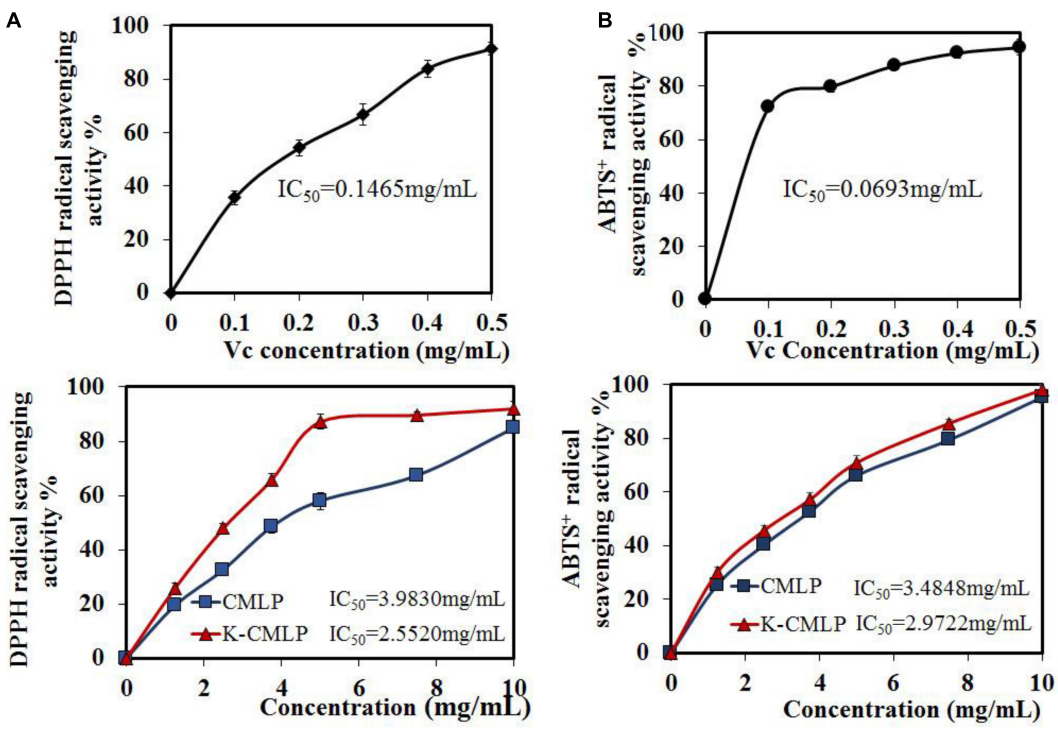

FIGURE 7 | Antioxidant activities of CMLP and K-CMLP: *DPPH*· radical-scavenging activity **(A)**; *ABTS*$^{+}$· radical-scavenging activity **(B)**. Values are the mean ± SD of three replicates.

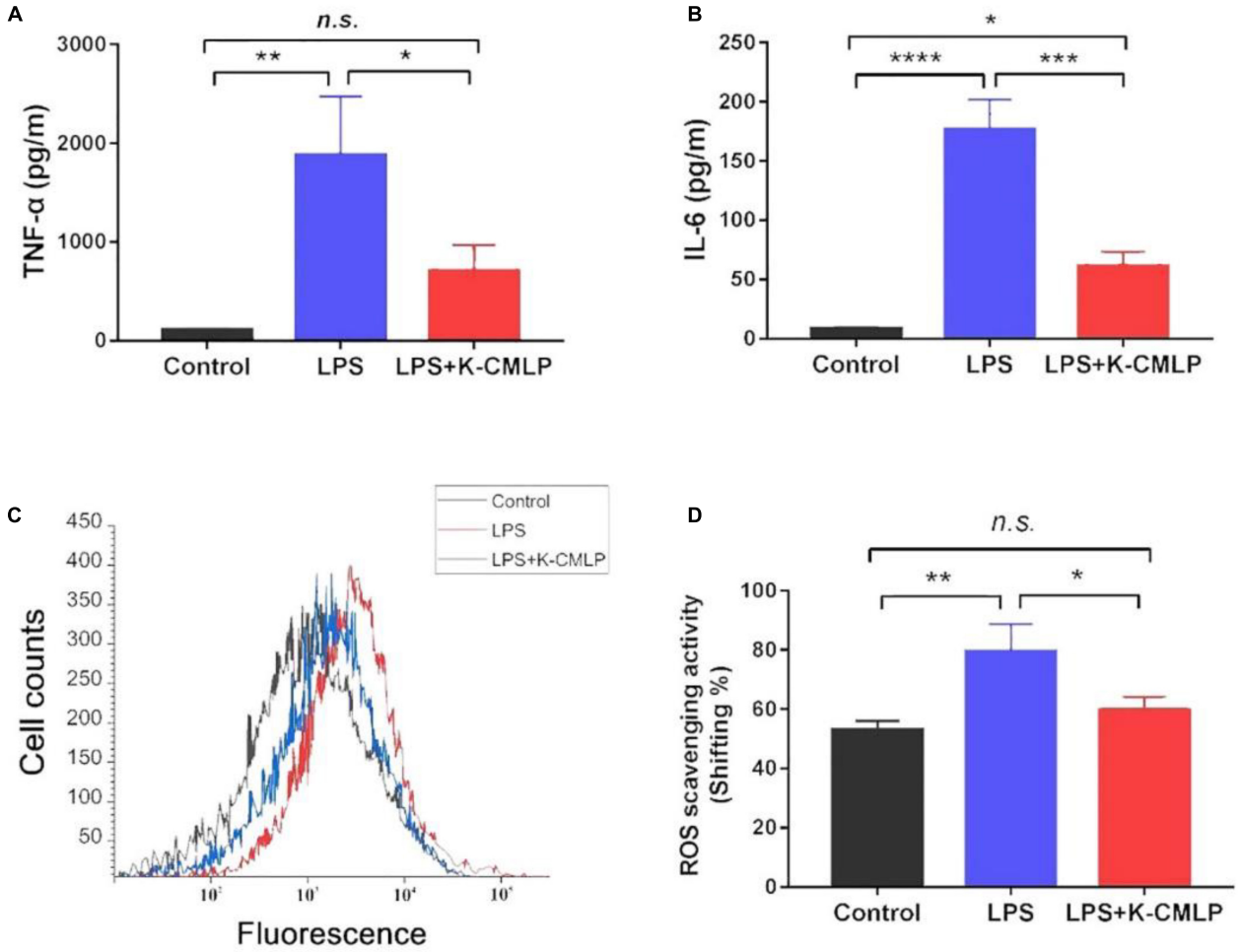

FIGURE 9 | Anti-inflammation effect of K-CMLP on production of pro-inflammatory cytokines [TNF-α **(A)**, IL-6 **(B)**], cell counts **(C)** and reactive oxygen species (ROS) scavenging activity **(D)** in LPS induced RAW 264.7 cells model. Values represent the mean ± SE (bars) from eight independent samples (n = 3). * Means $P < 0.05$, ** means $P < 0.05$, ***$P < 0.0005$, and ****$P < 0.0001$ compared with the only LPS treated group for incubating 24 h.

Rha-C2) and (Rha-H2, Gal-C1) indicated that the galactose residue was attached to O-2 of rhamnose. The structure of polysaccharides was very complex, and only the repetitive units in polysaccharides could be analyzed by methylation analysis and NMR analysis. However, more accurate structural information on polysaccharides needs to be combined with a lot of structural verification, such as partial acid hydrolysis, Smith degradation and so on. In summary, the repeating units of K-CMLP main chain were 1, 2-Rha and 1, 4-Gal alternately connected, and a small amount of glucose residues were connected to O-4 of rhamnose (**Figure 6**). The polysaccharide K-CMLP contains a large number of hydroxyl groups, forming intramolecular and intermolecular hydrogen bonds in an aqueous solution (29), so that they have strong water retention because the complex three-stage network structure formed by its intermolecular action has an aqueous solution with remarkable viscoelasticity (30, 31). It has been reported that enhancing the viscosity of the digesta could help some physiological responses, including constipation relief and blood glucose control (32), which suggested that the polysaccharide K-CMLP might help control blood glucose and cholesterol levels.

Antioxidant Activity of Citrus medica L. var. polysaccharide and K-CMLP

The *DPPH*· and $ABTS^{+}$· tests were widely used to evaluate the ability of compounds to scavenge free radicals *in vitro* (33). As shown in **Figure 7A**, CMLP and K-CMLP were able to scavenge *DPPH*· radicals to different degrees in a dose-dependent manner when the concentration ranged from 0 to 10.0 mg/mL. The higher *DPPH*· scavenging activity was displayed by the homogeneous polysaccharide K-CMLP with IC_{50} = 2.5520 mg/mL. Obtained results showed that K-CMLP is the main component in the crude polysaccharide which has antioxidant activity. In the case of $ABTS^{+}$· scavenging activity, the various samples showed the same trend, and K-CMLP was the most effective compared with CMLP (IC_{50} = 2.9722 mg/mL) (**Figure 7B**). These results revealed that

K-CMLP contains many hydroxyl groups, with high hydrogen-donating capacity.

Anti-inflammatory Activity of K-CMLP

The MTT test showed that K-CMLP had no cytotoxicity to RAW 264.7 macrophages at different concentrations (10, 100, 200, and 400 μg/mL), and cell viability was more than 95% (**Figure 8**). Macrophages, important components in the human immune defense system, respond actively to inflammation by releasing pro-inflammatory cytokines, such as TNF-α, IL-1β, and IL-6; high levels of these cytokines can cause systemic complications (34, 35). Lipopolysaccharide (LPS) was an outer membrane component of Gram-negative bacteria that can cause severe inflammation by triggering the production of various proinflammatory cytokines. When LPS was added to the cells, TNF-α and IL-6 increased significantly (36). However, the production of LPS-induced TNF-α ($P < 0.05$ **Figure 9A**) and IL-6 ($P < 0.0005$, **Figure 9B**) was significantly inhibited by the polysaccharide K-CMLP. Both systemic and local inflammation may foster an oxidative injury with the release of ROS (37). To investigate whether the anti-inflammatory effect of polysaccharide K-CMLP was related to its antioxidant activity, the production of ROS detected by the fluorescent probe DCFH-DA was evaluated. As shown in **Figures 9C,D**, LPS treatment significantly increased the ROS production of RAW 264.7 cells. However, when treated with the polysaccharide K-CMLP, the production of ROS was significantly inhibited. These data support the hypothesis that the anti-inflammatory effect of polysaccharide K-CMLP may be related to its antioxidant capacity.

CONCLUSION

In this study, a novel high molecular polysaccharide K-CMLP was purified from finger citron. K-CMLP is a new type of galactorhamnan with a molecular weight of 3.76×10^3 kDa. The main linkage types of K-CMLP were 1,2,4-Rha-linked-1, 4-Gal and were substituted by β-D-Gal*p* units at 4-OH of rhamnose. Up to now, the proportion of rhamnose in the reported polysaccharides isolated from finger citron is relatively less than arabinose, galactose, glucose, and xylose. Overall, K-CMLP was a new type of galactorhamnan. Both CMLP and K-CMLP exhibited potential antioxidant activities *in vitro*. Our findings suggest that K-CMLP is able to inhibit the production of pro-inflammatory cytokines (TNF-α, IL-6), as well as ROS in LPS-stimulated RAW 264.7 macrophages. In conclusion, this is the first report describing a novel galactorhamnan polysaccharide present in finger citron fruit, and the bioactivity data suggest that K-CMLP could be used as a function food for health.

DATA AVAILABILITY STATEMENT

The original contributions presented in this study are included in the article/supplementary material, further inquiries can be directed to the corresponding authors.

AUTHOR CONTRIBUTIONS

BL and PC contributed to the conception, design, and funding of the study. BL completed the purification of the polysaccharide and identified its structure. JL completed the antioxidant assay of polysaccharides. KL completed the anti-inflammatory assay of polysaccharides. PL and PC completed the writing and revision of the manuscript. All authors contributed to the article and approved the submitted version.

FUNDING

The work was supported by a key project at the central government level: the ability establishment of sustainable use for valuable Chinese medicine resources (2060302), Traditional Chinese Medicine Bureau of Guangdong Province (20212123), and Medical Scientific Research Foundation of Guangdong Province, China (B2021357).

REFERENCES

1. Yang L, Ye J, Guo WD, Wang CC, Hu HT. Differences in cold tolerance and expression of two fatty acid desaturase genes in the leaves between fingered citron and its dwarf mutant. *Trees.* (2012) 26:1193–201. doi: 10.1007/s00468-012-0695-6
2. Ma QG, Wei RR, Yang M, Huang XY, Wang F, Dong JH, et al. Isolation and characterization of neolignan derivatives with hepatoprotective and neuroprotective activities from the fruits of *Citrus medica* L. var. Sarcodactylis Swingle. *Bioorganic Chem.* (2021) 107:104622. doi: 10.1016/j.bioorg.2020.104622
3. He ZC, Liang FJ, Zhang YY, Pan YJ. Water-soluble polysaccharides from finger citron fruits (*Citrus medica* L. var. sarcodactylis). *Carbohydrate Res.* (2014) 388:100–4. doi: 10.1016/j.carres.2013.12.020
4. Peng B, Luo YY, Hu XJ, Song LY, Yang JN, Zhu JH, et al. Isolation, structural characterization, and immunostimulatory activity of a new water-soluble polysaccharide and its sulfated derivative from *Citrus medica* L. var. sarcodactylis. *Int J Biol Macromol.* (2019) 123:500–11. doi: 10.1016/j.ijbiomac.2018.11.113
5. Luo XG, Wang J, Chen HQ, Zhou AM, Song MY, Zhong QP, et al. Identification of flavoanoids from finger citron and evaluation on their antioxidative and antiaging activities. *Front Nutr.* (2020) 7:584900. doi: 10.3389/fnut.2020.584900
6. Taskinen MR, Lahdenperä S, Syvänne M. New insights into lipid metabolism in non-insulin-dependent diabetes mellitus. *Ann Med.* (1996) 28:335–40. doi: 10.3109/07853899608999090
7. Chen XA, Chen HQ, Xiao J, Liu JY, Tang N, Zhou AM. Variations of volatile flavour compounds in finger citron (*Citrus medica* L. var. sarcodactylis) pickling process revealed by E-nose, HS-SPME-GC-MS and HS-GC-IMS. *Food Res Int (Ottawa, Ont).* (2020) 138:109717. doi: 10.1016/j.foodres.2020.109717
8. Wang Y, Khan FA, Siddiqui M, Aamer M, Lu C, Atta Ur R, et al. The genus Schefflera: a review of traditional uses, phytochemistry and pharmacology. *J Ethnopharmacol.* (2021) 279:113675. doi: 10.1016/j.jep.2020.113675
9. Tayyab M, Farheen S, Mubeena MMP, Khanam N, Shahi MH. Antidepressant and neuroprotective effects of naringenin via sonic hedgehog-gli1 cell signaling pathway in a rat model of chronic unpredictable mild stress. *Neuromol Med.* (2019) 21:250–61. doi: 10.1007/s12017-019-08538-6

10. Li ZH, Cai M, Liu YS, Sun PL, Luo SL. Antibacterial activity and mechanisms of essential oil from *Citrus medica* L. var. sarcodactylis. *Molecules (Basel, Switzerland).* (2019) 24:1577. doi: 10.3390/molecules24081577
11. Chhikara N, Kour R, Jaglan S, Gupta P, Gat Y, Panghal A. *Citrus medica*: nutritional, phytochemical composition and health benefits - a review. *Food Funct.* (2018) 9:1978–92. doi: 10.1039/c7fo02035j
12. Chen H, Wang J, Liu X, Zhou A, Xiao J, Huang K, et al. Optimization in continuous phase-transition extraction of crude flavonoids from finger citron fruit and evaluation on their antiaging activities. *Food Sci Nutr.* (2020) 8:1636–48. doi: 10.1002/fsn3.1450
13. Wang E, Li Y, Maguy BL, Lou Z, Wang H, Zhao W, et al. Separation and enrichment of phenolics improved the antibiofilm and antibacterial activity of the fractions from *Citrus medica* L. var. sarcodactylis in vitro and in tofu. *Food Chem.* (2019) 294:533–8. doi: 10.1016/j.foodchem.2019.05.038
14. Barreca D, Mandalari G, Calderaro A, Smeriglio A, Trombetta D, Felice MR, et al. *Citrus* flavones: an update on sources, biological functions, and health promoting properties. *Plants (Basel, Switzerland).* (2020) 9:288. doi: 10.3390/plants9030288
15. Kim KN, Ko YJ, Yang HM, Ham YM, Roh SW, Jeon YJ, et al. Anti-inflammatory effect of essential oil and its constituents from fingered citron (*Citrus medica* L. var. sarcodactylis) through blocking JNK, ERK and NF-κB signaling pathways in LPS-activated RAW 264.7 cells. *Food Chem Toxicol.* (2013) 57:126–31. doi: 10.1016/j.fct.2013.03.017
16. Wu Z. Effect of different drying methods on chemical composition and bioactivity of finger citron polysaccharides. *Int J Biol Macromol.* (2015) 76:218–23. doi: 10.1016/j.ijbiomac.2015.02.043
17. Zhou T, Jiang Y, Wen LR, Yang B. Characterization of polysaccharide structure in *Citrus reticulate* 'Chachi' peel during storage and their bioactivity. *Carbohydrate Res.* (2021) 508:108398. doi: 10.1016/j.carres.2021.108398
18. Luo B, Dong LM, Xu QL, Zhang Q, Liu WB, Wei XY, et al. Characterization and immunological activity of polysaccharides from *Ixeris polycephala*. *Int J Biol Macromol.* (2018) 113:804–12. doi: 10.1016/j.ijbiomac.2018.02.165
19. Sevag MG, Lackman DB, Smolens J. The isolation of the components of streptococcal nucleoproteins in serologically active form. *J Biol Chem.* (1938) 124:42–9. doi: 10.1029/97PA02893
20. Chen P, Hei M, Kong L, Liu Y, Yang Y, Mu H, et al. One water-soluble polysaccharide from *Ginkgo biloba* leaves with antidepressant activities via modulation of the gut microbiome. *Food Funct.* (2019) 10:8161–71. doi: 10.1039/c9fo01178a
21. Masuko T, Minami A, Iwasaki N, Majima T, Nishimura S, Lee YC. Carbohydrate analysis by a phenol-sulfuric acid method in microplate format. *Anal Biochem.* (2005) 339:69–72. doi: 10.1016/j.ab.2004.12.001
22. Blumenkrantz N, Asboe-Hansen G. New method for quantitative determination of uronic acids. *Anal Biochem.* (1973) 54:484–9. doi: 10.1016/0003-2697(73)90377-1
23. Bradford MM. A rapid and sensitive method for the quantitation of microgram quantities of protein utilizing the principle of protein-dye binding. *Anal Biochem.* (1976) 72:248–54. doi: 10.1006/abio.1976.9999
24. Hakomori S. A rapid permethylation of glycolipid, and polysaccharide catalyzed by methylsulfinyl carbanion in dimethyl sulfoxide. *J Biochem.* (1964) 55:205–8. doi: 10.1093/oxfordjournals.jbchem.a127869
25. Ji X, Cheng Y, Tian J, Zhang S, Shi M. Structural characterization of polysaccharide from jujube (*Ziziphus jujube* Mill.) fruit. *Chem Biol Technol Agric.* (2021) 8:54. doi: 10.1186/s40538-021-00255-2
26. Chen L, Wu JE, Li ZM, Liu Q, Zhao X, Yang HS. Metabolomic analysis of energy regulated germination and sprouting of organic mung bean (*Vigna radiata*) using NMR spectroscopy. *Food Chem.* (2019) 286:87–97.
27. Huang H, Huang G. Extraction, separation, modification, structural characterization, and antioxidant activity of plant polysaccharides. *Chem Biol Drug Design.* (2020) 96:1209–22. doi: 10.1111/cbdd.13794
28. Abbou A, Kadri N, Debbache N, Dairi S, Remini H, Dahmoune F, et al. Effect of precipitation solvent on some biological activities of polysaccharides from *Pinus halepensis* Mill. seeds. *Int J Biol Macromol.* (2019) 141:663–70. doi: 10.1016/j.ijbiomac.2019.08.266
29. Yang DY, Gao S, Yang HS. Effects of sucrose addition on the rheology and structure of iota-carrageenan. *Food Hydrocolloids.* (2020) 99:105317.
30. Ran XL, Yang ZX, Chen YF, Yang HS. Konjac glucomannan decreases metabolite release of a plant-based fshball analogue during *in vitro* digestion by affecting amino acid and carbohydrate metabolic pathways. *Food Hydrocolloids.* (2022) 129:107623.
31. Huang M, Zhao X, Mao YH, Chen L, Yang HS. Metabolite release and rheological properties of sponge cake after *in vitro* digestion and the influence of a flour replacer rich in dietary fibre. *Food Res Int.* (2021) 144:110355.
32. Lentle R, Janssen P. Physical characteristics of digesta and their influence on flow and mixing in the mammalian intestine: a review. *J Comparat Physiol B Biochem Syst Environ Physiol.* (2008) 178:673. doi: 10.1007/s00360-008-0264-x
33. Ji XL, Guo JH, Ding DQ, Gao J, Hao LR, Guo XD, et al. Structural characterization and antioxidant activity of a novel high-molecular-weight polysaccharide from *Ziziphus Jujuba* cv. Muzao. *J Food Measurement Characterization.* (2022) 16:1–10. doi: 10.1007/s11694-022-01288-3
34. Xie Z, Wang Y, Huang J, Qian N, Shen G, Chen L. Anti-inflammatory activity of polysaccharides from *Phellinus linteus* by regulating the NF-κB translocation in LPS-stimulated RAW 264.7 macrophages. *Int J Biol Macromol.* (2019) 129:61–7. doi: 10.1016/j.ijbiomac.2019.02.023
35. Lee SY, Kim HJ, Han JS. Anti-inflammatory effect of oyster shell extract in LPS-stimulated RAW 264.7 cells. *Prevent Nutr Food Sci.* (2013) 18:23–9. doi: 10.3746/pnf.2013.18.1.023
36. Si MK, Mitaka C, Tulafu M, Abe S, Kitagawa M, Ikeda S, et al. Inhibition of poly (adenosine diphosphate-ribose) polymerase attenuates lung-kidney crosstalk induced by intratracheal lipopolysaccharide instillation in rats. *Respiratory Res.* (2013) 14:126. doi: 10.1186/1465-9921-14-126
37. Tien KJ, Chou CW, Lee SY, Yeh NC, Yang CY, Yen FC, et al. Obstructive sleep apnea and the risk of atopic dermatitis: a population-based case control study. *PLoS One.* (2014) 9:e89656. doi: 10.1371/journal.pone.0089656

Conflict of Interest: The authors declare that the research was conducted in the absence of any commercial or financial relationships that could be construed as a potential conflict of interest.

Publisher's Note: All claims expressed in this article are solely those of the authors and do not necessarily represent those of their affiliated organizations, or those of the publisher, the editors and the reviewers. Any product that may be evaluated in this article, or claim that may be made by its manufacturer, is not guaranteed or endorsed by the publisher.

Copyright © 2022 Luo, Lv, Li, Liao and Chen. This is an open-access article distributed under the terms of the Creative Commons Attribution License (CC BY). The use, distribution or reproduction in other forums is permitted, provided the original author(s) and the copyright owner(s) are credited and that the original publication in this journal is cited, in accordance with accepted academic practice. No use, distribution or reproduction is permitted which does not comply with these terms.

frontiers | Frontiers in Nutrition

ORIGINAL RESEARCH
published: 09 June 2022
doi: 10.3389/fnut.2022.912014

Ultrasound-Assisted Deep Eutectic Solvents Extraction of Polysaccharides From *Morchella importuna*: Optimization, Physicochemical Properties, and Bioactivities

Xu Pan[1], Lijing Xu[1,2], Junlong Meng[1,3]*, Mingchang Chang[1,3], Yanfen Cheng[1,2], Xueran Geng[1,2], Dongdong Guo[1] and Rongzhu Liu[1]*

[1] College of Food Science and Engineering, Shanxi Agricultural University, Jinzhong, China, [2] Shanxi Key Laboratory of Edible Fungi for Loess Plateau, Taigu, China, [3] Shanxi Engineering Research Center of Edible Fungi, Taigu, China

OPEN ACCESS

Edited by:
Xin Wang,
Northwest A&F University, China

Reviewed by:
Zichao Wang,
Henan University of Technology, China
Lei Yuan,
Tibet Agriculture and Animal Husbandry University, China

***Correspondence:**
Lijing Xu
xulijingsx@hotmail.com
Junlong Meng
mengjunlong@hotmail.com

Specialty section:
This article was submitted to Food Chemistry, a section of the journal Frontiers in Nutrition

Received: *03 April 2022*
Accepted: *27 April 2022*
Published: *09 June 2022*

Citation:
Pan X, Xu L, Meng J, Chang M, Cheng Y, Geng X, Guo D and Liu R (2022) Ultrasound-Assisted Deep Eutectic Solvents Extraction of Polysaccharides From Morchella importuna: Optimization, Physicochemical Properties, and Bioactivities. Front. Nutr. 9:912014. doi: 10.3389/fnut.2022.912014

In this study, a high-efficiency and non-pollution extraction procedure, ultrasound-assisted technique with deep eutectic solvents (DESs), was applied for extraction of polysaccharides from *Morchella importuna* (MIP-D). The results exhibited that the system of DES was: mole ratio between choline chloride and oxalic acid of 2:1, water content of 90% (v/v), and the optimal extraction parameters were as follows: extraction time of 31.2 min, extraction temperature of 62.1°C, and the liquid–solid ratio of 32.5:1 (v/w). Under these extraction parameters, the extraction yield of MIP-D was 4.5 times higher than hot water extraction (HWE) method and had higher carbohydrate (85.27%) and sulfate contents (34.16%). Moreover, high-performance liquid chromatography (HPLC) and Fourier-transform IR (FTIR) spectrum analysis indicated that MIP-D was comprised of glucosamine, galactose, glucose, and mannose, with molar ratios of 0.39:1.88:3.82:3.91, which contained the pyranose ring skeleton. High-performance gel permeation chromatography (HPGPC) analysis revealed that MIP-D showed three fractions with molecular weights of 2.6×10^6, 7.3×10^4, and 3.7×10^3 Da, which were lower than those of polysaccharides extracted by HWE. *In-vitro* tests proved that MIP-D possessed excellent antioxidant and inhibited α-amylase and α-glucosidase inhibitory activities. Therefore, DESs (choline chloride-oxalic acid) as a high-efficiency and non-pollution solvent alternative can be applied to the separation of bioactive polysaccharides from *Morchella importuna* (*M. importuna*).

Keywords: *Morchella importuna*, polysaccharides, deep eutectic solvent, ultrasound-assisted extraction, antioxidant activity, hypoglycemic activity

INTRODUCTION

Polysaccharide, comprising of more than ten monosaccharides, is one of the four basic substances that make up life, found in animal cell membranes and cell walls of plants and microorganisms (1). Previous studies have also demonstrated that polysaccharide has the effects of antitumor, antifatigue, postponing aging, reducing blood lipid, hypoglycemic activity, and so on (2, 3).

Moreover, traditional separation methods of polysaccharides from natural materials have been associated with longer extraction time, lower efficiency, and environmentally disastrous (4). Thus, efficient and green extraction methods of polysaccharides are required to overcome these problems.

The most effective methods for separating polysaccharides are chemical treatment. Chemical methods generally use strong alkali and acid to remove impurities, respectively, so they are not environmentally friendly. Compared with chemical methods, biological methods using enzymes are more environmentally friendly, but these methods not only have low extraction efficiency, but also are not conducive to large-scale industrial production (5). Recently, deep eutectic solvents (DESs) have been found to be composed of hydrogen bond donors (HBDs) and hydrogen bond acceptors (HBAs) in a certain proportion (6). They can provide or accept external electrons or protons to form hydrogen bonds (4). Therefore, they can dissolve a variety of substances, such as polysaccharides and salts (7). In addition, deep eutectic solvents (DESs) not only have good properties of ionic liquids, such as excellent solubility, chemical stability, and thermal stability (8), but also have simple preparation, low cost, and no pollution (9). Currently, some studies have shown that DESs can be used as alternative solvents to extract polysaccharides from natural samples.

Morchella importuna (*M. importuna*), belonging to the Ascomycota, is widely distributed in Europe, Asia, and America and known as one of the rare and precious edible fungi in the world (10). Previous studies have also demonstrated that polysaccharides are one of the main bioactive components in *M. importuna* (11). However, extraction of polysaccharides from *M. importuna* has been rarely reported. Especially, the effect of choline chloride-oxalic acid (ChCl-OA) as an extraction medium on the physicochemical properties and bioactivities of *M. importuna* polysaccharides (MIPs) has not been studied.

Therefore, a high-efficiency and non-pollution extraction procedure was developed for the extraction of polysaccharides from *Morchella importuna* by ultrasound-assisted extraction (UAE). The optimum extraction conditions were optimized with the response surface methodology (RSM) employing Box–Behnken design (BBD). Subsequently, the physical–chemical characteristics of MIP-D were investigated by high-performance liquid chromatography (HPLC), high-performance gel permeation chromatography (HPGPC), and Fourier-transform IR (FTIR) and the biological activities of MIP-D were evaluated based on its antioxidant and hypoglycemic abilities.

MATERIALS AND METHODS

Materials and Chemical Reagents

Standard monosaccharides were purchased from Sigma Chemical Corporation (United States). Reagents containing choline chloride, oxalic acid dihydrate, citric acid, glycerol, 1,4-butanediol, acetamide, urea, anhydrous ethanol, citric acid, α-amylase, α-glucosidase, 1,1-diphenyl-2-picrylhydrazyl (DPPH), 2,2′-Azinobis-(3-ethylbenzthiazoline-6-sulphonate) (ABTS), and OH assay kit were purchased from Solarbio Science (Beijing, China). Other chemicals used throughout the experiment were analytical grade.

Extraction Methods

Deep Eutectic Solvent Preparation

The preparation of DESs was conducted as previously described (12). Six different types of DES were prepared by the heating method and used as solvent for ultrasonic-assisted extraction of MIPs instead of water. The types of DESs are shown in **Supplementary Table 1**. DESs were produced by mixing HBDs and HBAs in water bath at 80°C according to a certain molar ratio until they were completely dissolved and a colorless and transparent thick liquid was formed at room temperature.

Preparation of *M. importuna* Polysaccharides

The *M. importuna* was dried to constant weight and crushed with a grinder (Zhejiang Hongjingtian Corporation Ltd., Zhejiang, China) and the powder was obtained through the 50-size mesh. The extraction process was performed in an ultrasonic cleaner (KQ5200DE type, 40 kHz, 10 L, 600 W, Kunshan Ultrasonic Instrument Corporation Ltd., Kunshan, China).

The powder was mixed with DES that had been prepared and the mixture was incubated at a constant temperature, followed by the collection of the supernatant *via* centrifugation under 5,000 *g* for 10 min (Allegra 64R Centrifuge, Beckman Coulter Incorporation, Brea, CA, United States). Then, the protein in the supernatant was removed by the potassium ferrocyanide-zinc acetate method and dialyzed with distilled water for 24 h. The quadruple volume of dehydrated ethanol was added in the resulting solution, which was then placed at 4°C overnight to complete precipitation and then collected the precipitation, dissolved it with an appropriate amount of water and freeze-dried to obtain the crude polysaccharide from *M. importuna*.

In order to evaluate the UAE of MIPs, the polysaccharide from *M. importuna* by hot water method (MIP-W) was studied. The *M. importuna* powder (1 g) was added to 30 ml of distilled water and incubated at 80°C for 2 h. After repeated extraction for three times, the supernatant was combined, dialyzed, precipitated, and dried according to the above method.

Optimization of Ultrasound-Assisted Extraction

Effects of DES-1 mole ratio (1.5:1, 2:1, 2.5:1, 3:1, and 3.5:1), water content of DES-1 (10, 30, 50, 70, 90, and 100%, w/w), extraction time (10, 20, 30, 40, and 50 min), extraction temperature (40, 50, 60, 70, and 80°C), and liquid–solid ratio (10, 20, 30, 40, and 50 v/w) on the extraction efficiency of MIPs were studied by single factor test. Under the conditions of other factors remaining unchanged, each experimental factor was optimized. Finally, the extraction time, extraction temperature, and liquid–solid ratio were determined as the main factors. Based on the results from the above experiment, the response surface methodology (RSM) employing Box–Behnken design (BBD) was used to optimize the three main parameters and the extraction efficiency of MIPs was regarded as the response. The experimental designs of the code levels of the three influencing factors were nominated as (−1, 0, and +1) and

actual experimental values of each variable are shown in **Supplementary Table 2**. Each experiment was carried out three times. The experimental data obtained from BBD were analyzed by regression analysis. Under the optimal parameters, the extraction experiment was repeated for three times to verify the accuracy of RSM. The polysaccharide from *M. importuna* (MIP-D) was extracted under optimized conditions to determine their structural characterizations and bioactivities.

Structural Characterizations and Bioactivities of *Morchella importuna*

Chemical Composition Determination

The extraction efficiency of MIPs (%) was determined as follows: the extraction efficiency of MIPs (%) = [Weight of dried MIPs (g) × Total carbohydrate content of MIPs (%)/Weight of dried *M. importuna* (g)]. The content of carbohydrate, protein, uronic acid, and polyphenol in MIPs was measured by the phenol-sulfuric acid method with glucose as a standard, Bradford method with bovine serum albumin (BSA) as a standard, sulfuric acid-carbazole method with galacturonic acid as a standard, and the Folin–Ciocalteu method with pyrogallic acid as a standard based on our previous study (13, 14). The content of sulfate radical was determined by ion chromatography method with potassium sulfate as a standard according to the reported method (15).

Monosaccharide Composition Determination

The constituent monosaccharides of MIPs were measured by HPLC analysis based on our previous study, which is slightly modified (16). The eluents were NaOH (15 mM) flowing at 0.3 ml/min and 5 μl sample (0.1 mg/ml) was injected at 30°C.

Molecular Weight Determination

The weight-average molecular weight (Mw) of the MIPs was measured by HPGPC analysis on the Agilent 1260 Series HPLC System, equipped with series-connected Ultrahydrogel^{TM} 2000 and Ultrahydrogel^{TM} 500 columns and refractive index detector (RID) (17). The column was calibrated by standard dextrans (T-3, T-10, T-40, T-70, and T-110 series). The eluent was 0.1 mol/l $NaNO_3$, which was injected at 0.5 ml/min and 20 μl sample (5.0 mg/ml) was injected at 35°C.

Ultraviolet Spectrum Analysis

Ultraviolet spectrophotometer (LabTech, UV9100A, Hopkinton, MA, United States) was employed to determine the protein content in range of 200–400 nm.

Fourier-Transform IR Spectroscopy

The MIPs were mixed and grounded with KBr at a weight ratio of 1:100, followed by pressing into tablets. Spectrometer (Tensor 27, Bruker, Germany) was employed to analyze the FTIR spectra of MIPs in the wavenumber region of 4,000–5,000 cm^{-1}.

In-vitro Antioxidant Activities Assays

The DPPH, ABTS, and OH radical scavenging abilities of MIP-D were measured strictly based on the methods of DPPH, ABTS, and OH kit, respectively.

In-vitro α-Amylase and α-Glucosidase Inhibitory Activities

The α-amylase and α-glucosidase inhibitory activities of MIPs were measured according to the reported method (18).

RESULTS AND DISCUSSION

Optimization of Ultrasound-Assisted Extraction

Effect of Deep Eutectic Solvent System

In the process of extracting target bioactive substances from the sample, the physicochemical properties of the extraction solvent were essential conditions for this study, which might be due to the permeability of the extractant in the sample matrix that can be determined directly by them (4). According to different hydrogen bond donors, six different types of DES were synthesized in order to select a suitable DES for the extraction of MIPs (19). As shown in **Figure 1A**, the extraction efficiency varied with different types of DES. By comparing the hot water extraction (HWE), DES-1 and DES-2 increased the extraction efficiency of MIPs by 3.4 and 2.8 times, respectively. There was no significant difference between DES-3 and DES-4 in the extraction yields of MIPs. Effects of DES-5 and DES-6 on the extraction yields of MIPs were significantly lower than those obtained by hot water. DES-1 exhibited higher extraction efficiency than others, which might be attributed to its stronger electrostatic interaction between DES-1 and MIPs than those of other DESs (20). Furthermore, oxalic acid and choline chloride are non-toxic substances and widely found in natural foods (21). Therefore, the DES system constructed by choline chloride-oxalic acid was considered for the follow-up experiments.

Effect of Mole Ratio of Deep Eutectic Solvent

As reported, the hydrogen bond interaction of DES was determined by the molar ratio of HBD and HBA in the deep eutectic solvent, which affects the viscosity and surface tension of DES. The physical properties of DES would further affect the extraction efficiency of polysaccharides (4). It was important to note that DES was crystallized when the molar ratio was more than 3.5:1, so increasing the content of choline chloride was not attempted. As shown in **Figure 1B**, we can see that the extraction efficiency of MIPs was significantly affected by the molar ratio of DES-1. Moreover, the extraction efficiency increased with the increasing ratio of choline chloride in DES-1, which might be due to choline chloride improved the viscosity and surface tension of DES-1, thus increasing the permeability of DES-1 in *M. importuna* (4). However, a large number of crystals were produced in the process of alcohol precipitation with a molar ratio of 2.5–3.5:1 in DES-1, which made the subsequent extraction procedure into trouble. Due to this, the mole ratio of ChCl-OA in DES-1 used in the subsequent experiments was 2:1.

Effect of Water Content of Deep Eutectic Solvent

Previous studies have also revealed that the high viscosity and weak mobility of DES would reduce the extraction efficiency

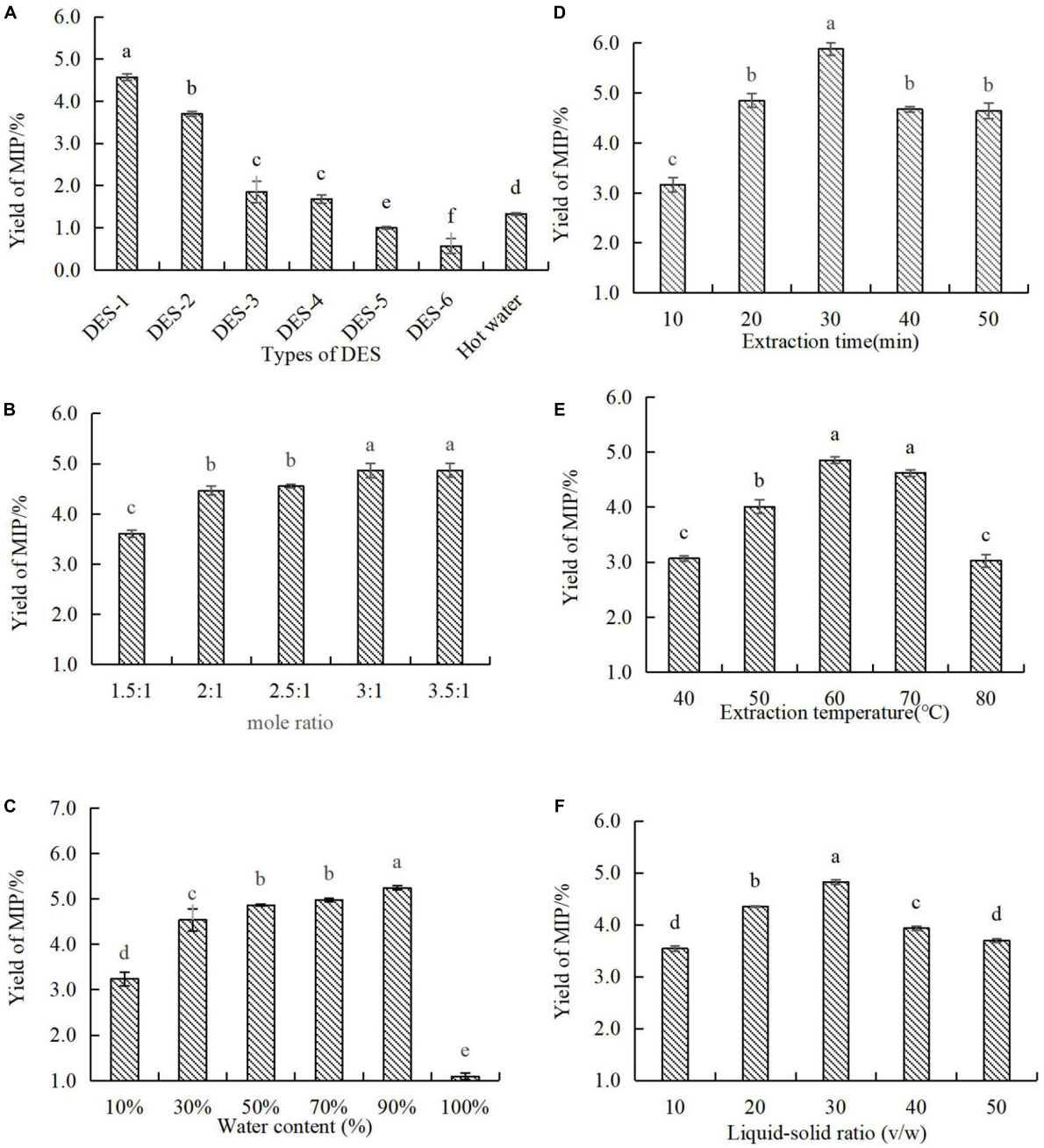

FIGURE 1 | Effect of different extraction parameters in the extraction yield of MIP-D. **(A)** Types of DESs, **(B)** mole ratio, **(C)** water content, **(D)** extraction time, **(E)** extraction temperature, and **(F)** ratio of liquid–solid. Data represent means ± *SD* ($n = 3$). Significant ($p < 0.05$) differences are shown by data bearing different letters (a–d).

of polysaccharides. However, the viscosity and polarity of DES were changed by the water content of DES system (22). Thus, it is essential to choose a suitable water content to improve the mass transfer rate and the processing efficiency. As shown in **Figure 1C**, extraction efficiency varied considerably dependent on DES water content. The extraction efficiency increased significantly with the increasing of the water content of DES-1 from 10 to 90%. This phenomenon might be attributed to the increase of water content in DES-1 leaded to a more suitable viscosity and polarity of DES-1 to improve interactions between polysaccharides and DES-1, which obtained a high extraction yield (4). However, the further increase of water content (100%) resulted in a significant decrease in extraction efficiency. In addition, DES-1 with the water content of 90% was not only easier to produce because of its low viscosity and high fluidity, but also had a lower cost. Therefore,

DES-1 with the water content of 90% was considered for the subsequent experiments.

Effect of Extraction Time

Previous studies had shown that the extraction efficiency was generally proportional to the extraction time (23). As shown in **Figure 1D**, the extraction efficiency of MIPs was affected by prolonging the extraction time. With the extension of extraction time, the extraction efficiency of MIP increased significantly from 3.16 to 5.88%, which might be due to the prolonging of extraction time that can destroy the cellular structure, increase the permeability, and can be conducive to polysaccharides extraction (23). However, when the extraction time increased from 30 to 50 min, the extraction efficiency of MIP dropped from 5.88 to 4.63%. This phenomenon might be related to the hydrolysis of MIPs at high temperature for a long time (24). Hence, the extraction time was selected in 30 min for the subsequent experiments.

Effect of Extraction Temperature

As reported, the extraction temperature is one of the vital factors influencing the extraction yield of polysaccharides (25). As shown in **Figure 1E**, the extraction efficiency of MIPs increased with the increase of extraction temperature from 40 to 60°C and reached the maximum polysaccharides yield (4.85%) at 60°C. This phenomenon might be due to the high temperature that may not only decrease the viscosity of DES-1 and increase the diffusion of DES-1, but also accelerate the mass transport of polysaccharides (19), which makes polysaccharides dissolve more in solvent and improve extraction yield. However, the higher temperature may decrease physical adsorption between the DES and MIPs (21), which will cause the target compounds to be separated from the DES hydrogen bond network. Thus, the extraction efficiency of MIPs decreased from 4.85 to 3.03%. In conclusion, the extraction temperature was selected at 60°C for the subsequent experiments.

Effect of Liquid–Solid Ratio

Study indicated that the liquid–solid ratio could affect the extraction efficiency of polysaccharides (20). As shown in **Figure 1F**, the effect of liquid–solid ratios on the extraction efficiency of MIPs was measured in this experiment. The extraction efficiency of MIPs increased with the increase of liquid–solid ratio from 10:1 to 50:1 and reached the maximum (4.82%) at 30:1 (v/w). However, a further increase of the liquid–solid ratio resulted in lower extraction efficiency. This phenomenon might be due to a small amount of DES-1 that could approach the extraction equilibrium, while a large amount of DES could increase the leaching of other compounds, resulting in the decrease of yield of MIPs. Moreover, the increase of liquid–solid ratio not only enhanced the difficulty of extracting polysaccharides, but also caused wastage of DES-1. Thus, 30:1 (v/w) was considered as the optimal liquid–solid ratio in this experiment.

In a word, the optimal system of DES was: a mole ratio between ChCl and OA of 2:1 and water content of 90% (v/v). Moreover, the preliminary optimization of experimental factors was: extraction time of 30 min, extraction temperature of 60°C, and liquid–solid ratio of 30:1 (v/w).

Optimization of Ultrasound-Assisted Extraction

Statistical Analysis

Based on the results of single-factor experiment, RSM was applied to study the influencing factors of UAE employing Design-Expert software (version 10.0.7). The data of 17 runs with three factors and three levels for optimizing the mutual effects of three parameters are shown in **Supplementary Table 3**. The data were analyzed by multiple regression analysis and the predicted MIPs yield was calculated using following equation:

$$Y = 5.84 + 0.19A + 0.37B + 0.14C - 0.23AB + 0.005976AC - 0.097BC - 0.60A^2 - 0.76B^2 - 0.24C^2$$

The results of the statistical summary are shown in **Table 1**. The F-value of the model was 52.33 ($P < 0.0001$), exhibiting that the model was significant (26). Additionally, the values of the determination coefficient (R^2) and adjusted determination coefficient (R^2_{adj}) were 0.9854 and 0.9665, respectively, which confirmed the highly goodness-of-fit of the model (27). Meanwhile, the value of the coefficient of variation (CV) was 2.28, which demonstrated the excellent reliability of the data (28). The p-values of 0.1793 and the F-value of 2.72 for lack of fit indicated the validity of the model. The linear coefficients (A, B, and C), cross-product coefficient (AB), and the quadratic term coefficients (A^2, B^2, and C^2) were all significant ($p < 0.05$), whereas cross-product coefficients (AC and BC) were not significant. We concluded that the order of three factors as follows: B ($P < 0.0001$) > A ($P = 0.0026$) > C ($P = 0.0128$).

Response Surface Analysis

The effect of the interaction of three factors on the extraction efficiency of MIPs could be visualized by the three-dimensional (3D) response surface (3D plots) and two-dimensional (2D) contour plots (2D plots). The mutual influences of various factors on the extraction efficiency of MIPs were reflected by the 3D plots and the significance of it was displayed by the 2D plots (26). The 3D plots in **Figures 2A,C,E** revealed that with the increase of extraction time (A), extraction temperature (B), and liquid–solid ratio (C), the extraction efficiency of polysaccharides

TABLE 1 | Chemical composition and sugar composition of MIPs.

Sample	Carbohydrate/%	Protein/%	Sulfate content/%	Polyphenols/%
MIP-D	85.27 ± 1.35	2.57 ± 0.06	34.16 ± 1.61	4.49 ± 0.39
MIP-W	57.89 ± 2.63	3.85 ± 0.03	24.43 ± 1.15	10.60 ± 0.35

Sugar composition (molar ratio)

	GlcN	Gal	Glc	Man
MIP-D	0.39	1.88	3.82	3.91
MIP-W	2.71	1.06	5.59	3.01

Each value represents the mean ± SD (n = 3).

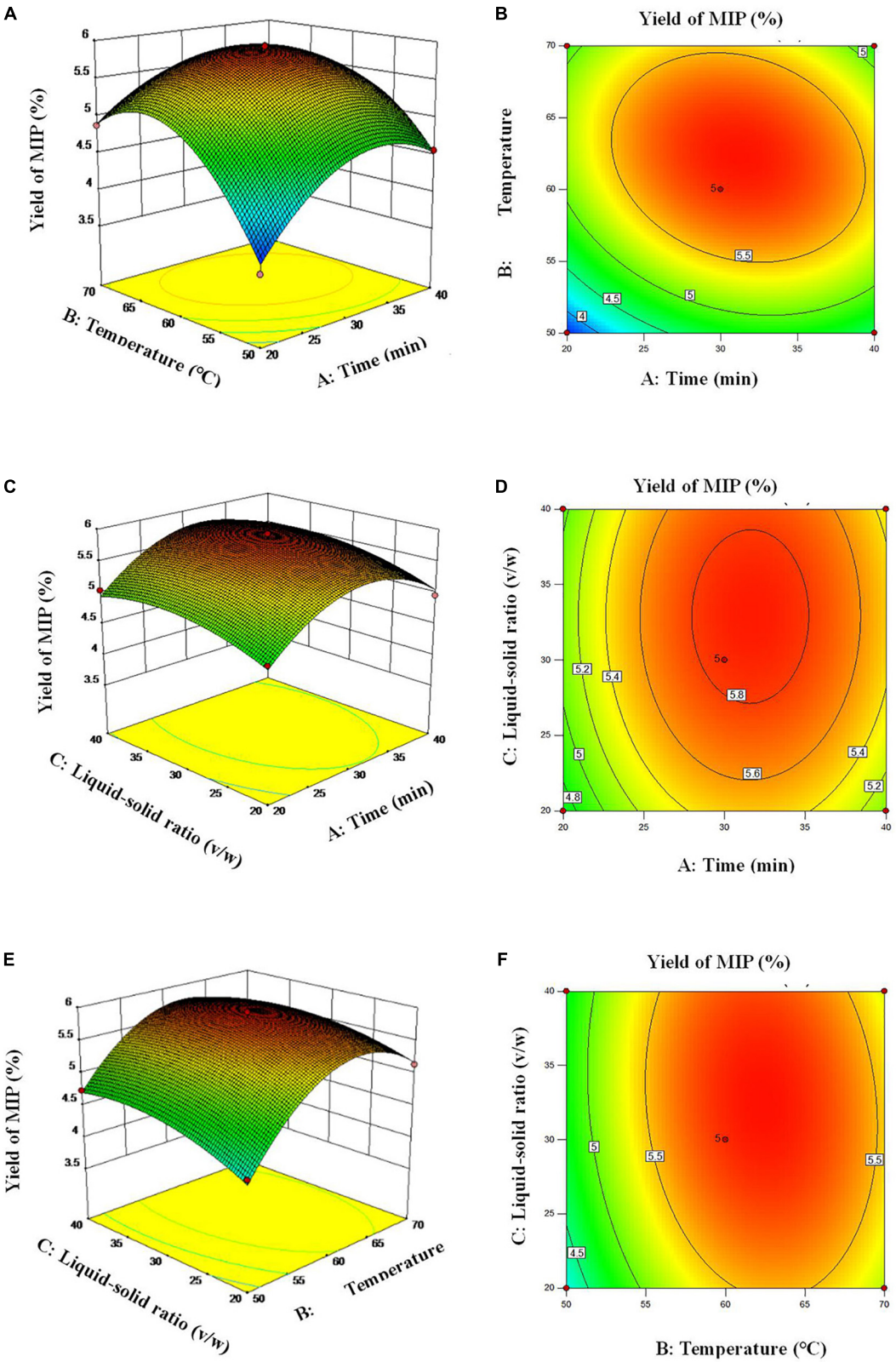

FIGURE 2 | Response surface plots **(A,C,E)** and response contour plots **(B,D,F)** showing the extraction time, extraction temperature and Liquid-solid ratio on the extraction yield of MIP.

increased first and then decreased. The 2D of **Figure 2B** showed that the interaction between A and extraction temperature B is significant. This observation agreed with the results of the *p*-value of cross-product coefficient (AB). **Figures 2D,F** illustrate that the interaction between AC and BC was insignificant.

Response Surface Results Optimization

By using Design-Expert software (version 10.0.7), the optimal conditions of three parameters were obtained and proposed as a practical response variable for the extraction: extraction time (A) of 31.2 min, extraction temperature (B) of 62.1°C, liquid–solid ratio (C) of 32.5:1, and the maximum estimated extraction values of 5.91%. Under the optimal parameters, the extraction experiment was repeated for three times to verify the accuracy of RSM and the extraction efficiency of MIPs was 5.93 ± 0.07%. The results confirmed that the experimental values of MIPs extraction were in good agreement with the predictive values of MIPs extraction. Compared with the HWE and UAE with water instead of DES, the UAE exhibited a higher extraction efficiency (4.5 and 5.4 times higher, respectively). Therefore, the response model was suitable for UAE procedure.

Chemical Composition, Monosaccharide Composition, and Molecular Weight Distribution of MIPs

The chemical compositions of MIPs are shown in **Table 2**. The carbohydrate, protein, sulfate, and polyphenol contents of MIP-D were measured to be 85.27, 2.57, 34.16, and 4.49%, respectively. The results obtained showed that MIP-D was an acidic heteropolysaccharide containing sulfate, which might exhibit excellent biological activity (29). Hu et al. also found that *Acanthopanax leucorrhizus* polysaccharide (ALP) shows better antioxidant activities after sulfated modification (30). After 24 h of dialysis and impurity removal, 4.49% of phenolic compounds were still detected in MIP-D, which indicated that natural polyphenolic-polysaccharide conjugates might exist in MIP-D. Liu et al. suggested that the conjugation of phenolic compounds can improve the antioxidant and enzyme inhibition effects of polysaccharides (31). Moreover, uronic acid was not detected in the chemical composition of MIP-D, which was agreed with the results of the previous study (1). To further evaluate the physicochemical properties of polysaccharides extracted by UAE, MIP-W was studied. Less carbohydrate (57.89%) and sulfate (24.43%) and more protein (3.85%) and polyphenol (10.60%) were found in MIP-W, which might be related to extraction method and solvent.

TABLE 2 | ANOVA of the experimental results of the Box–Behnken design (BBD).

Source	Sum of squares	df	Mean square	*F*-value	*p*-value
Model	6.3516	9	0.7057	52.33	<0.0001**
A	0.2819	1	0.2819	20.90	0.0026**
B	1.0800	1	1.0800	80.08	<0.0001**
C	0.1483	1	0.1483	10.99	0.0128*
AB	0.2167	1	0.2167	16.07	0.0051**
AC	0.0001	1	0.0001	0.01	0.9210
BC	0.0375	1	0.0375	2.78	0.1395
A^2	1.5003	1	1.5003	111.25	<0.0001**
B^2	2.4579	1	2.4579	182.26	<0.0001**
C^2	0.2375	1	0.2375	17.61	0.0041**
Residual	0.0944	7	0.0135		
Lack of fit	0.0633	3	0.0211	2.72	0.1793
Pure error	0.0311	4	0.0078		
Cor total	6.4460	16			

*CV%, 2.28; R^2, 0.9854; R^2_{ad}, 0.9665. *p < 0.05, **p < 0.01.*

As shown in **Table 2** and **Figure 3A**, MIP-D and MIP-W were composed of glucosamine (GlcN), galactose (Gal), glucose (Glc), and mannose (Man) with molar ratios of 0.39:1.88:3.82:3.91 and 2.71:1.06:5.59:3.01, respectively, according to elution time of monosaccharides standards. Moreover, uronic acid was not measured in the monosaccharide composition of MIPs, which was consistent with the results of chemical composition. Results suggested that UAE did not affect the monosaccharide composition of MIPs, but affected their molar ratios.

As shown in **Figures 3C,D**, MIP-D and MIP-W showed three peaks. The Mw values of MIP-D were measured to be 2.6×10^6, 7.3×10^4, and 3.7×10^3 Da and the Mw values of MIP-W were measured to be 4.1×10^6, 1.0×10^6, and 3.5×10^3 Da, respectively, according to the standard curve ($y = -0.5412x + 10.086$, $R^2 = 0.994$). Furthermore, the Mw of MIP-D was lower than MIP-W, which might be due to some high molecular weight fractions were ultrasonically degraded (32). Similar reports were also observed in previous studies (33). Therefore, these results indicated that UAE extraction method might extract lower molecular weight fractions of polysaccharides the traditional hot water extraction.

Ultraviolet and Fourier-Transform IR Spectroscopy

As shown in **Supplementary Figure 1**, MIP-D and MIP-W had no absorption peak at 260 and 280 nm, which indicated the absence of proteins and nucleic acids in MIPs. However, the protein contents were 2.57 and 3.85% in the chemical compositions of MIP-D and MIP-W, which might be related to the protein of MIPs being below the minimum detection of UV spectrophotometer.

The FTIR spectra were also applied for the determination of structural features of MIPs. As shown in **Figure 3B**, the absorption peaks at approximately 3,420 and 2,930 cm^{-1} were caused by O-H and C-H stretching vibration, respectively. The peak at 1,652 cm^{-1} was related to the C = O bending vibration (34). However, MIP-W had the absorption peak at 1,548 cm^{-1}, whereas MIP-W did not, indicating that MIP-W contained more protein, consistent with prior results (**Table 2**). Furthermore, the peak at 1,414 cm^{-1} was caused by the C = C bending vibration (34) and the weak peak at 1,253 cm^{-1} was assigned to the asymmetry stretching vibration of S = O, which indicated that MIPs contained sulfate radical (29). The peak at 1,030 cm^{-1} represented the C-O-C asymmetric stretching vibration, indicating the presence of the pyranose ring skeleton in MIPs (14). Finally,

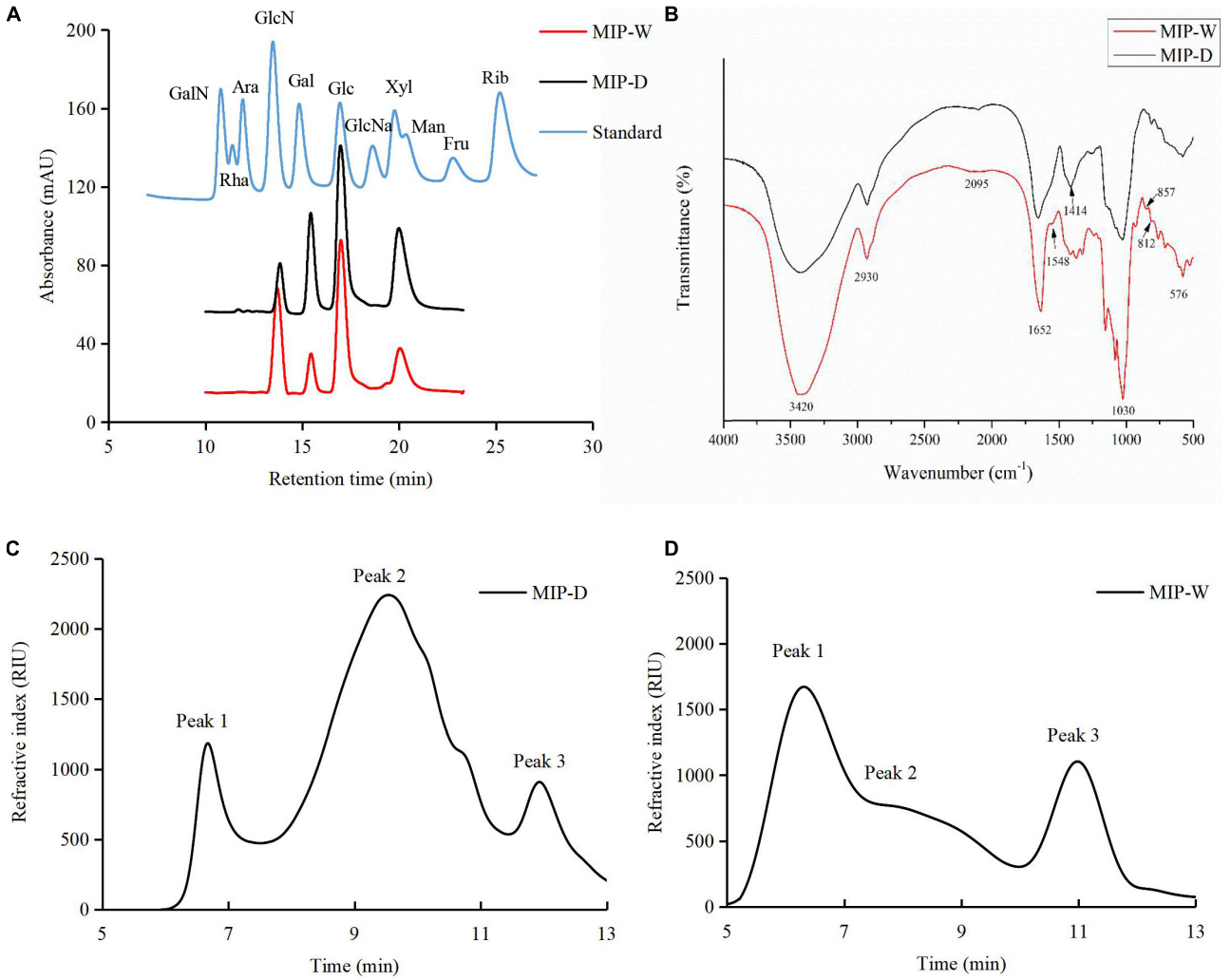

FIGURE 3 | (A) High performance liquid chromatography profiles of MIPs and monosaccharide standard; **(B)** fourier-transform IR (FTIR) spectra of MIPs over the frequency range of 4,000–5,000 cm^{-1}; high-performance gel permeation chromatography profiles of MIP-D **(C)** and MIP-W **(D)**.

the weak peaks at about 850 and 812 cm^{-1}, which might be attributed to the existence of α-type glycosidic linkages (29). Our results suggested that MIPs had the same FTIR spectra characteristic.

In-vitro Antioxidant Activity of the *Morchella importuna*

The DPPH is widely applied to measure the radical-scavenging ability of different bioactive substances separated from food products because of its stability (35). The ABTS is one of the vital radicals for determining the antioxidant ability of various bioactive substances from food products (36). Hydroxyl radical is one of the most toxic free radicals because it is associated with oxidative damage biomolecules in cells, such as alcohols, sugars, nucleic acids, and proteins, which can lead to tissue damage and even cell death (37). Therefore, to find bioactive substances that can remove OH radicals in nature, it is also very important.

The antioxidant activities of MIP-D are shown in **Figures 4A–C**. The DPPH, ABTS, and OH radical scavenging activities of MIP-D increased with increasing concentrations in the measurement range (0–4 mg/ml) and the highest radical scavenging activities were observed at concentrations of 4 mg/ml, which were 87.64, 81.61, and 89.39%, respectively. Furthermore, the IC_{50} values of the DPPH, ABTS, and OH radical scavenging activities of MIP-D were estimated to be approximately 0.55, 0.75, and 0.15 mg/ml, respectively, which were weaker than Vc (**Supplementary Table 4**).

In summary, the results indicated that the excellent antioxidant activities *in vitro* were observed in MIP-D and this phenomenon might be attributed to the content of sulfate radical and phenolic compounds that bonded with polysaccharides in MIP-D. Studies suggested that sulfated polysaccharides enhance its antioxidant activity by improving the hydrogen or electron donor capacity of its derivatives and the conjugation of phenolic compounds can improve the antioxidant nature of

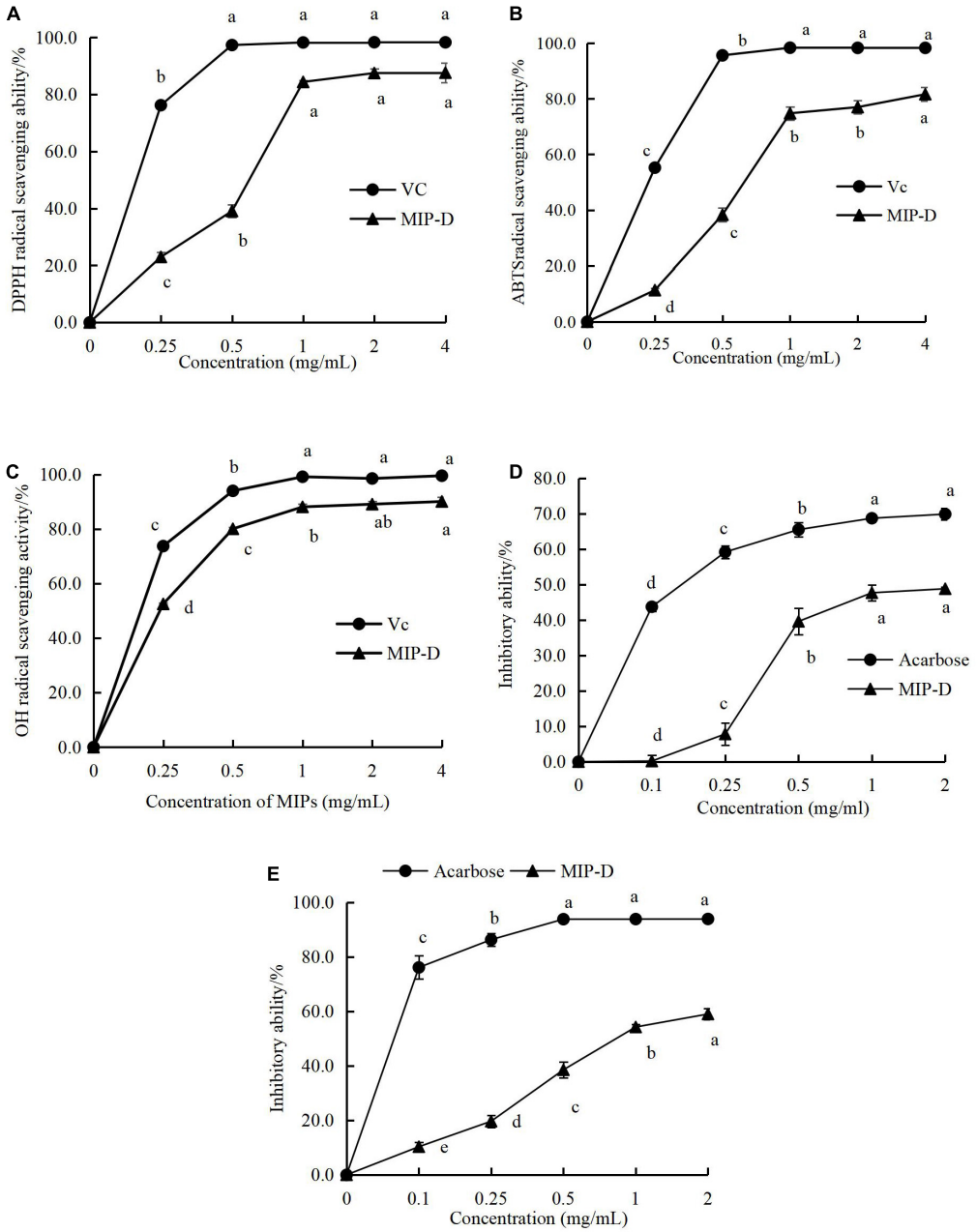

FIGURE 4 | Effect of MIP-D on antioxidant and hypoglycemic activity *in vitro*. **(A)** DPPH radical scavenging activity of MIP-D. **(B)** ABTS radical scavenging activity of MIP-D. **(C)** OH radical scavenging activity of MIP-D. **(D)** The inhibitory effects of MIP-D on α-glucosidase and **(E)** the inhibitory effects of MIP-D on α-amylase. Each value represents the mean ± *SD* (n = 3). Significant ($p < 0.05$) differences are shown by data bearing different letters (a–d).

polysaccharides (30, 31). However, the antioxidant mechanism and the structure–activity relationship of MIP-D are not clear and need further study.

In-vitro α-Amylase and α-Glucosidase Inhibitory Activities Assay

Hyperglycemia-related metabolism can be effectively improved by inhibiting the activities of α-glucosidase and α-amylase. The results showed that the polysaccharides from many fungi could inhibit α-amylase and α-glucosidase to some extent (38). Therefore, the UAE *in-vitro* inhibitory effects of polysaccharides from *M importuna* against target enzymes for type 2 diabetes were investigated. As given in **Figures 4D,E**, MIP-D exhibited obvious inhibitory activities on α-amylase and α-glucosidase and their inhibitory activities were positively correlated with their concentration. At 2.0 mg/ml, the highest inhibitions of α-amylase and α-glucosidase in MIP-D were determined to be

approximately 48.78 and 55.47%, respectively, but significantly lower than those of acarbose (69.85 and 93.87%). The IC_{50} value of α-glucosidase inhibitory activity of MIP-D was 0.15 mg/ml. Therefore, the results indicated that MIP-D exhibited excellent hypoglycemic activities and its inhibitory effect on α-amylase was stronger than that of α - glucosidase.

In summary, the results indicated that MIP-D presented excellent inhibitory effect on α-glucosidase and α-amylase, which could be explored further as a promising candidate for α-glucosidase and α-amylase inhibitors.

CONCLUSION

In this study, ChCl-OA was selected from a series of solvents for the extraction of polysaccharides from *M. importuna*. Based on the results of single-factor experiment, BBD and RSM were utilized to identify the main parameters and optimize the extraction conditions. Next, the effects of two extraction techniques (UAE and HWE) on the yields and characteristics of polysaccharides (MIP-D and MIP-W) were evaluated. Under the most suitable conditions, the extraction yield of MIP-D was 4.5 times higher than hot water extraction. Moreover, MIPs had the similar functional groups, but their chemical compositions, monosaccharide contents, and molecular weights were different. The results of bioactivities indicated that MIP-D exhibited excellent antioxidant activity and inhibited α-amylase and α-glucosidase inhibitory activities. However, more experiments need to be performed in the future, such as purification and bioactivity *in vivo*. Besides, we need to determine the configuration of glycosidic bonds in MIP-D structure in the future study. Overall, this study not only provides a green, efficiency, and economical alternative method for the extraction of polysaccharides from *M. importuna*, but also a scientific basis for the comprehensive utilization of *M. importuna* as a potential functional food.

DATA AVAILABILITY STATEMENT

The original contributions presented in the study are included in the article/**Supplementary Material**, further inquiries can be directed to the corresponding author/s.

AUTHOR CONTRIBUTIONS

LX: conceptualization, methodology, investigation, supervision, and writing-review and editing. XP: investigation and writing-original draft. YC: conceptualization and methodology. XG: software, formal analysis, and visualization. MC: resources, validation, and data curation. JM: resources and formal analysis. DG and RL: software and visualization. All authors contributed to the article and approved the submitted version.

FUNDING

This study was supported by the Shanxi Provincial Basic Research and Development Project (202103021224127) and the Scientific and Technological Innovation Programs of Higher Education Institutions in Shanxi (2021Y341).

SUPPLEMENTARY MATERIAL

The Supplementary Material for this article can be found online at: https://www.frontiersin.org/articles/10.3389/fnut.2022.912014/full#supplementary-material

REFERENCES

1. Wen Y, Peng D, Li C, Hu X, Bi S, Song L, et al. A new polysaccharide isolated from *Morchella importuna* fruiting bodies and its immunoregulatory mechanism. *Int J Biol Macromol.* (2019) 137:8–19. doi: 10.1016/j.ijbiomac.2019.06.171
2. Tao A, Feng X, Sheng Y, Song Z. Optimization of the *Artemisia* polysaccharide fermentation process by *Aspergillus niger*. *Front Nutr.* (2022) 9:842766. doi: 10.3389/fnut.2022.842766
3. Xu Y, Liu N, Fu X, Wang L, Yang Y, Ren Y, et al. Structural characteristics, biological, rheological and thermal properties of the polysaccharide and the degraded polysaccharide from raspberry fruits. *Int J Biol Macromol.* (2019) 132:109–18. doi: 10.1016/j.ijbiomac.2019.03.180
4. Zhang L, Wang M. Optimization of deep eutectic solvent-based ultrasound-assisted extraction of polysaccharides from *Dioscorea opposita* Thunb. *Int J Biol Macromol.* (2017) 95:675–81. doi: 10.1016/j.ijbiomac.2016.11.096
5. Kim H, Kang S, Li K, Jung D, Park K, Lee J. Preparation and characterization of various chitin-glucan complexes derived from white button mushroom using a deep eutectic solvent-based ecofriendly method. *Int J Biol Macromol.* (2021) 169:122–9. doi: 10.1016/j.ijbiomac.2020.12.081
6. Zhou Y, Wu YJ, Wang L, Han J, Wu JC, Li CM, et al. Natural deep eutectic solvents as green and biocompatible reaction medium for carbonic anhydrase catalysis. *Int J Biol Macromol.* (2021) 190:206–13. doi: 10.1016/j.ijbiomac.2021.08.221
7. Cvjetko Bubalo M, Curko N, Tomasevic M, Kovacevic Ganic K, Radojcic Redovnikovic I. Green extraction of grape skin phenolics by using deep eutectic solvents. *Food Chem.* (2016) 200:159–66. doi: 10.1016/j.foodchem.2016.01.040
8. Fernandes C, Melro E, Magalhaes S, Alves L, Craveiro R, Filipe A, et al. New deep eutectic solvent assisted extraction of highly pure lignin from maritime pine sawdust (*Pinus pinaster* Ait.). *Int J Biol Macromol.* (2021) 177:294–305. doi: 10.1016/j.ijbiomac.2021.02.088
9. Shafie MH, Samsudin D, Yusof R, Gan CY. Characterization of bio-based plastic made from a mixture of *Momordica charantia* bioactive polysaccharide and choline chloride/glycerol based deep eutectic solvent. *Int J Biol Macromol.* (2018) 118:1183–92. doi: 10.1016/j.ijbiomac.2018.06.103
10. Gursoy N, Sarikurkcu C, Cengiz M, Solak MH. Antioxidant activities, metal contents, total phenolics and flavonoids of seven *Morchella* species. *Food Chem Toxicol.* (2009) 47:2381–8. doi: 10.1016/j.fct.2009.06.032
11. Wang Z, Liu Y, Sun Y, Mou Q, Wang B, Zhang Y, et al. Structural characterization of LbGp1 from the fruits of *Lycium barbarum* L. *Food Chem.* (2014) 159:137–42. doi: 10.1016/j.foodchem.2014.02.171
12. Zdanowicz M. Deep eutectic solvents based on urea, polyols and sugars for starch treatment. *Int J Biol Macromol.* (2021) 176:387–93. doi: 10.1016/j.ijbiomac.2021.02.039
13. Wang Y, Liu Y, Huo J, Zhaoa X, Zheng J, Wei X. Effect of different drying methods on chemical composition and bioactivity of tea polysaccharides. *Int J Biol Macromol.* (2013) 62:714–9. doi: 10.1016/j.ijbiomac.2013.10.006

14. Yan JK, Yu YB, Wang C, Cai WD, Wu LX, Yang Y, et al. Production, physicochemical characteristics, and *in vitro* biological activities of polysaccharides obtained from fresh bitter gourd (*Momordica charantia* L.) *via* room temperature extraction techniques. *Food Chem.* (2021) 337:127798. doi: 10.1016/j.foodchem.2020.127798
15. Fan B, Luo J, Zhang H, Zhang X, Wang L, An Z, et al. Isolation, purification and composition analysis of polysaccharide from *Spirulina platensis*. *Food Sci*. (2022)43:160–6.
16. Yan JK, Wu LX, Qiao ZR, Cai WD, Ma H. Effect of different drying methods on the product quality and bioactive polysaccharides of bitter gourd (*Momordica charantia* L.) slices. *Food Chem.* (2019) 271:588–96. doi: 10.1016/j.foodchem.2018.08.012
17. Ma Q, Santhanam RK, Xue Z, Guo Q, Gao X, Chen H. Effect of different drying methods on the physicochemical properties and antioxidant activities of mulberry leaves polysaccharides. *Int J Biol Macromol.* (2018) 119:1137–43. doi: 10.1016/j.ijbiomac.2018.08.023
18. Yuan Q, Lin S, Fu Y, Nie XR, Liu W, Su Y, et al. Effects of extraction methods on the physicochemical characteristics and biological activities of polysaccharides from okra (*Abelmoschus esculentus*). *Int J Biol Macromol.* (2019) 127:178–86. doi: 10.1016/j.ijbiomac.2019.01.042
19. Zhang Q, De Oliveira Vigier K, Royer S, Jerome F. Deep eutectic solvents: syntheses, properties and applications. *Chem Soc Rev.* (2012) 41:7108–46. doi: 10.1039/c2cs35178a
20. Zhang W, Cheng S, Zhai X, Sun J, Hu X, Pei H, et al. Green and efficient extraction of polysaccharides from *Poria cocos* F.A. Wolf by deep eutectic solvent. *Nat Prod Commun.* (2020) 15, 54–56. doi: 10.1177/1934578x19900708
21. Shang XC, Chu D, Zhang JX, Zheng YF, Li Y. Microwave-assisted extraction, partial purification and biological activity *in vitro* of polysaccharides from bladder-wrack (*Fucus vesiculosus*) by using deep eutectic solvents. *Sep Purif Technol.* (2021) 259:118169. doi: 10.1016/j.seppur.2020.118169
22. Shah D, Mjalli FS. Effect of water on the thermo-physical properties of reline: an experimental and molecular simulation based approach. *Phys Chem Chem Phys.* (2014) 16:23900–7. doi: 10.1039/c4cp02600d
23. Xue H, Tan J, Li Q, Tang J, Cai X. Ultrasound-assisted deep eutectic solvent extraction of anthocyanins from blueberry wine residues: optimization, identification, and HepG2 antitumor activity. *Molecules.* (2020) 25:5456. doi: 10.3390/molecules25225456
24. Feng YN, Zhang XF. Polysaccharide extracted from *Huperzia serrata* using response surface methodology and its biological activity. *Int J Biol Macromol.* (2020) 157:267–75. doi: 10.1016/j.ijbiomac.2020.04.134
25. Kan Y, Chen T, Wu Y, Wu J, Wu J. Antioxidant activity of polysaccharide extracted from *Ganoderma lucidum* using response surface methodology. *Int J Biol Macromol.* (2015) 72:151–7. doi: 10.1016/j.ijbiomac.2014.07.056
26. Ma T, Sun X, Tian C, Luo J, Zheng C, Zhan J. Polysaccharide extraction from *Sphallerocarpus gracilis* roots by response surface methodology. *Int J Biol Macromol.* (2016) 88:162–70. doi: 10.1016/j.ijbiomac.2016.03.058
27. Wang J, Zhang J, Wang X, Zhao B, Wu Y, Yao J. A comparison study on microwave-assisted extraction of *Artemisia sphaerocephala* polysaccharides with conventional method: molecule structure and antioxidant activities evaluation. *Int J Biol Macromol.* (2009) 45:483–92. doi: 10.1016/j.ijbiomac.2009.09.004
28. Bai XL, Yue TL, Yuan YH, Zhang HW. Optimization of microwave-assisted extraction of polyphenols from apple pomace using response surface methodology and HPLC analysis. *J Sep Sci.* (2010) 33:3751–8. doi: 10.1002/jssc.201000430
29. Shi Y, Xiong Q, Wang X, Li X, Yu C, Wu J, et al. Characterization of a novel purified polysaccharide from the flesh of *Cipangopaludina chinensis*. *Carbohydr Polym.* (2016) 136:875–83. doi: 10.1016/j.carbpol.2015.09.062
30. Hu H, Li H, Han M, Cao Q, Liang H, Yuan R, et al. Chemical modification and antioxidant activity of the polysaccharide from *Acanthopanax* leucorrhizus. *Carbohydr Res.* (2020) 487:107890. doi: 10.1016/j.carres.2019.107890
31. Liu J, Bai R, Liu Y, Zhang X, Kan J, Jin C. Isolation, structural characterization and bioactivities of naturally occurring polysaccharide-polyphenolic conjugates from medicinal plants-A reivew. *Int J Biol Macromol.* (2018) 107:2242–50. doi: 10.1016/j.ijbiomac.2017.10.097
32. Jia Y, Gao X, Xue Z, Wang Y, Lu Y, Zhang M, et al. Characterization, antioxidant activities, and inhibition on alpha-glucosidase activity of corn silk polysaccharides obtained by different extraction methods. *Int J Biol Macromol.* (2020) 163:1640–8. doi: 10.1016/j.ijbiomac.2020.09.068
33. Wang B, Niu J, Mai B, Shi F, Li M, Chen L, et al. Effects of extraction methods on antioxidant and immunomodulatory activities of polysaccharides from superfine powder *Gynostemma pentaphyllum* Makino. *Glycoconj J.* (2020) 37:777–89. doi: 10.1007/s10719-020-09949-5
34. Meng X, Che C, Zhang J, Gong Z, Si M, Yang G, et al. Structural characterization and immunomodulating activities of polysaccharides from a newly collected wild *Morchella sextelata*. *Int J Biol Macromol.* (2019) 129:608–14. doi: 10.1016/j.ijbiomac.2019.01.226
35. Ahmadi S, Sheikh-Zeinoddin M, Soleimanian-Zad S, Alihosseini F, Yadav H. Effects of different drying methods on the physicochemical properties and antioxidant activities of isolated acorn polysaccharides. *Lwt.* (2019) 100:1–9. doi: 10.1016/j.lwt.2018.10.027
36. Hu S, Zhao G, Zheng Y, Qu M, Jin Q, Tong C, et al. Effect of drying procedures on the physicochemical properties and antioxidant activities of polysaccharides from *Crassostrea gigas*. *PLoS One.* (2017) 12:e0188536. doi: 10.1371/journal.pone.0188536
37. Wu Z. Effect of different drying methods on chemical composition and bioactivity of finger citron polysaccharides. *Int J Biol Macromol.* (2015) 76:218–23. doi: 10.1016/j.ijbiomac.2015.02.043
38. Ma L, Chen H, Zhu W, Wang Z. Effect of different drying methods on physicochemical properties and antioxidant activities of polysaccharides extracted from mushroom *Inonotus obliquus*. *Int Food Res J.* (2013) 50:633–40. doi: 10.1016/j.foodres.2011.05.005

Conflict of Interest: The authors declare that the research was conducted in the absence of any commercial or financial relationships that could be construed as a potential conflict of interest.

Publisher's Note: All claims expressed in this article are solely those of the authors and do not necessarily represent those of their affiliated organizations, or those of the publisher, the editors and the reviewers. Any product that may be evaluated in this article, or claim that may be made by its manufacturer, is not guaranteed or endorsed by the publisher.

Copyright © 2022 Pan, Xu, Meng, Chang, Cheng, Geng, Guo and Liu. This is an open-access article distributed under the terms of the Creative Commons Attribution License (CC BY). The use, distribution or reproduction in other forums is permitted, provided the original author(s) and the copyright owner(s) are credited and that the original publication in this journal is cited, in accordance with accepted academic practice. No use, distribution or reproduction is permitted which does not comply with these terms.

frontiers | Frontiers in Nutrition

ORIGINAL RESEARCH
published: 13 June 2022
doi: 10.3389/fnut.2022.940442

Structural Characterization of Polysaccharides in Waste Liquor Produced by Wet Decortication of Sesame Seeds

Yao-Ran Li[1,2], Shuai Xu[1], Run-Yang Zhang[1], Ming-Xuan Yang[1], Hua-Min Liu[1] and Xue-De Wang[1]**

[1] College of Food Science and Technology, Henan University of Technology, Zhengzhou, China, [2] College of Biosystems Engineering and Food Science, Zhejiang University, Hangzhou, China

OPEN ACCESS

Edited by:
Xiaolong Ji,
Zhengzhou University of Light Industry, China

Reviewed by:
Pai Peng,
Northwest A&F University, China
Shaolong Sun,
South China Agricultural University, China

***Correspondence:**
Hua-Min Liu
liuhuamin5108@163.com
Xue-De Wang
13903865584@126.com

Specialty section:
This article was submitted to Food Chemistry, a section of the journal Frontiers in Nutrition

Received: 10 May 2022
Accepted: 26 May 2022
Published: 13 June 2022

Citation:
Li Y-R, Xu S, Zhang R-Y, Yang M-X, Liu H-M and Wang X-D (2022) Structural Characterization of Polysaccharides in Waste Liquor Produced by Wet Decortication of Sesame Seeds. Front. Nutr. 9:940442. doi: 10.3389/fnut.2022.940442

The wet decortication of sesame seeds produces wastewater containing diverse minerals and organic pollutants that could be valuable resources for the food industry. This investigation aimed to reclaim, purify, and characterize the polysaccharides contained in the waste liquor from the sesame decortication industry. The purified polysaccharide fractions were characterized using monosaccharide analysis, GPC (high-performance gel permeation chromatography), FT-IR (Fourier-transform infrared) spectroscopy, methylation analysis, 1D and 2D Nucleai Magnetic Resonance (NMR) analysis, and thermal analysis. Four fractions were found (SSP-1,-2,-3, -4), of which SSP-2 was proportionately the largest and most interesting. The backbone of SSP-2 is mainly composed of (1→2,4)-β-$_D$-Xyl*p* residues with side chains connected to the O-4 position, with many T-β-$_D$-Gal*p* and (1→5)-α-$_L$-Ara*f* residues, and fewer (1→4)-α-$_D$-Glc*p*, (1→2)-α-$_L$-Rha*p*, T-α-$_L$-Ara*f*, and (1→2)-β-$_D$-Glc*p*A residues. An efficient method for removing the polysaccharides would simplify wastewater treatment while finding a use for them would benefit the sesame, food, and pharmaceutical industries.

Keywords: characterization, polysaccharide, waste liquor, wet decortication, sesame seeds

INTRODUCTION

Sesame (*Sesamum indicum* L.), primarily cultivated in Burma, Sudan, China, and India since ancient times, consisting 60% of the world's total yield, is one of the most important annual oilseed crops (1, 2). With its high content of protein and oil, sesame is a nutritious food, widely consumed in sweet and savory dishes and confections (3, 4). Typically, sesame seeds are dehulled before being used as human food. The meal left from oil extraction is high in protein, indigestible fiber, and oxalic acid. It is used to a limited extent as animal feed and might, with further treatment, be a source of protein for human food products (5, 6).

Among the current dehulling methods, two of the most common approaches are dry decortication and wet decortication. Dry decortication entails simply heating the sesame seeds. It is environmentally friendly as it produces no waste liquor; however, the long time and high temperature of the roasting process may change the appearance and flavor of the kernels (7). Wet

decortication involves the use of a strong alkali to remove the hulls. It is a conventional method that used to be widely adopted by the industry because the method can provide kernels with a more desirable appearance, taste, and yield than dry decortication. The use of lye, however, has significant disadvantages, such as its corrosive effect on equipment, the possible hazards of applying the hot (60°C) alkali, and the heat costs to keep the alkali at 60°C during the operation (7). The greatest drawback, however, is that a large volume of water is needed to wash off the lye, and the disposal of this waste lye liquor remains a common and serious problem confronting sesame producers all over the world (8).

Several studies have suggested that valuable nutrients can be reclaimed from the byproducts of sesame dehulling, and utilized in various ways (9). As for disposal of the wastewater, if this water could be further and efficiently processed to yield valuable resources, the benefits would be far-reaching. The waste lye liquor, one of the byproducts obtained during the process of wet decortication, is mainly composed of proteins and a range of polysaccharides, such as pectin, gums, celluloses, and hemicelluloses. Polysaccharides, very important bioactive macromolecules, have long been used as additives in healthy foods due to their various biological effects and in emulsions to improve texture, water retention, and stabilization (10). These molecules are proven to have antioxidative, hypolipidemic, and anti-tumor activities (11–13). The complex structures of polysaccharides, including the variety of monosaccharide components and the various linkage and configuration patterns, give them their diverse functional properties (14). To the best of our knowledge, the sugar composition and structural characterization of the sesame polysaccharides obtained from the waste liquor produced in the process of wet sesame dehulling have not been studied. We believe that these polysaccharides could be valuable resources for industry and that an efficient method for removing them would both benefit the sesame industry and simplify wastewater treatment.

Thus, the purpose of the present investigation aimed to develop an efficient, effective way to reclaim natural polysaccharides from the waste liquor produced by the wet decortication of sesame seeds. Polysaccharide fractions were reclaimed and purified, and the composition and structural features of the purified polysaccharide fractions were characterized using monosaccharide analysis, GPC (high-performance gel permeation chromatography), FT-IR (Fourier-transform infrared) spectroscopy, methylation analysis, 1D and 2D Nucleai Magnetic Resonance (NMR) analysis and thermal analysis.

MATERIALS AND METHODS

Materials

Sesame seeds (*Sesamum indicum* L.) were obtained from the Sesame Research Center, Henan Academy of Agricultural Sciences. After sieving to remove impurities, the seeds were dried for 24 h at 40°C and then kept in a sealed container at 4°C until decortication. Chemicals required for the assays, including dextran standards and standard monosaccharides ($_D$-glucose, $_D$-galactose, $_D$-mannose,$_D$-xylose,$_L$-rhamnose, $_L$-arabinose, $_D$-galacturonic acid, $_D$-glucuronic acid) were purchased from Sigma Chemical Co. (St. Louis, MO, United States). DEAE Cellulose-52 was obtained from Solarbio Science and Technology Ltd. (Beijing, China). All other chemical reagents were acquired from Tianjin Chemical Reagents Co. Ltd. (Tianjin, China) of analytical grade.

Sesame Wet Decortication Waste Liquor Collection

In brief, 500 g of sesame seeds were soaked in 3 L of 0.25% NaOH lye solution at 60°C for 5 min with stirring (500 rpm). The mixtures were passed through a 60-mesh sieve, and the sesame seeds were collected. After washing with rushing water to eliminate the residual lye, the seeds were rubbed for 5 min to decorticate the hulls. All hot-alkaline waste liquor was retained for further analysis.

Reclamation of Crude Polysaccharide

Firstly, the collected waste liquor was filtered to remove impurities. The pH of the filtrate was adjusted to 5.5, and the solution was centrifuged at 4,000 rpm (Backman, Avanti J-25, United States) for 15 min to precipitate sesame protein. The supernatant was collected and concentrated by a rotary evaporator (RE-3000A, Yarong Technology and Science Inc., Shanghai, China) and then precipitated with three times 95% (v/v) ethanol; solutions were left to settle for 3 h. The insoluble contents were collected by filtering through double layers of filters; afterward, the precipitate was washed with 70% ethanol. The precipitate was then decolorized with AB-8 macroporous resin and deproteinized by the Sevag method (15). To remove the salt and small molecule impurities, it was dialyzed for 3 days against water (molecular weight cut-off Mw 3,500 Da) and lastly lyophilized to obtain the refined crude polysaccharide (SSP).

Purification of the Polysaccharide Fractions

The crude SSP (500 mg/mL) was further dissolved in distilled water and separated on a DEAE cellulose-52 column (2.6 cm × 30 cm) by eluting with 0, 0.1, 0.2, 0.3, 0.5, and 0.7 M NaCl solution at a rate of 10 mL/tube (1.5 mL/min). The collected fraction was measured at 490 nm defining $_D$-glucose as a standard by the phenol-sulfuric acid method (16). The four main fractions corresponding to the four concentrations of NaCl solution (0.1, 0.2, 0.3, and 0.5 M), were collected and named SSP-1, SSP-2, SSP-3, and SSP-4, respectively.

Characterization

Monosaccharide Composition Analysis

A total of 5 mg of each polysaccharide sample was hydrolyzed by 3% H_2SO_4 at 105°C for 2.5 h. Samples were cooled to room temperature, then filtered through a 0.22 μm pore membrane filter. Subsequently, 1 mL of each extraction, diluted up to 3 mL with distilled water, was analyzed by HPAEC (High-Performance Anion Exchange Chromatography) with a carbopac PA-1 ion

exchange column (4.0 mm × 250 mm; Thermo Scientific Dionex, Sunnyvale, CA, United States) and a Dionex ICS-3000 system (Thermo Scientific Dionex, Sunnyvale, CA, United States).

Determination of Molecular Weight

High-performance gel permeation chromatography (1100 Series HPLC, Agilent) was used to analyze the molecular weights of the polysaccharide fractions. The HPLC was equipped with a differential refraction index detector and a TSK-G3000 PW_{XL} column constantly kept at 30°C. Dextran standards of different molecular weights (Dextran T1000, T500, T70, T40, T10, and T5) were examined in turn to plot the calibration curve according to the retention time and the logarithm of the corresponding molecular weights.

Fourier-Transform Infrared Analysis

Fourier transform infrared (FT-IR) spectra of every dried sample were determined using the KBr-pellet method with a Nicolet iN10 FT-IR spectroscope (Thermo Nicolet Corporation, Madison, WI, United States), at frequencies ranging from 4,000 cm^{-1} to 500^{-1} with a resolution of 4 cm^{-1} (17).

Methylation Analysis

The uronic acid reduction was carried out according to the literature with minor modifications (18). 20 mg of polysaccharide SSP-2 was dissolved in 5 mL of ice-cold 1 M imidazole-HCl, and 1 mL of 100 mg/mL $NaBD_4$ was added three times. Methylation with methyl iodide (CH_3I) was performed according to the published report (19). The carboxyl-reduced sample was then dissolved in 50 μm of DMSO/NaOH (60°C) slurry 50% (wt/wt) without ultrasonic treatment. Once ionized, the polysaccharide was treated with CH_3I. The methylated residue was hydrolyzed by treatment with 2 mL of 2 M TFA at 100°C for 6 h and was evaporated to get rid of the excess acid. The acquisition was finally acetylated with acetic anhydride and pyridine at 100°C for 1 h with the addition of $NaBH_4$ as a reducing agent. After acetylation, the resulting alditol acetates were analyzed with GC-MS (gas chromatography-mass spectrometry) system equipped with a DB-5 capillary column (0.25 mm × 30 m × 0.25 m, Thermo Finnigan Co., Santa Clara, CA, United States).

1D and 2D NMR Spectroscopy

1D nuclear magnetic resonance (NMR) spectra analysis of SSP-2 was carried out using a 500 MHz Bruker Avance III nuclear magnetic resonance instrument (Germany) with each sample dissolved in 1 mL of 99.8% D_2O. Two-dimensional spectra, including HSQC (heteronuclear single quantum coherence spectroscopy), COSY (^1H-^1H correlated spectroscopy), and HMBC (^1H detected heteronuclear multiple bond correlation spectroscopy) experiments were also ascertained by standard Bruker procedures at 25°C according to our previous method (20).

Thermal Analysis

Thermogravimetric analyses were performed on an SDT Q600 Simultaneous Thermal Analyzer (TA Instruments, United States) in a nitrogen atmosphere at 100 mL/min and scanned from 45°C to 700°C at a heating rate of 10°C/min.

DPPH Radicals Scavenging Activity

The 2,2 Diphenyl-1-picrylhydrazyl (DPPH) radicals scavenging activity of SSPs was measured according to the previous report (21). Briefly, 1.0 mL of SSPs solution at different concentrations was added to 3.0 mL 0.1 mM DPPH in methanol and incubated at room temperature for 60 min in the dark. The absorbance was determined using a microplate reader at 517 nm, and ascorbic acid was used as a positive control and antioxidant standard. The DPPH radical scavenging activity was calculated according to the following equation:

$$\text{DPPH radical scavenging activity (\%)} = [1 - (A_2 - A_1)/A_0]\,100\%$$

Where A_0 is the absorbance of the blank, in which distilled water was used in place of the sample, A_1 is the absorbance of the test sample solution, but the dehydrated alcohol instead of the DPPH solution. A_2 is the absorbance of the sample solution.

Iron Chelating Activity

The iron chelating activity of the polysaccharides was evaluated according to the method described by Shao et al. (22). Briefly, the reaction mixture containing 50 μL of SSPs at various concentrations, 100 μL of $FeSO_4{\cdot}7H_2O$ (0.5 mM), and 50 μL of ferrozine (5.0 mM), was distributed into a microplate. The mixture was incubated at room temperature for 30 min, using EDTA-2Na as the blank. After that, the absorbance was determined immediately at 562 nm. The iron chelation potential was expressed as the percentage inhibition and was calculated by the following equation:

$$Fe^{2+}\text{ chelating ability (\%)} = (1 - A_S/A_0)100\%$$

Where A_S is the absorbance of the sample, and A_0 is the absorbance of the blank, in which distilled water was used in place of the sample.

RESULTS AND DISCUSSION

Reclamation and Purification of Polysaccharide Fractions

The hot-alkaline waste liquor was obtained simulating the soaking process of wet decortication as described in section "Sesame Wet Decortication Waste Liquor Collection." The total yield of the crude polysaccharide SSP from the waste liquor was about 0.3% (based on dry matter of the sesame seeds) after extraction, ethanol precipitation, removal of proteins, dialysis, and lyophilization. Four main fractions were produced by fractionation with distilled water and NaCl solutions and were collected by preparative size-exclusion chromatography on a DEAE-52 column based on the total carbohydrate elution profile (**Figure 1A**). Following concentration, dialysis, and lyophilization, SSP-1, SSP-2, SSP-3, and SSP-4 fractions were finally obtained. They accounted for 15.7, 53.9, 12.1, and 11.8% of the total SSP content, respectively. SSP-1, SSP-3, and SSP-4 were each eluted as single and sharp symmetrical peaks,

which indicated their homogeneity. In contrast, the main fraction SSP-2 showed a shoulder on both the DEAE-52 column and GPC chromatographs, suggesting it was a polydispersed system composed of more than one compound.

Monosaccharide Compositions of the Polysaccharides

For the monosaccharide composition analysis, the molar content of each monosaccharide preparation was identified by comparison with monosaccharide standards; results are given in **Table 1**. The result indicated that all of the sesame polysaccharide fractions were rich in galactose and xylose, with notable differences in other chemical components. For instance, the monosaccharides of SSP-1, which was eluted by distilled water, markedly differed from the other three fractions. SSP-1 was neutral with no acidic sugar detected. The other fractions (SSP-2, SSP-3, and SSP-4) eluted at concentrations of 0.1, 0.2, and 0.3 M NaCl, respectively, and contained 8.2, 4.4, and 7.5% uronic acid, respectively. These results match those obtained by Hokputsa (23). Furthermore, glucose (28.4%) and mannose (11.2%) were the dominant components in SSP-1, while arabinose (29.1%) and galactose (23.9%) were the dominant components in SSP-2. Both SSP-3 and SSP-4 were mainly made up of galactose and xylose in molar ratios of 33.4:42.6 and 37.3:21.5, respectively. The high percentages of galactose, xylose, and arabinose with some mannose in the SSP fractions were considered to indicate correspondingly more arabinoxylan and galactomannan in sesame polysaccharides, whereas other sugars, presenting in lower amounts, might originate from different kinds of polysaccharides (24).

Average Molecular Weight

The homogeneity and average molecular mass of each purified fraction were calculated based on the calibration curve made with a group of standard dextran determined by HPLC. As shown in **Figure 1B**, molar mass distributions of SSP-1, SSP-3, and SSP-4 as shown by HPLC had narrow and symmetrical peaks, thus confirming their homogeneity. According to the calibration curve, l g Mw = -0.33t + 10.9 (R^2 = 0.996) (where t is the retention time, and R^2 represents the fitting coefficient); the average molecular weights of SSP-1, SSP-3, and SSP-4 were determined to be 3,300, 3,370, and 3,400 Da, respectively. However, the HPLC profile of SSP-2 appeared to be bimodal in shape. SSP-2 consisted of a polysaccharide calculated as 10,910 Da with a retention time of 21.2 min and another calculated as 3,500 Da with a retention time of 22.7 min. SSP-2 represented a large proportion of SSP, owing to both its high molecular weight and high content, shown as the large peak area in the elution profile. Nastaran et al. (25) suggested that the presence of NaOH would increase the degradation of the polysaccharides, thereby also increasing the quantity of low molecular weight (<50 kDa) polysaccharides. Carbonell-Barrachina et al. (8) observed that alkaline extraction relatively easily dissolved the polysaccharides with high molecular weights, while the lower-molecular-weight polysaccharide fractions were likely to be extracted with milder conditions like DMSO treatment (26). Thus, one possible explanation for the relatively low molecular weight is that the mild dehulling conditions combined with the alkaline degradation of polysaccharides counteracted the extraction effects of alkali liquor.

Fourier-Transform Infrared Analysis

Fourier-Transform Infrared spectroscopy, an effective analytical technique, is based on the fact that bonds and functional groups vibrate at characteristic frequencies (27). As shown in **Figures 1C–F**, the purified fractions from SSP had similar characteristic absorption peaks at around 3,397, 2,921, 1,632, 1,420, 1,119, 863, and 624 cm^{-1}, indicating that the structure did not obviously change during elution of the polysaccharides. The FT-IR spectra showed a strong and broadband at 3,411 cm^{-1} assigned to the O–H stretching vibration of the polysaccharides, while the peak at 2,926 cm^{-1} was attributed to the C–H stretching vibration (28). In good accord with the sugar composition, in the spectra for all the fractions except SSP-1, the symmetrical and asymmetrical stretching vibrations of the carboxylate group similarly showed two clear intense bands at 1,424 and 1,632 cm^{-1} (29, 30). Furthermore, the carbohydrates showed high absorbencies within the region of 1,200–1,000 cm^{-1}, indicating the presence of galactopyranose in the main chain (31, 32). The spectra of all four polysaccharides lacked a signal at 1,730 cm^{-1} for carbonyl stretching, which indicated that the mild dehulling process entirely saponified the acetyl groups and methyl esters.

Methylation Analysis

As listed in **Table 1**, SSP-2 was composed of rhamnose, arabinose, galactose, glucose, xylose, glucuronic acid, and galacturonic acid in the molar ratio of 16.3:29.1:23.9:9.0:13.5:6.2:2.0. To determine the monosaccharide linkages, SSP-2 was further methylated and hydrolyzed into alditol acetate derivatives, and then determined by methylation analysis (shown in **Table 2** and **Supplementary Figure 1**). The analysis indicated that the dominant modes of linkages were →5)-$_L$-Ara*f*-(1→, →2,4)-$_D$-Xyl-*p*-(1→, →2)-$_D$-Glc*p*A-(1→, →4)-$_D$-Glc*p*-(1→ and →6)-$_D$-Gal*p*-(1→, accompanied by small amounts of →2,3,4)-$_D$-Xyl*p*-(1→, →2)-$_L$-Rha*p*-(1→, →4)-$_L$-Ara*p*-(1→, →3,5)-$_L$-Ara*f*-(1→, →3)-$_D$-Gal*p*-(1→, →3,6)-$_D$-Glc*p*-(1→ and →2,4)-$_D$-Gal*p*-(1→. The major terminal linkages, which attached to the branch-points of the backbone, were detected as T-$_D$-Gal*p*, T-$_L$-Ara*f* and T-$_L$-Rha*p* residues. A tiny bit of →3)-$_L$-Rha*p*-(1→, →3,4)-$_L$-Rha*p*-(1→ and →2,3)-$_L$-Ara*p*-(1→ were also detected (each contain <2.2% of the total peak area). The results showed that the repeating elements of SSP-2 mainly consisted of a (1→5)-Ara*f* backbone with branches consisting of many (1→2,4)-Xyl*p* residues attached to O-3 of some xylose or a (1→2,4)-Xyl*p* backbone with branches consisting of many (1→5)-Ara*f* residues attached to O-4 of some xylose residues. The existence of large quantities of (1→2,3,4)-linked xylose suggested that the SSP-2 fraction is highly branched. According to the relative amounts of (1→2,3,4)-linked xylose, the theoretical branch ratios at the C-3 of the backbone arabinose may be approximately 64.8%. Similarly, 38.7% of (1→5)-linked arabinose were substituted at O-3 positions to form (1→3,5)-linked arabinose moieties.

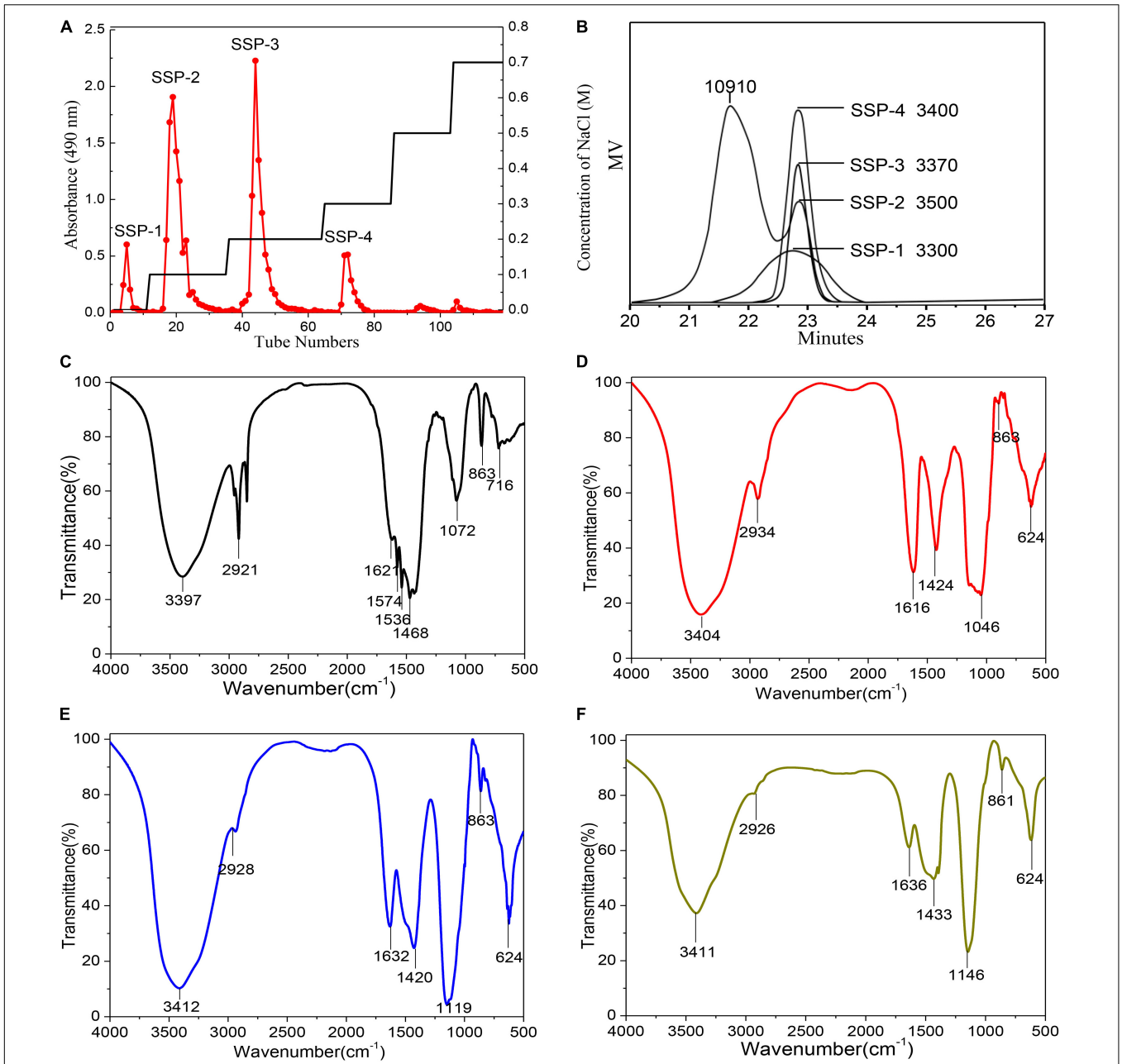

FIGURE 1 | Elution profile and physicochemical analysis: DEAE cellulose-52 column elution profile **(A)**; GPC profiles and molecular weights **(B)**; FT-IR spectra of SSP-1 **(C)**, SSP-2 **(D)**, SSP-3 **(E)**, and SSP-4 **(F)**.

TABLE 1 | Composition of monosaccharides in polysaccharides obtained from the waste liquor produced by wet decortication of sesame seeds.

Fractions	Monosaccharide composition (%)							
	Rha[a]	Ara[a]	Gal[a]	Glc[a]	Xyl[a]	Man[a]	GlcA[a]	GalA[a]
SSP-1	9.3	5.9	29.8	28.4	15.4	11.2	nd[b]	nd[b]
SSP-2	16.3	29.1	23.9	9.0	13.5	nd[b]	6.2	2.0
SSP-3	nd[b]	14.6	33.4	5.0	42.6	nd[b]	4.4	nd[b]
SSP-4	15.1	8.7	37.3	5.6	21.5	4.2	4.5	3.0

[a]*Rha, rhamnose; Ara, arabinose; Gal, galactose; Glc, glucose; Xyl, xylose; Man, mannose; GlcA, glucuronic acid; GalA, galacturonic acid.*
[b]*nd, not detected.*

TABLE 2 | Methylation analysis of SSP-2.

Methylated sugar	Linkages	Molar ratio (%)
2,3,4-Me_3-Rha*p*[a]	T-$_L$-Rha*p*-(1→	8.9
3,4-Me_2-Rha*p*	→2)-$_L$-Rha*p*-(1→	4.6
2,4-Me_2-Rha*p*	→3)-$_L$-Rha*p*-(1→	2.0
2-Me_1-Rha*p*	→3,4)-$_L$-Rha*p*-(1→	2.2
2,3,5-Me_3-Ara*f*	T-$_L$-Ara*f*-(1→	9.0
2,3-Me_2-Ara*p*	→4)-$_L$-Ara*p*-(1→	4.3
2,3-Me_2-Ara*f*	→5)-$_L$-Ara*f*-(1→	10.4
4-Me_1-Ara*p*	→2,3)-$_L$-Ara*p*-(1→	1.8
2-Me_1-Ara*f*	→3,5)-$_L$-Ara*f*-(1→	4.0
2,3,4,6-Me_4-Gal*p*	T-$_D$-Gal*p*-(1→	13.0
2,4,6-Me_3-Gal*p*	→3)-$_D$-Gal*p*-(1→	3.8
2,3,4-Me_3-Gal*p*	→6)-$_D$-Gal*p*-(1→	5.4
3,6-Me_2-Gal*p*	→2,4)-$_D$-Gal*p*-(1→	2.6
2,3,6-Me_3-Glc*p*	→4)-$_D$-Glc*p*-(1→	5.7
2,4-Me_2-Glc*p*	→3,6)-$_D$-Glc*p*-(1→	3.3
3-Me_1-Xyl*p*	→2,4)-$_D$-Xyl*p*-(1→	7.7
Xyl*p*[b]	→2,3,4)-$_D$-Xyl*p*-(1→	5.0
3,4,6-Me_3-Glc*p*A	→2)-$_D$-Glc*p*A-(1→	6.2

[a]*2,3,4-Me_3-Rhap, 1,5-di-O-acetyl-6-deoxy-2,3,4-tri-O-methyl-$_L$-mannitol, ect.*
[b]*Xylp = 1,2,3,4,5-penta-O-acetyl xylitol.*

Theoretically, 32.0% of the glycosyl residues presented as branch points, and 30.9% of terminal residues were detected. The result was in accord with the expectation that the sum of all the terminal residues should be roughly equal to the sum of branch point residues (33). According to the result, although not entirely identical, the proportions of the methylated derivatives were consistent with the polysaccharide monosaccharide composition.

NMR Spectroscopy

The main structural features of SSP-2 were further confirmed from the results of a combination of 1D and 2D NMR analysis, shown in **Figures 2A–E**, which revealed detailed structural information such as α- or β- configurations, monosaccharide composition, and sugar linkage patterns (34). The ^{1}H NMR spectrum (**Figure 2A**) demonstrated that the chemical shifts of anomeric protons present in the region from 4.43 to 5.30 ppm were higher or lower than 5.0 ppm, which indicated that both α- and β- anomeric configurations were present in the SSP-2 fraction (35). The typical signals at the high field (1.17–1.23 ppm) were attributed to the $-CH_3$ (C6) of rhamnose (36). The ^{13}C NMR spectrum (**Figure 2B**) of SSP-2 showed anomeric carbon signals corresponding to the proton signals from 97.68 to 109.34 ppm and multiple non-anomeric carbon signals in the region of 59.90 to 84.87 ppm. The corresponding chemical shifts of rhamnose for $-CH_3$ (C6) at 16.77 and 16.91 ppm in the ^{13}C NMR spectrum can be assigned according to the HSQC spectrum (**Figure 2D**). Furthermore, the peaks in the range of 174.99 to 176.87 ppm could be attributed to the carboxyl carbons of Glc*p*A (37).

The detailed sugar ring carbon/hydrogen signals were determined as far as possible by combining the results of methylation analysis, HSQC, COSY, and HMBC experiments with the literature data. In addition, the relative configuration of the residues was established on the basis of the characteristic chemical shifts of the anomeric carbons. By comparison with the results of the HSQC experiment, seven clear signals in the anomeric region of the ^{1}H NMR spectrum were observed, which could be attributed to anomeric protons. These seven resonances at 4.43–5.30 ppm were designated as A (H1)-G (H1) according to the decreasing chemical shifts of their anomeric protons. Other chemical shifts of sugar residues were not detected in the spectrum as described in the methylation analysis due to their relatively low content. To further confirm the detailed proton signals (**Table 2**), the corresponding sugar residues' chemical shifts were assigned based on the COSY spectrum (**Figure 2C**) and the literature. The proton chemical shifts of residues A, B, F, and G showed H-1 up to H-6 correlations, and the other residues (C, D, and E) were assigned in turn from H-1 to H-5 (**Table 3**). In succession, the carbon signals corresponding to the assigned protons were identified from the cross-peaks in the HSQC spectrum. The corresponding residues were tentatively assigned to (1→4)-α-$_D$-Glc*p* (A), (1→2)-α-$_L$-Rha*p* (B), (1→5)-α-$_L$-Ara*f* (C), T-α-$_L$-Ara*f* (D), (1→2,4)-β-$_D$-Xyl*p* (E), T-β-$_D$-Gal*p* (F) and (1→2)-β-$_D$-Glc*p*A (G), which was consistent with the methylation results and literature data ((38); Q. (37, 39–42)). According to the linked positions of the residues shown by the cross-peaks, the chemical shifts of individual residues produced by ^{1}H-^{1}H COSY and HSQC spectra were verified by the HMBC experiments. For instance, the H-5/C-6 signal of a long-range correlation appeared at 4.23/176.87 ppm in the HMBC spectrum (**Figure 2E**); hence the corresponding residue of this sugar could be identified as Glc*p*A.

Quite apart from confirming the above assignments, HMBC NMR analysis was used to clarify the linkages between the structural fragments. Both intra- and inter-connections among these different sugar residues were determined according to all the information given by the cross-peaks between anomeric protons and non-anomeric carbons of every sugar residue in HMBC. The cross peak for H-1 of (1→4)-α-$_D$-Glc*p* and C-4 of (1→2,4)-β-$_D$-Xyl*p* was observed, indicating that (1→4)-α-$_D$-Glc*p* is connected to the O-4 position of (1→2,4)-β-$_D$-Xyl*p*. Similarly, H-1 of (1→2)-α-$_L$-Rha*p* is linked to the O-4 position of (1→4)-α-$_D$-Glc*p* and (1→2,4)-β-$_D$-Xyl*p*; both H-1 of (1→2)-α-$_L$-Rha*p* and (1→5)-α-$_L$-Ara*f* are connected to the O-2 position of (1→2)-α-$_L$-Rha*p*; and H-1 of (1→2,4)-β-$_D$-Xyl*p* is linked to its O-2 position. H-1 of T-α-$_L$-Ara*f* was linked to the O-4 position of (1→2,4)-α-$_D$-Xyl*p* as indicated by a cross peak at 4.94/77.27 ppm (H-1 of Ara*f* and C-4 of (1→2,4)-α-$_D$-Xyl*p*), and (1→2)-β-$_D$-Glc*p*A were linked to the O-5 position of (1→5)-α-$_L$-Ara*f* at 4.43/76.71 ppm (H-1 of Glc*p*A and C-5 of Ara*f*). Similarly, H-1 of T-β-$_D$-Gal*p* was both connected to the O-4 position of (1→2,4)-α-$_D$-Xyl*p* and the O-2 position of (1→2)-β-$_D$-Glc*p*A as indicated by a cross peak at 4.53/77.27 ppm (H-1 of Gal*p* and C-5 of (1→2)-β-$_D$-Glc*p*A) and another at 3.37/101.46 ppm (H-1 of Gal*p* and C-2 of (1→2)-β-$_D$-Glc*p*A). And the cross peak present at 1.23/70.05 ppm (H-6 of and C-5 of Rha*p*) concurred with the structure of (1→2)-α-$_L$-Rha*p*. Based on the results above, a possible structure for SSP-2 is proposed as shown in **Figure 2F**. It is difficult to distinguish all the linkage patterns of the polysaccharide *via* NMR owing to its high degree of branching.

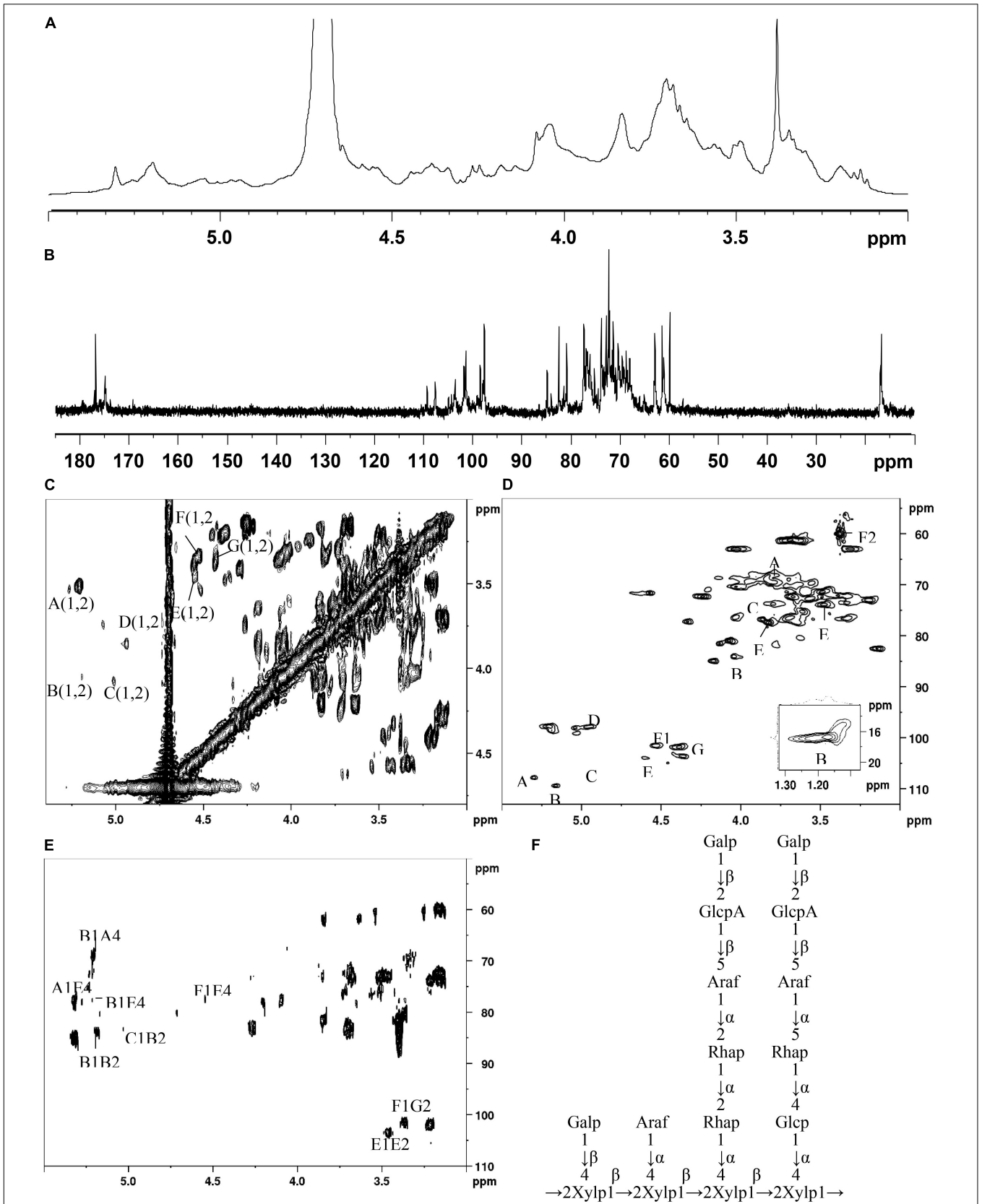

FIGURE 2 | ^{1}H **(A)**, ^{13}C **(B)**, COSY **(C)**, HSQC **(D)**, and HMBC **(E)** spectra of SSP-2 in D_2O; proposed structure of SSP-2 **(F)**.

TABLE 3 | Summary of ^{1}H and ^{13}C chemical shifts (δ,ppm) for SSP-2.

Residues	H1/C1	H2/C2	H3/C3	H4/C4	H5/C5	H6/C6
A: →4)-α-$_D$-Glc*p*-(1→	5.30	3.53	3.35	3.83	3.95	3.25
	107.76	77.17	71.40	68.79	69.57	72.31
B: →2)-α-$_L$-Rha*p*-(1→	5.20	4.06	3.82	3.35	3.78	1.23
	109.34	83.95	73.71	62.86	70.05	16.77
C: →5)-α-$_L$-Ara*f*-(1→	5.02	4.08	3.71	4.21	3.83	
	107.65	80.89	68.80	70.43	76.71	
D: T-α-$_L$-Ara*f*-(1→	4.94	3.86	4.19	3.64	3.84	
	97.80	78.84	68.50	69.82	81.60	
E:→2,4)-β-$_D$-Xyl*p*-(1→	4.56	3.45	3.64	3.86	4.08	
	103.85	73.85	69.66	77.27	80.89	
F: T-β-$_D$-Gal*p*-(1→	4.53	3.35	4.07	3.87	4.19	3.65
	101.46	72.12	76.23	73.64	81.40	72.57
G: →2)-β-$_D$-Glc*p*A-(1→	4.43	3.37	3.57	3.73	3.15	4.23
	101.91	59.87	71.40	70.05	82.41	176.87

Thermal Analysis

Thermal stability is a critical characteristic that determines applications. TG and DTG analyses were conducted to assess the thermal behavior of the samples and to figure out how thermal transitions associated with evaporation, decomposition, and oxidation could affect the structure (43). The residual mass of the prepared samples was measured as a function of temperature, as shown in **Supplementary Figure 2**. Peak temperatures for all of the derivative curves similarly showed two main stages of loss of mass. These values were susceptible to changes depending on the chemical composition, degrees of polymerization, molecular weight, and branching of the samples. There was a weight loss less than 17% at the first stage in the period of 100–150°C, which could be explained by the dissociation of absorbed and structural water and which coincided with the existence of hydrophilic groups in each polysaccharide (44). The second stage, including endothermic peaks between 150 and 550°C, was due to the heat degradation of the polysaccharides. Differences among samples could be observed in this stage. The results showed that SSP-1, with a higher Man/Gal ratio, had a high decomposition temperature, which was consistent with the literature (45). Na and Lee showed that high mannose content resulted in the greater binding energy of the polysaccharide chains. The slower degradation at the end of the second stage finished at 550°C with a large quantity of char, which was related to the inorganic compounds and volatile decomposition products in the samples, such as hydroxyl and carboxyl groups (46).

Antioxidant Activity and the Structure-Activity Relationship

DPPH Scavenging Activity

The scavenging of DPPH radicals could be used to indicate the hydrogen-donating ability of the purified polysaccharides. As shown in **Figure 3A**, the scavenging activity of SSP-1, SSP-2, SSP-3, SSP-4, and V_C against the DPPH radical was monitored at 517 nm. As can be seen, SSP-2 showed better scavenging activity of DPPH radicals than the other three polysaccharides.

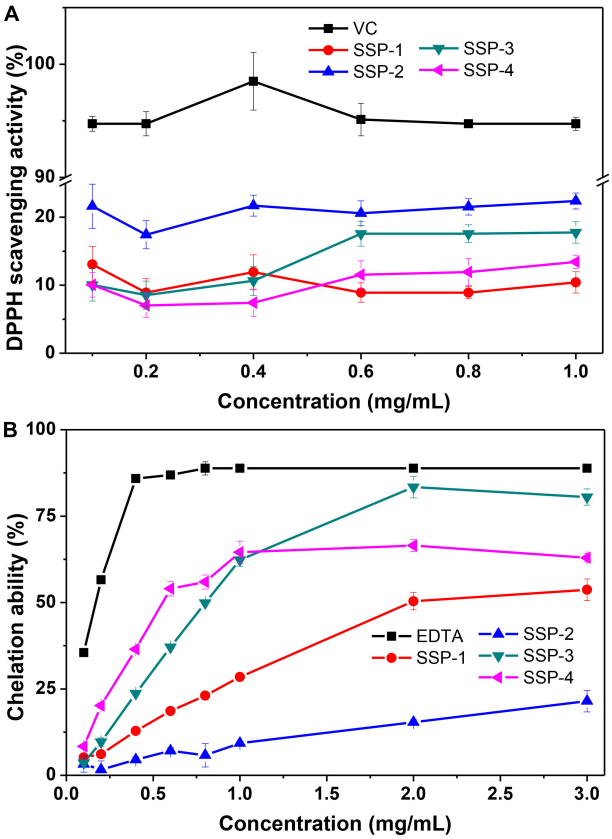

FIGURE 3 | DPPH radical scavenging assay **(A)** and ferrous ion chelating ability assay **(B)**.

However, the scavenging activity in all concentrations ranging from 0.1 to 1.0 mg/mL was no more than 25%, which was much lower than that of Vc. Niu (47) reported that the alkali-soluble heteropolysaccharide from *pentaphyllum* Makino showed lower absorbance capacities for DPPH than the water-soluble polysaccharide and the DPPH radical scavenging capacity of the alkali-soluble polysaccharide was calculated to be 2 μmol TE/g. The chemical structures, molecular weights, and monosaccharide compositions of the alkali-soluble polysaccharide were different from the polysaccharide extracted with hot water, which will result in different antioxidant activities.

Iron Chelating Activity

Fe^{2+} is a powerful pro-oxidant with active reactivity and it involves in the Fenton reaction which leads to the oxidation of lipid and protein. Therefore, the chelating activity of polysaccharides can be used as an obvious indicator of antioxidant capacity (48). The correlation between the concentration of the polysaccharides and their chelating activities to Fe^{2+} is shown in **Figure 3B**. This result indicated that the SSPs represent concentration-dependent chelation ability and SSP-3 had the best chelating ability with a chelating rate of 80.5% at the concentration of 3.0 mg/mL. At concentration

of 3.0 mg/mL, the chelating rates of SSP-1, SSP-2 and SSP-4 were 53.7.5, 21.5, and 63.0%, respectively. The results indicated that all of the SSPs possessed powerful Fe^{2+} chelating ability, which is still weaker than that of EDTA. The formation of SSPs -Fe^{3+} complex inhibited the occurrence of Fenton reaction, therefore the generation of hydroxyl radical is reduced. However, the way in which structure affects the antioxidant activities remains unknown.

Correlation of Structure and Antioxidant Activity

The biological activities of polysaccharides were mainly related to their molecular weight, monosaccharide composition, sulfate content, glycosidic linkage, and chain structure (49). Although the relationships between function and structure of polysaccharides remained unclear, some evidence can be inferred from our study as follows.

It is widely known that polysaccharides possess antioxidant effects due to the number of reductive hydroxyl groups in their structure. And polysaccharides with low molecule weight is more likely to present a stronger reducing power, because they may have a higher content of reducing end (available active hydroxyl group terminals) to accept and eliminate the free radicals. However, molecule weight is certainly not the deciding factor of the antioxidant effects. In our study, the SSP-2 fraction with a higher molecule weight (10.9 kDa) presented better DPPH scavenging activity than the other fractions, which was consistent with an investigation by Liang et al. (50). It was found that fraction MDP-2 with a higher molecule weight (1,700 kDa) from the *Mycena dendrobii* has better antioxidant activity than fraction MDP-1 (602 kDa).

In addition, the discrepancies of biological activities between the four fractions were probably owing to the difference in the ratio of monosaccharides. Their DPPH scavenging activities are in the order of ascorbic acid > SSP-2 > SSP-3 > SSP-4 > SSP-1, suggesting the probable relationship between the polysaccharides and their xylose content. And SSP-2 performed better in DPPH scavenging activities may be due to its high uronic acid content (51). At concentration of 3.0 mg/mL, the ferrous ion chelating activity of SSP-1, SSP-2, SSP-3, and SSP-4 are concentration-dependent and are in the order of SSP-3 > SSP-4 > SSP-1 > SSP-2. In addition, the xylose content in them was determined in the same order, indicating that the chelating ability of the four polysaccharides was probably due to their xylose content.

CONCLUSION

Four polysaccharide fractions (SSP-1, SSP-2, SSP-3, and SSP-4) were purified from the waste liquor obtained by simulating the soaking process of wet decortication of sesame seeds. Structural analysis revealed that the polysaccharides reclaimed from this process were low-molecular-weight polysaccharides. The main fraction, SSP-2, consisted of rhamnose, arabinose, galactose, glucose, xylose, glucuronic acid, and galacturonic acid in the molar ratio of 16.3:29.1:23.9:9.0:13.5:6.2:2.0. The results of monosaccharide composition, methylation, and NMR spectroscopic analyses indicated that the backbone of SSP-2 mainly consisted of (1→2,4)-β-$_D$-Xyl*p* residues with side chains connected to the O-4 position composed of a great deal of T-β-$_D$-Gal*p* and (1→5)-α-$_L$-Ara*f* residues, and lesser contents of (1→4)-α-$_D$-Glc*p*, (1→2)-α-$_L$-Rha*p*, T-α-$_L$-Ara*f*, and (1→2)-β-$_D$-Glc*p*A residues. Polysaccharides from the waste liquor have complex structures and may have potential as an ingredient in foods or as excipients in pharmaceuticals, and these possibilities merit further study. In addition, removing polysaccharides from the waste liquor will simplify wastewater treatment. Further studies on the bioactivity and chemistries of these four polysaccharide fractions are in progress.

DATA AVAILABILITY STATEMENT

The raw data supporting the conclusions of this article will be made available by the authors, without undue reservation.

AUTHOR CONTRIBUTIONS

Y-RL: conceptualization, writing-original draft preparation, and methodology. SX: data curation and visualization. R-YZ and M-XY: investigation. H-ML: writing-review and editing and validation. X-DW: supervision and writing-review and editing. All authors contributed to the article and approved the submitted version.

FUNDING

This work was financially supported by China Agricultural Research System of MOF and MARA, Natural Science Foundation of Excellent Youth for Henan (222300420038), the Key Project of Science and Technology of Henan Province (201300110600), and the Innovation and Entrepreneurship Training Program for Higher Education Students in Henan Province (202110463042, 202110463043, and 202110463040).

SUPPLEMENTARY MATERIAL

The Supplementary Material for this article can be found online at: https://www.frontiersin.org/articles/10.3389/fnut.2022.940442/full#supplementary-material

REFERENCES

1. Mikropoulou EV, Petrakis EA, Argyropoulou A, Mitakou S, Halabalaki M, Skaltsounis LA. Quantification of bioactive lignans in sesame seeds using HPTLC densitometry: comparative evaluation by HPLC-PDA. *Food Chem.* (2019) 288:1–7. doi: 10.1016/j.foodchem.2019.02.109
2. Liu HM, He MK, Yao YG, Qin Z, Cai XS, Wang XD. Pectic polysaccharides extracted from sesame seed hull: physicochemical and functional properties.

Int J Biol Macromol. (2021) 192:1075–83. doi: 10.1016/j.ijbiomac.2021.10.077
3. Mohamed IA, Uslu N, Musa Ozcan M, Al Juhaimi F, Ghafoor K, Babiker EE, et al. Effect of conventional oven roasting treatment on the physicochemical quality attributes of sesame seeds obtained from different locations. *Food Chem.* (2021) 338:128109. doi: 10.1016/j.foodchem.2020.128109
4. Rangkadilok N, Pholphana N, Mahidol C, Wongyai W, Saengsooksree K, Nookabkaew S, et al. Variation of sesamin, sesamolin and tocopherols in sesame (*Sesamum indicum* L.) seeds and oil products in Thailand. *Food Chem.* (2010) 122:724–30. doi: 10.1016/j.foodchem.2010.03.044
5. Besharati M, Palangi V, Taghizadeh A, Kaya A, Abachi S. Determining the effect of natural inhibitors on sesame meal degradability using in vitro three step method. *Vet Arh.* (2021) 91:513–21. doi: 10.24099/vet.arhiv.1138
6. Eom SJ, Zu HD, Lee J, Kang MC, Park J, Song KM, et al. Development of an ultrasonic system for industrial extraction of unheated sesame oil cake. *Food Chem.* (2021) 354:129582. doi: 10.1016/j.foodchem.2021.129582
7. Moharram YG, Osman HOA, Abou-Ei-Khier YIA. Wet decortication of sesame seeds by new methods. *Food Nutr Bull.* (1990) 12:1–6. doi: 10.1177/156482659001200126
8. Carbonell-Barrachina AA, Lluch MA, Perez-Munera I, Hernando I, Castillo S. Effects of chemical dehulling of sesame on color and microstructure. *Food Sci Technol Int.* (2009) 0:1–6. doi: 10.1177/1082013209339704
9. Elleuch M, Besbes S, Roiseux O, Blecker C, Attia H. Quality characteristics of sesame seeds and by-products. *Food Chem.* (2007) 103:641–50. doi: 10.1016/j.foodchem.2006.09.008
10. Yu Y, Shen M, Song Q, Xie J. Biological activities and pharmaceutical applications of polysaccharide from natural resources: a review. *Carbohydr Polym.* (2018) 183:91–101. doi: 10.1016/j.carbpol.2017.12.009
11. Guo R, Chen M, Ding Y, Yang P, Wang M, Zhang H, et al. Polysaccharides as potential anti-tumor biomacromolecules –a review. *Front Nutr.* (2022) 9:838179. doi: 10.3389/fnut.2022.838179
12. Kalita P, Ahmed AB, Sen S, Chakraborty R. A comprehensive review on polysaccharides with hypolipidemic activity: occurrence, chemistry and molecular mechanism. *Int J Biol Macromol.* (2022) 206:681–98. doi: 10.1016/j.ijbiomac.2022.02.189
13. Zhou S, Huang G. Extraction, derivatization, and antioxidant activity of *Morinda citrifolia* polysaccharide. *Chem Biol Drug Des.* (2022) 99:603–8. doi: 10.1111/cbdd.14023
14. Ji X, Guo J, Ding D, Gao J, Hao L, Guo X, et al. Structural characterization and antioxidant activity of a novel high-molecular-weight polysaccharide from *Ziziphus jujuba* cv. Muzao. *J Food Meas Charact.* (2022) 16:2191–200. doi: 10.1007/s11694-022-01288-3
15. Huo S, Wang H, Chen J, Hu X, Zan X, Zhang C, et al. A preliminary study on polysaccharide extraction, purification, and antioxidant properties of sugar-rich filamentous microalgae *Tribonema minus*. *J Appl Phycol.* (2022) 48:1–13. doi: 10.1007/s10811-021-02630-w
16. Dubois M, Gilles KA, Hamilton JK, Rebers PA, Smith F. Colorimetric method for determination of sugars and related substances. *Anal Chem.* (1956) 28:350–6. doi: 10.1021/ac60111a017
17. Ji X, Guo J, Pan F, Kuang F, Chen H, Guo X, et al. Structural elucidation and antioxidant activities of a neutral polysaccharide from arecanut (*Areca catechu* L.). *Front Nutr.* (2022) 9:853115. doi: 10.3389/fnut.2022.853115
18. Kim JB, Carpita NC. Changes in esterification of the uronic acid groups of cell wall polysaccharides during elongation of maize coleoptiles. *Plant Physiol.* (1992) 98:646–53. doi: 10.1104/pp.98.2.646
19. Pettolino FA, Walsh C, Fincher GB, Bacic A. Determining the polysaccharide composition of plant cell walls. *Nat Protoc.* (2012) 7:1590–607. doi: 10.1038/nprot.2012.081
20. Wang L, Liu HM, Xie AJ, Wang XD, Zhu CY, Qin GY. Chinese quince (*Chaenomeles sinensis*) seed gum: structural characterization. *Food Hydrocolloids.* (2018) 75:237–45. doi: 10.1016/j.foodhyd.2017.08.001
21. Chen J, Zhang X, Huo D, Cao C, Li Y, Liang Y, et al. Preliminary characterization, antioxidant and alpha-glucosidase inhibitory activities of polysaccharides from *Mallotus furetianus*. *Carbohydr Polym.* (2019) 215:307–15. doi: 10.1016/j.carbpol.2019.03.099
22. Shao LL, Xu J, Shi MJ, Wang XL, Li YT, Kong LM. Preparation, antioxidant and antimicrobial evaluation of hydroxamated degraded polysaccharides from *Enteromorpha prolifera*. *Food Chem.* (2017) 237:481–7. doi: 10.1016/j.foodchem.2017.05.119
23. Hokputsa S, Harding SE, Inngjerdingen K, Jumel K, Michaelsen TE, Heinze T, et al. Bioactive polysaccharides from the stems of the Thai medicinal plant *Acanthus ebracteatus*: their chemical and physical features. *Carbohydr Res.* (2004) 339:753–62. doi: 10.1016/j.carres.2003.11.022
24. Coll-Almela L, Saura-Lopez D, Laencina-Sanchez J, Schols HA, Voragen AG, Ros-Garcia JM. Characterisation of cell-wall polysaccharides from mandarin segment membranes. *Food Chem.* (2015) 175:36–42. doi: 10.1016/j.foodchem.2014.11.118
25. Khodaei N, Karboune S. Extraction and structural characterisation of rhamnogalacturonan I-type pectic polysaccharides from potato cell wall. *Food Chem.* (2013) 139:617–23. doi: 10.1016/j.foodchem.2013.01.110
26. Bian J, Peng F, Xu F, Sun RC, Kennedy JF. Fractional isolation and structural characterization of hemicelluloses from *Caragana korshinskii*. *Carbohydr Polym.* (2010) 80:753–60. doi: 10.1016/j.carbpol.2009.12.023
27. Long X, Hu X, Xiang H, Chen S, Li L, Qi B, et al. Structural characterization and hypolipidemic activity of *Gracilaria lemaneiformis* polysaccharide and its degradation products. *Food Chem. X.* (2022) 14:100314. doi: 10.1016/j.fochx.2022.100314
28. Ji X, Liu F, Peng Q, Wang M. Purification, structural characterization, and hypolipidemic effects of a neutral polysaccharide from *Ziziphus jujuba* cv. Muzao. *Food Chem.* (2018) 245:1124–30. doi: 10.1016/j.foodchem.2017.11.058
29. Saravana PS, Cho YN, Patil MP, Cho YJ, Kim GD, Park YB. Hydrothermal degradation of seaweed polysaccharide: characterization and biological activities. *Food Chem.* (2018) 268:179–87. doi: 10.1016/j.foodchem.2018.06.077
30. Wang ZB, Pei JJ, Ma HL, Cai PF, Yan JK. Effect of extraction media on preliminary characterizations and antioxidant activities of *Phellinus linteus* polysaccharides. *Carbohydr Polym.* (2014) 109:49–55. doi: 10.1016/j.carbpol.2014.03.057
31. Jeddou KB, Chaari F, Maktouf S, Nouri-Ellouz O, Helbert CB, Ghorbel RE. Structural, functional, and antioxidant properties of water-soluble polysaccharides from potatoes peels. *Food Chem.* (2016) 205:97–105. doi: 10.1016/j.foodchem.2016.02.108
32. Ji X, Cheng Y, Tian J, Zhang S, Jing Y, Shi M. Structural characterization of polysaccharide from jujube (*Ziziphus jujuba* Mill.) fruit. *Chem Biol Technol Agric.* (2021) 8:54. doi: 10.1186/s40538-021-00255-2
33. Nep EI, Carnachan SM, Ngwuluka NC, Kontogiorgos V, Morris GA, Sims IM, et al. Structural characterisation and rheological properties of a polysaccharide from sesame leaves (*Sesamum radiatum* Schumach. & Thonn.). *Carbohydr Polym.* (2016) 152:541–7. doi: 10.1016/j.carbpol.2016.07.036
34. Gao J, Zhang T, Jin ZY, Xu XM, Wang JH, Zha XQ, et al. Structural characterisation, physicochemical properties and antioxidant activity of polysaccharide from *Lilium lancifolium* Thunb. *Food Chem.* (2015) 169:430–8. doi: 10.1016/j.foodchem.2014.08.016
35. He L, Ji P, Cheng J, Wang Y, Qian H, Li W, et al. Structural characterization and immunostimulatory activity of a novel protein-bound polysaccharide produced by *Hirsutella sinensis* Liu, Guo, Yu & Zeng. *Food Chem.* (2013) 141:946–53. doi: 10.1016/j.foodchem.2013.04.053
36. Bruyn AD, Anteunis M, Gussem RD, Dutton GGS. 1H-N.m.r. study of L-rhamnose, methyl cc-L-rhamnopyranoside, and 4-O-β-D-galactopyranosyl-L-rhamnose in deuterium oxide. *Carbohydr Res.* (1976) 47:158–63. doi: 10.1016/s0008-6215(00)83559-4
37. Liu J, Wen XY, Kan J, Jin CH. Structural characterization of two water-soluble polysaccharides from black soybean (*Glycine max* (L.) Merr.). *J Agric Food Chem.* (2015) 63:225–34. doi: 10.1021/jf505172m
38. Ding HH, Cui SW, Goff HD, Chen J, Guo Q, Wang Q. Xyloglucans from flaxseed kernel cell wall: structural and conformational characterisation. *Carbohydr Polym.* (2016) 151:538–45. doi: 10.1016/j.carbpol.2016.05.094
39. Guo Q, Cui SW, Wang Q, Hu X, Wu Y, Kang J, et al. Structure characterization of high molecular weight heteropolysaccharide isolated from *Artemisia sphaerocephala* Krasch seed. *Carbohydr Polym.* (2011) 86:742–6. doi: 10.1016/j.carbpol.2011.05.018
40. Luo D. Structural investigation of a polysaccharide (DMB) purified from *Dioscorea nipponica* Makino. *Carbohydr Polym.* (2014) 103:261–6. doi: 10.1016/j.carbpol.2013.12.033

41. Xia YG, Liang J, Yang BY, Wang QH, Kuang HX. Structural studies of an arabinan from the stems of *Ephedra sinica* by methylation analysis and 1D and 2D NMR spectroscopy. *Carbohydr Polym.* (2015) 121:449–56. doi: 10.1016/j.carbpol.2014.12.058
42. Zhao J, Zhang F, Liu X, St Ange K, Zhang A, Li Q, et al. Isolation of a lectin binding rhamnogalacturonan-I containing pectic polysaccharide from pumpkin. *Carbohydr Polym.* (2017) 163:330–6. doi: 10.1016/j.carbpol.2017.01.067
43. Xie JH, Liu X, Shen MY, Nie SP, Zhang H, Li C. Purification, physicochemical characterisation and anticancer activity of a polysaccharide from *Cyclocarya paliurus* leaves. *Food Chem.* (2013) 136:1453–60. doi: 10.1016/j.foodchem.2012.09.078
44. Wang L, Zhang B, Xiao J, Huang Q, Li C, Fu X. Physicochemical, functional, and biological properties of water-soluble polysaccharides from *Rosa roxburghii* Tratt fruit. *Food Chem.* (2018) 249:127–35. doi: 10.1016/j.foodchem.2018.01.011
45. Na K, Lee KY. Characteristics of the lactan gum produced from various carbon sources by *Rahnella aquatilis*. *Biotechnol Lett.* (1997) 19:1193–5. doi: 10.1023/A:1018429719189
46. Pohjanlehto H, Setälä HM, Kiely DE, McDonald AG. Lignin-xylaric acid-polyurethane-based polymer network systems: preparation and characterization. *J Appl Polym Sci.* (2014) 131:39714–21. doi: 10.1002/app.39714
47. Niu Y, Shang P, Chen L, Zhang H, Gong L, Zhang X. Characterization of a novel alkali-soluble heteropolysaccharide from tetraploid *Gynostemma pentaphyllum* Makino and its potential anti-inflammatory and antioxidant properties. *J Agric Food Chem.* (2014) 62:3783–90. doi: 10.1021/jf500438s
48. Wang L, Liu HM, Qin GY. Structure characterization and antioxidant activity of polysaccharides from Chinese quince seed meal. *Food Chem.* (2017) 234:314–22. doi: 10.1016/j.foodchem.2017.05.002
49. Jahanbin K, Gohari AR, Moini S, Emam-Djomeh Z, Masi P. Isolation, structural characterization and antioxidant activity of a new water-soluble polysaccharide from *Acanthophyllum bracteatum* roots. *Int J Biol Macromol.* (2011) 49:567–72. doi: 10.1016/j.ijbiomac.2011.06.012
50. Liang XX, Gao YY, Pan Y, Zou YF, He M, He CL, et al. Purification, chemical characterization and antioxidant activities of polysaccharides isolated from *Mycena dendrobii*. *Carbohydr Polym.* (2019) 203:45–51. doi: 10.1016/j.carbpol.2018.09.046
51. Zeng WC, Zhang Z, Jia LR. Antioxidant activity and characterization of antioxidant polysaccharides from pine needle (*Cedrus deodara*). *Carbohydr Polym.* (2014) 108:58–64. doi: 10.1016/j.carbpol.2014.03.022

Conflict of Interest: The authors declare that the research was conducted in the absence of any commercial or financial relationships that could be construed as a potential conflict of interest.

Publisher's Note: All claims expressed in this article are solely those of the authors and do not necessarily represent those of their affiliated organizations, or those of the publisher, the editors and the reviewers. Any product that may be evaluated in this article, or claim that may be made by its manufacturer, is not guaranteed or endorsed by the publisher.

Copyright © 2022 Li, Xu, Zhang, Yang, Liu and Wang. This is an open-access article distributed under the terms of the Creative Commons Attribution License (CC BY). The use, distribution or reproduction in other forums is permitted, provided the original author(s) and the copyright owner(s) are credited and that the original publication in this journal is cited, in accordance with accepted academic practice. No use, distribution or reproduction is permitted which does not comply with these terms.

frontiers | Frontiers in Nutrition

ORIGINAL RESEARCH
published: 13 June 2022
doi: 10.3389/fnut.2022.917432

Hemicellulosic Polysaccharides From Bamboo Leaves Promoted by Phosphotungstic Acids and Its Attenuation of Oxidative Stress in HepG2 Cells

Zhuqian Xiao[1,2], Jiajie Li[1], Hongpeng Wang[1], Qiang Zhang[1], Qing Ge[1], Jianwei Mao[1] and Ruyi Sha[1]*

[1] Zhejiang Provincial Collaborative Innovation Center of Agricultural Biological Resources Biochemical Manufacturing, Zhejiang University of Science and Technology, Hangzhou, China, [2] College of Chemical Engineering, Zhejiang University of Technology, Hangzhou, China

In this work, we exploited an efficient method to release hemicellulosic polysaccharides (BLHP) from bamboo (*Phyllostachys pubescens Mazel*) leaves assisted by a small amount of phosphotungstic acid. Structural unit analysis proved that BLHP-A1 and BLHP-B1 samples possessed abundant low-branch chains in →4)-β-$_D$-Xyl*p*-(1→ skeleton mainly consisting of Xyl*p*, Man*p*, Glc*p*, Gal*p*, and Ara*f* residues. According to the results of the antioxidant activity assays *in vitro*, both of the two fractions demonstrated the activity for scavenging DPPH· and $ABTS^+$ radicals and exhibited relatively a high reducing ability compared to the recently reported polysaccharides. Moreover, the antioxidant activities of purified polysaccharides were evaluated against H_2O_2-induced oxidative stress damage in HepG2 cells. BLHP-B1 showed more activity for preventing damages from H_2O_2 in HepG2 cells by improving the enzyme activities of SOD, CAT, and GSH-Px and decreasing the production of MDA as well as suppressing reactive oxygen species (ROS) formation. This study implied that BLHP could demonstrate its attenuation ability for oxidative stress in HepG2 cells.

Keywords: bamboo leaves, hetero-polysaccharides, oxidative stress, HepG2 cells, phosphotungstic acid

OPEN ACCESS

Edited by:
Xiaolong Ji,
Zhengzhou University of Light Industry, China

Reviewed by:
Xufeng Wang,
Fuzhou University, China
Wei Li,
Korea Institute of Oriental Medicine, South Korea
Xuwei Long,
Nanjing University of Science and Technology, China

****Correspondence:***
Zhuqian Xiao
zustxzq@zust.edu.cn

Specialty section:
This article was submitted to Food Chemistry, a section of the journal Frontiers in Nutrition

Received: *11 April 2022*
Accepted: *10 May 2022*
Published: *13 June 2022*

Citation:
Xiao Z, Li J, Wang H, Zhang Q, Ge Q, Mao J and Sha R (2022) Hemicellulosic Polysaccharides From Bamboo Leaves Promoted by Phosphotungstic Acids and Its Attenuation of Oxidative Stress in HepG2 Cells. Front. Nutr. 9:917432. doi: 10.3389/fnut.2022.917432

INTRODUCTION

Free radicals [reactive oxygen species (ROS) and nitrogen species are included] act as essential active species in living tissues to maintain cellular homeostasis in organisms. The accumulation of radicals can lead to some serious diseases including Alzheimer's disease, Parkinson's disease, and even tumors (1–3). On the other hand, the activity of the antioxidant enzyme system, including catalase (CAT), superoxide dismutase (SOD), and glutathione peroxidase (GSH-Px), will be motivated to scavenge the active radicals, protecting cells from the invasion of ROS. Oxidative stress from ROS has been widely regarded as a significant factor in cell aging and immune injuries, and H_2O_2 is one of the general contributors to cause oxidative damage in model cells or animal tissue evaluation (4, 5). Recently, quite a few natural products from terrestrial and aquatic organisms, including peptides, glycoproteins, terpenoids, and polysaccharides, have been elucidated to possess promising antioxidant activity due to a particular structure (6–8). Polysaccharides, a polymer widely found in organisms, are rich in hydroxyl groups and functional side chains, exhibiting

excellent antioxidant activity (9). A quintessential example should be cited that distinct antioxidant, antitumor, and antimicrobial activities of polysaccharides extracted from Ganoderma have been reported previously (10). The type of glycosidic linkages, branching patterns, and linkages to proteins in Ganoderma polysaccharides are all concerning its antioxidant activity.

Bamboo, one of the agricultural and forestry cash crops, is widely cultivated in southeast Asia. Through the ages, the bamboo stem has been used as a resource for paper manufacturing due to its 40–48% of cellulose (11). Likewise, the contents of cellulose and hemicellulose in bamboo leaves are 20–40% and 35–45%, respectively (12). Particularly, the content of hemicellulose is more in the bamboo stem, which is suggestive of the occurrence of structural carbohydrate polymers with various branches. Bamboos encompass 1,250 species within 75 genera and share the desirable characteristics of high productivity and are fast-growing, and could be recognized as renewable resources to extract functional hetero-polysaccharides because of their abundant hemicelluloses (13). However, the extraction methods of plant-based polysaccharides were adopted as a physical process assisted by ultrasonic (14), microwave (15), and even hot water (16) directly, which proved to show low selectivity for specific components releasing. The crude hemicelluloses extracted from plant sources probably contain $_{D}$-galactose, $_{D}$-mannose, $_{L}$-rhamnose, $_{L}$-fucose, and even peptides, implying that it is a challenge to analyze the characteristic structure of polysaccharides after extraction using different physical methods. Phosphotungstic acid (HPW, $H_3PW_{12}O_{40}$), one of the heteropolyacids with Keggin structure, is a strong Brønsted acid. According to our previous study, a certain amount of HPW demonstrated high selectivity for xylose recovery (17). Hence, it is reasonable to apply phosphotungstic acid in the selective extraction of hemicellulosic polysaccharides. On the other hand, numerous publications elaborate that multitudinous polysaccharides extracted from plants exhibit strong free radicals scavenging ability as well as an excellent protective effect on oxidative damage of ROS in induced cells *in vitro* (18–20). Moreover, cancer cells with rapid proliferation capacity demonstrate a high utilization rate of inspired oxygen. It is believed that these cells are subjected to the influence of oxidative stress. Coupled with their easy culturing, we plan to employ H_2O_2-induced HepG2 cells damage *in vitro* as a model to evaluate their protective effects on the oxidative injury. The structure of the extracted polysaccharides samples will also be analyzed.

MATERIALS AND METHODS

Materials and Chemicals

One-year-old bamboo (*Phyllostachys pubescens Mazel*) leaves were collected from a mountain in Xihu District, Hangzhou, Zhejiang Province of China. All the raw materials were smashed into about 200 μm (all the particle sizes were measured on a Topsizer Plus laser particle size analyzer, Zhuhai OMEC Instruments Co., Ltd., Zhuhai, China) after oven drying. Dimethyl sulfoxide (DMSO), 1,1-diphenyl-2-picrylhydrazyl radical (DPPH), 2,2-azinobis-3 ethyl benzothiazoline-6-sulphonic acid (ABTS), standard monosaccharides including $_{D}$-glucose, $_{D}$-galactose, $_{L}$-arabinose, $_{L}$-rhamnose and $_{D}$-mannose, potassium ferricyanide were purchased from Sigma-Aldrich in China mainland. H_2O_2, $FeSO_4$, and phosphotungstic acid were from Sinopharm Chemical Reagent Co. Ltd., China. DEAE-Sepharose® fast flow column (2.0 cm × 40 cm, Cl^- form) is purchased from Sigma-Aldrich, Shanghai, China. Commercial assay kits for the determination of SOD, catalase (CAT), GSH-Px, and methylenedioxyamphetamine, (MDA) including Cell Counting Kit-8 (CCK-8), and BCA Protein Assay Kit, Radio Immunoprecipitation Assay (RIPA) lysis buffer, and Minimum Eagle's medium (MEM) were purchased from Beyotime Biotechnology Co. Ltd., Shanghai, China. Reactive Oxygen Species Assay Kit (DCFH-DA) was from MedChemExpress (Shanghai).

Bamboo Leaves Hetero-Polysaccharides Extraction and Purification

Bamboo leaves powder (BLP) was further ball-milled for 3.0 h to obtain tinnier particles in nearly 50 μm diameter (particle size analyzer measured). The milled powder was then dewaxed with 95% ethanol at 60°C before extraction. To measure the yield of polysaccharides, the dewaxed BLP was oven-dried till the moisture was nearly 4.0%. In a typical extracting process, briefly, 5.0 g BLP mixed with 0.1 g phosphotungstic acid was employed in the Teflon-lined ultrasonic reactor (100 ml, Yanzheng Instrument Co., Ltd., China) at 50 W and 60.0 ml deionized water was injected as the extracting medium. This weak hydrolysis occurred at 80°C for 2.0 h under N_2 atmosphere. After extraction, the liquid was filtrated, and the trace phosphotungstic acid was removed by dialysis (3,000 molecular cutoff by regenerated cellulose membrane from CMEC Biochemical Co. Ltd., China). The neutral filtrate was then concentrated by 95% alcohol precipitation and then centrifuged at 8,000 rpm for 20 min to yield crude bamboo leaves polysaccharides (CBLP). Successively, CBLP precipitates were freeze-dried to obtain CBLP powder. DEAE-Sepharose fast-flow column (2.0 cm × 40 cm, Cl^- form) was applied to the isolation of components. The concentrated NaCl solutions (0.1, 0.2, 0.4, 0.6, 1.0, and 2.0 mol/L) were added as the eluent at the rate of 1.0 ml/min after 500.0 ml deionized water elution. The concentration of isolated polysaccharides was measured according to the absorbance at 498 nm by the phenol-sulfuric acid method (21, 22). The tubes containing target components were then collected and evaporated to concentrate the polysaccharides solutions accordingly. The samples were further purified by the DEAE Sephacryl S-300 column to obtain purified bamboo leaves hetero-polysaccharides (BLHP). Finally, these concentrated solutions were freeze-dried at –60°C (nominated as BLHP-A1 and BLHP-B1).

Chemical Analysis and Physical Characterizations of Bamboo Leaves Hetero-Polysaccharides

The monosaccharides were detected by high-performance anion-exchange chromatography with pulsed amperometric detection (HPAEC-PAD, Dionex ICS-5000$^+$, Thermo Fisher Scientific,

United States). The hydrolysate was determined by an ED detector with a picomole level resolution. The analytical column was Carbo PAC^{TM} PA10 (4 mm × 250 mm) protected by PAC^{TM} PA10 (4 mm × 50 mm) column. The chromatographic pure sugars, including $_D$-glucose, $_D$-galactose, $_L$-arabinose, $_L$-rhamnose, $_D$-mannose, and the hydrolysate samples were injected into the detector with 200 mM NaOH eluent at 1.0 ml/min for 40 min. The column temperature was 40°C.

Fourier Transform Infrared Spectrometer

The characteristic covalent bonds and groups of BLHP fractions were analyzed on a Bruker V70 IR Spectrometer (Bruker, Germany) in 4,000–400 cm^{-1}. Before the performance, trace quantities of the sample were grounded with spectrographic grade potassium bromide and then pressed into a pellet under 12.0 MPa pressure.

Ultraviolet Analysis

The polysaccharides (1.0 mg) were dissolved into 1.0 ml ultrapure water, and then scanned and analyzed on a Ultraviolet (UV)-vis spectrophotometer (UV-5500PC, Metash Instruments Co. Ltd., Shanghai, China) within the wavelength range of 200–400 nm.

Scanning Electron Microscopy Characterization

To observe the morphologies of polysaccharides after freeze-drying, Scanning Electron Microscopy (SEM) analysis was performed on a HITACHI S 4800 SEM (HITACHI, Japan) with an accelerating voltage of 15.0 kV. The samples were coated with gold atoms to strengthen the conductivity.

Methylation Analysis

First, polysaccharides samples were vacuum dried for 24 h in a dryer with P_2O_5; 10.0 mg of sample was dissolved in 6.0 ml of DMSO and stirred for 15 h at 45°C. Then 30.0 mg NaOH was added to the solution above and stirred for 4.0 h at room temperature. Successively, 3.6 ml of methyl iodide was added into the solution under nitrogen protection in a dark place. After stirring for 1.0 h at 25°C, 6.0 ml of deionized water was introduced to terminate the reaction. The obtained mixture was extracted by trichloromethane and the water phase was removed. The residual organic phase was further extracted by deionized water five times. Then the organic phase was distilled to obtain methylated samples. This methylation procedure was repeated three times to ensure complete methylation. Afterward, the methylated samples were hydrolyzed with 2 M of TFA (2 ml) for 2 h at 120°C, and then reduced by NaBD4 (60 mg) overnight at room temperature. The dry reduced samples were then acetylated by acetic anhydride (0.5 ml) in pyridine (0.5 ml) at 100°C for 2 h to gain their partially methylated alditol acetates, which were analyzed by gas chromatography-mass spectrometry (GC–MS).

Gas Chromatography-Mass Spectrometry Analysis

The methylated alditol acetates were analyzed on an Agilent 7890A-5975C (Agilent Technology, Palo Alto, CA, United States) with an Rtx-5 quartz capillary column (0.25 mm × 0.25 mm × 30 m, Shimadzu Technology, Kyoto, Japan). The derived sample (1.0 μl) was injected with a He flow of 1.0 ml/min. The temperature program was set as follows: (1) initially 120°C for 5.0 min and then to 200°C at 5°C/min; (2) continuously increased to 215°C/min at 2°C/min; (3) increased to 270°C at 20°C/min and then maintained for 5 min. Mass spectra were recorded at a range of 40–500 m/z.

NMR Analysis

A total of 20.0 mg of polysaccharides powder was dissolved into 0.5 ml HDO in an NMR tube. The filtrates were recorded on a 600 MHz Digital spectrometer (AVANCE III 600 MHz, Bruker Corporation, New Castle, DE, United States) to obtain ^1H and ^{13}C spectra, and two-dimensional (2D) NMR spectra (COSY, HSQC, and HMBC).

The Chemical Antioxidant Activity Evaluation *in vitro* of Bamboo Leaves Hetero-Polysaccharides

DPPH· and ABTS$^+$ Free Radicals Scavenging

DPPH· free radical scavenging tests were performed according to the standard DPPH· assay method developed by Jiang (23) with a slight modification. A total of 4.0 ml of DPPH· solution (0.1 mM in 95% MeOH) was mixed with a specific volume of concentrated BLHP filtrate. A total of 45 μl of Tris-HCl buffer (450 mM, pH = 7.4) was injected into the mixture and then incubated in the dark for 30 min at 30°C after being vibrated well. The absorbance of the liquid was read at 517 nm. The radical scavenging activity was then calculated by Eq. (1):

$$DPPH\ scavenging\ rate(\%) = [1 - (A_1 - A_2)/A_0] \times 100\%$$

The ABTS$^+$ radical scavenging of BLHP was evaluated using the method developed by Ma (24).

Reducing Ability Test

The reducing ability of BLHP was measured according to our previous method (25) with minor modification. Briefly, 1.0 ml of concentrated BLHP solution was mixed with 2.5 ml of 0.2 M phosphate buffer (pH = 6.6) and 2.0 ml of $K_3Fe(CN)_6$ solution (1%, w/v). The mixture was centrifuged for 10 min after reacting for 20 min in a 50°C water bath. A total of 2.0 ml of supernatant and 2.0 ml of deionized water were then mixed before 0.4 ml $FeCl_3$ solution (1%, w/v) was added. This solution was stewed for 10 min at 25°C. Finally, the absorbance was recorded at 700 nm, and vitamin C (VC) was used as the positive control.

Bamboo Leaves Hetero-Polysaccharides Attenuation in Oxidative Stress Induced by H_2O_2 in HepG2 Cells

Cell Lines and Culture Conditions

The human hepatocellular carcinomas (HepG2, CL-0103) cell line was purchased from Procell Life Science and Technology Co. Ltd. (Wuhan, China), authenticated by Short Tandem Repeat (STR). After thawing, the cells were cultured in minimum Eagle's medium (MEM) with 10% FBS, 1% non-essential amino acids (NEAA), and 1 mM sodium pyruvate (NaP) and then incubated at 37°C under a 5% CO_2 atmosphere. In this work, HepG2

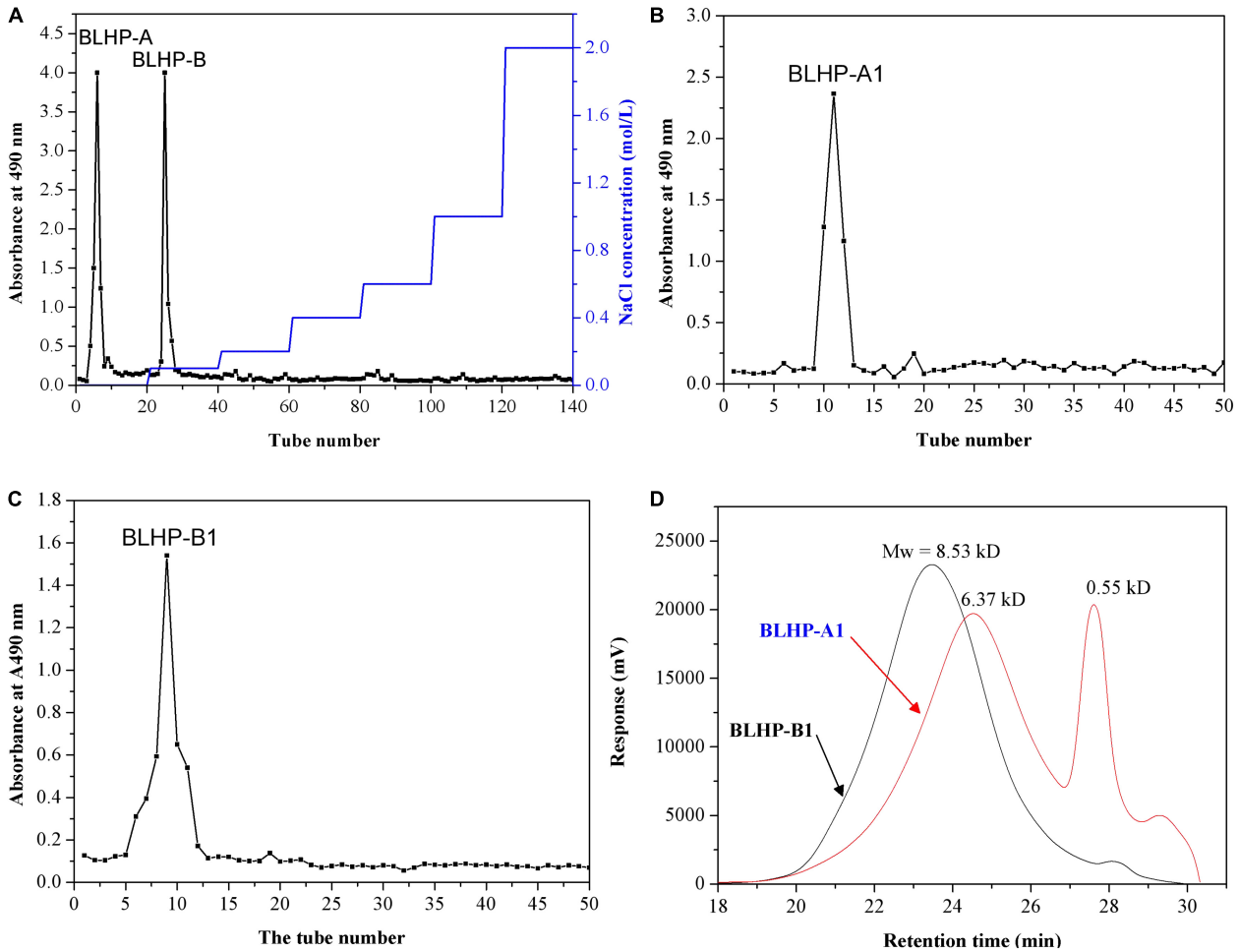

FIGURE 1 | Purification of the BLHP samples: **(A)** the crude polysaccharides were applied to DEAE-Sepharose fast flow column (2.0 cm × 40 cm, Cl^- form) to produce BLHP-A and BLHP-B fractions; **(B)** DEAE Sephacryl S-300 column (2.0 cm × 40 cm) was applied to purify BLHP-A sample; **(C)** DEAE Sephacryl S-300 column (2.0 cm × 40 cm) was applied to purify BLHP-B sample; **(D)** chromatogram of the molar mass distribution of BLHP-A1 and BLHP-B1 detected by GPC.

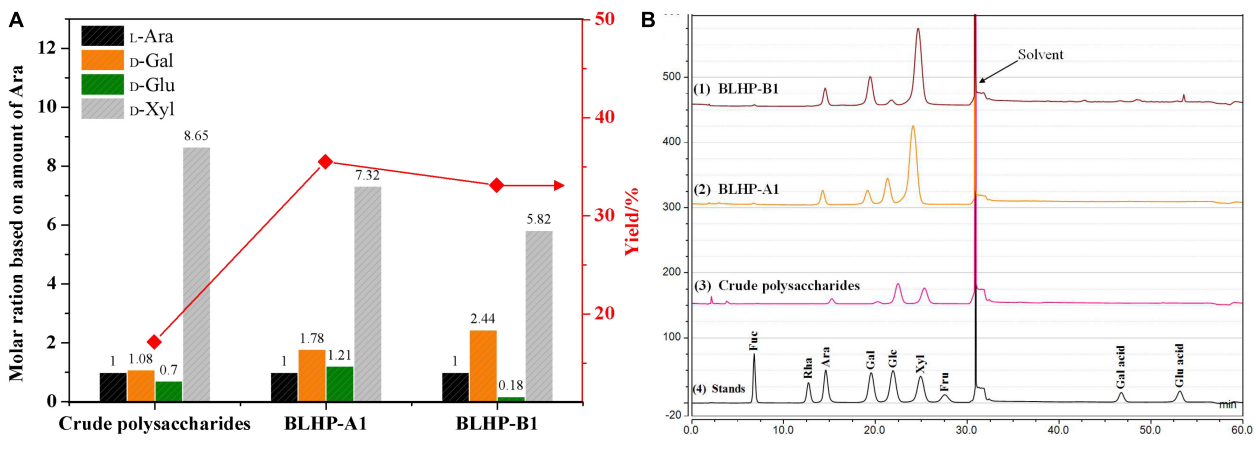

FIGURE 2 | The monosaccharide content in crude polysaccharides, BLHP-A1 and BLHP-B1 samples. **(A)** The relative molar ratios of monosaccharides among three samples based on the molar of arabinose. **(B)** HPACE spectrum for monosaccharide detection. All the samples were prepared at concentrations of 1.0 mg/ml.

cells were cultured for the measurement of the protective effect on H_2O_2-induced oxidative damage. The differentiation method was conducted according to previous studies (26). Cells were subcultured every 5 days by trypsinization with 0.05% trypsin-EDTA solution.

Cytotoxicity Assay

The toxicity of polysaccharides samples (BLHP-A1 and BLHP-B1) toward natural HepG2 cells was evaluated by the MTT method (27); 5×10^5 cells/well were plated in a flat-bottom (96-well microtiter plate) and incubated under the culturing condition for 24 h. Then the cells were treated with appropriate solutions of BLHP-A1 and BLHP-B1 (250, 500, 750, 1,000, 2,000, and 3,000 μg/ml) and incubated for 24 h at 37°C under a 5% CO_2 atmosphere. After that, the medium was replaced with a fresh medium and then 100 μl MTT (3-(4,5-dimethylthiazol-2)-2,5-diphenyltetrazolium bromide, 1.0 mg/ml in PBS buffer) was added (28). The plates were incubated for 1.0 h at 37°C. Successively, the medium was removed carefully and 200 μl DMSO (dimethyl sulfoxide) was introduced to dissolve the formazan crystals. After oscillating for 10 min in the dark, the absorbance at 570 nm was recorded in an ELISA instrument (SpectraMax iD3, Molecular Devices Co. Ltd., Shanghai, China).

H_2O_2-Induced Oxidative Damage of HepG2 Cells

Generally, H_2O_2 could react with metallic cations in low valence such as Fe^{2+} and Cu^{+}, and some hydroxyl radicals generated

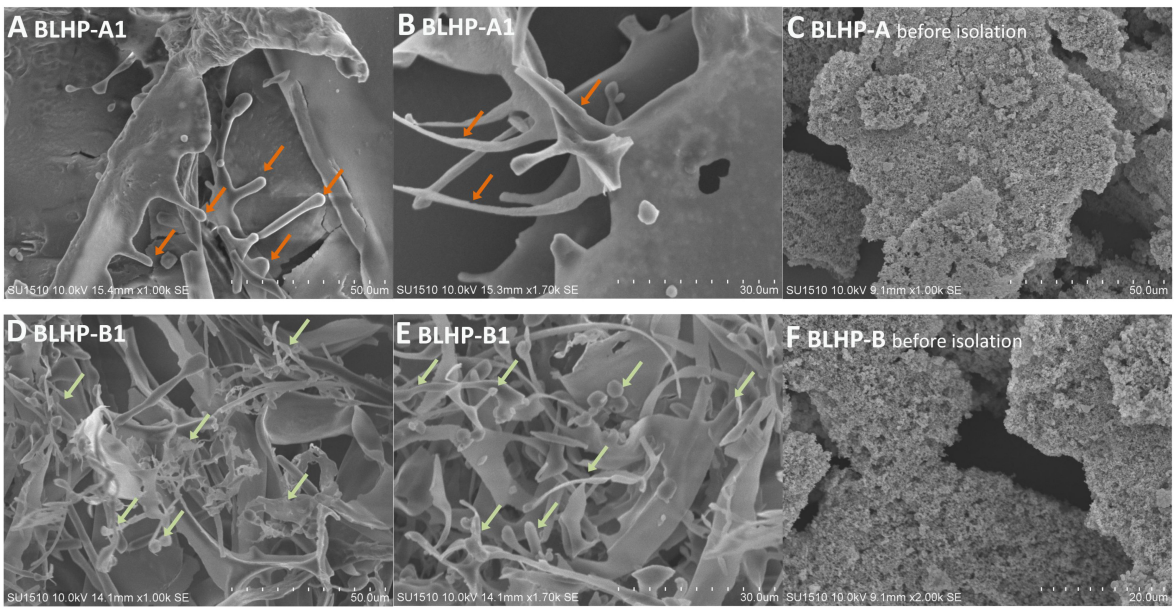

FIGURE 3 | The morphologies of polysaccharides extracted from bamboo leaves. **(A,B)** Represent BLHP-A1 fraction after being purified by DEAE-Sepharose fast-flow column. **(D,E)** Illustrate purified BLHP-B1 fraction by DEAE-Sepharose fast-flow column. **(C,F)** Are the morphologies of BLHP before further purification.

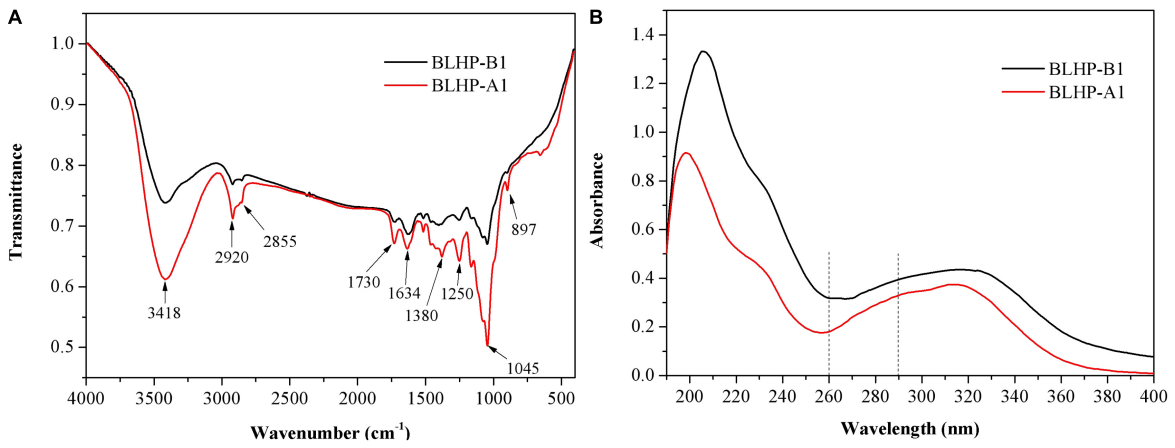

FIGURE 4 | FT-IR spectra analysis **(A)** and UV full scanning **(B)** of BLHP-A1 and BLHP-B1 fractions.

during the reaction would lead to oxidative damage in cells. The HepG2 cells were cultured under the same condition described before. For a typical H_2O_2-induced cell oxidative damage assay, briefly, the different concentrations (100–1,300 μmol/ml) of H_2O_2 were employed to treat the cultured HepG2 cells for 4.0 h. The absorbance at 540 nm was determined. MTT was introduced to each well. The blank group was treated with MEM in the absence of H_2O_2.

Reactive Oxygen Species Measurement

The intracellular ROS were measured by ROS assay kit with a modification of Ma's method (29). The cells in the logarithmic

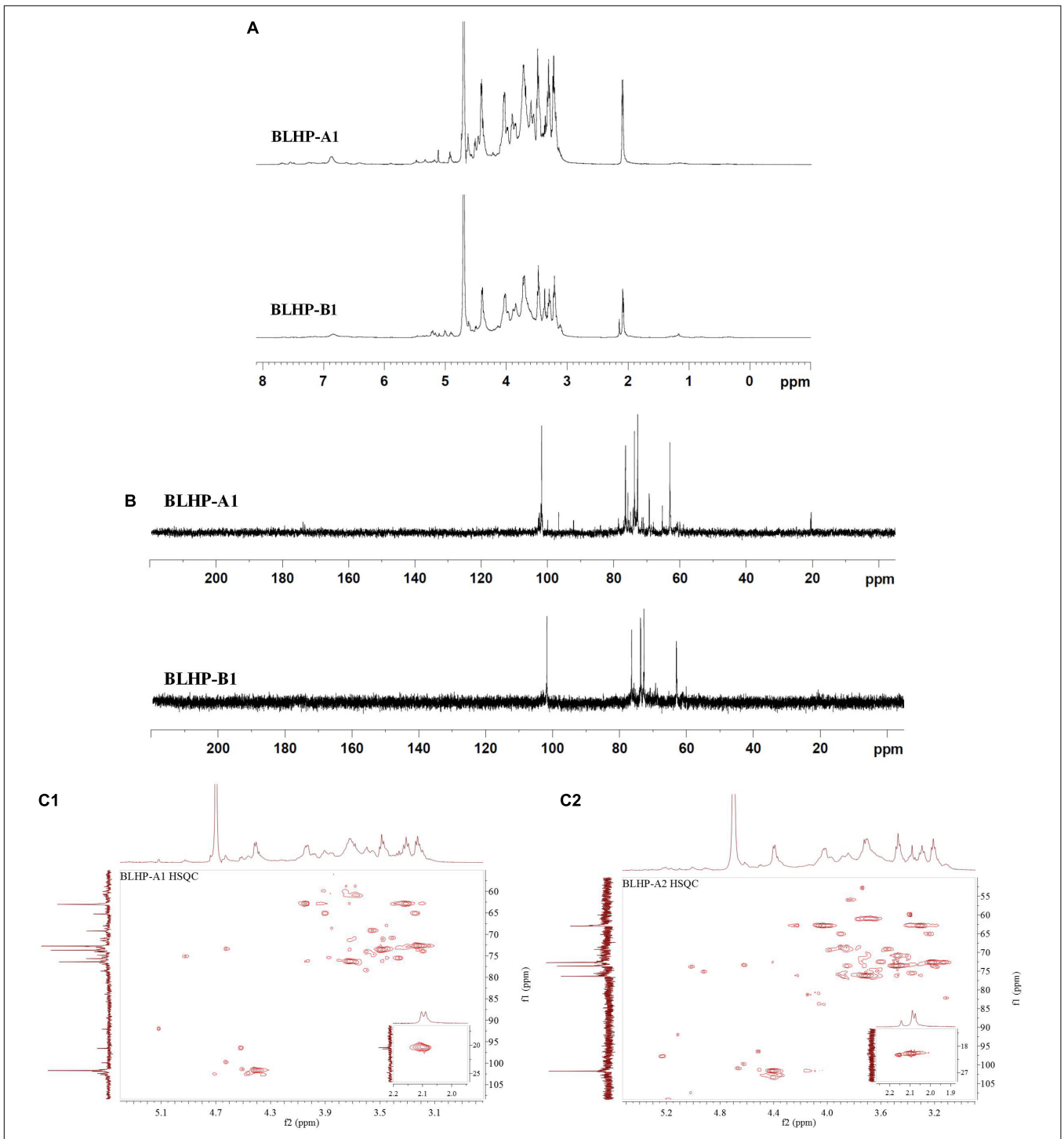

FIGURE 5 | ^{1}H **(A)** and ^{13}C **(B)** NMR spectra and HSQC for BLHP-A1 and BLHP-B1 samples **(C1,C2)** after deduction of some weak signal.

phase were inoculated in a 96-well microtiter plat with 1×10^6 cells/well and then incubated for 24 h at 37°C under a 5% CO_2 atmosphere. After being treated with the low, medium, and high concentrations of BLHP, 10 μmol/L of DCFH-DA fluorescent probe was introduced to the cell suspension. The intensity of ROS was determined on flow cytometry (CytoFLEX, Beckman Coulter Co. Ltd., Brea, CA, United States) with the analysis software of CytExpert.

Protective Measurement of Bamboo Leaves Hetero-Polysaccharides on H_2O_2-Induced Oxidative Damage in HepG2 Cells

In the previous description, the model of H_2O_2-induced HepG2 cells oxidative stress was established. To explore the protective effect of BLHP on damaged cells, HepG2 cells were cultured under the conditions described in the "Cell Lines and Culture Conditions" and "Cytotoxicity Assay" sections. After incubation for 24 h, the evaluations were conducted, respectively, as follows: (1) The final setting concentrations of BLHP samples (250, 1,000, and 3,000 μg/ml) were employed in the protected groups. (2) The damage group was treated with 600 μmoL/ml H_2O_2 without any BLHP in MEM. (3) The cells in the control group (NC) were cultured in MEM and then treated without any other agents. After 48 h treatment with the BLHP samples, the protected groups and damage groups were challenged with 600 μmoL/ml H_2O_2 for another 4.0 h to induce oxidative stress and the control group was treated with MEM at the same condition. After lysing of cells, the system was centrifuged for 5 min at 12,000 *g* at 4°C to separate solids and liquid. The liquid supernatant was collected for the assays of enzyme activities and the measurement of some characteristic products in cells. In detail, the activities of SOD, CAT, and GSH-Px enzymes were evaluated. Moreover, since MDA was the indicator for lipid oxidation degree, from this view, the content of MDA was determined by assay kits.

Statistical Analysis

All the data were expressed as the means ± standard error of the mean ($n = 3$). *SPSS 2.0* was used for the statistical analysis of experimental data and the one-way ANOVA test was applied for the analysis of the statistically significant difference. A *P*-value of less than 0.05 was represented as significantly different.

RESULTS AND DISCUSSION

Isolation and Purification of Bamboo Leave Hetero-Polysaccharides

The crude hemicellulosic polysaccharides from bamboo leaves were purified by a DEAE-Sepharose fast-flow column (2.0 cm × 40 cm, Cl^- form). According to absorbance statistics at 490 nm in **Figure 1A**, two fractions were obtained and denominated as BLHP-A and BLHP-B. The two fractions were from the elution of deionized water and 0.1 M NaCl solution, respectively. All assigned tubes were collected, concentrated, and freeze-dried to achieve BLHP-A and BLHP-B powder. Successively, the two samples were re-dissolved and further purified by DEAE Sephacryl S-300 column separately and the results are illustrated in **Figures 1B,C**. Interestingly, only one fraction was isolated from BLHP-A or BLHP-B despite BLHP-B1 showing wide molecular weight distribution in **Figure 1D**. This result indicated that BLHP-A and BLHP-B were homogeneous

TABLE 1 | The signal chemical shifts (ppm) of the major structures detected by NMR spectra of BLHP-A1 and BLHP-B1 samples.

Major units	Chemical shifts (δ_C/δ_H)/ppm						-CH_3
	C1/H1	C2/H2	C3/H3	C4/H4	C5/H5	C6/H6	
BLHP-A1							
β-$_D$-Man*p*-(1→	100.1/4.60	70.3/3.71	71.6/3.93	73.5/3.64	75.9/3.36	63.4/3.20	
α-$_D$-Glc*p*-(1→	98.6/5.17	71.2/3.63	73.9/3.80	73.2/3.86	72.8/3.92	60.7/3.75	
β-$_D$-Gal*p*-(1→	103.9/4.81	72.5/3.62	73.8/3.79	73.2/3.61	74.2/4.93	62.4/3.75[1	
→5)-β-$_D$-Man*p*-(1→	101.1/4.52	76.3/3.90	76.3.0/3.70	76.8/3.37	82.5/4.15	69.7/3.30	
→3)-β-$_D$-Gal*p*-(1→	101.9/4.41	72.7/3.55	78.1/4.04	68.2/3.91	75.6/3.72	65.3/3.70	
→4)-β-$_D$-Xyl*p*-(1→	101.7/4.46	74.0/3.21	74.9/3.48	76.4/3.71	63.0/4.04		
→5)-α-$_L$-Ara*f*-(1→ [a]	105.1/5.23	81.6/4.06	78.2/3.62	85.9/3.97	66.8/3.67		
2-*O*-acetyl group							20.07/2.08
BLHP-B1							
β-$_D$-Man*p*-(1→	100.1/4.60	70.3/3.71	71.6/3.93	73.5/3.64	75.9/3.36	63.4/3.20	
α-$_D$-Glc*p*-(1→	98.6/5.18	71.2/3.65	73.8/3.77	73.2/3.82	72.7/3.90	60.7/3.71	
β-$_D$-Gal*p*-(1→	103.9/4.81	72.5/3.62	73.8/3.79	73.2/3.61	74.2/4.93	62.4/3.75[1	
→5)-β-$_D$-Man*p*-(1→	101.1/4.52	76.3/3.90	76.3.0/3.70	76.8/3.37	82.5/4.15	69.7/3.30	
→6)-α-$_D$-Glc*p*-(1→	96.6/5.03	74.4/3.4	75.9/3.5	74.6/3.2	75.5/3.6	69.3/3.9[1	
→6)-β-$_D$-Gal*p*-(1→	102.4/4.48	73.6/3.74	68.6/3.58	72.1/3.39	63.9/3.79	73.6/3.19	
→4)-β-$_D$-Xyl*p*-(1→	101.7/4.42	73.7/3.25	74.9/3.52	76.4/3.73	67.0/3.38		
→5)-α-$_L$-Ara*f*-(1→ [a]	110.5/5.17	82.6/4.12	77.6/3.83	81.9/4.07	67.8/3.92		
2-*O*-acetyl group							20.01/2.10
3-*O*-acetyl group							22.30/2.18

[a] *→5)-α-$_L$-Araf-(1→ was determined by reported literature and NMR analysis while it was trace in methylation analysis.*

polysaccharides prepared by phosphotungstic acid hydrolysis. Moreover, according to gel permeation chromatography (GPC) analysis, the average molecular weights of BLHP-A1 and BLHP-B1 were 8.53 and 6.37 kDa, respectively. From these views, the addition of phosphotungstic acid during polysaccharides extraction will contribute significantly to controlling molecular weight to obtain polysaccharides in lower molecular weight (<10 kD). The trace phosphotungstic acid could be removed by dialysis easily. GPC analysis also exhibited two specific peaks in the BLHP-B fraction, probably implying the occurrence of oligosaccharides.

Chemical Compositions and Physical Characterizations of Bamboo Leaves Hetero-Polysaccharides

The monosaccharide compositions of BLHP-A1 and BLHP-B1 were detected quantitatively by HPAEC-PAD and the results are shown in **Figure 2A**. All the samples extracted from bamboo leaves seemingly demonstrated similar monosaccharide distributions, including $_D$-glucose, $_D$-xylose, $_L$-arabinose, and $_D$-galactose despite other trace monomers being detected in a specific sample. On the other hand, according to the high resolutions among monomers in **Figure 2B**, HPAEC could be an effective equipment for the separation of sugars. Especially, the relative contents of specific monosaccharides were different in samples. $_D$-Xylose was the dominating component in all samples, implying our extracting method mainly facilitated the disassembly of hemicelluloses from bamboo leaves, which was the reason for hetero-polysaccharides definition in this work. Considering the content of xylose and similar distribution of monosaccharides, BLHP-A1 and BLHP-B1 could be defined as hemicellulosic polysaccharides, discriminating from cellulosic polysaccharides.

The morphologies of BLHP are shown in **Figure 3**. The polysaccharides exhibited different surface structures before and after column purification. BLHP-A1 showed some irregular filaments at the margin of tiny flaps. BLHP-B1 analogously manifested a rough surface including sheet-like, rod-like, and lump-like structures. These parallel results were probably indicative of a filamentous structure formed by cross-linked chains, consistent with the structure of the purified polysaccharides extracted from auriculariales (30). It was universally acknowledged that the polysaccharides would recrystallize during freeze-dried and interpreted with inter- and intra-molecular hydrogen bonds. In contrast, polysaccharides exhibited uniform structures like granular aggregates and there was no significant discrepancy between BLHP-A and BLHP-B.

Ultraviolet and Fourier Transform Infrared Analysis

Fourier transform infrared (FT-IR) analysis in **Figure 4A** demonstrated significant differences between BLHP-A1 and BLHP-B1 according to the infrared absorption. Concretely, both samples gave the characteristic absorbance at 3,418 cm^{-1} for O–H, 2,920 and 2,855 cm^{-1} for C–H (asymmetrical stretching) structures (31). These bonds were indispensable in polysaccharides. The absorbance at 1,730 cm^{-1} was assigned to the stretching vibration of carbonyl groups. The peak at 1,634 cm^{-1} was relevant to the flexural vibration of O–H (32) since no considerable content of protein was characterized in **Figure 4B**. The occurrence of a characteristic peak at 1,380 cm^{-1} might be attributed to trace amide (33). The bending vibration of O–H was observed at about 1,250 cm^{-1}. The peak at 897 cm^{-1} was assigned to the stretching vibration of C–O–C and C–O–H, originating from pyranoid monosaccharides. On the other hand, the bands at 897 cm^{-1} were the characteristic absorption of β-configuration (22), which was consistent with NMR analysis. The absorbance at 1,045 cm^{-1} was suggestive of the presence of pyranose mainly from the cellulose fraction (34). The UV spectrum (**Figure 4B**) demonstrated no obvious absorbance peak at 260 and 290 nm approximately, which was indicative of the absence of free or combinative protein and nucleic acids in the two samples (35).

Methylation Analysis

The glycosidic linkage types of BLHP-A1 and BLHP-B1 were explored by methylation analysis. The methylated products of the two samples were hydrolyzed and detected by GC–MS. As a result, there were five alditol acetates in BLHP-A1, including 2,3,4,6-Me_4-Man*p*, 2,3,4,6-Me_4-Glc*p*, 2,3-Me_2-Xly*p*, 2,3,4,6-Me_4-Gal*p*, 3,4,6-Me_3-Man*p* and 2,4,6-Me_3-Gal*p*. Comparatively, 2,3,4,6-Me_4-Man*p*, 2,3,4,6-Me_4-Glc*p*, 2,3-Me_2-Xly*p*, 2,3,4,6-Me_4-Gal*p*, 3,4,6-Me_3-Man*p*, 2,3,4-Me_3-Glc*p* and 2,3,4-Me_3-Gal*p* derivative alditol acetates were detected in BLHP-B1. In addition, the linkage types of the two samples represented some differences; 1,6-linked-Gla*p* and 1,6)-linked-Glc*p* fragments were only present in BLHP-B1 while 1,3)-linked-Gal*p* was absent in BLHP-B1. However, the methylated alditol acetate about arabinose was absent in both polysaccharides despite a small quantity of arabinose being determined by HPAEC analysis probably due to incomplete methylation and isomerization during the derivatization process. Some extra groups including *O*-acetyl groups and terminal sugar needed confirmation by the NMR spectrum.

NMR Analysis

NMR analysis was the key technology in this work to provide sugar residue linkage sequence and anomeric configurations. ^1H and ^{13}C NMR spectra are shown in **Figure 5**. In the ^1H-NMR spectra, lower field resonance in the chemical shift range of 1.9 to 6.0 ppm indicated the presence of polysaccharides (36, 37). The chemical shifts about anomeric protons in branched polysaccharides were observed from 4.3 to 5.5 ppm. The chemical shifts in protons correlating with $C_{2,3}$ in sugar units varied from 3.2 to 4.2 ppm. Hence, the main monosaccharides were attributed to β-configuration since the signal peaks at 4.3–4.8 ppm demonstrated strong signals while the chemical shifts for α-configurations were near 5.0 ppm and lower chemical shifts. Notably, the main monosaccharide in both BLHP-A1 and BLHP-B1 was xylose according to the HPAEC analysis. Therefore, $_D$-Xyl*p* linkage was attributed to β-configuration. According to ^1H spectrum in **Figure 5A**, six anomeric proton

signals (5.17, 4.81, 4.60, 4.52, 4.46, and 4.41 ppm) appeared in BLHP-A1. And seven anomeric proton signals (5.18, 5.03, 4.81, 4.60, 4.52, 4.48, and 4.42 ppm), were observed in BLHP-B1. The chemical shift at δ 4.70 ppm was HDO. In ^{13}C spectrum in **Figure 5B**, the anomeric carbon signals were difficult to be determined because of the overlaps and trace amount. Still, we could also discriminate the main anomeric carbon signals, which delivered the structural information about hetero-branches in polysaccharides. The chemical shift at about 177 ppm was attributed to trace uronic acid in agreement with FT-IR analysis (38). The specific ^{1}H and ^{13}C cross assignments for chemical shifts of BLHP-A1 and BLHP-B1 are illustrated in **Table 1** accompanying a comparison with reported polysaccharide structures.

The 101.7/4.46 ppm was assigned to →4)-β-$_D$-Xyl*p*-(1→ due to strong β-configuration at 4.46 ppm in BLHP-A1 (39). On the other hand, HPAEC analysis also indicated xylose was the dominant sugar in hydrolysate. The other ^{1}H and ^{13}C cross assignments for this structure were confirmed according to the HSQC spectrum. In addition, the ^{1}H signals at about 2.1 ppm were attributed to *O*-acetyl groups linked as the terminal branches in the xylan skeleton (39). The trace and sporadic anomeric carbon signals at 109.1/5.32 ppm (in BLHP-A1) and 110.5/5.17 ppm (in BLHP-B1) in the HSQC spectrum (**Figures 5C1,C2**) were assigned to →5)-α-$_L$-Ara*f*-(1→structure (40, 41). According to previous literature and NMR spectrum, the anomeric carbon signals near 102 ppm were attributed to C1 in Gal*p* relevant units (36, 42). The cross-peaks at 99.7/5.12 and 100.5/5.12 ppm were ascribed to δ_{C1}/δ_{H1} of →4)-α-$_D$-Glc*p*-(1→ units in BLHP-A1 and BLHP-B1, respectively, as well as 98.6/5.17 and 98.6/5.18 ppm, were determined as α-$_D$-Glc*p*-(1→ (35, 43). Additionally, 59.7/3.36 ppm was attributed to OCH_3 (44), which implied that monosaccharides residues in both of the fractions might be methylated naturally and partially.

The Chemical Antioxidant Activities of Bamboo Leaves Hetero-Polysaccharides

To evaluate the chemical antioxidant activity, DPPH· and $ABTS^{+}$ radicals scavenging activities and reducing ability were measured

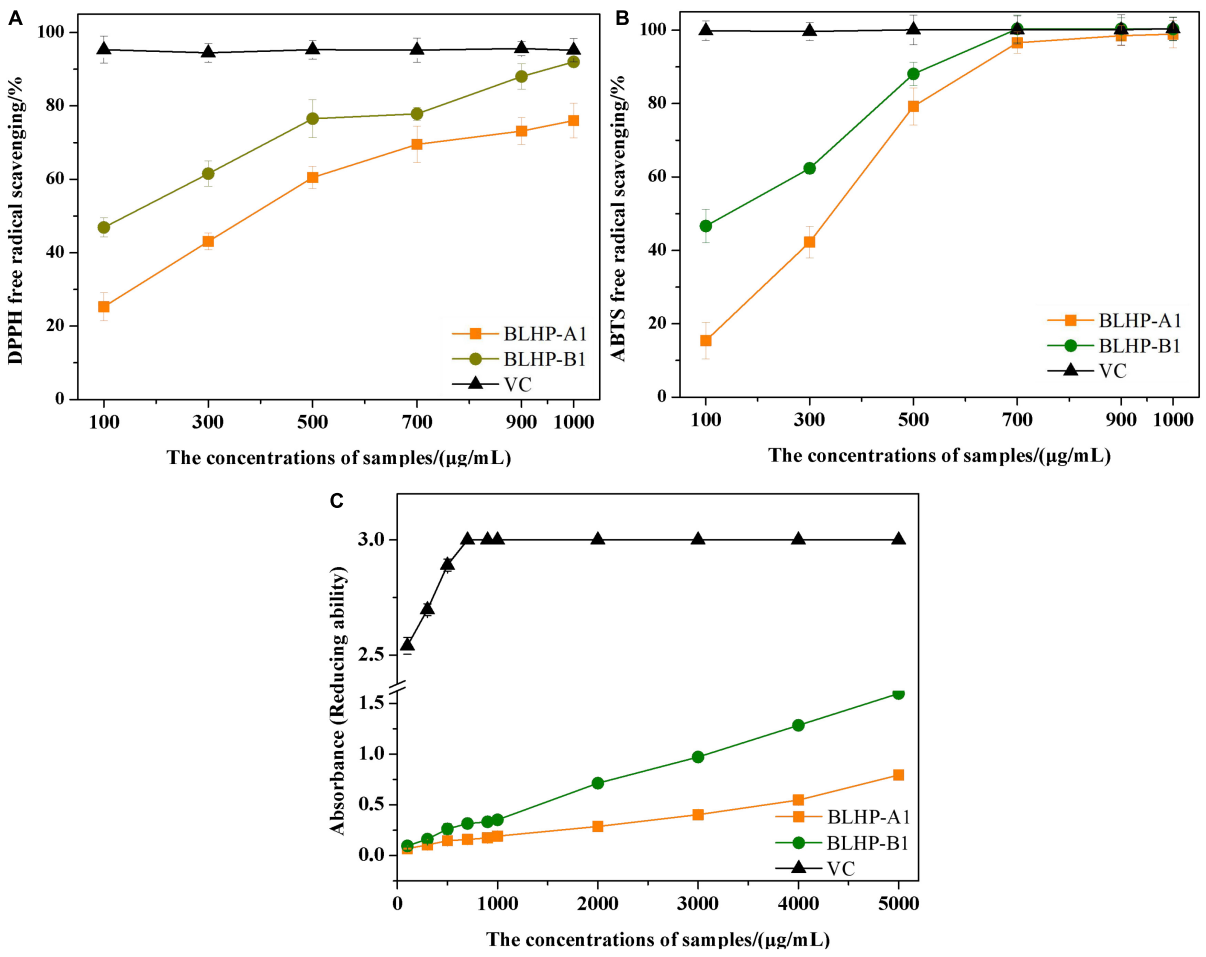

FIGURE 6 | The measurements of antioxidant activities of BLHP-A1 and BLHP-B1 in chemical view, compared with relevant abilities of VC. **(A)** DPPH· radicals scavenging of BLHP-A1 and BLHP-B1 samples in the concentration range of 100–1,000 μg/ml. **(B)** $ABTS^{+}$ radicals scavenging of BLHP-A1 and BLHP-B1 samples in the concentration range of 0.1–1.0 mg/ml. **(C)** Reducing ability of BLHP-A1 and BLHP-B1 samples. The absorbances were recorded at 700 nm.

TABLE 2 | A mini summary for DPPH· and $ABTS^+$ radical scavenging with molecular weight (MW) of some recent reported polysaccharides.

Polysaccharides source	Molar ratio of monosaccharides	MW/kDa	DPPH· scavenging activity (IC50)/(mg/ml)	$ABTS^+$ scavenging activity (IC50)/(mg/ml)	References
Mung bean skin	Rha[a], Ara, Gal, Glc, Xyl, fructose (Fru), and GalA	208	0.47	0.37	(23)
Auriculariales	Man(85.0), GlcA(0.6), GalA(0.03), Glc(0.03), Gal(10.0), Xyl(0.1), Ara(3.6) and Fuc(0.6)	1260	1.0	None	(30)
Sagittaria sagittifolia L.[b]	$_L$-Rha(8.47), $_D$-Ara(2.09), $_D$-Glu(75.01) and $_D$-Gal(14.43)	1984.0	∼2.2	∼1.4	(33)
Sagittaria sagittifolia L.	$_L$-Rha(1.24), $_D$-Ara(0.22),$_D$-Xly(0.49), $_D$-Man(0.33), $_D$-Glu(96.9) and $_D$-Gal(0.81)	294.9	∼5.0[c]	∼4.5	(46)
Holothuria leucospilota	Rha(39.08), Fucose (Fuc, 35.72), GlcA(10.72), Gal(8.43), Glc(4.23) and Xly(1.83)	52.8	∼0.2	∼0.5	(47)
Sargassum tenerrimum	Fuc(52.3), Gal(1.7), Man(3.8), Ara(4.1)	31.18	∼0.1	> 0.125	(48)
Plantago ovata Forssk seeds	$_L$-Rha(15.9), $_D$-Xly(57.3), $_L$-Ara(0.4), $_D$-Glc(26.0) and $_D$-Gal(0.4)	37.4	0.362	0.372	(49)
Oka	Gal(33.8–38.6), Glc(12.4–17.9), Rha(13.7–17.5), Ara(3.0–9.9) and GalA(19.0–21.2) and GlcA(6.7–8.3)	129	None	2.34	(50)
Sargassum pallidum	Fuc(14.93), Gal(26.63) and GalA(32.19)	510	∼0.5	∼0.5	(51)
Flaxseed hull	Glc, Gal, Xly and Ara	1696	∼0.5	∼0.31	(52)
Bamboo *(Phyllostachys pubescens Mazel)* leaves	$_L$-Ara(1.00), $_D$-Gal(2.44), $_D$-Glu(0.18) and $_D$-Xly(5.82)	8.53	0.14	0.13	*This work*

[a]*Molar ratio of monosaccharides was absent.*
[b]*Extracted by different methods.*
[c]*The IC50 value was estimated.*

and the results are illustrated in **Figure 6**. In this work, the concentrations of BLHP samples from 100 to 1,000 μg/ml were employed to explore the DPPH· and $ABTS^+$ radical scavenging. As depicted in **Figure 6A**, both BLHP-A1 and BLHP-B1 samples showed the DPPH· radical scavenging activity increased as the concentrations of BLHP rose while the same concentrations of vitamin C (VC) exhibited higher activity of radical scavenging. The scavenging rates of BLHP-A1 and BLHP-B1 for DPPH· were 76.0 and 92.0%, respectively, when 1,000 μg/ml of samples were introduced. Hence, both samples demonstrated antioxidant activity for DPPH· radicals scavenging. Moreover, the dosage-effect relationship was found between DPPH· radical scavenging and the concentration of samples. IC_{50} of BLHP-A1 and BLHP-B1 were 330 and 140 μg/ml, respectively. According to previous studies, some polysaccharides extracted from plants or their appurtenances showed similar antioxidant activities but different intensities. Li's group reported the polysaccharides from *Gynura procumbens* leaves acquired DPPH· radical scavenging activity with 2,070 μg/ml for IC_{50} value (45). The polysaccharides from mung bean skin exhibited relatively high antioxidant activity, indicating a moderate effect on DPPH· scavenging with the IC_{50} of 470 μg/ml (23).

$ABTS^+$ radical scavenging activity of BLHP samples (**Figure 6B**) demonstrated a similar dosage-effect relationship. Unlike DPPH· radical scavenging, the lower concentrations (300–700 μg/ml) of samples showed a relatively higher scavenging rate. When the concentration of BLHP was 700 μg/ml, $ABTS^+$ radical scavenging rates of BLHP-A1 and BLHP-B1 were up to 96.6 and 100%, implying BLHP exhibited significant scavenging ability on $ABTS^+$ in a concentration-dependent manner. IC_{50} of BLHP-A1 and BLHP-B1 for $ABTS^+$ scavenging were 270 μg/ml and 130 μg/ml, respectively. A similar scavenging rate for $ABTS^+$ by the polysaccharides from *Sagittaria sagittifolia* L needed 5,000 μg/ml which was significantly higher than that of BLHP (33). On the other hand, both DPPH· and $ABTS^+$ radical scavenging demonstrated that BLHP-B1 exhibited stronger activity than that of BLHP-A1. Probably, this promotion of the antioxidant activity was relevant to the linkage type in the structure of BLHP-B1. Moreover, high radical scavenging activities could be obtained as high concentrations of BLHP samples were employed (>700 μg/ml). From these views, the BLHP indicated moderate radical scavenging activities compared to positive control by concentrated VC.

The reducing ability was also regarded as a significant indicator of antioxidant activity. During the transformation of Fe^{3+} or ferricyanide complex to Fe^{2+}, the electron-donating ability of polysaccharides could be occupied. The absorbance served as the indicator was measured at 700 nm (**Figure 6C**). The absorbances of BLHP-A1 and BLHP-B1 improved as the sample concentrations increased, while the reducing ability of BLHP was lower than that of VC at the same concentration.

To have a macroscopical knowledge of the antioxidant activity, we gave a comparison with recently reported polysaccharides in **Table 2**. The polysaccharides extracted from diverse sources showed various free radical scavenging, indicated by IC50 values of DPPH· and $ABTS^+$ radical scavenging. According to the published results, the polysaccharides in this work demonstrated relatively higher DPPH· and $ABTS^+$ radical scavenging, inspiring some potential applications in antioxidant materials manufacturing. Moreover, different extraction methods brought distinct molecular weights and chemical compositions

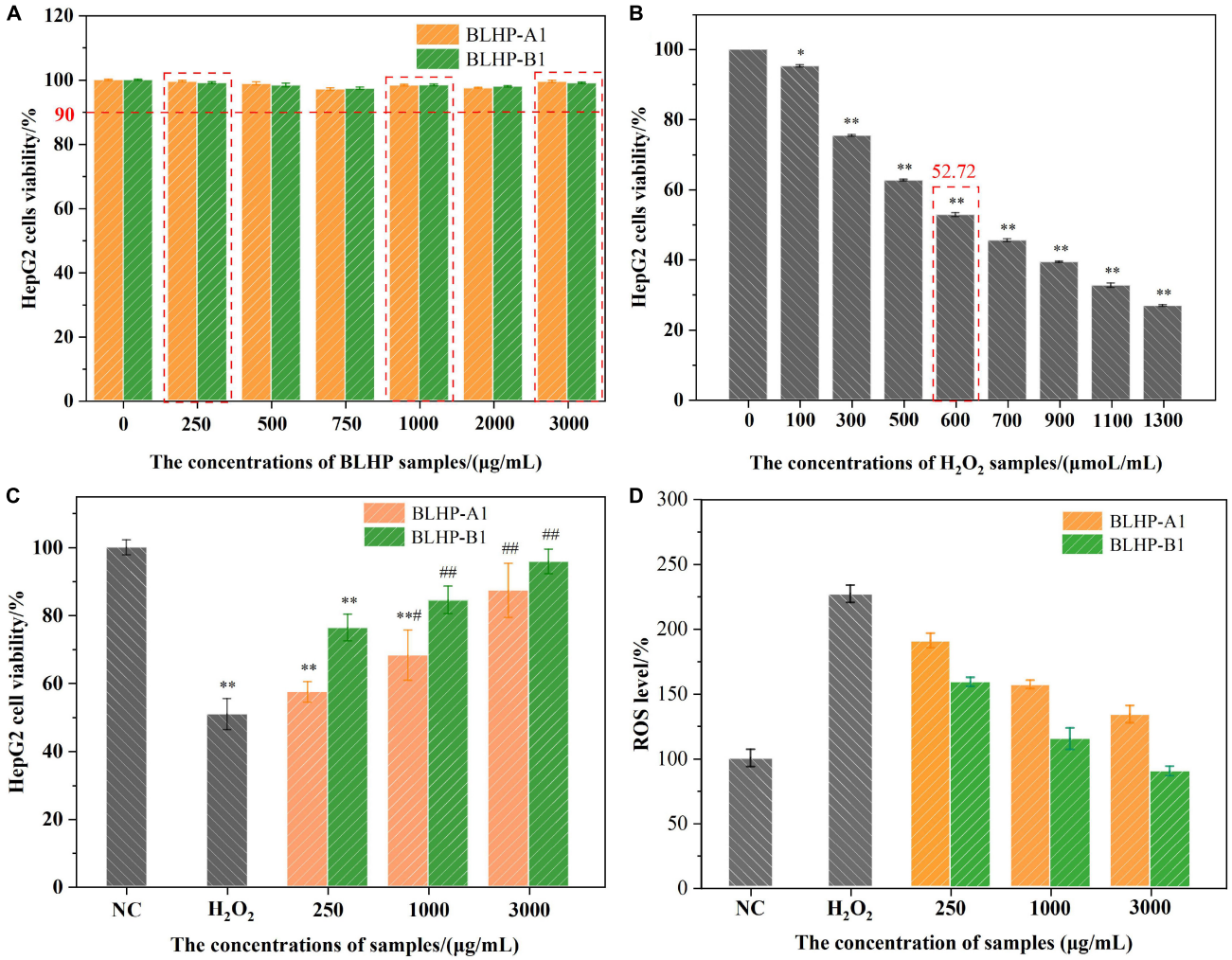

FIGURE 7 | The effects of BLHP and H_2O_2 concentrations on HepG2 cells viability. **(A)** The HepG2 cells were incubated with BLHP samples at different concentrations (0, 250, 500, 750, 1,000, 2,000, and 3,000 μg/ml). **(B)** The HepG2 cells were treated with H_2O_2 at different concentrations (0, 100, 300, 500, 600, 700, 900, 1,100, and 1,300 μmol/ml). **(C)** The treated concentrations of H_2O_2, BLHP samples in the oxidative stress model. **(D)** Variations in relative ROS levels compared to that of NC group. The selected concentration of H_2O_2 was 600 μmoL/ml. The selected concentrations of BLHP samples were 250, 1,000 and 3,000 μg/ml. (*$p < 0.05$, **$p < 0.01$ compared with the control group; #$p < 0.05$, ##$p < 0.01$ compared with the H_2O_2 group).

which were regarded as one of the main factors to affect its functions. However, up to now, efficient extraction methods to produce polysaccharides with uniform molecular weight have not been well developed yet. But, it was certain that all reported active polysaccharides possessed heterogeneous monosaccharides constituted by abundant branches.

Bamboo Leaves Hetero-Polysaccharides Attenuation in Oxidative Stress Induced by H_2O_2 in HepG2 Cells

Effect of Bamboo Leaves Hetero-Polysaccharides and H_2O_2 on the Viability of HepG2 Cells

The cytotoxicity of HepG2 cells affected by different concentrations of polysaccharides and H_2O_2 solutions was evaluated by the MTT method and the results are illustrated in **Figure 7**. Fortunately, the viability of the cells in BLHP solutions was more than 90% and near 98% in the concentration range of 250–3,000 μg/ml (**Figure 7A**), implying the toxicities of BLHP-A1 and BLHP-B1 were exceedingly weak. Comparatively, H_2O_2-induced cells exhibited apoptosis intensively depending on the H_2O_2 concentration from 100 to 1,300 μmoL/ml (**Figure 7B**). To be noted, 600 μmoL/ml of H_2O_2 could result in 52.72% of cell viability, close to half of the cell viability. These results inferred that the model of H_2O_2–induced HepG2 cells was established employing 600 μmoL/ml of H_2O_2. Moreover, 250, 1,000, and 3,000 μg/ml of BLHP samples should be introduced on behalf of low, medium, and high dosages as concluded in **Figure 7C**. What was worth mentioning was the practically 100% viability of HepG2 cells in the negative control (NC) group. Furthermore, H_2O_2 caused the production of larger quantities of ROS in HepG2 cells, indicating 2.5-folds higher

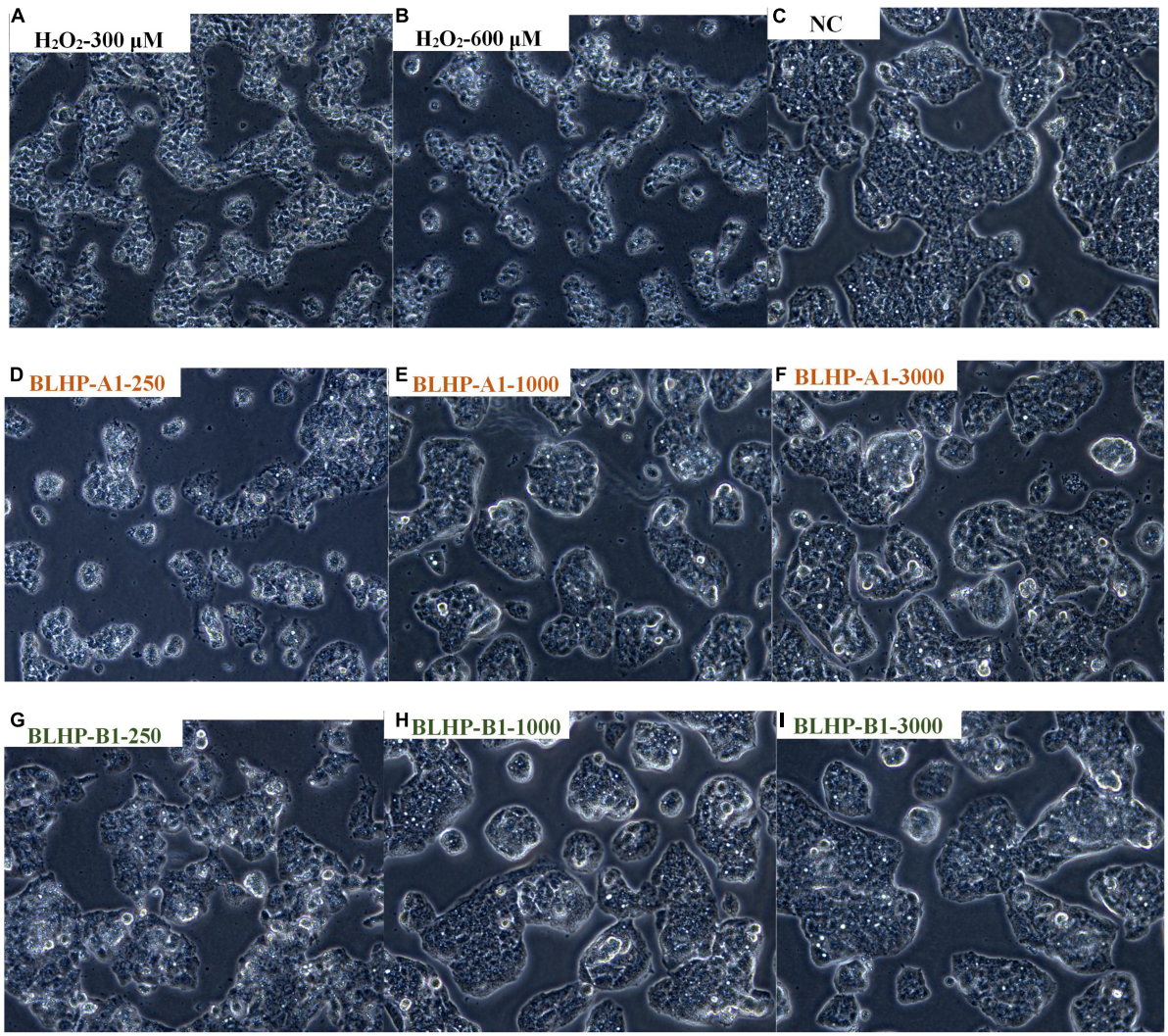

FIGURE 8 | The morphologies of HepG2 cells in different situations. **(A,B)** Were treated with 300 and 600 μmol/ml H_2O_2, respectively. **(C)** Represented natural cells in MEM without any treatment or protection. **(D–F)** Illustrated the protection effects in H_2O_2-induced cells by various concentrations (250, 1,000, and 3,000 μg/ml) of BLHP-A1. **(G–I)** Indicated the protection effects in H_2O_2-induced cells by various concentrations (250, 1,000, and 3,000 μg/ml) of BLHP-B1.

than that in non-induced cells (**Figure 7D**). The addition of BLHP samples inhibited the relative ROS level in H_2O_2-induced cells, implying BLHP possessed a potential protective function for oxidative damage.

H_2O_2-Induced Oxidative Damage of HepG2 Cells

The growth morphologies of HepG2 cells in positive, negative, and induced groups exhibited conspicuous differences. The cell counts in induced groups (**Figures 8A,B**) reduced significantly compared with the NC group (**Figure 8C**), suggesting the oxidative damage from H_2O_2 suppressed the cell viability. Notably, the normal HepG2 cells were epithelial-like growing as monolayers (adherent growth) in small aggregates. From the cell morphologies in positive groups (**Figures 8D–I**), we could easily conclude that BLHP was rewarding for protection against oxidative damage. Merely from the number of morphological mutants, BLHP-B1 seemingly possessed a more substantial protective effect than that of BLHP-A1 on oxidative damage, especially in low dosage (250 μg/ml). More adhered cells were observed in the BLHP-B1-treated group. Furthermore, with the increase of BLHP concentrations, the growing shapes of HepG2 cells dramatically changed along with natural orientation nearly in a concentration-dependent manner. The cells emerged as typical morphologies on the verge of that in the NC group as the concentration of BLHP-B1 was 3,000 μ g/ml.

Protective Measurement of Bamboo Leaves Hetero-Polysaccharides on H_2O_2-Induced Oxidative Damage in HepG2 Cells

According to the chemical antioxidant activities and the morphologies of HepG2 cells in positive groups, we might harbor the idea that BLHP, especially BLHP-B1, demonstrated

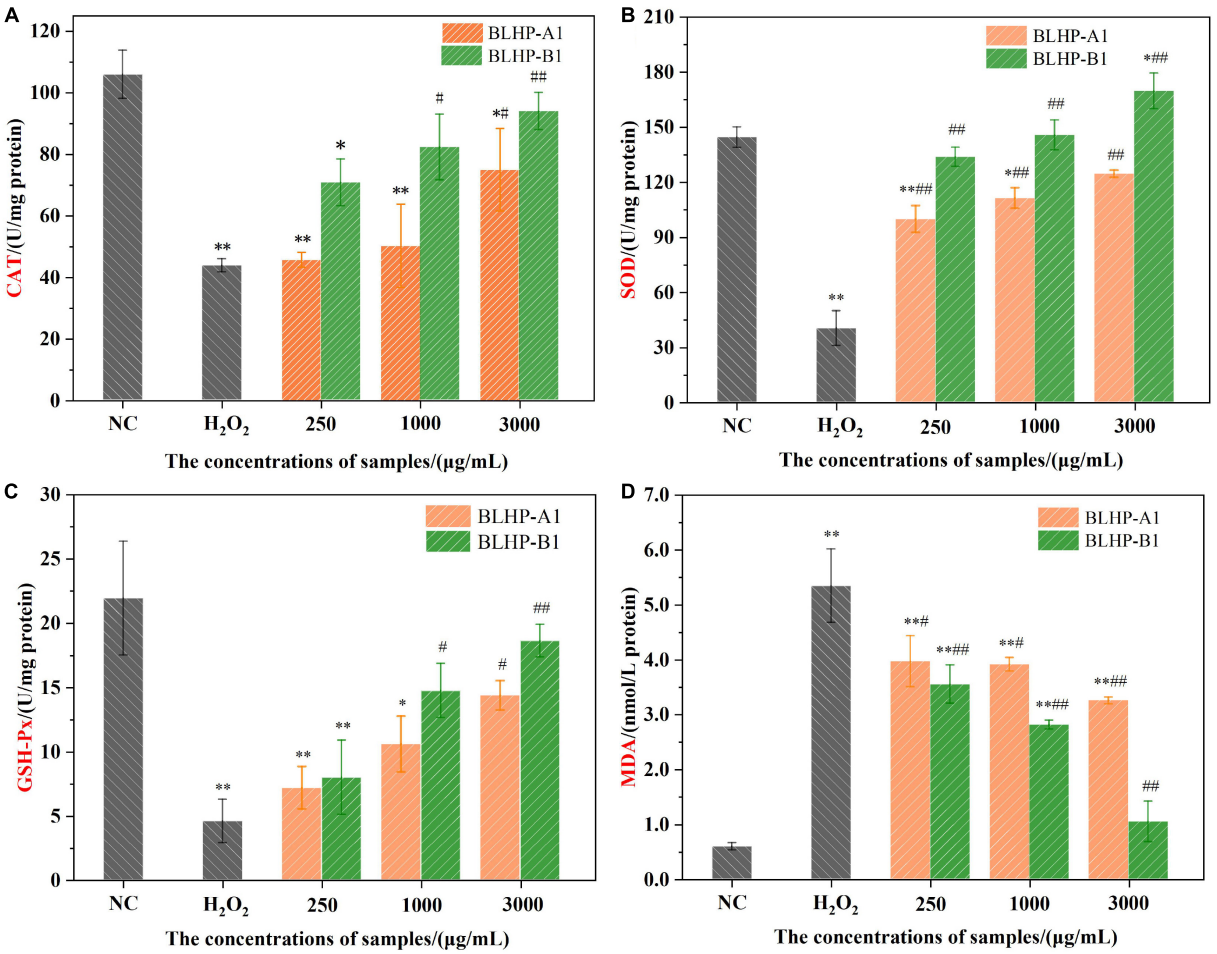

FIGURE 9 | The effects of BLHP samples on the concentrations of antioxidant enzymes CAT **(A)**, SOD **(B)**, GSH-Px **(C)** and MDA **(D)** product. NC, normal control; H_2O_2: H_2O_2 (600 μmoL/ml) induced group. (*$p < 0.05$, **$p < 0.01$ compared with the control group; #$p < 0.05$, ##$p < 0.01$ compared with the H_2O_2 group).

the promising ability to scavenge free radicals and prosperity of cell viability. These results captured our attention to further explore the protective effect on H_2O_2-induced oxidative damage in HepG2 cells. Hence, some indicators, including the activities of SOD, CAT, and GSH-Px enzymes, MDA products in oxidative stress, were evaluated and measured. Many polysaccharides could enhance enzyme activity or restore the antioxidant enzymes system to scavenge the accumulating free radicals in the body for retarding aging (53, 54). H_2O_2 was a quintessential inductive agent which could result in the accumulation of free radicals and damage the antioxidant enzymes (55, 56). In this study, we established H_2O_2-induced damaged HepG2 cells to investigate the protective effect of BLHP on oxidative stress. **Figure 9** illustrates the activities of CAT, SOD, and GSH-Px in H_2O_2-treated groups. In detail, the activities of CAT, SOD, and GSH-Px were decreased to 41.3, 27.8, and 20.8%, respectively, compared to that in the negative control group as illustrated in **Figures 9A–C**. Interestingly, the BLHP-treated groups overwhelmingly gave rise to the activities of CAT, SOD, and GSH-Px in H_2O_2-treated cells, even reverting or exceeding them to baselines. The activity of the SOD enzyme compared to that in the control group was even slightly enhanced when 3,000 μg/ml of BLHP-B1 was employed (**Figure 9B**). Furthermore, there was another phenomenon that fascinated us. BLHP-B1 sample expressed stronger protection even promoting the ability to the activities of CAT, SOD, and GSH-Px than those of BLHP-A1. Hence, the different structure fragments including →6)-β-$_D$-Gal*p*-(1→ and 3-*O*-acetyl group, might play an essential role in the attenuation of oxidative stress in HepG2 cells. Probably, the advanced structure of polysaccharides played a greater role in determining their bioactivities. However, we had enough advanced technologies to parse the secondary or even tertiary structure of these polysaccharides. Moreover, the enhancements for the enzyme system were all performed in a dosage-dependent manner in low, medium, and high concentrations of BLHP. A significant increase to 5.34 nmol/L of the MDA previously exposed to 600 μmol/ml H_2O_2 for 4.0 h (**Figure 9D**) while the negative control group showed trace concentrations of MDA. The MDA content in the BLHP-treated groups was extremely decreased

coinciding with the dosage effect. These findings elucidated that the H_2O_2-injured cells were remarkably attenuated after treatment with 250, 1,000, and 3,000 μ g/ml of BLHP.

Some endogenous antioxidant enzymes including catalase (CAT), SOD, and GSH-Px constituted a self-defense system against oxidative stress (57). The BLHP treatment increased the CAT activity, implying the cells possessed the capacity to purge H_2O_2 conversion directly to oxygen and water while H_2O_2 decreased the activity of the CAT enzyme. During the H_2O_2 treatment, some free radicals would release successively resulting in the accumulation of oxidizing species. Likewise, the SOD enzyme activity reflected the loading of intracellular antioxidants, further indicating the intracellular radical's levels. BLHP acted as a promoter of SOD activity besides scavenging free radicals as proved in **Figure 9B**. GSH-Px performed as one of the essential components in the antioxidant defense system, serving as an electron donor to insecure ROS. The metabolism of GSH was deduced to be regulated by bamboo leaves polysaccharides to avoid cell apoptosis. Previous studies of oxidative stress induced by H_2O_2 had emphasized that the caspase enzyme system could be inhibited by polysaccharides (58, 59). Besides, the expression of other proteins promoting the apoptosis process would be coincidentally inhibited by polysaccharides.

CONCLUSION

In this study, we extracted hetero-polysaccharides (BLHP) from bamboo leaves assisted by a small amount of phosphotungstic acid. Chemical and physical characterizations proved that BLHP-A1 and BLHP-B1 fractions belonged to hetero-polysaccharides. Successively, we evaluated the antioxidant activity of BLHP. As a result, both the fractions demonstrated the potential to scavenge DPPH· and $ABTS^+$ radicals and exhibited relatively high reducing ability in *vitro* antioxidant assays. Furthermore, BLHP-B1 showed more activity to prevent H_2O_2-induced damages in HepG2 cells. BLHP-B1 could suppress oxidant stress by improving the enzyme activities of SOD, CAT, and GSH-Px as well as decreasing the production of MDA. According to the morphologies of damaged HepG2 cells and the enzyme activities, it was proved that BLHP, especially BLHP-B1, could attenuate injury in oxidative stress in HepG2 cells. These results hinted that hemicellulosic polysaccharides extracted by heteropolyacid from bamboo leaves possessed the potential to be used as an antioxidant for the organism but further *in vivo* and mechanism studies need lucubrating.

DATA AVAILABILITY STATEMENT

The raw data supporting the conclusions of this article will be made available by the authors, without undue reservation.

AUTHOR CONTRIBUTIONS

ZX contributed to the conceptualization, methodology, and writing of the original draft. JL and QZ performed the investigation and collected resources. HW conducted a formal analysis. QG used software for analysis and validation. JM and RS contributed to the project administration and supervision. All authors contributed to the article and approved the submitted version.

FUNDING

This research was supported by the Zhejiang Provincial Public Welfare Technology Application and Research Project of China (No. LGC21B060001). Key project at central government level: the ability establishment of sustainable use for valuable Chinese medicine resources (No. 2060302). "Pioneer" and "Leading Goose" R&D Program of Zhejiang (No. 2022C02023), China.

REFERENCES

1. Yu S, Liu GC, Wang ML, Lv ZY, Du PG. A selenium polysaccharide from Platycodon grandiflorum rescues PC12 cell death caused by H2O2 via inhibiting oxidative stress. *Int J Biol Macromol.* (2017) 144:393–9. doi: 10.1016/j.ijbiomac.2017.06.052
2. Duračková Z. Some current insight into oxidative stress. *Physiol Res.* (2009) 59:459–69. doi: 10.33549/physiolres.931844
3. Bhat AH, Dar KB, Anees S, Zargar MA, Masood A, Sofi MA, et al. Oxidative stress, mitochondrial dysfunction and neurodegenerative diseases; a mechanistic insight. *Biomed Pharmacother.* (2015) 74:101–10. doi: 10.1016/j.biopha.2015.07.025
4. Li Y, Sun Y, Zhu MZ, Zhu RX, Zhang JZ, Zhou JC, et al. Sacculatane diterpenoids from the Chinese liverwort *Pellia epiphylla* with protection against H2O2-induced apoptosis of PC12 cells. *Phytochemistry.* (2019) 162:173–82. doi: 10.1016/j.phytochem.2019.03.007
5. Li XX, Rommelaere S, Kondo S, Lemaitre B. Renal purge of hemolymphatic lipidsprevents the accumulation of ROS-induced inflammatory oxidized lipids and protects drosophila from tissue damage. *Immunity.* (2020) 52:374–87.e6. doi: 10.1016/j.immuni.2020.01.008
6. Wong FC, Xiao JB, Wang SY, Ee KY, Chai TT. Advances on the antioxidant peptides from edible plant sources. *Trends Food Sci Technol.* (2020) 99:44–57. doi: 10.1016/j.tifs.2020.02.012
7. Li TT, Wu CE, Meng XY, Fan GJ, Tang Y. Structural characterization and antioxidant activity of a glycoprotein isolated from *Camellia oleifera* Abel seeds against D-galactose-induced oxidative stress in mice. *J Funct Foods.* (2020) 64:e103594. doi: 10.1016/j.jff.2019.103594
8. Ji XL, Cheng YQ, Tian JY, Zhang SQ, Jing YS, Shi MM. Structural characterization of polysaccharide from jujube (*Ziziphus jujuba* Mill.) fruit. *Chem Biol Technol Agric.* (2021) 8:54–60. doi: 10.1186/s40538-021-00255-2
9. Szpakowska N, Kowalczyk A, Kaczynski Z. The chemical structure of polysaccharides isolated from the *Ochrobactrum rhizosphaerae* PR17T. *Carbohydr Res.* (2020) 497:e108136. doi: 10.1016/j.carres.2020.108136
10. Ferreira I, Heleno SA, Reis FS, Stojkovic D, Queiroz MJ, Vasconcelos MH, et al. Chemical features of *Ganoderma polysaccharides* with antioxidant, antitumor and antimicrobial activities. *Phytochemistry.* (2015) 114:38–55. doi: 10.1016/j.phytochem.2014.10.011
11. Peng H, Wang N, Hu ZR, Yu ZP, Liu YH, Zhang JS, et al. Physicochemical characterization of hemicelluloses from bamboo (*Phyllostachys pubescens* Mazel) stem. *Ind Crop Prod.* (2012) 37:41–50.

12. Peng P, She D. Isolation, structural characterization, and potential applications of hemicelluloses from bamboo: a review. *Carbohyd Polym.* (2014) 112:701–20. doi: 10.1016/j.carbpol.2014.06.068
13. Gilbert HJ, Knox JP, Boraston AB. Advances in understanding the molecular basis of plant cell wall polysaccharide recognition by carbohydrate-binding module. *Curr Opin Struc Biol.* (2013) 23:669–77. doi: 10.1016/j.sbi.2013.05.005
14. Ji XL, Guo JH, Pan FB, Kuang FJ, Chen HM, Guo XD, et al. Structural elucidation and antioxidant activities of a neutral polysaccharide from Arecanut (*Areca catechu* L.). *Front Nutr.* (2022) 9:e853115. doi: 10.3389/fnut.2022.853115
15. Mirzadeh M, Arianejad MR, Khedmat L. Antioxidant, antiradical, and antimicrobial activities of polysaccharides obtained by microwave-assisted extraction method: a review. *Carbohyd Polym.* (2020) 229:e115421. doi: 10.1016/j.carbpol.2019.115421
16. Surayot US, Yelithao K, Tabarsa M, Lee DH, Palanisamy S, Prabhu NM, et al. Structural characterization of a polysaccharide from *Certaria islandica* and assessment of immunostimulatory activity. *Process Biochem.* (2019) 83:214–21. doi: 10.1016/j.procbio.2019.05.022
17. Xiao ZQ, Wang XL, Yang QQ, Xing C, Ge Q, Gai XK, et al. Ball milling promotes saccharification of agricultural biomass by heteropolyacid and enzyme: unlock the lignin cage for sugars recovery. *Biomass Convers Biorefin.* (2020) 9:12–22. doi: 10.1007/s13399-020-00950-4
18. Ji XL, Guo JH, Ding DQ, Gao J, Hao LR, Guo XD, et al. Structural characterization and antioxidant activity of a novel high-molecular-weight polysaccharide from *Ziziphus Jujuba* cv. Muzao. *J Food Meas Charact.* (2022) 2:e1288. doi: 10.1007/s11694-022-01288-3
19. Li WL, Lin K, Zhou M, Xiong Q, Li CY, Ru Q. Polysaccharides from *Opuntia milpa* alta alleviate alloxan-induced INS-1 cells apoptosis via reducing oxidative stress and upregulating Nrf2 expression. *Nutr Res.* (2020) 77:108–18. doi: 10.1016/j.nutres.2020.02.004
20. Wen ZS, Xue R, Du M, Tang Z, Xiang XW, Zheng B, et al. Hemp seed polysaccharides protect intestinal epithelial cells from hydrogen peroxide-induced oxidative stress. *Int J Biol Macromol.* (2019) 135:203–11. doi: 10.1016/j.ijbiomac.2019.05.082
21. Jeong HK, Lee D, Kim HP, Baek SH. Structure analysis and antioxidant activities of an amylopectin-type polysaccharide isolated from dried fruits of *Terminalia chebula*. *Carbohyd Polym.* (2019) 211:100–8. doi: 10.1016/j.carbpol.2019.01.097
22. Chaiklahana R, Chirasuwana N, Triratanaa P, Lohab V, Tiab S, Bunnag B. Polysaccharide extraction from *Spirulina* sp. and its antioxidant capacity. *Int J Biol Macromol.* (2013) 58:73–8. doi: 10.1016/j.ijbiomac.2013.03.046
23. Jiang L, Wang WJ, Wen PW, Shen MY, Li HR, Ren YM, et al. Two water-soluble polysaccharides from mung bean skin: physicochemical characterization, antioxidant and antibacterial activities. *Food Hydrocoll.* (2020) 100:e105412. doi: 10.1016/j.foodhyd.2019.105412
24. Ma JS, Liu H, Han CR, Zeng SJ, Xu XJ, Lu DJ, et al. Extraction, characterization and antioxidant activity of polysaccharide from *Pouteria campechiana* seed. *Carbohyd Polym.* (2020) 229:e115409. doi: 10.1016/j.carbpol.2019.115409
25. Xiao ZQ, Zhang Q, Dai J, Wang XL, Yang QQ, Cai CG, et al. Structural characterization, antioxidant and antimicrobial activity of water-soluble polysaccharides from bamboo (*Phyllostachys pubescens* Mazel) leaves. *Int J Biol Macromol.* (2020) 142:432–42. doi: 10.1016/j.ijbiomac.2019.09.115
26. Chale-Dzul J, Freile-Pelegrín Y, Robeldo D, Moo-Puc R. Protective effect of fucoidans from tropical seaweeds against oxidative stress in HepG2 cells. *J Appl Phycol.* (2017) 29:2229–38. doi: 10.1007/s10811-017-1194-3
27. Guo QW, Xu LL, Chen Y, Ma QQ, Santhanam RK, Xue ZH, et al. Structural characterization of corn silk polysaccharides and its effect in H2O2 induced oxidative damage in L6 skeletal muscle cells. *Carbohyd Polym.* (2019) 208:161–7. doi: 10.1016/j.carbpol.2018.12.049
28. Gao CP, Zhong LF, Jiang LP, Geng CY, Yao XF, Cao J. *Phellinus linteus* mushroom protects against tacrine-induced mitochondrial impairment and oxidative stress in HepG2 cells. *Phytomedicine.* (2013) 20:705–9. doi: 10.1016/j.phymed.2013.02.014
29. Mehmood T, Maryam A, Zhang H, Li YM, Khan M, Ma TH. Deoxyelephantopin induces apoptosis in HepG2 cells via oxidative stress, NF-κB inhibition and mitochondrial dysfunction. *Biofactors.* (2016) 43:63–72. doi: 10.1002/biof.1324
30. Su Y, Li L. Structural characterization and antioxidant activity of polysaccharide from four auriculariales. *Carbohyd Polym.* (2020) 229:e115407. doi: 10.1016/j.carbpol.2019.115407
31. Peng H, Zhou MY, Yu ZP, Zhang JS, Ruan R, Wan YQ, et al. Fractionation and characterization of hemicelluloses from young bamboo (*Phyllostachys pubescens* Mazel) leaves. *Carbohyd Polym.* (2013) 95:262–71. doi: 10.1016/j.carbpol.2013.03.007
32. Tang W, Liu CC, Liu JJ, Hu LY, Huang YS, Yuan L, et al. Purification of polysaccharide from *Lentinus edodes* water extract by membrane separation and its chemical composition and structure characterization. *Food Hydrocoll.* (2020) 105:e105851. doi: 10.1016/j.foodhyd.2020.105851
33. Gu JY, Zhang HH, Zhang JX, Wen CT, Ma HL, Duan YQ, et al. Preparation, characterization and bioactivity of polysaccharide fractions from *Sagittaria sagittifolia* L. *Carbohyd Polym.* (2020) 229:e115355. doi: 10.1016/j.carbpol.2019.115355
34. Zhu JX, Chen ZY, Chen L, Yu C, Wang HX, Wei XL, et al. Comparison and structural characterization of polysaccharides from natural and artificial Se-enriched green tea. *Int J Biol Macromol.* (2019) 130:388–98. doi: 10.1016/j.ijbiomac.2019.02.102
35. Cao JJ, Lv QQ, Zhang B, Chen HQ. Structural characterization and hepatoprotective activities of polysaccharides from the leaves of *Toona sinensis* (A. Juss) Roem. *Carbohyd Polym.* (2019) 212:89–101. doi: 10.1016/j.carbpol.2019.02.031
36. Chaves PFP, Iacomini M, Cordeiro LMC. Chemical characterization of fructooligosaccharides, inulin and structurally diverse polysaccharides from chamomile tea. *Carbohyd Polym.* (2019) 214:269–75. doi: 10.1016/j.carbpol.2019.03.050
37. Khemakhem I, Abdelhedi O, Trigui I, Ayadi MA, Bouaziz M. Structural, antioxidant and antibacterial activities of polysaccharides extracted from olive leaves. *Int J Biol Macromol.* (2018) 106:425–32. doi: 10.1016/j.ijbiomac.2017.08.037
38. Gong P, Wang SY, Liu M, Chen FX, Yang WJ, Chang XN, et al. Extraction methods, chemical characterizations and biological activities of mushroom polysaccharides: a mini-review. *Carbohydr Res.* (2020) 494:e108037. doi: 10.1016/j.carres.2020.108037
39. Wang KL, Wang B, Hu RB, Zhao XH, Li HL, Zhou GK, et al. Characterization of hemicelluloses in *Phyllostachys edulis* (moso bamboo) culm during xylogenesis. *Carbohyd Polym.* (2019) 221:127–36. doi: 10.1016/j.carbpol.2019.05.088
40. Zelaya VM, Fernández PV, Vega AS, Mantese AI, Federico AA, Ciancia M. Glucuronoarabinoxylans as major cell walls polymers from youngshoots of the woody bamboo *Phyllostachys aurea*. *Carbohyd Polym.* (2017) 167:240–9. doi: 10.1016/j.carbpol.2017.03.015
41. Li C, Dong ZP, Zhang B, Huang Q, Liu G, Fu X. Structural characterization and immune enhancement activity of a novel polysaccharide from *Moringa oleifera* leaves. *Carbohyd Polym.* (2020) 234:e115897. doi: 10.1016/j.carbpol.2020.115897
42. Seyfi R, Kasaai MR, Chaichi MJ. Isolation and structural characterization of a polysaccharide derived from a local gum: zedo (*Amygdalus scoparia* Spach). *Food Hydrocolloid.* (2019) 87:915–24. doi: 10.1016/j.foodhyd.2018.09.017
43. Shi WT, Zhong J, Zhang Q, Yan CY. Structural characterization and antineuroinflammatory activity of a novel heteropolysaccharide obtained from the fruits of *Alpinia oxyphylla*. *Carbohyd Polym.* (2020) 229:e115405. doi: 10.1016/j.carbpol.2019.115405
44. Lin YP, An FP, He H, Feng F, Song HB, Huang Q. Structural and rheological characterization of pectin from passion fruit (*Passiflora edulis* f. flavicarpa) peel extracted by high-speed shearing. *Food Hydrocoll.* (2021) 114:e106555. doi: 10.1016/j.foodhyd.2020.106555
45. Li C, Li X, You L, Fu X, Liu RH. Fractionation, preliminary structural characterization and bioactivities of polysaccharides from *Sargassum pallidum*. *Carbohyd Polym.* (2017) 155:261–70. doi: 10.1016/j.carbpol.2016.08.075
46. Gu JY, Zhang HH, Yao H, Zhou J, Duan YQ, Ma HL. Comparison of characterization, antioxidant and immunological activities of three polysaccharides from *Sagittaria sagittifolia* L. *Carbohyd Polym.* (2019) 133:11–20. doi: 10.1016/j.carbpol.2020.115939
47. Yuan YQ, Li C, Zheng QW, Wu JX, Zhu KX, Shen XR, et al. Effect of simulated gastrointestinal digestion in vitro on the antioxidant activity, molecular

weight and microstructure of polysaccharides from a tropical sea cucumber (*Holothuria leucospilota*). *Food Hydrocoll.* (2019) 89:735–41. doi: 10.1016/j.foodhyd.2018.11.040
48. Raguraman V, Abraham LS, Jyotsna J, Seedevi P, Kannan GS, Thirugnanasambandam R, et al. Sulfated polysaccharide from *Sargassum tenerrimum* attenuates oxidative stress induced reactive oxygen species production in in vitro and in zebrafish model. *Carbohyd Polym.* (2019) 203:441–9. doi: 10.1016/j.carbpol.2018.09.056
49. Patel MK, Tanna B, Gupta H, Mishra A, Jha B. Physicochemical, scavenging and anti-proliferative analyses of polysaccharides extracted from psyllium (*Plantago ovata* Forssk) husk and seeds. *Int J Biol Macromol.* (2019) 133:190–201. doi: 10.1016/j.ijbiomac.2019.04.062
50. Olawuyi IF, Kim SR, Hahn D, Lee WY. Influences of combined enzyme-ultrasonic extraction on the physicochemical characteristics and properties of okra polysaccharides. *Food Hydrocoll.* (2020) 100:e105396. doi: 10.1016/j.foodhyd.2019.105396
51. Yuan D, Li C, Huang Q, Fu X. Ultrasonic degradation effects on the physicochemical, rheological and antioxidant properties of polysaccharide from *Sargassum pallidum*. *Carbohyd Polym.* (2020) 239:e116230. doi: 10.1016/j.carbpol.2020.116230
52. Yuan B, Han JN, Cheng YL, Cheng SJ, Huang DC, Mcclements DJ, et al. Identification and characterization of antioxidant and immune-stimulatory polysaccharides in flaxseed hull. *Food Chem.* (2020) 315:e126226. doi: 10.1016/j.foodchem.2020.126266
53. Yan L, Xiong C, Zhu P, Xu J, Yang ZR, Ren H, et al. Structural characterization and in vitro antitumor activity of a polysaccharide from *Artemisia annua* L. (Huang Huahao). *Carbohyd Polym.* (2019) 213:361–9. doi: 10.1016/j.carbpol.2019.02.081
54. Kumar PP, Prashanth KVH. Low molecular weight chitosan (˜20 kDa) protects acrylamide induced oxidative stress in D. melanogaster by restoring dopamine and KIF5B levels. *Carbohyd Polym.* (2019) 222:e115005. doi: 10.1016/j.carbpol.2019.115005
55. Trinh MDL, Ngo DH, Tran DK, Tran QT, Vo TS, Dinh MH, et al. Prevention of H2O2-induced oxidative stress in Chang liver cells by 4-hydroxybenzyl-chitooligomers. *Carbohyd Polym.* (2014) 103:502–9. doi: 10.1016/j.carbpol.2013.12.061
56. Chinnapaka S, Zheng GX, Chen AS, Munirathinam G. Nitro aspirin (NCX4040) induces apoptosis in PC3 metastatic prostate cancer cells via hydrogen peroxide (H2O2)-mediated oxidative stress. *Free Radic Biol Med.* (2019) 143:494–509. doi: 10.1016/j.freeradbiomed.2019.08.025
57. Skalski B, Lis B, Pecio Ł, Kontek B, Olas B, Żuchowski J, et al. Isorhamnetin and its new derivatives isolated from sea buckthorn berries prevent H2O2/Fe–induced oxidative stress and changes in hemostasis. *Food Chem Toxicol.* (2019) 125:614–20. doi: 10.1016/j.fct.2019.02.014
58. Xiong C, Li Q, Chen C, Chen ZQ, Huang WL. Neuroprotective effect of crude polysaccharide isolated from the fruiting bodies of *Morchella importuna* against H2O2-induced PC12 cell cytotoxicity by reducing oxidative stress. *Biomed Pharmacother.* (2016) 83:569–76. doi: 10.1016/j.biopha.2016.07.016
59. Oh SH, Vo TS, Ngo DH, Kim SY, Ngo DN, Kim SK. Prevention of H2O2-induced oxidative stress in murine microglial BV-2 cells by chitin-oligomers. *Process Biochem.* (2016) 51:2170–5. doi: 10.1016/j.procbio.2016.08.015

Conflict of Interest: The authors declare that the research was conducted in the absence of any commercial or financial relationships that could be construed as a potential conflict of interest.

Publisher's Note: All claims expressed in this article are solely those of the authors and do not necessarily represent those of their affiliated organizations, or those of the publisher, the editors and the reviewers. Any product that may be evaluated in this article, or claim that may be made by its manufacturer, is not guaranteed or endorsed by the publisher.

Copyright © 2022 Xiao, Li, Wang, Zhang, Ge, Mao and Sha. This is an open-access article distributed under the terms of the Creative Commons Attribution License (CC BY). The use, distribution or reproduction in other forums is permitted, provided the original author(s) and the copyright owner(s) are credited and that the original publication in this journal is cited, in accordance with accepted academic practice. No use, distribution or reproduction is permitted which does not comply with these terms.

frontiers | Frontiers in Nutrition

ORIGINAL RESEARCH
published: 21 June 2022
doi: 10.3389/fnut.2022.935632

Characterization and Antibacterial Activity of a Polysaccharide Produced From Sugarcane Molasses by *Chaetomium globosum* CGMCC 6882

Li Ma[1], Xueliang Guo[1], Jiaoyang Yang[1], Xiangru Zeng[1], Kaili Ma[1], Lu Wang[2], Qi Sun[3] and Zichao Wang[2,4]**

[1] Henan Provincial Key University Laboratory for Plant-Microbe Interactions, College of Biology and Food, Shangqiu Normal University, Shangqiu, China, [2] School of Biological Engineering, Henan University of Technology, Zhengzhou, China, [3] College of Life Sciences, Chongqing Normal University, Chongqing, China, [4] National Engineering Laboratory, Key Laboratory of Henan Province, Henan University of Technology, Zhengzhou, China

OPEN ACCESS

Edited by:
Xiaolong Ji,
Zhengzhou University of Light Industry, China

Reviewed by:
Peng Lei,
Nanjing Tech University, China
Xin Zeng,
Huaibei Normal University, China

***Correspondence:**
Qi Sun
sunqi2017@cqnu.edu.cn
Zichao Wang
zcwang@haut.edu.cn

Specialty section:
This article was submitted to Food Chemistry, a section of the journal Frontiers in Nutrition

Received: 04 May 2022
Accepted: 30 May 2022
Published: 21 June 2022

Citation:
Ma L, Guo X, Yang J, Zeng X, Ma K, Wang L, Sun Q and Wang Z (2022) Characterization and Antibacterial Activity of a Polysaccharide Produced From Sugarcane Molasses by Chaetomium globosum CGMCC 6882. Front. Nutr. 9:935632. doi: 10.3389/fnut.2022.935632

As a by-product of the sugar industry containing many sugars, proteins, nitrogenous materials, and heavy metals, molasses is rarely used for polysaccharide production. In the present work, a *Chaetomium globosum* CGMCC 6882 polysaccharide was produced from sugarcane molasses (CGP-SM) was successfully produced from sugarcane molasses. The yield of CGP-SM was 5.83 ± 0.09 g/l and its protein content was 2.41 ± 0.12% (w/w). Structural analysis showed that CGP-SM was a crystalline and amorphous polysaccharide containing rhamnose, glucosamine, galactose, glucose, mannose, fructose, and glucuronic acid in the molar ratio of 10.31: 1.14: 2.07: 59.55: 42.65: 1.92: 9.63. Meanwhile, weight-average molecular weight (Mw), number-average molecular weight (Mn), and polydispersity (Mw/Mn) of CGP-SM were 28.37 KDa, 23.66 KDa, and 1.199, respectively. Furthermore, the bacteriostatic assay indicated that CGP-SM inhibited the growth of *Escherichia coli* and *Staphylococcus aureus* in a concentration-dependent manner, and its inhibitory effect on *S. aureus* was higher than that of *E. coli*. Above all, this work provides a green method for the production of bioactive polysaccharide from sugarcane molasses.

Keywords: sugarcane molasses, *Chaetomium globosum* CGMCC 6882, polysaccharide, structural characteristics, antibacterial activity

INTRODUCTION

Microbial polysaccharides, such as lipopolysaccharides (LPS), capsular polysaccharides (CPS), and exo-polysaccharides (EPS), are polymers of biological carbohydrates with high molecular weight and constitute an important part of renewable polymer resources (1). CPS is mainly associated with pathogenicity and toxin promoters in bacteria, LPS is present in the outer membrane of bacteria and important for human immune response, and EPS is a bacterial extracellular polymer (2). EPS usually consists of monosaccharide and non-carbohydrate substituent, which can be divided into two types according to the composition of sugar units, one is a homologous polysaccharide

composed of only one monosaccharide unit (3), and the other is heteropolysaccharide containing two or more monosaccharide units (4). EPS not only has superior rheological properties, bio-adhesion, non-toxicity, biocompatibility, and biodegradation (5, 6), but also can be produced from renewable resources and waste (7–9), which makes it popular in the food and other industries.

Molasses is the main accessory substance in the sugar manufacturing process, which contains about 50% (w/w) sugars, 1.0% (w/w) nitrogenous materials, and heavy metals (such as Fe^{2+}, Cu^{2+}, Mn^{2+}, Mg^{2+}, Ca^{2+}, etc.) (10). The total yearly yield of molasses is about 55 million tons worldwide, but it is simply discharged or applied to feed due to its thick, semi-flowing, and dark brown properties (11). With the rapid development of microbial fermentation and bio-catalysis transformation technologies in recent years, more and more value-added bio-products have been produced from molasses *via* microbial transformation, such as bio-fuels, enzymes, organic acids, etc. (12). Meanwhile, many polysaccharides have also been produced from molasses, including pullulan (13), welan gum (14), hyaluronic acid (4), and glucan (3). The above research provided help for the production of polysaccharides from low-cost molasses with an environmentally microbial process.

As an endophytic fungus isolated from *Gynostemma pentaphyllum* herb, *Chaetomium globosum* CGMCC 6882 could use many kinds of processing wastes as a carbon source to produce polysaccharides *via* submerged fermentation. For instance, crude glycerol could be used by *C. globosum* CGMCC 6882 to produce anticancer polysaccharides (15). At the same time, *C. globosum* CGMCC 6882 could use wheat straw and distillers' grain to produce antioxidant and anti-inflammatory polysaccharides (7, 9). However, the utilization of molasses for polysaccharide production by *C. globosum* CGMCC 6882 was neglected up to now. Therefore, a polysaccharide of CGP-SM was produced from sugarcane molasses by *C. globosum* CGMCC 6882 with submerged cultivation presently. On the one hand, the physicochemical properties of CGP-SM were characterized. On the other hand, the inhibition effects of CGP-SM against *Escherichia coli* and *Staphylococcus aureus* were assayed. We hope that this work could provide help for further developing the scope of bioactive polysaccharide production by microorganisms from molasses.

MATERIALS AND METHODS

Materials and Chemicals

Sugarcane molasses was purchased from Xinze biological Co. Ltd. (Zhengzhou, China), and contained 8% (w/w) glucose, 28% (w/w) sucrose, 2.1% (w/w) other carbohydrates, 12% (w/w) fructose, 3.6% (w/w) crude protein, 0.05% (w/w) crude fat, 8.2% (w/w) ash, 5.3% (w/w) salt, and 7.5% (w/w) metal ions. Rhamnose, fucose, fructose, galactose, glucose, glucosamine, xylose, mannose, arabinose, galacturonic acid, and glucuronic acid used in the present work were purchased from Sigma-Aldrich (Shanghai, China). Meanwhile, other chemical reagents were bought from Sinopharm Chemical Reagent Co., Ltd. (Shanghai, China).

Organisms

Chaetomium globosum CGMCC 6882 was stored in China General Microbiological Culture Collection Center (China). *E. coli* and *S. aureus* were bought from the China Center of Industrial Culture Collection (CICC), the collection numbers were CICC10899 and CICC10001, respectively.

Pre-treatment of Sugarcane Molasses

Pre-treatment of sugarcane molasses was based on the methods reported previously by Ai et al. (16) with some modifications. Briefly, crude sugarcane molasses was diluted by adding four folds (w/w) deionized water and filtered *via* a 0.45 μm drainage membrane filter (Beijing Solarbio Science & Technology Co., Ltd., Beijing, China). The filtrate was heated for 30 min at 100°C and centrifuged (TGL-16M, Xiangyi Centrifuge Instrument Co., Ltd.) at 10,000 × *g* for 15 min, then the supernatant was collected for further use.

Polysaccharide Production From Sugarcane Molasses

The fermentation medium used for CGP-SM production by *C. globosum* CGMCC 6882 contained only 40 g/l above the sugarcane molasses supernatant. Batch fermentation was carried out in a 7.0 L fermenter (BioFlo 115, New Brunswick, United States) at 28°C with 3.5 L medium, cultivation lasted for 7 days, inoculation volume was 5% (v/v), culture pH was kept between 6.80 and 7.20 with the addition of 4 mol/l NaOH and 4 mol/l HCl, the agitation was 100 rpm and the aeration was 0.8 vvm. CGP-SM extraction and purification were conducted according to the methods reported previously (17) with some modifications. After fermentation, the fermented liquid was filtered and centrifuged to remove impurities. Then the broth was concentrated at 60°C and 0.1 MPa. After that, the concentrated broth was de-proteinized by adding three volumes of Sevag solution. Finally, three volumes of cold alcohol was added and kept at 4°C overnight to precipitate CGP-SM, the precipitated CGP-SM was washed three times with 75% cold alcohol and lyophilized to obtain crude CGP-SM. The crude CGP-SM was re-dissolved in distilled water and de-pigmented with AB-8 macroporous resin. Then, the CGP-SM solution was dialyzed for 48 h in distilled water (M_W cut-off was 10 kDa). After that, the CGP-SM solution was filtered through a 0.22 μm filter and applied to a Sepharose CL-6B column (2.5 × 60 cm) for further purification, and eluted with 0.1 mol/l NaCl at a flow rate of 0.6 ml/min. In the end, the fraction was collected and freeze-dried for the following analysis.

Physicochemical Properties Analysis

Determination of Monosaccharide Composition and Protein Content

Protein content in CGP-SM was detected by the Coomassie Brilliant Blue method with bovine serum albumin as standard (18). Meanwhile, CGP-SM was dissolved in 2 mol/l trifluoroacetic acid (TFA) and hydrolyzed at 120°C for 2 h, then the hydrolysate was washed three times with methanol and evaporated to dryness for removing TFA. The hydrolyzed material was transferred

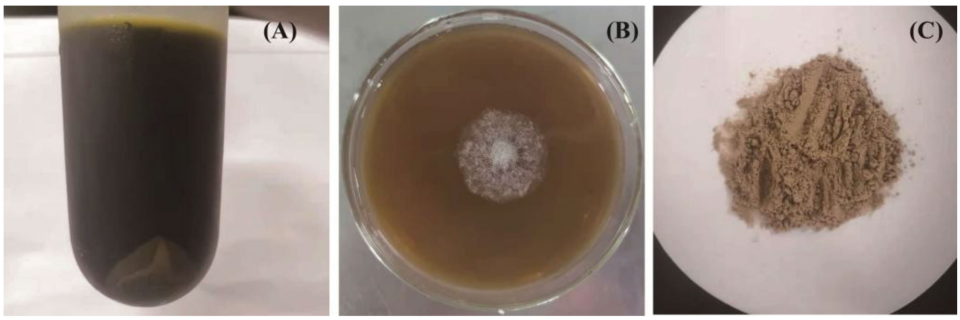

FIGURE 1 | The distilled, heated, and centrifuged sugarcane molasses **(A)**, growth profile of *Chaetomium globosum* CGMCC 6882 on sugarcane molasses plate **(B)**, polysaccharide (CGP-SM) powder obtained from submerged fermentation **(C)**.

into a 25 ml volumetric flask, diluted to 25 ml by adding deionized water, and detected using high-performance anion-exchange chromatography (HPAEC) equipped with Dionex ICS5000 system (Dionex, United States) and CarboPac PA20 column (ID 3 mm × 150 mm) as reported previously (19).

Determination of Molecular Weight

CGP-SM was dissolved in 0.1 mol/l $NaNO_3$ and filtered by a 0.5 μm microfiltration membrane. Then, the molecular weight of CGP-SM was detected by high-performance gel filtration chromatography (HPGFC) equipped with a refractive index detector and a Superose 12 column (1.0 cm × 30.0 cm) as the method reported by Li et al. (20) with some modifications.

Fourier Transform Infrared Spectroscopic Analysis

A Nexus 470 Fourier transform infrared (FT-IR) spectrometer (Nicolet, United States) was used to detect the FT-IR spectra of CGP-SM. Briefly, 5 mg CGP-SM was fully ground with 1 g KBr and pressed to a pallet for FT-IR spectra determination between 4,000 and 400 cm^{-1} as reported previously (17).

TABLE 1 | Characteristics of polysaccharide produced by *Chaetomium globosum* CGMCC 6882 from sugarcane molasses.

Parameters	CGP-SM
Polysaccharide yield (g/L)	5.83 ± 0.09
Protein content (w%)	2.41 ± 0.12
Monosaccharide composition (μmol/L)	
Rhamnose	10.31
Glucosamine	1.14
Galactose	2.07
Glucose	59.55
Mannose	42.65
Fructose	1.92
Glucuronic acid	9.63
Molecular weight (1 × 10^3 Da)	
Weight-average molecular weight (M_w)	28.37
Number-average molecular weight (M_n)	23.66
Polydispersity (M_w/M_n)	1.199

Nuclear Magnetic Resonance Analysis

The nuclear magnetic resonance (NMR) spectra of CGP-SM were recorded by a Bruker Avance 500 MHz spectrometer (Bruker Inc., Germany). Briefly, CGP-SM was dissolved in a 5 mm NMR tube with 1 ml D_2O and processed by ultrasonic treatment for 30 min as reported previously (19). Then, the ^1H NMR and ^{13}C NMR spectra of CGP-SM were recorded in parts per million.

Scanning Electron Microscopy Observation

Morphological images of CGP-SM were recorded by a Quant 200 scanning electron microscopy (SEM) (FEI, Netherlands) as reported by Yan et al. (21) with some modifications. Briefly, the freeze-dried CGP-SM sample was fixed onto a metal observation stage placed in a vacuum, and the accelerating voltage was 15 kV.

X-Ray Diffraction Analysis

A D8advance X-ray diffractometer (Bruker, Germany) was used to analyze the crystallinity of CGP-SM as reported previously with some modifications (22). Cu-Kα was used as the radiation source, the scanning angle range was set as 10–60° (2θ). The scanning voltage was 30 kV and the scanning current was 30 mA. Meanwhile, the scanning rate was 2°/min and the step size was 0.02°.

Antibacterial Activity Assay

Inhibitory effects of CGP-SM against *E. coli* and *S. aureus* were analyzed by using the inhibition zone method as reported previously (23) with some modifications. Briefly, CGP-SM was dissolved in deionized water to 0.125, 0.25, 0.5, 1.0, and 2.0 mg/ml, respectively, filtrated through a 0.22 μm drainage membrane filter (Beijing Solarbio Science & Technology Co., Ltd.). Then, nutrient agar (20 ml) was added into plates and solidified, after which, 150 μl test organism (10^6 CFU/ml) suspension was spread on the agar plate surface. Then, one sterilized 2 mm circular paper was placed onto the middle of the plate, and 10 μl of CGP-SM samples were injected onto the circular paper. The inhibition zone of each plate was measured by diameter after incubation at 37 ± 1°C for 24 h. Antibacterial activities of CGP-SM against *E. coli* and *S. aureus* were analyzed by determining the diameters of inhibition zones with a Vernier caliper.

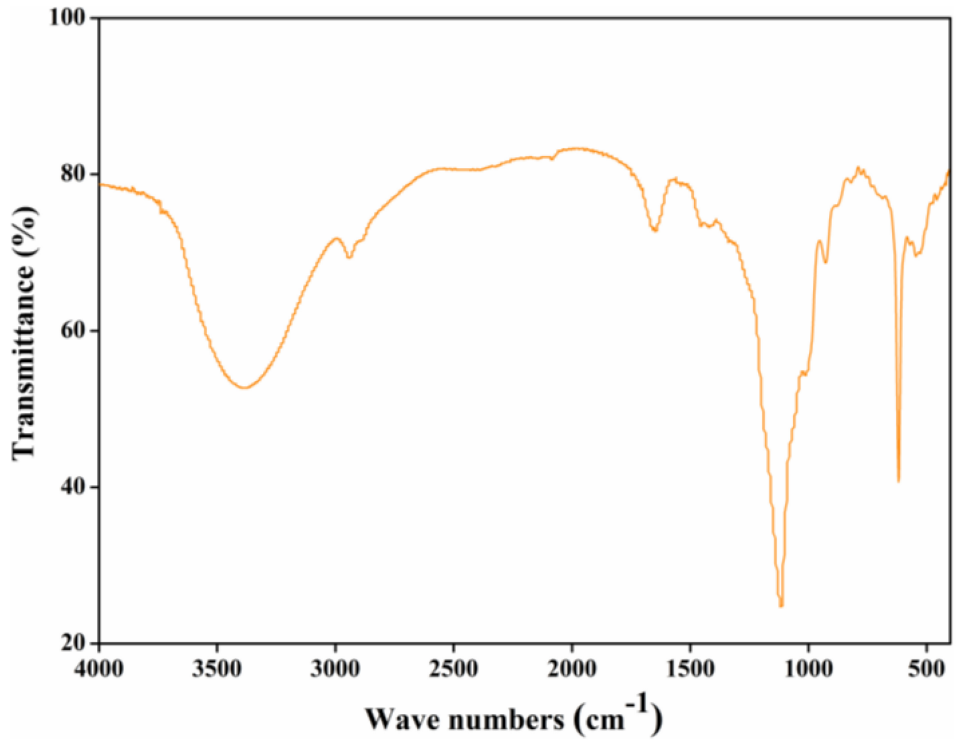

FIGURE 2 | Fourier-transform infrared (FT-IR) spectrum of CGP-SM.

Statistical Analysis

Data were expressed as means ± SD after triplicate repeats. Data were subjected to one-way ANOVA, and the significant differences were analyzed using SPSS version 19.0 (IBM, United States).

RESULTS AND DISCUSSION

Polysaccharide Production

In the present work, after sugarcane molasses was distilled, heated, and centrifuged, the supernatant (**Figure 1A**) could be used as the only carbon source for *C. globosum* CGMCC 6882 growth (**Figure 1B**), which demonstrated that sugarcane molasses is a promising substrate for metabolites production by *C. globosum* CGMCC 6882. Meanwhile, after submerged cultivation, extraction, and purification, a polysaccharide (CGP-SM) was obtained (**Figure 1C**) and its yield was 5.83 ± 0.09 g/l (**Table 1**), the color of CGP-SM might be due to the pigments in which it was left. This yield is lower than welan gum (37.65 g/l) (14) and sophorolipid (53 ± 3 g/l) (24) produced from molasses, but higher than chitosan (0.39 g/l) (25) and hyaluronic acid (3.48 g/l) (4) produced from molasses with submerged cultivation. Many factors, such as microbial species, culture conditions, and nutritional types, could affect polysaccharide yields (26), but submerged cultivation has the advantages of better controlling cultivation conditions, less pollution, less time consumption, high efficiency, and less space occupation. Meanwhile, **Table 1** showed that CGP-SM contained 2.41 ± 0.12% (w/w) protein, which might be due to the unused protein in sugarcane molasses bonded to CGP-SM during the extraction process.

Physicochemical Properties of CGP-SM

Monosaccharide Composition

Except for polysaccharide source, extraction, and purification methods, monosaccharide diversity of microbial exo-polysaccharide is mainly affected by the culture conditions and culture medium nutrients (27). As shown in **Table 1** and **Supplementary Figure 1**, the monosaccharide composition of CGP-SM was rhamnose, glucosamine, galactose, glucose, mannose, fructose, and glucuronic acid in the molar ratio of 10.31: 1.14: 2.07: 59.55: 42.65: 1.92: 9.63. Previously, when wheat straw was used as the only carbon source, the monosaccharide composition of polysaccharide produced by *C. globosum* CGMCC 6882 was rhamnose, glucosamine, galactose, glucose, xylose, fructose, and glucuronic acid in the molar ratio of 21.46: 1.58: 1.11: 55.15: 36.37: 7.04: 7.34 (9). When glucose was used as the only carbon source, the monosaccharide composition of polysaccharide produced by *C. globosum* CGMCC 6882 was arabinose, galactose, glucose, xylose, mannose, and glucuronic acid in the molar ratio of 0.64: 2.58: 23.53: 0.90: 2.47: 0.27 (19). At the same time, monosaccharide composition of polysaccharide produced by *C. globosum* CGMCC 6882 was rhamnose, arabinose, galactose, glucose, xylose, mannose, galacturonic acid, and glucuronic acid in the molar ratio of 4.11: 7.34: 13.31:

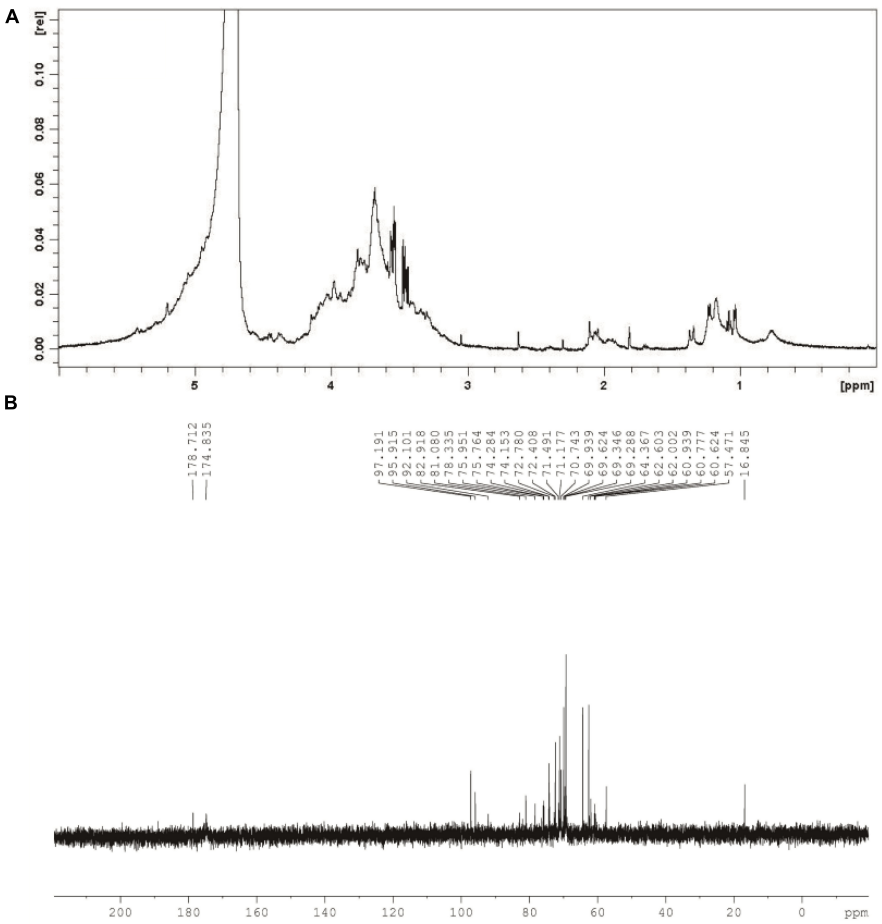

FIGURE 3 | ^{1}H nuclear magnetic resonance (NMR) spectrum **(A)** and ^{13}C NMR spectrum **(B)** of CGP-SM.

20.99: 1.07: 0.91: 4.75: 0.36 with distillers' grain as the only carbon source (7). However, monosaccharide compositions of polysaccharides produced by *C. globosum* CGMCC 6882 were galactose, glucose, mannose, and glucuronic acid in molar ratios of 5.95: 58.75: 5.65: 0.76 and 8.16: 43.77: 5.84: 0.43 with glycerol and crude glycerol were used as carbon source, respectively (15).

Molecular Weight

As shown in **Table 1**, the weight-average molecular weight (Mw) and number-average molecular weight (Mn) of CGP-SM were 28.37 and 23.66 KDa, respectively, and its polydispersity (Mw/Mn) was 1.199. Previously, Zhang et al. (28) found that molecular weight could affect the antibacterial activities of polysaccharides produced by *C. globosum* CGMCC 6882, and the lower molecular weight endowed polysaccharide with higher antibacterial activity. Meanwhile, Zheng et al. (29) found that the antioxidant activity of polysaccharide produced by *Pholiota nameko* PN-01 was enhanced with the decrease in its molecular weight. However, Dou et al. (30) reported that the antioxidant and α-glucosidase inhibitory activities of blackberry fruit polysaccharides were coincident with their molecular weights. Furthermore, Cai et al. (31) demonstrated that *Ganoderma lucidum* polysaccharide had higher anti-fatigue activity when its molecular weight was higher than 10 kDa.

Fourier-Transform Infrared Spectra

As can be seen from **Figure 2**, a broad peak at around 3,400 cm^{-1} might relate to the O-H stretching vibration of intra-molecular or inter-molecular hydrogen bonds (19). A typical peak at around 2,900 cm^{-1} might attribute to C-H tensile vibration such as CH, CH_2, and CH_3 groups, the absorption peak at around 2,400 cm^{-1} might relate to aliphatic C-H bonds stretching (7). The absorption peaks at around 1,700 and 1,250 cm^{-1} might be derived from C=O stretching vibration in the ester or carboxyl groups, and absorption peak at around 1,600 cm^{-1} might be induced by the symmetrical C=O stretching vibrations in carboxyl groups (9). The absorption peak at around 1,400 cm^{-1} might correspond to asymmetrical C=O stretching vibrations coupled with C-H bending vibrations, and absorption peaks between 1,000 and 1,200 cm^{-1} might assign to C-O-H and C-O-C stretching vibrations. Absorption peaks between 900 and 800 cm^{-1} might assign to the β-glycosidic bonds and α-type glycosidic linkages in CGP-SM.

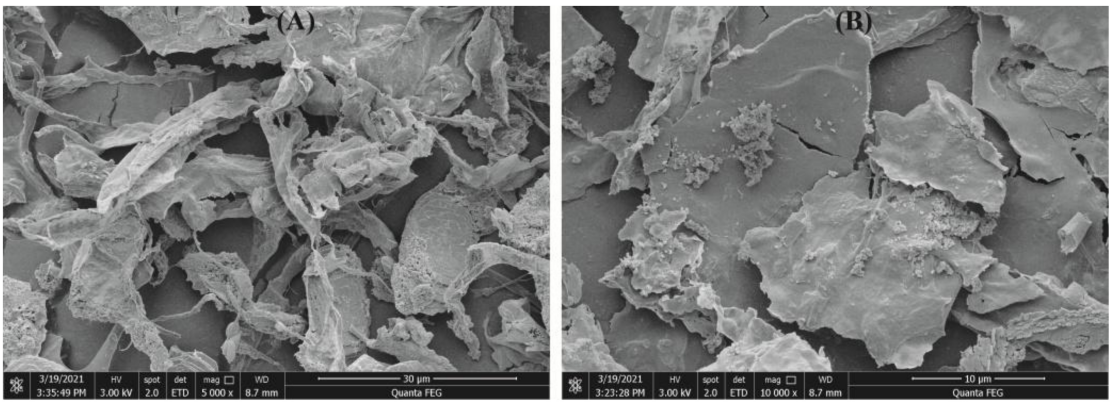

FIGURE 4 | Scanning electron microscopy (SEM) photographs of CGP-SM with different magnifications. **(A)** ×5,000, **(B)** ×10,000.

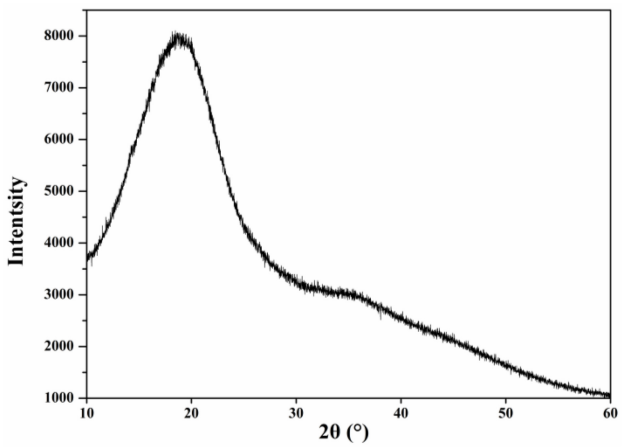

FIGURE 5 | X-ray diffractogram of CGP-SM.

Nuclear Magnetic Resonance Spectra

As can be seen from **Figure 3A**, chemical shift at around 4.8 ppm might assign to D_2O used in the present work. Meanwhile, singles between 4.0 and 3.4 ppm might relate to glycosyl residues in CGP-SM. The ^1H signal at approximately 2.0 ppm might relate to the *O*-acetyl groups in CGP-SM. Furthermore, singles at around 1.2 ppm might be due to the proton of the CH_3 group in Rha*p* residues (32). In addition, the ^{13}C NMR spectrum of CGP-SM showed several anomeric carbon signals ranging from 0.0 to 200.0 ppm (**Figure 3B**). The spectrum signals at around 175 and 180 ppm might relate to the ionic carboxyl group in uronic acid (33). The signal peaks at around 96 and 97 ppm might relate to anomeric carbons in Glc*p* and Ara*p*. The signals observed at around 60 and 80 ppm in the anomeric region of the ^{13}C NMR spectra might assign to the C-2, C-3, C-4, C-5, and C-6 of Glc*p* (34). Signal peak at around 16.8 ppm might relate to C-6 in Rha*p*.

Scanning Electron Microscopy

Scanning electron microscopy (SEM) is an effective instrument to observe the morphological image, shape, and porosity of polysaccharides (35). As shown in **Figure 4A**, CGP-SM had irregular structures and ribbons with branches. Meanwhile, **Figure 4B** showed that CGP-SM exhibited an irregular, fibrous, and smooth surface, which might relate to the low content of uronic acid leading to few interaction points among particle (30). These results are comparable to the polysaccharide reported by López-Legarda et al. (36), but different from the polysaccharide reported by Xiong et al. (37). The shape, structure, and surface morphology of polysaccharides are not only affected by the processes of extraction, solubility, purification, and lyophilization but also influenced by the culture conditions (36).

X-Ray Diffractometry

In the present work, the amorphous and crystalline information of CGP-SM were analyzed by an X-ray diffraction (XRD) and the results were shown in **Figure 5**. As can be seen from **Figure 5**, there was a broad diffraction peak appeared at around 20°, which indicated that CGP-SM was a crystalline and amorphous structure of polysaccharide. This structural feature was comparable to the *Fritillaria pallidiflora* Schrenk polysaccharide reported by Rozi et al. (38), but the XRD result of polysaccharide reported by Dou et al. (30) was different from the present work.

Antibacterial Activity

Bacteriostatic activities of CGP-SM against *E. coli* and *S. aureus* were analyzed by using inhibition zone diameter (mm) methods. **Figure 6** showed that the inhibitory effects of CGP-SM against *E. coli* and *S. aureus* increased with the increase of its concentration from 0.125 to 2.0 mg/ml, and its inhibitory effect on *S. aureus* was higher than that of *E. coli*. When the concentration of CGP-SM was 0.125 mg/ml, inhibition zones of CGP-SM against *E. coli* and *S. aureus* were 1.21 ± 0.17 mm and 1.57 ± 0.13 mm, respectively. When its concentration reached 2.0 mg/ml, inhibition zones of CGP-SM against *E. coli* and *S. aureus* were 25.12 ± 0.48 mm and 31.85 ± 0.39 mm (**Supplementary Figure 2**), respectively. Meanwhile, researchers obtained comparable bacteriostatic activity of polysaccharides against *E. coli* and *S. aureus*. For

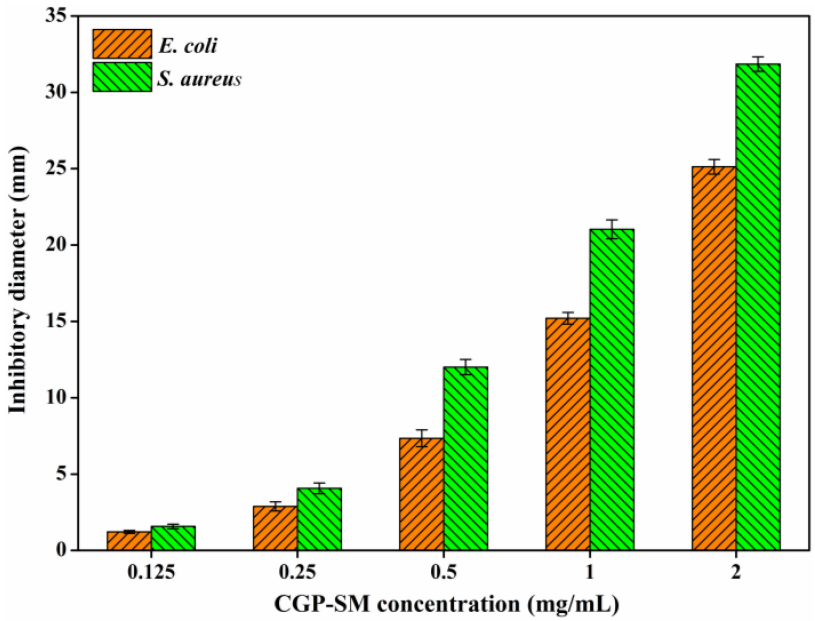

FIGURE 6 | Antibacterial activity of CGP-SM against *Escherichia coli* and *Staphylococcus aureus* with different concentrations.

instance, Qiu et al. (39) demonstrated that the antibacterial activity of β-glucan oligosaccharides against *S. aureus* and *E. coli* increased with the increase of its concentration, and its inhibitory effect on *S. aureus* was higher than that of *E. coli*. Meanwhile, Meng et al. (40) reported that a water-soluble *Diaphragma juglandis* polysaccharide had a higher inhibitory effect on *S. aureus* than *E. coli*. However, Jiang et al. (41) found that mung bean (*Vigna radiate*) skin polysaccharide had antibacterial activity against *S. aureus*, but not *E. coli*. There are many factors, such as environmental conditions, polysaccharide structure, and microbial species that could influence the bacteriostatic effect of polysaccharides, and the antibacterial mechanisms of different polysaccharides are also varied (42). Furthermore, the antibacterial mechanisms of CGP-SM against *S. aureus* and *E. coli* will be analyzed in future work.

CONCLUSION

With the rapid development of microbial fermentation and biocatalysis transformation technology over the last decade, increasing numbers of value-added bio-products have been produced from molasses by microbial conversion. In the present work, an antibacterial polysaccharide of CGP-SM was produced from sugarcane molasses by *C. globosum* CGMCC 6882 with submerged cultivation, but its yield was only 5.83 ± 0.09 g/l. Although this work provides help for the production of bioactive polysaccharide from low-cost molasses with the environmentally microbial process, how to achieve the efficient production of bioactive polysaccharides through molasses pretreatment, microbial gene reconstruction, and fermentation process optimization will be the focus of future research.

DATA AVAILABILITY STATEMENT

The original contributions presented in this study are included in the article/**Supplementary Material**, further inquiries can be directed to the corresponding authors.

AUTHOR CONTRIBUTIONS

LM contributed to the conception, design, and funding of the study. XG, JY, XZ, and KM organized the database. LW wrote the first draft of the manuscript. QS and ZW contributed to the writing—review and editing. All authors contributed to the article and approved the submitted version.

FUNDING

This work was supported by the Program for Science & Technology Innovative Research Team in University of Henan Province (21IRTSTHN025), the Natural Science Foundation of Henan Province (212300410131), the National Engineering Laboratory, Provincial Key Laboratory of Food Science Discipline, Henan University of Technology (NL2021006), and the Natural Science Foundation of Chongqing (cstc2019jcyj-msxmX0459).

SUPPLEMENTARY MATERIAL

The Supplementary Material for this article can be found online at: https://www.frontiersin.org/articles/10.3389/fnut.2022.935632/full#supplementary-material

REFERENCES

1. Hussain A, Zia KM, Tabasum S, Noreen A, Ali M, Iqbal R, et al. Blends and composites of exopolysaccharides; properties and applications: a review. *Int J Biol Macromol.* (2017) 94:10–27. doi: 10.1016/j.ijbiomac.2016.09.104
2. Wu J, Han X, Ye M, Li Y, Wang X, Zhong Q. Exopolysaccharides synthesized by lactic acid bacteria: biosynthesis pathway, structure-function relationship, structural modification and applicability. *Crit Rev Food Sci Nutrit.* [Online ahead of print]. (2022):1–22. doi: 10.1080/10408398.2022.2043822
3. Acosta SBP, Marchioro MLK, Santos VAQ, Calegari GC, Lafay CBB, Barbosa-Dekker AM, et al. Valorization of soybean molasses as fermentation substrate for the production of microbial exocellular β-glucan. *J Polym Environ.* (2020) 28:2149–60.
4. Amado IR, Vázquez JA, Pastrana L, Teixeira JA. Microbial production of hyaluronic acid from agro-industrial by-products: molasses and corn steep liquor. *Biochem Engine J.* (2017) 117:181–7.
5. Ji X, Peng B, Ding H, Cui B, Nie H, Yan Y. Purification, structure and biological activity of *Pumpkin* polysaccharides: a Review. *Food Rev Int.* (2021) 2021:1904973.
6. Ji X, Guo J, Ding D, Gao J, Hao L, Guo X, et al. Structural characterization and antioxidant activity of a novel high-molecular-weight polysaccharide from *Ziziphus Jujuba* cv. *Muzao*. *J Food Measure Characteriz.* (2022) 16:2191–200.
7. Wang Z, Liu X, Bao Y, Wang X, Zhai J, Zhan X, et al. Characterization and anti-inflammation of a polysaccharide produced by *Chaetomium globosum* CGMCC 6882 on LPS-induced RAW 264.7 cells. *Carbohydr Polymers.* (2021) 251:117129. doi: 10.1016/j.carbpol.2020.117129
8. Wang Z, Ning T, Gao K, He X, Zhang H. Utilization of glycerol and crude glycerol for polysaccharide production by an endophytic fungus *Chaetomium globosum* CGMCC 6882. *Preparat Biochem Biotechnol.* (2019) 49:807–12. doi: 10.1080/10826068.2019.1621895
9. Wang Z, Jia S, Cui J, Qu J, Yue Y, Sun Q, et al. Antioxidant activity of a polysaccharide produced by *Chaetomium globosum* CGMCC 6882. *Int J Biol Macromol.* (2019) 141:955–60.
10. Zhang S, Wang J, Jiang H. Microbial production of value-added bioproducts and enzymes from molasses, a by-product of sugar industry. *Food Chem.* (2021) 346:128860. doi: 10.1016/j.foodchem.2020.128860
11. Li M, Zi X, Zhou H, Hou G, Cai Y. Effects of sucrose, glucose, molasses and cellulase on fermentation quality and *in vitro* gas production of king grass silage. *Anim Feed Sci Technol.* (2014) 197:206–12.
12. Wu R, Chen D, Cao S, Lu Z, Huang J, Lu Q, et al. Enhanced ethanol production from sugarcane molasses by industrially engineered *Saccharomyces cerevisiae via* replacement of the *PHO4* gene. *RSC Adv.* (2020) 10:2267–76. doi: 10.1039/c9ra08673k
13. Singh RS, Kaur N, Kennedy JF. Pullulan production from agro-industrial waste and its applications in food industry: a review. *Carbohydr Polym.* (2019) 217:46–57. doi: 10.1016/j.carbpol.2019.04.050
14. Li Q, Zhou Y, Ke C, Bai Y, Liu X, Li S. Production of welan gum from cane molasses by *Sphingomonas* sp. FM01. *Carbohydr Polym.* (2020) 244:116485. doi: 10.1016/j.carbpol.2020.116485
15. Wang Z, Chen P, Tao N, Zhang H, Li R, Zhan X, et al. Anticancer activity of polysaccharides produced from glycerol and crude glycerol by an endophytic fungus *Chaetomium globosum* CGMCC 6882 on human lung cancer A549 cells. *Biomolecules.* (2018) 8:171. doi: 10.3390/biom8040171
16. Ai H, Liu M, Yu P, Zhang S, Suo Y, Luo P, et al. Improved welan gum production by *Alcaligenes* sp. ATCC31555 from pretreated cane molasses. *Carbohydr Polym.* (2015) 129:35–43. doi: 10.1016/j.carbpol.2015.04.033
17. Wang Z, Zhao X, Liu X, Lu W, Jia S, Hong T, et al. Anti-diabetic activity evaluation of a polysaccharide extracted from *Gynostemma pentaphyllum*. *Int J Biol Macromol.* (2019) 126:209–14. doi: 10.1016/j.ijbiomac.2018.12.231
18. Blumenkrantz N, Asboe-Hansen G. New method for quantitative determination of uronic acids. *Analyt Biochem.* (1973) 54:484–9.
19. Wang Z, Xue R, Cui J, Wang J, Fan W, Zhang H, et al. Antibacterial activity of a polysaccharide produced from *Chaetomium globosum* CGMCC 6882. *Int J Biol Macromol.* (2019) 125:376–82. doi: 10.1016/j.ijbiomac.2018.11.248
20. Li C, Fu X, Huang Q, Luo F, You L. Ultrasonic extraction and structural identification of polysaccharides from *Prunella vulgaris* and its antioxidant and antiproliferative activities. *Eur Food Res Technol.* (2015) 240:49–60.
21. Yan JK, Wang YY, Ma HL, Wang ZB. Ultrasonic effects on the degradation kinetics, preliminary characterization and antioxidant activities of polysaccharides from *Phellinus linteus* mycelia. *Ultrason Sonochem.* (2016) 29:251–7. doi: 10.1016/j.ultsonch.2015.10.005
22. Wang Z, He X, Yan L, Wang J, Hu X, Sun Q, et al. Enhancing enzymatic hydrolysis of corn stover by twin-screw extrusion pretreatment. *Industr Crops Products.* (2020) 143:111960. doi: 10.1016/j.biortech.2013.07.109
23. Wang Z, Yang Q, Wang X, Li R, Qiao H, Ma P, et al. Antibacterial activity of xanthan-oligosaccharide against *Staphylococcus aureus via* targeting biofilm and cell membrane. *Int J Biol Macromol.* (2020) 153:539–44. doi: 10.1016/j.ijbiomac.2020.03.044
24. Solaiman DKY, Ashby RD, Zerkowski JA, Foglia TA. Simplified soy molasses-based medium for reduced-cost production of sophorolipids by *Candida bombicola*. *Biotechnol Lett.* (2007) 29:1341–7. doi: 10.1007/s10529-007-9407-5
25. Chatterjee S, Guha AK, Chatterjee BP. Evaluation of quantity and quality of chitosan produce from *Rhizopus oryzae* by utilizing food product processing waste whey and molasses. *J Environ Manage.* (2019) 251:109565. doi: 10.1016/j.jenvman.2019.109565
26. Hou C, Yin M, Lan P, Wang H, Nie H, Ji X. Recent progress in the research of *Angelica sinensis* (Oliv.) Diels polysaccharides: extraction, purification, structure and bioactivities. *Chem Biol Technol Agricult.* (2021) 8:13.
27. Peng L, Qiao S, Xu Z, Guan F, Ding Z, Gu Z, et al. Effects of culture conditions on monosaccharide composition of *Ganoderma lucidum* exopolysaccharide and on activities of related enzymes. *Carbohydr Polym.* (2015) 133:104–9. doi: 10.1016/j.carbpol.2015.07.014
28. Zhang L, Ma L, Pan Y, Zheng X, Sun Q, Wang Z, et al. Effect of molecular weight on the antibacterial activity of polysaccharides produced by *Chaetomium globosum* CGMCC 6882. *Int J Biol Macromol.* (2021) 188:863–9. doi: 10.1016/j.ijbiomac.2021.08.059
29. Zheng L, Ma Y, Zhang Y, Meng Q, Yang J, Wang B, et al. Increased antioxidant activity and improved structural characterization of sulfuric acid-treated stepwise degraded polysaccharides from *Pholiota nameko* PN-01. *Int J Biol Macromol.* (2021) 166:1220–9. doi: 10.1016/j.ijbiomac.2020.11.004
30. Dou ZM, Chen C, Huang Q, Fu X. Comparative study on the effect of extraction solvent on the physicochemical properties and bioactivity of blackberry fruit polysaccharides. *Int J Biol Macromol.* (2021) 183:1548–59. doi: 10.1016/j.ijbiomac.2021.05.131
31. Cai M, Xing H, Tian B, Xu J, Li Z, Zhu H, et al. Characteristics and antifatigue activity of graded polysaccharides from *Ganoderma lucidum* separated by cascade membrane technology. *Carbohydr Polym.* (2021) 269:118329. doi: 10.1016/j.carbpol.2021.118329
32. Li B, Zhang N, Wang DX, Jiao L, Tan Y, Wang J, et al. Structural analysis and antioxidant activities of neutral polysaccharide isolated from *Epimedium koreanum* Nakai. *Carbohydr Polym.* (2018) 196:246–53. doi: 10.1016/j.carbpol.2018.05.037
33. Wang XT, Zhu ZY, Zhao L, Sun HQ, Meng M, Zhang JY, et al. Structural characterization and inhibition on α-d-glucosidase activity of non-starch polysaccharides from *Fagopyrum tartaricum*. *Carbohydr Polym.* (2016) 153:679–85. doi: 10.1016/j.carbpol.2016.08.024
34. Yu XH, Liu Y, Wu XL, Liu LZ, Fu W, Song DD. Isolation, purification, characterization and immunostimulatory activity of polysaccharides derived from American ginseng. *Carbohydr Polym.* (2017) 156:9–18. doi: 10.1016/j.carbpol.2016.08.092
35. Dou Z, Chen C, Fu X. The effect of ultrasound irradiation on the physicochemical properties and α-glucosidase inhibitory effect of blackberry fruit polysaccharide. *Food Hydrocoll.* (2019) 96:568–76.
36. López-Legarda X, Rostro-Alanis M, Parra-Saldivar R, Villa-Pulgarín JA, Segura-Sánchez F. Submerged cultivation, characterization and *in vitro* antitumor activity of polysaccharides from *Schizophyllum radiatum*. *Int J Biol Macromol.* (2021) 186:919–32. doi: 10.1016/j.ijbiomac.2021.07.084
37. Xiong F, Li X, Zheng L, Hu N, Cui M, Li H. Characterization and antioxidant activities of polysaccharides from *Passiflora edulis* Sims peel under different degradation methods. *Carbohydr Polym.* (2019) 218:46–52. doi: 10.1016/j.carbpol.2019.04.069

38. Rozi P, Abuduwaili A, Mutailifu P, Gao Y, Rakhmanberdieva R, Aisa HA, et al. Sequential extraction, characterization and antioxidant activity of polysaccharides from *Fritillaria pallidiflora* Schrenk. *Int J Biol Macromol.* (2019) 131:97–106. doi: 10.1016/j.ijbiomac.2019.03.029
39. Qiu Y, Ma Y, Huang Y, Li S, Xu H, Su E. Current advances in the biosynthesis of hyaluronic acid with variable molecular weights. *Carbohydr Polym.* (2021) 269:118320. doi: 10.1016/j.carbpol.2021.118320
40. Meng Q, Li Y, Xiao T, Zhang L, Xu D. Antioxidant and antibacterial activities of polysaccharides isolated and purified from *Diaphragma juglandis* fructus. *Int J Biol Macromol.* (2017) 105:431–7. doi: 10.1016/j.ijbiomac.2017.07.062
41. Jiang L, Wang W, Wen P, Shen M, Li H, Ren Y, et al. Two water-soluble polysaccharides from mung bean skin: physicochemical characterization, antioxidant and antibacterial activities. *Food Hydrocoll.* (2020) 100:105412.
42. Wang Z, Sun Q, Zhang H, Wang J, Fu Q, Qiao H, et al. Insight into antibacterial mechanism of polysaccharides: a review. *LWT Food Sci Technol.* (2021) 150:111929.

Conflict of Interest: The authors declare that the research was conducted in the absence of any commercial or financial relationships that could be construed as a potential conflict of interest.

Publisher's Note: All claims expressed in this article are solely those of the authors and do not necessarily represent those of their affiliated organizations, or those of the publisher, the editors and the reviewers. Any product that may be evaluated in this article, or claim that may be made by its manufacturer, is not guaranteed or endorsed by the publisher.

Copyright © 2022 Ma, Guo, Yang, Zeng, Ma, Wang, Sun and Wang. This is an open-access article distributed under the terms of the Creative Commons Attribution License (CC BY). The use, distribution or reproduction in other forums is permitted, provided the original author(s) and the copyright owner(s) are credited and that the original publication in this journal is cited, in accordance with accepted academic practice. No use, distribution or reproduction is permitted which does not comply with these terms.

frontiers | Frontiers in Nutrition

ORIGINAL RESEARCH
published: 21 June 2022
doi: 10.3389/fnut.2022.928972

Characterization of Structure and Antioxidant Activity of Polysaccharides From Sesame Seed Hull

Run-Yang Zhang, Jing-Hao Gao, Yi-Lin Shi, Yi-Fei Lan, Hua-Min Liu, Wen-Xue Zhu and Xue-De Wang**

Institute of Special Oilseed Processing and Technology, College of Food Science and Technology, Henan University of Technology, Zhengzhou, China

OPEN ACCESS

Edited by:
Qiu Li,
Qingdao Agricultural University, China

Reviewed by:
Ming-Guo Ma,
Beijing Forestry University, China
Diao She,
Northwest A&F University, China

***Correspondence:**
Hua-Min Liu
liuhuamin5108@163.com
Xue-De Wang
wangxuede1962@126.com

Specialty section:
This article was submitted to Food Chemistry, a section of the journal Frontiers in Nutrition

Received: *26 April 2022*
Accepted: *23 May 2022*
Published: *21 June 2022*

Citation:
Zhang R-Y, Gao J-H, Shi Y-L, Lan Y-F, Liu H-M, Zhu W-X and Wang X-D (2022) Characterization of Structure and Antioxidant Activity of Polysaccharides From Sesame Seed Hull. Front. Nutr. 9:928972. doi: 10.3389/fnut.2022.928972

Sesame seed hull is the major by-product of sesame seed processing and is rich in polysaccharides. In this work, sesame hull polysaccharides (SHP) were extracted by ultrasound-assisted alkali extraction methods with a yield of 6.49%. Three purified polysaccharide fractions were obtained after decolorization, deproteinization, and column chromatography. Then, their main composition and antioxidant activity were investigated. The dominant fraction was SHP-2 with a yield of 3.78%. It was composed of galacturonic acid (51.3%), glucuronic acid (13.8%), rhamnose (8.9%), glucose (8.4%), and others. The linkage types of SHP-2 have the α-D-Gal*p*A-(1,4)-linked, α-D-Glc*p*A-(1,2)-linked, β-T-D-Rha*p*-linked, β-D-Glc*p*-(1,6)-linked, β-T-D-Gal*p*-linked, α-L-Xyl*p*-(1,4)-linked, α-L-Ara*f*-(1,3,5)-linked, and β-D-Man*p*-(1,4)-linked. This study might provide some useful basic data for developing applications for sesame seed hull polysaccharides in the food and pharmaceutical industries.

Keywords: sesame seed, hull, polysaccharides, chemical structure, antioxidant activity

INTRODUCTION

Polysaccharide is a macromolecule found in almost all organisms. Structurally, polysaccharides are chains of monosaccharides connected by glycosidic linkages (1, 2). They have many functional and/or biological properties. The science of using polysaccharide-based substances in manufacturing health and biomedical products, cosmetics, human food, and animal feed is rapidly evolving (3–5). Rising demand is fueling the search for more and better sources of natural polysaccharides.

To meet this demand, particular attention has been paid to plant oil seeds, because the by-products of oil production are typically rich in polysaccharides (6). Sesame (*Sesamum indicum* L., Pedaliaceae) is a popular edible oil raw material in Asia and Africa (7). However, the oil derived from un-hulled sesame seeds is inferior due to the presence of bitter substances in the sesame hull, such as oxalic acid and tannin (8, 9). Therefore, dehulling is a critical operation during the

manufacture of sesame-based products, such as sesame oil, sesame protein, and sweetened sesame paste (10, 11). By weight, the hull constitutes 17.0–19.0% (see section "Materials and Chemical Reagents") of the whole sesame seed. Thus, during the dehulling process, a large amount of sesame hulls is produced as a production by-product. Currently, these hulls are usually simply discarded and not fully utilized, but it is rich in polysaccharides (42.7%) and contains high amounts of dietary fiber (25.6%) (12). Moreover, sesame hull was found to contain pectin with linear homogalacturonan as the main structure, with a yield of 9.72% and good free radical-scavenging ability (9). These characteristics suggest that sesame hulls might be a raw material of function polysaccharides and low-calorie foods. Nowadays, a wide range of polysaccharides has already found applications in human health, such as functional food and bioactive compounds. In addition, these polysaccharides generally have excellent antioxidant properties. According to epidemiological studies, natural antioxidants in the diet give rise to a lower probability of cardiovascular disease and cancer (2). Obviously, to promote the usage of waste sesame seed hulls, more information is needed as to chemical structure and biological activities of polysaccharides.

To date, most studies of dehulled sesame meals have been concerned with oil, flavonoids, and proteins (13). The polysaccharides of sesame have received little attention (9, 14). Furthermore, there is no research about the structural characterization of sesame hull polysaccharides. Therefore, the present knowledge of structural characterization and functional properties is deficient, and further study is required.

The aim of this work was to get purified polysaccharides from sesame hull and then characterizes its primary structure. In addition, the radical-scavenging assay and ferrous ion chelating assays were also carried out. These works might provide some useful information on the structural aspects of sesame hull polysaccharides for its applied research.

MATERIALS AND METHODS

Materials and Chemical Reagents

The seeds of sesame (*Zhengzhi 13,* white) were purchased from Henan Sesame Research Center and stored in the refrigerator (−20°C) before use. Sesame hulls were obtained according to previous reports (15, 16). The sesame seeds were soaked for 10 min in sufficient volume of distilled water at room temperature to allow the sesame skins to absorb water and swell and then knead them. The skins are broken into pieces and have broken away from the surface of the seeds, revealing the white-colored kernels. Both kernels and skins are then dried together in an oven (50°C) for 6 h. The crushed hulls shrink more and become smaller so that they can be sifted through a sieve (30 mesh) and collected. The ratio of hull mass to seed mass was between 17% and 19%, which was also the yield of hull. The dried hulls removed oil by the Soxhlet extraction method and placed in oven (50°C) for 6 h to evaporate excess solvent (16). Finally, samples were placed in desiccators before use. Furthermore, the protein content (4.41%) and ash content (33.05%) of defatted hulls were determined according to the AOCS methods (17). Potassium hydroxide, hydrochloric acid, ethanol, and toluene were analytical grade.

Isolation and Purification of Polysaccharide

This procedure was according to the previous studies (18, 19). Briefly, the dried defatted sesame hulls (1 g) were mixed with 25 mL KOH solution (5 wt%) at 50°C in an ultrasonic extractor for 30 min. Then, put in a water bath kettle with continuous magnetic stirring at 50°C for 3 h. After that, the filtrates were obtained through a suction filter and then neutralized to pH 5.5 with hydrochloric acid (6 mol/L). Then, the mixtures were centrifuged at 5,180 *g* for 35 min by a LD 5–10 centrifugal machine (Jingli Centrifuge Co., Beijing, China). Concentrate the liquid supernatant to 1/10 of its original volume by rotary vacuum evaporator and pour in 3 times anhydrous ethanol. After centrifugation, the precipitate was resolubilized and dialyzed for several days using a dialysis bag (Solarbio, 3,500 Da), until there is no salt in the dialysate. It is then concentrated again and freeze-dried for 48 h. At this stage, the yield of polysaccharides without deproteinization was 12.10%. It was then resolubilized, and the protein was removed by the Sevag method (20) and decolored with AB-8 resin (Solarbio). The polysaccharide solution was freeze-dried and labeled as SHP. Then, it was purified by column chromatography (cellulose DEAE-52, 55 mm × 300 mm, Solarbio) which eluted in sequence with NaCl solutions (0, 0.1,0.3, 0.5, and 0.7 mol/L) at 2 mL/min. Elution curves were drawn. The collected fractions were dialyzed and lyophilized. Three purified fractions were obtained and labeled as SHP-1, SHP-2, and SHP-3. The sugar content of the purified polysaccharides was detected by using the phenol–sulfuric acid method (21).

Monosaccharide Analysis

The monosaccharide composition was detected by the reported method (18). Briefly, samples (5.00 ± 0.05 mg) were blended with 125 μL 72% H_2SO_4 and 1.35 mL distilled water and then placed in a circulating hot air oven. Set the temperature to 105°C for 2.5 h. After that, the hydrolysate is neutralized and diluted 50 times with distilled water. Then, diluent was filtered through a filter (0.22 μm) and then was injected into the high-performance anion exchange chromatography (Dionex ICS-3000, Sunnyvale, CA, United States) which is equipped with CarbopacPA-20 column. The column temperature was set at 30°C, and flow rate was 0.5 mL/min; gradient elution was carried out at different times with different ratios of mobile phases: A (0.1 mol/L NaOH) and B (0.1 mol/L NaOH, 0.2 mol/L NaAc). The monosaccharide standards were also detected to make a standard curve graph. The peak areas of the corresponding compounds in the unknown samples were brought into the standard curve, and the concentrations were calculated.

Molecular Weight Distribution

The molecular weight distributions were determined according to Guo et al. (9, 22). The HPSEC (high-pressure size exclusion

chromatography, Malvern Viscotek TDA305max) is equipped with a Guard column, A6000M column, a refractive index detector (RID), and a low-angle light-scattering system (LALS). After preparation of polysaccharide solution (1 mg/mL), set parameters as follows: injection volume of 100 μL; the temperature of both column and detector temperature was 40°C; $NaNO_3$ (0.1 mol/L) containing NaN_3 (0.03 wt%) was used as the eluent solution with a flow rate of 0.7 mL/min.

Fourier Transform Infrared Spectrometer Analyses

Dried polysaccharide samples with KBr powder were ground. The Nicolet iN10 Fourier transform infrared spectrophotometer (Thermo Nicolet Corporation, United States) was used to characterize the FTIR (Fourier transform infrared spectrometry) spectra of the polysaccharide samples. The spectra were recorded between 400 cm^{-1} and 4,000 cm^{-1} (23).

Scanning Electron Microscopic Observations

A scanning electron microscope (SEM, Quanta 250FEG, FEI, United States) was used to characterize sample morphology according to the previous study (24). The polysaccharide sample was coated with gold, and then, images were captured using an accelerating potential of 3 kV with 1,000–5,000 × magnification under a high vacuum.

Thermal Measurements

Thermal stability was determined according to the previous study (25). The samples (about 10 mg) were weighed and placed in a NETZSCH STA-449C thermal gravimetric analyzer and then heated at a rate of 10°C /min from 45°C to 700°C with stable nitrogen flow at 50 mL/min.

Methylation and GC-MS of Polysaccharides

In this work, the SHP-2 was reduced to neutral polysaccharides with EDC and $NaBH_4$ according to the previous report (26). The methylation analysis was according to the previous studies (22, 27) with modifications. In brief, dissolve 2 mg reduced product in DMSO by heating in an ultrasonic water bath. About 20 mg of sodium hydroxide powder was added, charged with nitrogen, and sonicated for 20 min. After cooling, methyl iodine (0.3 mL) was added to start a methylation reaction. Then, the reaction was terminated by adding sodium thiosulfate solution. The methylated polysaccharide was extracted by chloroform and then was hydrolyzed at 120°C for 4 h in 0.5 mL TFA (2 mol/L). Then, it was cool to room temperature and blow-dry with nitrogen. The hydrolysis product was reduced with $NaBD_4$, acetylated with acetic anhydride/pyridine (1:1 v/v), and then finally extracted with dichloromethane. Then, the product was analyzed by the Agilent Technologies 7890B-7000C gas chromatography–mass spectrometry. The apparatus was equipped with a HP5-ms quartz capillary column, and the column size was 30 m × 0.25 mm × 0.25 μm. Experiment parameters were based on the literatures (28, 29). Set the temperature to 80°C and hold for 3 min, heat to 250°C at a rate of 10°C/min, and then hold for 10 min; carrier gas was helium (1 mL/min); injection temperature was 250°C, and injection volume was 1 μL. For the MS, electron impact ion source was used; set the temperature of ion source at 250°C, ionization energy of 70 eV, and mass range from 33 to 400 amu.

NMR Spectroscopy Analyses

The ^1H and ^{13}C NMR spectroscopy, HSQC (heteronuclear single-quantum coherence), ^1H-^1H COSY (correlation spectroscopy), and HMBC (heteronuclear multiple-bond correlation) spectroscopy were observed by a Bruker ARX500 NMR spectrometer (Brucker, Rheinstetten, Germany) at 297.3 K according to previous report (28). Sample (50 mg) was dissolved in deuterated water (D_2O, 99.9%, Sigma, United States) and freeze-dried and repeated several times to completely replace the H_2O by D_2O. Finally, the polysaccharide was dissolved in deuterated water (99.9%) and poured into the NMR tube. In the hydrogen spectrum, the peak of deuterated water was used to calibrate the chemical shift. For the determination of the carbon spectrum, the chemical shifts were calibrated using tetramethylsilane as an external standard. The data were analyzed by Bruker Topspin-NMR software 4.0.

Antioxidant Activities of Polysaccharides

The antioxidant activities of sesame hull polysaccharide were investigated as reported previously with modifications (30, 31). The various concentrations of polysaccharide solutions were prepared by dissolving polysaccharide samples in ultrapure water; they were then stored at 4°C until needed.

Hydroxyl Radical (OH)-Scavenging Activity Assay

$FeSO_4$ solution (50 μL, 1.8 mmol/L) and salicylic acid solution (50 μL, 1.8 mmol/L) were added to 50 μL polysaccharide solutions in turn. Then, 50 μL H_2O_2 solution (0.3%) was added. After 35 min, the absorbance of mixtures was detested at 510 nm. The same concentration of ascorbic acid (VC) solution was determined by the same method. The scavenging rate was obtained using the following formula:

$$\cdot OH \text{ scavenging activity } (\%) = \frac{A_0 - (A_1 - A_2)}{A_0} \times 100\% \quad (1)$$

where A_1 is the absorbance of the solution with the sample added, A_0 is the absorbance without sample, and A_2 is the absorbance of the sample solution without H_2O_2 solution.

DPPH (1,1-Diphenyl-2-Picrylhydrazy) Radical-Scavenging Activity

Polysaccharide solution (50 μL) was blended and reacted with 150 μL of 0.1 mmol/L DPPH solution for 30 min in a dark environment. A Multiskan FC automatic microplate reader (Thermo Fisher Scientific, Waltham, MA, United States) was used to obtain the absorbance. Ascorbic acid (VC) was also

detected as the positive control. The scavenging rate was obtained by the following formula:

$$\text{DPPH radical scavenging activity (\%)} = \frac{A_0 - (A_1 - A_2)}{A_0} \times 100\% \quad (2)$$

where A_0 is the absorbance of the mixture of deionized water and DPPH solution, A_1 is the absorbance of the mixture of polysaccharide solution with DPPH solution, and A_2 is the absorbance of the mixture of polysaccharide solution with deionized water.

DMPD (*N*, *N*-Dimethyl-p-Phenylenediamine Dihydrochloride) Radical-Scavenging Activity

One milliliter of DMPD solution (0.1 mol/L) was prepared and added to 100 mL 0.1 mol/L acetate buffer (pH 5.25). Then, 0.2 mL of 0.05 mol/L ferric chloride solution was added, thereby creating the $DMPD^{\cdot+}$ (colored radical cation) in the solution. Polysaccharide solution (50 μL) was added to the $DMPD^{+}$ solution (200 μL). After 10 min at 25°C, the absorbance was detected at 510 nm. The scavenging activity was calculated according to the following formula:

$$\text{DMPDradical scavenging activity(\%)} = \frac{A_0 - (A_1 - A_2)}{A_0} \times 100\% \quad (3)$$

where A_0 is the absorbance of the mixture of acetate buffer and $DMPD^{\cdot+}$ solution, A_1 is the absorbance of polysaccharide solution sample with $DMPD^{\cdot+}$ solution, and A_2 is the absorbance of polysaccharide solution sample with acetate buffer.

Ferrous Ion (Fe^{2+}) Chelating Ability

About 50 μL polysaccharide solution was prepared and mixed with 100 μL of 0.1 mmol/L $FeSO_4$ solution, and then, 50 μL ferrozine solution (2.0 mmol/L) was added. The mixed solution was placed in dark environment for 10 min. The absorbance of sample was observed at 562 nm. The EDTA-2Na (Ethylene diamine tetraacetic acid disodium salt) was used as the control. The result was obtained using the following formula (4):

$$Fe^{2+} \text{ chelating activity (\%)} = \frac{A_0 - (A_1 - A_2)}{A_0} \times 100\% \quad (4)$$

where A_0 is the absorbance of the blank control solution, A_1 is the absorbance of the mixture containing both reaction solution and sample, and A_2 is the absorbance of the mixture containing both deionized water and sample.

Statistical Analysis

The data were analyzed by SPSS Statistics 23.0. All of the data were expressed as mean ± standard deviation (SD). The significance of differences among mean comparisons was calculated using Duncan's multiple range test with a significance level of 0.05.

RESULTS AND DISCUSSION

Yield and Morphology of Purified Polysaccharide Fractions

The yield of SHP was 6.49%, which was based on the weight of sesame hull, before fractionation by ion-exchange chromatography. In a study that also used ultrasound assistance, the yield of polysaccharides extracted from mulberry fruits was 3.13% (32). In another study, the yield polysaccharides from the *Moringa oleifera* Lam. leaf by microwave extraction was about 2.96% (33). Hence, the polysaccharide content of the sesame hull is relatively rich. After fractionation, the elution curve (**Figure 1A**) revealed that SHP consisted mainly of three fractions and the yield is 1.40% (SHP-1), 3.78% (SHP-2), and 1.06% (SHP-3), respectively. The total sugar content was 93.90% (SHP-1), 98.00% (SHP-2), and 91.10% (SHP-3), respectively. The peaks were clearly separated, which indicated that the three fractions had been effectively isolated from SHP. Protein content, calculated using the Bradford procedure (34), was 0.78% (SHP-1), 1.67% (SHP-2), and 1.29% (SHP-3).

Morphologies of SHP-1, SHP-2, and SHP-3 are shown in **Figure 1E**. Actually, the surface morphology of dried samples *via* SEM was very likely to be related to their lyophilization method or process. In this study, the apparent appearance of several purified polysaccharides being lyophilized under the same conditions is presented. SHP-1 appears very chaotic, irregular, and fragmented, with strips, sheets, curls, and an uneven surface. In contrast, SHP-2 appears as smooth, large flakes (about 100 μm) with some holes, while SHP-3 is a long strip (< 40 μm), narrower than SHP-2. The differences might be associated with different network structures and branches inside the samples (35, 36).

Monosaccharide Composition

The sugar compositions of the purified polysaccharide fractions are shown in **Table 1**. The SHP-1 contained mostly galactose (41.4%), xylose (31.9 %), and arabinose (18.8%) with small amounts of glucose (2.3%), glucuronic acid (2.2%), and galacturonic acid (3.4%) units. In contrast, SHP-2 was rich in galacturonic acid (51.3%) and glucuronic acid (13.8%) together with arabinose (5.7%), galactose (4.7%), glucose (8.4%), xylose (5.9%), rhamnose (8.9%), and mannose (1.3%). SHP-3 also contained large amounts of galacturonic acid (64.1%), indicating that both SHP-2 and SHP-3 fractions were pectic-type polysaccharides (37, 38).

Molecular Weight Distribution

The biological and chemical activities of polysaccharides are closely related to molecular weight and distribution of molecular weights; hence, understanding these parameters is necessary for assessing their potential applications in industry (39, 40). The molecular weight distribution of these samples can be seen in **Figure 1B**. There was one peak in SHP-1 and SHP-2 and two peaks in SHP-3. This indicates that SHP-3 polysaccharide molecules had a wide molecular weight distribution characteristic, and the homogeneity of

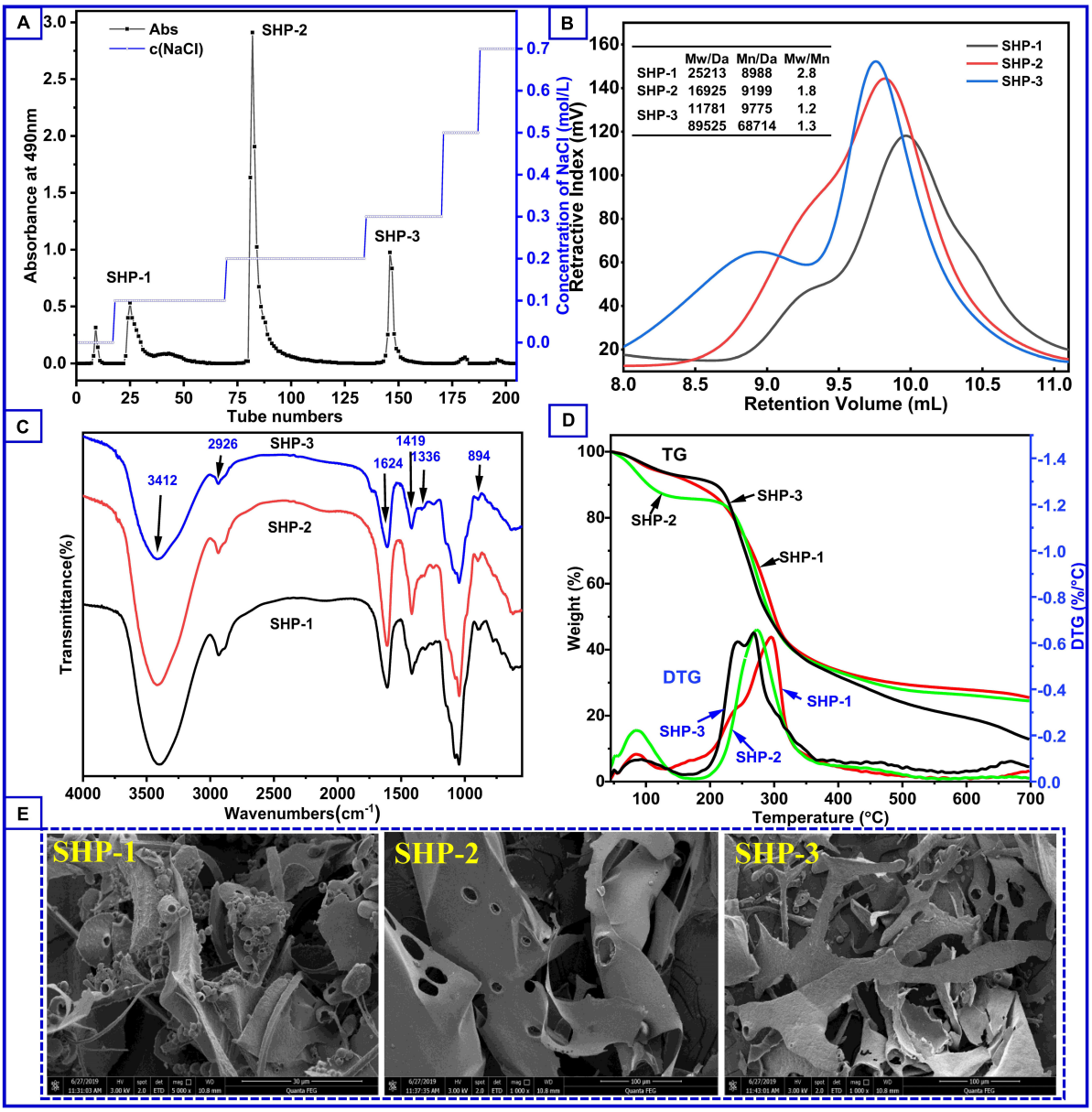

FIGURE 1 | (A) Content of polysaccharide fractions obtained by elution at different salt concentrations during column chromatography. **(B)** Molecular weight distribution of polysaccharide samples. **(C)** Fourier transform infrared spectroscopy of polysaccharide samples. **(D)** Thermogravimetry curves (left axis) and derivative thermogravimetry curves (right axis) of SHP-1, SHP-2, and SHP-3. **(E)** The scanning electron microscope of the samples.

SHP-3 was worse than other samples. Moreover, there were two components with different molecular weight in SHP-3, and weight average molecular weight (Mw) was 11,781 Da and 89,525 Da, respectively. Mw is an important data to measure chain length of polysaccharides molecules. The Mw of SHP-1 and SHP-2 was 25,213 Da and 16,925 Da, respectively. Their polydispersity indexes (Mw/Mn) were 2.805 (SHP-1) and 1.840 (SHP-2), respectively. Therefore, the polydispersity indexes of SHP-2 are smaller relative to the SHP-1, which indicates that SHP-2 has a better homogeneity than SHP-1.

FTIR Characterization

FTIR spectroscopy is commonly used to identify characteristic organic groups and some chemical bonds of polysaccharides (41, 42). The spectra of purified polysaccharide in the range from 4,000 to 500 cm^{-1} are shown in **Figure 1C**. These fractions showed similarity in the main absorption spectra, but exhibited difference in peak intensity. Two absorption bands (2,800–3,500 cm^{-1} and 500–1,700 cm^{-1}) were clearly observed for the three polysaccharides. The appearance of a sharp and strong peak between 3,600 and 3,200 cm^{-1} is associated with -OH stretching due to the large number of intra-molecular and inter-molecular

hydrogen bonds in samples (39, 43). Peaks at 2,926 cm^{-1} are associated with asymmetric and symmetric stretching of CH_2. Stretching peaks at around 1,624 cm^{-1} correspond to free carboxyl groups (1,700–1,600 cm^{-1}), while those at around 1,336 cm^{-1} and 1,419 cm^{-1} are associated with the vibration of C-O stretching in symmetric COO- (1,300–1,400 cm^{-1}) (44). The result suggests that there are uronic acid components in SHP-1, SHP-2, and SHP-3 and is in agreement with sugar composition analysis results (**Table 1**). The absorption band range from 1,300 to 1,000 cm^{-1} is designated as the fingerprint region and is characterized by vibrations of several types of bonds in carbohydrate rings, including C-O-C and C-O. These peaks indicate the presence of a pyran-type structure in all three fractions (45, 46). The peak at approximately 894 cm^{-1} is related to β-glycosidic linkages in polysaccharide chains, and the peak at 844 cm^{-1} can be associated with α-pyranose (22). Therefore, the FTIR spectra of these purified polysaccharide fractions all have absorption peaks typical of heteropolysaccharides.

Thermal Analysis

Thermal stability data represent information necessary for polysaccharides' applications in the food and biopharmaceuticals industries (23). The thermogravimetric curve can be used to analyze the weight loss and thermal behavior of samples. The DTG (derivative thermogravimetry) curve helps to determine the maximum value of a mass loss process and assists us in identifying some of the smaller mass loss processes. It can also be used in processes that indicate whether a chemical or physical reaction is taking place at a certain temperature stage. The thermogravimetric (TG) curve to temperature (or time) (**Figure 1D**) shows three stages of degradation. The initial stage of mass loss occurred from 45°C to 150°C and was because of the evaporation of water. The losses were 5.9% (SHP-1), 12.3% (SHP-2), and 5.6% (SHP-3). A significant peak in this temperature range can also be seen in the DTG curve, which indicates that a significant weight loss does occur. Moreover, SHP-2 volatilizes a large number of small molecules (i.e., water) compared to the other two fractions. The second stage (150–350°C) was associated with the decomposition and depolymerization of the chemical structure (9), and the fractions lost weight of 68.6% (SHP-1), 63.3% (SHP-2), and 81.6% (SHP-3). In the DTG curve, the maximum peak value represents the maximum rate of sample mass loss. Therefore, mass loss is fastest at this stage, with maximum loss rates at 294.8°C, 273.1°C, and 266.9°C for SHP-1, SHP-2, and SHP-3, respectively. Apparently, SHP-3 reached its fastest decomposition temperature much earlier. The third stage of mass loss was between 350 and 600°C, and the percentages of weight loss were found to be 25.5% (SHP-1), 24.5% (SHP-2), and 12.8% (SHP-3). The loss of quality at this stage is relatively small and might be related to the oxidation of carbonaceous organic material (16, 47). In general, if the polymers in the sample are relatively stable, then only the small molecular weight molecules are lost below 300°C in the nitrogen environment. Whereas range from 300 to 600°C, the organic polymers are mostly degraded and volatilized. Then, the stable inorganic compounds remain above 600°C. However, for the polymers containing ring and aromatic structures, they do not fully volatilize above 600°C, but form the charcoal residue. Therefore, the change in mass loss is almost minimal above 600°C, as can also be seen from the DTG curves (6, 18). By understanding the changes in these polysaccharide fractions, it is possible to provide these thermodynamic aspects for their application studies.

Methylation and NMR Spectra Analysis

From the results of the previous work, SHP-2 is the main component of sesame hull polysaccharides. Meanwhile, it has the most homogeneous molecular weight distribution and possesses a good antioxidant activity. Therefore, a more in-depth structural characterization of SHP-2 was carried out.

The methylation analysis is the most widely method to obtain the glycosidic linkages in structural polysaccharide chemistry. It involves exhaustive methylation and hydrolysis of the polysaccharide to a mixture of monomeric methylated sugars, which are then separated, identified, and quantified. The positions of glycosidic linkages in the polysaccharide correspond to the positions of unsubstituted hydroxyl groups in these methylated monosaccharides (48, 49). The Fourier infrared spectra of SHP-2 before and after methylation can be seen in **Supplementary Figure 1**. After methylation treatment, the peak of FTIR spectra near 3,400 cm^{-1} is almost disappeared, which proved that the methylation was completed. The GC-MS spectra of PMAAs (partially methylated alditol acetate) for SHP-2 are shown in **Supplementary Figure 2**. The analysis of PMAAs was assessed using the standard database from the Complex Carbohydrate Research Center of University of Georgia combining the ionization pattern of PMAAs, and then, the result

TABLE 1 | Monosaccharide compositions of purified polysaccharides of sesame hulls.

Samples	Molar composition[a] (mol%)							
	Ara[b]	Gal	Glc	Xyl	Rha	Man	GlcA	GalA
SHP-1	18.8	41.4	2.3	31.9	n.d.	n.d.	2.2	3.4
SHP-2	5.7	4.7	8.4	5.9	8.9	1.3	13.8	51.3
SHP-3	12.5	13.1	n.d.[c]	10.3	n.d.	n.d.	n.d.	64.1

[a] *Expressed in relative molar percentages.*
[b] *Ara, arabinose; Gal, galactose; Glc, glucose; Xyl, xylose; Fuc, fructose; Rib, ribose; Rha, Rhamnose; Man, mannose; GlcA, glucuronic acid; GalA, galacturonic acid; SHP-1, SHP-2, and SHP-3 were three purified fractions of sesame hulls polysaccharide, respectively.*
[c] *ND, not detectable.*

was shown in **Table 2**. The primary ions formed during the ionization of PMAA at EI follow a pattern: (1) The break between two methylated carbon atoms is the easiest and the resulting ions are more abundant; (2) when the break occurs between a methylated carbon atom and an acetylated carbon atom, the cationic fragment containing the methylated carbon atom is formed first; (3) the break between two acetylated carbon atoms is less likely to occur and therefore the resulting ions are less abundant. The resulting ion abundance is also very low. Besides, the groups, such the -HOAc (m/z 60), -CH_2CO (m/z 42), and -CH_3OH (m/z 32), break away from the primary ion to form the secondary ion with the corresponding ion abundance (28, 50). Taking 1,5-Tri-*O*-acetyl-1-deuterio-2,3,4,6-tri-*O*-methyl-D-galactitol (derived from 1-linked-D-Gal*p*) as an example, the mass fragmentation was mainly m/z 71, 87, 101, 102, 118, 129, 145, 161, 162, and 205. Similarly, all the inter-glycosidic linkage patterns were obtained as shown in the following: T-Rha*p*(1→, →4)-Xyl*p*(1→,T-Gal*p*(1→, →3,5)-Ara*f*(1→, →2)-Glc*p*(1→, →4)-Gal*p*(1→, →4)-Man*p*(1→, →6)-Glc*p*(1→ with the molar ratio of 12.2 : 4.6 : 3.2 : 4.2 : 21.1 : 42.1 : 2.9 : 9.7. The ratio was approximately consistent with the monosaccharide analysis.

The methylation analysis provides quantitative information but no information on the relative order of the sugar residues or on their anomeric nature. Determination of the complete structure of a polysaccharide requires complementary analyses, such as by NMR. The anomeric proton signal in low field (δ > 5.00 ppm) was generally attributed to the α-glycosidic conformation, and 4.30–5.00 ppm was assigned to β-glycosidic (49, 51). The anomeric proton signals were obtained from the ^{1}H NMR spectra at δ 4.54, 4.59, 5.24, 4.44, 5.34, 5.05, 4.98, and 4.92 ppm, respectively (**Figure 2A**). There was no absorption in the range of 6–8 ppm, indicating that there were no ferulic acid nor phenols in SHP-2 (52). The chemical shifts of anomeric carbons occur at 90.0–110.0 ppm. The ^{13}C NMR spectrum (**Figure 2B**) showed eight peaks: 101.3, 104.1, 97.6, 101.7, 107.5, 99.1, 97.6, and 103.3 ppm, respectively. Several typical peaks also corroborated the monosaccharide composition. The signals at 173.7 and 176.8 ppm implied the presence of glucuronic acid or galacturonic acid, respectively. There was a strong peak at 3.58 ppm in ^{1}H-NMR spectra, which confirmed the existence of -O-CH_3 group in glucuronic acid and galacturonic acid. The anomeric proton signals and carbon signals were matched one to one from the HSQC (heteronuclear single-quantum coherence) NMR spectra (**Figure 2D**). They were 101.3/4.54, 104.1/4.59, 97.6/5.24, 101.7/4.44, 107.5/5.34, 99.1/5.05, 97.6/4.98, and 103.3/4.92 ppm, respectively. The chemical shifts of β-*D* or α-L configurations were in the range of 100–110 ppm, the signals of α-D or β-L configuration were in the region of 90–100 ppm, and these rules can be used to determine their configurations (53, 54). Then, the analysis is continued by H, H-COSY (correlation spectroscopy) spectrum (**Figure 2C**) with the signal 101.3/4.54 as an example. δ 4.17 ppm can be assigned to H-2 due to its correlation with H-2 (4.54 ppm) from the COSY spectrum and published data. Similarly, the chemical shifts of H3, H4, H5, and H6 were assigned to 3.74, 3.51, 3.49, and 1.22 ppm, respectively. Then, the correlation with C-1 to C-6 can be found in the HSQC spectrum and was 101.3, 71.4, 81.1, 73.4, 72.3, and 17.4 ppm, respectively. Besides, it is also possible to verify the signal by capitalizing on two- and three-bond couplings in HBMC (Heteronuclear Multiple Bond Coherence) spectra

TABLE 2 | Methylation analysis result of SHP-2.

PMAAs (partially methylated alditol acetates)		Linkage patterns	Major mass fragment (*m/z*)	Retention time (min)	Relative amount /mol%
A	2,3,4-Me_2-Rha*p*	T-Rha*p*(1→	43, 59, 72, 89, 102, 118, 131, 162, 175, 203	11.90	12.2
B	2,3-Me_2-Xyl*p*	→4)-Xyl*p*(1→	43, 59, 71, 87, 102, 118, 129, 145, 162, 189, 207, 253	13.11	4.6
C	2,3,4,6-Me_4-Gal*p*	T-Gal*p*(1→	43, 59, 71, 87, 102, 118, 129, 145, 161, 162, 175, 205	13.94	3.2
D	2-Me-Ara*f*	→3,5)-Ara*f*(1→	43, 59, 74, 85, 99, 118, 130, 142, 160, 207, 261	14.41	4.2
E	3,4,6-Me_3-Glc*p*	→2)-Glc*p*(1→	43, 59, 71, 87, 101, 129, 145, 161, 174, 190, 205, 234	15.20	21.1
F	2,3,6-Me_3-Gal*p*	→4)-Gal*p*(1→	43, 57, 71, 85, 99, 118, 129, 147, 161, 233, 281, 305	15.61	42.1
G	2,3,6-Me_3-Man*p*	→4)-Man*p*(1→	43, 87, 99, 118, 129, 147, 173, 208, 233	15.81	2.9
H	2,3,4-Me_3-Glc*p*	→6)-Glc*p*(1→	43, 59, 71, 87, 102, 118, 129, 143, 162, 173, 189, 233	16.51	9.7

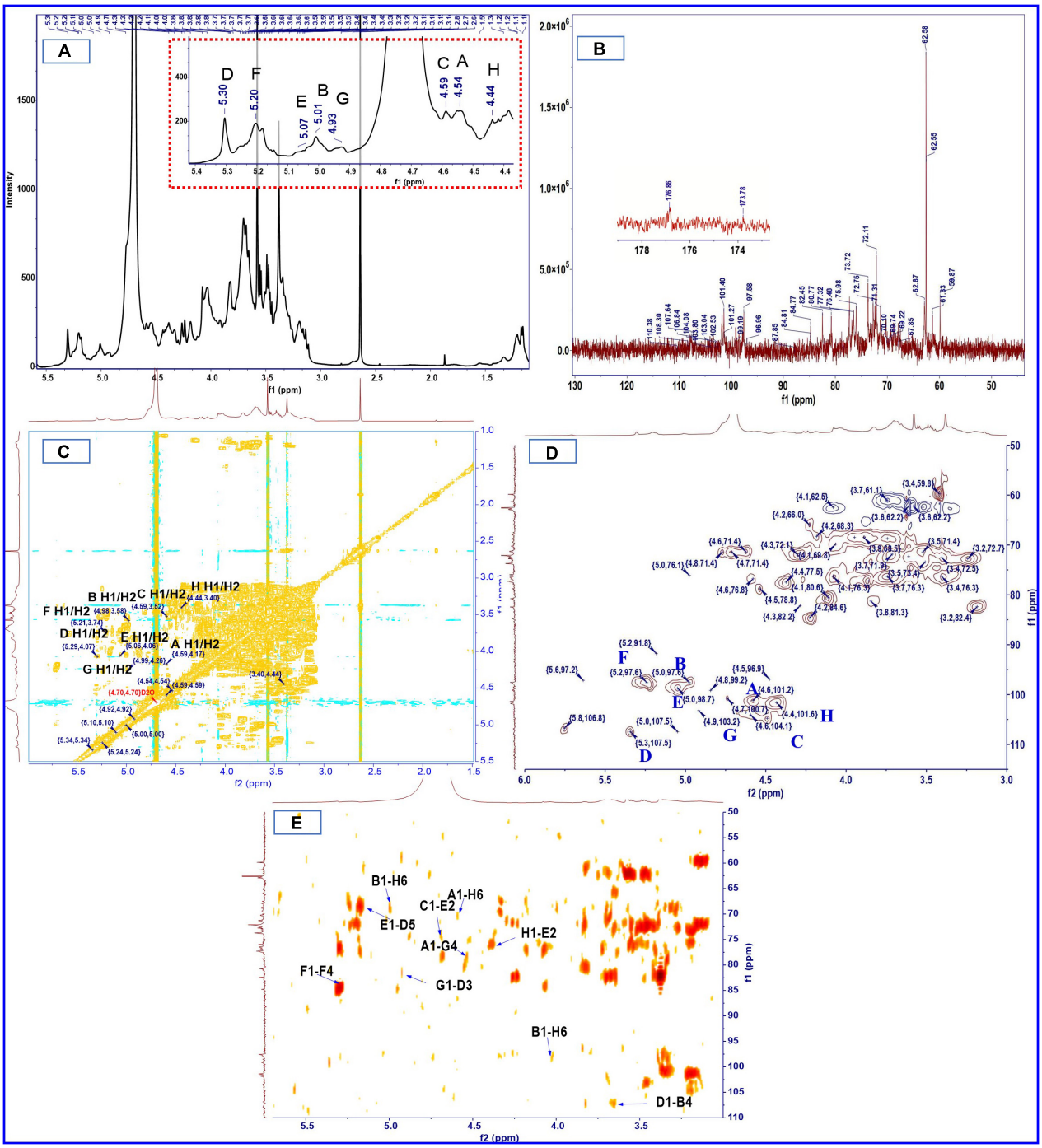

FIGURE 2 | ^{1}H **(A)**, ^{13}C **(B)**, COSY **(C)**, HSQC **(D)**, and HMBC **(E)** spectra of SHP-2.

(**Figure 2E**). For instance, the correlation can be found between C-2/C-3 and H-1 in one monosaccharide sugar unit or polymers. Therefore, combining the above analysis and reference (55), these chemical shifts were attributed to the T-β-L-Rha*p* (A). In the same way, through the analysis of data and references (56–63), every residue (A-H) was identified, and the chemical shifts are list in **Table 3**.

The order and position of the linkage between monosaccharide residues can be further inferred from HMBC. The HMBC spectrum (**Figure 2E**) indicated that C-1 of residue A (T-β-L-Rha*p*) was correlated with the H-6 of residue H (1,6-linked-β-D-Glc*p*) and H-4 of residue G (1,4-linked-β-D-Man*p*), namely A C1/H6 H; A C1/H4 G. Similarly, C-1 of residue H was correlated with the H-2 of 1, 2-linked-α-D-Glc*p*A (H C1/H2 E);

TABLE 3 | Chemical shifts of resonances in the ^{1}H and ^{13}C NMR spectra of SHP-2.

	Sugar residues	Chemical shifts (ppm)					
		C1/H1	C2/H2	C3/H3	C4/H4	C5/H5	C6/H6
A	T-β-L-Rha*p*(1→	101.3/4.54	71.4/4.17	81.1/3.74	73.4/3.51	72.3/3.49	17.4/1.22
B	→4)-α-D-Xyl*p*(1→	97.6/4.98	72.3/3.53	73.9/3.75	70.4/3.65	62.2/3.58	-
C	T-β-D-Gal*p*(1→	104.1/4.59	71.6/3.52	74.1/3.68	69.7/3.96	76.6/3.74	62.4/3.53
D	→3,5)-α-L-Ara*f*(1→	107.5/5.34	80.8/4.01	82.1/4.29	82.1/4.09	68.5/3.89	-
E	→2)-α-D-Glc*p*A(1→	99.1/5.05	76.3/4.10	72.4/3.74	72.1/4.30	71.4/4.60	173.7/-
F	→4)-α-D-Gal*p*A(1→	97.6//5.24	68.7/3.74	70.1/4.05	84.6/4.23	77.6/4.36	176.8/-
G	→4)-β-D-Man*p*(1→	103.3/4.92	71.9/4.32	74.5/3.98	78.1/4.04	76.4/3.73	62.6/4.09
H	→6)-β-D-Glc*p*(1→	101.7/4.44	72.3/3.40	76.3/3.55	69.2/3.58	76.3/3.61	69.8/4.07

C-1 of residue D corresponded to H-4 of 1,4-linked-α-D-Xyl*p* (D C1/H4 B); C-1 signal of 1, 2-linked-α-D-Glc*p*A correlates with the H-5 of 1,3,5-linked-α-L-Ara*f* (E C1/H5 D); H-6 of residue H was correlated with C-1 signal of residue B (B C1/H6 H); C-1 of residue G was corresponded to H-3 of residue D (G C1/H3 D). It is worth noting that C-1 signal of 1,4-linked-α-D-Gal*p*A correlates with the H-4 of 1,4-linked-α-D-Gal*p*A (F C1/H4 F), while C-4 of residue F correlates with the H-1 of another residue F (F C4/H1 F). No linkage signal seems to be found for residue F to other residues, so multiple residues F may be linked to each other to form a chain-like structure. In addition, a previous study of our laboratory also showed the presence of pectin polysaccharides in sesame hulls (9). Therefore, the HG (homogalacturonan) which is a linear polymer composed of 1,4-linked galacturonic acid and commonly found in pectin polysaccharides (64) might be present in SHP-2. In addition, based on the above-mentioned galacturonic acid of 51.3%, it can be inferred that HG is the dominant main component of SHP-2.

Antioxidant Activity *in vitro*

The antioxidant ability exerted by different antioxidants requires different evaluation methods (65). Accordingly, several different methods have been used for the assessment of antioxidant ability in this study, and the results are analyzed and discussed as follows.

Hydroxyl Radical (·OH) Scavenging Activity

The·OH can react readily association with many kinds of biomacromolecule in the body, such the lipids, proteins, and cell DNA, while excess free radicals would cause damage in tissue and even death of cell (66). Therefore, clearing excess hydroxyl radicals might be necessary to keep the human body healthy. The scavenging activity of polysaccharides is largely due to the hydrogen supplied from polysaccharides contact with radicals and stabilizing their chemical properties and then terminates the radical chain reaction of free radicals. Another possibility is that the polysaccharide combines with key radical ions in a chain reaction that causes the free radical chain to end (67). The results are presented in **Figure 3A**. Among all crude polysaccharide and purified fractions, the hydroxyl radical-scavenging ability can be ranked in the following order: SHP > SHP-3 > SHP-2 > SHP-1. The scavenging abilities of polysaccharide samples were lower than VC in terms of hydroxyl radical activity ($P < 0.05$). The scavenging activities were 83.06 %, 80.79 %, 63.19 %, 53.95 %, and 99.97% for the SHP, SHP-3, SHP-2, SHP-1, and ascorbic acid at a concentration of 5 mg/mL, respectively. This result demonstrated that SHP possessed the strongest scavenging activities, and SHP-3 showed the best activities among the purified fractions.

DPPH-Free Radical-Scavenging Assay

This experiment relies on the chromatic properties of stable radical cations and has been typically used to detect the antioxidative ability of pure or crude natural polysaccharides. The scavenging ability (**Figure 3B**) of SHP, SHP-1, SHP-2, SHP-3, and VC at 5.0 mg/mL had maximum values of 69.50%, 23.46%, 32.45%, 59.11%, and 95.72%, respectively. The radical-scavenging rates of SHP and SHP-3 markedly increased with increasing concentrations, while the rate of SHP-1 did not. The results indicate that the scavenging ability of DPPH-free radical for acidic polysaccharides was higher than that of neutral polysaccharides.

DMPD Radical-Scavenging Activity

The DMPD (*N, N dimethyl-p-phenylenediamine*) radical-scavenging activity experiment was commonly used to detect the oxidation resistance. The $DMPD^{\cdot+}$ (DMPD radical cation) with color was obtained in the presence of an oxidant. Antioxidant compounds are able to transfer the hydrogen atom to the $DMPD^{\cdot+}$, and then, the solution is discolored (65). The scavenging activity of the polysaccharides on DMPD free radicals showed a positive correlation in the concentrations of 0.1–5.0 mg/mL (**Figure 3C**). The scavenging abilities represented maximum values of 43.03% (SHP), 11.61% (SHP-1), 27.36% (SHP-2), 30.45% (SHP-3), and 89.19% (VC) at 5.0 mg/mL, respectively. Similar to other experiments, SHP showed the best antioxidant activity, followed by SHP-3 and SHP-2, and then SHP-1.

Ferrous Ion Chelating Ability

Electron transformation between Fe^{2+} and Fe^{3+} plays an essential role in physiological processes of the human body, such as enzymatic reactions in cellular metabolism and redox reactions (67, 68). However, a high level of ferrous ions (Fe^{2+}) accelerates oxidative reactions, which can compromise health. Therefore, the intake of compounds with metal chelation activity

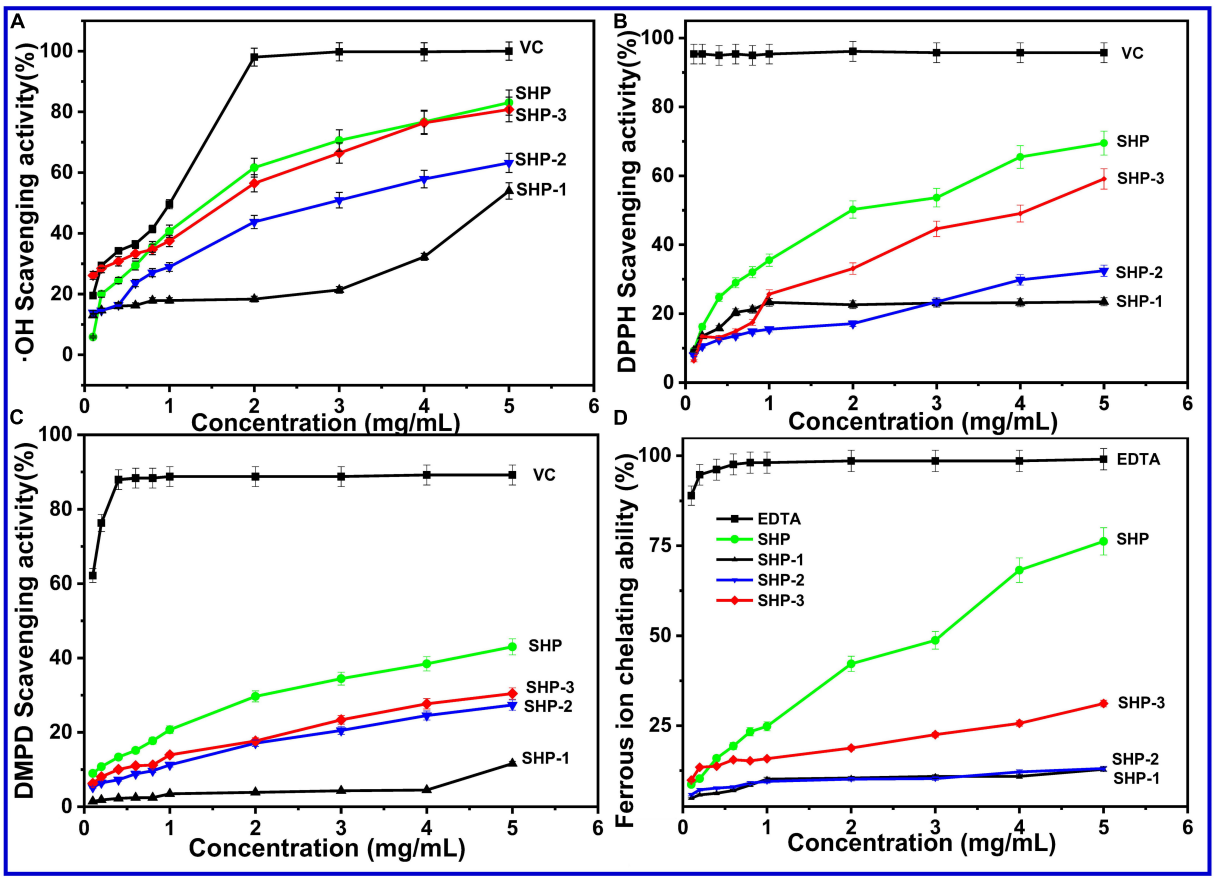

FIGURE 3 | (A) Hydroxyl radical (·OH) scavenging activity. **(B)** DPPH-free radical-scavenging assay. **(C)** DMPD radical-scavenging activity. **(D)** Ferrous ion chelating ability of SHP-1, SHP-2, SHP-3, and VC.

is important for protecting the health of the body (65). The results of chelating activities of SHP, SHP-1, SHP-2, and SHP-3 at various concentrations were measured and are shown in **Figure 3D**. The Fe^{2+} chelating activity of these polysaccharides was concentration-dependent and ranges from 0.1 to 5.0 mg/mL. In that range, SHP displayed a sharp increase (from 8.62 to 76.23%) with increasing concentration, which indicates that SHP has an effective chelating Fe^{2+} capacity.

In this work, the relatively weak activity of purified polysaccharide fractions compared with SHP might be because the purification processes might have removed some molecules, such as proteins, responsible for the antioxidant activity (67). This remains to be investigated in future studies. On the contrary, the antioxidant activity of SHP-3 and SHP-2 was much greater than that of SHP-1. Some publications have underlined the significance of functional groups in the polysaccharide side chains, monosaccharide composition, and average molecular weight for antioxidant activity (67, 68). This result might be related to the high abundant uronic acid of SHP-2 and SHP-3, because a previous study found that the anticancer activity of polysaccharides increases with uronic acid content (69, 70). Besides, SHP-3 and SHP-2 contain many smaller molecular weight polysaccharide molecules. The functional sites or active functional groups might be more likely to contact with free radicals or ferrous ions in an aqueous solution and thus show better antioxidant capacity (71, 72). The natural polysaccharides of sesame seed hull have the potential to be used as an antioxidant.

CONCLUSION

In this investigation, the SHP was extracted from sesame seed hull with a yield of 6.49%, and then, three fractions (SHP-1, SHP-2, and SHP-3) with molecular weights ranging from 11.7 to 89.5 kDa were obtained after exclusion ion-exchange column chromatography. SHP-2 with a yield of 3.78% was the dominant fragment in SHP. SHP-2 was the most homogeneous fraction in terms of molecular weight distribution compared to others. The galacturonic acid (51.3%) and glucuronic acid (13.8%) were found to be the major monosaccharide residues of SHP-2. Notably, the linear chain of 1,4-linked-α-D-Gal*p*A residues (linear homogalacturonan) was the dominant chemical structure presented in SHP-2 by NMR spectrum and methylation analysis. The SHP and purified fractions (SHP-3 and SHP-2) had good free

radical-scavenging ability. Therefore, the polysaccharides from sesame hull had potential prospect as antioxidant. This study provided some basic chemical structure information of sesame hull polysaccharides for its application.

DATA AVAILABILITY STATEMENT

The original contributions presented in the study are included in the article/**Supplementary Material**, further inquiries can be directed to the corresponding author/s.

AUTHOR CONTRIBUTIONS

R-YZ: conceptualization, writing—original draft preparation, and methodology. J-HG: data curation and visualization. Y-LS: investigation. Y-FL: software. H-ML: writing—reviewing and editing and validation. W-XZ: validation. X-DW: supervision and writing—reviewing and editing. All authors contributed to the article and approved the submitted version.

FUNDING

This work was supported by the Natural Science Foundation of Excellent Youth for Henan (222300420038), the Key Project of Science and Technology of Henan Province (201300110600), and the Innovation and Entrepreneurship Training Program for Higher Education Students in Henan Province (202110463042, 202110463043, and 202110463040).

SUPPLEMENTARY MATERIAL

The Supplementary Material for this article can be found online at: https://www.frontiersin.org/articles/10.3389/fnut.2022.928972/full#supplementary-material

REFERENCES

1. Wang BH, Cao JJ, Zhang B, Chen HQ. Structural characterization, physicochemical properties and α-glucosidase inhibitory activity of polysaccharide from the fruits of wax apple. *Carbohyd Polym.* (2019) 211:227–36. doi: 10.1016/j.carbpol.2019.02.006
2. Ji XL, Peng BX, Ding HH, Cui BB, Nie H, Yan YZ. Purification, structure and biological activity of pumpkin polysaccharides: a review. *Food Rev Int.* (2021). doi: 10.1080/87559129.2021.1904973 [Epub ahead of print].
3. Ji XL, Guo JH, Ding DQ, Gao J, Hao LR, Guo XD, et al. Structural characterization and antioxidant activity of a novel high-molecular-weight polysaccharide from *Ziziphus jujuba* cv. Muzao. *J Food Meas Charact.* (2022) 16:2191–200. doi: 10.1007/s11694-022-01288-3
4. Shi L. Bioactivities, isolation and purification methods of polysaccharides from natural products: a review. *Int J Biol Macromol.* (2016) 92:37–48. doi: 10.1016/j.ijbiomac.2016.06.100
5. Hu X, Goff HD. Fractionation of polysaccharides by gradient non-solvent precipitation: a review. *Trends Food Sci Tech.* (2018) 81:108–15.
6. Liu HM, Wang FY, Liu YL. Hot-compressed water extraction of polysaccharides from soy hulls. *Food Chem.* (2016) 202:104–9. doi: 10.1016/j.foodchem.2016.01.129
7. Merci A, Urbano A, Grossmann MVE, Tischer CA, Mali S. Properties of microcrystalline cellulose extracted from soybean hulls by reactive extrusion. *Food Res Int.* (2015) 73:38–43.
8. Chang LW, Yen WJ, Huang SC, Duh PD. Antioxidant activity of sesame coat. *Food Chem.* (2002) 78:347–54.
9. Liu HM, He MK, Yao YG, Qin Q, Cai XS, Wang XD. Pectic polysaccharides extracted from sesame seed hull: physicochemical and functional properties. *Int J Biol Macromol.* (2021) 192:1075–83. doi: 10.1016/j.ijbiomac.2021.10.077
10. Farran MT, Uwayjan MG, Miski AMA, Akhdar NM, Ashkarian VM. Performance of broilers and layers fed graded levels of sesame hull. *J Appl Poultry Res.* (2000) 9:453–9.
11. Anilakumar KR, Pal A, Khanum F, Bawa AS. Nutritional, medicinal and industrial uses of sesame (*Sesamum indicum* L.) seeds – an overview. *Agric Conspec Sci.* (2010) 75:159–68.
12. Elleuch M, Besbes S, Roiseux O, Blecker C, Attia H. Quality characteristics of sesame seeds and by-products. *Food Chem.* (2007) 103:641–50.
13. Das R, Bhattacharjee C. *Processing Sesame Seeds and Bioactive Fractions, Processing and Impact on Active Components in Food.* Cambridge, MA: Academic Press (2015). p. 385–94.
14. Elleuch M, Bedigian D, Besbes S, Blecker C, Attia H. Dietary fibre characteristics and antioxidant activity of sesame seed coats (Testae). *Int J Food Prop.* (2012) 15:25–37.
15. Carbonell-Barrachina AA, Lluch MA, Perez-Munera I, Hernando I, Castillo S. Effects of chemical dehulling of sesame on color and microstructure. *Food Sci Technol Int.* (2009) 15:229–34.
16. Zhang RY, Liu HM, Hou J, Yao YG, Ma YX, Wang XD. Cellulose fibers extracted from sesame hull using subcritical water as a pretreatment. *Arab J Chem.* (2021) 14:103178. doi: 10.1016/j.arabjc.2021.103178
17. AOCS. *Official Methods and Recommended Practices of the American oil Chemists' Society*. Champaign, IL: AOCS Press (1998).
18. Feng P, Ren JL, Feng X, Jing B, Sun RC. Comparative study of hemicelluloses obtained by graded ethanol precipitation from sugarcane bagasse. *J Agr Food Chem.* (2009) 57:6305–17. doi: 10.1021/jf900986b
19. Xu JY, Yuan TQ, Xiao L, Sun RC. Effect of ultrasonic time on the structural and physico-chemical properties of hemicelluloses from *Eucalyptus grandis*. *Carbohyd Polym.* (2018) 195:114–9. doi: 10.1016/j.carbpol.2018.04.067
20. Long X, Yan Q, Cai L, Li G, Luo X. Box-Behnken design-based optimization for deproteinization of crude polysaccharides in *Lycium barbarum* berry residue using the Sevag method. *Heliyon.* (2020) 6:e03888. doi: 10.1016/j.heliyon.2020.e03888
21. Nowotny A. Carbohydrate determination by phenol-sulfuric acid. In: Nowotny A editor. *Basic Exercises in Immunochemistry*. (Heidelberg: Springer) (1979). p. 171–3.
22. Guo Q, Cui S, Kang WJ, Ding H, Wang Q, Wang C. Non-starch polysaccharides from American ginseng: physicochemical investigation and structural characterization. *Food Hydrocolloid.* (2015) 44:320–7.
23. Zhang Z, Zhang Y, Liu H, Wang J, Zhong S. A water-soluble selenium–enriched polysaccharide produced by *Pleurotus ostreatus*: purification, characterization, antioxidant and antitumor activities in vitro. *Int J Biol Macromol.* (2021) 168:356–70. doi: 10.1016/j.ijbiomac.2020.12.070
24. Wang L, Liu HM, Xie AJ, Wang XD, Zhu CY, Qin GY. Chinese quince (*Chaenomeles sinensis*) seed gum: structural characterization. *Food Hydrocolloid.* (2018) 75:237–45.
25. Qin Z, Liu HM, Cheng XC, Wang XD. Effect of drying pretreatment methods on structure and properties of pectins extracted from Chinese quince fruit. *Int J Biol Macromol.* (2019) 137:801–8. doi: 10.1016/j.ijbiomac.2019.06.209
26. Liu W, Liu Y, Zhu R, Yu J, Lu W, Pan C, et al. Structure characterization, chemical and enzymatic degradation, and chain conformation of an acidic polysaccharide from *Lycium barbarum* L. *Carbohyd Polym.* (2016) 147:114–24. doi: 10.1016/j.carbpol.2016.03.087
27. Taylor RL, Conrad HE. Conrad, stoichiometric depolymerization of polyuronides and glycosaminoglycuronans to monosaccharides following reduction of their carbodiimide-activated carboxyl group. *Biochem.* (1972) 11:1383–8. doi: 10.1021/bi00758a009

28. Chen J, Li L, Zhang Z, Wan L, Zheng Q, Xu D, et al. Structural characterization of polysaccharide from *Centipeda minima* and its hypoglycemic activity through alleviating insulin resistance of hepatic HepG2 cells. *J Funct Foods.* (2021) 82:104478. doi: 10.1016/j.jff.2021.104478
29. Liu XX, Liu HM, Yan YY, Fan LY, Yang JN, Wang XD, et al. Structural characterization and antioxidant activity of polysaccharides extracted from jujube using subcritical water. *LWT Food Sci Technol.* (2020) 117:108645. doi: 10.1016/j.lwt.2019.108645
30. Thaipong K, Boonprakob U, Crosby K, Cisneros-Zevallos L, Byrne DH. Comparison of ABTS, DPPH, FRAP, and ORAC assays for estimating antioxidant activity from guava fruit extracts. *J Food Compos Anal.* (2012) 19:669–75.
31. Chen L, Huang G. The antiviral activity of polysaccharides and their derivatives. *Int J Biol Macromol.* (2018) 115:77–82. doi: 10.1016/j.ijbiomac.2018.04.056
32. Chen C, You LJ, Abbasi AM, Fu X, Liu RH. Optimization for ultrasound extraction of polysaccharides from mulberry fruits with antioxidant and hyperglycemic activity in vitro. *Carbohyd Polym.* (2015) 130:122–32. doi: 10.1016/j.carbpol.2015.05.003
33. Chen C, Zhang B, Huang Q, Fu X, Liu RH. Microwave-assisted extraction of polysaccharides from *Moringa oleifera* Lam. leaves: characterization and hypoglycemic activity. *Ind Crop Prod.* (2017) 100:1–11.
34. Bradford MM. A rapid and sensitive method for the quantitation of microgram quantities protein utilizing the principle of protein-dye binding. *Anal Biochem.* (1976) 72:248–59.
35. Hadidi M, Amoli PI, Jelyani AZ, Hasiri Z, Rouhafza A, Ibarz A, et al. Polysaccharides from pineapple core as a canning by-product: extraction optimization, chemical structure, antioxidant and functional properties. *Int J Biol Macromol.* (2020) 163:2357–64. doi: 10.1016/j.ijbiomac.2020.09.092
36. Zhang Y, Wu Z, Liu J, Zheng Z, Li Q, Wang HJ, et al. Identification of the core active structure of a *Dendrobium officinale* polysaccharide and its protective effect against dextran sulfate sodium-induced colitis via alleviating gut microbiota dysbiosis. *Food Res Int.* (2020) 137:109641. doi: 10.1016/j.foodres.2020.109641
37. Zhang B, Gao Y, Zhang L, Zhou Y. The plant cell wall: biosynthesis, construction, and functions. *J Integr Plant Biol.* (2020) 63:251–72. doi: 10.1111/jipb.13055
38. Dranca F, Oroian M. Extraction, purification and characterization of pectin from alternative sources with potential technological applications. *Food Res Int.* (2018) 113:327–50. doi: 10.1016/j.foodres.2018.06.065
39. Jiang H, Dong J, Jiang S, Liang Q, Kang W. Effect of durio zibethinus rind polysaccharide on functional constipation and intestinal microbiota in rats. *Food Res Int.* (2020) 136:109316. doi: 10.1016/j.foodres.2020.109316
40. Xiao Y, Shen M, Luo Y, Ren Y, Xie J. Effect of mesona Chinensis polysaccharide on the pasting, rheological, and structural properties of tapioca starch varying in gelatinization temperatures. *Int J Biol Macromol.* (2020) 156:137–43. doi: 10.1016/j.ijbiomac.2020.04.041
41. Myz A, Spn A, Jyy A, Myxa B. Ascorbic acid induced degradation of polysaccharide from natural products: a review. *Int J Biol Macromol.* (2020) 151:483–91. doi: 10.1016/j.ijbiomac.2020.02.193
42. Ji XL, Cheng YQ, Tian JY, Zhang SQ, Jing YS, Shi MM. Structural characterization of polysaccharide from jujube (*Ziziphus jujuba* Mill.) fruit. *Chem Biol Technol Ag.* (2021) 8:54. doi: 10.1186/s40538-021-00255-2
43. Ji XL, Guo JH, Pan FB, Kuang FJ, Chen HM, Guo XD, et al. Structural elucidation and antioxidant activities of a neutral polysaccharide from Arecanut (*Areca catechu* L.). *Front Nutr.* (2022) 9:853115. doi: 10.3389/fnut.2022.853115
44. Nep EI, Carnachan SM, Ngwuluka NC, Kontogiorgos V, Morris GA, Sims IM, et al. Structural characterization and rheological properties of a polysaccharide from sesame leaves (*Sesamum radiatum* Schumach. & Thonn.). *Carbohyd Polym.* (2016) 152:541–7. doi: 10.1016/j.carbpol.2016.07.036
45. Cernà M, Barros AS, Nunes A, Rocha SM, Delgadillo I, Copìkovà J. Use of FT-IR spectroscopy as a tool for the analysis of polysaccharide food additives. *Carbohyd Polym.* (2003) 51:383–9.
46. Cai WR, Xu HL, Xie LL, Sun J, Sun TT, Wu XY, et al. Purification, characterization and in vitro anticoagulant activity of polysaccharides from *Gentiana scabra* Bunge roots. *Carbohyd Polym.* (2016) 140:308–13.
47. Banerjee P, Jana S, Mukherjee S, Bera K, Majee SK, Ali I, et al. The heteropolysaccharide of *Mangifera indica* fruit: isolation, chemical profile, complexation with β-lactoglobulin and antioxidant activity. *Int J Biol Macromol.* (2020) 165:93–9. doi: 10.1016/j.ijbiomac.2020.09.161
48. Nie SP, Cui SW, Phillips AO, Xie MY, Phillipsd GO, Al-Assafd S, et al. Elucidation of the structure of a bioactive hydrophilic polysaccharide from cordyceps sinensis by methylation analysis and NMR spectroscopy. *Carbohyd Polym.* (2011) 84:894–9.
49. Li R, Tao A, Yang R, Fan M, Duan B. Structural characterization, hypoglycemic effects and antidiabetic mechanism of a novel polysaccharides from *Polygonatum kingianum* Coll. et Hemsl. *Biomed Pharmacother.* (2020) 131:10687. doi: 10.1016/j.biopha.2020.110687
50. Kamerling JP. *Comprehensive Glycoscience: From Chemistry to Systems Biology: Biochemistry of Glycocojugate Glycans. Carbohydrate-Mediated Interactions*. Amsterdam: Elsevier Science (2007).
51. Oliveira DM, Mota TR, Salatta FV, Sinzker RC, Santos W. Cell wall remodeling under salt stress: insights into changes in polysaccharides, feruloylation, lignification, and phenolic metabolism in maize. *Plant Cell Environ.* (2020) 43:2172–91. doi: 10.1111/pce.13805
52. Yao H, Wang JQ, Yin JY, Nie SP, Xie MY. A review of NMR analysis in polysaccharide structure and conformation: progress, challenge and perspective. *Food Res Int.* (2021) 143:110290. doi: 10.1016/j.foodres.2021.110290
53. Zhu Y, Yu X, Ge Q, Li J, Ouyang Z. Antioxidant and anti-aging activities of polysaccharides from *Cordyceps* cicadae. *Int J Biol Macromol.* (2020) 157:394–400. doi: 10.1016/j.ijbiomac.2020.04.163
54. Yang L, Zhang H, Zhao Y, Huang J, Zhu D, Wang S, et al. Chemical structure, chain conformation and rheological properties of pectic polysaccharides from soy hulls. *Int J Biol Macromol.* (2020) 148:41–8. doi: 10.1016/j.ijbiomac.2020.01.047
55. Jones MD, Vinogradov E, Nomellini JF, Smit J. The core and O-polysaccharide structure of the *Caulobacter crescentus* lipopolysaccharide. *Carbohyd Res.* (2015) 402:111–7.
56. Mahdi TAK, Kenneth CBW. The polysaccharides of agricultural lupin seeds. *Carbohyd Res.* (1992) 227:147–61. doi: 10.1016/0008-6215(92)85067-a
57. Westman EL, Mcnally DJ, Rejzek M, Miller WL, Kannathasan VS, Preston A, et al. Identification and biochemical characterization of two novel UDP-2,3-diacetamido-2,3-dideoxy-α-D-glucuronic acid 2-epimerases from respiratory pathogens. *Biochem J.* (2007) 405:123–30. doi: 10.1042/BJ20070017
58. Dobrochaeva K, Khasbiullina N, Shilova N, Antipova N, Obukhova P, Ovchinnikova T, et al. Specificity of human natural antibodies referred to as anti-Tn. *Mol Immuno.* (2020) 120:74–82. doi: 10.1016/j.molimm.2020.02.005
59. Merino S, Gonzalez V, Tomás JM. The first sugar of the repeat units is essential for the Wzy polymerase activity and elongation of the O-antigen lipopolysaccharide. *Future Microbiol.* (2016) 11:903–18. doi: 10.2217/fmb-2015-0028
60. Yu X, Torzewska A, Zhang X, Yin Z, Drzewiecka D, Cao H, et al. Genetic diversity of the O antigens of Proteus species and the development of a suspension array for molecular serotyping. *PLoS One.* (2017) 12:e0183267. doi: 10.1371/journal.pone.0183267
61. Paton JC, Trappetti C. *Streptococcus pneumoniae* capsular polysaccharide. *Microbiol Spectr.* (2019) 7:1–15. doi: 10.1128/microbiolspec.GPP3-0019-2018
62. Zhao D, Ding X, Hou Y, Hou W, Liu L, Xu T, et al. Structural characterization, immune regulation and antioxidant activity of a new heteropolysaccharide from *Cantharellus cibarius* Fr. *Int J Mol Med.* (2018) 41:2744–54. doi: 10.3892/ijmm.2018.3450
63. Li Y, Yi P, Wang N, Liu J, Liu X, Yan Q, et al. High level expression of β-mannanase (RmMan5A) in *Pichia pastoris* for partially hydrolyzed guar gum production. *Int J Biol Macromol.* (2017) 105:1171–9. doi: 10.1016/j.ijbiomac.2017.07.150
64. Debra M. Pectin structure and biosynthesis. *Curr Opin Plant Biol.* (2008) 11:266–77. doi: 10.1016/j.pbi.2008.03.006
65. Fogliano V, Verde V, Randazzo G, Ritieni A. Method for measuring antioxidant activity and its application to monitoring the antioxidant capacity of wines. *J Agr Food Chem.* (1999) 47:1035–40. doi: 10.1021/jf980496s

66. Yuan JF, Zhang ZQ, Fan ZC, Yang JX. Antioxidant effects and cytotoxicity of three purified polysaccharides from *Ligusticum chuanxiong* Hort. *Carbohyd Polym.* (2008) 74:822–7.
67. Jiang H, Dong J, Jiang S, Liang Q, Kang W. Metagenomic analysis of gut microbiota modulatory effects of jujube (*Ziziphus jujuba* Mill.) polysaccharides in a colorectal cancer mouse model. *Food Func.* (2020) 11:163–73. doi: 10.1039/c9fo02171j
68. Liu G, Li B, Liu Y, Feng Y, Zhou Y. Rapid and high yield synthesis of carbon dots with chelating ability derived from acrylamide/chitosan for selective detection of ferrous ions. *Appl Surf Sci.* (2019) 487:1167–75.
69. Westereng B, Coenen GJ, Michaelsen TE, Voragen AGJ, Samuelsen AB, Schols HA, et al. Release and characterization of single side chains of white cabbage pectin and their complement-fixing activity. *Mol Nutr Food Res.* (2009) 53:780–9. doi: 10.1002/mnfr.200800199
70. Singh A, Dutta PK, Kumar H, Kureel AK, Rai AK. Synthesis of chitinglucan-aldehyde-quercetin conjugate and evaluation of anticancer and antioxidant activities. *Carbohyd Polym.* (2018) 193:99–107.
71. Liu C, Chen J, Li E, Fan Q, Wang D, Li P, et al. The comparison of antioxidative and hepatoprotective activities of *Codonopsis pilosula* polysaccharide (CP) and sulfated CP. *Int Immunopharmacol.* (2015) 24:299–305.
72. Dey A, Rasane P, Singhal S, Kumar V, Kaur S, Singh J. Cactus cladode polysaccharide as cryoprotectant in frozen Paneer (Indian cottage cheese). *Int J Dairy Technol.* (2020) 73:215–25.

Conflict of Interest: The authors declare that the research was conducted in the absence of any commercial or financial relationships that could be construed as a potential conflict of interest.

Publisher's Note: All claims expressed in this article are solely those of the authors and do not necessarily represent those of their affiliated organizations, or those of the publisher, the editors and the reviewers. Any product that may be evaluated in this article, or claim that may be made by its manufacturer, is not guaranteed or endorsed by the publisher.

Copyright © 2022 Zhang, Gao, Shi, Lan, Liu, Zhu and Wang. This is an open-access article distributed under the terms of the Creative Commons Attribution License (CC BY). The use, distribution or reproduction in other forums is permitted, provided the original author(s) and the copyright owner(s) are credited and that the original publication in this journal is cited, in accordance with accepted academic practice. No use, distribution or reproduction is permitted which does not comply with these terms.

frontiers | Frontiers in Nutrition

TYPE Correction
PUBLISHED 29 July 2022
DOI 10.3389/fnut.2022.992487

Check for updates

OPEN ACCESS

APPROVED BY
Frontiers Editorial Office,
Frontiers Media SA, Switzerland

*CORRESPONDENCE
Hua-Min Liu
liuhuamin5108@163.com
Xue-De Wang
wangxuede1962@126.com

SPECIALTY SECTION
This article was submitted to Food Chemistry, a section of the journal Frontiers in Nutrition

RECEIVED 12 July 2022
ACCEPTED 15 July 2022
PUBLISHED 29 July 2022

CITATION
Zhang R-Y, Gao J-H, Shi Y-L, Lan Y-F, Liu H-M, Zhu W-X and Wang X-D (2022) Corrigendum: Characterization of structure and antioxidant activity of polysaccharides from sesame seed hull. *Front. Nutr.* 9:992487. doi: 10.3389/fnut.2022.992487

COPYRIGHT
© 2022 Zhang, Gao, Shi, Lan, Liu, Zhu and Wang. This is an open-access article distributed under the terms of the Creative Commons Attribution License (CC BY). The use, distribution or reproduction in other forums is permitted, provided the original author(s) and the copyright owner(s) are credited and that the original publication in this journal is cited, in accordance with accepted academic practice. No use, distribution or reproduction is permitted which does not comply with these terms.

Corrigendum: Characterization of structure and antioxidant activity of polysaccharides from sesame seed hull

Run-Yang Zhang, Jing-Hao Gao, Yi-Lin Shi, Yi-Fei Lan, Hua-Min Liu*, Wen-Xue Zhu and Xue-De Wang*

Institute of Special Oilseed Processing and Technology, College of Food Science and Technology, Henan University of Technology, Zhengzhou, China

KEYWORDS

sesame seed, hull, polysaccharides, chemical structure, antioxidant activity

A corrigendum on
Characterization of structure and antioxidant activity of polysaccharides from sesame seed hull

by Zhang, R.-Y., Gao, J.-H., Shi, Y.-L., Lan, Y.-F., Liu, H.-M., Zhu, W.-X., and Wang, X.-D. (2022). Front. Nutr. 9:928972. doi: 10.3389/fnut.2022.928972

In the published article, there was an error in Table 2 as published. In the second column of Table 2, the names of several linkage patterns are incorrect. The corrected Table 2 and its caption "Table 2 Methylation analysis result of SHP-2" appear below.

The authors apologize for this error and state that this does not change the scientific conclusions of the article in any way. The original article has been updated.

Publisher's note

All claims expressed in this article are solely those of the authors and do not necessarily represent those of their affiliated organizations, or those of the publisher, the editors and the reviewers. Any product that may be evaluated in this article, or claim that may be made by its manufacturer, is not guaranteed or endorsed by the publisher.

10.3389/fnut.2022.992487

TABLE 2 Methylation analysis result of SHP-2.

PMAAs (partially methylated alditol acetates)		Linkage patterns	Major mass fragment (*m/z*)	Retention time (min)	Relative amount /mol%
A	2,3,4-Me_2-Rha*p*	T-Rha*p*(1→	43, 59, 72, 89, 102, 118, 131, 162, 175, 203	11.90	12.2
B	2,3-Me_2-Xyl*p*	→4)-Xyl*p*(1→	43, 59, 71, 87, 102, 118, 129, 145, 162, 189, 207, 253	13.11	4.6
C	2,3,4,6-Me_4-Gal*p*	T-Gal*p*(1→	43, 59, 71, 87, 102, 118, 129, 145, 161, 162, 175, 205	13.94	3.2
D	2-Me-Ara*f*	→3,5)-Ara*f*(1→	43, 59, 74, 85, 99, 118, 130, 142, 160, 207, 261	14.41	4.2
E	3,4,6-Me_3-Glc*p*	→2)-Glc*p*(1→	43, 59, 71, 87, 101, 129, 145, 161, 174, 190, 205, 234	15.20	21.1
F	2,3,6-Me_3-Gal*p*	→4)-Gal*p*(1→	43, 57, 71, 85, 99, 118, 129, 147, 161, 233, 281, 305	15.61	42.1
G	2,3,6-Me_3-Man*p*	→4)-Man*p*(1→	43, 87, 99, 118, 129, 147, 173, 208, 233	15.81	2.9
H	2,3,4-Me_3-Glc*p*	→6)-Glc*p*(1→	43, 59, 71, 87, 102, 118, 129, 143, 162, 173, 189, 233	16.51	9.7

frontiers | Frontiers in Nutrition

ORIGINAL RESEARCH
published: 29 June 2022
doi: 10.3389/fnut.2022.942241

Chemical Structure and Immune Activation of a Glucan From *Rhizoma Acori Tatarinowii*

Wuxia Zhang, Jiaqi He, Yihua Hu, Jingwu Lu, Jinzhong Zhao and Peng Li**

Shanxi Key Laboratory for Modernization of TCVM, Department of Basic Sciences, Shanxi Agricultural University, Shanxi, China

Rhizoma Acori Tatarinowii is a traditional Chinese herb used to treat depression and coronary heart disease. Studies on its active components mainly focus on small molecular compounds such as asarone and other essential oil components, while the large molecular active components such as polysaccharides are ignored. In this study, we aimed to study the chemical structure and immune activation of polysaccharides from *Rhizoma Acori Tatarinowii*. In this study, a polysaccharide (RATAPW) was isolated and purified by DEAE-52 cellulose and Sephadex G-100 column chromatography from alkali extraction polysaccharide of *Rhizoma Acori Tatarinowii*. The average molecular weight of RATAPW was 2.51 × 10^4 Da, and the total carbohydrate contents of RATAPW were 98.23 ± 0.29%. The monosaccharide composition, methylation, and nuclear magnetic resonance (NMR) analysis results displayed that the polysaccharide was α-1,4-glucan with short α-1,6 branches. Immunofluorescence assay and inhibitor neutralization assay indicated that RATAPW could promote the TNF-α production of RAW264.7 macrophage through the nuclear factor kappa B (NF-κB) molecular signaling pathway. Treatment with 200 μg/ml of RATAPW enhanced a 38.77% rise in the proliferation rate of spleen lymphocytes. RATAPW also enhances ConA-induced T cells and lipopolysaccharide (LPS)-induced B cell proliferation in a dose-dependent effect. Our study lays a foundation for the discovery of natural polysaccharide immune modulators or functional food from *Rhizoma Acori Tatarinowii*.

Keywords: polysaccharide, structure, immune activity, *Rhizoma Acori Tatarinowii*, glucan

OPEN ACCESS

Edited by:
Xiaolong Ji,
Zhengzhou University of Light Industry, China

Reviewed by:
Deqiang Zhu,
Qilu University of Technology, China
Zichao Wang,
Henan University of Technology, China

****Correspondence:***
Wuxia Zhang
wuxia200758@163.com
Peng Li
lipengcuc@163.com

Specialty section:
This article was submitted to Food Chemistry, a section of the journal Frontiers in Nutrition

Received: *12 May 2022*
Accepted: *06 June 2022*
Published: *29 June 2022*

Citation:
Zhang W, He J, Hu Y, Lu J, Zhao J and Li P (2022) Chemical Structure and Immune Activation of a Glucan From Rhizoma Acori Tatarinowii. Front. Nutr. 9:942241. doi: 10.3389/fnut.2022.942241

INTRODUCTION

Herb medicine *Rhizoma Acori Tatarinowii* has appetizing, sedative, detumescent, and analgesic effects and is often used to treat joint pain, depression, and Alzheimer's disease syndrome (1). To date, *Rhizoma Acori Tatarinowii* has been studied for various biological activities, such as potentiating neuronal differentiation of PC12 cells (2), inhibiting the proliferation of cancer cells (3), and promoting the absorption and transport of compounds by inhibiting glycoprotein (4).

Abbreviations: MTT, 3-(4,5-dimethyl-2-triazolyl)-2,5-diphenyltetrazolium bromide; ConA, concanavalin A; BAY 11-7082, (E)-3-[(4-methylphenylsulfonyl]-2-propenenitrile; LPS, lipopolysaccharide; DAPI, 2- (4-Amidinophenyl)-6-indolecarbamidine dihydrochloride; TFA, trifluoroacetic acid; DMSO, dried dimethyl sulfoxide; ELISA, enzyme-linked immunosorbent assay; PMAA, partially methylated alditol acetates; APC, the antigen-presenting cell; MAPKs, mitogen-activated protein kinases.

However, studies on the active components of *Rhizoma Acori Tatarinowii* mainly focused on the small molecular compounds such as asarone and other essential oil components but ignored the large molecular components such as polysaccharides. In recent years, natural polysaccharides attracted extensive attention for their immunomodulatory activities (5). For example, a polysaccharide from the fruiting bodies of *Helvella leucopus* induced macrophage activation *via* the nuclear factor kappa B (NF-κB) signal pathway (6). The α-glucan from ginger could activate RAW264.7 cells to release cytokines (7).

Inspired by these studies, we speculated that the immune activity of *Rhizoma Acori Tatarinowii* may be related to the active polysaccharide components. Consistently, our previous studies showed that the polysaccharides obtained by water extraction have prominent immunological activity (8). However, the extraction yields, structures, and bioactivities of polysaccharides are strictly affected by the extraction process (9). Studies have shown that polysaccharides obtained by different extraction methods vary greatly. He et al. showed alkalic-extractable polysaccharides from *Ziziphus jujuba cv.* with higher antioxidant activity (10). In this study, we aimed to study the chemical structure and immune activation of polysaccharides from *Rhizoma Acori Tatarinowii*. We extracted the polysaccharide from the *Rhizoma Acori Tatarinowii* with the alkaline solution. The crude polysaccharide was isolated and purified by anion exchange and gel filtration chromatography. The chemical structure was characterized by monosaccharide compositions, infrared spectra (IR), methylation, and nuclear magnetic resonance (NMR) analyses. The immune activation of the polysaccharide was determined by enzyme-linked immunosorbent assay (ELISA), immunofluorescence assay, and inhibitor neutralization assay.

MATERIALS AND METHODS

Rhizoma Acori Tatarinowii and Chemical Reagents

Dried herb *Rhizoma Acori Tatarinowii* was produced in Sichuan Province, China. DEAE-52 cellulose, Sephadex G-100, and 3-(4,5-dimethyl-2-triazolyl)-2,5-diphenyltetrazolium bromide (MTT) were purchased from Beijing Solarbio. DAPI, BAY 11-7082, NF-κB p65 antibody, and FITC labeled Goat Anti-Rabbit IgG were supplied by Shanghai Beyotime Biotechnology. ELISA kits were manufactured in R&D Systems.

Isolation and Purification of Polysaccharide From *Rhizoma Acori Tatarinowii*

The dried *Rhizoma Acori Tatarinowii* was grounded into powder and then defatted with 95% ethanol. The solid residues were extracted with distilled water (1:10, w/v) at 80°C for 2 h, and this extraction process was repeated 3 times. The supernatants were pooled, collected, and studied previously (8). To obtain more kinds of polysaccharides, we further extracted polysaccharides from the residue by alkali extraction and alcohol precipitation. The solid residue was extracted 3 times with 0.2 M sodium hydroxide at 50°C for 2 h. Subsequently, the collected supernatants were concentrated, neutralized, and precipitated with 4 times absolute ethyl alcohol. The polysaccharide precipitates were collected and redissolved in distilled water. Then, the polysaccharide solution was dialyzed for 72 h in distilled water (change the water every 4 h and Mw cutoff: 3,500 Da). After freeze-drying, the alkali extracted crude polysaccharide was obtained. The crude polysaccharide was dissolved in deionized water, and the mixture was centrifuged. The supernatant was loaded on DEAE-52 cellulose (5 cm × 50 cm, Cl^- form) and eluted with distilled water and different concentrations of gradient NaCl solution (0.1, 0.2, and 0.5 M NaCl) at a constant flow rate consecutively. The total carbohydrate content of each fraction was detected using the phenol-sulfuric acid method (11). According to the solubility and content of polysaccharides, water elute was further purified using a Sephadex G-100 column. The collected components were eluted with distilled water at a flow rate of 0.2 ml/min. The eluent in the test tube with absorbance greater than 0.3 was collected, lyophilized, and named RATAPW.

Characterization of Polysaccharides

Molecular Weight Measurement

The purity and molecular weight of RATAPW were analyzed by high-performance gel permeation chromatography (HPGPC) performed on three columns (Waters Ultrahydrogel 250, 1,000, and 2,000; 30 cm × 7.8 mm; 6 μm particles) in series (12). The purified RATAPW was eluted with 3 mmol/L sodium acetate at 0.5 ml/min. Notably, 5.2, 11.6, 23.8, 48.6, 148, 273, and 410 kDa dextrans were used as standards. The calibration curve is calculated using Log (Mw) = –0.1719T + 11.585 (T: elution time).

Infrared Spectra Analysis

An amount of 2 mg dry RATAPW was mixed with 50 mg chromatographic pure KBr. Agate pestle and mortar were used for grounding the sample, and it was further analyzed using the Fourier transform infrared spectrophotometer (BRUCK, Germany) after pressing in pellets (13). The measurement wavenumber region ranged from 400 cm^{-1} to 4,000 cm^{-1}.

Chemical Component and Monosaccharide Composition Analysis

The phenol–sulfuric acid method and Bradford's method (14) were used to determine the total sugar and protein contents, respectively.

An amount of 10 mg RATAPW was hydrolyzed using the 3 M TFA at 120°C for 3 h (15). The hydrolysate was washed three times with methanol and evaporated. Finally, the hydrolyzed material was dissolved with 5 ml of deionized water, transferred to a 50 ml volumetric flask, and diluted to 50 ml. High-performance anion-exchange chromatography (HPAEC) equipped with ICS-5000 (Waltham, MA, United States) and a CarboPac^{TM} PA-20 analytical column (3 mm × 150 mm) was employed. Here, 15 mM NaOH and 100 mM sodium acetate were used as mobile phases for gradient elution at 0.3 ml/min (16). The monosaccharide kinds

of RATAPW were determined by comparing the retention times with fifteen monosaccharide standards (fucose, galactosamine, rhamnose, arabinose, glucosamine, galactose, glucose, N-acetyl-D-glucosamine, xylose, mannose, ribose, galacturonic acid, guluronic acid, glucuronic acid, and mannuronic acid).

Methylation and Glycosidic Linkage Analysis

The methylation analysis method was applied to confirm the glycosidic linkages of RATAPW based on the reference (17). In brief, the dried polysaccharide RATAPW (3 mg) was dissolved in 1 ml dried DMSO and dried NaOH powder, ultrasonically treated for 1 h. Subsequently, the methyl iodide was added under dark conditions and stirred at 30°C for 1 h to obtain the methylated product. Further hydrolyzed with 4 M TFA, reduced with $NaBH_4$, and acetylated with acetic anhydride. Ultimately, the partially methylated alditol acetates (PMAA) containing the linkage type of RATAPW were analyzed by chromatography-mass spectrometry (GC–MS) system (Shimadzu GCMS-QP 2010) equipped with an RXI-5 SIL MS column (30 m × 0.25 mm × 0.25 μ m).

Nuclear Magnetic Resonance Analysis

A Bruker 600 MHz spectrometer equipped with a $^{1}H/^{13}C$ double probe was used for NMR analysis at 25°C (18). An amount of 50 mg dried RATAPW was dissolved in 1 ml D_2O and frozen three times to exchange H protons into deuterium completely. The lyophilized sample was then dissolved in 0.5 ml D_2O overnight before NMR analysis. ^{1}H NMR, ^{13}C NMR, ^{1}H-^{1}H COSY, HSQC, HMBC, and NOESY spectra of RATAPW were recorded.

Measurement of TNF-α Cytokine Production Induced by RATAPW

The RAW264.7 cell was a kind gift from Prof. Jinyou Duan at Northwest A&F University. In 96-well plates, RAW 264.7 cells (1×10^5 cells/well) were incubated with different concentrations (50, 100, or 200 μg/ml) of RATAPW for 24 h. phosphate buffer saline (PBS) was used as the negative control and lipopolysaccharide (LPS) (2 μg/ml) was used as the positive control. The cell supernatants were collected. TNF-α proteins in the cell supernatants were measured using the ELISA kits (R&D) according to the instructions (19). To determine the effect of RATAPW on the growth profile of RAW264.7 cells, 0.5 mg/ml MTT was added to the plates and further incubated for 4 h at 37°C. The optical density was measured at 570 nm.

In addition, RAW 264.7 cells were pretreated with PBS or 3 μM BAY 11-7082 for 1 h and incubated with 200 μg/ml RATAPW or LPS (2 μg/ml) for 24 h. TNF-α cytokine content in the different wells was measured using the ELISA kits.

Immunofluorescence Tests for NF-κB Activation

After being treated with 200 μg/ml RATAPW or LPS (2 μg/ml) for 3 h, the primary NF-κB p65 antibody was added to RAW 264.7 cells for 1 h and then incubated with a FITC-labeled second antibody for 1 h. Finally, we added DAPI and viewed green p65 protein and blue nuclei fluoresce by laser confocal microscopy.

Effect of RATAPW on Lymphocyte Proliferation

The spleen lymphocyte suspension was obtained by grinding, sieving, and lysis of erythrocytes. Notably, 1×10^7 cells/well lymphocyte cells in 96-well plates were incubated with different concentrations of RATAPW or pre-added the mitotic inducer Con A (5 μg/ml) and LPS (2 μg/ml). After 48 h, the MTT method was used to evaluate the effect of RATAPW on lymphocyte proliferation *in vitro*.

Statistical Analysis

Dates were expressed as mean value ± standard deviation. One-way and two-way ANOVA were used for statistical significance analysis using the GraphPad Prism 8.0 software.

RESULTS

Alkali Extraction and Column Chromatography Purification of Polysaccharide

The crude polysaccharide was isolated from dried *Rhizoma Acori Tatarinowii* through alkali extraction (**Figure 1**). A polysaccharide designated RATAPW was obtained after DEAE-52 cellulose ion-exchange chromatography and gel filtration chromatography purification steps. The yield of RATAPW was 2.41 ± 0.27% from the crude polysaccharide.

Molecular Weight and Infrared Spectral Analysis

The HPGPC peak revealed that the polysaccharide RATAPW was homogeneous and of high purity, with only one symmetrical absorption peak (20). The weight-average molecular weight (Mw) of RATAPW was 2.51×10^4 Da (T: 41.803 min) according to the calibration curve (**Figure 2A**). In **Figure 2B**, the bands in the 3,369.63 cm^{-1}, 2,933.30 cm^{-1}, 1,643.24 cm^{-1}, and 1,370 cm^{-1} regions are characteristic absorption peaks of RATAPW (21). The typical vibration at 3,369.63 cm^{-1} corresponded to the -OH stretching. The bands at 2,933.30 cm^{-1} and 1,370 cm^{-1} were the characteristic absorption of C-H stretching vibration and the variable angular vibration of C-H. The absorbance band at 1,643.24 cm^{-1} represented asymmetric stretching vibrations of *C* = O bonds.

Chemical and Monosaccharide Composition of RATAPW

The total sugar contents in this fraction were 98.23 ± 0.29% after lyophilization. Only a trace amount of protein (1.52 ± 0.07%) was measurable in RATAPW. HPAEC results showed that RATAPW was mainly composed of glucose (**Figure 3**).

Glycosyl Linkage Types of RATAPW

After methylation, hydrolysis, and acetylation, the PMAAs of RATAPW were analyzed using gas chromatography-mass spectrometry (GC-MS). The major glycosyl linkage type

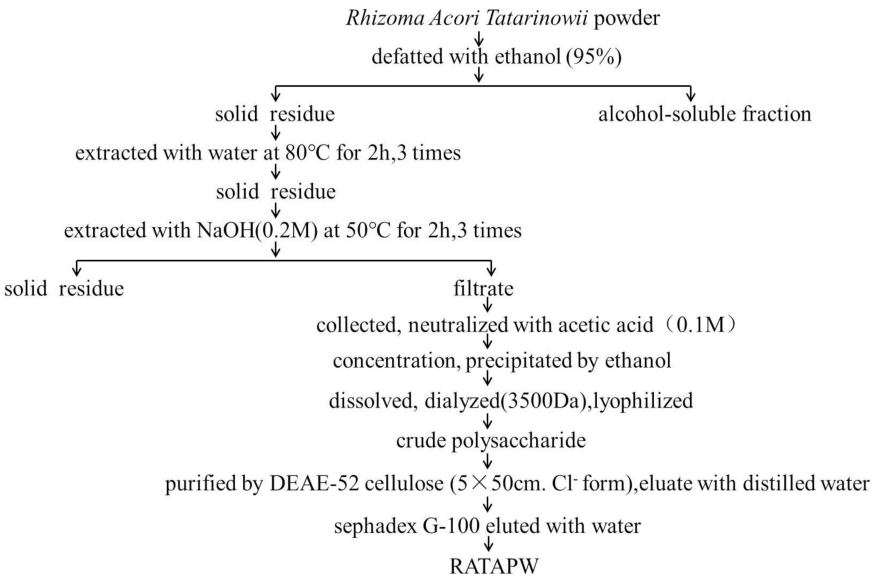

FIGURE 1 | Flowchart of purification polysaccharide RATAPW from *Rhizoma Acori Tatarinowii.*

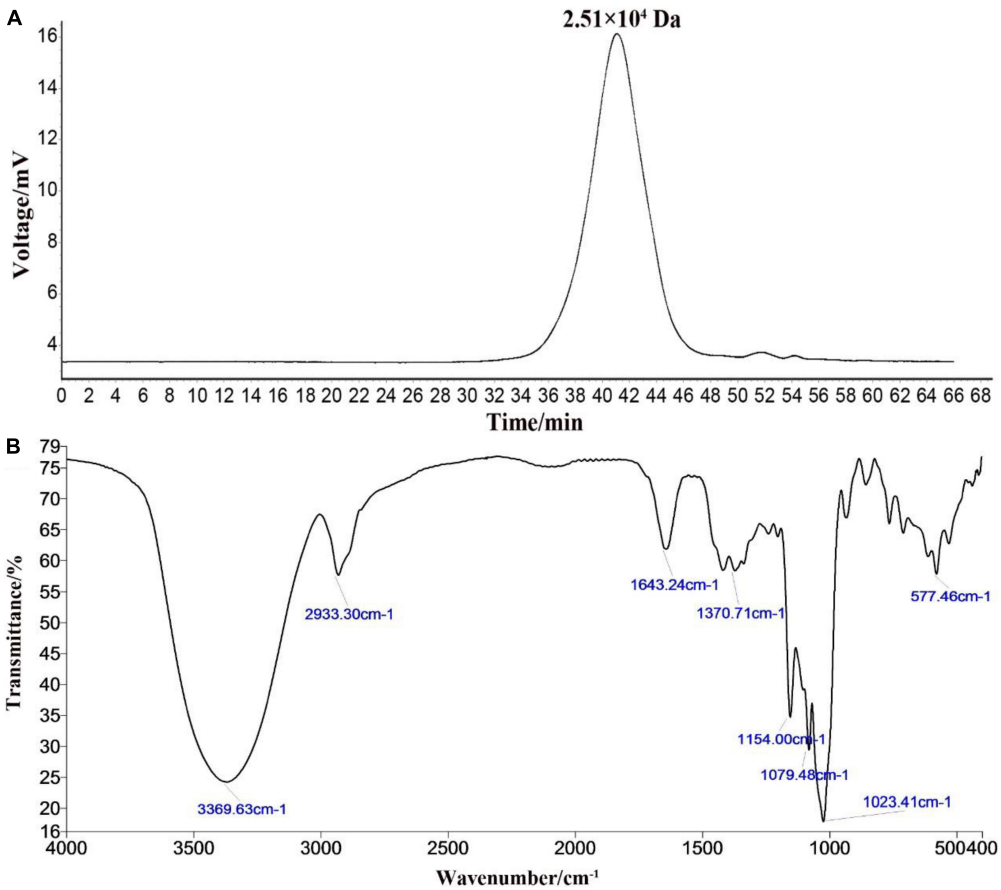

FIGURE 2 | High-performance gel permeation chromatography spectra **(A)** and infrared spectra **(B)** of RATAPW.

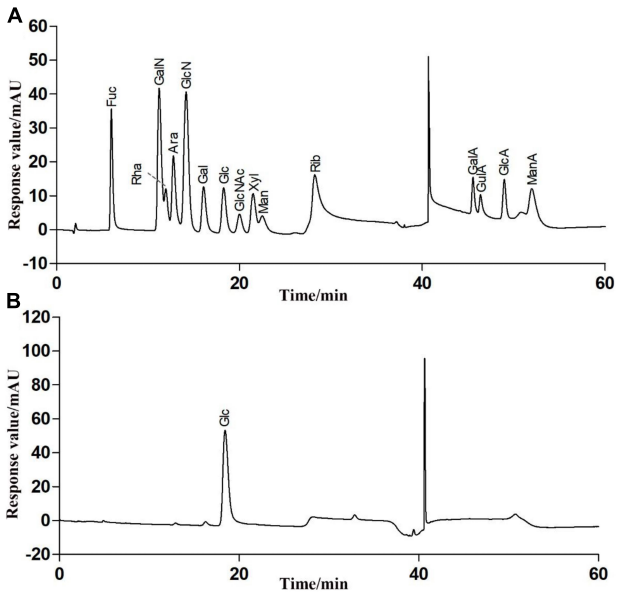

FIGURE 3 | High-performance anion exchange chromatogram of the fifteen mixed standard monosaccharaides **(A)** and purified polysaccharide RATAPW **(B)**.

was →4)-Glcp-(1→ in RATAPW (**Table 1**). In addition, 2.3% →4,6)-Glcp-(1→, 2.89% →6-Glcp-(1→ and 2.57% non-reducing terminals Glcp-(1→ were also detected. Therefore, the backbone of RATAPW should be 1,4-linked-Glcp, and there are three branches at C-6 for one hundred glucose residues in the backbone.

Nuclear Magnetic Resonance Analysis

The precise structural information of RATAPW was identified by NMR spectroscopy. The chemical shifts of main glycosyl linkage residues →4)-α-Glcp-(1→ and →6)-α-Glcp-(1→ were assigned (**Table 2**). The signals at 5.31 and 4.91 ppm in the ^{1}H NMR spectrum were attributed to the H1 of →4)-α-Glcp-(1→ and α-Glcp-(1→ (**Figure 4A**). The overlapping broad peaks around 5.31 ppm indicated the existence of branches in →4)-α-Glcp-(1→ residue. According to the literature (22), the main signal at δ 101.05 ppm was assigned to the C1 of →4)-α-Glcp-(1→ in ^{13}C NMR (**Figure 4B**).

The other signals of H/C were analyzed by COSY and HSQC spectrum (**Figures 4C,D**). In ^{1}H–^{1}H COSY, the cross-peaks at δH/H 5.31/3.55, 3.55/3.90, 3.90/3.58, and 3.58/3.78 ppm suggested that the signals at δ 5.31, 3.55, 3.65, 3.90, and 3.58 ppm corresponded to H1, H2, H3, H4, and H5 of →4)-α-Glcp-(1→ (residue **A**), respectively. HSQC showed that the H1 and C1 signals of →4)-α-Glcp-(1→ were 101.05 and 5.31 ppm. C1–C6 of the residue →4)-α-Glcp-(1→ were δ 101.05, 72.91, 74.56, 78.31, 72.53, and 61.89 ppm, respectively. In the HMBC spectrum (**Figure 4E**), cross-peaks at δ 5.31/78.31 and δ 3.58/101.05 ppm represented the correlation between H1/C4 and H4/C1 of residue →4)-α-Glcp-(1→, which suggested that the backbone of RATAPW was →4)-α-Glcp-(1→4)-α -Glcp-(1→.

The cross-peaks of H1/H4 and H3/H5 in the NOESY spectrum also indicate that the →4)-α-Glcp-(1→ residue was alpha configuration (**Figure 4F**). Based on the monosaccharide composition, methylation, and NMR analysis results, the possible structure of RATAPW was a 1,4-linked α-glucans and branched at C-6 every 32 →4)-α-Glcp-(1→ residue (**Figure 5**).

RATAPW Induced RAW 264.7 to Produce TNF-α *via* the NF-κB Pathway

The MTT results showed that different concentrations of RATAPW did not promote the proliferation of macrophages (**Supplementary Figure 1**). As shown in **Figure 6A**, TNF-α production of RAW 264.7 cells was significantly increased by RATAPW with a dose-dependent effect. Endotoxin contamination results showed that the endotoxin content is less than 0.01 EU, which ensures that the effect of RATAPW on RAW 264.7 cells was not due to endotoxin contamination (23).

TABLE 1 | Linkage type analysis of RATAPW using gas chromatography-mass spectrometry (GC-MS).

RT	Methylated sugar	Mass fragments (m/z)	Area ratios	Type of linkage
16.11	2,3,4,6-Me4-Glcp	43,45,71,87,101,118,129,145,162	2.57	Glcp-(1→
21.231	2,3,6-Me3-Glcp	43,45,87,99,101,113,118,129,131,162,173,233	92.24	→4)-Glcp-(1→
22.265	2,3,4-Me_3-Glcp	43,45,87,99,101,118,129,162,189,233	2.89	→6-Glcp-(1→
27.192	2,3-Me2-Glcp	43,85,87,99,101,118,127,159,162,201,261	2.3	→4,6)-Glcp-(1→

TABLE 2 | ^{1}H NMR and ^{13}C NMR spectral assignments for RATAPW.

Glycosyl residues	H1	H2	H3	H4	H5	H6a	H6b
	C1	C2	C3	C4	C5	C6	
→4)-α-Glcp-(1→	5.31	3.55	3.9	3.58	3.78	3.79	3.71
	101.05	72.91	74.56	78.31	72.53	61.89	
α-Glcp-(1→	4.91	3.53	3.67	–	–	–	–
	99.1	–	–	–	–	–	–

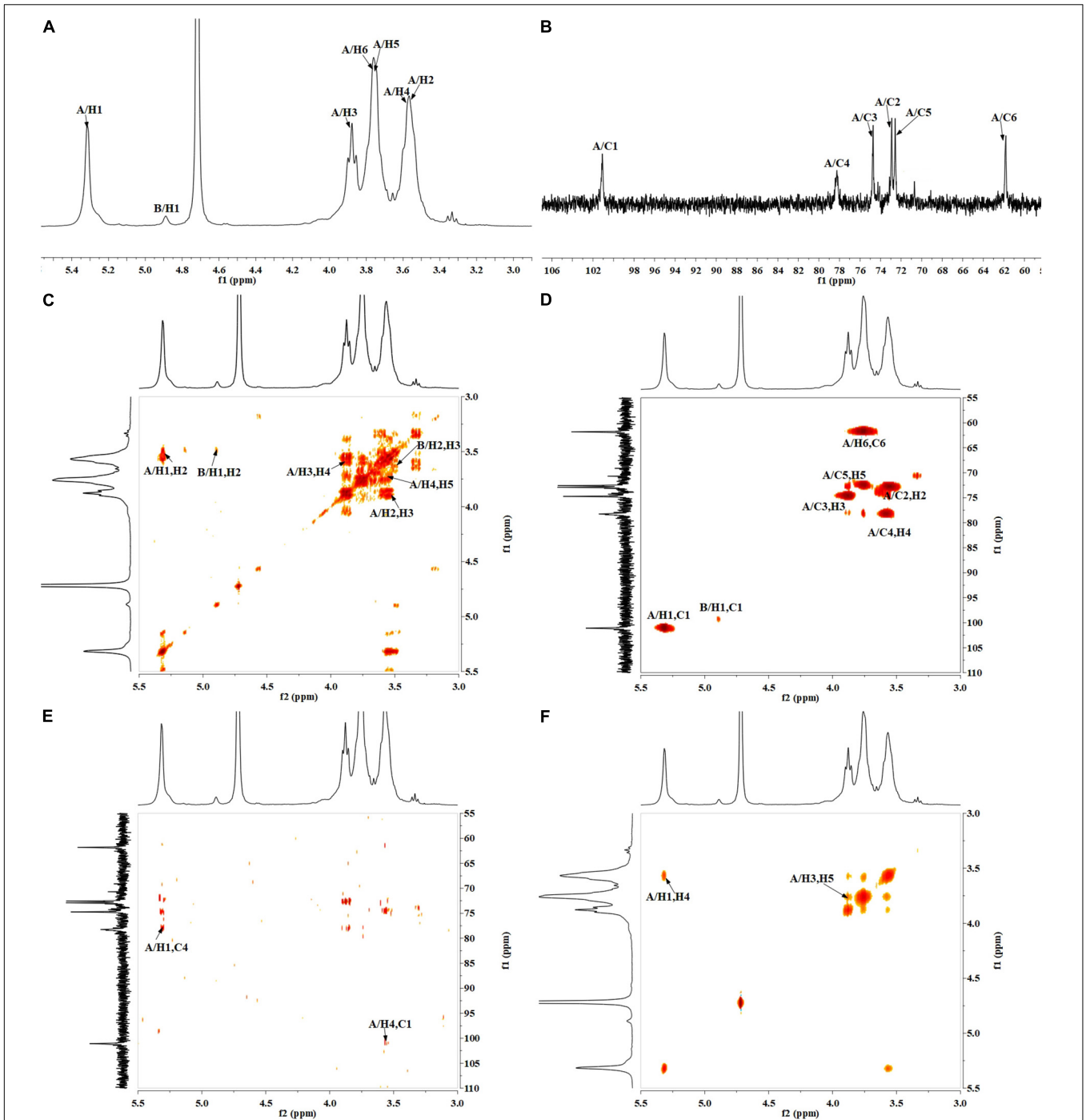

FIGURE 4 | NMR spectra of RATAPW: **(A)** ^{1}H NMR, **(B)** ^{13}C HMR, **(C)** ^{1}H-COSY, **(D)** HSQC, **(E)** HMBC, and **(F)** NOESY. In each figure, codes A and B represent the →4)-α-Glcp-(1→ and α-Glcp-(1→ residue, respectively.

Nuclear factor kappa B is a pivotal nuclear transcription factor, which is associated with multiple immune genes and manipulated the cytokine responses (24). External irritants can cause the inactive IκBα in the cytosolic phosphorylation and degradation and then induce p65 subunit translocation to the nucleus (25, 26). Thus, we detected the NF-κB activation in RAW264.7 cells by immunofluorescence assay. Results showed that RATAPW and LPS could activate NF-κB and make cytoplasmic NF-κB p65 protein translocated to the nucleus (**Figure 6B**). Furthermore, to validate whether the NF-κB activation was involved in RATAPW-induced cytokine production, 3 μM BAY 11-7082 (an NF-κB inhibitor) was added before adding RATAPW or

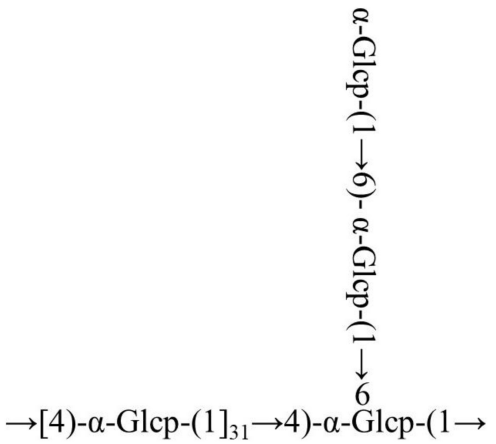

FIGURE 5 | Putative structure of RATAPW.

LPS. Experimental results showed that BAY 11-7082 overtly suppressed TNF-α secretion in RAW264.7 cells (**Figure 6C**). All these results show that RATAPW can activate macrophages *via* the NF-κ B pathway.

RATAPW Promotes Splenocyte Proliferation

As a major site of immune responses, the induction and regulation of spleen proliferation are very important for the immune system (27). Mouse primary splenocytes are mainly composed of T and B cells (28). Our results showed that RATAPW promoted the proliferation of spleen lymphocytes (**Figure 7A**). It also acted in concert to synergistically enhance ConA-stimulated T cells and LPS-induced B cell proliferation in a dose-dependent effect (**Figures 7B,C**).

DISCUSSION

In this study, a polysaccharide named RATAPW (molecular weight: 2.51 × 10^4 Da) was isolated from *Rhizoma Acori Tatarinowii* with alkali extraction and alcohol precipitation, and its primary chemical structure, physicochemical properties, and immune activity were characterized. The HPAEC results showed that RATAPW was mainly composed of glucose, combined with methylation analysis results and NMR spectra, and RATAPW was an α-1,4-glucans branched at C-6 every 32 glucose residues. The bioactivity tests showed that RATAPW could activate

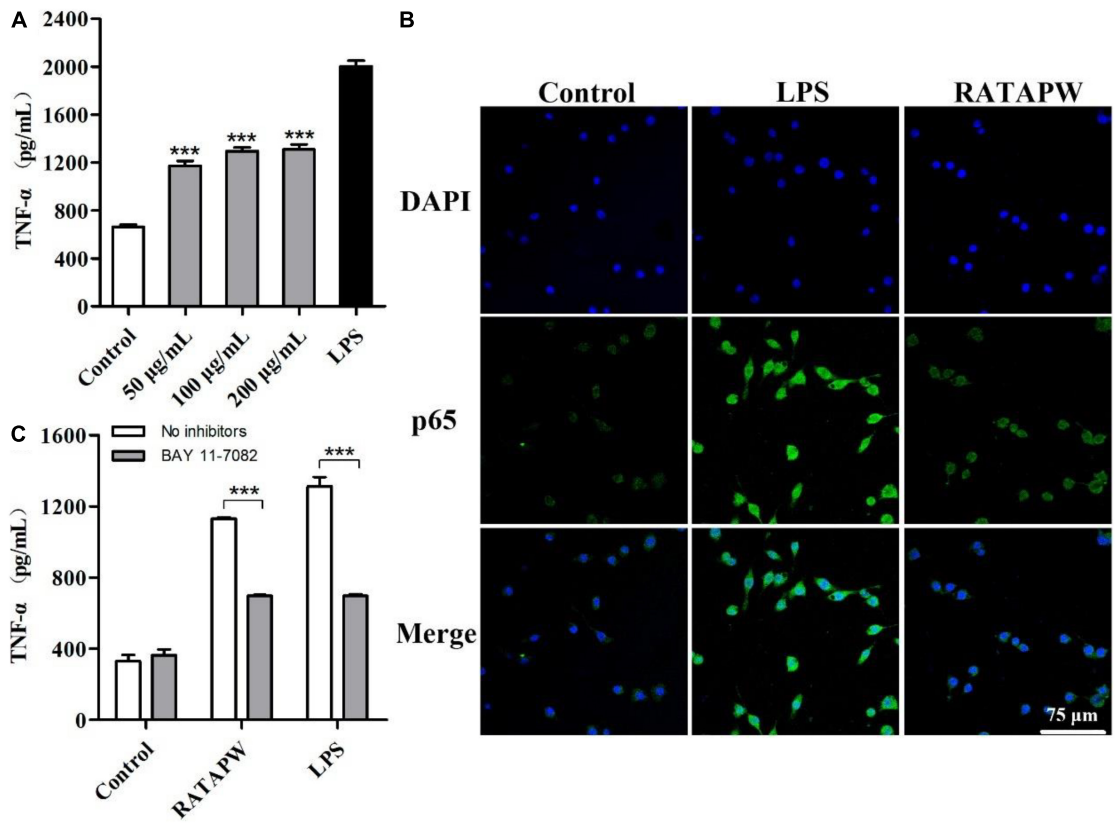

FIGURE 6 | RATAPW activates macrophages *via* the NF-κB pathway. **(A)** RAW264.7 cells were incubated with RATAPW for 24 h, and TNF-α production was tested. ***$p < 0.001$ were compared with the control group. **(B)** An amount of 200 μg/ml RATAPW or 2 μg/ml lipopolysaccharide (LPS) were added to RAW264.7 cells for 3 h, and p65 protein (green) in the nuclei (DAPI) was determined by laser confocal microscopy. **(C)** After being pretreated with PBS (no inhibitors) or BAY 11-7082 for 1 h, RAW264.7 cells were incubated with 200 μg/ml RATAPW or 2 μg/ml LPS for another 24 h. TNF-α production in the supernate was tested.

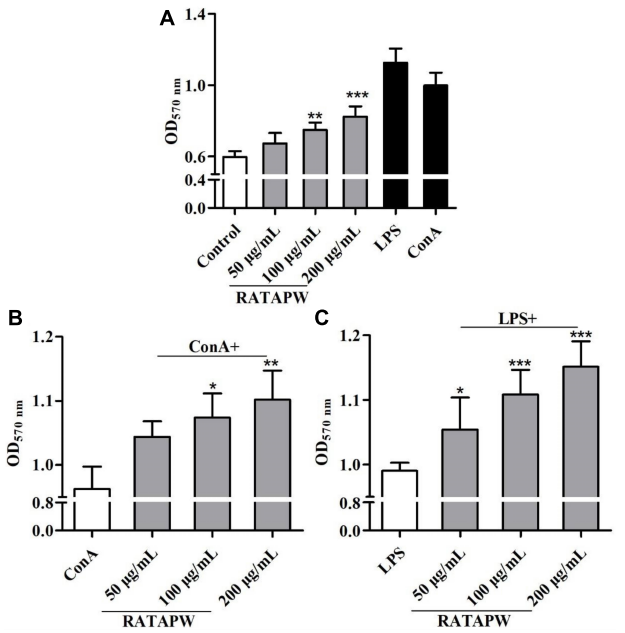

FIGURE 7 | RATAPW promoted splenocyte proliferation. Different concentrations of RATAPW **(A)**, in the presence of mitogens Con A (5 μg/ml) **(B)** or LPS (2 μg/ml) **(C)** were added to the spleen cells for 48 h, and the number was determined using 3-(4,5-dimethyl-2-triazolyl)-2,5-diphenyltetrazolium bromide (MTT) method. $^{***}p < 0.001$, $^{**}p < 0.01$, and $^{*}p < 0.05$ were compared with the control group **(A)**, ConA group **(B)**, or LPS group **(C)**, respectively.

the RAW 264.7 cells increasing TNF-α secretion by NF-κB pathways. Besides, RATAPW can also enhance T and B lymphocyte proliferation.

Glucans are divided into α- and β-conformation, and the linkage of the glucose can be either 1,4 or 1,6 glycoside bonds (29). Reports suggested that the chemical structure and chain conformation of glucan directly affect its biological activity (30). Therefore, it is necessary to detail the structure-activity relationships between glucans and immunoregulation. Till now, it has been known that many natural β-glucans exhibit significant immunomodulatory activities (31). A set of receptors for β-glucans have been revealed, such as toll-like receptors (TLRs), dectin-1, complement receptor 3 (CR3), and lactosylceramide (30). Similarly, a lot of studies have demonstrated that α-glucans also had kinds of immune activities, which can be directly influenced by the solubility, molecular weight, molecular charge, branching degree, and glycosidic bonds of α-glucans (32).

Reports suggest that the (1→3)-, (1→4)-, or (1→6)-α-glucans can stimulate immune cells to secrete cytokines to different degrees (33). Consistently, our results showed that RATAPW was an α-1,4-glucan with few (1→6) branches and can activate macrophages to release cytokines. Our previous study has displayed that two α-glucans from *Radix Paeoniae Alba* with a similar structure to RATAPW can also promote splenocyte proliferation and RAW264.7 phagocytic activity (34). The molecular weight is another important impact factor for macrophage stimulation and the production of cytokines. The molecular weight of RATAPW was 25.1 kDa, within the range of 10 kDa to 1,000 kDa. Previous reports have indicated that polysaccharides with molecular weights in this range have the highest immunoregulatory activities (35). The solubility can also affect the recognition of polysaccharides by the antigen-presenting cells (APCs) and cytokine production (36). It has been demonstrated that the increase of water solubility of α-glucans enhances its immunostimulant activity (37). The immune activity of RATAPW might also be linked to its high solubility. Therefore, it was speculated that the immunoregulatory activity of RATAPW might be attributed to its high solubility, moderate molecular weight, and low degree of branching.

Glucans are toll-like receptor 4 (TLR4) ligands on the macrophages' cell surface and activate immune cells through the TLR4/IKK/NK-κB pathway (38). α-Glucan could also activate the MAPK signaling pathway to promote the secretion of cytokines (9). Our results proved that RATAPW activates the RAW 264.7 cells and increases TNF-α secretion by the NF-κB pathways. The possible receptor and molecular pathway of RATAPW need to be further explored. In general, the glucan RATAPW could be explored as an immunomodulator in the field of health food and medicine.

DATA AVAILABILITY STATEMENT

The original contributions presented in this study are included in the article/**Supplementary Material**, further inquiries can be directed to the corresponding authors.

AUTHOR CONTRIBUTIONS

WZ designed the research, performed the experiments, analyzed the data, and wrote the manuscript. JH and YH performed the experiments. JL analyzed the experimental data. JZ analyzed the NMR data. PL supervised the work and wrote and reviewed the manuscript. All authors contributed to the article and approved the submitted version.

FUNDING

This study was supported by the Science and Technology Innovation Project of Colleges and Universities in Shanxi Province (2021L146), the National Natural Science Foundation of China (No. 31800678), the Fundamental Research Program of Shanxi Province (20210302124129), and the Special Guiding Projects for the Commercialization of Scientific and Technological Achievements of Shanxi Province (202104021301038).

SUPPLEMENTARY MATERIAL

The Supplementary Material for this article can be found online at: https://www.frontiersin.org/articles/10.3389/fnut.2022.942241/full#supplementary-material

REFERENCES

1. Fu Y, Yang Y, Shi J, Bishayee K, Lin L, Lin Y, et al. Acori tatarinowii rhizoma extract ameliorates Alzheimer's pathological syndromes by repairing myelin injury and lowering Tau phosphorylation in mice. *Pharmazie.* (2020) 75:395–400. doi: 10.1691/ph.2020.0492
2. Lam K, Huang Y, Yao P, Wang H, Dong T, Zhou Z, et al. Comparative study of different *Acorus* species in potentiating neuronal differentiation in cultured PC12 cells. *Phytother Res.* (2017) 31:1757–64. doi: 10.1002/ptr.5904
3. Wu J, Zhang X, Sun Q, Chen M, Liu S, Zhang X, et al. β-asarone inhibits gastric cancer cell proliferation. *Oncol Rep.* (2015) 34:3043–50. doi: 10.3892/or.2015.4316
4. Shi B, Liu J, Zhang Q, Wang S, Jia P, Bian L, et al. Effect of co-administration of Acori Tatarinowii Rhizoma volatile oil on pharmacokinetic fate of xanthotoxol, oxypeucedanin hydrate, and byakangelicin from *Angelicae dahuricae* Radix in rat. *J Sep Sci.* (2020) 43:2349–62. doi: 10.1002/jssc.201901250
5. Li Y, Wang X, Ma X, Liu C, Wu J, Sun C. Natural polysaccharides and their derivates: a promising natural adjuvant for tumor immunotherapy. *Front Pharmacol.* (2021) 12:621813. doi: 10.3389/fphar.2021.621813
6. Zhang W, Gong L, Zhou Z, Sun M, Li Y, Sun J, et al. Structural characterization and immunomodulatory activity of a mannan from *Helvella leucopus*. *Int J Biol Macromol.* (2022) 212:495–507. doi: 10.1016/j.ijbiomac.2022.05.132
7. Yang X, Wei S, Lu X, Qiao X, Simal-Gandara J, Capanoglu E, et al. A neutral polysaccharide with a triple helix structure from ginger: characterization and immunomodulatory activity. *Food Chem.* (2021) 350:129261. doi: 10.1016/j.foodchem.2021.129261
8. Zhang W, Song D, Xu D, Wang T, Chen L, Duan J. Characterization of polysaccharides with antioxidant and immunological activities from Rhizoma Acori Tatarinowii. *Carbohydr Polym.* (2015) 133:154–62. doi: 10.1016/j.carbpol.2015.07.018
9. Cui F, Jiang L, Qian L, Sun W, Tao T, Zan X, et al. A macromolecular α-glucan from fruiting bodies of *Volvariella volvacea* activating RAW264. 7 macrophages through MAPKs pathway. *Carbohydr Polym.* (2020) 230:115674. doi: 10.1016/j.carbpol.2019.115674
10. He Z, Zhu Y, Bao X, Zhang L, Li N, Jiang G, et al. Optimization of alkali extraction and properties of polysaccharides from *Ziziphus jujuba* cv. residue. *Molecules.* (2019) 24:2221. doi: 10.3390/molecules24122221
11. DuBois M, Gilles K, Hamilton J, Rebers P, Smith F. Colorimetric method for determination of sugars and related substances. *Anal Chem.* (2002) 28:350–6.
12. Zhang W, Chen L, Li P, Zhao J, Duan J. Antidepressant and immunosuppressive activities of two polysaccharides from Poria cocos (Schw.) Wolf. *Int J Biol Macromol.* (2018) 120:1696–704. doi: 10.1016/j.ijbiomac.2018.09.171
13. Kakar M, Li J, Mehboob M, Sami R, Benajiba N, Ahmed A, et al. Purification, characterization, and determination of biological activities of water-soluble polysaccharides from *Mahonia bealei*. *Sci Rep.* (2022) 12:8160. doi: 10.1038/s41598-022-11661-3
14. Bradford M. A rapid and sensitive method for the quantitation of microgram quantities of protein utilizing the principle of protein-dye binding. *Anal Biochem.* (1976) 72:248–54. doi: 10.1006/abio.1976.9999
15. Wang Z, Liu X, Bao Y, Wang X, Zhai J, Zhan X, et al. Characterization and anti-inflammation of a polysaccharide produced by *Chaetomium globosum* CGMCC 6882 on LPS-induced RAW 264.7 cells. *Carbohydr Polym.* (2021) 251:117129. doi: 10.1016/j.carbpol.2020.117129
16. Wang Z, Xue R, Cui J, Wang J, Fan W, Zhang H, et al. Antibacterial activity of a polysaccharide produced from *Chaetomium globosum* CGMCC 6882. *Int J Biol Macromol.* (2019) 125:376–82. doi: 10.1016/j.ijbiomac.2018.11.248
17. Ji X, Guo J, Ding D, Gao J, Hao L, Guo X, et al. Structural characterization and antioxidant activity of a novel high-molecular-weight polysaccharide from *Ziziphus Jujuba* cv. Muzao. *J Food Meas Character.* (2022) 16:2191–200. doi: 10.1007/s11694-022-01288-3
18. Ji X, Guo J, Pan F, Kuang F, Chen H, Guo X, et al. Structural elucidation and antioxidant activities of a neutral polysaccharide from Arecanut (*Areca catechu* L.). *Front Nutr.* (2022) 9:853115. doi: 10.3389/fnut.2022.853115
19. Zhang W, Hu Y, He J, Guo D, Zhao J, Li P. Structural characterization and immunomodulatory activity of a novel polysaccharide from Lycopi Herba. *Front Pharmacol.* (2021) 12:691995. doi: 10.3389/fphar.2021.691995
20. Ji X, Cheng Y, Tian J, Zhang S, Jing Y, Shi M. Structural characterization of polysaccharide from jujube (*Ziziphus jujuba* Mill.) fruit. *Chem Biol Technol Agric.* (2021) 8:54. doi: 10.1186/s40538-021-00255-2
21. He P, Dong Z, Wang Q, Zhan QP, Zhang MM, Wu H. Structural characterization and immunomodulatory activity of a polysaccharide from *Eurycoma longifolia*. *J Nat Prod.* (2019) 82:169–76. doi: 10.1021/acs.jnatprod.8b00238
22. Hu X, Huang Y, Dong Q, Song L, Yuan F, Yu R. Structure characterization and antioxidant activity of a novel polysaccharide isolated from pulp tissues of Litchi chinensis. *J Agric Food Chem.* (2011) 59:11548–52. doi: 10.1021/jf203179y
23. Zhang W, Mu H, Dong D, Wang D, Zhang A, Duan J. Alteration in immune responses toward N-deacetylation of hyaluronic acid. *Glycobiology.* (2014) 24:1334–42. doi: 10.1093/glycob/cwu079
24. Cao L, Li R, Chen X, Xue Y, Liu D. Neougonin a inhibits lipopolysaccharide-induced inflammatory responses *via* downregulation of the NF-kB signaling pathway in RAW 264.7 macrophages. *Inflammation.* (2016) 39:1939–48. doi: 10.1007/s10753-016-0429-9
25. Yan J, Han Z, Qu Y, Yao C, Shen D, Tai G, et al. Structure elucidation and immunomodulatory activity of a β-glucan derived from the fruiting bodies of *Amillariella mellea*. *Food Chem.* (2018) 240:534–43. doi: 10.1016/j.foodchem.2017.07.154
26. Mendes Sdos S, Candi A, Vansteenbrugge M, Pignon MR, Bult H, Boudjeltia KZ, et al. Microarray analyses of the effects of NF-kappaB or PI3K pathway inhibitors on the LPS-induced gene expression profile in RAW264.7 cells: synergistic effects of rapamycin on LPS-induced MMP9-overexpression. *Cell Signal.* (2009) 21:1109–22. doi: 10.1016/j.cellsig.2009.02.025
27. Batista F, Harwood N. The who, how and where of antigen presentation to B cells. *Nat Rev Immunol.* (2009) 9:15–27. doi: 10.1038/nri2454
28. Huang Y, Tsai K, Tan S, Kang S, Ford M, Harder K, et al. 2B4-SAP signaling is required for the priming of naive CD8(+) T cells by antigen-expressing B cells and B lymphoma cells. *Oncoimmunology.* (2017) 6:e1267094. doi: 10.1080/2162402x.2016.1267094
29. Wagener J, Striegler K, Wagener N. α- and β-1,3-glucan Synthesis and Remodeling. *Curr Top Microbiol Immunol.* (2020) 425:53–82. doi: 10.1007/82_2020_200
30. Jin Y, Li P, Wang F. β-glucans as potential immunoadjuvants: a review on the adjuvanticity, structure-activity relationship and receptor recognition properties. *Vaccine.* (2018) 36:5235–44. doi: 10.1016/j.vaccine.2018.07.038
31. Córdova-Martínez A, Caballero-García A, Roche E, Noriega DC. β-glucans could be adjuvants for SARS-CoV-2 virus vaccines (COVID-19). *Int J Environ Res Public Health.* (2021) 18:12636. doi: 10.3390/ijerph182312636
32. Moreno-Mendieta S, Guillén D, Hernández-Pando R, Sánchez S, Rodríguez-Sanoja R. Potential of glucans as vaccine adjuvants: a review of the α-glucans case. *Carbohydr Polym.* (2017) 165:103–14. doi: 10.1016/j.carbpol.2017.02.030
33. Koppada R, Norozian FM, Torbati D, Kalomiris S, Ramachandran C, Totapally BR. Physiological effects of a novel immune stimulator drug, (1,4)-α-D-glucan, in rats. *Basic Clin Pharmacol Toxicol.* (2009) 105:217–21. doi: 10.1111/j.1742-7843.2009.00383.x
34. Zhang W, Li P, Song D, Niu H, Shi S, Wang S, et al. Structural characterization and biological activities of two α-glucans from radix paeoniae alba. *Glycoconj J.* (2016) 33:147–57. doi: 10.1007/s10719-015-9647-x
35. Zhang X, Qi C, Guo Y, Zhou W, Zhang Y. Toll-like receptor 4-related immunostimulatory polysaccharides: primary structure, activity relationships, and possible interaction models. *Carbohydr Polym.* (2016) 149:186–206. doi: 10.1016/j.carbpol.2016.04.097
36. Wismar R, Brix S, Laerke HN, Frøkiaer H. Comparative analysis of a large panel of non-starch polysaccharides reveals structures with selective

regulatory properties in dendritic cells. *Mol Nutr Food Res.* (2011) 55:443–54. doi: 10.1002/mnfr.201000230

37. Bao X, Duan J, Fang X, Fang J. Chemical modifications of the (1→3)-alpha-D-glucan from spores of *Ganoderma lucidum* and investigation of their physicochemical properties and immunological activity. *Carbohydr Res.* (2001) 336:127–40. doi: 10.1016/s0008-6215(01)00238-5
38. Złotko K, Wiater A. A Report on Fungal (1→3)-α-d-glucans: properties. *Funct Appl.* (2019) 24:3972. doi: 10.3390/molecules24213972

Conflict of Interest: The authors declare that the research was conducted in the absence of any commercial or financial relationships that could be construed as a potential conflict of interest.

Publisher's Note: All claims expressed in this article are solely those of the authors and do not necessarily represent those of their affiliated organizations, or those of the publisher, the editors and the reviewers. Any product that may be evaluated in this article, or claim that may be made by its manufacturer, is not guaranteed or endorsed by the publisher.

Copyright © 2022 Zhang, He, Hu, Lu, Zhao and Li. This is an open-access article distributed under the terms of the Creative Commons Attribution License (CC BY). The use, distribution or reproduction in other forums is permitted, provided the original author(s) and the copyright owner(s) are credited and that the original publication in this journal is cited, in accordance with accepted academic practice. No use, distribution or reproduction is permitted which does not comply with these terms.

frontiers | Frontiers in Nutrition

ORIGINAL RESEARCH
published: 30 June 2022
doi: 10.3389/fnut.2022.934769

Two Novel Polysaccharides From *Clitocybe squamulosa*: Their Isolation, Structures, and Bioactivities

Dongdong Guo[1†], Jiayu Lei[1†], Lijing Xu[1,2], Yanfen Cheng[1,2], Cuiping Feng[1,2], Junlong Meng[1,3], Mingchang Chang[1,3] and Xueran Geng[1,2*]*

[1] College of Food Science and Engineering, Shanxi Agricultural University, Taigu, China, [2] Shanxi Key Laboratory of Edible Fungi for Loess Plateau, Taigu, China, [3] Shanxi Engineering Research Center of Edible Fungi, Taigu, China

OPEN ACCESS

Edited by:
Xiaolong Ji,
Zhengzhou University of Light Industry, China

Reviewed by:
Shuang Zhao,
Beijing Academy of Agriculture and Forestry Sciences, China
Qin Liu,
Henan Academy of Agricultural Sciences (HNAAS), China
Yingyin Xu,
Sichuan Academy of Agricultural Sciences, China

***Correspondence:**
Mingchang Chang
sxndcmc@163.com
Xueran Geng
gengxueran2007@163.com

[†] These authors have contributed equally to this work

Specialty section:
This article was submitted to Food Chemistry, a section of the journal Frontiers in Nutrition

Received: 03 May 2022
Accepted: 23 May 2022
Published: 30 June 2022

Citation:
Guo D, Lei J, Xu L, Cheng Y, Feng C, Meng J, Chang M and Geng X (2022) Two Novel Polysaccharides From Clitocybe squamulosa: Their Isolation, Structures, and Bioactivities. Front. Nutr. 9:934769. doi: 10.3389/fnut.2022.934769

The crude polysaccharides from the fruiting bodies of *Clitocybe squamulosa* (CSFP) were isolated by hot-water extraction. Two novel polysaccharides, CSFP1-β and CSFP2-α, were further purified by DEAE-52 anion exchange and Sephacryl S-400 gel filtration chromatography, and the purities reached 98.44 and 97.83%, respectively. The structural characteristics and bioactivities of CSFP, CSFP1-β, and CSFP2-α were identified by the combination of chemical and instrumental analysis. Results showed that CSFP was formed by the aggregation of honeycomb spherical materials; CSFP1-β and CSFP2-α were interwoven by reticular and fibrous structures, respectively. Purified components of both CSFP1-β and CSFP2-α showed typical infrared absorption peaks of polysaccharides, and contents of nucleic acid and protein decreased significantly. Simultaneously, CSFP with a molecular weight (Mw) of 1.948×10^4 Da were composed mainly of glucose, mannose, galactose, and rhamnose. CSFP1-β was composed mainly of glucose, galactose, and mannose, while CSFP2-α was composed of glucose, and both their *Mw* distributions were uneven. Compared with CSFP, the antioxidant activities of CSFP1-β and CSFP2-α were significantly improved ($p < 0.05$), and they both showed good abilities to bind free cholesterol and bile acid salts *in vitro*. The binding abilities of the two compounds were found to be 68.62 and 64.43%, and 46.66 and 45.05 mg/g, respectively. CSFP, CSFP1-β, and CSFP2-α had good bacteriostatic effects with a linear increasing relationship to increasing concentration. In addition, CSFP promoted the growth of RAW264.7 cells and has potential immunomodulatory, anti-inflammatory, and anti-tumor activities.

Keywords: *Clitocybe squamulosa* polysaccharides, purification, structural characterization, bioactivity, physicochemical properties

HIGHLIGHTS

- *Clitocybe squamulosa* is a precious wild edible fungus, which is rich in a variety of nutrients.
- Two polysaccharides named CSFP1-α and CSFP2-β were isolated from *Clitocybe squamulosa*.
- CSFP1-α and CSFP2-β show good biological activity.
- CSFP can promote RAW264.7 cell growth.

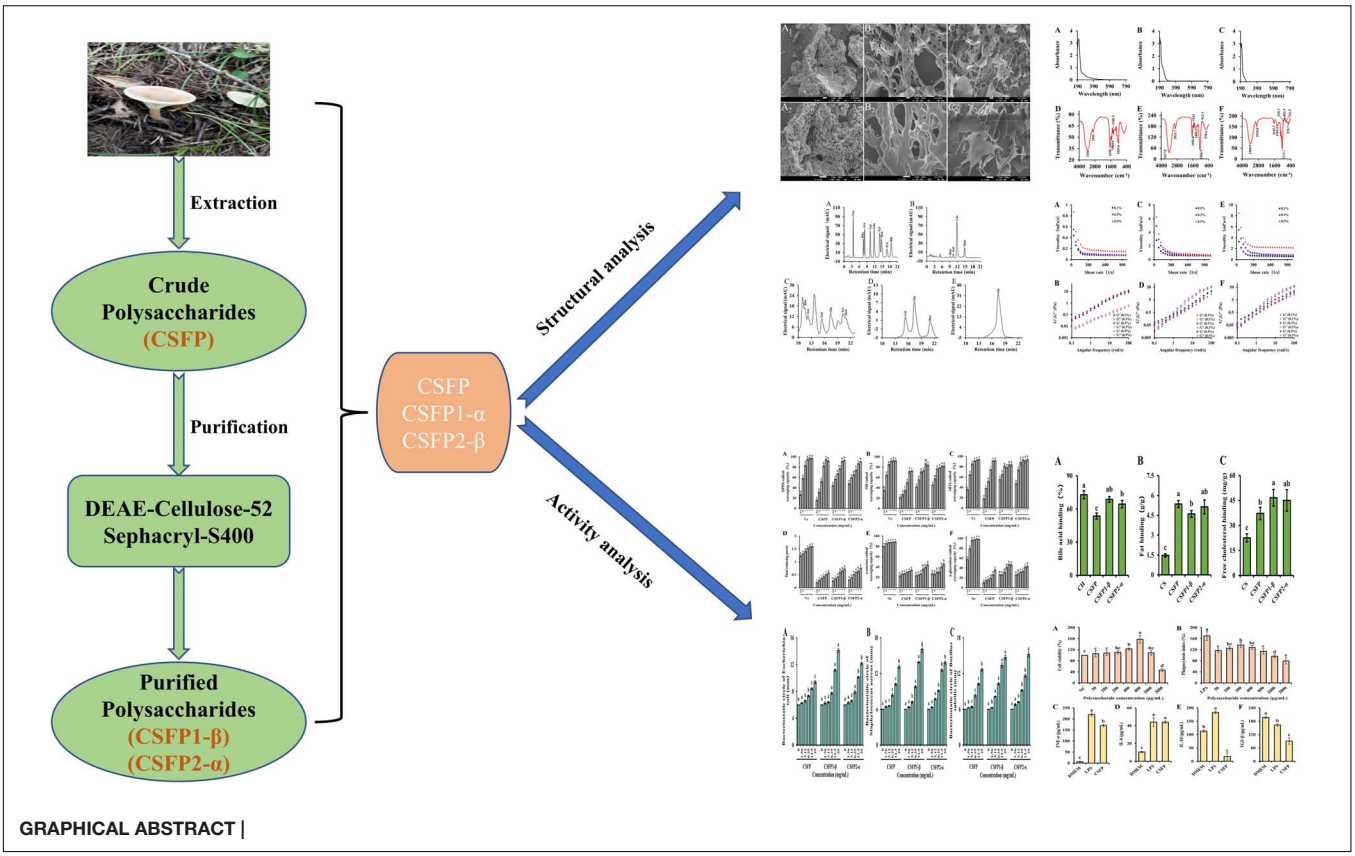

GRAPHICAL ABSTRACT |

INTRODUCTION

Polysaccharides are a natural biomaterial, widely present in animals, plants, and microorganisms. Previous research found that polysaccharides exhibit a variety of health promotion and drug regulation effects, such as antioxidant (1), anti-tumor (2), and immune regulation (3), and also have the potential to prevent the effects of hyperglycemia and high cholesterol (4). In recent years, functional mushroom-derived polysaccharides have been widely applied in medicine, food, and other fields because of their multiple biological effects and low toxicity, and lack of severe side effects (5, 6). So far, studies have reported the *in vitro* bioactivities of a variety of natural mushroom polysaccharides. For example, a novel acid heteropolysaccharide isolated from a spent mushroom substrate of *Pleurotus eryngii* exhibited strong superoxide radical [EC 50 = (0.33 ± 0.02) mg/ml], hydroxyl radical [EC 50 = (1.19 ± 0.02) mg/ml], and DPPH radical [EC 50 = (0.52 ± 0.02) mg/ml] scavenging rates in a dose-dependent manner (7). Hao et al. (8) proved that *Pleurotus citrinopileatus* polysaccharides showed non-competitive inhibition of α-glucosidase activity (IC 50 = 0.556 mg/ml) and could reduce the oxidative stress in HepG2-IR cells. Wang et al. (9) prepared polysaccharides from *Armillariella tabescens* mycelia (PAT) with a remarkable inhibitory effect on the growth of typical food-borne pathogenic bacteria using a green technique. The results showed that PAT could inhibit the growth of *Escherichia coli*, *Proteus vulgaris*, *Bacillus subtilis*, and *Staphylococcus aureus* cells, with minimum inhibitory concentrations of 0.5, 1.0, 4.0, and 4.0 mg/ml, respectively. Moreover, Xiao et al. (10) extracted and purified a rare wild *Lactarius deliciosus* fruiting body polysaccharides (LDP-1). LDP-1 with a *Mw* of 9.8×10^5 Da showed immunological activity against RAW264.7 cells, which can promote the proliferation and phagocytosis of RWA264.7. The cytokines of TNF-α, IL-1β, and IL-6 were secreted in a concentration-dependent manner (at 4.83, 17.8, and 11 times that of the control, respectively). Therefore, mushroom polysaccharides with natural activity have very important research value.

In addition, the bioactivity and structural characteristics of mushroom polysaccharides have been explored using various analytical methods, which found that there was a close relationship between them (11). Ji et al. (12) discovered that ginseng (*Panax ginseng C. A. Meyer*) polysaccharides rich in uronic acid often have higher biological effects, and the α-(1→4)-GalpA and α-(1→4)-Galp components in the main chain are essential for their anti-inflammatory and antiviral effects. Li et al. (13) implied that *Hericium erinaceus* polysaccharide (HEP) with immune activity usually had a relatively large *Mw* and that with low *Mw* had strong antioxidant activity. The activity of HEP was significantly correlated with *Mw*. Moreover, more electron-withdrawing groups such as carboxyl or carbonyl groups in a polysaccharide could lower the dissociation energy of the O-H bond, thus resulting in the greater release of hydrogen atoms. Chen et al. (14) purified a homogeneous *Lentinus edodes*

polysaccharide (LEPA1), which contains no uronic acid and exhibited weak scavenging activity on superoxide radicals, as compared with other polysaccharide fractions containing uronic acid and ascorbic acid. Therefore, it is important to develop new polysaccharide resources from mushrooms and explore their structure–activity relationship in practical production and application.

Clitocybe squamulosa is a precious wild edible mushroom, which is widely distributed in Wutai Mountain Ecological Park, Shanxi Province, China. Its fruiting bodies have a firm and tender texture, unique flavor, and are rich in nutrients, making them popular among consumers (15). Due to the differences in purity and structure–activity relationships of polysaccharides, mushroom-derived polysaccharides from different sources impart different physiological functions. So far, most of the research on *C. squamulosa* polysaccharides (CSFP) has focused on the extraction and utilization of crude polysaccharides, which is not conducive to the in-depth exploration of the structure–activity relationship of polysaccharides. There have been no reports until now concerning the isolation, purification, and structural elucidation of CSFP. The main purpose of this study is to determine the processing and structural characteristics of high-purity polysaccharides isolated from *C. squamulosa* and evaluate their potential biological activities *in vitro*. The research may provide a theoretical basis for further understanding of the structure–activity relationship of polysaccharides.

MATERIALS AND METHODS

Materials and Chemical Reagents

The *Clitocybe squamulosa* were provided by the Edible Fungi Center of Shanxi Agricultural University (Shanxi Province, China). Mouse monocyte macrophage RAW264.7 cells were purchased from Shanghai Zhongqiao Xinzhou Biotechnology Co., Ltd (Shanghai Province, China). DEAE-cellulose-52 and Sephacryl S-400 were purchased from Solarbio (Beijing, China) and GE Healthcare (Chicago, IL, United States). All other chemical reagents were of analytical grade.

Extraction and Purification of CSFP

The CSFP could be extracted according to a previously reported method (16). In short, the *C. squamulosa* fruiting body powder was mixed with ultrapure water in a ratio of 1:30 (*w/v*). Then, the mixture was filtered after 3.6 h in a water bath at 80°C and concentrated with a rotary evaporator (IKA, China). The zinc acetate potassium ferrocyanide method was adopted for protein removal, followed by ultrapure water dialysis (molecular retention 3,500 Da). The dialysate and absolute ethanol were alcohol-precipitated overnight in the ratio of 1:4, and the sediment was collected, freeze-dried, and stored at low temperature for later assays. CSFP could be further isolated and purified according to the previously reported method (2). Briefly, CSFP could be fully dissolved in ultrapure water, configured into an aqueous solution (10 mg/ml), loaded into a DEAE-cellulose-52 ion exchange column (2.8 cm × 32 cm), and then eluted successively with 0, 0.1, and 0.3 mol/L NaCl solution (flow rate: 4 ml/min). The eluted components were collected and reloaded into a gel permeation chromatography column (Sephacryl S-400 (XK26 × 100 cm)), and then eluted with 0.2 mol/L NH_4HCO_3 solution at a flow rate of 3 ml/min. The content of polysaccharides in the collecting tube was determined by a phenol-sulfuric acid method (17), and the elution curve was drawn according to OD_{490} data. The main fraction was collected for subsequent analyses.

Chemical Composition

The method of determination of polysaccharide content was consistent with that described in section "Extraction and Purification of CSFP," and glucose was used as the standard. The reducing sugar (C_R) content was determined by the DNS method with glucose as a standard (18). The content of uronic acids was determined by the sulfuric acid-carbazole method with galacturonic acid as a standard (18). The protein content was determined by Coomassie brilliant blue method with BSA as a standard (19).

Structural Analysis

Scanning Electron Microscopy

Three different polysaccharide samples (CSFP, CSFP1-β, and CSFP2-α) were coated on the sample sticking table, respectively, and gold-spray-coated. Scanning Electron Microscopy (SEM) with a 20.0-kV accelerating voltage (Zeiss Merlin, Germany) was adopted to observe the morphological characteristics of the samples at different magnifications (2).

Ultraviolet–Visible Absorption Spectra

Freeze-dried samples (CSFP, CSFP1-β, and CSFP2-α) were prepared into 1 mg/ml solutions with ultrapure water, respectively. The absorption peaks of polysaccharide samples at 260 and 280 nm were measured using a Cary60 UV spectrophotometer (Agilent, United States) in the range of 190–800 nm (20).

Fourier-Transformed Infrared Spectroscopy

The powdered samples (CSFP, CSFP1-β, and CSFP2-α, respectively) weighing 1 mg and dry KBr powder (150 mg) were mixed evenly, pressed in an FW-4A powder tablet press, and the pressed samples were analyzed using a spectrophotometer (TENSOR 27, Bruker, Germany) in the range of 400–4,000 cm^{-1}.

Monosaccharide Composition

The monosaccharide composition of different samples (CSFP, CSFP1-β, and CSFP2-α) was measured by using ICS5000 + ion chromatography (Thermo Scientific, United States). The sample loading quantity was 20 μl, and the chromatographic conditions included mobile phase A (ultrapure water), mobile phase B (100 mmol/L NaOH solution), and column temperature (30°C) (21).

Molecular Weight Distribution

The *Mw* of different samples (CSFP, CSFP1-β, and CSFP2-α) was measured by high-performance gel permeation chromatography (HPGPC) with 18-angle laser light scattering (Wyatt Technology, United States). We eluted 0.1 mol/L $NaNO_3$ (at a flow rate of 0.5 ml/min), and then injected 20 μl samples (5.0 mg/ml) at 35°C (22).

Rheological Properties

The effects of CSFP, CSFP1-β, and CSFP2-α samples at different concentrations (1, 3, and 5%) on the viscosity of polysaccharide solution were measured using MCR 102 rheometer (loaded with lamina CP 50-1, diameter 50 mm, Anton Paar, Graz, Austria). Similarly, the variations in storage modulus (*G'*) and loss modulus (*G"*) of 1, 3, and 5% polysaccharide solutions at oscillation frequencies from 0.1 to 100 rad/s were also studied (23).

In vitro Bioactivity Analysis

Antioxidant Activities

The DPPH, ·OH, and ABTS radical scavenging abilities of different samples (CSFP, CSFP1-β, and CSFP2-α) were determined strictly based on the methods of a correlation test kit (Solarbio Science, Beijing, China). The total reducing power of different samples could be determined according to the previously reported method (24, 25). In short, we added 1 ml of polysaccharide solution, 2.5 ml of phosphoric acid buffer (pH 6.6, 0.2 mol/L), and 2.5 ml of 1% potassium ferricyanide solution to the test tube, mixed these evenly, and placed the specimen in a water bath at 50°C for 20 min. We then added 2.5 ml of 10% trichloroacetic acid solution and centrifuged the specimen at 1,000 rpm for 10 min. We mixed 2.5 ml of supernatant, 2.5 ml of distilled water, and 6.5 ml of 0.1% ferric chloride solution evenly, stood it for 10 min, and measured the absorbance at 700 nm. The reducing power was represented by the absorbance value. Vitamin C (Vc) was used as a positive control.

Enzymatic Inhibitory Activities

The α-glucosidase and α-amylase inhibitory activities of different samples (CSFP, CSFP1-β, and CSFP2-α) were assessed according to the previously reported methods (26, 27). Acarbose (Ac) was used as a positive control.

In vitro Binding Properties

The binding capacities (bile acid, fat, and free cholesterol) of different samples (CSFP, CSFP1-β, and CSFP2-α) *in vitro* were estimated according to the previously reported methods (28). Carboxymethylcellulose sodium (CS) and cholestyramine (CH) were used as positive controls, respectively.

In short, the method for the determination of fat-binding capacity is as follows: we fully dissolved 0.5 g of polysaccharide in 10 ml of ultrapure water, adjusted the pH of the solution to 2.0 with 0.1 mol/L HCl, added 10 g soybean oil, mixed well, incubated at 37°C for 2 h, removed it, adjusted the pH to 7.6 with 0.1 mol/L NaCl solution, incubated at 37°C for 2 h, and then centrifuged it at 4,000 rpm for 20 min. Then carefully removed the unbound oil from the upper layer and weighed it, and the total amount of oil minus the amount of unbound oil is the weight of the combined fat in the sample (expressed in grams per gram of polysaccharide bound soybean oil (g/g)).

The method for determining the binding capacity of polysaccharides to cholesterol includes the following steps. Preparation of micelle solution: 1 ml of micelle solution contained 100 mmo1/L sodium taurocholate, 20 mmol/L cholesterol, 50 mmol/L oleic acid, 1,320 mmol/L sodium chloride, and 150 mmol/L phosphate buffer (pH 7.4). This solution was combined with the polysaccharide in a micellar solution, and the mixed solution was incubated at 37°C for 2 h and centrifuged at 10,000 rpm for 20 min. The supernatant was collected and the cholesterol content was determined using a kit (Solarbio Science, Beijing, China), which was expressed as the amount of bound cholesterol in milligrams per gram of polysaccharide bound cholesterol (mg/g).

The method for determining the binding capacity of polysaccharides to cholate is as follows. We took a certain amount of polysaccharide sample and mixed it with 5 ml of 0.1 mol/L hydrochloric acid solution. Afterward, the mixture was incubated at 37°C for 2 h, the pH of the mixture was adjusted to 7.6 with 0.1 mol/L sodium hydroxide solution, 10 ml of 0.1 mol/L phosphate buffer (containing 0.5 mg/ml cholate) was added, and the solution was incubated at 37°C for 2 h. The content of cholate in the supernatant was analyzed. The amount of polysaccharide bound bile salt was calculated from the difference between the total amount of bile acid salt and the amount of unbound bile salt (expressed in milligrams per gram of polysaccharide bound bile salt (mg/g)).

Bacteriostatic Activity

The antibacterial activities were studied against three bacterial species (*E. coli*, *S. aureus*, and *B. subtilis*) from the Engineering Technology Research Center of Edible Fungi (Shanxi, China) (following a published method (29), with slight modification). Using the K-B filter paper method, CSFP, CSFP1-β, and CSFP2-α solutions with different concentrations (0, 1.56, 3.12, 6.25, 12.5, and 25 mg/ml) were prepared, respectively, and 6-mm filter paper pieces were soaked in the prepared polysaccharide solutions. We then absorbed 100 μl of the activated strain suspension and evenly applied it on a plate prepared with LB medium. The filter paper pieces with the different polysaccharide concentrations were placed on the plate coated with a bacterial solution at equal intervals, and each group of tests could be repeated three times. The filter paper pieces soaked with sterile water were used as blank control. The plate was placed in a constant temperature incubator suitable for strain growth for 48 h, and the diameter of the bacteriostatic circle was recorded.

Effect of CSFP on the Growth of RAW264.7 Cells

Cell Culturing

Converted macrophage RAW264.7 cells were placed in the complete medium containing 1% double antibody and cultured in the incubator at 37°C and 5% CO_2. CSFP solutions

with different concentration gradients were prepared, filtered using a 0.22-um aqueous phase filter membrane, and retained for later assay.

Determination of Cell Viability and Phagocytic Index

The MTT method (2) was used to detect cell viability as follows: the RAW264.7 cell concentration in the logarithmic growth period was adjusted to 1×10^6 pieces/ml. We added 150 μl of sample solution to a cell plate for culture over 12 h at 37°C and 5% CO_2, discarded the medium, and added 150 μl of DMEM complete culture medium containing different concentrations of CSFP. The specimens were cultured for 24 h. Afterward, discarded the supernatant, added 10 μl of 5 mg/ml MTT solution to each well of the plate, cultured them for 4 h at 37°C, discarded the supernatant, and then added 150 μl of DMSO to each well. A normal control group and a blank control group were established at the same time. The absorbance was measured at 490 nm by a microplate reader (SpectraMax i3X, Shanghai, China).

The neutral red method (30) was used to detect cell phagocytic activity. The culture of RAW264.7 cells and the preparation of CSFP solution were the same as in the MTT method. After adding different concentrations of CSFP solution and incubating for 24 h, we removed the supernatant, added 100 μl of 0.075% neutral red PBS solution, cultured for 2 h, discarded the supernatant, washed it three times with PBS, added 100 μl of cell lysate to each well, and allowed the specimens to stand at 4°C for 12 h. The absorbance was measured at 540 nm by a microplate reader (using LPS as the positive control).

Determination of Cytokine Content

Taking RAW264.7 cells in the logarithmic growth period, the cell concentration was adjusted to 1×10^6 pieces/ml. Then, 150 μl of 200 μg/ml CSFP complete medium was added to the test group, and 150 μl of complete medium was added to the blank control group and positive control group, respectively. Each group was cultured at 37°C and 5% CO_2 for 12 h, whereafter the supernatant was removed. Then 150 μl of 1.0 μg/ml LPS DMEM high-sugar medium was added to the experimental group and positive control group, respectively. Next, 150 μl of DMEM high-sugar medium was added to the negative control group, and the determination was conducted after continuous culture for 4 h. The contents of TNF-α, IL-6, IL-10, and TGF- β in the cell culture medium were detected in strict accordance with the instructions supplied with the Enzyme-Linked Immunosorbent Assay (ELISA) Kits (Shanghai, China).

Statistical Analysis

MS-Excel® was used to plot the charts herein. All tests were repeated in triplicate. The results were presented as mean ± standard deviation (SD). Statistical significance analysis was undertaken using SPSS 20.0 software (IBM Inc., Chicago, IL, United States). Analysis of variance (ANOVA) and Duncan's multiple range test ($p < 0.05$) were performed to evaluate differences between the samples.

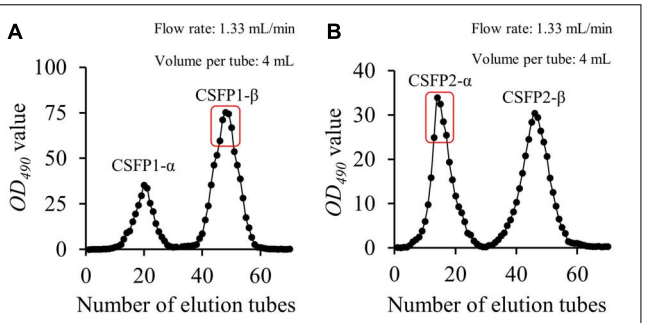

FIGURE 1 | Elution profiles of CSFP in Sephacryl S-400. The sample of CSFP is loaded into the DEAE-52 anion exchange column. The collected component was named as CSFP1 after washing with ultrapure water, and then the collected component was named as CSFP2 after adding 0.1 M NaCl solution. **(A)** Elution profiles of CSFP1 in Sephacryl S-400 of the, and **(B)** Elution profiles of CSFP2 in Sephacryl S-400.

TABLE 1 | The content of polysaccharides, proteins, uronic acid, and reducing sugars in CSFP, CSFP1-β, and CSFP2-α .

Content (%)	Polysaccharide	Protein	Uronic acid	Reducing sugar
CSFP	63.72 ± 4.91^b	3.05 ± 0.10^a	11.81 ± 0.99^a	2.60 ± 0.12^a
$CSFP_1$-β	98.44 ± 1.93^a	1.17 ± 0.08^b	8.97 ± 0.70^b	1.98 ± 0.07^b
$CSFP_2$-α	97.83 ± 1.42^a	1.19 ± 0.05^b	9.42 ± 0.51^b	1.95 ± 0.02^b

Values represent mean ± standard deviation, and different superscript lowercase letters indicate significance ($p < 0.05$) in each row.

RESULTS AND DISCUSSION

Extraction, Purity, and Chemical Composition of CSFP, CSFP1-β, and CSFP2-α

The CSFP (yield, 4.15%) could be obtained after hot-water extraction and ethanol precipitation, and further purified using a DEAE-cellulose-52 ion exchange column and a Sephacryl S-400 gel permeation chromatography column. The main fraction (**Figure 1**) was collected and freeze-dried to obtain the pure polysaccharide (CSFP1-β and CSFP2-α) for structural characterization (**Table 1**). The polysaccharide contents of CSFP, CSFP1-β, and CSFP2-α were 63.72, 98.44, and 97.83%, respectively, and the protein contents were 3.05, 1.17, and 1.19%, respectively. The results showed that purification could reduce the amounts of small molecules, such as pigments, protein, and other impurities, in crude polysaccharide samples and thereby improve the purity (2). In addition, compared with CSFP, the uronic acid contents of CSFP1-β and CSFP2-α decreased significantly ($p < 0.05$), which were 8.97 and 9.42%, respectively. It was found that the uronic acid content of natural polysaccharide may be closely related to its antioxidant activity, binding properties, and α-glucosidase inhibitory effect (30, 31). Moreover, compared with CSFP, the values of C_R of CSFP1-β and CSFP2-α were also significantly reduced ($p < 0.05$), but there was no significant difference between CSFP1-β and CSFP2-α .

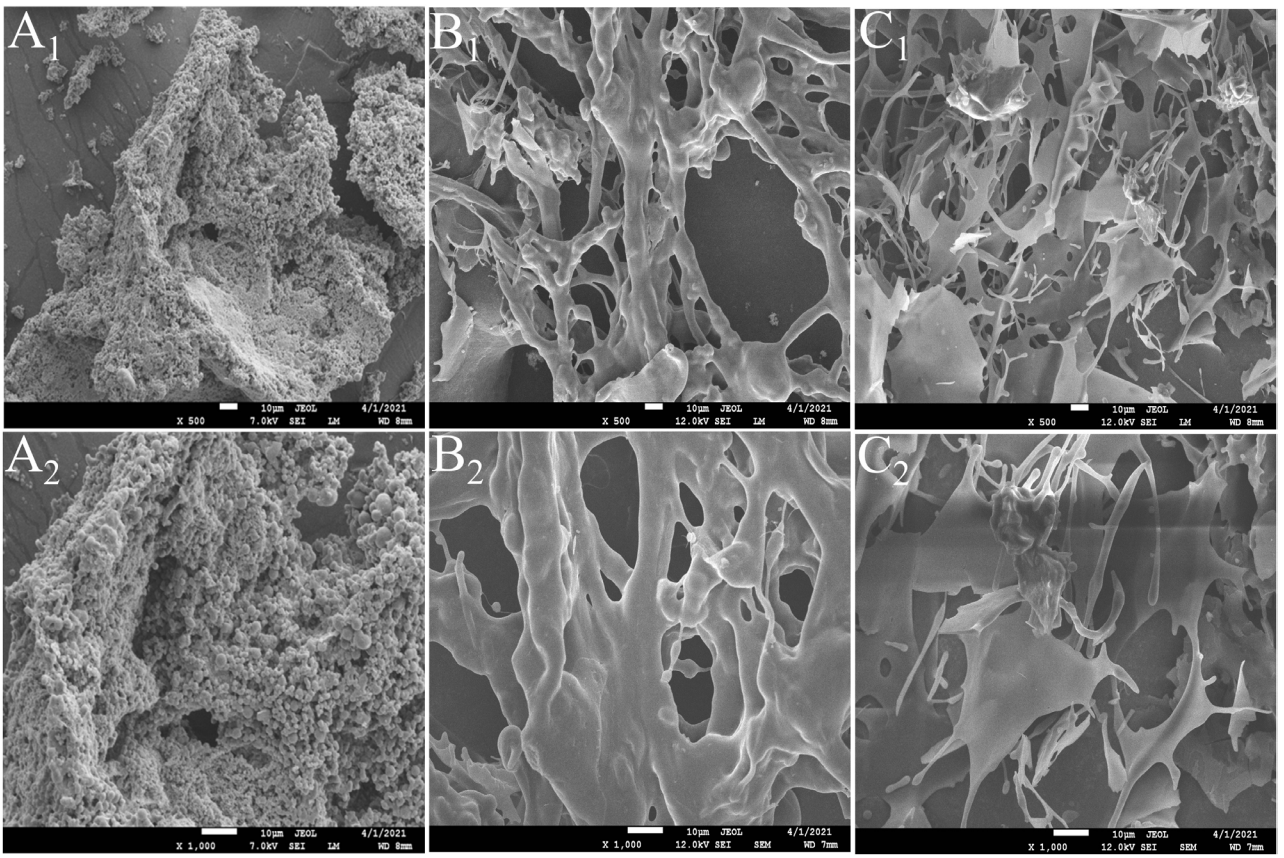

FIGURE 2 | SEM images of CSFP, CSFP1-β, and CSFP2-α at ×500 and ×1,000 magnifications. **(A_1,A_2)** CSFP; **(B_1,B_2)** CSFP1-β; and **(C_1,C_2)** CSFP2-α.

Structural Characteristics Analysis of CSFP, CSFP1-β, and CSFP2-α

Scanning Electron Microscopy Analysis

Different micro-morphological characteristics were found to be the key factors leading to the complexity of polysaccharides (32). The microstructure of CSFP, CSFP1-β, and CSFP2-α was investigated using SEM analysis (**Figure 2**). The results show that CSFP could be formed by irregular spherical particle clusters in a dense honeycomb shape. After purification, there were significant differences in the microstructure between the dialyzed CSFP and the purified polysaccharide fractions (CSFP1-β and CSFP2-α). The apparent morphology of CSFP1-β was rough, and the structure remained intact and was randomly cross-linked by the network structure. However, CSFP2-α was observed to be smooth and uniform, comprising a fibrous structure similar to columnar and flake-like forms. Research showed that the surface structure of CSFP2-α was akin to that of the purified HEFP-2b component of *H. erinaceus* fruiting body polysaccharides (2). Ji et al. (33) speculated that the network structure aggregation of polysaccharide molecules may be closely related to the presence of a variety of carboxyl and hydroxyl groups. It was found that the higher content of hydroxyl and carbonyl groups in the polysaccharide chains appeared to strengthen the intermolecular and intramolecular interactions, resulting in strong molecular chain aggregation and more stable polysaccharide molecules (34).

Ultraviolet–Visible Absorption Spectra and Fourier-Transformed Infrared Spectroscopy Spectroscopic Analyses

The Ultraviolet-Visible absorption spectra (UV spectra) of CSFP, CSFP1-β, and CSFP2-α are shown in **Figures 3A–C**. No absorption peaks were observed at 260 and 280 nm, indicating that three samples contain negligible amounts of nucleic acids and proteins (35). This was consistent with the results of chemical composition wherein little protein was detected in these polysaccharide fractions (**Table 1**). Fourier-transformed infrared spectroscopy was mainly used to distinguish and identify some functional groups, chemical bond substituents, and pyranose ring and furanose ring structures in the natural polysaccharides (36). As shown in **Figures 3D–F**, briefly, the characteristic peaks of CSFP, CSFP1-β, and CSFP2-α at 3,350 cm^{-1}, 3,417.8 cm^{-1}, and 3,384.9 cm^{-1} were due to the tensile vibrations of O-H bonds, which displayed typical polysaccharide peaks (37). The absorption peaks at 2,934 cm^{-1}, 2,931.7 cm^{-1}, and 2,929.8 cm^{-1} were due to the vibrations of C-H bonds (38). The absorption bands at 1,650 cm^{-1}, 1,656.8 cm^{-1}, and 1,643.3 cm^{-1} were caused by the stretching

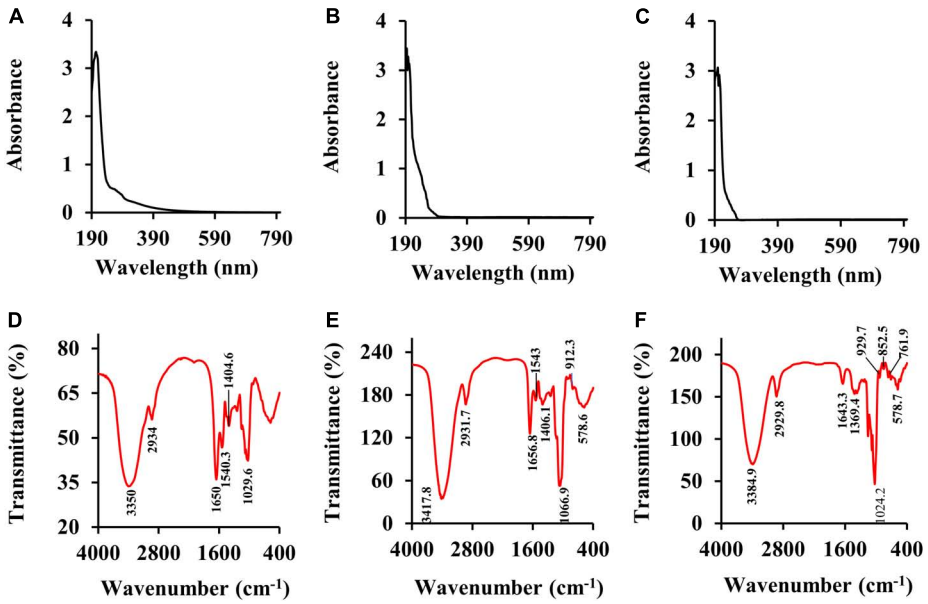

FIGURE 3 | The UV spectra and FT-IR spectra of CSFP, CSFP1-β, and CSFP2-α. **(A–C)** The UV spectra, and **(D–F)** the FT-IR spectra.

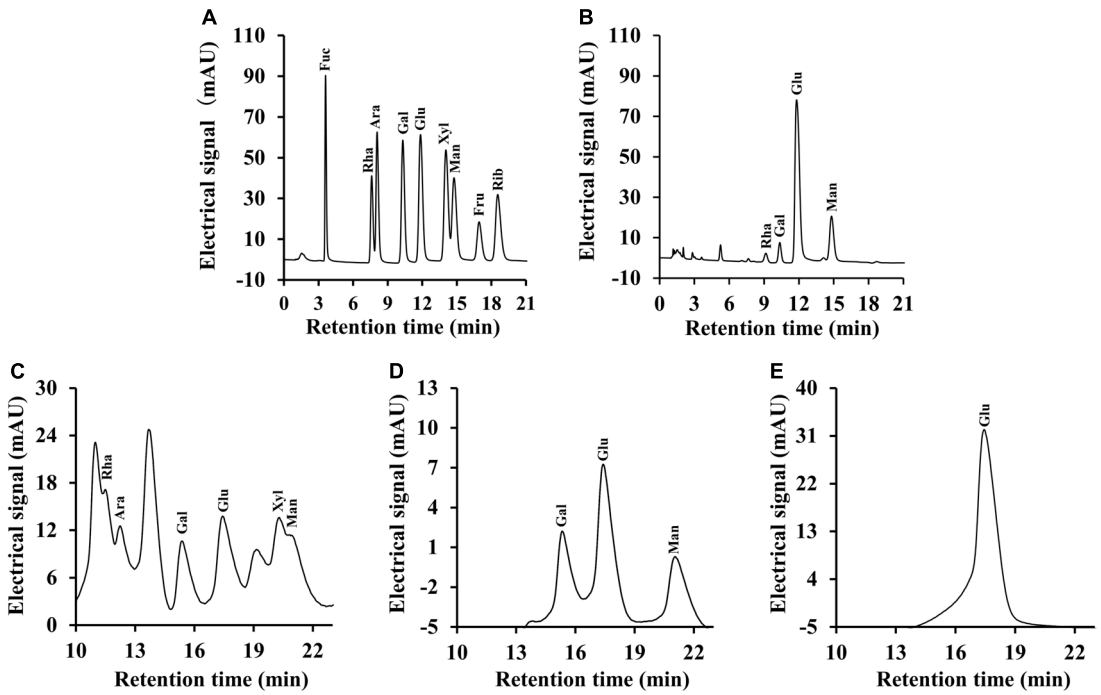

FIGURE 4 | Ion chromatography profiles of the monosaccharide standards, CSFP, CSFP1-β, and CSFP2-α. **(A,C)** The monosaccharide standards, **(B)** CSFP, **(D)** CSFP1-β, and **(E)** CSFP2-α. Fuc, Ara, Rha, Gal, Glc, Xyl, Man, Fru, and Rib represent fucose, arabinose, rhamnose, galactose, glucose, xylose, mannose, fructose, and ribose, respectively.

vibrations of C=O and COO- bonds, indicating the presence of -COOH groups in CSFP, CSFP1-β, and CSFP2-α (39). The absorption peaks at 1,404.6 cm^{-1}, 1,406.1 cm^{-1}, and 1,369.4 cm^{-1} were attributed to the stretching vibration of C-O bonds, indicating the presence of -OCH_3 groups (40). Moreover, the absorption bands at 1,043 cm^{-1}, 1,066.9 cm^{-1}, and 1,024.2 cm^{-1} might be a result of O-H variable-angle vibrations, indicating that CSFP, CSFP1-β, and CSFP2-α

TABLE 2 | Changes in molecular weight (*Mw*) and molar ratio of monosaccharide compositions of CSFP, CSFP1-β, and CSFP2-α .

Sample	CSFP	CSFP1-ß	CSFP2-a
Peak 1 *Mw* (Da)	1.948×10^4	5.16×10^4	4.029×10^6
Percentage ratio (%)	100	30.62	87.12
Peak 2 *Mw* (Da)		2.462×10^4	1.579×10^3
Percentage ratio (%)		38.58	12.88
Peak 3 *Mw* (Da)		7.086×10^3	
Percentage ratio (%)		30.81	
Monosaccharide composition and mole ratio			
Glucose	1.07	3.92	1
Mannose	0.38	2.44	
Galactose	0.11	3.61	
Rhamnose	0.02		

contained a pyranose ring structure (41). The absorption peaks at 912.3–929.7 cm^{-1} and 850 cm^{-1} showed that both CSFP1-β and CSFP2-α contained a β-glycosidic bond and α-glycosidic bond (19).

Monosaccharide Composition and Molecular Weight Analysis

It is well-known that polysaccharides are formed by a series of monosaccharides linked by glycosidic bonds. On the basis of monosaccharide composition, polysaccharides can be divided into homopolysaccharides and heteropolysaccharides (42). For heteropolysaccharides, in addition to the different types and ordering of their monosaccharide units, heteropolysaccharides also have various types and sequences of glycosidic bonds, which also result in structural diversity (43). As shown in **Figure 4**, the monosaccharide composition analysis indicated that CSFP were mainly composed of glucose, mannose, galactose, and rhamnose in molar ratios of 1.07: 0.38: 0.11: 0.02. CSFP1-β was mainly composed of glucose, galactose, and mannose in molar ratios of 3.92: 3.61: 2.44. Furthermore, CSFP2-α was a key component of glucose. The results showed that glucose was the most abundant of the three polysaccharides, and CSFP purified by DEAE-cellulose-52 and Sephacryl S-400 could not only change its monosaccharide composition, but also affect its molar ratio. Furthermore, to a certain extent, the monosaccharide composition of polysaccharides affects the biological activity of polysaccharides (44). Liu et al. (45) found that the active substance that played an antioxidant role in the *Agrocybe cylindracea* may be attributed to the presence of Glc and Gal. Hen et al. (46) found that the antioxidant effect of *P. eryngii* may be due to the presence of Man, Rha, and GalA.

In general, the *Mw* distribution of polysaccharides determines its many physico-chemical properties and biological activity (47). Therefore, the *Mw* values of CSFP and its purified components (CSFP1-β, CSFP2-α) were determined by HPGPC in this study. As shown in **Table 2**, the *Mw* of CSFP was 1.948×10^4 Da. After DEAE-cellulose-52 and Sephacryl S-400 purification, all HPGPC chromatograms of the CSFP1-β and CSFP2-α exhibited two or three peaks, indicating that they were heteropolysaccharides. Results showed that three peaks of CSFP1-β were present at 5.16×10^4 Da (30.62%), 2.462×10^4 Da (38.58%), and 7.086×10^3 Da (30.81%), respectively. In addition, two peaks of CSFP2-α were found at 4.029×10^6 Da (87.12%) and 1.579×10^3 Da (12.88%), respectively. Results showed that the *Mw* values of purified components (CSFP1-β, CSFP2-α) were higher than that of the pectic polysaccharides in okra (*Abelmoschus esculentus*) (48). In addition, polysaccharides with high *Mw* may have better biological activities. Studies have shown that the *Mw* of *Lentinan* is roughly 500 kDa and *Lentinus edodes* polysaccharide is a common, well-established medicinal fungal polysaccharide that has been used as a pharmaceutical agent (49, 50). A polysaccharide-like substance, also called sizofiran, is produced by Schizophyllum, which has a *Mw* of 100–200 kDa (51). Studies have shown that low-*Mw* polysaccharides can penetrate immune cells and stimulate. The superior activity of high-*Mw* polysaccharides may be due to a better binding affinity for carbohydrate receptors of immune cells (52). All in all, the role of *Mw* in the biological activity of polysaccharides is very important.

Rheological Characterization

The rheological properties of natural polysaccharides are related to their antioxidant activities. Owing to their excellent viscosity, they are now widely used in industry to make gelling agents, thickeners, and emulsifiers (44, 53). As shown in **Figures 5A,C,E**, the apparent viscosity of different samples (CSFP, CSFP1-β, and CSFP2-α) was dose-dependent. This characteristic may be related to the mutual stacking and overlapping of polysaccharide molecules and the increase in the degree of polymerization (54). In addition, the study also found that the apparent viscosity of different samples at different concentrations decreased with the increase in shear rate, and showed the shear-thinning behavior of a Newtonian fluid in the range of high shear rate. The author speculates that the shear-thinning behavior of polysaccharides may be related to the unwinding of molecular chains in solution (55, 56). Moreover, compared with CSFP, the apparent viscosity of purified components (CSFP1-β and CSFP2-α) increased significantly at the same concentration, which may be related to their *Mw* and polydispersity (57). Dynamic rheology techniques can be used to detect the solid or liquid properties of polysaccharides (58). As shown in **Figures 5B,D,F**. At 25°C, with the increase of angular frequency of CSFP, CSFP1-β, and CSFP2-α, the storage modulus (*G*') and loss modulus (*G*") also increase. The change in this characteristic may be related to the increase in polymer chain complexity and the number of connections in the sample between the areas of high concentration (59). In addition, *G*' and *G*" represent elastic and viscous properties, respectively. When the loss modulus (*G*") of the sample is greater than the storage modulus (*G*'), it indicates that the sample exhibits liquid-like behavior; otherwise, the sample exhibits solid-like behavior (60). When the concentrations of different sample solutions were 0.1, 0.3, and 0.5%, respectively, *G*' and *G*" values of CSFP suggested no cross-linking, while cross-formation occurred and the gel formation and elastic properties of CSFP1-β and CSFP2-α increased with increasing concentrations. Hu et al. (61) extracted polysaccharide (DTMP) from "deer tripe

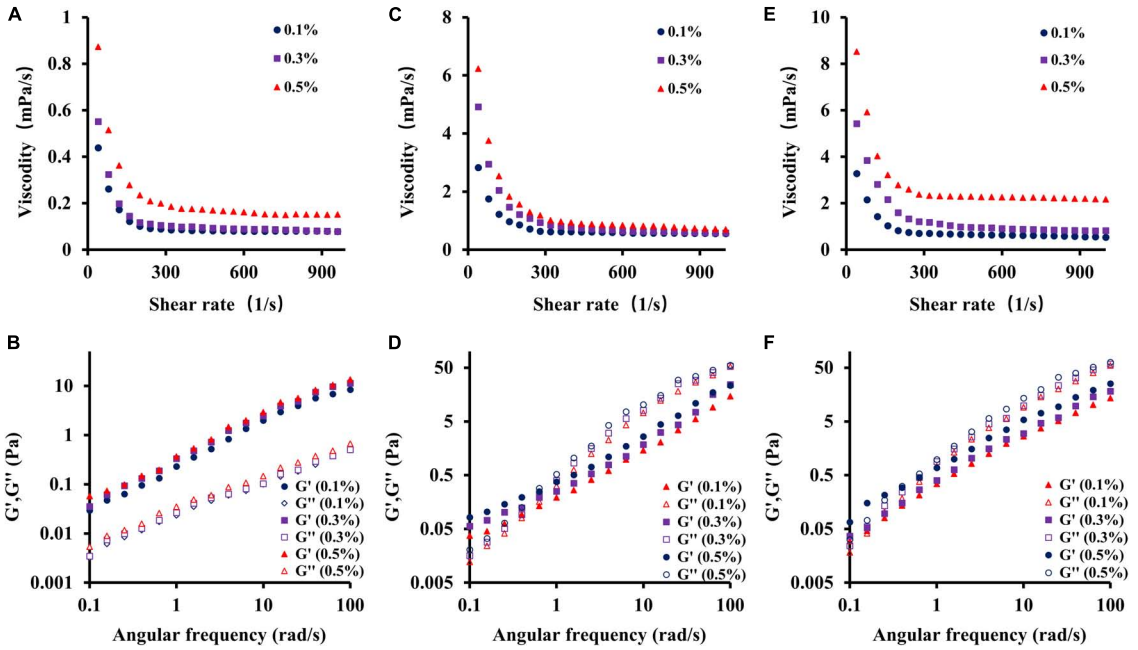

FIGURE 5 | Dependence of apparent viscosity on the shear rate and plots of storage modulus *G'* and loss modulus *G"* against frequency for CSFP, CSFP1-β, and CSFP2-α. **(A,B)** Rheological characteristic diagram of CSFP, **(C,D)** Rheological characteristic diagram of CSFP1-β, and **(E,F)** Rheological characteristic diagram of CSFP2-α.

mushroom" and studied its rheological and gel properties. The results indicated that the DTMP solution showed shear-thinning behavior (pseudoplasticity), and its pseudoplasticity was more obvious at a concentration of 2%. In addition, DTMP also showed a gel-like behavior ($G' > G''$), and the strength of gel increased with the increase of concentration (from 2 to 10%). In addition, Wang et al. (62) prepared alkali-extracted polysaccharide (HEAEP-0.5) from the water-insoluble residue of *H. erinaceus*. It was found that HEAEP-0.5 was a high-viscosity polysaccharide (its intrinsic viscosity was 1.43 L/g). It exhibited strong shear-thinning behavior and could form weak gels as the concentration increased. Polysaccharides from *Clitocybe squamulosa* have significant rheological properties. This study can provide a theoretical basis for its application in the field of the food industry.

Bioactivity of CSFP, CSFP1-β, and CSFP2-α

Antioxidant Activities

Previous studies have shown that the CSFP has good antioxidant activity (16); however, the antioxidant activity of purified components of CSFP has not been studied. Therefore, this experiment will explore and compare the antioxidant activities of CSFP, CSFP1-β, and CSFP2-α. As shown in **Figures 6A–D**, compared with Vc, each of CSFP, CSFP1-β, and CSFP2-α showed significant antioxidant activity, and the antioxidant activity of purified components (CSFP1-β and CSFP2-α) was significantly higher than that of CSFP. The IC_{50} values of the DPPH radical scavenging capacity of CSFP, CSFP1-β, and CSFP2-α were 0.828, 0.364, and 0.303 mg/ml, respectively. The IC_{50} values of ·OH radical scavenging capacity were 1.763, 0.346, and 0.239 mg/ml, respectively. The IC_{50} values of ABTS radical scavenging capacity were 0.819, 0.106, and 0.203 mg/ml, respectively. Furthermore, three different samples also showed a certain potential for reduction. Research shows that polysaccharides from mushrooms, such as *Volvariella Volvacea*, *Agaricus biporous*, *L. edodes*, and *Pleurotus ostreatus,* exhibited significant antioxidant properties relevant to their health-protecting functions (63–65). Antioxidant heteroglycan (PS, $Mw \sim 1.98 \times 10^5$ Da) obtained from the aqueous extract of an edible mushroom *Termitomyces clypeatus* (R. Heim) (66) showed ferrous ion chelating ability, superoxide radical scavenging activities, and high reducing power with EC 50 values of 475, 180, and 260 μg/ml, respectively. In addition, polysaccharides rich in uronic acid often have stronger biological effects. Luo et al. (67) confirmed that acidic polysaccharides have more significant antioxidant activity through *in vitro* antioxidant tests on the purified components of ginseng polysaccharides. It was speculated that the antioxidant activity of natural functional polysaccharides was also closely related to their chemical properties and *Mw* distribution (30, 68). Therefore, the polysaccharide component of *C. squamulosa* can be used as a natural antioxidant and has the potential for application in the functional food industry.

Enzymatic Inhibitory Activities

Diabetes is another major chronic disease that threatens people's health. Most hypoglycemic methods on the market include insulin injection and western medicine to control blood sugar

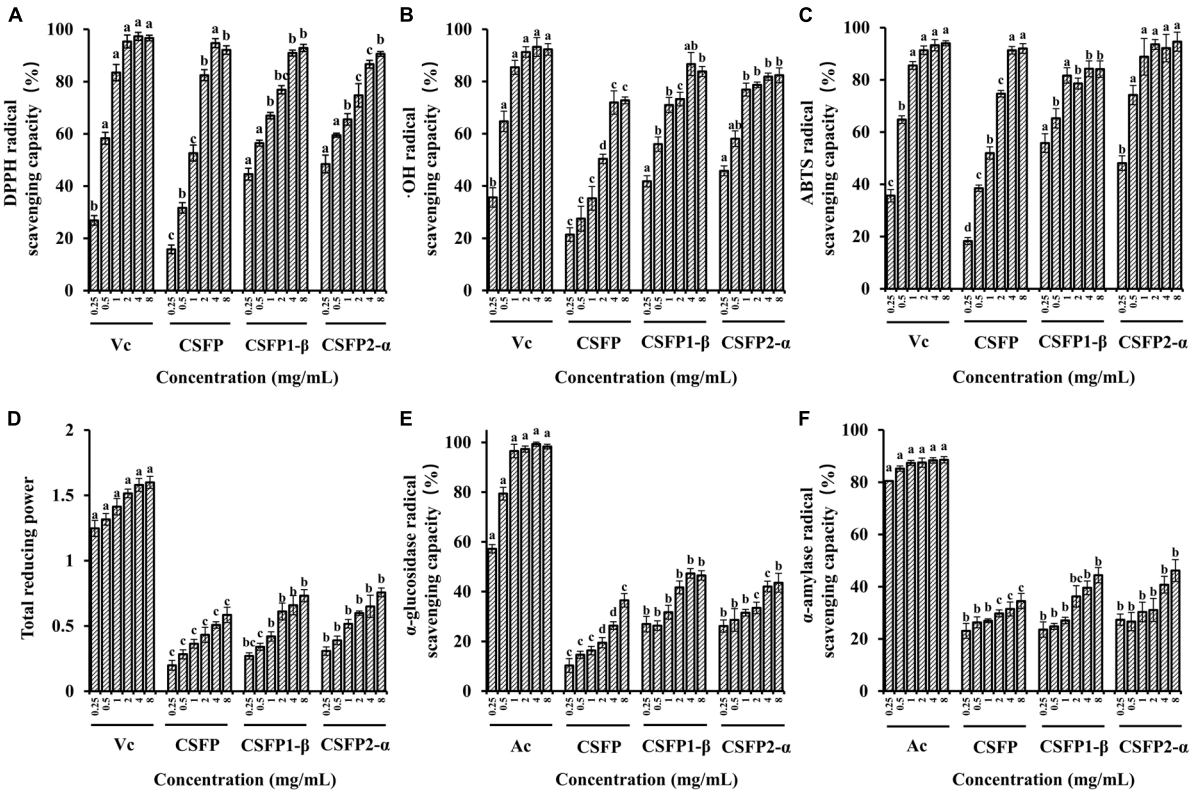

FIGURE 6 | Antioxidant activity and inhibitory enzyme activity of CSFP, CSFP1-β, and CSFP2-α. **(A)** DPPH radical scavenging capacity, **(B)** ·OH radical scavenging capacity, **(C)** ABTS radical scavenging capacity, **(D)** total reducing power, **(E)** α-glucosidase inhibition capacity, and **(F)** α-amylase inhibition capacity. Data are expressed as the mean ± standard deviation values (n = 3), and different lowercase letters denote statistical significance ($p < 0.05$).

concentrations (acarbose, metformin hydrochloride, glimepiride, etc.). The search for new treatments can also reveal new ways to treat diabetes. Studies have shown that the inhibition of α-glucosidase release is one of the main strategies used to combat metabolic symptoms associated with type 2 diabetes and hyperglycemia (69). As shown in **Figures 6E,F**, CSFP, CSFP1-β, and CSFP2-α have significantly inhibited (*in vitro*) the action of α-glucosidase. Indeed, The IC_{50} values of inhibitory α-glucosidase activity of CSFP, CSFP1-β, and CSFP2-α were 5.20, 8.68, and 22.68 mg/ml, respectively. Compared with Ac, CSFP, CSFP1-β, and CSFP2-α had relatively weak inhibitory effects on α-glucosidase. Moreover, inhibition of α-amylase activity also plays a crucial role in diabetes patients. The IC_{50} values of inhibitory α-amylase activity of CSFP, CSFP1-β, and CSFP2-α were 17.01, 16.85, and 20.92 mg/ml, respectively. Compared with Ac, CSFP, CSFP1-β, and CSFP2-α showed moderate α-amylase inhibitory activity. Studies have shown that the hypoglycemic activity of mushroom polysaccharides is related to its high uridine acid, high degree of esterification, and high *Mw* (28, 70). In addition, the study also reported the hypoglycemic activity of a variety of polysaccharides found in edible fungi. For example, Zhu et al. (71) used the polysaccharide purified from *Ganoderma lucidum* to orally feed diabetic mice for 4 weeks. The results showed that *G. lucidum* polysaccharides decreased fasting blood glucose levels and improved endothelium-dependent aortic relaxation. Chen et al. (72) obtained a heteropolysaccharide from *Grifola frondosa,* and experiments have shown that it could significantly increase glucose uptake, thereby reducing insulin resistance in HepG2 cells and improving glucose levels and glucose tolerance in type 2 diabetic mice. Polysaccharides of edible fungi show good competitiveness in hypoglycemic activity and have the potential for further development.

Binding Capacities

Excessive intake of bile acids, free cholesterol, and fat often leads to problems such as diabetes, cardiovascular disease, obesity, and so on (44, 73). CSFP can exert good effects on reducing blood lipid and cholesterol content (16). Therefore, this experiment will evaluate and compare the binding ability of purified components of CSFP to fat, cholesterol, and bile acids *in vitro*. As illustrated in **Figure 7**, the bile acid and cholesterol binding capacities of CSFP were 53.64% and 37.24 mg/g, respectively. After purification, the ability to bind bile acid salt and cholesterol of CSFP1-β and CSFP2-α *in vitro* was significantly improved ($p < 0.05$) to 68.62% and 46.66 mg/g, and 64.43% and 45.05 mg/g, respectively. In addition, although the fat-binding capacity of CSFP1-β and CSFP2-α decreased slightly, they remained significantly higher than that of the positive control ($p < 0.05$). Research showed that the binding ability *in vitro* may be related to the degree of esterification

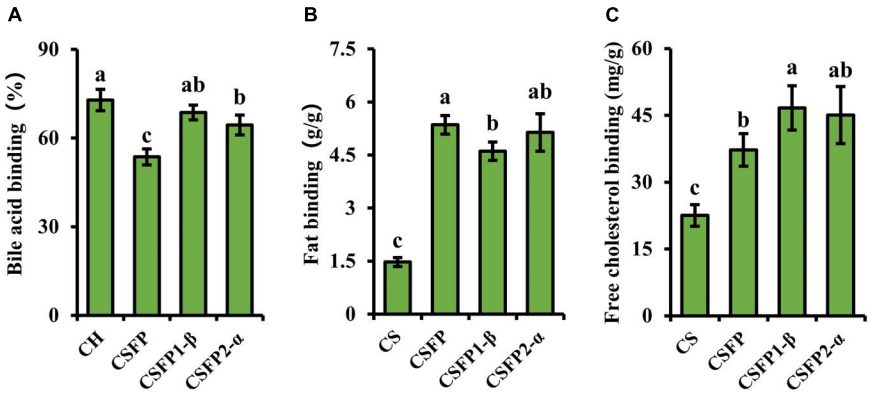

FIGURE 7 | Binding ability of CSFP, CSFP1-β, and CSFP2-α *in vitro*. **(A)** Bile acid, **(B)** Fat, and **(C)** Free cholesterol. Data are expressed as the mean ± standard deviation ($n = 3$) values, and different lowercase letters denote statistical significance ($p < 0.05$).

and *Mw* distribution of natural polysaccharides (28, 44). Fu et al. (74) extracted and purified a water-soluble polysaccharide from *Acanthopanax senticosus*. In alloxan-induced mice, oral *A. Senticosus* polysaccharide can reduce the levels of total cholesterol, triglycerides, and low-density lipoprotein cholesterol in mice. In conclusion, all results show that CSFP, CSFP1-β, and CSFP2-α have the potential for application in the prevention of high cholesterol and hyperlipidemia.

Antibacterial Activity

Nowadays, because many harmful bacteria have developed resistance to antibiotics, it has become even more necessary to control bacterial infections. Therefore, it is necessary to find a new natural pollution-free material for research (75). In this study, the bacteriostatic potential of CSFP, CSFP1-β, and CSFP2-α *in vitro* was evaluated. As shown in **Figure 8**, within the test concentration range, CSFP, CSFP1-β, and CSFP2-α showed different degrees of antibacterial activity against the three tested strains (*E. coli*, *S. aureus*, and *B. subtilis*). The inhibition zones of CSFP, CSFP1-β, and CSFP2-α for *E. coli* were in the range of 6.36–9.52, 6.24–14.09, and 6.29–12.16 mm, respectively. Studies have shown that *E. coli* is a Gram-negative bacterium, which can cause gastrointestinal or urethral infection in animals under certain conditions. Furthermore, at the same concentration, CSFP1-β has the most significant inhibitory effect on *E. coli*. Polysaccharides from *Periploca laevigata* root barks also showed a good inhibitory effect on *E. coli* (76), which was consistent with the results of this study. Meanwhile, CSFP, CSFP1-β, and CSFP2-α also showed moderate antibacterial activity against *S. aureus* and *B. subtilis*. The antibacterial diameters were (6.41–13.08 mm, 6.36–16.11 mm, and 6.33–13.82 mm) and (6.25–12.65 mm, 6.27–14.68 mm, and 6.80–15.20 mm), respectively. Previous studies have shown that *Cyclocarya paliurus* polysaccharides also show moderate antibacterial activity against *E. coli*, *S. aureus*, and *B. subtilis*. When the concentration of polysaccharide solution was 1 mg/ml, the diameter of the antibacterial ring was 6.54, 6.57, and 6.93 mm, respectively (77). Manna et al. (78) synthesized nanoparticles using a *Lentinus squarrosulus* hetero-polysaccharide and successfully demonstrated its use against *E. coli* and other bacteria. The nanoparticles were better than normal particles in inhibiting bacteria and viruses. Mushroom polysaccharides shielded mice against *Salmonella* lipopolysaccharide-induced septic shock (79). *Auricularia auricula-judae* crude polysaccharides were active against *E. coli* and *S. aureus* (80). A sulfated polysaccharide from oyster mushrooms showed antibacterial activity against food-borne *E. coli* and *S. aureus* (81). The bacteriostatic effect of polysaccharides has been confirmed by many studies, but its related mechanism warrants further studies to provide theoretical support for practical industrial production.

Effects of CSFP on RAW264.7 Cells

Macrophages are key immune cells for host defense, and stimulating the activity and phagocytosis of macrophages is an important way of enhancing immune function. The MTT assay and the neutral red assay were used to determine the effect of CSFP on the proliferation of RAW264.7 cells. As shown in **Figures 9A,B**, within the tested concentration range (50–2,000 μg/ml), CSFP could promote RAW264.7 increment in a dose-dependent manner. When the concentration of CSFP solutions was 800 and 200 μg/ml, respectively, the cell viability and phagocytosis index of macrophages reached their maxima. In addition, the effect of CSFP on the phagocytosis index of RAW264.7 was lower than that of LPS. Research finds that *Glehniae radix* polysaccharide promoted the proliferation of RAW264.7 cells, which suggested that *Glehniae radix* polysaccharide may exhibit potential anti-inflammatory, anti-tumor, and immunoregulation activities (82) in a manner consistent with our study. Therefore, taking the phagocytosis index as the reference, 200 μg/ml of CSFP was selected to treat RAW264.7 macrophages in further studies. RAW264.7 cells were incubated in a high-glucose medium containing 200 μg/ml of CSFP for 12 h and then stimulated with LPS for 4 h. As shown in **Figures 9C–F**, except for TGF-β, in the determination of TNF-α, IL-4, and IL-10, the LPS group was significantly higher than the DMEM group ($p < 0.05$). In addition, compared with the LPS group, CSFP had a significant effect on the content of cytokines in RAW264.7

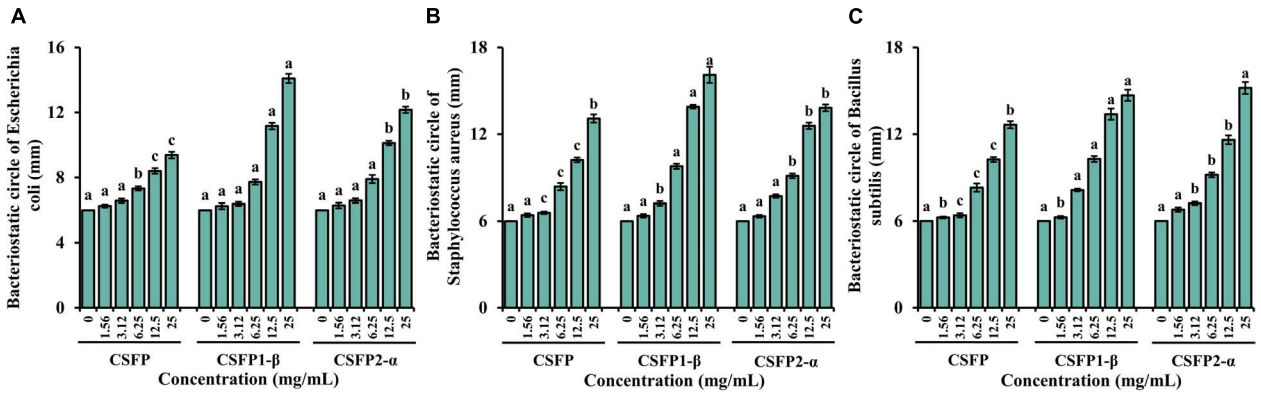

FIGURE 8 | Bacteriostatic test results of CSFP, CSFP1-β, and CSFP2-α. **(A)** *Escherichia coli*, **(B)** *Staphylococcus aureus*, and **(C)** *Bacillus subtilis*. Data are expressed as the mean ± standard deviation values (n = 3), and different lowercase letters denote statistical significance ($p < 0.05$).

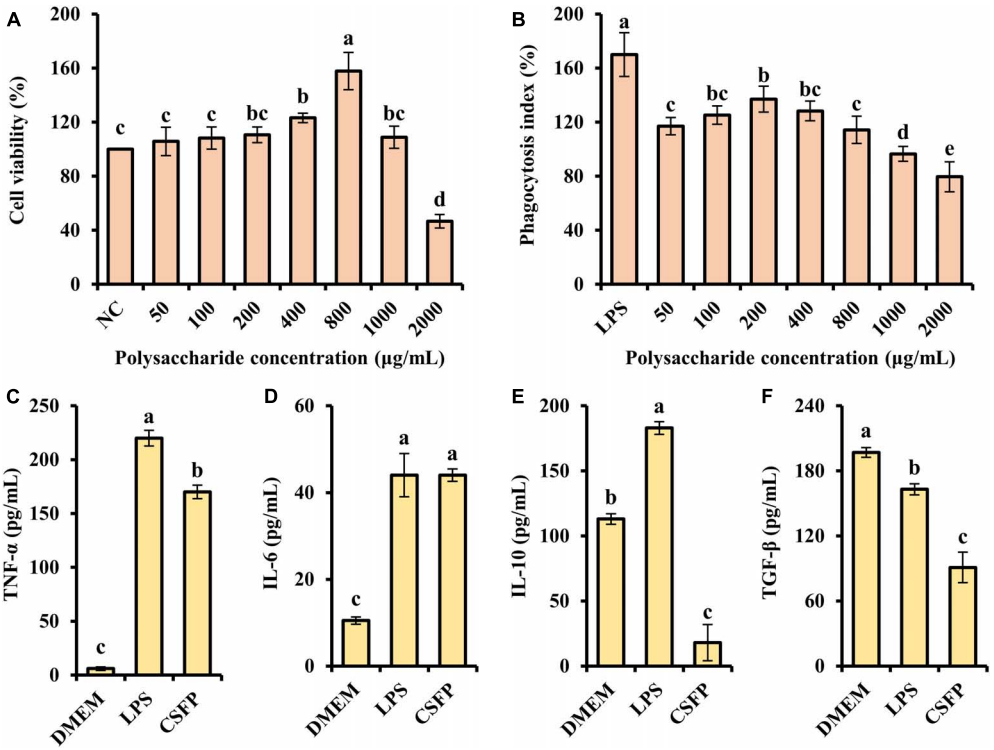

FIGURE 9 | Effect of CSFP on the growth of RAW264.7 cell *in vitro*. **(A)** Cell viability, **(B)** Phagocytosis index, **(C–F)** Secretion of cytokines TNF-α, IL-6, IL-10, and TGF-β. Data are expressed as the mean ± standard deviation values (n = 3), and different lowercase letters denote statistical significance ($p < 0.05$).

cell supernatant (except in the case of IL-6). Furthermore, *Pleurotus nebrodensis* polysaccharides enhanced immunity and inflammatory responses by activating macrophages (83). A previous study indicated the mechanism of macrophage activation induced by a novel polysaccharide (PLCM) extracted from the culture broth of *Cordyceps militaris*. The results showed that PLCM could enhance the immunostimulatory activity of RAW264.7 macrophages, including the release of toxic molecules (NO and SOD), release of cytokine tumor necrosis factor (TNF-α), and the phagocytosis of macrophages (84). The results showed that CSFP could alter the concentrations of inflammatory and anti-inflammatory factors in RAW264.7 cells, thus playing a beneficial role in immune regulation.

CONCLUSION

In this study, two new polysaccharides (CSFP1-β and CSFP2-α) were isolated and purified from *C. squamulosa*. The results show

that CSFP1-β was mainly composed of glucose, galactose, and mannose, while the main component of CSFP2-α was glucose, and the *Mw* distribution of both was uneven. In addition, purified components (CSFP1-β and CSFP2-α) exhibited good antioxidant activity *in vitro* and have the potential to control post-prandial hyperglycemia and reduce the level of lipids in serum. The study also found that CSFP, CSFP1-β, and CSFP2-α demonstrated a good bacteriostatic effect and showed a linear increasing concentration gradient relationship. CSFP could also significantly promote the proliferation of RAW264.7 cells. Therefore, CSFP, CSFP1-β, and CSFP2-α were expected to become functional food to promote body health for further development and future utilization.

DATA AVAILABILITY STATEMENT

The original contributions presented in this study are included in the article/supplementary material, further inquiries can be directed to the corresponding authors.

AUTHOR CONTRIBUTIONS

DG: conceptualization, methodology, and writing — original draft. JL: software development. LX: investigation and resources. YC: formal analysis and visualization. CF: resources and formal analysis. JM: conceptualization and methodology. MC: resources and data curation. XG: supervision and reviewing and editing of the manuscript. All authors contributed to the article and approved the submitted version.

FUNDING

This study was financially supported by the Youth Project of Basic Research Program in Shanxi (20210302124071), Key Research and Development Program of Shanxi Province (201803D221009-1), Key Project of Coal-based Science and Technology of Shanxi Province (FT2014-03-01), and Key Team of Scientific and Technological Innovation of Edible Fungi of Shanxi Province (201805D131009).

REFERENCES

1. Wang L, Li L, Gao J, Huang J, Yang Y, Xu Y, et al. Characterization, antioxidant and immunomodulatory effects of selenized polysaccharides from dandelion roots. *Carbohydr Polym.* (2021) 260:117796. doi: 10.1016/j.carbpol.2021.117796
2. Liu JY, Hou XX, Li ZY, Shan SH, Chang MC, Feng CP, et al. Isolation and structural characterization of a novel polysaccharide from *Hericium erinaceus* fruiting bodies and its arrest of cell cycle at S-phage in colon cancer cells. *Int J Biol Macromol.* (2020) 157:288–95. doi: 10.1016/j.ijbiomac.2020.04.162
3. Jin M-Y, Li M-Y, Huang R-M, Wu X-Y, Sun Y-M, Xu Z-L. Structural features and anti-inflammatory properties of pectic polysaccharides: a review. *Trends Food Sci Technol.* (2021) 107:284–98. doi: 10.1016/j.tifs.2020.10.042
4. Zhu K, Nie S, Li C, Lin S, Xing M, Li W, et al. A newly identified polysaccharide from *Ganoderma atrum* attenuates hyperglycemia and hyperlipidemia. *Int J Biol Macromol.* (2013) 57:142–50. doi: 10.1016/j.ijbiomac.2013.03.009
5. Ma GX, Du HJ, Hu QH, Yang WJ, Pei F, Xiao H, et al. Health benefits of edible mushroom polysaccharides and associated gut microbiota regulation. *Crit Rev Food Sci Nutr.* (2021) 2:1–18. doi: 10.1080/10408398.2021.1903385
6. Yin C, Noratto GD, Fan X, Chen Z, Yao F, Shi D, et al. The impact of mushroom polysaccharides on gut microbiota and its beneficial effects to host: a review. *Carbohydr Polym.* (2020) 250:116942. doi: 10.1016/j.carbpol.2020.116942
7. Yin ZH, Sun-Waterhouse DX, Wang JM, Ma CY, Waterhouse GI, Kang W. Polysaccharides from edible fungi *Pleurotus spp.*: advances and perspectives. *J. Future Foods.* (2021) 12:128–40. doi: 10.1016/j.jfutfo.2022.01.002
8. Hao YL, Sun HQ, Zhang XJ, Wu LR, Zhu ZY. A novel acid polysaccharide from fermented broth of *Pleurotus citrinopileatus*: hypoglycemic activity *in vitro* and chemical structure. *J Mol Struct.* (2020) 1220:128717. doi: 10.1016/j.molstruc.2020.128717
9. Zhang K, Huang Y, Wu Q, Guo W, Chen H, Zhang W, et al. Antibacterial effect and mechanism against *Escherichia coli* of polysaccharides from *Armillariella tabescens mycelia*. *J Fish China.* (2022) 207:750–9. doi: 10.11964/jfc.20170310732
10. Cheng XD, Wu QX, Zhao J, Su T, Lu YM, Zhang WN, et al. Immunomodulatory effect of a polysaccharide fraction on RAW 264.7 macrophages extracted from the wild *Lactarius* deliciosus. *Int J Biol Macromol.* (2019) 128:732–9. doi: 10.1016/j.ijbiomac.2019.01.201
11. Ji XL, Guo JH, Ding DQ, Gao J, Hao LR, Guo XD, et al. Structural characterization and antioxidant activity of a novel high-molecular-weight polysaccharide from *Ziziphus Jujuba cv. Muzao*. *J Food Meas Charact.* (2022) 6:2191–200. doi: 10.1007/s11694-022-01288-3
12. Ji XL, Hou CY, Shi MM, Yan YZ, Liu YQ. An insight into the research concerning *panax ginseng C. A. Meyer* polysaccharides: a review. *Food Rev Int.* (2020) 2020:1–17. doi: 10.1080/87559129.2020.1771363
13. Li T, Li C, Wu D, Yang Y, Jin Y. Studies on the acid degradation process and *in vitro* immune activity of the polysaccharide h6pc20 in *Hericium erinaceus*. *IOP Confer Ser Mater Sci Engi.* (2018) 392:052014. doi: 10.1088/1757-899X/392/5/052014
14. Chen H, Ju Y, Li J, Min Y. Antioxidant activities of polysaccharides from *Lentinus edodes* and their significance for disease prevention. *Int J Biol Macromol.* (2012) 501:214–8. doi: 10.1016/j.ijbiomac.2011.10.027
15. Guo DD, Lei JY, Peng ZJ, Liu RZ, Chang MC, Geng XR, et al. Extraction optimization, structural characterization and physicochemical properties of polysaccharides from *Clitocybe squamulosa* fruiting body. *Acta Edulis Fungi.* (2021) 28:39.
16. Guo DD, Lei JY, He C, Peng ZJ, Liu RZ, Pan X, et al. *In vitro* digestion and fermentation by human fecal microbiota of polysaccharides from *Clitocybe squamulosa*. *Int J Biol Macromol.* (2022) 208:343–55. doi: 10.1016/j.ijbiomac.2022.03.126
17. Huang F, Liu Y, Zhang RF, Bai YJ, Dong LH, Liu L, et al. Structural characterization and *in vitro* gastrointestinal digestion and fermentation of litchi polysaccharide. *Int J Biol Macromol.* (2019) 140:965–72. doi: 10.1016/j.ijbiomac.2019.08.170
18. Hu L, Liu R, Wu T, Sui WJ, Zhang M. Structural properties of homogeneous polysaccharide fraction released from wheat germ by hydrothermal treatment. *Carbohydr Polym.* (2020) 240:116238. doi: 10.1016/j.carbpol.2020.116238
19. Yuan Q, He Y, Xiang PY, Wang SP, Cao ZW, Gou T, et al. Effects of simulated saliva-gastrointestinal digestion on the physicochemical properties and bioactivities of okra polysaccharides. *Carbohydr Polym.* (2020) 238:116183. doi: 10.1016/j.carbpol.2020.116183
20. Qiao YB, Ye Y, Cai TX, Li S, Liu XQ. Anti-fatigue activity of the polysaccharides isolated from Ribes stenocarpum Maxim. *J Funct Foods.* (2022) 89:104947. doi: 10.1016/j.jff.2022.104947
21. Wang YF, Yu L, Wei XL. Monosaccharide composition and bioactivity of tea flower polysaccharides obtained by ethanol fractional precipitation and stepwise precipitation. *CyTA J Food.* (2012) 10:1–4. doi: 10.1080/19476337.2010.523901
22. Zheng L, Ma YH, Zhang YJ, Meng QJ, Yang JH, Wang BL, et al. Increased antioxidant activity and improved structural characterization of sulfuric acid-treated stepwise degraded polysaccharides from Pholiota nameko PN-01. *Int J Biol Macromol.* (2021) 166:1220–9. doi: 10.1016/j.ijbiomac.2020.11.004
23. Yuan Q, He Y, Xiang PY, Huang YJ, Cao ZW, Shen SW, et al. Influences of different drying methods on the structural characteristics and multiple

bioactivities of polysaccharides from okra (*Abelmoschus esculentus*). *Int J Biol Macromol.* (2020) 147:1053–63. doi: 10.1016/j.ijbiomac.2019.10.073
24. Liu Y, Zhou YF, Liu MD, Wang Q, Li Y. Extraction optimization, characterization, antioxidant and immunomodulatory activities of a novel polysaccharide from the wild mushroom *Paxillus involutus*. *Int J Biol Macromol.* (2018) 112:326–32. doi: 10.1016/j.ijbiomac.2018.01.132
25. Zhao YM, Song JH, Wang J, Yang JM, Wang ZB, Liu YH. Optimization of cellulase-assisted extraction process and antioxidant activities of polysaccharides from *Tricholoma* mongolicum Imai. *J Sci Food Agric.* (2016) 96:4484–91. doi: 10.1002/jsfa.7662
26. Floris S, Fais A, Medda R, Pintus F, Piras A, Kumar A, et al. Washingtonia filifera seed extracts inhibit the islet amyloid polypeptide fibrils formations and alpha-amylase and alpha-glucosidase activity. *J Enzyme Inhib Med Chem.* (2021) 36:517–24. doi: 10.1080/14756366.2021.1874945
27. Xu YQ, Niu XJ, Liu NY, Gao YK, Wang LB, Xu G, et al. Characterization, antioxidant and hypoglycemic activities of degraded polysaccharides from blackcurrant (*Ribes nigrum L.*) fruits. *Food Chem.* (2018) 243:26–35. doi: 10.1016/j.foodchem.2017.09.107
28. Fu Y, Yuan Q, Lin S, Liu W, Du G, Zhao L, et al. Physicochemical characteristics and biological activities of polysaccharides from the leaves of different loquat (*Eriobotrya japonica*) cultivars. *Int J Biol Macromol.* (2019) 135:274–81. doi: 10.1016/j.ijbiomac.2019.05.157
29. Cheng HR, Feng SL, Shen SA, Zhang L, Yang RW, Zhou YH, et al. Extraction, antioxidant and antimicrobial activities of *Epimedium acuminatum* Franch. polysaccharide. *Carbohydr Polym.* (2013) 961:101–8. doi: 10.1016/j.carbpol.2013.03.072
30. Duan MY, Shang HM, Chen SL, Li R, Wu HX. Physicochemical properties and activities of comfrey polysaccharides extracted by different techniques. *Int J Biol Macromol.* (2018) 115:876–82. doi: 10.1016/j.ijbiomac.2018.04.188
31. Chen HX, Zhang M, Qu ZH, Xie BJ. Antioxidant activities of different fractions of polysaccharide conjugates from green tea (*Camellia Sinensis*). *Food Chem.* (2008) 106:559–63. doi: 10.1016/j.foodchem.2007.06.040
32. Xu YQ, Liu GJ, Yu Z, Song X, Li X, Yang Y, et al. Purification, characterization and antiglycation activity of a novel polysaccharide from *black currant*. *Food Chem.* (2016) 199:694–701. doi: 10.1016/j.foodchem.2015.12.078
33. Ji XL, Cheng YQ, Tian JY, Zhang SQ, Jing YS, Shi MM, et al. Structural characterization of polysaccharide from jujube (*Ziziphus jujuba Mill.*) fruit. *Chem Biol Technol Ag.* (2021) 81:1–7. doi: 10.1186/s40538-021-00255-2
34. Wei L, Hong W, Yu JP, Liu YM, Gao YC. Structure, chain conformation, and immunomodulatory activity of the polysaccharide purified from Bacillus Calmette Guerin formulation. *Carbohydr Polym.* (2016) 150:149–58. doi: 10.1016/j.carbpol.2016.05.011
35. Pu XY, Ma XL, Liu L, Ren J, Li HB, Li XY, et al. Structural characterization and antioxidant activity *in vitro* of polysaccharides from angelica and astragalus. *Carbohydr Polym.* (2016) 137:154–64. doi: 10.1016/j.carbpol.2015.10.053
36. Suleman E, Mtshali MS, Lane EJ. Investigation of false positives associated with loop-mediated isothermal amplification assays for detection of Toxoplasma gondii in archived tissue samples of captive felids. *J Vet Diagn Invest.* (2016) 28:536–42. doi: 10.1177/1040638716659864
37. You Q, Yin X, Zhang S, Jiang ZJ. Extraction, purification, and antioxidant activities of polysaccharides from *Tricholoma* mongolicum Imai. *Carbohydr Polym.* (2014) 99:1–10. doi: 10.1016/j.carbpol.2013.07.088
38. Chen C, Zhang B, Fu X, You LJ, Abbasi AM, Liu RH. The digestibility of mulberry fruit polysaccharides and its impact on lipolysis under simulated saliva, gastric and intestinal conditions. *Food Hydrocolloid.* (2016) 58:171–8. doi: 10.1016/j.foodhyd.2016.02.033
39. Ye Z, Wang W, Yuan Q, Ye H, Sun Y, Zhang H, et al. Box-Behnken design for extraction optimization, characterization and *in vitro* antioxidant activity of *Cicer arietinum L. hull* polysaccharides. *Carbohydr Polym.* (2016) 147:354–64. doi: 10.1016/j.carbpol.2016.03.092
40. Meng X, Che C, Zhang J, Gong Z, Si M, Yang G, et al. Structural characterization and immunomodulating activities of polysaccharides from a newly collected wild *Morchella sextelata*. *Int J Biol Macromol.* (2019) 129:608–14. doi: 10.1016/j.ijbiomac.2019.01.226
41. Shi YY, Xiong QP, Wang XL, Li X, Yu CH, Wu J, et al. Characterization of a novel purified polysaccharide from the flesh of Cipangopaludina chinensis. *Carbohydr Polym.* (2016) 136:875–83. doi: 10.1016/j.carbpol.2015.09.062
42. Wang Q, Wang F, Xu ZH, Ding ZY. Bioactive mushroom polysaccharides: a review on monosaccharide composition, biosynthesis and regulation. *Molecules.* (2017) 6:955. doi: 10.3390/molecules22060955
43. Ruthes AC, Smiderle FR, MarcelloIacominia. Mushroom heteropolysaccharides: a review on their sources, structure and biological effects. *Carbohydr Polym.* (2016) 136:358–75. doi: 10.1016/j.carbpol.2015.08.061
44. Yuan Q, Lin S, Fu Y, Nie XR, Liu W, Su Y, et al. Effects of extraction methods on the physicochemical characteristics and biological activities of polysaccharides from okra (*Abelmoschus esculentus*). *Int J Biol Macromol.* (2019) 127:178–86. doi: 10.1016/j.ijbiomac.2019.01.042
45. Liu M, Jing HJ, Zhang JJ, Che G, Zhou M, Gao Z, et al. Optimization of mycelia selenium polysaccharide extraction from *Agrocybe cylindracea* SL-02 and assessment of their antioxidant and anti-ageing activities. *PLoS One.* (2016) 118:e0160799. doi: 10.1371/journal.pone.0160799
46. Chou CH, Sung TJ, Hu YN, Lu HY, Yang LC, Cheng KC, et al. Chemical analysis, moisture-preserving, and antioxidant activities of polysaccharides from *Pholiota nameko* by fractional precipitation. *Int J Biol Macromol.* (2019) 131:1021–31. doi: 10.1016/j.ijbiomac.2019.03.154
47. Lin S, Guo H, Lu M, Lu MY, Gong JD, Wang L, et al. Correlations of molecular weights of OI–glucans from Qingke (*Tibetan hulless barley*) to their multiple bioactivities. *Molecules.* (2018) 23:1710. doi: 10.3390/molecules23071710
48. Wang KL, Li M, Wen X, Chen XS, He ZY, Ni YY. Optimization of ultrasound-assisted extraction of okra (*Abelmoschus esculentus* (L.) Moench) polysaccharides based on response surface methodology and antioxidant activity. *Int J Biol Macromol.* (2018) 114:1056–63. doi: 10.1016/j.ijbiomac.2018.03.145
49. Thakur MP, Singh HK. Mushrooms, their bioactive compounds and medicinal uses: a review. *Med Plants Int J Phytomed Indust.* (2013) 51:1–20. doi: 10.5958/j.0975-6892.5.1.004
50. Mizuno M, Nishitani Y. Immunomodulating compounds in Basidiomycetes. *J ClinBiochem Nutr.* (2013) 523:202–7. doi: 10.3164/jcbn.13-3
51. Giavasis I. Bioactive fungal polysaccharides as potential functional ingredients in food and nutraceuticals. *Curr Opin Biotechnol.* (2014) 26:162–73. doi: 10.1016/j.copbio.2014.01.010
52. El Enshasy HA, Hatti-Kaul R. Mushroom immunomodulators: unique molecules with unlimited applications. *Trends Biotechnol.* (2013) 3112:668–77. doi: 10.1016/j.tibtech.2013.09.003
53. Yuan YQ, Li C, Zheng QW, Wu JX, Zhu KX, Shen XR, et al. Effect of simulated gastrointestinal digestion *in vitro* on the antioxidant activity, molecular weight and microstructure of polysaccharides from a tropical sea cucumber (*Holothuria leucospilota*). *Food Hydrocolloid.* (2019) 89:735–41. doi: 10.1016/j.foodhyd.2018.11.040
54. Bae IY, Oh IK, Lee S, Yoo SH, Lee HG. Rheological characterization of levan polysaccharides from *Microbacterium laevaniformans*. *Int J Biol Macromol.* (2008) 42:10–3. doi: 10.1016/j.ijbiomac.2007.08.006
55. Benchabane A, Bekkour KJC, Science P. Rheological properties of carboxymethyl cellulose (CMC) solutions. *Cooloid Polym Sci.* (2008) 286:1173–80. doi: 10.1007/s00396-008-1882-2
56. Jin Q, Cai Z, Li X, Yadav MP, Zhang H. Comparative viscoelasticity studies: corn fiber gum versus commercial polysaccharide emulsifiers in bulk and at air/liquid interfaces. *Food Hydrocolloid.* (2017) 64:85–98. doi: 10.1016/j.foodhyd.2016.11.002
57. Zhong K, Zhang Q, Tong L, Liu L, Zhou X, Zhou S. Molecular weight degradation and rheological properties of schizophyllan under ultrasonic treatment. *Ultrason Sonochem.* (2015) 23:75–80. doi: 10.1016/j.ultsonch.2014.09.008
58. Chen Y, Zhang JG, Sun HJ, Wei ZJ. Pectin from Abelmoschus esculentus: optimization of extraction and rheological properties. *Int J Biol Macromol.* (2014) 70:498–505. doi: 10.1016/j.ijbiomac.2014.07.024
59. Simas-Tosin FF, Barraza RR, Petkowicz CLO, Silveira JLM, Sassaki GL, Santos EMR, et al. Rheological and structural characteristics of peach tree gum exudate. *Food Hydrocolloid.* (2010) 24:486–93. doi: 10.1016/j.foodhyd.2009.12.010
60. Wang L, Zhang B, Xiao J, Huang Q, Li C, Fu X. Physicochemical, functional, and biological properties of water-soluble polysaccharides from Rosa roxburghii Tratt fruit. *Food Chem.* (2018) 249:127–35. doi: 10.1016/j.foodchem.2018.01.011

61. Hu HW, Teng X, Zhang SS, Liu TT, Li X, Wang DW. Structural characteristics, rheological properties, and antioxidant activity of novel polysaccharides from "Deer Tripe Mushroom". *J Food Qual.* (2021) 2021:1–12. doi: 10.1155/2021/6593293
62. Wang XY, Xu R, Yin JY, Wang YX, Ma LY, Nie SP, et al. Physicochemical, structural and rheological properties of alkali-extracted polysaccharide from fruiting body of *Hericium erinaceus*. *LWT.* (2019) 115:108330. doi: 10.1016/j.lwt.2019.108330
63. Yang JH, Lin HC, Mau JL. Antioxidant properties of several commercial mushrooms. *Food Chem.* (2002) 772:229–35. doi: 10.1016/S0308-8146(01)00342-9
64. Chen Y, Li XH, Zhou LY, Li W, Liu L, Wang DD, et al. Structural elucidation of three antioxidative polysaccharides from *Tricholoma lobayense*. *Carbohydr Polym.* (2017) 157:484–92. doi: 10.1016/j.carbpol.2016.10.011
65. Liu Q, Tian GT, Yan H, Geng XR, Cao QP, Wang HX, et al. Characterization of polysaccharides with antioxidant and hepatoprotective activities from the wild edible mushroom *Russula vinosa Lindblad*. *J Agric Food Chem.* (2014) 6235:8858–66. doi: 10.1021/jf502632c
66. Pattanayak M, Samanta S, Maity P, Sen IK, Nandi AK, Manna DK, et al. Heteroglycan of an edible mushroom *Termitomyces clypeatus*: structure elucidation and antioxidant properties. *Carbohyd Res.* (2015) 413:30–6. doi: 10.1016/j.carres.2015.05.005
67. Luo DH, Fang BS. Structural identification of ginseng polysaccharides and testing of their antioxidant activities. *Carbohydr Polym.* (2008) 723:376–81. doi: 10.1016/j.carbpol.2007.09.006
68. Sheng JW, Sun YL. Antioxidant properties of different molecular weight polysaccharides from *Athyrium multidentatum* (Doll.) Ching. *Carbohydr Polym.* (2014) 108:41–5. doi: 10.1016/j.carbpol.2014.03.011
69. Podsedek A, Majewska I, Redzynia MG, Sosnowska D, Kozio E, Kiewicz MJ, et al. *In vitro* inhibitory effect on digestive enzymes and antioxidant potential of commonly consumed fruits. *J Agric Food Chem.* (2014) 62:4610–7. doi: 10.1021/jf5008264
70. Espinal-Ruiz M, Parada-Alfonso F, Restrepo-Sánchez LP, Narváez-Cuenca CE. Inhibition of digestive enzyme activities by pectic polysaccharides in model solutions. *Bioact Carbohydr Diet Fibre.* (2014) 4:27–38. doi: 10.1016/j.bcdf.2014.06.003
71. Zhu KX, Nie SP, Li C, Gong DM, Xie MY. *Ganoderma atrum* polysaccharide improves aortic relaxation in diabetic rats *via* PI3K/Akt pathway. *Carbohydr Polym.* (2014) 103:520–7. doi: 10.1016/j.carbpol.2013.12.080
72. Chen YQ, Liu YY, Sarker MR, Yan X, Yang CF, Zhao LN, et al. Structural characterization and antidiabetic potential of a novel heteropolysaccharide from Grifola frondosa *via* IRS1/PI3K-JNK signaling pathways. *Carbohydr Polym.* (2018) 198:452–61. doi: 10.1016/j.carbpol.2018.06.077
73. Guo H, Lin S, Lu M, Gong JD, Wang L, Zhang Q, et al. Characterization, *in vitro* binding properties, and inhibitory activity on pancreatic lipase of beta-glucans from different Qingke (*Tibetan hulless barley*) cultivars. *Int J Biol Macromol.* (2018) 120:2517–22. doi: 10.1016/j.ijbiomac.2018.09.023
74. Fu JF, Fu JF, Liu Y, Li RY, Gao B, Zhang NY, et al. Modulatory effects of one polysaccharide from Acanthopanax senticosus in alloxan-induced diabetic mice. *Carbohydr Polym.* (2012) 873:2327–31. doi: 10.1016/j.carbpol.2011.10.068
75. Bancalari E, Martelli F, Bernini V, Neviani E, Gatti M. Bacteriostatic or bactericidal? Impedometric measurements to test the antimicrobial activity of Arthrospira platensis extract. *Food Control.* (2020) 118:107380. doi: 10.1016/j.foodcont.2020.107380
76. Hajji M, Hamdi M, Sellimi S, Ksouda G, Laouer H, Li S, et al. Structural characterization, antioxidant and antibacterial activities of a novel polysaccharide from Periploca laevigata root barks. *Carbohydr Polym.* (2019) 206:380–8. doi: 10.1016/j.carbpol.2018.11.020
77. Xie JH, Shen MY, Xie MY, Nie SP, Chen Y, Li C, et al. Ultrasonic-assisted extraction, antimicrobial and antioxidant activities of Cyclocarya paliurus (*Batal.*) Iljinskaja polysaccharides. *Carbohydr Polym.* (2012) 89:177–84. doi: 10.1016/j.carbpol.2012.02.068
78. Manna DK, Nandi AK, Pattanayak M, Maity P, Tripathy S, Mandal AK, et al. A water soluble β-glucan of an edible mushroom *Termitomyces heimii*: structural and biological investigation. *Carbohydr Polym.* (2015) 134:375–84. doi: 10.1016/j.carbpol.2015.07.099
79. Hu SH, Cheung PC, Hung RP, Chen YK, Wang JC, Chang SJ. Antitumor and immunomodulating activities of exopolysaccharide produced by big cup culinary-medicinal mushroom clitocybe maxima (*higher basidiomycetes*) in liquid submerged culture. *Int J Med Mushrooms.* (2015) 17:891–901. doi: 10.1615/intjmedmushrooms.v17.i9.90
80. Signoretto C, Marchi A, Bertoncelli A, Burlacchini G, Papetti A, Pruzzo C, et al. The anti-adhesive mode of action of a purified mushroom (*Lentinus edodes*) extract with anticaries and antigingivitis properties in two oral bacterial pathogens. *BMC Complem Altern M.* (2014) 141:1–9. doi: 10.1186/1472-6882-14-75
81. Cai M, Lin Y, Luo YL, Liang HH, Sun P. Extraction, antimicrobial, and antioxidant activities of crude polysaccharides from the wood ear medicinal mushroom Auricularia auricula-judae (*higher basidiomycetes*). *Int J Med Mushrooms.* (2015) 7:591. doi: 10.1615/IntJMedMushrooms.v17.i6.90
82. Du B, Fu Y, Wang X, Jiang H, Lv Q, Du R, et al. Isolation, purification, structural analysis and biological activities of water-soluble polysaccharide from *Glehniae radix*. *Int J Biol Macromol.* (2019) 128:724–31. doi: 10.1016/j.ijbiomac.2019.01.159
83. Wang XM, Zhang J, Wu LH, Zhao YL, Li T, Li JQ, et al. A mini-review of chemical composition and nutritional value of edible wild-grown mushroom from China. *Food Chem.* (2014) 151:279–85. doi: 10.1016/j.foodchem.2013.11.062
84. Lee JS, Kwon DS, Lee KR, Park JM, Ha SJ, Hong EK. Mechanism of macrophage activation induced by polysaccharide from *Cordyceps militaris* culture broth. *Carbohydr Polym.* (2015) 120:29–37. doi: 10.1016/j.carbpol.2014.11.059

Conflict of Interest: The authors declare that the research was conducted in the absence of any commercial or financial relationships that could be construed as a potential conflict of interest.

Publisher's Note: All claims expressed in this article are solely those of the authors and do not necessarily represent those of their affiliated organizations, or those of the publisher, the editors and the reviewers. Any product that may be evaluated in this article, or claim that may be made by its manufacturer, is not guaranteed or endorsed by the publisher.

Copyright © 2022 Guo, Lei, Xu, Cheng, Feng, Meng, Chang and Geng. This is an open-access article distributed under the terms of the Creative Commons Attribution License (CC BY). The use, distribution or reproduction in other forums is permitted, provided the original author(s) and the copyright owner(s) are credited and that the original publication in this journal is cited, in accordance with accepted academic practice. No use, distribution or reproduction is permitted which does not comply with these terms.

frontiers | Frontiers in Nutrition

ORIGINAL RESEARCH
published: 30 June 2022
doi: 10.3389/fnut.2022.916271

Hypoglycemic Effects of *Lycium barbarum* Polysaccharide in Type 2 Diabetes Mellitus Mice *via* Modulating Gut Microbiota

*Qingyu Ma, Ruohan Zhai, Xiaoqing Xie, Tao Chen, Ziqi Zhang, Huicui Liu, Chenxi Nie, Xiaojin Yuan, Aobai Tu, Baoming Tian, Min Zhang, Zhifei Chen and Juxiu Li**

College of Food Science and Engineering, Northwest A&F University, Yangling, China

This study aims to explore the molecular mechanisms of *Lycium barbarum* polysaccharide (LBP) in alleviating type 2 diabetes through intestinal flora modulation. A high-fat diet (HFD) combined with streptozotocin (STZ) was applied to create a diabetic model. The results indicated that LBP effectively alleviated the symptoms of hyperglycemia, hyperlipidemia, and insulin resistance in diabetic mice. A high dosage of LBP exerted better hypoglycemic effects than low and medium dosages. In diabetic mice, LBP significantly boosted the activities of CAT, SOD, and GSH-Px and reduced inflammation. The analysis of 16S rDNA disclosed that LBP notably improved the composition of intestinal flora, increasing the relative abundance of *Bacteroides*, *Ruminococcaceae_UCG-014*, *Intestinimonas*, *Mucispirillum*, *Ruminococcaceae_UCG-009* and decreasing the relative abundance of *Allobaculum*, *Dubosiella*, *Romboutsia*. LBP significantly improved the production of short-chain fatty acids (SCFAs) in diabetic mice, which corresponded to the increase in the beneficial genus. According to Spearman's correlation analysis, *Cetobacterium*, *Streptococcus*, *Ralstonia*. *Cetobacterium*, *Ruminiclostridium*, and *Bifidobacterium* correlated positively with insulin, whereas *Cetobacterium*, *Millionella*, *Clostridium_sensu_stricto_1*, *Streptococcus*, and *Ruminococcaceae_UCG_009* correlated negatively with HOMA-IR, HDL-C, ALT, AST, TC, and lipopolysaccharide (LPS). These findings suggested that the mentioned genus may be beneficial to diabetic mice's hypoglycemia and hypolipidemia. The up-regulation of peptide YY (PYY), glucagon-like peptide-1 (GLP-1), and insulin were remarkably reversed by LBP in diabetic mice. The real-time PCR (RT-PCR) analysis illustrated that LBP distinctly regulated the glucose metabolism of diabetic mice by activating the IRS/PI3K/Akt signal pathway. These results indicated that LBP effectively alleviated the hyperglycemia and hyperlipidemia of diabetic mice by modulating intestinal flora.

Keywords: ***Lycium barbarum*** **polysaccharide, type 2 diabetes mellieus, gut microbiota, hypoglycemia, hypolipidemia**

OPEN ACCESS

Edited by:
Qiu Li,
Qingdao Agricultural University, China

Reviewed by:
Zichao Wang,
Henan University of Technology, China
Ding-Tao Wu,
Chengdu University, China

***Correspondence:**
Juxiu Li
lijuxiu@nwafu.edu.cn

Specialty section:
This article was submitted to Food Chemistry, a section of the journal Frontiers in Nutrition

Received: *09 April 2022*
Accepted: *12 May 2022*
Published: *30 June 2022*

Citation:
Ma Q, Zhai R, Xie X, Chen T, Zhang Z, Liu H, Nie C, Yuan X, Tu A, Tian B, Zhang M, Chen Z and Li J (2022) Hypoglycemic Effects of Lycium barbarum Polysaccharide in Type 2 Diabetes Mellitus Mice via Modulating Gut Microbiota. Front. Nutr. 9:916271. doi: 10.3389/fnut.2022.916271

INTRODUCTION

The global burden of diabetes mellitus has risen rapidly in recent decades, however, many individuals go undiagnosed (1). According to the latest research by the International Diabetes Federation (IDF, 10th edition), the global diabetes prevalence is expected to be 10.5% (537 million) in 2021, rising to 12.2% (783 million) in 2045 (2). Diabetes mellitus is a chronic metabolic condition

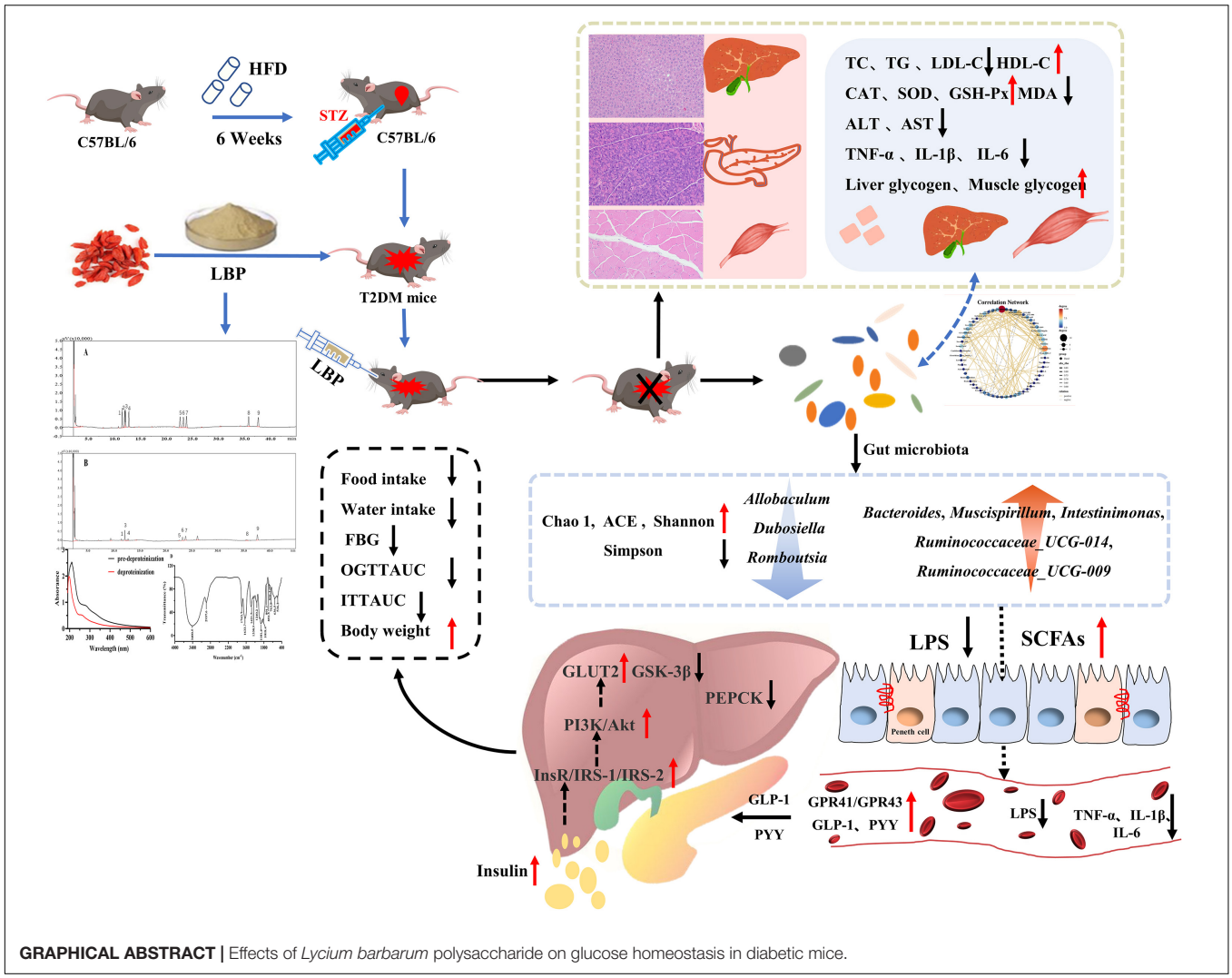

GRAPHICAL ABSTRACT | Effects of *Lycium barbarum* polysaccharide on glucose homeostasis in diabetic mice.

that has been linked to several factors, including age, genetic predisposition, lifestyle, dietary patterns, as well as physical and mental health (3). Type 1 diabetes mellitus (T1DM), type 2 diabetes mellitus (T2DM), and gestational diabetes mellitus (GDM) are the three basic kinds of diabetes (2). T2DM is defined as a relative insulin shortage induced by pancreatic β-cell dysfunction and failure, which gradually leads to insulin resistance in the tissues, liver, and skeletal muscle over time (4). T2DM accounts for nearly 90% of the total and the global burden of diabetes is expected to reach 1,054 billion USD by 2045, accompanied by increased health expenditures for public care of this disease (2). Long-time high blood glucose exposure elevated the development of reactive oxygen species (ROS), which could be harmful to the host's health (5). Several factors, including food, lifestyle changes, medication, and bariatric surgery, can prevent or delay the onset and progression of T2DM. Metformin, insulin secretagogues, glycosidase inhibitors, glucagon-like peptide-1 (GLP-1), analogs, DPP-4 inhibitors, SGLT-2 inhibitors, as well as insulin and its agonists are used to treat diabetes (6). Although therapeutic medicines are efficient at managing blood glucose levels, they can also cause a variety of side effects, including blood glucose fluctuations, hypoglycemia, gastrointestinal reactions, and liver, pancreatic, and kidney injuries (7). As a result, researchers must devise a new strategy to combat T2DM.

The growing evidence has implicated that host health is inextricably linked to intestinal flora (8). Some studies have linked the altered intestinal flora composition to the onset of obesity, diabetes, peripheral tissue inflammation, and gastrointestinal disorders (9, 10). The disorder and dysfunction of intestinal flora may lead to an increase of opportunistic pathogens, such as *Betaproteobacteria* and *Clostridium bolteae*, which may be able to damage the host (9). The decline of *Faecalibacterium prausnitzii* could reduce the production of SCFAs, which should be accompanied by an increase in destructive inflammatory cytokines (10). Intestinal flora dysbiosis can cause tissue and organ dysfunction, interfere with endogenous metabolites in the host, and cause other harm to the organism (11). Polysaccharides have been shown to play an important role in the prevention of the onset and progression of T2DM by modulation of intestinal

flora (12–14). Polysaccharides isolated from *Vigna angularis* and mulberry leaf alleviated diabetes in diabetic rats by activating the signaling pathway of insulin/PI3K/AKT or blocking islet cell apoptosis (15). Furthermore, *Ganoderma lucidum* polysaccharide reversed gut dysbiosis and decreased the Firmicutes–Bacteroidetes ratio (16). Another study found that by altering the composition of intestinal flora, *G. lucidum* polysaccharide reduced inflammation, and delayed the onset and progress of diabetes (17). Polysaccharides isolated from *Holothuria leucospilota* significantly increased the proportion of SCFAs-producing bacteria in diabetic mice, including *Lactobacillus* and *Bifidobacterium* (14). These studies revealed that polysaccharides may be useful in regulating the composition of intestinal flora and selectively increased the proportion of beneficial bacteria.

Type 2 diabetes mellitus is a chronic metabolic disease characterized by uncontrolled insulin secretion, hyperglycemia, and hyperlipidemia (1). Many recent studies have demonstrated that *Lycium barbarum* polysaccharide (LBP) could help with T2DM in a variety of ways (18, 19). Some reports have shown that LBP can influence the composition and structure of gut microbiota (18–21). *Lycium barbarum* is a well-known traditional Chinese herb and is a popular food in China and other Asian countries (22). The concentrated juice or extracts of this fruit are added to beverages to improve liver function and reduce oxidative stress damage (21). LBP is regarded as one of the most important active components with numerous biological activities, including antioxidant, anti-tumor, anti-inflammatory, anti-hyperglycemic, and anti-hyperlipidemic properties (21, 22). LBP's biological activities are primarily determined by its chemical structure, chain conformations, and molecular weight (MW) (23). LBP has a MW range of 10–2,300 kDa (24). Although different extraction methods cause variations in the composition of LBP, its monosaccharide mainly is primarily composed of xylose (Xyl), glucose (Glc), rhamnose (Rha), mannose (Man), galactose (Gal), arabinose (Ara), fructose (Fru), fucose (Fuc), ribose (Rib), galacturonic acid (GalA), and glucuronic acid (GlcA) (24). Furthermore, the biological activities of LBP are also closely related to its chemical structures. A reported review summarized that the backbones of LBP are mainly composed of (1 → 3)-β-Gal*p*, (1 → 4)-β-Gal*p*, (1 → 6)-β-Gal*p*, (1 → 6)-α-glucans, and (1 → 4)-α polygalacturonans with various branches and terminals (24). Even though it has been well documented that LBP can alleviate diabetic symptoms by modulating intestinal flora. However, the potential molecular mechanism of LBP in diabetes alleviation from the perspective of the gut microbiota has not been fully elucidated. As a result, the goal of this study is to gain a better understanding of the molecular mechanism of LBP by modulating intestinal flora in the treatment of T2DM. The LBP's hypoglycemic and hypolipidemic effects, as well as its modulation of the gut microbiota, were investigated. This study estimated the mRNA expression of critical genes involved in glucose metabolism. Furthermore, we performed a Spearman correlation between gut microbiota and biochemical parameters. These findings may help to elucidate the potential mechanism of LBP in the treatment of diabetes and its complications.

MATERIALS AND METHODS

Materials and Reagents

The dried fruits of *L. barbarum* were provided by the National Wolfberry Engineering Research Center of Ningxia Academy of Agricultural and Forestry Sciences (Yinchuan, China). 3-Methyl-1-phenyl-2-pyrazoline-5-one (PMP), monosaccharide standards, and streptozotocin (STZ) were obtained from Sigma Chemical Co., Ltd. (St. Louis, MO, United States). Standards of SCFAs were obtained from Shanghai Yuanye Biotechnology Co., Ltd. (Shanghai, China). A commercial company supplied the mouse feeds (Trophic Animal Feed High-Tech Co., Ltd., Nantong, China). All the other chemicals and solvents used in this study were analytical grade and obtained from Sinopharm Chemical Reagent Co., Ltd. (Shanghai, China).

Preparation of *Lycium barbarum* Polysaccharide

Lycium barbarum polysaccharide was prepared by referring to the works of literature with appropriate modifications (25–27). Briefly, the dried powder of *L. barbarum* was treated with ethanol solution (v/v, 80%) for 2 h to remove small molecules, e.g., monosaccharides, oligosaccharides, pigments, and polyphenols, as well as alcohol-soluble fats, before drying the residues at 60°C overnight. The extraction procedure was as follows: the dried residues were mixed with distilled water (w/v, 1:20) and ultrasonicated (60°C, 180 W) for 15 min before being extracted at 90°C for 105 min. The extraction procedure described above was repeated two times and combined. The extracts were concentrated under reduced pressure at 50°C using a rotary evaporator. The concentrated solution was mixed with absolute ethanol (v/v, 1:4) overnight (4°C). Centrifugation was used to obtain the precipitate (3,500 rpm, 10 min). Repeat the concentrated operation three times after resolving in deionized water. The reported method was used to remove proteins (28). Finally, after removing the small molecule with a dialysis membrane (3.5 kDa), the mixture solution was collected, concentrated, and lyophilized to obtain LBP.

Characterization of *Lycium barbarum* Polysaccharide

The total carbohydrates, protein, and uronic acid contents were determined using previously published methods (29–31). A UV-3100 spectrophotometer was used to scan the UV spectrum of LBP (Mapada Inc., Shanghai, China). LBP samples were formulated with ultrapure water (1 mg/ml) and scanned at the wavelengths ranging from 190 to 610 nm, with ultrapure water served as a blank control (32). The Fourier-transformed infrared (FTIR) spectra were obtained using the Bruker Vetex70 FT-IR instrument (Vetex70, Bruker Co., Germany) within the frequency range of 4,000–400 cm^{-1} (33). The MW of LBP was determined using Infinity Liquid Chromatography (Agilent Technologies Inc., Wilmington, DE, United States) equipped with the TSKgel G5000PWXL column (7.5 mm × 30 cm; TOSOH Corporation, Japan) and the Agilent 1260 refractive index detector (34). In brief, the flow phase was ultrapure water (0.5 ml/min), LBP

was formulated at 2.0 mg/ml and a 10 μl solution was injected to be analyzed; the column temperature was kept at 30°C. The calibration equation was lg MW = −0.3259t + 10.949 (R^2 = 0.9957) based on the retention of standards dextran. The monosaccharide composition of LBP was analyzed by GC–MS, and the procedure was carried out using chromatography (Shimadzu 2014C, Japan) equipped with the DB-17 column (30 m × 0.25 mm × 0.25 μm) (35). The monosaccharide standard mixture was consistently treated with LBP.

Animal Experiments

The specific pathogen-free C57BL/6 mice (male, 6-week-old, SCXK-2018-001) were provided by Xi'an Jiaotong University (Xi'an, China). All mice were housed in accredited animal facilities in an environment with a 12-h reverse light–dark cycle (temperature 22 ± 2°C, humidity 55 ± 5%). **Figure 1** depicts the experiment after 1 week of adaptation, which was carried out using previous methods with appropriate modifications (32). Mice fed a high-fat diet (HFD, TP 23300, 60% kcal from fat) were prepared for insulin resistance in mice, while mice in the normal control group (NC) were fed with normal feed (LAD 3001G, 16.7% kcal from fat). All mice were fed with HFD for 6 weeks and then starved for 6 h before receiving an intraperitoneal injection of fresh-prepared STZ buffer (pH 4.2–4.5, 0.1 mol/L in sodium citrate solution, 40 mg/kg) within 30 min. Mice in the normal control group received the same volume of sodium citrate solution. After 72 h, the level of fasting blood glucose (FBG) was measured using a glucose analyzer, and FBG above 11.1 mmol/L was considered in diabetic mice (36). Food and water intake, body weight (BW), and FBG levels in mice were all recorded. All mice were anesthetized and executed, and the main organs were weighed after the removal of surface blood. All experimental procedures were approved by the Animal Ethics Committee of Xi'an Jiaotong University.

Oral Glucose Tolerance Test and Insulin Tolerance Test

The oral glucose tolerance test (OGTT) and insulin tolerance test (ITT) were performed in the final week of the animal experiment (37). OGTT loaded glucose (2 g/kg BW) by gavage after 12-h fasting. FBG levels in blood from the tail vein were measured before and after glucose administration at 15, 30, 60, 90, and 120 min. The mice were fasting for 4 h, ITT was conducted by injecting intraperitoneally (0.5 IU/kg BW) and then measuring FBG in blood from the tail vein at the same point in time as OGTT. As described previously (38), the homeostasis model assessment for insulin resistance (HOMA-IR) and homeostasis model assessment for beta cell (HOMA-β) was calculated as (FBG × INS)/22.5, and 20 × INS/(FBG − 3.5), respectively.

Biochemical Parameter Analysis

Levels of glycated serum protein (GSP), glycogen (liver and muscle), and other biochemical parameters were determined with commercial kits purchased from the Nanjing Jiancheng Bioengineering Institute (Nanjing, China). ELISA kits were used to measure hemoglobin A1c (HbA1c), LPS, interleukin-6 (IL-6), interleukin-1β (IL-1β), GLP-1, peptide YY (PYY), tumor necrosis factor-α (TNF-α), and insulin (INS) (Colorful Gene, Wuhan, China).

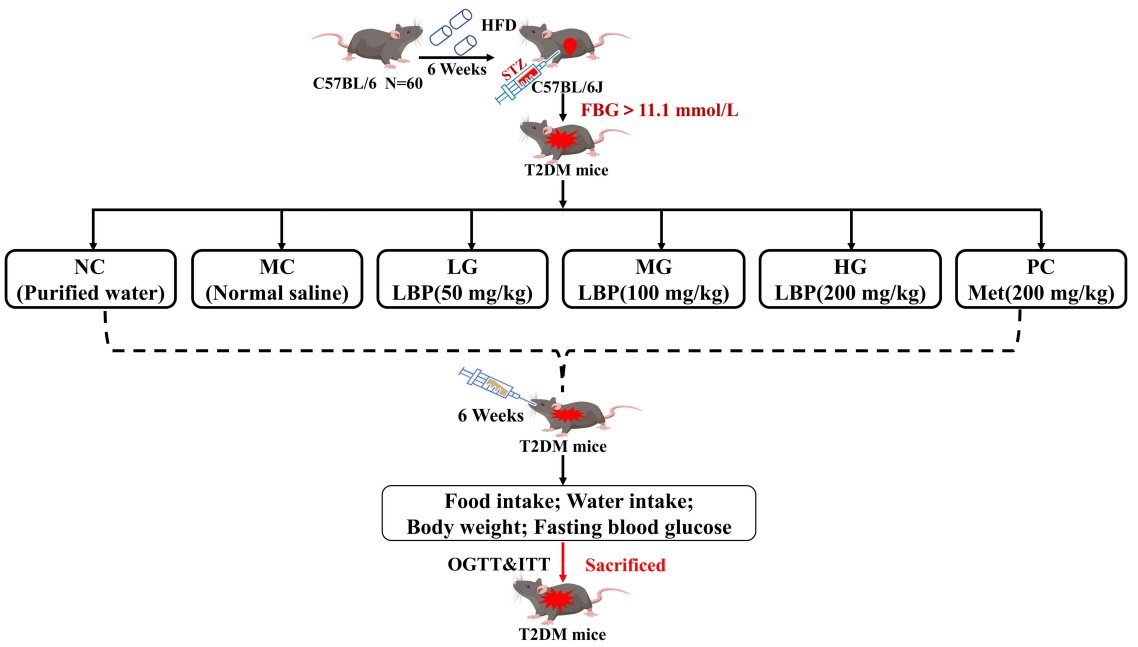

FIGURE 1 | Animal experimental protocol and design. All the mice were divided into a normal group (administrated with normal saline) and diabetic groups (injected with multiple low dosages of STZ at the beginning of the seventh week, 40 mg/kg/day × 3). The diabetic mice were divided randomly into five groups: model control group (MC), low dosage group (LG), medium dosage group (MG), high dosage group (HG), and positive control group (PC).

Histopathological Analysis of Liver, Pancreas, and Skeleton Muscle

Histopathological examinations of the liver, pancreas, and skeletal muscle were performed by previously reported methods (32). A small section of the tissues was fixed in 10% formalin, dehydrated in alcohol, embedded in paraffin, and stained with hematoxylin–eosin (H&E).

Quantification of Short-Chain Fatty Acids in Fecal Samples

Gas chromatography was used to determine SCFAs in feces samples based on previously reported methods with appropriate modifications (39). In brief, approximately 200 mg of feces were dissolved with ultrapure water (w/v, 1:5) in a 5 ml centrifuge tube, and dissolved material from the vortexes was mixed thoroughly. Afterward, the mixture was centrifuged (12,000 rpm, 10 min), 0.75 ml supernatant fluid was mixed with 0.15 ml H_2SO_4 (v/v), and then mixed with 1.6 ml of diethyl ether, followed by incubating in shaking table (160 rpm, 30 min), while simultaneously mixing 10 times. The mixed solution was then centrifuged for 10 min at 4°C and 12,000 rpm to collect the organic phase in the upper layer. The organic phase was concentrated with liquid nitrogen from 1.5 to 0.3 ml and then passed through a 0.25 μm organic filter for further analysis as described below: the initial temperature was 50°C (1 min) and raised to 120°C (15°C/min), increased to 170°C (5°C/min), raised to 220°C (15°C/min, maintained 5 min), injection volume 2.0 μl. The temperatures of the injector and detector were 250 and 270°C, respectively.

16S rDNA Sequencing and Bioinformatics Analysis

Fresh fecal pellets from eight mice per group were collected for microbial analysis of intestinal flora (40). According to the manufacturer's instructions, bacterial genomic DNA extracted from feces was obtained by a QIAamp DNA stool Mini Kit from Qiagen (Hilden, Germany). The V3 and V4 regions of 16S rDNA were amplified by 338F (5′-ACTCCTACGGGCAGCAG-3′) and 806R (5′-GGACTACHVGGGTWTCTAAT-3′) universal primers with dual-index barcodes to tag each sample. The concentrations of PCR products were measured using a QuantiFluor-St Fluorometer (Promega, United States). The fecal samples of PCR products in equimolar concentrations were examined on the Illumina MiSeq platform following the manufacturer's manual by Shanghai Biotree Biomedical Technology Co., Ltd. (Shanghai, China).

Quantitative Real-Time PCR Analysis

Total RNA was extracted from colon and liver tissues using the TRIzol reagents (Jingcai Bio., Xi'an, China), and reverse transcription reagents were used to synthesize cDNA (Tiangen, Beijing, China). Real-time PCR (RT-PCR) was used to measure gene expression on a CFX96 RT-PCR detection system (Bio-Rad, Hercules, CA, United States) using the SYBR Green master mix (Tiangen, Beijing, China). The $2^{-\Delta\Delta CT}$ method was used to normalize gene expression to that of the housekeeping gene (β-actin). **Supplementary Table 1** shows the primer sequences used in this study.

Statistical Analysis

Statistical analysis of data was analyzed by SPSS V22.0 software (IMB, Chicago, IL, United States). The differences were conducted using a one-way analysis of variance (ANOVA) test followed by Duncan's test. Results were presented as mean ± SD. Values with $p < 0.05$ were considered to be statistically significant.

RESULTS AND ANALYSIS

Characterization of *Lycium barbarum* Polysaccharide

The yield of LBP is 2.76 ± 0.33%. LBP mainly consisted of carbohydrates, uronic acid, and protein of 62.27 ± 2.37, 25.03 ± 1.27, and 2.92 ± 0.17%. **Figures 2A,B** show the GC chromatograms of the monosaccharide standards and LBP, respectively. The GC chromatogram in **Figure 2B** revealed that LBP was made up of eight monosaccharides, with a molar ratio of 0.23: 1.90: 0.26: 0.20: 1.0: 1.26: 0.44: 1.49 for Rha, Ara, Xyl, Man, Glc, Gal, GlcA, GalA residues. The retention time (18.283 min) was used to compute the MW of LBP, which was found to be 98.0 kDa. In **Figure 2C**, UV spectroscopy examination of LBP revealed no significant absorption at 260–280 nm, indicating that the LBP does not include protein or nucleic acid (32). **Figure 2D** shows the results of FT-IR spectroscopy used to characterize LBP. Polysaccharide absorption peaks were found at 800–1,200, 1,450–1,800, 2,900–3,000, and 3,200–3,600 cm^{-1} in the spectra. The hydroxyl group (O-H) had a characteristic significant broad stretch peak at 3,400.5 cm^{-1}, while the C-H stretching vibration had a band at 2,937.6 cm^{-1} (41). The broadband at 1633.7 cm^{-1} was created by bound water (18). The absorbance of a carboxylic group (COO-) is responsible for a strong band of 1,743.7 cm^{-1} and a weak band of 1,421.5 cm^{-1}, indicating that LBP included uronic acid (35). The C = O stretching vibration is responsible for the frequency band at 1330.9 cm^{-1} (42). The fingerprint of molecules is a wavelength range between 950 and 1,200 cm^{-1} that is used to determine the position and intensity of distinctive bands in polysaccharides (43). The presence of C-O bonds and furanose rings in the monosaccharide blocks of LBP is attributed to the intense stretching peaks at 1,101.4 and 1,018.4 cm^{-1}. The presence of α-glycosidic, β-glycosidic linkages, and pyranose rings in the monosaccharide blocks of LBP was confirmed by the band at 831.3, 852.5, and 891.1 cm^{-1}, respectively. The α-glycosidic bond is prevalent in LBP, as evidenced by the moderate absorbance at 831.3 and 852.5 cm^{-1}, and the weak absorbance at 891.1 cm^{-1} (18).

Effects of *Lycium barbarum* Polysaccharide on Body Weight, Food Intake, and Water Intake in Mice

Figure 3A and **Supplementary Table 2** show that mice in the MC group consumed more food and water intake

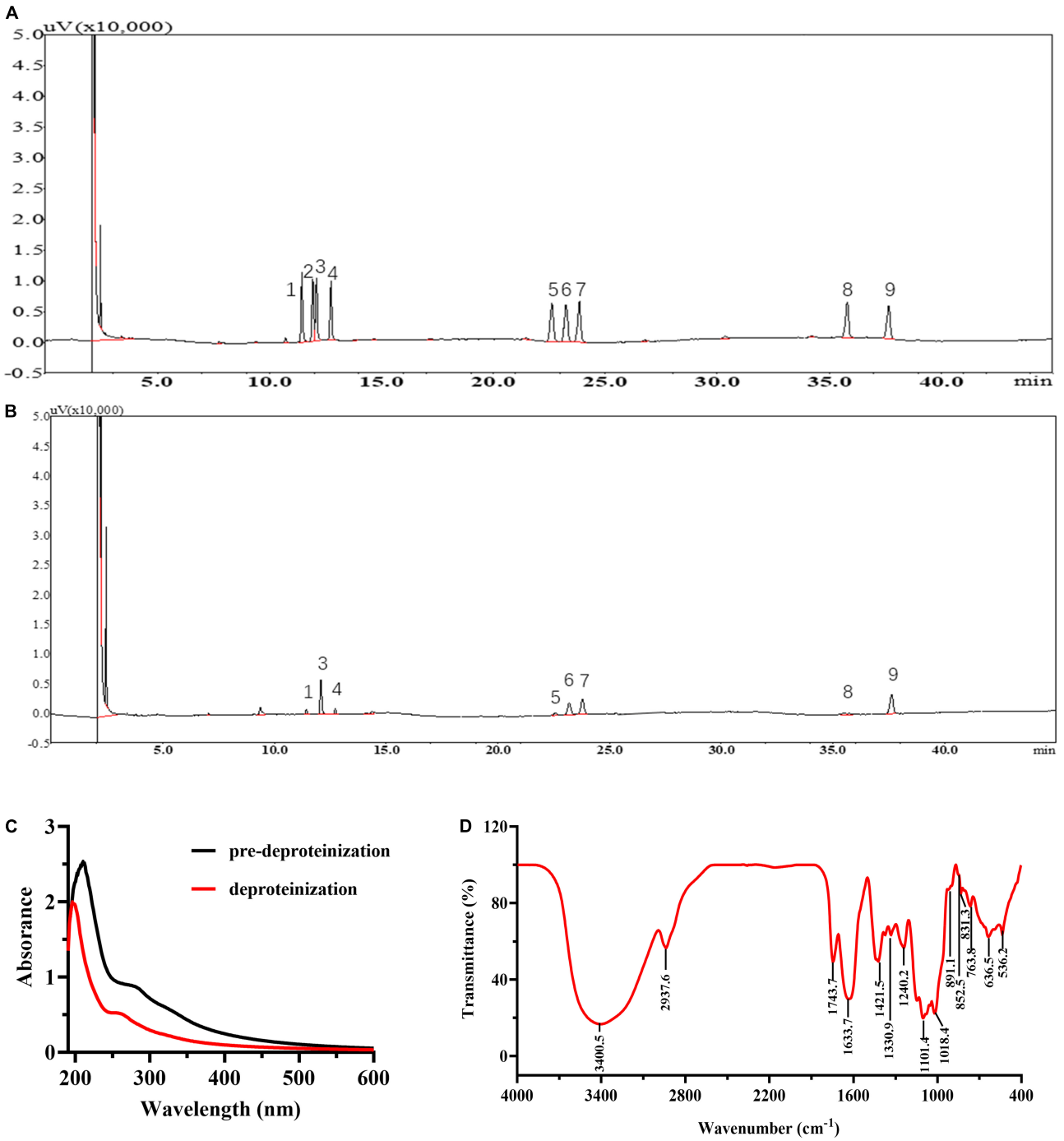

FIGURE 2 | Chemical information of LBP. GC chromatogram of the monosaccharide standards **(A)**, and LBP **(B)**. The peaks in monosaccharide standards and LBP represent (1) rhamnose, (2) fructose, (3) arabinose, (4) xylose, (5) mannose, (6) glucose, (7) galactose, (8) glucuronic acid, (9) galacturonic acid; the **(C)** UV spectra of LBP, **(D)** FTIR spectra of LBP.

than that in the NC group ($p < 0.05$). In diabetic mice, LBP reversed BW loss and reduced food and water intake ($p < 0.05$). In comparison with the NC group, the MC group's total food and water intake increased by 23.44 and 36.30%, respectively. Total food intake reduced by 5.11, 9.22, 14.18, and 11.84% in the LG, MG, HG, and PC groups, respectively, compared with the MC group, while total water intake declined by 17.42, 20.26, 22.60, and 13.55%. These findings showed that LBP reduced BW loss, and food and water intake in diabetic mice.

Effects of *Lycium barbarum* Polysaccharide on Fasting Blood Glucose, Oral Glucose Tolerance Test, Insulin Tolerance Test, HbA1c, Glycated Serum Protein, Glucagon-Like Peptide-1, Peptide YY, Insulin, and HOMA-IR in Mice

Figure 3B shows that FBG in the MC group increased by 149.57% when compared with the NC group. FBG levels in the LG, MG, HG, and PC groups decreased by 24.25, 25.52, 33.02, and 26.50%, respectively, as compared with the MC group. In **Figures 3C,D**, LBP notably reduced the levels of OGTTAUC, ITTAUC, and HOMA-IR **Figure 3O** in comparison with the MC group ($p < 0.05$). As shown in **Figure 3C**, after loading glucose, the blood glucose levels reached a peak in each group within 30 min. Furthermore, at each time point, blood glucose in the MC group was higher than that in the other groups in (**Figures 3G,H**). LBP significantly reduced OGTTAUC and ITTAUC levels in the LG, MG, and HG groups compared with the NC group ($p < 0.05$), with a decrease of 25.98, 27.67,

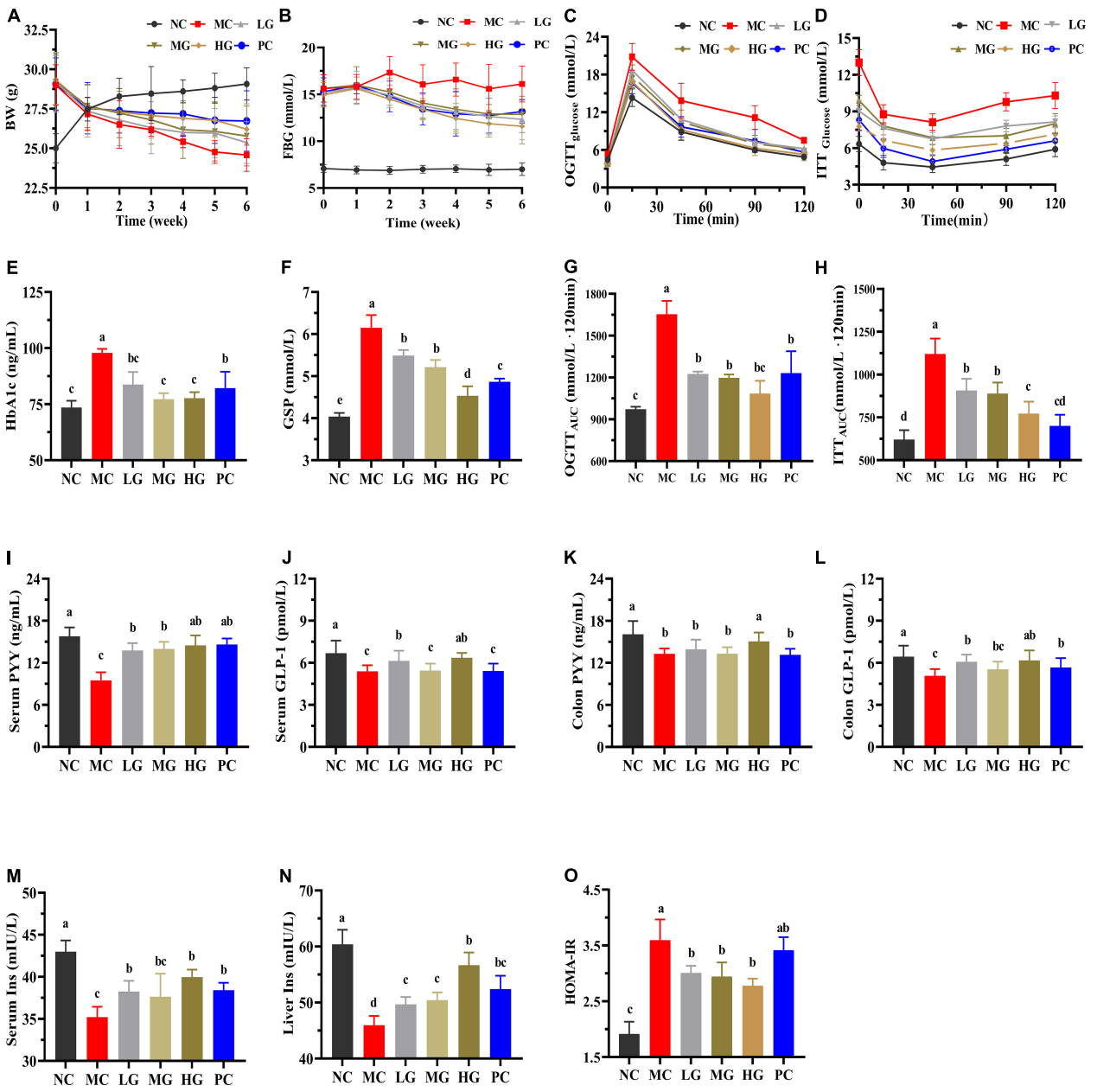

FIGURE 3 | Effects of LBP on biochemical parameters. **(A)** BW; **(B)** FBG; **(C)** OGTT; **(D)** ITT; **(E)** HbA1c; **(F)** GSP; **(G)** OGTTAUC; **(H)** ITTAUC; **(I)** serum PYY; **(J)** serum GLP-1; **(K)** colon PYY; **(L)** colon GLP-1; **(M)** serum INS; **(N)** liver INS; and **(O)** HOMA-IR. Different letters denote significant differences at $p < 0.05$.

and 34.50% (OGTTAUC), 18.99, 20.62 and 31.04% (ITTAUC), respectively. HbA1c (**Figure 3E**), GSP (**Figure 3F**), and HOMA-IR (**Figure 3O**) levels were significantly higher in the MC group than those in the NC group, while GLP-1 (**Figures 3J,L**), PYY (**Figures 3I**,**K**), and insulin (**Figures 3M,N**) levels were significantly lower in the MC group than those in the NC group ($p < 0.05$). As compared with the MC group, LBP reduced HbA1c, GSP, and HOMA-IR levels, improved GLP-1 and PYY levels (serum and colon), and decreased insulin (serum and liver) ($p < 0.05$). These results disclosed that LBP improved insulin sensitivity, alleviated insulin resistance, and improved blood glucose metabolism in diabetic mice.

Effects of *Lycium barbarum* Polysaccharide on Blood Lipids, Oxidative Stress, and Cytokines in Mice

Table 1 shows that the NC group's TC, TG, and LDL-C levels were significantly lower than those in the MC group ($p < 0.05$), while TBA and HDL-C levels notably increased ($p < 0.05$). LBP significantly decreased TC, TG, and LDL-C levels ($p < 0.05$), and improved TBA and HDL-C levels in diabetic mice compared to the MC group ($p < 0.05$), indicating that LBP alleviated dyslipidemia. Furthermore, the MC group's increment of AST and ALT was significantly higher than that in the NC group ($p < 0.05$). When compared to the MC group, LBP remarkably reduced the levels of ALT and AST ($p < 0.05$). These results demonstrated that LBP effectively reversed the abnormal lipid metabolism in diabetic mice.

In **Table 2**, the levels of CAT, SOD, GSH, GSH-Px, and TAOC (serum and liver) in the MC group were significantly lower than that in the NC group ($p < 0.05$), while the level of MDA was higher than that in the NC group ($p < 0.05$). LBP exhibited an ascendency in promoting the levels of CAT, SOD, GSH-Px, and TAOC, while decreasing MDA in the liver as compared with the MC group ($p < 0.05$).

In **Figure 4**, levels of IL-6, IL-1β, TNF-α, and LPS in the MC group were significantly higher than those in the NC group ($p < 0.05$). In comparison to the MC group, LBP significantly reduced the levels of IL-6, IL-1β, TNF-α, and LPS (serum and liver) in the LG, MG, and HG groups ($p < 0.05$), demonstrating that LBP effectively relieved the inflammation of diabetic mice. According to the results, LBP markedly mitigated dyslipidemia, oxidative stress, and inflammation in diabetic mice.

Histopathological Observations and Glycogen Measurements

H&E stating images of the panceras, liver, and skeletal muscle sections are shown in **Figure 5**. In **Figure 5A**, the pancreas staining in the NC group exhibited a uniform arrangement of structure and the pancreatic islets contained several pancreatic β-cells, whereas the pancreatic islet in the MC group displayed significant damage compromising and deforming its shape accompanied by a reduction in pancreatic β-cells. LBP partially repaired the damaged state and improved the number of pancreatic β-cells. In **Figure 5B**, the level of HOMA-β in the NC group was significantly lower than that in the MC group ($p < 0.05$). After treatment of LBP, the HOMA-β level in the HG group was significantly decreased as compared with the MC group ($p < 0.05$). In **Figure 5C**, the liver cells were normal and neatly arranged without clearly lipid accumulation in the NC group. In contrast, cytoplasmic vacuoles were found in the liver sections of mice in the MC group, indicating that LBP partly mitigated the damage caused by diabetes. The hepatocytes structure of mice in the HG group was almost completely restored to normal. As shown in **Figure 5E**, in comparison with the NC group, the pathological damages of skeletal muscle sections in the MC group were partially ameliorated by LBP.

TABLE 1 | Effects of LBP on levels of biochemical parameters in serum and liver.

		Group					
	Items	**NC**	**MC**	**LG**	**MG**	**HG**	**PC**
Serum	TC (mmol/L)	2.57 ± 0.14 c	3.83 ± 0.07 a	2.89 ± 0.14 bc	2.81 ± 0.27 b	2.68 ± 0.12 bc	2.74 ± 0.11 c
	TG (mmol/L)	0.63 ± 0.07 c	1.05 ± 0.06 a	6.80 ± 0.13 bc	0.88 ± 0.06 b	0.80 ± 0.10 bc	0.73 ± 0.05 c
	LDL-C (mmol/L)	2.32 ± 0.20 d	3.57 ± 0.18 a	2.86 ± 0.14 bc	2.99 ± 0.07 b	2.48 ± 0.24 cd	2.64 ± 0.14 c
	HDL-C (mmol/L)	3.72 ± 0.19 a	2.33 ± 0.13 d	2.96 ± 0.05 c	2.88 ± 0.08 c	3.42 ± 0.15 b	2.45 ± 0.21 d
	ALT (U/L)	7.04 ± 0.61 c	14.90 ± 1.59 a	10.80 ± 1.48 b	10.64 ± 1.40 b	10.32 ± 1.11 b	8.95 ± 1.50 bc
	AST (U/L)	8.40 ± 0.81 d	15.15 ± 1.11 a	12.56 ± 0.97 b	12.11 ± 0.95 b	10.28 ± 0.41 c	13.10 ± 0.67 b
	TBA (μmol/L)	3.35 ± 0.36 a	2.16 ± 0.05 c	2.75 ± 0.19 b	2.78 ± 0.15 b	2.72 ± 0.13 b	2.76 ± 0.10 b
Liver	TC (mmol/gprot)	0.11 ± 0.01 e	0.29 ± 0.02 a	0.19 ± 0.01 c	0.18 ± 0.02 c	0.15 ± 0.01 d	0.24 ± 0.03 b
	TG (mmol/gprot)	0.056 ± 0.004 b	0.128 ± 0.011 a	0.08 ± 0.009 b	0.065 ± 0.012 b	0.060 ± 0.008 b	0.071 ± 0.014 b
	LDL-C (mmol/gprot)	0.074 ± 0.006 b	0.094 ± 0.004 a	0.079 ± 0.003 b	0.079 ± 0.004 b	0.071 ± 0.009 b	0.087 ± 0.003 ab
	HDL-C (mmol/gprot)	0.050 ± 0.001 a	0.035 ± 0.003 c	0.044 ± 0.002 b	0.044 ± 0.003 b	0.043 ± 0.002 b	0.050 ± 0.003 ab
	ALT (U/gprot)	4.77 ± 0.92 d	10.76 ± 1.20 a	8.05 ± 0.74 b	6.46 ± 0.70 c	7.12 ± 0.47 bc	7.79 ± 0.66 bc
	AST (U/gprot)	4.47 ± 0.90 b	8.31 ± 1.34 a	6.02 ± 0.86 b	5.43 ± 0.66 b	5.06 ± 0.53 b	6.66 ± 1.12 ab
	TBA (μmol/L)	16.13 ± 0.65 a	12.47 ± 0.54 b	13.46 ± 0.72 b	15.06 ± 0.69 a	15.61 ± 1.07 a	13.67 ± 0.85 b

Values are presented as the mean ± SD. Different letters denote significant differences at $p < 0.05$.

TABLE 2 | Effects of LBP on levels of oxidative stress parameters in mice.

		Group					
	Items	**NC**	**MC**	**LG**	**MG**	**HG**	**PC**
Liver	CAT (U/mgprot)	31.08 ± 1.80 a	20.12 ± 1.89 c	24.10 ± 1.49 b	25.32 ± 1.72 b	29.92 ± 2.71 a	25.20 ± 1.62 b
	SOD (U/mgprot)	196.20 ± 13.82 a	136.15 ± 4.67 c	174.33 ± 8.86 b	166.42 ± 9.29 b	173.14 ± 13.64 b	177.72 ± 10.52 b
	GSH (μmol/gprot)	4.47 ± 0.27 a	2.99 ± 0.23 c	3.63 ± 0.19 bc	3.72 ± 0.22 bc	3.96 ± 0.24 b	3.32 ± 0.31 c
	GSH-Px (U/gprot)	285.28 ± 7.33 a	203.61 ± 11.81 d	234.55 ± 10.88 c	240.61 ± 9.17 bc	252.26 ± 11.42 b	244.60 ± 9.37 bc
	MDA (nmol/mgprot)	1.28 ± 0.03 a	1.78 ± 0.08 a	1.61 ± 0.17 b	1.46 ± 0.07 bc	1.41 ± 0.05 c	1.46 ± 0.08 bc
	TAOC (mmol/gprot)	0.084 ± 0.012 a	0.050 ± 0.005 c	0.058 ± 0.004 c	0.059 ± 0.005 c	0.072 ± 0.004 b	0.068 ± 0.002 bc
Serum	TAOC (mM Trolox)	0.68 ± 0.03 a	0.51 ± 0.03 b	0.65 ± 0.01 ab	0.67 ± 0.05 a	0.67 ± 0.01 a	0.61 ± 0.02 b

Values are presented as the mean ± SD. Different letters denote significant differences at $p < 0.05$.

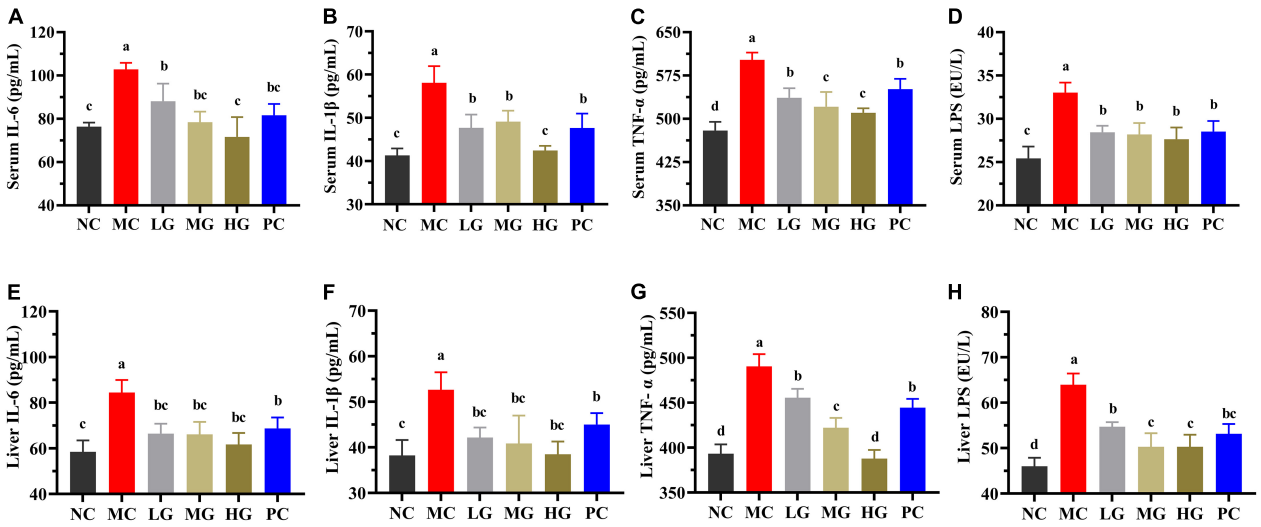

FIGURE 4 | Effects of LBP on **(A)** serum IL-6; **(B)** serum IL-1β; **(C)** serum TNF-α; **(D)** serum LPS; **(E)** liver IL-6; **(F)** liver IL-1β; **(G)** liver TNF-α; and **(H)** liver LPS. Different letters denote significant differences at $p < 0.05$.

Figures 5D,F show the levels of glycogen in the liver and skeletal muscle, respectively. Glycogen levels in the MC group were significantly lower than that in the NC group ($p < 0.05$). LBP remarkably improved the contents of glycogen as compared with the MC group ($p < 0.05$), indicating that LBP promoted the accumulation of glycogen in diabetic mice. These findings disclosed that LBP effectively protected the liver, pancreas, and skeletal muscle from oxidative damage in diabetic mice.

Effects of *Lycium barbarum* Polysaccharide on Gut Microbiota in Mice

Effects of *Lycium barbarum* Polysaccharide on Diversities of Gut Microbiota

In **Figures 6A,B**, Chao 1 and ACE in the NC group were remarkably higher than those in the MC group ($p < 0.05$), illustrating that gut microbiota richness was significantly decreased in diabetic mice. LBP notably increased ACE and Chao 1 indexes in the LG, MG, and HG groups compared with the MC group ($p < 0.05$), indicating that LBP was effective in regulating the community richness of intestinal flora. **Figures 6C,D** show that Shannon was higher in the NC group than that in the MC group ($p < 0.05$), while the Simpson index was notably lower in the NC group ($p < 0.05$). We used principal coordinates analysis (PCoA) and non-metric multidimensional scaling (NMDS) to calculate beta diversity in this study. **Figures 6E,F** shows the results of PCoA in the MC group were different from those in the LG group. In the same way, NMDS analysis also showed a significant difference between the MC group and the LG group.

Effects of *Lycium barbarum* Polysaccharide on the Composition of Gut Microbiota

The top 10 phyla of intestinal flora are shown in **Figure 7**. In each group, the relative abundance of four predominant phyla was Firmicutes, Bacteroides, Actinobacteria, and Proteobacteria (**Figure 7A**), accounting for 95.77, 95.65, 91.59, 85.65, 95.16, and 94.18%, respectively. In **Figure 7C**, the relative abundance of Firmicutes was dramatically higher than that in the MC group compared to the NC, LG, and MG groups ($p < 0.05$). In **Figure 7F**, the ratio of Firmicutes–Bacteroides (F/B) in the MC group was higher than that in the NC group

($p < 0.05$). In this study, the top 30 genera were isolated in **Figure 7B** and analyzed in **Figures 7G–N**. As compared with the MC group, the relative abundance of *Allobaculum*, *Dubosiella*, and *Romboutsia* in the NC, LG, MG, HG, and PC groups were significantly decreased ($p < 0.05$), oppositely, the relative abundance of *Bacteroides*, *Ruminococcaceae_UCG-014*, *Mucispirillum*, *Intestinimonas*, *Ruminococcaceae_UCG-009* were remarkably increased ($p < 0.05$). These results indicated that LBP had a significant impact on the composition and structure of intestinal flora.

The linear discriminant analysis effect size (LEfSe) method was conducted to further identify the specific bacteria taxa (**Figures 8A,B**), and the calculation of effect size for variation-rich features was founded on linear discriminant analysis (LDA). In the NC, MC, LG, MG, HG, and PC groups (**Figure 8A**), we found 57 OTUs that were significantly different from other groups with 4, 7, 22, 6, 13, and 4 OTUs in each group, respectively. In the NC group, Actinobacteria (phylum level), Actinobacteria (class level), Bifidobacteriales (order level), Bifidobacteriaceae (family level), and *Bifidobacterium* (genus level) were more abundant, whereas Tenericutes (phylum level), Erysipelotrichia (class level), Erysipelotrichales (order level), Erysipelotrichaceae (family level), and *Allobaculum* (genus level) were enriched in the MC group. Proteobacteria and Deferribacteres (phylum level), Clostridia and Deferribacteres (class level), Clostridiales and Deferribacterales (order level), Lachnospiraceae, Ruminococcaceae, Bacteroidaceae, and Deferribacteraceae (family level), and *Bacteroides*, *Lachnospiraceae*, *Blautia*,

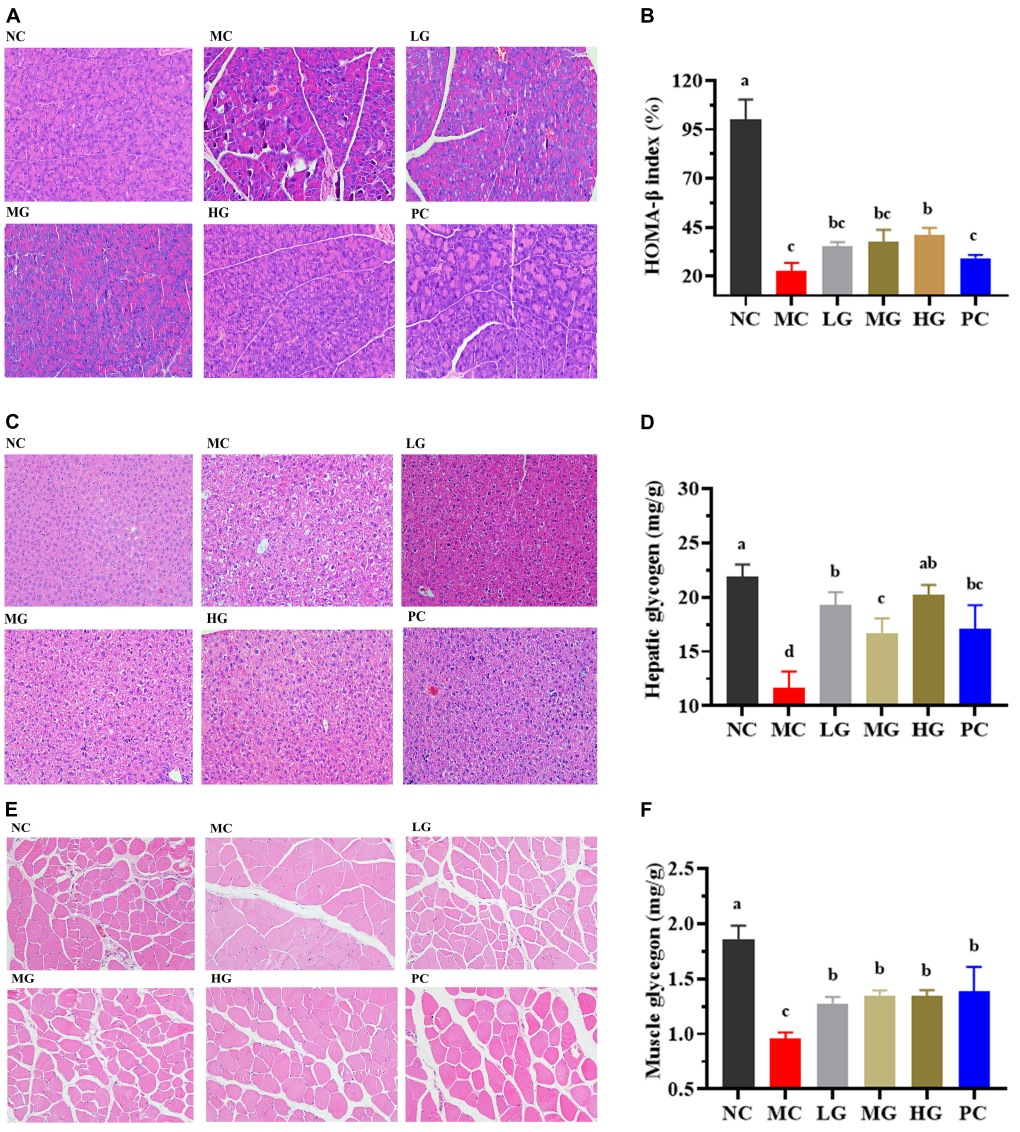

FIGURE 5 | Effects of LBP on pancreas, liver, skeletal muscle, hepatic glycogen, and muscle glycogen. **(A)** H&E staining of pancreas; **(B)** HOMA-β; **(C)** H&E staining of liver; **(D)** hepatic glycogen; **(E)** H&E staining of muscle; and **(F)** muscle glycogen. Different letters denote significant differences at $p < 0.05$.

Mucispirillum, *Intestinimonas*, and *Ruminclostridium_9* (genus level), *Lachnospiraceae_bacterium_09*, and *Mucispirillum_achaedleri_ASF457* (species level) were biomarkers in the LG group. Verrucomicrobia (phylum level), Verrucomicrobiae (class level), Verrucomicrobiales (order level), Akkermansiaceae (family level), and *Akkermansia* (genus level) were more abundant in the MG group. Actinobacteria (phylum level), Bacilli and Coriobacteriia (class level), Lactobacillales and Coribacteriales (order level), Lactobacillaceae and Atopobiaceae (family level), and *Dubosiella*, *Lactobacillus*, and *Coriobacteriaceae_UCG_002* (genus level) were enriched in the HG group. In the PC group, *Faecalibaculum* and *Ruminococcaceae_UCG_014* were enriched. These results indicated that LBP modulated the composition of intestinal flora.

Effects of *Lycium barbarum* Polysaccharide on Short-Chain Fatty Acids in Mice Feces

In **Table 3**, the SCFAs levels in the MC group were significantly lower than that in the NC group ($p < 0.05$). As compared with the MC group, contents of acetate, propionate, butyrate, iso-butyrate, and total SCFAs were remarkably increased in the MG and HG groups ($p < 0.05$). Additionally, levels of valerate and iso-valerate in the HG group, as well as isovalerate in the MG group were increased as compared with the MC group ($p < 0.05$). These results illustrated that LBP significantly improved the levels of SCFAs in diabetic mice, particularly the contents of acetate, propionate, and butyrate.

Potential Interactions Between Gut Microbiota and Biochemical Parameters

To assess the potential interaction between the gut microbiota and biochemical parameters, a Spearman's correlation analysis was performed on the relative abundance of significantly changed gut microorganisms (**Figure 8D**, $p < 0.05$). Spearman's rank analysis revealed that the relative abundance of *Ruminoccaceae_UCG-009*, *UBA1819*, *Streptococcus*, *Cetobacterium*, *Ralstonia*, *Millionella*, *Lactococcus*, *Leuconostoc*, *Bifidobacterium*, *Lactobacillus*, *Alloprevotella*, *Coriobacteriaceae_UCG-002*, *Bradyrhizobium*, *Rikenellaceae_RC9_gut_group*, *Lachnospiraceae_UCG-006*, *Anaerovorax*, *Ruminococcaceae_UCG-004*, *Bacteroides*, *Negativibacillus*, *ASF356* was negatively correlated with ITTAUC, OGTTAUC, FBG, GSP, HbA1c, HOMA-IR, as well as levels of TC, TG, LDL-C, ALT, AST, LPS, IL-6, IL-1β, TNF-α (serum and liver), while positively correlated with HOMA-β, BW, acetate, isovalerate, valerate, iso-butyrate, muscle glycogen, butyrate, propionate, and levels of Insulin, TBA, TAOC, HDL-C (serum and liver). Apart from that, the visual network of correlation analysis (**Figure 8C**) showed a close correlation between intestinal flora and biochemical profiles ($|r| > 0.7$). The results of correlation analysis showed that the relative abundance of *Cetobacterium*, *Millionella*, *Clostridium_sensu_stricto_1*, *Streptococcus*, *Ruminococcaceae_UCG_009* was negatively correlated with HOMA-IR and HDL-C, ALT, AST, TC, LPS in the liver. A significant positive correlation was observed between insulin (serum and liver) and *Cetobacterium*, *Streptococcus*, as well as *Ralstonia*. *Cetobacterium*, *Ruminiclostridium*, *Bifidobacterium*, and *Streptococcus* exhibited a positive correlation with HDL-C and serum insulin, liver glycogen, GSH, and CAT, as well as propionate, butyrate, and iso-butyrate. *Butyricimonas* was positively correlated with TG, GSP, and MDA. Similarly, *Ruminococcaceae_UCG-009* was positively correlated with TBA and TAOC (serum), HDL-C in the liver, muscle glycogen, iso-butyrate, and iso-valerate. Additionally, *Millionella* was negatively correlated with valerate, propionate, and TAOC (serum).

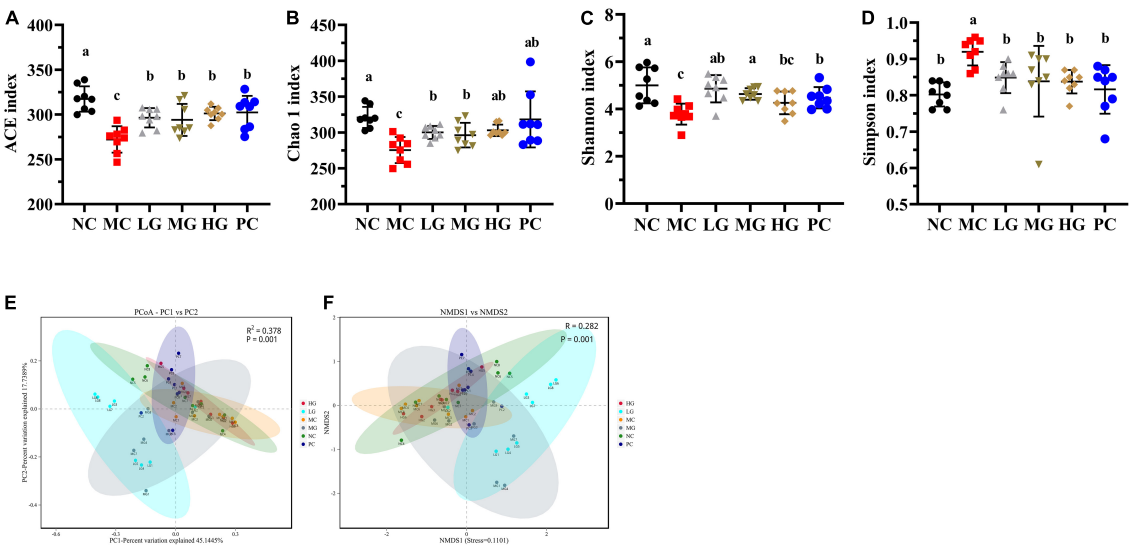

FIGURE 6 | Effects of LBP on alpha diversity and beta diversity. **(A)** ACE index; **(B)** Chao 1 index; **(C)** Shannon index; **(D)** Simpson index; **(E)** PCoA; and **(F)** NMDS. Different letters denote significant differences at $p < 0.05$.

Effects of *Lycium barbarum* Polysaccharide on the mRNA Expression of Colon and Liver in Mice

The underlying molecular mechanisms of LBP in diabetes alleviation were investigated using RT-PCR in this study. In **Figures 9A–D**, PYY, GLP-1, GPR43 (also known as free fatty acid receptor 2, FFAR2), and GPR41 (also known as FFAR3) relative expression levels were significantly higher in the NC, LG, MG, and HG groups as compared with those in the MC group ($p < 0.05$). In the MC group, the relative expression levels of insulin receptor (InsR), insulin receptor substrate-1 (IRS-1), insulin receptor substrate-2 (IRS-2), phosphatidylinositol 3-kinase (PI3K), protein kinase B (PKB, also known as Akt), and translocating glucose transporter-2 (GLUT2) were significantly lower than those in the NC group ($p < 0.05$). LBP reduced the levels of InsR (**Figure 9E**), IRS-1 (**Figure 9F**), IRS-2 (**Figure 9G**), PI3K (**Figure 9H**), Akt (**Figure 9I**), and GLUT2 (**Figure 9J**) in the LG, MG, and HG groups compared with the MC group ($p < 0.05$). In contrast, the MC group had a significantly

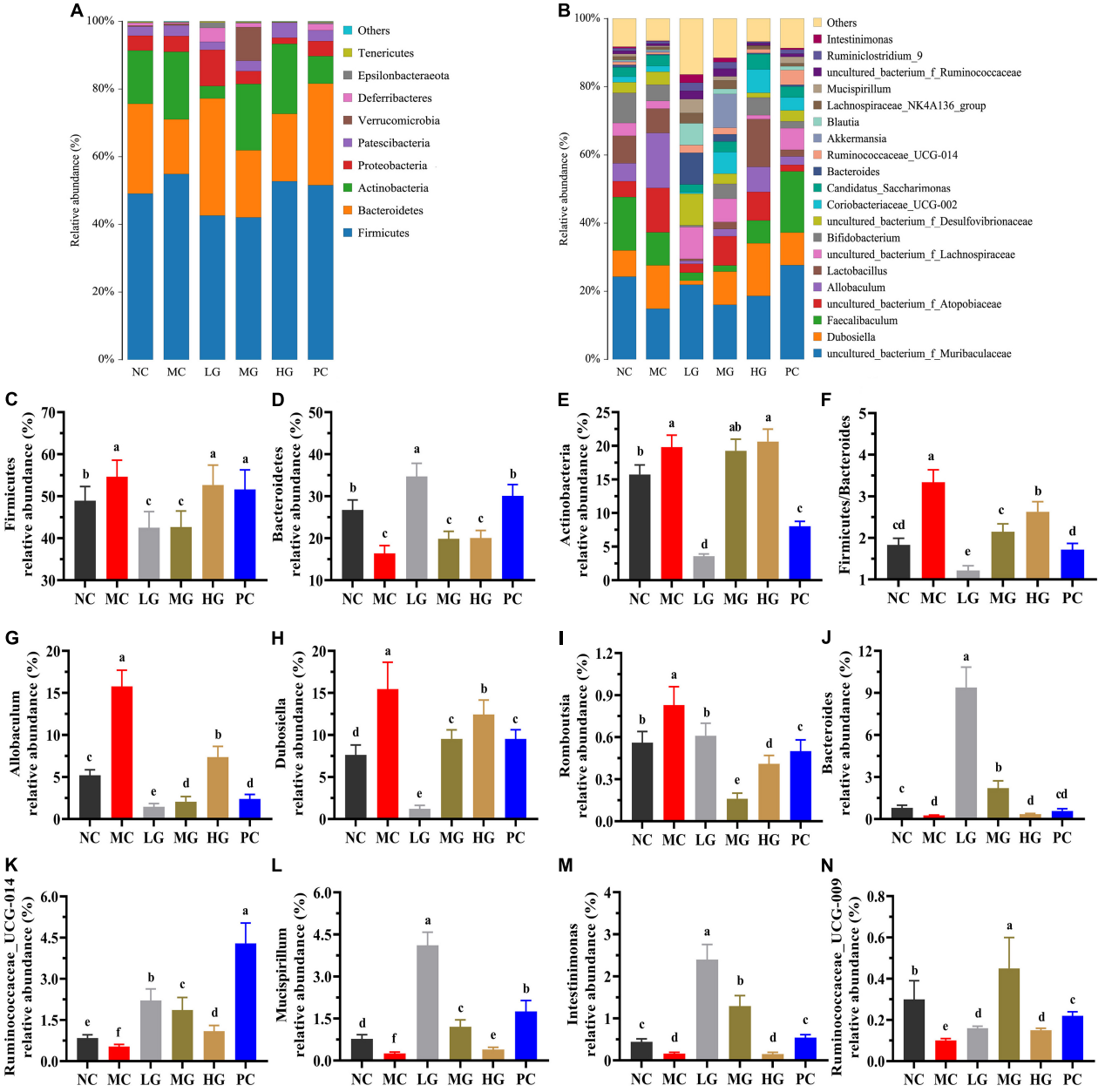

FIGURE 7 | Effects of LBP on the relative abundance of gut microbiota at levels of phylum and genus. **(A)** Phylum (top 10); **(B)** genus (top 30); **(C)** Firmicutes; **(D)** Bacteroidetes; **(E)** Actinobacteria; **(F)** ratio of Firmicutes/Bacteroidetes; **(G)** Allobaculum; **(H)** Dubosiella; **(I)** Romboutsia; **(J)** Bacteroides; **(K)** Ruminococcaceae_UCG-014; **(L)** Mucispirillum; **(M)** Intestinimonas; and **(N)** Ruminococcaceae_UCG-009. Different letters denote significant differences at $p < 0.05$.

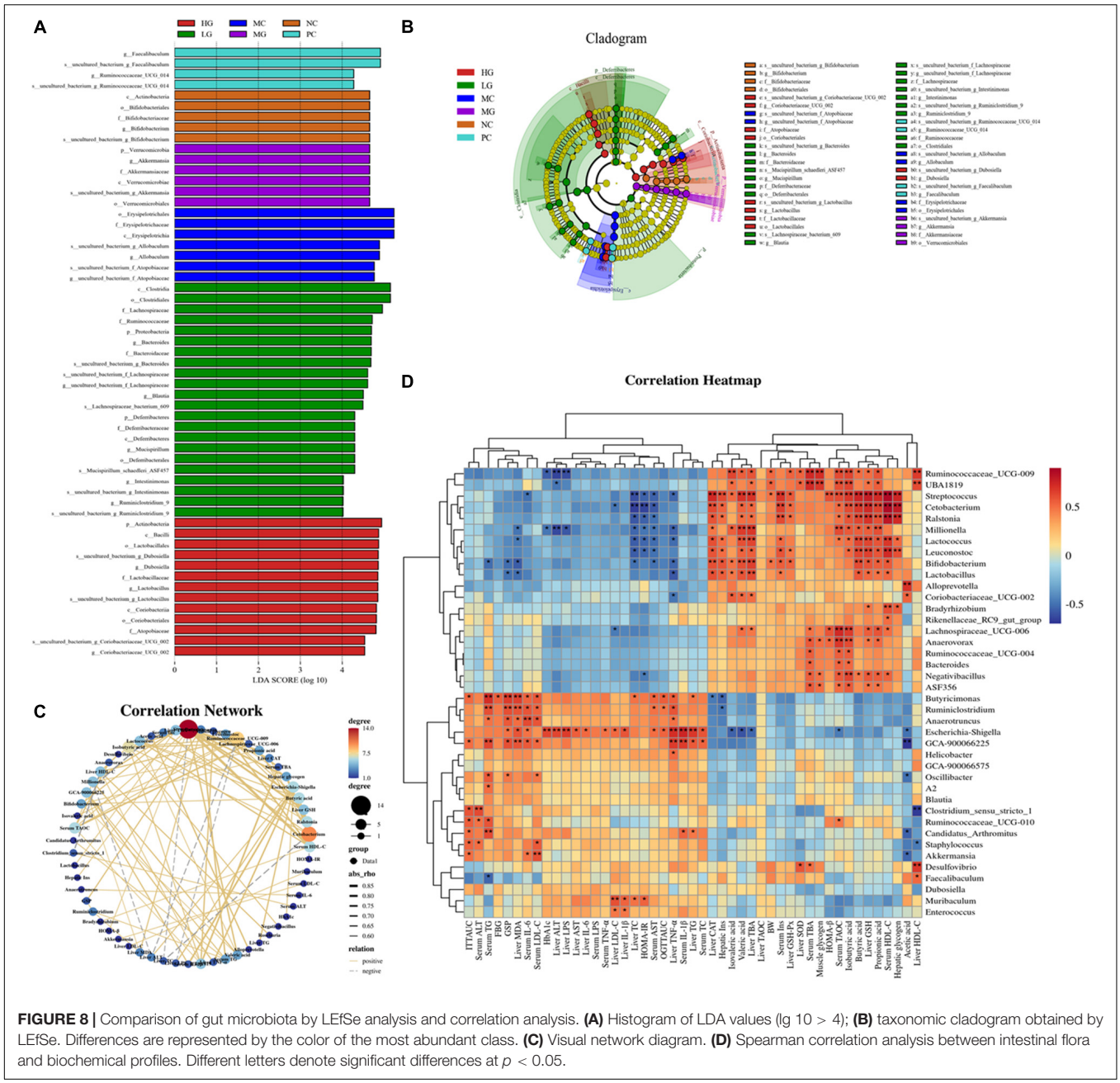

FIGURE 8 | Comparison of gut microbiota by LEfSe analysis and correlation analysis. **(A)** Histogram of LDA values (lg 10 > 4); **(B)** taxonomic cladogram obtained by LEfSe. Differences are represented by the color of the most abundant class. **(C)** Visual network diagram. **(D)** Spearman correlation analysis between intestinal flora and biochemical profiles. Different letters denote significant differences at $p < 0.05$.

TABLE 3 | Effects of LBP on levels of SCFAs in mice feces.

	Group					
Item	**NC**	**MC**	**LG**	**MG**	**HG**	**PC**
Acetate (μmol/g)	10.52 ± 0.50 a	8.00 ± 0.28 c	7.59 ± 0.25 c	9.07 ± 0.55 b	10.76 ± 1.19 a	10.59 ± 1.05 a
Propionate (μmol/g)	9.49 ± 0.42 b	8.79 ± 0.18 c	9.88 ± 0.62 b	10.03 ± 0.72 b	10.86 ± 0.78 a	9.26 ± 0.29 c
Isobutyrate (μmol/g)	2.58 ± 0.14 a	2.28 ± 0.04 b	2.63 ± 0.23 a	2.74 ± 0.36 a	2.67 ± 0.10 a	2.50 ± 0.07 ab
Butyrate (μmol/g)	1.44 ± 0.07 b	1.26 ± 0.03 c	10.37 ± 0.02 bc	1.60 ± 0.07 a	1.65 ± 0.12 a	1.31 ± 0.07 c
Isovalerate (μmol/g)	1.24 ± 0.08 a	1.08 ± 0.02 b	1.14 ± 0.02 b	1.21 ± 0.06 ab	1.23 ± 0.07 a	1.17 ± 0.04 ab
Valerate (μmol/g)	1.21 ± 0.06 ab	1.02 ± 0.02 c	1.13 ± 0.03 b	1.15 ± 0.05 b	1.23 ± 0.09 a	1.10 ± 0.02 bc
Total SCFAs (μmol/g)	27.14 ± 1.95 a	22.94 ± 0.52 c	23.76 ± 1.65 b	24.78 ± 1.79 b	28.86 ± 1.45 a	27.51 ± 1.13 a

Values are presented as the mean ± SD. Different letters denote significant differences at $p < 0.05$.

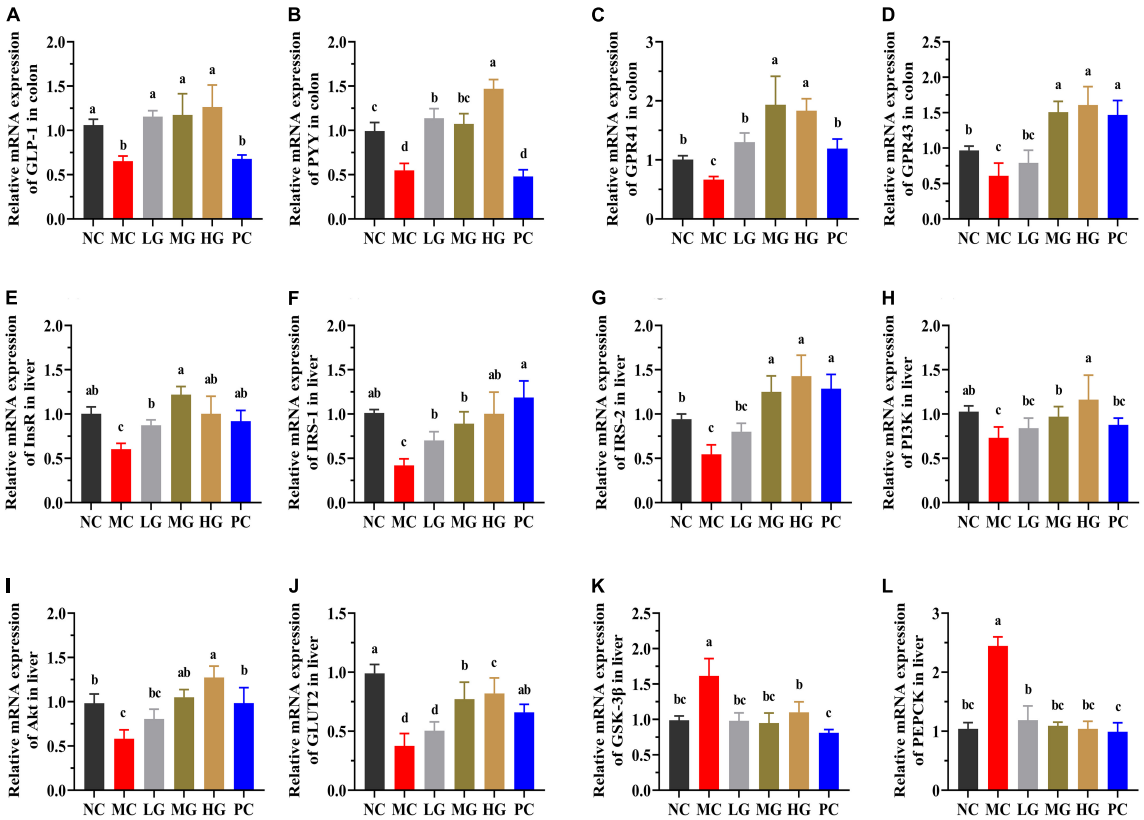

FIGURE 9 | The mRNA expressions were determined using the real-time PCR and normalized with the β-actin expression. **(A)** GLP-1; **(B)** PYY; **(C)** GPR41; **(D)** GPR43; **(E)** InsR; **(F)** IRS-1; **(G)** IRS-2; **(H)** PI3K; **(I)** Akt; **(J)** GLUT2; **(K)** GSK-3β; and **(L)** PEPCK. Different letters denote significant differences at $p < 0.05$.

higher relative expression of phosphorylated glycogen synthase kinase-3β (GSK-3β) (**Figure 9K**) and phosphoenolpyruvate carboxykinase (PEPCK) (**Figure 9L**) than those in the NC, LG, MG, and HG groups, respectively ($p < 0.05$). These results indicated that LBP effectively regulated the expression levels of genes involved in blood glucose modulation in diabetic mice.

DISCUSSION

In this study, we assessed the LBP's hypoglycemic and hypolipidemic activity, as well as its effects on the gut microbiota of diabetic mice. The yield of LBP in this study is 2.76 ± 0.33%, which is slightly lower than that in previously reported study (3.08%) (25). Carbohydrates (62.27 ± 2.37%), uronic acid (25.03 ± 1.27%), and protein (2.92 ± 0.17%) predominate in LBP, which is consistent with previous research with 60.96 ± 5.58, 20.98 ± 2.49, and 5.30 ± 0.12%, respectively (20). According to a previous report (19), the spectroscopy results disclosed that LBP was a complex glycoconjugate composed of acidic heteropolysaccharides and polypeptides. LBP is primarily composed of Rha, Ara, Xyl, Man, Glc, Gal, GlcA, and GalA residues with a molar ratio of 0.23: 1.90: 0.26: 0.20: 1.0: 1.26: 0.44: 1.49. And Ara, Gal, and GlcA are dominant in it, these results are consistent with the reported research on LBP (20). Polysaccharide physicochemical properties are closely linked to their MW, and only polysaccharide fractions in the appropriate MW mass range of the same source have the best biological activities (44). According to a published review, LBP had a MW range of 10–2300 kDa (24). Furthermore, a previous study reported the identification of numerous pharmacologically active polysaccharides with MWs ranging from 3.5 to 160 kDa (45). In this study, the MW of LBP is 98.0 kDa, which is closed to the specified range, indicating that LBP may have an excellent biological function. The hypoglycemic results of LBP in this study have confirmed the conclusion.

In the animal experiments, we conducted OGTT and ITT (**Supplementary Figure S1**) in HFD-induced mice to ensure that the diabetic mice employed in this study exhibited significant insulin resistance and typical T2DM characteristics before LBP intervention. In diabetic mice, LBP treatment significantly reversed the typical symptoms, including the decrease of FBG, decrease in food consumption and water intake, as well as prevention of BW loss. When compared with the NC group, these profiles in the MC group were significantly higher. A previous study found that weight loss in diabetics was caused by impaired energy metabolism, blood glucose imbalances, and underutilization of carbohydrates (46). In diabetic mice, LBP effectively regulated the levels of BW, FBG, as well as food and water intake. These findings demonstrated that LBP elevated

energy metabolism by increasing the uptake and utilization of blood glucose in diabetic mice. LBP not only markedly restored the impaired glucose tolerance but also improved the insulin tolerance in diabetic mice. The levels of HbA1c and GSP reflected the average blood glucose level over 2–3 weeks (47). In comparison with the MC group, LBP reduced HbA1c and GSP levels in the LG, MG, and HG groups, implying that LBP continuously maintained blood glucose homeostasis under control. Historically, hyperglycemia has been linked to hyperinsulinemia, the possible reason is that the host requires more insulin to maintain glucose homeostasis (7). As a result, the maintenance of insulin concentrations is critical for maintaining blood glucose homeostasis (48). LBP significantly improved the levels of insulin secretion and sensitivity, as well as alleviated insulin resistance in diabetic mice. The liver and skeletal muscle are the central target organs of insulin and play a vital role in the maintenance of glucose homeostasis (49). LBP promoted glycogen accumulation in diabetic mice, both in the liver and skeletal muscle, and the probable reason is that insulin facilitates glycogen synthesis or inhibits hepatic gluconeogenesis (7). Consequently, the pancreas, liver, and skeletal muscles are indispensable tissues or organs for mitigating diabetes (50). In this study, H&E staining revealed that LBP restored the pathological changes in the pancreas, liver, and skeletal muscle caused by diabetes.

Type 2 diabetes mellitus is frequently associated with complications, which pose a greater threat to diabetics than diabetes itself (51). As a result, reducing diabetes-related complications is critical to improving diabetes (4). According to a reported study, high levels of TC, TG, and LDL-C may cause intestinal endothelial dysfunction and worsen the onset and progression of atherosclerosis (52). TBA, ALT, and AST levels are regarded as critical indicators of hepatocellular injury and liver dysfunction (53). LBP increased the levels of TBA and HDL-C while decreasing TC, TG, LDL-C, ALT, and AST levels. The reported literature has proved that oxidative stress can cause cardiovascular disease, diabetic nephropathy, and insulin dysfunction in the host, increasing the risk of developing diabetes (54). LBP increased the activities of CAT, SOD, and GSH-Px, while decreasing MDA levels, indicating that LBP acted as a hepatoprotective agent and mitigated oxidative damage in diabetic mice. Furthermore, LBP reduced inflammatory factors, such as IL-1β, IL-6, and TNF-α (serum and liver), which is consistent with previous studies of *G. lucidum* polysaccharide in alleviating diabetic mouse inflammation (16, 17). LPS is primarily derived from the metabolism of certain intestinal microorganisms and can cause inflammation and insulin resistance in target tissues and organs (55). In addition to this, the host's chronic hyperglycemia and hyperlipidemia may result in the production of excessive ROS (56).

The gut microbiota is important in the treatment of T2DM (57). The biodiversity of gut microbiota in the MC group of mice was significantly lower than that in the NC group. A previous study reported that the increased ratio of the phyla Firmicutes–Bacteroidetes was associated with obesity and the balance of intestinal flora (58). The F/B ratio is critical in reflecting the impact of gut flora on health, and an elevated ratio frequently indicates an unhealthy physiological state *in vivo* (59). In this study, LBP significantly decreased F/B levels in the LG, MG, and HG groups when compared with the MC group ($p < 0.05$), indicating that the LBP's hypoglycemic effects may be mediated by regulating the composition of intestinal microbiota in diabetic mice. By comparing specific bacteria, we investigated the modulatory effect of LBP on the microbiome. In comparison with the MC group, the relative abundance of *Bacteroides*, *Ruminococcaceae_UCG-014*, *Ruminococcaceae_UCG-009*, *Mucispirillum*, and *Intestinimonas* was significantly higher in the NC group, while *Allobaculum*, *Dubosiella*, and *Romboutsia* were significantly lower ($p < 0.05$). LBP reversed the decrease of *Bacteroides*, *Ruminococcaceae_UCG-014*, *Mucispirillum*, *Intestinimonas*, *Ruminococcaceae_UCG-009*, and the increase of *Allobaculum*, *Dubosiella*, *Romboutsia* in the LG, MG, and HG groups as compared with the MC group ($p < 0.05$). *Bacteroidetes* is a vital Bacteroidetes phylum member that increased in LBP-treated mice compared with the MC group. A previous study found that *Bacteroides* improved metabolic function and immune dysfunction in HFD-induced mice (60). The increased relative abundance of *Bacteroides* is consistent with a previously reported study (61). *Ruminococaceae* degraded and fermented LBP, which was then used for its growth and predominance. Additionally, certain *Ruminococaceae* genera can produce both butyrate and acetate, which is advantageous for *Roseburia* to produce butyrate (62). LBP contains many glycosides and has been shown to restrain the decline of *Ruminococaceae_UCG-014* and *Ruminococcaceae_UCG-009* in diabetic mice (**Figures 7K,N**). In this study, *Ruminococaceae_UCG-014* is a SCFAs-producing bacteria that was enriched by LBP (62). *Mucispirillum*, which lives in the gut mucous layer of rodents' guts, uses SCFAs for energy metabolism but doesn't produce them (62). A recent study found that *Mucispirillum schaedleri* protected mice from colitis by antagonizing *Salmonella* (63). LBP increased *Mucispirillum* abundance in this study (**Figure 7L**). *Intestinimonas*, a butyrate-producing genus found in the mouse intestine (64), was enriched in LBP-treated groups (**Figure 7M**). *Allobaculum* is an important functional phylotype of metabolic dysbiosis, as well as a harmful genus of bacteria that is more prevalent in diabetics (65). The relative abundance of *Allobaculum* remarkably increased in the MC group but decreased in LBP-treated groups as compared with that in the NC group, indicating that LBP effectively decreased the relative abundance of *Allobaculum* in diabetic mice. A previous study reported that *Grifola frondosa* heteropolysaccharide increased the relative abundance of *Allobaculum*, implying that it may helped the host to fight against non-alcoholic fatty liver disease (NAFLD) (66). On the contrary, the proportion of *Allobaculum* in LBP-treated groups was significantly lower than that in the MC group ($p < 0.05$). *Romboutsia* is another SCFAs-producing genus that is regarded to have beneficial effects on the regulation of intestinal homeostasis (67, 68). It has also been linked to circulating inflammatory (IL-1β) and behavioral outcomes, such as lethargy, and anxiety-like behavioral (67). In this study, *Sargassum fusiforme* polysaccharide caused an increase in *Romboutsia* (68), whereas LBP decreased it in this study. These

disparate or opposite results of *Allobaculum* and *Romboutsia* suggested that the same genus could play different roles under different physiological states. A reported study showed that *Dubosiella* was positively related to acetate (69). LBP inhibited the increase of *Dubosiella* in diabetic mice in this study, which was consistent with another study (70). To summarize, LBP improved the abundance of beneficial bacteria, while decreasing the abundance of harmful bacteria, protecting the host from damages caused by harmful microorganisms and their metabolites. Changes in the composition of intestinal flora have been linked to the emergence and progression of diabetes (71). Recent studies disclosed that many metabolic diseases were caused by the changes in gut microbiota, and reshaping intestinal flora was critically important to the host's health (72). As a result, we investigated the relationship between intestinal flora and biochemical profiles. The relative abundance of *Cetobacterium*, *Millionella*, *Clostridium_sensu_stricto_1*, *Streptococcus*, *Ruminococcaceae_UCG-009* was negatively correlated with HDL-C, HOMA-IR, ALT, AST, TC, and LPS in the liver. A positive and significant correlation was found between insulin (serum and liver) and *Cetobacterium*, *Streptococcus*, as well as *Ralstonia*. *Cetobacterium*, *Ruminiclostridium*, *Bifidobacterium*, and *Streptococcus* showed a positive correlation with HDL-C and insulin (serum), hepatic glycogen, GSH, and CAT in the liver. Furthermore, *Bifidobacterium* was involved in liver injury and inflammation. These results indicated that *Cetobacterium*, *Millionella*, *Clostridium_sensu_stricto_1*, *Streptococcus*, *Ruminococcaceae_UCG-009*, *Cetobacterium*, *Streptococcus*, *Ralstonia*. *Cetobacterium*, *Ruminiclostridium*, *Bifidobacterium*, and *Streptococcus* may be related to hepatic injury and insulin resistance. Our study demonstrated that LBP not only alleviated inflammation, and altered the composition of intestinal flora, but also improved the production of SCFAs. SCFAs are important metabolites that are produced by beneficial microorganisms during the fermentation of indigestible polysaccharides and fibrates (73, 74). SCFAs influence glucose homeostasis by modulating glucose absorption and utilization in metabolically active tissues or organs (75). Acetate, propionate, and butyrate are metabolic substrates for the synthesis of cholesterol, and gluconeogenesis is important for controlling blood glucose, cholesterol, and lipid metabolism (76). Furthermore, propionate inhibits cholesterol and fatty acid synthesis in the liver (14). Butyrate is the most abundant energy substance in colonocytes and has a variety several beneficial effects, including the activities of immunomodulation, anti-inflammatory, and antimicrobial properties (77). The rise of acetate, propionate, and butyrate corresponded to the effects of LBP on the alleviation of hypertriglyceridemia, hyperglycemia, and hypercholesterolemia in T2DM mice. Isobutyric acid and isovaleric acid are byproducts of protein fermentation, most notably microbial protein fermentation (78). The possible cause for the increase of the isobutyric acid and isovaleric acid could be related to the content of protein in LBP (79). In this study, SCFAs changes in diabetic mice were linked to LBP modulation in *Bacteroides*, *Ruminococcaceae_UCG-014*, *Intestinimonas*, *Ruminococcaceae_UCG-009*, and *Romboutsia*. In addition to this, the genera *Allobaculum*, *Mucispirillum*, and *Dubosiella* could not be classified as either pro-inflammatory or anti-inflammatory bacteria (80). These results suggested that reshaping the composition and structure of the gut microbiota was an important strategy for diabetes risk reduction.

Several studies have shown that SCFAs helped to improve energy metabolism. SCFAs can directly activate G-protein-coupled receptors (GPCRs), mainly including GPR109A, GPR43, and GPR41 (8). Both GPR41 and GPR43 could be activated by SCFAs, particularly acetate and propionate (8). After stimulation by SCFAs, GPR41, and GPR43 could enhance the secretion of GLP-1 and PYY from intestinal L cells (8). The increased GLP-1 and PYY expression may improve insulin sensitivity and inhibits gluconeogenesis by promoting insulin secretion (37, 81). In this study, LBP significantly increased the expression of GPR41, GPR43, GLP-1, and PYY, while decreasing HOMA-IR. Insulin resistance of the liver has been linked to the onset and progression of T2DM, and it is widely acknowledged that the regulation of some critical metabolic pathways may be an excellent treatment option (68). The IRS/PI3K/Akt signaling pathway is widely acknowledged to play a critical role in the transmission of insulin signals and modulation of glucose metabolism (7, 68). IRS-1 and IRS-2 are downstream signal factors of InsR, and those are the critical kinase of glucose uptake and the target of insulin resistance (13). The increased insulin could stimulate the phosphorylation of InsR, promoting IRS-2 binding to PI3K while inhibiting IRS-1 signal transmission (13). The dysfunction of PI3K may affect the process of activated Akt, causing disruptions in glucose metabolism (68). In addition to this, insulin stimulation activates phosphorylated Akt, which not only improves glucose uptake by promoting GLUT2 to the hepatocyte membrane but also regulates the inhibition of GSK-3β in regulating the process of glycogen synthesis (13, 68). In this study, LBP significantly increased the expression of InsR, IRS-1, IRS-2, PI3K, and Akt in the liver of diabetic mice. LBP increased blood glucose absorption and utilization in diabetic mice, indicating that diabetes may be alleviated by enhancing IRS/PI3K/Akt signaling pathways. Apart from this, PEPCK is a gluconeogenic enzyme and is elevated in diabetics (82). In addition, hyperglycemia is caused by excessive hepatic glycogen and glucose production. LBP decreased the relative expression of PEPCK in this study. Particularly, the expression of IRS-1, IRS-2, PI3K, GLUT2, and Akt was significantly higher in the HG group than those in the LG and MG groups, demonstrating that the HG group's superior ability to modulate the glucose production of high-dosage LBP. As a result, LBP reduced insulin resistance in T2DM mice by promoting the absorption and utilization of excess blood glucose and suppressing gluconeogenesis.

CONCLUSION

In this study, LBP significantly reduced food and water intake, alleviated hyperglycemia and insulin resistance, decreased lipid accumulation, and inhibited weight loss in diabetic mice by increasing blood glucose uptake and utilization. LBP increased the activities of SOD, CAT, and GSH-Px, indicating that LBP could protect the liver and pancreas from oxidative damage

in diabetic mice. The 16S rDNA analysis illustrated that LBP significantly changed the intestinal composition, decreasing *Allobaculum*, *Dubosiella*, and *Romboutsia*, increasing *Bacteroides*, *Ruminococcaceae_UCG-014*, *Mucispirillum*, *Intestinimonas*, and *Ruminococcaceae_UCG-009*. The SCFAs level in LBP-treated mice was significantly increased, which was accompanied by the increase in SCFAs-producing genera. The RT-PCR analysis revealed that LBP up-regulated the expressions of GLP-1, PYY, GPR41, GPR43, activated InsR/PI3K/AKT signal pathway, and down-regulated the expressions of GSK-3β and PEPCK of diabetic mice. In conclusion, these findings suggested that LBP may alleviate hyperglycemia and hyperlipidemia by modulating intestinal flora and could be used as a beneficial ingredient adjuvant in T2DM.

DATA AVAILABILITY STATEMENT

The raw sequencing data uploaded at https://www.ncbi.nlm.nih.gov/Traces/study/?acc=PRJNA826571.

ETHICS STATEMENT

The animal study was reviewed and approved by the Animal Care Committee of Xi'an Jiaotong University.

AUTHOR CONTRIBUTIONS

QM contributed to conceptualization, wrote the original draft, and investigation. RZ, TC, and ZZ investigated the study. XX contributed to data curation. HL contributed to software. CN, XY, AT, BT, and ZC contributed to software and validation. MZ validated the study. JL contributed to methodology and revising and supervising the study. All authors contributed to the article and approved the submitted version.

FUNDING

This work was sponsored by the Shaanxi Provincial Science and Technology Innovation Team, China (grant/program no. 2022TD-15); Natural Sciences Foundation of Shaanxi Province Youth Project, China (grant/program no. 2021JQ-141); and Northwest A&F University, China.

SUPPLEMENTARY MATERIAL

The Supplementary Material for this article can be found online at: https://www.frontiersin.org/articles/10.3389/fnut.2022.916271/full#supplementary-material

REFERENCES

1. DeFronzo RA, Ferrannini E, Groop L, Henry RR, Herman WH, Holst JJ, et al. Type 2 diabetes mellitus. *Nat Rev Dis Primers.* (2015) 1:1–22. doi: 10.1038/nrdp.2015.19
2. Sun H, Saeedi P, Karuranga S, Pinkepank M, Ogurtsova K, Duncan BB, et al. IDF diabetes atlas: global, regional and country-level diabetes prevalence estimates for 2021 and projections for 2045. *Diabetes Res Clin Pract.* (2022) 183:109119–31. doi: 10.1016/j.diabres.2021.109119
3. Panwar H, Rashmi HM, Batish VK, Grover S. Probiotics as potential biotherapeutics in the management of type 2 diabetes – prospects and perspectives. *Diabetes Metab Res Rev.* (2013) 29:103–12. doi: 10.1002/dmrr.2376
4. Zhang L, Zhou W, Zhan L, Hou S, Zhao C, Bi T, et al. Fecal microbiota transplantation alters the susceptibility of obese rats to type 2 diabetes mellitus. *Aging.* (2020) 12:17480–502. doi: 10.18632/aging.103756
5. Fiorentino TV, Prioletta A, Zuo P, Folli F. Hyperglycemia-induced oxidative stress and its role in diabetes mellitus related cardiovascular diseases. *Curr Pharm Des.* (2013) 19:5695–703. doi: 10.2174/13816128113193 20005
6. You Y, Ren T, Zhang S, Shirima GG, Cheng Y, Liu X. Hypoglycemic effects of zanthoxylum alkylamides by enhancing glucose metabolism and ameliorating pancreatic dysfunction in streptozotocin-induced diabetic rats. *Food Funct.* (2015) 6:3144–54. doi: 10.1039/c5fo00432b
7. Jia R-B, Li Z-R, Wu J, Ou Z-R, Sun B, Lin L, et al. Antidiabetic effects and underlying mechanism of an anti-digestive dietary polysaccharide from *Sargassum fusiforme* in rats. *Food Funct.* (2020) 11:7023–36. doi: 10.1039/D0FO01166E
8. Tan J, McKenzie C, Potamitis M, Thorburn AN, Mackay CR, Macia L. The role of short-chain fatty acids in health and disease. *Adv Immunol.* (2014) 121:91–119. doi: 10.1016/B978-0-12-800100-4.00003-9
9. Chen M, Xiao D, Liu W, Song Y, Zou B, Li L, et al. Intake of *Ganoderma lucidum* polysaccharides reverses the disturbed gut microbiota and metabolism in type 2 diabetic rats. *Int J Biol Macromol.* (2020) 155:890–902. doi: 10.1016/j.ijbiomac.2019.11.047
10. Cani PD, Osto M, Geurts L, Everard A. Involvement of gut microbiota in the development of low-grade inflammation and type 2 diabetes associated with obesity. *Gut Microbes.* (2012) 3:279–88. doi: 10.4161/gmic.19625
11. Wu Q, Chen T, El-Nezami H, Savidge TC. Food ingredients in human health: ecological and metabolic perspectives implicating gut microbiota function. *Trends Food Sci Technol.* (2020) 100:103–17. doi: 10.1016/j.tifs.2020.04.007
12. Pan Y, Wang C, Chen Z, Li W, Yuan G, Chen H. Physicochemical properties and antidiabetic effects of a polysaccharide from corn silk in high-fat diet and streptozotocin-induced diabetic mice. *Carbohydr Polym.* (2017) 164:370–8. doi: 10.1016/j.carbpol.2017.01.092
13. Zhu Q, Lin L, Zhao M. Sulfated fucan/fucosylated chondroitin sulfate-dominated polysaccharide fraction from low-edible-value sea cucumber ameliorates type 2 diabetes in rats: new prospects for sea cucumber polysaccharide based-hypoglycemic functional food. *Int J Biol Macromol.* (2020) 159:34–45. doi: 10.1016/j.ijbiomac.2020.05.043
14. Zhao F, Liu Q, Cao J, Xu Y, Pei Z, Fan H, et al. A sea cucumber (*Holothuria leucospilota*) polysaccharide improves the gut microbiome to alleviate the symptoms of type 2 diabetes mellitus in Goto-Kakizaki rats. *Food Chem Toxicol.* (2020) 135:1–9. doi: 10.1016/j.fct.2019.110886
15. Wu G, Bai Z, Wan Y, Shi H, Huang X, Nie S. Antidiabetic effects of polysaccharide from azuki bean (*Vigna angularis*) in type 2 diabetic rats via insulin/PI3K/AKT signaling pathway. *Food Hydrocolloids.* (2020) 101:105456. doi: 10.1016/j.foodhyd.2019.105456
16. Chang CJ, Lin CS, Lu CC, Martel J, Ko YF, Ojcius DM, et al. Corrigendum: *Ganoderma lucidum* reduces obesity in mice by modulating the composition of the gut microbiota. *Nat Commun.* (2017) 8:16130. doi: 10.1038/ncomms16130
17. Xu S, Dou Y, Ye B, Wu Q, Wang Y, Hu M, et al. *Ganoderma lucidum* polysaccharides improve insulin sensitivity by regulating inflammatory cytokines and gut microbiota composition in mice. *J Funct Foods.* (2017) 38:545–52. doi: 10.1016/j.jff.2017.09.032
18. Zhu J, Liu W, Yu J, Zou S, Wang J, Yao W, et al. Characterization and hypoglycemic effect of a polysaccharide extracted from the fruit of *Lycium barbarum* L. *Carbohydr Polym.* (2013) 98:8–16. doi: 10.1016/j.carbpol.2013.04.057

19. Zhang XR, Zhou WX, Zhang YX, Qi CH, Yan H, Wang ZF, et al. Macrophages, rather than T and B cells are principal immunostimulatory target cells of *Lycium barbarum* L. polysaccharide LBPF4-OL. *J Ethnopharmacol.* (2011) 136:465–72. doi: 10.1016/j.jep.2011.04.054
20. Ding Y, Yan Y, Peng Y, Chen D, Mi J, Lu L, et al. In vitro digestion under simulated saliva, gastric and small intestinal conditions and fermentation by human gut microbiota of polysaccharides from the fruits of *Lycium barbarum*. *Int J Biol Macromol.* (2019) 125:751–60. doi: 10.1016/j.ijbiomac.2018.12.081
21. Masci A, Carradori S, Casadei MA, Paolicelli P, Petralito S, Ragno R, et al. *Lycium barbarum* polysaccharides: extraction, purification, structural characterisation and evidence about hypoglycaemic and hypolipidaemic effects. A review. *Food Chem.* (2018) 254:377–89. doi: 10.1016/j.foodchem.2018.01.176
22. Zhou SF, Jiang C, Zhou ZW, Sheng HP, He LJ, Fan XW, et al. An evidence-based update on the pharmacological activities and possible molecular targets of *Lycium barbarum* polysaccharides. *Drug Design Dev Ther.* (2014) 2015:33–78. doi: 10.2147/DDDT.S72892
23. Jin M, Lu Z, Huang M, Wang Y, Wang Y. Sulfated modification and antioxidant activity of exopolysaccahrides produced by *Enterobacter cloacae* Z0206. *Int J Biol Macromol.* (2011) 48:607–12. doi: 10.1016/j.ijbiomac.2011.01.023
24. Jin M, Huang Q, Zhao K, Shang P. Biological activities and potential health benefit effects of polysaccharides isolated from *Lycium barbarum* L. *Int J Biol Macromol.* (2013) 54:16–23. doi: 10.1016/j.ijbiomac.2012.11.023
25. Liu W, Xu J, Zhu R, Zhu Y, Zhao Y, Chen P, et al. Fingerprinting profile of polysaccharides from *Lycium barbarum* using multiplex approaches and chemometrics. *Int J Biol Macromol.* (2015) 78:230–7. doi: 10.1016/j.ijbiomac.2015.03.062
26. Hou C, Yin M, Lan P, Wang H, Nie H, Ji X. Recent progress in the research of *Angelica sinensis* (Oliv.) diels polysaccharides: extraction, purification, structure and bioactivities. *Chem Biol Technol Agric.* (2021) 8:13–26. doi: 10.1186/s40538-021-00214-x
27. Liu Y, Gong G, Zhang J, Jia S, Li F, Wang Y, et al. Response surface optimization of ultrasound-assisted enzymatic extraction polysaccharides from *Lycium barbarum*. *Carbohydr Polym.* (2014) 110:278–84. doi: 10.1016/j.carbpol.2014.03.040
28. Zha X-Q, Luo J-P, Luo S-Z, Jiang S-T. Structure identification of a new immunostimulating polysaccharide from the stems of *Dendrobium huoshanense*. *Carbohydr Polym.* (2007) 69:86–93. doi: 10.1016/j.carbpol.2006.09.005
29. Dubois M, Gilles HA, Hamilton JK, Rebers PA, Smith F. Colorimetric method for determination of sugars and related substances. *Anal Chem.* (1956) 28:22–5. doi: 10.1021/ac60111a017
30. Bradford MM. A rapid and sensitive method for the quantitation of microgram quantities of protein utilizing the principle of protein-dye binding. *Anal Biochem.* (1976) 72:248–54. doi: 10.1016/0003-2697(76)90527-3
31. Filisetti-Cozzi TMCC, Carpita NC. Measurement of uronic acids without interference from neutral sugars. *Anal Biochem.* (1991) 197:157–62. doi: 10.1016/0003-2697(91)90372-Z
32. Ma Q, Yuan L, Zhuang Y. Preparation, characterization and in vivo antidiabetic effects of polysaccharides from *Pachyrrhizus erosus*. *Int J Biol Macromol.* (2018) 114:97–105. doi: 10.1016/j.ijbiomac.2018.03.099
33. Ji X, Yan Y, Hou C, Shi M, Liu Y. Structural characterization of a galacturonic acid-rich polysaccharide from *Ziziphus jujuba* cv. muzao. *Int J Biol Macromol.* (2020) 147:844–52. doi: 10.1016/j.ijbiomac.2019.09.244
34. Liu Z, Zhang Z, Qiu L, Zhang F, Xu X, Wei H, et al. Characterization and bioactivities of the exopolysaccharide from a probiotic strain of *Lactobacillus plantarum* WLPL04. *J Dairy Sci.* (2017) 100:6895–905. doi: 10.3168/jds.2016-11944
35. Lin X, Ji X, Wang M, Yin S, Peng Q. An alkali-extracted polysaccharide from *Zizyphus jujuba* cv. muzao: structural characterizations and antioxidant activities. *Int J Biol Macromol.* (2019) 136:607–15. doi: 10.1016/j.ijbiomac.2019.06.117
36. Yuan Q-C, Zhan B-Y, Du M, Chang R, Li T-G, Mao X-Y. Dietary milk fat globule membrane regulates JNK and PI3K/Akt pathway and ameliorates type 2 diabetes in mice induced by a high-fat diet and streptozotocin. *J Funct Foods.* (2019) 60:1–9. doi: 10.1016/j.jff.2019.103435
37. Zheng X, Chen T, Jiang R, Zhao A, Wu Q, Kuang J, et al. Hyocholic acid species improve glucose homeostasis through a distinct TGR5 and FXR signaling mechanism. *Cell Metab.* (2020) 33:1–13. doi: 10.1016/j.cmet.2020.11.017
38. Lundsgaard A-M, Holm JB, Sjøberg KA, Bojsen-Møller KN, Myrmel LS, Fjære E, et al. Mechanisms preserving insulin action during high dietary fat intake. *Cell Metab.* (2019) 29:50–63.e4. doi: 10.1016/j.cmet.2018.08.022
39. Qu W, Yuan X, Zhao J, Zhang Y, Hu J, Wang J, et al. Dietary advanced glycation end products modify gut microbial composition and partially increase colon permeability in rats. *Mol Nutr Food Res.* (2017) 61:1–14. doi: 10.1002/mnfr.201700118
40. Tian B, Liu M, An W, Yu L, Zhang J, Liu Y, et al. *Lycium barbarum* relieves gut microbiota dysbiosis and improves colonic barrier function in mice following antibiotic perturbation. *J Funct Foods.* (2020) 71:1–13. doi: 10.1016/j.jff.2020.103973
41. Li F, Pak S, Zhao J, Wei Y, Zhang Y, Li Q. Structural characterization of a neutral polysaccharide from *Cucurbia moschata* and its uptake behaviors in caco-2 cells. *Foods.* (2021) 10:2357. doi: 10.3390/foods10102357
42. Ji X, Guo J, Ding D, Gao J, Hao L, Guo X, et al. Structural characterization and antioxidant activity of a novel high-molecular-weight polysaccharide from *Ziziphus jujuba* cv. muzao. *J Food Meas Char.* (2022). 16:2191–2200. doi: 10.1007/s11694-022-01288-3
43. Fellah A, Anjukandi P, Waterland MR, Williams MAK. Determining the degree of methylesterification of pectin by ATR/FT-IR: methodology optimisation and comparison with theoretical calculations. *Carbohydr Polym.* (2009) 78:847–53. doi: 10.1016/j.carbpol.2009.07.003
44. Thambiraj SR, Phillips M, Koyyalamudi SR, Reddy N. Yellow lupin (*Lupinus luteus* L.) polysaccharides: antioxidant, immunomodulatory and prebiotic activities and their structural characterisation. *Food Chem.* (2018) 267:319–28. doi: 10.1016/j.foodchem.2018.02.111
45. Cho Y-J, Son H-J, Kim K-S. A 14-week randomized, placebo-controlled, double-blind clinical trial to evaluate the efficacy and safety of ginseng polysaccharide (Y-75). *J Transl Med.* (2014) 12:283–9. doi: 10.1186/s12967-014-0283-1
46. Oršolić N, Sirovina D, Odeh D, Gajski G, Balta V, Šver L, et al. Efficacy of caffeic acid on diabetes and its complications in the mouse. *Molecules.* (2021) 26:3262–87. doi: 10.3390/molecules26113262
47. Lo H-Y, Li C-C, Chen F-Y, Chen J-C, Hsiang C-Y, Ho T-Y. Gastro-resistant insulin receptor-binding peptide from *Momordica charantia* improved the glucose tolerance in streptozotocin-induced diabetic mice via insulin receptor signaling pathway. *J Agric Food Chem.* (2017) 65:9266–74. doi: 10.1021/acs.jafc.7b03583
48. Song JX, Ren H, Gao YF, Lee CY, Li SF, Zhang F, et al. Dietary capsaicin improves glucose homeostasis and alters the gut microbiota in obese diabetic ob/ob mice. *Front Physiol.* (2017) 8:602–14. doi: 10.3389/fphys.2017.00602
49. Yang CF, Lai SS, Chen YH, Liu D, Liu B, Ai C, et al. Anti-diabetic effect of oligosaccharides from seaweed *Sargassum confusum* via JNK-IRS1/PI3K signalling pathways and regulation of gut microbiota. *Food Chem Toxicol.* (2019) 131:110562–72. doi: 10.1016/j.fct.2019.110562
50. Thomas RM, Jobin C. Microbiota in pancreatic health and disease: the next frontier in microbiome research. *Nat Rev Gastroenterol Hepatol.* (2020) 17:53–64. doi: 10.1038/s41575-019-0242-7
51. Deng X, Sun L, Lai X, Xiang L, Li Q, Zhang W, et al. Tea polypeptide ameliorates diabetic nephropathy through RAGE and NF-κB signaling pathway in type 2 diabetes mice. *J Agric Food Chem.* (2018) 66:11957–67. doi: 10.1021/acs.jafc.8b04819
52. Rosenblit PD. Common medications used by patients with type 2 diabetes mellitus: what are their effects on the lipid profile? *Cardiovasc Diabetol.* (2016) 15:95–108. doi: 10.1186/s12933-016-0412-7
53. Hu X-Q, Thakur K, Chen G-H, Hu F, Zhang J-G, Zhang H-B, et al. Metabolic effect of 1-deoxynojirimycin from mulberry leaves on db/db diabetic mice using liquid chromatography-mass spectrometry based metabolomics. *J Agric Food Chem.* (2017) 65:4658–67. doi: 10.1021/acs.jafc.7b01766
54. Wu T, Shen M, Liu S, Yu Q, Chen Y, Xie J. Ameliorative effect of *Cyclocarya paliurus* polysaccharides against carbon tetrachloride induced oxidative stress in liver and kidney of mice. *Food Chem Toxicol.* (2020) 135:111014–24. doi: 10.1016/j.fct.2019.111014
55. Winer DA, Luck H, Tsai S, Winer S. The intestinal immune system in obesity and insulin resistance. *Cell Metab.* (2016) 23:413–26. doi: 10.1016/j.cmet.2016.01.003

56. Liao X, Yang L, Chen M, Yu J, Zhang S, Ju Y. The hypoglycemic effect of a polysaccharide (GLP) from *Gracilaria lemaneiformis* and its degradation products in diabetic mice. *Food Funct.* (2015) 6:2542–9. doi: 10.1039/c4fo01185f
57. Wu J, Wang K, Wang X, Pang Y, Jiang C. The role of the gut microbiome and its metabolites in metabolic diseases. *Protein Cell.* (2021) 12:360–73. doi: 10.1007/s13238-020-00814-7
58. Turnbaugh PJ, Ley RE, Mahowald MA, Magrini V, Mardis ER, Gordon JI. An obesity-associated gut microbiome with increased capacity for energy harvest. *Nature.* (2006) 444:1027–31. doi: 10.1038/nature05414
59. Zhang X, Zhang N, Kan J, Sun R, Tang S, Wang Z, et al. Anti-inflammatory activity of alkali-soluble polysaccharides from *Arctium lappa* L. and its effect on gut microbiota of mice with inflammation. *Int J Biol Macromol.* (2020) 154:773–87. doi: 10.1016/j.ijbiomac.2020.03.111
60. Cano PG, Santacruz A, Sanz MÁY, Bereswill S. *Bacteroides uniformis* CECT 7771 ameliorates metabolic and immunological dysfunction in mice with high-fat-diet induced obesity. *PLoS One.* (2012) 7:e41079–95. doi: 10.1371/journal.pone.0041079
61. Xu H, Huang W, Hou Q, Kwok LY, Laga W, Wang Y, et al. Oral administration of compound probiotics improved canine feed intake, weight gain, immunity and intestinal microbiota. *Front Immunol.* (2019) 10:666–80. doi: 10.3389/fimmu.2019.00666
62. Tian B, Zhao J, Zhang M, Chen Z, Ma Q, Liu H, et al. *Lycium ruthenicum* anthocyanins attenuate high-fat diet-induced colonic barrier dysfunction and inflammation in mice by modulating the gut microbiota. *Mol Nutr Food Res.* (2021) 65:1–16. doi: 10.1002/mnfr.202000745
63. Herp S, Brugiroux S, Garzetti D, Ring D, Jochum LM, Beutler M, et al. *Mucispirillum schaedleri* antagonizes *Salmonella virulence* to protect mice against colitis. *Cell Host Microbe.* (2019) 25:681–94.e8. doi: 10.1016/j.chom.2019.03.004
64. Kläring K, Hanske L, Bui N, Charrier C, Blaut M, Haller D, et al. *Intestinimonas butyriciproducens* gen. nov., sp. nov., a butyrate-producing bacterium from the mouse intestine. *Int J Syst Evol Microbiol.* (2013) 63:4606–12. doi: 10.1099/ijs.0.051441-0
65. Nobel YR, Cox LM, Kirigin FF, Bokulich NA, Yamanishi S, Teitler I, et al. Metabolic and metagenomic outcomes from early-life pulsed antibiotic treatment. *Nat Commun.* (2015) 6:7486–501. doi: 10.1038/ncomms8486
66. Li X, Zeng F, Huang Y, Liu B. The positive effects of *Grifola frondosa* heteropolysaccharide on NAFLD and regulation of the gut microbiota. *Int J Mol Sci.* (2019) 20:5302–18. doi: 10.3390/ijms20215302
67. Qin R, Wang J, Chao C, Yu J, Copeland L, Wang S, et al. RS5 produced more butyric acid through regulating the microbial community of human gut microbiota. *J Agric Food Chem.* (2021) 69:3209–18. doi: 10.1021/acs.jafc.0c08187
68. Li Z-R, Jia R-B, Wu J, Lin L, Ou Z-R, Liao B, et al. *Sargassum fusiforme* polysaccharide partly replaces acarbose against type 2 diabetes in rats. *Int J Biol Macromol.* (2021) 170:447–58. doi: 10.1016/j.ijbiomac.2020.12.126
69. Guo C, Wang Y, Zhang S, Zhang X, Du Z, Li M, et al. *Crataegus pinnatifida* polysaccharide alleviates colitis via modulation of gut microbiota and SCFAs metabolism. *Int J Biol Macromol.* (2021) 181:357–68. doi: 10.1016/j.ijbiomac.2021.03.137
70. Bao M, Hou K, Xin C, Zeng D, Cheng C, Zhao H, et al. *Portulaca oleracea* L. extract alleviated type 2 diabetes via modulating the gut microbiota and serum branched-chain amino acid metabolism. *Mol Nutr Food Res.* (2022). 2101030. doi: 10.1002/mnfr.202101030
71. Liu G, Liang L, Yu G, Li Q. Pumpkin polysaccharide modifies the gut microbiota during alleviation of type 2 diabetes in rats. *Int J Biol Macromol.* (2018) 115:711–7. doi: 10.1016/j.ijbiomac.2018.04.127
72. Tanca A, Abbondio M, Palomba A, Fraumene C, Manghina V, Cucca F, et al. Potential and active functions in the gut microbiota of a healthy human cohort. *Microbiome.* (2017) 5:79–94. doi: 10.1186/s40168-017-0293-3
73. Bartolomaeus H, Balogh A, Yakoub M, Homann S, Markó L, Höges S, et al. Short-chain fatty acid propionate protects from hypertensive cardiovascular damage. *Circulation.* (2019) 139:1407–21. doi: 10.1161/CIRCULATIONAHA.118.036652
74. Ji X, Hou C, Gao Y, Xue Y, Yan Y, Guo X. Metagenomic analysis of gut microbiota modulatory effects of jujube (*Ziziphus jujuba* Mill.) polysaccharides in a colorectal cancer mouse model. *Food Funct.* (2020) 11:163–73. doi: 10.1039/c9fo02171j
75. Chen Y, Guo J, Qian G, Fang D, Shi D, Guo L, et al. Gut dysbiosis in acute-on-chronic liver failure and its predictive value for mortality. *J Gastroenterol Hepatol.* (2015) 30:1429–37. doi: 10.1111/jgh.12932
76. LeBlanc JG, Chain F, Martín R, Bermúdez-Humarán LG, Courau S, Langella P. Beneficial effects on host energy metabolism of short-chain fatty acids and vitamins produced by commensal and probiotic bacteria. *Microb Cell Fact.* (2017) 16:79–89. doi: 10.1186/s12934-017-0691-z
77. Chen R, Liu B, Wang X, Chen K, Zhang K, Zhang L, et al. Effects of polysaccharide from *Pueraria lobata* on gut microbiota in mice. *Int J Biol Macromol.* (2020) 158:740–9. doi: 10.1016/j.ijbiomac.2020.04.201
78. Williams BA, Zhang D, Lisle AT, Mikkelsen D, McSweeney CS, Kang S, et al. Soluble arabinoxylan enhances large intestinal microbial health biomarkers in pigs fed a red meat–containing diet. *Nutrition.* (2016) 32:491–7. doi: 10.1016/j.nut.2015.10.008
79. Rasmussen HS, Holtug K, Mortensen PB. Degradation of amino acids to short-chain fatty acids in humans: an in vitro study. *Scand J Gastroenterol.* (1988) 23:178–82. doi: 10.3109/00365528809103964
80. Zhang Y, Liu W, Zhang D, Yang Y, Wang X, Li L. Fermented and germinated processing improved the protective effects of foxtail millet whole grain against dextran sulfate sodium-induced acute ulcerative colitis and gut microbiota dysbiosis in C57BL/6 mice. *Front Nutr.* (2021) 8:694936. doi: 10.3389/fnut.2021.694936
81. Yao Y, Yan L, Chen H, Wu N, Wang W, Wang D. *Cyclocarya paliurus* polysaccharides alleviate type 2 diabetic symptoms by modulating gut microbiota and short-chain fatty acids. *Phytomedicine.* (2020) 77:153268–82. doi: 10.1016/j.phymed.2020.153268
82. Jia R-B, Li Z-R, Wu J, Ou Z-R, Liao B, Sun B, et al. Mitigation mechanisms of *Hizikia fusifarme* polysaccharide consumption on type 2 diabetes in rats. *Int J Biol Macromol.* (2020) 164:2659–70. doi: 10.1016/j.ijbiomac.2020.08.154

Conflict of Interest: The authors declare that the research was conducted in the absence of any commercial or financial relationships that could be construed as a potential conflict of interest.

Publisher's Note: All claims expressed in this article are solely those of the authors and do not necessarily represent those of their affiliated organizations, or those of the publisher, the editors and the reviewers. Any product that may be evaluated in this article, or claim that may be made by its manufacturer, is not guaranteed or endorsed by the publisher.

Copyright © 2022 Ma, Zhai, Xie, Chen, Zhang, Liu, Nie, Yuan, Tu, Tian, Zhang, Chen and Li. This is an open-access article distributed under the terms of the Creative Commons Attribution License (CC BY). The use, distribution or reproduction in other forums is permitted, provided the original author(s) and the copyright owner(s) are credited and that the original publication in this journal is cited, in accordance with accepted academic practice. No use, distribution or reproduction is permitted which does not comply with these terms.

frontiers | Frontiers in Nutrition

ORIGINAL RESEARCH
published: 01 July 2022
doi: 10.3389/fnut.2022.925050

Determining Methyl-Esterification Patterns in Plant-Derived Homogalacturonan Pectins

Yang Yu[1], Liangnan Cui[1], Xianbin Liu[1], Yuwen Wang[1], Chenchen Song[1], UnHak Pak[1], Kevin H. Mayo[2], Lin Sun[1] and Yifa Zhou[1]**

[1] *Jilin Provincial Key Laboratory on Chemistry and Biology of Changbai Mountain Natural Drugs, Engineering Research Center of Glycoconjugates of Ministry of Education, School of Life Sciences, Northeast Normal University, Changchun, China,* [2] *Department of Biochemistry, Molecular Biology and Biophysics, The University of Minnesota, Minneapolis, MN, United States*

Homogalacturonan (HG)-type pectins are nutrient components in plants and are widely used in the food industry. The methyl-esterification pattern is a crucial structural parameter used to assess HG pectins in terms of their nutraceutical activity. To better understand the methyl-esterification pattern of natural HG pectins from different plants, we purified twenty HG pectin-rich fractions from twelve plants and classified them by their monosaccharide composition, Fourier transform-infrared spectroscopy (FT-IR) signatures, and NMR analysis. FT-IR shows that these HG pectins are all minimally esterified, with the degree of methyl-esterification (DM) being 5 to 40%. To examine their methyl-esterification pattern by enzymatic fingerprinting, we hydrolyzed the HG pectins using endo-polygalacturonase. Hydrolyzed oligomers were derivatized with 2-aminobenzamide and subjected to liquid chromatography-fluorescence-tandem mass spectrometry (HILIC-FLR-MS^n). Twenty-one types of mono-/oligo-galacturonides having DP values of 1–10 were found to contain nonesterified monomers, dimers, and trimers, as well as oligomers with 1 to 6 methyl-ester groups. In these oligo-galacturonides, MS^n analysis demonstrated that the number of methyl-ester groups in the continuous sequence was 2 to 5. Mono- and di-esterified oligomers had higher percentages in total methyl-esterified groups, suggesting that these are a random methyl-esterification pattern in these HG pectins. Our study analyzes the characteristics of the methyl-esterification pattern in naturally occurring plant-derived HG pectins and findings that will be useful for further studying HG structure-function relationships.

Keywords: HG pectin, endo-polygalacturonase, enzymatic fingerprinting, methyl-esterification, oligogalacturonides

OPEN ACCESS

Edited by:
Xin Wang,
Northwest A&F University, China

Reviewed by:
Vincenzo Lionetti,
Sapienza University of Rome, Italy
Tao Huang,
Ningbo University, China

****Correspondence:***
Lin Sun
sunl925@nenu.edu.cn
Yifa Zhou
zhouyf383@nenu.edu.cn

Specialty section:
This article was submitted to Food Chemistry, a section of the journal Frontiers in Nutrition

Received: *21 April 2022*
Accepted: *23 May 2022*
Published: *01 July 2022*

Citation:
Yu Y, Cui L, Liu X, Wang Y, Song C, Pak U, Mayo KH, Sun L and Zhou Y (2022) Determining Methyl-Esterification Patterns in Plant-Derived Homogalacturonan Pectins. Front. Nutr. 9:925050. doi: 10.3389/fnut.2022.925050

INTRODUCTION

Pectin is a family of covalently linked, galacturonic-rich acidic polysaccharides widely found in the cell walls of plants. These are usually divided into homogalacturonan (HG), rhamnogalacturonan I (RGI), and rhamnogalacturonan II (RGII) domains (1). HG is the most abundant pectin, accounting for more than 65% of the total pectin (1). HG is a linear homopolymer that is

primarily composed of α-1,4-linked D-galacturonic acid (GalA) residues with DP values of 30–100 (2), although shorter chains have also been reported (3). GalA residues in HG pectins can be methyl-esterified at their C-6 carboxyl group (4), with their degree of methyl-esterification (DM) and methyl-ester distribution being major structural characteristics of HG pectins. HG pectin is synthesized in the Golgi of plants and transported to the cell wall by vesicles (5). During synthesis, HG pectins can be modified by HG-methyltransferase (HG-MT) to form highly esterified pectin (6, 7), which can be de-esterified by pectin-methylesterases (PMEs) (8, 9). The methyl-esterification pattern in HG pectins is involved in normal physiology, as well as in plant pathology, e.g., in regulating growth (10), morphology, development (11), and defense (12, 13).

Homogalacturonan pectin, a crucial dietary nutrient in plants, has anti-inflammatory properties, as well as the ability to modulate immunity and intestinal flora. Due to this, HG pectin is regarded as a key functional factor in healthy foods that improve intestine health and metabolism (14). Many properties and nutraceutical functions of HG pectins are related to their DM values (15). Compared with high DM pectin, low DM pectin shows better antioxidant, anti-inflammatory, and immunomodulatory properties and is more conducive to regulating intestinal flora (14). Recently, it was reported that not only the DM value but also methyl-ester distribution can influence anti-inflammatory and immunoregulation properties of pectin. Low DM pectins, as well as intermediate DM pectins with blockwise distributions of nonesterified GalA residues, are beneficial for anti-inflammatory effects *via* inhibition of TLR2-1 receptors (16, 17). In addition, low DM pectins with a higher blockwise distribution of nonesterified GalA residues, as well as intermediate DM pectins, have been confirmed to increase the frequency of intestinal T-helper (Th)1 and Th2 cells in mice (18). Therefore, it is necessary to analyze methyl-esterification patterns in HG pectins to further investigate the relationship between their structural features and their nutritional functions.

Due to the high molecular weight of HG pectins, it is difficult to directly assess methyl-esterification patterns. Enzymes such as endo-polygalacturonase (Endo-PG), endo-polygalacturonase (PL), and pectin methyl esterase (PME) (19, 20) have been used to hydrolyze and modify HG pectins for structural analyses. HG-related oligomers produced by enzyme hydrolysis have been separated and analyzed using high-performance anion-exchange chromatography (HPAEC at pH 5) and capillary electrophoresis (21, 22). Nevertheless, the structural characteristics of these oligogalacturonides remain unknown. In recent years, hydrophilic interaction liquid chromatography (HILIC), coupled with electrospray ionization ion trap mass spectrometry (ESI-MS^n), has been employed in the analysis of oligosaccharides (23–25), an approach that can be used to separate oligogalacturonides and analyze their structures simultaneously. However, it has been difficult to distinguish B/C and Y/Z fragment ions of these oligosaccharides in HILIC-ESI-MS^n, thus leading to inaccurate structural results (26).

Derivatization is often used prior to MS analysis of oligosaccharides, e.g., by using reductive amination to add a fluorescent probe at the reducing end of the oligosaccharides (27, 28). In this approach, the fluorescence detector only observes oligosaccharides that have fluorescent markers, whereas impurities will not be detected (29). Oligosaccharide isomers with different chiralities are excluded, as the reducing end is labeled, making the chromatogram more easy to analyze. In this regard, a variety of fluorescent probes have been used, including 2-aminobenzamide (2-AB), 2-aminobenzoic acid (2-AA), 2-aminopyridine (2-AP), and 2-aminoacridone (AMAC) (29–32). HG methyl-ester distribution can be determined by analyzing the structural characteristics and quantifying oligogalacturonides produced.

To characterize the methyl-esterification pattern in HG pectins, we used a series of descriptive parameters, including the degree of blockness (DB) and the absolute degree of blockiness (DB_{abs}) (20, 24, 33). DB values were calculated as the amount of nonesterified monogalacturonic, digalacturonic, and trigalacturonic acid residues released by endo-PG relative to the total unesterified GalA (20). However, determining the DB value may be complicated by the DM value of a pectin, especially those with high DM values. Due to this, we used DB_{abs} values to provide information about the absolute number of blocks in the pectin without correction for DM and values that are calculated as the number of unesterified GalA residues in enzymatic oligogalacturonides relative to the total GalA (33). Both DB and DB_{abs} have been commonly used to characterize random and blockwise patterns of methyl-esterification in HG pectins (24). PL has also been used to degrade HG pectins in order to study their methyl-esterification pattern in highly esterified pectins, as well as the degree of blockiness and the absolute degree of blockiness in highly methylesterified stretches (DB_{Me} and DB_{absMe}, respectively) (20). Using the combined degradation of two glycosidases to study the methyl ester distribution in HG pectins has also been reported in recent years, and the concept of the pectin degree of hydrolysis (DH) has been proposed to describe methyl-esterification patterns (24).

Recently, we have been carrying out a program about comparing pectin structures of plants, which are used as food or herbs in China (34, 35). In this study, we reported the results of twenty HG pectins purified from twelve plants first. These twenty HG pectins were hydrolyzed using Endo-PG, and the resulting HG oligomers were derivatized with 2-AB and analyzed using HILIC-FLR-MS^n. DB and DB_{abs} parameters were calculated and used to assess the distribution of methyl-ester groups. Our study reveals the characteristics of methyl-esterification patterns from natural HG pectins from plants and findings that will provide a basis for studying their structure-function relationships and formulating the use of HG pectins in healthy foods.

MATERIALS AND METHODS

Materials and Reagents

DEAE-cellulose, Sepharose CL-6B, Sephadex G25, and aminobenzamide (2AB) were purchased from Sigma-Aldrich. Endo-polygalacturonase (Endo-PG, EC 3.2.1.15 from *Aspergillus niger*) was purchased from Megazyme. All chemicals used were analytical grade and produced in China.

Homogalacturonan pectins were extracted from the following plants: *Panax japonicus*, *Pseudostellaria heterophylla*, *Schisandra chinensis*, *Prunella vulgaris*, *Panax Notoginseng*, *Polygonum orientale*, *Anemarrhena asphodeloides*, *Kadsura longipedunculata*, *Isatis indigotica*, *Aconitum carmichaelii*, *Coptis chinensis*, and *Sophora flavescens*.

Preparation of HG Pectins

The total polysaccharide was extracted from dried plants (MP) as previously described (34) and fractioned using DEAE cellulose ion-exchange chromatography with distilled water and 0.5 M NaCl as eluents to obtain neutral (MPP-N) and acidic polysaccharides (MPP-A). Total pectin extracts were loaded onto a DEAE cellulose column and eluted using a stepwise gradient of aqueous NaCl (0, 0.2, and 0.3 M) to acquire a charge distribution of homogenous fractions. These fractions were further purified using a Sepharose CL-6B column to obtain HG pectins (HG-MP). Elution curves were monitored by determining the sugar content.

General Methods

Total carbohydrate content was determined using the phenol-sulfuric acid method (36). UV spectra are shown in **Supplementary Methods 1**. The molecular weight distribution was determined as shown in **Supplementary Methods 2**. Monosaccharide composition is shown in **Supplementary Methods 3**. ^{13}C NMR spectra were obtained and are shown in **Supplementary Methods 4**.

Degree of Polymerization

The degree of polymerization was analyzed using HPSEC-RI-MALLS. This system is comprised of one column (Shodex OH-Pack SB-803 HQ) connected to a multi-angle light scattering detector (DAWN HELEOSII, Wyatt Technology Corp., Santa Barbara, CA, United States) and a refractive index detector (OptilabrEX, Wyatt Technology Corp). The eluent was a solution of 0.2 M NaCl containing 0.02% NaN_3. MWs were calculated using Astra (Version 6.1.1.84) software. Finally, the degree of polymerization was estimated by MW.

Estimation of the Degree of Methyl-Esterification

The degree of methyl-esterification (DM) was calculated using Fourier transform-infrared spectroscopy (FT-IR) (Perkin Elmer, United States) spectroscopy as previously described (37). DM values are proportional to the ratio of the area from the band at 1,740 cm^{-1} over the sum of the areas of bands at 1,740 and 1,630 cm^{-1}. To quantify the DM of samples, a calibration curve was constructed based on pectin standards of known DM (0, 22, 44, 66, and 88%).

Enzymatic Hydrolysis

Homogalacturonan pectins (5 mg ml^{-1}) were solubilized in 50 mM ammonium acetate buffer (pH 4.5). Notably, 1 μl of endo-polygalacturonase II (1,100 U ml^{-1}) was added prior to incubation for 12 h at 40°C, and enzymatic hydrolysis was repeated once. The enzyme was inactivated by boiling at 100 °C for 10 min. After cooling, digests were centrifuged at 12,000 rpm for 5 min, and the supernatant was analyzed for the molecular weight distribution using high-performance size-exclusion chromatography. Oligo-galacturonides were purified on a Sepahdex-G25 column.

Derivatization of Oligogalacturonides With Aminobenzamide (2-AB)

Oligogalacturonides were lyophilized and reconstituted with 10 μl of a 0.1 M 2-AB solution in glacial acetic acid/dimethyl sulfoxide (DMSO) (3:7, v v^{-1}) and 10 μl of a freshly prepared solution of 1 M sodium cyanoborohydride in glacial acetic acid/dimethyl sulfoxide (DMSO) (3:7, v v^{-1}). Solutions were centrifuged at 12,000 rpm for 1 min at room temperature. The reaction mixture was then incubated at 65°C for 3 h and concentrated to 200 ng μl^{-1} using 50% acetonitrile-water at a 1:1 ratio (vol vol^{-1}) prior to analysis using HILIC-FLR/ESI-MS^n (32).

HILIC-FLR/ESI-MS^n Analysis

Fluorescently labeled galacturonate-based oligosaccharides were analyzed using a UPLC system (Waters Acquity H-Class, United States) coupled to a fluorescence detector (Waters Acquity H-Class, United States) and an ESI-IT-MS^n-detector (Amazon speed ETD, Bruker, Germany). Chromatographic separation was performed on an Acquity UPLC BEH amide column (1.7 m, 2.1 mm × 150 mm) in combination with a Van Guard pre-column (1.7 m, 2.1 mm × 5 mm; Waters Corporation, Milford, MA, United States). HILIC-FLR/ESI-MS^n elution procedures and detection methods are described in **Supplementary Methods 5**. Quantification of oligogalacturonides was verified using this procedure as illustrated in **Supplemental Methods 6**.

Determination of the Degree of Blocked Segments and the Absolute Degree of Blocked Segments

The calculation of two parameters, namely, degree of blocked segments (DB) and absolute degree of blocked segments (DB_{abs}) was determined using HILIC-FLR-MSn for quantification with 20 types of HG pectins. As previously described, DB and DB_{abs} were calculated as the number of unesterified GalA residues in oligogalacturonides relative to the total unesterified GalA and all the GalA residues in the polymer. These parameters were used to characterize the random or blocked patterns of methyl-esterification in HG pectins (18, 22, 31). The calculation formula is shown as follows:

$$DB = \frac{\sum_{n=1-3} \left[OligoGalA_n\right]_{unesterified} \times n}{GalA_{unesterified}} \quad (1)$$

$$DB_{abs} = \frac{\sum_{n=1-3} \left[OligoGalA_n\right]_{unesterified} \times n}{GalA_{total}} \quad (2)$$

RESULTS AND DISCUSSION

Preparation of HG Pectins From Plants

Homogalacturonan pectins were prepared from 20 plants according to the protocol as shown in **Figure 1**. In brief, total polysaccharide was obtained from each plant by hot water extraction and ethanol precipitation. Neutral (MPP-N) and acidic polysaccharides (MPP-A) were separated from total polysaccharides by ion-exchange chromatography. The acidic polysaccharides from different plants were all pectins, which were further separated by ion-exchange chromatography using different elution concentrations of sodium chloride solution. For some plants (*Isatis indigotica, Aconitum carmichaelii, Coptis chinensis,* and *Sophora flavescens*), MPP-A2 was the dominant fraction, whereas for other plants, both MPP-A2 and MPP-A3 were the major fractions. MPP-A2 from four plants and MPP-A2 and MPP-A3 from eight plants were then purified by size exclusion chromatography, and one major acidic fraction was obtained from each of them. Therefore, twenty pectin fractions came from twelve plants. Those fractions with relatively high yields and with homogenous molecular weight distributions (**Supplementary Figure 1**) were selected for further analysis. In UV-Vis spectra of all purified pectin fractions, no UV absorption was observed at 260 or 280 nm, indicating that they were free of proteins and nucleic acids (**Supplementary Figure 2**). The sugar content in these pectins ranged from 86.3 to 92.6%, indicating relatively high purity. Monosaccharide composition analysis showed that the GalA content in these fractions was over 70%, showing that HG was the major component in them. HPSEC-RI-MALLS analysis indicated that their weight-average molecular weights (MWs) ranged between 8 and 55 kDa (**Supplementary Figure 1** and **Table 1**).

^{13}C-NMR Analysis of HG Pectins

^{13}C-NMR was used to analyze the chemical structures of HG pectins (**Figure 2**). Signals at 99.36, 68.64, 67.97, 77.79, 71.08, and 175.04 ppm were assigned to the C-1, C-2, C-3, C-4, C-5, and C-6 atoms of →4)-α-D-GalA*p*-(1→, and the signal at 170.81 ppm was due to C-6 of →4)-α-D-MeGalA*p*-(1→, respectively. These chemical shifts suggested that HG is the dominant structure in these pectin fractions. The resonance at 52.74 ppm was attributed to the -OCH_3 group, indicating that these HG pectins were methyl-esterified. The absence of a (or a very weak) signal at ∼19.16 ppm indicated that these HG pectins contained no (or only very small amounts of) acetyl groups. Aside from characteristic signals from the HG backbone, some weak signals at 98.91 and 16.44 ppm were identified as C-1 and C-6 of →2)-α-L-Rha*p*-(1→, respectively, and signals at 104.26 ppm and 106.92 ppm were from C-1 of β-D-Gal*p* and α-L-Ara*f*, respectively. These results indicated that few RG-I domains are also present in these fractions, consistent with monosaccharide composition. The major signals in ^{13}C-NMR spectra of these HG pectins were similar, whereas the pectin fraction with a small RG-I content had a more complicated spectrum. In addition, signal intensities at 52.74 and 170.81 ppm (attributable to methyl and methyl ester groups, respectively) were different, suggesting that the degree of methyl-esterification (DM) may be different.

FT-IR Analysis of the DM of HG Pectins

Based on our NMR analysis, these HG pectins were all methyl-esterified. To determine the DM of these HG pectins, FT-IR analysis was performed. The FT-IR spectra of 20 HG pectins (**Figure 3** and **Supplementary Figure 3**) exhibited similar characteristic peaks from 400 to 4,000 cm^{-1}, as well as absorption peaks at 1,740 and 1,630 cm^{-1} that were attributed to C = O vibrations of the methyl-esterified GalA and GalA in the acidic forms, respectively. However, the peak areas at 1,740 cm^{-1} and 1,630 cm^{-1} were distinct for some pectins. Based on these two peak areas, DM values were calculated as described in the "Methods" section. As shown in **Table 2**, the DM of these HG pectins was all less than 50%, suggesting that their HGs have relatively low methyl-esterification. According to DM values, these HG pectins were divided into four classes with DM values of (I) 0–10%, (II) 10–20%, (III) 20–30%, and (IV) more than 30%. We choose HG-PN-2, HG-PJ-1, HG-CC, and HG-KL-1 from each class of pectin as examples in the following methyl-esterification pattern analysis.

Quantitative and Methyl-Ester Distribution of Mono-/Oligo-Galacturonides

Due to the relatively large molecular weight distributions in HG pectins, specific sites of methyl-esterification are difficult to determine directly using chemical or spectroscopic approaches. Therefore, enzymatic hydrolysis was employed to degrade the HGs into mono-/oligo-galacturonides. By a quantitative analysis of nonesterified and esterified mono/oligo-galacturonides and by analyzing the structures of esterified oligogalacturonides, methyl-esterification patterns were estimated (38).

Endo-Polygalacturonase Hydrolysis of HG Pectins

Endo-PG was used to degrade HG pectins because they were only minimally esterified. Endo-PG [EC 3.2.1.15] is purified from *Aspergillus aculeatus* that can hydrolyze at least four continuous unesterified α-(1-4)-GalA linkages. This enzyme cannot hydrolyze glycosidic bonds between esterified α-(1-4)-GalA groups (39). The products of Endo-PG degradation were monitored using HPGPC (**Supplementary Figure 4**). Oligosaccharides with MW < 2 kDa were the major products. In addition, a small number of large and medium molecular weight fractions were also produced, which arise from RG-I and RG-II domains (34, 35, 40). Following degradation, hydrolysates were separated using Sephadex G-25 to remove polymers, thus yielding mono-/oligo-galacturonides (yield∼50–80%).

HILIC-FLR-MS Analysis of Mono-/Oligo-Galacturonides

In this study, 2-AB was used to label mono-/oligo-galacturonides that were produced by enzymatic hydrolysis of HG pectins. This labeling protocol stoichiometrically links one fluorescent probe per reducing end of an oligosaccharide, with labeling efficiency reaching greater than 85% (41). Fluorescently labeled

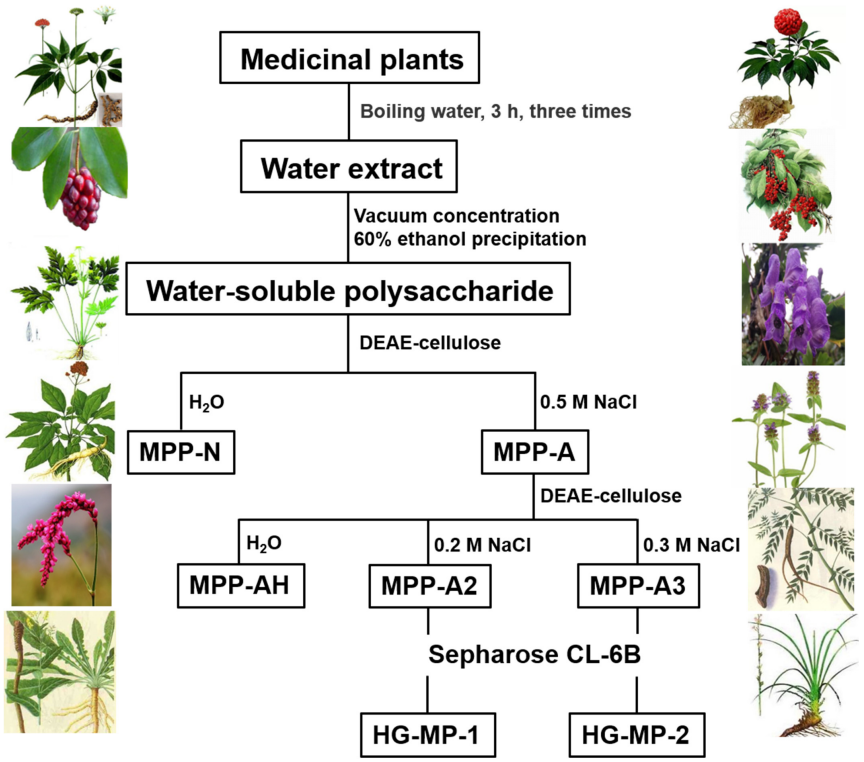

FIGURE 1 | Separation and purification of homogalacturonan (HG) pectins from plants.

TABLE 1 | Basic physicochemical properties of twenty kinds of homogalacturonan (HG) pectin.

Plant	Fraction[a]	Sugar content (% w)	Mw (KDa)	Monosaccharide composition (mol %)			
				GalA	Rha	Gal	Ara
Panax japonicus	HG-PJ-1	89.4	13.4	83.9	3.2	5.8	5.1
	HG-PJ-2	90.1	18.5	91.0	2.6	2.5	2.4
Pseudostellaria eterophylla	HG-PH-1	87.3	18.7	80.6	3.8	7.0	8.6
	HG-PH-2	86.4	26.0	81.1	4.2	6.2	8.5
Schisandra chinensis	HG-SC-1	91.5	51.0	90.8	2.5	3.3	1.9
	HG-SC-2	88.6	13.0	81.9	3.8	6.4	5.8
Prunella vulgaris	HG-PV-1	92.5	11.3	80.4	5.3	8.2	6.1
	HG-PV-2	90.6	21.0	78.1	8.9	7.4	5.6
Panax Notoginseng	HG-PN -1	91.6	11.8	74.6	5.1	9.3	8.0
	HG-PN-2	89.4	18.7	75.4	6.5	8.3	8.2
Polygonum orientale	HG-PO-1	86.3	26.9	75.9	9.4	8.7	6.0
	HG-PO-2	87.2	23.0	74.0	9.4	10.1	6.5
Anemarrhena sphodeloides	HG-AA-1	88.9	10.1	81.7	3.4	4.8	10.2
	HG-AA-2	91.2	15.5	74.6	5.9	4.9	14.6
Kadsura longipedunculata	HG-KL-1	92.6	19.1	81.1	4.2	7.5	7.2
	HG-KL-2	91.5	27.9	73.6	9.6	10.9	5.9
Isatis indigotica	HG-II	89.1	35.7	72.2	11.6	6.1	10.1
Aconitum carmichaelii	HG-AC	87.6	43.4	78.3	10.0	5.0	6.7
Coptis chinensis	HG-CC	88.0	16.1	70.6	4.8	7.4	17.2
Sophora flavescens	HG-SF	89.1	48.0	71.2	7.6	7.2	13.9

[a] *The pectin fractions were named "HG-binomial nomenclature of plants (initials)."*

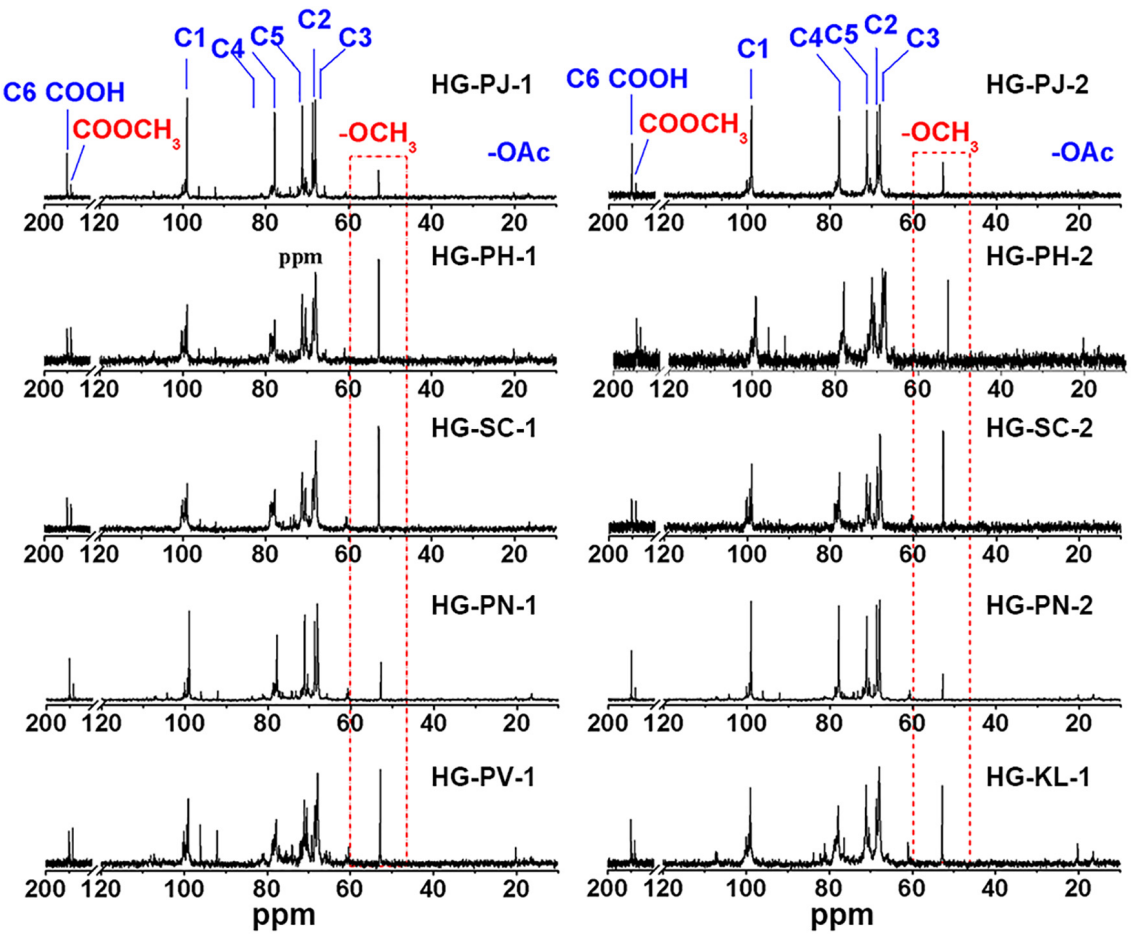

FIGURE 2 | ^{13}C NMR spectrum of HG pectin.

mono-/oligo-galacturonides were completely separated by HILIC. In this study, four fractions were taken to exemplify our analytical approach. **Figure 4** shows the total ion chromatogram (TIC) of the mono-/oligo-galacturonides by HILIC-FLR-MS analysis. The HILIC-MS elution pattern showed that the derivatized oligogalacturonides have masses lower than ∼1,200 exhibiting mostly $[M\text{-}H]^{-1}$ ions, and oligomers greater than ∼1,200 were represented by both $[M\text{-}H]^{-1}$ and $[M\text{-}H]^{-2}$ ions. Nonesterified mono-/oligo-galacturonides were monomers (313), dimers (417), and trimers (647). Methyl-esterified oligogalacturonides with different DP values and different numbers of methyl-ester groups were observed, including DP 3–5 containing a single methyl-ester group, DP 4–6 containing two methyl-ester groups, DP 5–8 containing three methyl-ester groups, DP 7–9 containing four methyl-ester groups, DP 8–10 containing five methyl-ester groups, and DP 9–10 containing six methyl-ester groups.

Quantification of Mono-/Oligo-Galacturonides by HILIC-FLR Analysis

To quantify the content of mono/oligo-galacturonides from different HG pectins, a set of standard mono-/oligo-galacturonides (DP1-6) at different concentrations were first analyzed by HILIC-FLR (**Figure 5A**). Calibration curves showed excellent linearity over the entire concentration range (15.6 to 1,000 μM) with R^2 values falling between 0.9955 and 0.9996 (**Supplementary Table 1**). The limit of detection (LOD) and limit of quantitation (LOQ) ranges were within 0.1–0.3 and 0.4–1.2 μM, respectively (**Supplementary Table 1**). By comparing standard curves with different DPs, we found that the slope (K) of the GalA standard curve was the highest, whereas other oligomers (DP2-6) had slopes that tended to be relatively smooth (**Figure 5B**). Therefore, we used the DP6 standard curve to calculate the content of oligomers with DP > 6. As methyl-esterified oligogalacturonide standards were not available, the content of methyl-esterified oligogalacturonide was estimated using a standard curve of nonesterified oligogalacturonides with the same DP. The molar percentage of mono-/oligo-galacturonides from different HG pectins in HILIC-FLR was calculated using standard curves, and the results are shown in **Supplementary Table 2**. Among these mono-/oligo-galacturonides, nonesterified monomers, dimers, and trimers had the largest amounts of total mono-/oligo-galacturonides. The variety of oligogalacturonides from HG

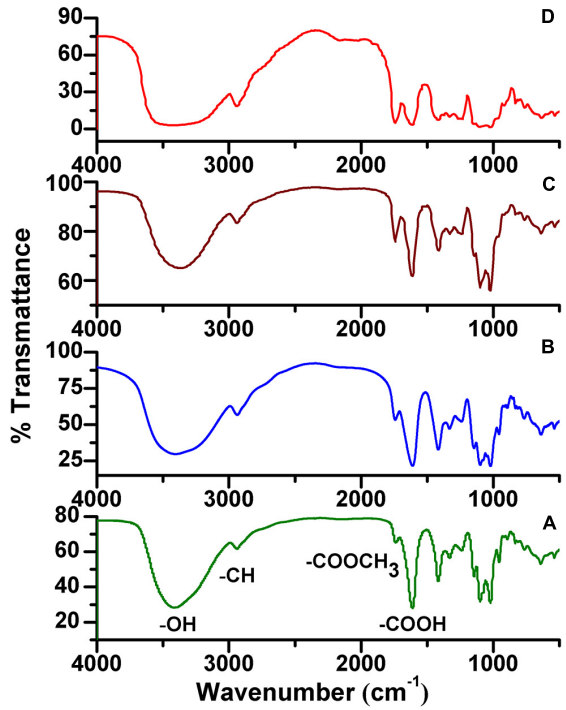

FIGURE 3 | Fourier transform-infrared spectroscopy (FT-IR) spectra of HG pectins from plants. **(A)** HG-PN-2 (Class I); **(B)** HG-PJ-1 (Class II); **(C)** HG-CC-1 (Class III); and **(D)** HG-KL-1 (Class IV).

TABLE 2 | The degree of methyl-esterification (DM) of 20 HG pectins.

Class	Fraction	DM (%)
I	HG-AC	5.0
	HG-PN-2	6.6
	HG-PJ-2	9.6
II	HG-PN-1	11.2
	HG-PJ-1	17.6
	HG-PV-2	19.8
III	HG-PH-2	21.8
	HG-AA-2	23.5
	HG-SF	23.7
	HG-PH-1	25.0
	HG-AA-1	25.2
	HG-PO-1	27.2
	HG-PO-2	27.7
	HG-CC	28.9
IV	HG-PV-1	30.3
	HG-KL-2	31.0
	HG-SC-2	33.5
	HG-SC-1	34.8
	HG-II	39.0
	HG-KL-1	40.2

pectin with higher DM values was more abundant than those with lower DM values, and the content of oligogalacturonides decreased gradually along with the increase in DP.

Methyl-Ester Group Distribution in Oligogalacturonides

To elucidate sites of methyl-esterification in HG pectin oligosaccharides, we used MS^2 fragmentation analysis. The reducing end of these oligosaccharides was labeled with the fluorescent probe 2-AB. Using the negative mode MS detection, we found that the cleavage of Z and Y ions increased by 102 over the *m/z* value, whereas C and B ions remained unchanged. Fragmentation patterns were annotated according to Domon and Costello (42). We used HILIC-MS^2 to analyze 18 oligogalacturonides with different numbers of methyl-ester groups, six of which are analyzed in detail and shown below.

Mass spectrometry results demonstrated that the $[M-H]^{-1}$ ion at *m/z* 819 corresponded to the mono methyl-esterified tetramer of galacturonic acid, and fragment peaks at *m/z* 369 $[C2]^-$, *m/z* 559 $[C3+Me]^-$, and *m/z* 643 $[Z3+Me]^-$ in MS^2 analysis confirmed the structure as GalA-GalA-$GalA_{Me}$-GalA-2AB (**Figure 6A**). For di-methyl-esterified pentamers of galacturonic acid (*m/z* 1,027 $[M-H]^-$ ion), fragment peaks at *m/z* 383 $[C2+Me]^-$ and *m/z* 749 $[C4+2Me]^-$ and their complementary *m/z* 453 $[Z2]^-$, *m/z* 643 $[Z3+Me]^-$, and *m/z* 833 $[Z4+3Me]^-$ in MS^2 spectra were observed. These data indicated that the oligogalacturonide sequence was GalA-$GalA_{Me}$-$GalA_{Me}$-GalA-GalA-2AB (**Figure 6B**). The $[M-H]^-$ ion at *m/z* 1,217 corresponded to a tri-methyl-esterified hexamer of galacturonic acid. Fragment peaks at *m/z* 383 $[C2+Me]^-$, *m/z* 573 $[C3+2Me]^-$ and their complementary *m/z* 453 $[Z2]^-$, *m/z* 643 $[Z3+Me]^-$, *m/z* 833 $[Z4+2Me]^-$, and *m/z* 1,023 $[Z5+3Me]^-$ in MS^2 spectra were found, suggesting the oligogalacturonide sequence of GalA-$GalA_{Me}$-$GalA_{Me}$-$GalA_{Me}$-GalA-GalA-2AB (**Figure 6C**).

Oligomers having molecular weights greater than ∼1,200 Da showed mostly di-deprotonated $[M-2H]^{2-}$ ions in MS^2 spectra, such as the single-charged *m/z* 1,583 $[M-H]^-$ ion and the di-deprotonated species at *m/z* 791 $[M-H]^{2-}$ ion associated with the tetra-esterified octamer of galacturonic acid. Furthermore, the presence of fragment ions at *m/z* 527 $[C3]^-$, *m/z* 367 $[C4+Me]^{2-}$, *m/z* 462 $[C5+2Me]^{2-}$, *m/z* 557 $[C6+3Me]^{2-}$, and *m/z* 277 $[Z1]^-$ in MS^2 spectrum confirmed the sequence of the heptamer as GalA-GalA-GalA-$GalA_{Me}$-$GalA_{Me}$-$GalA_{Me}$-$GalA_{Me}$-GalA-2AB (**Figure 7A**). The penta-methyl-esterified nonamer (*m/z* 886 $[M-H]^{2-}$) showed peaks at *m/z* 527 $[B3]^-$, *m/z* 735 $[C4+Me]^-$, *m/z* 462 $[C5+2Me]^{2-}$, *m/z* 557 $[C6+3Me]^{2-}$, *m/z* 652 $[C7+4Me]^{2-}$, and *m/z* 747 $[C8+5Me]^{2-}$ in MS^2 spectra, and the structure was determined to be GalA-GalA-GalA-$GalA_{Me}$-$GalA_{Me}$-$GalA_{Me}$-$GalA_{Me}$-$GalA_{Me}$-GalA-2AB (**Figure 7B**). The hexa-methyl-esterified nonamer (*m/z* 893 $[M-H]^{2-}$) with peaks at *m/z* 383 $[C2+Me]^-$, *m/z* 573 $[C3+2Me]^-$, *m/z* 763 $[C4+3Me]^{2-}$, *m/z* 469 $[C5+4Me]^{2-}$, *m/z* 564 $[C6+4Me]^{2-}$, *m/z* 659 $[C7+5Me]^{2-}$, and *m/z* 754 $[C8+6Me]^{2-}$ in MS^2 spectra, having the structure of GalA-$GalA_{Me}$-$GalA_{Me}$-$GalA_{Me}$-GalA-$GalA_{Me}$-$GalA_{Me}$-$GalA_{Me}$-GalA-2AB (**Figure 7C**). The structures of another 12 different methyl-esterified oligogalacturonides are shown in **Supplementary Figure 4**.

Based on these analyses, we could see that the most continuously distributed methyl-ester group was five in these oligomers. With the increase in DP of the oligogalacturonides,

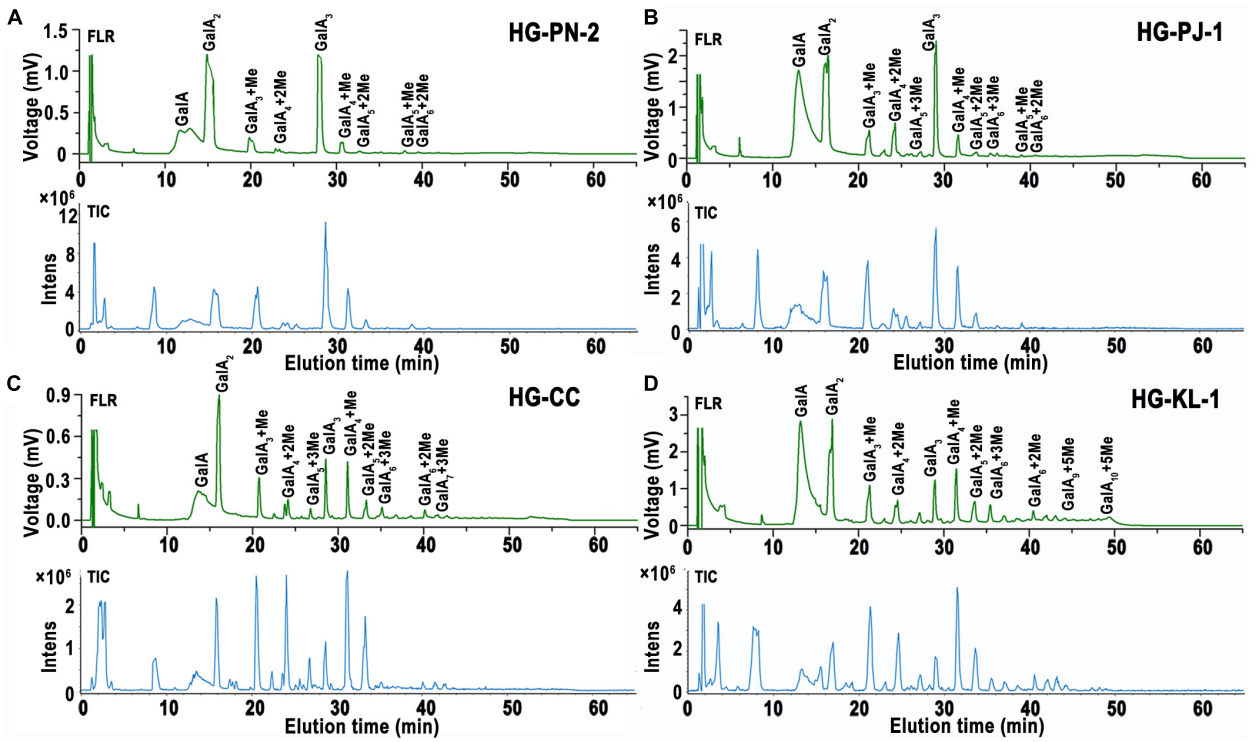

FIGURE 4 | HILIC elution patterns of GalA-oligomers produced from HG pectins with different degrees of methyl-esterification (DM). **(A)** HG-PN-2 (Class I); **(B)** HG-PJ-1 (Class II); **(C)** HG-CC-1 (Class III); and **(D)** HG-KL-1 (Class IV).

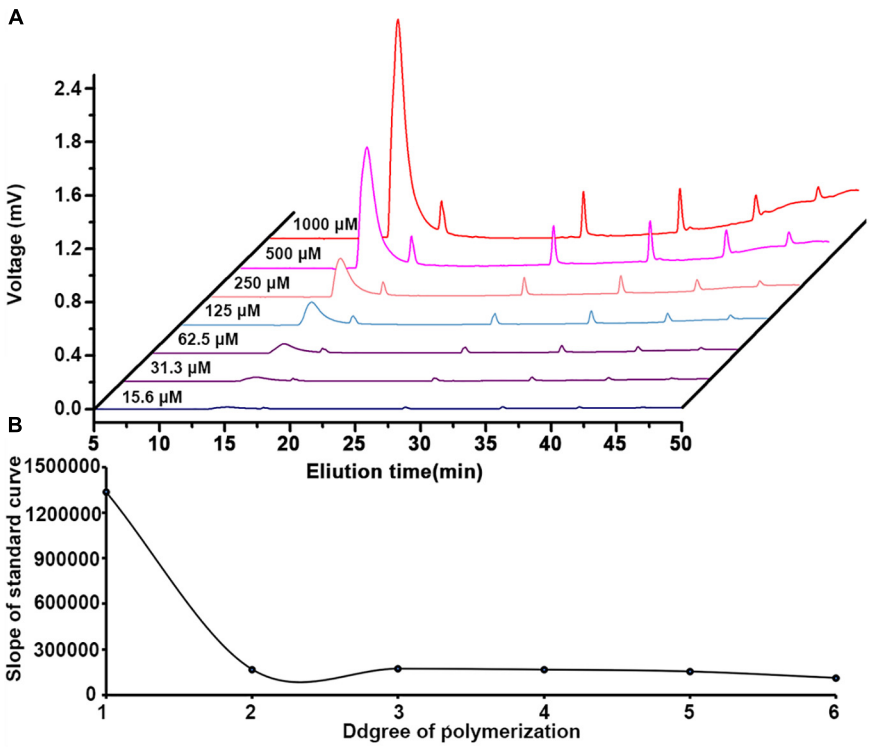

FIGURE 5 | (A) HILIC-FLR elution curves of oligogalacturonide standards (DP1-6) at different concentrations. **(B)** Comparison of the slope of GalA standard curve.

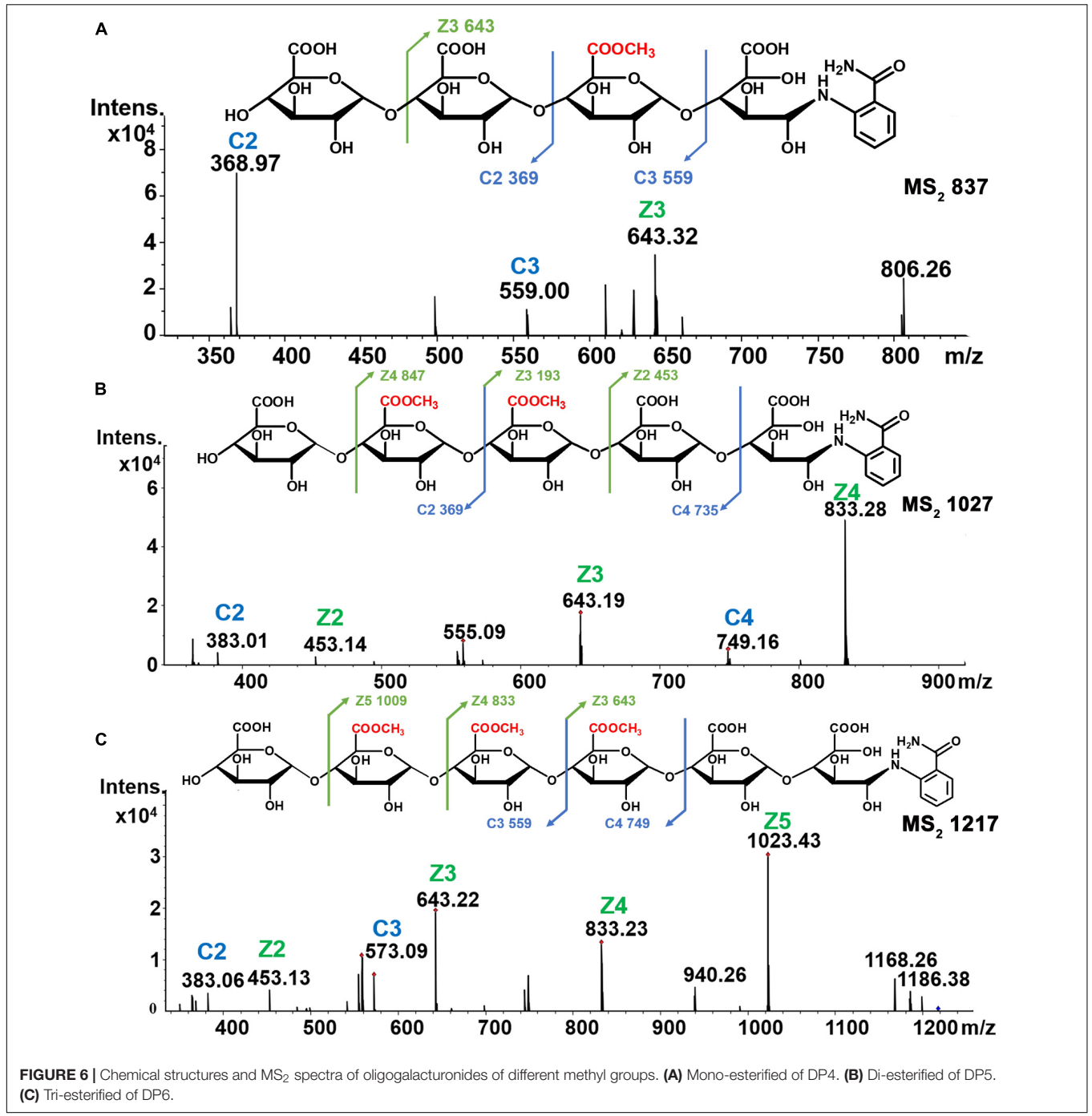

FIGURE 6 | Chemical structures and MS_2 spectra of oligogalacturonides of different methyl groups. **(A)** Mono-esterified of DP4. **(B)** Di-esterified of DP5. **(C)** Tri-esterified of DP6.

1-2 GalA residue gaps also existed between methyl ester groups. Oligomers carrying a maximum of 3 consecutive methyl-ester groups have been reported (19, 43). Pectin lyase (EC 4.2.2.10), which cleaves between methyl-esterified GalA residues in HG regions by β-elimination, was used (together with Endo-PG in some studies) to analyze high DM pectins (19, 20) that may result in a decrease of consecutive methyl-ester groups in GalA-oligomers. Due to the low DM values of these 20 HG pectins, pectin lyase was not used in our study. During our analysis of the methyl-ester group sites in these oligogalacturonides, there may be characteristic mass spectrum peaks of the corresponding isomers; however, their fine structures could not be resolved due to having only small amounts of material.

Methyl-Esterification Pattern of 20 HG Pectins

Quantification and distribution of methyl-ester groups in pectin-derived HG oligosaccharides with different DM values were systematically investigated (**Figure 8**). We found that large

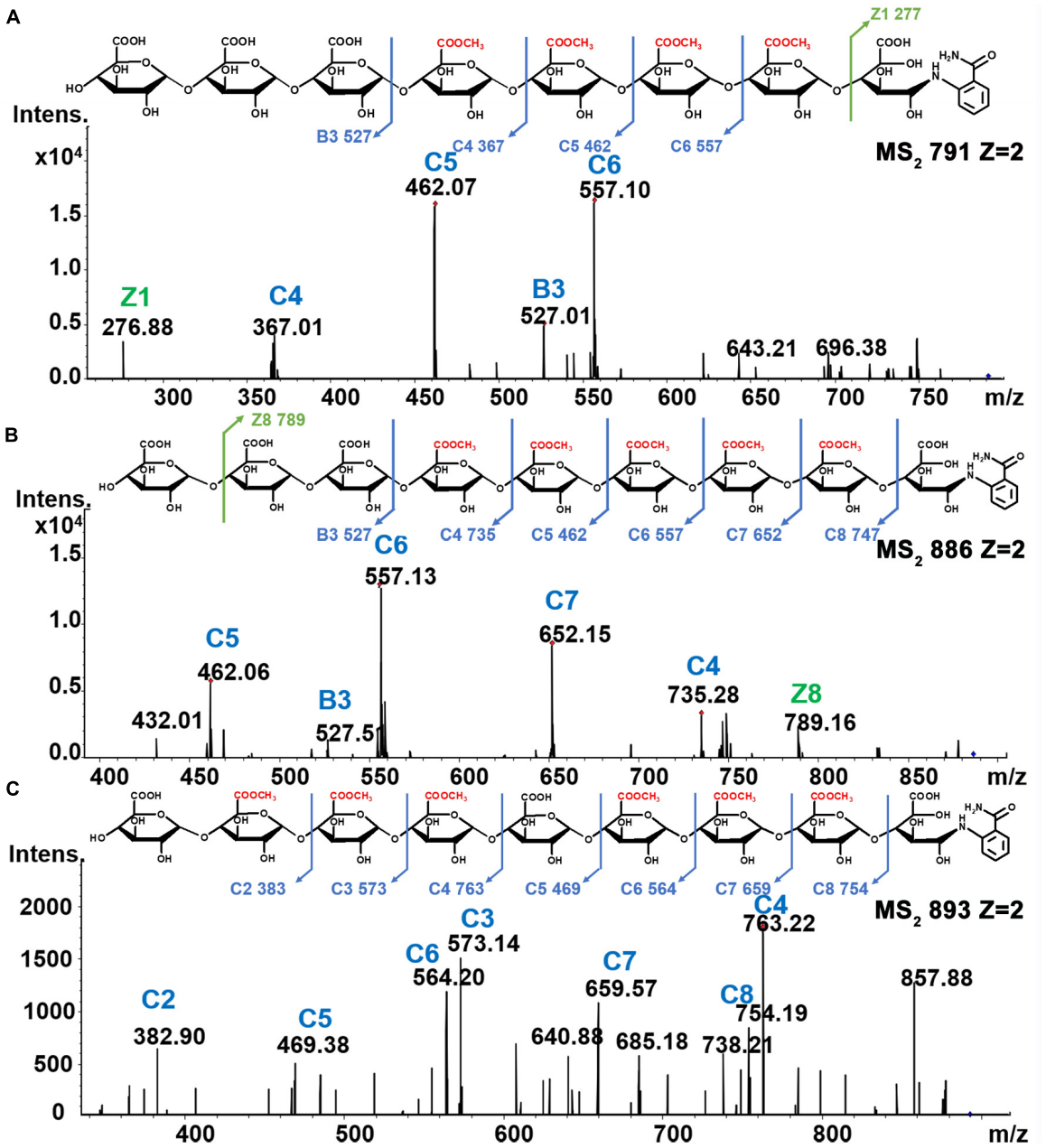

FIGURE 7 | (A) Tetra-esterified of DP8 **(B)** penta-esterified of DP9 and **(C)** hex-esterified of DP9.

amounts of nonesterified monomers, dimers, and trimers were released on Endo-PG degradation. Monomers and dimers were only present as nonesterified oligomers, consistent with previous studies (38, 44). For the total amount of nonesterified oligomer, the higher the DM of the pectin, the smaller the percentage of trimmer. This suggested a gradual decrease in the average size of nonesterified GalA fragments in HG pectins with DM values increasing. In addition, the higher DM of the pectin, the larger the amount of methyl-esterified oligomers. We noticed that mono- and di-esterified oligomers had a larger percentage in total methyl-esterified oligomers, and the amounts and types of methyl-esterified oligomers were quite abundant in higher DM pectins, indicating a relatively random pattern of methyl-ester distribution in these 20 HG pectins (19). Although the plant PMEs were reported as a kind of pectin methylesterase [leading to the appearance of de-esterified stretches or blocks (20, 45)], we assumed that the de-esterification of pectins in plants is a more complex process than using various PMEs (46). Furthermore, although some of these twenty HG pectins were purified from plants and used in medicines and foods, others were derived from plants and used only for drugs. We noticed that there was no difference between their structural

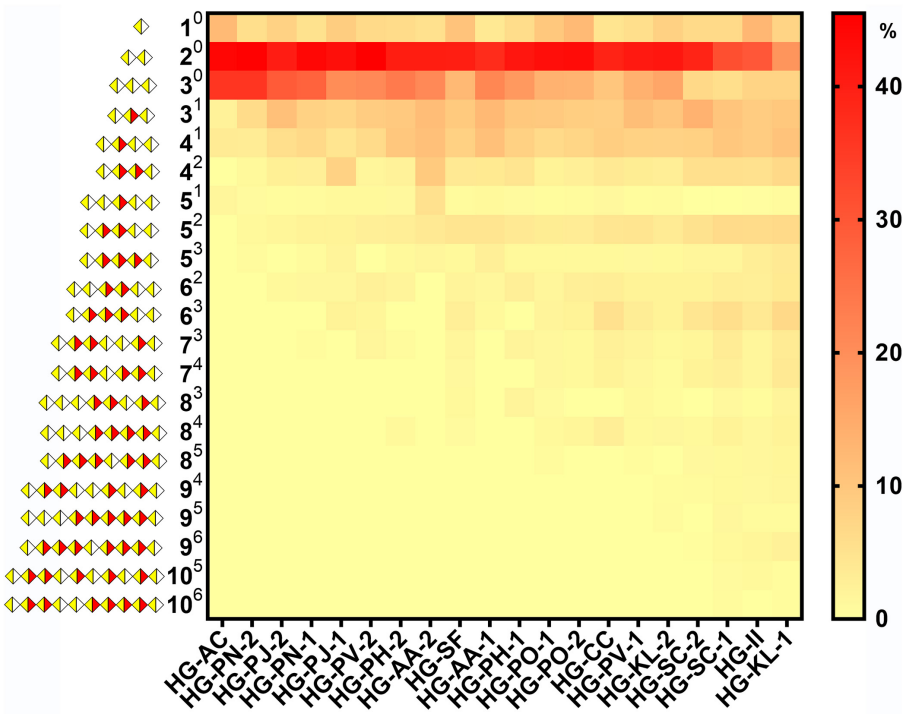

FIGURE 8 | The heatmap of species and quantification of HG pectin oligosaccharides in different plants (A^B A is the degree of galacturonic acid; B is the number of methyl groups; ◇ GalA; ◆ methylesterified GalA).

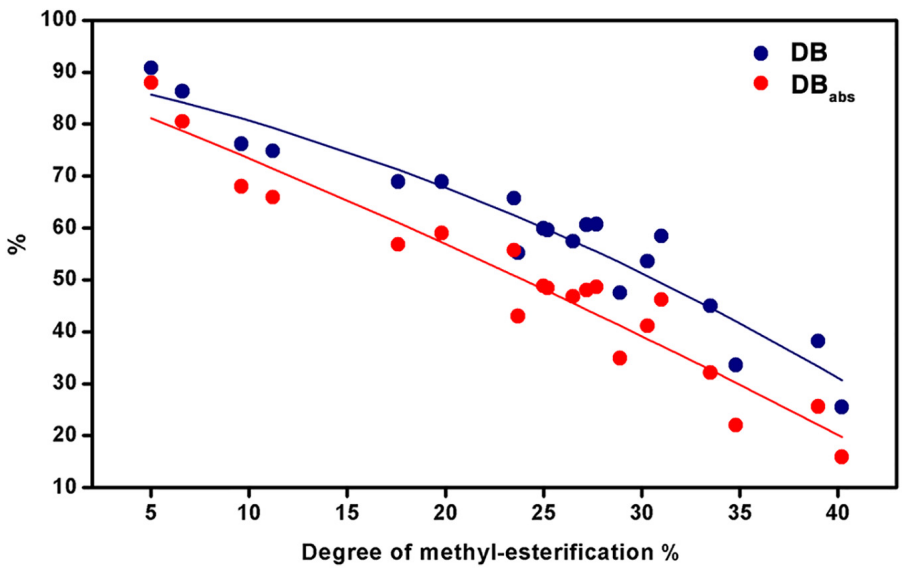

FIGURE 9 | DB and DB_{abs} as a function of the degree of methylesterification for the 20 HG pectins.

features, including methyl-esterification distribution patterns. This suggests that toxic side effects from medicinal plant products may not be caused by their HG pectins and that these HG pectins may be safely used.

Furthermore, the DB and DB_{abs} values of 20 HG pectins were calculated to characterize their methyl-esterification patterns (**Supplementary Table 3**). In this study, we found a gradual decrease in DB or DB_{abs} values with increasing DM values (**Figure 9**). These DB and DB_{abs} values indicate a random or blockwise pattern of methyl-esterification. Pectins with similar DM values, but with different DB or DB_{abs} values, may have a nonidentical pattern of methyl-esterification (38, 47). Among

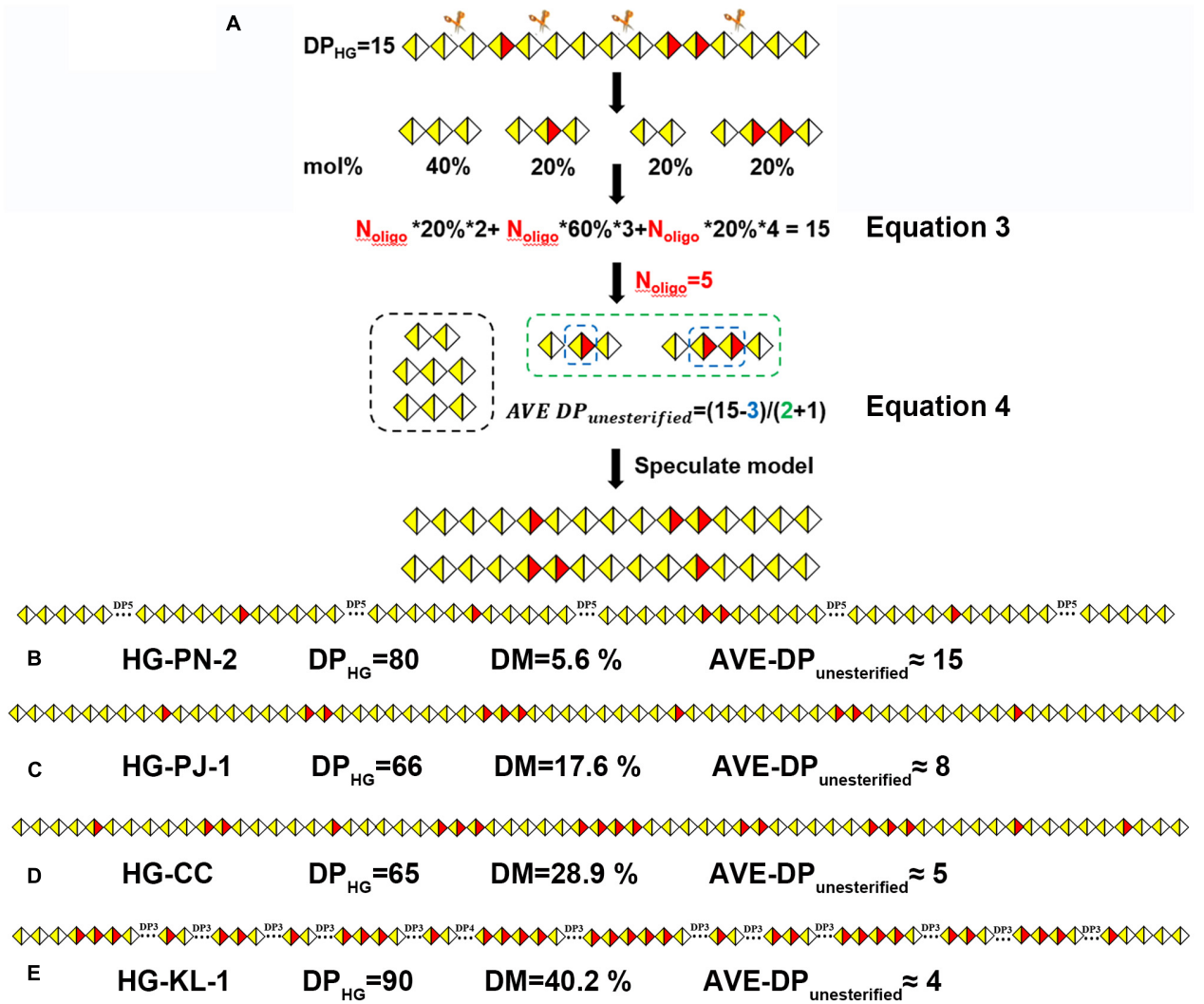

FIGURE 10 | (A) The calculation process of the number of oligogalacturonides (N_{oligo}); methyl-esterification distribution models of HG pectins with different DM: **(B)** HG-PN-2(Class I); **(C)** HG-PJ-1 (Class II); **(D)** HG-CC (Class III); **(E)** HG-KL-1 (Class IV).

the pectins with smaller DM values, DB or DB_{abs} values were relatively close to each other, suggesting similar degrees of methyl-esterification (**Figure 9**). It has been reported that DM and DB values of HG pectins are both related to function. Low DM pectins (DM≈20) and intermediate DM pectins (DM≈50) with high DB values (DB60) can strongly inhibit TLR2-1. DM50 pectins with low DB values (DB33) and those with high DM values (DM≈80) did not inhibit TLR2-1 (16, 17). Moreover, DM20 pectins with high DB values (DB94), as well as DM50 pectins, showed a capacity to regulate T cell-based immunity, whereas DM20 pectins with low DB values (DB86) did not (18). Therefore, HG pectins with various DM and DB values may well possess diverse functions, something that needs to be further explored in the future.

According to our results, the average size of nonesterified GalA regions in these pectins could not be obtained using DB and DB_{abs} values because their DP values and degree and position of methyl-esterification were not considered. To better illustrate the methyl-esterification pattern in HG pectins, we have established a new approach. By using a model HG pectin with a degree of polymerization (DP_{HG}) of 15 as an example (**Figure 10A**), four types of oligogalacturonides, namely GalA-GalA (20%), GalA-GalA-GalA (40%), GalA-$GalA_{Me}$-GalA (20%), and GalA-$GalA_{Me}$-$GalA_{Me}$-GalA (20%), were obtained on Endo-PG digestion. The total amount of enzymatically hydrolyzed HG oligosaccharides (N_{oligo}) was calculated using DP_{HG}, the molar percentage of each oligogalacturonide, and its corresponding DP value (equation 3). Each amount of resulting oligogalacturonide (equal to N_{oligo} multiplied by the molar percentage) was calculated as 1, 2, 1, and 1, respectively. We defined $GalA_{Me}$ in each oligogalacturonide as a "block," and unesterified GalA was equally distributed between "blocks." The average size of unesterified GalA (AVE $DP_{unesterified}$) imbedded in the "blocks" was calculated from the difference in DP_{HG} and $GalA_{Me}$ values

divided by the "block" amount (N_{block}) plus one (equation 4). The AVE $DP_{unesterified}$ was four in this distribution model, allowing two models to be inferred (**Figure 10A**).

$$N_{oligo} = \frac{DP_{HG}}{\sum_{n=1-10}[OligoGalA_n\%] \times n} \quad (3)$$

$$AVE\ DP_{unesterified} \approx (DP_{HG} - GalA_{Me})/(N_{block} + 1) \quad (4)$$

Using this approach, we analyzed the methyl-ester distribution pattern for Class IV (HG-KL-1). HPSEC-RI-MALLS showed that the MW of HG-KL-1 is 30 kDa, with the DP_{HG} value being calculated (MW × GalA % of monosaccharide)/176 as ∼90. Different mono-/oligo-galacturonides were quantified using HILIC-FLR (**Supplementary Table 2**), and approximately 20 oligogalacturonide fragments were calculated according to equation 3 (N_{oligo} = 20). The product of N_{oligo} × molar percentage yielded the number of GalA, GalA-GalA, and GalA-GalA-GalA blocks in these oligosaccharides, which were found to be 1, 4, and 1, respectively. Similarly, the "blocks" containing 1–5 esterified groups were calculated to be 5, 3, 3, 2, and 1, respectively, reaching N_{block} = 14 along with $GalA_{Me}$ = 33. In this regard, the AVE $DP_{\text{unesterified}}$ was estimated to be 4. The proposed model for HG-KL-1 was established using these results (**Figure 10E**), along with the models of the other three classes of HG pectins (**Figures 10B–D**).

Among our 20 HG pectins, the ratio of $N_{\text{block}}/N_{\text{oligo}}$ was larger in higher DM pectins. The AVE $DP_{unesterified}$ of these four classes of HG pectins was calculated as a range of 18–15, 12–8, 8–5, and 6–4, respectively, suggesting that the average size of nonesterified GalA regions in these pectins was decreased on increasing DM values (**Figure 10** and **Supplementary Table 3**). We also calculated DM values based on these models, with results being consistent with FT-IR data. In general, DB values could not provide information as to whether the pectin may contain one large block or several smaller blocks of nonesterified GalA residues. When two pectins have similar DM and DB values, but different functions, it becomes difficult to use DB values to explain the relationship between methyl-ester distribution and function. In contrast, the parameter AVE $DP_{unesterified}$ could be introduced to analyze methyl-ester distribution and function of the pectin.

Nevertheless, some limitations to our approach remain. First, our analytical strategy is only suitable for use with low methyl-esterified HG pectins. For the methyl-ester group distribution analysis with high DM pectins, PL should be used with Endo-PG completely degrading the pectins (48). Furthermore, we assumed that blocks are evenly separated in our models, whereas the actual distribution of esterified-GalA residues is likely to be more complex, and the sequence of different block lengths remains uncertain. In this study, we only showed one type of random distribution model. Nevertheless, we identified a class of oligosaccharides with discontinuous methyl-ester groups using HILIC-FLR-MS^n analysis, but these did not show up in our methyl-esterification distribution models due to their low content.

CONCLUSION

In this study, 20 HG pectins were prepared from twelve plants. The DM of these HG pectins ranged from 5 to 40%. Enzymatic fingerprinting of HG pectins with different DM values was performed by enzymatic hydrolysis, fluorescence labeling of mono/oligo-galacturonides, and HILIC-FLR-MS^n analysis. According to the quantitative and methyl-esterification distribution analysis of oligogalacturonides, we inferred the random methyl-esterification pattern in these HG pectins and proposed possible models for them. Our study reveals the characteristics of methyl-esterification patterns in natural HG pectins from plants and provides the basis for developing their structure-function relationships. In turn, our findings can be applied to the use of HG pectins in healthy foods.

DATA AVAILABILITY STATEMENT

The original contributions presented in the study are included in the article/**Supplementary Material**, further inquiries can be directed to the corresponding author/s.

AUTHOR CONTRIBUTIONS

YY: investigation and writing—original draft. LC, XL, and YW: investigation. CS: formal analysis. UP: modify the manuscript. KM, LS, and YZ: writing—review and editing. All authors contributed to the article and approved the submitted version.

FUNDING

This study was supported by the National Natural Science Foundation of China (22007011), the Scientific and Technologic Foundation of Jilin Province (20200201004JC), and Innovation Platform Project of Qinghai Province (2021-ZJ-T02).

SUPPLEMENTARY MATERIAL

The Supplementary Material for this article can be found online at: https://www.frontiersin.org/articles/10.3389/fnut.2022.925050/full#supplementary-material

REFERENCES

1. Ovodov YS. Current views on pectin substances. *Russ J Bioorg Chem.* (2009) 35:293–310. doi: 10.1134/S1068162009030017

2. Round AN, Rigby NM, Macdougall A, Morris VJ. A new view of pectin structure revealed by acid hydrolysis and atomic force microscopy. *Carbohydr Res.* (2010) 345:487–97. doi: 10.1016/j.carres.2009.12.019

3. Thibault JF, Renard CMGC, Axelos MAV, Roger P, Crépeau MJ. Studies of the length of homogalacturonic regions in pectins by acid hydrolysis. *Carbohydr Res.* (1993) 238:271–86. doi: 10.1016/0008-6215(93)87019-O
4. Remoroza C, Cord-Landwehr S, Leijdekkers AG, Moerschbacher BM, Schols HA, Gruppen H. Combined HILIC-ELSD/ESI-MSn enables the separation, identification and quantification of sugar beet pectin derived oligomers. *Carbohydr Polym.* (2012) 90:41–8. doi: 10.1016/j.carbpol.2012.04.058
5. Nebenführ A, Staehelin LA. Mobile factories: golgi dynamics in plant cells. *Trends Plant Sci.* (2001) 6:160–7. doi: 10.1016/S1360-1385(01)01891-X
6. Mohnen D. Pectin structure and biosynthesis. *Curr Opin Plant Biol.* (2008) 11:266–77. doi: 10.1016/j.pbi.2008.03.006
7. Thierry B, Annick SG, Marie-Pierre BV, Claudine M. Various pectin methyltransferase activities with affinity for low and highly methylated pectins. *Plant Cell Physiol.* (1997) 38:259–67. doi: 10.1093/oxfordjournals.pcp.a029161
8. Pelloux J, Rustérucci C, Mellerowicz EJ. New insight into pectin methylesterase structure and function. *Trends Plant Sci.* (2007) 2:267–77. doi: 10.1016/j.tplants.2007.04.001
9. Vincent RR, Cucheval A, Hemar Y, Williams M. Bio-inspired network optimization in soft materials—insights from the plant cell wall. *Eur Phys J E Soft Matter.* (2009) 28:79–87. doi: 10.1140/epje/i2008-10416-2
10. Haas KT, Wightman R, Meyerowitz EM, Peaucelle A. Pectin homogalacturonan nanofilament expansion drives morphogenesis in plant epidermal cells. *Science.* (2020) 367:1003–7. doi: 10.1126/science.aaz5103
11. Sirisomboon P, Tanaka M, Fujita S, Kojima T. Relationship between the texture and pectin constituents of japanese pear. *J Texture Stud.* (2010) 31:679–90. doi: 10.1111/j.1745-4603.2000.tb01028.x
12. Coculo D, Lionetti V. The plant invertase/pectin methylesterase inhibitor superfamily. *Front Plant Sci.* (2022) 13:863892. doi: 10.3389/fpls.2022.863892
13. Del Corpo D, Fullone MR, Miele R, Lafond M, Pontiggia D, Grisel S, et al. AtPME17 is a functional *Arabidopsis thaliana* pectin methylesterase regulated by its PRO region that triggers PME activity in the resistance to *Botrytis cinerea*. *Mol Plant Pathol.* (2020) 21:1620–33. doi: 10.1111/mpp.13002
14. Blanco-Pérez F, Steigerwald H, Schülke S, Vieths S, Toda M, Scheurer S. The dietary fiber pectin: health benefits and potential for the treatment of allergies by modulation of gut microbiota. *Curr Allergy Asthma Rep.* (2021) 21:1–19. doi: 10.1007/s11882-021-01020-z
15. Naqash F, Masoodi FA, Rather SA, Wani SM, Gani A. Emerging concepts in the nutraceutical and functional properties of pectin—a review. *Carbohydr Polym.* (2017) 168:227–39. doi: 10.1016/j.carbpol.2017.03.058
16. Beukema M, Jermendi É, Berg M, Faas MM, Vos PD. The impact of the level and distribution of methyl-esters of pectins on TLR2-1 dependent anti-inflammatory responses. *Carbohydr Polym.* (2021) 251:117093. doi: 10.1016/j.carbpol.2020.117093
17. Martin B, Éva J, Taco K, Kohji K, Bart JH, Marco AB, et al. Attenuation of doxorubicin-induced small intestinal mucositis by pectins is dependent on pectin's methyl-ester number and distribution. *Mol Nutr Food Res.* (2021) 65:1–8. doi: 10.1002/mnfr.202100222
18. Beukemaa M, Jermendib É, Oerlemansa MMP, Logtenbergb MJ, Akkermana R, An R, et al. The level and distribution of methyl-esters influence the impact of pectin on intestinal T cells, microbiota, and Ahr activation. *Carbohydr Polym.* (2022) 286:119280. doi: 10.1016/j.carbpol.2022.119280
19. Remoroza C, Broxterman S, Gruppen H, Schols HA. Two-step enzymatic fingerprinting of sugar beet pectin. *Carbohydr Polym.* (2014) 108:338–47. doi: 10.1016/j.carbpol.2014.02.052
20. Ralet MC, Williams M, Tanhatan-Nasseri A, Ropartz D, Quéméner B, Bonnin E. Innovative enzymatic approach to resolve homogalacturonans based on their methyl-esterification pattern. *Biomacromolecules.* (2012) 13:1615. doi: 10.1021/bm300329r
21. Daas PJH, Voragen AGJ, Schols HA. Study of the methyl ester distribution in pectin with endo-polygalacturonase and high-performance size-exclusion chromatography. *Biopolymers.* (2001) 58:195–203. doi: 10.1002/1097-0282(200102)58:23.0.CO;2-C
22. Coenen GJ, Kabel MA, Schols HA, Voragen AG. CE-MSn of complex pectin-derived oligomers. *Electrophoresis.* (2010) 29:2101–11. doi: 10.1002/elps.200700465
23. Ognyanov M, Remoroza C, Schols HA, Georgiev YN, Krystyjan M. Structural, rheological and functional properties of galactose-rich pectic polysaccharide fraction from leek. *Carbohydr Polym.* (2019) 229:115549. doi: 10.1016/j.carbpol.2019.115549
24. Remoroza C, Buchholt HC, Gruppen H, Schols HA. Descriptive parameters for revealing substitution patterns of sugar beet pectins using pectolytic enzymes. *Carbohydr. Polym.* (2014) 101:1205–15. doi: 10.1016/j.carbpol.2013.10.034
25. Leijdekkers AGM, Sanders MG, Schols HA, Gruppen H. Characterizing plant cell wall derived oligosaccharides using hydrophilic interaction chromatography with mass spectrometry detection. *J Chromatogr A.* (2011) 1218:9227–35. doi: 10.1016/j.chroma.2011.10.068
26. Mendis PM, Sasiene ZJ, Ropartz D, Rogniaux H, Jackson GP. Structural characterization of isomeric oligogalacturonan mixtures using ultrahigh-performance liquid chromatography-charge transfer dissociation mass spectrometry. *Anal Chem.* (2021) 93:2838–47. doi: 10.1021/acs.analchem.0c04142
27. Anumula KR. Advances in fluorescence derivatization methods for high-performance liquid chromatographic analysis of glycoprotein carbohydrates. *Anal Biochem.* (2006) 350:1–23. doi: 10.1016/j.ab.2005.09.037
28. Ruhaak LR, Zauner G, Huhn C, Bruggink C, Deelder AM, Wuhrer M. Glycan labeling strategies and their use in identification and quantification. *Anal Bioanal Chem.* (2010) 397:3457–81. doi: 10.1007/s00216-010-3532-z
29. Volpi N, Galeotti F, Bo Y, Linhardt RJ. Analysis of glycosaminoglycan-derived, precolumn, 2-aminoacridone-labeled disaccharides with LC-fluorescence and LC-MS detection. *Nat Protoc.* (2014) 9:541–58. doi: 10.1038/nprot.2014.026
30. Melmer M, Stangler T, Schiefermeier M, Brunner W, Premstaller A. HILIC analysis of fluorescence-labeled N-glycans from recombinant biopharmaceuticals. *Anal Bioanal Chem.* (2010) 398:905–14. doi: 10.1007/s00216-010-3988-x
31. He L, Sato K, Abo M, Okubo A, Yamazaki S. Separation of saccharides derivatized with 2-aminobenzoic acid by capillary electrophoresis and their structural consideration by nuclear magnetic resonance. *Anal Bioanal Chem.* (2003) 314:128–34. doi: 10.1016/S0003-2697(02)00633-4
32. Hase S. High-performance liquid chromatography of pyridylaminated saccharides. *Methods Enzymol.* (1994) 230:225–37. doi: 10.1016/0076-6879(94)30015-1
33. Guillotin SE, Bakx EJ, Boulenguer P, Mazoyer J, Schols HA, Voragen AGJ. Populations having different gala blocks characteristics are present in commercial pectins which are chemically similar but have different functionalities. *Carbohydr Polym.* (2005) 60:391–8. doi: 10.1016/j.carbpol.2005.02.001
34. Ning X, Liu Y, Jia MD, Wang QD, Sun ZY, Ji L, et al. Pectic polysaccharides from radix *Sophorae tonkinensis* exhibit significant antioxidant effects. *Carbohydr Polym.* (2021) 262:117925. doi: 10.1016/j.carbpol.2021.117925
35. Zhang M, Zu H, Zhuang X, Yu Y, Wang Y, Zhao Z, et al. Structural analyses of the HG-type pectin from *Notopterygium incisum* and its effects on galectins. *Int J Biol Macromol.* (2020) 162:1035–43. doi: 10.1016/j.ijbiomac.2020.06.216
36. Dubois M, Gilles KA, Hamilton JK, Rebers PA, Smith F. Colorimetric method for determination of sugars and related substances. *Anal Chem.* (1956) 28:350–6. doi: 10.1021/ac60111a017
37. Yu Y, Wang Y, Liu X, Liu Y, Ji L, Zhou Y, et al. Comparison of analytical methods for determining methyl-esterification and acetylation of pectin. *Appl. Sci Basel.* (2021) 11:4461. doi: 10.3390/app11104461
38. Amicucci MJ, Nandita E, Galermo AG, Castillo JJ, Lebrilla CB, Park D. A nonenzymatic method for cleaving polysaccharides to yield oligosaccharides for structural analysis. *Nat Commun.* (2020) 11:3963. doi: 10.1038/s41467-020-17778-1
39. Daas PJH, Alebeek V, Voragen AGJ, Schols HA. Determination of the distribution of non-esterified galacturonic acid in pectin with endo-polygalacturonase. *Gums Stab Food Ind.* (2000) 26:3–18. doi: 10.1533/9781845698355.1.3
40. Pak U, Yu Y, Ning X, Ho C, Ji L, Mayo KH, et al. Comparative study of water-soluble polysaccharides isolated from leaves and roots of isatis indigotica fort. *Int J Biol Macromol.* (2022) 206:642–52. doi: 10.1016/j.ijbiomac.2022.02.187
41. Bigge JC, Patel TP, Bruce JA, Goulding PN, Charles SM, Parekh RB. Nonselective and efficient fluorescent labeling of glycans using 2-amino benzamide and anthranilic acid. *Anal Biochem.* (1995) 230:229–38. doi: 10.1006/abio.1995.1468

42. Domon B, Costello CE. A systematic nomenclature for carbohydrate fragmentations in FAB-MS/MS spectra of glycoconjugates. *Glycoconjugate J.* (1988) 5:397–409. doi: 10.1007/BF01049915
43. Daas PJH, Voragen AGJ, Schols HA. Characterization of non-esterified galacturonic acid sequences in pectin with endopolygalacturonase. *Carbohydr Res.* (2000) 326:120–9. doi: 10.1016/S0008-6215(00)00037-9
44. Cameron RG, Luzio GA, Goodner K, Williams M. Demethylation of a model homogalacturonan with a salt-independent pectin methylesterase from citrus: I. Effect of pH on demethylated block size, block number and enzyme mode of action. *Carbohydr Polym.* (2008) 71:287–99. doi: 10.1016/j.carbpol.2007.07.007
45. Wu HC, Bulgakov VP, Jinn TL. Pectin methylesterases: cell wall remodeling proteins are required for plant response to heat stress. *Front Plant Sci.* (2018) 9:1612. doi: 10.3389/fpls.2018.01612
46. Ognyanov M, Remoroza C, Schols HA, Georgiev Y, Kratchanova M, Kratchanov C. Isolation and structure elucidation of pectic polysaccharide from rose hip fruits (*Rosa canina* L.). *Carbohydr Polym.* (2016) 151:803–11. doi: 10.1016/j.carbpol.2016.06.031
47. Tanhatan-Nasseri A, Crépeau MJ, Thibault JF, Ralet MC. Isolation and characterization of model homogalacturonans of tailored methyl-esterification patterns. *Carbohydr Polym.* (2011) 86:1236–43. doi: 10.1016/j.carbpol.2011.06.019
48. Jermendi É, Beukema M, Berg MA, de Vos P, Schols HA. Revealing methyl-esterification patterns of pectins by enzymatic fingerprinting: beyond the degree of blockiness. *Carbohydr Polym.* (2022) 277:118813. doi: 10.1016/j.carbpol.2021.118813

Conflict of Interest: The authors declare that the research was conducted in the absence of any commercial or financial relationships that could be construed as a potential conflict of interest.

Publisher's Note: All claims expressed in this article are solely those of the authors and do not necessarily represent those of their affiliated organizations, or those of the publisher, the editors and the reviewers. Any product that may be evaluated in this article, or claim that may be made by its manufacturer, is not guaranteed or endorsed by the publisher.

Copyright © 2022 Yu, Cui, Liu, Wang, Song, Pak, Mayo, Sun and Zhou. This is an open-access article distributed under the terms of the Creative Commons Attribution License (CC BY). The use, distribution or reproduction in other forums is permitted, provided the original author(s) and the copyright owner(s) are credited and that the original publication in this journal is cited, in accordance with accepted academic practice. No use, distribution or reproduction is permitted which does not comply with these terms.

frontiers | Frontiers in Nutrition

ORIGINAL RESEARCH
published: 04 July 2022
doi: 10.3389/fnut.2022.938290

Anti-cancer Potential of Polysaccharide Extracted From *Polygonatum sibiricum* on HepG2 Cells via Cell Cycle Arrest and Apoptosis

Mo Li[1,2†], *Yumeng Liu*[1†], *Henan Zhang*[1], *Yanfeng Liu*[1], *Weiming Wang*[3], *Shengbo You*[4], *Xinyu Hu*[1], *Meijun Song*[1], *Rina Wu*[1*] and *Junrui Wu*[1*]

[1] College of Food Science, Shenyang Agricultural University, Liaoning Engineering Research Center of Food Fermentation Technology, Shenyang Key Laboratory of Microbial Fermentation Technology Innovation, Shenyang, China, [2] College of Criminal Science and Technology, Criminal Investigation Police University of China, Shenyang, China, [3] Heilongjiang Academy of Traditional Chinese Medicine, Harbin, China, [4] Institute of Crop Germplasm Resources, Shandong Academy of Agricultural Sciences, Jinan, China

OPEN ACCESS

Edited by:
Xiaolong Ji,
Zhengzhou University of Light Industry, China

Reviewed by:
Haitian Fang,
Ningxia University, China
Guochuan Jiang,
Jilin Agriculture University, China

***Correspondence:**
Rina Wu
wrn6956@163.com
Junrui Wu
junruiwu@126.com

[†] These authors have contributed equally to this work

Specialty section:
This article was submitted to Food Chemistry, a section of the journal Frontiers in Nutrition

Received: 07 May 2022
Accepted: 23 May 2022
Published: 04 July 2022

Citation:
Li M, Liu Y, Zhang H, Liu Y, Wang W, You S, Hu X, Song M, Wu R and Wu J (2022) Anti-cancer Potential of Polysaccharide Extracted From Polygonatum sibiricum on HepG2 Cells via Cell Cycle Arrest and Apoptosis. Front. Nutr. 9:938290. doi: 10.3389/fnut.2022.938290

Polygonatum sibiricum is one of the most widely used traditional Chinese medicine in China. *Polygonatum sibiricum* polysaccharide (PSP) is the main functional component of *Polygonatum sibiricum*. In this study, a water-soluble polysaccharide (PSP-1) was first isolated from *Polygonatum sibiricum* with a molecular weight of 38.65 kDa. Structural analysis was performed via methylation and FT-IR spectroscopy analyses, which in combination with NMR spectroscopy, revealed that PSP-1 has a → 4-α-D-Glcp-1→ backbone with the substitution at O-6 with the β-D-Glcp-1→ residues. Furthermore, PSP-1 exhibited potent and concentration-dependent anticancer effects, inducing HepG2 cell apoptosis and arresting the cell cycle at the G1 phase. Moreover, PSP-1 also decreased the mitochondrial membrane potential, damaged the nucleus of HepG2 cells, and increased the activity of caspase-9 and−3 in the intrinsic apoptotic pathways to induce HepG2 cell apoptosis. To conclude, PSP-1 might be a good candidate for the treatment of liver cancer, and this work provides important information for understanding the relationship between structure and antitumor activity of PSP-1, which is relevant for the treatment of hepatocellular carcinoma in clinic.

Keywords: *Polygonatum sibiricum* polysaccharide, structural characterization, antitumor activity, HepG2 cells, cell apoptosis

INTRODUCTION

Hepatocellular carcinoma (HCC) is a leading cause of cancer-related mortality worldwide. Traditional methods for the treatment of HCC consist of surgery and medication. However, over 80% of HCC patients are not suited to surgical treatment due to severe liver injury (1). Although medication has an initial therapeutic effect, the long-term use of anti-cancer drugs commonly gives rise to drug resistance, in addition to being associated with various side effects (2). Therefore, the development of highly effective and non-toxic natural compounds is seen as a good alternative for the treatment of liver cancer. In recent years, many studies have shown that natural polysaccharides have significant inhibitory effects on tumors (3–6). Natural polysaccharides have become the main research focus for anti-tumor drugs since they are less toxic and have no side effects in humans.

Polygonatum sibiricum (PS) extracts are associated with many beneficial pharmacological functions and are used widely in treatments against hypercholesterolemia, diabetes, cancer, and inflammatory diseases, among others (7, 8). Of these, polysaccharides play a significant role in PS-based therapeutics (9). The biological activities of polysaccharides are closely related to their complex structure, including their molecular weight, monosaccharide composition, glycosidic linkages, substituents, and degree of branching (10–12). For instance, the high-molecular-weight (>300 kDa) polysaccharides of *Hirsutella sinensis* and *Ganoderma lucidum* are known to play a predominant against obesity (13, 14), while the low-molecular-weight polysaccharides of *Tremella fuciformis* and *Enteromorpha linza* have been shown to exhibit high levels of antioxidant activity (15, 16). Furthermore, polysaccharides with a high uronic acid content have been shown to exert significantly high levels of antioxidant activity (17). Therefore, the identification of the polysaccharide structure is essential to determine the relationship between the structure and biological activities of these molecules.

In few studies, it was revealed that *Polygonatum sibiricum* polysaccharide (PSP) have inhibitory effects on lung cancer and cervical cancer (8, 18). In addition, PSP also has protective effect on liver, which can significantly alleviate the chemical damage of hard storage and prevent the acute heart failure induced by adriamycin which indicate that PSP can act on the liver to resist some diseases (19, 20). Nevertheless, less is known for the anticancerous effects of PSP against HCC and the relationship between structure and antitumor activity. Therefore, there is an urgent need to characterize the structure and antitumor activity of PSP.

In the present study, a water-soluble polysaccharide (PSP-1) was extracted and purified from *Polygonatum sibiricum* using Sephrose DEAE-52 cellulose and Sephadex G-100 HR column chromatography. The structure of PSP-1 was analyzed using High performance liquid chromatography (HPLC), Gas Chromatography and Mass Spectrometry (GC-MS), Fourier-transform infrared spectroscopy (FT-IR), Scanning electron microscopy (SEM), and Nuclear magnetic resonance (NMR) spectroscopy. Furthermore, *in vitro* experiments using human hepatoma HepG2 cells were conducted to assess the effect of PSP-1 on the proliferation, metastasis, and apoptosis of HepG2 cells.

MATERIALS AND METHODS

Materials

Polygonatum sibiricum were purchased from a local market (Shenyang, Liaoning, China). HepG2 cell line was purchased from Stem Cell Bank, Chinese Academy of Sciences. DEAE-52 cellulose and Sephadex G-100 were obtained from Solarbio Co., Ltd (Beijing China). Monosaccharide standards (D-glucose, D-mannose, D-galactose, L-arabinose, D-xylose, L-rhamnose, and D-fucose) were purchased from Shanghai yuanye Bio-Technology Co., Ltd (Shanghai China). Fetal bovine serum (FBS), Dulbecco's Modified Eagle Medium (DMEM), trypsin EDTA, penicillin and streptomycin were obtained from Gibco (Grand Island, NY, USA). Caspase-3 and caspase-9 kit were purchased from KeyGEN Biotechnology Co., Ltd. (Jiangsu, China). All other chemicals were of reagent grade.

Extraction and Purification of PSP

Polygonatum sibiricum was washed and dried at 50°C for 48 h. The dried *Polygonatum sibiricum* was then crushed into a powder using a micronizer and filtered through a 100-mesh sieve. The resulting powder was pretreated with petroleum ether at 25°C for 6 h to remove any fats, followed by extraction using 85% ethanol for 24 h to remove any pigments and small organic compounds. After suction filtration, the filter residue was dried at 50°C and extracted using distilled water (1:20, g/mL) at 90°C for 2 h under continuous stirring. The extraction solution was centrifuged (4,000 rpm, 15 min), and the resulting supernatant was concentrated to an appropriate volume by decompression at 70°C in a rotary evaporator. The supernatant was precipitated with ethanol (1:4, v/v) for 12 h, collected by centrifugation (4,000 rpm, 10 min), and deproteinized using Sevag reagent. The extracts were precipitated again using ethanol (1:4, v/v) for 12 h and centrifuged (4,000 rpm, 10 min). Lastly, the precipitates were dialyzed against water for 48 h (cut-off Mw 8–14 kDa) and lyophilized as crude polysaccharides.

The crude polysaccharides were dissolved in distilled water and loaded onto a DEAE-52 cellulose column (2.6 × 40 cm), and eluted stepwise using NaCl solutions (0, 0.1, 0.2, 0.3, 0.4, and 0.5 M) at a flow rate of 1 mL/min. The sugar elute was collected in tubes (5 min/tube) and then combined under the monitor using the phenol sulfuric acid method. The major fractions were concentrated, dialyzed (cut-off Mw 3,500 Da), and lyophilized. The dried polysaccharides were dissolved for further purification using a Sephadex G-100 gel filtration column (1.6 × 30 cm) at a flow rate of 1 mL/min. The top fractions of the elution peak (5 min/tube) were collected and lyophilized to obtain the purified polysaccharides. The overall procedure used to purify PSP is illustrated schematically in **Figure 1A**. The extraction yield of the polysaccharides was calculated using the following formula:

$$\text{Extraction yield}(\%) = (W_1/W_0) \times 100 \quad (1)$$

where W_1 is the weight of dried crude polysaccharides and W_0 is the weight of dry *Polygonatum sibiricum*.

The PSP-1 with the highest antitumor activity in different purified single-component polysaccharides which was selected by MTT assay (data not provided). In this study, we focused on the research of PSP-1.

Characterization of PSP-1

Chemical Composition Analysis

Contents of total carbohydrates, uronic acid, and protein in PSP-1 were determined by the phenol-sulphuric acid assay (21), m-hydroxydiphenyl assay (22), and coomassie brilliant blue assay (23), respectively.

Monosaccharide Composition Analysis

The monosaccharide composition of PSP-1 was analyzed by high-performance liquid chromatography (HPLC), as described

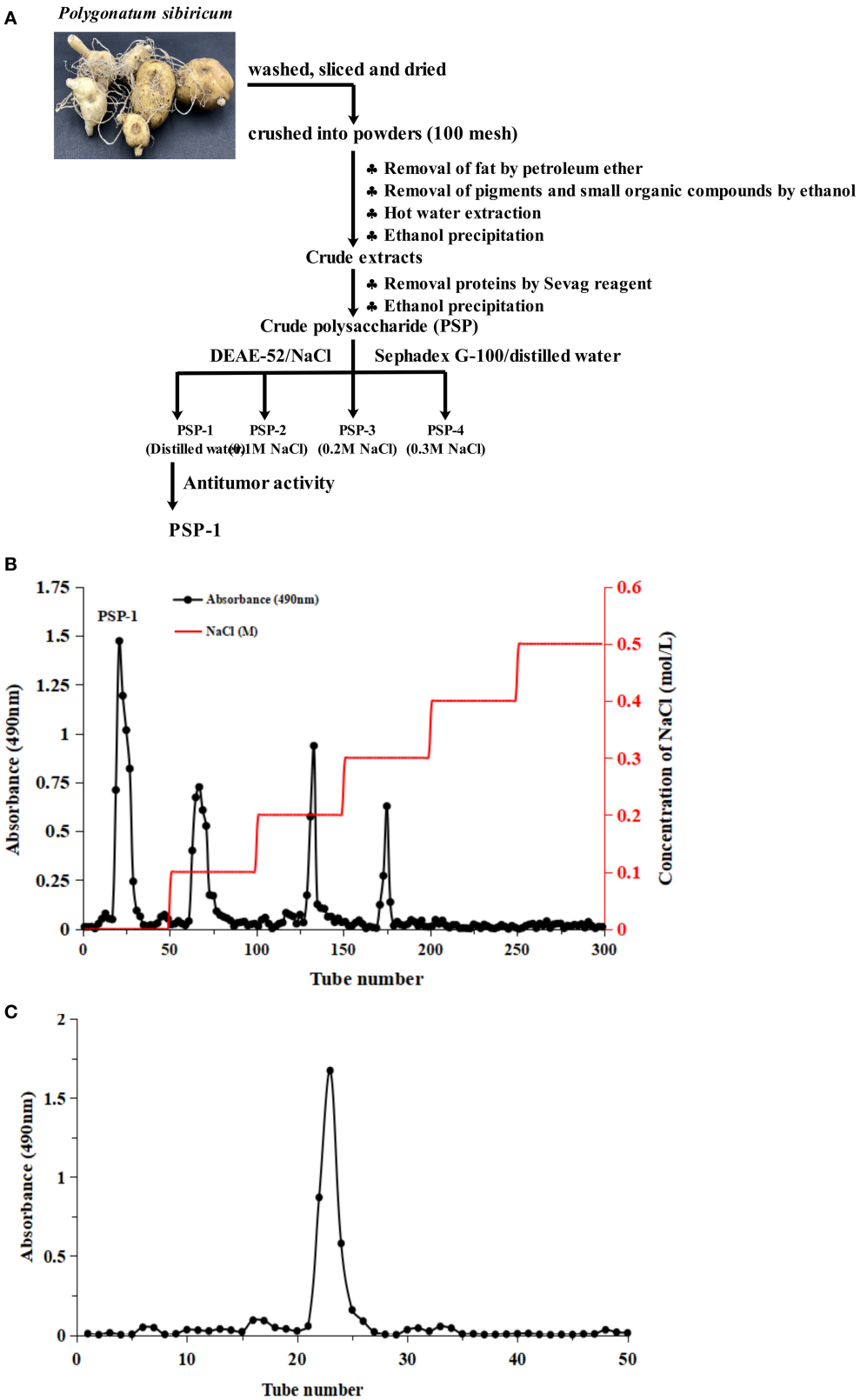

FIGURE 1 | Continued

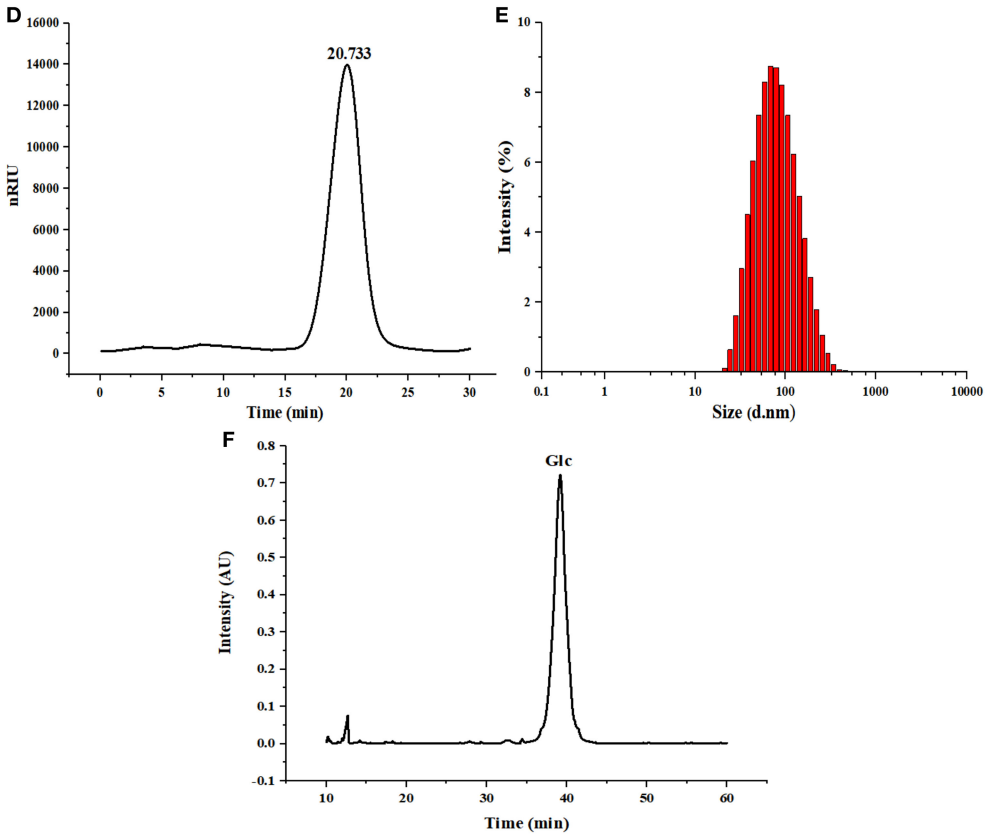

FIGURE 1 | Diagram of extraction process of *Polygonatum sibiricum* polysaccharide fraction 1 (PSP-1) **(A)** Chromatography of PSP-1 by DEAE-52 cellulose column **(B)** and Sephadex G-100 chromatography **(C)** HPGPC chromatograms of PSP-1 **(D)** Particle size distribution of PSP-1 **(E)** Monosaccharide composition of PSP-1 **(F)**.

previously (24) and the detail methods were presented in **Supplementary Method S1**.

Molecular Weight Distribution and Particle Size Analysis

The molecular weight distribution of PSP-1 was determined by HPGPC as described before. The PSP-1 was dissolved in ultrapure water (4.0 mg/mL) and filtered through a 0.45 μm membrane before injection. Then 10 μL sample solution was analyzed by HPGPC-RID.

Particle size distributions of PSP-1 solution (1 mg/mL) were done using A Zetasizer Nano-ZS90 (Malvern, Britain) at 25°C.

Scanning Electron Microscopy (SEM) Analysis

The PSP-1 samples were thinly coated with gold powder and visualized by an SEM system (S4800, Tokyo, Japan).

Fourier Transform Infrared (FI-IR) Analysis

The infrared spectrum of PSP-1 was determined using a FT-IR (Nicolet 6700, Thermo Scientific, USA) within the frequency range of 4,000-400 cm^{-1}.

Methylation Analysis

Methylation analysis of PSP-1 was performed according to a previously described method with some modifications (10) and the specific experimental methods were presented in **Supplementary Method S2**.

Nuclear Magnetic Resonance (NMR) Spectroscopy Analysis

The ^{1}HNMR spectra and ^{13}CNMR spectra of PSP-1 were recorded using a Bruker AV-400 NMR spectrometer (Bruker Instrumental Inc.,Billerica, Massachusetts, USA) at 25°C. Before measurement, the PSP-1 was dissolved with D_2O.

Antitumor Activity of PSP-1

Cell Culture

The HepG2 cells were cultured in DMEM with FBS (10% v/v) and penicillin (1% v/v) in 5% CO_2 humidified atmosphere at 37°C.

Cell Proliferation Assay and Colony Formation Assay

The effect of PSP-1 on HepG2 cell proliferation was assessed using the MTT assay and the detail methods were presented in **Supplementary Method S3**.

Cell Migration Assay

The effect of PSP-1 on tumor cell migration was assessed using a wound-healing assay (25) and the detail methods were presented in **Supplementary Method S4**.

The Morphology of HepG2 After Treatment With PSP-1

Cell suspensions (1 mL) (5×10^5 cells/mL) were inoculated in six-well-plates for 24 h. The culture medium was removed, and 1 mL PSP-1 solution (0, 100, 200, and 400 μg/mL) was added and incubated for 72 h. The supernatant was removed, washed with PBS three times, followed by the addition of acridine orange (AO) and ethidium bromide (EB) double staining kits for staining for 10–15 min. Observation was performed using confocal laser scanning microscopy (CLSM). AO passes through the cell membrane of living cells, chimeric with DNA, and shows green fluorescence under CLSM. EB cannot cross the cell membrane of living cells, but is able to cross the cell membrane of apoptotic cells and show red fluorescence.

The HepG2 cell suspension (1 mL) (5×10^5 cells/mL) was inoculated in six-well-plates for 24 h. The culture medium was removed, and 1 mL of PSP-1 solution (0, 100, 200, and 400 μg/mL) was added and incubated for 72 h. HepG2 cells were then stained with Hoechst 33,342 (1 μg/mL) for 15 min at 37°C. After washing with PBS three times, nuclear morphology was observed under CLSM.

Mitochondrial Membrane Potential (MMP) Level

HepG2 cells were seeded in six-well-microplates and incubated at 37°C for 24 h to allow the cells to adhere. Then, PSP-1 was added and incubated for 72 h. The cells were harvested and washed with PBS, followed by incubation with JC-1 (1 mL) for 20 min at 37°C in the dark. The cells were covered with anti-fluorescence quenching agents after washing and observed by CLSM.

Cell Cycle and Apoptosis Assay

The detail methods of the cell cycle and apoptosis assay were presented in **Supplementary Method S5**

Determination of Apoptosis-Related Enzyme Activity

HepG2 cells were seeded in 6-well-plates. The PSP-1 solution (0, 100, 200, 400 μg/mL) was added. After incubation for 72 h, the cells were washed and lysed by lysis. The caspase-3 and caspase-9 activities were measured according to the guidelines for the caspase-3 and caspase-9 activity assay kits (C1116, C1158; Beyotime Biotechnology).

Statistical Analysis

All experiments were conducted three times. The data were analyzed by SPSS 19.0 statistical software. The experimental results were expressed as mean ± standard deviation. The difference was $p < 0.05$.

RESULTS AND DISCUSSION

Physicochemical Properties and Monosaccharide Composition of PSP-1

PSP-1 was isolated using a DEAE-52 cellulose column and Sephadex G-100 after elution with distilled water. The resulting elution profile is shown in **Figures 1B,C**. The yield of PSP-1 was 3.01 ± 0.29%, based on the dry matter, with a total carbohydrate, protein and uronic acid content of 93.63 ± 1.81%, 0.44 ± 0.06%, and 0.98 ± 0.21%, respectively. The molecular weight of PSP-1 was measured by HPGPC using dextran as a standard, as shown in **Figure 1D**, which indicated that PSP-1 was a homogeneous polysaccharide. Based on the calibration curve ($y = -0.2959x + 10.722$, $R^2 = 0.9926$), the molecular weight of PSP-1 was determined to be 38.65 kDa. In a previous study, Zhang et al. isolated a polysaccharide PS-WNP from *Polygonatum sibiricum* and determined its molecular weight to be 76 kDa (15). Wang et al. reported that a novel polysaccharide (PSP3) with the molecular weight of 7.743 kDa was isolated and purified from *Polygonatum sibiricum* (7). Different molecular weight distributions indicate that there are significant differences among polysaccharides (24, 26). In the present study, the molecular weight of PSP-1 was found to differ from other reported polysaccharides from *Polygonatum sibiricum*. Several studies have shown that the molecular weight of polysaccharides is closely related to their antitumor activity (10, 27).

The size distribution of PSP-1 in aqueous solution (**Figure 1E**) revealed a symmetrical narrow peak at approximately 101.3 nm. The polydispersity index of PSP-1 (0.276), which measures the uniformity of the particle size distribution of a polymer, indicated that PSP-1 was a homogenous polysaccharide.

The monosaccharide composition of PSP-1 was analyzed using HPLC. As shown in **Figure 1F**, PSP-1 was composed of glucose.

Structure of PSP-1

SEM Analysis of PSP-1

The microstructure of PSP-1 was determined by SEM at a magnifications of 5.00× and 10.00×, as shown in **Figures 2A,B**. PSP-1 exhibited a smooth and porous surfaces consisting of flake-like lamellae. Seen from the image at 1,000× augmentation, a flake layer with unregular curls was observed in polygahatous polysaccharides. Representative Glc-rich natural polysaccharides show the aforementioned lamellar structure (28). The apparent structure of polysaccharides is closely related to the solubility and water absorption of polysaccharides (29). In addition, polysaccharides with an even and smooth sheet-like structure have better antitumor activity (25).

FT-IR Analysis

Infrared spectroscopy is commonly used to identify the primary structure of polysaccharides (30). The infrared absorption spectrum of PSP-1 is shown in **Figure 2C**. The sample was found to have a broad and strong absorption peak at 3416.16 cm^{-1}, indicating that there is O-H group stretching vibration. The absorption band at 2925.22 cm^{-1} indicates that there is an asymmetric CH_2 stretching vibration (31). The peaks were

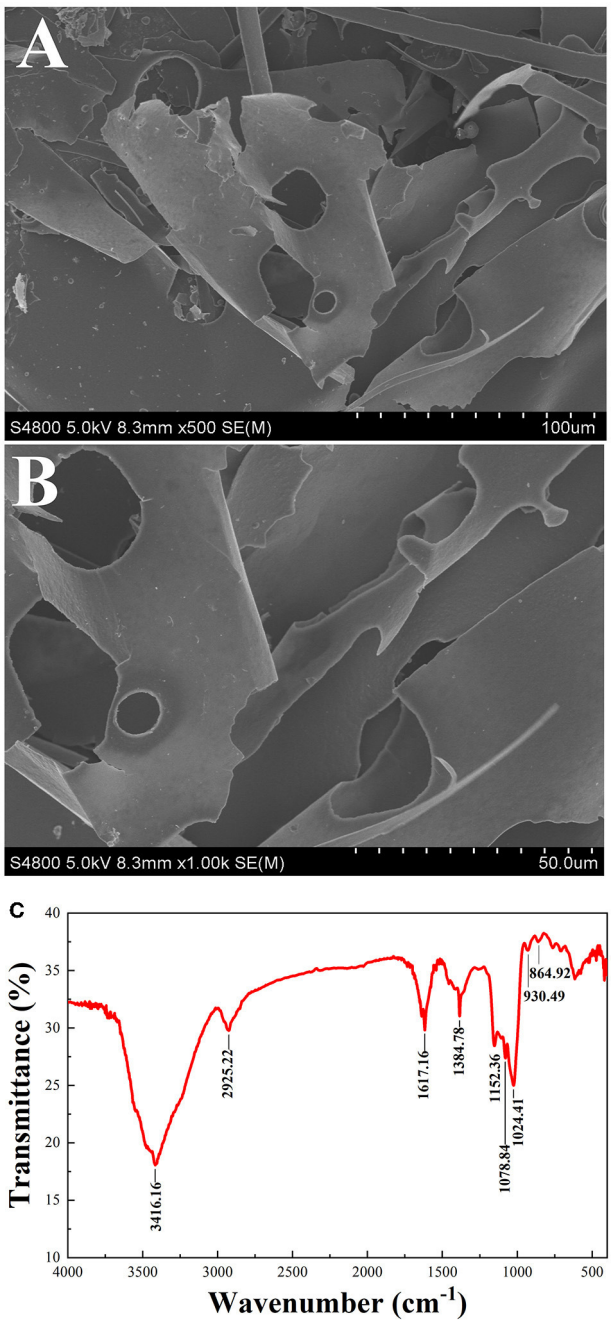

FIGURE 2 | SEM (500× 1,000×) of PSP-1 **(A,B)** FT-IR spectra of PSP-1 in the range of 4,000–400 cm^{-1} **(C)**.

observed at 1617.16 cm^{-1} and 1384.78 cm^{-1} may be due to the symmetrical stretching vibration of COO- (32). The three absorption peaks observed at 1152.36, 1078.84, and 1024.41 cm^{-1} indicate the presence of pyran rings in the PSP-1. The characteristic absorption bands at 930.49 cm^{-1} and 864.92 cm^{-1} indicated that PSP-1 contained α- and β-anomeric units (24, 26, 33). These results confirmed that PSP-1 showed typical polysaccharide absorption peaks.

Methylation Analysis of PSP-1

PSP-1 was methylated, depolymerized, and analyzed by GC–MS to determine the linkage patterns of the sugar units (**Table 1**), indicating the presence of two components named 2,3,6-Me_3-Glcp, 2,3,4,6-Me_3-Glcp and 2,3-Me_2-Glcp were shown in **Table 1**. These compounds are in a ratio of 79.18: 10.32: 10.50. Based on their comparison with mass spectrum patterns from the literature (34–36), and the standard data, the linkages of Glc were deduced to be →4)-α-D-Glcp-(1→, D-Glcp-(1→ and →4,6)-α-D-Glcp-(1→, respectively.

NMR Spectrum of PSP-1

The ^{1}H and ^{13}C NMR spectra of PSP-1 are shown in **Figures 3A,B**. The entire assignment shifts of ^{1}H and ^{13}C NMR for PSP-1 were identified with reference to the previous literatures (35, 37–39) and illustrated in **Table 2**. The anomeric proton signals (5.33, 4.89, and 4.46 ppm) and the anomeric carbon signals (99.6, 97.9, and 102.9 ppm) corresponded to H-1 and C-1 of →4)-α-D-Glc*p*-(1→, →4,6)-α-D-Glc*p*-(1→, and β-D-Glc*p*-(1→. The NMR results were consistent with the results of monosaccharide composition and methylation analysis.

Combining all the results from monosaccharide composition analysis, the methylation analysis, and the NMR spectroscopy, the structure of PSP-1 was a water-soluble polysaccharide mainly composed of →4)-α-D-Glcp-(1→, →4,6)-α-D-Glcp-(1→ and β-D-Glcp-(1→ groups. Among them, the content of →4)-α-D-Glcp-(1→was the highest. These findings suggest that the main chain of the polysaccharide is→4)-α-D-Glcp-(1→, while the branch chain was β-D-Glcp-(1→ and linked at the C6-position of →4,6)-α-D-Glcp-(1→.

Antitumor Activity of PSP-1

Inhibitory Effect of PSP-1 on HepG2 Cells

To evaluate the effects of PSP-1 on the proliferation of HepG2 cells, HepG2 cells were treated with PSP-1 or vehicle and analyzed by MTT and colony formation assays. The results of the MTT assay indicated that the proliferation of HepG2 cells treated with PSP-1 was significantly inhibited compared to the control ($P < 0.05$) (**Figure 4A**). The MTT results further confirmed that HepG2 cells were more susceptible to PSP-1 at a dose of 72 h.

In the colony formation assay, HepG2 cells treated with different concentrations of PSP-1 (100, 200, and 400 μg/mL) formed fewer colonies than the untreated control group, a phenomenon that was concentration-dependent (**Figures 4B,C**). The results indicate the inhibitory effect of PSP-1 on the clonogenic ability of HepG2 cells.

Effect of PSP-1 on Cell Migration

Wound healing assays are commonly used to evaluate tumor cell invasiveness and migration. As shown in **Figure 4D**, PSP-1 was found to inhibit the wound healing of HepG2 cells in a time-dependent manner. The scratch closure change in **Figure 4E** indicates that PSP-1 can significantly prevent wound healing. At a PSP-1 concentration of 0, 100, 200, and 400 μg/mL, after 72 h, the rate of scratch closure change of PSP-1 was 63.64, 47.83, 30.43, and 25.00%, respectively. These

TABLE 1 | Glycosyl linkages analysis of PSP-1.

Numbers	Characteristic fragments (m/z)	Methylated sugar	Molar ratio (%)	Linkage type	References
1	43, 45, 57, 85, 87, 99, 101, 113, 117, 161, 173, 233	2,3,6-Me_3-Glcp	79.18	→4)-Glcp-(1→	Gou et al. (34)
2	59, 71, 87, 102, 118, 129,145, 162,175, 205	2,3,4,6-Me_3-Glcp	10.32	D-Glcp-(1→	Zeng et al. (35)
3	57, 85, 99, 101, 117, 127, 161, 201, 261	2,3-Me_2-Glcp	10.50	→4,6)-Glcp-(1→	Zhang et al. (36)

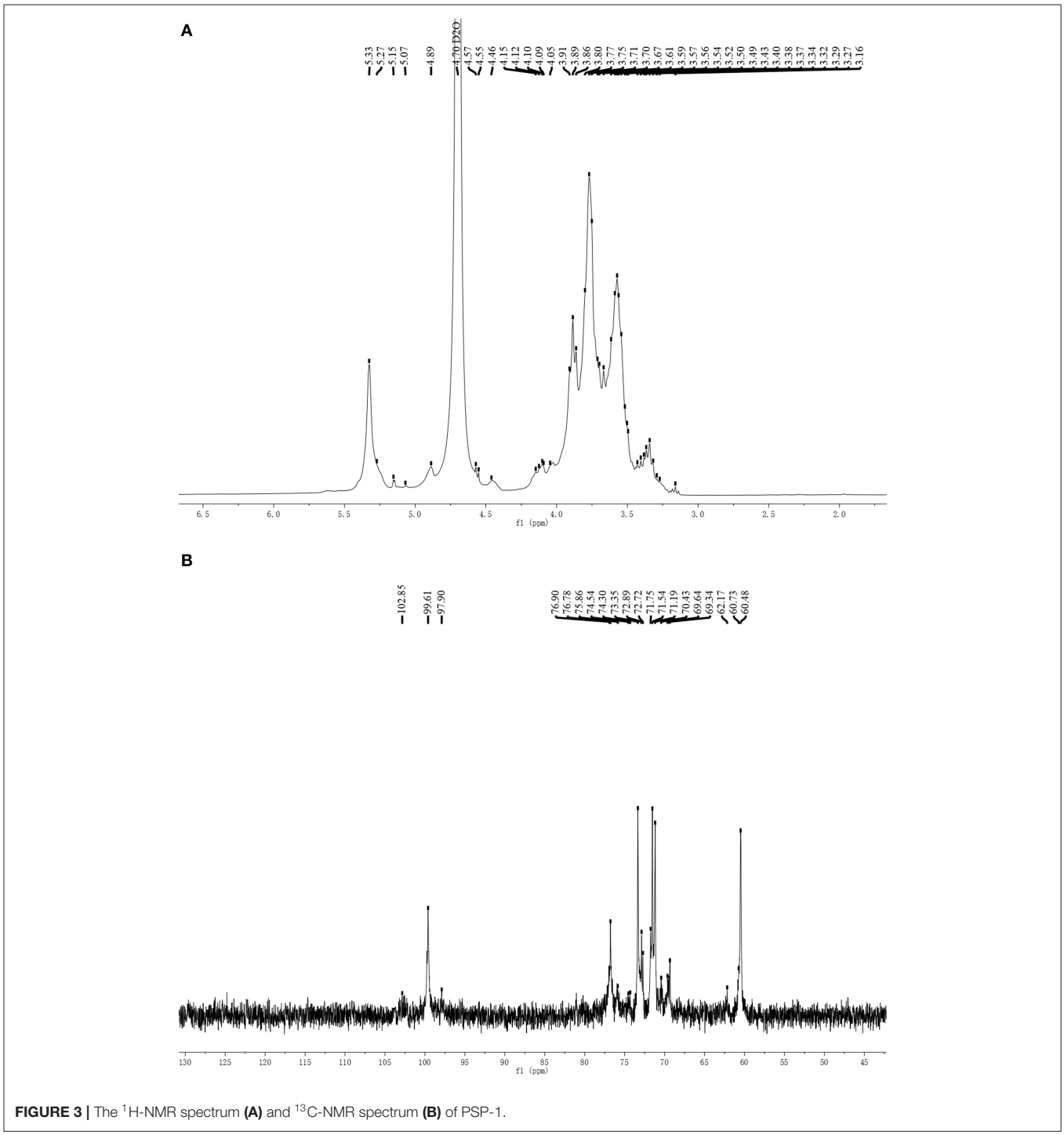

FIGURE 3 | The ^{1}H-NMR spectrum **(A)** and ^{13}C-NMR spectrum **(B)** of PSP-1.

TABLE 2 | ^{13}C and ^{1} H NMR chemical shifts (ppm, δ) for PSP-1.

Sample	H-1/C-1	H-2/C-2	H-3/C-3	H-4/C-4	H-5/C-5	H-6/C-6	Reference
→4)-α-D-Glcp-(1→	5.33/99.6	3.56/71.5	3.91/73.3	3.59/76.8	3.78/71.2	3.77/60.5	Ghosh et al. (37)
β-D-Glcp-(1→	4.46/102.9	3.34/72.9	3.40/75.9	3.37/69.3	3.67/76.9	3.76/60.7	Agrawal (38); Ghosh et al. (37)
→4,6)-α-D-Glcp-(1→	4.89/97.9	3.49/71.2	3.16/71.5	3.67/76.8	3.89/70.4	4.02/69.4	Shi et al. (39)

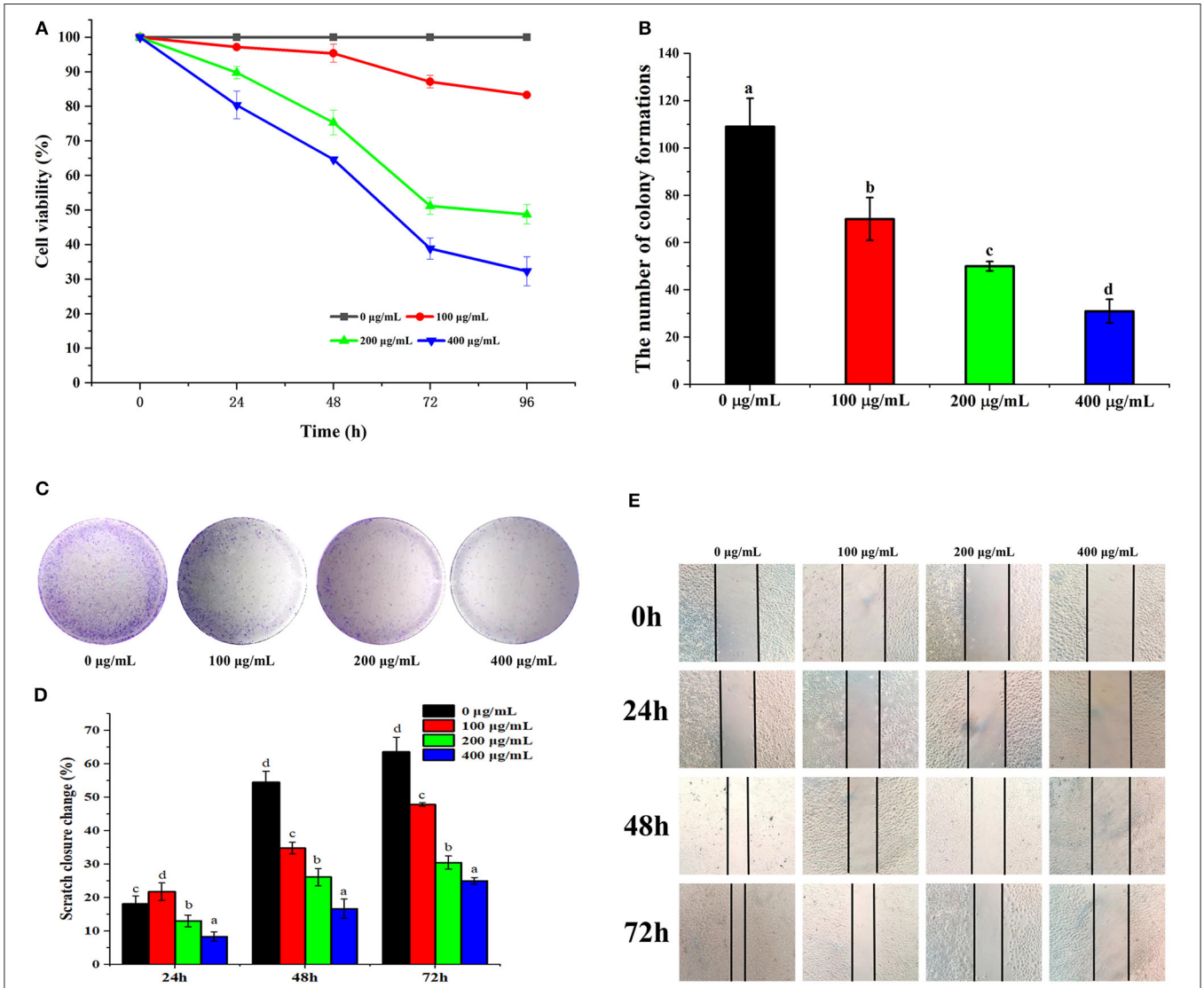

FIGURE 4 | PSP-1 inhibits HepG2 cells proliferation *in vitro*. HepG2 cells were treated with different concentration (0, 100, 200, 400 μg/mL) of PSP-1 for 0, 24, 48, 72, and 96 h. The effect of PSP-1 on cell proliferation was evaluated by MTT assay. **(A)** The clonogenicity of the indicated cells were detected after treatment with different concentration of PSP-1. **(B,C)** Scratch image and scratch closure change of HepG2 cells after treatment with different concentration of PSP-1 **(D,E)**. Data are presented as the mean ± SD, $n = 3$. Different letters above the bars indicate significant difference.

results indicate that PSP-1 is able to inhibit the migration of HepG2 cells.

Effect of PSP-1 on Cell Morphology

The apoptosis of HepG2 cells after treatment with PSP-1 was observed using LSCM (**Figure 5A1**). There was almost no apoptosis of HepG2 cells in the control group under LSCM. Compared to the HepG2 cells in the control group, the number of living HepG2 cells decreased and the number of apoptotic cells increased significantly after 72 h of incubation with an increasing PSP-1 concentration. The number of apoptotic cells was the highest at a concentration of PSP-1

of 400 μg/mL. These results indicated that SPS-1 exerted a significant inhibitory effect on the growth and proliferation of HepG2 cells, with an apoptosis effect that was concentration-dependent.

Hochest 33342 staining was used to observe the PSP-1-induced apoptotic nucleus of HepG2 cells. After Hoechst 33342 staining was performed on HepG2 cells incubated with different concentrations of PSP-1 for 72 h, the nuclei morphology of HepG2 cells were detected using LSCM. The results showed that HepG2 cells treated with PSP-1 exhibited nuclear apoptotic morphologies, such as condensed chromatin, nuclear pyknosis, and apoptotic bodies (**Figure 5A2**), but no evidence of abnormal nuclear morphology was present in the control group, which displayed intact nuclei. These results suggested that PSP-1 might induce HepG2 cell apoptosis by damaging its nucleus.

Determination of Mitochondrial Membrane Potential (MMP, $\Delta\psi m$)

Tetrechloro-tetraethylbenzimidazol carbocyanine iodide (JC-1) is a fluorescent probe that is widely used to detect the mitochondrial membrane potential (MMP, $\Delta\psi m$). When MMP is high, JC-1 aggregates in the matrix of mitochondria to form J-aggregates, which produce red fluorescence. When the mitochondrial membrane potential is low, JC-1 does not gather in the matrix of mitochondria and exists in monomer form, which generates green fluorescence. Therefore, changes in mitochondrial membrane potential were detected by changes in fluorescence color. The decrease in mitochondrial membrane potential is a landmark event in the early stages of apoptosis. Changes in the membrane potential of HepG2 cells treated with different concentrations of PSP-1 for 72 h are shown in **Figure 5B**. In the absence of PSP-1, HepG2 cells had intact membranes and exhibited uniform red fluorescence. However, as the concentration of PSP-1 increased, a decrease in red fluorescence and an increase in green fluorescence were observed, indicating that the mitochondrial membrane potential of HepG2 cells decreased significantly in a concentration-dependent manner after PSP-1 treatment. When J-aggregates and monomers merged, the cells emitted yellow-green fluorescence, indicating cell apoptosis and even necrosis. Taken together, the results of merged staining indicated that PSP-1 induces apoptosis in cancer cells.

Effect of PSP-1 on Cell Cycle and Apoptosis

Cell cycle analysis showed that the cell percentage markedly increased in the G1 phase and declined in the S phase after 72 h of PSP-1 treatment compared with the vehicle group (**Figure 5C**). At a PSP-1 concentration of 400 μg/mL, PSP-1 significantly increased the portion of HepG2 cells in G1 phase from 41.44 to 74.15% and significantly decreased the portion of HepG2 cells in S phase from 46.56 to 22.22% for HepG2 cells. These results suggested that PSP-1 could induce HepG2 cell cycle arrest in G1 phase.

Next, we measured the effect of PSP-1 on apoptosis in HepG2 cells. The cells were treated with different concentrations of PSP-1 for 72 h, and the apoptosis rate was analyzed by flow cytometry. The results showed that the rate of apoptosis in HepG2 cells was significantly higher in the PSP-1 group than in the vehicle group in a concentration-dependent manner (**Figure 5D**). At a PSP-1 concentration of 400 μg/mL, the cell population of total apoptotic cells increased from 17.4 to 53.6% in HepG2 cells. These results indicate that PSP-1 significantly inhibited proliferation and induced the apoptosis of HepG2 cells in *vitro*.

TABLE 3 | Caspase-3 and caspase-9 activity of HepG2 cell after PSP-1 treatment.

Sample	Caspase-3 ($\times 10^6$ U/mg prot)	Caspase-9 ($\times 10^6$ U/mg prot)
Control	8.92 ± 0.86^a	8.17 ± 0.83^a
100 μg/mL	10.87 ± 0.96^b	10.54 ± 0.72^b
200 μg/mL	12.62 ± 0.36^{bc}	12.46 ± 0.75^c
400 μg/mL	14.22 ± 1.46^c	13.57 ± 0.29^c

Data were shown as means ± S.D (n = 3). Numbers followed by different letters are significantly different at the level of $p < 0.05$ according to the Duncan test.

PSP-1 Activated Caspase-3 and-9

A molecular hallmark of apoptosis is the activation of caspases, which are a family of intracellular aspartate-specific cysteine proteases that execute cell death through proteolytic cleavage in the induction of apoptosis (40). To determine whether caspase activation contributes to PSP-1-induced apoptosis, the activities of initiator caspase (caspase-9) and effector caspase (caspase-3) were assessed using colorimetric assay kits after the treatment of HepG2 cells with PSP-1 (0, 100, 200, and 400 μg/mL) for 72 h. The results showed a concentration-dependent increase in the activities of caspase-9 and−3 in the PSP-1-treated cells (**Table 3**), suggesting the simultaneous involvement of the intrinsic apoptotic pathways in PSP-1-induced apoptosis in HepG2 cells. The polysaccharides from *Artemisia annua* L. (Huang Huahao) also showed a similar mechanism of inducing apoptosis in HepG2 cells (40).

The antitumor activity of polysaccharides is strongly attributed to their structural features, including their microstructure, monosaccharide composition, Mw, glycosidic linkages, and triple-helix conformation (25, 27, 41). Previous studies have reported that polysaccharides with a smooth lamellar structure exhibit high levels of antitumor activity, which made the active site of action of polysaccharides fully exposed and contributed to its anti-tumor activity (25). Moreover, polysaccharides with lower molecular weights have been found to exhibit stronger binding to receptors on the surface of immune cells due to the occurrence of cross-link receptors, which show higher tumor inhibition due to stronger immune responses (41, 42). The polysaccharide with $\rightarrow$ 4)-α-D-Glcp-(1$\rightarrow$ structure has high levels of immunoregulatory activity (43), and the rank of glycogen is closely related to its biological activity. Highly branched glycogen is more conducive to antitumor and immunomodulatory activities (44). In this study, the low Mw

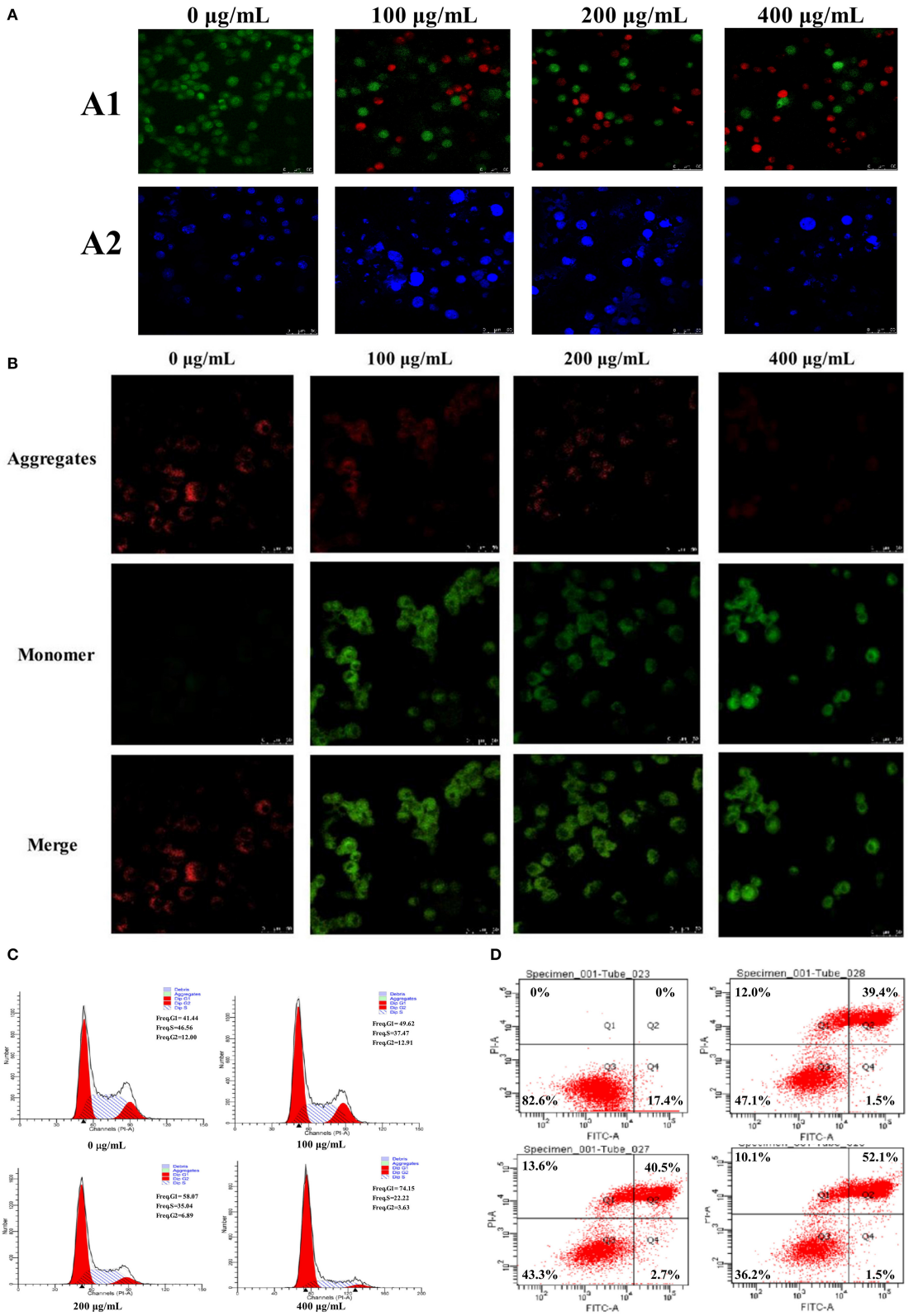

FIGURE 5 | The morphological changes of HepG2 cells treated with 0, 100, 200, and 400 μg/mL of PSP-1 for 72 h **(A)**, the morphological characterization of HepG2 cells was observed and photographed under a Confocal laser scanning microscope **(A1)**, nuclear morphological changes induced by PSP-1 in HepG2 cells after DAPI staining. **(A2)** Effect of PSP-1 on MMP **(B)** Cell cycle progression was assessed using propidium iodide staining detected by fluorescence activated cell sorting. **(C)** The apoptotic rates of the indicated cells induced by PSP-1 at different concentrations for 72 h were detected by ANNexin V/PI double-staining asssy **(D)**.

and the smooth lamellar structure in PSP-1 may be the main factors contributing to its antitumor activity.

CONCLUSIONS

In this study, a water-soluble polysaccharide (PSP-1) was obtained from *Polygonatum sibiricum*. The molecular weight of PSP-1 was approximately 38.65 kDa with a particle size of approximately 101.3 nm. The results of monosaccharide analysis, methylation analysis, and NMR indicated that PSP-1 is mainly composed of → 4)-α-D-Glcp-(1→, → 4,6)-α-D-Glcp-(1→ and β-D-Glcp-(1→ groups, which has a backbone consisting of a → 4)-α-D-Glcp-(1→ backbone with the substitution at O-6 with the β-D-Glcp-(1→ residues. PSP-1 was found to exert potential anti-hepatocellular activity *in vitro*, which could cause nuclear damage and decrease the mitochondrial membrane potential of HepG2 cells. Moreover, PSP-1 was found to significantly inhibit the proliferation and induce the apoptosis of HepG2 cells *in vitro*, increasing the activity of caspase-9 and -3 in the intrinsic apoptotic pathways to induce apoptosis in HepG2 cells. Taken together, our results clearly indicate that PSP-1 shows potential as an antitumor agent. Meanwhile, further research is needed to explore more antitumor mechanisms *in vitro* and *vivo*.

DATA AVAILABILITY STATEMENT

The original contributions presented in the study are included in the article/**Supplementary Material**, further inquiries can be directed to the corresponding author/s.

AUTHOR CONTRIBUTIONS

ML and YuL: investigation, data curation, methodology, formal analysis, writing—original draft, and software. HZ, YaL, WW, and SY: methodology, formal analysis, and writing—review and editing. XH and MS: data curation, validation, software, investigation, data curation, software, and investigation. RW: supervision, funding acquisition, and project administration. JW: conceptualization, supervision, project administration, writing review and editing.

FUNDING

This work was supported by the Joint project of National Natural Science Foundation of China [Grant No. U20A20400]. The Liaoning Provincial Natural Science Foundation regional joint fund project [2020-MZLH-34]. Shenyang young and middle-aged science and technology innovation Leading Talents Project [RC200495]. Guiding Plan of Natural Science Foundation of Liaoning Province [2019-ZD-0714] is revised to Shenyang Science and technology innovation platform project [21-103-0-14, 21-104-0-28].

SUPPLEMENTARY MATERIAL

The Supplementary Material for this article can be found online at: https://www.frontiersin.org/articles/10.3389/fnut.2022.938290/full#supplementary-material

REFERENCES

1. Li W, Wang J, Chen Z, Gao X, Chen Y, Xue Z, et al. Physicochemical properties of polysaccharides from Lentinus edodes under high pressure cooking treatment and its enhanced anticancer effects. *Int. J. Biol. Macromol.* (2018) 115:994–1001. doi: 10.1016/j.ijbiomac.2018.04.094
2. Iwamoto T. Clinical application of drug delivery systems in cancer chemotherapy: review of the effificacy and side effects of approved drugs. *Biol Pharm Bull.* (2013) 36:715–8. doi: 10.1248/bpb.b12-01102
3. Zhang Z, Zhang Y, Liu H, Wang J, Wang D, Deng Z, et al. water-soluble selenium-enriched polysaccharide produced by Pleurotus ostreatus: Purifification, characterization, antioxidant and antitumor activities in vitro. *Int J Biol Macromol.* (2021) 168:356–70. doi: 10.1016/j.ijbiomac.2020.12.070
4. Wu J, Yan D, Liu Y, Luo X, Li Y, Cao C, et al. Purification, structural characteristics, and biological activities of exopolysaccharide isolated from leuconostoc mesenteroides SN-8. *Front Microbiol.* (2021) 12:644226. doi: 10.3389/fmicb.2021.644226
5. Feng Y, Zhang J, Wen C, Dzah C, Juliet I, Duan Y, Zhang H. Recent advances in Agaricus bisporus polysaccharides: Extraction, purification, physicochemical characterization and bioactivities. *Process Biochem*. (2020) 94:39–50. doi: 10.1016/j.procbio.2020.04.010
6. Ji X, Guo J, Pan F, Kuang F, Chen H, Guo X, Liu Y. Structural elucidation and antioxidant activities of a neutral polysaccharide from Arecanut (*Areca catechu L*). *Front Nutr.* (2022) 9:853115. doi: 10.3389/fnut.2022.853115
7. Wang Y, Liu N, Xue X, Li Q, Sun D, Zhao Z. Purification, structural characterization and in vivo immunoregulatory activity of a novel polysaccharide from *Polygonatum sibiricum*. *Int J Biol Macromol.* (2020) 160:688–94. doi: 10.1016/j.ijbiomac.2020.05.245
8. Long T, Liu Z, Shang J, Zhou X, Yu S, Tian H, et al. *Polygonatum sibiricum* polysaccharides play anti-cancer effect through TLR4-MAPK/NF-κB signaling pathways. *Int J Biol Macromol.* (2018) 111:813–21. doi: 10.1016/j.ijbiomac.2018.01.070
9. Zhu X, Li Q, Lu F, Wang H, Yan S, Wang Q, et al. Antiatherosclerotic potential of Rhizoma Polygonati polysaccharide in hyperlipidemia-induced atherosclerotic hamsters. *Drug Res.* (2015) 65:479–83. doi: 10.1055/s-0034-1387756
10. Wu Q, Luo M, Yao X, Yu L. Purification, structural characterization, and antioxidant activity of the COP-W1 polysaccharide from Codonopsis tangshen Oliv. *CarbohydPolym.* (2020) 236:116020. doi: 10.1016/j.carbpol.2020.116020
11. Ren Y, Zheng G, You L, Wen L, Li C, Fu X, et al. Structural characterization and macrophage immunomodulatory activity of a polysaccharide isolated from Gracilaria lemaneiformis. *J Funct Foods.* (2017) 33:286–96. doi: 10.1016/j.jff.2017.03.062
12. Ji X, Guo J, Ding D, Gao J, Hao L, Guo X, et al. Structural characterization and antioxidant activity of a novel high-molecular-weight polysaccharide from Ziziphus Jujuba cv. *Muzao J Food Meas Charact.* (2022). doi: 10.1007/s11694-022-01288-3
13. Wu TR, Lin CS, Chang CJ, Lin TL, Martel J, Ko YF, et al. Gut commensal Parabacteroides goldsteinii plays a predominant role in the anti-obesity effects of polysaccharides isolated from *Hirsutella sinensis*. *Gut.* (2018) 68:248–62. doi: 10.1136/gutjnl-2017-315458
14. Chang CJ, Lin CS, Lu CC, Martel J, Ko YF, Ojcius DM, et al. *Ganoderma lucidum* reduces obesity in mice by modulating the composition of the gut microbiota. *Nat Commun.* (2017) 6:7489. doi: 10.1038/ncomms16130

15. Zhang H, Cao Y, Chen L, Wang J, Tian Q, Wang N, et al. A polysaccharide from *Polygonatum sibiricum* attenuates amyloid-β-induced neurotoxicity in PC12 cells. *Carbohyd Polym*. (2015) 117:879–86. doi: 10.1016/j.carbpol.2014.10.034
16. Zhang Z, Wang X, Mo X, Qi H. Degradation and the antioxidant activity of polysaccharide from *Enteromorpha linza*. *Carbohyd. Polym*. (2013) 92:96. doi: 10.1016/j.carbpol.2012.11.096
17. Liu Y, Zhang B, Ibrahim SA, Gao SS, Yang H, Huang W. Purification, characterization and antioxidant activity of polysaccharides from Flammulina velutipes residue. *Carbohyd. Polym*. (2016) 145:71–7. doi: 10.1016/j.carbpol.2016.03.020
18. Li L, Thakur K, Cao YY, Liao BY, Zhang JG, Wei ZJ. Anticancerous potential of polysaccharides sequentially extracted from Polygonatum cyrtonema Hua in Human cervical cancer Hela cells. *Int J Biol Macromol*. (2020) 148:843–50. doi: 10.1016/j.ijbiomac.2020.01.223
19. Cui X, Wang S, Cao H, Guo H, Li Y, Xu F, et al. A review: the bioactivities and pharmacological applications of *Polygonatum sibiricum* polysaccharides. *Molecules*. (2018) 23:1170–5. doi: 10.3390/molecules23051170
20. Zhu X, Wu W, Chen X, Yang F, Zhang J, Hou J. Protective effects of Polygonatum sibiricum polysaccharide on acute heart failure in rats. *Acta Cir Bras*. (2018) 33:868–78. doi: 10.1590/s0102-865020180100000001
21. Wang D, Zhao Y, Jiao Y, Yu L, Yang S, Yang X. Antioxidative and hepatoprotective effects of the polysaccharides from Zizyphus jujube cv. *Shaanbeitanzao CarbohydPolym*. (2012) 88:1453–9. doi: 10.1016/j.carbpol.2012.02.046
22. Filisetti-Cozzi TM, Carpita NC. Measurement of uronic acids without interference from neutral sugars. *Anal Biochem*. (1991) 197:157–62. doi: 10.1016/0003-2697(91)90372-Z
23. Blumenkrantz N, Asboe-Hansen G. New method for quantitative determination of uronic acids. *Academic Press*. (1973) 54:484–9. doi: 10.1016/0003-2697(73)90377-1
24. Li M, Ma F, Li R, Ren G, Yan D, Zhang H, et al. Degradation of tremella fuciformis polysaccharide by a combined ultrasound and hydrogen peroxide treatment: process parameters, structural characteristics, and antioxidant activities. *Int J Biol Macromol*. (2020)160: 979–90. doi: 10.1016/j.ijbiomac.2020.05.216
25. Li Y, Qin G, Chen C, Yuan B, Huang D, Cheng S, et al. Purification, characterization and anti-tumor activities of polysaccharides from Ecklonia Kurome obtained by three different extraction methods. *Int J Biol Macromol*. (2019) 150:1000–10. doi: 10.1016/j.ijbiomac.2019.10.216
26. Dong XD, Feng YY, Liu YN, Ji HY, Yu J. A novel polysaccharide from *Castanea mollissima Blume*: Preparation, characteristics and antitumor activities in vitro and in vivo. *Carbohyd. Polym*. (2020) 240:116323. doi: 10.1016/j.carbpol.2020.116323
27. Ji X, Cheng Y, Tian J, Zhang S, Jing Y, Shi M. Structural characterization of polysaccharide from jujube (Ziziphus jujuba Mill) fruit. *Chem Biol Technol Ag*. (2021) 8:54. doi: 10.1186/s40538-021-00255-2
28. Cheng X, Shi S, Su J, Xu Y, Ordaz-Ortiz JJ, Li N, et al. Structural characterization of a heteropolysaccharide from fruit of Chaenomelese speciosa (Sweet) Nakai and its antitumor activity. *Carbohyd Polym*. (2020) 236:116065. doi: 10.1016/j.carbpol.2020.116065
29. Bertoft E. Tetlow IJ. Understanding starch structure: recent progress. *Agronomy*. (2017) 7:7030056. doi: 10.3390/agronomy 7030056
30. Chen Z, Zhao Y, Zhang M, Yang X, Yue P, Tang D, et al. Structural characterization and antioxidant activity of a new polysaccharide from *Bletilla striata* fibrous roots. *CarbohydPolym*. (2020) 227:115362. doi: 10.1016/j.carbpol.2019.115362
31. Chen Y, Zhang H, Wang Y, Nie S, Li C, Xie M. Acetylation and carboxymethylation of the polysaccharide from Ganoderma atrum and their antioxidant and immunomodulating activities. *Food Chem*. (2014) 156:279–88. doi: 10.1016/j.foodchem.2014.01.111
32. Liu Y, Liu Y, Mu D, Yang H, Feng Y, Ji R, et al. Preparation, structural characterization and bioactivities of polysaccharides from mulberry (Mori Fructus). *Food Biosci*. (2022) 46:101604. doi: 10.1016/j.fbio.2022.101604
33. Manhivi VE, Venter S, Amonsou EO, Kudanga T. Composition, thermal and rheological properties of polysaccharides from amadumbe (*Colocasia esculenta*) and cactus (*Opuntia spp.*). *Carbohyd Polym*. (2018) 195:163–9. doi: 10.1016/j.carbpol.2018.04.062
34. Gou Y, Sun J, Liu J, Chen H, Jin C. Structural characterization of a water-soluble purple sweet potato polysaccharide and its effect on intestinal inflammation in mice. *J Funct Foods*. (2019) 61:103502. doi: 10.1016/j.jff.2019.103502
35. Zeng F, Chen W, He P, Zhan Q, Wang Q, Wu H, et al. Structural characterization of polysaccharides with potential antioxidant and immunomodulatory activities from Chinese water chestnut peels. *Carbohyd Polym*. (2020) 246:116551. doi: 10.1016/j.carbpol.2020.116551
36. Zhang WN, Su RN, Gong LL, Yang WW, Chen J, Yang R, et al. Structural characterization and in vitro hypoglycemic activity of a glucan from *Euryale ferox Salisb. Seeds CarbohydPolym*. (2019) 209:363–71. doi: 10.1016/j.ijbiomac.2019.01.158
37. Ghosh K, Chandra K, Ojha AK, Islam SS, NMR. and MALDI-TOF analysis of a water-soluble glucan from an edible mushroom, Volvariella diplasia. *CarbohydRes*. (2008) 343:2834–40. doi: 10.1016/j.carres.2008.05.011
38. Agrawal PK, NMR. spectroscopy in the structural elucidation of oligosaccharides and glycosides. *Phytochemistry*. (1991) 31:3307–30. doi: 10.1016/0031-9422 (92)83678-R
39. Shi H, Bi S, Li H, Li J, Li C, Yu R, et al. Purification and characterization of a novel mixed-linkage α,β-D-glucan from Arca subcrenata and its immunoregulatory activity. *Int J Biol Macromol*. (2021) 182:207–16. doi: 10.1016/j.ijbiomac.2021.03.196
40. Yan L, Xiong C, Xu P, Zhu J, Yang Z, Ren H, et al. Structural characterization and in vitro antitumor activity of A polysaccharide from Artemisia annua L. *(Huang Huahao) Carbohyd Polym*. (2019) 213:361–9. doi: 10.1016/j.carbpol.2019.02.081
41. Zheng X, Lu F, Xu X, Zhang L. Extended chain conformation of b-glucan and its effect on antitumor activity. *J Mater Chem B*. (2017) 5:5623. doi: 10.1039/C7TB01324H
42. Ping Z, Xu H, Liu T, Huang J, Meng Y, Xu X, et al. Anti-hepatoma activity of the stiff branched β-d-glucan and effects of molecular weight. *J Mater Chem B*. (2016) 4:1299. doi: 10.1039/C6TB01299J
43. Li R, Chen W, Wang W, Tian W, Zhang X. Extraction, characterization of Astragalus polysaccharides and its immune modulating activities in rats with gastric cancer. *CarbohydPolym*. (2009) 78:738–42. doi: 10.1016/j.carbpol.2009.06.005
44. Gong Y, Cao C, Ai C, Wen C, Wang L, Zhao J, et al. Structural characterization and immunostimulatory activity of a glucan from Cyclina sinensis. *Int J Biol Macromol*. (2020) 161:779–86. doi: 10.1016/j.ijbiomac.2020.06.020

Conflict of Interest: The authors declare tha the research was conducted in the absence of any commercial or financial relationships that could be construed as a potential conflict of interest.

Publisher's Note: All claims expressed in this article are solely those of the authors and do not necessarily represent those of their affiliated organizations, or those of the publisher, the editors and the reviewers. Any product that may be evaluated in this article, or claim that may be made by its manufacturer, is not guaranteed or endorsed by the publisher.

Copyright © 2022 Li, Liu, Zhang, Liu, Wang, You, Hu, Song, Wu and Wu. This is an open-access article distributed under the terms of the Creative Commons Attribution License (CC BY). The use, distribution or reproduction in other forums is permitted, provided the original author(s) and the copyright owner(s) are credited and that the original publication in this journal is cited, in accordance with accepted academic practice. No use, distribution or reproduction is permitted which does not comply with these terms.

frontiers | Frontiers in Nutrition

ORIGINAL RESEARCH
published: 07 July 2022
doi: 10.3389/fnut.2022.945804

Preparation and Structure Characterization of High-Value *Laminaria digitata* Oligosaccharides

Kit-Leong Cheong[1,2], *Jia-Kang Li*[1,2] *and Saiyi Zhong*[1]*

[1] Guangdong Provincial Key Laboratory of Aquatic Product Processing and Safety, College of Food Science and Technology, Guangdong Ocean University, Zhanjiang, China, [2] Department of Biology, College of Science, Shantou University, Shantou, China

Algae-derived marine oligosaccharides have been reported to be promising bioactive compounds because of their various properties with health benefits and potential significance in numerous applications in industrial biotechnology. In this study, laminaran oligosaccharides (LOs) with varying degrees of polymerization were obtained through partial acid hydrolysis of laminaran derived from *Laminaria digitata*. Based on response surface methodology, the optimum LOs yield was obtained for acid hydrolysis laminaran at a hydrolysis time of 55 min, temperature of 71°C, and acid concentration of 1.00 mol/L. The size-exclusion resin Bio-Gel P-2 was considered to be a better option for LOs purification. The structure of the purified oligosaccharides was analyzed through mass spectrometry and nuclear magnetic resonance. They demonstrated the main oligosaccharide structure corresponding to the connection of glucose with β-D-Glc*p*-(1→3)-β-D-Glc*p*, which was identified as laminaribiose (DP2), laminaritriose (DP3), laminaritetrose (DP4), and laminaripentaose (DP5). LOs demonstrate excellent antioxidant activities, as evidenced from their reactions with oxidizing free radicals, 1, 1-diphenyl-2-picryl-hydrazyl, and 2, 2′-azino-bis (3-etilbenzotiazoline-6-sulfonic acid) radicals. LOs exhibited a prebiotic effect on the growth of *Bifidobacterium adolescentis* and *Lactobacillus plantarum*. Therefore, we propose the development of LOs as natural antioxidants and prebiotics in the functional food and pharmaceutical industries.

Keywords: laminaran, oligosaccharide, *Laminaria digitata*, size exclusion chromatography, biological activity

OPEN ACCESS

Edited by:
Qiu Li,
Qingdao Agricultural University, China

Reviewed by:
Yujiao Sun,
Shaanxi University of Science and Technology, China
Xiao-Jia Chen,
University of Macau, China

***Correspondence:**
Saiyi Zhong
zhongsy@gdou.edu.cn

Specialty section:
This article was submitted to Food Chemistry, a section of the journal Frontiers in Nutrition

Received: *16 May 2022*
Accepted: *06 June 2022*
Published: *07 July 2022*

Citation:
Cheong K-L, Li J-K and Zhong S (2022) Preparation and Structure Characterization of High-Value Laminaria digitata Oligosaccharides. Front. Nutr. 9:945804. doi: 10.3389/fnut.2022.945804

INTRODUCTION

Marine algae, an important component of the coastal marine ecosystem, are a good source of phenolic compounds, carotenoids, vitamins, minerals, peptides, proteins, and polysaccharides (1, 2). *Laminaria digitata* is a large brown alga in the family Laminariaceae that is extensively cultivated in China, where it is traditionally used for human consumption because of its excellent taste and nutritional value. It is an important and commercially valuable resource for food, animal fodder, and pharmaceuticals (3). *L. digitata* is rich in polysaccharides known as laminaran, which has garnered increasing attention from scientists. This macromolecule has been demonstrated to have potential to improve human health and impart various biological functions such as antitumor, anticoagulant, antiallergic, antiviral, antitumor, and antibacterial properties (4, 5).

Laminaran is a β-glucan with a backbone of β-1, 3-glycosidic linkages and is branched with small amounts of β-1, 6-glycosidic linkages. In general, the bioactivity of laminaran is closely

correlated to its molecular weight, linkage type, degree of branching, and content. Laminaran with large molecular weight and size are usually poorly soluble, and it is difficult to span the membranes to exert their biological effects (6). Laminaran oligosaccharides (LOs) are known to have a low molecular weight with a degree of polymerization (DP) in the range of 2–10, and in recent years, they have garnered increasing interest because of their potential biological activities. Choi et al. reported that laminaran was degraded by gamma irradiation to produce low-molecular-weight laminaran, which exhibited better 2, 2-diphenyl-1-picrylhydrazyl (DPPH) radical-scavenging activity and protection of lipid peroxidation compared to laminaran (7). Wu reported that oligosaccharides derived from *L. japonica* exhibited high hydroxyl radical scavenging activity (91.31%) at a concentration of 100 μg/mL (8). Antioxidant activity is an important physiological role of functional foods. Consumption of antioxidants helps scavenge free radicals in human biological systems and could reduce the incidences of chronic diseases such as heart disease and cancer (9). Purified oligosaccharides can be identified more accurately by assessing their activities and demonstrating their pharmacological mechanism (10). However, the biological activities of LOs have been investigated with the crude LOs fraction in recent studies, whereas purified LOs have seldom been performed. Further studies are required to clarify the antioxidant activity of purified LOs.

The production of marine algae oligosaccharides through hydrolysis generally requires the extraction of polysaccharides from marine algae, followed by depolymerization. The degradation products prepared by different methods differed in the structures. Enzymatic method is highly specific for oligosaccharide production but the relatively high costs of enzyme production, which makes them unfavorable from an economic point of view. Chemical methods for the preparation of marine algae oligosaccharides are considered useful and widely used because they are relatively simple, inexpensive, and controllable (11). The mixture of LOs derived from chemical methods needs to be further purified because the purity of oligosaccharides is also important for the potentiation of their physiological effects and to obtain a marketable product. Purification of LOs with varying DP remains a challenge because of their high polarity and laborious procedures for obtaining high-purity oligosaccharides. Thus far, there have been only a few reports on the preparation and purification of LOs. However, pure LOs are necessary for quantification analysis and clarification of their related biological activity mechanisms for the development of marine functional food, drugs, and related products (12). Therefore, it is important to develop a high-resolution, automated, and simple procedure for the preparation and purification of LOs. Fast protein liquid chromatography (FPLC) is generally applied only for protein and peptide purification because it only has an ultraviolet detector. Because oligosaccharides do not absorb ultraviolet light, auto-peak collection may be difficult (13). Traditionally, colorimetric assays have been used for offline detection of oligosaccharide fractions (14). However, they have several drawbacks such as being laborious, slow, and consuming large amounts of hazardous reagents. Recently, FPLC coupled with the refractive index detection (RID) method has been successfully applied in the separation and purification of oligosaccharides, and has been proven to be highly automated with a high resolution (15).

In this study, LOs were produced from *L. digitata* polysaccharides through partial acid hydrolysis. LOs with varying DPs were purified by an FPLC system coupled with a refractive index detector, which is usually used to detect carbohydrates and fulfill the automated collection of the oligosaccharide fraction. The effects of DP on antioxidant properties, including DPPH and ABTS radical scavenging activities, and the prebiotic activities of the purified LOs were investigated.

MATERIALS AND METHODS

Materials and Chemicals

Sephadex G-10 and Sephadex LH-20 were purchased from GE Healthcare (Uppsala, Sweden). Bio-gel P-2 extra fine was purchased from the Bio-Rad company (California, United States). HPLC-grade acetonitrile and trifluoroacetic acid (TFA) were purchased from Aladdin Chemical Co. (Shanghai, China). The DPPH and ABTS were acquired from Sigma-Aldrich. The *Bifidobacterium adolescentis* and *Lactobacillus plantarum* were purchased from China Center of Industrial Cultural Collection. All other chemicals and reagents were of analytical grade.

Preparation of Laminaran

The dried *L. digitata* was homogenized in a blender. The powder was first extracted with methanol/ dichloromethane/ water (4:2:1; *v/v/v*) to remove small molecular weight compounds, color matter, and lipids (16). The laminaran was obtained according to previous report with minor modifications (17). The residue was collected by centrifugation at 4,000 × g for 10 min. After dried in an oven at 50 °C until a constant weight, the residue was extracted with hot water in a ratio of 1:40 (*w/v*, g/mL) at 90°C for 2 h. After cooling to room temperature, the aqueous extract was filtrated and then added three times volume of 95% (*v/v*) ethanol, and the precipitated was collected through centrifugation (3,500 × g, 10 min). The pellet was re-dissolved in hot water and left overnight 4°C, the supernatant thus obtained was centrifuged to remove the insoluble matter. Subsequently, the supernatant was then mixed with aqueous calcium chloride (2%, *w/v*) and centrifuged at 3,500 × g for 10 min. The precipitates dissolve in water and dialysis (molecular weight cut-off 500 Da) against water. Further purification involved the separation of fractions loaded on to solid phase extraction cartridges (Thermo Fisher Scientific, HyperSep Silica, silica bed 500 mg). Fractions were collected and lyophilized.

Controlled Acid Hydrolysis of Laminaran

LOs were produced from laminaran by partial acid hydrolysis. In this study, response surface methodology (RSM) was used to optimize and investigate the influence of independent variables on the preparation of LOs from laminaran. Experiments were established based on a Box–Behnken Design (BBD) with three

factors and three levels. The BBD design consisted of 17 experimental points, 5 replicates at the center of the design were used to allow for estimation of a pure error sum of squares. The partial acid hydrolysis of laminaran conditions include hydrolysis time (X_1, 45–80 min), temperature for hydrolysis (X_2, 60–80°C), and TFA concentration (X_3, 0.75–1.25 mol/L). After partial acid hydrolysis, the reactant was immediately cooled in an ice bath to room temperature. The yield of LOs (include DP 2–5, mg/mL) was determined using high performance liquid chromatography and fitted to a quadratic polynomial model as follows formula:

$$Y = \beta_0 + \sum \beta_i X_i + \sum \beta_{ii} X_i^2 + \sum \beta_{ij} X_i X_j$$

where, Y is the predicted response (LOs yield mg/mL) associated with each factor level combination, β_0, β_i, β_{ii}, and β_{ij} are the regression coefficients for intercept, linear, quadratic, and interaction terms, respectively; X_i and X_j are the independent variables.

The statistical analyses of data were carried out using BBD to establish the mathematical model, interpret the interaction and estimate the response of the independent variables. Experimental data were analyzed to fit a second-order polynomial model. The models were predicted through statistical analysis and regression analysis (ANOVA) using Design Expert V8. This software was also used to obtain the coefficients of the quadratic polynomial model. The quality of the fitted model was expressed by the coefficient of determination R^2, and its statistical significance was checked with an *F*-test.

High Performance Liquid Chromatography Analysis of Laminaran Oligosaccharides

High performance liquid chromatography (HPLC) analysis was carried out in an Alltech 1200 HPLC system (Alltech, United States) equipped with a LT-II evaporative light scattering detector (ELSD, Shimadzu Corporation, Japan). The analysis of sample was evaluated on a NH_2 column (250 × 4.6 mm i.d., 5 μm). The column temperature was maintained at 35°C The eluent solutions were water (A) and acetonitrile (B) with a gradient solution of 75% B at 0–5 min, 75–55% B at 5–20 min, 55–40% B at 20–35 min, and 40% B at 35–40 min. The flow rate was 0.5 mL/min and the injection volume was 20 μL. ELSD conditions were as follows: temperature of drift tube was 50°C, the value of gain was 4, and the flow rate of nitrogen gas was 2 mL/min.

Fast Protein Liquid Chromatography Purification of Laminaran Oligosaccharides

LOs were separated and purified by FPLC using a modified method as described previously (15). FPLC analysis was carried on an Akta FPLC system (AKTA Pure, GE Healthcare, Uppsala, Sweden) coupled with a refractive index detector (Agilent Technologies, Palo Alto, CA, United States). The LOs (0.5 g) were dissolved in distilled water (1 mL), and filtered using a 0.45 μm membrane before injected into the GE Healthcare column XK 16/100 packed with Sephadex LH-20. The LOs with different fractions were eluted with water at a flow rate of 0.5 mL/min. The collection volume was 3 mL per tube. The liquid corresponded to a single peak was collected for further analysis. The rest were concentrated and further purified using Bio-Gel P-2 extra fine.

Electron Spray Ionization-Mass Spectrometry

The molecular masses of purified oligosaccharide with different degree of polymerization were measured using a Thermo TSQ Endura liquid chromatograph–mass spectrometer system (LC–MS system, Thermo Fisher Scientific, United States). Ionization was carried out using electrospray ionization (ESI) with a positive ion mode. The ionization mode was performed using the following conditions: temperature 300°C, source voltage 3.5 kV, drying gas N_2 of 0.7 L/min, nebulizer pressure 25 psi, isolation width 4, fragment amplification 1.5, and masses scanned from 50 to 2,000 *m/z*. Before ESI-MS analysis, samples were prepared as previously described method (18). In brief, freeze-dried samples (10 mg) were submersed in 1 mL of acetonitrile/water solution (5%, *v/v*), and filtered through a 0.45 μ m membrane.

Nuclear Magnetic Resonance Analyses

Each purified oligosaccharide sample (50 mg) with different degree of polymerization was loaded into nuclear magnetic tube and dissolved in D_2O at room temperature. The ^1H spectrum and ^{13}C nuclear magnetic resonance (NMR) spectrum were recorded on a Bruker AVANCE 500 spectrometer (Bruker BioSpin Corporation, Billerica, MA, United States).

Antioxidant Activities of Laminaran Oligosaccharides

The DPPH radical scavenging activity of LOs was investigated by a previous method with slight modification (19). In brief, 100 μL different concentrations (0.1–2.0 mg/mL) of LOs were added to 100 μL of 50 mmol/L DPPH in ethanol. Then the mixture was shaken and incubated in dark place for 30 min, and the value of absorbance was measured at 517 nm. Ascorbic acid was used as a positive control. The ability of DPPH scavenging was calculated using the following equation:

$$\text{DPPH scavenging activity (\%)} = [1 - (A_i - A_j)/A_0] \times 100\%$$

Where A_0 was the absorbance of blank (ethanol instead of sample), A_i was the absorbance of sample (sample with DPPH-methanol solution), A_j was the absorbance of control (sample without DPPH-methanol solution).

The potential of LOs in scavenging ABTS radicals was evaluated as described earlier with some adjustments (20). Briefly, ABTS radical solution was prepared as follows: 7 mmol/L of ABTS solution (5 mL) was incubated with 2.45 mmol/L of potassium persulfate (88 μL) at room temperature for 16 h. Next, 2 mL ABTS radical solution were added into LOs samples (1 mL) with various concentrations (0.0625, 0.125, 0.25, 0.5, 1, and 2 mg/mL), respectively. After rection at room temperature

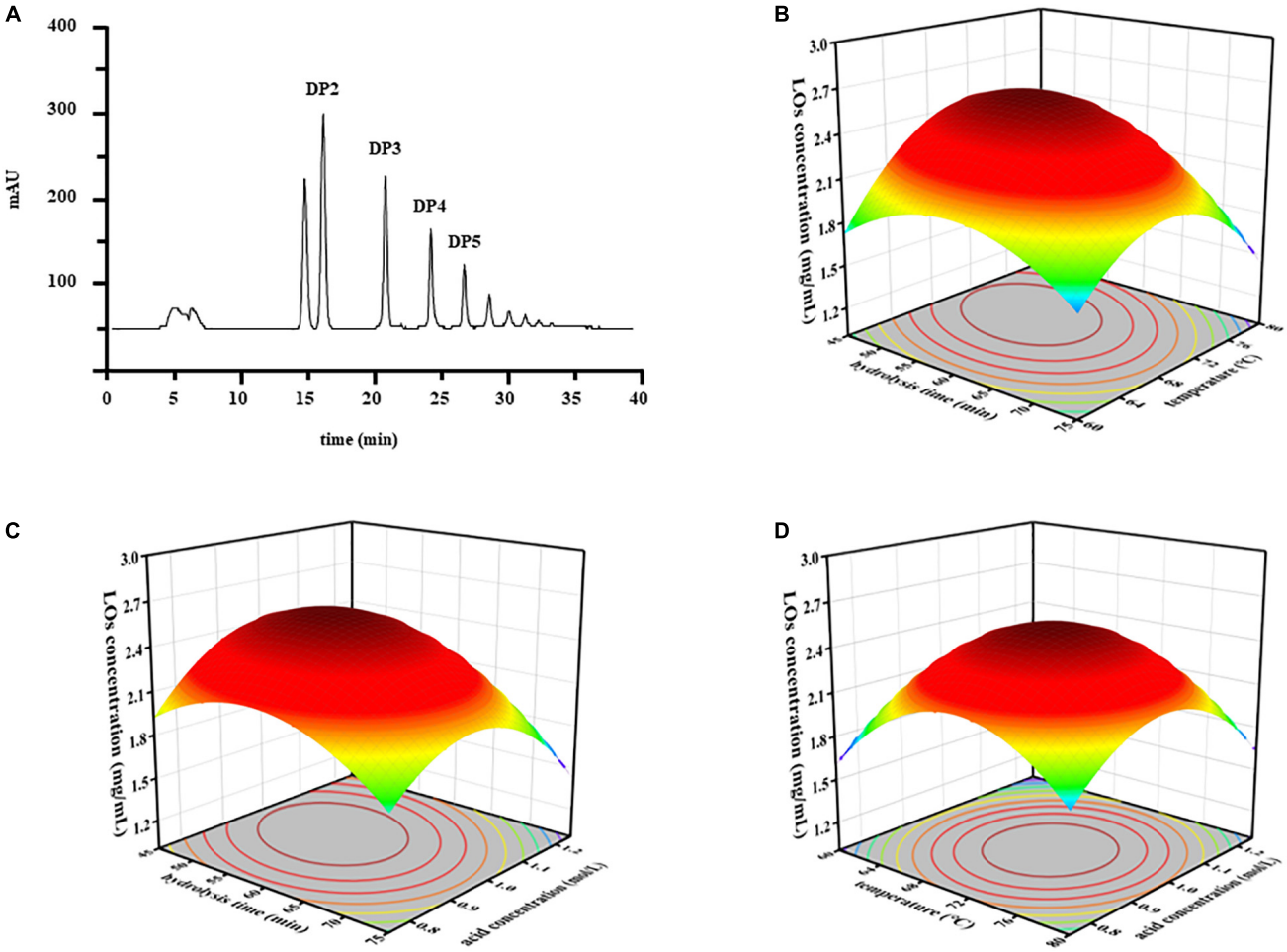

FIGURE 1 | (A) The chromatograms of LOs separated by HPLC-ELSD. The response surface plots of the interaction effects of independent variables on the LOs production. **(B)** Hydrolysis time and temperature; **(C)** hydrolysis time and acid concentration; **(D)** temperature and acid concentration.

(in dark place) for 10 min, the value of absorbance was measured at 734 nm. Ascorbic acid was used as the positive control. The ABTS radical scavenging activity (%) was calculated as DPPH radical scavenging activity equation above.

Prebiotic Effect of Laminaran Oligosaccharides

The prebiotic effect of the LOs on *Bifidobacterium adolescentis* and *Lactobacillus plantarum* were carried in batch cultures according to previous study with minor modification (21). Tubes containing the basal MRS medium were supplemented with LOs, inoculated with *B. adolescentis* and *L. plantarum*, and incubated at 37°C for 48 h under anaerobic conditions. For comparative purposes, additional experiments were performed with media containing fructo-oligosaccharide (FOS) as positive control. The growth of each strain was monitored by measuring the optical density (OD) of the cultures at 600 nm. The OD_{600} values (expressed as mean ± *SD*, $n = 3$) were measured using a spectrophotometer.

RESULTS AND DISCUSSION

Optimization of Hydrolysis Conditions

Response surface methodology (RSM) is an effective collection of statistical analysis methods that can be used to optimize different environmental processes and evaluate the effects of multiple variables, which helps reduce the process parameters with a minimum number of experiments. The yield of LOs was determined by HPLC-ELSD (**Figure 1A**). ANOVA was used to examine the significant variables and fitness of the regression model. The BBD results are listed in **Table 1**. Based on these results, the model *P*-value (possibility) was < 0.0001, indicating that the model was significant for responses in partial hydrolysis yield. The model *F*-value of 127.53 implies that there is only a 0.01% chance of occurrence owing to noise. The *P*-value of the lack-of-fit and *F*-value were 0.059 and 0.9787, respectively, which demonstrated that the lack-of-fit was insignificantly relative to the pure error and confirmed the validity of the model. Furthermore, the regression model exhibits a high degree of correlation between the experimental and predicted values. The

TABLE 1 | The box Behnken design with three independent variables, include hydrolysis time, temperature, and acid concentration for the LOs production.

Hydrolysis time (min)	Temperature (°C)	Acid concentration (mol/L)	LOs concentration (mg/mL)
45	60	1.00	1.72
75	60	1.00	1.65
45	80	1.00	2.20
75	80	1.00	1.43
45	70	0.75	1.91
75	70	0.75	1.75
45	70	1.25	2.05
75	70	1.25	1.43
60	60	0.75	1.61
60	80	0.75	1.76
60	60	1.25	1.56
60	80	1.25	1.62
60	70	1.00	2.55
60	70	1.00	2.62
60	70	1.00	2.57
60	70	1.00	2.56
60	70	1.00	2.44

coefficients of determination R^2 and adjusted R^2 were 0.9939 and 0.9861, respectively, whereas a relatively low coefficient of variation (2.60%) indicated better precision and reliability of the experiments.

The quadratic equation model estimated by observed data was as follows: LOs yield (mg/mL) = $2.55 - 0.20\ X_1 + 0.059\ X_2 - 0.046\ X_3 - 0.18\ X_1X_2 - 0.12\ X_1X_3 - 0.022\ X_2X_3 - 0.33\ {X_1}^2 - 0.47\ {X_2}^2 - 0.44\ {X_3}^2$, where X_1, X_2, and X_3 denote hydrolysis time, temperature, and acid concentration, respectively. To determine the optimum levels of each variable for maximum yield of LOs, RSM plots were constructed using two independent variables. The relationships between LOs production and the three different variables (hydrolysis time X_1, temperature X_2, and acid concentration X_3) using RSM are shown in **Figures 1B–D**. Based on the results, the predicted optimum yield of LOs (2.59 mg/mL) was computed as hydrolysis time of 54.84 min, temperature of 71.26 °C, and acid concentration of 1.00 mol/L. Considering the error from the actual operation, the experiment was conducted under these modified optimal conditions: hydrolysis time of 55 min, temperature of 71°C, and acid concentration of 1.00 mol/L, and LOs were obtained in a yield of 2.59 mg/mL. The controlled acid hydrolysis of laminaran seems to be the best choice for LOs production on a large scale because of its simplicity, affordability, and reproducibility.

Selection of Size-Exclusion Chromatography Resins for Purification

FPLC is a form of preparative liquid chromatography that is often used to purify mixtures of proteins. It has advantages of high resolution, high automation (including auto sampler and peak collection), gradient program control, and availability of stationary phases in most common chromatography modes. Although the method was originally developed for purification of proteins, it has also been widely applied in separation and purification of other kinds of samples, such as RNA, oligonucleotides, polysaccharides, oligosaccharides. An appropriate size-exclusion chromatography (SEC) resin is the key parameter for obtaining high-purity oligosaccharides with varying DPs. Generally, Sephadex G-10, Sephadex LH-20, and Bio-Gel P-2 are commercially available and are used for the separation of carbohydrates with molecular weights in the range of 150–2,000 Da. Sephadex G-10 and LH-20 are beaded gel filtration media prepared by cross-linking dextran, which has been reported to yield excellent separation results for hyaluronan oligosaccharides (22) and arabinoxylan oligosaccharides (23), respectively. Kumar et al. separated fructo-oligosaccharides from onions using Bio-Gel P-2 (24). Therefore, the performance of these three different SEC resins (Sephadex G-10, Sephadex LH-20, and Bio-Gel P-2) for the purification of LOs from crude oligosaccharides was investigated and compared, and Bio-Gel P-2 was screened as a favorable resin. Enrichment of purified DP 2–5 from crude LOs exhibited excellent purification performance using Bio-Gel P-2.

Identification of Laminaran Oligosaccharides

Mass spectrometry has been proven to be a sensitive, fast, and effective technique for analyzing the structure of oligosaccharides. This technique can provide detailed oligosaccharide structure information, such as molecular weight, monosaccharide composition, linkages, fragment patterns, and location of chemical modifications of the oligosaccharides (25, 26). Purified LOs were subjected to ESI-MS analysis. **Figure 2** shows the ESI-MS profiles of the purified LOs. In the spectrum, peaks were observed that showed the $[M + Na]^+$ ions at *m/z* 365.1 (**Figure 2A**), *m/z* 527.1 (**Figure 2B**), *m/z* 689.2 (**Figure 2C**), and *m/z* 851.2 (**Figure 2D**), corresponding to DP 2, DP 3, DP 4, and DP 5 lamirabiose-derived oligosaccharides, respectively. A similar mass spectra result was reported by Yang et al., with the hydrolysis products of laminaritriose plus Na at m/z 527 and laminaritetraose plus Na at m/z 689 (27).

Structural information at the molecular level is directly related to the chemical structural properties and biological interaction modes. The structural aspects of the purified LOs were assessed using ^{1}H NMR and ^{13}C NMR spectroscopy. NMR is one of the most effective non-destructive methods. This method is commonly used for the structural analysis of oligosaccharides. NMR data provide information about the oligosaccharide structure, including the monosaccharide composition, presence of α-type or β-type carbohydrates, linkage features, and sequences of the monosaccharide units (28).

The NMR spectra of the purified LOs are shown in **Figure 3** and the chemical shifts of ^{1}H and ^{13}C signals are summarized in **Table 2**. The anomeric proton of non-reducing D-glucopyranosyl chemical shift at 4.60 ppm and anomeric carbon chemical shift is at 102.8 ppm, which denoted its β-anomeric form. The chemical

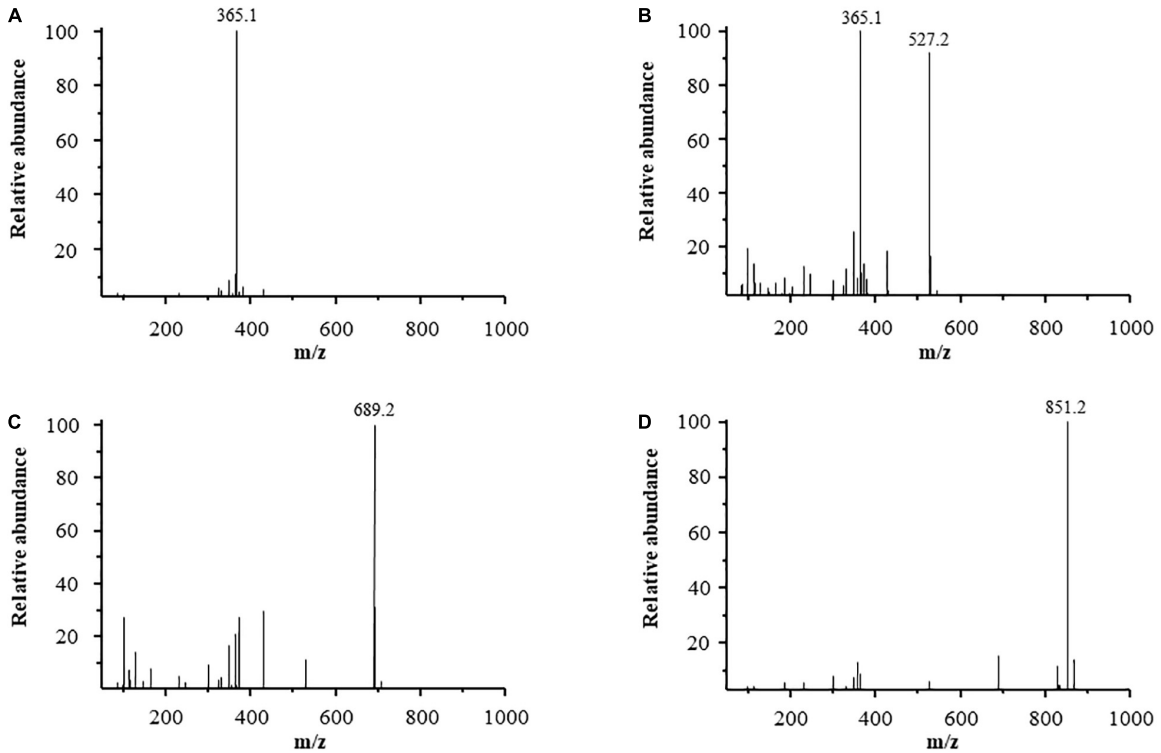

FIGURE 2 | ESI-MS of purified LOS, **(A)** laminaribiose, **(B)** laminaritriose, **(C)** laminaritetrose, **(D)** laminaripentaose.

shifts at 4.69 ppm were assigned to the H-1 and C-1 protons and signals of 1→3-linked-β-D-Glc*p*.

The ^{13}C NMR signals in the region in the range of 68.1–84.7 ppm were attributed to C-2→C-5 carbons of the pyranoid rings of 1→3-linked-β-D-Glc and β-D-Glc. In the spectrum of ^{1}H NMR, a significant chemical shift in the range of 3.43–3.46 ppm was observed and assigned to H-3 of 1→3-linked-β-D-Glc*p*. It also included resonances characteristic of 1→3-linked-β-D-Glc and β-D-Glc such as signals from ring protons (H-2→H-5) in the range of 3.38–3.59 ppm. These data were in accordance with those of previous studies (29, 30), which indicated that laminaran is a non-reducing glucosyl end linked to various numbers of 1→3-linked-β-D-Glc*p*. The structure of laminaran derived from *Sargassum duplicatum* reported by Usoltseva et al. consists primarily of a linear sugar chain of 1→3-linked-β-D-Glc*p* residues with a terminal β-D-Glc*p* residue (31).

MS was used to determine the molecular weight of LOs while ^{1}H and ^{13}C NMR were employed to determine the sugar residue sequences. From the results of structural analyses, it can be concluded that the repeating units of LOs are 1→3-linked-β-D-Glc*p* with non-reducing terminal β-D-Glc*p* residues at C-3. The probable structures of the LOs are shown in **Figure 3C**.

Antioxidant Effects of Different Purified Laminaran Oligosaccharides

Reactive oxygen species, including superoxide anions, hydrogen peroxide, and hydroxyl radicals are produced in cells through oxygen metabolism and function. In contrast, several reactive oxygen species can contribute to various oxidative stress-induced diseases such as diabetes, cancer, cardiovascular, and neurodegenerative diseases (32). Recently, oligosaccharides have been demonstrated to play an important role as free-radical scavengers and prevent oxidative damage in living organisms. Their ability strongly depends on chemical structures such as monosaccharide composition, type of glyosidic, and molecular weight (25). The *in vitro* experiments of antioxidant activities are generally determined through DPPH radical scavenging, lipid peroxide inhibition, ferric reducing antioxidant power, nitric oxide scavenging, and ABTS radical scavenging with the advantages of simplicity, cost effectiveness, and ease of interpretation. In this study, DPPH and ABTS radical scavenging assays were used to investigate the antioxidant activities of LOs.

DPPH is a stable radical that can be used to determine the antioxidant activity of LOs by measuring the decrease in absorbance at 517 nm. As shown in **Figure 4A**, the scavenging abilities of all the samples were concentration-dependent. The scavenging of the DPPH radical of oligosaccharides was due to their hydrogen-donating ability that led to the formation of a stable molecule (33). These results are similar to those of other neutral oligosaccharides produced from natural polysaccharides such as xylo-oligosaccharides and gluco-oligosaccharides. Kallel et al. reported that half-maximal inhibitory concentration (IC_{50}) of xylo-oligosaccharides from garlic straw xylan was 0.45 mg/mL (33). In addition, IC_{50} of β-gluco-triose and β-gluco-tetraose hydrolysis from β-glucan was 1.8 mg/mL (34).

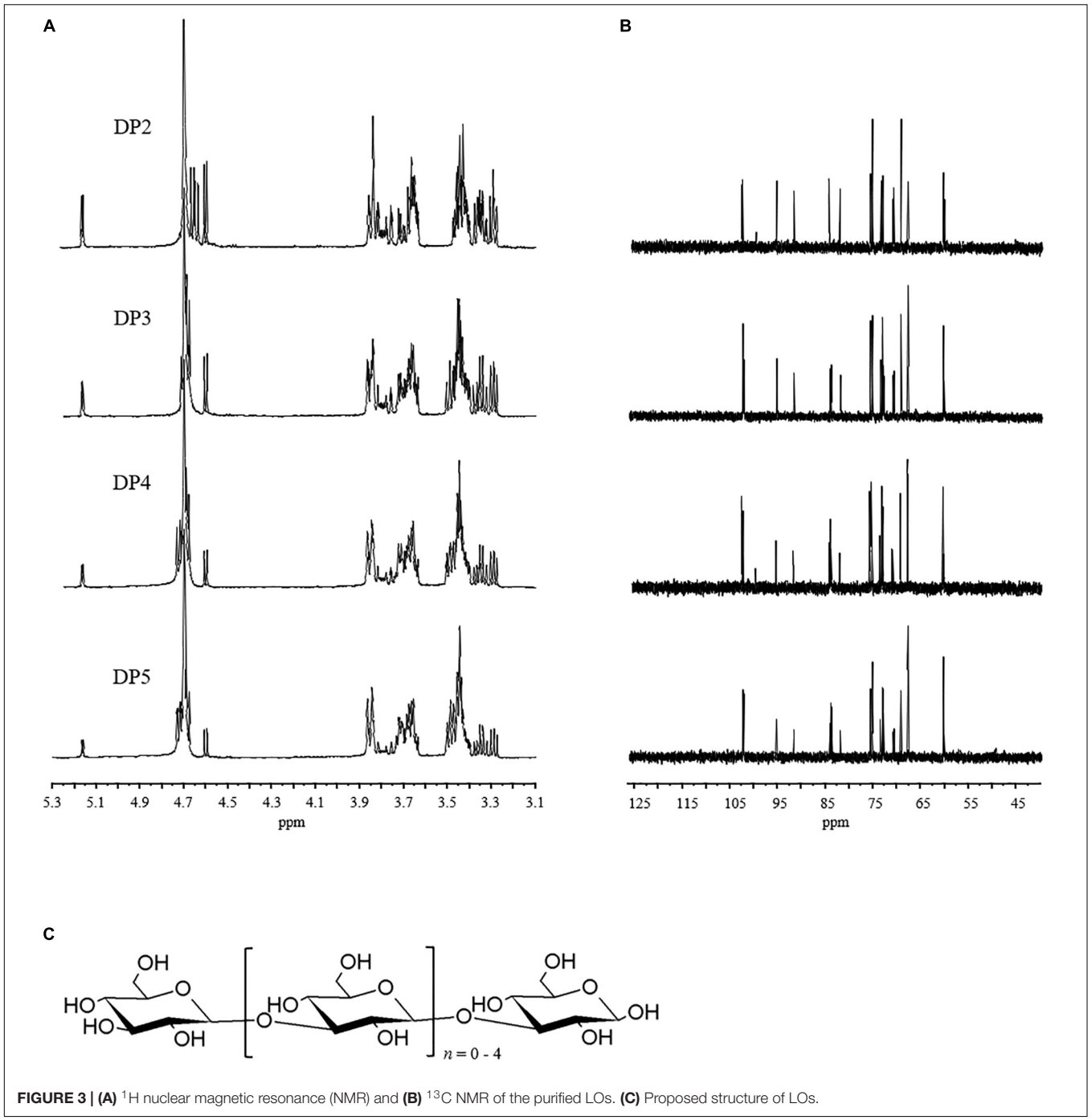

FIGURE 3 | (A) ^{1}H nuclear magnetic resonance (NMR) and **(B)** ^{13}C NMR of the purified LOs. **(C)** Proposed structure of LOs.

TABLE 2 | ^{1}H nuclear magnetic resonance (NMR) and ^{13}C NMR chemical shifts of laminaran oligosaccharides DP2-DP5 (D_2O, δ in ppm).

Residue	1	2	3	4	5	6
A	95.66–95.68/ 4.69–4.73	73.77–73.83/ 3.41–3.49	84.48–84.66/ 3.67–3.77	68.07–68.11/ 3.49–3.55	75.55–75.62/ 3.47–3.59	60.66–60.69/ 3.86–3.95; 3.75–3.84
B	102.48–102.51/ 4.68–4.78	73.36–73.45/ 3.38–3.46	84.23–84.27/ 3.43–3.46	68.08–68.11/ 3.43–3.4 6	75.57–75.63/ 3.49–3.59	60.66–60.69/ 3.84; 3.73–3.82

A, →3)β-D-Glc; B, →3)-β-D-Glc-(1→3).

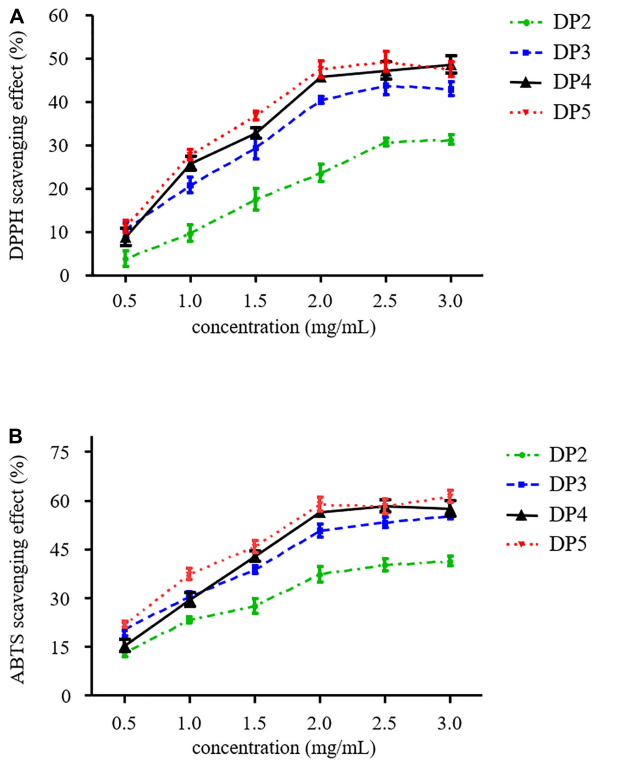

FIGURE 4 | (A) DPPH scavenging effect and **(B)** ABTS scavenging effect of purified LOs.

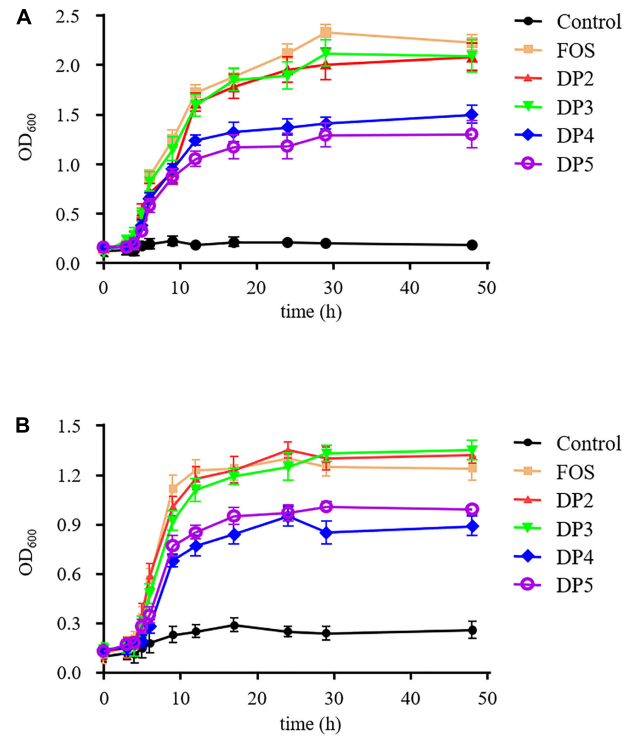

FIGURE 5 | The growth curves for *B. adolescentis* **(A)** and *L. plantarum* **(B)** grown in basal medium supplemented with purified LOs. The growth curves for each strain with a range of test samples were determined by measuring the OD of the cultures at 600 nm intermittently over a 48 h period.

ABTS radical scavenging ability is another commonly used method in functional food research to measure antioxidant activity. **Figure 4B** illustrates that a correlation was established between LOs concentration and ABTS radical-scavenging ability. At low concentrations, this ability was enhanced rapidly with an increase in concentration; however, the rising trend slowed when the concentration of LOs was more than 2.0 mg/mL. The ABTS radical scavenging rates of DP2 and DP5 at a concentration of 2 mg/mL were 37.3 and 58.8%, respectively. DP3–5 exhibited higher ABTS radical scavenging activity, whereas DP2 exhibited relatively low ability. Therefore, the antioxidant activity of the LOs in this study may be attributed to the DP of the oligosaccharides.

The mechanism of the ABTS radical scavenging ability of oligosaccharides may be similar to that of the DPPH radical scavenging mechanism. In general, C-2 and C-6 hydroxyls of oligosaccharides are mainly involved in H-atom transfer reactions toward the ABTS radical (35). It is hypothesized that hydrogen abstraction occurs at C-2 or C-6 positions of LOs captured at these positions to yield a stable ABTS-oligosaccharide form. Furthermore, Kang et al. reported agaro-oligosaccharide production through enzymatic hydrolysis of agarose, where the scavenging activities of agaro-oligosaccharides against ABTS radicals ranged from 60.34 to 83.84% (35). Choi et al. reported that low-molecular-weight laminaran from laminaran degraded by gamma irradiation exhibited high antioxidant activities (7).

These aforementioned antioxidant activity results reveal that LOs are free radical inhibitors and primary antioxidants that scavenge free radicals. This indicates that LOs could potentially be exploited in the preparation of functional food products.

Prebiotic Activities of Laminaran Oligosaccharides

Prebiotics are mainly targeted to enhance the growth of beneficial bacteria, such as bifidobacteria and lactobacilli in the gut (12, 36). Therefore, we tested the potential prebiotic effects of LOs. The proliferation of probiotics in the media with different purified LOs as carbon sources is shown in **Figure 5**. *B. adolescentis* strains grown in FOS-, DP2, and DP3 supplemented media exhibited similar and rapid growth with high final OD 600 values; however, they grew significantly slower in DP4 and DP5 supplemented media. The results demonstrated that the varying DPs of LOs had different effects on the growth of *B. adolescentis* and *L. plantarum*. The growth of *L. plantarum* in DP4 and DP5 resulted in lower absorbance levels of 0.95 and 1.01, respectively. This lower level of growth is likely related to the DP of the LOs. A lower DP generally induced faster growth of the probiotics because the lower DP oligosaccharides were cleaved into monosaccharides as energy sources.

These findings are similar to those made by Zhang et al. who reported that neoagaro-oligosaccharides with DP3 exhibited

the best growth stimulation for *Sterptococcus thermophilus*, and its OD_{600} reached 0.94 after 72 h of incubation. The order of prebiotic effects of neoagaro-oligosaccharides was DP3 > DP5 > DP8 (37). In this study, LOs exhibited beneficial effects on the growth of probiotic strains such as bifidobacteria and lactobacilli. Therefore, LOs could be regarded as prebiotics, which might have the same benefits as FOS.

CONCLUSION

LOs were obtained using controlled acid hydrolysis of laminaran from *L. digitata*. BBD was applied to determine the optimum process parameters that afforded a high LOs yield. By analyzing the second-order polynomial model, a maximum LOs yield of 2.59 mg/mL was obtained under the following conditions: hydrolysis time of 55 min, temperature of 71°C, and acid concentration of 1.00 mol/L. Subsequently, large-scale pure LOs were automatically and efficiently separated and purified using the FPLC-RID technique, whereas the Bio-Gel P-2 size exclusion resin was suitable for LOs separation. These are useful for pharmaceutical application and for the qualitative and quantitative analyses of LOs as additives in health foods.

The obtained results clearly demonstrate that each LOs fraction exhibits antioxidant activity, which follows a concentration-dependent response for DPPH and ABTS radicals scavenging activities. In particular, DP5 exhibited excellent antioxidant capacity. Prebiotic experiments demonstrated the growth of *B. adolescentis* and *L. plantarum* in LOs. LOs with DP3 exhibited remarkable prebiotic activity. Although *in vitro* assessment of the functionality of oligosaccharides has some limitations, the results provide a direction for future research and application and improve our understanding of the potential applications of LOs. These results suggest that LOs exhibit antioxidant and prebiotic activities, indicating their potential application in functional foods aimed at improving human gastrointestinal health and preventing gut diseases.

DATA AVAILABILITY STATEMENT

The original contributions presented in this study are included in the article/supplementary material, further inquiries can be directed to the corresponding author.

ETHICS STATEMENT

The protocol for these experiments was approved by the Ethics Committee of Guangdong Ocean University.

AUTHOR CONTRIBUTIONS

K-LC and SZ designed the research. K-LC conducted the research. K-LC, J-KL, and SZ analyzed the data. K-LC and J-KL wrote the manuscript. SZ edited the manuscript. All authors read and approved the final manuscript.

FUNDING

This research was financially supported by Key-Area Research and Development Program of Guangdong Province (2020B1111030004), the Innovative Team Program of High Education of Guangdong Province (2021KCXTD021), and the Special Project of Guangdong Science and Technology Department (210718205862114).

REFERENCES

1. Brown ES, Allsopp PJ, Magee PJ, Gill CI, Nitecki S, Strain CR, et al. Seaweed and human health. *Nutr Rev.* (2014) 72:205–16. doi: 10.1111/nure.12091
2. Qiu S-M, Aweya JJ, Liu X, Liu Y, Tang S, Zhang W, et al. Bioactive polysaccharides from red seaweed as potent food supplements: a systematic review of their extraction, purification, and biological activities. *Carbohydr Polym.* (2022) 275:118696. doi: 10.1016/j.carbpol.2021.118696
3. Gupta S, Abu-Ghannam N. Bioactive potential and possible health effects of edible brown seaweeds. *Trends Food Sci Technol.* (2011) 22:315–26. doi: 10.1016/j.tifs.2011.03.011
4. Ermakova S, Men'shova R, Vishchuk O, Kim S-M, Um B-H, Isakov V, et al. Water-soluble polysaccharides from the brown alga *Eisenia bicyclis*: structural characteristics and antitumor activity. *Algal Res.* (2013) 2:51–8. doi: 10.1016/j.algal.2012.10.002
5. Kadam SU, Donnell CP, Rai DK, Hossain MB, Burgess CM, Walsh D, et al. Laminarin from Irish brown seaweeds *Ascophyllum nodosum* and *Laminaria hyperborea*: ultrasound assisted extraction, characterization and bioactivity. *Mar Drugs.* (2015) 13:4270–80. doi: 10.3390/md13074270
6. Kim S-K, Rajapakse N. Enzymatic production and biological activities of chitosan oligosaccharides (COS): a review. *Carbohydr Polym.* (2005) 62:357–68. doi: 10.1016/j.carbpol.2005.08.012
7. Choi JI, Kim HJ, Lee JW. Structural feature and antioxidant activity of low molecular weight laminarin degraded by gamma irradiation. *Food Chem.* (2011) 129:520–3. doi: 10.1016/j.foodchem.2011.03.078
8. Wu S-J. Preparation and antioxidant activity of the oligosaccharides derived from *Laminaria japonica*. *Carbohydr Polym.* (2014) 106:22–4. doi: 10.1016/j.carbpol.2014.01.098
9. Jin M, Liu H, Hou Y, Chan Z, Di W, Li L, et al. Preparation, characterization and alcoholic liver injury protective effects of algal oligosaccharides from *Gracilaria lemaneiformis*. *Food Res Int.* (2017) 100:186–95. doi: 10.1016/j.foodres.2017.08.032
10. Nicola V, Francesca M, Suwan J, Linhardt RJ. Electrophoresis for the analysis of heparin purity and quality. *Electrophoresis.* (2012) 33:1531–7. doi: 10.1002/elps.201100479
11. Zhu B, Ni F, Xiong Q, Yao Z. Marine oligosaccharides originated from seaweeds: source, preparation, structure, physiological activity and applications. *Crit Rev Food Sci Nutr.* (2021) 61:60–74. doi: 10.1080/10408398.2020.1716207
12. Xie, X-T, Cheong K-L. Recent advances in marine algae oligosaccharides: structure, analysis, and potential prebiotic activities. *Crit Rev Food Sci Nutr.* (2021) 1–16. doi: 10.1080/10408398.2021.1916736
13. Bai W, Fang X, Zhao W, Huang S, Zhang H, Qian M. Determination of oligosaccharides and monosaccharides in Hakka rice wine by precolumn derivation high-performance liquid chromatography. *J Food Drug Anal.* (2015) 23:645–51. doi: 10.1016/j.jfda.2015.04.011

14. Zhenmin Y, Yongtao Y, Chuanchuan G, Dengke H, Jun H, Mingyue Z. Isolation of inulin-type oligosaccharides from Chinese traditional medicine: *Morinda officinalis* how and their characterization using ESI-MS/MS. *J Sep Sci.* (2010) 33:120–5. doi: 10.1002/jssc.200900396
15. Li J, Cheong KL, Zhao J, Hu DJ, Chen XQ, Qiao CF, et al. Preparation of inulin-type fructooligosaccharides using fast protein liquid chromatography coupled with refractive index detection. *J Chromatogr A.* (2013) 1308:52–7. doi: 10.1016/j.chroma.2013.08.012
16. Xu SY, Aweya JJ, Li N, Deng RY, Chen WY, Tang J, et al. Microbial catabolism of *Porphyra haitanensis* polysaccharides by human gut microbiota. *Food Chem.* (2019) 289:177–86. doi: 10.1016/j.foodchem.2019.03.050
17. Rajauria G, Ravindran R, Garcia-Vaquero M, Rai DK, Sweeney T, O'Doherty J. Molecular characteristics and antioxidant activity of laminarin extracted from the seaweed species *Laminaria hyperborea*, using hydrothermal-assisted extraction and a multi-step purification procedure. *Food Hydrocolloid.* (2021) 112:106332. doi: 10.1016/j.foodhyd.2020.106332
18. Zhang X, Aweya JJ, Huang Z-X, Kang Z-Y, Bai Z-H, Li K-H, et al. In vitro fermentation of *Gracilaria lemaneiformis* sulfated polysaccharides and its agaro-oligosaccharides by human fecal inocula and its impact on microbiota. *Carbohydr Polym.* (2020) 234:115894. doi: 10.1016/j.carbpol.2020.115894
19. Khan BM, Qiu H-M, Xu S-Y, Liu Y, Cheong K-L. Physicochemical characterization and antioxidant activity of sulphated polysaccharides derived from *Porphyra haitanensis*. *Int J Biol Macromol.* (2020) 145:1155–61. doi: 10.1016/j.ijbiomac.2019.10.040
20. Xu S-Y, Liu J-P, Huang X, Du L-P, Shi F-L, Dong R, et al. Ultrasonic-microwave assisted extraction, characterization and biological activity of pectin from jackfruit peel. *LWT.* (2018) 90:577–82. doi: 10.1016/j.lwt.2018.01.007
21. Hongpattarakere T, Cherntong N, Wichienchot S, Kolida S, Rastall RA. In vitro prebiotic evaluation of exopolysaccharides produced by marine isolated lactic acid bacteria. *Carbohydr Polym.* (2012) 87:846–52. doi: 10.1016/j.carbpol.2011.08.085
22. Lv M, Wang M, Cai W, Hao W, Yuan P, Kang Z. Characterisation of separated end hyaluronan oligosaccharides from leech hyaluronidase and evaluation of angiogenesis. *Carbohydr Polym.* (2016) 142:309–16. doi: 10.1016/j.carbpol.2016.01.052
23. Schendel RR, Becker A, Tyl CE, Bunzel M. Isolation and characterization of feruloylated arabinoxylan oligosaccharides from the perennial cereal grain intermediate wheat grass (*Thinopyrum intermedium*). *Carbohydr Res.* (2015) 407:16–25. doi: 10.1016/j.carres.2015.01.006
24. Kumar VP, Prashanth KVH, Venkatesh YP. Structural analyses and immunomodulatory properties of fructo-oligosaccharides from onion (*Allium cepa*). *Carbohydr Polym.* (2015) 117:115–22. doi: 10.1016/j.carbpol.2014.09.039
25. Cheong KL, Qiu HM, Du H, Liu Y, Khan BM. Oligosaccharides derived from red seaweed: production, properties, and potential health and cosmetic applications. *Molecules.* (2018) 23:18. doi: 10.3390/molecules23102451
26. Kailemia MJ, Ruhaak LR, Lebrilla CB, Amster IJ. Oligosaccharide analysis by mass spectrometry: a review of recent developments. *Anal Chem.* (2014) 86:196–212. doi: 10.1021/ac403969n
27. Yang J, Xu Y, Miyakawa T, Long L, Tanokura M, Zhou N-Y. Molecular basis for substrate recognition and catalysis by a marine bacterial laminarinase. *Appl Environ Microbiol.* (2020) 86:e1796–20. doi: 10.1128/AEM.01796-20
28. Jana UK, Kango N. Characteristics and bioactive properties of mannooligosaccharides derived from agro-waste mannans. *Int J Biol Macromol.* (2020) 149:931–40. doi: 10.1016/j.ijbiomac.2020.01.304
29. Menshova RV, Ermakova SP, Anastyuk SD, Isakov VV, Dubrovskaya YV, Kusaykin MI, et al. Structure, enzymatic transformation and anticancer activity of branched high molecular weight laminaran from brown alga *Eisenia bicyclis*. *Carbohydr Polym.* (2014) 99:101–9. doi: 10.1016/j.carbpol.2013.08.037
30. Malyarenko OS, Usoltseva RV, Shevchenko NM, Isakov VV, Zvyagintseva TN, Ermakova SP. In vitro anticancer activity of the laminarans from Far Eastern brown seaweeds and their sulfated derivatives. *J Appl Phycol.* (2017) 29:543–53. doi: 10.1007/s10811-016-0915-3
31. Usoltseva RV, Anastyuk SD, Shevchenko NM, Surits VV, Silchenko AS, Isakov VV, et al. Polysaccharides from brown algae *Sargassum duplicatum*: the structure and anticancer activity in vitro. *Carbohydr Polym.* (2017) 175:547–56. doi: 10.1016/j.carbpol.2017.08.044
32. Priyan Shanura Fernando I, Kim K-N, Kim D, Jeon Y-J. Algal polysaccharides: potential bioactive substances for cosmeceutical applications. *Crit Rev Biotechnol.* (2019) 39:99–113. doi: 10.1080/07388551.2018.1503995
33. Kallel F, Driss D, Chaabouni SE, Ghorbel R. Biological activities of xylooligosaccharides generated from garlic straw xylan by purified xylanase from Bacillus mojavensis UEB-FK. *Appl Biochem Biotechnol.* (2015) 175:950–64. doi: 10.1007/s12010-014-1308-1
34. Chaari F, Belghith-Fendri L, Zaouri-Ellouzi S, Driss D, Blibech M, Kallel F, et al. Antibacterial and antioxidant properties of mixed linkage beta-oligosaccharides from extracted β-glucan hydrolysed by *Penicillium occitanis* EGL lichenase. *Nat Prod Res.* (2016) 30:1353–9. doi: 10.1080/14786419.2015.1056185
35. Kang OL, Ghani M, Hassan O, Rahmati S, Ramli N. Novel agaro-oligosaccharide production through enzymatic hydrolysis: physicochemical properties and antioxidant activities. *Food Hydrocolloid.* (2014) 42:304–8. doi: 10.1016/j.foodhyd.2014.04.031
36. Wu D-T, Liu W, Yuan Q, Gan R-Y, Hu Y-C, Wang S-P, et al. Dynamic variations in physicochemical characteristics of oolong tea polysaccharides during simulated digestion and fecal fermentation in vitro. *Food Chem. X* (2022) 14:100288. doi: 10.1016/j.fochx.2022.100288
37. Zhang Y-H, Song X-N, Lin Y, Xiao Q, Du X-P, Chen Y-H, et al. Antioxidant capacity and prebiotic effects of *Gracilaria neoagaro* oligosaccharides prepared by agarase hydrolysis. *Int J Biol Macromol.* (2019) 137:177–86. doi: 10.1016/j.ijbiomac.2019.06.207

Conflict of Interest: The authors declare that the research was conducted in the absence of any commercial or financial relationships that could be construed as a potential conflict of interest.

Publisher's Note: All claims expressed in this article are solely those of the authors and do not necessarily represent those of their affiliated organizations, or those of the publisher, the editors and the reviewers. Any product that may be evaluated in this article, or claim that may be made by its manufacturer, is not guaranteed or endorsed by the publisher.

Copyright © 2022 Cheong, Li and Zhong. This is an open-access article distributed under the terms of the Creative Commons Attribution License (CC BY). The use, distribution or reproduction in other forums is permitted, provided the original author(s) and the copyright owner(s) are credited and that the original publication in this journal is cited, in accordance with accepted academic practice. No use, distribution or reproduction is permitted which does not comply with these terms.

frontiers | Frontiers in Nutrition

ORIGINAL RESEARCH
published: 12 July 2022
doi: 10.3389/fnut.2022.921892

Antitumor Potential and Structure Characterization of Polysaccharides From *Lagotis brevituba* Maxim in the Tibetan Plateau

*Ruixue Gong†, Weiguo Cao†, Haijun Huang, Bao Yu, Huan Chen, Wei Tao, Quji Luorong, Juan Luo and Dan Zhang**

College of Traditional Chinese Medicine, Chongqing Medical University, Chongqing, China

This study purified two polysaccharides (LBMPs) from *Lagotis brevituba* Maxim in several steps. The chemical structure of LBMP-2 was determined by HPGPC, FT-IR, IC, ^{1}H and ^{13}C NMR, AFM, SEM, and TEM. The results show that LBMP-2 was mainly composed of GalA, and the Mw of LBMP-2 is 23.799 kDa. In addition, the antioxidant activity, and the antitumor activity *in vitro* and *in vivo* were studied. LBMP-2 has excellent antioxidant and antitumor capacity. The inhibition of tumor cell proliferation *in vitro* may result in the inhibition of aerobic respiration and glycolysis. Tumor growth inhibition *in vivo* may inhibit the expression of AMPK in tumors and enhance spleen function. Compared with conventional chemotherapy drug cyclophosphamide, LBMP-2 is less harmful to the body and safer. Therefore, LBMP-2 provides a potential source of antitumor drugs.

Keywords: isolation, purification, structure analysis, antioxidant, antitumor

OPEN ACCESS

Edited by:
Xin Wang,
Northwest A&F University, China

Reviewed by:
Guangli Yu,
Ocean University of China, China
Jing Li,
Nanchang University, China

***Correspondence:**
Dan Zhang
zhangdan01234567@hotmail.com

†These authors have contributed equally to this work and share first authorship

Specialty section:
This article was submitted to Food Chemistry, a section of the journal Frontiers in Nutrition

Received: *16 April 2022*
Accepted: *06 June 2022*
Published: *12 July 2022*

Citation:
Gong R, Cao W, Huang H, Yu B, Chen H, Tao W, Luorong Q, Luo J and Zhang D (2022) Antitumor Potential and Structure Characterization of Polysaccharides From Lagotis brevituba Maxim in the Tibetan Plateau. Front. Nutr. 9:921892. doi: 10.3389/fnut.2022.921892

INTRODUCTION

Lagotis brevituba Maxim (*L. brevituba*) is a traditional Chinese herb of the Scrophulariaceae family and is mainly distributed over alpine grasslands and gravel slopes at altitudes of 3,000–4,420 m in southwestern Gansu, eastern Qinghai and Tibet (1). At present, there are still relatively few studies on *L. brevituba*, mainly focusing on the chemical components and pharmacological activities.

Due to the plateau situation, plateau plants contain more polysaccharides than ordinary plants. For example, the crude polysaccharides of *Cordyceps sinensis* on the plateau had a total sugar content of 45.6% (2). Recent studies have demonstrated that polysaccharides have strong biological properties. Among them, antioxidant activity (3), antitumor activity and immunomodulatory activity (4) are particularly prominent, and polysaccharides also have fewer toxic and side effects. Therefore, they are widely used in various health products and medicines.

We previously compared the antioxidant activities of *L. brevituba in vivo* and *in vitro* (5), and found that the water extract has strong 1,1-Diphenyl-2-picrylhydrazyl Free Radical (DPPH) free radical scavenging activity. We also found that *L. brevituba* had many polysaccharides. Combined with the relevant modern pharmacological research of *L. brevituba* and polysaccharides, it is speculated that the polysaccharides of *L. brevituba* may have antioxidant activity, regulating immunity and antitumor activity. However, no attention has been given to the characterization or antitumor activity of polysaccharides from *L. brevituba*. Therefore, this study analyzes the structure of the polysaccharides of *L. brevituba,* verifies its antioxidant, immune-regulating and antitumor activities, and explores the relationship between

antitumor activity and molecular structure in a more comprehensive manner. Our results provide new structural information on polysaccharides from *L. brevituba* and promote the development and utilization for medicinal use.

MATERIALS AND METHODS

Polysaccharide Isolation and Purification

Following a previous report with some modifications, the whole plant of *L. brevituba* polysaccharides was extracted by boiling water (6).

Extraction

L. brevituba was shredded and refluxed with 95% ethanol 3 times for 2 h to remove lipids. Then, refluxed with boiling water 3 times for 2 h. A threefold volume of 95% ethanol was mixed with the liquid and left at 4°C overnight. Crude polysaccharides were centrifuged for 10 min at 4,000 rpm and dissolved in 1,000 mL of deionized water.

Purification

To separate the water-soluble fraction from the insoluble fraction, a DEAE-cellulose column was used with a gradient of 0–1 mol/L NaCl and a flow rate of 1 mL/min. Eluent (5 mL/tube) was collected automatically. The total carbohydrate content of the elution was determined by the phenol–sulfuric acid method (7). The results showed two large elution peaks, named LBMP-1 and LBMP-2. The samples were dialyzed for 48 h in deionized water with a dialysis bag (molecular weight cutoff 3,500 Da). Under reduced pressure, the samples were concentrated and lyophilized to obtain pure polysaccharides.

Chemical Analysis

A phenol–sulfuric acid method was used to estimate total carbohydrates (7). The m-hydroxybiphenyl method was used to measure uronic acid (8). Bradford method was used to measure protein content (9). The total polyphenols were determined by using the Follin-Ciocalteu method (10).

Structural Characteristics of Polysaccharides

Molecular Weight

LMBP-2 molecular weight was determined by HPGPC using a Shimadzu HPLC system equipped with a TSKgel G4000PWXL column (7.8 × 300 mm) and a Shimadzu RID-10A refractive index detector (11). The experimental conditions: the detector temperature was 40°C; the column temperature was 35°C; 0.2 mol/L NaCl was used for the elution; the flow rate was 0.3 mL/min, and the injection volume was 10 μL. The standard curve was established using 210, 150, 80, 50, 25, 12, 5, and 1 kDa standard dextran (Aladdin), LabSolutions GPC software was used to calculate the molecular weight of LMBP-2.

Monosaccharide Composition

LBMP-2 monosaccharide compositions were determined using high-performance ion chromatography (HPIC) (ICS5000, Thermo Fisher Scientific, United States) and a DionexCarbopac^{TM}PA20 column (3 * 150 mm) (12). Trifluoroacetic acid (3 mol/L, 10 mL) hydrolyzed LBMP-2 for 3 h at 120°C in a sealed tube. Then, the hydrolysate was dried with a nitrogen blower at 60°C. Sample dissolved in deionized water at 0.2 mg/mL. After centrifuging the sample solution at 12,000 rpm for 5 min, the supernatant fraction was collected and loaded onto the IC system. Fuc, Ara, Rha, Gal, Xly, Glc, Man, Fru, Rib, GlcA, GalA, GulA, ManA, GalN, GlcN, and GlcNAc were used as standards.

FT-IR Analysis

LBMP-2′s FT-IR spectrum was determined with a Spotlight 300 spectrometer (PerkinElmer, United Kingdom).

NMR Analysis

A BrukerAscend^{TM}600 MHz NMR spectrometer was used to measure the ^{13}C and ^{1}H NMR spectra of 30 mg of LBMP-2 dissolved in 0.5 mL of D_2O.

Atomic Force Microscope Analysis

BrukerDension Icon atomic force microscopes (AFMs) were used for LBMP-2 AFM imaging. Polysaccharides were dissolved in deionized water and diluted to 3 μg/mL. An AFM was used to image the prepared sample.

Scanning Electron Microscope Analysis

SEM imaging was conducted with a scanning electron microscope (SEM) (S-3000N, Hitachi, Japan). LBMP-2 polysaccharides were freeze-dried, fixed with double-sided tape, sputtered with gold, and scanned under a high vacuum.

Transmission Electron Microscope Analysis

The sample of LBMP-2 (0.25 mg/mL) was diffused in hot water at 80°C for 10 min, dropped on a carbon-supported copper mesh, dried naturally at room temperature, and observed by a transmission electron microscope (TEM).

Antioxidant Activity *in vitro*

Reducing Ability

The reducing power was determined using the method described previously (13). The positive control was BHT.

DPPH Radical Scavenging Activity

The DPPH radical-scavenging activities of LBMP-2 were determined using the method described previously (13). BHT was used as the positive control.

ABTS Radical Scavenging Activity

The 2,2′-Azinobis (3-ethylbenzothiazoline -6-sulfonic Acid Ammonium Salt) (ABTS) radical-scavenging activities of LBMP-2 were determined using the method described previously (13). BHT served as a positive control.

Antitumor Activity *in vitro*

Cell Culture

Shanghai Cell Bank of the Chinese Academy of Sciences provided the B16-F10 cell lines.

Cell Viability Assay

The antiproliferative activity of the compounds was assessed using the MTT assay (14). 1×10^5 cells/mL were seeded in 96-well microplates. After 12 h of cell culture, the cells were treated with nine concentrations (0, 1.95, 3.9, 7.8, 15.625, 31.25, 62.5, 125, and 250 μg/mL) for 24 h. The 0 μg/mL group was the blank group. Each group had 6 parallel controls.

Cellular Metabolic Flux Assay

2.5×10^4 cells/mL were seeded in XFp eight-well cell culture miniplates (Seahorse XF HS Mini, Agilent). LBMP-2 was added to cells at 250 μg/mL for 24 h, then the manufacturer's protocol was followed during the energy phenotype test, mito stress test and glycolysis stress test (Seahorse XFp Cell Energy Phenotype Test Kit, Seahorse XFp Cell Mito Stress Test Kit, Seahorse XFp Glycolysis Stress Test Kit). The metabolic data of the cells were normalized to the total cellular protein content. Lysates were salvaged and BCA Protein Assay Kit (Beyotime, China) was used to measure total protein.

Antitumor Activity *in vivo*

Animals

A temperature- and humidity-controlled room with a 12-h light/12-h dark cycle was used to maintain mice of male 6-week-old C57BL/6 (20 ± 2 g). All mice were provided with free access to food and water in an SPF-grade environment. The right flank back of C57BL/6 mice was shaved before injection. 4×10^5 cells/mL B16-F10 cells (100 μL) were injected subcutaneously into the right flank of the mice. After 4 days, five groups of mice ($n = 8$) were randomly selected. (1) Model group: normal saline (NS) was intraperitoneally injected into the mice (20 mL/kg); (2) CTX group (Positive group): CTX (cyclophosphamide) was intraperitoneally injected into the mice (20 mg/kg). (3) High dose: LBMP-2 were intraperitoneally injected into the mice (30 mg/kg); (4) Low dose group: LBMP-2 were intraperitoneally injected into the mice (15 mg/kg); (5) Control group: water and food are available for free in an SPF-rated environment. After 11 consecutive days of daily administration, mice were sacrificed with 1% sodium pentobarbital and high-concentration carbon dioxide. A tissue sample was collected for further analysis. Chongqing Medical University's ethics committee approved all animal husbandry and experimental protocols.

Histopathological Examination

As described previously, a histologic examination was performed (15). Paraffin-embedded spleen tissue and tumor tissue were stained with H&E and immunohistochemistry. A primary antibody against AMPK (Servicebio, China) was incubated with tumor tissue sections, and incubation of the spleen tissue sections with primary antibodies against $CD3^+$, $CD4^+$, $CD8^+$ (Servicebio, China). The percent of staining areas was calculated using ImageProPlus.

Statistical Analysis

All data are expressed as the mean ± standard deviation (S.D.). Statistical analyses were performed by one-way ANOVA using the SPSS statistical package (SPSS. Inc., Chicago, United States). A value of $P < 0.05$ was considered to be statistically significant.

RESULTS AND DISCUSSION

Extraction, Isolation and Purification of LBMP-2

The structure of polysaccharides is complex and diverse. Extraction, separation and purification from natural plants are still the main way to obtain polysaccharides. DEAE-cellulose was used to fractionate the LBMP (**Figure 1A**). The LBMP-1 and LBMP-2 were obtained using a NaCl gradient (0, 0.2 mol/L). The yield of crude polysaccharides was 21.3 ± 1.5%. The purified polysaccharides of LBMP-1 were obtained with a yield of 0.28 ± 0.23% based on the dried whole plant of *L. brevituba*. The purified polysaccharides of LBMP-2 were obtained with a yield of 1.62 ± 0.43% based on the dried whole plant of *L. brevituba*. The content of uronic acid was as high as 67.6 ± 0.32%, and no protein or phenolic acid was detected. The influence of phenolics and proteins on subsequent testing was excluded. Compared with LBMP-2 (1.62 ± 0.43%), the yield of LBMP-1 was low, so no research has been done on LBMP-1.

Characterization of the LBMP-2

Molecular Weight

The molecular weight of polysaccharides was related to their biological activity. HPGPC analysis of LBMP-2 showed a single peak (**Figure 1B**). LabSolutions GPC software was used to obtain the standard curve: $Y = -2.157975e\text{-}003X^3 - 0.1740564X^2 - 4.843469X + 51.09103$; $R^2 = 0.9982101$. The Mw of LBMP-2 was 23.799 kDa, and the Mn of LBMP-2 was 23.776 kDa. The Mw/Mn ratio was 1, indicating that LBMP-2 was a homogeneous polysaccharide (16).

Monosaccharide Composition

In order to determine LBMP-2′s monosaccharide composition, HPIC was chosen instead of GC–MS due to its ability to identify uronic acid with ease (12). As shown in **Figure 1C**, monosaccharides were composed of Rha, Ara, Gal, Glc, and GalA in molar ratios of 0.156:0.144:0.107:0.114:0.480. Therefore, it can be determined that GalA was the major monosaccharide composition. *In vitro* and *in vivo*, polysaccharides with high uronic acid content, especially high galacturonic acid content, have better antioxidant activity (16, 17).

FT-IR Analysis

In FT-IR analysis, LMBP-2 showed absorption peaks characteristic of polysaccharides in the range of 4,000–400 cm^{-1} (**Figure 1D**). Historically, the broad stretched absorption peak at 3,418 cm^{-1} was considered to be the signature of the O-H bond. At 2,941 cm^{-1}, the absorption was caused by the C-H stretching of CH, CH_2, and CH_3 groups, which was characteristic of polysaccharides. The peaks at 1,747 and 1,612 cm^{-1} were characteristic absorption peaks of the C = O band for the carboxylate groups. The relatively strong absorption peak at 1,200–1,000 cm^{-1} revealed C-O-C and C-O-H link

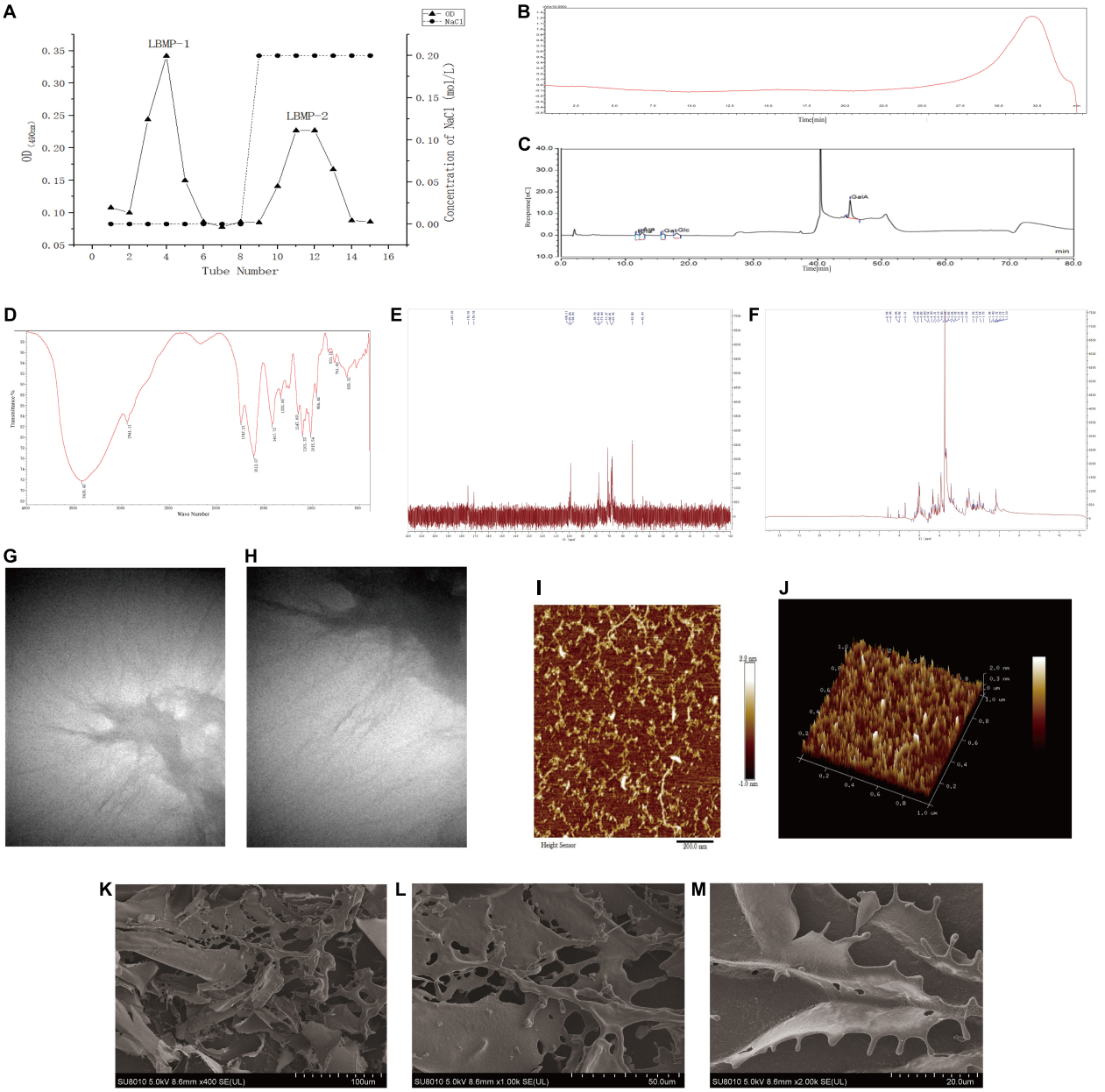

FIGURE 1 | Characterization of LBMP-2. **(A)** Isolation and purification of LBMP-2. **(B)** HPGPC of LBMP-2. **(C)** IC of LBMP-2. **(D)** FT-IR spectra of LBMP-2. **(E,F)** NMR spectra of LBMP-2. **(G–M)** Microstructure analyses of LBMP-2.

bonds, which indicated that the pyranose ring was present. The peak at 831 cm^{-1} suggests that the pyranose ring was in the α-configuration. There was no peak at 1,600–1,500 cm^{-1}, indicating that protein was not present in LBMP-2. Those results were consistent with the Bradford method (17, 18).

NMR Analysis

NMR spectrometer can provide detailed information about polysaccharide structure, including α- or β-anomeric configuration, monosaccharide composition, connection mode, and sugar unit sequence (19). We investigated the structure of LBMP-2 with NMR analysis, in particular its sugar units and linkage patterns. Based on the component, linkage analysis, and literature values, the main chemical shifts of LBMP-2 were found, and they are presented in **Table 1**. **Figures 1E,F** show the NMR spectrum of LBMP-2. The signals in the range of δ5.50–4.40 ppm (^{1}H NMR) and δ90–110 ppm (^{13}C NMR) are assigned to α-D-Glc*p* residues, α-D-Gal*p* residues, α-L-Rha*p* residues, and α-D-Ara*f* residues (19). In the ^{13}C NMR spectrum (**Figure 1E**), the signals in the range of δ170–180 ppm are attributed to the Gal*p*A residue, and the signal in the range of δ52.86 ppm is attributed to the O-CH_3 group of pectin. In the ^{1}H

TABLE 1 | The ^{1}H NMR and ^{13}C NMR data of LBMP-2 (in D_2O solvent).

δ C (ppm)	δ H (ppm)
187.03; 175.01; 170.95 (Gal*p*A)	2.14; 2.07 (2-O- and 3-O-GalA)
52.86 (O-CH_3 group of pectin)	3.82 (GalA)
100.11	5.08 (T-α-L-Rha*p*)
99.06, 98.94	5.18 (T-ara*f*)
78.79, 77.86	6.58;6.44;6.04
77.44	5.99;5.71
71.27	4.89, 4.60, 4.52, 4,40, 4.31, 4.19, 4.06
68.81	3.69, 3.65, 3.42, 3.27
67.95	2.85, 2.62, 2.29
45.24	1.92, 1.79, 1.48, 1.40, 1.32,1.23, 1.17, 1.10

NMR spectrum (**Figure 1F**), the concentration of chemical shifts at δ3–5 ppm is considered a typical feature of polysaccharides (16), and most α-anomeric protons usually appear at δ5–6 ppm shifts (20). The signal in the range of δ3.82 ppm is attributed to the methyl group in the carboxyl group of GalA, and the signals in the range of δ2.14 and δ2.07 ppm are attributed to the acetyl group at 2-O- and 3-O-GalA. The signal in the range of δ5.18 ppm is attributed to T-ara*f*, and the signal in the range of δ5.08 ppm is attributed to T-α-L-Rha *p* (21, 22). This result also confirms the infrared result.

Atomic Force Microscope Analysis

AFM has been widely used in biology and medicine. High-resolution imaging and nanomechanical characterization can be performed to obtain surface topography information, undulation information, roughness information and height information of nanomaterials, polymer materials, biological samples, metal materials, ceramic materials, and thin-film materials (23, 24). AFM was used to analyze the morphology of polysaccharides to gain insight into their chain conformation. **Figures 1I,J** shows AFM topography images of LBMP-2. Irregular chains could be seen on LBMP-2, its length ranged from 10 to 398 nm, its maximal height was 224 pm, and its maximal width was 15 nm.

Scanning Electron Microscope Analysis

The apparent structure of LBMP-2 was studied by SEM (**Figures 1K–M**). SEM is one of the most effective means of analyzing biopolymer structure, including size, shape, and porosity (25). **Figure 1K** shows that solid LBMP-2 has a loose and porous sheet structure, and **Figures 1L,M** clearly shows the highly branched structure of LBMP-2.

Transmission Electron Microscope Analysis

The apparent structure of LBMP-2 was studied by TEM (**Figures 1G,H**). It can be seen in **Figure 1G** at low magnification (1.4 w times) that polysaccharide chains will form large aggregates through the self-assembly process in water. The random diffusion of polysaccharide chains can be seen under the high magnification lens (2.6 w times) in **Figure 1H**. This result indicates that the easy aggregation of LBMP-2 in an aqueous solution may be related to the self-assembly process of polysaccharide chains. The random coiling of polysaccharides promotes the interaction between polysaccharides and platelets and can also promote the binding of some specific receptors to cause physiological effects (26).

According to AFM, SEM, and TEM images, LBMP-2 molecules are dendritic multi-branched structures. And it indicated that the spatial structure of LBMP-2 may be a helical structure, and there are many special binding sites. It was reported earlier that either single-helix or multi-helix structure can improve biological immunity and enhance the activity of lymphocytes to achieve the purpose of anti-tumor (27, 28). Therefore, we infer that lbmp-2 had good antitumor activity.

Antioxidant Activity *in vitro*

One of the main causes of aging and disease is oxidative stress. According to the literature, oxidative stress plays a key role in the development and occurrence of cancer (29). Therefore, antioxidants are beneficial for the prevention and treatment of cancer. To determine *in vitro* the antioxidant properties of LBMP-2, DPPH radicals, ABTS radicals and reducing power analysis were conducted, and **Figure 2** shows the scavenging ability at concentrations ranging from 0.01 to 2 mg/mL. **Figure 2A** shows the concentration-dependent scavenging activity of LBMP-2 on DPPH free radicals. The IC_{50} value of LBMP-2 was 0.3 mg/mL, and the IC_{50} value of BHT in the positive control group was 0.26 mg/mL. The DPPH scavenging ability of LBMP-2 showed superior scavenging capacity. **Figures 2B,C** shows that at a concentration of 2 mg/mL, the scavenging rate of LBMP-2 on ABTS free radicals was only approximately 7%, and the reducing power was much lower than that of BHT.

The reducing power was based on the evaluation method of the single electron transfer mechanism (SET). The DPPH and ABTS methods evaluate the oxidation resistance of the sample based on the hydrogen atom transfer mechanism (HAT) and the single electron transfer mechanism (SET). ABTS prefers the SET evaluation mechanism, while DPPH relies more on the HAT mechanism (30). Based on the different detection principles of the DPPH method, ABTS method, and reduction experiments, LBMP-2 had a superior scavenging capacity *in vitro*. Probably because LBMP-2 contains a lot of uronic acid and lower molecular weight. The uronic acid increased in the number of carboxyl and carbonyl groups and double bonds (31), and the low molecular weights would have a looser structure and more reductive hydroxyl group terminals (32). These special structures increase the possibility of LBMP-2 accepting and eliminating the free radicals.

Antitumor Activity *in vitro*

With increasing LBMP-2 concentration, the viability of B16-F10 cells decreased gradually. After 24 h of intervention, the survival rate of each group is shown in **Figure 3**. When the LBMP-2 concentrations in the culture medium were 1.95 and 3.9 μg/mL, there was no inhibitory effect on B16-F10 cells. When the concentration was 62.5, 125, 250 μg/mL, the cell survival rate decreased to 55.30, 49.34, and 46.53% ($P < 0.001$). Because of the ability to inhibit cell growth, we chose 250 μg/mL for the follow-up study.

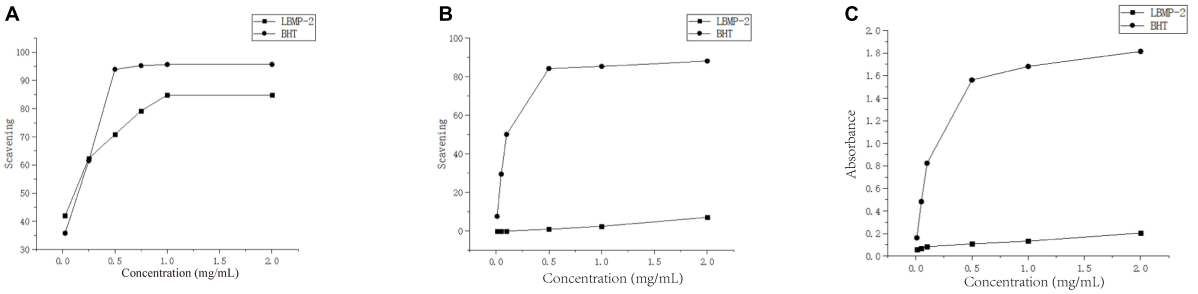

FIGURE 2 | Antioxidant activities of LBMP-2 *in vitro*. **(A)** Scavenging abilities on DPPH radicals. **(B)** Scavenging abilities on ABTS radicals. **(C)** Reducing power.

With Seahorse XF, two major energy-producing pathways, cellular mitochondrial respiration and glycolysis, can be measured simultaneously. We monitored the OCR (oxygen consumption rate) and ECAR (extracellular acidification rate) in real-time (**Figures 4A–C**) in response to treatment with LBMP-2 (250 μg/mL) for 24 h in B16-F10 cells. Compared to the control, the treated cells had no significant difference in metabolic potential. However, the OCR and ECAR of the cells were decreased relative to the control. The cell glycolytic ability and mitochondrial function were further tested. LBMP-2 significantly reduced the basal glycolysis and maximal glycolytic capacity compared with the control (**Figures 4D,E**). LBMP-2 also significantly reduced cell mitochondrial respiration compared with the control (**Figures 4F,G**), suggesting that LBMP-2 damages the mitochondrial function of B16-F10 cells. Mammalian cells have two key energy metabolism pathways, namely, oxidative phosphorylation (aerobic respiration) and glycolysis. Warburg (33) reported that in malignant tumor cells, glycolysis is the main pathway for their energy supply. LBMP-2 may block the energy supply of cells by simultaneously inhibiting the aerobic respiration and anaerobic respiration of B16-F10 cells, thereby inhibiting cell proliferation.

Antitumor Activity *in vivo*

Regulating the energy metabolism pathway to inhibit tumor growth may be one of the important mechanisms of antitumor drugs. AMPK is the regulating center of energy metabolism balance. It can not only cause an acute metabolic response but also promote metabolic reprogramming and adaptation by regulating specific transcription factors and coactivators (34). At the same time, there are many studies that prove that boosting immunity can inhibit tumor growth (35). To investigate the antitumor activity of LBMP-2 *in vivo*, we subcutaneously implanted a mouse melanoma model. A significant inhibitory effect of LBMP-2 was observed after 11 days of administration. **Figure 5** shows that the model group's average tumor weight was 2.400 ± 0.229 g, while the high dose group was reduced to 1.091 ± 0.1901 g, the low dose group was decreased to 1.460 ± 0.4440 g, and the CTX group was decreased to 0.2588 ± 0.1249 g (**Figure 5A**). The tumor inhibition rates were 54.53, 39.15, and 89.22%, respectively. In **Figure 5B**, the mice's actual body weights were displayed. The CTX group exhibited markedly decreased body weight. The administration group's spleen index was significantly higher than the model group, while the CTX group's spleen index was significantly lower (**Figure 5C**). The results showed that LBMP-2 can effectively increase the spleen index of mice, indicating that LBMP-2 can inhibit the growth of tumors while increasing the immune level of the body, which is safer than CTX.

In order to further assess LBMP-2′s antitumor efficacy, histological H&E staining assays and immunohistochemistry were applied to tumor tissues (**Figure 6**). A high tumor cell density was seen in the model group, and the nucleus was enlarged and stained deeply (15). Tumors that received CTX or LBMP-2 exhibited massively incomplete structures. According to the data, LBMP-2 inhibits the growth of melanoma tumors in mice. Contrary to the CTX group, there was a significant reduction in AMPK expression in the administration group. AMPK deletion did not accelerate solid tumor growth (36). These results suggest that LBMP-2 inhibits the growth of melanoma by reducing the expression of AMPK. In some cases, AMPK inhibition led to tumor cell death (37). The Seahorse energy metabolism meter found that LBMP-2 can reduce the overall metabolism of B16-F10 cells, which may be achieved by reducing the expression of AMPK.

Tumor occurrence and conventional treatment are often accompanied by a decline in immune function (38). The

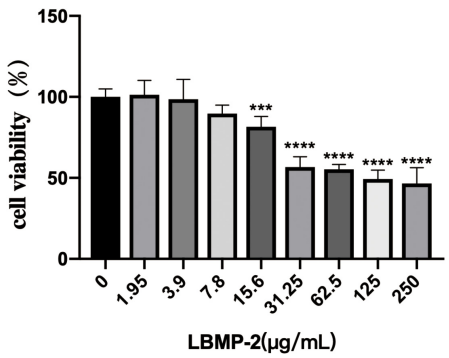

FIGURE 3 | The effect of LBMP-2 on the viability of B16-F10 cells ($n = 6$, $^{***}p < 0.001$, $^{****}p < 0.0001$).

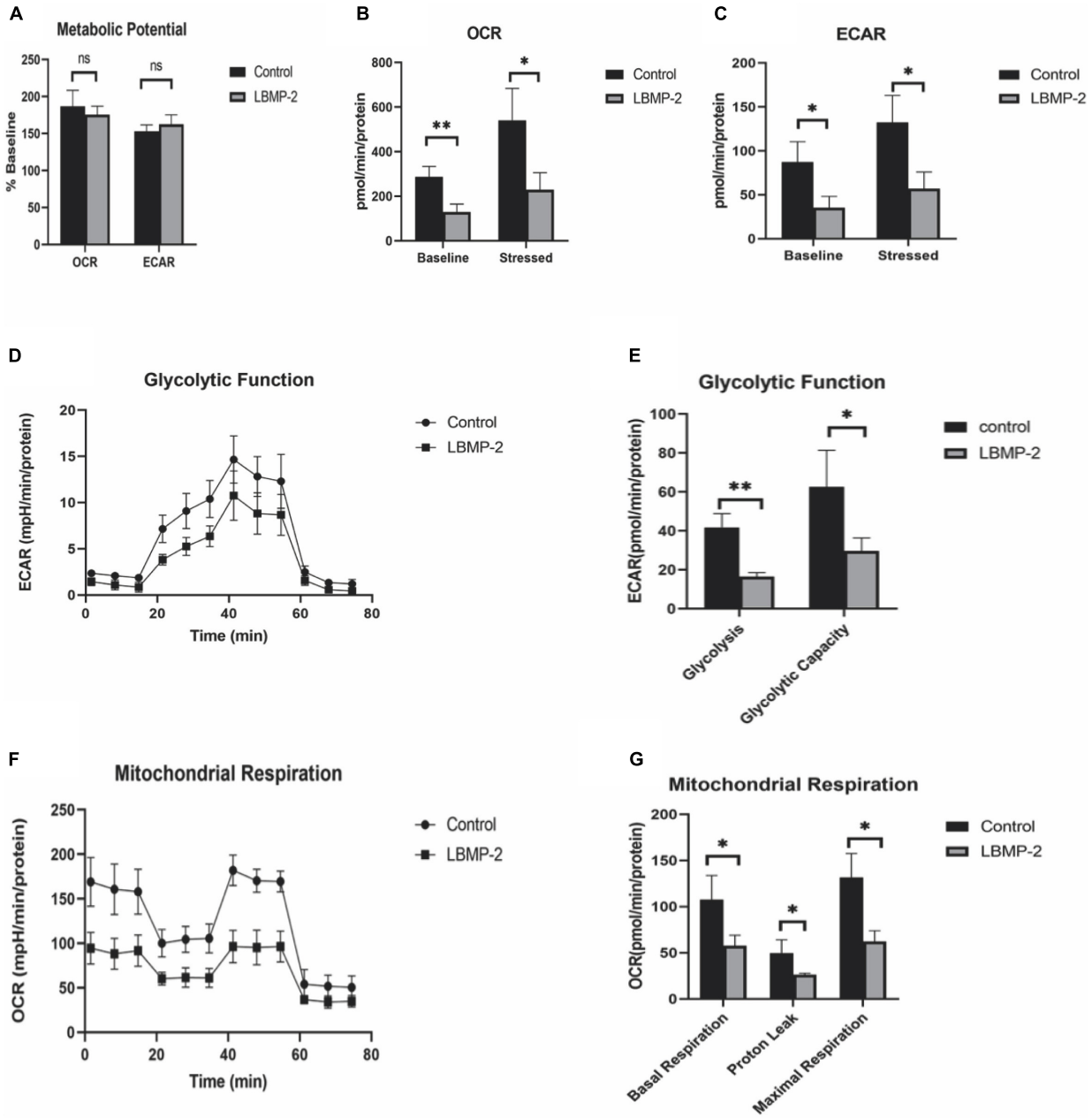

FIGURE 4 | The effect of LBMP-2 on the metabolism of B16-F10 cells. **(A–C)** Energy metabolism phenotype. **(D,E)** Glycolytic metabolism. **(F,G)** Aerobic Respiratory. (*$P < 0.05$, **$P < 0.01$, and ns: no significant difference).

spleen is one of the most important immune organs of the body and the main location of T lymphocytes. The level of the spleen index can evaluate the body's immune level (39). To determine whether the antitumor effect of LBMP-2 is related to its action on immune organs, histological H&E staining assays and immunohistochemistry were conducted (**Figure 7**). As shown in **Figures 7A–E**, the white arrows indicate white pulp, and the red arrows show red pulp. In the spleen tissue, CTX treatment severely damaged the architecture, the cells were arranged loosely. LBMP-2 treatment repaired the cell structure of the white and red pulp, increasing the proportion of white pulp. The immunohistochemistry results showed that compared to the control group, the model group $CD4^+$ cells ratio did not change, while the CTX group $CD4^+$ cells ratio was significantly lower, while the administration group $CD4^+$ cells ratio was significantly higher. The ratio of $CD4^+/CD8^+$ cells decreased in all groups compared to the control group. The CTX group's $CD4^+/CD8^+$ ratio decreased compared with the model group, whereas that of the administration group increased. No significant

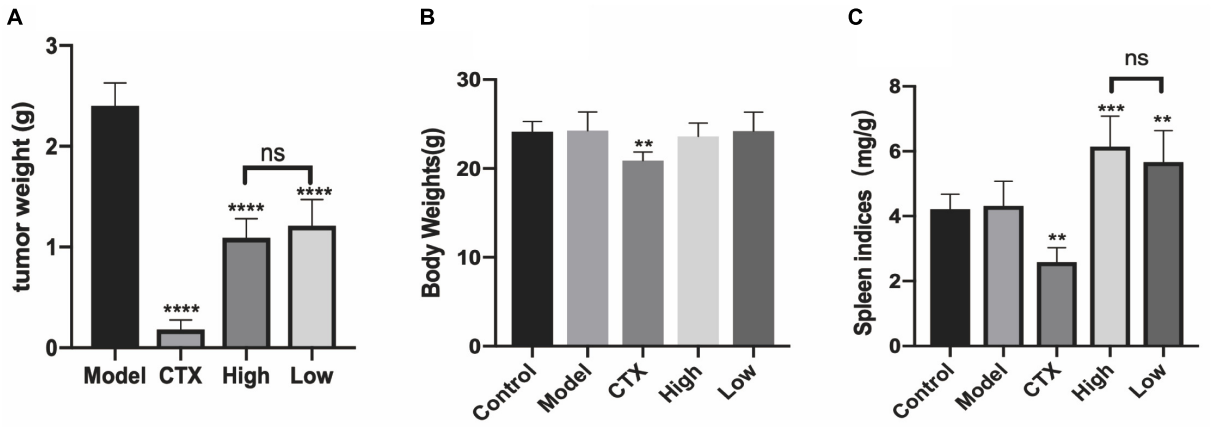

FIGURE 5 | LBMP-2 inhibited tumor growth in melanoma tumor-bearing mice. **(A)** The tumor weight from melanoma tumor-bearing mice; **(B)** the body weight of mice; **(C)** the spleen indices of mice ($N = 8$, $^{**}p < 0.01$, $^{***}p < 0.001$, $^{****}p < 0.0001$, and ns: no significant difference).

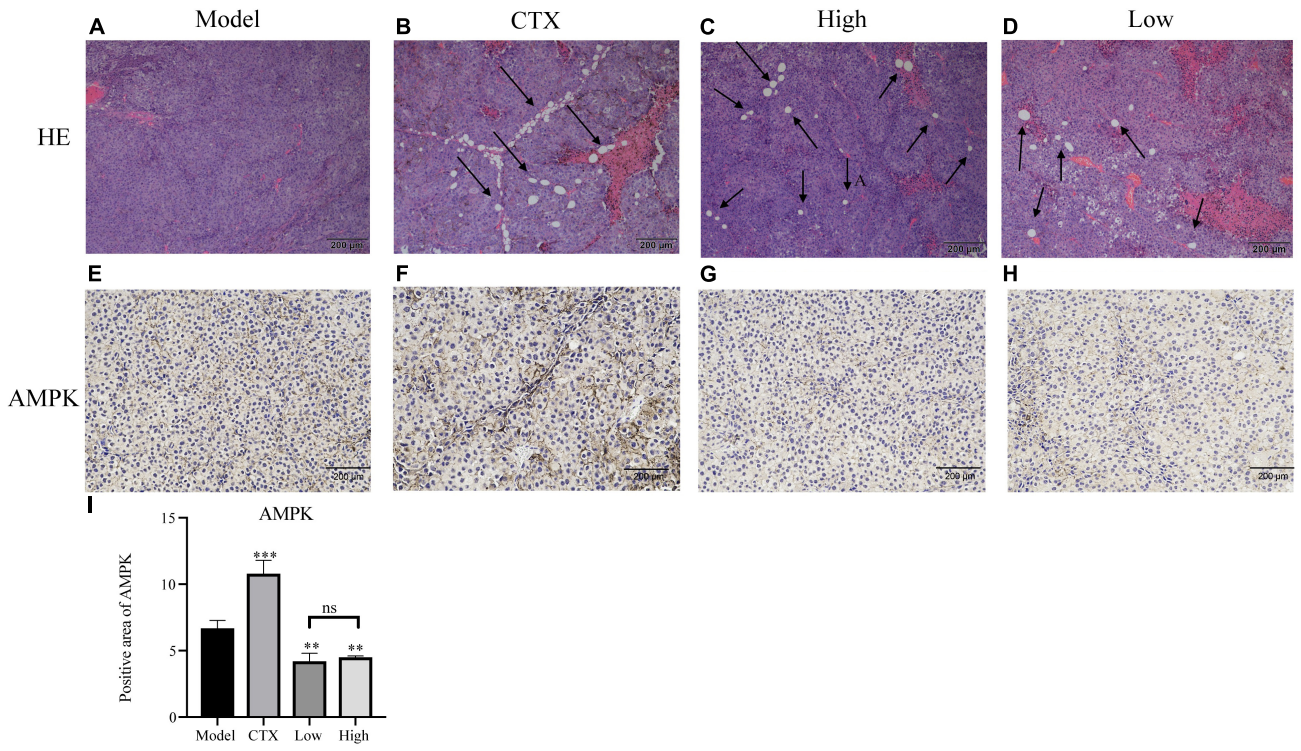

FIGURE 6 | Effects of LBMP-2 on tumors in melanoma tumor-bearing mice. **(A–D)** Representative H&E staining images of tumor sections separated from melanoma tumor-bearing mice. **(E–H)** Representative immunohistochemistry images of tumor sections separated from melanoma tumor-bearing mice. **(I)** Positive area of AMPK ($^{**}p < 0.01$, $^{***}p < 0.001$, and ns: no significant difference).

difference was found between the doses (**Figures 7F–I**). T lymphocytes are counted by the $CD3^+$ signal. $CD4^+$ cells, or Regulatory T cells, play an important role in the immune response. $CD8^+$ cells, or suppressor T cells, play the role of negative immunoregulation. Together, they recognize, respond to, and eliminate antigen substances. Immune function can be reflected in their levels. The $CD4^+/CD8^+$ ratio, specifically, was directly related to the immune system's function (40). This study shows that the increase in $CD3^+$ in all experimental groups may be related to the occurrence of tumors that activate the immune system. The spleen index, H&E and immunohistochemical results of the CTX group all showed that cyclophosphamide can destroy the structure of the spleen and reduce the immune function of the body, while these data of the administration group show that LBMP-2 can improve the function of the spleen and enhance immunity.

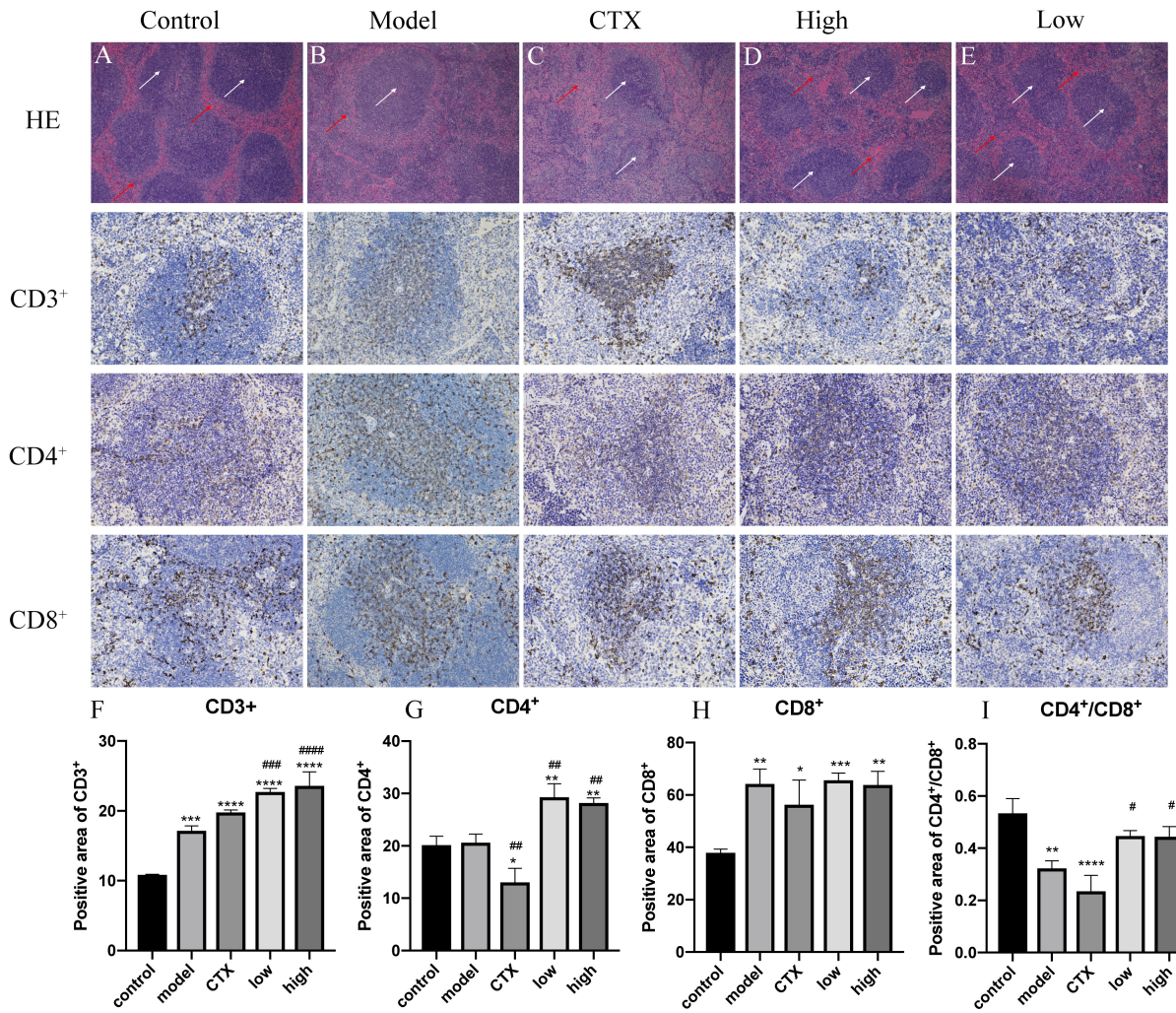

FIGURE 7 | Effects of LBMP-2 on spleen morphology in melanoma tumor-bearing mice. **(A–E)** H&E-staining result, **(F–I)** positive area of immunohistochemistry. $^{*}p < 0.05$, $^{**}p < 0.01$, $^{***}p < 0.001$, $^{****}p < 0.0001$ compared with the control group. $^{\#}p < 0.05$, $^{\#\#}p < 0.01$, $^{\#\#\#}p < 0.001$, $^{\#\#\#\#}p < 0.0001$ compared with the model group.

The results suggest that the antitumor effect of LBMP-2 may be related to improving the spleen function of B16-F10 tumor-bearing mice.

CONCLUSION

Based on our results, LBMP-2 from *L. brevituba* has antioxidation, inhibits tumor cell proliferation effects *in vitro*, and inhibits tumor growth in tumor-bearing mice. The low molecular weight and high uronic acid content might explain these biological activities. Its antitumor mechanism may be related to inhibiting tumor energy metabolism by down-regulating the expression of AMPK protein while regulating the immune function of the spleen. This research shows that LBMP-2 has potential application value in antitumor drug therapy.

DATA AVAILABILITY STATEMENT

The original contributions presented in this study are included in the article/supplementary material, further inquiries can be directed to the corresponding author/s.

ETHICS STATEMENT

The animal study was reviewed and approved by the Ethics Committee of Chongqing Medical University.

AUTHOR CONTRIBUTIONS

RG: investigation, methodology, and writing—original draft. WC: conceptualization, formal analysis, writing—original draft, funding acquisition, and project administration. HC, WT, QL,

JL, HH, and BY: conceptualization, data curation, validation, and methodology. DZ: project administration, supervision, validation, funding acquisition, and writing—review and editing. All authors contributed to the article and approved the submitted version.

FUNDING

This work was supported by the Chongqing Technology Innovation and Application Development Project (grant no. cstc2020jscx-dxwtBX0054).

REFERENCES

1. Yuan X, Zhao J, Wang H, Yu R, Wen H, Liu Z, et al. Antiproliferative activity of phenylpropanoids isolated from *Lagotis brevituba* maxim. *Phytother Res.* (2017) 31:1509–20. doi: 10.1002/ptr.5875
2. Bi S, Huang W, Chen S, Huang C, Li C, Guo Z, et al. *Cordyceps militaris* polysaccharide converts immunosuppressive macrophages into M1-like phenotype and activates T lymphocytes by inhibiting the PD-L1/PD-1 axis between TAMs and T lymphocytes. *Int J Biol Macromol.* (2020) 150:261–80. doi: 10.1016/J.IJBIOMAC.2020.02.050
3. Li S, Liu H, Wang W, Wang X, Zhang C, Zhang J, et al. Antioxidant and anti-aging effects of acidic-extractable polysaccharides by *Agaricus bisporus*. *Int J Biol Macromol.* (2018) 106:1297–306. doi: 10.1016/J.IJBIOMAC.2017.08.135
4. Chen X, Sheng Z, Qiu S, Yang H, Jia J, Wang J, et al. Purification, characterization and in vitro and in vivo immune enhancement of polysaccharides from mulberry leaves. *PLoS One.* (2019) 14:e0208611. doi: 10.1371/journal.pone.0208611
5. Dan Z, Lihong T, Ling Y, Wei T, Ruixue G, Quji L, et al. In vitro and in vivo antioxidative activity against radiation-induced damage and the systematic chemical components of different extracts of maxim. *Evid Based Complement Alternat Med.* (2020) 2020:9726431. doi: 10.1155/2020/9726431
6. Yuan R, Tao X, Liang S, Pan Y, He L, Sun J, et al. Protective effect of acidic polysaccharide from *Schisandra chinensis* on acute ethanol-induced liver injury through reducing CYP2E1-dependent oxidative stress. *Biomed Pharmacother.* (2018) 99:537–42. doi: 10.1016/J.BIOPHA.2018.01.079
7. Masuko T, Minami A, Iwasaki N, Majima T, Nishimura SI, Lee YC. Carbohydrate analysis by a phenol–sulfuric acid method in microplate format. *Anal Biochemist.* (2005) 339:69–72. doi: 10.1016/J.AB.2004.12.001
8. Blumenkrantz N, Asboe-Hansen G. New method for quantitative determination of uronic acids. *Anal Biochemist.* (1973) 54:484–9. doi: 10.1016/0003-2697(73)90377-1
9. Bradford MM. A rapid and sensitive method for the quantitation of microgram quantities of protein utilizing the principle of protein-dye binding. *Anal Biochemist.* (1976) 72:248–54. doi: 10.1016/0003-2697(76)90527-3
10. Tan L-H, Zhang D, Yu B, Zhao S-P, Cao W-G. Antioxidant activity of the different polar solvent extracts of *Magnolia officinalis* leaves and purification of main active compounds. *Eur Food Res Technol.* (2014) 240:815–22. doi: 10.1007/s00217-014-2387-5
11. Kan L, Chai Y, Li X, Zhao M. Structural analysis and potential anti-tumor activity of *Sporisorium reilianum* (Fries) polysaccharide. *Int J Biol Macromol.* (2020) 153:986–94. doi: 10.1016/J.IJBIOMAC.2019.10.228
12. Liu S, Yang Y, Qu Y, Guo X, Yang X, Cui X, et al. Structural characterization of a novel polysaccharide from *Panax notoginseng* residue and its immunomodulatory activity on bone marrow dendritic cells. *Int J Biol Macromol.* (2020) 161:797–809. doi: 10.1016/J.IJBIOMAC.2020.06.117
13. Chen Z, Zhang D, Guo JJ, Tao W, Gong RX, Yao L, et al. Active components, antioxidant, inhibition on metabolic syndrome related enzymes, and monthly variations in mature leaf Hawk tea. *Molecules.* (2019) 24:657. doi: 10.3390/molecules24040657
14. Lin RK, Choong CY, Hsu WH, Tai CJ, Tai CJ. Polysaccharides obtained from mycelia of cordyceps militaris attenuated doxorubicin-induced cytotoxic effects in chemotherapy. *Afr Health Sci.* (2019) 19:2156–63. doi: 10.4314/ahs.v19i2.40
15. Yang Y, Sun X, Zhao Y, Ge W, Ding Z, Liu J, et al. Anti-tumor activity and immunogenicity of a succinoglycan riclin. *Carbohydr Polym.* (2021) 255:117370. doi: 10.1016/J.CARBPOL.2020.117370
16. Zhu R, Zhang X, Wang Y, Zhang L, Zhao J, Chen G, et al. Characterization of polysaccharide fractions from fruit of *Actinidia arguta* and assessment of their antioxidant and antiglycated activities. *Carbohydr Polym.* (2019) 210:73–84. doi: 10.1016/J.CARBPOL.2019.01.037
17. Li W, Wang K, Jiang N, Liu X, Wan M, Chang X, et al. Antioxidant and antihyperlipidemic activities of purified polysaccharides from *Ulva pertusa*. *J Appl Phycol.* (2018) 30:2619–27. doi: 10.1007/s10811-018-1475-5
18. Liang XX, Gao YY, Pan Y, Zou YF, He M, He M, et al. Purification, chemical characterization and antioxidant activities of polysaccharides isolated from *Mycena dendrobii*. *Carbohydr Polym.* (2019) 203:45–51. doi: 10.1016/J.CARBPOL.2018.09.046
19. Gao J, Zhang T, Jin ZY, Xu XM, Wang JH, Zha XQ, et al. Structural characterisation, physicochemical properties and antioxidant activity of polysaccharide from *Lilium lancifolium* Thunb. *Food Chem.* (2015) 169:430–8. doi: 10.1016/J.FOODCHEM.2014.08.016
20. He S, Wang X, Zhang Y, Wang J, Sun H, Wang J, et al. Isolation and prebiotic activity of water-soluble polysaccharides fractions from the bamboo shoots (*Phyllostachys praecox*). *Carbohydr Polym.* (2016) 151:295–304. doi: 10.1016/J.CARBPOL.2016.05.072
21. Tamaki Y, Konishi T, Fukuta M, Tako M. Isolation and structural characterisation of pectin from endocarp of *Citrus depressa*. *Food Chem.* (2008) 107:352–61. doi: 10.1016/J.FOODCHEM.2007.08.027
22. Kang J, Cui SW, Phillips GO, Chen J, Guo Q, Wang Q. New studies on gum ghatti (*Anogeissus latifolia*) part II. Structure characterization of an arabinogalactan from the gum by 1D, 2D NMR spectroscopy and methylation analysis. *Food Hydrocoll.* (2011) 25:1991–8. doi: 10.1016/J.FOODHYD.2010.11.021
23. Svetličić V, Žutić V, Pletikapić G, Mišić Radić T. Marine polysaccharide networks and diatoms at the nanometric scale. *Int J Mole Sci.* (2013) 14:20064–78. doi: 10.3390/ijms141020064
24. Jena BP, Hörber JKH editors. *Force Microscopy: Applications in Biology and Medicine*. Hoboken, NJ: John Wiley & Sons, Inc. (2005). doi: 10.1002/0470007702
25. Rozi P, Abuduwaili A, Mutailifu P, Gao Y, Rakhmanberdieva R, Aisa HA, et al. Sequential extraction, characterization and antioxidant activity of polysaccharides from *Fritillaria pallidiflora* Schrenk. *Int J Biol Macromol.* (2019) 131:97–106. doi: 10.1016/J.IJBIOMAC.2019.03.029
26. Lin S, Al-Wraikat M, Niu L, Zhou F, Zhang Y, Wang M, et al. Degradation enhances the anticoagulant and antiplatelet activities of polysaccharides from *Lycium barbarum* L. leaves. *Int J Biol Macromol.* (2019) 133:674–82. doi: 10.1016/J.IJBIOMAC.2019.04.147
27. Yi Y, Zhang MW, Liao ST, Zhang RF, Deng YY, Wei ZC, et al. Effects of alkali dissociation on the molecular conformation and immunomodulatory activity of longan pulp polysaccharide (LPI). *Carbohydr Polym.* (2012) 87:1311–7.
28. Bao XF, Dong Q, Fang JN. Structure and conformation behavior of a glucan from spores of *Ganoderma lucidum* (Fr.) karst. *Acta Biochimica et Biophysica Sinica.* (2000) 32:557–61.
29. Liang D, Zhou Q, Gong W, Wang Y, Nie Z, He H, et al. Studies on the antioxidant and hepatoprotective activities of polysaccharides from *Talinum triangulare*. *J Ethnopharmacol.* (2011) 136:316–21. doi: 10.1016/J.JEP.2011.04.047
30. Apak R, Özyürek M, Güçlü K, Çapano$_1$lu E. Antioxidant activity/capacity measurement. 1. Classification, physicochemical principles, mechanisms, and electron transfer (ET)-based assays. *J Agric Food Chem.* (2016) 64:997–1027. doi: 10.1021/acs.jafc.5b04739
31. Wu H, Min T, Li X, Li L, Lai F, Tang Y, et al. Physicochemical properties and antioxidant activities of acidic polysaccharides from wampee seeds. *Int J Biol Macromol.* (2013) 59:90–5. doi: 10.1016/J.IJBIOMAC.2013.04.020
32. Wang J, Hu S, Nie S, Yu Q, Xie M. Review article reviews on mechanisms of in vitro antioxidant activity of polysaccharides. *Oxid Med Cell Longev.* (2016) 2016:5692852. doi: 10.1155/2016/5692852

33. Warburg O, Wind F, Negelein E. The metabolism of tumors in the body. *J Gen Physiol.* (1927) 8:519–30. doi: 10.1085/jgp.8.6.519
34. Collodet C, Foretz M, Deak M, Bultot L, Metairon S, Viollet B, et al. AMPK promotes induction of the tumor suppressor FLCN through activation of TFEB independently of mTOR. *FASEB J.* (2019) 33:12374–91. doi: 10.1096/fj.201900841R
35. Jiang S, Wang S, Zhang L, Tian L, Li L, Liu Z, et al. Hesperetin as an adjuvant augments protective anti-tumour immunity responses in B16F10 melanoma by stimulating cytotoxic CD8+ T cells. *Scand J Immunol.* (2020) 91:e12867. doi: 10.1111/sji.12867
36. Eichner LJ, Brun SN, Herzig S, Young NP, Curtis SD, Shackelford DB, et al. Genetic analysis reveals AMPK Is required to support tumor growth in murine Kras-dependent lung cancer models. *Cell Metabol.* (2019) 29:285–302.e7. doi: 10.1016/j.cmet.2018.10.005
37. Kishton RJ, Barnes CE, Nichols AG, Cohen S, Gerriets VA, Siska PJ, et al. AMPK is essential to balance glycolysis and mitochondrial metabolism to control T-all cell stress and survival. *Cell Metabol.* (2016) 23:649–62. doi: 10.1016/j.cmet.2016.03.008
38. Bhatia A, Kumar Y. Cellular and molecular mechanisms in cancer immune escape: a comprehensive review. *Exp Rev Clin Immunol.* (2014) 10:41–62. doi: 10.1586/1744666X.2014.865519
39. Yoo JH, Lee YS, Ku SK, Lee HJ. *Phellinus baumii* enhances the immune response in cyclophosphamide-induced immunosuppressed mice. *Nutr Res.* (2020) 75:15–31. doi: 10.1016/J.NUTRES.2019.12.005
40. Xiong W, Liu ZG, Xiong L, Xiong MC, Lei GH, Wu Y, et al. CD3+, CD4+, and CD8+ expression in cells in peripheral blood of silicosis patients and intervention effect of Thymalfasin. *Ann Clin Lab Sci.* (2019) 49:368–71.

Conflict of Interest: The authors declare that the research was conducted in the absence of any commercial or financial relationships that could be construed as a potential conflict of interest.

Publisher's Note: All claims expressed in this article are solely those of the authors and do not necessarily represent those of their affiliated organizations, or those of the publisher, the editors and the reviewers. Any product that may be evaluated in this article, or claim that may be made by its manufacturer, is not guaranteed or endorsed by the publisher.

Copyright © 2022 Gong, Cao, Huang, Yu, Chen, Tao, Luorong, Luo and Zhang. This is an open-access article distributed under the terms of the Creative Commons Attribution License (CC BY). The use, distribution or reproduction in other forums is permitted, provided the original author(s) and the copyright owner(s) are credited and that the original publication in this journal is cited, in accordance with accepted academic practice. No use, distribution or reproduction is permitted which does not comply with these terms.

frontiers | Frontiers in Nutrition

ORIGINAL RESEARCH
published: 13 July 2022
doi: 10.3389/fnut.2022.961875

Pectin Stabilized Fish Gelatin Emulsions: Physical Stability, Rheological, and Interaction Properties

*Sheng Huang[1,2], Hui Wang[1,2], Shu Wang[1,2], Xiaomei Sha[2,3], Ning Chen[1,2], Yueming Hu[1,2] and Zongcai Tu[1,2,3]**

[1] State Key Laboratory of Food Science and Technology, Nanchang University, Nanchang, China, [2] National R&D Center for Freshwater Fish Processing, Jiangxi Normal University, Nanchang, China, [3] Engineering Research Center for Freshwater Fish High-Value Utilization of Jiangxi, Jiangxi Normal University, Nanchang, China

Pectin, a kind of natural polysaccharide, shows the attractive potential as a natural stabilizer for protein emulsion. The aim of this study is to investigate the effect of pectin on the physical stability, rheology, interface, and interaction properties of the fish gelatin (FG) emulsion, as pectin was utilized to improve the stability of FG, fish oil emulsion. During the study, when pH $<$ 6, the FG-pectin emulsion displayed better storage stability and salinity tolerance. Analyzing the result, pectin could avoid phase separation at the freeze-thaw process and prevent the liquid-gel transition of FG emulsions during storage. On the other hand, when pH $\geq$ 6, the emulsion displayed high viscosity due to the complex flocculation and stratified during long-term storage. Electrostatic interactions, hydrophobic interactions, and hydrogen bonding of the FG-pectin complexes in the emulsion were all reduced. Overall, pectin improved the stability of FG emulsions through electrostatic repulsion, hydrophobic interactions, and steric hindrance.

Keywords: pectin, fish gelatin, emulsions, non-covalent interactions, interface performance, rheological properties

OPEN ACCESS

Edited by:
Xiaolong Ji,
Zhengzhou University of Light Industry, China

Reviewed by:
Ping Shao,
Zhejiang University of Technology, China
Hui Zhang,
Zhejiang University, China
Jianhua Liu,
Zhejiang University of Technology, China

***Correspondence:**
Zongcai Tu
tuzc_mail@aliyun.com

Specialty section:
This article was submitted to Food Chemistry, a section of the journal Frontiers in Nutrition

Received: *05 June 2022*
Accepted: *23 June 2022*
Published: *13 July 2022*

Citation:
Huang S, Wang H, Wang S, Sha X, Chen N, Hu YM and Tu ZC (2022) Pectin Stabilized Fish Gelatin Emulsions: Physical Stability, Rheological, and Interaction Properties. Front. Nutr. 9:961875. doi: 10.3389/fnut.2022.961875

INTRODUCTION

Pectin is an anionic polysaccharide derived from plant cell walls and intercellular extracted from orange peel, apple peel, or jujube (1, 2). It is a dietary fiber, which is conducive to weight control and intestinal health, universally utilized as a food additive or medicine carrier material (3). Gelatin is the most commonly used emulsifier, gel, and food supplement needed for upholding the tissues of the human body (4). Based on material sources, it can be divided into mammalian gelatin (e.g., pig and cow), poultry gelatin, and fish gelatin (FG) among others (5). Among them, FG is extracted from various fish byproducts (skin/scale/bone), which have a cheap raw material (fish scale) and low risk of zoonotic diseases (6).

Many studies have focused on the interaction and application of pectin and gelatin. They can form a complex through complex coacervation, edible film, or emulsion to enhance performance on both sides as drug or nutrient delivery systems (7–9). The entrapment and transportation of functional oils by biomacromolecule emulsion are a hot topic in the nutrient delivery process

(10). Fish oil has been widely studied because it is rich in docosahexaenoic acid (DHA, C22:6n3) and eicosapentaenoic acid (EPA, C20:5n3), which can effectively reduce plasma triglycerides (11). FG-pectin-embedded fish oil is more conducive to health production and application. But the emulsifying performance of pectin is not ideal; its emulsifying ability is limited by its composition (degree of methyl esterification, protein residues, neutral sugar side chain, and molecular weight), and pectin as an emulsifier is sensitive to environmental pH and ionic strength (12). Although the foaming and water absorption properties of FG are better than those of mammalian gelatin, the emulsifying properties of FG are worse than those of mammalian gelatin (13). Moreover, FG is a linear protein, and its emulsification stability is not as good as that of spherical protein similar to whey protein. Therefore, the application of pectin or FG as a natural emulsifier in production and processing is still limited. In addition, the binding of FG-pectin, similar to most polysaccharide–protein molecules, produces phase separation, which is closely related to their concentrations and other factors (14).

Studies have shown that plant polysaccharides can improve protein emulsion stability (15). For example, gum Arabic enhances the emulsion stability of whey protein isolate (16). Porcine gelatin–pectin-mixed solution was incubated for 4 h under alkaline conditions for conjugation to improve emulsion stability, however, the non-heat-treated gelatin–pectin emulsion was layered after storage for 1 day (8). Besides that, few studies have focused on interfacial rheological changes and interaction forces in the formation of the FG-pectin-stabilized emulsion process. Therefore, the purpose of this study was to improve the storage stability of FG emulsion *via* non-covalent effect and investigate the effect of pectin on the interfacial rheological changes and interaction forces of FG emulsion. The effects of different concentrations of pectin, environmental factors (freeze-thaw, heating, and pH changes), and long-term storage on emulsion stability were investigated, and the underlying mechanisms were analyzed.

MATERIALS AND METHODS

Materials

Pectin (from citrus peel, GalA $\geq$ 74%, methoxylation degree 54%) was bought from Sigma Co., Ltd. (Shanghai, China). FG (*Tilapia mossambica*, type A, 260 Bloom) was obtained from Ding Biological Technology Co., Ltd. (Suzhou, China). Deep-sea fish oils (DHA + EPA $\geq$ 80%) were purchased from Guanchen Biological Technology Co., Ltd. (Shanghai, China). All other chemicals were of analytical grade and obtained from commercial sources.

Preparation of Fish Oil-Loaded Pectin-Fish Gelatin-Stabilized Emulsions

Fish gelatin (2% w/v) and pectin (2%, 3% w/v) were heated to 60°C with continuous stirring to dissolve thoroughly. The emulsions were prepared by "layer-by-layer" approach (**Supplementary Figure 1**). The 4 mL fish oil was added into the 20 mL FG solution and mechanically sheared by a T18 homogenizer with a 15-mm head at speed of 12,000 rpm for 60 s. Then, 20 mL pectin was added to the previous solution and sheared at the same rate for 30 s. The controlled group was added 20 mL of deionized water instead. To detect the effect of pH on the emulsions, three groups (FG 1.0% w/v and pectin 1.0% w/v, pH 4.2) were adjusted pH values at 6, 8, and 10 with 0.1 M NaOH. To compare the mix method with the layer-by-layer method, 1.0% (w/v) pectin and 1.0% (w/v) FG were mixed before adding fish oil, then following the above process. All the primary emulsions were added into a high-pressure homogenizer (UH-06, Union-Biotech, Shanghai, China) at 100 Mpa pressure of 2 min. Therefore, the final FG concentration of emulsions was 1.0% (w/v) and the aqueous solution to fish oil ratio was 10:1. The fresh emulsion was centrifuged in a high-speed refrigerated centrifuge (10,000 $\times$ *g*, 1 h, 4°C) to observe the stratification.

Different concentrations of pectin (0.5%, 1.0%, 1.5% w/v) in emulsions named 0.5%, 1.0%, 1.5%. The emulsion-added deionized water instead of pectin was set as a control group named FE. The various pH groups were pH6, pH8, and pH10. After storage at 25°C a day, the pH6 and pH10 groups were adjusted to pH 4.2 with 0.1 M HCl (referred to as pH6-A and pH10-A, respectively).

Particle Size and Zeta Potential

Particle size measurements were conducted by the Malvern laser particle size analyzer (Ms3000, Malvern, United Kingdom). The refractive index of the emulsion particles and the aqueous dispersion medium were 1.46 and 1.33 (17). The emulsions were dripped into the test container (diluted by deionized water) until the sample concentration reached the detection limit.

Zeta potential measurements were performed by the Malvern laser particle size analyzer (Nano ZSP, Malvern, United Kingdom). The emulsions were diluted 100-fold with deionized water.

Emulsion Stability Analysis

The dynamic physical stability (DPS) was determined with a LUMi-Sizer (L.U.M. GmbH, Berlin, Germany) according to the previous report (18). The machine detects emulsions stability *via* horizontal centrifugal force. The centrifugation speed was set at 4,000 rpm for 30 min and the temperature was constant at 25°C.

Freeze-thaw stability test: Froze 5 mL emulsion sample at −20°C for 22 h and then thaw at 30°C for 2 h. Repeat this Freeze-thaw cycle four times to determine DPS, particle size, and zeta potential.

Heat treatment stability test: Heat 5 mL emulsion sample to 60 and 70°C for 30 min in a water bath. DPS, particle size, and potential are then measured after cooling to room temperature.

Influence of salt concentration: Mix 5 mL emulsion sample with NaCl solution, the final NaCl concentrations are 0, 300, 600 mmol/L and total volume is 10 mL, then measure the particle size and potential.

Storage Measurement

Macroscopic observations: The 3.5 mL of emulsions containing 0.01% (w/v) sodium azide were transferred to a glass container

and reserved at 25°C 50% RH. The stratification of the emulsion was observed during the storage.

Optical microscope observations: during the storage, 4 μL emulsion was dropped on a glass slide and then covered by a coverslip. The samples were observed using an inverted microscope (Olympus Co., Ltd., Tokyo, Japan) with a built-in camera with 40-fold objective lens.

Confocal Laser Scanning Microscopy

The microstructure of emulsions was analyzed by Confocal Laser Scanning Microscopy (CLSM) (Leica TCS SP8 SMD, Germany) according to the method of Miao et al. (19). The emulsion (1 mL) was mixed with 40 μL dye (0.1% Nile red dye and 1.0% Nile blue) and protected from light. Then, 4 μL of samples were added onto a glass slide to observe. Two lasers (488 and 633 nm) were used to excite Nile red and Nile blue, respectively.

Surface Hydrophobicity

Emulsion surface hydrophobicity was determined by the 8-anilino-1-naphthalenesulfonic acid fluorescent probe (ANS) method according to the method of Li et al. (20) with some modifications. The emulsion (0.5 mL) was mixed with 25 μL 8 mM ANS and 4.5 mL of deionized water. The mix stood in the dark at room temperature for 1 h then measured at λex = 370 nm and λem = 400–600 nm.

Rheology Properties

The rheological properties of emulsions were determined based on the procedure using the Paar-Physica MCR 302 rheometer (Anton Paar, Ostfildern, Germany) described by Xu et al. (21) with some modifications.

Dynamic frequency sweep: The emulsion (about 17 mL) was poured into a concentric barrel and kept at 25°C for 5 min. The frequency was ranging from 0.1 to 100 rad/s, and the strain value was fixed at 0.5%.

Flow sweep test: The shear rate was increased from 1 1/s to 100 1/s with a fixed strain of 0.5%. The apparent viscosity (AV, η, Pa·s) was recorded. AV was modeled as:

$$\eta = D\gamma^{n-1}, \quad (1)$$

Where D is the consistency index (Pa·s^n), γ is the shear rate (1/s), and n is the flow behavior index.

Interfacial Properties

An optical contact angle measuring instrument (Optical contact angle system OCA, Germany) was used to detect the change in the interface pressure at the oil-water interface. Before the test, the density of water, pectin, FG, and FG-pectin were detected by flat-bottomed spherical density bottles after being treated with T18 homogenizer at speed of 12,000 rpm for 60 s. The 1.0% (w/v) pectin and 1.0% (w/v) FG were mixed and homogenized at 100 Mpa pressure for 2 min, which is named HP 1.0%. Using a syringe with a straight needle, the sample is drawn and got rid of disturbance of bubbles in the liquid. Then, the needle was immersed in a transparent glass tank filled with fish oil. A droplet of 20 μL was applied to analyze the droplet shape in an adsorption time (at least 180 min).

Interaction Force Analysis

Surface hydrophobicity analysis was measured by the method of Li et al. (20) with some modifications. The method was to add 0.5 mL emulsion and 25 μL of 8 mM ANS to 4.5 mL of deionized water, wait reaction performed at room temperature for 1 h in the dark, then analyzed with a fluorescence spectrometer in λ_{ex} = 370 nm and λ_{em} = 400–600 nm.

The emulsion (1 mL) was poured into EP tubes, after being freeze-dried, and was subjected to infrared spectroscopic analysis with 32 scans from 500 to 4,000 cm^{-1}, according to the method described by Ren et al. (22).

Statistical Analysis

Three or more replicates were tested independent experiments, and the results were expressed as mean values ± standard deviations. Data analyses were subjected to one-way ANOVA, with the significance level set at $p < 0.05$. The SPSS 22.0 software (SPSS Inc., Chicago, IL, United States) and Origin Pro 9.0 software were used for statistical and graphical analysis.

RESULTS AND DISCUSSION

Effect of Preparation Method on the Properties of Emulsions

Generally, emulsions stabilized by polysaccharide–protein complexes are fabricated by two alternative methods (23). (1) For mixing before the emulsification method, for example, soy polysaccharide and soy protein mixture are utilized to fabricate soybean oil emulsion (24). (2) For the layer-by-layer method, shear and homogenization are used to form a primary emulsion with gelatin–oil; the primary emulsion is then mixed with pectin to prepare two-layer emulsions. In this study, DPS was used to affect the stability of emulsions (**Figure 1A**). After centrifugation, different mass phases were divided, resulting in variations in light transmission. These variations were detected by near-infrared spectroscopy. The worse the stability of the emulsion, the greater the variation in transmittance with centrifugal time and the larger the instability index. FE emulsion had a high DPS, which means the disability of pure FG emulsion. Group 1% and Mix had similar DPS ($p > 0.05$) which were lower than FE ($p < 0.05$), indicating that the complex emulsion fabricated by the two methods had good stability. Although some research reported that the layer-by-layer method had a primary problem, its emulsion was prone to bridging or depletion in the flocculation. As such, the mixed emulsion method has better stability than the layer-by-layer method (25). On the other hand, researchers commonly prepare stable emulsion with proteins and polysaccharides through the layer-by-layer method (26). The difference in emulsion stability prepared by the two methods was not obvious in this study.

To further study the difference between the two methods, the difference among FG emulsion, group 1% (layer-by-layer

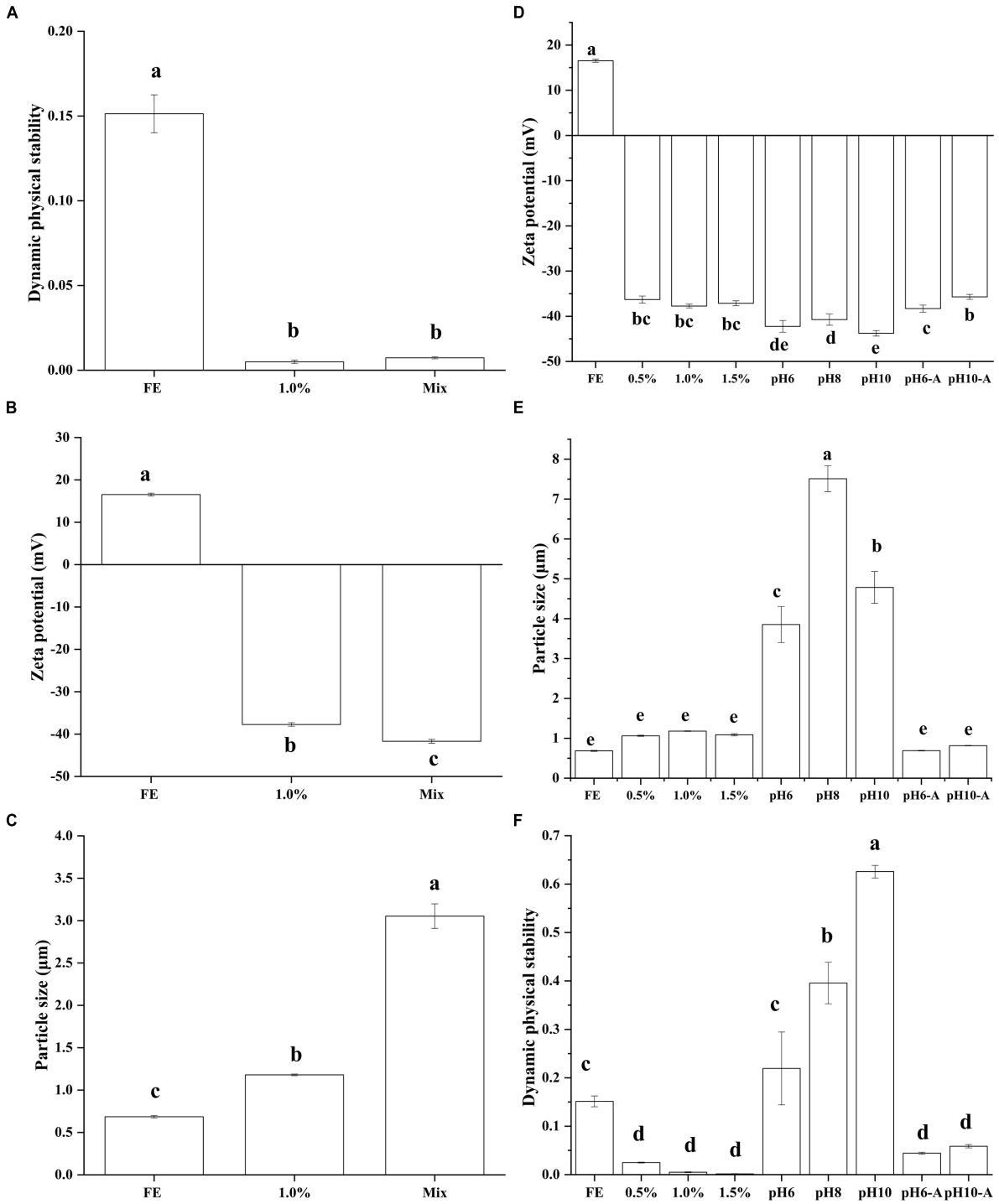

FIGURE 1 | Effect of preparation method on the dynamic physical stability **(A)**, zeta potential **(B)**, particle size **(C)** of complex emulsions; effect of pectin and pH on the zeta potential **(D)**, particle size **(E)**, and dynamic physical stability **(F)** of complex emulsions.

method), and Mix (mixing before emulsification method) in zeta potential and particle size (D_{43}) were compared (**Figures 1B,C**). Zeta potential and particle size are considerable indicators to evaluate the stability of an emulsion system. Pectin brought abundant negative charge from -COO^- leading to the negative of the complex emulsion zeta potential. The zeta potential of group Mix was lower than group 1% ($p < 0.05$). The particle size is closely related to the surface properties and dispersing ability of

the material. Generally speaking, a smaller particle size emulsion has better spatial stability (27). Pectin complex emulsion had a higher particle size than FG emulsion ($p < 0.05$). The particle size of group Mix (3.05 μm) was nearly 2.6 times that of group 1% (1.18 μm). From these results, it can be speculated that pectin provides steric hindrance to the emulsion droplets, resulting in larger particle size but better emulsion stability. Similar research reported that dextran may enhance soy protein isolate steric hindrance leading to the better physical and structural stability of complex emulsion (28). Then, whether the complex formed by pectin and FG will affect the emulsification ability of FG will be analyzed in the subsequent interfacial properties analysis.

Effect of Pectin and pH on the Properties of Complex Emulsions

Zeta Potential, Particle Size, and Dynamic Physical Stability of Complex Emulsions

Zeta potential and particle size are considerable indicators to evaluate the stability of an emulsion system. The zeta potential of each emulsion is shown in **Figure 1D**. The pI of FG was about pH 9; thus, the FE emulsion (pH 5.9) showed a positive charge. With the addition of pectin, the zeta potential transformed from a positive charge (18.97 mV) to a negative charge (−44.96 mV). Because the chains of pectin carry abundant -COOH (12), the zeta potential of complex emulsions became negative. The absolute value was much higher than that of the control FE. A previous study revealed that the high absolute zeta potential enhances emulsion stability (29). Van der Waals force and electrostatic interaction force in colloid constitute the main interaction between the two particles (30). Electrostatic repulsion in FG-pectin emulsion was dominant. FG-pectin emulsions were prone to more negative charges with the intensified alkalinity of solutions. However, the differences in zeta potentials at pH 6, 8, and 10 emulsions were not significant ($p > 0.05$). Because most -COOH in the FG or pectin chains transformed to -COO^-, the negative charges were saturated. After emulsions were centrifuged (**Supplementary Figure 2**), the bottom layer of FG-pectin emulsions (pH < 6) were cloudy and the others were transparent. Gelatin and pectin can form coacervates *via* electrostatic interaction (31), so the cloudy of bottom layer was FG-pectin coacervates. With the increase of pH, the electrostatic interaction between FG and pectin weakened, making it difficult to form coacervates. The acid adjustment enhanced the zeta potential of emulsions, which were similar to 1.0% ($p > 0.05$).

The volume average particle size of emulsions is shown in **Figure 1E**. The particle size of emulsions increased first and then decreased as the pectin concentration increased. The particle size of emulsions containing 1 or 1.5% pectin was similar to that of FG emulsion ($p > 0.05$). High pectin content provided sufficient negative charge to enhance electrostatic and spatial repulsion. Similarly, previous research demonstrated that a large electrostatic repulsion force is exerted between the neighboring carrageenan (anionic polysaccharide) chains, and the carrageenan forms a much smaller complex with lentil protein in the solution (32). As solution alkalinity increased, the emulsion of pH 6 to 10 had a larger particle size from 3.85 to 7.51 μm. By comparison, pH 8 had the highest D_{43} ($p < 0.05$) possibly because it was close to the pI of FG. Under alkaline conditions, the electrostatic interactions between pectin and FG weakened, and the interactions of FG-pectin were dominated by surface patch binding (33). The acid adjustment group had a decreased particle size similar to 1.0% ($p > 0.05$).

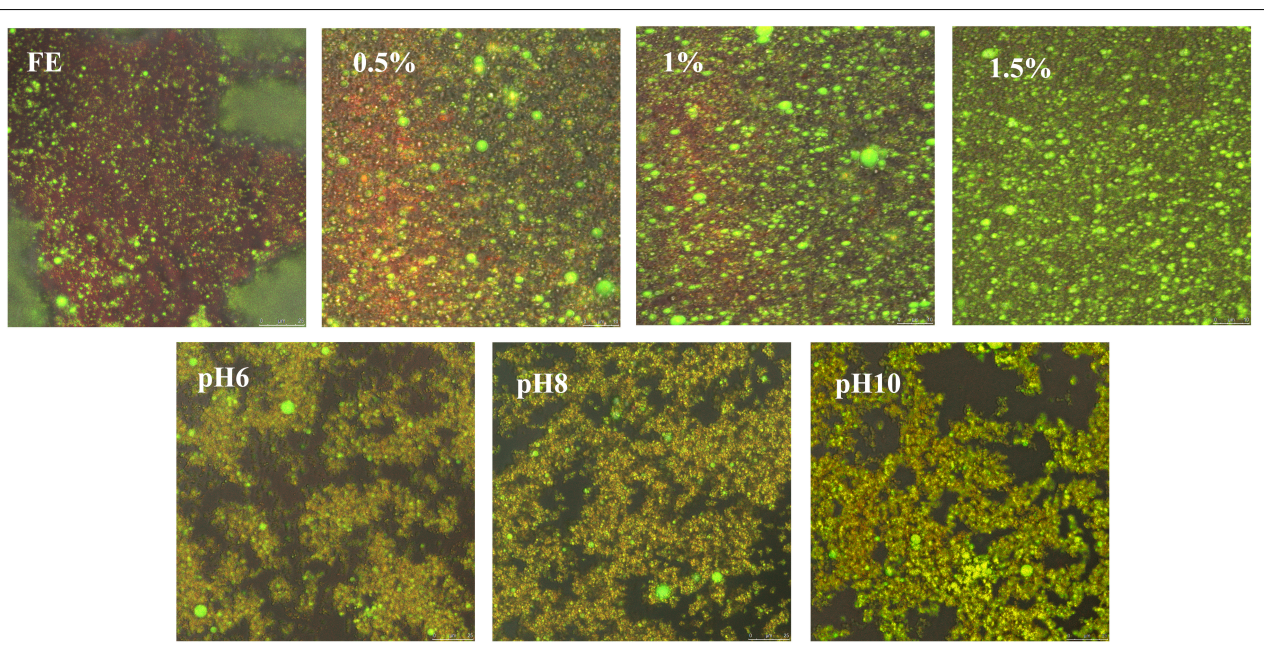

FIGURE 2 | Confocal laser scanning microscopy of complex emulsions.

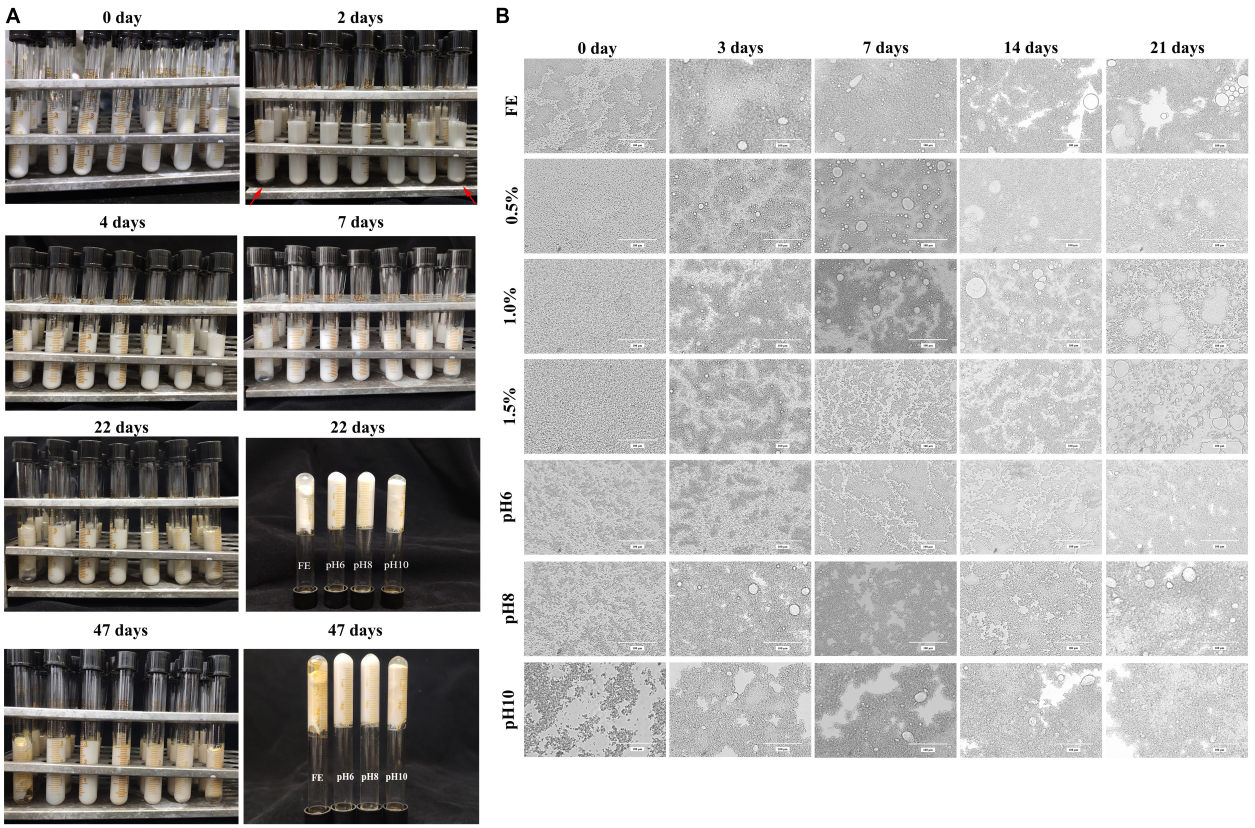

FIGURE 3 | Storage measurement **(A)** and optical microscope observations **(B)** of complex emulsions.

Although the FG emulsion had the lowest particle size, the instability index of the FG emulsion was higher than that of FG-pectin emulsions (**Figure 1F**). Consistent with the zeta potential, the results showed that the stability of FG emulsion strengthened as pectin was mixed. The difference in DPS in the 0.5 to 1.5% pectin group was not significant ($p > 0.05$) during 30 min of centrifugation. In the comparison of the effect of pH on the DPS of emulsions, emulsions at pH 6 to 10 had the highest instability index, which indicated that the alkali-adjusted FG-pectin emulsions were unstable. This finding might be due to the weakened positive charge of FG and the larger particle size of the emulsion as in the previous analysis. During acid adjustment, DPS decreased evidently ($p < 0.05$). The results of zeta potential, particle size, and DPS indicated that the pH adjustment of the composite emulsion was reversible.

Microstructure of Complex Emulsions

After being dyed, all fresh emulsions were immediately observed through CLSM (**Figure 2**). Nile blue was used to label the protein–polysaccharide content with green color intensity during the CLSM observation, and Nile red was utilized to label the internal oil phase (19). Amphiphilic substances converged at the oil–water interface and wrapped the oil droplets to form a sphere to prevent their aggregation. The oil droplets in the CLSM images were spherical, indicating that the oil droplet was successfully wrapped by the emulsifier. However, large accumulations were observed in the FG emulsion, demonstrating that FG molecules were prone to flocculation. Flocculation is a ubiquitous phenomenon that affects the emulsion, appearance, and rheology of O/W emulsions stabilized by proteins (34). On the contrary, FG emulsion mixed with pectin led to the disappearance of aggregates and a large number of loaded oil droplets. More loaded oil droplets formed because of the increase in the pectin content. When pH $\geq$ 6, clusters existed and the number of oil droplets decreased. The results showed that the inhomogeneity of alkali emulsions increased.

Storage Test of Complex Emulsions

During storage, unstable emulsions are prone to phase separation, flocculation, oil creaming, and precipitation (18). The storage stability of emulsions was determined during long-term storage at 25°C. The fresh emulsions of all the groups were white and fluid (**Figure 3A**). The FG emulsion was slightly stratified after 2 days of storage. With the extension of storage time, stratification became more serious. The emulsion at pH 10 was also stratified after 2 d of storage, which was slighter than the FG emulsion. In particular, the four emulsions (FG, pH 6 to 10) solidified after 22 d of storage. Consistent with our findings, previous results showed that gelatin emulsions undergo liquid–gel transition after 28 days of storage (10). By contrast, 0.5,

1.0, and 1.5% emulsions were not stratified and remained fluid during the whole storage. According to our previous research, pectin hinders the formation of FG gel networks (6), resulting in the loss of liquid–gel transition.

Optical microscope observations were performed to analyze the changes in the microstructure of emulsions during storage (**Figure 3B**). The oil droplets of fresh emulsions were small and non-conspicuous. Fresh FG emulsions flocculated to groups and FG-pectin emulsions (pH 6–10) were clustered, which were consistent with CLSM results. Conversely, FG-pectin emulsions (0.5, 1.0, and 1.5%) were uniform because polysaccharides can inhibit droplet movement (35). Combining with polysaccharides is an effective strategy to control and inhibit the flocculation of protein emulsions (34). As the storage time was extended, large oil droplets increased, implying that the droplets coalesced during this test. If oil droplets were not fully covered by particles, they tended to combine, thereby forming larger oil droplets (36). Interestingly, the clusters of FG-pectin emulsions (pH 6–10) assembled in groups in common with the observations of the FG emulsion. Thus, FG-pectin emulsions (pH 6–10) and FG emulsions were gelled in storage.

Environmental Stability of Complex Emulsions

When emulsions are used in beverage or drug delivery, complex environments (high temperature, freeze-thaw, high salt) are often encountered, and the environmental stability of emulsions is indispensable at this time. The influence of thermal treatment on FG-pectin emulsions is shown in **Figures 4A–C**. The zeta potential, particle size, and DPS results indicated that FG emulsion was thermally stable. Although the high-temperature treatment weakened the stability of complex emulsions, the DPS of complex emulsions was still better than that of FG emulsion.

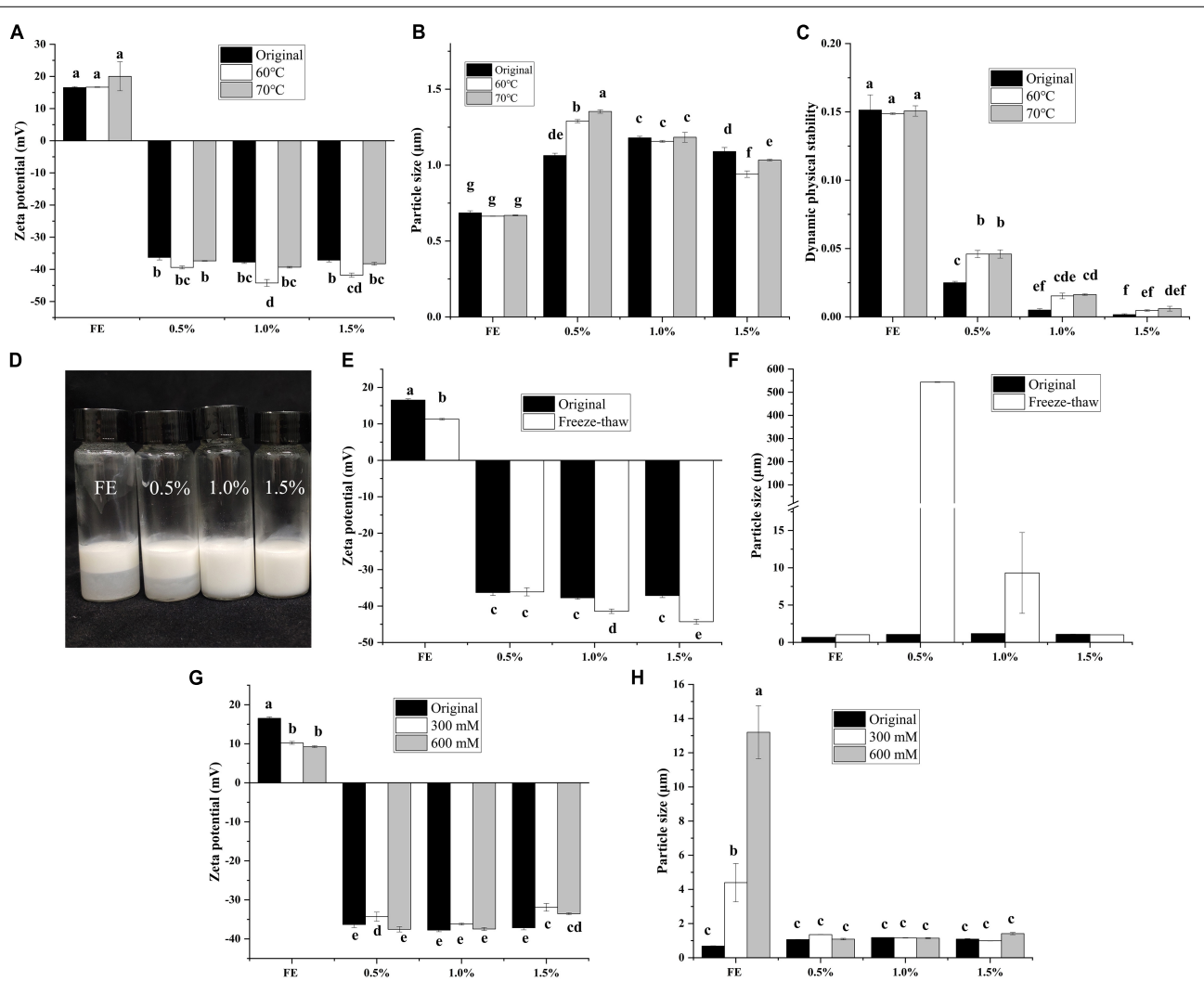

FIGURE 4 | Effect of heat treatment on zeta potential **(A)**, particle size **(B)**, and dynamic physical stability **(C)** of complex emulsions; effect of freeze-thaw treatment on appearance **(D)**, zeta potential **(E)**, and particle size **(F)** of the complex emulsion; effect of freeze-thaw treatment on zeta potential **(G)** and particle size **(H)** of complex emulsion.

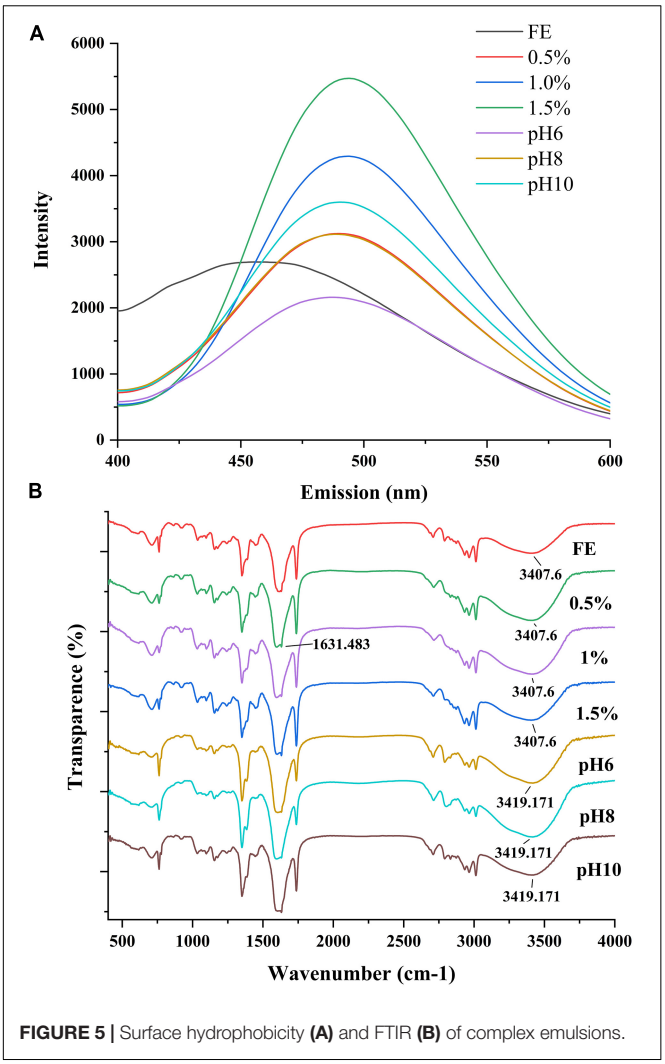

FIGURE 5 | Surface hydrophobicity **(A)** and FTIR **(B)** of complex emulsions.

All emulsions except 1.0 and 1.5% emulsions stratified after the freeze-thaw treatment (**Figure 4D**). After the freeze-thaw treatment, FG emulsions had a decreased zeta potential and enhanced particle size (**Figures 4E,F**). Most notably, abundant floccules appeared at 0.5% FG-pectin emulsions after the freeze-thaw treatment. Moreover, the particle size was larger than that of other groups, whereas the zeta potential did not change appreciably. Because of phase separation, polysaccharides and proteins combine to form insoluble agglomerates (14). When the emulsions were dominated by pectin, particle size and zeta potential decreased. This result demonstrated that the higher proportion of pectin in a composite emulsion was more conducive to the effect of freezing and thawing.

The influence of salt treatment on FG-pectin emulsions is shown in **Figures 4G,H**. FG emulsions were susceptible to salt concentration. The zeta potential decreased, and the particle size increased sharply. On the contrary, the complex emulsions were insensitive to changes in environmental salt concentrations. Therefore, FG-pectin emulsions were stable at high temperatures and could tolerate salt environments. When the pectin content in the composite emulsion was low, phase separation was likely to occur during the freeze-thaw process, but increasing the pectin content could avoid phase separation.

Interaction Force Analysis

Hydrophobicity is related to the stability and functionality of proteins because of its effect on the conformation of proteins in solutions. The surface hydrophobicity of emulsions is shown in **Figure 5A**. FG emulsion had a peak at 456 nm with fluorescence intensity of 2,694. However, the fluorescence peaks were red-shift after mixing with pectin, and the fluorescence intensity improved as the pectin concentration increased. Therefore, the hydrophobic interaction of complex was promoted. This result was consistent with previous findings, which indicated that more hydrophobic groups of proteins are exposed because of the addition of polysaccharides (9). When the solution pH became neutral, the fluorescence intensity decreased because of the attenuation of FG-pectin binding. Then, as the solution became alkaline, the fluorescence intensity increased again. Under alkaline conditions, the FG chains aggregated because of the strengthened hydrophobic interaction (37).

FTIR was conducted to further detect the interaction force of the effect of pectin on FG emulsions (**Figure 5B**). The wide peak at around 3,407 cm^{-1} presented the N–H stretching and stretching vibration of hydroxyl groups, which are characteristic of amide A (38, 39). This peak did not change with the increase of pectin. However, in the alkali-adjusted groups, the peak at 3,407 cm^{-1} moved to 3,418 to 3,419 cm^{-1}, which indicated that hydrogen bonds weakened. The peaks at 1,631 cm^{-1} belonged to amide I corresponded to C = O stretching or hydrogen bonds coupled with COO^{-} (9). Amide I in all the emulsions had no significant changes. Because of the stronger amide I absorption, the peaks at 1,616 cm^{-1} (1° amide II) were obscured by amide I. The 1° amide II corresponded to CN stretching and NH bending (38), which were moved to a lower wavenumber as the pectin concentrations increased. Conversely, these peaks at amide II initially moved to a higher wavenumber (pH < pI) and then moved to lower wavenumber (pH > pI) in the alkaline-adjusted emulsions.

The secondary structure of FG in emulsions was analyzed using the second derivative of the FTIR spectra in the amide I region (1,700–1,600 cm^{-1}). The peaks corresponded to β-sheet (1,610–1,642 cm^{-1}), random coil (1,642–1,650 cm^{-1}), α-helix (1,650–1,660 cm^{-1}), β-turn (1,660–1,680 cm^{-1}), and anti-parallel β-sheets (1,680–1,700 cm^{-1}) conformations (40). In **Supplementary Figure 3**, the secondary structures of FG in all emulsions were dominated by β-sheet, which was similar to a previous report (38). In addition, α-helix and random coil were reduced as pectin concentration increased to 1.0%; furthermore, the β-sheet substantially increased. This observation may be caused by the transformation from α-helix/random coil to β-sheet and the interaction between protein–lipid (41) and protein–polysaccharide molecules. The enhancement of the ordered structure indicated the higher stability of FG molecules. Phoon et al. (42) believed that the transition from a loose coil/α-helix to an intermolecular β-sheet is the key to establishing an effective interface barrier between oil and water. In the

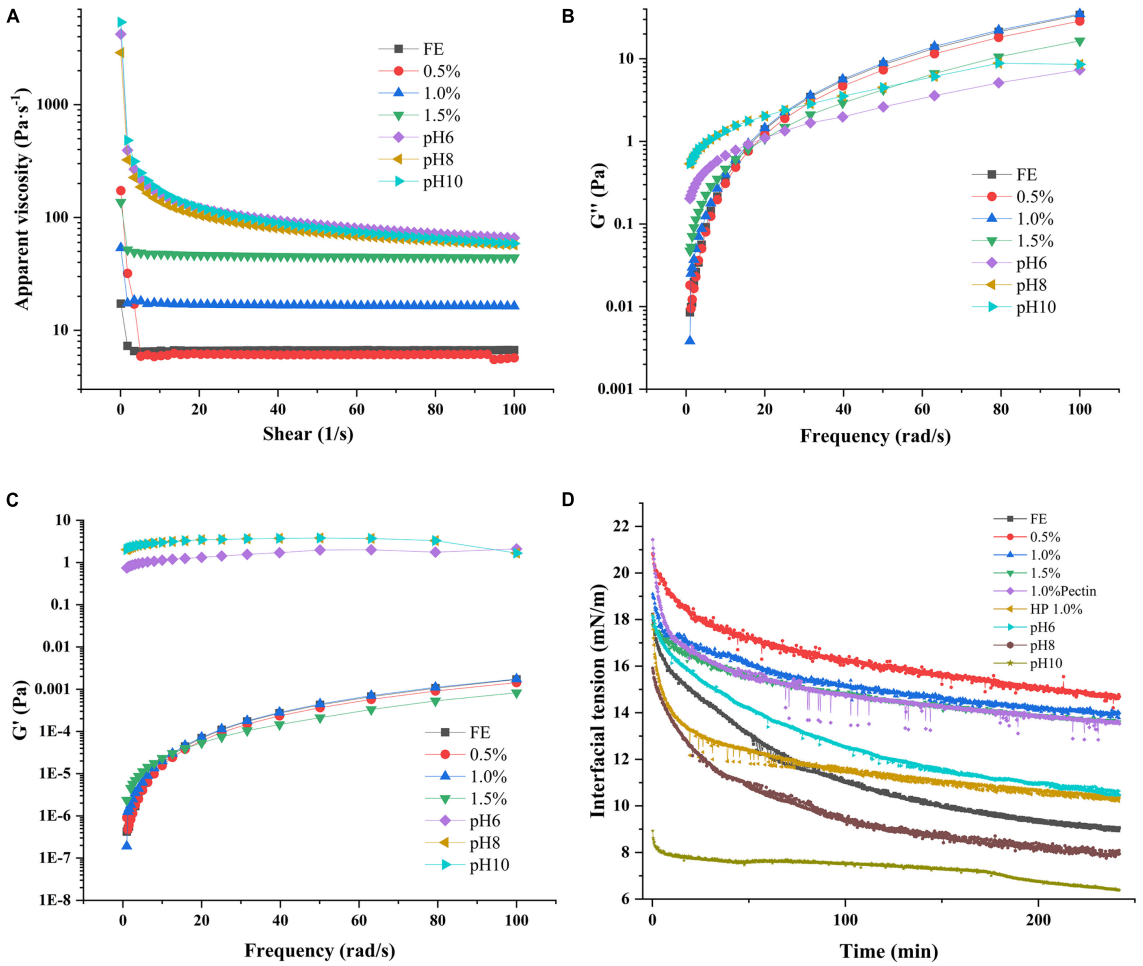

FIGURE 6 | Apparent viscosity **(A)**, loss modulus **(B)**, storage modulus **(C)**, and interfacial tension **(D)** of complex emulsions.

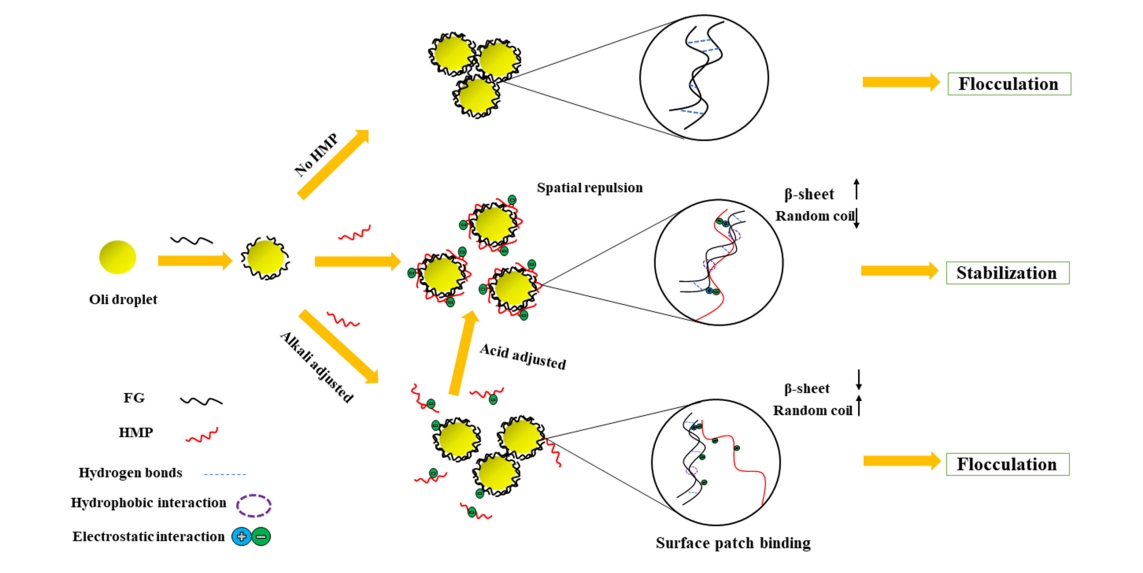

FIGURE 7 | Schematic mechanism of FG-pectin complex emulsions.

pH-adjusted groups, the β-sheet content decreased, but the random coil content initially increased and then decreased as pH increased. The growing tendency among the unordered secondary structures of FG displayed the increased openness and flexibility of protein molecules (42). It might also result in the flocculation of emulsions (pH 6–10).

Rheology Properties of Complex Emulsion Analysis

The flow sweep test revealed the AV and fluid properties (Newtonian or non-Newtonian fluid) of emulsions. A Newtonian fluid is any fluid whose viscosity remains constant regardless of any external stress applied to it. On the contrary, the viscosity of a non-Newtonian fluid can change under force (6). As shown in **Figure 6A,** FG and FG-pectin emulsions (pH < 6) from 1 1/s to 100 1/s had constant AV, and the low pectin content of complex emulsions had a similar AV to that of the FG emulsion. High pectin concentrations positively affected the AV of emulsions, consistent with previous research that the viscosity of the polysaccharides-protein emulsion increased linearly with the polysaccharides concentration (43). Polysaccharides can strengthen the viscosity of emulsions and improve emulsion stability because of the extended network formation in the aqueous phase (44). Nevertheless, the AV of the emulsion at pH 6 to 10 groups was the highest, and it declined as the shear rate increased, displaying the features of a non-Newtonian fluid. This finding was due to the high flocculation of emulsion droplets during microstructure morphology observation. Compared with the nonflocculated FG-pectin emulsion, the flocculating emulsion showed an enhanced viscosity and shear-thinning behavior because some of the continuous phases were retained in the structure. These flocculates were destroyed by an external force, resulting in a shear-thinning behavior (29). As such, alkali-adjusted emulsions had a higher instability index but were only slightly stratified during storage.

Dynamic frequency sweep revealed the elasticity and viscosity of emulsions (**Figures 6B,C**). G′ (storage modulus) represents the elastic properties of emulsions and G″ (loss modulus) denotes the viscous properties of emulsions. The G″ of FE and FG-pectin emulsion (0.5–1.5%) under dynamic frequency scanning were much greater than that of G′, denoting that the viscous trend in the structure was dominant. Otherwise, alkali-adjusted emulsions had the highest G′ under low-frequency conditions, and G′ > G″ because of a high flocculation degree (45). With the increased frequency, G″ of alkali-adjusted emulsions approached G′, which was consistent with the flow sweep test results, that is, flocculation dispersed.

Interfacial Properties Analysis

The interaction between polysaccharide and protein is affected by the pH value of the solution, the ratio of biopolymers, the order of adding biopolymers, and other factors (46), and these effects may further affect the surface activity of biopolymers. The change in the surface pressure of FG and pectin adsorbed on the oil–water interface with adsorption time was analyzed and detected *via* dynamic drop analysis. The interfacial tension of FG and FG-pectin is presented in **Figure 6D**. All interfacial tension–time curves are divided into rapid and slow reduction stages. For the FG emulsion, the interfacial tension decreased to 9.05 (mM/m) near the steady phase, indicating a good surface activity. However, the same concentration of pectin decreased to 13.53 (mM/m) near the steady phase, showing a poor surface activity because of the lack of a hydrophobic unit (12), which limited their adsorption at the oil–water interface. After FG was mixed with pectin *via* stirring and shearing, the interfacial tension increased. As the pectin content increased, the curves were similar to those of pectin. When the amount of pectin was enough, the interfacial tension slightly changed. This result is similar to that reported by Wang et al. (32), who demonstrated that the interaction between a lentil protein isolate and an anionic polysaccharide binding complex may limit the rearrangement of correct protein localization at the interface; as a result, interfacial tension increases. The interfacial tension of the complex at pH 6-10 were decreased due to the formation FG-pectin coacervate were prevented. In the case of pH 8/10, the interfacial tension of the composite emulsion is below the pure FG emulsion. These results show that an alkaline environment is more conducive to FG molecules' adsorption. The alkaline environment contributes to the interfacial properties of gelatin (47). Thus, the higher the solution pH, the lower the interfacial tension value.

Interfacial property analysis consequence of emulsifiers revealed that the pectin and FG mixing had an antagonistic effect on the adsorption of oil–water interface. This antagonism effect may be owing to the adsorption of pectin at the interface to prevent FG molecules from approaching or the decrease of adsorption capacity of the FG-pectin coacervate. To further explore this question, the high-pressure homogenization group was designed. HP 1.0% group had a lower interfacial tension than the mixing 1.0%. During homogenization, pectin chains and proteins are rapidly activated and strengthened under shear force (14). High-pressure homogenization deepened the interaction between FG and pectin and improved the surface activity of the composite.

Schematic Model of Fish Gelatin-Pectin Complex Emulsion Interactions

The proposed potential mechanism of FG-pectin emulsion interactions is illustrated in **Figure 7**. In the presence of amphiphilic macromolecular particles at high concentrations, they can quickly adsorb to the oil surface and prevent their coalescence through space and electrostatic repulsion (36). According to the theory of bridging (48), FG emulsion could easily flocculate because of the intermolecular hydrogen bonds effect, leading to emulsion stratification and liquid–gel transition behavior. When pH < 6, the AV of the FG-pectin emulsion was higher than that of the FE emulsion. When pectin was added, the β-sheet of the complex increased and the random coil decreased. FG emulsion flocculation was prevented by increasing the hydrophobic interaction and electrostatic interaction of the FG-pectin system, ultimately enhancing the emulsion stability. The salinity tolerance of complex emulsions was improved by

pectin. But the low-pectin-content emulsions underwent phase separation to form an insoluble complex during the freeze-thaw treatment. Hence, complex emulsions should contain a high amount of pectin, which was more stable in freeze-thaw and heat treatment processes. When pH $\geq$ 6, the emulsion was a non-Newtonian fluid whose AV and G′ were higher than those of emulsions at pH $<$ 6. Emulsion clusters with a large particle size formed. During long-term storage, the emulsions were prone to stratification and gelling but were still lighter than the FE emulsion. Although the total potential decreased, the electrostatic barrier between particles was destroyed. The electrostatic interaction of FG-pectin shifted to surface patch binding, whereas the hydrophobic interaction and hydrogen bonds were decreased. Therefore, FG and pectin formed a compatible phase system, resulting in emulsion flocculation. However, this process could be reversed by acid adjustment and homogenization, making it simpler and more convenient in practical applications.

CONCLUSION

Pectin greatly prolonged the storage property of fish gelatin emulsion, prevented delamination and gelation during storage, and enhanced the salt ion tolerance of FG emulsion. The fish gelatin emulsion was easy to delaminate during the freeze-thaw process, and the high pectin content improved the freeze-thaw stability of the fish gelatin emulsion. Since both FG and pectin are biological macromolecules, antagonism occurred during the adsorption process on the surface of oil droplets, increasing surface tension of the complex. High-pressure homogenization was required to allow sufficient interaction of FG and pectin, thereby enhancing the surface activity of the complex. The pH had a great influence on the complex emulsion, and the emulsion was unstable when pH $\geq$ 6. However, the stability of FG-pectin emulsion induced by pH adjustment was reversible due to the non-covalent interactions of FG-pectin. Pectin could make up for the corresponding defects of FG in emulsifying properties and form stable emulsions. This study showed great potential for nutrient or drug delivery and needed further studies.

DATA AVAILABILITY STATEMENT

The original contributions presented in this study are included in the article/**Supplementary Material**, further inquiries can be directed to the corresponding author.

AUTHOR CONTRIBUTIONS

SH carried out the major experiments and data analysis and writing – original draft preparation. ZT contributed to the supervision, funding, and review the manuscript. HW carried out the part of the experiments and analyzed the relative data. XS reviewed the manuscript. SW contributed to the software and validation. NC assisted to carry out the experiments. YH reviewed the manuscript. All authors contributed to the article and approved the submitted version.

FUNDING

This study was supported by the National Natural Science Foundation of China (No. 31860428), the Earmarked Fund for China Agriculture Research System (CARS-45), the Research Project of the State Key Laboratory of Food Science and Technology (SKLF-ZZB-202126), and the Open Project Program of State Key Laboratory of Food Science and Technology (No. SKLF-KF-202005).

SUPPLEMENTARY MATERIAL

The Supplementary Material for this article can be found online at: https://www.frontiersin.org/articles/10.3389/fnut.2022.961875/full#supplementary-material

REFERENCES

1. Chan SY, Choo WS, Young DJ, Loh XJ. Pectin as a rheology modifier: origin, structure, commercial production and rheology. *Carbohydr Polym.* (2017) 161:118–39. doi: 10.1016/j.carbpol.2016.12.033
2. Ji X, Yan Y, Hou C, Shi M, Liu Y. Structural characterization of a galacturonic acid-rich polysaccharide from Ziziphus Jujuba cv. Muzao. *Int J Biol Macromol.* (2020) 147:844–52. doi: 10.1016/j.ijbiomac.2019.09.244
3. Wongkaew M, Tangjaidee P, Leksawasdi N, Jantanasakulwong K, Rachtanapun P, Seesuriyachan P, et al. Mango pectic oligosaccharides: a novel prebiotic for functional food. *Front Nutr.* (2022) 9:798543. doi: 10.3389/fnut.2022.798543
4. Nag M, Lahiri D, Dey A, Sarkar T, Pati S, Joshi S, et al. Seafood discards: a potent source of enzymes and biomacromolecules with nutritional and nutraceutical significance. *Front Nutr.* (2022) 9:879929. doi: 10.3389/fnut.2022.879929
5. Wasswa J, Tang R, Gu XH. Utilization of fish processing by-products in the gelatin industry. *Food Rev Int.* (2007) 23:159–74. doi: 10.1080/87559120701225029
6. Huang S, Tu ZC, Sha XM, Wang H, Hu YM, Hu ZZ. Gelling properties and interaction analysis of fish gelatin-low-methoxyl pectin system with different concentrations of Ca2+. *Lwt-Food Sci Technol.* (2020) 132:109826. doi: 10.1016/j.lwt.2020.109826
7. Huang T, Tu ZC, Shangguan XC, Sha XM, Wang H, Zhang L, et al. Fish gelatin modifications: a comprehensive review. *Trends Food Sci Tech.* (2019) 86:260–9. doi: 10.1016/j.tifs.2019.02.048
8. Diftis NG, Pirzas TA, Kiosseoglou VD. Emulsifying properties of gelatin conjugated to pectin under alkaline conditions. *J Sci Food Agric.* (2005) 85:804–8. doi: 10.1002/jsfa.2029
9. Huang S, Tu ZC, Sha XM, Hu YM, Chen N, Wang H. Fabrication and performance evaluation of pectin-fish gelatin-resveratrol preservative films. *Food Chem.* (2021) 361:129832. doi: 10.1016/j.foodchem.2021.129832
10. Zhang T, Ding MZ, Tao LN, Liu LJ, Tao NP, Wang XC, et al. Octenyl succinic anhydride modification of bovine bone and fish skin gelatins and their application for fish oil-loaded emulsions. *Food Hydrocoll.* (2020) 108:106041. doi: 10.1016/j.bbalip.2011.10.011
11. Shearer GC, Savinova OV, Harris WS. Fish oil – how does it reduce plasma triglycerides? *Biochim Biophys Acta.* (2012) 1821:843–51.
12. Fan CH, Chen XL, He JJ. Effect of calcium chloride on emulsion stability of methyl-esterified citrus pectin. *Food Chem.* (2020) 332:127366. doi: 10.1016/j.foodchem.2020.127366
13. Sha X-M, Hu Z-Z, Tu Z-C, Zhang L-Z, Duan D-L, Huang T, et al. Influence of dynamic high pressure microfluidization on functional properties and

structure of gelatin from bighead carp (*Hypophthalmichthys nobilis*) scale. *J Food Proc. Preserv.* (2018) 42:e13607.
14. Wusigale L, Liang L, Luo Y. Casein and pectin: structures, interactions, and applications. *Trends Food Sci Tech.* (2020) 97:391–403.
15. Shao P, Feng J, Sun P, Xiang N, Lu B, Qiu D. Recent advances in improving stability of food emulsion by plant polysaccharides. *Food Res Int.* (2020) 137:109376.
16. Zhang HX, Fan Q, Li D, Chen X, Liang L. Impact of gum Arabic on the partition and stability of resveratrol in sunflower oil emulsions stabilized by whey protein isolate. *Colloid Surf B.* (2019) 181:749–55. doi: 10.1016/j.colsurfb.2019.06.034
17. Cao YP, Dai YP, Lu XL, Li RY, Zhou W, Li JH, et al. Formation of shelf-stable pickering high internal phase emulsion stabilized by *Sipunculus nudus* water-soluble proteins (WSPs). *Front Nutr.* (2021) 8:770218. doi: 10.3389/fnut.2021.770218
18. Xu J, Zhou L, Miao JY, Yu WZ, Zou LQ, Zhou W, et al. Effect of cinnamon essential oil nanoemulsion combined with ascorbic acid on enzymatic browning of cloudy apple juice. *Food Bioproc Tech.* (2020) 13:860–70.
19. Miao JY, Xu N, Cheng C, Zou LQ, Chen J, Wang Y, et al. Fabrication of polysaccharide-based high internal phase emulsion gels: enhancement of curcumin stability and bioaccessibility. *Food Hydrocoll.* (2021) 117:106679.
20. Li C, Dai T, Chen J, Li X, Li T, Liu C, et al. Protein-polyphenol functional ingredients: the foaming properties of lactoferrin are enhanced by forming complexes with procyanidin. *Food Chem.* (2021) 339:128145. doi: 10.1016/j.foodchem.2020.128145
21. Xu W, Li ZF, Sun HM, Zheng SQ, Li H, Luo DL, et al. High internal-phase pickering emulsions stabilized by xanthan gum/lysozyme nanoparticles: rheological and microstructural perspective. *Front Nutr.* (2022) 8:744234. doi: 10.3389/fnut.2021.744234
22. Ren YM, Jiang L, Wang WJ, Xiao YH, Liu SC, Luo Y, et al. Effects of mesona chinensis benth polysaccharide on physicochemical and rheological properties of sweet potato starch and its interactions. *Food Hydrocoll.* (2020) 99:105371.
23. Ghosh AK, Bandyopadhyay P. Polysaccharide-protein interactions and their relevance in food colloids. In: Karunaratne DN editor. *The Complex World of Polysaccharides.* London: IntechOpen (2012). doi: 10.5772/50561
24. Yin B, Deng W, Xu K, Huang L, Yao P. stable nano-sized emulsions produced from soy protein and soy polysaccharide complexes. *J Colloid Interface Sci.* (2012) 380:51–9. doi: 10.1016/j.jcis.2012.04.075
25. Camino NA, Sánchez CC, Rodríguez Patino JM, Pilosof AMR. Hydroxypropylmethylcellulose at the oil–water interface. Part I. Bulk behaviour and dynamic adsorption as affected by pH. *Food Hydrocoll.* (2011) 25:1–11.
26. Rehman A, Ahmad T, Aadil RM, Spotti MJ, Bakry AM, Khan IM, et al. Pectin polymers as wall materials for the nano-encapsulation of bioactive compounds. *Trends Food Sci Tech.* (2019) 90:35–46.
27. Al-Maqtari QA, Ghaleb ADS, Mahdi AA, Al-Ansi W, Noman AE, Wei MP, et al. Stabilization of water-in-oil emulsion of *Pulicaria* jaubertii extract by ultrasonication: fabrication, characterization, and storage stability. *Food Chem.* (2021) 350:129249. doi: 10.1016/j.foodchem.2021.129249
28. Zhou Y, Teng F, Tian T, Sami R, Wu CL, Zhu Y, et al. The impact of soy protein isolate-dextran conjugation on capsicum oleoresin (*Capsicum annuum* L.) nanoemulsions. *Food Hydrocoll.* (2020) 108:105818.
29. Zhang XY, Qi BK, Xie FY, Hu M, Sun YF, Han L, et al. Emulsion stability and dilatational rheological properties of soy/whey protein isolate complexes at the oil-water interface: Influence of pH. *Food Hydrocoll.* (2021) 113:106391.
30. Chang YI, Chang P-K. The role of hydration force on the stability of the suspension of *Saccharomyces cerevisiae*–application of the extended DLVO theory. *Colloids Surf A.* (2002) 211:67–77.
31. Muhoza B, Xia S, Cai J, Zhang X, Duhoranimana E, Su J. Gelatin and pectin complex coacervates as carriers for cinnamaldehyde: effect of pectin esterification degree on coacervate formation, and enhanced thermal stability. *Food Hydrocoll.* (2019) 87:712–22.
32. Wang YX, Ghosh S, Nickerson MT. Effect of pH on the formation of electrostatic complexes between lentil protein isolate and a range of anionic polysaccharides, and their resulting emulsifying properties. *Food Chem.* (2019) 298:125023. doi: 10.1016/j.foodchem.2019.125023
33. Joshi N, Rawat K, Bohidar HB. pH and ionic strength induced complex coacervation of pectin and gelatin a. *Food Hydrocoll.* (2018) 74:132–8.
34. Dickinson E. Strategies to control and inhibit the flocculation of protein-stabilized oil-in-water emulsions. *Food Hydrocoll.* (2019) 96:209–23.
35. Zhang RY, Belwal T, Li L, Lin XY, Xu YQ, Luo ZS. Recent advances in polysaccharides stabilized emulsions for encapsulation and delivery of bioactive food ingredients: a review. *Carbohydr. Polym.* (2020) 242:116388.
36. Lv SS, Zhou HL, Bai L, Rojas OJ, McClements DJ. Development of food-grade pickering emulsions stabilized by a mixture of cellulose nanofibrils and nanochitin. *Food Hydrocoll.* (2021) 113:106451.
37. Xu J, Li TD, Tang XL, Qiao CD, Jiang QW. Effect of aggregation behavior of gelatin in aqueous solution on the grafting density of gelatin modified with glycidol. *Colloid Surf B.* (2012) 95:201–7. doi: 10.1016/j.colsurfb.2012.02.041
38. Sow LC, Kong K, Yang HS. Structural modification of fish gelatin by the addition of gellan, kappa-carrageenan, and salts mimics the critical physicochemical properties of pork gelatin. *J Food Sci.* (2018) 83:1280–91. doi: 10.1111/1750-3841.14123
39. Liu X-X, Liu H-M, Yan Y-Y, Fan L-Y, Yang J-N, Wang X-D, et al. Structural characterization and antioxidant activity of polysaccharides extracted from jujube using subcritical water. *LWT.* (2020) 117:108645.
40. Xu JM, Zhang T, Zhang YY, Yang LL, Nie YH, Tao NP, et al. Silver carp scale gelatins for the stabilization of fish oil-loaded emulsions. *Int J Biol Macromol.* (2021) 186:145–54. doi: 10.1016/j.ijbiomac.2021.07.043
41. Xu LL, Lv YQ, Su YJ, Chang CH, Gu LP, Yang YJ, et al. Enhancing gelling properties of high internal phase emulsion-filled chicken gels: effect of droplet fractions and salts. *Food Chem.* (2022) 367:130663. doi: 10.1016/j.foodchem.2021.130663
42. Phoon PY, San Martin-Gonzalez MF, Narsimhan G. Effect of hydrolysis of soy β-conglycinin on the oxidative stability of O/W emulsions. *Food Hydrocoll.* (2014) 35:429–43.doi: 10.1016/j.foodhyd.2013.06.024
43. Niu B, Shao P, Feng S, Qiu D, Sun P. Rheological aspects in fabricating pullulan-whey protein isolate emulsion suitable for electrospraying: application in improving β-carotene stability. *LWT.* (2020) 129:109581. doi: 10.1016/j.lwt.2020.109581
44. Bai L, Liu F, Xu X, Huan S, Gu J, McClements DJ. Impact of polysaccharide molecular characteristics on viscosity enhancement and depletion flocculation. *J Food Eng.* (2017) 207:35–45. doi: 10.1016/j.jfoodeng.2017.03.021
45. Ercelebi EA, Ibanoglu E. Rheological properties of whey protein isolate stabilized emulsions with pectin and guar gum. *Eur Food Res Technol.* (2009) 229:281–6. doi: 10.1007/s00217-009-1056-6
46. Raei M, Shahidi F, Farhoodi M, Jafari SM, Rafe A. Application of whey protein-pectin nano-complex carriers for loading of lactoferrin. *Int J Biol Macromol.* (2017) 105:281–91. doi: 10.1016/j.ijbiomac.2017.07.037
47. Zhang T, Ding M, Wang X, Zhong J. Droplet and creaming stability of fish oil-loaded gelatin/surfactant-stabilized emulsions depends on both the adsorption ways of emulsifiers and the adjusted pH. *Food Sci Hum Wellness.* (2020) 9:280–8. doi: 10.1016/j.fshw.2020.04.002
48. Baraniak BM, Waleriańczyk E. FLOCCULATION. 2nd edn. In: Caballero B, Trugo LC, Finglas PM editors. *Encyclopedia of Food Sciences and Nutrition.* Oxford: Academic (2003). p. 2531–5. doi: 10.1016/B0-12-227055-X/00485-5

Conflict of Interest: The authors declare that the research was conducted in the absence of any commercial or financial relationships that could be construed as a potential conflict of interest.

Publisher's Note: All claims expressed in this article are solely those of the authors and do not necessarily represent those of their affiliated organizations, or those of the publisher, the editors and the reviewers. Any product that may be evaluated in this article, or claim that may be made by its manufacturer, is not guaranteed or endorsed by the publisher.

Copyright © 2022 Huang, Wang, Wang, Sha, Chen, Hu and Tu. This is an open-access article distributed under the terms of the Creative Commons Attribution License (CC BY). The use, distribution or reproduction in other forums is permitted, provided the original author(s) and the copyright owner(s) are credited and that the original publication in this journal is cited, in accordance with accepted academic practice. No use, distribution or reproduction is permitted which does not comply with these terms.

frontiers | Frontiers in Nutrition

TYPE Review
PUBLISHED 18 July 2022
DOI 10.3389/fnut.2022.965073

Check for updates

OPEN ACCESS

EDITED BY
Xin Wang,
Northwest A&F University, China

REVIEWED BY
Xuewei Ye,
Zhejiang University, China
Lei Yuan,
Tibet Agriculture and Animal Husbandry University, China

*CORRESPONDENCE
Lin Li
lilin29pumc@163.com
Yizhe Yan
yanyizhe@zzuli.edu.cn

†These authors have contributed equally to this work

SPECIALTY SECTION
This article was submitted to Food Chemistry, a section of the journal Frontiers in Nutrition

RECEIVED 09 June 2022
ACCEPTED 30 June 2022
PUBLISHED 18 July 2022

CITATION
He Y, Li L, Chang H, Cai B, Gao H, Chen G, Hou W, Jappar Z and Yan Y (2022) Research progress on extraction, purification, structure and biological activity of *Dendrobium officinale* polysaccharides. *Front. Nutr.* 9:965073. doi: 10.3389/fnut.2022.965073

COPYRIGHT
© 2022 He, Li, Chang, Cai, Gao, Chen, Hou, Jappar and Yan. This is an open-access article distributed under the terms of the Creative Commons Attribution License (CC BY). The use, distribution or reproduction in other forums is permitted, provided the original author(s) and the copyright owner(s) are credited and that the original publication in this journal is cited, in accordance with accepted academic practice. No use, distribution or reproduction is permitted which does not comply with these terms.

Research progress on extraction, purification, structure and biological activity of *Dendrobium officinale* polysaccharides

Yuan He[1†], Lin Li[2*†], Hao Chang[3], Bin Cai[4], Huajun Gao[4], Guoyu Chen[1], Wen Hou[2], Zubaydan Jappar[2] and Yizhe Yan[1*]

[1]College of Food and Bioengineering, Henan Key Laboratory of Cold Chain Food Quality and Safety Control, Zhengzhou University of Light Industry, Zhengzhou, China, [2]College of Life Sciences, Zhengzhou Normal University, Zhengzhou, China, [3]Cigar Research Institute, Anhui Tobacco Technology Center, Bengbu, China, [4]Haikou Cigar Research Institute, Hainan Provincial Branch of CNTC, Haikou, China

Dendrobium officinale Kimura et Migo (*D. officinale*) is a traditional medicinal and food homologous plant that has been used for thousands of years in folk medicine and nutritious food. Recent studies have shown that polysaccharide is one of the main biologically active components in *D. officinale*. *D. officinale* polysaccharides possess several biological activities, such as anti-oxidant, heptatoprotective, immunomodulatory, gastrointestinal protection, hypoglycemic, and anti-tumor activities. In the past decade, polysaccharides have been isolated from *D. officinale* by physical and enzymatic methods and have been subjected to structural characterization and activity studies. Progress in extraction, purification, structural characterization, bioactivity, structure-activity relationship, and possible bioactivity mechanism of polysaccharides *D. officinale* were reviewed. In order to provide reference for the in-depth study of *D. officinale* polysaccharides and the application in functional food and biomedical research.

KEYWORDS

***Dendrobium officinale*, polysaccharides, structural characterization, biological activity, structure-activity relationship**

Introduction

Dendrobium officinale Kimura et Migo (*D. officinale*), commonly known as *Tiepi Shihu*, belongs to the orchid family *Dendrobium* genus (1), largely distributed in tropical and subtropical regions, especially in southern China, Japan, India, Australia, and other regions (2). There are more than 1,500 species of *Dendrobium* in the world, and in China has reported more than 80 species of *Dendrobium*.

Dendrobium is a precious Chinese herbal medicine with a long history of medicinal use in China. Modern pharmacological studies show that *D. officinale*

has anti-inflammatory, nourishing the spleen and stomach, immunomodulatory, and prolonging life effects (3). Importantly, *D. officinale* is rich in a variety of bioactive components, such as polyphenols, flavonoids, alkaloids, polysaccharides, amino acids, and vitamins, etc., of which polysaccharides are considered to be the main active substances in *D. officinale* (4–8). *D. officinale* polysaccharides obtained by different extraction and separation methods have different physicochemical properties and biological activities, including anti-cancer (9), anti-inflammatory (10), antioxidant (11), hypoglycemic (12), immune regulation (13), gastrointestinal tract protection (14), and liver protection (15) effects.

In recent years, some scholars have reviewed *D. officinale* polysaccharides. For example, Chen et al. (1) reviewed the research progress on the separation, structural properties and biological activities of *D. officinale* polysaccharides. Yue et al. (16) summarized the isolation methods, structural properties, and biological activities of *D. officinale* polysaccharides. Li et al. (17) systematically summarized the preparation, structural characterization and bioactive molecular mechanism of *D. officinale* polysaccharides. However, there is a lack of systematic overview of the structural characteristics, biological activity mechanism, and structure-activity relationship of *D. officinale* polysaccharides. Therefore, this paper systematically reviews the extraction, separation, purification, structural properties, biological activities, and mechanism of action of *D. officinale* polysaccharides, and focuses on structure-activity relationship of *D. officinale* polysaccharides.

Extraction, isolation, and purification methods

To obtain more bioactive polysaccharide from *D. officinale*, it needs to be extracted, separated and purified as shown in **Figure 1**. First, fresh *D. officinale* was washed and dried at low temperature and ground into powder. Next, the powder was soaked in a water bath (70°C) for 3 h in 90–95% ethanol to inactivate the enzyme and remove small molecular substances such as oligosaccharides, amino acids, lipids, and pigments (18). Then, the ethanol is filtered and evaporated to dryness. Finally, the solid residue is extracted by different methods, for example hot water extraction (19), ultrasonic-assisted extraction (20), enzyme-assisted extraction (21), microwave-assisted extraction (22), supercritical fluid extraction (23), and freeze-thaw cold pressing (24).

Hot water extraction is the most commonly used extraction method in laboratory and industry because it is simple, convenient and safe, but hot water extraction is long and inefficient. Other methods are also usually used to assist extraction, such as ultrasonic-assisted extraction and microwave-assisted extraction. He et al. (24) conducted experiments for comparing the extraction of polysaccharides from hot water, ultrasonic assisted hot water extraction, and microwave assisted hot water extraction, the yield of polysaccharides from *D. officinale* was the highest at 20.55%, followed by microwave-assisted hot-water extraction at 17.74%. Ultrasound and microwave could damage the cell wall, causing an outflow of substances within the cell, which increases the efficiency of polysaccharide extraction, but long-term use leads to structural destruction of polysaccharides (25). In addition to the physical extraction method, enzymes are also used to assist the extraction of *D. officinale* polysaccharides. Currently, the enzymes used to prepare polysaccharides mainly include cellulase, pectinase, and protease. Enzymes could soften the cell wall, change the permeability of the cell wall, and make the cell contents easier to dissolve, thereby improving the extraction efficiency (26). He et al. (24) used cellulase-assisted extraction of *D. officinale* stem polysaccharides, and the extraction rate was 18.50%, which was much higher than that of hot water extraction. To sum up, the hot water extraction method is simple and convenient, but the extraction rate is low and time-consuming; ultrasonic-assisted, and microwave-assisted extraction methods can improve the extraction efficiency, but long-term ultrasonic or microwave irradiation could degrade polysaccharides and change the structure of polysaccharides; enzyme-assisted extraction method has the advantages of mild reaction conditions and high efficiency, but it has high production costs and strict environmental requirements.

It is worth mentioning that the yield of *D. officinale* polysaccharides is not only related to the extraction method, but also to the extraction conditions (such as solid-liquid ratio, extraction time, and extraction temperature). The different extraction conditions of polysaccharides were optimized by response surface methodology and orthogonal method. For example, Pan et al. (27) found that the optimal enzyme-assisted extraction conditions of *D. officinale* polysaccharides were: solid-liquid ratio 1:25, pH 5.5, cellulase 10 m/L, extraction temperature at 40°C and extraction time of 3 h, the polysaccharide yield was 8.41 g/100 g dry weight, which was 1.25 times that of hot water extraction. Guo et al. (20) found that when the ultrasonic power was 144 W, the extraction time was 150 min, the extraction temperature was 353.15 K, and the solid-liquid ratio was 60:1, the highest yield of *D. officinale* polysaccharide was 43.7%.

The crude extract of *D. officinale* polysaccharide usually contains some impurities such as pigments, proteins, and other small molecules. Therefore, decolorization and deproteinization are the keys to purify *D. officinale* polysaccharide. At present, the decolorization of *D. officinale* polysaccharide is mainly carried out by activated carbon adsorption method, hydrogen peroxide method, and resin adsorption method (1). Among different decolorization methods, the hydrogen peroxide method has the best decolorization effect, but the amount of hydrogen peroxide should be strictly controlled, otherwise it will destroy the polysaccharide structure and even lead to polysaccharide

10.3389/fnut.2022.965073

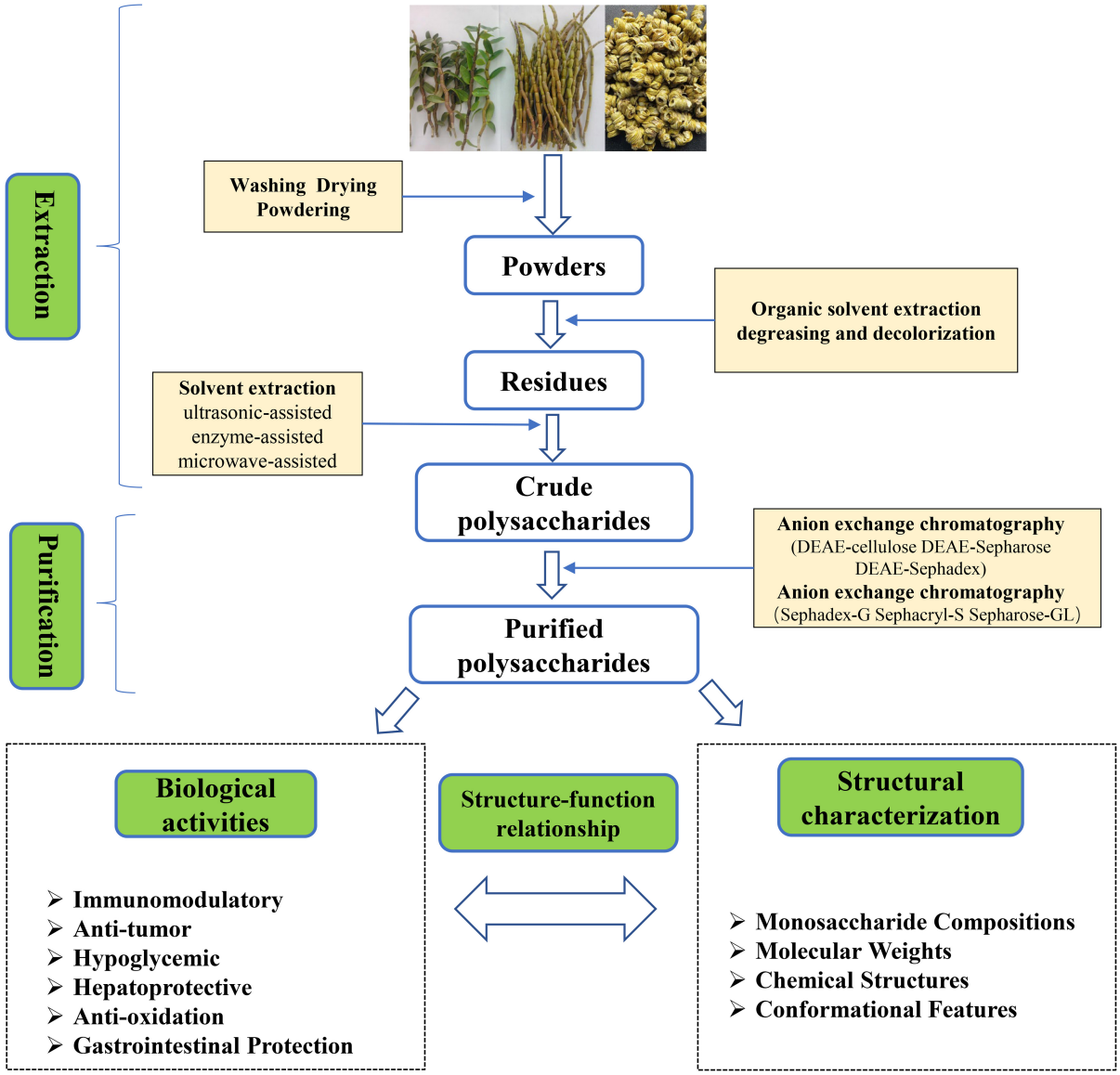

FIGURE 1
Schematic representation of the extraction, purification, and bioactivity of polysaccharides from *Dendrobium officinale*.

degradation. Compared with the oxidation method, the activated carbon adsorption method has little effect on the polysaccharide structure, but due to its porous structure, the polysaccharide retention rate was low. Macroporous resin adsorption has high stability and selective adsorption, which is an ideal decolorization method for polysaccharides (28–30). Till now, the protein in polysaccharide is mainly removed by Sevag and trichloroacetic acid. Among them, trichloroacetic acid has the best protein removal effect and high polysaccharide retention rate, but excessive trichloroacetic acid will lead to polysaccharide degradation. The Sevag reagent is often used for deproteinization of *D. officinale* polysaccharides due to its mild reaction. However, the Sevag reagent has low deproteinization efficiency, low polysaccharide retention rate and toxic reagent residues (17, 31, 32). In the future, safer and more environmentally friendly methods such as enzymatic hydrolysis, resin adsorption, and ultrafiltration could be used to deproteinize *D. officinale* polysaccharides.

It is reported that *D. officinale* polysaccharide is a heteropolysaccharide containing different components, and the separation of *D. officinale* polysaccharide into a single component is the basis for studying the chemical structure (33). To date, step-by-step alcohol precipitation has become a method for the initial separation of polysaccharides. As the molecular weight of polysaccharides increases, the solubility of polysaccharides in ethanol decreases. Based on

this principle, different concentrations of ethanol are used to separate polysaccharides of different components (34). Xing et al. (35) successfully separated four components from DOP by fractional alcohol precipitation (40, 50, 60, and 70% v/v) method. Although the fractional precipitation method is simple, the molecular weight distribution of the polysaccharide after separation is wide, which is a rough separation method. In addition, column chromatography is a commonly used method for the separation and purification of polysaccharides. It could be divided into anion exchange chromatography and gel filtration chromatography. Neutral polysaccharides and acidic polysaccharides were separated by anion exchange chromatography with different concentrations of NaCl, and polysaccharides of different molecular weight were separated by gel filtration chromatography (36, 37). Currently, anion chromatography columns (DEAE-cellulose and DEAE-Sepharose Fast Flow) separated acidic polysaccharides and medium polysaccharides according to polysaccharide polarity (37–39). Gel filtration chromatography (Sephadex-G series and sephacryl-S series) separated polysaccharides based on molecular weight differences (40–42). For instance, Xie et al. (39) used a DEAE-Cellulose column (1.6 cm × 60 cm) to elute with water and 0.05 M NaCl solution to obtain two separated fractions (DOP-W and DOP-S). Sun et al. (43) isolated three major polysaccharide components (DCPP-I, DCPP-I-a, and DCPP-II) from DCPP by DEAE-Cellulose-52 and Sephadex G-200 column, wherein DCPP-I-a was composed of xylose, glucose, galactose was composed in a molar ratio of 1.44:6.93:12.79 and had a molecular weight of 67 KDa. Besides column chromatography, other purification techniques such as salting out, ultrafiltration, metal coordination are also used for polysaccharide purification (37).

Physiochemical and structural characterization

The physicochemical structural characteristics of plant polysaccharides mainly include monosaccharide composition, molecular weight, chemical structures, type and position of glycosidic bonds, and spatial conformation (44). A variety of polysaccharide components were isolated from *D. officinale* polysaccharides, and their chemical structures could be determined by a combination of chemical analysis, spectroscopic analysis, and chromatographic analysis, such as high performance gel permeation chromatography (HPGPC), high-performance liquid chromatography (HPLC), gas chromatography (GC), gas chromatography-mass spectroscopy (GC-MS), fourier transform infrared spectroscopy (FT-IR), nuclear magnetic resonance (NMR), scanning electron microscope (SEM), atomic force microscope (AFM), methylation analysis, Smith degradation, periodate oxidation, etc (37, 44–46). The structural characteristics of *D. officinale* polysaccharides such as monosaccharide composition, molecular weight, chemical structure and biological activity are summarized in **Table 1**.

Monosaccharide compositions

In the research on the structural characteristics, physicochemical properties, and structure-activity relationship of plant polysaccharides, the composition of monosaccharides is the most basic and core research object. In most cases, analysis of monosaccharide composition includes polysaccharide hydrolysis, chemical modification, and quantitative detection by HPLC, GC (44, 57). The monosaccharide composition of polysaccharides obtained from different varieties, origins and extraction methods is obviously different. However, most *D. officinale* polysaccharides consisted mainly of glucose, mannose, and galactose according to different moles (1). In one study, for example, Huang et al. (5) purified two polysaccharides (DOPA-1 and DOPA-2) through Sephacryl S-300 chromatography with different molar ratios of mannose to glucose as shown in **Table 1**. Meanwhile, Tian et al. (58) compared before and after fermentation, the monosaccharide composition *D. officinale* polysaccharide changed little. Interestingly, He et al. (24) obtained *D. officinale* polysaccharides by different extraction methods, which consisted of different molar ratios of mannose and glucose.

Molecular weights

Molecular weight of polysaccharide is usually determined by HPLC, HPGPC, and high performance size exclusion chromatography multiangle laser light scattering (HPSEC-MALLS) (29, 33). It could be concluded from **Table 1** that the molecular weight distribution of *D. officinale* polysaccharides was wide, and the molecular weight ranged from 2.53 to 1,930 kDa. At the same time, the molecular weight of *D. officinale* polysaccharides was affected by the source of raw materials and the method of extraction, separation, and purification. Zhang et al. (10) used Sephadex G-100 column to separate two polysaccharides (DLP-1, DLP-2) from *D. officinale* leaves with molecular weights of 28.342 and 41.143 kDa. Comparing the effect of different extraction methods on the molecular weight of *D. officinale* polysaccharide, compared with hot water extraction and enzyme-assisted extraction, ultrasonic-assisted extraction had the lowest molecular weight (197.1 kDa), because long time ultrasonic extraction could destroy the polysaccharide chain structure and cause polysaccharide degradation (24).

TABLE 1 The polysaccharides isolated from *Dendrobium officinale*.

No.	Compound name	Source	Mw (Da)	Monosaccharide composition	Structures	Biological activities	References
1	DOP-W3-b	Stems of *D. officinale*	1.543×10^4	Man, Glc in the ratio of 4.5:1.0	Backbone consisting of β-(1→4)-D-Man*p*, β-(1→4)-D-Glc*p* and β-(1→3,6)-D-Man*p* residues; branch consisting of β-(1→4)-D-Man*p*, β-(1→4)-D-Glc*p* and terminal β-D-Glc*p*, and O-acetyl groups attached to 2-O-2 of β-(1→4)-D-Man*p*	Immunoregulation	39
2	DPOa	*Tiepi Fengdou*	8.1×10^5	Man, Glc in the ratio of 5.6:1.0	Backbone consisting of β-(1→4)-D-Man*p*, β-(1→4)-D-Glc*p* residues	Immunoregulation	47
3	DOPb	*Tiepi Fengdou*	6.7×10^5	Man, Glc in the ratio of 5.9:1.0	Backbone consisting of β-(1→4)-D-Man*p*, β-(1→4)-D-Glc*p* residues	Immunoregulation	
4	DOP	Stems of *D. officinale*	8.5×10^3	Man, Glc, Ara, GalA in the ratio of 6.2:2.3:2.1:0.1	Backbone consisting of β-(1→4)-D-Man*p*, β-(1→4)-D-Glc*p* residues	Antioxidant	41
5	HPS-1B23	Herba *Dendrobii*	2.2×10^4	Glc, Man, Gal in the ratio of 31:10:8	Backbone consisting of α-(1→6)-D-Glu*p*, α-(1→4)-D-Glc*p*,α-(1→3,6)-D-Man*p*	Immunoregulation	42
6	FP	*D. officinale*	2.53×10^3	Glc, Gal, Man in the ratio of 2.1:3.4:3.9	Backbone consisting of →3,6)-β-L-Man*p*-(1→, α-D-Glc*p*-(1→, →4)-α-D-Glc*p*-(1→, →3,6)-β-D-Gal*p*-(1→, →6)-β-D-Gal*p*-(1→	Antioxidant, immunoregulation	48
7	DOPS-1	*D. officinale*	1.57×10^6		Backbone consisting of (1→4)-β-D-Glc*p*, (1→4)-β-D-Man*p* and 2-O-acetyl-(1→4)-β-D-Man*p*	Antioxidant, antitumor	40
8	DDFPs50	*D. devonianum*	5.63×10^5	Man, Glc, Gal, Rha, Ara, Fru, GlcA in the ratio of 8.45:2.93:1.00:0.06:0.37:0.04:0.2		Antioxidant	34
9	DOPA-1		2.29×10^5	Man, Glc, Gal in the ratio of 1:0.42:0.27	contain (1 → 3), (1 → 2), and (1 → 6) linkages in the main or branch chains	Anti-tumor	49
10	DOPA-1	Fresh stems of *D. officinale*	3.94×10^5	Man, Glc in the ratio of 5.8:1	Backbone consisting of β-(1→4)-D-Man*p*, β-(1→4)-D-Glc*p* residues	Antioxidant, immunoregulation	5
11	DOPA-2	Fresh stems of *D. officinale*	3.62×10^5	Man, Glc in the ratio of 4.5:1	Backbone consisting of β-(1→4)-D-Man*p*, β-(1→4)-D-Glc*p* residues	Antioxidant, immunoregulation	
12	DOP-1	*D. officinale*	6.8×10^3	Man, Glc in the ratio of 5.18:1	Backbone consisted of →4)-β-D-Glc*p*-(1→, →4)-β-D-Man*p*-(1→, →4)-2-O-acetyl-β-D-Man*p*-(1→ and →4)-3-O-acetyl-β-D-Man*p*-(1→	Hypoglycemic	50
13	DOP-2	*D. officinale*	1.43×10^4	Man, Glc in the ratio of 4.78:1	Backbone consisted of →4)-β-D-Glc*p*-(1→, →4)-β-D-Man*p*-(1→, →4)-2-O-acetyl-β-D-Man*p*-(1→ and →4)-3-O-acetyl-β-D-Man*p*-(1→	Hypoglycemic	
14	DLP- 1	*D. officinale* leaves	1.38×10^6	Man, Glc in the ratio of 3.13:1	Backbone consisted of (1→4)-β-D- Man*p*, (1→4)-β-D- Glc*p*, and (1→4)-2-O-acetyl-β-D-Man*p*	Immunoregulation	51
15	DLP- 2	*D. officinale* leaves	1.93×10^6	Rha, Ara, Gal in the ratio of 1.37:0.94:1	Backbone consisted of (1→4)-β-D-Man*p*, (1→4)-β-D-Glc*p*	Immunoregulation	
16	DOP1-1	*D. officinale*	1.78×10^5	Man, Gal in the ratio of 5.9:1	*O*-acetylated glucomannan with β-D configuration	Immunoregulation	52
17	DCP	Fresh *D. catenatum* stems	2.21×10^5	Glc, Man, GalA in the ratio of 30.2:69.5:0.3	Backbone consisted of (1→4)-β-D-Man*p*, 2-*O*-acetyl-(1→4)-β-D-Man*p*, (1→6)-α-D-Glc*p*, and (1→4)-α-D-Glc*p* residues	Immunoregulation	53
18	LDOP	Leaf of *D. officinale*	9.18×10^4	Man, Gla, Glc, GlcA, and Ara in the ratio of 2.0:1.3:1.6:1.7:0.7	Backbone consisting of α-(1→4)-D-Man*p*, α-(1→6)-D-Glc*p*	Anti-inflammatory	54
19	DOA1a	Dried stems of *D. officinale*	3.7×10^4	Ara, Xyl, Glc, 4-*O*-methylglucuronic acid(4-MGA), Rha, Gal in the ratio of 8.9: 62.7: 8.5: 12.3: 3.9: 3.7	Backbone consisting of β-(1→4)-D-xylan; branch consisting of α-(1→4)-D-Glc*p*, α-(1→3)-L-Rha*p*	Anti-angiogenesis	55
20	DOP-1	*D. officinale* Kimura et Migo	4.47×10^5	Gal, Glc, Man in the ratio of 1:1.79:6.71	Backbone consisting of →4)-α-D-Glc*p*-(1→4)-α-D-Man*p*-(1→4)-α-D-Man*p*-(1→4,6)-α-D-Man*p*-(1→	Antioxidant, anti-tumor	56

Chemical structures

In addition to the research on the monosaccharide composition and average molecular weight of *D. officinale* polysaccharides, the chemical structure characterization of polysaccharides has also gradually attracted attention (**Table 1**). At present, the chemical structures of polysaccharides have been analyzed by methylation analysis, periodic acid oxidation, Smith degradation, GC-MS, infrared spectroscopy, FT-IR, and NMR (32, 37, 57). So far, several studies have reported the chemical structure of *D. officinale* polysaccharides (**Figure 2**). Zha et al. (42) elucidated the structure of a polysaccharide (HPS-1B23) isolated by DEAE-Cellulose anion-exchange column, Sephacryl S-200 column, Sephadex G-75 column. According to the results of periodate oxidation, methylation analysis and NMR, the repeating unit of HPS-1B23 was constructed as shown in **Figure 2A**. They also found that the C-3 position of the (1→6)-linked glucose was partially substituted by an acetyl group. And the molar ratio of (1→6)-linked glucose, (1→4)-linked glucose, (1→3,6)-linked mannose, and (1→3,6)-linked mannose in backbone is 4:2:1:2.2.

Kuang et al. (50) characterized the structure of two component polysaccharides (DOP-1, DOP-2) isolated from *D. officinale*. Studies have shown that both DOP-1 and DOP-2 were composed of mannose and glucose, and it is speculated that their backbone structures are both composed of →4)-β-D-Glc*p*-(1→, →4)-β-D-Man*p*-(1→, →4)-2-O-acety-β-D-Man*p*-(1→ (**Figure 2B**).

Yue et al. (55) isolated a novel polysaccharide (S32) from the crude polysaccharide of *D. officinale* extracted with DEAE Sepharose Fast Flow and Sephacryl S-300. Studies have shown that it was composed of arabinose, xylose, glucose, 4-MGA, and a small amount of galactose and rhamnose. We infer that the structural repeat unit of S32 was shown in **Figure 2C**, and it contained a backbone of 1,4-linked β-D-xylan, with branches of 1,4-linked α-D-glucose, 1,3-linked α-L-rhamnose, and terminal-linked α-L-arabinose, β-D-galactose, 4-MGA, and β-D-xylose directly or indirectly attached to C-2 position of glycosyl residues on backbone (55).

Tao et al. (59) isolated two polysaccharide components (DOW-1 and DOPW-2) from *D. officinale*, and characterized the polysaccharide structure based on methylation analysis and NMR, inferring the repeating unit structure of DOPW-1 and DOPW-2 (**Figure 2D**). Meanwhile, methylation analysis revealed that both DOPW-1 and DOPW-2 possessed the same backbones of →4)-β-D-Man*p*-(1→, →4)-β-D-Glc*p*-(1→, although with different percentages.

He et al. (52) isolated a fraction of neutral heteropolysaccharide (DOP1-1) from *D. officinale* and analyzed their physicochemical properties. NMR and FT-IR analysis indicated that partial structure of DOP-1-1 is an *O*-acetylated glucomannan with β-D configuration in pyranose sugar forms.

Conformational features

Till now, the primary structure of *D. officinale* polysaccharide has been studied by lots of experiments, but there were few reports on the solution properties and conformation features of *D. officinale* polysaccharide (1). At present, the advanced structure characterization of polysaccharide mainly includes Congo red experiment, SEM, AFM, circular dichroism, and X-ray diffraction (XRD) (36, 44). Zhong et al. (51) isolated two polysaccharides (DLP-1 and DLP-2) from *D. officinale* leaves, both of which could form complexes with Congo red in the Congo red experiment, indicating that DLP-1 and DLP-2 had triple helices structure. Besides, the surface structure of DLP-1 was irregular large flakes with smooth surface and porous interior. In contrast, the surface of DLP-2 was rough, loose, and uneven, consisting of large spongy particles, which might be due to the binding of polysaccharides to different macromolecules and the freeze-drying and dehydration processes affecting the morphology of polysaccharides. In the future, more advanced technology is needed to conduct research in order to better understand the structure-activity relationship of *D. officinale* polysaccharides.

Biological activities

In recent years, *D. officinale* polysaccharides have attracted extensive attention in the field of biological and medical for their various biological properties and pharmacological functions. Studies *in vitro* and *in vivo* have shown that *D. officinale* polysaccharides have a variety of pharmacological activities, including immunomodulatory (60), antioxidant (56), anti-tumor (49), gastrointestinal protection (61), anti-aging (3), hepatoprotective (62), hypoglycemic (50), and anti-inflammatory (63). Among them, immune regulation, anti-oxidation, anti-cancer and gastrointestinal protection are the main activities of *D. officinale* polysaccharide. The activity of *D. officinale* polysaccharides and the corresponding mechanism are shown in **Figure 3**.

Immunomodulatory

Immune regulation is one of the most important physiological of *D. officinale* polysaccharides. It could regulate the immune system in animals by binding to receptors on the surface of immune cells and activating different signaling pathways. (44). The immunomodulatory mechanism of *D. officinale* polysaccharide was shown in **Figure 4**. *D. officinale* polysaccharide relieved immunosuppression by regulating the proportion and differentiation status of immune cells (such as $CD4^+$ T cells, $CD8^+$ T cells, B lymphocytes, macrophages, and natural killer cells) (1, 16, 28). In general, they could enhance

10.3389/fnut.2022.965073

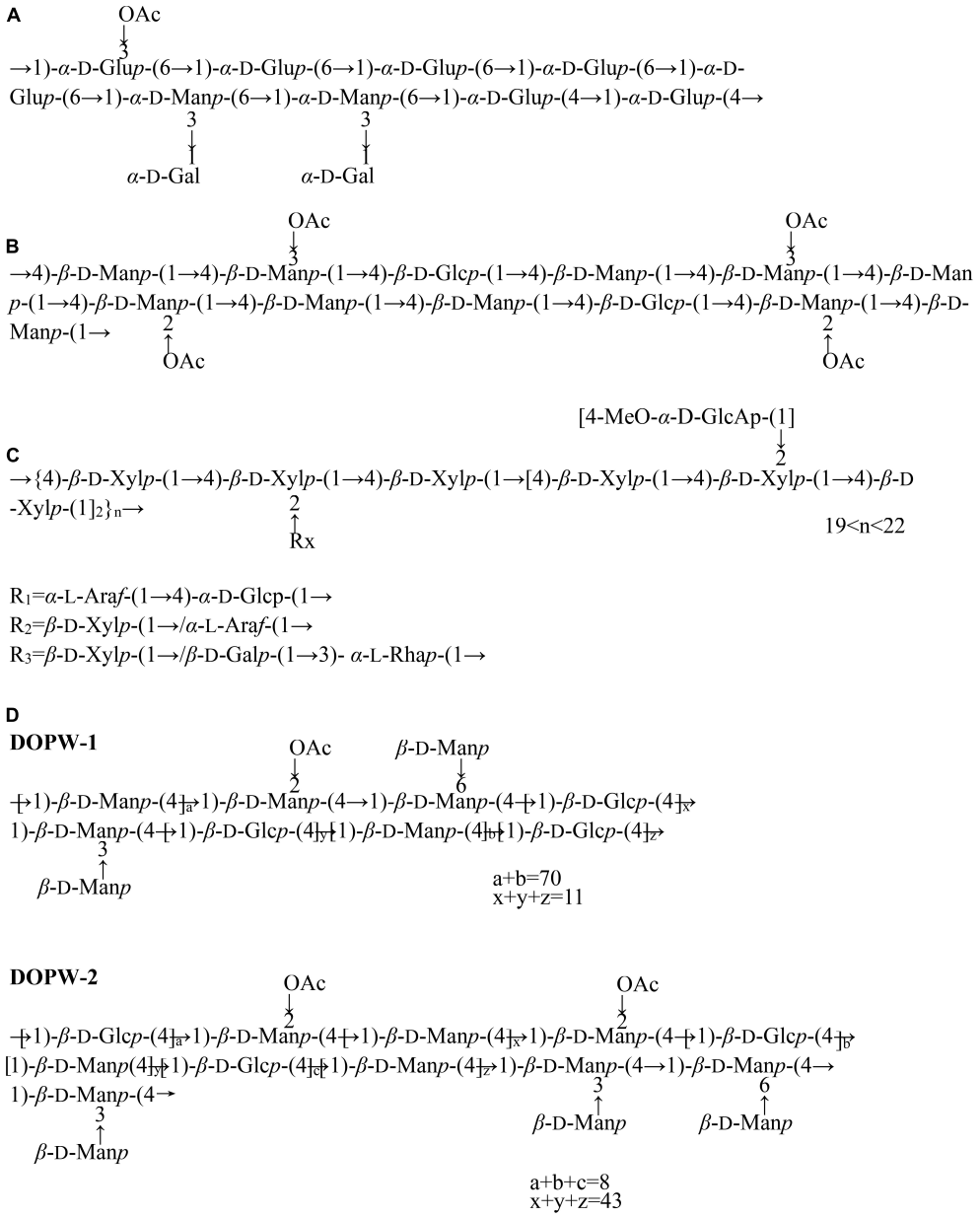

FIGURE 2
The chemical structure of *D. officinale* polysaccharides. **(A)** The *D. huoshanense* polysaccharide (HPS-1B23), **(B)** two component polysaccharides (DOP-1, DOP-2), **(C)** a novel polysaccharide (S32), **(D)** two novel polysaccharide fractions (DOW-1, DOPW-2).

the phagocytic ability of macrophages through non-specific immunomodulatory functions and promote the production of certain cytokines [such as interleukin-2 (IL-2), interleukin-6 (IL-6), interferon-γ (IFN-γ), tumor necrosis factor-α (TNF-α)] and other inflammatory factors [such as reactive oxygen species (ROS), nitric oxide (NO)] (17).

Huang et al. (60) studied the immunomodulatory activity of polysaccharides (DOP-1-1) isolated from the stems of *D. officinale*. The results suggested that DOP-1-1 induced an immune response through the nuclear factor-kappa B (NF-κB) mediated by TLR4 signaling pathway, confirming that CCL4 and IP10 may be new targets of DOP-1-1-stimulated immune response.

In one case, a polysaccharide (DOP-W3-b) with more intestinal immune activity was isolated from the stem of *D. officinale*. Oral administration showed that DOP-W3-b promoted Peyer's patches (PPs) and mesenteric by changing the structure of the intestinal mucosa. Lymph nodes (MLNs) cytokines secreted IFN-γ and IL-4 effectively modulated intestinal mucosal immune activity and increased the production of secretory immunoglobulin A (sIgA) (39).

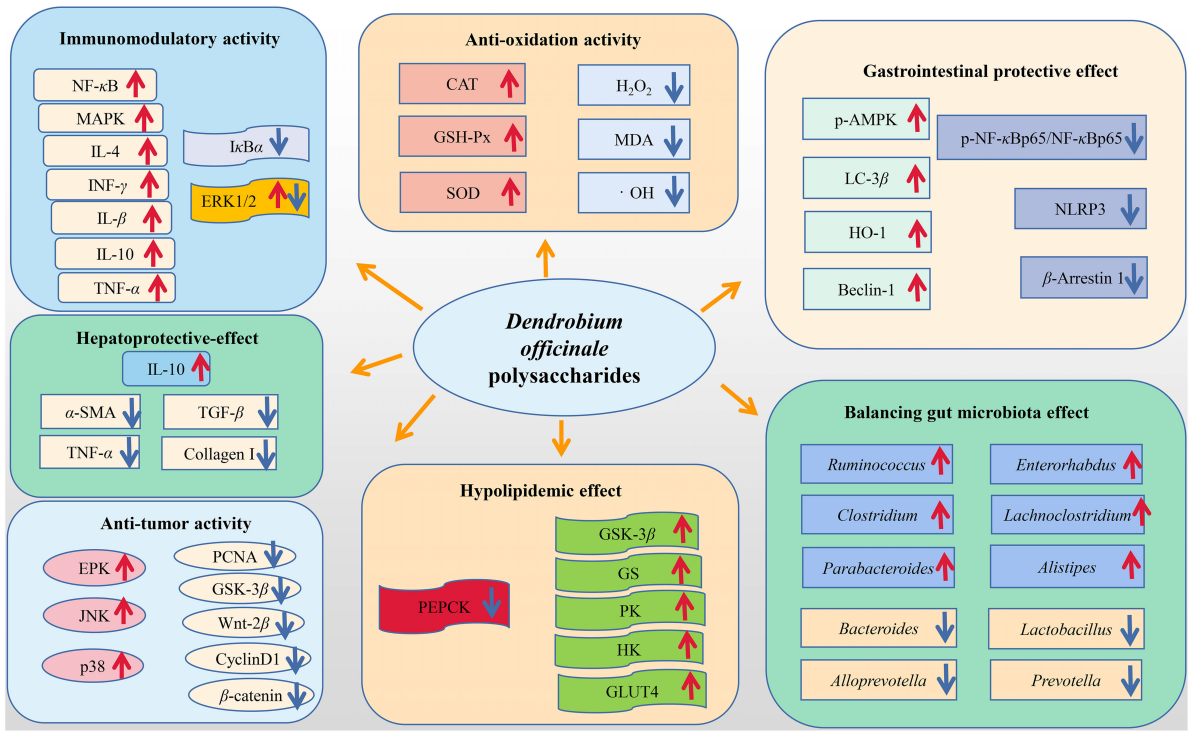

FIGURE 3
Bioactivities of *D. officinale* polysaccharides.

Two novel component polysaccharides (DLP-1 and DLP-2) were isolated from *D. officinale* leaves, both of which could stimulate the proliferation and phagocytosis of RAW 264.7 cells, and promote the secretion of NO, IL-6, IL-1β, and TNF-α. Moreover, the immunomodulatory activity of DLP-2 was higher than that of DLP-1 at the same concentration. Thus, DLP-1 and DLP-2 could be used as functional food additives (51). Similarly, DCP also has immunostimulatory activity *in vitro*, the mechanism of which was similar to that of DLP-1 and DLP-2 (53). Meanwhile, two component polysaccharides (DOP-1 and DOP-2) were isolated from *D. officinale* by DEAE cellulose and Sephacryl S-400, which caused a significant stimulation of cytokine secretion of both splenocytes and macrophages. DOP-1 had a greater effect on lymphocyte activation and DOP-2 on macrophage activation (64). In conclusion, the immunomodulatory effect of ferric polysaccharide was mainly achieved by inhibiting MAPK and NF-κB activation, promoting cytokine secretion and macrophages activity.

Anti-tumor

Tumors are caused by different factors such as genetics, environment, and lifestyle. Tumorgenesis is a complex process, closely related to immune and inflammatory processes. Its anti-tumor activity mechanism is mainly to enhance immune regulation, inhibit tumor cell proliferation, and regulate tumor cell microenvironment (1, 65, 66).

Wei et al. (49) determined the antitumor cell activity of purified DOPA-1 by cell experiments. They found that DOPA-1 inhibited the growth of HepG-2 cells in a dose-dependent manner. The levels of ROS in HepG-2 cells treated with DOPA-1 increased, the mitochondrial membrane potential decreased, and the expressions of P53, Bax, and Bak were up-regulated, and the expressions of Bcl-2 and Mcl-1 were down-regulated as shown in **Figure 5**. Liang et al. (9) found that DOPS could restore the intestinal barrier function and enhance the intestinal anti-tumor immune response, thereby inhibiting the occurrence of colorectal tumors. Xing et al. (35) reported that four component polysaccharides (DOP-40, DOP-50, DOP-60, and DOP-70) induced apoptosis in HepG-2 cells through Bcl-2 and Bax-dependent pathways. In addition, purified polysaccharides (DCPP-I, DCPP-I-a, and DCPP-II) showed stronger inhibitory effect on SPC-A-1 cell proliferation than crude polysaccharides (43).

Comparing the antitumor activities of different polysaccharides in DOP122, DOP20, DOP8, and DOP2, we found that DOP20 had the strongest inhibitory effect on the proliferation of osteosarcoma (OS) U2OS and Saos-2 cells (67). In addition, DOP20 promoted DDP-induced cell apoptosis by the mitochondrial pathway by up-regulates the expression of P53, Bax, Bak; down-regulated the expression of Bcl-2 and

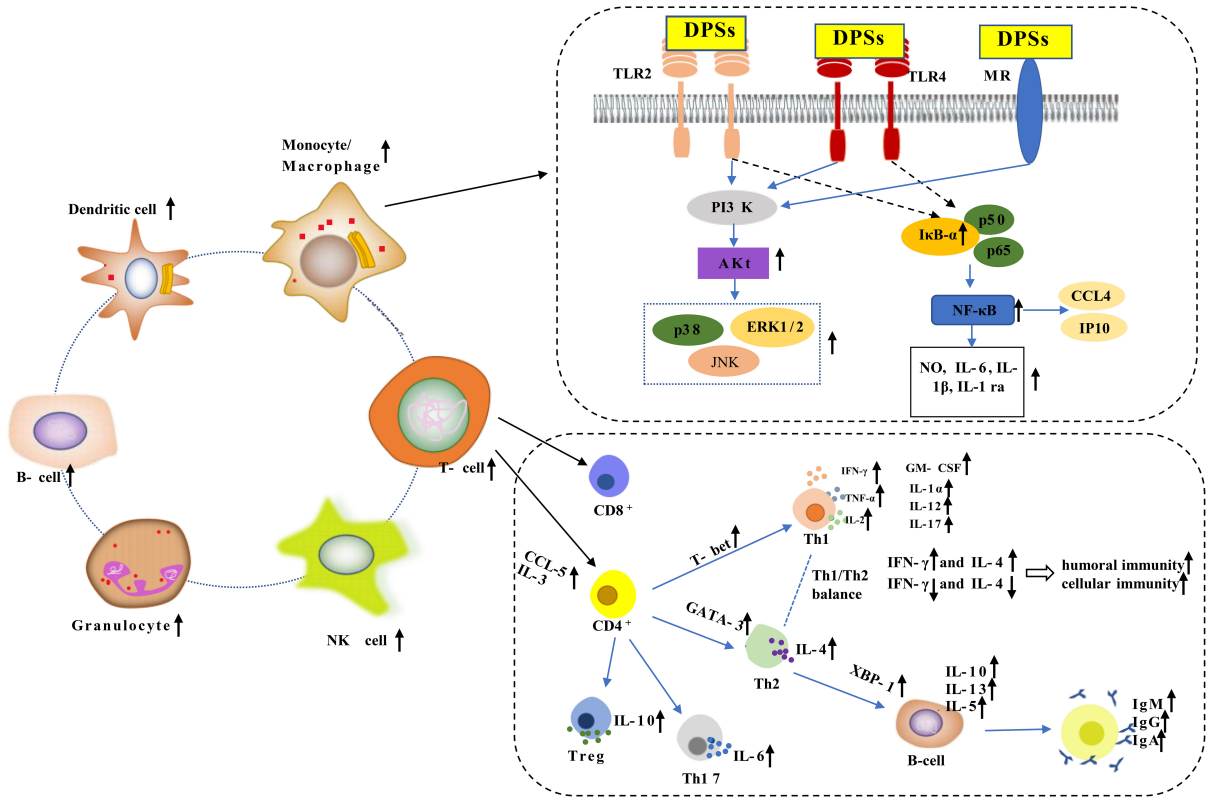

FIGURE 4
The potential immunomodulatory mechanisms of *D. officinale*.

Mcl-1; increased the proportion of Cleaved caspase9/Caspase9, Cleaved caspase3/Caspase3, and Cleaved PARP/PARP (67). Besides, the anti-tumor activity of DOPs on OS cells was superior to that of mannose-containing monosaccharides and oligosaccharides, and the molecular weight was also an important factor affecting the anti-tumor activity. In the future, polysaccharides with relatively appropriate molecular weight or molecular weight range should be found for application.

Hypoglycemic

Diabetes mellitus is a metabolic disease caused by insufficient secretion of the pancreas, characterized by elevated blood sugar levels (33). Studies have shown that *D. officinale* polysaccharides could promote insulin secretion and inhibit glucagon secretion, and achieve the purpose of extrapancreatic hypoglycemia by inhibiting epinephrine-induced hepatic glycogenolysis and promoting hepatic glycogen synthesis (17, 68, 69). Liu et al. (70) explored the hypoglycemic mechanism of DOP from the glucagon-mediated signaling pathway and the structure of hepatic glycogen that catalyzes hepatic glucose metabolism. The results showed that DOP significantly inhibited the glucagon-mediated cAMP-PKA signaling pathway, increased the GS expression and decrease GP expression, thereby promoting hepatic glycogen synthesis and inhibiting hepatic glycogen degradation. Furthermore, through the glucagon-mediated Akt/FoxO1 signaling pathway, the expression of G6Pase and PEPCK was reduced, and hepatic gluconeogenesis was inhibited in diabetic mice (**Figure 6**).

Taking alloxan-induced diabetic mice as the research object, the hypoglycemic activities of different varieties of *D. officinale* polysaccharides (DHP, DOP, DNP, and DCP) were compared. The results of serum FBG levels and Serum insulin level showed that DHP, DOP, and DNP had significant hypoglycemic activity (71). In addition, different doses of DOPs were fed to diabetic rats, and it was found that DOPs had obvious hypoglycemic activity and increased serum insulin and GLP-1 levels in diabetic rats. Moreover, The Ca^{2+}/CaM/CaMKII and MAPK pathways were involved in DOP-induced GLP-1 secretion in STC-1 cells *in vitro* (50). Nowadays, long-term use of hypoglycemic drugs and insulin injections could cause serious side effects to the body. *D. officinale* polysaccharide had the effect of repairing islet cells, and the potential to become a new anti-diabetic drug in the future. However, a large number of clinical trials are still needed to study the hypoglycemic activity of *D. officinale* polysaccharide.

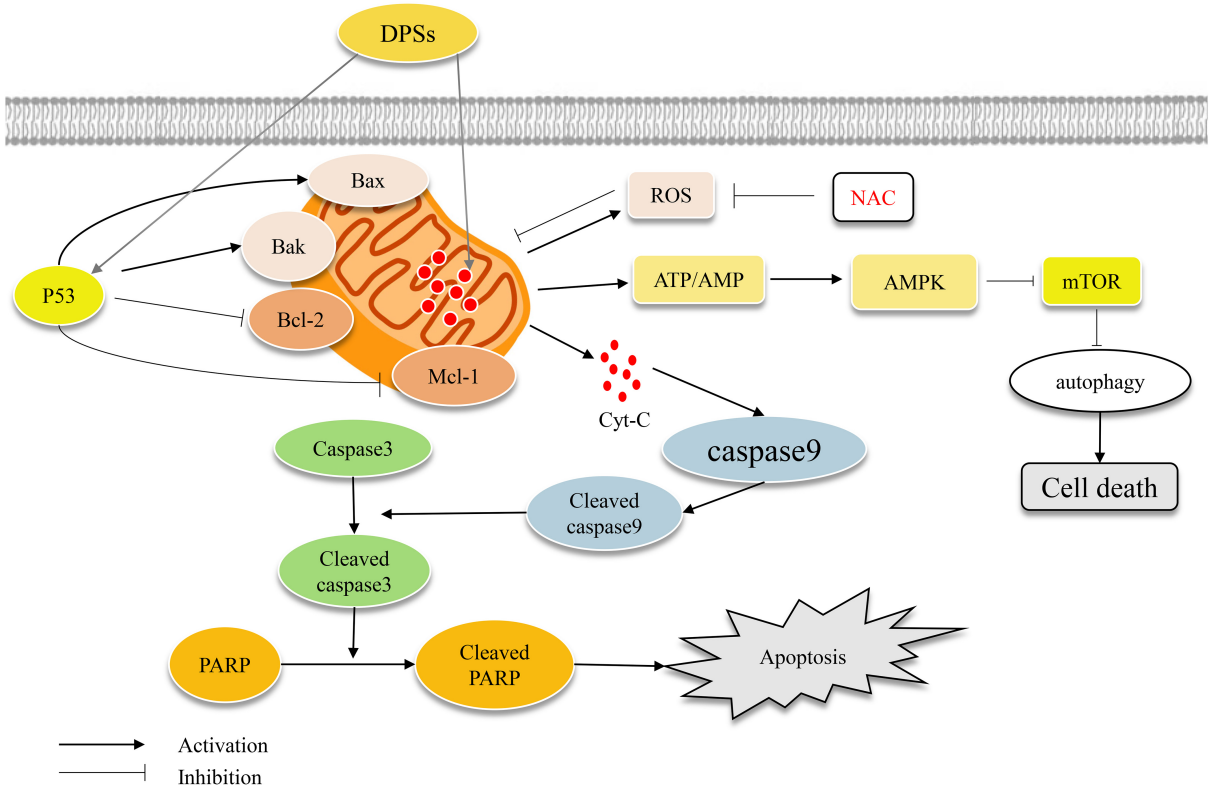

FIGURE 5
The potential anti-tumor mechanisms of *D. officinale*.

Hepatoprotective

The liver is the largest digestive gland in the human body, a place for material metabolism, and an important detoxification organ to maintain the body's homeostasis. Some drugs or chemical substances induce liver damage and cause various diseases including hepatitis, alcoholic liver injury, liver fibrosis, liver cancer, etc (72). In a male Sprague–Dawley rat model of alcoholic liver injury, after oral administration of *D. officinale* polysaccharide (DOP) 400 and 100 mg/kg, ASF content in serum and liver tissue decreased, inflammatory cytokines (such as IL-1β, IL- 6, and TNF-α) were significantly decreased, and NF-κB phosphorylation was inhibited. *In vitro*, DOP increased LO2 cell viability, inhibited LDH release, and decreased IL-1β, IL-6, and TNF-α secretion (73). Lin et al. (62) studied that DOP feeding for 30 days could protect liver injury induced by acetaminophen (APAP), and further studies showed that DOP exerted hepatoprotective effect by inhibiting oxidative stress and activating the Nrf2-Keap1 signaling pathway. A study by Wang et al. showed that *D. officinale* polysaccharide (DOP) could protect ccl4-induced liver fibrosis by maintaining intestinal homeostasis and inhibiting the activation of LPS-TLR4-NF-κB signaling pathway (74).

Anti-oxidation

With the deepening of scientific research, it has been gradually recognized that many diseases are related to oxidative stress, such as diabetes, cardiovascular disease, hypertension, and other chronic diseases, so antioxidant strategies have received more and more attention. *D. officinale* contains high activity of superoxide dismutase (SOD), peroxidase (POD), catalase (CAT), and has good antioxidant activity *in vitro* and *in vivo* (3).

Huang et al. (75) compared the antioxidant activity of *D. officinale* polysaccharide crude and purified in cyclophosphamide-induced mice. The results showed that the bold and purified compounds had good antioxidant activities against CTX-induced oxidative stress, including increased liver and thymus indices, increased antioxidant enzyme activity, and decreased malondialdehyde (MND) levels in serum, thymus, and liver. Wang et al. (56) isolated two polysaccharides (DOP-1 and DOP-2) from fermented *D. officinale* polysaccharides, and their antioxidant activities were concentration-dependent in DPPH free radical and hydroxyl radical scavenging tests. And the hydroxyl radical scavenging rate of DOP-1 was better than that of DOP-2. Fan et al. (76) separated six polysaccharides from *D. officinale* by a step-by-step alcohol precipitation method.

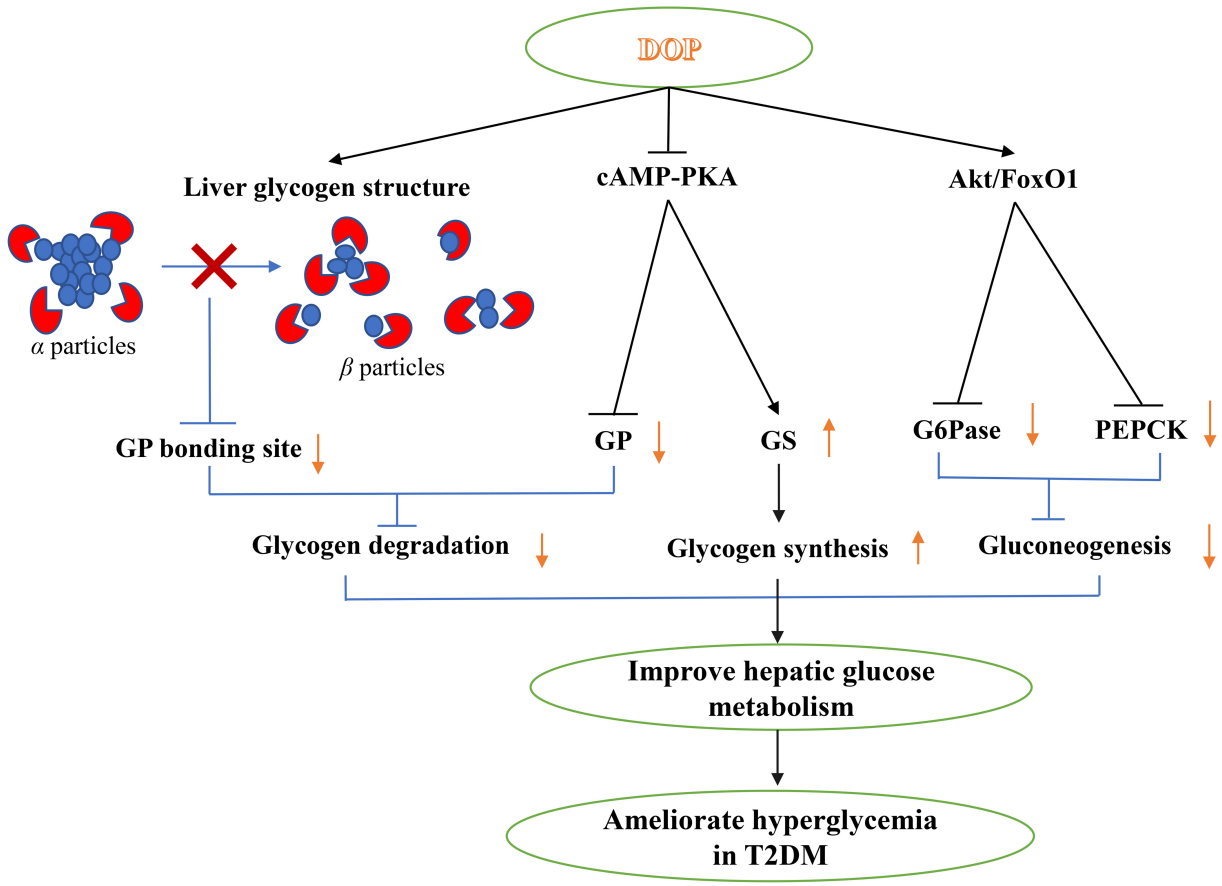

FIGURE 6
The potential hypoglycemic mechanisms of *D. officinale*.

The antioxidant test *in vitro* showed that the six components all had strong antioxidant activities, and the smaller the molecular weight, the stronger the antioxidant activity.

Gastrointestinal protection

Modern pharmacological studies indicated that plant polysaccharides protected gastrointestinal mucosa, regulate intestinal flora, and prevent colorectal cancer (1, 77). Studies have found that *D. officinale* polysaccharide has a protective effect on the gastrointestinal tract, and because it is not easily digested and absorbed, it has the effect of regulating intestinal flora (39, 78).

The polysaccharide fraction (LOP-1) isolated from *D. officinale* leaves had protective effect of ethanol-induced gastric mucosal injury (61). The results showed that the mechanism of action of LOP-1 was to activate the expression levels of p-AMPK, LC3β, and Beclin-1, inhibit the expression levels of p-mTOR and p62, and increase the proportion of Bcl-2 and Bax, thereby reduce gastric mucosal damage and pathological damage (61). Liang et al. (15) found that *D. officinale* polysaccharide (DOP-G-3) could reduce inflammatory damage, reduce colon pathological damage, and protect colon from dextran sulfate sodium (DSS)-induced colitis. Ma et al. (79) found that *D. officinale* polysaccharide could reduce the expression of IL-6, Raf-2, MEK1, MEK2, and ERK by promoting the expression of EGFR and TFF-1 expression, thus reducing the level of inflammatory factors and protecting the gastric mucosa.

Polysaccharides could not be directly digested, the behavior in the intestinal tract is considered a "ridge" between microbiota and host communication. The gastrointestinal tract is often referred to as the "second brain" of the human body. It was reported that the abundance of gut bacteria increased after 25 days of *D. officinale* (DOW-5b) treatment, especially beneficial microorganisms such as butyrate-producing Clostridium, Parabacteroides and anti-inflammatory *Akkermansia*, while harmful bacteria such as *Proteobacteria* decreased (80). In addition, when studying the effect of *D. officinale* (DOP) fermentation on human intestinal flora, the results showed that DOP could increase the abundance

of *Firmicutes* and *Bacteroidetes*, and decrease the abundance of *Proteobacteria* (81). At the same time, the content of short-chain fatty acids (SCFA) mainly composed of acetic acid, propionic acid and butyric acid increased significantly (81). In conclusion, *D. officinale* polysaccharides could improve the disease and maintain physiological activities by increasing the diversity of human intestinal flora, regulating the proportion of intestinal flora, and promoting the growth and proliferation of beneficial flora.

Other

Except as mentioned above biological activities, other biological activities of *D. officinale* polysaccharides were also evaluated. Yue et al. (55) isolated a novel sulfated polysaccharide (S32S) from *D. officinale* stems, which has obvious anti-angiogenic effects by inhibiting the migration and tube formation of human microvascular endothelial cells (HMEC-1). Moreover, *D. officinale* polysaccharide was also found to have neuroprotective activity. Feng et al. (82) proved that *D. officinale* polysaccharide (DOP) could alleviate the cognitive decline in SAMP8 mice by inhibiting the activation of microglia in the hippocampus of SAMP8 mice. Zhang et al. (83) found that fermented *D. officinale* polysaccharide (FDOP) had the effect of reducing antioxidant damage and anti-aging. The results showed that FDOP reduced antioxidant damage and anti-aging effects by upregulating Nrf2/Keap1 and (TGF-β)/Smads signaling pathways.

Structure-function relationship

It is generally believed that the bioactivity of polysaccharides is closely related to their structural properties, including monosaccharide composition, molecular weight, chain conformation, and glycosidic bond types (44). Due to the complex structure of *D. officinale* polysaccharides and the limited understanding of the structure-activity relationship, it is of great significance to explore the structure-activity relationship of *D. officinale* polysaccharides for the development and application of *D. officinale* polysaccharides.

As we all know that the bioactivity of plant polysaccharides is mainly related to the monosaccharide composition, wherein the more complex the monosaccharide composition, the better the biological activity (3). Two polysaccharides rich in mannose (DOPA-1, DOPA-2) were isolated from *D. officinale*. Studies have shown that high mannose content has mild immunostimulatory activity and antioxidant activity (5). Liang et al. (84) isolated two novel polysaccharides (DOP1, DOP2) from *D. officinale* by the DES method, which consisted of glucose and mannose in molar ratios of 2.2:1 and 3.7:1, respectively. The study found that both components had strong antioxidant activity, and the higher the mannose content, the stronger the activity. Molecular weight was also a factor that affects the activity of *D. officinale* polysaccharides. Many scholars have found that the molecular weight of polysaccharides was positively correlated with activity, and polysaccharides with a molecular weight greater than 100 kDa show better activity (3, 16, 17). For example, Huang et al. (5) isolated two component polysaccharides (DOPA-1, DOPA-2) from *D. officinale* with molecular weights of 394 and 362 kDa, respectively, and the results showed that the higher molecular weight component DOPA-1 was more active. In addition, polysaccharide conformation and backbone may also affect polysaccharide biological activity (37, 44). Huang et al. (75) found that the structure containing (1→4)-β-D-Man*p* and O-acetyl was the main reason for the immune activity of polysaccharides.

In general, most studies on the structure-activity relationship of *D. officinale* polysaccharides are single rather than systematic. At present, scholars still need to conduct systematic research on the structure-activity relationship of *D. officinale* polysaccharides, which is conducive to the further development of polysaccharide preparations with specific functions.

Conclusions and perspectives

With the study of biomacromolecules, such as nucleic acids and proteins, developing rapidly, our understanding of the crucial nature of polysaccharides has dramatically expanded over the last few decades. *D. officinale* polysaccharides have received extensive attentions due to their extremely high pharmacological effects and excellent biological properties. This paper summarizes the latest research progress of *D. officinale* polysaccharides, including the extraction, isolation and purification, structure analysis, biological activity, mechanism of action, and structure-activity relationship of *D. officinale* polysaccharides. Although there are many studies on *D. officinale* polysaccharides, there are still many problems to be solved in terms of the current research results.

First, the structurally active relationship of polysaccharides from *D. officinale* was not fully elucidated. Therefore, in-depth research on the structure analysis and structure-activity relationship of *D. officinale* polysaccharides is necessary; the accurate structures of polysaccharides are obtained by applying the latest science and technology to further study their biological activities; the structure-activity relationship database of *D. officinale* polysaccharides is constructed to eliminate the limitations of research. Secondly, the current structural analysis of *D. officinale* polysaccharides mainly focuses on the primary structure of monosaccharide composition, molecular weight,

main chain and side chain, and further analysis of the advanced structure is required. Third, with the study of new technologies "omics," such as metabolomics, microbiomics, proteomics, genomics, transcriptomics, and bioinformatics are widely used in the study of biological activity mechanisms. Fourth, the immune activity of polysaccharides and gut microbiota has received extensive attention. The current mainstream opinion is that the relative molecular mass and polymer length affect the participation of polysaccharides in the recognition and glycolysis processes between microorganisms. It is necessary to strengthen the study of the relationship between the structure of natural polysaccharides and their regulation of intestinal microecology. The human race is experiencing a novel coronavirus outbreak and investigators are eager to find an immunopotentiator to deal with the virus problem.

In summary, *D. officinale* polysaccharides have great application prospects in the fields of biology, medicine, functional food and so on.

Author contributions

YH, HC, BC, HG, and YY contributed to the conception and design of the study. YH wrote the first draft of the manuscript. GC, WH, and ZJ wrote the sections of the manuscript. LL and YY contributed to the funding of the study and writing — review and editing. All authors contributed to the article and approved the submitted version.

Funding

This study was supported by the Key Scientific Research Projects of Colleges and Universities in Henan Province (21B416001), the Key Specialized Research and Development Breakthrough Program in Henan Province (212102310901); the College Students' Scientific Research Innovation Project of Zhengzhou Normal University (2021004), and the Leading Program Project of National Tobacco Corporation (110202103017).

Conflict of interest

The authors declare that the research was conducted in the absence of any commercial or financial relationships that could be construed as a potential conflict of interest.

Publisher's note

All claims expressed in this article are solely those of the authors and do not necessarily represent those of their affiliated organizations, or those of the publisher, the editors and the reviewers. Any product that may be evaluated in this article, or claim that may be made by its manufacturer, is not guaranteed or endorsed by the publisher.

References

1. Chen WH, Wu JJ, Li XF, Lu JM, Wu W, Sun YQ, et al. Isolation, structural properties, bioactivities of polysaccharides from *Dendrobium officinale* Kimura et. Migo: a review. *Int J Biol Macromol.* (2021) 184:1000–13. doi: 10.1016/j.ijbiomac.2021.06.156

2. Wang Z, Zhao M, Cui H, Li J, Wang M. Transcriptomic landscape of medicinal *Dendrobium* reveals genes associated with the biosynthesis of bioactive components. *Front Plant Sci.* (2020) 11:391. doi: 10.3389/fpls.2020.00391

3. Guo L, Qi J, Du D, Liu Y, Jiang X. Current advances of *Dendrobium officinale* polysaccharides in dermatology: a literature review. *Pharm Biol.* (2020) 58:664–73. doi: 10.1080/13880209.2020.1787470

4. Li M, Trapika I, Tang SYS, Cho JL, Qi Y, Li CG, et al. Mechanisms and active compounds polysaccharides and bibenzyls of medicinal Dendrobiums for diabetes management. *Front Nutr.* (2021) 8:811870. doi: 10.3389/fnut.2021.811870

5. Huang K, Li Y, Tao S, Wei G, Huang Y, Chen D, et al. Purification, characterization and biological activity of polysaccharides from *Dendrobium officinale*. *Molecules.* (2016) 21:701. doi: 10.3390/molecules21060701

6. Zhou C, Xie Z, Lei Z, Huang Y, Wei G. Simultaneous identification and determination of flavonoids in *Dendrobium officinale*. *Chem Cent J.* (2018) 12:40. doi: 10.1186/s13065-018-0403-8

7. Liu ZP, Guo YY, Iu JJ, Si JP, Wu LS, Zhang XF. Effect of strains and parts on amino acids of *Dendrobium officinale*. *China J Chin Mater Med.* (2015) 40:1468–72.

8. Zhu Y, Zhang A, He B, Zhang X, Yu Q, Si J. Quantitative variation of total alkaloids contents in *Dendrobium officinale*. *China J Chin Mater Med.* (2010) 35:2388–91.

9. Liang J, Li H, Chen J, He L, Du X, Zhou L, et al. *Dendrobium officinale* polysaccharides alleviate colon tumorigenesis via restoring intestinal barrier function and enhancing anti-tumor immune response. *Pharmacol Res.* (2019) 148:104417. doi: 10.1016/j.phrs.2019.104417

10. Zhang M, Wu J, Han J, Shu H, Liu K. Isolation of polysaccharides from *Dendrobium officinale* leaves and anti-inflammatory activity in LPS-stimulated THP-1 cells. *Chem Cent J.* (2018) 12:109. doi: 10.1186/s13065-018-0480-8

11. Kim S, Jo K, Byun BS, Han SH, Yu KW, Suh HJ, et al. Chemical and biological properties of puffed *Dendrobium officinale* extracts: evaluation of antioxidant and anti-fatigue activities. *J Funct Foods.* (2020) 73:104144. doi: 10.1016/j.jff.2020.104144

12. Wang K, Wang H, Liu Y, Shui W, Wang J, Cao P, et al. *Dendrobium officinale* polysaccharide attenuates type 2 diabetes mellitus via the regulation of PI3K/Akt-mediated glycogen synthesis and glucose metabolism. *J Funct Foods.* (2018) 40:261–71. doi: 10.1016/j.jff.2017.11.004

13. Yang LC, Lu TJ, Hsieh CC, Lin WC. Characterization and immunomodulatory activity of polysaccharides derived from Dendrobium tosaense. *Carbohydr Polym.* (2014) 111:856–63. doi: 10.1016/j.carbpol.2014.05.007

14. Zheng Q, Qiu D, Liu X, Zhang L, Cai S, Zhang X. Antiproliferative effect of Dendrobium catenatum Lindley polypeptides against human liver, gastric and breast cancer cell lines. *Food Funct.* (2015) 6:1489–95. doi: 10.1039/c5fo00060b

15. Liang J, Chen S, Hu Y, Yang Y, Yuan J, Wu Y, et al. Protective roles and mechanisms of Dendrobium officinal polysaccharides on secondary liver injury in acute colitis. *Int J Biol Macromol.* (2018) 107:2201–10. doi: 10.1016/j.ijbiomac.2017.10.085

16. Yue H, Zeng H, Ding K. A review of isolation methods, structure features and bioactivities of polysaccharides from Dendrobium species. *Chin J Nat Med.* (2020) 18:1–27. doi: 10.1016/s1875-5364(20)30001-7

17. Li X, Wang X, Wang Y, Liu X, Ren X, Dong Y, et al. A systematic review on polysaccharides from Dendrobium genus: recent advances in the preparation, structural characterization, bioactive molecular mechanisms, and applications. *Am J Chin Med.* (2022) 50:471–509. doi: 10.1142/S0192415X22500185

18. Ji X, Han L, Liu F, Yin S, Peng Q, Wang M. A mini-review of isolation, chemical properties and bioactivities of polysaccharides from buckwheat (Fagopyrum Mill). *Int J Biol Macromol.* (2019) 127:204–9. doi: 10.1016/j.ijbiomac.2019.01.043

19. Wang C, Xu L, Guo X, Cui X, Yang Y. Optimization of the extraction process of polysaccharides from *Dendrobium officinale* and evaluation of the in vivo immunmodulatory activity. *J Food Process Preserv.* (2018) 42:e13598. doi: 10.1111/jfpp.13598

20. Guo X, Liu S, Wang Z, Zhang G. Ultrasonic-assisted extraction of polysaccharide from *Dendrobium officinale*: kinetics, thermodynamics and optimization. *Biochem Eng J.* (2022) 177:108227. doi: 10.1016/j.bej.2021.108227

21. Hu JM, Li JL, Feng P, Zhang XD, Zhong M. Optimization of enzymatic extraction of polysaccharide from *Dendrobium officinale* by box-Behnken design and response surface methodology. *J Chin Med Mater.* (2014) 37:130–3. doi: 10.13863/j.issn1001-4454.2014.01.001

22. Netramai S, Kijchavengkul T, Samsudin H, Lertsiri S. Data of microwave assisted extraction and conventional hot water extraction of Dendrobium Sonia 'Earsakul' orchid flower. *Data Brief.* (2020) 31:105906. doi: 10.1016/j.dib.2020.105906

23. Razgonova MP, Zakharenko AM, Kalenik TK, Nosyrev AE, Stratidakis AK, Mezhuev YO, et al. Supercritical fluid technology and supercritical fluid chromatography for application in ginseng extracts. *Farmacia.* (2019) 67:202–12. doi: 10.31925/farmacia.2019.2.2

24. He L, Yan X, Liang J, Li S, He H, Xiong Q, et al. Comparison of different extraction methods for polysaccharides from *Dendrobium officinale* stem. *Carbohydr Polym.* (2018) 198:101–8. doi: 10.1016/j.carbpol.2018.06.073

25. Ji X, Peng B, Ding H, Cui B, Nie H, Yan Y. Purification, structure and biological activity of Pumpkin polysaccharides: a review. *Food Rev Int.* (2021). doi: 10.1080/87559129.2021.1904973

26. Fan Y, Lin M, Luo A. Extraction, characterization and antioxidant activities of an acidic polysaccharide from *Dendrobium devonianum*. *J Food Meas Charact.* (2022) 16:867–79. doi: 10.1007/s11694-021-01211-2

27. Pan LH, Wang J, Ye XQ, Zha XQ, Luo JP. Enzyme-assisted extraction of polysaccharides from *Dendrobium chrysotoxum* and its functional properties and immunomodulatory activity. *LWT Food Sci Technol.* (2015) 60:1149–54. doi: 10.1016/j.lwt.2014.10.004

28. Chen G, Yuan Q, Saeeduddin M, Ou S, Zeng X, Ye H. Recent advances in tea polysaccharides: extraction, purification, physicochemical characterization and bioactivities. *Carbohydr Polym.* (2016) 153:663–78. doi: 10.1016/j.carbpol.2016.08.022

29. Wang Y, Zhang H. Advances in the extraction, purification, structural-property relationships and bioactive molecular mechanism of *Flammulina velutipes* polysaccharides: a review. *Int J Biol Macromol.* (2021) 167:528–38. doi: 10.1016/j.ijbiomac.2020.11.208

30. Yin Z, Zhang W, Zhang J, Kang W. Isolation, purification, structural analysis and coagulatory activity of water-soluble polysaccharides from *Ligustrum lucidum* Ait flowers. *Chem Cent J.* (2017) 11:98. doi: 10.1186/s13065-017-0332-y

31. Qiu SM, Aweya JJ, Liu X, Liu Y, Tang S, Zhang W, et al. Bioactive polysaccharides from red seaweed as potent food supplements: a systematic review of their extraction, purification, and biological activities. *Carbohydr Polym.* (2022) 275:118696. doi: 10.1016/j.carbpol.2021.118696

32. Fang J, Wang Z, Wang P, Wang M. Extraction, structure and bioactivities of the polysaccharides from *Ginkgo biloba*: a review. *Int J Biol Macromol.* (2020) 162:1897–905. doi: 10.1016/j.ijbiomac.2020.08.141

33. Hou C, Yin M, Lan P, Wang H, Nie H, Ji X. Recent progress in the research of *Angelica sinensis* (Oliv.) Diels polysaccharides: extraction, purification, structure and bioactivities. *Chem Biol Technol Agric.* (2021) 8:13. doi: 10.1186/s40538-021-00214-x

34. Wang D, Fan B, Wang Y, Zhang L, Wang F. Optimum extraction, characterization, and antioxidant activities of polysaccharides from Flowers of *Dendrobium devonianum*. *Int J Anal Chem.* (2018) 2018:3013497. doi: 10.1155/2018/3013497

35. Xing S, Zhang X, Ke H, Lin J, Huang Y, Wei G. Physicochemical properties of polysaccharides from *Dendrobium officinale* by fractional precipitation and their preliminary antioxidant and anti-HepG2 cells activities in vitro. *Chem Cent J.* (2018) 12:100. doi: 10.1186/s13065-018-0468-4

36. Ji X, Yin M, Nie H, Liu Y. A review of isolation, chemical properties, and bioactivities of polysaccharides from *Bletilla striata*. *Biomed Res Int.* (2020) 2020:5391379. doi: 10.1155/2020/5391379

37. Ji X, Hou C, Shi M, Yan Y, Liu Y. An insight into the research concerning Panax ginseng C. A. Meyer polysaccharides: a review. *Food Rev Int.* (2020) 38:1149–65. doi: 10.1080/87559129.2020.1771363

38. Song TH, Chen XX, Tang SCW, Ho JCM, Lao LX, Ng TB, et al. *Dendrobium officinale* polysaccharides ameliorated pulmonary function while inhibiting mucin-5AC and stimulating aquaporin-5 expression. *J Funct Foods.* (2016) 21:359–71. doi: 10.1016/j.jff.2015.12.015

39. Xie SZ, Liu B, Zhang DD, Zha XQ, Pan LH, Luo JP. Intestinal immunomodulating activity and structural characterization of a new polysaccharide from stems of *Dendrobium officinale*. *Food Funct.* (2016) 7:2789–99. doi: 10.1039/c6fo00172f

40. Wang LX, Li CY, Hu C, Gong PS, Zhao SH. Purification and structural characterization of *Dendrobium officinale* polysaccharides and its activities. *Chem Biodivers.* (2021) 18:e2001023. doi: 10.1002/cbdv.202001023

41. Luo QL, Tang ZH, Zhang XF, Zhong YH, Yao SZ, Wang LS, et al. Chemical properties and antioxidant activity of a water-soluble polysaccharide from *Dendrobium officinale*. *Int J Biol Macromol.* (2016) 89:219–27. doi: 10.1016/j.ijbiomac.2016.04.067

42. Zha XQ, Luo JP, Luo SZ, Jiang ST. Structure identification of a new immunostimulating polysaccharide from the stems of *Dendrobium huoshanense*. *Carbohyd Polym.* (2007) 69:86–93. doi: 10.1016/j.carbpol.2006.09.005

43. Sun YD, Wang ZH, Ye QS. Composition analysis and anti-proliferation activity of polysaccharides from *Dendrobium chrysotoxum*. *Int J Biol Macromol.* (2013) 62:291–5. doi: 10.1016/j.ijbiomac.2013.08.046

44. Ji X, Peng Q, Yuan Y, Shen J, Xie X, Wang M. Isolation, structures and bioactivities of the polysaccharides from jujube fruit (*Ziziphus jujuba* Mill.): a review. *Food Chem.* (2017) 227:349–57. doi: 10.1016/j.foodchem.2017.01.074

45. Ji X, Hou C, Guo X. Physicochemical properties, structures, bioactivities and future prospective for polysaccharides from *Plantago* L. (Plantaginaceae): a review. *Int J Biol Macromol.* (2019) 135:637–46. doi: 10.1016/j.ijbiomac.2019.05.211

46. Guo Q, Liang S, Xiao Z, Ge C. Research progress on extraction technology and biological activity of polysaccharides from edible fungi: a review. *Food Rev Int.* (2022). doi: 10.1080/87559129.2022.2039182

47. Wei W, Feng L, Bao WR, Ma DL, Leung CH, Nie SP, et al. Structure characterization and immunomodulating effects of polysaccharides isolated from *Dendrobium officinale*. *J Agric Food Chem.* (2016) 64:881–9. doi: 10.1021/acs.jafc.5b05180

48. Zeng YJ, Yang HR, Ou XY, Su HH, Zong MH, Yang JG, et al. Fungal polysaccharide similar with host *Dendrobium officinale* polysaccharide: preparation, structure characteristics and biological activities. *Int J Biol Macromol.* (2019) 141:460–70. doi: 10.1016/j.ijbiomac.2019.08.238

49. Wei Y, Wang L, Wang D, Wang D, Wen C, Han B, et al. Characterization and anti-tumor activity of a polysaccharide isolated from *Dendrobium officinale* grown in the Huoshan County. *Chin Med.* (2018) 13:47. doi: 10.1186/s13020-018-0205-x

50. Kuang MT, Li JY, Yang XB, Yang L, Xu JY, Yan S, et al. Structural characterization and hypoglycemic effect via stimulating glucagon-like peptide-1 secretion of two polysaccharides from *Dendrobium officinale*. *Carbohyd Polym.* (2020) 241:116326. doi: 10.1016/j.carbpol.2020.116326

51. Zhong C, Tian W, Chen H, Yang Y, Xu Y, Chen Y, et al. Structural characterization and immunoregulatory activity of polysaccharides from *Dendrobium officinale* leaves. *J Food Biochem.* (2022) 46:e14023. doi: 10.1111/jfbc.14023

52. He TB, Huang YP, Yang L, Liu TT, Gong WY, Wang XJ, et al. Structural characterization and immunomodulating activity of polysaccharide from *Dendrobium officinale*. *Int J Biol Macromol.* (2016) 83:34–41. doi: 10.1016/j.ijbiomac.2015.11.038

53. Liu J, Yu L, Wang C, Zhang Y, Xi H, Si J, et al. Preparation, structural features and in vitro immunostimulatory activity of a glucomannan from fresh *Dendrobium catenatum* stems. *Front Nutr.* (2021) 8:823803. doi: 10.3389/fnut.2021.823803

54. Yang K, Lu T, Zhan L, Zhou C, Zhang N, Lei S, et al. Physicochemical characterization of polysaccharide from the leaf of *Dendrobium officinale* and effect on LPS induced damage in GES-1 cell. *Int J Biol Macromol.* (2020) 149:320–30. doi: 10.1016/j.ijbiomac.2020.01.026

55. Yue H, Liu Y, Qu H, Ding K. Structure analysis of a novel heteroxylan from the stem of *Dendrobium officinale* and anti-angiogenesis activities of its sulfated derivative. *Int J Biol Macromol.* (2017) 103:533–42. doi: 10.1016/j.ijbiomac.2017.05.097

56. Wang X, Zhou X, Wang K, Cao X. Structural characterisation and bioactivity of polysaccharides isolated from fermented *Dendrobium officinale*. *J Sci Food Agric.* (2022) 102:280–90. doi: 10.1002/jsfa.11356

57. Ji X, Guo J, Ding D, Gao J, Hao L, Guo X, et al. Structural characterization and antioxidant activity of a novel high-molecular-weight polysaccharide from *Ziziphus*

Jujuba cv. Muzao. *J Food Meas Charact.* (2022) 16:2191–200. doi: 10.1007/s11694-022-01288-3

58. Tian W, Dai L, Lu S, Luo Z, Qiu Z, Li J, et al. Effect of Bacillus sp. DU-106 fermentation on *Dendrobium officinale* polysaccharide: structure and immunoregulatory activities. *Int J Biol Macromol.* (2019) 135:1034–42. doi: 10.1016/j.ijbiomac.2019.05.203

59. Tao S, Lei Z, Huang K, Li Y, Ren Z, Zhang X, et al. Structural characterization and immunomodulatory activity of two novel polysaccharides derived from the stem of *Dendrobium officinale* Kimura et Migo. *J Funct Foods.* (2019) 57:121–34. doi: 10.1016/j.jff.2019.04.013

60. Huang YP, He TB, Cuan XD, Wang XJ, Hu JM, Sheng J. 1,4-beta-d-Glucomannan from *Dendrobium officinale* activates NF-small ka, CyrillicB via TLR4 to regulate the immune response. *Molecules.* (2018) 23:2658. doi: 10.3390/molecules23102658

61. Ke Y, Zhan L, Lu T, Zhou C, Chen X, Dong Y, et al. Polysaccharides of *Dendrobium officinale* Kimura & Migo leaves protect against ethanol-induced gastric mucosal injury via the AMPK/mTOR signaling pathway in vitro and vivo. *Front Pharmacol.* (2020) 11:526349. doi: 10.3389/fphar.2020.526349

62. Lin G, Luo D, Liu J, Wu X, Chen J, Huang Q, et al. Hepatoprotective effect of polysaccharides isolated from *Dendrobium officinale* against acetaminophen-induced liver injury in mice via regulation of the Nrf2-Keap1 signaling pathway. *Oxid Med Cell Longev.* (2018) 2018:6962439. doi: 10.1155/2018/6962439

63. Zhang L, Peng H, Xu J, Xu Y, Yin Y, He B, et al. Effects of *Dendrobium officinale* polysaccharides on brain inflammation of epileptic rats. *Int J Polym Sci.* (2019) 2019:1–6. doi: 10.1155/2019/9058161

64. Xia L, Liu X, Guo H, Zhang H, Zhu J, Ren F. Partial characterization and immunomodulatory activity of polysaccharides from the stem of *Dendrobium officinale* (Tiepishihu) in vitro. *J Funct Foods.* (2012) 4:294–301. doi: 10.1016/j.jff.2011.12.006

65. Zhang L, Wang F, Ren X. Inhibitory effect of *Dendrobium officinale* polysaccharide on human gastric cancer cell xenografts in nude mice. *Food Sci Techol.* (2017) 38:78–83. doi: 10.1590/1678-457x.00917

66. Yu W, Ren Z, Zhang X, Xing S, Tao S, Liu C, et al. Structural characterization of polysaccharides from *Dendrobium officinale* and their effects on apoptosis of hela cell line. *Molecules.* (2018) 23:2484. doi: 10.3390/molecules23102484

67. Zhang X, Duan S, Tao S, Huang J, Liu C, Xing S, et al. Polysaccharides from *Dendrobium officinale* inhibit proliferation of osteosarcoma cells and enhance cisplatin-induced apoptosis. *J Funct Foods.* (2020) 73:104143. doi: 10.1016/j.jff.2020.104143

68. Wang YH. Traditional uses, chemical constituents, pharmacological activities, and toxicological effects of Dendrobium leaves: a review. *J Ethnopharmacol.* (2021) 270:113851. doi: 10.1016/j.jep.2021.113851

69. Chen H, Nie Q, Hu J, Huang X, Huang W, Nie S. Metabolism amelioration of *Dendrobium officinale* polysaccharide on type II diabetic rats. *Food Hydrocoll.* (2020) 102:105582. doi: 10.1016/j.foodhyd.2019.105582

70. Liu Y, Yang L, Zhang Y, Liu X, Wu Z, Gilbert RG, et al. *Dendrobium officinale* polysaccharide ameliorates diabetic hepatic glucose metabolism via glucagon-mediated signaling pathways and modifying liver-glycogen structure. *J Ethnopharmacol.* (2020) 248:112308. doi: 10.1016/j.jep.2019.112308

71. Pan LH, Li XF, Wang MN, Zha XQ, Yang XF, Liu ZJ, et al. Comparison of hypoglycemic and antioxidative effects of polysaccharides from four different Dendrobium species. *Int J Biol Macromol.* (2014) 64:420–7. doi: 10.1016/j.ijbiomac.2013.12.024

72. Lin L, Yang S, Xiao Z, Hong P, Sun S, Zhou C, et al. The inhibition effect of the seaweed polyphenol, 7-phloro-eckol from Ecklonia cava on alcohol-induced oxidative stress in HepG2/CYP2E1 cells. *Mar Drugs.* (2021) 19:158. doi: 10.3390/md19030158

73. Yang K, Zhan L, Lu T, Zhou C, Chen X, Dong Y, et al. *Dendrobium officinale* polysaccharides protected against ethanol-induced acute liver injury in vivo and in vitro via the TLR4/NF-kappaB signaling pathway. *Cytokine.* (2020) 130:155058. doi: 10.1016/j.cyto.2020.155058

74. Wang K, Yang X, Wu Z, Wang H, Li Q, Mei H, et al. *Dendrobium officinale* polysaccharide protected CCl4-induced liver fibrosis through intestinal homeostasis and the LPS-TLR4-NF-kappaB signaling pathway. *Front Pharmacol.* (2020) 11:240. doi: 10.3389/fphar.2020.00240

75. Huang X, Nie S, Cai H, Zhang G, Cui SW, Xie M, et al. Study on *Dendrobium officinale* O-acetyl-glucomannan (Dendronan§): part VI. Protective effects against oxidative stress in immunosuppressed mice. *Food Res Int.* (2015) 72:168–73. doi: 10.1016/j.foodres.2015.01.035

76. Fan H, Meng Q, Xiao T, Zhang L. Partial characterization and antioxidant activities of polysaccharides sequentially extracted from *Dendrobium officinale*. *J Food Meas Charact.* (2018) 12:1054–64. doi: 10.1007/s11694-018-9721-8

77. Ng TB, Liu J, Wong JH, Ye X, Wing Sze SC, Tong Y, et al. Review of research on Dendrobium, a prized folk medicine. *Appl Microbiol Biotechnol.* (2012) 93:1795–803. doi: 10.1007/s00253-011-3829-7

78. Wang Q, Liang J, Liu H. In vitro effects of four polysaccharides containing β-D-Glup on intestinal function. *Int J Food Prop.* (2019) 22:1064–76. doi: 10.1080/10942912.2019.1628778

79. Ma S, Wu Q, Zhao Z, Xiong J, Niu J, Liu C, et al. Mechanisms of *Dendrobium officinale* polysaccharides in repairing gastric mucosal injuries based on mitogen-activated protein kinases (MAPK) signaling pathway. *Bioengineered.* (2022) 13:71–82. doi: 10.1080/21655979.2021.2006951

80. Li M, Yue H, Wang Y, Guo C, Du Z, Jin C, et al. Intestinal microbes derived butyrate is related to the immunomodulatory activities of *Dendrobium officinale* polysaccharide. *Int J Biol Macromol.* (2020) 149:717–23. doi: 10.1016/j.ijbiomac.2020.01.305

81. Fu Y, Zhang J, Chen K, Xiao C, Fan L, Zhang B, et al. An in vitro fermentation study on the effects of *Dendrobium officinale* polysaccharides on human intestinal microbiota from fecal microbiota transplantation donors. *J Funct Foods.* (2019) 53:44–53. doi: 10.1016/j.jff.2018.12.005

82. Feng CZ, Cao L, Luo D, Ju LS, Yang JJ, Xu XY, et al. Dendrobium polysaccharides attenuate cognitive impairment in senescence-accelerated mouse prone 8 mice via modulation of microglial activation. *Brain Res.* (2019) 1704:1–10. doi: 10.1016/j.brainres.2018.09.030

83. Zhang Y, You S, Wang D, Zhao D, Zhang J, An Q, et al. Fermented *Dendrobium officinale* polysaccharides protect UVA−induced photoaging of human skin fibroblasts. *Food Sci Nutr.* (2022) 10:1275–88. doi: 10.1002/fsn3.2763

84. Liang J, Zeng Y, Wang H, Lou W. Extraction, purification and antioxidant activity of novel polysaccharides from *Dendrobium officinale* by deep eutectic solvents. *Nat Prod Res.* (2019) 33:3248–53. doi: 10.1080/14786419.2018.1471480

frontiers | Frontiers in Nutrition

TYPE Original Research
PUBLISHED 19 July 2022
DOI 10.3389/fnut.2022.941524

Check for updates

OPEN ACCESS

EDITED BY
Xin Wang,
Northwest A&F University, China

REVIEWED BY
Deqiang Zhu,
Qilu University of Technology, China
Hongzhen Luo,
Huaiyin Institute of Technology, China
QiaoPeng Tian,
Jiangnan University, China

*CORRESPONDENCE
Qi Sun
sunqi2017@cqnu.edu.cn
Zichao Wang
zcwang@haut.edu.cn

SPECIALTY SECTION
This article was submitted to Food Chemistry, a section of the journal Frontiers in Nutrition

RECEIVED 11 May 2022
ACCEPTED 24 June 2022
PUBLISHED 19 July 2022

CITATION
Li S, Wang Y, Dun W, Han W, Xu C, Sun Q and Wang Z (2022) Effect of ultrasonic degradation on the physicochemical property and bioactivity of polysaccharide produced by *Chaetomium globosum* CGMCC 6882.
Front. Nutr. 9:941524.
doi: 10.3389/fnut.2022.941524

COPYRIGHT
© 2022 Li, Wang, Dun, Han, Xu, Sun and Wang. This is an open-access article distributed under the terms of the Creative Commons Attribution License (CC BY). The use, distribution or reproduction in other forums is permitted, provided the original author(s) and the copyright owner(s) are credited and that the original publication in this journal is cited, in accordance with accepted academic practice. No use, distribution or reproduction is permitted which does not comply with these terms.

Effect of ultrasonic degradation on the physicochemical property and bioactivity of polysaccharide produced by *Chaetomium globosum* CGMCC 6882

Shiwei Li[1,2], Yingna Wang[1], Weipeng Dun[1], Wanqing Han[1], Chunping Xu[3], Qi Sun[4]* and Zichao Wang[5]*

[1]College of Life Sciences and Agronomy, Zhoukou Normal University, Zhoukou, China, [2]College of Food Science and Technology, Henan University of Technology, Zhengzhou, China, [3]College of Food and Bioengineering, Zhengzhou University of Light Industry, Zhengzhou, China, [4]College of Life Sciences, Chongqing Normal University, Chongqing, China, [5]School of Biological Engineering, Henan University of Technology, Zhengzhou, China

Similar to the enzymatic process, there might also be an active fragment in polysaccharides, how to obtain is important for investigating the bioactivity and pharmacological mechanism of polysaccharides. Presently, a *Gynostemma pentaphyllum* endophytic fungus *Chaetomium globosum* CGMCC 6882 polysaccharide [Genistein Combined Polysaccharide (GCP)] was degraded by ultrasonic treatment, two polysaccharide fragments of GCP-F1 and GCP-F2 were obtained. Physicochemical results showed that GCP-F1 and GCP-F2 had the same monosaccharide composition of arabinose, galactose, glucose, xylose, mannose, and glucuronic acid as compared to GCP with slightly different molar ratios. However, weight-average molecular weights of GCP-F1 and GCP-F2 decreased from 8.093 **x** 10^4 Da (GCP) to 3.158 × 10^4 Da and 1.027 × 10^4 Da, respectively. *In vitro* scavenging assays illustrated that GCP-F1 and GCP-F2 had higher antioxidant activity against 2,2′-azinobis-(3-ethylbenzothiazoline-6-sulfonic acid (ABTS) radical, 2,2-diphenyl-1-picrylhydrazyl (DPPH) radical, superoxide anions, and hydroxyl radical than GCP, the order was GCP < GCP-F1 < GCP-F2. Meanwhile, antibacterial tests showed that ultrasonic degradation increased the antibacterial activity of GCP-F1 as compared to GCP, but GCP-F2 almost lost its antibacterial activity with further ultrasound treatment. Changes in the antioxidant and antibacterial activities of GCP-F1 and GCP-F2 might be related to the variation of their molecular weights.

KEYWORDS

***Chaetomium globosum* CGMCC 6882, polysaccharide, ultrasonic degradation, molecular weight, biological activity**

Introduction

As a macromolecule consisting of more than ten monosaccharides through α-glycosidic or β-glycosidic bonds, polysaccharide is one of the essential substances for organism and has many bioactivities, such as antioxidant, antibacteria, anti-inflammatory, antidiabetic, antitumor, regulating intestinal micro-ecology, improving immunity, and promoting growth (1, 2). Even in fighting against COVID-19, polysaccharide also shows an excellent potential application (3). Meanwhile, polysaccharide also has good applications in food, breeding, planting, industrial, and agricultural fields. For instance, *Mesona chinensis* Benth polysaccharide could improve the pasting viscosity, viscoelasticity, gelling properties, and water-retention capacity of rice starch and shows a good prospect of application in food modification (4). Chitosan oligosaccharides could destroy cellular permeability and alter cellular metabolism of food spoilage fungi *Aspergillus Flavus* and *Aspergillus Fumigatus* and potentially be used as antiseptics in food (5). Xantho-oligosaccharide could inhibit phytopathogenic *Xanthomonas campestris* pv. *campestris* and be used as a biopesticide in the planting industry (6). *Ganoderma lucidum* polysaccharide could promote pig health and improve pork quality and be used as a potential feed additive in the breeding industry (7).

The structural feature of polysaccharide is the basis of its biological activity, and the structural difference will endow polysaccharide with different bioactivities. For example, the fucose ratio in the monosaccharide composition of *Pleurotus geesteranus* polysaccharide affected its antioxidant and hepatoprotective effects (8). Triple-helix lentinan exhibited the highest antitumor activity against *Sarcoma* 180 solid tumor *in vivo* (9). Spherical molecular shape was important for apoptosis-inducing activity of *Lycium barbarum* polysaccharide against human hepatoma cells (10). The sulfated group and β-glycosidic bond affected the antitumor activity of exo-polysaccharides from *Lactobacillus plantarum* 70810 (11). Meanwhile, molecular weight influenced the hypoglycemic effects of konjac glucomannan on type 2 diabetic rats (12). Homoplastically, almost all structural characteristics of polysaccharides affect their biological activities, in addition to the detection and analysis methods of polysaccharides lagging behind protein and DNA, it is difficult to uncover the relationship between structural features and biological activities of polysaccharides presently. Based on this, we select the easily controlled structural feature of molecular weight and study its effect on polysaccharide bioactivity (13), thus providing guidance for the analysis of the structure-activity relationship of polysaccharides.

Chaetomium globosum CGMCC 6882 was an endophytic fungus extracted from *Gynostemma pentaphyllum*, which could use some carbon sources to produce different bioactive polysaccharides (14, 15), but how structure affects the biological activity of polysaccharides produced by *C. globosum* CGMCC 6882 was not clear. Meanwhile, Zhang et al. (16) found that molecular weight influenced the activity of polysaccharides produced by *C. globosum* CGMCC 6882. Therefore, an antibacterial polysaccharide of Genistein Combined Polysaccharide (GCP) produced by *C. globosum* CGMCC 6882 was degraded by ultrasonic treatment in the present work for seeking the potential active fragment. On the one hand, physicochemical properties of GCP before and after ultrasonic degradation were compared. On the other hand, activities of pristine and ultrasound-degraded GCP fragments were assessed.

Materials and methods

Materials and chemicals

Production, extraction, and purification of polysaccharide GCP produced by *C. globosum* CGMCC 6882 were conducted according to the methods previously reported (1). Standard monosaccharides of fucose, rhamnose, arabinose, glucosamine, galactose, glucose, xylose, mannose, fructose, galacturonic acid, and glucuronic acid were bought from Sigma-Aldrich (Sigma Chemicals, St. Louis, United States). Dextran standards were purchased from Shanghai Aladdin Biochemical Technology Co., Ltd. (Shanghai, China). Trifluoroacetic acid (TFA), potassium bromide (KBr), 2,2-diphenyl-1-picrylhydrazyl (DPPH), ascorbic acid (Vc), and other chemicals were purchased from Sinopharm Chemical Reagent Co. (Beijing, China).

Ultrasonic degradation of Genistein Combined Polysaccharide

Ultrasound degradation of GCP was carried out on a JY98-IIIDN Ultrasonic Processor (Xinzhi Bio-Sciences Co., Ltd., Ningbo, China). GCP was dissolved in distilled water and stirred overnight at room temperature to a solution of 1 mg/ml, then subjected to ultrasound treatment at a frequency of 20 kHz and 1,000 W power level in a certain pulse mode (5 s on and 5 s off) with different time. During the degradation process, a 6 mm diameter tip probe was immersed into the solution at 3 cm depth. Although Hu et al. (17) verified that the thermal effects during ultrasonic irradiation would not affect polysaccharide change if the internal temperature of ultrasonication was not over 100°C, the beaker of the polysaccharide solution was inserted into an ice-cold bath for

avoiding the high temperature. When the ultrasonic time was sustained for 30 min, one group of the resulting solution was taken out and the other one was extended for 120 min degradation. After which, two ultrasonic degradation solutions were dialyzed against distilled water for 48 h (changed the water every 4 h and molecular weight cutoff was 8,000 Da). After that, GCP solutions were filtered through a 0.22 μm filter, applied to a Sepharose CL-6B column (2.5 cm × 60 cm) for further purification, and eluted with 0.1 mol/L NaCl solution at a flow rate of 0.6 ml/min. Then, the purified GCP fractions were respectively dialyzed against distilled water with a 3,500 Da dialysis bag for desalination. In the end, the dialyzed fractions were collected and freeze dried, the obtained polysaccharide fragments were named GCP-F1 (30 min) and GCP-F2 (120 min), respectively.

Physicochemical properties analysis

Determination of monosaccharide composition

Genistein Combined Polysaccharide, GCP-F1, and GCP-F2 were dissolved in 2 mol/L TFA and hydrolyzed at 120°C for 2 h, respectively. The hydrolysate was washed three times with methanol and evaporated. Finally, the hydrolyzed material was transferred to a 25 ml volumetric flask, diluted to 25 ml with deionized water, and analyzed using high-performance anion exchange chromatography (HPAEC) according to the methods reported previously (1).

Determination of molecular weight

Genistein Combined Polysaccharide, GCP-F1, and GCP-F2 were dissolved to a concentration of 2 mg/ml, respectively. After which, their molecular weights were detected by high-performance size exclusion chromatography (HPSEC) according to the methods reported previously (1).

Fourier transform infrared spectroscopic analysis

Fourier transform infrared spectra of GCP, GCP-F1, and GCP-F2 were obtained using a Nexus 470 FT-IR Spectrometer (Nicolet, United States). The FT-IR spectra of GCP, GCP-F1, and GCP-F2 were recorded using a KBr pallet containing 0.1% GCP (GCP-F1 or GCP-F2), the wave number was set from 4,000 to 400 cm^{-1}.

Nuclear magnetic resonance analysis

Genistein Combined Polysaccharide, GCP-F1, and GCP-F2 were dissolved in D_2O in 5 mm NMR tubes, respectively, a Bruker Avance 500 MHz Spectrometer (Bruker Inc., Germany) was used to record the ^1H NMR and ^{13}C NMR spectra of GCP, GCP-F1, and GCP-F2 at 30°C. Chemical shifts for ^1H NMR and ^{13}C NMR spectra were recorded in parts per million.

Antioxidant activity assay

2,2′-azinobis-(3-ethylbenzothiazoline-6-sulfonic acid (ABTS) radical scavenging activity

2,2′-azinobis-(3-ethylbenzothiazoline-6-sulfonic acid radical scavenging activities of GCP, GCP-F1, and GCP-F2 were detected according to the method reported previously (18). An equal volume of 7 mmol/L ABTS and 1.4 mmol/L potassium persulfate was mixed and stored in dark for 16 h at room temperature to prepare ABTS radical. Before use, ABTS radical solution was diluted with distilled water to an absorbance of 0.70 ± 0.02 at 734 nm. Then, 0.1 ml of polysaccharide solution with various concentrations (0.5, 1.0, 1.5, 2.0, 2.5, and 3.0 mg/ml) was added into 0.9 ml ABTS radical solution and mixed vigorously. After the mixture was reacted at room temperature for 5 min, the absorbance of the mixture was measured at 734 nm. ABTS radical scavenging activity was (%) = $[1 - (A_i - A_j)/A_0] \times 100\%$. Where A_0 is the absorbance of control group without polysaccharide solution, A_i is the absorbance of polysaccharide solution, and A_j is the absorbance of background without ABTS radical. Meanwhile, Vc was used as a positive control in the following antioxidant tests.

2,2-diphenyl-1-picrylhydrazyl radical scavenging activity

2,2-diphenyl-1-picrylhydrazyl radical scavenging activities of GCP, GCP-F1, and GCP-F2 were determined according to the method reported previously (14). DPPH was dissolved in alcohol to a concentration of 0.1 mmol/L, then 2 ml of polysaccharide solution with various concentrations (0.5, 1.0, 1.5, 2.0, 2.5, and 3.0 mg/ml) was added to 2 ml of alcoholic DPPH. The system was fully mixed and kept in dark for 30 min at room temperature. Finally, the absorbance of the mixture was measured at 517 nm with a microplate reader (Thermo, United States). DPPH radical scavenging activity was (%) = $(A_0 - A_i + A_j)/A_0 \times 100\%$. Where A_0 is the absorbance of the control group without polysaccharide solution, A_i is the absorbance of polysaccharide solution, and A_j is the absorbance of background without DPPH radical.

Superoxide anions scavenging activity

Superoxide anions' scavenging activities of GCP, GCP-F1, and GCP-F2 were detected by pyrogallic acid method (2). Tris-HCl buffer of 2.5 ml (0.05 mol/L, pH = 8.2) was added into 0.4 ml of polysaccharide solutions with various concentrations (0.5, 1.0, 1.5, 2.0, 2.5, and 3.0 mg/ml). The mixture solution was reacted at 25°C for 10 min, then, 0.1 ml of pyrogallic acid was added and reacted for 20 min. The reaction was quenched by adding 0.5 ml of HCl and the absorbance of the mixture was measured at 380 nm. Superoxide anions scavenging activity was (%) = $(1 - A/A_0) \times 100\%$. Where A is the absorbance of

polysaccharide solution and A_0 is the absorbance of the control group without polysaccharide solution.

Hydroxyl radical scavenging activity

Hydroxyl radical scavenging activities of GCP, GCP-F1, and GCP-F2 were detected according to the method reported by Hu et al. (19). In total, 2 ml of 6 mmol/L $FeSO_4$ and 2 ml of 6 mmol/L H_2O_2 were added to 2 ml of polysaccharide solutions at various concentrations (0.5, 1.0, 1.5, 2.0, 2.5, and 3.0 mg/ml), the system was fully mixed and reacted at room temperature for 10 min. Then, 2 ml of 6 mmol/L ortho-hydroxybenzoic acid was added and reacted for another 30 min. The absorbance of the mixture was measured at 510 nm. Hydroxyl radical scavenging activity was (%) = $(A_0 - A_i + A_j)/A_0 \times 100\%$. Where A_0 is the absorbance of polysaccharide solution replaced by distilled water, A_i is the absorbance of polysaccharide solution, and A_j is the absorbance of H_2O_2 replaced by distilled water.

Antibacterial activity assay

Antibacterial activities of GCP, GCP-F1, and GCP-F2 against *Escherichia coli* and *Staphylococcus aureus* were assayed by the agar diffusion method (1). Polysaccharides were dissolved in distilled water to various concentrations (0.4, 0.8, 1.2, 1.6, and 2.0 mg/ml) and filtrated by 0.22 μm millipore filter. In total, 15 ml of nutrient agar was added to each glass plate and solidified, then 100 μl of 10^6 CFU/ml of test organisms suspension was spread on the agar plate surface and a filter paper disk (diameter: 6 mm, thickness: 1 mm) containing 30 μl of polysaccharide solution was placed in the center of the plate. These glass plates were incubated at 37°C for 24 h. The antibacterial activities of GCP, GCP-F1, and GCP-F2 were evaluated by determining the diameters of inhibition zones with a vernier caliper.

Statistical analysis

Data were expressed as means ± SD after triplicate repeats. Data were subjected to one-way ANOVA, and significant differences were analyzed using SPSS version 19.0 (IBM, United States).

Results and discussion

Ultrasonic degradation

As shown in **Figure 1**, after GCP is degraded by ultrasonic treatment at 20 kHz and 1,000 W power levels at different times, two elution curves (GCP-F1 and GCP-F2) are found on the separation and purification results of Sepharose CL-6B column, indicating that two polysaccharide fragments are obtained *via* ultrasonic treatment. Except for the regulations of metabolic pathway and fermentation conditions (13, 15), with enzymatic degradation, chemical degradation, physical degradation, and other degradation methods (20, 21), many researchers obtained similar de-polymerized polysaccharides to present work. Meanwhile, Yan et al. (22) demonstrated that polysaccharide fragments with different degrees of polymerization could also be obtained by controlling the treatment process and extraction methods.

Effects of ultrasonic degradation on physicochemical properties

Monosaccharide composition

The composition of monosaccharides could affect the charge of polysaccharides, thus influencing their biological activities and physicochemical properties (23). **Table 1** shows that the obtained ultrasonic fragments of GCP-F1 and GCP-F2 contain the same kind of neutral monosaccharides (arabinose, galactose, glucose, xylose, and mannose) and acid monosaccharide (glucuronic acid) as compared to GCP in the similar molar ratios. Interestingly, Yan et al. (24) found that monosaccharide composition of polysaccharides extracted from *Phellinus linteus* mycelia was not affected by ultrasonic treatment, and the molar ratios were slightly

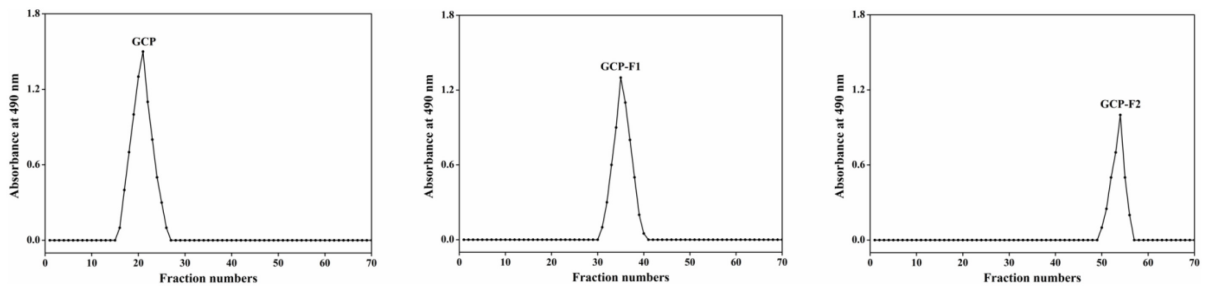

FIGURE 1
Elution curve of Genistein Combined Polysaccharide (GCP), GCP-F1, and GCP-F2 on Sepharose CL-6B column (2.5 cm × 60 cm).

TABLE 1 Monosaccharide compositions and molecular weights of Genistein Combined Polysaccharide (GCP), GCP-F1, and GCP-F2.

Items	GCP	GCP-F1	GCP-F2
Monosaccharide composition			
Arabinose (μmol/L)	0.64	0.66	0.67
Galactose (μmol/L)	2.58	2.62	2.53
Glucose (μmol/L)	23.53	21.88	22.07
Xylose (μmol/L)	0.90	0.85	1.01
Mannose (μmol/L)	2.47	2.53	2.58
Glucuronic acid (μmol/L)	0.27	0.21	0.23
Molecular weight			
Weight-average molecular weight (Mw)	8.093×10^4 Da	3.158×10^4 Da	1.027×10^4 Da
Number-average molecular weight (Mn)	7.982×10^4 Da	3.117×10^4 Da	1.016×10^4 Da
Polydispersity (Mw/Mn)	1.014	1.013	1.011

different. Wang et al. (25) demonstrated that monosaccharide composition and a molar ratio of yellow tea polysaccharide were almost not altered by ultrasonic degradation. Meanwhile, Yang et al. (26) also suggested that ultrasound treatment did not affect the monosaccharide composition and molar ratio of polysaccharides.

Molecular weight

In general, polysaccharides with high molecular weight can form a gel layer on the surface of bacteria and exert better antibacterial activity (27), but low molecular weight polysaccharides usually have higher biological activities (28). As shown in Table 1, the weight-average molecular weight (Mw) of GCP is 8.093×10^4 Da, Mw of GCP-F1 is decreased to 3.158×10^4 Da with 30 min ultrasound treatment, and Mw of GCP-F2 is reduced to 1.027×10^4 Da with 120 min ultrasonic time. Meanwhile, polydispersities of GCP, GCP-F1, and GCP-F2 were 1.014, 1.013, and 1.011, respectively. Many scholars found that the decrease in molecular weight could increase the physicochemical property and bioactivity of polysaccharides, such as rheological profiles, antitumor activity, antioxidant activity, moisture-preserving activity, and antibacterial activity (29, 30). However, Yang et al. (31) found that the anticancer activity of polysaccharides extracted from *Flammulina velutipes* was decreased with the reduction of their molecular weights. Meanwhile, Guo et al. (32) demonstrated that when the molecular weight of fucoidan was reduced too small by ultrasonic treatment, the antioxidant activity of which was also decreased.

Fourier transform infrared

As can be seen from Figure 2, the absorption peak between 3,400 and 3,200 cm^{-1} might attribute to O-H stretching vibration of hydrogen bonds (1), the absorption peak at around 2,940 cm^{-1} might assign to asymmetric stretching vibration of C-H in CH, CH_2, and CH_3 groups (33), absorbance peaks at around 1,600 and 1,400 cm^{-1} might due to symmetrical C = O stretching vibrations and asymmetrical C = O stretching vibrations (2), absorbance peak at around 1,100 cm^{-1} might correspond to vibration absorption of C-O-H and C-O-C (34), and absorption peaks between 900 and 600 cm^{-1} might belong to β-glycosidic bonds and α-glycosidic linkages, respectively. However, Figure 2 shows that the intensity of the characteristic peaks in GCP, GCP-F1, and GCP-F2 was different, suggesting that the number and type of functional groups in GCP, GCP-F1, and GCP-F2 might be different and which will be analyzed in our future work.

Nuclear magnetic resonance

As shown in Figure 3A of ^{1}H-NMR chemical shift data, peaks between 3.5 and 3.6 ppm might belong to the CH2 linked to -OH in glucose and galactose, peaks between 3.6 and 3.8 ppm might relate to CH2 in the -O-CH2-OH of arabinose and the CH associated with -OH in monosaccharide, peaks between 3.8

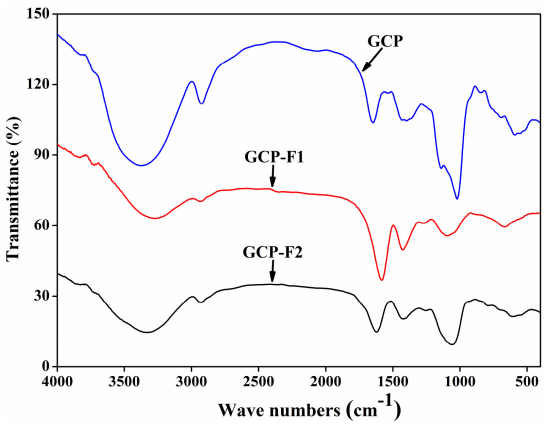

FIGURE 2
Fourier transform infrared (FT-IR) spectra of Genistein Combined Polysaccharide (GCP), GCP-F1, and GCP-F2.

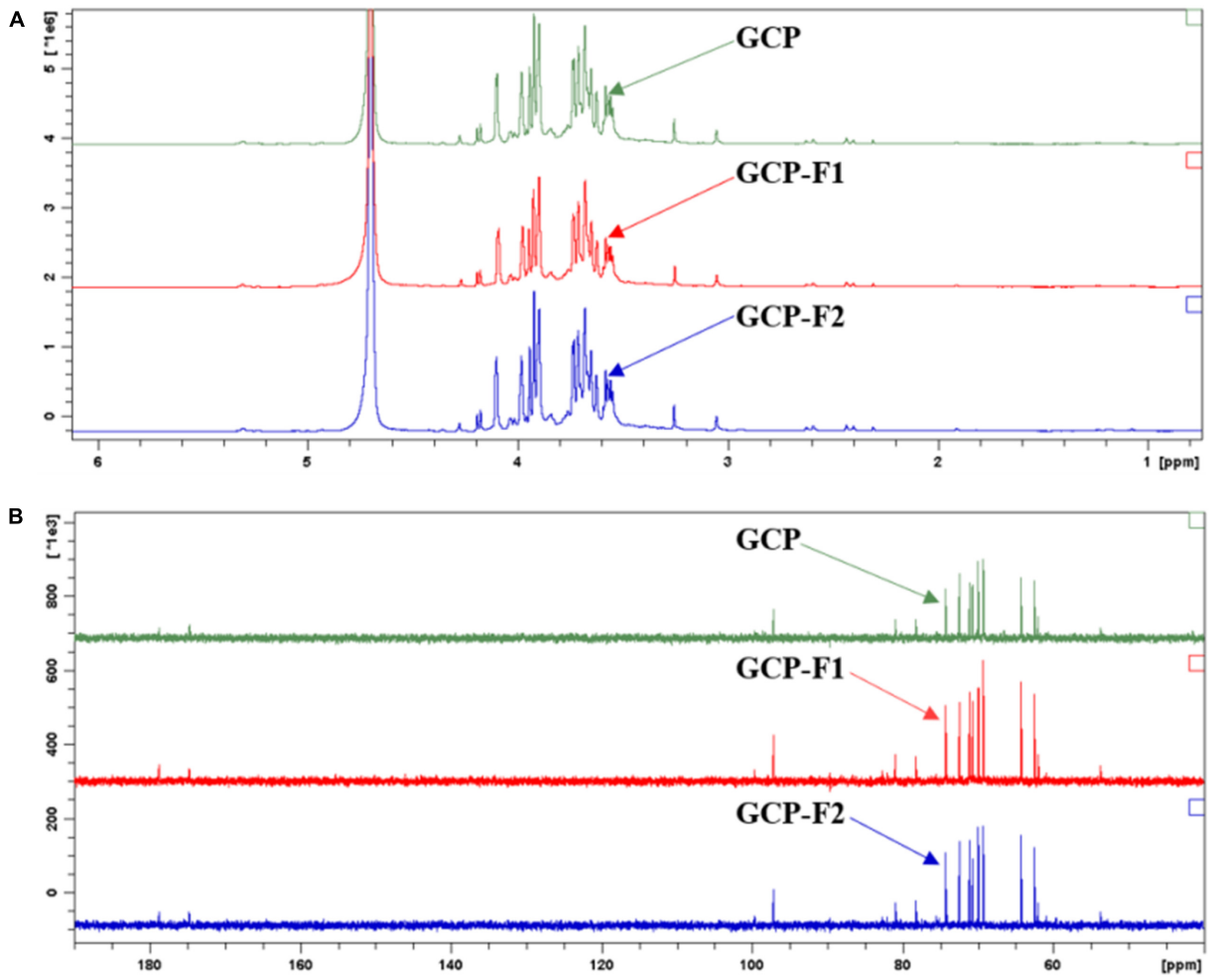

FIGURE 3
Nuclear magnetic resonance (NMR) spectroscopic analysis of Genistein Combined Polysaccharide (GCP), GCP-F1, and GCP-F2. **(A)** ^{1} H-NMR; **(B)** ^{13} C-NMR.

and 4.0 ppm might attribute to CH in the -O-CH-COOH of glucuronic acid and in the HO-CH-CHO of glucose, and peak at about 4.1 ppm might relate to CH in the -O-CH-OH of monosaccharide, which was due to the movement of - O-, -OH, and -CHO-COOH as an electron-withdrawing group to the lower field with the connected CH. Meanwhile, hydrogen ions in -OH and -COOH of monosaccharides will be deuterated or dissociative in solvent D_2O, thus no characteristic absorption peaks were shown on ^{1}H NMR spectra (14). As can be seen from **Figure 3B** of ^{13} C-NMR results, peaks between 60 and 65 ppm might relate to the CH2 in glucose, arabinose, xylose, and galactose, peaks between 69 and 74 ppm might be due to the CH in monosaccharide, peak at 78.2 ppm might attribute to CH in the -O-CH-CH2OH of galactose, peak at 80.9 ppm might relate to CH in the -O-CH-COOH of glucuronic acid, peak at 97.1 ppm might relate to CH in the -O-CH-OH of monosaccharide, and peaks at 174.7 and 178.7 ppm might relate to CHO in glucose and COOH in glucuronic acid, respectively (1). The NMR spectra results of GCP, GCP-F1, and GCP-F2 indicated that they might have similar chemical structures.

Effects of ultrasonic degradation on antioxidant activity

As shown in **Figure 4**, GCP-F1 and GCP-F2 have higher antioxidant activities on ABTS radical, DPPH radical, superoxide anions, and hydroxyl radical in a concentration-dependent manner than those of GCP, though are lower than those of Vc. The scavenging activity order was GCP < GCP-F1 < GCP-F2 < Vc. At the concentration of 3.0 mg/ml, the maximum scavenging rates on ABTS radical, DPPH radical, superoxide anions, and hydroxyl radical were 53.18 ± 1.42%, 62.85 ± 1.91%, 50.04 ± 1.61%, and 71.93 ± 1.53% for

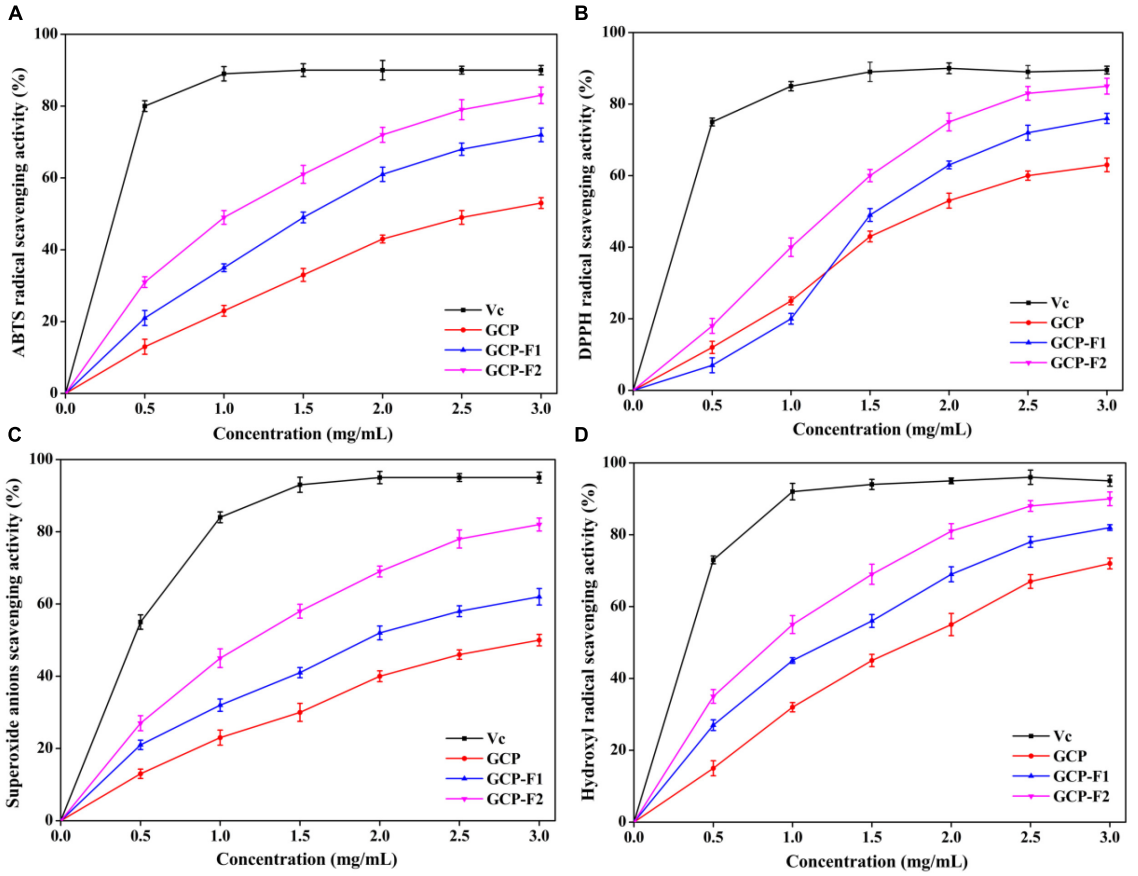

FIGURE 4
Scavenging effects of GCP, GCP-F1, and GCP-F2 on 2,2′-azinobis-(3-ethylbenzothiazoline-6-sulfonic acid (ABTS) radical **(A)**, 2,2-diphenyl-1-picrylhydrazyl (DPPH) radical **(B)**, superoxide anions **(C)**, and hydroxyl radical **(D)**.

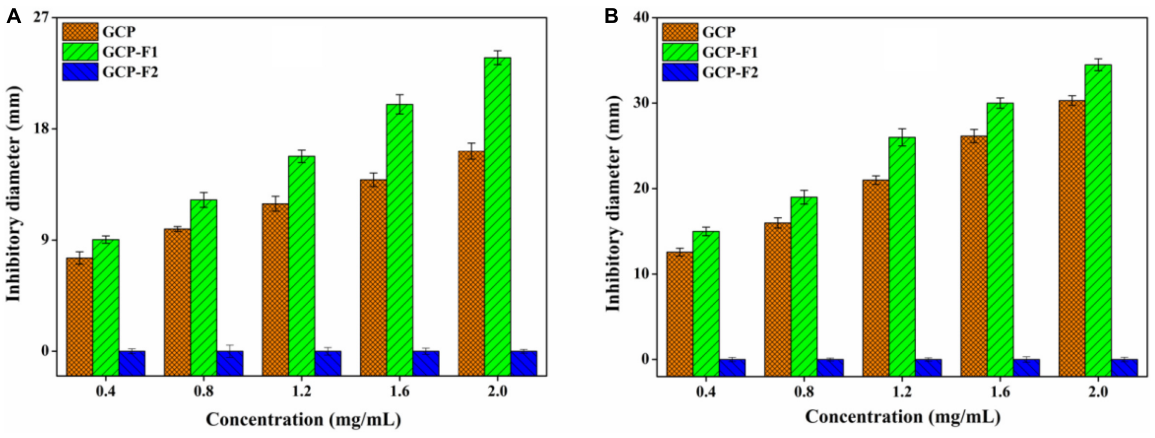

FIGURE 5
Antibacterial activities of Genistein Combined Polysaccharide (GCP), GCP-F1, and GCP-F2 against *E. coli* **(A)** and *S. aureus* **(B)**.

GCP, 72.31 ± 1.88%, 76.04 ± 1.37%, 61.97 ± 2.35%, and 81.07 ± 0.86% for GCP-F1, and 83.55 ± 2.31%, 85.08 ± 2.21%, 82.16 ± 1.84%, and 90.08 ± 1.94% for GCP-F2, respectively.

There might be many reasons for the increased scavenging activities of GCP-F1 and GCP-F2. On the one hand, ultrasonic degradation might not only increase hydroxyl groups and

create new functional groups in GCP-F1 and GCP-F2 but also form radicals during water sonolysis, which will endow GCP-F1 and GCP-F2 had better antioxidant activities (21, 35). On the other hand, the content and ratio of arabinose, galactose, glucose, mannose, and glucuronic acid might also influence the antioxidant activity of GCP-F1 and GCP-F2 (36–38). Last but not least, GCP-F1 and GCP-F2 might have less compacted structures with the reduction of molecular weight after ultrasound treatment, which donated more electrons to react with free radicals (39, 40). However, the detailed action mechanism will be further analyzed in our future work.

Effects of ultrasonic degradation on antibacterial activity

As can be seen from **Figure 5A**, GCP and GCP-F1 show a concentration-dependent manner against *E. coli*, and the inhibitory effect of GCP-F1 is higher than that of GCP. At the concentration of 2.0 mg/ml, inhibitory zones of GCP and GCP-F1 against *E. coli* were 16.23 ± 0.59 and 23.76 ± 0.51 mm, respectively, indicating that ultrasound treatment increased the antibacterial activity of GCP-F1. However, GCP-F2 almost lost its antibacterial activity against *E. coli* (**Figure 5A**). Meanwhile, **Figure 5B** shows a similar antibacterial trend of GCP, GCP-F1, and GCP-F2 against *S. aureus* to those of *E. coli*, inhibitory zones of GCP and GCP-F1 against *S. aureus* are 30.25 ± 0.48 and 34.51 ± 0.66 mm at 2.0 mg/ml but not for GCP-F2. Researchers found that hydroxyl and carboxyl groups in polysaccharide can chelate metal ions and influence the nutrient uptake of bacteria, thus playing its antibacterial activity (41). The increased antibacterial activity of GCP-F1 might be related to the more exposure to hydroxyl and carboxyl groups induced by the decrease of molecular weight and breaking of intermolecular hydrogen bonding (21, 42). Meanwhile, monosaccharide composition and the molar ratio will also affect the antibacterial activity of GCP-F1 and GCP-F2 (43). Furthermore, a low molecular weight of GCP-F1 might allow it to enter the bacteria and exert its antibacterial activity by affecting protein, nucleic acid, and energy metabolism of the cell (44–46). However, a too low molecular weight of GCP-F2 with further degradation prevents it from forming an active structure (13, 32), which might be the reason that GCP-F2 lost its antibacterial activity.

Conclusion

Physicochemical property and biological activity of polysaccharide GCP and its fragments (GCP-F1 and GCP-F2) obtained by ultrasonic degradation were analyzed. Compared to GCP, a lower molecular weight of GCP-F1 and GCP-F2 showed higher antioxidant activities in a concentration-dependent manner. Though ultrasonic degradation increased the antibacterial activity of GCP-F1 by reducing its molecular weight, GCP-F2 almost lost its antibacterial activity with further ultrasonic degradation and molecular weight reduction. Therefore, there might also be specific active units in polysaccharides as compared to an enzymatic process, and it is very important to obtain appropriate polymerization of polysaccharides for their better bioactivities.

Data availability statement

The original contributions presented in this study are included in the article/supplementary material, further inquiries can be directed to the corresponding author/s.

Author contributions

SL contributed to conception, design, and funding of the study. YW, WD, and WH organized the database. CX wrote the first draft of the manuscript. QS and ZW contributed to writing—review and editing. All authors approved it for publication.

Funding

This work was supported by the Science and Technology Research Project of Henan Province (182102310687), Henan Provincial Education Department Project (19B550010), the Natural Science Foundation of Henan Province (212300410131), and the Natural Science Foundation of Chongqing (cstc2019jcyj-msxmX0459).

Conflict of interest

The authors declare that the research was conducted in the absence of any commercial or financial relationships that could be construed as a potential conflict of interest.

Publisher's note

All claims expressed in this article are solely those of the authors and do not necessarily represent those of their affiliated organizations, or those of the publisher, the editors and the reviewers. Any product that may be evaluated in this article, or claim that may be made by its manufacturer, is not guaranteed or endorsed by the publisher.

References

1. Wang Z, Xue R, Cui J, Wang J, Fan W, Zhang H, et al. Antibacterial activity of a polysaccharide produced from *Chaetomium globosum* CGMCC 6882. *Int J Biol Macromol.* (2019) 125:376–82. doi: 10.1016/j.ijbiomac.2018.11.248

2. Wang Z, Liu X, Bao Y, Wang X, Zhai J, Zhan X, et al. Characterization and anti-inflammation of a polysaccharide produced by *Chaetomium globosum* CGMCC 6882 on LPS-induced RAW 264.7 cells. *Carbohydr Polym.* (2021) 251:117129. doi: 10.1016/j.carbpol.2020.117129

3. Chen R, Li Y, Chen J, Lu C. A review for natural polysaccharides with anti-pulmonary fibrosis properties, which may benefit to patients infected by 2019-nCoV. *Carbohydr Polym.* (2020) 247:116740. doi: 10.1016/j.carbpol.2020.116740

4. Ren Y, Rong L, Shen M, Liu W, Xiao W, Luo Y, et al. Interaction between rice starch and *Mesona chinensis* Benth polysaccharide gels: pasting and gelling properties. *Carbohydr Polym.* (2020) 240:116316. doi: 10.1016/j.carbpol.2020.116316

5. Ke Y, Ding B, Zhang M, Dong T, Fu Y, Lv Q, et al. Study on inhibitory activity and mechanism of chitosan oligosaccharides on *Aspergillus Flavus* and *Aspergillus Fumigatus*. *Carbohydr Polym.* (2022) 275:118673.

6. Qian F, An L, He X, Han Q, Li X. Antibacterial activity of xantho-oligosaccharide cleaved from xanthan against phytopathogenic *Xanthomonas campestris* pv. *Campestris*. *Process Biochem.* (2006) 41:1582–8.

7. Li XL, He LP, Yang Y, Liu FJ, Cao Y, Zuo JJ. Effects of extracellular polysaccharides of *Ganoderma lucidum* supplementation on the growth performance, blood profile, and meat quality in finisher pigs. *Livest Sci.* (2015) 178:187–94.

8. Song X, Shen Q, Liu M, Zhang C, Zhang L, Ren Z, et al. Antioxidant and hepatoprotective effects of intracellular mycelium polysaccharides from *Pleurotus geesteranus* against alcoholic liver diseases. *Int J Biol Macromol.* (2018) 114:979–88. doi: 10.1016/j.ijbiomac.2018.04.001

9. Zhang L, Li X, Xu X, Zeng F. Correlation between antitumor activity, molecular weight, and conformation of lentinan. *Carbohydr Res.* (2005) 340:1515–21.

10. Zhang M, Tang X, Wang F, Zhang Q, Zhang Z. Characterization of *Lycium barbarum* polysaccharide and its effect on human hepatoma cells. *Int J Biol Macromol.* (2013) 61:270–5.

11. Wang K, Li W, Rui X, Chen X, Jiang M, Dong M. Structural characterization and bioactivity of released exopolysaccharides from *Lactobacillus plantarum* 70810. *Int J Biol Macromol.* (2014) 67:71–8. doi: 10.1016/j.ijbiomac.2014.02.056

12. Deng J, Zhong J, Long J, Zou X, Wang D, Song Y, et al. Hypoglycemic effects and mechanism of different molecular weights of konjac glucomannans in type 2 diabetic rats. *Int J Biol Macromol.* (2020) 165:2231–43. doi: 10.1016/j.ijbiomac.2020.10.021

13. Qiu Y, Ma Y, Huang Y, Li S, Xu H, Su E. Current advances in the biosynthesis of hyaluronic acid with variable molecular weights. *Carbohydr Polym.* (2021) 269:118320. doi: 10.1016/j.carbpol.2021.118320

14. Wang Z, Jia S, Cui J, Qu J, Yue Y, Sun Q, et al. Antioxidant activity of a polysaccharide produced by *Chaetomium globosum* CGMCC 6882. *Int J Biol Macromol.* (2019) 141:955–60.

15. Wang Z, Chen P, Tao N, Zhang H, Li R, Zhan X, et al. Anticancer activity of polysaccharides produced from glycerol and crude glycerol by an endophytic fungus *Chaetomium globosum* CGMCC 6882 on human lung cancer A549 cells. *Biomolecules.* (2018) 8:171. doi: 10.3390/biom8040171

16. Zhang L, Ma L, Pan Y, Zheng X, Sun Q, Wang Z, et al. Effect of molecular weight on the antibacterial activity of polysaccharides produced by *Chaetomium globosum* CGMCC 6882. *Int J Biol Macromol.* (2021) 188:863–9. doi: 10.1016/j.ijbiomac.2021.08.059

17. Hu JL, Nie SP, Li C, Wang S, Xie MY. Ultrasonic irradiation induces degradation and improves prebiotic properties of polysaccharide from seeds of *Plantago asiatica* L. during *in vitro* fermentation by human fecal microbiota. *Food Hydrocoll.* (2018) 76:60–6.

18. Wang Z, Wang Z, Huang W, Suo J, Chen X, Ding K, et al. Antioxidant and anti-inflammatory activities of an anti-diabetic polysaccharide extracted from *Gynostemma pentaphyllum* herb. *Int J Biol Macromol.* (2020) 145:484–91. doi: 10.1016/j.ijbiomac.2019.12.213

19. Hu X, Wang K, Yu M, He P, Qiao H, Zhang H, et al. Characterization and antioxidant activity of a low-molecular-weight xanthan gum. *Biomolecules.* (2019) 9:730. doi: 10.3390/biom9110730

20. Li S, Xia H, Xie A, Wang Z, Ling K, Zhang Q, et al. Structure of a fucose-rich polysaccharide derived from EPS produced by *Kosakonia* sp. CCTCC M2018092 and its application in antibacterial film. *Int J Biol Macromol.* (2020) 159:295–303. doi: 10.1016/j.ijbiomac.2020.05.029

21. Qin Y, Xie J, Xue B, Li X, Gan J, Zhu T, et al. Effect of acid and oxidative degradation on the structural, rheological, and physiological properties of oat β-glucan. *Food Hydrocoll.* (2021) 112:106284.

22. Yan JK, Wu LX, Qiao ZR, Cai WD, Ma H. Effect of different drying methods on the product quality and bioactive polysaccharides of bitter gourd (*Momordica charantia* L.) slices. *Food Chem.* (2019) 271:588–96. doi: 10.1016/j.foodchem.2018.08.012

23. Yuan Q, He Y, Xiang PY, Wang SP, Cao ZW, Gou T, et al. Effects of simulated saliva-gastrointestinal digestion on the physicochemical properties and bioactivities of okra polysaccharides. *Carbohydr Polym.* (2020) 238:116183. doi: 10.1016/j.carbpol.2020.116183

24. Yan JK, Wang YY, Ma HL, Wang ZB. Ultrasonic effects on the degradation kinetics, preliminary characterization and antioxidant activities of polysaccharides from *Phellinus linteus* mycelia. *Ultrason Sonochem.* (2016) 29:251–7. doi: 10.1016/j.ultsonch.2015.10.005

25. Wang H, Chen J, Ren P, Zhang Y, Omondi Onyango S. Ultrasound irradiation alters the spatial structure and improves the antioxidant activity of the yellow tea polysaccharide. *Ultrason Sonochem.* (2021) 70:105355. doi: 10.1016/j.ultsonch.2020.105355

26. Yang H, Bai J, Ma C, Wang L, Li X, Zhang Y, et al. Degradation models, structure, rheological properties and protective effects on erythrocyte hemolysis of the polysaccharides from *Ribes nigrum* L. *Int J Biol Macromol.* (2020) 165:738–46. doi: 10.1016/j.ijbiomac.2020.09.093

27. Albuquerque PBS, de Oliveira WF, dos Santos Silva PM, dos Santos Correia MT, Kennedy JF, Coelho LCBB. Epiphanies of well-known and newly discovered macromolecular carbohydrates – A review. *Int J Biol Macromol.* (2020) 156:51–66. doi: 10.1016/j.ijbiomac.2020.04.046

28. Zheng L, Ma Y, Zhang Y, Meng Q, Yang J, Wang B, et al. Increased antioxidant activity and improved structural characterization of sulfuric acid-treated stepwise degraded polysaccharides from *Pholiota nameko* PN-01. *Int J Biol Macromol.* (2021) 166:1220–9. doi: 10.1016/j.ijbiomac.2020.11.004

29. Li J, Li S, Zheng Y, Zhang H, Chen J, Yan L, et al. Fast preparation of rhamnogalacturonan I enriched low molecular weight pectic polysaccharide by ultrasonically accelerated metal-free Fenton reaction. *Food Hydrocoll.* (2019) 95:551–61.

30. Liu M, Liu Y, Cao MJ, Liu GM, Chen Q, Sun L, et al. Antibacterial activity and mechanisms of depolymerized fucoidans isolated from *Laminaria japonica*. *CarbohydrPolym.* (2017) 172:294–305. doi: 10.1016/j.carbpol.2017.05.060

31. Yang W, Pei F, Shi Y, Zhao L, Fang Y, Hu Q. Purification, characterization and anti-proliferation activity of polysaccharides from *Flammulina velutipes*. *Carbohydr Polym.* (2012) 88:474–80.

32. Guo X, Ye X, Sun Y, Wu D, Wu N, Hu Y, et al. Ultrasound effects on the degradation kinetics, structure, and antioxidant activity of sea cucumber fucoidan. *J Agric Food Chem.* (2014) 62:1088–95. doi: 10.1021/jf404717y

33. Wang Z, Zhao X, Liu X, Lu W, Jia S, Hong T, et al. Anti-diabetic activity evaluation of a polysaccharide extracted from *Gynostemma pentaphyllum*. *Int J Biol Macromol.* (2019) 126:209–14. doi: 10.1016/j.ijbiomac.2018.12.231

34. Yang Y, Qiu Z, Li L, Vidyarthi SK, Zheng Z, Zhang R. Structural characterization and antioxidant activities of one neutral polysaccharide and three acid polysaccharides from *Ziziphus jujuba* cv. *Hamidazao*: a comparison. *Carbohydr Polym.* (2021) 261:117879. doi: 10.1016/j.carbpol.2021.117879

35. Ogutu FO, Mu TH. Ultrasonic degradation of sweet potato pectin and its antioxidant activity. *Ultrason Sonochem.* (2017) 38:726–34. doi: 10.1016/j.ultsonch.2016.08.014

36. Lo TCT, Chang CA, Chiu KH, Tsay PK, Jen JF. Correlation evaluation of antioxidant properties on the monosaccharide components and glycosyl linkages of polysaccharide with different measuring methods. *Carbohydr Polym.* (2011) 86:320–7.

37. Lin L, Cui F, Zhang J, Gao X, Zhou M, Xu N, et al. Antioxidative and renoprotective effects of residue polysaccharides from *Flammulina velutipes*. *Carbohydr Polym.* (2016) 146:388–95. doi: 10.1016/j.carbpol.2016.03.071

38. Yang W, Wang Y, Li X, Yu P. Purification and structural characterization of Chinese yam polysaccharide and its activities. *Carbohydr Polym.* (2015) 117:1021–7.

39. Khedmat L, Izadi A, Mofid V, Mojtahedi SY. Recent advances in extracting pectin by single and combined ultrasound techniques: a review of techno-functional and bioactive health-promoting aspects. *Carbohydr Polym.* (2020) 229:115474. doi: 10.1016/j.carbpol.2019.115474

40. Cui R, Zhu F. Ultrasound modified polysaccharides: a review of structure, physicochemical properties, biological activities and food applications. *Trends Food Sci Technol.* (2021) 107:491–508.

41. Gülçin I. Antioxidant and antiradical activities of $_L$-carnitine. *Life Sci.* (2006) 78:803–11.

42. Khan AA, Gani A, Masoodi FA, Amin F, Wani IA, Khanday FA, et al. Structural, thermal, functional, antioxidant & antimicrobial properties of β-d-glucan extracted from baker's yeast (*Saccharomyces cereviseae*)—Effect of γ-irradiation. *Carbohydr Polym.* (2016) 140:442–50.

43. Han Q, Wu Z, Huang B, Sun L, Ding C, Yuan S, et al. Extraction, antioxidant and antibacterial activities of *Broussonetia papyrifera* fruits polysaccharides. *Int J Biol Macromol.* (2016) 92:116–24. doi: 10.1016/j.ijbiomac.2016.06.087

44. Zhang Y, Wu YT, Zheng W, Han XX, Jiang YH, Hu PL, et al. The antibacterial activity and antibacterial mechanism of a polysaccharide from *Cordyceps cicadae*. *J Funct Foods.* (2017) 38:273–9.

45. Chen X, Tao L, Ru Y, Weng S, Chen Z, Wang J, et al. Antibacterial mechanism of *Tetrastigma hemsleyanum* Diels et Gilg's polysaccharides by metabolomics based on HPLC/MS. *Int J Biol Macromol.* (2019) 140:206–15. doi: 10.1016/j.ijbiomac.2019.08.097

46. Wang Z, Zhu J, Li W, Li R, Wang X, Qiao H, et al. Antibacterial mechanism of the polysaccharide produced by *Chaetomium globosum* CGMCC 6882 against *Staphylococcus aureus*. *Int J Biol Macromol.* (2020) 159:231–5. doi: 10.1016/j.ijbiomac.2020.04.269

frontiers | Frontiers in Nutrition

TYPE Review
PUBLISHED 22 July 2022
DOI 10.3389/fnut.2022.961507

Check for updates

OPEN ACCESS

EDITED BY
Xiaolong Ji,
Zhengzhou University of Light Industry, China

REVIEWED BY
Jinyuan Ma,
Henry Ford Health System, United States
Fengchao Lang,
National Institutes of Health (NIH), United States
Yanqing Liu,
Columbia University, United States

*CORRESPONDENCE
Baoming Tian
tbm2020@zjut.edu.cn
Yajun Hu
huyajun711@163.com

SPECIALTY SECTION
This article was submitted to Food Chemistry, a section of the journal Frontiers in Nutrition

RECEIVED 04 June 2022
ACCEPTED 04 July 2022
PUBLISHED 22 July 2022

CITATION
Chen Y, Pan X, Tian B and Hu Y (2022) Polysaccharide immunization and colorectal cancer: A systematic review and network meta-analysis. *Front. Nutr.* 9:961507. doi: 10.3389/fnut.2022.961507

COPYRIGHT
© 2022 Chen, Pan, Tian and Hu. This is an open-access article distributed under the terms of the Creative Commons Attribution License (CC BY). The use, distribution or reproduction in other forums is permitted, provided the original author(s) and the copyright owner(s) are credited and that the original publication in this journal is cited, in accordance with accepted academic practice. No use, distribution or reproduction is permitted which does not comply with these terms.

Polysaccharide immunization and colorectal cancer: A systematic review and network meta-analysis

Yuefeng Chen[1], Xinnan Pan[2], Baoming Tian[3,4,5]* and Yajun Hu[1]*

[1]Department of Medical College of Shaoxing University, Shaoxing, China, [2]Department of Medical College of Wenzhou Medical University, Wenzhou, China, [3]College of Food Science and Technology, Zhejiang University of Technology, Hangzhou, China, [4]Zhejiang Institute of Modern TCM and Natural Medicine Co., Ltd., Hangzhou, China, [5]School of Pharmaceutical Sciences, Zhejiang Chinese Medical University, Hangzhou, China

Polysaccharides have a variety of biological activities, and in the anti-tumor field, they produce tumor suppressive effects by regulating the polarization of tumor-associated macrophages (TAMs). In immunotherapy, it has significant activities in modulating cytokines and antibody production. We reviewed them and selected CD24, an immune target, for meta-analysis with colorectal cancer (CRC) to investigate the correlation between CD24 expression and CRC. Correlation of CD24 positive expression with clinical-pathological features: age, sex, Duke's stage, diameter, depth of invasion, degree of differentiation, and lymph node metastasis. It showed that: CD24 expression in CRC was significantly correlated with advanced nuclear grade of CRC, lymph node metastasis, Duke's stage of CRC and age of CRC patients, while there was no significant correlation with gender, tumor diameter and invasion depth. The aim is to clarify the specific mechanism of polysaccharide immune anti-tumor, combined with targeted site-specific anti-solid tumor.

KEYWORDS

colorectal cancer, CD24, prognosis, polysaccharides, immune

TCM (Traditional Chinese medicine) has multiple benefits by altering the microenvironment and enhancing the action of the immune system (1). Plant polysaccharides as TCM-derived components have been widely studied. Many biological properties of plant polysaccharides have been discovered, including anticancer, antioxidant, and immunomodulatory effects (2). Ginseng polysaccharide is effective against non-small cell lung cancer (3, 4), astragalus polysaccharide is effective against liver cancer (5), and shiitake mushroom polysaccharide is effective against CRC (6). Jujube polysaccharides also improve intestinal flora and inhibit CRC progression (7). TAMs have been implicated in anti-tumor processes. M1 macrophages can limit tumor cell proliferation in diverse tumor microenvironments (TME), but M2 macrophages have pro-tumor effects. TAMs infiltration and polarization in TME

can be regulated by plant polysaccharides, which can enhance M1 polarization, M2 to M1 polarization, and inhibit M2 function. *Radix Codonopsis* polysaccharide increases macrophage activation and polarization to M1, impairs TME, and prevents cancer cells from evading the immune system (8). Epimedium polysaccharide modulates the TME, reverses TAM phenotype, boosts T cell expression, and boosts tumor immunity (9). The CD14 pathway is activated by Poria polysaccharide, which promotes the conversion of M2 to M1. Plant polysaccharides mainly regulate TAMs in terms of regulating infiltration and regulating polarization, which play a role in improving the tumor microenvironment and anti-tumor effects. The study of signaling pathways plays a crucial role in this job. In TAMs, IAPS-2 (An acidic polysaccharide extracted from the roots of an herb called Ilex asprella) inhibits STAT3 phosphorylation while increasing STAT1 phosphorylation, facilitating M1 polarization (10). Ganoderma lucidum polysaccharide PSG-1 induces activation of TAMs through TLR4-mediated NF-κB and MAPK signaling pathways, increases TNF-α and NO expression, promotes M1 properties, and exerts anti-tumor activity (11). In addition, dendrobium officinale polysaccharide can significantly inhibit tumor growth in mice by directly targeting TLR2 and promoting the polarization of TAMs toward M1 (12). JAK/STAT, PI3K/Akt, JNK, and other signaling pathways are also involved in modulating TAMs phenotype.

NF-κB pathway, PD-L1 and leukocyte differentiation antigens are important targets for the biological activities of proliferation, differentiation, and migration of solid tumors such as colorectal. EG, MG, HXRARG, and HXRA, four polysaccharide active components of ryegrass, induce P65 and IκBα phosphorylation to begin the NF-κB pathway, increase NO, TNF-α, and IL-6 production, and boost immunological activity (13). *Ganoderma lucidum* polysaccharide inhibits STAT3 phosphorylation, suppresses PD-L1 expression, boosts PD-L1 antibody effectiveness, and reduces the side effects of targeted inhibitors such wasting and anemia (14). The expression of CD40, CD53, CD80, CD86, and CD83 molecules on the surface of dendritic cells was significantly increased by Erysipelas polysaccharides, as was the expression of cytokines such as IL-12 p40 and IL-10 (15, 16). Momordica charantia was able to reduce the expression levels of inflammatory factors, such as IL-1β, IL-6, IFN-γ, and TNF-α (17).

CD24, as the major histocompatibility complex on the surface of dendritic cells, is a highly glycosylated mucin-like cell surface adhesion molecule with a relative molecular weight of 35–45 kDa. It is anchored to the cell surface by Glycosylphosphatidylinositol (GPI). It regulates cell adhesion in cell-cell cell-matrix interactions and is significantly related to tumor cell infiltration and proliferation (18, 19). Under physiological conditions, it is expressed in developmental or regenerated tissues and granulocytes, pre-B cells, keratinocytes, and renal tubular epithelial cells (20–22). Barkal et al. found on tumor cells that CD24 was able to bind to the protein Siglec-10 on macrophages and inhibit the anti-tumor effect of phagocytosis. And the $CD24^-$ deficient tumors infiltrating TAMs showed enhanced phagocytosis and lower growth than controls. After cycle culture, polyclonal $CD24^-$ tumors became mostly $CD24^+$, consistent with the selection of $CD24^-$ cells by TAMs and the appearance of $CD24^+$ cell subclones without the double allele CD24 deletion. Suggesting that TAMs-mediated increase in $CD24^-$ cell clearance is responsible for the reduction in tumor load (23). Not surprisingly, there are few studies that address such issues as polysaccharide regulation of CD24 or CD24 affecting polysaccharide regulation. Extensive data search was able to identify that they could have a common role in TAMs polarization, etc. In summary, we can block CD24 expression by monoclonal antibodies to enhance the phagocytosis of polysaccharide-regulated TAMs and significantly improve the anti-solid tumor effect.

CRC is a long-term, multi-programmed process involving in a series of oncogenes, tumor suppressor genes, and RNA gene mutations, resulting in changes in the function of important intracellular regulatory factors (24). Several studies have shown that high expression of CD24 in tumor cells and its involvement in CRC cell proliferation and invasion is a poor prognostic factor for CRC (25). Colorectal adenoma, a precancerous lesion of CRC, has an expression of CD24 comparable to that found in CRC at 90%. In contrast, CD24 expression in normal tissue near the lesion was almost 0 (26). Therefore, a complete understanding of the relationship between the expression of CD24 in CRC and its clinical characteristics is of great significance for the treatment and prognosis of CRC.

Correlation between CD24 and colorectal cancer

It is well known that colorectal adenoma is the most crucial precancerous disease of CRC. Studies have shown that the positive rate of CD24 is as high as 60% when the diameter of colorectal polyp is less than 2.0 cm. Moreover, CD24 increased with age, the diameter of colorectal polyps, the type of dysplasia of colorectal polyps, the metastasis of CRC, and the degree of differentiation of CRC, which showed a significant positive correlation (27, 28). This suggests that the change in the expression of CD24 is an early event in the development of CRC. At the same time, a series of experiments indicate that CD24 is involved in the occurrence and development of CRC (29–31). For example, Tan et al. used flow cytometry to study the expression of CD24 on peripheral blood CD3 cells in patients with CRC (observation group) and healthy controls (control group). It was found that the fluorescence intensity of CD24 on CD3 cells in the observation group was 337.02 ± 27.92 and that in the control group was 293.84 ± 9.54. There was a significant difference between the two groups. Some studies have shown

that CD24 has a great relationship with CRC treatment and can be used as a target for targeted therapy of CRC (32, 33).

The role of CD24 in the growth, invasion, recurrence, and metastasis of colorectal cancer

CD24 is highly expressed in most tumor specimens and is significantly related to the infiltration and proliferation of tumor cells. CD24 is a glycosylated phosphatidylinositol cell surface protein that mediates cancer cells, activated platelets, vascular endothelial cells, lymphatic circulation, and blood migration, resulting in tumor invasion and distal metastasis (34, 35). However, there is no transmembrane structure in CD24. When CD24 is expressed in CRC cell lines, some literature has shown that CD24 transduces the MAPK signal pathway through the activation of Src family kinases to promote the growth and invasion of CRC and enhance the invasive ability of CRC cells through Lyn. Lyn is one of the members of the Src family kinase family.

It has been reported that the expression of CD24, CD24 in 92.5% of human CRC tissue, can promote the growth of CRC cells. The positive expression rate of CD24 in the tumor diameter $\geq$ 5 cm group is as high as 87.0%, which is significantly higher than that in the tumor diameter $<$ 5 cm group. To some extent, this shows that CD24 promotes the growth of CRC cells.

The expression of CD24 in liver metastasis of CRC increases gradually, and a significant positive correlation can indicate the metastasis of CRC. P-selectin is a calcium-dependent endogenous lectin, rapidly expressed on the surface of activated vascular endothelial cells and platelets induced by inflammation and trauma. P-selectin is the earliest recognized and the only known ligand of CD24. In the pathological state of CD24, the organ can capture tumor cells and form distant metastasis by binding to P-selectin on the surface of vascular endothelial cells of distant organs or by interacting with platelets (23, 36).

Correlation between CD24 expression and clinicopathological features in colorectal cancer

CD24 gradually increased with the degree of differentiation of CRC, showing a significant positive correlation. With the increase of the degree of differentiation of CRC, the expression of CD24 gradually increased (37). The increase in the expression rate of CD24 can be used as the basis for the malignant transformation of colorectal polyps. With the increase in the diameter of colorectal polyps, the degree of polyp dysplasia, and the degree of differentiation of CRC, the expression rate of CD24 increases.

The expression level of CD24 in CRC is related to the clinicopathological features of CRC. The expression level of CD24 in CRC without serosa invasion was 0.7495 ± 0.0392, and in serosa invasion, CRC was 0.8935 ± 0.0521. The difference was statistically significant; that is, the expression level of CD24 in CRC increased with the degree of invasion of CRC.

The correlation between the expression of CD24 in colorectal cancer and the prognosis of colorectal cancer

A colorectal adenomatous polyp is a crucial precancerous lesion of CRC. Early detection of colorectal adenomatous polyp is helpful to the prognosis of CRC, and it has been reported that 95% of CRC is malignant from adenoma (38). In the early stage of the multistage progression of CRC, CD24 is highly expressed and malignant (39). The expression rate of CD24 in normal mucosa, inflammatory polyp, tubular adenoma, villous adenoma, and adenocarcinoma of CRC increased gradually, and the expression rate of CD24 increased with the degree of differentiation of CRC. Therefore, early analysis of CD24 expression can reduce the probability of colorectal polyps deteriorating into CRC and promote the prognosis of CRC (37).

Su et al. showed that the average survival time of the CD24 low expression group was 55.299 months, while the average survival time of the high expression group was 36.324 months. There was a significant difference in survival rate between the low expression group and the increased expression group. The survival rate of the expanded expression group was lower than that of the joint expression group, which could be used as an independent factor affecting the prognosis of patients with CRC.

Objectives

A meta-analysis of the correlation between CD24 expression and clinicopathological features and prognosis in colorectal cancer was conducted.

Materials and methods

Inclusion criteria

(1) The subjects were all people with CRC confirmed by pathology.

(2) It is necessary to include data on the correlation between the expression of CD24 in CRC and clinicopathological features.

Exclusion criteria

(1) Editorials, reviews, previews, abstracts, letters, and non-human basic research.

(2) Research in which data cannot be extracted.

(3) The language of the literature except for Chinese and English.

(4) Research that does not contain up-to-date data has been repeatedly published.

Retrieval strategy

The computer searches the Embase, PubMed, Web of Science. Subject search words include "CRC," "CD24," and so on. Free words include "age," "sex," "stage," "diameter," "depth of invasion," "degree of differentiation," "lymph node metastasis" and so on. The method of combination of subject words and free words is used for retrieval. The retrieval time is from establishing the database to April 1, 2022, to improve the literature search and accuracy. The list of references that have been included in the study is also searched manually to ensure the recall rate. In addition, manual search excludes important meetings in case reports, abstracts, reviews, letters, animal experiments, and oncology.

Statistical method

Statistical software and analysis

All the data included in this meta-analysis were merged and analyzed by Review Manager 5.4 software. The I^2-value judges the heterogeneity among the studies. If $I^2 > 50\%$, it can be considered that there is significant heterogeneity among the included studies, and the random effect model is selected to combine the effects; if $I^2 < 50\%$, it means that the included studies are homogeneous, and the fixed effect model is chosen to combine the results. Higgins et al. believe that the value of I^2 is between 0 and 100%, and the higher the value of I^2, the more significant the heterogeneity among the included studies. When the I^2-value is 25%, it indicates mild heterogeneity among the included studies, and the existence of $I^2 = 50\%$ suggests that there is moderate heterogeneity among the studies. In contrast, when $I^2 = 75\%$, it indicates a high degree of heterogeneity among the studies. It is generally believed that when $I^2 > 50\%$, the heterogeneity among the included studies is higher.

Sensitivity analysis

The heterogeneity between studies was detected by observing the value of I^2. If there is moderate or high heterogeneity between studies, the source of heterogeneity needs to be determined by sensitivity analysis. After the single study was excluded, the effects of the remaining studies were excluded, and the heterogeneity was compared with the total heterogeneity. Suppose the combined heterogeneity changes significantly compared with the total heterogeneity or outside the 95% confidence interval of the point estimated total effect of the combined effect amount in the forest map of sensitivity analysis. In that case, the results of this study are unstable. The study should be analyzed in-depth to determine the source of heterogeneity to draw cautious conclusions.

Publication bias

There are few studies on the survival outcomes of patients in this meta-analysis, so this study uses Egger's test and Begg's test to evaluate whether the included studies had publication bias when the $P > 0.10$ of the Egger's test and $P > 0.05$ of the Beggles test suggested no publication bias.

Results

Literature retrieval results

According to the established retrieval strategy, 133 related articles were retrieved electronically, and 13 duplicate articles were excluded. In strict accordance with the criteria of nano-arrangement, 70 pieces that were not following the meeting minutes, abstracts, reviews, non-human studies, and non-Chinese and English literature were excluded, and 50 other articles were excluded. After carefully reading the complete text, 41 articles that did not conduct a separate study on CD24 and whose data could not be extracted were banned. Finally, 9 studies that met the inclusion criteria were obtained, with 1,105 patients with CRC (**Figure 1**). [(1) Chen (40), Study of c-myc and CD24 expression in colorectal cancer and polyps. (2) Chen et al. (41), Expression of CD24 in colorectal cancer and its significance. (3) Su et al. (42), Expression of CD24 and Src in colorectal cancer tissues and their significance. (4) Su (43), The role and mechanism of Lyn in the regulation of colorectal cancer invasion by CD24. (5) Hua et al. (44), Expression of CD44 and CD24 in colorectal cancer and adenoma and their tumorigenic and invasive abilities. (6) Su (45), Expression of CD24 and CD166/ALCAM in colorectal cancer and their relationship with tumor cell proliferation and angiogenesis. (7) Shu (46), Study of CD24 and Lgr5 expression in colorectal polyps and colorectal cancer. (8) Xue et al. (47), Expression of CD24 and Lgr5 in colorectal polyps and colorectal cancer. (9) Zhang (48), Expression analysis of CD24 and Lgr5 in colorectal polyps and CRC].

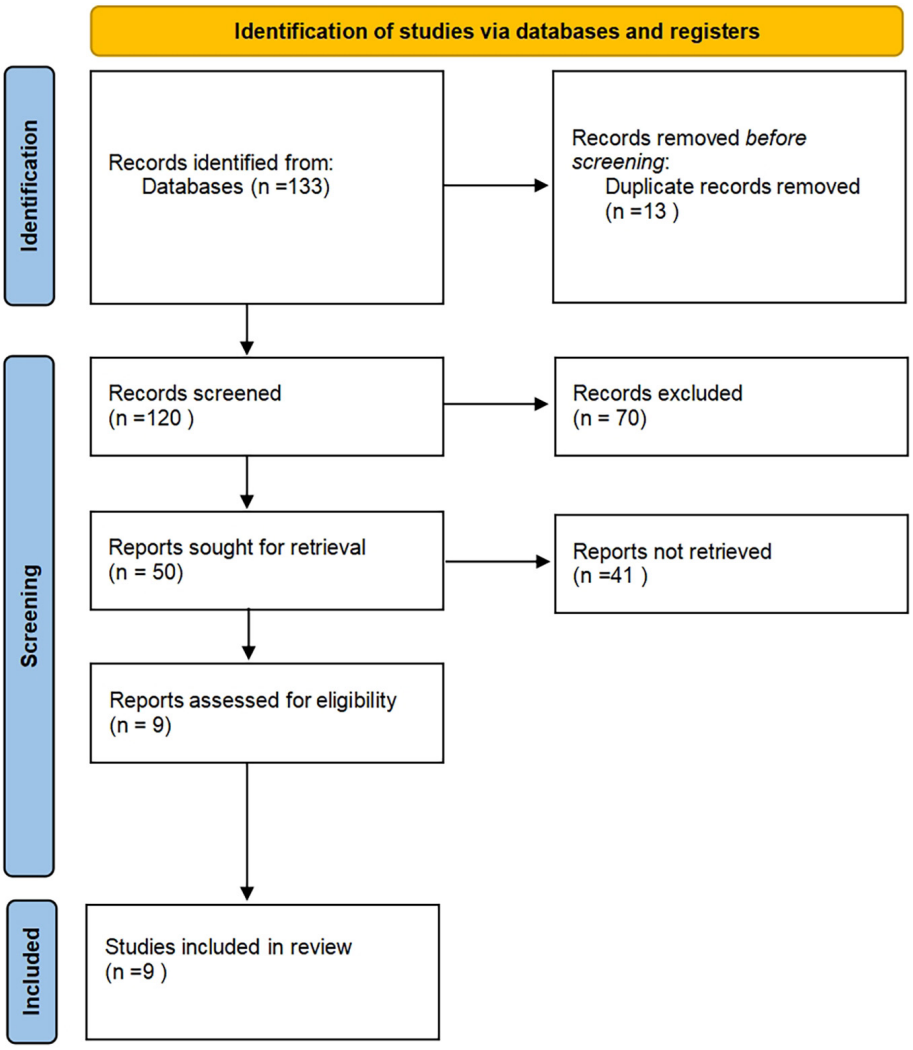

FIGURE 1
Document retrieval flow chart.

Correlation between CD24 expression and clinicopathological features in colorectal cancer

Correlation between the expression of CD24 in colorectal cancer and high-grade nuclear grade

A total of 4 studies were included in the evaluation of the correlation between the expression of CD24 and the degree of differentiation in CRC. A total of 528 patients with CRC were included, including 403 patients in the high and middle differentiation group and 125 patients in the low differentiation group (Figure 2). The heterogeneity test (I^2 = 66%, P = 0.03) showed that the heterogeneity was small, so the fixed effect model combined the effects. The results show a significant correlation between the expression of CD24 in CRC and the degree of differentiation of patients (RR = 0.56, 95% CI:0.45–0.71, $P < 0.00001$).

Correlation between expression of CD24 and lymph node metastasis in colorectal cancer

A total of 511 CRC patients were included in four studies to evaluate the correlation between CD24 expression and lymph node metastasis, including 198 patients with lymph node metastasis and 313 patients without lymph node metastasis (Figure 3). The heterogeneity test results showed that I^2 was 82%, P = 0.0008. The results showed considerable heterogeneity among studies, so the random effect model combined the effect. The results showed a significant correlation between the expression of CD24 in CRC and lymph node metastasis (RR = 1.90, 95% CI: 1.24–2.91, P = 0.003).

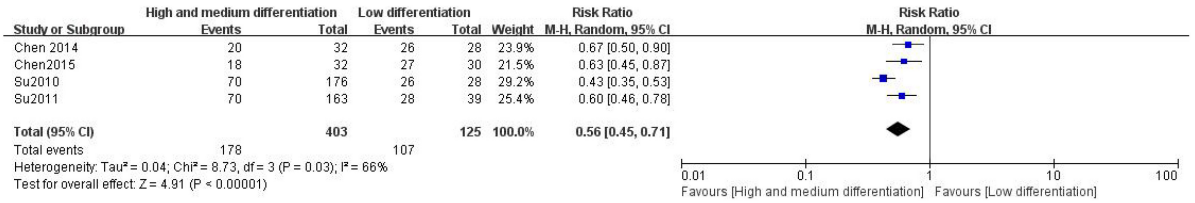

FIGURE 2
Forest map of correlation between CD24 expression and high-level nuclear classification.

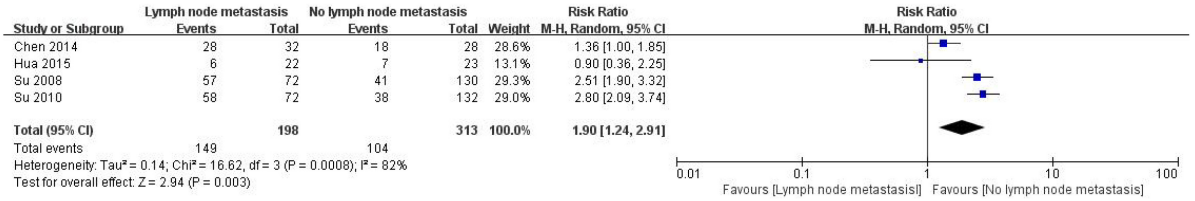

FIGURE 3
Forest map of correlation between CD24 expression and lymph node metastasis.

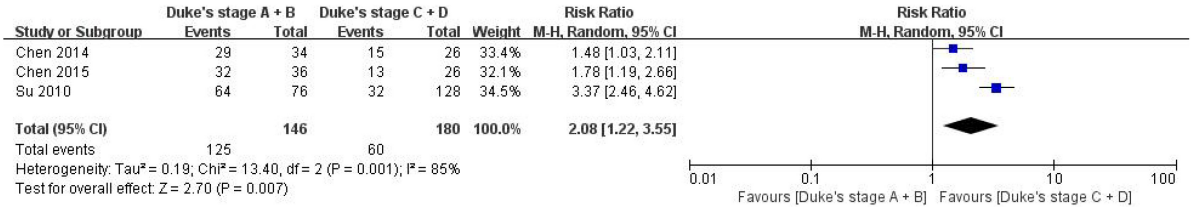

FIGURE 4
Forest map related to CD24 expression and dukes staging.

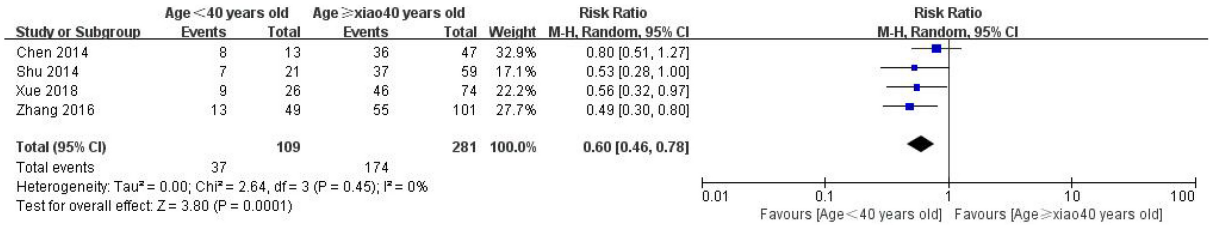

FIGURE 5
Forest map related to CD24 expression and age.

Correlation between expression of CD24 in colorectal cancer and dukes staging

Three studies were included in evaluating the correlation between the expression of CD24 in CRC and Duke's stage, including 125 patients with Duke's stage A&B and 60 patients with Duke's stage C&D stage (Figure 4). The heterogeneity test results showed that I^2 = 85%, P = 0.001, suggesting that the heterogeneity among the studies was enormous, so the random effect model was used to combine the effect. The results showed a significant correlation between the expression of CD24 in CRC and Duke's staging (RR = 2.08, 95% CI: 1.22–3.55, P = 0.007).

Correlation between age and expression of CD24 in colorectal cancer

A total of 4 studies were included in the evaluation of the correlation between the expression of CD24 and age in CRC, including 281 patients in the age ≥ 40 group and 109

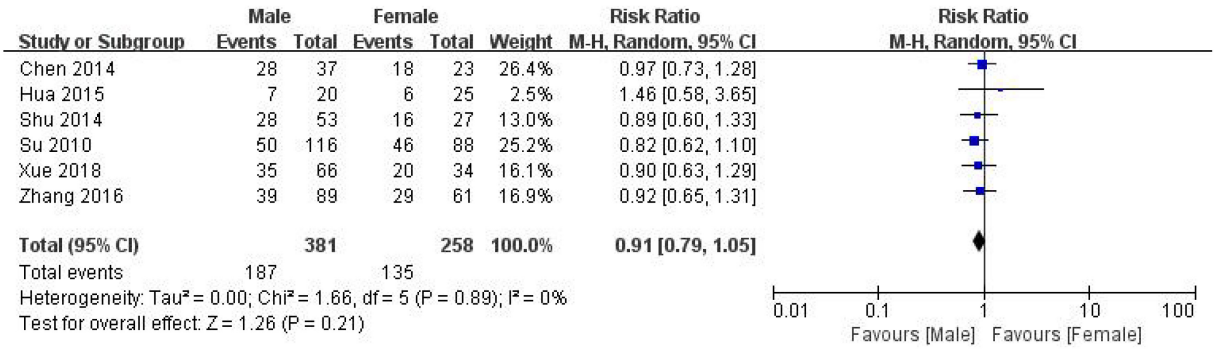

FIGURE 6
Forest map related to CD24 expression and gender.

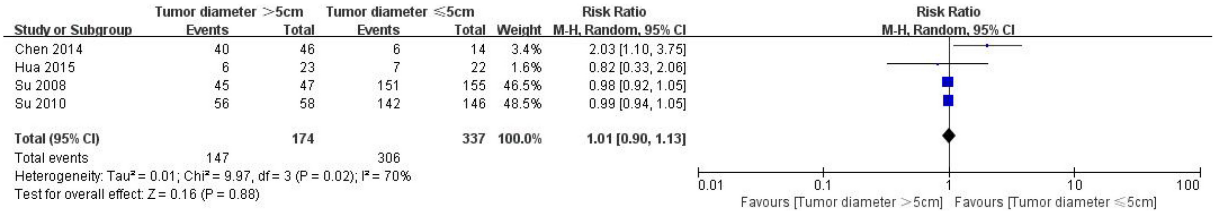

FIGURE 7
Forest map related to CD24 expression and tumor diameter.

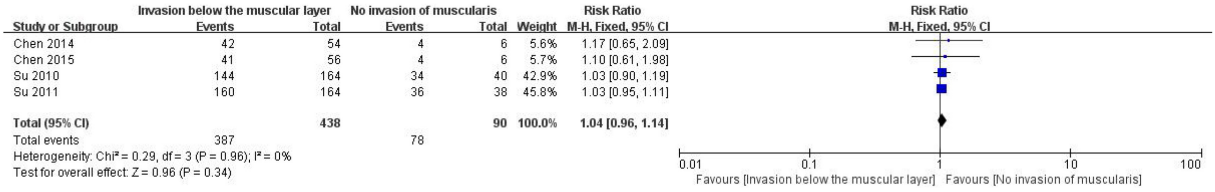

FIGURE 8
Forest map related to CD24 expression and infiltration depth.

patients in the age < 40 groups (Figure 5). The heterogeneity test results showed that I^2 = 0%, P = 0.0001, suggesting that the heterogeneity among the studies was small, so the random effect model was used to combine the effects. The results show a significant correlation between the expression of CD24 in CRC and the age of the patients (RR = 0.60, 95% CI: 0.46–0.7, P = 0.0001).

Correlation between gender and expression of CD24 in colorectal cancer

639 CRC patients, including 381 males and 258 females, were included in 6 studies to evaluate the correlation between CD24 expression and lymph node metastasis in CRC (Figure 6). The heterogeneity results (I^2 = 0%, P = 0.89) suggested that the heterogeneity among the studies was not significant, and the random effect model was selected to combine the effects. The results showed no significant correlation between the expression of CD24 and gender in CRC (RR = 0.91, 95% CI:0.79–1.05, P = 0.21).

Correlation between CD24 expression and tumor diameter in colorectal cancer

A total of 511 patients with colon cancer were included in 4 studies to evaluate the correlation between the expression of CD24 in colon cancer and tumor diameter, including 174 patients with tumor diameter > 5 cm and 337 patients with tumor diameter ≤ 5 cm (Figure 7). The heterogeneity test results (I^2 = 70%, P = 0.02) showed that the heterogeneity of each study was significant, so the random effect model was used to combine the effect. The results showed no significant correlation between the expression of CD24 in CRC and the diameter of the tumor (RR = 1.01, 95% CI: 0.90–1.13, P = 0.88).

Correlation between the expression of CD24 and the depth of invasion in colorectal cancer

A total of 528 patients with CRC were included in four studies to evaluate the correlation between CD24 expression and lymph node metastasis, including 387 patients with invasion of the muscular layer and 78 patients without charge of the muscular layer (**Figure 8**). The heterogeneity test results (I^2 = 0%, P = 0.96) showed that the heterogeneity of each study was small, so the random effect model was used to combine the effect. The results showed no significant correlation between the expression of CD24 and the depth of invasion in CRC (RR = 1.04, 95% CI: 0.96–1.14, P = 0.34).

Conclusion

The expression of CD24 in CRC was significantly correlated with a high-grade nuclear grade, lymph node metastasis, Duke's stage, and age, but not with gender, tumor diameter, and depth of invasion.

Discussion

Although the theoretical basis for plant polysaccharides' immune antitumor and clinical applications has been established by their modulatory effects on TAMs, the current body of research is still limited to the bioactive effects on solid tumors, and the mechanism by which they cause this effect needs further investigation. There are several signaling pathways and targets associated with malignant tumors, thus it is yet unknown if there are regulatory mechanisms particular to polysaccharides that can prevent tumors or malignant disorders. TAMs are one of the possible targets of immunological anti-tumor since they are a significant part of TME. Since CD24 is related to the plant polysaccharide-regulating CRC pathway and has a regulatory polarizing impact on TAMs during the conclusion process, we chose CD24 for the CRC correlation study.

CD24 still faces significant challenges before it is used in the clinic. First of all, the clinical detection method of CD24 is immunohistochemical, and there is no unified standard for the definition of its critical value, which will be a significant limitation for the practical application of CD24 in clinical practice. Secondly, CRC with different differentiation may show other clinical characteristics and biological behavior. Still, due to the lack of data collected, our meta-analysis does not evaluate the relationship between CD24 and clinicopathological parameters of CRC with different differentiation, which needs further study.

In addition, there are some shortcomings in this meta-analysis, which are shown in the following aspects: (1) the methods for detecting tumor markers in our studies are all realized by immunohistochemistry. However, there is a certain degree of bias due to the differences in antibody types, drug concentrations, and critical values used in different studies. (2) The literature languages included in this study are limited to Chinese and English, excluding studies in other languages, which may lead to the exclusion of other appropriate studies, which may also lead to bias; (3) there are not many studies on the relationship between CD24 expression and prognosis, which is the reason why the results may be biased. (4) Most published studies lack the necessary data on patient treatment, creating additional inconsistencies and leading to potential selection bias.

Although this study has some limitations, this meta-analysis is still the first independent systematic evaluation of the correlation between CD24 expression and clinicopathology and prognosis in CRC. The meta-analysis of the above results shows that the expression of CD24 in CRC can reduce the overall and disease-free survival of patients with CRC and has a specific correlation with clinicopathological parameters, such as lymph node metastasis TNM stage and so on. It may have a particular reference value in future tumor differential diagnosis and targeted therapy. Examples include exosomal MiR-155 and MiR-665 as new hepatocellular carcinoma biomarkers (49), and ITGs as indicators of immune escape in NSCLC (50). Tumor-related markers can be analyzed from multiple perspectives and in multiple dimensions to consider the development of tumors and their prognosis. What is worth further thinking about is whether we can block the expression of CD24 in CRC in some way to inhibit the proliferation of tumor cells and prevent lymph node metastasis, to provide new ideas for clinical diagnosis and treatment to improve the prognosis of patients with CRC. However, the number of studies and sample size included in this meta-analysis is relatively tiny. In future studies, a large sample of prospective studies is needed to evaluate further the correlation between CD24 and clinicopathological features and prognosis to provide a sufficient theoretical basis for clinical treatment guidance of CD24.

Plant polysaccharides offer a significant advantage in the production of immune adjuvants due to their extensive diversity and low toxicity. Different immune adjuvants now in use play a vital role in tumor immunotherapy. Clinical application of several plant polysaccharides as effective all-natural immune adjuvants and anticancer adjuvants has previously occurred. In order to facilitate the targeted binding of CD24 antibodies and particular anti-CRC, they can also be molecularly altered.

Author contributions

YC, XP, and BT: conception and design. YC and YH: administrative support, data analysis, interpretation, and independent evaluation of each eligible study. YC and XP: database management and statistical analysis, collection, and

assembly of data. All authors contributed to the article and approved the final mauscript.

Acknowledgments

This work was sponsored by the School-Enterprise Cooperation Project Fund of Zhejiang University of Technology (KYY-HX-20211132).

Conflict of interest

BT was employed by Zhejiang Institute of Modern TCM and Natural Medicine Co., Ltd.

The remaining authors declare that the research was conducted in the absence of any commercial or financial relationships that could be construed as a potential conflict of interest.

Publisher's note

All claims expressed in this article are solely those of the authors and do not necessarily represent those of their affiliated organizations, or those of the publisher, the editors and the reviewers. Any product that may be evaluated in this article, or claim that may be made by its manufacturer, is not guaranteed or endorsed by the publisher.

References

1. Xu J, Zhang J, Wang J. The application of traditional Chinese medicine against the tumor immune escape. *J Transl Int Med.* (2020) 8:203–4. doi: 10.2478/jtim-2020-0032

2. Wang W, Xue C, Mao X. Radioprotective effects and mechanisms of animal, plant and microbial polysaccharides. *Int J Biol Macromol.* (2020) 153:373–84. doi: 10.1016/j.ijbiomac.2020.02.203

3. Huang J, Liu D, Wang Y, Liu L, Li J, Yuan J, et al. Ginseng polysaccharides alter the gut microbiota and kynurenine/tryptophan ratio, potentiating the antitumour effect of antiprogrammed cell death 1/programmed cell death ligand 1 (anti-PD-1/PD-L1) immunotherapy. *Gut.* (2022) 71:734–45. doi: 10.1136/gutjnl-2020-321031

4. Ji X, Hou C, Shi M, Yan Y, Liu Y. An insight into the research concerning *Panax ginseng* C. A. Meyer polysaccharides: a review. *Food Rev Int.* (2022) 38:1149–65. doi: 10.1080/87559129.2020.1771363

5. Li C, Pan XY, Ma M, Zhao J, Zhao F, Lv YP. *Astragalus polysacharin* inhibits hepatocellular carcinoma-like phenotypes in a murine HCC model through repression of M2 polarization of tumour-associated macrophages. *Pharm Biol.* (2021) 59:1533–9. doi: 10.1080/13880209.2021.1991384

6. Liu Y, Zhao J, Zhao Y, Zong S, Tian Y, Chen S, et al. Therapeutic effects of lentinan on inflammatory bowel disease and colitis-associated cancer. *J Cell Mol Med.* (2019) 23:750–60. doi: 10.1111/jcmm.13897

7. Ji X, Hou C, Gao Y, Xue Y, Yan Y, Guo X. Metagenomic analysis of gut microbiota modulatory effects of jujube (*Ziziphus jujuba* Mill.) polysaccharides in a colorectal cancer mouse model. *Food Funct.* (2020) 11:163–73. doi: 10.1039/C9FO02171J

8. Chen M, Li Y, Liu Z, Qu Y, Zhang H, Li D, et al. Exopolysaccharides from a *Codonopsis pilosula* endophyte activate macrophages and inhibit cancer cell proliferation and migration. *Thorac Cancer.* (2018) 9:630–9. doi: 10.1111/1759-7714.12630

9. Wang C, Feng L, Su J, Cui L, Dan L, Yan J, et al. Polysaccharides from *Epimedium koreanum* Nakai with immunomodulatory activity and inhibitory effect on tumor growth in LLC-bearing mice. *J Ethnopharmacol.* (2017) 207:8–18. doi: 10.1016/j.jep.2017.06.014

10. Li Q, Hao Z, Hong Y, He W, Zhao W. Reprogramming tumor associated macrophage phenotype by a polysaccharide from *Ilex asprella* for sarcoma immunotherapy. *Int J Mol Sci.* (2018) 19:3816. doi: 10.3390/ijms19123816

11. Zhang S, Nie S, Huang D, Huang J, Wang Y, Xie M. Polysaccharide from *Ganoderma atrum* evokes antitumor activity via toll-like receptor 4-mediated NF-kappaB and mitogen-activated protein kinase signaling pathways. *J Agric Food Chem.* (2013) 61:3676–82. doi: 10.1021/jf4004225

12. Wang HY, Ge JC, Zhang FY, Zha XQ, Liu J, Li QM, et al. *Dendrobium officinale* polysaccharide promotes M1 polarization of TAMs to inhibit tumor growth by targeting TLR2. *Carbohydr Polym.* (2022) 292:119683. doi: 10.1016/j.carbpol.2022.119683

13. Wei J, Wang B, Chen Y, Wang Q, Ahmed AF, Zhang Y, et al. The immunomodulatory effects of active ingredients from *Nigella sativa* in RAW264.7 cells through NF-κB/MAPK signaling pathways. *Front Nutr.* (2022) 9:899797. doi: 10.3389/fnut.2022.899797

14. He J, Zhang W, Di T, Meng J, Qi Y, Li G, et al. Water extract of sporoderm-broken spores of *Ganoderma lucidum* enhanced pd-l1 antibody efficiency through downregulation and relieved complications of pd-l1 monoclonal antibody. *Biomed Pharmacother.* (2020) 131:110541. doi: 10.1016/j.biopha.2020.110541

15. Lin YL, Liang YC, Lee SS, Chiang BL. Polysaccharide purified from *Ganoderma lucidum* induced activation and maturation of human monocyte-derived dendritic cells by the NF-kappaB and p38 mitogen-activated protein kinase pathways. *J Leukoc Biol.* (2005) 78:533–43. doi: 10.1189/jlb.0804481

16. Lin YL, Lee SS, Hou SM, Chiang BL. Polysaccharide purified from *Ganoderma lucidum* induces gene expression changes in human dendritic cells and promotes T helper 1 immune response in BALB/c mice. *Mol Pharmacol.* (2006) 70:637–44. doi: 10.1124/mol.106.022327

17. Semiz A, Ozgun Acar O, Cetin H, Semiz G, Sen A. Suppression of inflammatory cytokines expression with bitter melon (*Momordica charantia*) in TNBS-instigated ulcerative colitis. *J Transl Int Med.* (2020) 8:177–87. doi: 10.2478/jtim-2020-0027

18. Kryczek I, Liu S, Roh M, Vatan L, Szeliga W, Wei S, et al. Expression of aldehyde dehydrogenase and CD133 defines ovarian cancer stem cells. *Int J Cancer.* (2012) 130:29–39. doi: 10.1002/ijc.25967

19. Chantziou A, Theodorakis K, Polioudaki H, de Bree E, Kampa M, Mavroudis D, et al. Glycosylation modulates plasma membrane trafficking of CD24 in breast cancer cells. *Int J Mol Sci.* (2021) 22:8165. doi: 10.3390/ijms22158165

20. Ayre DC, Elstner M, Smith NC, Moores ES, Hogan AM, Christian SL. Dynamic regulation of CD24 expression and release of CD24-containing microvesicles in immature B cells in response to CD24 engagement. *Immunology.* (2015) 146:217–33. doi: 10.1111/imm.12493

21. Bombelli S, Meregalli C, Grasselli C, Bolognesi MM, Bruno A, Eriani S, et al. PKH^{high}/CD133+/CD24- renal stem-like cells isolated from human nephrospheres exhibit in vitro multipotency. *Cells.* (2020) 9:1805. doi: 10.3390/cells9081805

22. Gilliam DT, Menon V, Bretz NP, Pruszak J. The CD24 surface antigen in neural development and disease. *Neurobiol Dis.* (2017) 99:133–44. doi: 10.1016/j.nbd.2016.12.011

23. Barkal AA, Brewer RE, Markovic M, Kowarsky M, Barkal SA, Zaro BW, et al. CD24 signalling through macrophage Siglec-10 is a target for cancer immunotherapy. *Nature.* (2019) 572:392–6. doi: 10.1038/s41586-019-1456-0

24. Cancer Genome Atlas Network. Comprehensive molecular characterization of human colon and rectal cancer. *Nature.* (2012) 487:330–7. doi: 10.1038/nature11252

25. Sagiv E, Starr A, Rozovski U, Khosravi R, Altevogt P, Wang T, et al. Targeting CD24 for treatment of colorectal and pancreatic cancer by monoclonal antibodies

or small interfering RNA. *Cancer Res.* (2008) 68:2803–12. doi: 10.1158/0008-5472.CAN-07-6463

26. Ahmed MA, Al-Attar A, Kim J, Watson NF, Scholefield JH, Durrant LG, et al. CD24 shows early upregulation and nuclear expression but is not a prognostic marker in colorectal cancer. *J Clin Pathol.* (2009) 62:1117–22. doi: 10.1136/jcp.2009.069310

27. Okano M, Konno M, Kano Y, Kim H, Kawamoto K, Ohkuma M, et al. Human colorectal CD24+ cancer stem cells are susceptible to epithelial-mesenchymal transition. *Int J Oncol.* (2014) 45:575–80. doi: 10.3892/ijo.2014.2462

28. Seo KJ, Kim M, Kim J. Prognostic implications of adhesion molecule expression in colorectal cancer. *Int J Clin Exp Pathol.* (2015) 8:4148–57.

29. Su N, Peng L, Xia B, Zhao Y, Xu A, Wang J, et al. Lyn is involved in CD24-induced ERK1/2 activation in colorectal cancer. *Mol Cancer.* (2012) 11:43. doi: 10.1186/1476-4598-11-43

30. Wang W, Wang X, Peng L, Deng Q, Liang Y, Qing H, et al. CD24-dependent MAPK pathway activation is required for colorectal cancer cell proliferation. *Cancer Sci.* (2010) 101:112–9. doi: 10.1111/j.1349-7006.2009.01370.x

31. Baumann P, Thiele W, Cremers N, Muppala S, Krachulec J, Diefenbacher M, et al. CD24 interacts with and promotes the activity of c-src within lipid rafts in breast cancer cells, thereby increasing integrin-dependent adhesion. *Cell Mol Life Sci.* (2012) 69:435–48. doi: 10.1007/s00018-011-0756-9

32. Muraro MG, Mele V, Daster S, Han J, Heberer M, Cesare Spagnoli G, et al. CD133+, CD166+CD44+, and CD24+CD44+ phenotypes fail to reliably identify cell populations with cancer stem cell functional features in established human colorectal cancer cell lines. *Stem Cells Transl Med.* (2012) 1:592–603. doi: 10.5966/sctm.2012-0003

33. Jaggupilli A, Elkord E. Significance of CD44 and CD24 as cancer stem cell markers: an enduring ambiguity. *Clin Dev Immunol.* (2012) 2012:708036. doi: 10.1155/2012/708036

34. Bray F, Ferlay J, Soerjomataram I, Siegel RL, Torre LA, Jemal A. Global cancer statistics 2018: GLOBOCAN estimates of incidence and mortality worldwide for 36 cancers in 185 countries. *CA Cancer J Clin.* (2018) 68:394–424. doi: 10.3322/caac.21492

35. Weng CC, Ding PY, Liu YH, Hawse JR, Subramaniam M, Wu CC, et al. Mutant Kras-induced upregulation of CD24 enhances prostate cancer stemness and bone metastasis. *Oncogene.* (2019) 38:2005–19. doi: 10.1038/s41388-018-0575-7

36. Ayre DC, Pallegar NK, Fairbridge NA, Canuti M, Lang AS, Christian SL. Analysis of the structure, evolution, and expression of CD24, an important regulator of cell fate. *Gene.* (2016) 590:324–37. doi: 10.1016/j.gene.2016.05.038

37. Li Y, Zhang M, Wang X, Liu W, Wang H, Yang YG. Vaccination with CD47 deficient tumor cells elicits an antitumor immune response in mice. *Nat Commun.* (2020) 11:581. doi: 10.1038/s41467-019-14102-4

38. Park DH, Kim HS, Kim WH, Kim TI, Kim YH, Park DI, et al. Clinicopathologic characteristics and malignant potential of colorectal flat neoplasia compared with that of polypoid neoplasia. *Dis Colon Rectum.* (2008) 51:43–9; discussion 49. doi: 10.1007/s10350-007-9091-5

39. Choi Y-L, Lee S-H, Kwon G-Y, Park C-K, Han J-J, Choi JS, et al. Overexpression of CD24: association with invasiveness in urothelial carcinoma of the bladder. *Arch Pathol Lab Med.* (2007) 131:275–81. doi: 10.5858/2007-131-275-OOCAWI

40. Chen W. Study of c-MYC and CD24 expression in colorectal cancer and polyps. *Qingdao Univ.* (2014) 1–39.

41. Chen WJ, Dong SH, Tian ZB, Qu L, Mu GF. Expression of CD24 in colorectal cancer and its significance. *Weihai Matern Child Health Hosp.* (2015).

42. Su N, Yan Anne C, Liang Y, Peng L, Wang J, Jiang B, et al. Expression of CD24 and Src in colorectal cancer tissues and their significance. *Mod Dig Interv.* (2010) 15.

43. Ning S. The role and mechanism of Lyn in the regulation of colorectal cancer invasion by CD24. *South Med Univ.* (2011) 1–75.

44. Hua YQ, Wu YJ, Tan YQ, Liu LP, Ba CX. Expression of CD44 and CD24 in colorectal cancer and adenoma and their tumorigenic and invasive abilities. *J Inner Mong Med Univ.* (2015) 37:407–12. doi: 10.16343/j.cnki.issn.2095-512x.2015.05.002

45. Su Z. Expression of CD24 and CD166/ALCAM in colorectal cancer and their relationship with tumor cell proliferation and angiogenesis. *Fujian Med Univ.* (2008) 1–76.

46. Shu D. Study of CD24 and Lgr5 expression in colorectal polyps and colorectal cancer. *Soochow Univ.* (2014) 1–62.

47. Xue WC, Wang JL, Xu JC, Wu CX, Gao JH. Expression of CD24 and Lgr5 in colorectal polyps and colorectal cancer. *Chin J Gerontol.* (2018) 38:3116–9.

48. Zhang H. Expression analysis of CD24 and Lgr5 in colorectal polyps and CRC. *J Clin Exp Med.* (2016) 15:1059–62.

49. Mohamed AA, Omar AAA, El-Awady RR, Hassan SMA, Eitah WMS, Ahmed R, et al. MiR-155 and MiR-665 role as potential non-invasive biomarkers for hepatocellular carcinoma in egyptian patients with chronic hepatitis C virus infection. *J Transl Int Med.* (2020) 8:32–40. doi: 10.2478/jtim-2020-0006

50. Wang Y, Hou K, Jin Y, Bao B, Tang S, Qi J, et al. Lung adenocarcinoma-specific three-integrin signature contributes to poor outcomes by metastasis and immune escape pathways. *J Transl Int Med.* (2021) 9:249–63. doi: 10.2478/jtim-2021-0046

frontiers | Frontiers in Nutrition

TYPE Review
PUBLISHED 25 July 2022
DOI 10.3389/fnut.2022.914679

Check for updates

OPEN ACCESS

EDITED BY
Xiaolong Ji,
Zhengzhou University of Light Industry, China

REVIEWED BY
Yiming Niu,
University of Macau, China
Fancheng Meng,
Southwest University, China
Ren-You Gan,
Institute of Urban Agriculture (CAAS), China

*CORRESPONDENCE
Yan Qu
quyan028@126.com
Chen Zhang
chenzhang_1990@126.com

†These authors have contributed equally to this work

SPECIALTY SECTION
This article was submitted to Food Chemistry, a section of the journal Frontiers in Nutrition

RECEIVED 07 April 2022
ACCEPTED 04 July 2022
PUBLISHED 25 July 2022

CITATION
Yue X, Chen Z, Zhang J, Huang C, Zhao S, Li X, Qu Y and Zhang C (2022) Extraction, purification, structural features and biological activities of longan fruit pulp (Longyan) polysaccharides: A review. *Front. Nutr.* 9:914679. doi: 10.3389/fnut.2022.914679

COPYRIGHT
© 2022 Yue, Chen, Zhang, Huang, Zhao, Li, Qu and Zhang. This is an open-access article distributed under the terms of the Creative Commons Attribution License (CC BY). The use, distribution or reproduction in other forums is permitted, provided the original author(s) and the copyright owner(s) are credited and that the original publication in this journal is cited, in accordance with accepted academic practice. No use, distribution or reproduction is permitted which does not comply with these terms.

Extraction, purification, structural features and biological activities of longan fruit pulp (Longyan) polysaccharides: A review

Xuan Yue[1†], Zhejie Chen[2†], Jinming Zhang[1], Chi Huang[1], Shiyi Zhao[1], Xuebo Li[1], Yan Qu[1*] and Chen Zhang[1*]

[1]State Key Laboratory of Southwestern Chinese Medicine Resources, School of Pharmacy, Chengdu University of Traditional Chinese Medicine, Chengdu, China, [2]State Key Laboratory of Quality Research in Chinese Medicine, Institute of Chinese Medical Sciences, University of Macau, Macau, China

Dimocarpus longan Lour. (also called as longan) is a subtropical and tropical evergreen tree belonging to the Sapindaceae family and is widely distributed in China, Southeast Asia and South Asia. The pulp of longan fruit is a time-honored traditional medicinal and edible raw material in China and some Asian countries. With the advancement of food therapy in modern medicine, longan fruit pulp as an edible medicinal material is expected to usher in its rapid development as a functional nutrient. As one of the main constituents of longan fruit pulp, longan fruit pulp polysaccharides (LPs) play an indispensable role in longan fruit pulp-based functional utilization. This review aims to outline the extraction and purification methods, structural characteristics and biological activities (such as immunoregulatory, anti-tumor, prebiotic, anti-oxidant, anti-inflammatory and inhibition of AChE activity) of LPs. Besides, the structure-activity relationship, application prospect and patent application of LPs were analyzed and summarized. Through the systematic summary, this review attempts to provide a theoretical basis for further research of LPs, and promote the industrial development of this class of polysaccharides.

KEYWORDS

longan fruit pulp polysaccharide, extraction, structures, bioactivities, immune regulation, antitumor

Introduction

Dimocarpus longan Lour. (also called as longan) is a subtropical and tropical evergreen tree widely distributed in warm climates around the world, and mainly concentrated in southern China, Southeast Asia and South Asia, especially in China where longan has been cultivated for more than 2,000 years. Longan trees are mostly cultivated on embankment and gardens, and their fruits are generally picked in autumn. Longan fruits are perishable, have a short storage period, and are susceptible to post-harvest diseases. Longan fruit is divided into pulp, pericarp and core. Modern

research focuses on longan fruit pulp, longan fruit pulp polysaccharides (LPs) are the main components of the water extract of longan fruit pulp (Figure 1). In Chinese traditional medical and botany classics, such as Shennong's Classic of Materia Medica (Simplified Chinese: 神農本草經) and the Nanfang caomu Zhuang (Simplified Chinese: 南方草木狀), the precursory medical scientists and botanists have deeply summarized the medicinal and nutritive values and related cultivation history of longan fruit pulp (fruit flesh). Longan fruit pulp can be eaten fresh and dried, it has been demonstrated that the pulp of longan fruit is rich in dietary fiber, vitamins, phosphor, protein, polysaccharides and minerals, which contributes to the high nutritional value and the beneficial effect of spleen and brain (1). Based on the theory of food and drug homology, Chinese medicine practitioners have concluded through long practice and experience that the nutritional value of longan fruit pulp provides an irreplaceable premise for it to become an outstanding tonic. Generally, the dried longan fruit pulp (also known as Guiyuan) is combined with other herbs to treat diseases caused by body deficiency, such as Guipi Decoction and Jade Ling Ointment. Besides, in other Asian countries such as Thailand, Vietnam and Indonesia, longan fruit pulp is also employed as a food therapy material for amnesia, insomnia, neurasthenia, heart palpitations and fatigue of traditional medicines (2).

As a tonic, longan fruit pulp is rich in nutritional value, among which longan fruit pulp polysaccharides (Usually denoted as "Longan polysaccharides," abbreviated as LPs), as one of the material bases of longan fruit pulp health effects, have been proved to have immunomodulatory, anti-tumor and anti-oxidant physiological effects. So far, with the gradual improvement of separation and purification technology and the progress of biomedical research, scholars have conducted extensive research on the structural characteristics and biological activities of LPs. LPs are heterogeneous polysaccharides mainly composed of glucose (Glc), galactose (Gal), mannose (Man), rhamnose (Rha), ribose (Rib), glucuronic acid (GlcA) and galacturonic acid (GalA). Crude LPs were extracted from longan fruit pulp by different extraction methods, and then further purification could yield relatively pure and homogeneous LPs. In addition, the modification of polysaccharides has been a hot topic in modern polysaccharide research. In order to improve the biological activity of LPs and broaden their applications, scholars have also modified LPs according to their structures, such as chemical modifications like sulfation and phosphorylation, and biological modifications like enzymatic modifications and fermentation modifications of LPs. In addition, pharmacological studies of LPs have been carried out in an orderly manner, showing a variety of biological activities, such as LPs can enhance the ability of scavenging free radicals, immunomodulation, anti-tumor, and also exert the ability to regulate the dynamic balance of intestinal flora and enhance memory. For example, polysaccharides extracted from longan fruit pulp were shown to result in better learning and memory in mice by passive avoidance tests (3). Therefore, LPs have great commercial potential for functional food development, disease adjuvant therapy and cosmetics development.

To date, there are plenty of studies on LPs, but there is no systematic review on LPs. The purpose of this paper is to comprehensively summarize the extraction and purification methods, structural characteristics, and multiple biological activities (e.g., immunomodulatory, anti-tumor, prebiotic, anti-oxidant, anti-inflammatory, and AChE inhibitory activities) of LPs. Besides, the structural modifications, patent statistics as well as the application prospects of the LPs are also summarized (Figure 2). These contents provide the theoretical basis for the further study of LPs and will contribute to the further diversified industrial development of LPs.

Methods of extraction and purification

Extraction

The extraction of LPs is the first step in their basic research and commercial application, and our qualitative and quantitative studies of their active ingredients depend mainly on the choice of extraction methods. In general, the extraction process of LPs has three main steps: (1) Removal of pericarp, core and other impurities from longan fruit; (2) Disruption of the cell wall of longan fruit pulp cells, and the results of studies on plant cell walls indicated that plant polysaccharides are one of the main structural components of plant cell walls, so the extraction method that can effectively decompose the cell wall and release LPs without destroying the polysaccharide structure as much as possible should be selected (4); (3) Determination of the actual extraction rate, content and structure of LPs. At present, the extraction methods of LPs are generally mainly conventional extraction methods such as hot water method, microwave method, ultrasonic method and enzymatic method. In contrast, ultra-high pressure (UHP) technology and auxiliary extraction methods such as microwave-assisted extraction (MAE), ultrasonic-assisted extraction (UAE), ultra-high pressure (UHP)-assisted enzymes and ultrafine crushing-assisted enzymes can improve the original extraction process to a certain extent and obtain higher extraction efficiency. The researchers investigated the extraction temperature, solvent pH, extraction time and material-to-liquid ratio in LPs extraction methods to obtain the conditions for maximum extraction rate.

Hot water extraction

HWE is the most widespread and simple extraction method. Under high temperature water environment, plant cell walls are softened and polysaccharides are easily released and solubilized.

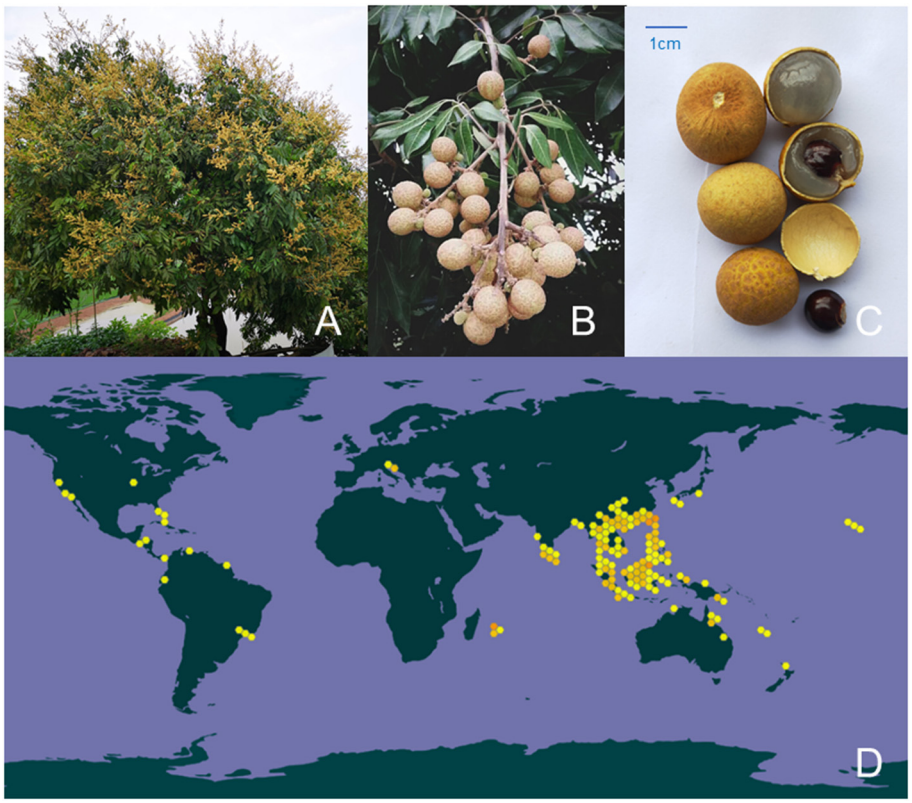

FIGURE 1
Botanical characteristics and the distribution of longan in the world. **(A)** The plant of longan, **(B)** the fruit of longan, and **(C)** different parts of longan fruit. **(D)** The approximate distribution of longan in the world (Data from the Global Biodiversity Information Facility, color figure can be viewed at wileyonlinelibrary.com).

The HWE method has the advantages of good permeability, high leaching rate and simple operation scheme, but it also has disadvantages such as time consuming, high temperature requirement, easy starch pasting and easy polysaccharide hydrolysis (5). Usually, prior to HWE of LPs, dried longan fruit pulp was crushed with a high-speed grinder and then the sample was pre-treated with a solvent (e.g., ethanol, acetone, or methanol) to remove low molecular weight (Mw) substances such as pigments, monosaccharides, and oligosaccharides. Distilled water (1:20 to 1:40, W/V) was used to extract the longan fruit pulp at 50°C to 90°C for 90–240 min, followed by filtration to obtain the extract, and the filtrate was concentrated to a certain amount under reduced pressure at no more than 65°C. Then, a certain amount of anhydrous ethanol was added to make the polysaccharides precipitate out as much as possible, and the crude LPs were precipitated after being stored at 4°C for 12 h. The content of LPs was determined by phenol-sulfuric acid method. For example, Zhong et al. optimized the HWE process of LPs by response surface methodology (RSM), and they concluded that the yield of LPs could reach 0.413% under the optimal conditions of liquid to solid ratio of 4:5, and extraction time of 4.5 h (6). However, many water-soluble non-polysaccharides were also dissolved in solution during HWE of LPs. So, the crude LPs obtained during this process need to be further purified.

Enzyme-assisted extraction

Enzyme technology is a biotechnology that has been widely applied to the extraction of active ingredients in recent years. In the extraction of LPs, the use of enzymes can temper the extraction conditions and accelerate the release of LPs under relatively mild conditions. This is mainly because pectin, cellulose and hemicellulose in longan fruit pulp are the main cell wall polysaccharides that play an important role in maintaining the texture of ripe fruits, however, EAE can break the cell wall by specifically catalyzing the degradation of these cell wall polysaccharides, thus releasing LPs in large quantities and achieving improved extraction efficiency (7). Therefore, the strategy of EAE for effective enrichment of LPs is characterized by high extraction rate, simple operation and high reproducibility (8, 9), and commonly used enzymes include cellulase (10, 11), dextranase, amylase, papain, hemicellulase and pectinase (12). It is important to note that when

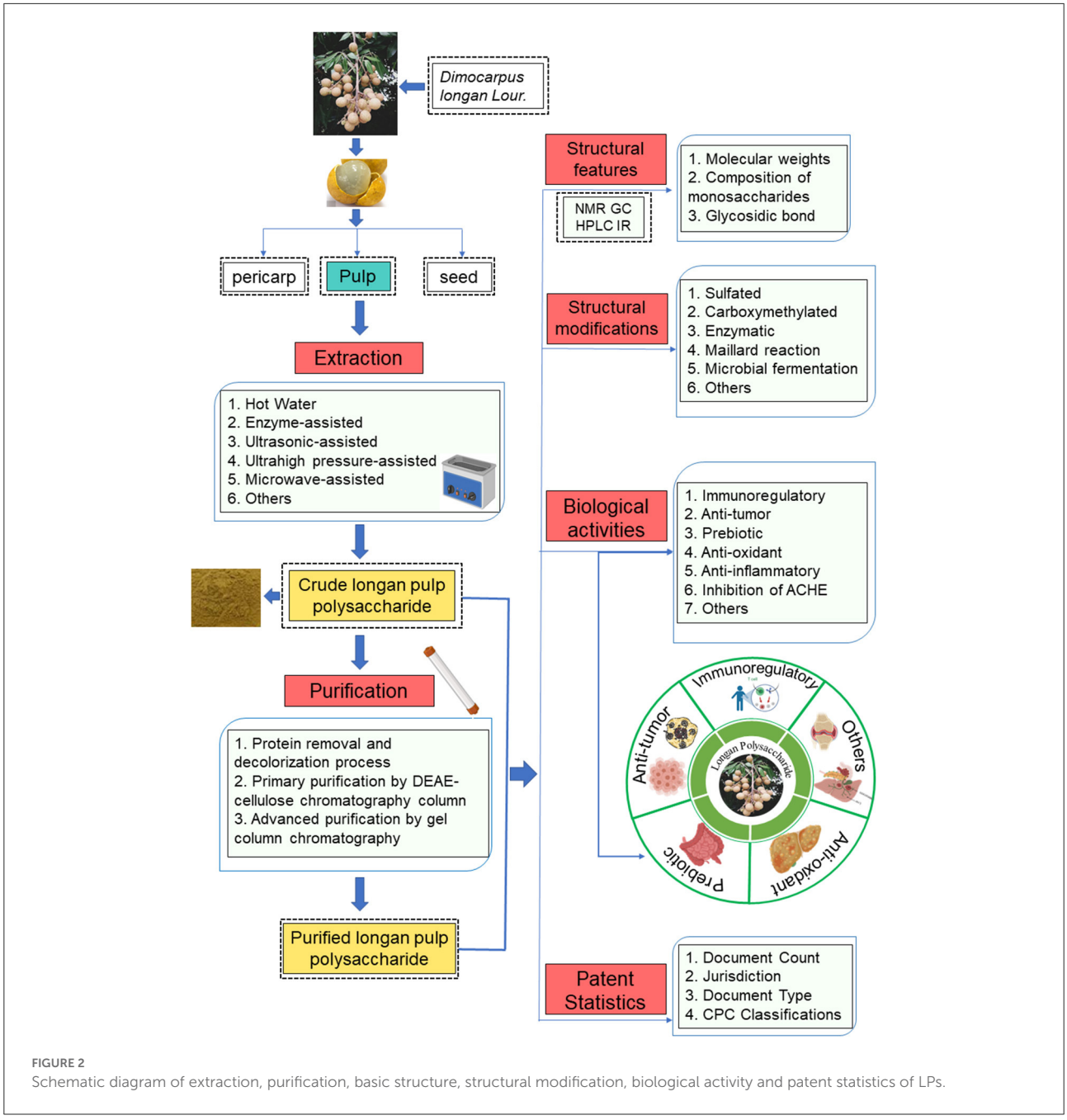

FIGURE 2
Schematic diagram of extraction, purification, basic structure, structural modification, biological activity and patent statistics of LPs.

extracting LPs, enzymes are usually added during maceration, when enzymatic reactions (enzymatic dissolution of cell surface structures and intercellular associations) are most likely to occur, followed by HWE in order to achieve polysaccharide solubilization. Cheng et al. produced transformed longan fruit pulp with low sucrose content and rich in Fructo-oligosaccharide (Fos) by treating fresh longan fruit pulp with 300 mg of complex plant hydrolase Viscoozyme L at pH = 6.0 and 55°C. Viscoozyme L has potent arabinose hydrolase and pectinase activities and can be used to degrade such cell wall polysaccharides to release water-soluble LPs. The results of content determination showed that the content of water-soluble LPs obtained from the enzymatically treated extracts increased significantly from 3.61 to 8.30 mg/g, while the insoluble fiber content decreased significantly with increasing enzymatic digestion time. This was because during enzymatic digestion, a large amount of insoluble fiber could be hydrolyzed into oligomers, which are recycled into the water-soluble LPs group (13). However, enzymatic digestion of LPs has some disadvantages, such as some enzymes are expensive and not

easily available; strict control of temperature and pH is required during the experimental process, and changes in conditions may lead to inactivation of the enzymes; and may also destroy the advanced structure of some LPs.

Ultrasonic-assisted extraction

In recent years, UAE has been widely used for the extraction of LPs. The enhanced extraction efficiency of ultrasound is mainly attributed to its mechanical and cavitation effects, the former greatly facilitating mass transfer between immiscible phases through hyper-stirring, especially at low frequencies. The latter can disrupt the cell wall by cavitation, resulting in the reduction of particle size and enhanced mass transfer through the cell wall (14). Compared with the conventional HWE method, UAE can better improve the extraction efficiency, save operation time, simplify the operation process, and depolymerize polysaccharides to a limited Mw. Based on the combination of artificial neural network and genetic algorithm, Yang et al. derived an optimal condition for ultrasonic extraction of LPs at 120 watts, 12 min and 57°C (15). In addition, Zhong et al. employed ultrasonic technique to extract LPs from dried longan fruit pulp. On the basis of single factor experiment, the optimal extraction conditions for LPs were ultrasonic power of 680 W, extraction time of 4.5 min, and water-to-material ratio of 25 mL/g. At this time, the yield of LPs was 4.455 ± 0.093%, which is in good agreement with the predicted value of 4.469% (16). Notably, UAE led to some changes in the structure and properties of LPs to some extent, depended on the parameters of applied power and operating conditions, so further studies on the UAE of LPs are needed (17).

Ultrahigh pressure (UHP)-assisted extraction

UHP-assisted extraction is an emerging extraction technique developed on the basis of food UHP technology, and modern research has applied it to the extraction of polysaccharides. The UHP-assisted extraction efficiency of LPs was greatly improved due to the rapid pressure changes in a short period of time that accelerated the rupture of cell walls and enhanced the release of intracellular products and the penetration of solvents into cells. Thus, UHP-assisted extraction achieved high yield of the target product with reduced processing time, temperature and energy input, which is efficient, time-saving and environmentally friendly (18). Bai et al. to consider the yield and structure of LPs as well as to facilitate practical extraction, they optimized the conditions of UHP-assisted enzymatic extraction of LPs by RSM and analytical design. The optimized conditions were: water to pretreatment material ratio of 42 mL/g, enzyme to pretreatment material ratio of 1:100, enzymatic digestion time of 1.7 h, and ultra-high pressure of 407 MPa for 6 min, which resulted in a yield of 8.55% of LPs (3). However, scholars have noticed that the yield of water-soluble LPs decreases instead after a period of UHP treatment, which may be due to the excessive depolymerization of the structure of LPs as the holding time increases, and their yield decreases as a result. But it was undeniable that the extraction rate of total polysaccharides from longan fruit pulp was still largely enhanced after UHP-assisted extraction within the suitable conditions (18).

Microwave-assisted extraction

MAE is a combination of microwave and traditional solvent extraction methods that directly converts microwave energy into thermal energy through simultaneous molecularly occurring dual polarization and ionic conduction, allowing the sample to be heated almost immediately, thus extracting bioactive compounds from the material matrix into solution (19). Thus, MAE of polysaccharides has the significant advantage of simultaneously increasing their yield and bioactivity (20). Li et al. used the microwave pretreatment-HWE method to extract LPs. Within the investigated experimental range, they arrived at the optimal extraction process conditions for LPs by single-factor investigation and orthogonal experiments as follows: the microwave pretreatment power was kept at 700 W, the treatment time maintained at 60 s, HWE material-liquid ratio controlled at 1:15, extraction temperature at 100°C, extraction time at 7 h, and stirring speed at 240 r/min, when the yield of LPs can reach 9 mg/g (21). Nevertheless, excessive microwave power and other factors could cause rapid heating of longan fruit pulp cells and then severed water loss, resulting in the destruction of the structure and activity of LPs.

Others

Superfine grinding is an emerging technology that refers to the preparation of ultrafine powders with small solid particles (1 nm−100 mm) and good surface properties, which has the advantages of time saving, solvent saving and energy saving. After the pulp of longan fruit was ultra-micronized, the size of the extracted LPs particles decreased and the surface area increased, and their adsorption and water permeability were enhanced, which eventually led to the better dissolution of LPs in the solvent and the extraction efficiency was effectively enhanced (22). It is worth noting that modern research on the extraction process of LPs focuses on the dynamic balance of yield and activity. All current extraction methods effectively improve the extraction rate of LPs, but the treatments taken during the extraction process (e.g., high temperature, pH, high pressure, ultrasonic and microwave) may lead to changes in the structure of LPs, which in turn may affect their biological activity. Therefore, the research on the extraction methods of LPs needs to be further strengthened.

Purification

As with other plant polysaccharides, crude LPs obtained through the extraction process usually also contain impurities such as proteins, nucleic acids, small molecules and other compounds. Therefore, further purification is required to remove these compounds. According to the literature, the main methods for the deproteinization of plant polysaccharides are the trifluoro-trichloroethane method, the trichloroacetic acid method, the Sevag method, the bio-enzymatic method, and a combination of several methods. Among them, the application of Sevage reagent is considered as one of the most common strategies to remove crude protein from LPs because it can be used repeatedly to remove additional protein residues. However, the Sevag deproteinization method also has disadvantages such as time-consuming, severe loss of LPs, and the organic reagents used tend to cause structural changes of LPs. Moreover, the acid precipitation method can cause degradation of some polysaccharides, so that the yield of LPs is affected. Although the protease method is safe, the enzymatic digestion is usually insufficient and the degree of refinement is low, therefore, researchers usually use a mixture of several methods for better protein removal. Modern studies have also shown that small pigment molecules are often adsorbed by activated carbon; Macroporous resins can effectively remove pigments and proteins from LPs with mild conditions and simple processes, and also help to maintain the activity of LPs; Column chromatography is the most widely applied in the purification of LPs because of its simple operation, good purification performance and a wide variety of purifiable substances; In addition, there are also a few reports on the separation and purification of bioactive polysaccharides by high-speed counter-current chromatography (23).

Usually, LPs obtained by deproteinization and decolorization processes also contain polysaccharide fractions of various properties. Therefore, in order to obtain single polysaccharide fractions with different molecular weights, we need further purification. LPs are macromolecular carbohydrates consisting of aldose or ketose, which are weakly acidic and can be adsorbed by ion exchange with anion exchange resins in neutral solutions, but the application of strong alkaline anion exchange resins is limited because LPs are prone to isomerization or decomposition in a strongly alkaline environment. Thus, the diethyl-aminoethyl (DEAE) cellulose column was invented by taking advantage of the property that the cis-dihydroxy group in polysaccharides can form complex salts with boric acid, and was widely applied in the separation and purification process of LPs. However, this method was mainly used for the primary purification of LPs. Gel chromatography is currently the most commonly applied advanced purification method for LPs, and the commonly used gels are dextran gel G100 (Sephadex G100), agarose gel 4B (Sepharose 4B) and propylated dextran gel S-400 (Sephacryl S-400). In the separation and purification process, the gel column acts as a molecular sieve, allowing LPs of different molecular weights to be separated. For instance, Meng et al. used HWE, alcohol precipitation and deproteinization to extract crude LPs. Then separated by DEAE-cellulose anion exchange and Sephacryl S-300 high-resolution (HR) gel filtration chromatography to obtain a single water-soluble polysaccharide LP1 (24). This suggests that the use of a combination of purification methods is indispensable to obtain LPs with relatively well-defined structures.

Structural features

Basic structures

The structural characteristics of LPs are mainly determined by the Mw, the composition and sequence of monosaccharides, the conformation and position of glycosidic bonds, the type of branched chains and the degree of polymerization. Different polysaccharide compositions and structures influence its biological activity (25, 26). So far, dozens of polysaccharide components have been extracted from longan fruit pulp. After the purification of crude LPs, the basic structural characteristics of LPs are generally studied accordingly by partial acid hydrolysis, periodate oxidation, Smith degradation, gel permeation chromatography, high performance liquid chromatography (HPLC), gas chromatography (GC), Fourier transform infrared spectroscopy (FT-IR), gas chromatography-mass spectrometry (GC-MS) and nuclear magnetic resonance (NMR) spectroscopy. Due to the differences in raw materials, extraction and purification processes and other conditions, the results of various reported studies on the structural characteristics and monosaccharide composition of LPs are diverse. Therefore, to clarify the current research status and better grasp the structural characteristics of LPs, we summarized the structure and some chemical parameters of LPs by classification in Table 1, and mapped the structure of homogeneous LPs with more definite Mw extracted in recent years in Figure 3.

Polysaccharides are monosaccharide polymers linked by glycosidic bonds and contain one or more different monosaccharide units. Most of the LPs reported so far are heteropolysaccharides, which have molecular weights ranging from 8.7 to 4800 kDa and contain roughly 9 different ratios of monosaccharides, namely glucose (Glc), galactose (Gal), arabinose (Ara), rhamnose (Rha), mannose (Man), xylose (Xyl), fucose (Fuc), fructose (Fru) and ribose (Rib), and possibly glucuronic acid (GlcA) and galacturonic acid (GalA) as well (43). Their specific structural information is mentioned in some literature. For example, Zhu et al. extracted a water-soluble LP from longan fruit pulp and obtained a pure polysaccharide with a calculated molecular weight of

TABLE 1 The extraction, purification, and structural characterization of polysaccharides from the longan fruit pulp.

No.	Component name	Extraction method	Purification method	Monosaccharide composition	Mw (Da)	Structures features	Structure-activity relationship	References
1	LPS1	Hot water	Gel filtration and anion-exchange chromatography	Glc (Consists of 661 glucose residues)	1.08×10^5	(1→6)-α-*D*-glucan	Immunomodulatory and anti-cancer	(27)
2	LP-H	Hot water	Sevage	Rha:Ara:Man:Glc:Gal = 1.2:4.6:1:3:2.2	2.38×10^5	Mainly consisted of →3)-α-*L*-Ara*f*-(1→, →3,6)-β-*D*-Gal*p*-(1→, α-*L*-Rha*p*-(1→, →4)-β-*D*-Glc*p*-(1→	Prebiotic	(22)
3	LP-S	Superfine grinding		Rha:Ara:Man:Glc:Gal = 1.2:4.9:1:2.1:4	2.28×10^5	Mainly consisted of →3)-α-*L*-Ara*f*-(1→, →3,6)-β-*D*-Gal*p*-(1→, α-*L*-Rha*p*-(1→, →4)-β-*D*-Gal*p*-(1→	Prebiotic	
4	LP-SE	Superfine grinding-assisted enzymatic		Rha:Ara:Man:Glc:Gal = 1.1:4.3:1:1.5:2.8	1.90×10^5	Mainly consisted of →3)-α-*L*-Ara*f*-(1→, →3,6)-β-*D*-Gal*p*-(1→, α-*L*-Rha*p*-(1→, →5)-α-*L*-Ara*f*-(1→	With better prebiotic	
5	LP-UE	Ultra-high pressure-assisted enzyme	Sevage	Rha:Ara:Xyl:Man:Glc:Gal = 5.8:40.8:1:2.3:32.5:26.7	2.91×10^5	β-type glycosidic bond	Moderate acetylcholinesterase inhibitory	(3)
6	LP-H	Hot water		Rha:Ara:Xyl:Man:Glc:Gal = 1.1:11.9:1:1.6:12.2:11.1	1.19×10^5		Slight acetylcholinesterase inhibitory	
7	LP-U	Ultra-high pressure		Rha:Ara:Xyl:Man:Glc:Gal = 1.2:11.7:1.2:1:10:12.4	1.32×10^5			
8	LP-E	Enzymatic method		Rha:Ara:Xyl:Man:Glc:Gal = 5.9:46.2:1:6:22.2:33.7	3.18×10^5			
9	LP	Unfermented, hot water	Sevage	Rha:Ara:Xyl:Man:Glc:Gal = 5.7:28.5:1:1.5:15.3:13.3	2.22×10^5	Mainly consisted of α-type and β-type glycosidic bond	Immunomodulatory and prebiotic	(28)
10	LP-F	After fermentation, hot water	Sevage	Rha:Ara:Xyl:Man:Glc:Gal = 5.1:26.5:1:1.8:7.8:12.4	1.11×10^5		Stronger immunomodulatory and prebiotic	
11	LPs	Water extraction, alcohol precipitation	Gel filtration chromatography	Man:Rib:Rha:GlcA:GalA:Glu:Gal = 4:1.25:3.75:3:1:25:5.25	$(2.13–7.07)\times10^3$	N/A	Immunostimulatory and free radical scavenging	(29)

(Continued)

10.3389/fnut.2022.914679

TABLE 1 Continued

No.	Component name	Extraction method	Purification method	Monosaccharide composition	Mw (Da)	Structures features	Structure-activity relationship	References
12	MLPs	Water extraction, alcohol precipitation	Gel filtration chromatography	Man:Rib:Rha:GlcA:GalA:Glu:Gal = 19:1:17:13:3:100:24	2.78 × 10^4-1.00 × 10^6	Possess more branched structures	Stronger free radical scavenging abilities and immune-stimulating effects, but weaker growth-inhibitory activities against cancer cells	
13	LP1	Hot water	Sevage, chromatography of DEAE-cellulose and Sephadex G-100	N/A	1.23×10^3	N/A	Immunomodulatory and anti-tumor	(30)
14	LP1-S	Hot water	Sevage, chromatography of DEAE-cellulose and Sephadex G-100	N/A	1.05×10^5	N/A	Immunomodulatory and stronger anti-tumor	
15	LPIIa	Ultrahigh pressure-assisted enzymatic	HiPrep 26/60 Sephacryl S-300 HR column	Rib:Ara:Xyl:Glc:Gal = 1.05:1:22.88:1.01:2.59:34.58	1.59×10^5	The backbone consisted of (1→3,4)-α-Rha*p*, (1→4)-β-Gal*p*, (1→6)-β-Gal*p*, (1→3,6)-β-Gal*p*, with branches at the O-4 of Rha and O-3 of Gal, consisting of side chains of α-Ara*f*, β-Gal*p*, and α-Glc*p*	Anti-inflammatory and protective intestinal barrier function	(31)
16	LP3	After extraction with distilled water, cellulase enzymolysis and ultrasonic cell disintegration were used.	Anion exchange resin D301-F	Rib:Rha:Ara:Xyl:Man:Glc:Gal = 4.85:1.06:14.55:1.00:28.36:70.89:8.58	N/A	N/A	Strong immunoregulatory	(32)
17	LPP	N/A	Sephadex G-100 gel column and gel filtration chromatogram	N/A	3.75×10^4	N/A	The combination of FITC pre-labeling and HPSEC-FD makes the quantitative determination of LPP possible in mouse plasma, spleen and lung samples	(33)

(Continued)

10.3389/fnut.2022.914679

TABLE 1 Continued

No.	Component name	Extraction method	Purification method	Monosaccharide composition	Mw (Da)	Structures features	Structure-activity relationship	References
18	LPPF	N/A	Sephadex G-100 gel column and gel filtration chromatography	N/A	3.9×10^4	N/A		
19	LPI	N/A	DEAE-cellulose anion-exchange chromatography	Rib:Rha:Ara:Xyl:Man:Glc:Gal = 0.57:0.01:1.00:0.20:9.64:21.84:0.73	1.459×10^4	Mainly consisted of (1→6)-*α*-*D*-Glc*p*, (1→5)-*α*-*L*-Ara*f* and (1→4)-*β*-*D*-Man*p*	Except for LPI, the other three significantly stimulated lymphocyte proliferation in the dose range of 100–400 μg/mL and their stimulations on normal/LPS-induced proliferation and depressions on ConA-Induced proliferation could be ordered as LPIII > LPIV > LPII > LPI. All the fractions had the optimal dose of 100 μg/mL on enhancing macrophage phagocytosis. Among them, LPII had the considerable yield and activity for exploiting as a potential immunoadjuvant	(34)
20	LPII			Rib:Rha:Ara:Xyl:Man:Glc:Gal = 1.00:0.22:3.00:0.21:5.85:14.62:1.77	6.834×10^4	Mainly consisted of (1→6)-*α*-*D*-Glc*p*, (1→5)-*α*-*D*-Ara*f* and *β*-*D*-Gal*p*		
21	LPIII			Rib:Rha:Ara:Xyl:Man:Glc:Gal = 1.00:3.21:4.70:0.56:0.41:0.66:2.18	1.074×10^5	Mainly consisted of (1→4)-*β*-*D*-Rha*p* and (1→5)-*α*-*L*-Dra*f*		
22	LPIV			Rib:Rha:Ara:Xyl:Man:Glc:Gal = 7.52:7.58:7.69:7.82:9.59:9.70:9.91	5.282×10^6	N/A		

(Continued)

10.3389/fnut.2022.914679

TABLE 1 Continued

No.	Component name	Extraction method	Purification method	Monosaccharide composition	Mw (Da)	Structures features	Structure-activity relationship	References
23	LPD2	Hot water	Weak anion exchanger	Ara:Ma:Glc:Gal = 0.25:0.49:1:0.5	9.64×10^6	The main linkages of the sugar residues were (1→4)-β-Glc and (1→6)-β-Man	Significantly enhanced the lymphocytes proliferation, phagocytosis and NO and IL-6 secretion by macrophage	(35)
24	LPIa	Hot water	Sevage, DEAE-Sepharose Fast Flow chromatography and HiPrep 26/60 Sephacryl S-300 HR chromatography	Rha:Rib:Fuc:Ara:Xyl:Man:Glc:Gal = 0.99:1.37:34.61:1.48:1.73:5.86:55.16	1.47×10^5	Mainly consisted of →3)-α-Ara$f$-(1→, →3,6)-β-Gal$p$-(1→, α-Ara$f$-(1→ and →5)-α-Ara$f$-(1→	Both LPIa and LPIIa have higher intestinal barrier protection and immunoregulatory activities than LPIIIa and LPIVa	(36)
25	LPIIa			Rha:Rib:Ara:Xyl:Glc:Gal = 1.05:1.00:22.88:1.01:2.59:34.58	1.593×10^5	Mainly consisted of →3)-α-Ara$f$-(1→, →3,6)-β-Gal$p$-(1→, α-Ara$f$-(1→ and →5)-α-Ara$f$-(1→		
26	LPIIIa			Rha:Rib:Fuc:Ara:Man:Glc:Gal = 14.46:1.85:2.31:46.17:1.00:1.97:20.99	1.94×10^4	Mainly consisted of →3)-α-Ara$f$-(1→, →3,6)-β-Gal$p$-(1→, →3)-β-Gal$p$A-(1→ and α-Rha$p$-(1→		
27	LPIVa			Rha:Rib:Ara:Man:Glc:Gal = 4.71:0.38:25.03:1.00:2.53:15.50	4.4×10^4	Mainly consisted of →3)-α-Ara$f$-(1→, →3,6)-β-Gal$p$-(1→, →3)-β-Gal$p$A-(1→ and α-Rha$p$-(1→		
28	LPPMs	Alkali-extraction and acid-precipitation	N/A	N/A	N/A	N/A	Anti-oxidation, anti-tumor and immune stimulation activity were enhanced	(37)
29	LP1			Rib:Rha:Ara:Xyl:Man:Glc:Gal = 6.1:4.9:52.2:1:11.1:72.2:20.3		N/A	The immunoregulatory activity was weaker than that of LP2 and LP3	(38)
30	LP2	Ultrasound-assisted enzymatic method	Gel column chromatograms	Rib:Rha:Ara:Xyl:Man:Glc:Gal = 2:1:16.7:23.7:57.2:114.3:2.2	$>10^5$	Mainly composed of glucosyl residues in the α-pyranose form	Immunoregulatory activity	
31	LP3			Rib:Rha:Ara:Xyl:Man:Glc:Gal = 11.7:1:33.3:4.7:213.3:472:13.3			Immunoregulatory activity	

(Continued)

10.3389/fnut.2022.914679

TABLE 1 Continued

No.	Component name	Extraction method	Purification method	Monosaccharide composition	Mw (Da)	Structures features	Structure-activity relationship	References
32	LP1	Hot water extraction and alcohol precipitation	DEAE-cellulose anion-exchange and Sephacryl S-300 HR gel chromatography	Glc:GalA:Ara:Gal = 5.39:1.04:0.74:0.21	1.16×10^2	Consisted of a backbone of→4)-α-*D*-Glc*p*-(1→4)-α-*D*-Gal*p*A-(1→4)-α-*D*-Glc*p*-(1→4)-β-*D*-Glc*p*-(1→ units with poly saccharide side chains composed of →2)-β-*D*-Fru*f*-(1→2)-*L*-sorbose-(1→ attached to the O-6 position of the α-*D*-Glc*p* residues	Natural anti-tumor agent with immunomodulatory activity	(24)
33	LPIIa	Hot water	Ion exchange chromatography, gel filtration chromatography	Glc:Ara:Man:Gal = 7.55:1.45:1.22:1.00	4.47×10^4	Mainly composed of→6)-Glc-(1→, →5)-Ara-(1→, →4)-Man-(1→ and →6)-Gal-(1→	Strong immunoregulatory	(39)
34	LPS-N	Hot water-assisted microwave pretreatment and ethanol precipitation method	DEAE- Cellulose anion exchange chromatography	Xyl:Glc = 1:1.9	1.38×10^4	Belong to β-type heteropolysaccharide with pyran group	N/A	(40)
35	LPS-A1			Rha:Xyl:Ara:Gal = 1:1.64:4.33:2.28	1.382×10^3			
36	LPS-A2			Only Rha	5.71×10^5			
37	LWP	Longan juice ferments	Ultrafiltration	Glc:Man:Gal:Ara:GalA: GlcA = 167.72:3.38:3.13:3.46:2.33:1	$(1–3)\times 10^4$	Mainly composed of β-type	Hypoglycemic activity and free radical scavenging	(41)
38	LPsx	Hot water extraction and alcohol Precipitation	HPGPC system coupled with Ultrahydragel columns 500 and 250 gel columns at 60°C	Glu:Ara:Gal:Man:Xyl = 95.9:2.1:1.0:0.6:0.4	4.102×10^3	Mainly composed of (1→6)-α-*D*-Glu and (1→6)-β-*D*-Glu, branched with α-*D*-Glu-(1→	The immunomodulatory activity study showed that LPsx significantly increased the phagocytosis of macrophages, and strongly promoted the production of NO, IL-1β, IL-6 and TNF-α. Moreover, LPsx could inhibit the inflammatory response induced by lipopolysaccharide.	(42)

10.3389/fnut.2022.914679

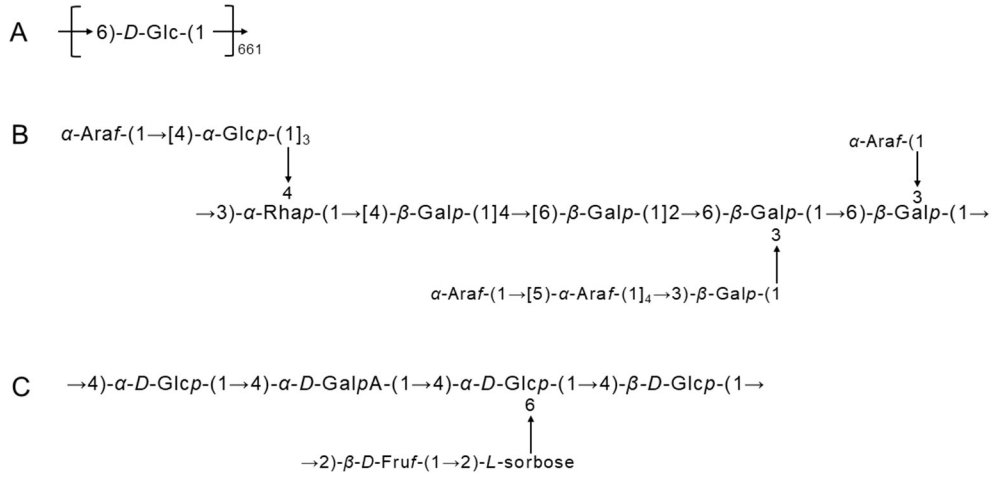

FIGURE 3
The structures of longan pulp polysaccharides. **(A)** LPS1, **(B)** LPIIa, and **(C)** LP1.

108 kDa and 661 glc residues by column purification, and named LPS1 (Figure 3A). Chromatographic analysis showed that LPS1 is a high polysaccharide of glc with a glycosidic bond of →6)-*D*-Glc-(1→; NMR spectroscopy pointed that the configuration of the anomeric carbon in the glc residue is α-type; C6 chemical shift further confirmed that the structure of LPS1 is (1→6)-α-*D*-glucan (27). Bai et al. purified four acidic polysaccharides from LPs, named LPIa, LPIIa, LPIIIa and LPIVa, whose average molecular weights and polysaccharide compositions can be seen in Table 1. The structural resolution of LPIa indicated that LPIa has a higher Mw and, in particular, contains two other specific glycosidic bonds →5)-α-Ara*f*-(1→ and α-Ara*f*-(1→, as well as a complex reticulated surface structure. These may be the main reason for the better biological activity of LPIa than the other three LPs (36). Notably, they also elaborated the detailed structure of LPIIa, in which there are branches at Gal-O-3 and Rha-O-4, and the branches consist of side chains of α-Glc*p*, α-Ara*f* and β-Gal*p* (Figure 3B) (31). In addition, a new water-soluble polysaccharide (LP1) was successfully purified from longan fruit pulp by DEAE-cellulose anion exchange and S-300 HR gel chromatography. The chemical structure was determined by IR, GC and NMR analysis (Table 1) and its detailed structure was mapped (Figure 3C) (24). After purification of LPs by DEAE-cellulose anion-exchange chromatography, Yi et al. obtained 4 fractions of crude LPs, including 1 neutral polysaccharide (LPI) and 3 acidic polysaccharides (LPII-IV), each with different monosaccharide composition, Mw and structural characteristics. The solution properties of the 4 fractions were analyzed by size exclusion chromatography combined with laser scattering (SEC-LLS), viscometry measurement, Congo red complex formation and atomic force microscopy. The study showed that LPI has both a spherical conformation and a triple helix structure, while LPII-IV exists in the form of flexible chains (34). The corresponding structural analysis is shown in Table 1.

Meanwhile, it has been demonstrated that the different structures of LPs largely depend on the different methods of extraction and purification (44). For example, Huang et al. extracted LPs by hot water, superfine grinding and superfine grinding-assisted enzymatic treatment, and obtained LP-H, LP-S and LP-SE, respectively. Compared with LP-H and LP-S, although the Mw, apparent viscosity, particle size and glucose content of LP-SE decreased to a certain extent, the yield, solubility, sugar content, arabinose and mannose content of LPs were increased. All three LPs contained similar glycosidic bonds of α-*L*-Rha*p*-(1→, →3)-α-*L*-Ara*f*-(1→ and →3,6)-β-*D*-Gal*p*-(1→, while each of them had a specific glycosidic bond of →4)-β-*D*-Glc*p*-(1→, →4)-β-*D*-Gal*p*-(1→ and →5)-α-*L*-Ara*f*-(1→, respectively (22). Besides, there are many other relevant examples. We summarized all the structures of LPs reported in Table 1. These studies will provide a theoretical basis for the functional development and potential utilization of LPs.

Structural modifications

LPs as natural plant polysaccharides have many excellent bioactivities, and the expression of these bioactivities is closely related to their structures. To further improve the physicochemical properties and bioactivities of LPs and enhance the application properties of LPs, researchers have carried out structural modifications of LPs. Commonly, various physical, chemical and biological means are used to modify the structure of LPs (45). It has been suggested that the biological activities of LPs, such as immunomodulatory, anti-viral, anti-inflammatory and anti-tumor, were enhanced after structural modification

TABLE 2 The modification approaches, containing reaction conditions, reaction principles and typical structures of modification products for different structural modifications.

No.	Structural modification method	Specific reaction and reaction principle	Reaction conditions/specific reaction methods	Determination of the degree of modification	Typical structures of the modification products (specific features of the structures and biological activities can be found in Table 1)	References
1	Sulfated modification	Concentrated sulfuric acid method - using the principle of sulfuric acid esterification reaction, concentrated sulfuric acid de-hydroxylation, alcohol de-hydrogenation in polysaccharides for the reaction, the introduction of sulfuric acid groups in polysaccharides, its reversible reaction.	Briefly, the mixture of concentrated sulfuric acid and butanol complex (3:1) was prepared in ice bath. Then, 125 mg ammonium sulfate was added and stirred for 10 min at temperature 0 °C (ice-water bath). LP1 (500 mg) was then dripped in slowly. The reaction mixture was stirred for 3 h at 10°C and was then neutralized with sodium hydroxide solution and precipitated with 95% ethanol. The sediment was redissolved with water, followed by dialysis, and freeze-dried.	Barium sulfate turbidimetry method	LP1-S、LYRP4	(30, 47)
2	Carboxymethylated modification	Sodium hydroxide-monochloroacetic acid (MCA) method - Introduction of carboxymethyl group on the -OH of polysaccharide by this substitution reaction system.	Dissolve LPs in alkaline solution, add a certain concentration of monochloroacetic acid (MCA), react for a period of time at a specific temperature, then dialyze the reaction solution after adjusting it to neutral, and the solution is concentrated, alcoholic precipitation, and vacuum dried.	UV spectrophotometry	CM-LYP、CM-LYP2	(48, 49)
3	Enzymatic modification	Enzymatic reaction -Certain structures can be recognized for catalytic degradation/cleavage.	Firstly, the appropriate enzyme was selected and its optimal reaction temperature and pH were determined; then a certain amount of longan fruit pulp was reacted in the vessel for a period of time and the treated sample was heated in a 90°C water bath for 3 min immediately after the reaction to stop the enzyme reaction. Finally, extraction or collection was performed.	The content of water-soluble polysaccharides was determined using the phenol-sulfuric acid colorimetry (Glucose was used as the standard). The content of soluble pectin was determined by the spectrophotometry method.	Fructo-oligosaccharides (Fos) such as 1-kestose and nystose	(50)

(Continued)

10.3389/fnut.2022.914679

TABLE 2 Continued

No.	Structural modification method	Specific reaction and reaction principle	Reaction conditions/specific reaction methods	Determination of the degree of modification	Typical structures of the modification products (specific features of the structures and biological activities can be found in Table 1)	References
				Quantitative analysis of ethanol-soluble sugars using HPLC. Determination of reducing sugars by UV spectrophotometry.		
4	Maillard reaction modification	Carbonyl ammonia reaction - based on the reduction between the carbonyl group of the sugar and the amino group of the amino compound.	LPs and amino acids were dissolved together in 100 mL NaOH solution (pH 9.0) to the final concentration of 2.5 mg/mL. Ten milliliters of the solution were added into a 25 mL penicillin bottle and sealed. The bottles were placed in a 100°C water bath for 1–6 h, and then transferred to an ice-water bath to end the MR between LPs and amino acids.	The browning degree was determined by the 420 nm absorbance; the Mw distribution was analyzed by a high-performance size exclusion chromatography (HPSEC) method.	MLPs (LPs-Lys)	(29, 37)
5	Microbial fermentation modification	Enzymatic reactions - Lactic acid bacteria or other microorganisms can affect polysaccharide composition by secreting different carbohydrate enzymes. These enzymes can degrade the insoluble pectocellulosic cell wall of fruit into soluble polysaccharides, resulting in increased yield of water-soluble polysaccharides as well as changes to Mw and monosaccharide composition of the extracted polysaccharides.	Fermentation experiments were conducted in aluminum foil sealed Erlenmeyer flasks, each containing 100 mL of pasteurized longan juice without any supplementary nutrients. Inoculum (1 mL) containing 7.0 log cfu/mL of activated *Lactobacillus fermentum* was added to each of the Erlenmeyer flasks. Fermentation was then allowed to proceed at 37 °C for 72 h. Samples were taken at 0, 6, 12, 24, 48 and 72 h for viable cell count, pH, and polysaccharides extraction.	Neutral polysaccharide content was determined using the phenol-sulfuric acid method (Glucose was used as the standard). Protein concentration was determined using the Bradford assay with a bovine serum albumin standard curve.	LP-F (*Lactobacillus fermentum*)	(28, 41)

(Continued)

10.3389/fnut.2022.914679

TABLE 2 Continued

No.	Structural modification method	Specific reaction and reaction principle	Reaction conditions/specific reaction methods	Determination of the degree of modification	Typical structures of the modification products (specific features of the structures and biological activities can be found in Table 1)	References
				Uronic acid content was determined using a modified m-hydroxydiphenyl method with galacturonic acid standards. The monosaccharide composition was determined using (GC-MS).		
6 Others	Alkali dissociation	Depolymerization reaction - sodium hydroxide could depolymerize polysaccharides with compact and high-organized conformation, to obtain its derivatives. Their activity could be enhanced by increasing chain stiffness	50 mg LPI was dissolved in 50 mL distilled water, then 50 mL of NaOH solution was added and the pH was neutralized with 5 mol/L hydrochloric acid solution after alkaline dissociation at room temperature for 10 min. The mixture was dialyzed, concentrated and lyophilized.	The molecular conformations were examined by size exclusion chromatography combined with multi-angle laser light scattering (SEC-MALLS), Congo red test and atomic force microscopy (AFM).	LPI1 and LPI2	(51)
	Phosphorylation modification	Esterification reaction - Phosphorylation modification of LPs using POCl3 (phosphorus oxychloride) as an esterifying agent	The dissolved LPs solution was slowly added to the $POCl_3$-pyridine mixture for 60 min (kept in a reaction bath at 0°C or in an ice-water mixture environment), and at the end of the reaction, the appropriate amount of sodium hydroxide solution was added to adjust to neutral. Finally, dialysis, alcohol precipitation and drying under reduced pressure were performed.	Phosphomolybdate blue spectrophotometric determination	LYP2-P	(52)

(Continued)

10.3389/fnut.2022.914679

TABLE 2 Continued

No.	Structural modification method	Specific reaction and reaction principle	Reaction conditions/specific reaction methods	Determination of the degree of modification	Typical structures of the modification products (specific features of the structures and biological activities can be found in Table 1)	References
	Acetylation modification	Acetic anhydride method - Acetylation modification is the addition of acetyl groups to the branched chains of polysaccharides, so that the branched chains of polysaccharides are fully unfolded, exposing more sugar hydroxyl or carboxyl groups inherent in the sugar, thus improving its water solubility and more conducive to activity	The pH of the reaction system was always maintained in the range of 8.0–10.0 by adding sodium hydroxide solution and acetic anhydride alternately under certain temperature conditions until the acetic anhydride was added, and the reaction was adjusted to neutral with hydrochloric acid solution after stirring for a period of time. Finally, dialysis, concentration, alcohol precipitation and freeze-drying were performed.	Hydroxylamine colorimetric assay	Ac-LYP2	(53)

(46). Therefore, structural modifications based on activity optimization are particularly significant for the study of LPs (29). The existing structural modification methods of LPs were classified and summarized as follows, specific details can be found in Table 2.

Sulfated modification

Among the chemical modification methods, sulfation is widely used in molecular modification of polysaccharides (54), because it not only increases the solubility of polysaccharides, but also provides and creates new physiological functions. Specifically, the principle is to add sulfuric acid groups to the sugar groups of polysaccharides to change the structure of polysaccharides, thus increasing their biological activities, such as immunomodulatory (55), anti-tumor (56), anti-oxidant (57), hypoglycemic (58) and anti-viral (54) activities. After sulfation modification, the chemical composition, Mw and monosaccharide composition of LPs were changed, and the activities of anti-glycosylation and anti-coagulant were also significantly enhanced (59). The sulfated derivative of LPs (LP1-S) was prepared by sulfation by Jiang et al., and the degree of substitution (DS) was determined to be 2.011. Two characteristic absorption bands (1223 and 640 cm^{-1}) appeared in FT-IR spectrum of LP1-S, indicating that the sulfation reaction did take place, the structural characteristics are shown in Table 1. Preliminary in *vitro* experiments demonstrated that LP1-S exhibits higher anti-proliferative activity than LP1 against human nasopharyngeal carcinoma (HONE1) cells, which may be due to the sulfate moiety in its structure. Therefore, these results suggested that LP1-S may be more useful than LP1 for the development of safe antitumor drugs or health foods (30). In addition, several studies have shown that the biological activity of sulfated LPs is mainly reflected in the sulfate groups. The number and location of the sulfate groups were different, and the biological activities were also different. Generally, the higher the degree of sulfation, the stronger the biological activity, which affects the degree of sulfation substitution. Huang et al. experimentally determined that the factors affecting the degree of sulfation substitution are: reaction time > reaction temperature > amount of reagent addition (47). The modification of LPs by sulfation aimed to produce sulfated LPs with low cost, high product volume and high biological activity (60).

Carboxymethylated modification

Carboxymethylation refers to the introduction of carboxymethyl groups on the branched chains of polysaccharides (61). Studies have shown that the introduction of carboxymethyl groups enhances the water solubility of LPs, and even the degree of substitution (DS) of carboxymethylation is proportional to its water solubility, which is one of the key

factors to promote its active role (62). Wei et al. used RSM to optimize the preparation process of carboxymethylated LPs (CM-LYP). The response surface analysis was performed by single-factor test on the concentration of monochloroacetic acid (MCA), reaction temperature and reaction time with the degree of carboxymethyl substitution as a measure, and a regression model between the degree of carboxymethyl substitution and each influencing factor was established. They finally obtained the optimal process conditions for the preparation of CM-LYP as MCA concentration of 1.2 mol/L, reaction temperature of 73°C, and reaction time of 3.2 h, at which the carboxymethyl substitution degree of LPs was as high as 1.053. Meanwhile, the results of antioxidant activity experiments pointed out that at the same dose concentration (3200 μg/mL), the scavenging rate of hydroxyl radicals and superoxide anion radicals as well as the inhibition of lipid peroxidation and H_2O_2-induced erythrocyte hemolysis were stronger with CM-LYP than with LYP before modification. The results of *in vivo* immunoreactivity assay also pointed out that CM-LYP has better immunoreactivity than LYP in terms of increasing spleen index, promoting serum hemolysin formation, and increasing lysozyme content in serum and spleen of immunosuppressed mice. This indicated to some extent that the introduction of carboxymethyl is beneficial to improve the immunomodulatory and antioxidant activities of LYP (49).

Enzymatic modification

We stated earlier that enzyme technology can be used to assist in the extraction of LPs, and in addition to that, enzymes can also be used to modify the structure of LPs. Compared with chemical modifications, enzymatic modification has the advantages of high specificity and high efficiency. After modification by enzymatic degradation, the Mw of LPs was reduced, their relative molecular masses were relatively uniform, and the process had little effect on the backbone of LPs (63). The aim of enzymatic modification was to utilize the specificity and selectivity of enzymes to specifically modify the structure of LPs to make better produce biopolymers with ameliorative mechanical and/or biological functional properties (64). Modern research has found that polysaccharides, when present in the form of oligosaccharides (defined as compounds containing 2–10 glycosidic bonds polymerized), act as prebiotics. Consuming these oligosaccharides can be used to modulate the intestinal microbiota, helping to create a healthy intestinal ecology and improve mineral absorption in the colon. Cheng et al. used a commercial enzyme, Viscozyme L, from *Aspergillus aculeatus*, a mixture containing pectinase, glucanase, cellulase and Fructo-furanosidase (FFase), in juicing longan fruit pulp. The purpose of using it was to increase the juice yield and clarity based on pectinase, glucanase and cellulase, and then converted the sucrose in it to Fructo-oligosaccharide by transfructosylation of FFase. They determined the content of water-soluble LPs on the basis of colorimetric method using phenol-sulfuric acid colorimetric method. The experimental results showed that the content of water-soluble LPs such as pectin increased significantly after enzyme treatment, while the sucrose content decreased significantly, and at the same time, a lot of fructo-oligosaccharides, including 1-kestose and nystose, were synthesized. In addition, the results of High-Performance Gel Permeation Chromatography (GPS) experiments showed that the content of fraction 1, representing the largest size of LPs, was significantly decreased after enzyme treatment, while the content of smaller size fractions 3 and 5 was increased, indicating that large polysaccharides could be hydrolyzed into small molecules by enzymatic digestion. Afterwards, they investigated the *in vitro* stimulation of *Lactobacillus* by LPs obtained before and after enzyme treatment. The experimental results pointed out that the stimulation of *Streptococcus thermophilus*, *Lactobacillus acidophilus* and *Lactobacillus delbrueckii* reference strains by LPs and Fos in longan juice was significantly improved after enzyme treatment (65). In conclusion, the content and molecular size distribution of LPs in longan juice changed significantly after enzyme treatment, implying that enzymes modify the structure of LPs and thus affect the expression of their biological activities. These showed the good potential of enzyme-treated LPs as functional foods, nutraceuticals and dietary prebiotics (50).

Maillard reaction modification

Maillard reaction (MR) is based on the carbonyl ammonia reaction between the carbonyl group of reducing sugar and the amino group of amino compounds (66), which involves a series of reactions such as condensation, degradation, cracking and polymerization (67), ultimately producing complex compounds such as ketones, pyrans and pyridines (68). MR also known as "non-enzymatic browning reaction," is a natural, non-toxic and widely available non-enzymatic browning in the food industry that allows effective macromolecular modification under mild and safe conditions and without additional chemicals (29, 69). Modern studies have shown that some amino acids, such as lysine (Lys), proline (Pro) or glycine (Gly), among others, are present in the samples obtained after the extraction and purification of LPs. Under certain conditions, they might form an MR system with LPs, whereby trigger MR (37). The changes in browning degree and Mw distribution can indicate the binding state of LPs and amino acids (70). For example, Yi et al. found that the reaction of LPs and Lys at pH = 9 and T = 100 °C for 4 h resulted in MR, which could yield the product MLPs. There were significant differences in the physicochemical properties of MLPs compared to unreacted LPs. This was demonstrated by the significantly higher browning of the MLPs and the fact that 6% of the LPs had a component Mw >7.07 kDa, while 45% of the MLPs had a component Mw >264.1 kDa. Then they also investigated the chemical

composition and structural characteristics of MLPs and found that the formation of MLPs from LPs and Lys by MR may be due to the fact that the tight conformation of LPs dissociates in alkaline and high temperature environments and the lysine molecule binds to the carbonyl group of LPs mainly through a free amino group (29). In addition, the results of bioactivity studies showed that MLPs have stronger free radical scavenging and immunostimulatory effects on macrophages compared to LPs, but weaker growth inhibition of cancer cells. These changes are related to lysine modifications and moreover to complex conformational relationships.

Secondly, MR between LPs and proteins is also a major feature of MR modification. The structural features of LPs-protein complexes can be monitored by measuring their free amino content, ultraviolet-visible spectrum (UV-Vis), FT-IR and Mw distribution to determine whether a MR occurs between LPs and proteins (71). Furthermore, *In vitro* activity evaluation showed that dry-heat-induced MR effectively enhances the anti-oxidant, anti-tumor and immune-stimulating activities of LPs (72). Meanwhile, the LPs-protein polymers formed by MR usually exhibit better properties, such as emulsification, thermal stability and solubility, than pure proteins or simple mixtures of protein-LPs. Actually, substances containing polysaccharides and proteins can undergo MR under heating conditions, which can be used for further processing and storage of these substances. Longan fruit pulp contains a large number of polysaccharides and protein, and it has a short storage period due to its high perishability and susceptibility to post-harvest diseases (73). Therefore, the methods of heating and drying are often utilized to store longan fruit pulp. During the heat process, there is a MR (also known as glycosylation reaction) between longan fruit pulp protein and LPs (74). LPs are linked to protein through the covalent bond between the free amino group of amino acids (mainly lysine and arginine) and the carbonyl groups of LPs (69). Therefore, the LP-protein Maillard modification is a good method to promote the biological activity of LPs and better storage of longan fruit pulp, but the relationship between its effect and the reaction stage remains to be further studied (37).

In conclusion, the MR reaction not only promoted changes in the primary structure of LPs but also triggered a series of changes in their higher-level structures, and these changes proved that MR is a promising method for modifying natural polysaccharides to obtain better biological properties. Therefore, MR-based probing of the effects of binding amino compounds on the structure and bioactivity of LPs can help to understand the structure-activity relationship of LPs (69).

Microbial fermentation modification

Chemical modification can change the structure of LPs by introducing substituents to affect their biological activities. However, chemical modification generally requires the use of organic solvents, strong acids or strong bases, which to some extent limits its application in practical production. Simultaneously, other modification methods, such as microbial biotransformation and enzyme modification, have attracted more and more attention due to their advantages of high efficiency, high specificity and products containing less harmful substances. Notably, fermentation using Lactic acid bacteria is an important fruit and vegetable processing technique that has been reused in recent years because of its ability to maintain and/or enhance the safety, nutrition, sensory and shelf-life characteristics of fruits and vegetables (75, 76). Recently, researches have applied fermentation technology to the structural modification of plant polysaccharides to make better physicochemical properties and biological activity of polysaccharides (77, 78). For example, Huang et al. applied *Lactobacillus fermentum* without producing extracellular polysaccharides to ferment longan fruit pulp juice at 37°C for 24 h, and then extracted LPs with hot water. The LPs isolated from unfermented and fermented longan fruit pulp juice were named as LP and LP-F. After structure analysis, it was found that LP-F has lower Mw, and contains less Glc, neutral sugar and uronic acid, but contains more Gal, Man, Ara and Rha. This revealed to some extent that LP and LP-F have some structural differences (28). In addition, they compared the physicochemical and prebiotics properties of LP-F extracted at different fermentation times and found that at different fermentation time points, the yield of LP-F, monosaccharide composition, Mw, content of neutral sugar and uronic acid changed obviously. The structural characteristics are shown in Table 1. After fermented by lactic acid bacteria, the structures of LPs were modified by lactic acid bacteria, and the prebiotic activity was improved accordingly. Among the tested fermented LPs, LP-12 showed the strongest prebiotic activity (41). The results of the fermentation experiments also showed that LPs are fermented by the intestinal microbiota after entering the human body for 48 h. The LP-F fermentation cultures contained higher levels of total short-chain fatty acids (SCFAs) and acetic acid, followed by higher numbers of *Enterococcus*, *Bifidobacterium* and *Clostridium* than LP fermentation cultures, but LP-F fermentation cultures showed lower pH and lower carbohydrate percentages than LP. Thus, LP-F was more susceptible to fermentation by the human intestinal microbiota than LP. This effect might also be attributed to the special chemical properties and structure of LP-F, including good solubility, low apparent viscosity, particle size, Mw, and different composition of monosaccharides (79).

Others

In addition to the structural modification methods above, there was some other methods also involved in some literatures. For example, alkali dissociation was one of the traditional methods to prepare modified LPs. In the study, longan

fruit pulp polysaccharides (LPI) were treated with sodium hydroxide, the alkali solution first cleaved the glycosidic bond of LPI, and degraded LPI into fragments with low Mw. Thus, alkali dissociation depolymerized LPI with tight and high tissue conformation to obtain its derivatives whose solubility and biological activity were strengthened (51). Similar to sulfation modification, phosphorylation modification involved the introduction of phosphate groups into LPs. After modification, the stability of LPs was improved and the antigenic properties of LPs in the body could be maintained. Studies had shown that longan fruit pulp polysaccharide (LYP2) is phosphorylated and modified. Phosphorylated-LYP2 had a triple helix structure, and the triple helix structure was a characteristic structure of polysaccharides with anti-tumor activity (52). There was also a small amount of literature mentioning acetylated modified LPs (53). In short, molecular modification changed the size structure, Mw, and the type, number and position of substituents of LPs, thereby affecting its biological activity.

Biological activities

It has been documented that both natural and modified polysaccharides usually exhibit a variety of biological activities. The Mw and chemical structure of polysaccharides are two main factors that determine the biological activities. Modern pharmacological activity studies have shown that LPs have immunomodulatory, anti-tumor, anti-oxidation, anti-glycosylation and hepatoprotective activities. Generally, diversified extraction and purification technologies, unequal treatment and application methods and different research techniques will affect the biological activities of LPs. Biological activity testing and research of LPs are mainly based on longan fruit pulp crude polysaccharides, which also brings obstacles to prove the exact active substances. Therefore, to promote the product development and functional application of LPs, we systematically reviewed the biological activities of LPs to provide a comprehensive reference for the basic research of LPs.

Immunoregulatory activity

Immunomodulatory activity is considered to be one of the important strategies to ameliorate the overall defense mechanisms in normal individuals and cancer patients. Experimental evidence *in vivo* and *in vitro* suggests that polysaccharides can exhibit immunomodulatory functions by stimulating cellular and humoral immune responses. In the meantime, the immunomodulatory function of polysaccharides might start from activating effector cells, such as natural killer (NK) cells, lymphocytes and macrophages, and the proliferation of spleen cells and the enhanced phagocytosis of macrophages were also indicators of enhanced immune regulation (80). Several recent reports have shown that LPs have certain immunomodulatory activities *in vivo* and *in vitro*, and their immunomodulatory mechanisms are diverse. However, the variety of LPs in these reports suggests that there may be multiple LPs involved in immunomodulation (44). Therefore, to better revealed the immunomodulatory activity mechanism of LPs and their structure-activity relationships, modern studies had characterized the structures of LPs by GC-MS, FT-IR and NMR *etc.*, and evaluated the immunomodulatory activities of LPs by relevant experiments.

First, it was noted that LPs stimulate the proliferation of splenic lymphocytes and phagocytosis of macrophages (81). And among them, macrophages play an extremely critical role in innate and acquired immune regulation (82). In general, delayed-type hypersensitivity (DTH) was considered to be the diagnostic expression of related immune responses. The medium-dose (200 mg/kg) and low-dose (100 mg/kg) LPs extracted by ultrasound showed strong immunoregulatory effects on mice model. Compared with the model control group, it could significantly enhance the DTH response, macrophage phagocytic function and concanavalin A (ConA)-stimulated spleen cell proliferation in mice (83). Min et al. prepared longan fruit pulp homogenous polysaccharide-protein complexes (LPP) by alkali extraction and acid precipitation method, it enhanced the immune function of mice through several ways, such as enhanced the production of anti-chicken red blood cell anti-body and phagocytosis of macrophage, promoted the proliferation of ConA-induced splenocyte and the secretion of cytokines in serum (33). Secondly, based on this, Yi et al. obtained LPIIa from longan fruit pulp and investigated its physicochemical properties and immune-stimulating effects on macrophages. Studies have shown that in the dose range of 100–400 μg/mL, LPIIa enhances the nitric oxide (NO) production and macrophage phagocytosis function. Moreover, at a dose of 200 μg/mL, LPIIa significantly increased the activity of macrophage inducible nitric oxide synthase (iNOS), and the secretion of interleukin-6 (IL-6) and tumor necrosis factor-α (TNF-α). However, these effects were significantly reduced after Toll-like receptor 4 (TLR4) or TLR2 was blocked. Similarly, specific inhibitors such as p38 mitogen-activated protein kinase (MAPK), protein kinase C (PKC), phosphatidyl inositol 3-kinase and nuclear factor-κB (NF-κB) also selectively inhibited LPIIa immune-stimulating activity against macrophages. These results suggested that its immunostimulatory signal may be mediated by TLR4 and TLR2, and subsequently activate the p38MAPK and NF-κB pathways. Therefore, LPIIa had strong immunomodulatory activity by stimulating macrophages and could be used as an adjuvant for immunotherapy (39). Besides, Yi et al. obtained four fractions (LPI-IV) from the LPs water extract by DEAE anion exchange column chromatography, and evaluated the immunomodulatory activity of these polysaccharides *in vitro*. They concluded that compared with normal control group, except for LPI, the other three

polysaccharides significantly stimulate lymphocyte proliferation within the dose range of 100–400 μg/mL, and also selectively stimulate B cells but not T cells. Furthermore, their promoting effects on lipopolysaccharide (LPS) -induced cell proliferation and their inhibitory effects on ConA-induced cell proliferation were LPIII > LPIV > LPII > LPI, respectively. The optimal dose of all components was 100 μg/mL, and all of them could enhance the phagocytosis of macrophages. Among them, LPII as a potential immunoadjuvant had high yield and activity (34). In addition, they also studied the relationship between molecular conformation and immunomodulatory activity of LPs. LPI had a spherical and rigid rod-like conformation, had no immune stimulation on NK and splenocytes cells in the dose range of 100–400 μg/mL. LPI1 or LPI2, as the alkali dissociative derivative of LPI, significantly enhanced the proliferation of splenocyte and cytotoxicity of NK cells due to the existence of slightly dissociated spherical conformation or single-helix chain. However, its contribution to macrophage phagocytosis was weak (51). Rong et al. investigated the immunomodulatory activity of LPs by comparing the effects of polysaccharides on the phagocytosis of macrophages. They isolated an active polysaccharide (LPD2) from longan fruit pulp and studied its structure and activity. Immune activity tests showed that LPD2 significantly promotes the phagocytic function and proliferation of lymphocytes, and promotes the secretion of IL-6 and NO by macrophages, suggesting that LPD2 can effectively induce the functional activation of macrophages. Meanwhile, LPD2 had a strong stimulating effect on the proliferation of splenic lymphocytes, which are important participants in innate immunity and adaptive immunity, suggesting that LPD2 has a significant impact on the activation of immune function in the body (Figure 4) (35). In addition, LPs also mediated immune-stimulating activity by interacting with various receptors and/or regulating intracellular signaling pathways after binding to various receptors, such as TLR4 (84), the lectin receptor of dectin-1, and complement receptor (85), *etc*. In short, the immunostimulatory activity of LPs might be due to direct or indirect interaction with immune system components, triggering different cellular and molecular events. The direct stimulation of immune cells such as macrophages, lymphocytes, neutrophils, monocytes, dendritic cells and complement proteins involved specific recognition receptors, which determine the final response (86).

It is worth mentioning that LPs can also exert immunomodulatory activity by acting on the intestine. Intestinal tract is the largest immune organ in the host, proper intestinal immune response of the steady state as well as the health of the host play an important role in maintaining intestinal barrier (87). The Mw of LPs is relatively large, generally more than 104 Da, so they are difficult to be absorbed directly through the gut. However, studies have displayed that the host indigestible polysaccharides are the most important food source of intestinal flora, so a diet rich in these polysaccharides was crucial for maintaining a healthy gut (88). Zhang et al. studied the effects of LPs on mice gut microbiota and its interaction with the host immune system using a multi-omics method. The results noted that LPs significantly increase the typical intestinal immune indexes of mice, and the changes caused by LPs in the microbiota are related to the immunomodulatory activity (44). In addition, there were studies aiming to investigate the effects of LPs on the systemic immunity and intestinal mucosal immunity of immunosuppressed mice by observing the synthesis and secretion of intestinal secretory immunoglobulin A (SIgA). And the results showed that the LPs improve cyclophosphamide (CTX)-treated in mice thymus and spleen indexes. The level of serum immunoglobulin A (IgA) and the secretion of SIgA in the intestinal lumen were also increased by the action of LPs. Therefore, appropriate consumption of LPs helped to strengthen the mucosal barrier by promoting the secretion of intestinal SIgA, thereby enhancing systemic immunity and intestinal mucosal immunity (Figure 5) (89).

It is also noteworthy that the structurally modified LPs have greater immunomodulatory activity. For example, Yi et al. studied the immunomodulatory effects of LP-protein complex (LP3) in immunosuppressed mice models. Oral administration of 100 $mg{\cdot}kg^{-1}{\cdot}d^{-1}$ LP3 could stimulate macrophage/lymphocyte activation and anti-body/cytokine secretion, and could also enhance splenocyte proliferation, anti-body production, cytokine secretion, macrophage phagocytosis and NK cytotoxicity in immunosuppressed mice. However, the structural characteristics of LP3 and the structural/immunomodulatory relationship need to be further studied (32). Jiang et al. indicated that all experimental doses (25–100 μg/mL) of sulfated LP1 (LP1-S) and LP1 significantly increased the proliferation of lymphocyte cells, spleen cells and LPS-induced proliferation of spleen cells, but LP1-S showed higher immunomodulatory activity than LP1. It might be caused by the sulfate group in the structure of LP1-S (30). Phosphorylation and acid hydrolysis were also used to modify LPs. Compared with unmodified LPs, their derivatives showed stronger effects in enhancing macrophage phagocytosis, stimulating lymphocyte proliferation and regulating cytokines, *etc*. (28). Therefore, to understand the structural characteristics of longan fruit pulp active polysaccharide was helpful to understand the application mechanism of LPs as an immune regulator.

Anti-tumor activity

According to the antitumor mechanism of polysaccharides, the antineoplastic activity of polysaccharides can be divided into two types: (1) polysaccharides inhibit the proliferation of cancer cells by activating the immune system of the body; (2) polysaccharides directly inhibit the proliferation of tumor cells (90). At present, the mortality rate of tumor-related diseases is

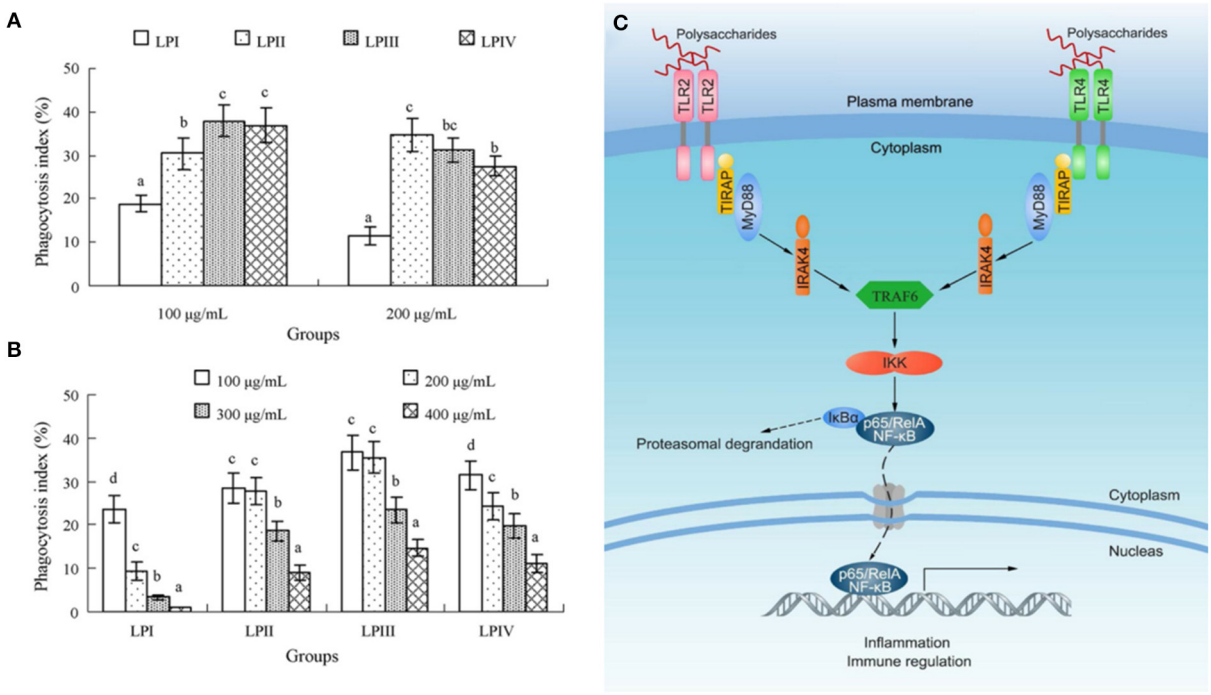

FIGURE 4
The activation of macrophages and the enhancement of phagocytic function are indicators of the enhancement of LPs immunomodulation, anti-tumor and anti-inflammatory activities. **(A)** The comparison of phagocytosis indexes of LPI–IV at 100 or 200 μg/mL. **(B)** The phagocytosis indexes of LPI-IV in the dose range of 100–400 μg/mL (34). **(C)** Possible molecular mechanism of LPs activating macrophages (35).

quite high, and the effectiveness of cancer treatment is limited. Many anti-cancer drugs are known to be immunosuppressants, which inhibit tumor growth and impair the immune system. Therefore, the discovery and identification of new anti-tumor drugs that can play an immunomodulatory role has become an important target of immunopharmacology and oncology therapy (91). Zhong et al. noted that UELP (ultrasound-extracted LPs) has a good anti-tumor effect on S180 tumors *in vivo*. Importantly, the experimental dose (200 mg/kg) of UELP had extreme anti-tumor effects, with a maximum inhibition rate of nearly 85% (83). At the same time, LPs also had anti-tumor effects in S180 tumor mice, which may be shown by the immunomodulatory mechanism as an immune adjuvant for the treatment of cancer. However, their direct inhibitory effect on tumor cells was not available (43). Meng et al. extracted and successfully purified a new WPS (LP1) from longan fruit pulp. *In vitro* experiments had shown that LP1 has significant anti-tumor activity against HO8910 and SKOV3 tumor cells, with inhibition rates of 50 and 40%, respectively. Meanwhile, LP1 was observed to prevent the development of tumor cells by directly killing tumor cells *in vitro* and in mice and improving immune activity. Therefore, LP1 has significant anti-tumor potential and can be used as a safe and effective reagent to treat corresponding diseases (24). LPs could also directly inhibit the proliferation of tumor cells cultured *in vitro*. Yi et al. obtained three kinds of LPs with different structures through different extraction methods, named LPI, LPII and LPIII. Anti-tumor studies had shown that in the range of 50–400 μg/mL, those three LPs showed direct inhibitory effects on HepG2, A549 and HeLa cells in a positive dose-dependent manner, and the inhibition rate of 400 μg/mL was significantly higher than other doses. In addition, the activity of 400 μg/mL LPIII, especially its inhibitory effect on the proliferation of hepatoma, was stronger than other activities, which may be related to its flexible conformation (92). The anti-tumor activity of LPs was also improved after modification by structural modification. Jiang et al. used purified longan fruit pulp WSP (LP1) as the raw material to prepare a sulfated derivative (LP1-S) by sulfuric acid method, and the measured DS was 2.011. Studies had shown that LP1-S has stronger anti-tumor activity compared with LP1, which may be related to its sulfate content (46). Anti-cancer tests showed that LP1-S has a certain inhibitory effect on the growth of hepatoma cells. However, it did not show any cytotoxicity against MCF-7 cells. In conclusion, LPs can be used as a potential anti-tumor adjuvant in food and drug therapy, but its anti-tumor activity and structure-activity relationship *in vivo* need further study (30).

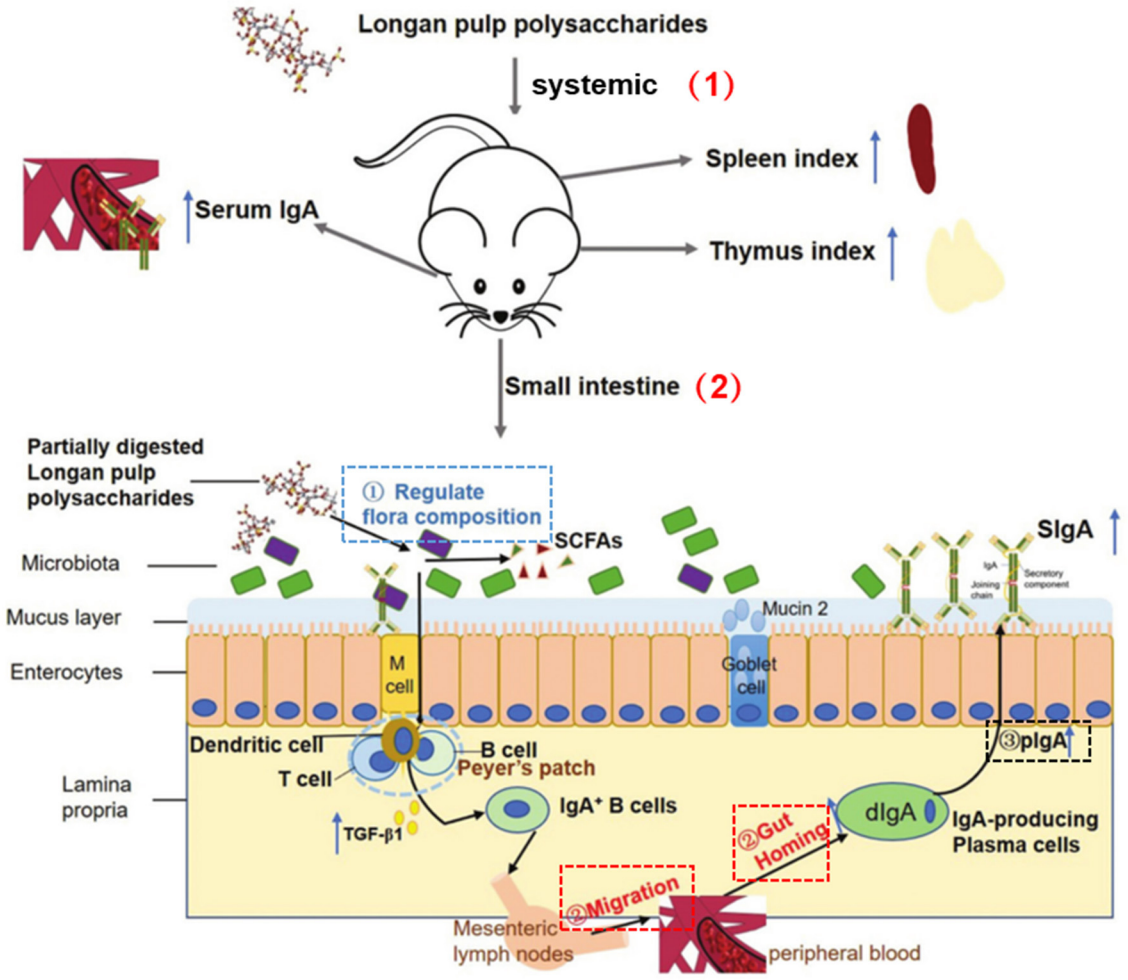

FIGURE 5
LP regulated systemic and intestinal immunity (89). (1) Systemic immunity: LP increased spleen and thymus indexes and serum IgA level. (2) Intestinal immunity: ① LP regulated intestinal microbiota composition *via* utilization by partial commensal bacteria; ② LP promoted the migration and gut homing of IgA+ plasma cells; ③ LP directly stimulated transcytosis of dIgA-pIgR and pIgR.

Prebiotic activity

Current literatures have shown that the prebiotics activity LPs mainly related to its influence on gut microbiota. The adjustment of the microbiota can ameliorate insulin resistance, blood glucose and glucose tolerance control and reduce inflammation (93), so LPs can be used as prebiotics and become a potential treatment tool for the treatment and prevention of obesity (94). Besides, LPs can selectively benefit a number of living microbial species called prebiotics in the human gut, and exert its health benefits by boosting the number of prebiotics in the gut and regulating its metabolites (95, 96). Therefore, evaluating the prebiotic activity of LPs is crucial to evaluate the possible health effects of LPs. Huang et al. showed that LP-SE has stronger prebiotic activity than LP-H and LP-S. Firstly, LP-SE had a higher extraction efficiency than LP-H and LP-S, so it had a higher sugar content and a lower Mw. LP-SE was considered to have a better proliferation effect. Secondly, the monosaccharide composition and glycosidic bond of LPs affected the prebiotic activity. Studies have shown that LP-SE has better prebiotic activity, which may be due to the fact that it contains more Ara and Gal, as well as the specific glycosidic bond →5)-*α*-*L*-Ara*f* -(1→. Moreover, the viscosity and solubility of LPs were also one of the important factors affecting the prebiotics activity. LP-SE with good water solubility and low viscosity was more likely to be quickly and completely utilized by prebiotics, so it showed stronger prebiotics activity than LP-H and LP-S (22). Furthermore, the prebiotic activity of enzyme-modified LPs was improved to some extent. Cheng et al. investigated the use of commercial Viscozyme L in the obtained longan fruit pulp juice, which has the potential to convert sucrose into fructo-oligosaccharides. The results showed

that enzyme treatment significantly changes the Mw distribution and monosaccharide composition of WPS. In addition, the enzyme-treated longan fruit pulp juice and its ethanol-soluble polysaccharide components enhanced the stimulating effect on the growth of intestinal probiotics, such as the growth of *Lactobacillus delbrueckii*, *Streptococcus thermophiles* and *Lactobacillus acidophilus*. All of them indicated that the oligo-polysaccharides contained in the enzyme-treated longan fruit pulp juice have better prebiotics activity (50).

Anti-oxidant activity

The anti-oxidant activity of polysaccharides is mainly demonstrated by the direct scavenging effect on hydroxyl radical (•OH), superoxide anion radical ($\bullet O^{2-}$) and hydrogen peroxide (H_20_2) (97). Free radicals are produced by aerobic reactions in the body. They poison the body in different ways and are closely related to the occurrence of multiple diseases (98, 99). When Zhong et al. investigated the radical scavenging activity of UELP, they found that experimental concentrations (5–35 mg/mL) of UELP have excellent scavenging activity for •OH and •DPPH, and both scavenging rates were significantly enhanced with increasing UELP concentrations, and a larger dose (35 mg/mL) of UELP showed almost complete scavenging effect (83). Liu et al. obtained longan wine solution by fermenting longan fruit pulp juice with *Saccharomyces cerevisiae*. Longan fruit pulp wine polysaccharide (LWP), the main functional component of longan fruit pulp wine, was separated into 4 fragments with different Mw by ultrafiltration system. It was showed that with the increase of Mw, the •DPPH scavenging rate of longan fruit pulp wine and four LP sections was gradually increased. Compared with longan fruit pulp wine, LWP with a Mw of 10–30 kDa or a <3 kDa had significant anti-oxidant activity in the volume range of 0.2–2.0 mL. When the sample volume was >1.6 mL, the 10–30 kDa LWP had the highest •DPPH scavenging rate (100). It is well-known that oxidative stress caused by free radicals and/or reactive oxygen species can cause organ damage. Chen et al. studied focal cerebral ischemia/reperfusion injury and its mechanism. The results showed that compared with the ischemia/reperfusion group, the LPs can significantly reduce the nervous system score, the cerebral infarction volume, the brain water content, malondialdehyde (MDA) content, myeloperoxidase (MPO) activity, TNF-α and IL-1β levels, Bax expression, and increase superoxide dismutase (SOD), glutathione (GSH), glutathione peroxidase (GSH-Px) activity and expression of Bcl-2. Therefore, LPs could be used as an effective polysaccharide with significant protective effect on cerebral ischemia/reperfusion injury, which may be related to the mechanism of reducing oxidative stress *in vivo* and *in vitro* (101). In addition, compared with unmodified LPs, MLPs, acetylated and carboxymethylated LPs derivatives had stronger anti-oxidant activity (102).

Anti-inflammatory activity

Inflammation is a defense response of the body to stimulation, which is characterized by redness, swelling, heat, pain and dysfunction. Chronic inflammations and disorders may lead to secondary injury and immunopathology in the host (103). LPIIa was purified from longan fruit pulp, and a co-culture model of Caco-2 cells and Raw264.7 macrophages was used to study its anti-inflammatory activity and intestinal barrier protection. The results showed that LPIIa inhibits the production of inflammatory mediators, including TNF-α, IL-6, NO (104) and PGE2, and reduces the expression of iNOS and cyclooxygenase-2 (COX-2) genes in LPS-induced Raw264.7 macrophages. In addition, LPIIa also decreased the expression of the intestinal tight junction channel protein Claudin-2 and increased the expression of the tight junction barrier protein ZO-1 in Caco-2 cells. These results indicated that LPIIa has a certain therapeutic effect on inflammatory bowel disease (IBD) (31).

Inhibition of AChE activity

Longan fruit pulp has been reported to have beneficial effects on memory in humans and is often used in Chinese medicine to treat amnesia, yet the mechanism by which longan fruit pulp affects memory function is unclear. Some studies have pointed out that acetylcholine plays an important role in memory function in the brain, and a large body of evidence supports the mechanism by which choline has the ability to regulate learning and memory function. And increasing acetylcholine levels with acetylcholinesterase (AChE) inhibitors is currently one of the most effective strategies for the treatment of Alzheimer's disease (105). Bai et al. compared the AChE inhibitory activity of LPs obtained by different extraction methods. All LPs showed moderate and concentration-dependent inhibition of AChE at concentrations ranging from 0.1 to 3.0 mg/mL. At a concentration of 3.0 mg/mL, the AChE inhibitory activities of LP-H, LP-E, LP-U and LP-UE were 18.15%, 19.31%, 20.17% and 25.40%, respectively. These results indicated that EAE and UHP-assisted extraction can improve the biological activity of LPs. Compared with the other three types of LPs, LP-UE had the highest AChE inhibitory activity, suggesting that LP-UE may have the potential to meliorate cognitive dysfunction. Thus, LP-UE may be a potential AChE inhibitor, and the regulation of the cholinergic system may be one of the pharmacological mechanisms of LPs to ameliorate memory impairment (3).

Others

In addition to the above activities, LPs also has some biological activities in intestinal protection, promoting cartilage growth and other aspects. Studies have shown that early intake of LPs can reduce the intestinal mucosal damage caused by chemotherapy by increasing the expression of mucin, adherence junction (AJ) and tight junction (TJ) complexes, thereby promoting the renewal of the intestinal mucosal and the morphological integrity of the intestine *in vivo*, so as to achieve the protective effect of LPs on the intestine (36). In addition, the effects of LPs on rabbit articular chondrocytes were explored by detecting the activity, morphology, cartilage-specific gene expression and glycosaminoglycan synthesis. The results showed that, similar to the positive group using TGF-β growth factor, LPs effectively promote the growth of chondrocytes and enhance the secretion and synthesis of cartilage extracellular matrix by up-regulating the expression levels of sox9, aggrecan and collagen II. Compared with the negative control group, the expression of type I collagen gene was down-regulated, indicating that LPs inhibit chondrocyte dedifferentiation. All these suggested that LPs can replace growth factor in the treatment of autologous chondrocyte implantation (ACI), which lays the foundation for the development of new drugs for the treatment of articular cartilage defects (106).

Patent registration of LPs

Currently, there are 630 patents related to LPs worldwide, of which 82.2% are patent applications, 17.3% are granted patents and <1% are limited patents. Among them, the jurisdiction of these patents is mainly distributed in China, the United States of America, Would Intellectual Property Organization (WO-WIPO), Europe and Australia. According to the relevant data, China and the United States have the largest number of patents, accounting for 67% of the total. In these patents, LPs are mainly used as food or food processing products, health products and dietary supplements. Some studies have specified that LPs and other substances together to make powder preparations with enhancing immune function broadens the utilization of LPs as a kind of health food. In addition, some patents also introduced that LPs can be used to make solid drinks to regulate Qi deficiency (a TCM term describing "chronic fatigue syndrome") constitution, powder with enhancing immunity, herbal composition to treat nervous system diseases and improve memory damage, pharmaceutical composition to treat cardiovascular and cerebrovascular diseases and as hair growth agent, *etc*. Their preparation methods and applications were also mentioned in turn. All these provided a theoretical basis for the patent development of LPs. In a word, although many scholars have made great contributions to the research of LPs in terms of basic research, the commercial and industrial development of LPs products is still in the initial stage, and there are still some difficulties in the development of most LP-related products in the actual industrial production. The analysis of 630 patents browsed was obtained by Lens.org using the search term "Longan polysaccharide," the patent details of LPs are shown in Figure 6.

Conclusions and perspectives

Longan fruit pulp, as one of the representative substances of medicinal and food homology, has attracted more and more attention from researchers because of its high edible and adjuvant therapeutic value. LPs, as one of the main biologically active components in longan fruit pulp, has been proven to be able to obtain homogeneous LPs with different structural characteristics from longan fruit pulp through different extraction and purification methods, and they also exhibit different biological activities. In recent years, researchers have conducted several studies on the structure and bioactivity of LPs, which focused on the traditional HWE, chemical composition, structure, immunostimulatory and antioxidant activities of LPs. Meanwhile, several more efficient methods have been applied in the extraction of LPs, such as EAE, UAE, UHP-assisted extraction, MAE and superfine grinding extraction, in order to improve the yield of LPs and reduce the extraction time. These extraction methods are all processed based on the HWE method, which can be useful from different angles according to different extraction needs. In addition, to further improve the biological activity of LPs and broaden their application scope, researchers have also modified LPs according to their structures. For example, LPs could be both extracted and structurally modified by enzymatic techniques. In this process, the extraction efficiency of LPs was improved. At the same time, the further modification of the structure also enhanced the immune regulation and anti-tumor activities of LPs. These results had a certain relationship with the type, dosage and concentration of enzymes. LPs are mainly composed of Glc, Ara, Man and Gal, which have different types of glycosidic bonds due to their different structures. Structures such as $\rightarrow$6)-Gal-($\rightarrow$1 and $\rightarrow$4)-β-Glc$\rightarrow$1 are often present in homogeneous LPs. Studies on biological activities have demonstrated that LPs have a variety of biological activities, including immunomodulatory, anti-oxidant, anti-tumor, prebiotic and anti-inflammatory, which provides a solid foundation for its application in the positive intervention of physiological dysfunction.

However, in general, there are still some shortcomings in the current research on LPs. For example, (1) LPs obtained by modern methods of extraction and purification are still crude LPs, which mostly belong to a class of macromolecules with diverse structures. We lack more clearer and more targeted extraction and purification methods. As a result, many studies have had many difficulties in characterizing their structures, and many higher-level structures are difficult to be elucidated. (2) the research on structural characteristics and activity is not

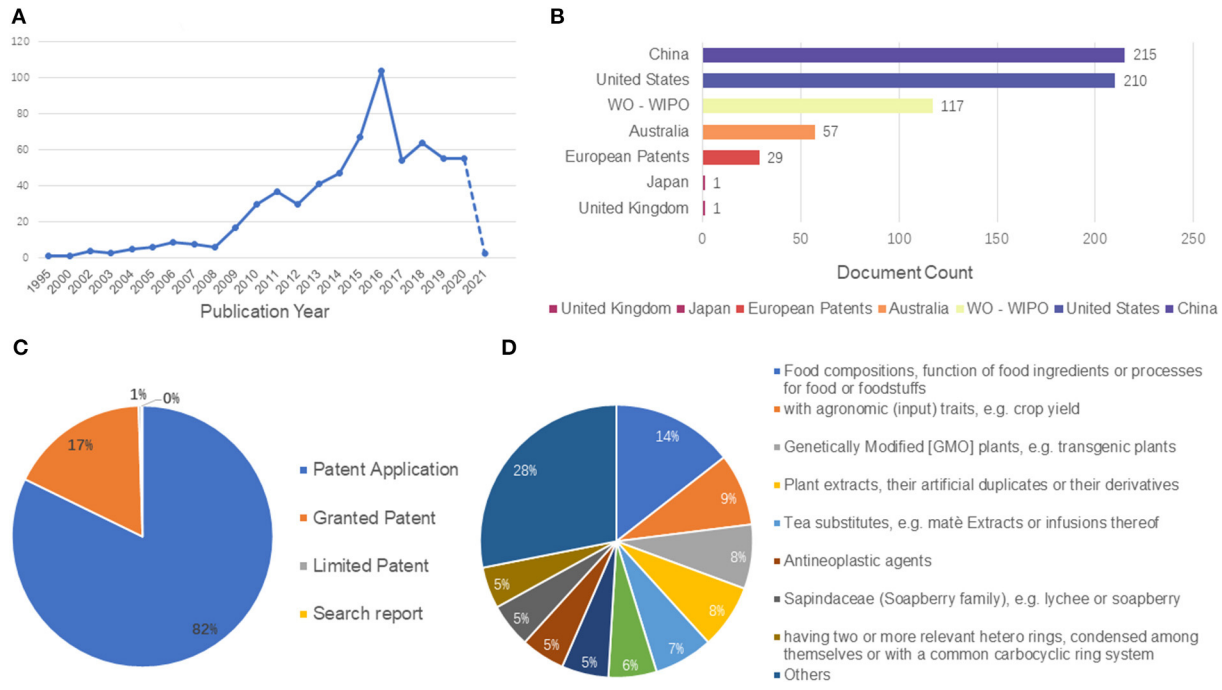

FIGURE 6
The analysis of 630 patents browsed was obtained by Lens.org using the search term "Longan polysaccharide." **(A)** Patent applications per years, **(B)** Document type, **(C)** Jurisdictions, and **(D)** CPC Classification.

in-depth. We need to carry out high-level structural analysis and structure-biological activity evaluation of LPs, as well as extensive research on the cellular and molecular mechanisms of biological activity. The research results of structure-activity relationship can guide the direction of molecular modification of LPs and provide theoretical support for the design, research and development of LPs agents. Furthermore, more *in vivo* experiments are also needed, which will help to better understand the functional effects of LPs and provide new ideas for further development of natural resources. (3) Although LPs, as natural plant polysaccharides, have no toxic side effects and high affinity to the human body, in order to better apply them to the protection and treatment of human diseases, we still lack systematic and credible quality control standards for LPs. Therefore, the quality evaluation research of LPs and their related products is indispensable to ensure the efficacy and safety of the product. The physical and chemical properties of this polysaccharide are also essential for quality control through quantitative and qualitative analysis.

In summary, the bioactive polysaccharides derived from longan fruit pulp are well-known and widely used in Asia as part of traditional diets and adjuvant therapeutic agents. In the past decades, people have been focused on the composition analysis, structural characterization and biological activity of LPs. LPs can be potentially employed in alternative medicine fields due to its unique physicochemical properties, structural diversity and biological effects, and has a broad application prospect as an immune stimulant or adjuvant anti-cancer agent. Therefore, this paper mainly reviews the LPs from the above aspects, which is helpful to establish a better application of the functional effects of LPs and provide new ideas for the further development of natural resources, for further scientific research and commercial development of LPs.

Author contributions

XY: methodology, investigation, and writing—original draft. ZC: validation and writing—review and editing. JZ: formal analysis and software. CH: resources. SZ: data curation. XL: visualization. YQ: supervision and funding acquisition. CZ: conceptualization and project administration. All authors contributed to the article and approved the submitted version.

Funding

This work was supported by the National Natural Science Foundation of China (Grant No. 81603309), National Natural Science Foundation of China (No. 81603281), Health Commission of Sichuan Province (21PJ108), National Interdisciplinary Innovation Team of Traditional Chinese Medicine (Grant No. ZYYCXTD-D-202209), China

Postdoctoral Science Foundation (No. 2021M690488), and the Xinglin Scholar Research Promotion Project of Chengdu University of Traditional Chinese Medicine (Grant no. QNXZ2018020).

Conflict of interest

The authors declare that the research was conducted in the absence of any commercial or financial relationships that could be construed as a potential conflict of interest.

The reviewer YN declared a shared affiliation, with no collaboration, with one of the authors ZC, to the handling editor at the time of the review.

Publisher's note

All claims expressed in this article are solely those of the authors and do not necessarily represent those of their affiliated organizations, or those of the publisher, the editors and the reviewers. Any product that may be evaluated in this article, or claim that may be made by its manufacturer, is not guaranteed or endorsed by the publisher.

References

1. Park SJ, Park DH, Kim DH, Lee S, Yoon BH, Jung WY, et al. The memory-enhancing effects of Euphoria longan fruit extract in mice. *J Ethnopharmacol.* (2010) 128:160–5. doi: 10.1016/j.jep.2010.01.001

2. Yang B, Jiang Y, Shi J, Chen F, Ashraf M. Extraction and pharmacological properties of bioactive compounds from longan (Dimocarpus longan Lour.) fruit — A review. *Food Res Int.* (2011) 44:1837–42. doi: 10.1016/j.foodres.2010.10.019

3. Bai Y, Liu L, Zhang R, Huang F, Deng Y, Zhang M. Ultrahigh pressure-assisted enzymatic extraction maximizes the yield of longan pulp polysaccharides and their acetylcholinesterase inhibitory activity *in vitro*. *Int J Biol Macromol.* (2017) 96:214–22. doi: 10.1016/j.ijbiomac.2016.11.105

4. Yuan L, Gong J, Yang M, Huyan H, Xu Y, Li X. Extraction techniques and methods of polysaccharides in plants. *Jilin Animal Husbandry Vet Med.* (2011) 32:13–8. doi: 10.3969/j.issn.1672-2078.2011.02.004

5. Huang H, Huang G. Extraction, separation, modification, structural characterization, and antioxidant activity of plant polysaccharides. *Chem Biol Drug Des.* (2020) 96:1209–22. doi: 10.1111/cbdd.13794

6. Han M. *Invesigation on the Structural and Bioactive Changes of Longan Pulp Polysaccharides by Different Maillard Reaction Systems.* Master: Wuhan Polytechnic University (2018).

7. Sharma HP, Patel H, Sugandha. Enzymatic added extraction and clarification of fruit juices-A review. *Crit Rev Food Sci Nutr.* (2017) 57:1215–27. doi: 10.1080/10408398.2014.977434

8. Liu Y, Gong G, Zhang J, Jia S, Li F, Wang Y, et al. Response surface optimization of ultrasound-assisted enzymatic extraction polysaccharides from Lycium barbarum. *Carbohydr Polym.* (2014) 110:278–84. doi: 10.1016/j.carbpol.2014.03.040

9. Song YR, Sung SK, Jang M, Lim TG, Cho CW, Han CJ, et al. Enzyme-assisted extraction, chemical characteristics, and immunostimulatory activity of polysaccharides from Korean ginseng (Panax ginseng Meyer). *Int J Biol Macromol.* (2018) 116:1089–97. doi: 10.1016/j.ijbiomac.2018.05.132

10. Li S, Han D, Row KH. Optimization of enzymatic extraction of polysaccharides from some marine algae by response surface methodology. *Korean J Chem Eng.* (2012) 29:650–6. doi: 10.1007/s11814-011-0221-3

11. Liu X, Zhang M, Guo K, Jia A, Shi Y, Gao G, et al. Cellulase-assisted extraction, characterization, and bioactivity of polysaccharides from Polygonatum odoratum. *Int J Biol Macromol.* (2015) 75:258–65. doi: 10.1016/j.ijbiomac.2015.01.040

12. Cheng Z, Song H, Yang Y, Liu Y, Liu Z, Hu H, et al. Optimization of microwave-assisted enzymatic extraction of polysaccharides from the fruit of Schisandra chinensis Baill. *Int J Biol Macromol.* (2015) 76:161–8. doi: 10.1016/j.ijbiomac.2015.01.048

13. Cheng Y. *Study on the Enzymatic Preparation and Functionality of Longan Juice Rich in Fructo-Oligosaccarides.* Doctor, South China Agricultural University (2019).

14. Li H, Guo H, Luo Q, Wu DT, Zou L, Liu Y, et al. Current extraction, purification, and identification techniques of tea polyphenols: An updated review. *Crit Rev Food Sci Nutr.* (2021) 2021:1–19. doi: 10.1080/10408398.2021.1995843

15. Yang B, Zhao M, Jiang Y. Optimization of tyrosinase inhibition activity of ultrasonic-extracted polysaccharides from longan fruit pericarp. *Food Chem.* (2008) 110:294–300. doi: 10.1016/j.foodchem.2008.01.067

16. Zhong K, Wang Q. Optimization of ultrasonic extraction of polysaccharides from dried longan pulp using response surface methodology. *Carbohydr Polym.* (2010) 80:19–25. doi: 10.1016/j.carbpol.2009.10.066

17. Jiang G, Jiang Y, Yang B, Yu C, Tsao R, Zhang H, et al. Structural characteristics and antioxidant activities of oligosaccharides from longan fruit pericarp. *J Agric Food Chem.* (2009) 57:9293–8. doi: 10.1021/jf902534v

18. Yang B, Jiang Y, Wang R, Zhao M, Sun J. Ultra-high pressure treatment effects on polysaccharides and lignins of longan fruit pericarp. *Food Chem.* (2009) 112:428–41. doi: 10.1016/j.foodchem.2008.05.097

19. Liu Y, Liu HY, Li SH, Ma WT, Li, HB, et al. Cannabis sativa bioactive compounds and their extraction, separation, purification, and identification technologies: An updated review. *TrAC Trends Analytical Chem.* (2022) 2022:149. doi: 10.1016/j.trac.2022.116554

20. Mirzadeh M, Arianejad MR, Khedmat L. Antioxidant, antiradical, and antimicrobial activities of polysaccharides obtained by microwave-assisted extraction method: A review. *Carbohydr Polym.* (2020) 229:115421. doi: 10.1016/j.carbpol.2019.115421

21. Yang C, Li Q, Ling X, Shao W, Xu H. Hot water extraction of longan polysaccharide assisted by microwave pretreatment. *CIESC J.* (2007) 8:2004–9. doi: 10.3321/j.issn:0438-1157.2007.08.020

22. Huang F, Liu H, Zhang R, Dong L, Liu L, Ma Y, et al. Physicochemical properties and prebiotic activities of polysaccharides from longan pulp based on different extraction techniques. *Carbohydr Polym.* (2019) 206:344–51. doi: 10.1016/j.carbpol.2018.11.012

23. Yang Y, Khan BM, Zhang X, Zhao Y, Cheong KL, Liu Y. Advances in separation and purification of bioactive polysaccharides through High-speed Counter-Current Chromatography. *J Chromatogr Sci.* (2020) 58:992–1000. doi: 10.1093/chromsci/bmaa063

24. Meng FY, Ning YL, Qi J, He Z, Jie J, Lin JJ, et al. Structure and antitumor and immunomodulatory activities of a water-soluble polysaccharide from Dimocarpus longan pulp. *Int J Mol Sci.* (2014) 15:5140–62. doi: 10.3390/ijms15035140

25. Zeng P, Li J, Chen Y, Zhang L. The structures and biological functions of polysaccharides from traditional Chinese herbs. *Prog Mol Biol Transl Sci.* (2019) 163:423–44. doi: 10.1016/bs.pmbts.2019.03.003

26. He Y, Chen Z, Nie X, Wang D, Zhang Q, Peng T, et al. Recent advances in polysaccharides from edible and medicinal Polygonati rhizoma: From bench to market. *Int J Biol Macromol.* (2021) 195:102–16. doi: 10.1016/j.ijbiomac.2021.12.010

27. Zhu Q, Jiang Y, Lin S, Wen L, Wu D, Zhao M, et al. Structural identification of (1–>6)-alpha-d-glucan, a key responsible for the health benefits of longan, and evaluation of anticancer activity. *Biomacromolecules.* (2013) 14:1999–2003. doi: 10.1021/bm400349y

28. Huang F, Hong R, Zhang R, Yi Y, Dong L, Liu L, et al. Physicochemical and biological properties of longan pulp polysaccharides modified by Lactobacillus fermentum fermentation. *Int J Biol Macromol.* (2019) 125:232–7. doi: 10.1016/j.ijbiomac.2018.12.061

29. Yi Y, Han MM, Huang F, Wang LM, Min T, Wang HX. Effects of a Lysine-involved Maillard reaction on the structure and in vitro activities of polysaccharides from Longan pulp. *Molecules.* (2019) 24:972. doi: 10.3390/molecules24050972

30. Jiang J, Meng FY, He Z, Ning YL, Li XH, Song H, et al. Sulfated modification of longan polysaccharide and its immunomodulatory and antitumor activity in vitro. *Int J Biol Macromol.* (2014) 67:323–9. doi: 10.1016/j.ijbiomac.2014.03.030

31. Bai Y, Jia X, Huang F, Zhang R, Dong L, Liu L, et al. Structural elucidation, anti-inflammatory activity and intestinal barrier protection of longan pulp polysaccharide LPIIa. *Carbohydr Polym.* (2020) 246:116532. doi: 10.1016/j.carbpol.2020.116532

32. Yi Y, Liao ST, Zhang MW, Zhang RF, Deng YY, Yang B, et al. Immunomodulatory activity of polysaccharide-protein complex of longan (Dimocarpus longan Lour.) pulp. *Molecules.* (2011) 16:10324–36. doi: 10.3390/molecules161210324

33. Min T, Sun J, Yi Y, Wang HX, Hang F, Ai YW, et al. Microanalysis, pharmacokinetics and tissue distribution of polysaccharide-protein complexes from Longan pulp in mice. *Int J Mol Sci.* (2015) 16:24403–16. doi: 10.3390/ijms161024403

34. Yi Y, Zhang MW, Liao ST, Zhang F, Deng YY, Wei Z, et al. Structural features and immunomodulatory activities of polysaccharides of longan pulp. *Carbohydr Polym.* (2012) 87:636–43. doi: 10.1016/j.carbpol.2011.08.034

35. Rong Y, Yang R, Yang Y, Wen Y, Liu S, Li C, et al. Structural characterization of an active polysaccharide of longan and evaluation of immunological activity. *Carbohydr Polym.* (2019) 213:247–56. doi: 10.1016/j.carbpol.2019.03.007

36. Bai Y, Huang F, Zhang R, Dong L, Jia X, Liu L, et al. Longan pulp polysaccharides relieve intestinal injury in vivo and in vitro by promoting tight junction expression. *Carbohydr Polym.* (2020) 229:115475. doi: 10.1016/j.carbpol.2019.115475

37. Han MM, Yi Y, Wang HX, Huang F. Investigation of the Maillard reaction between polysaccharides and proteins from Longan pulp and the improvement in activities. *Molecules.* (2017) 22:938. doi: 10.3390/molecules22060938

38. Yi Y, Liao ST, Zhang MW, Shi J, Zhang RF, Deng YY, et al. Physicochemical characteristics and immunomodulatory activities of three polysaccharide-protein complexes of longan pulp. *Molecules.* (2011) 16:6148–64. doi: 10.3390/molecules16076148

39. Yi Y, Wang H, Zhang R, Min T, Huang F, Liu L, et al. Characterization of polysaccharide from longan pulp as the macrophage stimulator. *RSC Adv.* (2015) 5:97163–70. doi: 10.1039/C5RA16044H

40. Yang C, He N, Ling X, Ye M, Zhang C, Shao W, et al. The isolation and characterization of polysaccharides from longan pulp. *Separation Purification Technol.* (2008) 63:226–30. doi: 10.1016/j.seppur.2008.05.004

41. Huang F, Hong R, Zhang R, Dong L, Bai Y, Liu L, et al. Dynamic variation in biochemical properties and prebiotic activities of polysaccharides from longan pulp during fermentation process. *Int J Biol Macromol.* (2019a) 132:915–21. doi: 10.1016/j.ijbiomac.2019.04.032

42. Lan H, Cheng Y, Mu J, Huang Y, Chen H, Zhao L, et al. Glucose-rich polysaccharide from dried 'Shixia' longan activates macrophages through Ca(2+) and CR3- mediated MAPKs and PI3K-AKT pathways. *Int J Biol Macromol.* (2021) 167:845–53. doi: 10.1016/j.ijbiomac.2020.11.040

43. Huang D, Chen Q, Chen J, Xu H. Analysis of monosaccharide composition in polysaccharide of Arillus Longan by High Performance Liquid Chromatography. *J Guangxi Acad Sci.* (2010) 26:234–36. doi: 10.13657/j.cnki.gxkxyxb.2010.03.047

44. Zhang J, Yang G, Wen Y, Liu S, Li C, Yang R, et al. Intestinal microbiota are involved in the immunomodulatory activities of longan polysaccharide. *Mol Nutr Food Res.* (2017) 61:e700466. doi: 10.1002/mnfr.201700466

45. Li S, Xiong Q, Lai X, Li X, Wan M, Zhang J, et al. Molecular modification of polysaccharides and resulting bioactivities. *Compr Rev Food Sci Food Saf.* (2016) 15:237–50. doi: 10.1111/1541-4337.12161

46. Huang G, Huang H. The derivatization and antitumor mechanisms of polysaccharides. *Future Med. Chem.* (2017) 9:1931–8. doi: 10.4155/fmc-2017-0132

47. Huang X. *Studies on Sulfation of Polysaccharide From Arillus Longan and Antitumor Activities of the Polysaccharide and Its Sulfated Derivative in vitro*. Master: Guangxi Medical University (2011).

48. Wang J. *Study on the Preparation, Antioxidant and Immunomodulatory Activities of Acetylated and Carboxymethylated Polysaccharides From Dimocarpus Longan Pulp*. Master, Guangxi Medical University (2016).

49. Wei Y, He Z, Tian H, Wang J, Nini W, Huang J, et al. Optimization of preparation of carboxymethylated polysaccharides from Longan (Dimocarpus longan) pulp by response surface methodology and their antioxidant activity and immunoregulatory activity. *Food Sci.* (2017) 38:275–83. doi: 10.7506/spkx1002-6630-201722041

50. Cheng Y, Lan H, Zhao L, Wang K, Hu Z. Characterization and prebiotic potential of longan juice obtained by enzymatic conversion of constituent sucrose into fructo-oligosaccharides. *Molecules.* (2018) 23:2596. doi: 10.3390/molecules23102596

51. Yi Y, Zhang MW, Liao ST, Zhang F, Deng YY, Wei ZC, et al. Effects of alkali dissociation on the molecular conformation and immunomodulatory activity of longan pulp polysaccharide (LPI). *Carbohydr Polym.* (2012) 87:1311–7. doi: 10.1016/j.carbpol.2011.09.014

52. Ning Y. *Study on the Preparation, Immunomodulatory and Antioxidant Activities of Phosphorylated and Acid Hydrolyzed Polysaccharides From Longan Pulp*. Master, Guangxi Medical University (2013).

53. Wang J, Wu N, Huang J, Wei Y, Yang Y, Li X, et al. Optimization of preparation of acetylated polysaccharides from Longan (Dimocarpus longan) pulp by response surface methodology and its antioxidant ability. *Food Sci.* (2016) 37:63–8. doi: 10.7506/spkx1002-6630-201616010

54. Huang X, Wang D, Hu Y, Lu Y, Guo Z, Kong X, et al. Effect of sulfated astragalus polysaccharide on cellular infectivity of infectious bursal disease virus. *Int J Biol Macromol.* (2008) 42:166–71. doi: 10.1016/j.ijbiomac.2007.10.019

55. Chen F, Huang G. Preparation and immunological activity of polysaccharides and their derivatives. *Int J Biol Macromol.* (2018) 112:211–6. doi: 10.1016/j.ijbiomac.2018.01.169

56. Wei D, Wei Y, Cheng W, Zhang L. Sulfated modification, characterization and antitumor activities of Radix hedysari polysaccharide. *Int J Biol Macromol.* (2012) 51:471–6. doi: 10.1016/j.ijbiomac.2012.06.004

57. Wang Z, Xie J, Yang Y, Zhang F, Wang S, Wu T, et al. Sulfated Cyclocarya paliurus polysaccharides markedly attenuates inflammation and oxidative damage in lipopolysaccharide-treated macrophage cells and mice. *Sci Rep.* (2017) 7:40402. doi: 10.1038/srep40402

58. Wang Y, Peng Y, Wei X, Yang Z, Xiao J, Jin Z. Sulfation of tea polysaccharides: Synthesis, characterization and hypoglycemic activity. *Int J Biol Macromol.* (2010) 46:270–4. doi: 10.1016/j.ijbiomac.2009.12.007

59. Li XL, Xiao JJ, Zha XQ, Pan LH, Asghar MN, Luo JP. Structural identification and sulfated modification of an antiglycation Dendrobium huoshanense polysaccharide. *Carbohydr Polym.* (2014) 106:247–54. doi: 10.1016/j.carbpol.2014.02.029

60. Huang X, Li X, Huang Y, Li F. Study on orthogonal optimization of sulfation reaction conditions of Longan pulp polysaccharide. *Chin J Modern Drug App.* (2011) 5:124–5. doi: 10.3969/j.issn.1673-9523.2011.05.111

61. Chakka VP, Zhou T. Carboxymethylation of polysaccharides: Synthesis and bioactivities. *Int J Biol Macromol.* (2020) 165:2425–31. doi: 10.1016/j.ijbiomac.2020.10.178

62. Wang J. *Study on the Preparation, Antioxidant and Immunomodulatory Activities of Acetylated and Carboxymethylated Polysaccharides from Dimocarpus Longan* pulp. Master: Guangxi Medical University (2016).

63. Rhein-Knudsen N, Ale MT, Meyer AS. Seaweed hydrocolloid production: an update on enzyme assisted extraction and modification technologies. *Mar Drugs.* (2015) 13:3340–59. doi: 10.3390/md13063340

64. Karaki N, Aljawish A, Humeau C, Muniglia L, Jasniewski J. Enzymatic modification of polysaccharides: Mechanisms, properties, and potential applications: A review. *Enzyme Microb Technol.* (2016) 90:1–18. doi: 10.1016/j.enzmictec.2016.04.004

65. Miao M, Jia X, Hamaker BR, Cui SW, Jiang B, Huang C. Structure–prebiotic properties relationship for α-D-glucan from Leuconostoc citreum SK24.002. *Food Hydrocoll.* (2016) 57:246–52. doi: 10.1016/j.foodhyd.2016.02.002

66. ALjahdali N, Carbonero F. Impact of Maillard reaction products on nutrition and health: Current knowledge and need to understand their fate in the human digestive system. *Crit Rev Food Sci Nutr.* (2019) 59:474–87. doi: 10.1080/10408398.2017.1378865

67. Henning C, Glomb MA. Pathways of the Maillard reaction under physiological conditions. *Glycoconj J.* (2016) 33:499–512. doi: 10.1007/s10719-016-9694-y

68. Liu P, Lu X, Li N, Zheng Z, Qiao X. Characterization, variables, and antioxidant activity of the Maillard reaction in a fructose (-) histidine model system. *Molecules.* (2018) 24:56. doi: 10.3390/molecules24010056

69. Teodorowicz M, van Neerven J, Savelkoul H. Food processing: The influence of the Maillard reaction on immunogenicity and

allergenicity of food proteins. *Nutrients.* (2017) 9:835. doi: 10.3390/nu9080835

70. Hamdi M, Nasri R, Azaza YB, Li S, Nasri M. Conception of novel blue crab chitosan films crosslinked with different saccharides via the Maillard reaction with improved functional and biological properties. *Carbohydr Polym.* (2020) 241:e116303. doi: 10.1016/j.carbpol.2020.116303

71. Sun T, Xu H, Zhang H, Ding H, Cui S, Xie J, et al. Maillard reaction of oat β-glucan and the rheological property of its amino acid/peptide conjugates. *Food Hydrocoll.* (2018) 76:30–4. doi: 10.1016/j.foodhyd.2017.07.025

72. Somjai C, Siriwoharn T, Kulprachakarn K, Chaipoot S, Phongphisutthinant R, Wiriyacharee P. Utilization of Maillard reaction in moist-dry-heating system to enhance physicochemical and antioxidative properties of dried whole longan fruit. *Heliyon.* (2021) 7:e07094. doi: 10.1016/j.heliyon.2021.e07094

73. Chen Y, Xie H, Tang J, Lin M, Hung YC, Lin H. Effects of acidic electrolyzed water treatment on storability, quality attributes and nutritive properties of longan fruit during storage. *Food Chem.* (2020) 320:126641. doi: 10.1016/j.foodchem.2020.126641

74. Fournet M, Bonte F, Desmouliere A. Glycation damage: A possible hub for major pathophysiological disorders and aging. *Aging Dis.* (2018) 9:880–900. doi: 10.14336/AD.2017.1121

75. Di Cagno R, Coda R, De Angelis M, Gobbetti M. Exploitation of vegetables and fruits through lactic acid fermentation. *Food Microbiol.* (2013) 33:1–10. doi: 10.1016/j.fm.2012.09.003

76. Septembre-Malaterre A, Remize F, Poucheret P. Fruits and vegetables, as a source of nutritional compounds and phytochemicals: Changes in bioactive compounds during lactic fermentation. *Food Res Int.* (2018) 104:86–99. doi: 10.1016/j.foodres.2017.09.031

77. Wang Y, Shao S, Xu P, Chen H, Lin-Shiau SY. Fermentation process enhanced production and bioactivities of oolong tea polysaccharides. *Food Res Int.* (2012) 46:158–66. doi: 10.1016/j.foodres.2011.11.027

78. Zhang ZH, Fan ST, Huang DF, Yu Q, Liu XZ, Li C, et al. Effect of Lactobacillus plantarum NCU116 fermentation on Asparagus officinalis polysaccharide: Characterization, antioxidative, immunoregulatory activities. *J Agric Food Chem.* (2018) 66:10703–11. doi: 10.1021/acs.jafc.8b03220

79. Huang F, Hong R, Yi Y, Bai Y, Dong L, Jia X, et al. In vitro digestion and human gut microbiota fermentation of longan pulp polysaccharides as affected by Lactobacillus fermentum fermentation. *Int J Biol Macromol.* (2020) 147:363–8. doi: 10.1016/j.ijbiomac.2020.01.059

80. Yin M, Zhang Y, Li H. Advances in research on immunoregulation of macrophages by plant polysaccharides. *Front Immunol.* (2019) 10:145. doi: 10.3389/fimmu.2019.00145

81. Lan H, Nunes C, Lopes GR, Wang K, Zhao L, Coimbra MA, et al. *In vitro* immunomodulatory activity of water-soluble glucans from fresh and dried Longan (Dimocarpus longan Lour.). *Carbohydr Polym.* (2021) 266:118106. doi: 10.1016/j.carbpol.2021.118106

82. Yu Y, Shen M, Wang Z, Wang Y, Xie M, Xie J. Sulfated polysaccharide from Cyclocarya paliurus enhances the immunomodulatory activity of macrophages. *Carbohydr Polym.* (2017) 174:669–76. doi: 10.1016/j.carbpol.2017.07.009

83. Zhong K, Wang Q, He Y, He X. Evaluation of radicals scavenging, immunity-modulatory and antitumor activities of longan polysaccharides with ultrasonic extraction on in S180 tumor mice models. *Int J Biol Macromol.* (2010) 47:356–60. doi: 10.1016/j.ijbiomac.2010.05.022

84. Zhang X, Qi C, Guo Y, Zhou W, Zhang Y. Toll-like receptor 4-related immunostimulatory polysaccharides: Primary structure, activity relationships, and possible interaction models. *Carbohydr Polym.* (2016) 149:186–206. doi: 10.1016/j.carbpol.2016.04.097

85. Lyu F, Xu X, Zhang L. Natural polysaccharides with different conformations: extraction, structure and anti-tumor activity. *J Mater Chem B.* (2020) 8:9652–67. doi: 10.1039/D0TB01713B

86. Ferreira SS, Passos CP, Madureira P, Vilanova M, Coimbra MA. Structure-function relationships of immunostimulatory polysaccharides: A review. *Carbohydr Polym.* (2015) 132:378–96. doi: 10.1016/j.carbpol.2015.05.079

87. Huang X, Nie S, Xie M. Interaction between gut immunity and polysaccharides. *Crit Rev Food Sci Nutr.* (2015) 57:2943–55. doi: 10.1080/10408398.2015.1079165

88. Cockburn DW, Koropatkin NM. Polysaccharide degradation by the intestinal microbiota and its influence on human health and disease. *J Mol Biol.* (2016) 428:3230–52. doi: 10.1016/j.jmb.2016.06.021

89. Bai Y, Huang F, Zhang R, Ma Q, Dong L, Su D, et al. Longan pulp polysaccharide protects against cyclophosphamide-induced immunosuppression in mice by promoting intestinal secretory IgA synthesis. *Food Funct.* (2020) 11:2738–48. doi: 10.1039/C9FO02780G

90. Chen L, Huang G. Antitumor activity of polysaccharides: An overview. *Curr Drug Targets.* (2018) 19:89–96. doi: 10.2174/1389450118666170704143018

91. Luo Y, Li J, Hu Y, Gao F, Pak-Heng Leung G, Geng F, et al. Injectable thermo-responsive nano-hydrogel loading triptolide for the anti-breast cancer enhancement via localized treatment based on "two strikes" effects. *Acta Pharm Sin B.* (2020) 10:2227–45. doi: 10.1016/j.apsb.2020.05.011

92. Yi Y, Huang F, Zhang MW, Zhang RF, Deng YY, Wei ZC, et al. Solution properties and in vitro anti-tumor activities of polysaccharides from longan pulp. *Molecules.* (2013) 18:11601–13. doi: 10.3390/molecules180911601

93. Ge Y, Ahmed S, Yao W, You L, Zheng J, Hileuskaya K. Regulation effects of indigestible dietary polysaccharides on intestinal microflora: An overview. *J Food Biochem.* (2021) 45:e13564. doi: 10.1111/jfbc.13564

94. Choque Delgado GT, Tamashiro W. Role of prebiotics in regulation of microbiota and prevention of obesity. *Food Res Int.* (2018) 113:183–8. doi: 10.1016/j.foodres.2018.07.013

95. Markowiak P, Slizewska K. Effects of probiotics, prebiotics, and synbiotics on human health. *Nutrients.* (2017) 9:1021. doi: 10.3390/nu9091021

96. Singh SP, Jadaun JS, Narnoliya LK, Pandey A. Prebiotic oligosaccharides: Special focus on fructooligosaccharides, its biosynthesis and bioactivity. *Appl Biochem Biotechnol.* (2017) 183:613–35. doi: 10.1007/s12010-017-2605-2

97. Xie JH, Jin ML, Morris GA, Zha XQ, Chen HQ, Yi Y, et al. Advances on bioactive polysaccharides from medicinal plants. *Crit Rev Food Sci Nutr.* (2016) 56:S60–84. doi: 10.1080/10408398.2015.1069255

98. Liu Y, Sun Y, Huang G. Preparation and antioxidant activities of important traditional plant polysaccharides. *Int J Biol Macromol.* (2018) 111:780–6. doi: 10.1016/j.ijbiomac.2018.01.086

99. Chen W, Jia Z, Zhu J, Zou Y, Huang G, Hong Y. Optimization of ultrasonic-assisted enzymatic extraction of polysaccharides from thick-shell mussel (Mytilus coruscus) and their antioxidant activities. *Int J Biol Macromol.* (2019) 140:1116–25. doi: 10.1016/j.ijbiomac.2019.08.136

100. Liu G, Sun J, He X, Tang Y, Li J, Ling D, et al. Fermentation process optimization and chemical constituent analysis on longan (Dimocarpus longan Lour.) wine. *Food Chem.* (2018) 256:268–79. doi: 10.1016/j.foodchem.2018.02.064

101. Chen J, Chen X, Qin J. Effects of polysaccharides of the Euphoria Longan (Lour.) Steud on focal cerebral ischemia/reperfusion injury and its underlying mechanism. *Brain Inj.* (2011) 25:292–9. doi: 10.3109/02699052.2010.546824

102. Xu H, Zhang X, Karangwa E, Xia S. Correlating enzymatic browning inhibition and antioxidant ability of Maillard reaction products derived from different amino acids. *J Sci Food Agric.* (2017) 97:4210–8. doi: 10.1002/jsfa.8295

103. Strowig T, Henao-Mejia J, Elinav E, Flavell R. Inflammasomes in health and disease. *Nature.* (2012) 481:278–86. doi: 10.1038/nature10759

104. Kunworarath N, Rangkadilok N, Suriyo T, Thiantanawat A, Satayavivad J. Longan (Dimocarpus longan Lour.) inhibits lipopolysaccharide-stimulated nitric oxide production in macrophages by suppressing NF-kappaB and AP-1 signaling pathways. *J Ethnopharmacol.* (2016) 179:156–61. doi: 10.1016/j.jep.2015.12.044

105. Tsai CH, Yen YH, Yang JPW. Finding of polysaccharide-peptide complexes in Cordyceps militaris and evaluation of its acetylcholinesterase inhibition activity. *J Food Drug Anal.* (2015) 23:63–70. doi: 10.1016/j.jfda.2014.05.006

106. Zhu S, Zhou B, Liu Q, Wu H, Zheng L. Effect of Longan polysaccharides on proliferation and phenotype maintenance in rabbit articular chondrocytes *in vitro*. *Med Biol Eng Comput.* (2016) 54:607–17. doi: 10.1007/s11517-015-1352-1

frontiers | Frontiers in Nutrition

TYPE Original Research
PUBLISHED 28 July 2022
DOI 10.3389/fnut.2022.946736

Check for updates

OPEN ACCESS

EDITED BY
Qiu Li,
Qingdao Agricultural University, China

REVIEWED BY
Yichen Hu,
Chengdu University, China
Emmanuel Anyachukwu Irondi,
Kwara State University, Nigeria
Ren-You Gan,
Institute of Urban Agriculture (CAAS), China

*CORRESPONDENCE
Li Wu
wuli02@caas.cn
Yang Yao
yaoyang@caas.cn

SPECIALTY SECTION
This article was submitted to Food Chemistry, a section of the journal Frontiers in Nutrition

RECEIVED 17 May 2022
ACCEPTED 30 June 2022
PUBLISHED 28 July 2022

CITATION
Zhu Y, Dun B, Shi Z, Wang Y, Wu L and Yao Y (2022) Structural characterization and bioactivity evaluation of water-extractable polysaccharides from chickpeas (*Cicer arietinum* L.) seeds. *Front. Nutr.* 9:946736. doi: 10.3389/fnut.2022.946736

COPYRIGHT
© 2022 Zhu, Dun, Shi, Wang, Wu and Yao. This is an open-access article distributed under the terms of the Creative Commons Attribution License (CC BY). The use, distribution or reproduction in other forums is permitted, provided the original author(s) and the copyright owner(s) are credited and that the original publication in this journal is cited, in accordance with accepted academic practice. No use, distribution or reproduction is permitted which does not comply with these terms.

Structural characterization and bioactivity evaluation of water-extractable polysaccharides from chickpeas (*Cicer arietinum* L.) seeds

Yingying Zhu[1,2], Baoqing Dun[1], Zhenxing Shi[1,3], Yuanji Wang[1], Li Wu[1]* and Yang Yao[1]*

[1]Institute of Crop Science, Chinese Academy of Agricultural Sciences, Beijing, China, [2]Henan Key Laboratory of Cold Chain Food Quality and Safety Control, College of Food and Bioengineering, Zhengzhou University of Light Industry, Zhengzhou, China, [3]School of Food Science and Technology, Henan University of Technology, Zhengzhou, China

Two water-extractable polysaccharide fractions designated as CWP (7. 37 × 10^5 Da) and CWP-0.2 (1.58 × 10^4 Da) were isolated and purified from chickpea (*Cicer arietinum* L.) seeds. The chemical structure of the two polysaccharides was characterized by various methods. Monosaccharide composition and methylation analysis showed that CWP was composed of Man and Glc in a molar ratio of 44.6:55.4, and CWP-0.2 was composed of Rha, Ara, Man, Glc, and Gal in a molar ratio of 10.6:23.3:5.2:4.9:56. Further structural characterization indicated that the main chain connection of CWP was → (2-β-d-Fru*f*-1) n→ , and the main chain connection of CWP-0.2 was explored as → 2,4)-α-l-Rha*p*-(1→ 3)-α-d-Gal*p*-(1→ with the branched chain of → 2,4)-α-l-Rha*p*-(1→ o-4. Besides, both CWP and CWP-0.2 had antioxidant and immunoregulatory activity *in vitro*, through scavenging DPPH· and $ABTS^{\cdot+}$ as well as stimulating production of NO, IL-6, TNF-α and MCP-1 in RAW 264.7 macrophages. CWP-0.2 revealed significantly higher bioactivity than CWP.

KEYWORDS

chickpea, polysaccharides, chemical structural, antioxidant, immunoregulatory

Introduction

Chickpea (*Cicer arietinum* L.) is the third most important legume in the world (1), with a long planting and application history in China, and is especially used in traditional Chinese Uygur medicine (2). Chickpea possesses high-quality starch, protein, fat and dietary fiber (3), and plays an important role in human diets. Previous studies have shown that chickpea possesses various biological activities, such as antioxidant (4), anti-inflammatory (5), amylase inhibitor (6), and angiotensin I-converting enzyme (ACE) inhibitory (7) activities.

Plant polysaccharides are natural high-macromolecular polymers with diverse potential medicinal characteristics and biological functions, with low cytotoxic side effects (8–12). Thus, they have received increased interests in recent years. Previous studies

reported that chickpeas hulls are good source of plant polysaccharides with excellent functional properties and biological activities (4, 7, 13). To explore structural characteristics of polysaccharides from chickpea hulls (CHP), Ye et al. (4) optimized the extraction conditions for isolation of CHP, and reported the molecular weight and monosaccharide composition (4). Mokni Ghribi et al. (7) and Akhtar et al. (13) further explored the structure of CHP with CP/MAS ^{13}C nuclear magnetic resonance spectroscopy (NMR), and demonstrated the presence of 1,4-d-galacturonan with methyl-esterified carboxyl group, 1,4-α-d-galactopyranosyluronan and methyl carbons of the methyl ester ($COOCH_3$) (7, 13). As reported, polysaccharides are not only existed in chickpeas hulls, the cell walls of endosperm also contain various plant polysaccharides. However, the recent studies mainly focused on the CHP, researches on the structure of polysaccharides from chickpea seeds are still limited. Besides, more detail information on the structural characteristics of plant polysaccharides can be explored from the ^{1}H-NMR, Dept135, HSQC, HHCOSY, and HMBC 2 D spectral data (14). A comprehensive understanding of the structures of chickpea polysaccharides is remained to be studied. In addition, the relationship between the bioactivity and chemical structure of chickpea polysaccharide is ambiguous and needs to be explored.

Therefore, the purpose of the present study was to obtain purified water-extracted polysaccharides from chickpea seeds with ion-exchange chromatography and to further characterize their chemical structure; to evaluate their antioxidant activity and immunoregulatory activity *in vitro*; and to analyze the correlation between the chemical structure and bioactivity of water-extracted chickpea polysaccharides.

Materials and methods

Materials and chemicals

Chickpea seeds were obtained from the National Gene Bank (Beijing, China). DEAE Sepharose Fast Flow was obtained from GE Healthcare Bio-Sciences Co. (Piscataway, NJ, USA). Dextran with different molecular weight (5,000–670,000 Da), griess reagent, arabinose (Ara), rhamnose (Rha), mannose (Man), galactose (Gal), glucose (Glc), 1,1-diphenyl-2-picrylhydrazyl (DPPH), 2,2'-azinobis-(3-ethyl-benzothiazolin-6-sulfonic acid) diammonium salt (ABTS), and 3-(4,5-dimethylthiazol-2-yl)-2,5-diphenyltetrazolium bromide (MTT) were purchased from Sigma-Aldrich (St. Louis, MS, USA). RPMI 1640 media, lipopolysaccharide (LPS), phosphate-buffered saline (PBS), and fetal bovine serum (FBS) were obtained from Gibco BRL Life Technologies (Thermo Fisher Scientific, NY, USA). Raw murine macrophage 264.7 (RAW 264.7) cells were purchased from the Cell Resources Center of the Chinese Academy of Sciences (Shanghai, China). OptEIA ELISA kits for tumor necrosis factor-α (TNF-α), MCP-1 and interleukin-6 (IL-6) were purchased from BD Biosciences (San Diego, CA, USA). A PathScan Antibody Array Kit was purchased from Cell Signaling Technology (Shanghai, China). All other chemicals and solvents used were analytical grade, unless otherwise specified.

Isolation and purification

The chickpea water-extracted crude polysaccharides (CWCP) from chickpea seeds were obtained according to the method of Yao et al. (15). Briefly, chickpea seeds were ground and passed through a 0.5-mm sieve, and the chickpea flour was pre-extracted with 95% ethanol (1:10 w/v) for 3 days to remove fat and small molecules. The residue was extracted twice with distilled water (1:20 w/v) at 90°C for 4 h. After centrifugation (4,000 g, 15 min), the supernatant was collected and deproteinated by the Savag method (16). The CWCP was obtained by freeze-drying. Then, CWCP (210 mg) was dissolved in distilled water (7 mL) and centrifuged at 10,000 g for 10 min, and then the supernatant was loaded onto the ÄKTA explorer 100 purification system with a DEAE Sepharose Fast Flow column. The column (100 cm × 2.6 cm) was first eluted with ultrapure water and then stepwise eluted with 0 to 2.0 M NaCl at a flow rate of 5 mL/min. The fractions (10 mL/tube) were collected using an automatic fraction collector, and 1 mL was removed from each tube and mixed with 1 mL of distilled water, 0.5 mL of 6% phenol solution and 5 mL of sulfuric acid. The absorbance was determined at 490 nm after reaction for 20 min using an ELISA reader (MULTISKAN GO, Thermo Fisher Scientific, USA). Four final fractions were collected, dialyzed and lyophilized, namely, CWP, CWP-0.2, CWP-0.5 and CWP-2, with yields of 35.10, 27.32, 0.83, and 0.98%, respectively. Due to the low yields of CWP-0.5 and CWP-2, only CWP and CWP-0.2 were further used to analyze the purity, chemical structure and biological activity. The purities of CWCP, CWP and CWP-0.2 were determined by the phenol-sulfuric acid method (17).

Analysis of molecular weight

The high-performance gel permeation chromatography (HPGPC) method was used to analyze the molecular weight (18). The sample and dextran with different molecular weight were prepared at 5 mg/mL and centrifuged (12,000 rpm, 10 min). The supernatant was filtered through a micropore filter with an injection volume of 20 μL. The high-performance liquid chromatography (HPLC) analysis system (Shimadzu LC-10A) was equipped with a BRT102 gel column (8 × 300 mm) (Borui Saccharide, Biotech. Co. Ltd.). The experimental conditions were as follows: column oven temperature: 40°C, flow rate: 0.8 mL/min, and mobile phase: ultrapure water.

Analysis of monosaccharide composition

Gas chromatography (GC) was used for the identification and quantification of monosaccharide components. CWP and CWP-0.2 (5 mg/mL) were hydrolysed with trifluoroacetic acid (2 M) at 120°C for 4 h. The released monosaccharides were converted into trimethysilylated derivatives and analyzed by GC on an Agilent 6890 instrument (Agilent Technologies, Santa Clara, CA, USA) equipped with an HP-5MS column (0.25 mm × 30 m × 0.25 μm) and were determined using a flame ionization detector (FID). The column temperature and other parameters were set according to a previous method (19).

Methylation analysis

Methylation analysis was performed by a previously described method (20). Briefly, 10 mg of CWP or CWP-0.2 and 2 mg of NaOH were dissolved in 100 μL of DMSO, and then methyl iodide was added to the reaction. Methylated polysaccharide was taken, and 2 M trifluoroacetic acid (1 mL) was hydrolysed for 90 min and then evaporated to dryness by a rotary evaporator. The residues were hydrolysed with 10 mL of 2 M trifluoroacetic acid (10 mL) at 100°C for 8 h, the hydrolysates were dissolved in 4 mL of cold 1% (w/w) NaOH, and then 3 mL of toluene was added. Samples were concentrated under reduced pressure and evaporated to dryness. The acetylated product was dissolved in 3 mL of chloroform and transferred to a separatory funnel. The chloroform layer was dried with anhydrous sodium sulfate, and the volume was fixed at 10 mL. The analysis was performed using a Shimadzu GCMS-QP 2010 gas chromatography-mass spectrometer.

Nuclear magnetic resonance spectroscopy (NMR) spectroscopic analysis

In a D_2O solution at 20°C, Bruker Avance 600 and Bruker Avance 500 NMR spectrometers (Bruker, Ettlingen Germany) were used to record proton NMR and ^{13}C APT NMR spectra (operating frequencies of 1H: 600.1 MHz and 499.8 MHz, operating frequencies of ^{13}C: 150.9 MHz and 125.7 MHz). MestReNova 10.0 (Mestrelab Research, Santiago de Compostela, Spain) and Origin 6.0 (Microsoft Windows, Redmond, USA) were used to analyse the data and generate NMR spectra. ^{1}H and ^{13}C spectra, Dept135, HSQC, HHCOSY and HMBC spectra and CWP and CWP-0.2 spectra were recorded at 30 MHz with an MBC spectrometer (Bruker, Rheinstetten, Germany). Tetramethoxysilane was used as an internal standard.

Assay of antioxidant activity

DPPH·radical scavenging activity

The DPPH·radical scavenging capability of CWP and CWP-0.2 was evaluated according to our previous method with slight modification (21). CWP and CWP-0.2 were dissolved in distilled water at different proportions (0.5–2.5 mg/mL), and 2 mL of the polysaccharide solution was added to tubes mixed with 2 mL of DPPH· solution (0.2 mM). The mixture was co-incubated for 30 min in the dark at room temperature. The absorbance of the resulting solution was detected at 517 nm, and Trolox was used as a positive control.

Scavenging rate (%) $= [1-(A_i\text{-}A_j)/A_0]\times 100$ (I)

where A_0 is the absorbance of the control (distilled water instead of samples), A_i is the absorbance in the presence of the sample and DPPH·, and A_j is the absorbance of the sample blank (ethanol instead of DPPH·).

ABTS·$^+$ radical scavenging activity

The ABTS·$^+$ radical scavenging capability of CWP and CWP-0.2 was measured using the reported method with some modifications (22). The ABTS·$^+$ reaction solution was prepared using a balanced mixture of ABTS (7.4 mM) and potassium persulfate (2.6 mM), and the mixture was incubated at 25°C for 12 h. The absorbance was adjusted to 0.7 ± 0.02 at 734 nm. For each sample, 0.4 mL of CWP and CWP-0.2 (0.5–2.5 mg/mL) were mixed with 1.6 mL of $ABTS^+$, and the mixture was co-incubated for 6 min in the dark at room temperature. The absorbance was measured at 734 nm, and Trolox was used as a positive control.

Scavenging rate (%) $= [1-(A_i\text{-}A_j)/A_0]\times 100$ (II)

where A_0 is the absorbance of the control (distilled water instead of samples), A_i is the absorbance in the presence of the sample and the $ABTS^+$ reaction solution, and A_j is the absorbance of the sample blank (PBS instead of the $ABTS^+$ reaction solution).

The free radical scavenging activity was expressed as trolox antioxidant equivalent capacity (TAEC, μM/g).

Assay of immunological activity

Cell cultures and treatment

The cell culture followed a published procedure with slight modification (23). Mouse RAW 264.7 macrophage cells were cultured in RPMI 1640 medium supplemented with 10% FBS, 1% streptomycin and 1% penicillin. Cells were seeded in 96-well tissue culture plates at a density of 2.5×10^6 cells per well, with various concentrations of CWP and CWP-0.2 (20, 40, 60 μg/mL) or LPS (1 μg/mL) as a positive control group treated with RPMI 1640 medium instead of sample. The 96-well tissue culture plates were incubated at 37°C in 5% CO_2/95% air for 24 h, and NO,

10.3389/fnut.2022.946736

TABLE 1 Purity, molecular weight, and monosaccharids composition of CWP and CWP-0.2.

Polysaccharides	Purity (%)	Molecular weight (Da)	Monosaccharids composition ratios	
			Monosaccharids	Ratio (mol%)
CWP	92.26 ± 1.38	7.37×10^5	Man	44.6
			Glc	55.4
CWP-0.2	94.45 ± 2.01	1.58×10^4	Rha	10.6
			Ara	23.3
			Man	5.2
			Glc	4.9
			Gal	56

MCP-1, TNF-α, and IL-6 levels in the culture medium were measured to determine the production of cytokines.

Quantification of NO, TNF-α, MCP-1, and IL-6

The production of NO by 2.5×10^6 cells/well in a 96-well tissue culture plate induced by 20, 40, and 60 μg/mL CWP and CWP-0.2 was determined after 24 h. TNF-α, MCP-1, and IL-6 concentrations in the supernatants from cell cultures were measured using ELISA kits according to the manufacturer's instructions. NO production was analyzed as the accumulation of nitrite in the 96-well tissue culture plate, determined with Griess reagent. Briefly, culture supernatant (50 μL) was pipetted from the 96-well tissue culture plate and mixed with 50 μL of Griess reagent. After incubation for 15 min in a cell incubator, the absorbance was measured using a SpectraMax 384 plus ELISA reader (Molecular Devices, Sunnyvale, CA, USA) at a 540 nm wavelength using Maxpro 6.2.1 software (Molecular Devices) (24). The concentration of nitrite was calculated based on a standard curve of sodium nitrite (0–100 μM).

Statistical analyses of data

All data are expressed as the mean ± standard deviation (SD). Statistical analysis was performed using SPSS (version 17.0). ANOVA with Dunnett's *post hoc* test was used to determine the significant differences between group means at $p < 0.05$. All analyses were processed at least three times.

Results and discussion

Purity and molecular weight

The purity of CWCP isolated from chickpea seeds was 80.34%. Chromatographic purification enabled two required fractions to be collected, and the purities of CWP and CWP-0.2 were 92.26 and 94.45%, respectively (Table 1). As shown in Figure 1A, CWP and CWP-0.2 showed single and symmetrical peaks, and the higher peaks, at 47 min, were NaCl in the mobile phase. The analysis indicated that the average molecular weights (Mw) of CWP and CWP-0.2 were 7.37×10^5 Da and 1.58×10^4 Da, respectively (Figures 1B,C; Table 1). Previous studies

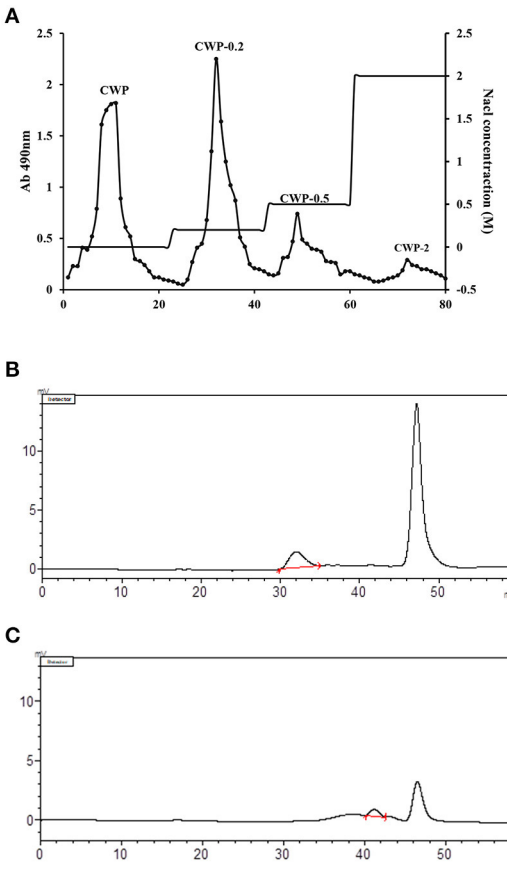

FIGURE 1
(A) Elution curve of chickpea polysaccharide on a DEAE Sepharose Fast Flow column. The crude polysaccharide was dissolved in distilled water and applied to the column, with elution with distilled water and NaCl (0.0–2.0 M). The eluent solution was collected and the carbohydrate content of the collected fraction was monitored using the phenol-sulfuric acid method. GPC chromatogram of **(B)** CWP and **(C)** CWP-0.2 for molecular weight determination with the size exclusion method Chromatography (SEC).

10.3389/fnut.2022.946736

TABLE 2 Monosaccharide linkage analysis of CWP and CWP-0.2 (molar ratios %).

Polysaccharides	RT	Methylated sugar	Mass fragments (m/z)	Ratios	Type of linkage
CWP	19.761	2,3,4,6-Me4-Glc*p*	43,71,87,101,117,129,145,161,205	16.04	Glc*p*-(1→
	24.583	3,4,6-Me3-Man*f*	43,71,87,99,101,129,145,161,189	40.51	→ 1)-Man*f*-(2→
	24.754	3,4,6-Me3-Glc*f*	43,71,87,99,101,129,145,161,189	43.43	→ 1)-Glc*f*-(2→
CWP-0.2	9.569	2,3,4-Me_3-Ara*f*	43,71,87,101,117,129,145,161	8.2	Ara*f*-(1→
	14.691	2,3-Me_2-Ara*f*	43,71,87,99,101,117,129,161,189	8.2	→ 5)-Ara*f*-(1→
	14.967	2,3-Me_2-Ara*p*	43,71,87,99,101,117,129,161,189	6.9	→ 4)-Ara*p*-(1→
	17.591	2,3,4,6-Me_4-Gal*p*	43,71,87,101,117,129,145,161,205	12.4	Gal*p*-(1→
	18.901	3-Me_1-Rha*p*	43,87,101,117,129,143,159,189	10.6	→ 2,4)-Rha*p*-(1→
	20.846	2,4,6-Me_3-Man*p*	43,71,87,99,101,129,145,161,189	8.2	→ 2)-Man*p*-(1→
	21.143	2,3,6-Me_3-Gal*p*	43,87,99,101,113,117,129,131,161,173,233	7.9	→ 4)-Gal*p*-(1→
	21.436	2,3,6-Me_3-Glc*p*	43,87,99,101,113,117,129,131,161,173,233	7.3	→ 4)-Glc*p*-(1→
	22.241	2,4,6-Me_3-Gal*p*	43,87,99,101,117,129,161,173,233	10.7	→ 3)-Gal*p*-(1→
	24.49	2,3,4-Me_3-Gal*p*	43,87,99,101,117,129,161,189,233	9.6	→ 6)-Gal*p*-(1→
	29.619	2,4-Me_2-Gal*p*	43,87,117,129,159,189,233	10	→ 3,6)-Gal*p*-(1→

Data are expressed as mol % and represent the mean of three analysis. The PMAA derivative of a 5-linked-L-arabinofuranosyl* residue 1,4,5-Tri-O-acetyl-1-deuterio-2,3-di-O-methyl-D-arabinitol; The PMAA derivative of a 4-linked-L-arabinopyranosyl residue 1,4,5-Tri-O-acetyl-1-deuterio-2,3-di-O-methyl-D-arabinitol.

have uncovered that the molecular weight of polysaccharides extracted from chickpea hulls is 7.8×10^5 Da to 3.1×10^6 (4, 13). The present results showed that molecular weights of polysaccharides extracted from chickpea seeds were lower than that from chickpea hulls.

Monosaccharide compositions and linkage analysis

CWP consisted of Man and Glc with a molar percent of 44.6:55.4. CWP-0.2 was composed of Rha, Ara, Man, Glc, and Gal with a molar percent of 10.6:23.3:5.2:4.9:56, respectively (Table 1). The molar percentages of Gal are large (more than 50%) in CWP-0.2. Ye et al. (4) uncovered the monosaccharide compositions of polysaccharides from chickpea, which consisted of Man, Rha, GalA, Glc, Gal and Ara, with a molar ratio of 0.03:0.43:0.06:0.06:0.43:0.11; CHPS-2 was composed of Man, Rha, GalA, Gal, Xyl, and Ara, with a molar ratio of 0.03:0.22:0.17:0.43:0.06:0.09; and CHPS-3 consisted of Rha, GalA and Gal, with a molar ratio of 0.34:0.08:0.57 (4). Akhtar et al. (13) also analyzed the monosaccharide compositions of CHPS, in which the molar percentages of galacturonic acid and galactose were 42.17 and 23.15%, respectively (13). Thus, our results were mutually confirmed.

To determine the linkage types, CWP and CWP-0.2 were subjected to methylation analysis (Table 2). The results showed that the main glycosidic bonds of CWP and CWP-0.2 were different. For CWP, the main glycosidic bonds were→ 1)-Glc*f*-(2→ , → 1)-Man*f*-(2→ and Glc*p*-(1→ . The results of monosaccharide composition showed that CWP was composed of mannose and glucose. Whereas, the methylation results suggested that CWP was composed of fructan, because fructose was a ketose, it would be isomerized into mannose and glucose in the reduction process. For CWP-0.2, 11 glycosidic bonds were detected, and the main glycosidic bonds were Gal*p*-(1→ , → 3)-Gal*p*-(1→ and → 2, 4)-Rha*p*-(1→ . The se results were almost consistent with the ratio of monosaccharide. For the → 5)-Ara*f*-(1→ and → 4)-Ara*p*-(1→ in CWP-0.2, → 5)-Ara*f*-(1→ was common in polysaccharide, while → 4)-Ara*p*-(1→ usually appeared in the form of xyl*p*1–4. Therefore, we compared the results of monosaccharide composition and it was arabinose not xylose. There was no doubt that two forms of arabinoside bonds existed, isomerism. The same phenomenon was reported in a previous study (25).

NMR spectroscopy

All NMR spectra of CWP and CWP-0.2 are shown in Figures 1, 2, respectively. The major chemical shifts are listed in Table 2. Signals were assigned using literature values (26, 27). 1D NMR spectra, including ^{1}H, ^{13}C and DEPT135 (Figures 2A–C, 3A–C), in CWP and CWP-0.2 had obvious differences. For the proton spectrum signals, the ^{1}H-NMR signals of CWP mainly focused on 3.0–5.5 ppm (Figure 2A), while CWP-0.2 ^{1}H-NMR signals were focused on 1–8 ppm (Figure 3A). The 0–3.2 ppm peaks were attributed to the hydrogen signals of aliphatic alkanes. The 3.2–5.5 ppm peaks belonged to the hydrogen signals of polysaccharides, while the 6.5–8 ppm peaks belonged

10.3389/fnut.2022.946736

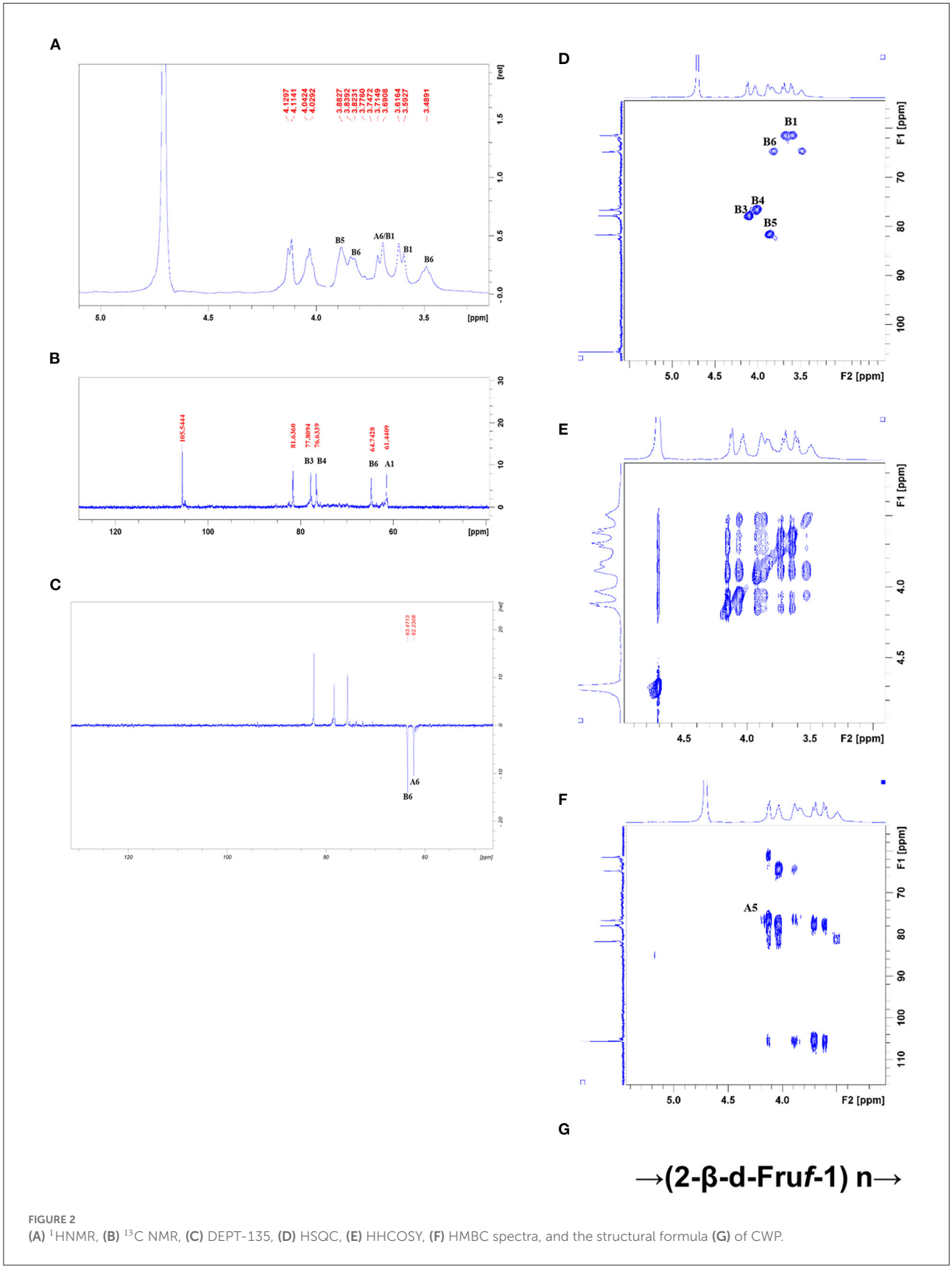

FIGURE 2
(A) ^{1}HNMR, **(B)** ^{13}C NMR, **(C)** DEPT-135, **(D)** HSQC, **(E)** HHCOSY, **(F)** HMBC spectra, and the structural formula **(G)** of CWP.

10.3389/fnut.2022.946736

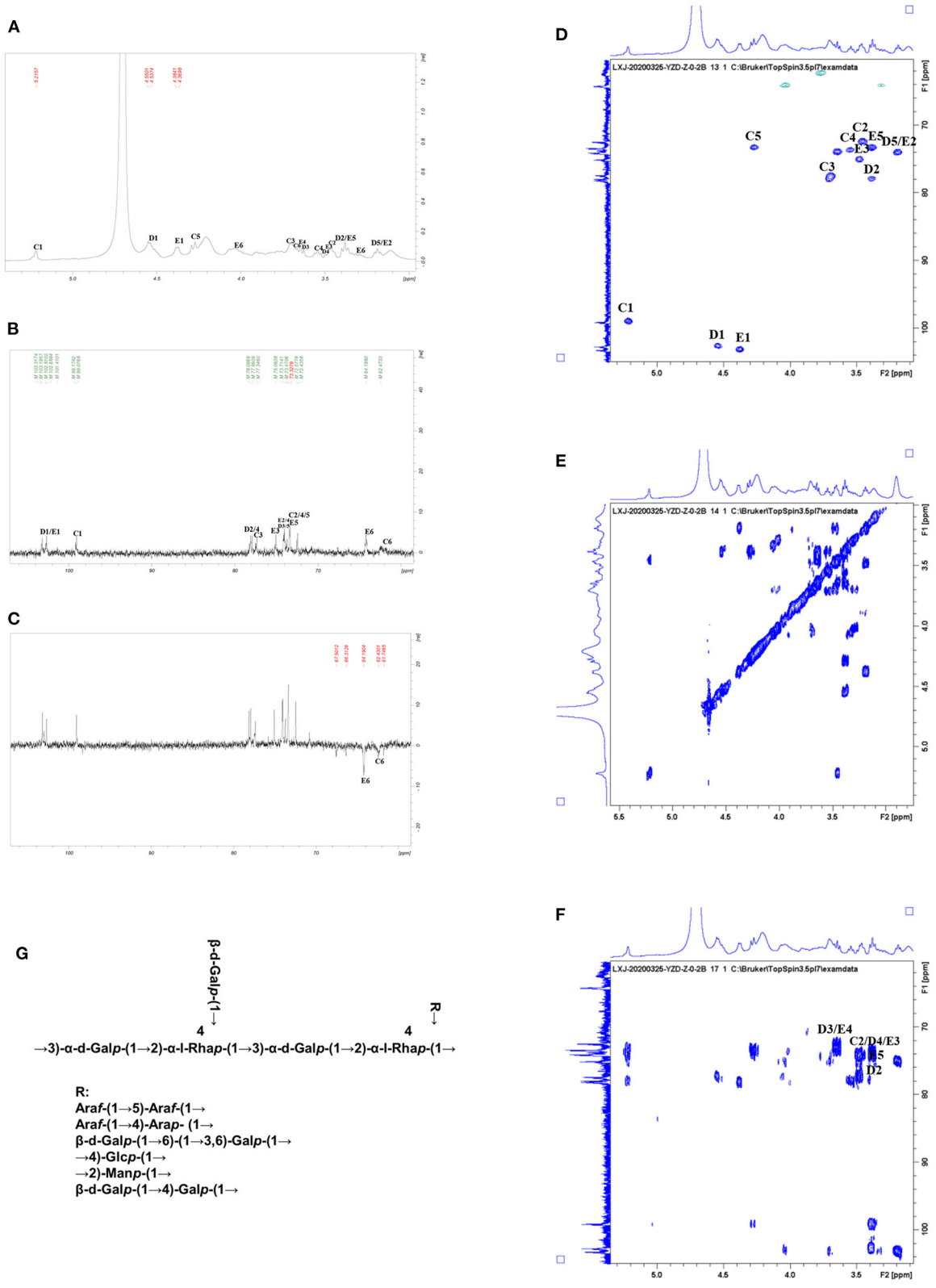

FIGURE 3
(A) ^{1}HNMR, **(B)** ^{13}C NMR, **(C)** DEPT-135, **(D)** HSQC, **(E)** HHCOSY, **(F)** HMBC spectra, and the structural formula **(G)** of CWP-0.2.

10.3389/fnut.2022.946736

TABLE 3 The major ^{13}C NMR Chemical shift (ppm) for CWP and CWP-0.2.

Polysaccharide	Glycosyl residues	H1a C1	H1b C1	H2 C2	H3 C3	H4 C4	H5 C5	H6a C6a	H6b C6b
CWP	**Residue B:** β-d-Fru*f*-2,1	3.6	3.68		4.1	4.01	3.87	3.48	3.82
		61.31		104.54	77.77	76.56	81.86	64.62	
CWP-0.2	**Residue C:** → 3)-α-d-Gal*p*-(1→	5.21		3.46	3.7	3.54	4.28	3.66	3.66
		99.12		72.5	77.43	73.43	73.17	62.05	62.05
	Residue D: → 2,4)-α-d-Rha*p*-(1→	4.54		3.39	3.64	3.48	3.19	1.27	
		102.8		77.92	73.99	77.67	74.04	17.71	
	Residue E: β-d-Gal*p*-(1→	4.38		3.19	3.47	3.65	3.39	3.3	4.04
		103.15		74.04	75.09	73.99	73.25	64.14	

TABLE 4 The antioxidant activity of CWP and CWP-0.2.

Polysaccharide	DPPH· free radical scavenging activity (TAEC, μM/g)	$ABTS^{\cdot+}$ radical scavenging activity (TAEC, μM/g)
CWP	2.35 ± 0.39^{b}	6.99 ± 0.44^{b}
CWP-0.2	4.92 ± 0.95^{a}	17.04 ± 0.87^{a}

Data are expressed as mean ± standard. Means within each column with different lowercase letters are significantly different ($p < 0.05$).

to aromatic hydrogen signals. According to Figure 3A, CWP-0.2 was mainly composed of galactose, which was consistent with the details of Table 1. In the ^{13}C NMR (126 MHz, D_2O) carbon spectra, the ^{13}C NMR signals of CWP and CWP-0.2 were both mainly concentrated from 60 to 120 ppm. As shown in Figure 2B of CWP, the main anomeric carbon signal peaks were δ105.54, 81.64, 77.81, 76.63, 64.74 and 61.44. For Figure 3B of CWP-0.2, the anomeric carbon signal peaks were mainly δ103.32, 103.20, 102.81, 102.69, 101.41, 99.18, 99.08, 78.10, 77.89, 77.35, 75.09, 73.71, 73.47, 73.33, 72.58, 72.44, 64.20 and 62.47. In the Dept135 spectra, for the CWP, we found that the methylene signal peaks δ 62.23 and δ 63.47 belonged to C1 and C6 of the fructose residues, respectively (Figure 2C). Regarding CWP-0.2, the peaks of 67.50, 66.31, 64.19, 62.43 and 61.75 were inverted, indicating that 67.50, 66.31, 64.19, 62.43 and 61.75 might be the chemical shifts of C6 (Figure 3C). Combined with the ^{13}C NMR and Dept135 spectra of CWP-0.2 (Figures 3B,C), the methylene signal peaks were mainly δ 23.40-67.51 ppm, the peaks at 67.51, 66.32, 64.20, 62.44 and 61.76 ppm were the C6 signal peaks of sugar and 14.51, 19.93, 21.61 PPM were methyl signals. According to the HSQC (Figures 2D, 3D) and ^{1}H-$^{1}HCOSY$ (Figures 2E, 3E) 2D spectra of CWP and CWP-0.2, the chemical displacements of ^{1}H NMR and ^{13}C NMR of the main residues were classified in Table 3. For the CWP, in HHCOSY analysis, three groups of chemical displacements located at 4.10/4.01, 4.01/3.87, and 3.87/3.48 represent the correlations of H3–H4, H4–H5, and H5–H6 on the fructose residue (Figure 2E). For the CWP-0.2, 99.12 ppm of anomeric carbon and 5.21 ppm of anomeric hydrogen were determined in the HSQC spectrum (Figure 3D). Then, according to HHCOSY (Figure 3E), the signals of H1–2, H2–3, H3–4, and H4–5 were 3.54/4.28, 5.21/3.46, 3.46/3.70, 3.70/3.54, and 3.54/4.28, respectively. Therefore, we inferred that H1, H2, H3, H4, and H5 of the signals were 5.21, 3.46, 3.7, 3.54 and 4.28 ppm, respectively. The corresponding C1–5 signals were 99.12, 72.5, 77.43, 73.43, and 73.17 ppm, and the chemical shift of C6 was 64.14. Therefore, the signal should go to → 3)-α-d-Gal*p*-(1→ . Similarly, connection modes of → 2,4)-α-l-Rha*p*-(1→ and β-d-Gal*p*-(1→ were also detected. HMBC 2D spectra analyses of CWP and CWP-0.2 were shown in Figures 2F, 3F. From the HMBC spectrum of CWP (Figure 2F), δ104.56 and δ3.60, 3.68 had correlation peaks, which were classified as C2 (β-d-Fru*f*-2,1)-H1a,b (β-d-Fru*f*-2,1), indicating → 2-β-d-Fru*f*-1→ 2-β-d-Fru*f*-1→ . At the same time, we also detected H3(β-d-Fru*f*-2,1)-C2 (β-d-Fru*f*-2,1), H5(β-d-Fru*f*-2,1)-C2 (β-d-Fru*f*-2,1). Meanwhile, the cross peaks of H4 (β-d-Fru*f*-2,1)-C5 (β-d-Fru*f*-2,1), H3 (β-d-Fru*f*-2,1)-C5 (β-d-Fru*f*-2,1) and H1a, b (β-d-Fru*f*-2,1)-C3 (β-d-Fru*f*-2,1) were observed in the HSQC scheme (Figure 2D). These results were consistent with the NMR analysis results. Regarding the HMBC spectrum of CWP-0.2 (Figure 3F), the anomeric carbon of → 3)-α-d-Gal*p*-(1→ and H2 of the → 2,4)-α-l-Rha*p*-(1→ correlation peaks were detected. Meanwhile, the anomeric hydrogen of → 3)-α-d-Gal*p*-(1→ and C2 of the → 2,4)-α-l-Rha*p*-(1→ correlation peaks were also detected. These two findings suggest the existence

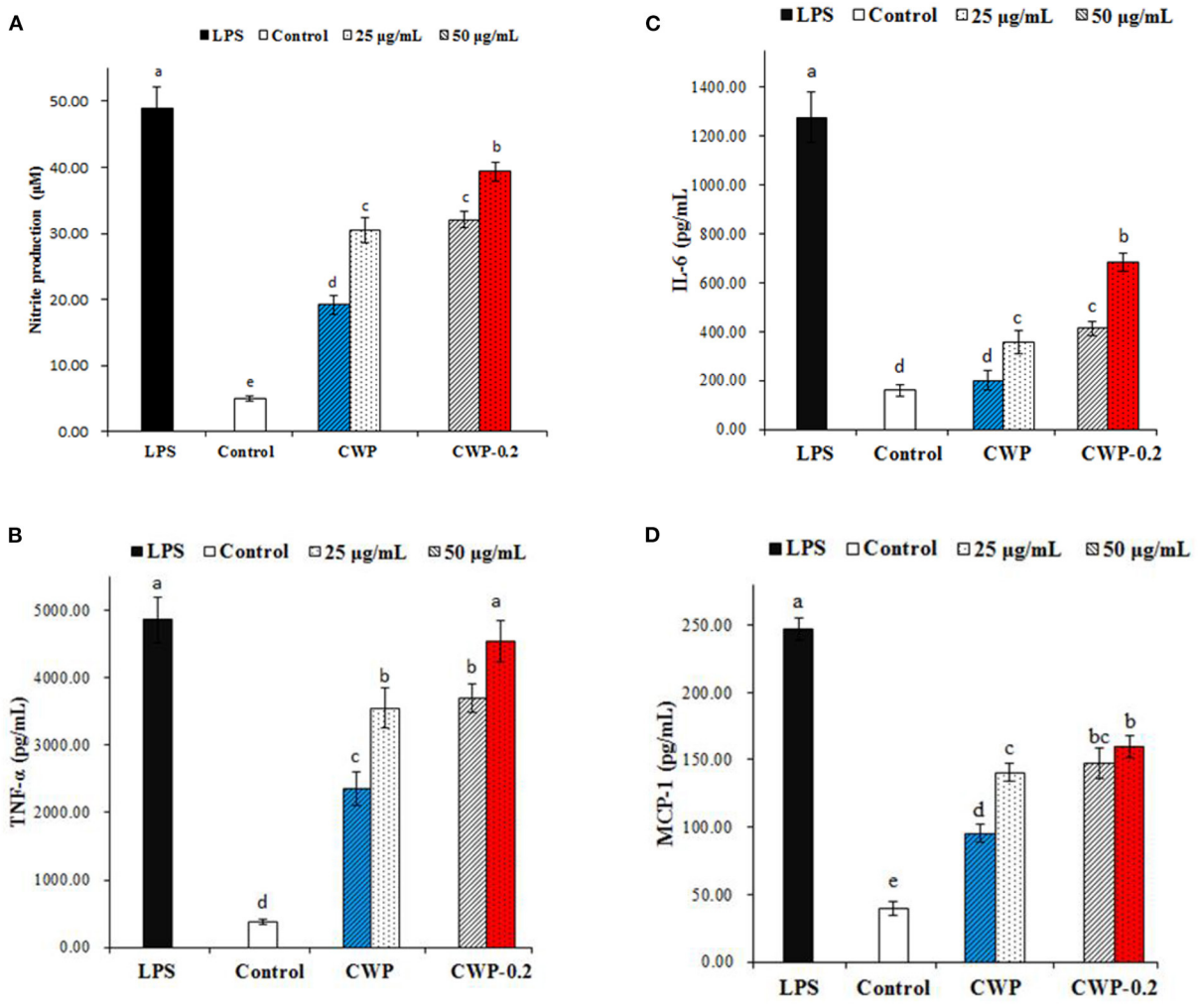

FIGURE 4
Effects of polysaccharides CWP and CWP-0.2 on RAW 264.7 macrophage **(A)** NO, **(B)** TNF-α, **(C)** IL-6, and **(D)** MCP-1 production. Values are the mean ± SD ($n = 3$). The different small letters in different columns represent significant difference at 0.05 level.

of → 3)-α-d-Gal*p*-(1→ 2,4)-α-l-Rha*p*-(1→ . Similarly, the correlation peaks, the anomeric carbon of → 2,4)-α-l-Rha*p*-(1→ and H3 of → 3)-α-d-Gal*p*-(1→ , the anomeric hydrogen of → 2,4)-α-l-Rha*p*-(1→ and C3 of → 3)-α-d-Gal*p*-(1→ , are consistent, indicating the presence of → 2,4)-α-l-Rha*p*-(1→ 3)-α-d-Gal*p*-(1→ . At the same time, the anomeric carbon of β-d-Gal*p*-(1→ and H4 of → 2,4)-α-l-Rha*p*-(1→ had correlation peaks, indicating the existence of β-d-Gal*p*-(1→ 2,4)-α-l-Rha*p*-(1→.

Therefore, the main chain connection of CWP was → (2-β-d-Fru*f*-1) n→ (Figure 2G). Regarding the main chain connection of CWP-0.2, the → 2,4)-α-l-Rha*p*-(1→ 3)-α-d-Gal*p*-(1→ was backbone, and the branched chain was linked to the backbone by → 2,4)-α-l-Rha*p*-(1→ o-4 (Figure 3G). According to the results of monosaccharide composition and NMR, it can be confirmed that the polysaccharide is inulin polysaccharide.

Antioxidant activities

It has been reported that plant polysaccharides could protect the body from oxidative damage (28). The antioxidant activities of CWP and CWP-0.2 were measured using DPPH· and $ABTS^{\cdot+}$ assays, which have been widely used in evaluating the antioxidant activities of various natural extracts. As shown in Table 4, all polysaccharide fractions exhibited antioxidant activity, and CWP-0.2 showed a higher scavenging activity against DPPH· and $ABTS^{\cdot+}$ than CWP. Yao et al. (9) reported that the scavenging activity of polysaccharides may be related to the molecular weight. Due to the lower molecular weight of CWP-0.2, it had a higher free radical scavenging capacity, both for DPPH· and $ABTS^{\cdot+}$ assays. Ye et al. (4) reported that polysaccharides from chickpea hulls (CHPS-1, CHPS-2, and CHPS-3) showed significant antioxidant activity against DPPH and ABTS free radicals, superoxide

anion radicals and reducing power (4). All results suggested that polysaccharides from chickpea could be developed as potential antioxidants in the food, pharmacy, and cosmetic industries.

Immunoregulatory activities

Nitric oxide (NO) is a significant signaling molecule in many tissues that play important roles in regulating varieties of physiological processes. Nitrite concentrations in the supernatant of polysaccharide-stimulated macrophages were determined as a reflection of NO production. Figure 4A showed the effects of different concentrations (25 and 50 μg/mL) of CWP and CWP-0.2 on the production of NO on RAW 264.7 cells. Compared with the control group, the production of NO significantly increased in CWP and CWP-0.2 in a dose-dependent manner at concentrations ranging from 25 to 50 μg/mL. In addition, CWP-0.2 showed significantly higher NO production than CWP at both concentrations, indicating a higher influence on macrophage activation.

Previous research has shown that activated macrophages play a significant role in mediating innate and adaptive immune responses via the production of a signaling chemical (NO) and cytokines (29). In this work, we also evaluated the effect of polysaccharides on the production of TNF-α, IL-6, and MCP-1 by RAW 264.7 macrophages, which were multifunctional cytokines associated with the production of NO and had a net effect on balancing its proinflammatory and immunosuppressive activities (30). As shown in Figures 4B–D, CWP or CWP-0.2 (25 and 50 μg/mL) treatment significantly increased the production of TNF-α, IL-6, and MCP-1 in RAW 264.7 cells in a concentration-dependent manner. CWP-0.2 showed stronger auxo-actions on TNF-α, IL-6, and MCP-1 production than CWP at both concentrations, which was similar to the production of NO. This might be because CWP-0.2, with its lower molecular weight, easily entered macrophages and even increased the strength of interactions between functional groups (hydroxyl or carboxylic groups) and proteins of RAW264.7 cells (29). Similar to these results, in our previous study, we obtained four fractions of water-extractable polysaccharides from adzuki bean, AAP-1 (94.2 kDa), AAP-1' (63.1 kDa), AAP-2 (82.3 kDa), and AAP-2' (60.4 kDa), and AAP-2', with the smallest molecular weight, showed the most potential activities and induced statistically higher NO production (29). It has been extensively shown that the immunomodulatory activity of polysaccharides was dependent on their chemical composition, molecular weight, conformation, glycosidic linkage, and degree of branching (31). However, studies on the immunoregulatory activities of chickpea polysaccharides were still limited. Further study should be focused on the immunoregulatory activities and the relationship between the immunoregulatory mechanism and the structure of chickpea polysaccharides.

Conclusion

In conclusion, two polysaccharide fractions, were obtained and purified from chickpea seeds. Their molecular weight was determined to be 7.37×10^5 Da and 1.58×10^4 Da, respectively. Further structural characterization indicated that the main chain connection of CWP was → (2-β-d-Fru*f*-1) n→ , and the main chain connection of CWP-0.2 was explored as → 2,4)-α-l-Rha*p*-(1→ 3)-α-d-Gal*p*-(1→ with the branched chain of → 2,4)-α-l-Rha*p*-(1→ o-4. The antioxidant and immunoregulatory activities of the two fractions were also demonstrated, and CWP-0.2 revealed significantly higher activity than CWP. These results will expand the knowledge of chickpea polysaccharides, and contribute to clarifying the benefits of chickpea foods.

Data availability statement

The original contributions presented in the study are included in the article/supplementary material, further inquiries can be directed to the corresponding author/s.

Author contributions

YZ, ZS, and YW contributed to conception and design of the study. YZ, ZS, YY, and BD organized the database. ZS and YW performed the statistical analysis. YZ wrote the first draft of the manuscript. ZS, YW, and BD wrote sections of the manuscript. All authors contributed to manuscript revision, read, and approved the submitted version.

Funding

This work was supported by the Special National Key Research and Development Plan (2021YFD1600100), Key Laboratory of Grain Crop Genetic Resources Evaluation and Utilization, Chia Agriculture Research System of MOF and MARA (CARS-08-G21) (Food Legumes).

Conflict of interest

The authors declare that the research was conducted in the absence of any commercial or financial relationships that could be construed as a potential conflict of interest.

Publisher's note

All claims expressed in this article are solely those of the authors and do not necessarily represent those of their affiliated organizations, or those of the publisher, the editors and the reviewers. Any product that may be evaluated in this article, or claim that may be made by its manufacturer, is not guaranteed or endorsed by the publisher.

References

1. Viveros A, Brenes A, Elices R, Arija I, Canales R. Nutritional value of raw and autoclaved Kabuli and Desi chickpeas (*Cicer arietinum* L.) for growing chickens. *Br Poult Sci.* (2001) 42:242–51. doi: 10.1080/00071660120048500

2. Ma H, Wang J, Qi H, Gao Y, Pang L, Yang Y, et al. Assessment of the estrogenic activities of chickpea (*Cicer arietinum* L) sprout isoflavone extract in ovariectomized rats. *Acta Pharmacol Sin.* (2013) 34:380–6. doi: 10.1038/aps.2012.160

3. Jukanti AK, Gaur PM, Gowda CLL, Chibbar RN. Nutritional quality and health benefits of chickpea (*Cicer arietinum* L.): a review. *Br J Nutr.* (2012) 108:S11––26. doi: 10.1017/S0007114512000797

4. Ye Z, Wang W, Yuan Q, Ye H, Sun Y, Zhang H, et al. Box–Behnken design for extraction optimization, characterization and *in vitro* antioxidant activity of *Cicer arietinum* L. hull polysaccharides. *Carbohydr Polym.* (2016) 147:354–64. doi: 10.1016/j.carbpol.2016.03.092

5. Zia-Ul-Haq M, Khan BA, Landa P, Kutil Z, Ahmed S, Qayum M, et al. Platelet aggregation and anti-inflammatory effects of garden pea, Desi chickpea and Kabuli chickpea. *Acta Pol Pharm.* (2012) 69:707–11. doi: 10.4103/0253-7613.99352

6. Wang Z, Chen M, Zhu Y, Qian P, Zhou Y, Wei J, et al. Isolation, identification and characterization of a new type of lectin with α-amylase inhibitory activity in chickpea (*Cicer arietinum* L.). *Protein Pept Lett.* (2017) 24:1008–20. doi: 10.2174/0929866524666170711120501

7. Mokni Ghribi A, Sila A, Maklouf Gafsi I, Blecker C, Danthine S, Attia H, et al. Structural, functional, and ACE inhibitory properties of water-soluble polysaccharides from chickpea flours. *Int J Biol Macromol.* (2015) 75:276–82. doi: 10.1016/j.ijbiomac.2015.01.037

8. Klaus A, Kozarski M, Niksic M, Jakovljevic D, Todorovic N, Van Griensven LJLD. Antioxidative activities and chemical characterization of polysaccharides extracted from the basidiomycete Schizophyllum commune. *LWT Food Sci Technol.* (2011) 44:2005–11. doi: 10.1016/j.lwt.2011.05.010

9. Yao Y, Zhu Y, Ren G. Antioxidant and immunoregulatory activity of alkali-extractable polysaccharides from Mung bean. *Int J Biol Macromol.* (2016) 84:289–94. doi: 10.1016/j.ijbiomac.2015.12.045

10. Ji X, Guo J, Pan F, Kuang F, Chen H, Guo X, et al. Structural elucidation and antioxidant activities of a neutral polysaccharide from Arecanut (*Areca catechu* L.). *Front Nutr.* (2022) 9:853115. doi: 10.3389/fnut.2022.853115

11. Paulsen B. Plant polysaccharides with immunostimulatory activities. *Curr Org Chem.* (2001) 5:939–50. doi: 10.2174/1385272013374987

12. Zhu Y, Dong L, Huang L, Shi Z, Dong J, Yao Y, et al. Effects of oat β-glucan, oat resistant starch, and the whole oat flour on insulin resistance, inflammation, and gut microbiota in high-fat-diet-induced type 2 diabetic rats. *J Funct Foods.* (2020) 69:103939. doi: 10.1016/j.jff.2020.103939

13. Akhtar HMS, Abdin M, Hamed YS, Wang W, Chen G, Chen D, et al. Physicochemical, functional, structural, thermal characterization and α-amylase inhibition of polysaccharides from chickpea (*Cicer arietinum* L.) hulls. *LWT.* (2019) 113:108265. doi: 10.1016/j.lwt.2019.108265

14. Ji X, Cheng Y, Tian J, Zhang S, Shi M. Structural characterization of polysaccharide from jujube (*Ziziphus jujuba* Mill.) fruit. *Chem Biol Technol Agric.* (2021) 8:54. doi: 10.1186/s40538-021-00255-2

15. Yao Y, Shi Z, Ren G. Antioxidant and immunoregulatory activity of polysaccharides from quinoa (*Chenopodium quinoa* willd.). *Int J Mol Sci.* (2014) 15:19307–18. doi: 10.3390/ijms151019307

16. Yu X, Yang X, Cui B, Wang L, Ren G. Antioxidant and immunoregulatory activity of alkali-extractable polysaccharides from North American ginseng. *Int J Biol Macromol.* (2014) 65:357–61. doi: 10.1016/j.ijbiomac.2014.01.046

17. Mizuno T, Iwata Y. Application of the phenol-sulufuric acid method for fractional determination of polysaccharides. *J Japan Soc Food Sci Technol.* (2010) 11:395–9. doi: 10.3136/nskkk1962.11.395

18. Qi J, Kim SM. Effects of the molecular weight and protein and sulfate content of Chlorella ellipsoidea polysaccharides on their immunomodulatory activity. *Int J Biol Macromol.* (2017) 107(Pt. A):70–77. doi: 10.1016/j.ijbiomac.2017.08.144

19. Beretta G, Granata P, Ferrero M, Orioli M, Facino RM. Standardization of antioxidant properties of honey by a combination of spectrophotometric/fluorimetric assays and chemometrics. *Anal Chim Acta.* (2005) 533:185–91. doi: 10.1016/j.aca.2004.11.010

20. Tang W, Lu J, Xie L, Huang J, Wang N, Chu B, et al. Structural characterization and antifatigue effect *in vivo* of Maca (*Lepidium meyenii* Walp) polysaccharide: structural characteristics and antifatigue effect of MP. *J Food Sci.* (2017) 82:759–66. doi: 10.1111/1750-3841.13619

21. Yao Y, Ren G. Effect of thermal treatment on phenolic composition and antioxidant activities of two celery cultivars. *LWT Food Sci Technol.* (2011) 44:181–5. doi: 10.1016/j.lwt.2010.07.001

22. Arnao MB, Cano A, Acosta M. The hydrophilic and lipophilic contribution to total antioxidant activity. *Food Chem.* (2001) 73:239–44. doi: 10.1016/S0308-8146(00)00324-1

23. Methacanon P, Madla S, Kirtikara K, Prasitsil M. Structural elucidation of bioactive fungi-derived polymers. *Carbohydr Polym.* (2005) 60:199–203. doi: 10.1016/j.carbpol.2004.12.006

24. Wang L, Yang X, Yu X, Yao Y, Ren G. Evaluation of antibacterial and anti-inflammatory activities of less polar ginsenosides produced from polar ginsenosides by heat-transformation. *J Agric Food Chem.* (2013) 61:12274–82. doi: 10.1021/jf404461q

25. Li N, Shi C, Shi S, Wang H, Yan J, Wang S. An inulin-type fructan isolated from Artemisia japonica and its anti-arthritic effects. *J Funct Foods.* (2017) 29:29–36. doi: 10.1016/j.jff.2016.11.033

26. Ratnayake RMS, Sims IM, Newman RH, Melton LD. Effects of cooking on the cell walls (dietary fiber) of Scarlet Warren winter squash (*Cucurbita maxima*) studied by polysaccharide linkage analysis and solid-state 13C NMR. *J Agric Food Chem.* (2011) 59:7186–93. doi: 10.1021/jf104784g

27. Wang H, Shi S, Bao B, Li X, Wang S. Structure characterization of an arabinogalactan from green tea and its anti-diabetic effect. *Carbohydr Polym.* (2015) 124:98–108. doi: 10.1016/j.carbpol.2015.01.070

28. Ji X, Guo J, Ding D, Gao J, Hao L, Guo X, et al. Structural characterization and antioxidant activity of a novel high-molecular-weight polysaccharide from Ziziphus Jujuba cv. Muzao. *J Food Mea Charact.* (2022) 16:2191–200. doi: 10.1007/s11694-022-01288-3

29. Yao Y, Zhu Y, Gao Y, Ren G. Effect of ultrasonic treatment on immunological activities of polysaccharides from adlay. *Int J Biol Macromol.* (2015) 80:246–52. doi: 10.1016/j.ijbiomac.2015.06.033

30. Ernandez T, Mayadas T. Immunoregulatory role of TNFα in inflammatory kidney diseases. *Kidney Int.* (2009) 76:262–76. doi: 10.1038/ki.2009.142

31. Dai Z, Su D, Zhang Y, Sun Y, Hu B, Ye H, et al. Immunomodulatory activity *in vitro* and *in vivo* of verbascose from mung beans (*Phaseolus aureus*). *J Agric Food Chem.* (2014) 62:10727–35. doi: 10.1021/jf503510h

frontiers | Frontiers in Nutrition

TYPE Original Research
PUBLISHED 02 August 2022
DOI 10.3389/fnut.2022.963318

Check for updates

OPEN ACCESS

EDITED BY
Qiu Li,
Qingdao Agricultural University, China

REVIEWED BY
Guangjing Chen,
Guiyang University, China
Zihan Song,
Insititute of Vegetables and Flowers (CAAS), China

*CORRESPONDENCE
Xin Lü
xinlu@nwsuaf.edu.cn
Manshun Liu
msliu9299@nwafu.edu.cn

†These authors have contributed equally to this work

SPECIALTY SECTION
This article was submitted to Food Chemistry, a section of the journal Frontiers in Nutrition

RECEIVED 07 June 2022
ACCEPTED 11 July 2022
PUBLISHED 02 August 2022

CITATION
Yue F, Zhang J, Xu J, Niu T, Lü X and Liu M (2022) Effects of monosaccharide composition on quantitative analysis of total sugar content by phenol-sulfuric acid method. *Front. Nutr.* 9:963318. doi: 10.3389/fnut.2022.963318

COPYRIGHT
© 2022 Yue, Zhang, Xu, Niu, Lü and Liu. This is an open-access article distributed under the terms of the Creative Commons Attribution License (CC BY). The use, distribution or reproduction in other forums is permitted, provided the original author(s) and the copyright owner(s) are credited and that the original publication in this journal is cited, in accordance with accepted academic practice. No use, distribution or reproduction is permitted which does not comply with these terms.

Effects of monosaccharide composition on quantitative analysis of total sugar content by phenol-sulfuric acid method

Fangfang Yue[1], Jinrui Zhang[1], Jiaxin Xu[1], Tengfei Niu[1], Xin Lü[1]*† and Manshun Liu[1,2]*†

[1]College of Food Science and Engineering, Northwest A&F University, Yangling, China, [2]College of Enology, Northwest A&F University, Yangling, China

Phenol-sulfuric acid method is one of the most common methods applied to the analysis of total sugar content during polysaccharides study. However, it was found that the results obtained from the phenol-sulfuric acid method was generally lower than the real total sugar content, especially when acidic monosaccharides were contained in the polysaccharides samples. Therefore, the present study focused to unveil the proposed problem. Based on the optimization of colorimetric conditions, such as optimal wave length of absorption, linearity range, color reaction time and temperature, it indicated that the phenol-sulfuric acid method was a convenient and accurate way for the total sugar content analysis. In addition, the color-rendering capabilities of 10 common monosaccharides were systematically analyzed to obtain a relative correction factor for each monosaccharide relative to glucose, which was proved to be the main reason for the deviation in the detection of total sugar content. Moreover, the key points during the application of phenol-sulfuric acid method were suggested. This study provides a scientific theoretical basis and a reliable experimental research method for the accurate determination of total sugar content by the phenol-sulfuric acid method, and which will also promote the application of this convenient method in the polysaccharides study.

KEYWORDS

phenol-sulfuric acid method, total sugar content, polysaccharides, monosaccharides, color-rendering capabilities

Introduction

In recent years, polysaccharide, as an important natural macromolecule, have been found to have various functional activities, such as antioxidant (1, 2), immune regulation (3), anti-tumor (4, 5), alleviation of obesity (6) and so on. Although the research biological activities of polysaccharides have been widely studied (7), the detection methods of the physicochemical properties of polysaccharides still need to be further optimized and perfected. The total sugar content is one of the important indicators of the physicochemical characteristics of polysaccharides.

10.3389/fnut.2022.963318

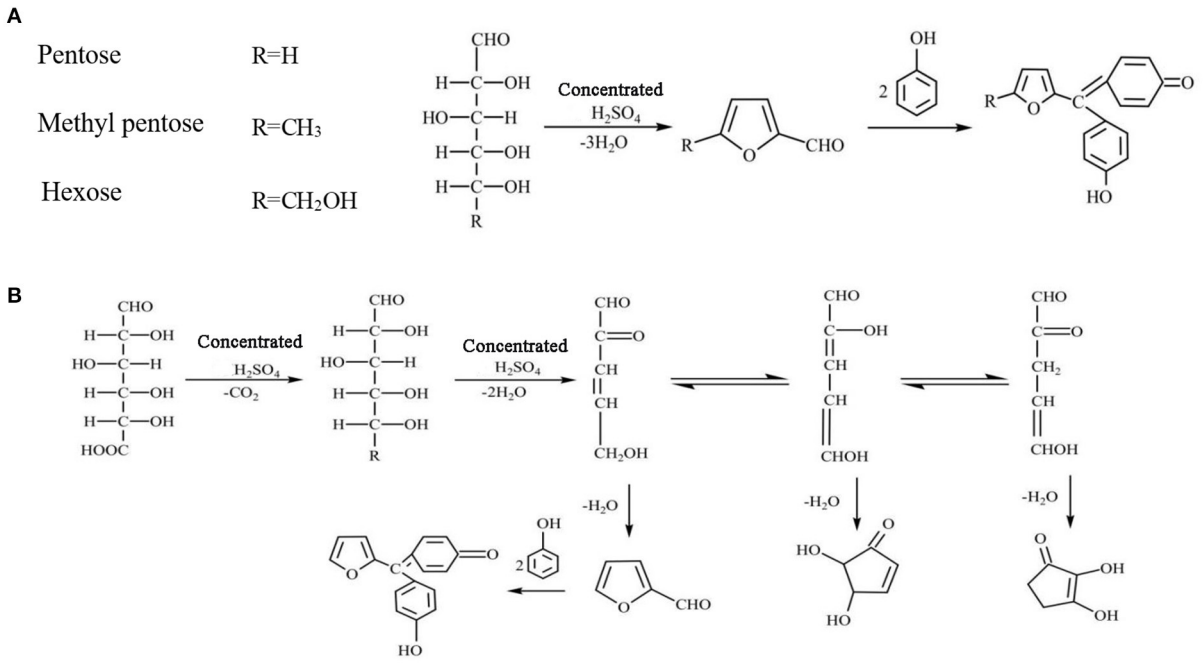

FIGURE 1
Principle of phenol-sulfuric acid method. **(A)** Pentose, methyl pentose and hexose reaction principle. **(B)** Uronic acid reaction principle.

In the industrial production process of polysaccharides, it is often necessary to measure and monitor the content of polysaccharides (8). Due to the wide variety of polysaccharides, the content and existing forms of polysaccharides are also variable (9, 10). Therefore, choosing an appropriate detection method is crucial. The total sugar represents the sum of reducing sugars (glucose, fructose, lactose, etc.) and oligosaccharides (sucrose, etc.) that can be hydrolyzed into reducing sugars under the measurement conditions (11, 12). The determination methods of total sugar content mainly include phenol-sulfuric acid method (2), anthrone-sulfuric acid method (13), full-wavelength enzyme labeling method (14), and direct titration method (15). In the current research, due to the simple detection method, good stability and high sensitivity, phenol-sulfuric acid method is widely used (16). In addition, phenol-sulfuric acid method can also measure methylated sugars, pentoses and polysaccharides, and is not affected by proteins (17, 18).

The determination principle of the phenol-sulfuric acid method is that concentrated sulfuric acid dehydrates polysaccharides to form uronic acid and hydroxyurea formaldehyde, and then condenses with phenol to form orange-red compounds (Figure 1). Within a certain concentration range, the color depth is proportional to the sugar content, which can be determined at OD 490 nm wavelength. However, experimental conditions, such as color development wavelength, color development time, color development temperature, and detection range play an important role in the accuracy of the determination of total sugar content (19). In addition, the calculation of the specific total sugar content needs to be obtained according to the standard curve drawn by standard monosaccharides. At present, glucose is often used as a standard in experiments, which leads to large errors in the determination of sugar content, especially for heteropolysaccharides. Apart from glucose, the hydrolysis of heteropolysaccharides may also generate other monosaccharides, and different monosaccharides have significant differences in structure and physicochemical properties. For example, in terms of functional groups, glucose is aldohexose and fructose is ketohexose (20). Also, ribose, xylose, and arabinose are pentose. And glucose, mannose, galactose, and fructose are hexose (21). In addition, in the process of phenol-sulfuric acid method, pentoses are more likely to react than hexose, the reaction rate of uronic acid is relatively slow, and uronic acid cannot be completely converted. Therefore, it is speculated that there may be significant differences in the color development ability of different monosaccharides after condensation with phenol. Although a great deal of research has been done to improve the phenol-sulfuric acid method, little attention has been paid to the errors caused by standard monosaccharides.

Therefore, this study explored the effect of different monosaccharide compositions on the quantitative analysis of total sugars. Through the independent quantitative analysis of a variety of different monosaccharides, a complete set of color development system for quantitative analysis of total sugars in phenol sulfate was established. The method is conducive to more accurate determination of the total sugar content contained in the present product, and makes up for the defect that the total sugar yield deviates from the actual content due to the large difference in color development of different types of monosaccharides. This experiment improves the rigor and accuracy of total sugar quantitative analysis, and provides a scientific theoretical basis and reliable experimental research methods for future applications in chemical industry, molecular detection and other fields.

Materials and methods

Materials and reagents

Glucose (Glu), Fructose (Fru), Mannose (Man), Galactose (Gal), Xylose (Xyl), Arabinose (Ara), Rhamnose (Rha), Fucose (Fuc), Galactose Uronic acid (GalUA), glucuronic acid (GlcUA), purity ≥ 98%, β-dextran (purity ≥ 80%), fructo oligosaccharide (purity ≥ 95%), xylan (purity ≥ 98%) and polygalacturonic acid (purity ≥ 90%) were purchased from Yuanye Biotechnology Co., Ltd. D-trehalose (purity ≥ 99%) was purchased from Shanghai McLean Biochemical Technology Co., Ltd. All of other chemicals and reagents were analytical grade.

Moisture content detection of monosaccharide standards

Quickly weigh a certain specification of standard monosaccharide. Then, it was dried in an oven with a temperature of 80°C and standard atmospheric pressure for 12 h, and the quality of the standard monosaccharide after drying in the oven was recorded. Calculate the moisture content of the standard monosaccharide by making the difference twice. If the difference between the two weighings does not exceed 0.002 g, it is recorded as constant weight.

Optimization of the phenol-sulfuric acid method

Using glucose as the standard solution, the detection conditions of the phenol-sulfuric acid method for the determination of total sugar were preliminarily determined by optimizing the color wavelength (300–700 nm), color stability (color stability of 10, 40, 80 μg/mL standard grape solution during the detection process), detection range (0–1,000 μg/mL standard grape solution), and heating conditions at 100°C or room temperature (RT).

Monosaccharide ultraviolet absorption spectroscopic analysis

First accurately prepare 100 μg/mL standard solutions of 10 kinds of monosaccharides, then accurately draw 0.8 mL of each monosaccharide standard solution, add distilled water to make up to 2.0 mL, and prepare a monosaccharide standard solution with a solution concentration of 40 μg/mL. Then accurately prepare 80% phenol-ethanol solution and store it in a brown bottle at 4°C away from light. Accurately draw 7.5 mL of 80% phenol solution and dissolve it in 96 mL of absolute ethanol to prepare a 6% phenol solution.

Add 1.0 mL of 6% phenol solution (currently prepared) to the working solutions of 10 monosaccharides, respectively, then quickly add 5.0 mL of concentrated sulfuric acid, mix well in time, and stand at RT for 20 min. Distilled water was used as blank control. Use Ultraviolet-2550 (UV-2550) dual-beam UV spectrophotometer and UV Probe software to measure the full absorption wavelength spectrum of the monosaccharide standard solution and find the maximum absorption peak.

Determination of standard curve of monosaccharide solution

Ten monosaccharide concentration gradient solutions were prepared (10, 20, 30, 40, 50, 60, 70, 80, and 90 μg/mL). Added 1.0 mL of 6% phenol solution, then quickly added 5.0 mL of concentrated sulfuric acid, mixed well in time, and leaved at RT for 20 min. Distilled water was used as blank control. The absorbance of each concentration gradient solution was measured with a 722s visible light spectrophotometer at a wavelength of 490 nm or 480/482/483 nm. A standard curve was made with the concentration as the abscissa and the absorbance as the ordinate. In addition, in order to obtain the correction factor of other monosaccharides relative to glucose, it is necessary to ensure the consistency of other detection conditions. Therefore, the optimal detection conditions (490 nm) for glucose were selected in this study. And the ratio of the slopes of glucose to the monosaccharides is the relative correction factors for different monosaccharides relative to glucose.

Practical application

Five representative polysaccharides, such as β-dextran, D-trehalose, fructo oligosaccharide, xylan and polygalacturonic

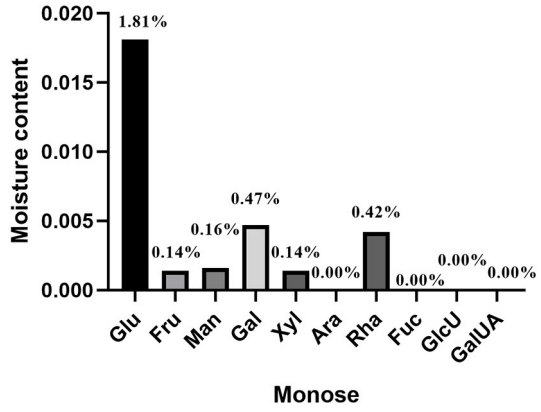

FIGURE 2
Monosaccharide water content measurement results.

acid, were selected for verification of correction factors. A polysaccharide solution with a concentration of about 40 μg/mL was prepared respectively, and the OD490 absorbance value of the polysaccharide solution was obtained by the phenol-sulfuric acid method, then the total sugar content was calculated.

Results

Moisture content analysis of monosaccharide standard

Molecular configurations of different monosaccharides lead to differences in water content. In addition, RT, pressure, altitude and other factors also affect the water content of sugar molecules. The water content has a certain influence on the concentration of monosaccharide molecules. In phenol-sulfuric acid method, the concentration of the monosaccharide solution is an important measurement index. Therefore, the moisture content of 10 monosaccharides was detected. The results showed that the highest water content of glucose was 1.81%, the water content of rhamnose and galactose was about 0.40%, the water content of xylose, mannose and fructose was about 0.14%, and other monosaccharides such as fucose and arabinose and acidic monosaccharides (galacturonic acid and glucuronic acid) are relatively low in water content and can be ignored (Figure 2).

Optimization of the phenol-sulfuric acid method

After the phenol-sulfuric acid reaction, the glucose standard solution has two characteristic absorption peaks at 330 and 490 nm, and the absorption intensity at 490 nm is higher than 330 nm, so 490 nm is used as the detection wavelength of the phenol-sulfuric acid method (Figure 3A). During the detection process, the color stability of 10, 40, and 80 μg/mL standard grape solutions were tested. As shown in Figure 3B, the absorbance increased within 10 min after adding 6% phenol solution, reached equilibrium after 20 min, and remained stable within 1 h. The results show that the color development time of 20 min is sufficient to ensure that the absorbance of the solution to be tested reaches a stable value, and the absorbance remains stable within 1 h. At the same time, the detection results of each standard solution showed a good linear concentration relationship, which ensured the accuracy of quantitative detection.

To determine the quantitative detection range of the phenol-sulfuric acid method, a standard grape solution of 0–1,000 μg/mL was selected for testing and analysis, and the results were linearly fitted to determine the linear range. As shown in Figure 3C, the phenol-sulfuric acid method can achieve accurate and quantitative detection of total sugar in the range of 0–100 μg/mL. When the concentration exceeds 100 μg/mL, the increase in absorbance value will deviate from the range of linear quantification. Since the more accurate linear range of absorbance value is 0.2–0.8, 0–80 μg/mL standard glucose solution is selected to measure the standard curve. And the correlation coefficient R^2 of the linear regression equation is 0.9992, indicating that within this range, the phenol-sulfuric acid method can accurately determine the total sugar content of the liquid to be tested.

The current study is controversial in the color development process of the phenol-sulfuric acid method. Through the study (Figure 3D), it was found that under unheated conditions, it showed a good linear trend at 10–80 μg/mL, while the absorbance value of standard glucose solution below 10 μg/mL was close to 0. Under heating conditions, both 1 and 5 μg/mL were within the linear quantitative range, indicating that heating treatment can extend the linear detection range and reduce the detection limit of the method. At the same time, in the detection range of 20–80 μg/mL, the detection results under the two conditions were highly consistent. It shows that heating does not affect the final detection result, but only reduces the detection limit of the method.

According to the experimental analysis results, the final detection wavelength of the phenol-sulfuric acid method was determined to be 490 nm, and the color development condition was static for 20 min at RT.

Improvement of phenol-sulfuric acid method

By detecting the optimal absorption wavelength of the monosaccharide standard solution. It can be discovered that the spectral absorption maxima of glucose (Figure 4A), fructose

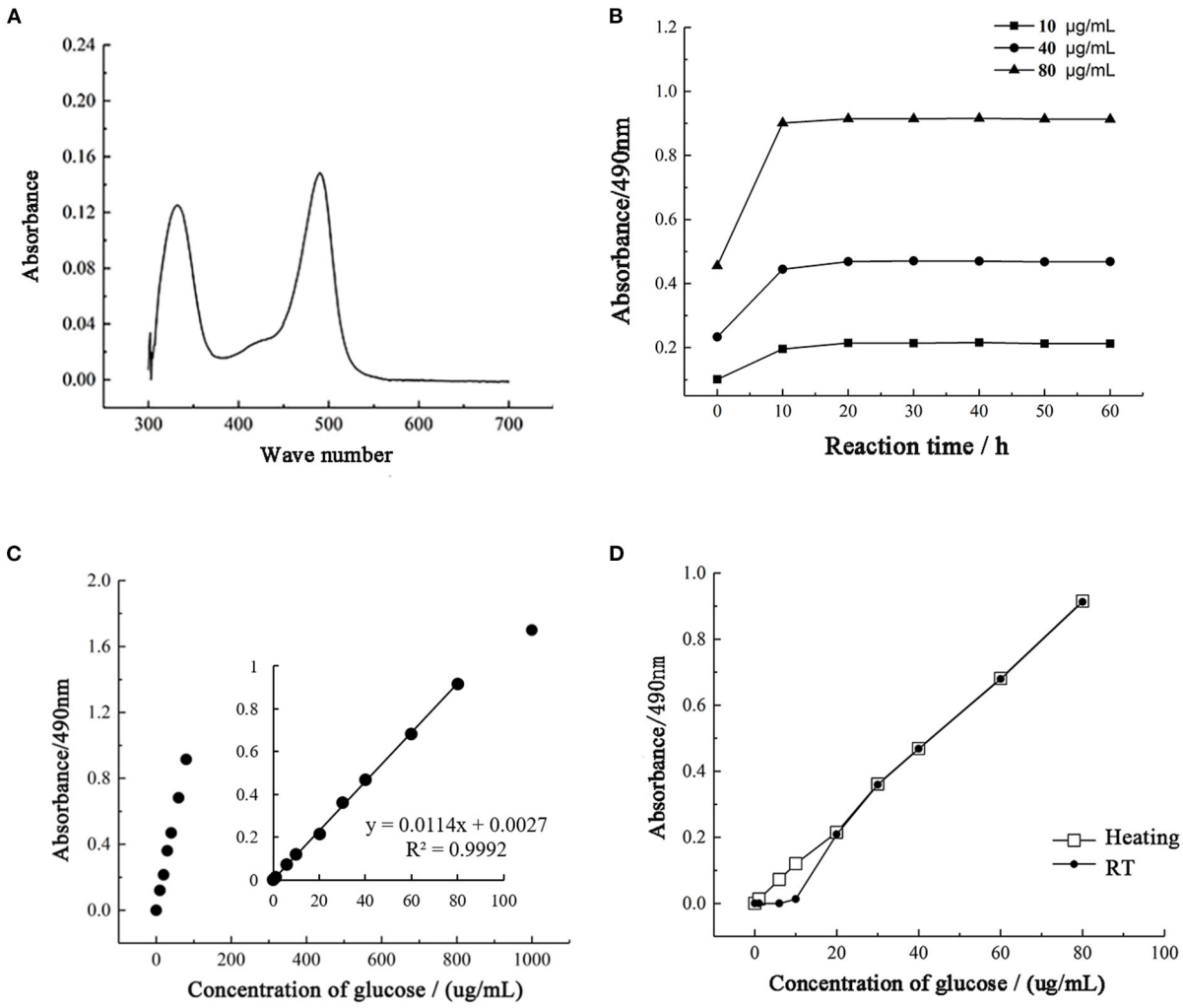

FIGURE 3
Optimization of the phenol-sulfuric acid method. **(A)** The UV-spectrum of samples. **(B)** The coloration stability of phenol sulfuric acid assay. **(C)** The range of detection for total sugar by phenol sulfuric acid assay. **(D)** The influence of heating on the phenol sulfuric acid assay.

(Figure 4B), mannose (Figure 4C) and galactose (Figure 4D) are around 490 nm. Rhamnose (Figure 4E) and fucose (Figure 4F), also known as 6-deoxy-L-mannose and 6-deoxy-L-galactose, have a spectral maximum absorption wavelength around 480 nm. The spectral maximum absorption wavelengths of xylose (Figure 4G) and arabinose (Figure 4H) in the pentoses are also around 480 nm. Acidic sugars, such as galacturonic acid (Figure 4I) and glucuronic acid (Figure 4J), have spectral absorption maxima around 483 nm.

Standard curves of monosaccharides at their corresponding absorption maximum wavelengths were also obtained (Figures 5A–D, J–P). The slope represents the color rendering power of the monosaccharide in the phenol-sulfuric acid method. Through comparative analysis, it was found that when the monosaccharide was at the maximum absorption wavelength, the slope of the detected standard curve was larger. Although 490 nm is generally used as the detection wavelength of the phenol-sulfuric acid method in a large number of studies, for heteropolysaccharide samples with low concentrations, it is best to choose the maximum absorption wavelength of the sample as the detection wavelength, which is beneficial to alleviate the experimental error caused by low absorbance values. In addition, to find the rule of monosaccharide color developing ability, the standard curves of all monosaccharides at 490 nm (Figures 5A–J) were compared and analyzed. And the ratio of the slopes of glucose to the monosaccharides is the relative correction factors for different monosaccharides relative to glucose (Table 1). Since the larger the slope, the stronger the color rendering ability of the monosaccharide. The closer the relative correction factor is to 1, the smaller the difference

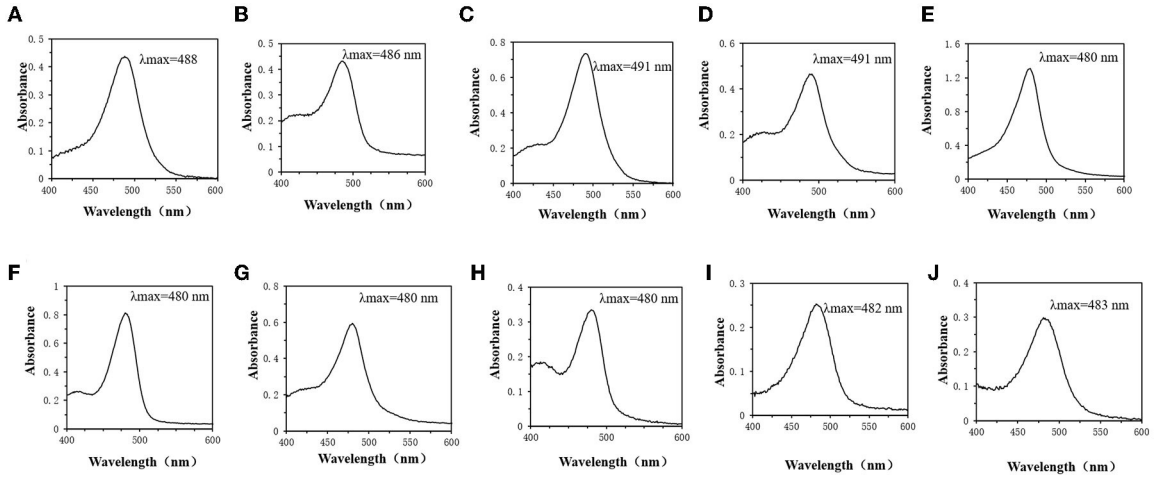

FIGURE 4
Monosaccharide UV absorption spectrum. **(A)** Glucose. **(B)** Fructose. **(C)** Mannose. **(D)** Galactose. **(E)** Rhamnose. **(F)** Xylose. **(G)** Fucose. **(H)** Arabinose. **(I)** Galactose Uronic acid. **(J)** Glucuronic acid.

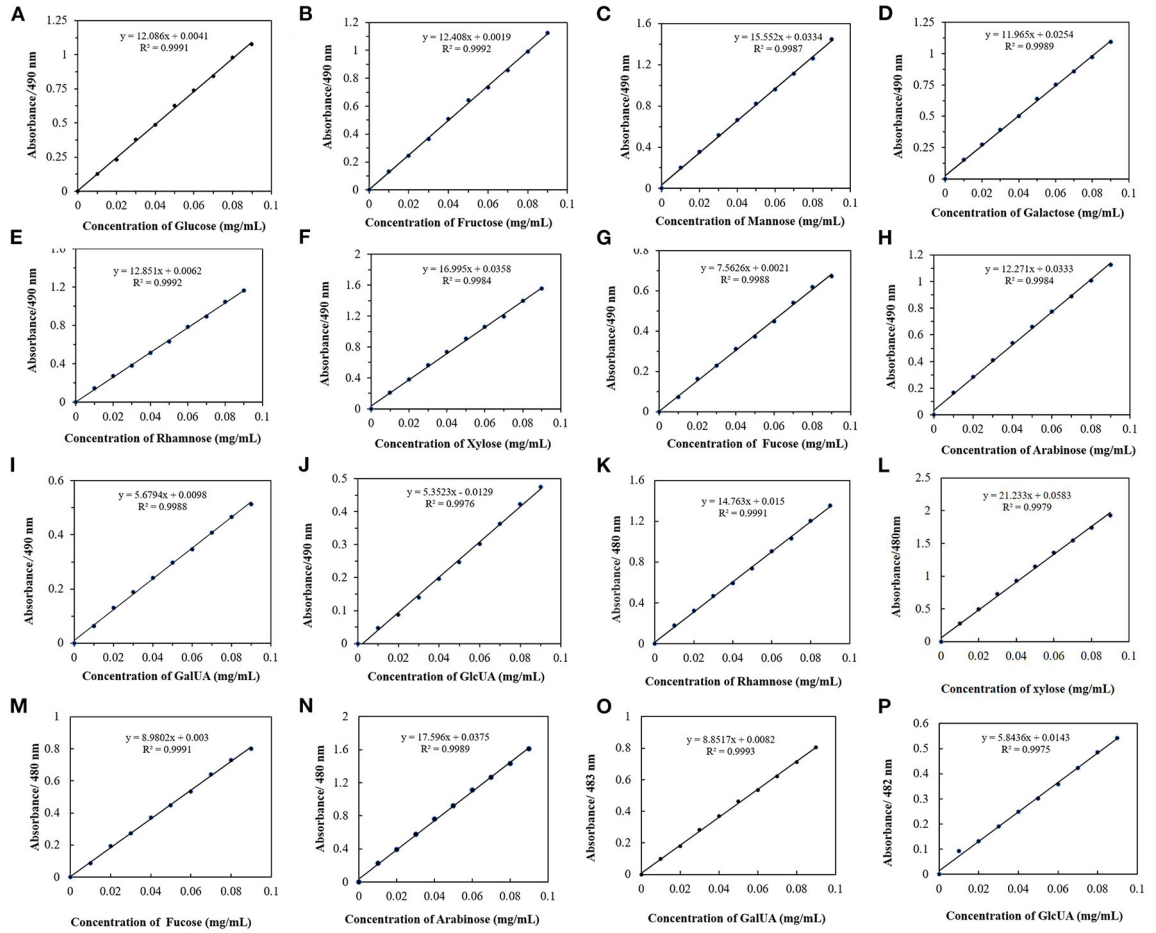

FIGURE 5
Monosaccharide UV absorption standard curves. **(A–J)** Standard curve of ten monosaccharides at 490 nm. **(K–P)** Standard curves of six monosaccharides at their maximum absorption wavelengths.

TABLE 1 Regression equation and relative correction factors of glucose and other monoses.

Monose	Regression equation	*r*	Relative correction factor
Glu	A = 12.086C + 0.0041	0.9991	—
Fru	A = 12.408C + 0.0019	0.9992	0.97
Man	A = 15.552C + 0.0334	0.9987	0.78
Gal	A = 11.965C + 0.0254	0.9989	1.01
Rha	A = 12.851C + 0.0062	0.9992	0.94
Xyl	A = 16.995C + 0.0358	0.9984	0.71
Fuc	A = 7.5626C + 0.0021	0.9988	1.6
Ara	A = 12.271C + 0.0333	0.9984	0.98
GalUA	A = 5.6794C + 0.0098	0.9988	2.13
GlcUA	A = 5.3523C-0.0129	0.9976	2.26

A, absorbance; C, concentration.

in color rendering ability between the monosaccharide and glucose. By comparing the slopes and correction factors of monosaccharides, it can be found that the slopes of fructose, galactose, rhamnose, and arabinose are basically the same, and the relative correction factor is close to 1, while the slopes of mannose and xylose are similar, and their color rendering ability higher than glucose. The fucose and the representative of acidic sugars (galacturonic acid and glucuronic acid) were significantly lower than those of glucose. For monosaccharides with weak color rendering ability, the amount detected in the reaction system is usually low, and it is difficult to detect the accurate content in a complex solution environment. Therefore, according to this study, the total sugar content of heteropolysaccharides composed of fructose, galactose, rhamnose, and arabinose can be directly calculated using the standard curve of glucose. The heteropolysaccharides composed of xylose and mannose, fucose and acid sugar can be multiplied by the correction factor to obtain the corrected total sugar content.

Practical application verification

To verify the accuracy of the correction factor, 5 heteropolysaccharides were selected from three types. β-dextran refers to a homopolysaccharide composed of glucose as a monosaccharide. D-trehalose is a disaccharide formed by two glucoses through α,α-1→1 bonds. Fructooligosaccharides are mainly composed of glucose and fructose. Xylan and polygalacturonic acid are composed of xylose and galacturonic acid, respectively. Through the detection of total sugar content, it was found that using glucose as the standard, the detected concentrations of glucan, D-trehalose and fructooligosaccharide (Table 2) were 35–37 μg/mL, which was close to 40 μg/mL, and the concentration of xylan was 57.08 μg/mL, slightly higher than the true concentration of xylan (42.6 μg/mL). while the concentration of polygalacturonic acid is about 20.8 μg/mL, which is much lower than the true concentration of polygalacturonic acid (41.6 μg/mL). After correction by the correction factor, the concentration of xylan was 40.53 μg/mL, and the concentration of polygalacturonic acid was 44.34 μg/mL, which was close to the real concentration of polysaccharide. Therefore, this experiment verifies the accuracy of the correction factor, and at the same time, the phenol-sulfuric acid color developing system can have higher accuracy through the correction.

Discussion

The phenol-sulfuric acid method is one of the main methods to detect total sugar content (22, 23). With the increasing number of polysaccharide species, accurate quantitative analysis by the phenol-sulfuric acid method becomes more difficult and challenging (24, 25). Numerous studies have improved the phenol-sulfuric acid method for different samples (26, 27). For example, in a sludge sample containing excess persulfate, NaSO was pre-added to prevent persulfate from affecting the determination of total sugar content by the traditional phenol-sulfuric method (28). In addition, the phenol-sulfuric acid method typically uses glucose (or a monosaccharide) as a standard to quantify the total sugar content of a sample (29, 30). However, there are significant differences in the structures and functional groups of different monosaccharides (31). For some heteropolysaccharides containing multiple monosaccharides, using glucose (or a certain monosaccharide) as the standard will lead to large errors in the detected total sugar content. Therefore, in this study, on the basis of determining the optimal detection conditions, the influence of different monosaccharide compositions on the quantitative analysis of total sugar measured by phenol-sulfuric acid method was explored, and the calibration factor of each monosaccharide relative to glucose was further obtained. In the improved

TABLE 2 Practical application of correction factors in polysaccharides.

	β-dextran	D-Trehalose	Fructooligosaccharides	Polygalacturonic acid	Xylan
True concentration/(ug/mL)	37.6	38.4	39.2	41.6	42.6
Detection concentration /(ug/mL)	35.35	35.65	37.22	20.81	57.08
Relative correction factor	-	-	0.97	2.13	0.71
Corrected concentration/(ug/mL)	35.35	35.65	36.11	44.34	40.53

phenol-sulfuric acid method, glucose can be used as the standard, combined with the monosaccharide composition of the heteropolysaccharide, and the accurate total sugar content can be obtained through the correction of the correction factor. Finally, through comparative analysis, the color rendering ability of monosaccharides was preliminarily evaluated and classified, and the monosaccharides with large deviations were corrected according to the correction factor, which provided a reference for more accurate calculation of the total sugar content of heteropolysaccharides in actual samples.

There is a close relationship between the moisture content of the sample and the concentration (32). During the measurement of total sugar content, the moisture content of the standard product was too high, which may lead to inaccurate test results. In this study, the water content of 10 common monosaccharides was determined. The water content of glucose, mannose and galactose was relatively high, and the water content of glucose was as high as 1.81% (Figure 2). Therefore, the drying and dehydration of glucose is an important step in making the standard curve of glucose. In addition, the detection conditions of the phenol-sulfuric acid method are different in different literature reports. For example, one study used heating at 100°C for 20 min during color development (25), but in another study, no heat treatment was performed (33). Therefore, in this study, the temperature, detection range, static time and other detection conditions of the phenol-sulfuric acid method were evaluated. When glucose was used as the standard, the final detection conditions of the phenol-sulfuric acid method were static for 20 min at RT for color development and detection of absorbance at 490 nm.

The difference in the color rendering ability of monosaccharides may be the main factor affecting the inaccuracy of the detection of total sugar content (34, 35). In this study, the standard solutions of 10 monosaccharides were scanned at full wavelength to determine the maximum absorption wavelengths of different monosaccharides. It was found that hexoses, such as glucose, fructose, mannose and galactose, have spectral absorption maxima around 490 nm. In addition, according to some functional groups, hexoses can be classified as aldose or ketose (36). Glucose is aldohexose, while fructose is ketohexose (37). Glucose also has two different structural forms, and the ring-shaped fructose also has two different structures, alpha and beta. Due to the similar structure of the hexose (38), the reactions produced in the phenol-sulfuric acid method are relatively consistent. There is no significant difference in the color rendering power, which may be the reason that the measured spectral range and absorbance are almost the same. Rhamnose, fucose, and pentose (xylose and arabinose) have maximum absorption wavelengths around 480 nm. Rhamnose and fucose, also known as 6-deoxy-L-mannose and 6-deoxy-L-galactose, respectively (39, 40). It can be found that the wavelength of maximum absorption changes as the hydroxyl groups of mannose and galactose are replaced by hydrogen (Figure 4). While it may be due to the low solubility of pentose in ethanol (41), and the low concentration of pentose leads to a lower optimal wavelength of absorbance and UV absorption in the phenol-sulfuric acid color developing system. In addition, acidic sugars such as galacturonic acid and glucuronic acid have spectral absorption maxima around 483 nm. Therefore, for heteropolysaccharides with different monosaccharide compositions, the maximum absorption wavelength may be in the range of 480–490 nm.

To obtain a more accurate total sugar content by using the phenol-sulfuric acid method, 10 different monosaccharides were used to create a standard curve in this study. The other monosaccharides were corrected with glucose as the standard to obtain the correction factor. By comparative analysis of correction factors, the 10 monosaccharides were divided into 3 categories according to their color rendering ability. And selected representative heteropolysaccharides in three categories to verify the accuracy of the correction factor. It is clear that the total sugar content of heteropolysaccharides composed of fructose, galactose, rhamnose, and arabinose can be directly calculated using the standard curve of glucose. While the heteropolysaccharides composed of xylose and mannose, fucose and acid sugar can be multiplied by the correction factor to obtain the corrected total sugar content.

The improved phenol-sulfuric acid method not only did not increase the complexity of the experiment, but also made the detection more accurate, especially significantly improved the accuracy of the total sugar content of acidic heteropolysaccharides. However, since this method ignores the influence of different proportions of monosaccharides on the quantitative analysis of total sugar content, the detection accuracy of heteropolysaccharides composed of different types of monosaccharides may be lower than that

of heteropolysaccharides composed of the same type of monosaccharides. Therefore, in future studies, the experimental scheme can be further optimized by discussing the proportion of different types of monosaccharides in the heteropolysaccharide, which improves the rigor and accuracy of the quantitative analysis of total sugars.

Conclusion

Based on the traditional phenol-sulfuric acid method for the determination of total sugar content in substances, this study revealed the influence of the sample moisture content, heating conditions, reaction time, and optimal absorption wavelength on the stability and accuracy of the phenol-sulfuric acid method. In addition, using 10 monosaccharides as target detection substances, a phenol-sulfuric acid chromogenic system for the determination of total sugar content in heteropolysaccharides was constructed. And the other monosaccharides were corrected with glucose as the standard, and the correction factors were obtained. The 10 monosaccharides were preliminarily divided into 3 categories according to the correction factor. Then, the known concentration of heteropolysaccharide was selected for verification, and it was preliminarily proved that the correction of the relative correction factor could obtain a more accurate total sugar content. This study not only significantly improves the accuracy of the phenol-sulfuric acid method, but also classifies the color rendering abilities of different monosaccharides, further simplifying the experiment, which has better application potential in the detection of total sugar content in actual complex samples.

Data availability statement

The original contributions presented in the study are included in the article/supplementary material, further inquiries can be directed to the corresponding authors.

Author contributions

FY, XL, and ML: conceptualization and methodology. FY: investigation and writing. JZ, JX, and TN: data curation and review. XL and ML: funding acquisition. All authors contributed to the article and approved the submitted version.

Funding

This work was financially supported by Chinese Universities Scientific Fund (Grant No. 2452022025), and Key point Research and Invention Program of Shannxi Province (Grant No. 2021ZDLNY05-06).

Conflict of interest

The authors declare that the research was conducted in the absence of any commercial or financial relationships that could be construed as a potential conflict of interest.

Publisher's note

All claims expressed in this article are solely those of the authors and do not necessarily represent those of their affiliated organizations, or those of the publisher, the editors and the reviewers. Any product that may be evaluated in this article, or claim that may be made by its manufacturer, is not guaranteed or endorsed by the publisher.

References

1. Ji XL, Guo JH, Ding DQ, Gao J, Hao LR, Guo XD, et al. Structural characterization and antioxidant activity of a novel high-molecular-weight polysaccharide from Ziziphus Jujuba cv. Muzao. *J Food Meas Charact*. (2022) 16:2191–200. doi: 10.1007/s11694-022-01288-3

2. Chen F, Huang G L. Antioxidant activity of polysaccharides from different sources of ginseng. *Int J Biol Macromol*. (2019) 125:906–8. doi: 10.1016/j.ijbiomac.2018.12.134

3. Sun Y, Zhang ZP, Cheng L, Zhang X, Liu YA, Zhang RL, et al. Polysaccharides confer benefits in immune regulation and multiple sclerosis by interacting with gut microbiota. *Food Res Int*. (2021) 149:110675. doi: 10.1016/j.foodres.2021.110675

4. Shen J, Park H S, Xia Y M, Kim G S, Cui S W. The polysaccharides from fermented ganoderma lucidum mycelia induced miRNAs regulation in suppressed HepG2 cells. *Carbohydr Polym*. (2014) 103:319–24. doi: 10.1016/j.carbpol.2013.12.044

5. Yue F, Xu J, Zhang S, Hu X, Wang X, Lu X. Structural features and anticancer mechanisms of pectic polysaccharides: a review. *Int J Biol Macromol*. (2022). doi: 10.1016/j.ijbiomac.2022.04.073

6. Xu Y, Zhang M, Wu T, Dai SD, Xu JL, Zhou ZK. The anti-obesity effect of green tea polysaccharides, polyphenols and caffeine in rats fed with a high-fat diet. *Food Funct*. (2015) 6:297–304. doi: 10.1039/C4FO00970C

7. Xia SL, Zhai YC, Wang X, Fan QR, Dong XY, Chen M, et al. Phosphorylation of polysaccharides: a review on the synthesis and bioactivities. *Int J Biol Macromol*. (2021) 184:946–54. doi: 10.1016/j.ijbiomac.2021.06.149

8. Wei ZH, Liu LL, Guo XF, Li YJ, Hou BC, Fan QL, et al. Sucrose fed-batch strategy enhanced biomass, polysaccharide, and ganoderic acids production in fermentation of Ganoderma lucidum 5.26. *Bioprocess Biosyst Eng*. (2016) 39:37–44. doi: 10.1007/s00449-015-1480-x

9. Fimbres-Olivarria D, Lopez-Elias J A, Carvajal-Millan E, Marquez-Escalante J A, Martinez-Cordova L R, Miranda-Baeza A, et al. Navicula sp sulfated

polysaccharide gels induced by Fe(III): rheology and microstructure. *Int J Mol Sci*. (2016) 17:8. doi: 10.3390/ijms17081238

10. Liu W, Liu YM, Zhu R, Yu JP, Lu WS, Pan C, et al. Structure characterization, chemical and enzymatic degradation, and chain conformation of an acidic polysaccharide from Lycium barbarum L. *Carbohydr Polym.* (2016) 147:114–24. doi: 10.1016/j.carbpol.2016.03.087

11. Zhao JH, Li HX, Xi WP, An W, Niu LL, Cao YL, et al. Changes in sugars and organic acids in wolfberry (Lycium barbarum L) fruit during development and maturation. *Food Chemist.* (2015) 173:718–24. doi: 10.1016/j.foodchem.2014.10.082

12. Asghari FS, Yoshida H. Acid-catalyzed production of 5-hydroxymethyl furfural from D-fructose in subcritical water. *Ind Eng Chem Res.* (2006) 45:2163–73. doi: 10.1021/ie051088y

13. Chen YF, Yang H, Shen ZZ, Ye JR. Whole-Genome Sequencing and Potassium-Solubilizing Mechanism of Bacillus aryabhattai SK1-7. *Front Microbiol*. (2022) 12:722379. doi: 10.3389/fmicb.2021.722379

14. Yun YH, Wei YC, Zhao XB, Wu WJ, Liang YZ, Lu HM. A green method for the quantification of polysaccharides in dendrobium officinale. *Rsc Advances*. (2015) 5:57–105065. doi: 10.1039/C5RA21795D

15. Kim JM, Nguyen L, Barr MF, Morabito M, Stringer D, Fitton JH, et al. Quantitative determination of fucoidan using polyion-sensitive membrane electrodes. *Anal Chim Acta.* (2015) 877:1–8. doi: 10.1016/j.aca.2015.04.020

16. DuBois M, Gilles KA, Hamilton JK, Rebers PA, Smith F. Colorimetric method for determination of sugars and related substances.pdf. *Anal Chem*. (1956) 28:350–6. doi: 10.1021/ac60111a017

17. Masuko T, Minami A, Iwasaki N, Majima T, Nishimura SI, Lee YC. Carbohydrate analysis by a phenol-sulfuric acid method in microplate format. *Anal Biochem*. (2005) 339:69–72. doi: 10.1016/j.ab.2004.12.001

18. Wang YG, Jing YJ, Leng FF, Wang SW, Wang F, Zhuang Y, et al. Establishment and application of a method for rapid determination of total sugar content based on colorimetric microplate. *Sugar Tech*. (2017) 19:424–31. doi: 10.1007/s12355-016-0473-7

19. Zhang HF, Niu LL, Yang XH, Li L. Analysis of water-soluble polysaccharides in an edible medicinal plant epimedium: method development, validation, and application. *J Aoac Int*. (2014) 97:784–90. doi: 10.5740/jaoacint.12-379

20. Nagy G, Pohl NLB. Complete hexose isomer identification with mass spectrometry. *J Am Soc Mass Spectrom*. (2015) 26:677–85. doi: 10.1007/s13361-014-1072-z

21. Yan JP, Liu SJ. Hot water pretreatment of boreal aspen woodchips in a pilot scale digester. *Energies*. (2015) 8:1166–80. doi: 10.3390/en8021166

22. Liu H, Yang S, Shi JS, Xu XY, Liu HB, Fu B. Towards understanding the dewatering mechanism of sewage sludge improved by bioleaching processing. *Sep Purif Technol.* (2016) 165:53–9. doi: 10.1016/j.seppur.2016.03.037

23. Yu GH, He PJ, Shao LM. Characteristics of extracellular polymeric substances (EPS) fractions from excess sludges and their effects on bioflocculability. *Bioresour Technol.* (2009) 100:3193–8. doi: 10.1016/j.biortech.2009.02.009

24. Rasouli M, Ostovar-Ravari A, Shokri-Afra H. Characterization and improvement of phenol-sulfuric acid microassay for glucose-based glycogen. *Eur Rev Med Pharmacol Sci*. (2014) 18:2020–4.

25. Zeng CB, Ye GY, Li GC, Cao H, Wang ZH, Ji SG. RID serve as a more appropriate measure than phenol sulfuric acid method for natural water-soluble polysaccharides quantification. *Carbohydr Polym*. (2022) 278:118928. doi: 10.1016/j.carbpol.2021.118928

26. Taylor K. A modification of the phenol sulfuric-acid assay for total carbohydrates giving more comparable absorbances. *Appl Biochemist Biotechnol*. (1995) 53:207–14. doi: 10.1007/BF02783496

27. Buysse J, Merckx R. An improved colorimetric method to quantify sugar content of plant-tissue. *J Exp Bot*. (1993) 44:1627–9. doi: 10.1093/jxb/44.10.1627

28. Zhang WH, Wu J, Weng LY, Zhang HJ, Zhang J, Wu AB. An improved phenol-sulfuric acid method for the determination of carbohydrates in the presence of persulfate. *Carbohydr Polym*. (2020) 227:115332. doi: 10.1016/j.carbpol.2019.115332

29. Boshagh F. Measurement methods of carbohydrates in dark fermentative hydrogen production- a review. *Int J Hydrogen Energy*. (2021) 46:24028–50. doi: 10.1016/j.ijhydene.2021.04.204

30. Jiang YP, Qi XH, Gao K, Liu WJ, Li N, Cheng NB, et al. Relationship between molecular weight, monosaccharide composition and immunobiologic activity of Astragalus polysaccharides. *Glycoconj J*. (2016) 33:755–61. doi: 10.1007/s10719-016-9669-z

31. Ji XL, Hou CY, Shi MM, Yan YZ, Liu YQ. An insight into the research concerningpanax ginseng c. a. meyer polysaccharides: a review. *Food Rev Int*. (2020) 38:1149–65. doi: 10.1080/87559129.2020.1771363

32. Xu JX, Wang DN, Lei YP, Cheng LJ, Zhuang WJ, Tian YT. Effects of combined ultrasonic and microwave vacuum drying on drying characteristics and physicochemical properties of Tremella fuciformis. *Ultrason Sonochem*. (2022) 84:105963. doi: 10.1016/j.ultsonch.2022.105963

33. Albalasmeh AA, Berhe AA, Ghezzehei TA. A new method for rapid determination of carbohydrate and total carbon concentrations using UV spectrophotometry. *Carbohydr Polym*. (2013) 97:253–61. doi: 10.1016/j.carbpol.2013.04.072

34. Luo YT, Tu YQ, Ren FZ, Zhang H. Characterization and functional properties of Maillard reaction products of beta-lactoglobulin and polydextrose. *Food Chemist*. (2022) 377:131749. doi: 10.1016/j.foodchem.2021.131749

35. Chen Y, Chefetz B, Rosario R, van Heemst JDH, Romaine CP, Hatcher PG. Chemical nature and composition of compost during mushroom growth. *Compost Sci Util*. (2000) 8:347–59. doi: 10.1080/1065657X.2000.10702008

36. Li Y, Liang J, Gao JN, Shen Y, Kuang HX, Xia YG. A novel LC-MS/MS method for complete composition analysis of polysaccharides by aldononitrile acetate and multiple reaction monitoring. *Carbohydr Polym*. (2021) 272:118478. doi: 10.1016/j.carbpol.2021.118478

37. Scruel O, Sener A, Malaisse WJ. Hexose metabolism in pancreatic islets: effect of D-glucose upon D-fructose metabolism. *Mol Cell Biochemist*. (1999) 197:209–16. doi: 10.1023/A:1006910201767

38. Zhu P, Meier S, Saravanamurugan S, Riisager A. Modification of commercial Y zeolites by alkaline-treatment for improved performance in the isomerization of glucose to fructose. *Mol Catal*. (2021) 510:111686. doi: 10.1016/j.mcat.2021.111686

39. Doan TNT, Prabhu P, Kim JK, Ahn YJ, Natarajan S, Kang LW, et al. Crystallization and preliminary X-ray crystallographic analysis of L-rhamnose isomerase with a novel high thermostability from Bacillus halodurans. *Acta Crystallogr F Struct Biol Commun*. (2010) 66:677–80. doi: 10.1107/S174430911001256X

40. Shafer CM, Molinski TF. Practical synthesis of 2,6-dideoxy-D-lyxo-hexose ("2-deoxy-D-fucose") from D-galactose. *Carbohydr Res*. (1998) 310:223–8. doi: 10.1016/S0008-6215(98)00160-8

41. Li SC, Yang XM, Ma HL, Yan JK, Guo DZ. Purification, characterization and antitumor activity of polysaccharides extracted from Phellinus igniarius mycelia. *Carbohydr Polym.* (2015) 133:24–30. doi: 10.1016/j.carbpol.2015.07.013

frontiers | Frontiers in Nutrition

TYPE Original Research
PUBLISHED 05 August 2022
DOI 10.3389/fnut.2022.962584

Check for updates

OPEN ACCESS

EDITED BY
Xiaolong Ji,
Zhengzhou University of Light Industry, China

REVIEWED BY
Guangjing Chen,
Guiyang University, China
Zhenyuan Zhu,
Tianjin University of Science and Technology, China
Qingbin Guo,
Tianjin University of Science and Technology, China

*CORRESPONDENCE
Bing Yang
yangbing4329@126.com
Yaxin Sang
yxsang1418@163.com

†These authors have contributed equally to this work and share first authorship

SPECIALTY SECTION
This article was submitted to Food Chemistry, a section of the journal Frontiers in Nutrition

RECEIVED 06 June 2022
ACCEPTED 15 July 2022
PUBLISHED 05 August 2022

CITATION
Zhang N, Yang B, Mao K, Liu Y, Chitrakar B, Wang X and Sang Y (2022) Comparison of structural characteristics and bioactivity of *Tricholoma mongolicum* Imai polysaccharides from five extraction methods.
Front. Nutr. 9:962584.
doi: 10.3389/fnut.2022.962584

COPYRIGHT
© 2022 Zhang, Yang, Mao, Liu, Chitrakar, Wang and Sang. This is an open-access article distributed under the terms of the Creative Commons Attribution License (CC BY). The use, distribution or reproduction in other forums is permitted, provided the original author(s) and the copyright owner(s) are credited and that the original publication in this journal is cited, in accordance with accepted academic practice. No use, distribution or reproduction is permitted which does not comply with these terms.

Comparison of structural characteristics and bioactivity of *Tricholoma mongolicum* Imai polysaccharides from five extraction methods

Nan Zhang†, Bing Yang*†, Kemin Mao, Yuwei Liu, Bimal Chitrakar, Xianghong Wang and Yaxin Sang*

College of Food Science and Technology, Hebei Agricultural University, Baoding, China

Tricholoma mongolicum Imai is an edible fungus rich in various health-promoting compounds, such as polysaccharides, polypeptides, polyunsaturated fatty acids, etc., and among them, polysaccharides have gotten more attention in recent research trends. This study explored the extraction of polysaccharides from *T. mongolicum* Imai by five extraction methods, including hot water extraction, ultrasound extraction, enzyme-assisted extraction, 0.1 M HCL extraction, and 0.1 M NaOH extraction. The effects of these extraction methods on the yield, chemical structure, apparent morphology, and the antioxidant activities of *Tricholoma mongolicum* Imai polysaccharides (TMIPs) were investigated in this study. The data showed that 0.1 M NaOH extraction produced the highest extraction yield compared to the other extraction methods. The results of high-performance gel permeation chromatography (HPGPC) and scanning electron microscopy (SEM) showed that different extraction methods had significant effects on the molecular weight and morphology of TMIPs. The results of Fourier transform infrared (FT-IR), X-ray diffraction (XRD), and thermogravimetric analysis showed that the extraction methods had no significant difference in functional groups, crystal structure, and thermal stability of TMIPs. The antioxidant activity of TMIPs extracted by ultrasound extraction was more prominent among the five polysaccharides, which might be related to a large number of low-molecular-weight components in molecular weight distribution.

KEYWORDS

***Tricholoma mongolicum* Imai, polysaccharide, extraction methods, structure characteristics, antioxidant activity**

Introduction

Tricholoma mongolicum Imai is a rare edible fungus growing in grasslands. Due to the deteriorating natural environment and over picking, the yield of *T. mongolicum* Imai has extremely reduced, and the producing area is distributed in Xilin Gol League, Hulunbuir League, Inner Mongolia, and Zhangjiakou, Hebei, China. *T. mongolicum* Imai is a world-famous wild edible fungus variety with thick, fragrant, and delicious meat and excellent taste. It is known as the first of the "eight treasures of grass" (1). *T. mongolicum* Imai is rich in polysaccharides, polypeptides, polyunsaturated fatty acids, and other bioactive substances, giving it various functional properties, such as anti-oxidation (2), anti-aging (1), anti-tumor (3), hepatoprotective effects (4), other medical and healthcare regulating human metabolism (5), and enhancing immunity (6). In recent years, there are few studies on the polysaccharides of *T. mongolicum* Imai's fruiting bodies or spores.

Polysaccharide is a chain polymer formed by a linear or branched connection of aldoses or ketoses through a glycosidic bond, which is the most abundant biopolymer in nature. As one of the important sources of polysaccharides, fungal polysaccharides are widely present in the cell walls of higher macrofungi. Fungal polysaccharides are active substances extracted from true mycelium mycelia and their fermented broth, which have antioxidant (7), anti-aging (8), anti-inflammatory (9), anti-tumor (10), hypoglycemic (11), immunoregulation (12), and other healthcare functions. At present, the commercialized fungal polysaccharides are derived from *Lentinus edodes*, *Polyporus umbellatus*, *Ganoderma lucidum*, *Coriolus versicolor*, tree tongue, etc. In recent years, the research on fungal polysaccharides in the world mainly focused on the molecular mechanism and application of *Lentinus edodes* and *Ganoderma lucidum* polysaccharides as immune activators to enhance immunity and anti-tumor (13, 14), while there were only a few reports on *T. mongolicus* Imai polysaccharides. Generally speaking, the biological activity of polysaccharides is closely related to its structural parameters, including sugar composition, molecular weight, and surface morphology, therefore, revealing that its chemical composition and structure are of great significance for further study of its biological activity. It has been widely accepted that the extraction methods of polysaccharides have an important impact on their structural and physicochemical properties (15).

Polysaccharide extraction methods include hot water-, ultrasound- assisted-, enzyme- treated-, acid- assisted-, alkali-assisted-extraction, and so on. Polysaccharide extraction requires cell wall destruction to improve extraction efficiency. Hot water extraction is generally easy to operate and does not cause polysaccharide degradation. However, the extraction is only from the outside of the cell wall with low extraction rates and longer extraction times (16). Ultrasound-assisted and enzyme-assisted extractions hydrolyze or mechanically destroy the cell wall (17, 18), but the structures of the polysaccharides may also be destroyed by rigorous extraction conditions of ultrasound or the enzymes used. Acid extraction is based on the feature that certain polysaccharides are soluble in dilute hydrochloric acid (19), where the cell wall fully absorbs water, then swells and breaks, thereby releasing polysaccharides and achieving the purpose of extraction. During the extraction process, other components such as protein and phenolic compounds may also be extracted, therefore, the yield of polysaccharides shows a higher amount than the actual value. In alkali-assisted extraction, hydroxyl ions interfere with the hydrogen bond between polysaccharides and release them into the solution to improve the polysaccharide yield (20). During acidic or alkaline extraction, the final extract needs to be neutralized to prevent the degradation of the target polysaccharide.

The above-mentioned extraction methods determine the structural and functional properties of the extracted polysaccharides (15). Therefore, this study aimed to extract the polysaccharides from *T. mongolicum* Imai by five methods, hot water, ultrasonic- and enzyme-assisted extraction, 0.1 M HCl, and 0.1 M NaOH. The antioxidant activity, microstructure, monosaccharide composition, and molecular weight of polysaccharides extracted by the five methods were compared. This study can provide basic data for further extraction, development, and utilization of *T. mongolicum* Imai polysaccharides.

Materials and methods

Materials and reagents

Dried fruiting bodies of *T. mongolicum* Imai were obtained from Zhangjiakou, Hebei Province, China. 1,1-Diphenyl-2-picrylhydrazyl (DPPH) was purchased from Solarbio Science and Technology Co., Ltd. (Beijing, China). The total antioxidant capacity assay kit for the ABTS method was purchased from Beyotime Co., Ltd. (Shanghai, China). Monosaccharide standards (mannose, ribose, rhamnose, glucuronic acid, galacturonic acid, *N*-acetyl-D-glucosamine, *N*-acetyl-D-galactosamine, glucose, galactose, xylose, arabinose, and fucose) were purchased from Shanghai Yuanye Bio-Technology Co., Ltd. (Shanghai, China). All the reagents and chemicals used in this study were analytical or HPLC grade.

Extraction of polysaccharide from *Tricholoma mongolicum* Imai fruiting bodies

Pretreatment of *Tricholoma mongolicum* Imai fruiting bodies

The whole dried *T. mongolicum* Imai fruiting bodies were dried in an oven at 60°C for 8 h and then ground into a

powder using a kitchen grinder. The powdered *T. mongolicum* Imai was treated with petroleum ether (30–60°) at a ratio of 1:5 (w:v) for 10 h to degrease. Then, the residue after decantation was treated with 75% ethanol at a ratio of 1:5 (w:v) for 4 h to remove the pigmented compounds and small molecular impurities. The residue was decanted and dried at 50°C for 8 h to obtain pretreated dry powder for further use.

Hot water extraction

The hot-water extraction of TMIPs was carried out according to the method of (21) with some modifications. Briefly, the pretreated powder of *T. mongolicum* Imai (20 g) was extracted with distilled water (500 ml) at 85°C with continuous stirring for 3 h. Then, the mixture was centrifuged at 4,600 r/min for 15 min to separate the supernatant from the solid residue, which was again extracted following the same procedure two more times. The supernatants were collected and then concentrated to 100 ml by a vacuum rotary evaporator under 55°C. To the concentrated extract, absolute alcohol was added at a 1:3 (v/v) ratio to precipitate the polysaccharides; the precipitate was washed successively with ether, acetone, and n-hexane after filtering, which was freeze-dried to get extracted polysaccharides (Named as TMIPs-H).

Ultrasound-assisted extraction

The ultrasound-assisted extraction of TMIPs was carried out according to the method of (22) with some modifications. Briefly, the powder of *T. mongolicum* Imai (20 g) was extracted with distilled water (400 ml) at 60°C for 35 min using a 300 W ultrasonic cleaning apparatus (Geneng, G-100S, Guangzhou). After centrifugation (4,600 r/min, 15 min), absolute ethanol was added at a 1:3 (v/v) ratio to precipitate the polysaccharides; the precipitate was washed successively with ether, acetone, and n-hexane after filtering, which was freeze-dried to get extracted polysaccharides (Named as TMIPs-U).

Enzyme-assisted extraction

The enzyme-assisted extraction of TMIPs was carried out by following the method of (23) with slight modifications. Briefly, the powder of *T. mongolicum* Imai (20 g) was extracted with distilled water (500 ml), which was mixed with 1.5% cellulase and 2% pectinase enzymes (Food grade). The pH was maintained at 5 for enzymolysis reaction at 50°C for 100 min. Then, the extraction was carried out in a water bath at 75°C for 4 h. After centrifugation, the supernatant was collected and concentrated to 100 ml in a vacuum rotary evaporator. To the concentrated extract, absolute alcohol was added at a 1:3 (v/v) ratio to precipitate the polysaccharides; the precipitate was washed successively with ether, acetone, and n-hexane after filtering, which was then freeze-dried to get extracted polysaccharides (Named as TMIPs-E).

Acid-assisted extraction

The method of (15) was used to extract TMIPs by acid-assisted extraction (15) with some modification. Briefly, the powder of *T. mongolicum* Imai was extracted with HCl (0.1 M) at a 10 ml/g solid–liquid ratio for 1 h; the extraction temperature was maintained at 90°C using a water bath. Then, the pH of the mixture was adjusted to 7.0 and centrifuged at 4,600 r/min for 15 min. The supernatant was concentrated in a vacuum rotary evaporator at 55°C, which was then precipitated with three times the volume of 95% ethanol. The precipitate was washed successively with ether, acetone, and n-hexane after filtering, which was then freeze-dried to get the extracted polysaccharides (Named as TMIPs-Ac).

Alkali-assisted extraction

The method was the same as section "Acid-assisted extraction", except that the extracting solvent was 0.1 M NaOH and the freeze-dried polysaccharide was named TMIPs-Al.

Each sample after freeze-drying was weighed and its yield was calculated according to the following formula:

$$\textit{Crude polysaccharide yield}\ (\%) = \frac{m}{M} \times 100 \qquad (1)$$

where, m is the mass of dried crude polysaccharide (g) and M is the mass of *T. mongolicum* Imai powder (g).

Chemical composition analysis

Phenol–sulfuric acid method was used to determine the total sugar content (24), and the standard mixture was prepared with glucose. The glucose used was dried to a constant weight in an oven at 60°C. Protein content was measured by the method of Coomassie brilliant blue with bovine serum albumin (BSA) as the standard (25). Contents of uronic acid were analyzed by the 3-phenylphenol colorimetric method with galacturonic acid as the standard (26).

Molecular weight determination

High-performance liquid gel permeation chromatography (HPGPC) was used to determine the molecular weight distribution of polysaccharides from *T. mongolicum* Imai by using Agilent 1260 high-performance liquid chromatography, TSK-Gel G4000 SWXL (7.8 mm × 300 mm) gel chromatography column, and refractive index detector (RID). Each dextran standard was dissolved and prepared into a standard solution with a concentration of 4.0 mg/ml, which was then analyzed by high-performance liquid chromatography through a 0.22-μm aqueous phase filtration membrane. Taking the retention time (x, min) of each standard as the horizontal axis and the logarithm of the dextran standard

molecule (y, log M_W) as the vertical axis to fit the regression equation, the corresponding regression equation was $y = -0.2415x + 7.740$. The specific detection conditions were as follows: injection volume of 15 μl, column temperature of 30°C, a flow rate of 0.7 ml/min, using ultrapure water as the mobile phase.

Monosaccharide composition

The monosaccharide composition of *T. mongolicum* Imai polysaccharides was determined by phenyl-3-methyl-5-pyrazolinone (PMP) pre-column derivatization. The 10-ml polysaccharide sample was hydrolyzed with 5.0 ml of 2 mol/L trifluoroacetic acid (TFA) at 120°C for 4 h. After acidolysis, methanol was added and TFA was dried by a nitrogen blowing apparatus. Then 250 μl sample solution was accurately absorbed into a 5-ml Eppendorf (EP) tube, and then 250 μl of 0.6 mol/L NaOH and 500 μl of 0.4 mol/L PMP–methanol were added at 70°C for 1 h. After cooling in cold water for 10 min, 500 μl of 0.3 mol/L HCl was added for neutralization; then, 1 ml of chloroform was added to whirlpool for 1 min and centrifuged at 3,000 r/min for 10 min. The supernatant was carefully taken and extracted 3 times, and the aqueous phase was analyzed by HPLC. The HPLC system consisted of an LC-20AD system equipped with an Agilent ZORBAX Eclipse Xtimate C18 column (5 μm, 4.6 mm × 200 mm) at a temperature of 30°C. The mobile phase consisted of 0.05 M phosphate buffer solution (pH 6.7) and acetonitrile (83:17, v/v) at a flow rate of 1 ml min^{-1}, with the sample injection volume of 20 μl. The DAD detector was set at 250 nm to acquire chromatograms. Mannose, ribose, rhamnose, glucuronic acid, galacturonic acid, N-acetyl-glucosamine, glucose, N-acetyl-galactosamine, galactose, xylose, arabinose, and fucose were used as the standards.

Fourier transform-infrared spectroscopy analysis

A total of 1 mg of each of the dried crude polysaccharides (TMIPs-H, TMIPs-U, TMIPs-E, TMIPs-Ac, and TMIPs-Al) was mixed with 100 mg of dried KBr to prepare the tablet for Fourier transform-infrared (FT-IR) experiment. The IR spectra were recorded at the wavenumber range of 4,000–400 cm^{-1} by a Nicolet FT-IR spectrophotometer (PerkinElmer, Waltham, MA, United States).

Thermogravimetric analysis

The thermal property of the TMIPs sample was studied using simultaneous thermal analysis (STA2500, NETZSCH, Germany). The heating rate was 10° min^{-1}, the heating range was 25–550°C, and the flow rate was 30 ml min^{-1} under a nitrogen atmosphere.

X-ray diffraction analysis

The dried *T. mongolicum* Imai polysaccharide samples were evenly placed in the sample pool and the sample pool was placed in the X-ray diffractometer (Ultima IV, Neo-Confucianism) operated at 40 kV and 40 mA, while 2θ ranged from 5 to 80°C at a scanning rate of 2°/min.

Scanning electron microscopy

The surface morphology of each sample was observed by a scanning electron microscope (SEM, ZEISS Gemini 300, Oberkochen, Germany) at an accelerating voltage of 5 kV. Before observation, the dry sample was sputtered with a gold layer, and SEM images were collected by a scanning electron microscope at 500 × and 2,000 × magnification.

Antioxidant activity

Diphenyl-2-picrylhydrazyl radical scavenging activity

The ability of polysaccharide samples to scavenge DPPH free radicals was evaluated according to the previously reported methods of (27). The DPPH solution (1.0 ml; 0.4 mmol/L), prepared with anhydrous ethanol, was mixed with 3.0 ml polysaccharide solution of different concentrations (0.125, 0.5, 1.0, 2.0, 3.0, and 4.0 mg/ml) and place in the dark at room temperature for 30 min. The absorbance of the sample was measured at 517 nm using a UV–Vis spectrophotometer. Ascorbic acid (0.125, 0.5, 1.0, 2.0, 3.0, and 4.0 mg/ml) was used as the positive control. The DPPH scavenging rate was calculated as follows:

$$DPPH\ radicals\ scavenging\ rate\ (\%) = 1 - \frac{A_S - A_0}{A_b} \times 100 \quad (2)$$

where, A_s is the absorbance of the sample group, A_0 is the absorbance value of anhydrous ethanol solution instead of DPPH solution, and A_b is the absorbance value of the polysaccharide sample replaced by deionized water.

ABTS radical scavenging activity

The ABTS free radical scavenging of five samples was measured by the readymade kit using ascorbic acid as the positive control. The following formula was used to calculate ABTS free radical scavenging activity of *T. mongolicum* Imai

polysaccharides:

$$ABTS\ radicals\ scavenging\ rate\ (\%) \quad 1 - \frac{A_s - A_0}{A_b} \times 100 \tag{3}$$

where, A_s is the absorbance value of polysaccharide sample solution, A_0 is the absorbance value of deionized water instead of ABTS+ solution, and A_b is the absorbance value of deionized water instead of polysaccharide sample.

Hydroxyl radical scavenging activity

The assay was performed with a slight modification referring to the method of (28). One milliliter of *T. mongolicum* Imai polysaccharide samples at different concentrations (0.125, 0.5, 1.0, 2.0, 3.0, and 4.0 mg/ml) was taken into the test tubes and the following reagents were successively added: 0.75 mm/L 1,10-phenanthroline (1.0 ml); 0.75 mm/L ferrous sulfate (1.0 ml); 0.01% (v/v) hydrogen peroxide (1.0 ml); and 0.15 mol/L sodium phosphate buffer solution with pH 7.4 (1.5 ml). The mixture was vortex-mixed and incubated at 37°C for 60 min. After the reaction, the absorbance was measured at 536 nm with ascorbic acid (0.125, 0.5, 1.0, 2.0, 3.0, and 4.0 mg/ml) as the positive control and deionized water as the blank control. The hydroxyl radical scavenging rate of the polysaccharide was calculated as follows:

$$Hydroxyl\ radicals\ scavenging\ rate\ (\%) = \frac{A_s - A_b}{A_0 - A_b} \times 100 \tag{4}$$

where, A_s is the absorbance of the sample group, A_{bji} is the absorbance value of the polysaccharide sample replaced by deionized water, A_0 is the absorbance value of deionized water instead of the polysaccharide sample and H_2O_2 solution.

Statistical analysis

All experiments were repeated three times. The results were expressed as mean ± SD. Every data point was analyzed using SPSS 26 (SPSS, IBM, United States). Duncan's multiple-range test was used for the analysis of variance. The difference was considered statistically significant when $p < 0.05$ and $p < 0.01$.

Results and discussion

Extraction yields and physicochemical properties of *Tricholoma mongolicum* Imai polysaccharides

The yield of the polysaccharide isolated from *T. mongolicum* Imai ranged from 6.64 to 13.16% depending on the extraction method. It can be seen from **Table 1** that the output of TMIPs-Al was higher than the rest four methods, which might be due to the destruction and hydrolysis of the cell wall by the alkaline environment, promoting the diffusion of polysaccharides (29). The yield of TMIPs-Ac was the second highest. These results were similar to those reported by (30). Ultrasonic-assisted extraction rate was the lowest, which might be due to the degradation of polysaccharides during ultrasonic treatment, resulting in smaller molecular weight and a decrease in the yield of the polysaccharide during alcohol precipitation process (29). This explanation was further confirmed by the results of molecular weight distribution.

The total sugar content of the five *T. mongolicum* Imai polysaccharides ranged from 26.48 to 36.24%. The total sugar contents of TMIPs-H, TMIPs-E, and TMIPs-Al were significantly ($p < 0.05$) higher than that of the remaining two polysaccharides. The protein content of TMIPs-Al (16.31%) was significantly higher than the other four polysaccharides of *T. mongolicum* Imai ($p < 0.05$), which was in agreement with the study of (31), where the protein extraction was higher under alkaline condition. The reason might be that the amide bonds in proteins were easily hydrolyzed by the alkali, thus increasing

TABLE 1 Extraction yield and chemical composition of polysaccharides from *Tricholoma mongolicum* Imai extracted by five different extraction methods.

Item	Sample				
	TMIPs-H	TMIPs-U	TMIPs-E	TMIPs-Ac	TMIPs-Al
Yield (%)	6.64	4.41	5.87	10.83	13.16
Total sugar (%)	36.24 ± 3.44^{a}	26.48 ± 0.48^{c}	32.96 ± 1.84^{a}	29.04 ± 0.56^{bc}	32.84 ± 0.04^{ab}
Protein (%)	4.93 ± 0.65^{d}	4.56 ± 0.27^{d}	7.67 ± 0.84^{c}	10.18 ± 0.33^{b}	16.31 ± 0.18^{a}
Uronic acid (%)	3.02 ± 0.82^{a}	2.95 ± 0.19^{a}	5.13 ± 0.24^{b}	2.73 ± 0.13^{a}	3.49 ± 0.60^{a}
Monosaccharide composition (molar ratio, %)					
Mannose	16.80	16.08	15.66	15.03	16.18
ribose	6.30	4.03	4.58	4.50	5.88
Glucuronic acid	1.59	1.72	0.95	0.52	0.19
Glucose	54.65	51.12	57.66	59.75	61.36
Galactose	13.98	20.15	14.63	14.08	9.24
Xylose	2.40	1.65	1.60	1.38	2.16
Fucose	3.50	4.23	3.94	3.72	3.99

Different letters in the same row represent significant differences at $p < 0.05$.

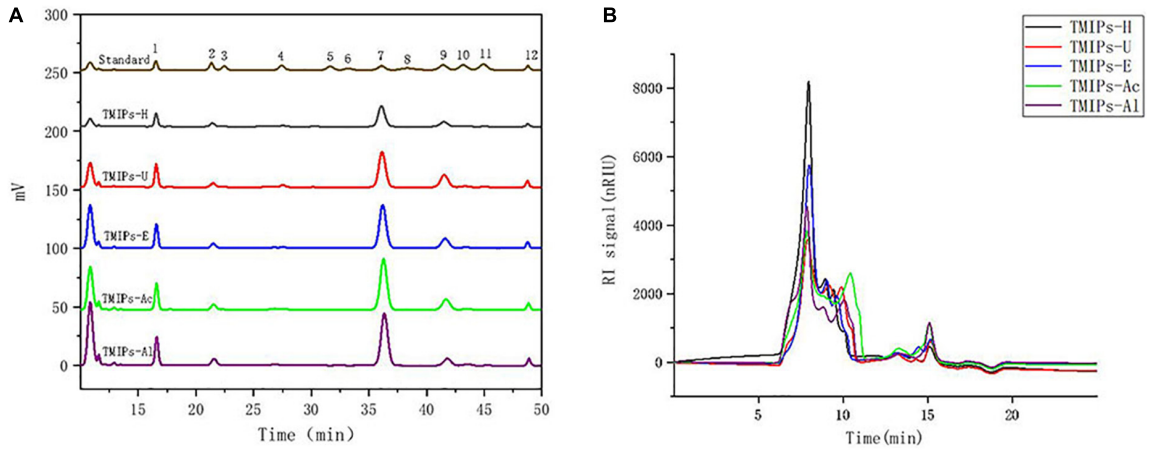

FIGURE 1
HPLC chromatograms of PMP derivatives of standard monosaccharides and TMIPs **(A)**; 1 – mannose; 2 – ribose; 3 – rhamnose; 4 – glucuronic acid; 5 – galacturonic acid; 6 – N-acetyl-glucosamine; 7 – glucose; 8 – N-acetyl-galactosamine; 9 – galactose; 10 – xylose; 11 – arabinose; 12 – fucose. Molecular weight distribution curve of TMIPs **(B)**.

the amounts of protein extracts. TMIPs-E showed the highest uronic acid content ($p < 0.05$), indicating that the uronic acid content of polysaccharides was related to the extraction method.

Molecular weight of *Tricholoma mongolicum* Imai polysaccharides

The biological activity of polysaccharides is affected by molecular weight distribution (32). To analyze the molecular weight distribution of the polysaccharides extracted by these five methods, High-performance gel permeation chromatography (HPGPC) method was used. As shown in **Figure 1B**, HPGPC spectra of different TMIPs were similar and multiple peaks appeared, indicating that all TMIPs were heteropolysaccharides. Except for TMIPs-Ac, the molecular weight of peak 1 and peak 2 of the other four polysaccharides were similar, ranging from 645.6 to 695.5 kDa and 334.6 to 407.3 kDa, respectively. It can be seen from **Table 2** that compared with the molecular weight distribution of TMIPs-H, the proportion of peaks 1 in the molecular weight distribution of TMIPs-U and TMIPs-E decreased and the proportion of peaks 2 and 3 increased, indicating that ultrasound and complex enzyme treatment resulted in an increase in the low molecular weight fraction of the polysaccharides. The reason might be that the polysaccharide was degraded by ultrasound and enzyme to some extent, which converted a part of the high-molecular-weight components into low-molecular-weight components, resulting in the increase of the low-molecular-weight components (29). Similar to our results, Chen and coworkers also proved that the ultrasonic treatment caused the polysaccharides to decompose into smaller molecules (33). The results showed that the molecular weight of TMIPs extracted by alkali and acid extraction was higher than those by hot water extraction, ultrasonic extraction, and enzymic extraction. These findings are consistent with previous reports that ultrasound, complex enzyme, and acid–alkaline treatment can effectively modify the glycosidic bonds (31). In general, the higher the molecular weight of polysaccharides, the greater their tensile strength, impact resistance, and elasticity (34). However, excessively high molecular weights can affect the solubility, rheological properties, processing applications, and even the biological activities of polymers to a certain extent (35). It is reported that polysaccharides with smaller molecular

TABLE 2 Average molecular weight and peak area of different peaks of TMIPs.

Sample	Molecular weight distribution		
	Peak number	Mv (kDa)	Peak area (%)
TMIPs-H	1	657.87	68.63
	2	382.33	11.23
	3	289.69	10.91
TMIPs-U	1	679.20	46.50
	2	334.56	18.55
	3	224.18	19.47
TMIPs-E	1	645.65	57.26
	2	362.05	15.21
	3	260.35	14.77
TMIPs-Ac	1	7,100.35	0.16
	2	692.79	55.77
	3	167.05	27.70
TMIPs-Al	1	695.49	52.39
	2	407.35	11.49
	3	202.83	21.27

weights usually play a more important role in determining the biological activity than those with larger molecular weights because smaller polysaccharide chains are easier to pass through biofilms and thus can play a more effective role.

Monosaccharide composition

The monosaccharide in TMIPs samples was identified by comparing the retention times with those of the standards. As shown in **Figure 1A** and **Table 1**, *T. mongolicum* Imai polysaccharide was composed of mannose, ribose, glucuronic acid, glucose, galactose, xylose, and fucose. The polysaccharides obtained by the five extraction methods were mainly composed of three monosaccharides, glucose, mannose, and galactose. The molar mass percentage of the three monosaccharides of TMIPs-H was 54.6, 16.8, and 13.9%, respectively, and the molar mass percentage of the three monosaccharides of TMIPs-U was, respectively, 51.1, 16.1, and 20.1%. The molar mass percentage of glucose, mannose, and galactose in TMIPs-E was 57.7, 15.7, and 14.6%. The molar mass percentage of three monosaccharides in TMIPs-Ac was 59.7, 15.0, and 14.1%; the molar mass percentage of the three monosaccharides of TMIPs-Al was 61.4, 16.2, and 9.2%, respectively. These polysaccharides were glucans, which were similar to the results of polysaccharide from *Agrocybe cylindracea* as reported by (36). The composition of monosaccharides had no obvious change, but the molar ratio of monosaccharides was different, which largely depended on the extraction conditions. This finding was consistent with previous reports by (37). The main reason might be that the polysaccharide molecules were partially degraded and the intermolecular hydrogen bond was broken under high temperature and high pressure, ultrasonic or acid-base conditions, resulting in the change in monosaccharide composition. The contents of glucuronic acid and galacturonic acid of the five polysaccharides were low, which was consistent with the results of uronic acid content.

Fourier transform infrared spectra analysis

Fourier transform infrared spectroscopy is usually used for the identification of the characteristic functional groups of polysaccharides. As shown in **Figure 2**, except that some characteristic bands showed the changes in absorbance and wave number, the polysaccharide samples extracted by the five extraction methods had similar general spectral characteristics, confirming the similar chemical compositions of the resultant polysaccharides. Fu and coworkers also proposed that the polysaccharides from loquat (*Eriobotrya japonica*) leaves, prepared by different methods, had similar structures (38). The characteristic peaks of polysaccharides appeared in all the five TMIPs. The broad and intense peak around 3,430 cm^{-1} was observed due to the stretching vibration of the O-H group (39). A weak band around 2,925 cm^{-1} was a characteristic of C-H stretching (40). In addition, the infrared analysis showed that no obvious absorption peak was detected near 1,730 cm^{-1}, indicating that the uronic acid in the five polysaccharides from *T. mongolicum* Imai was unesterified uronic acid. The strong peak around 1,640 cm^{-1} was attributed to C=O asymmetric stretching vibration of carboxyl group. The band at about 1,000–1,100 cm^{-1} showed the presence of C-O-C and C-O-H bonds, which was the characteristic peak of pyranose (41). The results

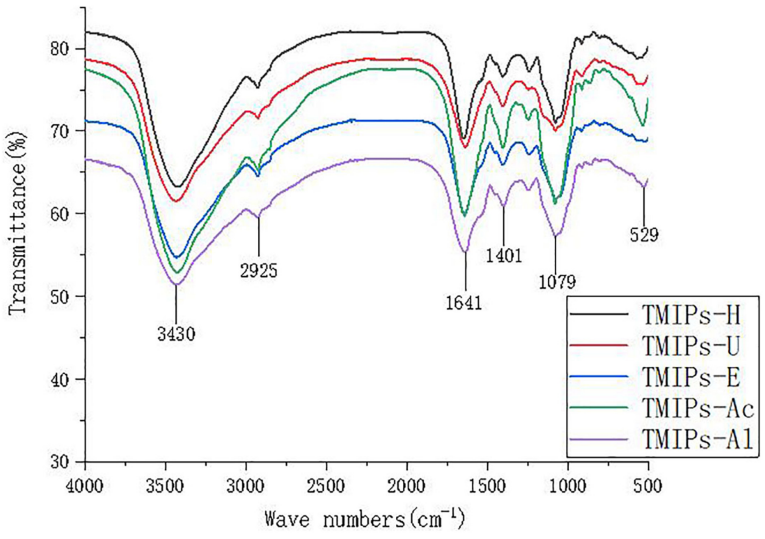

FIGURE 2
The FT-IR spectrum of TMIPs.

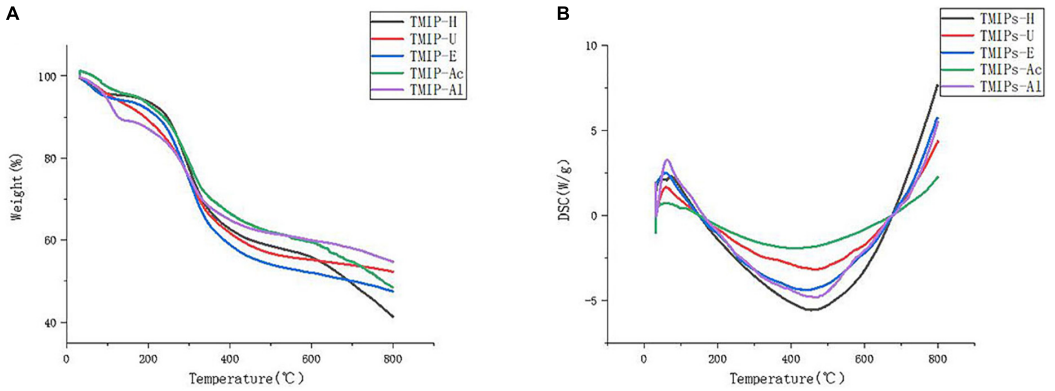

FIGURE 3
Thermogravimetric analysis of TMIPs. **(A)** TG curve and **(B)** DSC curve.

of IR spectroscopy indicated that the five extraction methods did not cause damage to the characteristic functional groups and skeletal structures of crude polysaccharides.

Thermogravimetric analysis and differential scanning calorimetry analysis

The thermodynamic properties of polysaccharides were studied by TGA and DSC. TGA curves showed that TMIPs experienced two main mass loss processes. The first mass loss mainly occurred at 25–120°C, which was attributed to the loss of free water in the sample. The second rapid weight loss stage occurred at 575–650°C, which might be related to the thermal decomposition of the polysaccharides (42). Differential scanning calorimetry (DSC) was used to estimate exothermic or endothermic changes with increasing temperature (43). The five polysaccharides exhibited an endothermic behavior at 20–120°C, which indicates that TMIPs are accompanied by the disintegration and mutation of homomorphic configuration during heating and an exothermic behavior at 380–500°C. This difference in thermal stability may be related to the differences in extraction methods, chemical composition, and structure of polysaccharides. Figure 3 shows that polysaccharides from different extraction methods had similar trends in thermodynamic curves, but there are certain differences in their endothermic and exothermic valleys. This difference in thermal stability might be related to the extraction method, chemical composition, and the structure of polysaccharides.

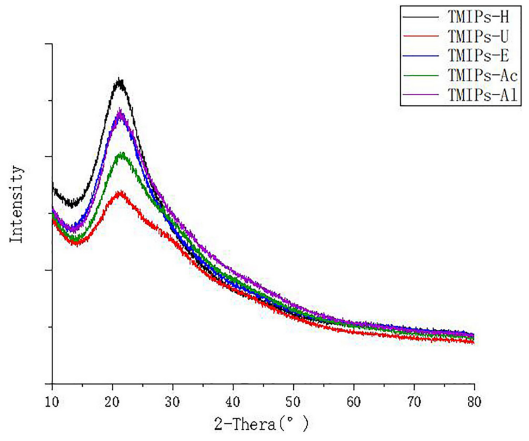

FIGURE 4
XRD analysis of different polysaccharides from TMIPs.

X-ray diffraction analysis

X-ray diffraction (XRD) is sensitive to the crystal structure analysis of plant polysaccharides. As shown in Figure 4, TMIPs with different intensities showed a single peak of passivation diffraction, when 2θ ranged from 21.17 to 21.47°, indicating that there was an amorphous or semi-crystalline structure inside (44). The XRD patterns displayed the characteristic diffraction curves of polysaccharides. Different extraction methods did not change the crystal structure of *T. mongolicum* Imai polysaccharide significantly.

Scanning electron microscopy analysis

The surface morphology of *T. mongolicum* Imai polysaccharides is displayed in Figure 5 as observed by scanning electron microscope (40). The polysaccharides obtained by different extraction methods had different shapes and sizes in micromorphology (45). TMIPs-H (Figure 5A) showed a massive and rough surface, covered with many

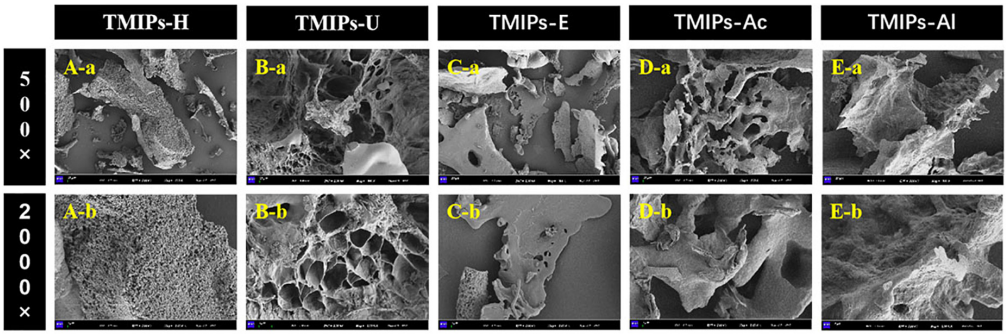

FIGURE 5
Scanning electron microscopy (SEM) micrographs of TMIPs. **(A)** TMIPS-H; **(B)** TMIPS-U; **(C)** TMIPS-E; **(D)** TMIPS-Ac; **(E)** TMIPS-Al; a. 500 × magnification; b. 2,000 × magnification.

small holes and the surface seemed very loose. TMIPs-U (**Figure 5B**) exhibited a much larger aperture than TMIPs-H and the structure appeared to be more robust with smooth and flat surface (43). This showed that ultrasound might produce acoustic cavitation, causing physical changes. TMIPs-E (**Figure 5C**) had a large number of small and compact spherical structures. The dense surface morphology of polysaccharides obtained by ultrasound and enzymatic hydrolysis might be attributed to their mild treatment conditions, which didn't reduce the interaction force and molecular crosslinking degree of polysaccharides completely. Thus, the yield of these two polysaccharides was lower than others. In addition, TMIPs-Ac (**Figure 5D**) displayed multilayered folds, while the surface of TMIPs-Al (**Figure 5E**) was rough and uneven, which might be due to the degradation and destruction of cell wall, facilitating the overflow of intracellular substances, improving the extraction efficiency of polysaccharides (37). The results indicated that different extraction methods had obvious influence on the microstructure of TMIPs.

Antioxidant activities *in vitro*

Scavenging activity of *Tricholoma mongolicum* Imai polysaccharides on Diphenyl-2-picrylhydrazyl radical

The DPPH radical scavenging abilities of TMIPs are shown in **Figure 6A**. The IC_{50} values of TMIPs-H, TMIPs-U, TMIPs-E, TMIPs-Ac, and TMIPs-Al were 0.94, 0.80, 1.27, 3.43, and 1.20 mg/ml, respectively. Ultrasonic extraction showed better DPPH inhibitory activity, which might be attributed to the increase of small molecular weight components of polysaccharides after ultrasonic treatment. Similar results were also reported by Chen and coworkers that low molecular weight usually had high biological activity (46). At the same mass concentration, polysaccharides with lower molecular weight usually have more free hydroxyl groups and higher reducing sugar content, thus having a strong antioxidant capacity. However, the antioxidant activity of polysaccharides is not determined by a single factor, but by comprehensive factors such as chemical composition, molecular weight, and chemical structure (47). The results showed that the antioxidant activity of the polysaccharide extracted by acid and alkali was weak; the reason might be that the internal structure of the polysaccharide was seriously damaged by acid and alkali treatment, which affects their biological activity.

Scavenging activity on ABTS radical of *Tricholoma mongolicum* Imai polysaccharides

The free radical scavenging ability of ABTS was often used to evaluate the antioxidant capacity of polysaccharides. It can be seen from **Figure 6B** that all the *T. mongolicum* Imai polysaccharides showed concentration-dependent scavenging activities. All five polysaccharides exhibited excellent ABTS free radical inhibitory activity. At a concentration of 4 mg/ml, the ABTS radical scavenging rate of TMIPs-H, TMIPs-U, TMIPs-E, TMIPs-Ac, and TMIPs-Al were 82.21, 86.16, 84.51, 73.90, and 84.43 mg/ml, respectively. Although samples' antioxidant capacities of ABTS were good, they did not exceed those of ascorbic acid. These results indicated that all the extracted TMIPs had the ability to scavenge ABTS free radicals, but the extraction method had an effect on the degree of scavenging activity. These apparent differences in scavenging activity may be related to differences in polysaccharide structure, such as different monosaccharide compositions, which can inhibit the formation of free radicals to varying degrees (31).

Scavenging activity of *Tricholoma mongolicum* Imai polysaccharides on hydroxyl radical

The hydroxyl radical is one of the most powerful oxidants and the most active natural free radicals. They disrupt cellular structures closest to the site of their formation and readily attack nucleic acids, proteins, and lipids. Therefore,

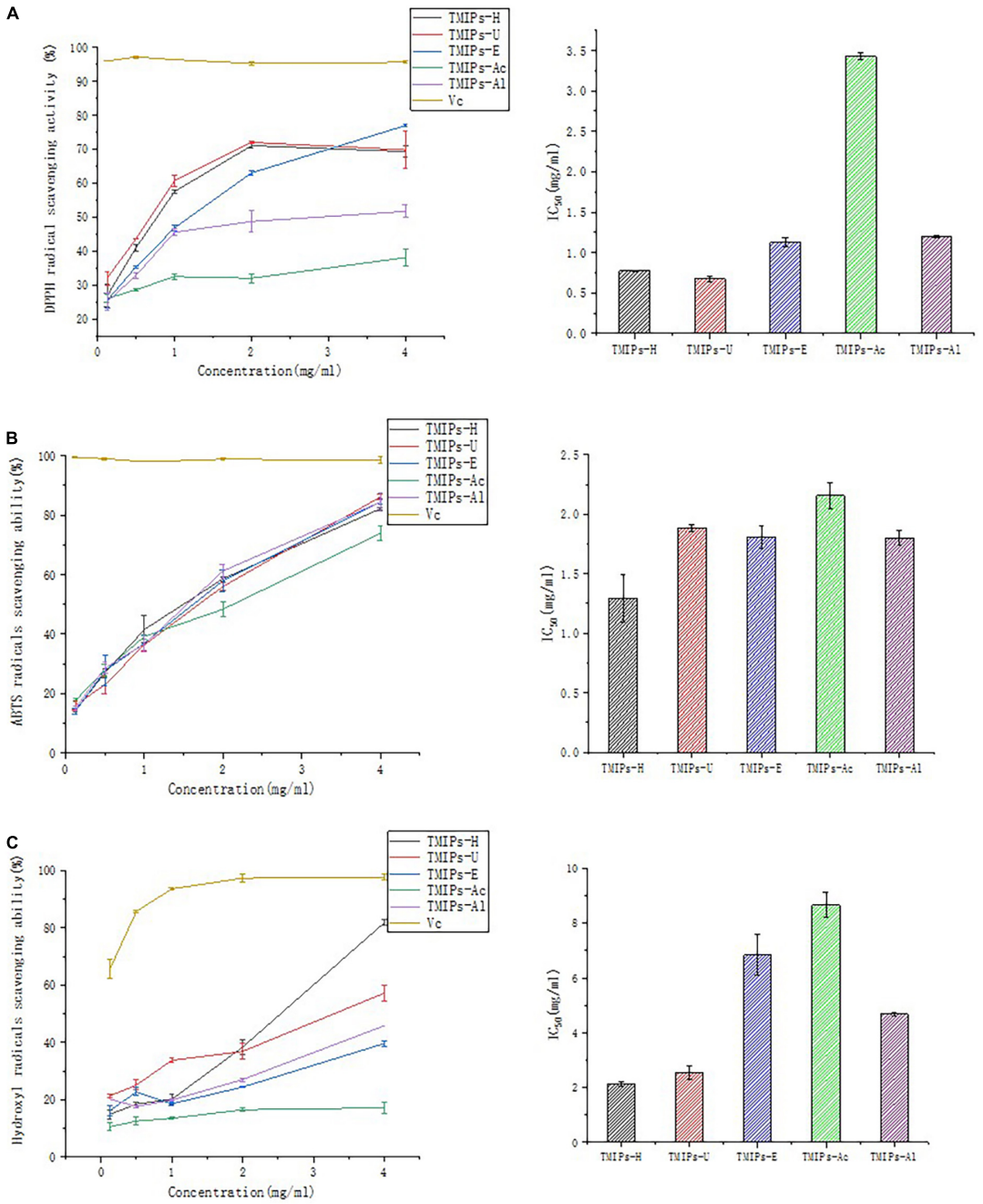

FIGURE 6
Antioxidant activity of TMIPs. **(A)** DPPH free radical scavenging ability. **(B)** ABTS free radical scavenging ability. **(C)** Hydroxyl radicals scavenging ability.

scavenging hydroxyl radicals is essential to protect living systems (48). As shown in **Figure 6C**, at a concentration of 0.125–4 mg/ml, the five polysaccharides showed different degrees of antioxidant activity in a concentration-dependent manner. The hydroxyl radical scavenging abilities of TMIPs were similar to their DPPH radical scavenging activities and followed the order TMIPs-H >TMIPs-U > TMIPs-Al > TMIPs-E > TMIPs-Ac. Despite this disparity, these polysaccharides are suitable for application as free radical scavengers. The IC_{50} of TMIPs-H and TMIPs-U were lower than that of the other TMIPs, indicating a better hydroxyl radical scavenging activity, which might be related to a

large number of low molecular weight components and different apparent morphologies.

Conclusion

In this study, the effects of five extraction methods on the chemical composition, structural characteristics, antioxidant activity, and hypoglycemic activity of TMIPs were evaluated. The results showed that all five polysaccharides had typical infrared spectroscopic characteristics of polysaccharides, and different extraction methods had little effect on their crystal structure and thermodynamic properties, showing similar trends. However, the extraction method had effects on its chemical composition, molecular weight distribution, monosaccharide content, and morphology. The yield and protein content of polysaccharides extracted by acid and alkali were higher than other methods. These structural differences led to different biological activities. TMIPs-U had a high DPPH and hydroxyl free radical scavenging capacity.

Studies have shown that different extraction methods affect the chemical composition and structural properties of polysaccharides, which together lead to the pros and cons of their biological activities. The anti-oxidant activity of *T. mongolicum* Imai polysaccharide obtained by ultrasonic and hot water extraction was better, but its extraction rates were lower than that of others. However, ultrasonic extraction can be selected as a more suitable polysaccharide extraction method not only because of the mild extraction conditions but also because the extracted polysaccharide has good biological activity. Therefore, TMIPs-U can be used for mass purification of the polysaccharide in further steps.

Data availability statement

The raw data supporting the conclusions of this article will be made available by the authors, without undue reservation.

Author contributions

NZ: conceptualization. NZ, KM, and BY: methodology, writing – original draft preparation, and visualization. BY: software. KM, YL, and BC: validation. BY: formal analysis. KM and XW: investigation. NZ, YL, and YS: resources and supervision. KM, XW, and BY: data curation. NZ, BC, BY, and YS: writing – review and editing. NZ, YL, and YS: project administration. YS: funding acquisition. All authors have read and agreed to the published version of the manuscript.

Funding

This work was financially supported by Introduced Talent Research Project of Hebei Agricultural University (YJ2021007), the National Natural Science Foundation of China (No. 32101911), and the National Key Research and Development Program of China (2019YFD0902003).

Conflict of interest

The authors declare that the research was conducted in the absence of any commercial or financial relationships that could be construed as a potential conflict of interest.

Publisher's note

All claims expressed in this article are solely those of the authors and do not necessarily represent those of their affiliated organizations, or those of the publisher, the editors and the reviewers. Any product that may be evaluated in this article, or claim that may be made by its manufacturer, is not guaranteed or endorsed by the publisher.

References

1. Xu W, Qian J, Ya M, Guo Y, Guo L. Research progress on *Tricholoma mongolicum* polysaccharide. *Heilongjiang Agric Sci.* (2018) 4:150–3.

2. You Q, Yin X, Zhang S, Jiang Z. Extraction, purification, and antioxidant activities of polysaccharides from *Tricholoma mongolicum* Imai. *Carbohyd Polym.* (2014) 99:1–10. doi: 10.1016/j.carbpol.2013.07.088

3. Su R, Bao H, Tu L, Yang S, Sun X. Anti-tumor activity of *Tricholoma mongolicum* fruit bodies. *Food Sci.* (2012) 33:280–4.

4. Liu Q, Tian G, Yan H, Geng X, Cao Q, Wang H, et al. Characterization of polysaccharides with antioxidant and hepatoprotective activities from the wild edible mushroom *Russula vinosa* Lindblad. *J Agric Food Chem.* (2014) 62:8858–66. doi: 10.1021/jf502632c

5. Zhang H, Jiang F, Zhang J, Wang W, Li L, Yan J. Modulatory effects of polysaccharides from plants, marine algae and edible mushrooms on gut microbiota and related health benefits: A review. *Int J Biol Macromol.* (2022) 204:169–92. doi: 10.1016/J.IJBIOMAC.2022.01.166

6. Liu Y, He S, Wei Y, Wang Y, Pei H, Bao H. Effects of *Tricholoma mongolicum* fruiting body extract on immune function in immunocompromised mice. *Acta Edulis Fungi.* (2020) 27:91–100. doi: 10.16488/j.cnki.1005-9873.2020.04.011

7. Guo L, Dai H, Ma J, Wang J, Hua Y, Zhou L. Isolation, structure characteristics and antioxidant activity of two water-soluble polysaccharides from *Lenzites betulina*. *BMC Chem.* (2021) 15:19. doi: 10.1186/S13065-021-00741-6

8. Sheng K, Wang C, Chen B, Kang M, Wang M, Liu K, et al. Recent advances in polysaccharides from *Lentinus edodes* (Berk.): Isolation, structures and

bioactivities. *Food Chem.* (2021) 358:129883. doi: 10.1016/J.FOODCHEM.2021.129883

9. Ji X, Hou C, Shi M, Yan Y, Liu Y. An insight into the research concerning Panax ginseng C. A. Meyer polysaccharides: A review. *Food Rev Int.* (2020) 38:1–17. doi: 10.1080/87559129.2020.1771363

10. Guo C, Guo D, Fang L, Sang T, Wu J, Guo C, et al. *Ganoderma lucidum* polysaccharide modulates gut microbiota and immune cell function to inhibit inflammation and tumorigenesis in colon. *Carbohyd Polym.* (2021) 267:118231. doi: 10.1016/J.CARBPOL.2021.118231

11. Chopra H, Kumar MA, Amin BA, Kumar MT, Kishore MY, Hyun BK. Narrative review: Bioactive potential of various mushrooms as the treasure of versatile therapeutic natural product. *J Fungi.* (2021) 7:728. doi: 10.3390/JOF7090728

12. Peng D, Wen Y, Bi S, Huang C, Yang J, Guo Z, et al. A new GlcNAc-containing polysaccharide from *Morchella importuna* fruiting bodies: Structural characterization and immunomodulatory activities in vitro and in vivo. *Int J Biol Macromol.* (2021) 192:1134–49. doi: 10.1016/J.IJBIOMAC.2021.10.051

13. Zhang Y, Liu Y, Zhou Y, Zheng Z, Tang W, Song M, et al. Lentinan inhibited colon cancer growth by inducing endoplasmic reticulum stress-mediated autophagic cell death and apoptosis. *Carbohyd Polym.* (2021) 267:118154. doi: 10.1016/J.CARBPOL.2021.118154

14. Liu G, Zhang J, Hou T, An S, Guo B, Liu C, et al. Extraction kinetics, physicochemical properties and immunomodulatory activity of the novel continuous phase transition extraction of polysaccharides from *Ganoderma lucidum*. *Food Funct.* (2021) 12:9708–18. doi: 10.1039/D1FO02185K

15. Dou Z, Chen C, Huang Q, Fu X. Comparative study on the effect of extraction solvent on the physicochemical properties and bioactivity of blackberry fruit polysaccharides. *Int J Biol Macromol.* (2021) 183:1548–59. doi: 10.1016/J.IJBIOMAC.2021.05.131

16. Wang Y, Zhang T, Huang X, Yin J, Nie S. Heteroglycans from the fruiting bodies of *Agrocybe cylindracea*: Fractionation, physicochemical properties andstructural characterization. *Food Hydrocoll.* (2020) 114:106568. doi: 10.1016/J.FOODHYD.2020.106568

17. Leong YK, Yang FC, Chang JS. Extraction of polysaccharides from edible mushrooms: Emerging technologies and recent advances. *Carbohyd Polym.* (2021) 251:117006. doi: 10.1016/j.carbpol.2020.117006

18. Zhao Y, Song J, Wang J, Yang J, Wang Z, Liu Y. Optimization of cellulase-assisted extraction process and antioxidant activities of polysaccharides from *Tricholoma mongolicum* Imai. *J Sci Food Agric.* (2016) 96:4484–91. doi: 10.1002/jsfa.7662

19. Yi Y, Xu W, Wang H, Huang F, Wang L. Natural polysaccharides experience physiochemical and functional changes during preparation: A review. *Carbohyd Polym.* (2020) 234:115896. doi: 10.1016/j.carbpol.2020.115896

20. Klaus A, Kozarski M, Niksic M, Jakovljevic D, Todorovic N, Van Griensven L. Antioxidative activities and chemical characterization of polysaccharides extracted from the basidiomycete *Schizophyllum commune*. *LWT-Food Sci Technol.* (2011) 44:2005–11. doi: 10.1016/j.lwt.2011.05.010

21. Chen X, Zhang H, Du W, Qian L, Xu Y, Huang Y, et al. Comparison of different extraction methods for polysaccharides from *Crataegus pinnatifida* Bunge. *Int J Biol Macromol.* (2020) 150:1011–9. doi: 10.1016/j.ijbiomac.2019.11.056

22. Qiu K, Li Z, Long Y, Lu Z, Zhu W. Study on extraction methods of polysaccharides from a processed product of *Aconitum carmichaeli* Debx. *RSC Adv.* (2021) 11:21259–68. doi: 10.1039/D1RA03628A

23. Li Y, Qin G, Cheng C, Yuan B, Huang D, Cheng S, et al. Purification, characterization and anti-tumor activities of polysaccharides from *Ecklonia kurome* obtained by three different extraction methods. *Int J Biol Macromol.* (2020) 150:1000–10. doi: 10.1016/j.ijbiomac.2019.10.216

24. Dubois M, Gilles KA, Hamilton JK, Rebers PA, Smith F. Colorimetric method for determination of sugars and related substances. *Anal Chem.* (2002) 28:350–6. doi: 10.1021/ac60111a017

25. Zor T, Selinger Z. Linearization of the bradford protein assay increases its sensitivity: Theoretical and experimental studies. *Anal Chem.* (1996) 236:302–8. doi: 10.1006/abio.1996.0171

26. Blumenkrantz N, Asboe-Hansen G. New method for quantitative determination of uronic acid. *Anal Biochem.* (1973) 54:484–9. doi: 10.1016/0003-269790377-1

27. Chen Z, Zhao Y, Zhang M, Yang X, Wei X. Structural characterization and antioxidant activity of a new polysaccharide from *Bletilla striata* fibrous roots. *Carbohyd Polym.* (2020) 227:115362. doi: 10.1016/j.carbpol.2019.115362

28. Liu W, Wang H, Yao W, Gao X, Yu L. Effects of sulfation on the physicochemical and functional properties of a water-insoluble polysaccharide preparation from *Ganoderma lucidum*. *J Agric Food Chem.* (2010) 58:3336–41. doi: 10.1021/jf903395g

29. Jia Y, Gao X, Xue Z, Wang Y, Lu Y, Zhang M, et al. Characterization, antioxidant activities, and inhibition on a-glucosidase activity of corn silk polysaccharides obtained by different extraction methods. *Int J Biol Macromol.* (2020) 163:1640–8. doi: 10.1016/j.ijbiomac.2020.09.068

30. Bai L, Zhu P, Wang W, Wang M. The influence of extraction pH on the chemical compositions, macromolecular characteristics, and rheological properties of polysaccharide: The case of okra polysaccharide. *Food Hydrocoll.* (2020) 102:105586. doi: 10.1016/j.foodhyd.2019.105586

31. Chen X, Chen G, Wang Z, Kan J. A comparison of a polysaccharide extracted from ginger (*Zingiber officinale*) stems and leaves using different methods: Preparation, structure characteristics, and biological activities. *Int J Biol Macromol.* (2020) 151:635–49. doi: 10.1016/j.ijbiomac.2020.02.222

32. Wassie T, Niu K, Xie C, Wang H, Xin W. Extraction techniques, biological activities and health benefits of marine algae *Enteromorpha prolifera* polysaccharide. *Front Nutr.* (2021) 8:747928. doi: 10.3389/FNUT.2021.747928

33. Chen X, Qi Y, Zhu C, Wang Q. Effect of ultrasound on the properties and antioxidant activity of hawthorn pectin. *Int J Biol Macromol.* (2019) 131:273–81. doi: 10.1016/j.ijbiomac.2019.03.077

34. Ji Y, Liao A, Huang J, Thakur K, Li X, Wei Z. Physicochemical and antioxidant potential of polysaccharides sequentially extracted from *Amana edulis*. *Int J Biol Macromol.* (2019) 131:453–60. doi: 10.1016/j.ijbiomac.2019.03.089

35. Wang L, Wu Q, Zhao J, Lan X, Yao K, Jia D. Physicochemical and rheological properties of crude polysaccharides extracted from *Tremella fuciform* is with different methods. *CYTA J Food.* (2021) 19:247–56. doi: 10.1080/19476337.2021.1884607

36. Wang Y, Zhang T, Xin Y, Huang X, Nie S. Comprehensive evaluation of alkali-extracted polysaccharides from *Agrocybe cylindracea*: Comparison on structural characterization. *Carbohyd Polym.* (2021) 255:117502. doi: 10.1016/J.CARBPOL.2020.117502

37. Chen C, Wang P, Huang Q, You L, Liu R, Zhao M, et al. A comparison study on polysaccharides extracted from Fructus Mori using different methods: Structural characterization and glucose entrapment. *Food Funct.* (2019) 10:3684–95. doi: 10.1039/c9fo00026g

38. Fu Y, Li F, Ding Y, Li H, Xiang X, Ye Q, et al. Polysaccharides from loquat (*Eriobotrya japonica*) leaves: Impacts of extraction methods on their physicochemical characteristics and biological activities. *Int J Biol Macromol.* (2020) 146:508–17. doi: 10.1016/j.ijbiomac.2019.12.273

39. Yuan Q, Lin S, Fu Y, Nie X, Liu W, Su Y, et al. Effects of extraction methods on the physicochemical characteristics and biological activities of polysaccharides from okra (*Abelmoschus esculentus*). *Int J Biol Macromol.* (2019) 127:178–86. doi: 10.1016/j.ijbiomac.2019.01.042

40. Ji X, Cheng Y, Tian J, Zhang S, Shi M. Structural characterization of polysaccharide from jujube (*Ziziphus jujuba* Mill.) fruit. *Chem Biol Technol Agric.* (2021) 8:54. doi: 10.1186/S40538-021-00255-2

41. Hou X, Huang X, Li J, Jiang G, Shen G, Li S. Extraction optimization and evaluation of the antioxidant and α-glucosidase inhibitory activity of polysaccharides from *Chrysanthemum morifolium* cv. Hangju. *Antioxidants.* (2020) 9:59. doi: 10.3390/antiox9010059

42. Long H, Gu X, Zhou N, Zhu Z, Wang C, Liu X, et al. Physicochemical characterization and bile acid-binding capacity of water-extract polysaccharides fractionated by stepwise ethanol precipitation from *Caulerpa lentillifera*. *Int J Biol Macromol.* (2020) 150:654–61. doi: 10.1016/j.ijbiomac.2020.02.121

43. Abuduwaili A, Rozi P, Mutailifu P, Gao Y, Nuerxiati R, Aisa HA, et al. Effects of different extraction techniques on physicochemical properties and biological activities of polysaccharides from *Fritillaria pallidiflora* Schrenk. *Process Biochem.* (2019) 83:189–97. doi: 10.1016/j.procbio.2019.05.020

44. Cheng S, He F, Fu L, Zhang Y. Polysaccharide from rubescens: Extraction, optimization, characterization and antioxidant activities. *RSC Adv.* (2021) 11:18974–83. doi: 10.1039/D1RA01365C

45. Zhu J, Chen Z, Zhou H, Yu C, Han Z, Shao S, et al. Effects of extraction methods on physicochemical properties and hypoglycemic activities of polysaccharides from coarse green tea. *Glycoconj J.* (2020) 37:1–10. doi: 10.1007/s10719-019-09901-2

46. Chen H, Zeng J, Wang B, Cheng Z, Chen K. Structural characterization and antioxidant activities of *Bletilla striata* polysaccharide extracted by different methods. *Carbohyd Polym.* (2021) 266:118149. doi: 10.1016/J.CARBPOL.2021.118149

47. Ji X, Guo J, Ding D, Gao J, Hao L, Guo X, et al. Structural characterization and antioxidant activity of a novel high-molecular-weight polysaccharide from *Ziziphus Jujuba* cv. Muzao. *J Food Meas Charact.* (2022) 16:2191–200. doi: 10.1007/S11694-022-01288-3

48. Peng Z, Min L, Fang Z, Zhang Q. In vitro antioxidant effects and cytotoxicity of polysaccharides extracted from *Laminaria japonica*. *Int J Biol Macromol.* (2012) 50:1254–9. doi: 10.1016/j.ijbiomac.2012.04.006

frontiers | Frontiers in Nutrition

TYPE Original Research
PUBLISHED 09 August 2022
DOI 10.3389/fnut.2022.946606

Check for updates

OPEN ACCESS

EDITED BY
Xiaolong Ji,
Zhengzhou University of Light Industry, China

REVIEWED BY
Jianhua Xie,
Nanchang University, China
Jie Gao,
Guangxi University, China
Lei Liu,
Xihua University, China

*CORRESPONDENCE
Hehe Li
xyzhehe@126.com

SPECIALTY SECTION
This article was submitted to Food Chemistry, a section of the journal Frontiers in Nutrition

RECEIVED 17 May 2022
ACCEPTED 15 July 2022
PUBLISHED 09 August 2022

CITATION
Wu Z, Qin D, Li H, Guo D, Cheng H, Sun J, Huang M, Ye X and Sun B (2022) Physicochemical and functional properties of *Lycium ruthenicum* pectin by different extraction methods.
Front. Nutr. 9:946606.
doi: 10.3389/fnut.2022.946606

COPYRIGHT
© 2022 Wu, Qin, Li, Guo, Cheng, Sun, Huang, Ye and Sun. This is an open-access article distributed under the terms of the Creative Commons Attribution License (CC BY). The use, distribution or reproduction in other forums is permitted, provided the original author(s) and the copyright owner(s) are credited and that the original publication in this journal is cited, in accordance with accepted academic practice. No use, distribution or reproduction is permitted which does not comply with these terms.

Physicochemical and functional properties of *Lycium ruthenicum* pectin by different extraction methods

Ziyang Wu[1,2,3], Dan Qin[1,2,3], Hehe Li[2,3]*, Dongqi Guo[1], Huan Cheng[1], Jinyuan Sun[2,3], Mingquan Huang[2,3], Xingqian Ye[1] and Baoguo Sun[2,3]

[1]Zhejiang Key Laboratory for Agro-Food Processing, National-Local Joint Engineering Laboratory of Intelligent Food Technology and Equipment, College of Biosystems Engineering and Food Science, Zhejiang University, Hangzhou, China, [2]Beijing Laboratory for Food Quality and Safety, Beijing Technology and Business University, Beijing, China, [3]Key Laboratory of Brewing Molecular Engineering of China Light Industry, Beijing Technology and Business University, Beijing, China

Three different extraction methods were used to extract high-temperature water-extracted pectin (HWp), high-temperature acid-extracted pectin (HAp), and high-temperature alkali-extracted pectin (HALp) from *Lycium ruthenicum*. The physicochemical properties, structure, and functional properties of three different pectins were studied. The results showed that HWp and HALp can extract rhamnogalacturonan-I (RG-I) from *L. ruthenicum* better. Through structural feature analysis, HWp and HALp have a branched structure, and HWp has a higher degree of esterification than HAp and HALp. Zeta potential results show that HWp solution is more stable. The thermal analysis results show that the thermal stability is HALp > HAp > HWp. HWp has the highest viscosity. The inhibitory activity results showed that HWp, HAp, and HALp have a certain inhibitory effect on α-glucosidase activity. This study shows the effects of different extraction methods on the properties of *L. ruthenicum* pectin and aims to provide a theoretical basis for the pharmaceutical and food industries to choose more suitable pectin extraction methods.

KEYWORDS

***Lycium ruthenicum*, pectin, extraction methods, physicochemical properties, functional properties**

Introduction

Pectin represents a group of structurally heterogeneous polysaccharides widely distributed in primary cell walls and the middle lamella of higher plants, which are rich in galacturonic acid (1). It is synthesized in the Golgi apparatus, released through exocytosis, and is commonly found in the primary wall of plant cell walls and the middle

layer of cells. The pectin content in the primary cell wall of dicot plants is higher than that in the cell walls of gramineous plants. Pectin is considered to be a complex plant heteropolysaccharide. In some species, 35% of the primary cell wall is made up of pectin. Pectin is the most complex polysaccharide in nature and plays an important role in many industries (2). Commercial pectin consists of at least 65% galacturonic acid monomers. Commercial pectin is mainly composed of homogalacturonan (HG) with very low content of rhamnogalacturonan-I (RG-I). A more common method for producing pectin is to extract it using an acidic aqueous solution at 60–100°C under the condition of pH 1.5–3. The pectin thus extracted can achieve a more uniform quality. In the past few years, people have started to focus on the health properties of pectin. Studies have shown that chain conformation is an important parameter of polysaccharides and is closely related to the biological activity of polysaccharide (3). Therefore, the side chain of pectin has received extensive attention (4). Studies have shown that substituted rhamnogalacturonic acid (RGs) pectin can prevent cancer (5) by inducing apoptosis (6) in cancer cells. Through structural characterization, pectin has side chains and shows prebiotic potential.

Lycium ruthenicum Murr is a perennial wild thorny shrub belonging to the Solanaceae family, distributed in the salinized desert areas of northwest China (7). According to Chinese classical pharmacy books, the fruit of *L. ruthenicum* Murr is known by the common name "black wolfberry" in China. *L. ruthenicum* Murr is considered a traditional Chinese herbal remedy for menopause, menstrual irregularities, and heart disease (8). *L. ruthenicum* Murr has been studied in recent years because of its functional properties, and it has many functional components, such as pectin (9), flavonoids (10), anthocyanins (11), phenolic acid (12), alkaloids (13), and essential oils (14), which have good biological activity. The literature shows that pectin has antioxidant (15), hypoglycemic (16), and antifatigue activities (17). Nowadays, the structural and functional properties of pectin from *L. ruthenicum* have attracted extensive attention.

According to literature, different extraction methods result in different physicochemical properties and chemical structures of polysaccharides (18). Due to the extremely strong water solubility and alcohol insolubility of pectin, ethanol precipitation after extraction with water is the most commonly used extraction method in the extraction of pectin. This study aims to compare the structure and biological characteristics of pectin using three different extraction methods (water extraction, acid extraction, and alkaline extraction). Finding the difference between different extraction methods of pectin provides a certain theoretical basis for actual production.

Materials and methods

Materials and reagents

Lycium ruthenicum was purchased from Qinghai Province, China. All *L. ruthenicum* were dried and then grounded sufficiently into powder (50 mesh) and stored in desiccators until further use. Standard monosaccharides were purchased from Sigma-Aldrich (Shanghai) Trading Co., Ltd. (Shanghai, China). Ethanol (≥99%), HCl (37%), NaOH (≥99%) K_2HPO_4 (≥99%), and KH_2PO_4 (≥ 99%) were purchased from Sinopharm Chemical Reagent Co., Ltd. (Shanghai, China), 4-nitrobenzene-α-D-glucopyranoside (BR), α-glucosidase (≥99%), and acarbose (≥99%) were purchased from Mreda (Beijing, China). All ultrapure water and deionized water were obtained from Milli-Q system (Advantage A10, Billerica, United States).

Extraction of *Lycium ruthenicum* pectin

Lycium ruthenicum consists of lots of phenolic compounds (19). The high-concentration alcohol solution can extract phenolic compounds well without destroying pectin or polysaccharides (20, 21). Therefore, *L. ruthenicum* powder was first treated with an 80% ethanol solution at 180 rpm for 48 h two times. The *L. ruthenicum* powder from which the free phenolic compounds were initially removed was obtained. Then, the obtained solid was degreased three times with n-hexane and dried at 40°C. The dried *L. ruthenicum* powder (30 g) was weighed and 900 ml deionized water was added. The high-temperature water extraction (HWE) directly extracted the sample after adding water. The high-temperature acid extraction (HAE) adjusted the sample with HCl (6 mol/L) to pH = 1. The high-temperature alkaline extraction (HALE) adjusted the sample with sodium hydroxide (NaOH) (6 mol/L) to pH = 13. Constant temperature heating magnetic stirrer (Yuhua Instrument Equipment Co., Ltd., Gongyi, China) was used to extract pectin at 85°C for 6 h, and then the extracted solution was cooled to room temperature. The pH of solutions that cooled to room temperature was adjusted to 7. Then, ethanol was added to the solution until the ethanol concentration was 80%. This solution was placed in a refrigerator at 4°C overnight. The overnight solution was centrifuged at 10,000 rpm for 15 min to obtain precipitated pectin. The supernatant was decanted, and the precipitate was dissolved with deionized water. The precipitate was placed in a water bath and heated at 70°C for 2 h to remove residual ethanol. Finally, the purified pectin was freeze-dried by freeze dryer (Alpha 1–4 LSCbasic, CHRIST, Osterode, Germany) for further analysis. The pectins obtained

from HWE, HAE, and HALE were named HWp, HAp, and HALp, respectively.

The calculation method of the extraction rate is to divide the mass of the freeze-dried gum by the mass of the initial fruit powder.

Physicochemical properties of *Lycium ruthenicum* pectin

Total sugar, total protein, and total phenols

For the sample chemical composition index, the total sugar, total protein, and total phenol of the sample were determined. The total sugar content was quantitatively determined using phenol-sulfuric acid colorimetric assay, in which glucose was used as a standard. The total protein content was determined using Bradford assay (Beyotime Biotechnology, China). The total phenolic content of the obtained samples was measured in gallic acid equivalent (GAE, μg/mg, dry weight basis) using the Folin–Ciocalteu colorimetric method.

Monosaccharide composition

The monosaccharide contents of samples were calculated according to Hu et al. with small modifications (4). The sample (2 mg) was added to 4 M trifluoroacetic acid and hydrolyzed at 110°C for 8 h. Trifluoroacetic acid was removed by nitrogen blowing (25°C). After diluting the samples with ionized water, they were filtered and analyzed. Rhamnose (Rha), glucuronic acid (GluA), glucose (Glu), galacturonic acid (GalA), arabinose (Ara), galactose (Gal), fucose (Fuc), and xylose (Xyl) were used as a monosaccharide standard. The prepared samples and monosaccharide standard mixture were assayed at 30°C using a Dionex system (ICS-5000, Thermo Fisher, Waltham, MA, United States) with a pulsed electrochemical detector and a Carbopac^{TM} PA10 analytical column. The separation was performed by isocratic elution with 18 mM NaOH for 15 min, followed by 18 mM NaOH in 100 mM NaOAc for the next 35 min.

Molecular weight parameters

The molecular weight of the samples was determined using size-exclusion chromatography coupled to multi-angle laser light scattering. The molecules were separated by hydrodynamic volume (SEC column, OHpak SB-G guard column, SB-806 HQ and SB-804 HQ columns, 7.8 × 300 mm, Shodex, Japan). After the sample was separated in a column connected to an HPLC system, the molecules were passed through a MALS detector and detected by a laser beam. MALS quantifies and displays molecular weight by analyzing the signal and differential refractive index (dRI) signal. The specific parameters were elution with 0.15 M NaCl (pH 7.0) on the SEC column. The system run time was 90 min, and the sample injection volume was 100 μl. The dn/dc (refractive index increment) value was defined as 0.138 ml/g for all samples (22). All data were analyzed using the ASTRA software (7.1.2, Wyatt Technology, United States).

Structural properties and stability of pectin

The structure of the samples was analyzed using Fourier transform infrared (FT-IR), and the pectin samples were ground with KBr and pressed into flakes for testing. Tablets were measured in the 4,000–400 cm^{-1} range using transmission mode and 32 scans on a spectrophotometer (Nicolet 5,700, Thermo Fisher Scientific, Waltham, United States). The calculation of the degree of esterification of pectin refers to the method of Monsoor (23). The peaks at 1,740 and 1,630 cm^{-1} in the infrared spectrum correspond to the C = O stretching vibrations of $COOCH_3$ and COO^- on pectin GalA, respectively. The formula for calculating the degree of esterification (DE value) of pectin is as follows:

$$DE(\%) = \frac{Area_{1740}}{Area_{1740} + Area_{1630}} \times 100 \quad (1)$$

where $Area_{1740}$ is the peak area of 1,740 cm^{-1} in the infrared absorbance spectrum, and $Area_{1630}$ is the peak area of 1,630 cm^{-1} in the infrared absorbance spectrum. The analysis of the peak area was performed using OMNIC 7.3 (Thermo Fisher Scientific, Waltham, United States).

Congo red experiment was used to detect whether the pectin of different extraction methods had a triple-helix conformation. Congo red solution (80 μmol/L) and NaOH solution (1 mol/L) were configured. Then, 1 mg of HWp, HAp, and HALp and 2 ml of Congo red solution were added to different centrifuge tubes, respectively. The amounts of substances added to the NaOH solution were 0, 0.1, 0.2, 0.3, 0.4, and 0.5 mol/L, respectively. All solutions were diluted to 5 ml. Vortex shaker (IKA, Baden-Württemberg, Germany) was used to mix the solution and let it stand for 10 min at room temperature. After zeroing the UV-Vis spectrophotometer (UV-2700 220V CH, Shimadzu Instrument Mfg. Co., Ltd., Suzhou, China) with deionized water, the samples were scanned in the range of 400–600 nm. The maximum UV absorption wavelength of samples at different concentrations of NaOH was determined.

Zeta potential analysis was based on the classical dynamic light scattering theory. The zeta potential mode of the Malvern Zetasizer Pro laser particle size analyzer (Malvern, United Kingdom) was used to measure the zeta potential of

the *L. ruthenicum* pectin solution. To avoid multiple scattering effects, 1% (w/v) pectin solution was diluted 100 times, and its potential was measured at 25°C.

Atomic force microscopy and scanning electron microscope

The pectin samples were dissolved in deionized water to make a 1 mg/ml solution. The solutions were continuously stirred at 50°C for 12 h and then diluted to 10 μg/ml. The diluted pectin solutions (10 μl) were added dropwise on fresh matrix-cut mica and air-dried at 25°C. Atomic force microscope (AFM) images were collected with Cipher-S AFM (Asylum Research Instruments, United States) using a silicon cantilever (Si_3N_4) probe with a spring constant of 0.2 N/m and a resonance frequency of 13 kHz. Image analysis was performed using Nanoscope Analysis version 1.9 (Bruker, Rheinstetten, Germany).

Scanning electron microscope (SEM) (ZEISS, Oberkochen, Germany) was used to observe and take photograph of the surface microstructure of pectin under different extraction methods. All samples were fixed on the sample stage with double-sided sticky tape and covered with gold in a vacuum evaporator. Acceleration voltage was 3.0 kV, and the working distance was 10.6 mm. The surface and shape were collected at an appropriate magnification.

Thermal analysis

For the determination of thermal stability of pectin samples, samples were characterized using a thermogravimetric analyzer (TGA 3+) (Mettler Toledo, Switzerland) in the temperature range of 50–600°C. Samples (3 mg) were analyzed in standard aluminum sample pans using high-purity N_2 as the purge gas.

Rheological characterization and dispersion stability

The rheological properties of the pectin samples were analyzed with an MCR302 Rheo-Stress rheometer (Anton Paar, Austria) with PP50 planar geometry. A 15% (w/v) solution of the sample was subjected to stable rate sweep testing over a shear rate range of 1–100 s^{-1} in logarithmic increments at 25°C. The data fit uses the following equation:

$$\eta = \kappa \cdot \gamma^{(n-1)} \quad (2)$$

where η is the apparent viscosity (Pa·s), κ (Pa·sn) is the consistency index, γ is the shear rate (s-1), and n is the flow behavior index. Strain sweeps were used to determine the linear viscoelastic range. Changes in storage modulus (G′) and loss modulus (G″) of the mixed solution were measured over a frequency sweep from 1 to 100 Hz.

Inhibition of α-glucosidase by *Lycium ruthenicum* pectin

α-Glucosidase inhibitors can competitively bind enzymes, inhibit the rate of carbohydrate hydrolysis in the intestinal tract, reduce the body's absorption of carbohydrates, and achieve the purpose of controlling blood sugar. The inhibitory activity of HWp, HAp, and HALp on α-glucosidase was determined. The measurement method refers to the method of Lordan (24), and some adjustments have been made. The α-glucosidase solution (0.5 U/ml), 4-nitrophenyl α-D-glucopyranoside solution (5 mM), and HWp, HAp, and HALp pectin solutions (0.1, 0.2, 0.4, 0.6, 0.8, 1.0, and 2.0 mg/ml) were configured with a phosphate-buffered solution (0.1 M) with pH 6.9. The concentration of Na_2CO_3 solution was 0.2 M. Each reactant was added to a 96-well plate, and each group of experiments was repeated three times. Acarbose was used as a positive control.

The samples obtained in G_a, G_b, G_c, and G_d measured the absorbance at 405 nm with a microplate reader (SpectraMax M2, Molecular Devices, San Jose, United States). The inhibitory efficiency of HWp, HAp, and HALp on glucosidase can be calculated according to the following formula:

$$\text{Inhibitory efficiency} = \left[1 - \frac{(G_d - G_c)}{(G_b - G_a)}\right] \times 100\% \quad (3)$$

Results and discussion

Physicochemical properties of high-temperature water-extracted pectin, high-temperature acid-extracted pectin, and high-temperature alkali-extracted pectin

Chemical composition

As shown in **Table 1**, the chemical compositions of HWp, HAp, and HALp were different. The yields of HAp (6.77 ± 0.54%) and HALp (6.19 ± 0.71%) are significantly higher than that of HWp (3.83 ± 0.73%), suggesting the contribution of acid or alkaline treatments in pectin extraction. This is due to the fact that acids and bases are good at breaking down the cell walls and releasing pectin. Compared with HWp (11.96 ± 1.65 μg GAE/mg), HAp (18.91 ± 1.69 μg GAE/mg) and HALp (17.09 ± 1.64 μg GAE/mg) had a higher phenolic content. Phenolic compounds are widely present in plants and

TABLE 1 Yields and the chemical compositions of HWp, HAp, and HALp.

	HWp	HAp	HALp
Yield (%, w/w)	3.83 ± 0.73^{b}	6.77 ± 0.54^{a}	6.19 ± 0.71^{a}
Total sugar (%, w/w)	65.86 ± 1.74^{b}	65.15 ± 2.68^{b}	70.85 ± 1.17^{a}
Total phenolic content (μg GAE/mg)	11.96 ± 1.65^{b}	18.91 ± 1.69^{a}	17.09 ± 1.64^{a}
Total protein content (%, w/w)	4.77 ± 0.64^{b}	5.82 ± 0.77^{a}	6.43 ± 0.41^{a}
Monosaccharide (%)			
Fuc	0.92 ± 0.15^{a}	0.59 ± 0.11^{a}	0.81 ± 0.01^{a}
Rha	2.70 ± 1.45^{b}	6.02 ± 0.54^{ab}	8.12 ± 0.91^{a}
Ara	38.16 ± 3.73^{a}	0.81 ± 0.06^{b}	38.31 ± 1.46^{a}
Gal	20.67 ± 2.40^{b}	26.94 ± 1.37^{a}	18.46 ± 0.94^{b}
Glu	5.35 ± 1.50^{b}	11.40 ± 1.02^{a}	3.00 ± 0.16^{b}
Xyl	5.31 ± 1.90^{b}	17.69 ± 4.29^{a}	4.98 ± 0.50^{b}
GalA	23.23 ± 4.77^{b}	33.22 ± 0.37^{a}	23.60 ± 0.77^{b}
GluA	3.66 ± 0.32^{a}	3.33 ± 0.13^{a}	2.73 ± 0.03^{a}
HG	20.53 ± 3.30^{b}	27.20 ± 0.39^{a}	15.48 ± 0.26^{b}
RG-I	64.23 ± 9.03^{a}	39.79 ± 0.23^{b}	73.00 ± 4.21^{a}
(Gal+Ara)/Rha	21.79 ± 2.27^{a}	4.61 ± 0.24^{c}	6.99 ± 0.30^{b}

^{a,b}Means that the data has significant differences.

are closely linked to plant cell walls through ester and ether bonds (20). The difference in total phenolic content among the three pectins may be due to the fact that the hydrogen bond between the cell wall and the polyphenols is broken under acidic or basic conditions, which leads to the release of more phenolic compounds (4). Compared with ordinary commercial pectin (1.46 μg GAE/mg pectin) and citrus pectin (5.89 ± 0.05 μg GAE/mg and 2.20 ± 0.16 μg GAE/mg) (25), the content of phenolic compounds in *L. ruthenicum* pectin is higher. This may be caused by the higher content of phenolic compounds in *L. ruthenicum* (26, 27). The total sugar content of HALp is significantly higher than that of HWp and HAp. The total protein content of HAp is significantly higher than that of HWp. Alkali-extracted pectin had more side chains, while acid-degraded pectin had more side chains. Given that arabinogalactose protein in *L. ruthenicum* pectin is an important glycoconjugate, a large part of the neutral sugar branch of RG-I in *L. ruthenicum* pectin should be tightly bound to the protein (28).

The monosaccharide composition of the three pectin samples was determined by comparing the retention times of the chromatograms of the pectin samples with that of the monosaccharide standard. As shown in **Table 1**, all samples were composed of Fuc, Rha, Ara, Gal, Glu, Xyl, GalA, and GluA. HWE, HAE, and HALE will not change the type of monosaccharides, but the compositions of monosaccharides extracted from pectin by different extraction methods are different. The contents of GalA in the three pectin were relatively high, proving that they have better antioxidant activity (29). The content of GalA of HAp is significantly higher than those of HWp and HALp. The decrease in GalA content in pectin may be attributed to β-elimination reaction, which is one of the mechanisms of non-enzymatic degradation of pectin that will cleave the HG skeleton and de-esterify it when treated with alkaline medium (30). The pectin side chain is mainly composed of Ara and Gal (4). As shown in **Table 1**, the content of Gal of HAp is significantly higher than those of HWp and HALp. The Ara mol% of HWp and HALp was about 45 times higher than that in HAp. This phenomenon can be attributed to the degradation effect of acid treatment. Glu may come from residues of soluble sugars that were not completely removed during the extraction process (31). For acid hydrolysis, the content of Gal and Ara in acid degradation of citrus pectin decreases (32), which may be because Ara and Gal are the most unstable, while GalA is the most resistant to acid hydrolysis (33, 34). Therefore, the content of GalA in HAp is higher. For Fuc and GluA, different extraction methods have little effect on their contents. The molar ratio of (Gal + Ara)/Rha can demonstrate the contribution of the RG region in the pectin structure and the length of the branch connecting to RG-I (35). In this study, the molar ratios of (Gal + Ara)/Rha for HWp, HAp, and HALp were 21.79 ± 2.27, 4.61 ± 0.24, and 6.99 ± 0.30, respectively. The (Gal + Ara)/Rha molar ratios of HWp and HALp are high, hence the presence of long-chain branched RG-I domains in these two pectins. The molar percentage of HG in HAp was 27.20 ± 0.39 mol%, which was significantly higher than that in HWp and HALp. Therefore, the HG region of HAp dominates.

Molecular weight

The molecular weight of pectin plays an important role in the biological activity and use of pectin (36). **Table 2** shows the molecular parameters of HWp, HAp, and HALp. For the three pectins, two symmetrical peaks were observed in the RI elution profile. In HWp and HAp, the concentration of the component with the highest molecular weight is lower, and the component with the lower molar mass is dominant. Compared with HWE, HAE can decompose pectin into smaller molar masses. In HALp, compared to HWp, HALE can decompose pectin into smaller molar masses, but 53.1% of pectin still maintains a high molar mass. These results showed that HWp, HAp, and HALp underwent degradation effect. Among them, HAp experienced the most serious degradation, followed by HALp. Although HWp has also undergone degradation, its effect is weaker than that of HAp and HALp. Polydispersity coefficients (Mw/Mn) of HALp (3.641 and 1.240) were a little higher than in HWp (1.464 and 1.084) and HAp (1.592 and 1.120). This indicates a broad molecular weight distribution of polysaccharides in HALp. The root mean square radii of the pectin samples from different treatments also varied, with values ranging from 25.600 to 138.900 nm. The above results indicate that the polysaccharides produced by the three treatment methods are all partially hydrolyzed. However, the polysaccharide sample treated with HALE maintains a higher molar mass.

Structural properties of pectin

Fourier transform infrared analysis

As identified in Figure 1A, the three absorption bands appearing at 3,422, 3,421, and 3,421 cm^{-1} represent the stretching vibration of hydroxyl (-OH); the absorption band at 2,926 cm^{-1} represents stretching vibration of C–H. The absorption bands at 1,744, 1,745, and 1,746 cm^{-1} can be considered to be esterified carboxyl groups ($COCH_3$), and the signals at 1,626 and 1,632 cm^{-1} show carboxylate groups. The degree of methoxylation (DM) of pectin can be determined from the percentage of peak area, which can be determined from

TABLE 2 The molecular parameters of HWp, HAp, and HALp.

Mass fraction(%)	HWp		HAp		HALp	
	Peak 1	Peak 2	Peak 1	Peak 2	Peak 1	Peak 2
	34.8	65.2	19.7	80.3	53.1	46.9
Mw (g/mol)	$(3.445 \pm 0.029) \times 10^6$	$(1.271 \pm 0.017) \times 10^5$	$(2.469 \pm 0.028) \times 10^5$	$(3.973 \pm 0.149) \times 10^4$	$(5.311 \pm 0.020) \times 10^6$	$(9.440 \pm 0185) \times 10^4$
Mn (g/mol)	$(2.353 \pm 0.017) \times 10^6$	$(1.173 \pm 0.017) \times 10^5$	$(1.551 \pm 0.024) \times 10^5$	$(3.547 \pm 0.147) \times 10^4$	$(1.459 \pm 0.005) \times 10^6$	$(7.615 \pm 0.143) \times 10^4$
Polydispersity (Mw/Mn)	1.464 ± 0.016	1.084 ± 0.021	1.592 ± 0.030	1.120 ± 0.063	3.641 ± 0.019	1.240 ± 0.034
Rz (nm)	138.900 ± 0.972	38.400 ± 1.382	25.600 ± 1.536	44.600 ± 3.390	49.900 ± 0.349	52.700 ± 1.634

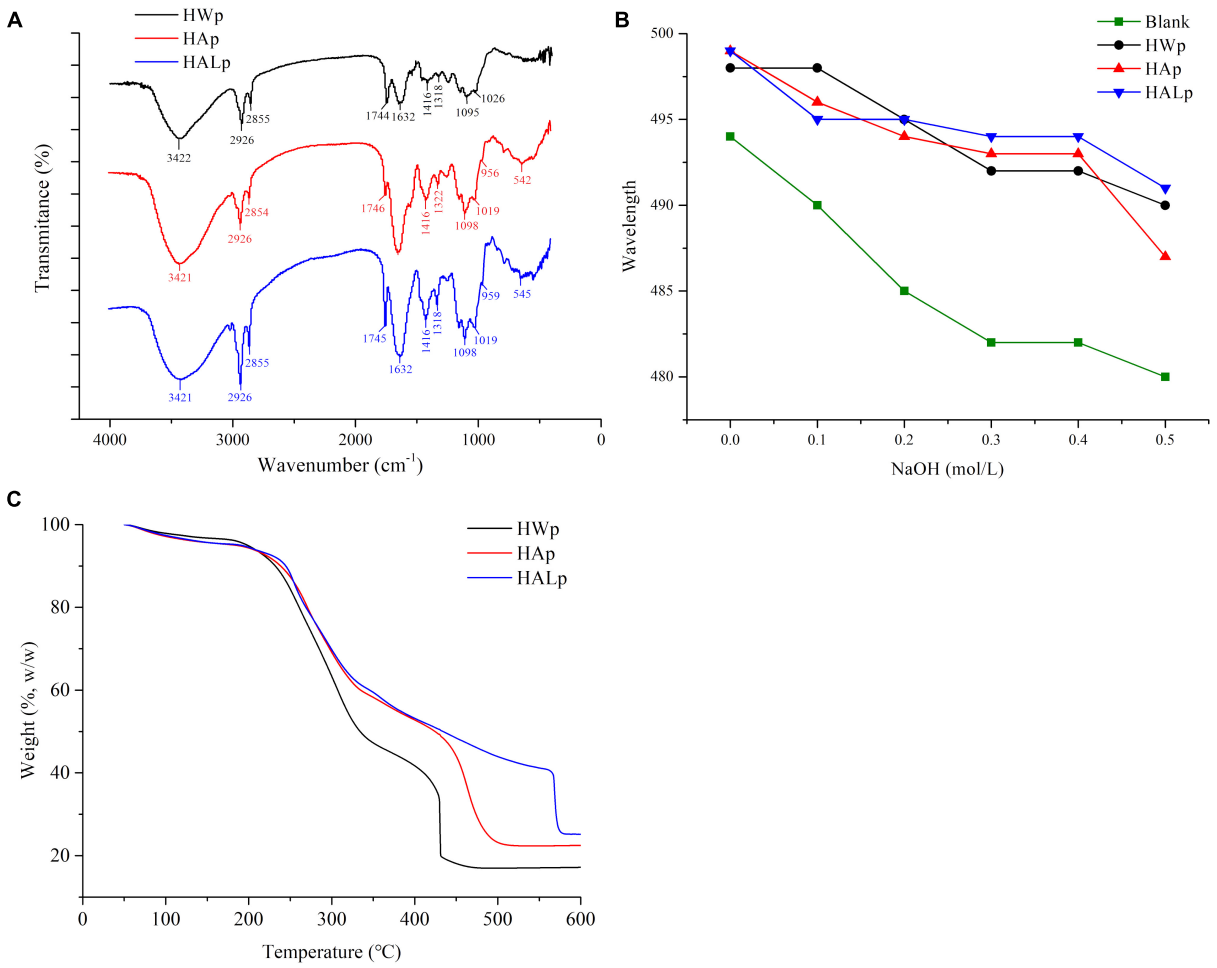

FIGURE 1
(A) FT-IR spectra of HWp, HAp, and HALp; **(B)** characterization of pectin helical structure at different concentrations; **(C)** thermodynamic properties of HWp, HAp, and HALp: TGA analysis.

the ratio of the area of the 1,740 cm^{-1} absorption band to the sum of the areas of the 1,740 and 1,633 cm^{-1} absorption bands (37). Figure 1A shows that HWp is a high methoxyl pectin, which is consistent with the results of the DM assay. The COO- absorption peaks at 1,746 and 1,626 cm^{-1} indicate that HALp has the lowest DM level. It may be that the de-esterification of alkali leads to the lower methoxy group of HALp, and the alkaline condition is the optimal condition for the production of low methoxyl pectin (30). The absorption peak of monosaccharides may exist below 1,100 cm^{-1}. The characteristic peaks of β-galactan generally appear around 1,080 cm^{-1}, while the characteristic peaks of arabinan mostly appear at 1,040 cm^{-1} (22). Furanose and pyranose rings may appear as peaks in the 920–950 cm^{-1} range. Above all, HALE can effectively reduce the level of DM.

According to Figure 1A and Formula (1), the degree of esterification of HWp is 31.03%, the degree of esterification of HAp is 2.96%, and the degree of esterification of HALp is 8.60%. Different extraction processes have a great influence on the degree of esterification, and the de-esterification effects of HAE and HALE are obvious.

Helical structure of pectin

Congo red is an acid dye that is soluble in water and ethanol. Congo red dyes can form complexes with polysaccharides with a three-strand helical chain conformation, and the ultraviolet maximum absorption wavelength of the complexes is red-shifted compared with Congo red solution. When the concentration of NaOH reaches a certain value, the maximum absorption wavelength will drop sharply. If the maximum absorption wavelength of the sample has a red shift, it proves that the sample has a helical structure. As shown in Figure 1B, compared with the Congo red solution, the UV maximum absorption wavelengths of HWp, HAp, and HALp all have a red shift, and they decrease as the concentration of NaOH increases. In summary, HWp, HAp, and HALp all have a triple helix structure.

Solution stability

Zeta potential refers to the potential difference between the surface of the dispersed droplets and the interior of the continuous phase in the emulsion, and is usually used to characterize the stability of the emulsion system. *L. ruthenicum* pectin is an anionic acidic polysaccharide that is negatively charged, and the measured potential of the emulsion is negative. The zeta potential of HWp is -46.07 ± 1.37, HAp is -35.08 ± 0.51, and HALp is -34.98 ± 0.95. The results show that the absolute value of the potential of HALp is the smallest, but there is no significant difference from HAp, and the absolute value of the zeta potential of HWp is large. This may be because HWE increases the degree of ionization of pectin, so that the surface of the solution droplets can absorb negatively charged molecules, the absolute value of the potential value increases, the mutual force is strong, and the solution is stable (38). Different extraction methods have significant effects on the zeta potential of *L. ruthenicum* pectin.

Thermal analysis

According to Figure 1C, the weight decrease trend of the three samples is similar. At the beginning, a slight weight loss was observed for the three pectins, and their weight remained largely unchanged before 250°C. At 200–250°C, the

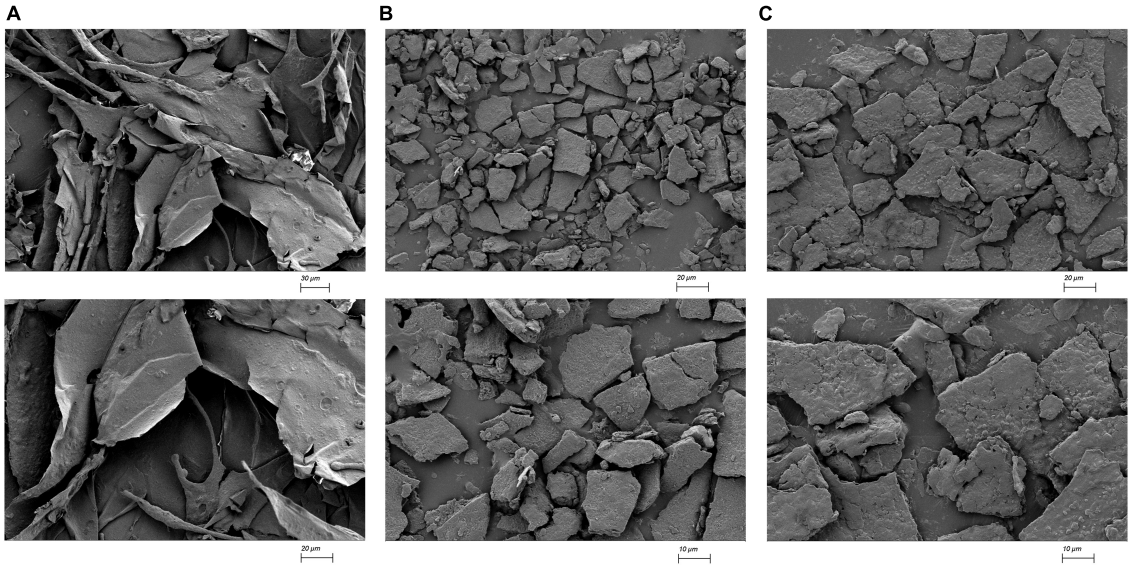

FIGURE 2
SEM imaging of HWp **(A)**, HAp **(B)**, and HALp **(C)**.

weight loss of the three pectins was mainly due to the loss of bound water in the pectin. Next, the weights of the three pectins dropped significantly during 250–350°C. The weight of HWp loss experienced slowed down in the range of 350–430°C and remain unchanged after 430°C. The weight of HAp loss experienced slowed down in the range of 350–500°C and remained unchanged after 500°C. The weight of HALp loss experienced slowed down in the range of 350–570°C and remained unchanged after 570°C. During the rapid weight loss phase, the weight loss onset for HWp, HAp, and HALp at 215.1, 232.6, and 233.4°C was caused by polysaccharide pyrolytic decompositions. At this time, the three kinds of pectins were thermally degraded under the action of temperature, the polysaccharide chain was decomposed, the acid group was decarboxylated, and the carbon–carbon double bond in the pyran ring was decomposed (39). Extensive pyrolysis of carbon occurs at 400–600°C. According to Figure 1C, the total mass loss of HWp is 82.8%, that of HAp is 77.5%, and that of HALp is 74.8%. Compared with HAE and HWE, the pectin samples prepared by HALE have better thermal stability, which can provide certain data support for choosing different pectin extraction method in the future.

Atomic force microscope and scanning electron microscope imaging of high-temperature water-extracted pectin, high-temperature acid-extracted pectin, and high-temperature alkali-extracted pectin

As shown in Figure 2, the results showed that the different material induced different physical changes. The microstructure of HWp is smooth and thin. The microstructure of HAp is relatively smooth and finely fragmented. The microstructure of HALp is a large block with irregular particles on the surface. The dense structure of HWEs causes them to cross-link with each other. This is also the reason for the high apparent viscosity of HWE. For HAE and HALE, the sheet-like structure is in a

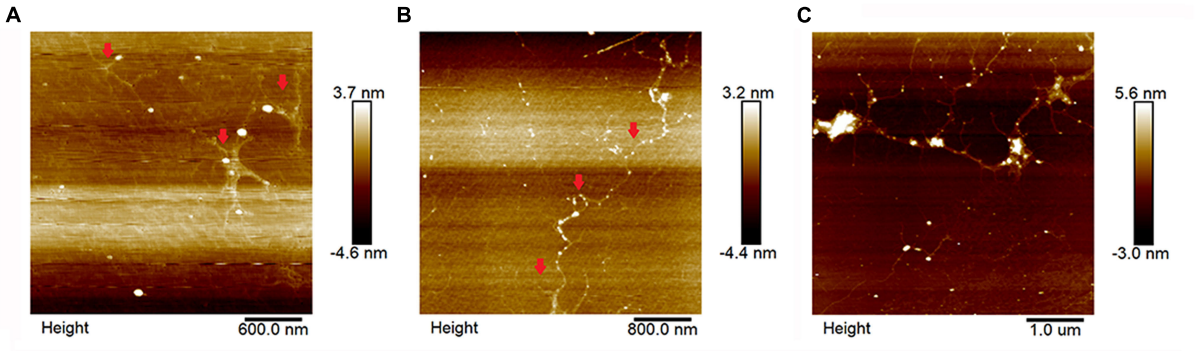

FIGURE 3
AFM imaging of HWp **(A)**, HAp **(B)**, and HALp **(C)**.

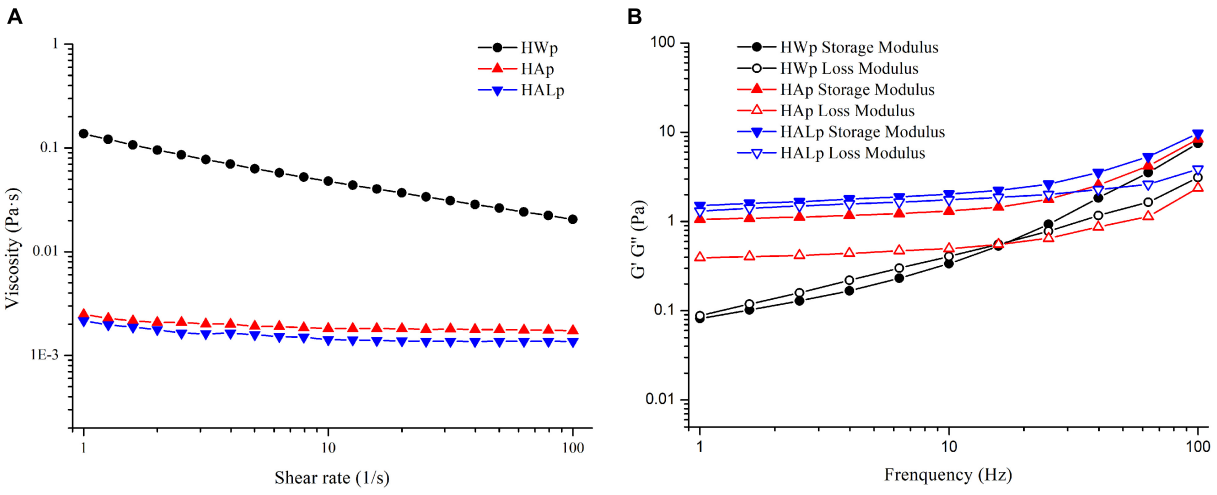

FIGURE 4
Rheological characterization of HWp, HAp, and HALp: **(A)** flow behavior and **(B)** frequency sweep of modulus G′ and G″.

TABLE 3 Parameters of flow curves obtained by fitting to power law model.

Sample	Concentration (w/v %)	κ (Pa·s^n)	n	R^2
HWp	15%	0.126	0.595	0.996
HAp	15%	0.002	0.913	0.830
HALp	15%	0.002	0.938	0.823

dispersed and stretched state, resulting in a low overall viscosity of the solution.

AFM can be used to visually observe the surface morphology of pectin samples. As shown in Figure 3, HWp and HALp are mainly a branched structure, while HAp is a chain structure. HWp, HAp, and HALp displayed heights of 2.3, 2.0, and 2.8 nm, respectively, on the mica flakes, which indicated that the polysaccharide chains of pectin were also slightly aggregated at low concentrations and would not be completely decomposed. Compared with the three pectins in Figure 3, HWp and HALp have branched structure, and HAp mainly has a linear structure, suggesting that HWE and HALE may lead to a high RG-I pectin region content.

Rheological characterization

The change in apparent viscosity with shear rate is illustrated in Figure 4A. The apparent viscosity of the three pectin solutions decreased with increasing shear stress (1–100 s^{-1}), so the samples all behaved as non-Newtonian pseudoplastic fluids. Other sources of pectin, such as those from apple peels (40) and lime peel (41), exhibited similar properties. Table 3 shows the specific parameters of the power-law model constructed according to Equation (2), with larger κ values reflecting the increase in flow resistance and viscosity. By eye observation, the viscosity of the three pectin solutions was the largest in HWp and the smallest in HALp. The molar mass parameters, substituent distribution, and branching together determine the rheological properties of pectin solutions (42). In this study, the branched structure of HWp may have contributed to the high viscosity of the solution.

Storage modulus G′ refers to the ability of a viscoelastic material to store energy in a cycle under the action of alternating stress, usually referring to elasticity; energy dissipation modulus G″ refers to the ability to consume energy in a changing cycle, usually referring to viscosity. The dynamic viscoelastic properties of HWp, HAp, and HALp are shown in Figure 4B. The degree of elastic deformation of HAp is higher than that of HWp and HALp. Both HAp and HALp at 15 w/v% appeared as thick liquids and could be defined as weak gels as G′ > G″ (43). This result shows that the molecular chain entanglement of pectin at this time belongs to the gel system, the elasticity is strong, and the pectin is mainly elastic. The intersection of the storage modulus and loss modulus of HWp indicates that HWE can enhance the gelation of pectin. It may be due to

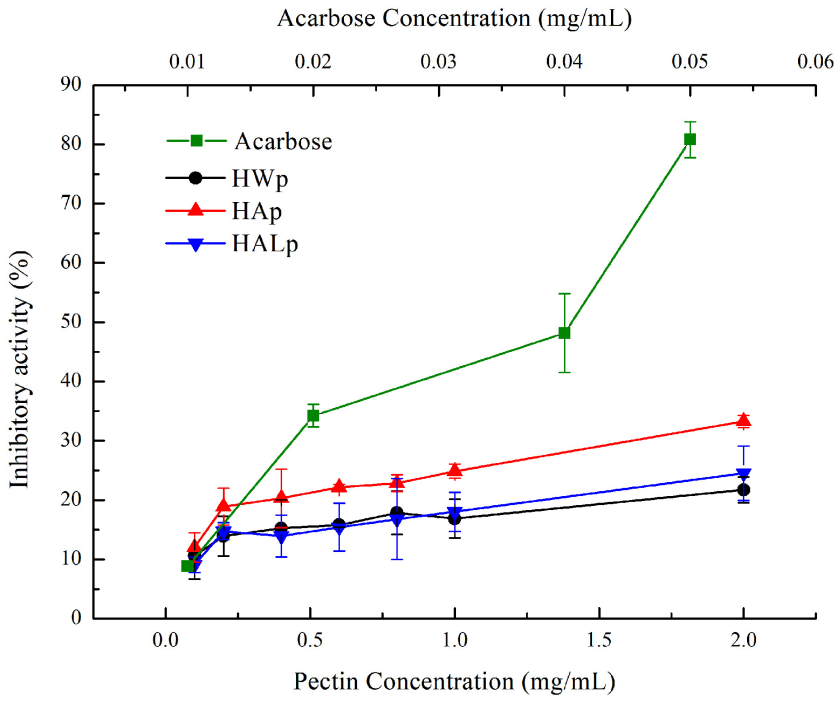

FIGURE 5
Different concentrations of HWp, HAp, HALp, and acarbose glucosidase inhibition efficiency.

the exposure of many connecting regions during the process of HWE extraction of pectin, the interaction of pectin chains is greater, and the cross-linking system formed is stronger, showing typically dynamic rheological properties of gel. It may be that the high RG-I domains lead to the creation of branched structures, resulting in the rheological properties of HWp. This has also been reported in other pectins rich in RG-I (44). The branched structure of the pectin extracted with HALE may be destroyed by the alkali solution, resulting in a less viscous solution, which is consistent with the molecular weight data.

Inhibit enzyme activity

As shown in Figure 5, different concentrations of HWp, HAp, and HALp reacted with α-glucosidase. Among them, the inhibition of α-glucosidase by HWp, HAp, and HALp was in a significant dose-dependent relationship, and the inhibition efficiency increased as the concentration increased. When the concentration of HWp, HAp, and HALp was 2 mg/ml, the inhibitory efficiency of α-glucosidase reached 21.73 ± 2.19%, 33.28 ± 1.03%, and 24.54 ± 4.60%, respectively. Compared with acarbose, HWp, HAp, and HALp have inhibitory effects on α-glucosidase. When the concentration of acarbose is 0.05 mg/ml, the inhibitory efficiency of α-glucosidase is 80.80%. Therefore, HWp, HAp, and HALp have a certain inhibitory effect on α-glucosidase activity, but the inhibitory intensity is much smaller than the control acarbose, and the order of the inhibitory intensity is HWp < HALp < HAp < acarbose.

Conclusion

Three different extraction methods were used to extract HWp, HAp, and HALp from *L. ruthenicum*. The yields of HAp (6.77%) and HALp (6.19%) are significantly higher than HWp (3.83%). Analysis of monosaccharide composition shows that the Ara content of HALp and HWp is significantly higher than that of HAp, and the Gal, Glu, xyl, and GalA contents of HAp are significantly higher than that of HWp and HALp. The RG-I contents of HALp (73.00%) and HWp (64.23%) are significantly higher than that of HAp (39.79%). The results show that HWE and HALE can extract RG-I from *L. ruthenicum* better. The physicochemical properties, structure, and functional properties of three different pectins were studied. FT-IR results show that different extraction processes have a great influence on the degree of esterification, and the de-esterification effects of HAE and HALE are obvious. AFM results show that HWp and HALp have a branched structure, and HAp has a chain structure. The crystallinities of the three pectins are similar. Zeta potential results show that HWp solution is more stable. The thermal analysis results show that the thermal stability is HALp > HAp > HWp. The rheological properties of the extracted pectin were studied. The dynamic modulus of HWp is more dependent on frequency, indicating that the pectin obtained by HAE is more liquid-like than HAp and HALp. HWp has the highest viscosity. The inhibitory activity results showed that HWp, HAp, and HALp have a certain inhibitory effect on α-glucosidase activity. This study provides new insights into the impact of different extraction methods on pectin and aims to provide a theoretical basis for the pharmaceutical and food industries to choose more suitable pectin extraction methods.

Data availability statement

The raw data supporting the conclusions of this article will be made available by the authors, without undue reservation.

Author contributions

ZW: methodology, software, and writing—original draft. DQ: methodology and software. HL: conceptualization and funding acquisition. DG: methodology. HC: funding acquisition. JS and MH: writing—review and editing. XY and BS: supervision and funding acquisition. All authors contributed to the article and approved the submitted version.

Funding

This study was supported by the Fundamental Research Funds for the Central Universities (2020FZZX003-02-05), the Key Research and Development program of Zhejiang Province (2021C02001), and the National Natural Science Foundation of China (No. 32172340).

Conflict of interest

The authors declare that the research was conducted in the absence of any commercial or financial relationships that could be construed as a potential conflict of interest.

Publisher's note

All claims expressed in this article are solely those of the authors and do not necessarily represent those of their affiliated organizations, or those of the publisher, the editors and the reviewers. Any product that may be evaluated in this article, or claim that may be made by its manufacturer, is not guaranteed or endorsed by the publisher.

References

1. Dranca F, Oroian M. Extraction, purification and characterization of pectin from alternative sources with potential technological applications. *Food Res Int.* (2018) 113:327–50. doi: 10.1016/j.foodres.2018.06.065

2. Liew SQ, Teoh WH, Yusoff R, Ngoh GC. Comparisons of process intensifying methods in the extraction of pectin from pomelo peel. *Chem Eng Process Process Intensif.* (2019) 143:107586. doi: 10.1016/j.cep.2019.107586

3. Ji X, Hou C, Shi M, Yan Y, Liu Y. An insight into the research concerning panax ginseng C. A. Meyer polysaccharides: A review. *Food Rev Int.* (2022) 38:1149–65. doi: 10.1080/87559129.2020.1771363

4. Hu W, Chen S, Wu D, Zhu K, Ye X. Physicochemical and macromolecule properties of Rg-I enriched pectin from citrus wastes by manosonication extraction. *Int J Biol Macromol.* (2021) 176:332–41. doi: 10.1016/j.ijbiomac.2021.01.216

5. Fan Y, Sun L, Yang S, He C, Tai G, Zhou Y. The roles and mechanisms of homogalacturonan and rhamnogalacturonan I pectins on the inhibition of cell migration. *Int J Biol Macromol.* (2018) 106:207–17. doi: 10.1016/j.ijbiomac.2017.08.004

6. Maxwell EG, Colquhoun IJ, Chau HK, Hotchkiss AT, Waldron KW, Morris VJ, et al. Rhamnogalacturonan I containing homogalacturonan inhibits colon cancer cell proliferation by decreasing Icam1 expression. *Carbohydr Polym.* (2015) 132:546–53. doi: 10.1016/j.carbpol.2015.06.082

7. Zhang S, He F, Chen X, Ding K. Isolation and structural characterization of a pectin from *Lycium ruthenicum* Murr and its anti-pancreatic ductal adenocarcinoma cell activity. *Carbohydr Polym.* (2019) 223:115104. doi: 10.1016/j.carbpol.2019.115104

8. Wu T, Lv H, Wang F, Wang Y. Characterization of polyphenols from *Lycium ruthenicum* fruit by Uplc-Q-Tof/Mse and their antioxidant activity in Caco-2 cells. *J Agric Food Chem.* (2016) 64:2280–8. doi: 10.1021/acs.jafc.6b00035

9. Wang H, Li J, Tao W, Zhang X, Gao X, Yong J, et al. *Lycium ruthenicum* studies: Molecular biology, phytochemistry and pharmacology. *Food Chem.* (2018) 240:759–66. doi: 10.1016/j.foodchem.2017.08.026

10. Zhang Q, Chen W, Zhao J, Xi W. Functional constituents and antioxidant activities of eight Chinese native Goji genotypes. *Food Chem.* (2016) 200:230–6. doi: 10.1016/j.foodchem.2016.01.046

11. Zheng J, Ding C, Wang L, Li G, Shi J, Li H, et al. Anthocyanins composition and antioxidant activity of wild *Lycium ruthenicum* Murr. From Qinghai-Tibet Plateau. *Food Chem.* (2011) 126:859–65. doi: 10.1016/j.foodchem.2010.11.052

12. Zhao J, Xu F, Ji T, Li J. A New spermidine from the fruits of *Lycium ruthenicum*. *Chem Nat Compd.* (2014) 50:880–3. doi: 10.1007/s10600-014-1105-7

13. Jin H, Zhao J, Zhou W, Shen A, Yang F, Liu Y, et al. Preparative separation of a challenging anthocyanin from *Lycium ruthenicum* Murr. By two-dimensional reversed-phase liquid chromatography/hydrophilic interaction chromatography. *RSC Adv.* (2015) 5:62134–41. doi: 10.1039/C5RA08713A

14. Altintas A, Kosar M, Kirimer N, Baser KHC, Demirci B. Composition of the essential oils of *Lycium barbarum* and L. Ruthenicum Fruits. *Chem Nat Compd.* (2006) 42:24–5. doi: 10.1007/s10600-006-0028-3

15. Su Y, Li L. Structural characterization and antioxidant activity of polysaccharide from four auriculariales. *Carbohydr Polym.* (2020) 229:115407. doi: 10.1016/j.carbpol.2019.115407

16. Liu J, Zhao Y, Wu Q, John A, Jiang Y, Yang J, et al. Structure characterisation of polysaccharides in vegetable "Okra" and evaluation of hypoglycemic activity. *Food Chem.* (2018) 242:211–6. doi: 10.1016/j.foodchem.2017.09.051

17. Jie RKL. Treating bimaxillary protrusion and crowding with the invisalign G6 first premolar extraction solution and invisalign aligners. *APOS Trends Orthod.* (2016) 12:219–24. doi: 10.4103/apos.apos_67_18

18. Sucheta, Misra NN, Yadav SK. Extraction of pectin from black carrot pomace using intermittent microwave, ultrasound and conventional heating: Kinetics, characterization and process economics. *Food Hydrocoll.* (2020) 102:105592. doi: 10.1016/j.foodhyd.2019.105592

19. Peng Y, Yan Y, Wan P, Dong W, Huang K, Ran L, et al. Effects of long-term intake of anthocyanins from *Lycium ruthenicum* Murray on the organism health and gut microbiota in vivo. *Food Res Int.* (2020) 130:108952. doi: 10.1016/j.foodres.2019.108952

20. Wu Z, He F, Qin D, Li H, Sun J, Sun X, et al. Determination of phenolic compounds in alcoholic fermentation materials and spent grains by ultrasound-assisted alkali alcohol extraction coupled with Hplc. *Anal Methods.* (2019) 11:5366–75. doi: 10.1039/c9ay01739a

21. Li X, Xie Q, Huang S, Shao P, You L, Pedisić S. Digestion & fermentation characteristics of sulfated polysaccharides from *Gracilaria* chouae using two extraction methods in vitro and in vivo. *Food Res Int.* (2021) 145:110406. doi: 10.1016/j.foodres.2021.110406

22. Wei C, Zhang Y, Zhang H, Li J, Tao W, Linhardt RJ, et al. Physicochemical properties and conformations of water-soluble peach gums via different preparation methods. *Food Hydrocoll.* (2019) 95:571–9. doi: 10.1016/j.foodhyd.2018.03.049

23. Monsoor MA, Kalapathy U, Proctor A. Improved method for determination of pectin degree of esterification by diffuse reflectance fourier transform infrared spectroscopy. *J Agric Food Chem.* (2001) 49:2756–60. doi: 10.1021/jf0009448

24. Lordan S, Smyth TJ, Soler-Vila A, Stanton C, Ross RP. The A-amylase and α-glucosidase inhibitory effects of Irish Seaweed extracts. *Food Chem.* (2013) 141:2170–6. doi: 10.1016/j.foodchem.2013.04.123

25. Buathongjan C, Israkarn K, Sangwan W, Outrequin T, Gamonpilas C, Methacanon P. Studies on chemical composition, rheological and antioxidant properties of pectin isolated from riang (*Parkia timoriana* (Dc.) Merr.) pod. *Int J Biol Macromol.* (2020) 164:4575–82. doi: 10.1016/j.ijbiomac.2020.09.079

26. Singh B, Singh JP, Kaur A, Singh N. Phenolic composition, antioxidant potential and health benefits of citrus peel. *Food Res Int.* (2020) 132:109114. doi: 10.1016/j.foodres.2020.109114

27. Islam T, Yu X, Badwal TS, Xu B. Comparative studies on phenolic profiles, antioxidant capacities and carotenoid contents of red Goji Berry (*Lycium barbarum*) and black Goji Berry (*Lycium ruthenicum*). *Chem Cent J.* (2017) 11:59. doi: 10.1186/s13065-017-0287-z

28. Alba K, Kontogiorgos V. Pectin at the oil-water interface: Relationship of molecular composition and structure to functionality. *Food Hydrocoll.* (2017) 68:211–8. doi: 10.1016/j.foodhyd.2016.07.026

29. Ji X, Cheng Y, Tian J, Zhang S, Jing Y, Shi M. Structural characterization of polysaccharide from Jujube (*Ziziphus jujuba* Mill.) fruit. *Chem Biol Technol Agric.* (2021) 8:54. doi: 10.1186/s40538-021-00255-2

30. Fracasso AF, Perussello CA, Carpiné D, Petkowicz CLO, Haminiuk CWI. Chemical modification of citrus pectin: Structural, physical and rheologial implications. *Int J Biol Macromol.* (2018) 109:784–92. doi: 10.1016/j.ijbiomac.2017.11.060

31. Ma X, Wang D, Chen W, Ismail BB, Wang W, Lv R, et al. Effects of ultrasound pretreatment on the enzymolysis of pectin: Kinetic study, structural characteristics and anti-cancer activity of the hydrolysates. *Food Hydrocoll.* (2018) 79:90–9. doi: 10.1016/j.foodhyd.2017.12.008

32. Zhang L, Zhang X, Liu D, Ding T, Ye X. Effect of degradation methods on the structural properties of citrus pectin. *LWT Food Sci Technol.* (2015) 61:630–7. doi: 10.1016/j.lwt.2014.11.002

33. Round AN, Rigby NM, MacDougall AJ, Morris VJA. New view of pectin structure revealed by acid hydrolysis and atomic force microscopy. *Carbohydr Res.* (2010) 345:487–97. doi: 10.1016/j.carres.2009.12.019

34. Thibault J-F, Renard CMGC, Axelos MAV, Roger P, Crépeau M-J. Studies of the length of homogalacturonic regions in pectins by acid hydrolysis. *Carbohydr Res.* (1993) 238:271–86. doi: 10.1016/0008-6215(93)87019-O

35. Hosseini SS, Khodaiyan F, Kazemi M, Najari Z. Optimization and characterization of pectin extracted from sour orange peel by ultrasound assisted method. *Int J Biol Macromol.* (2019) 125:621–9. doi: 10.1016/j.ijbiomac.2018.12.096

36. Ji X, Guo J, Ding D, Gao J, Hao L, Guo X, et al. Structural characterization and antioxidant activity of a novel high-molecular-weight polysaccharide from *Ziziphus jujuba* Cv. Muzao. *J Food Meas Charact.* (2022) 16:2191–200. doi: 10.1007/s11694-022-01288-3

37. Vriesmann LC, de Oliveira Petkowicz CL. Polysaccharides from the Pulp of Cupuassu (*Theobroma grandiflorum*): Structural characterization of a pectic fraction. *Carbohydr Polym.* (2009) 77:72–9. doi: 10.1016/j.carbpol.2008.12.007

38. Joshi M, Aldred P, Panozzo JF, Kasapis S, Adhikari B. Rheological and microstructural characteristics of lentil starch–lentil protein composite pastes and gels. *Food Hydrocoll.* (2014) 35:226–37. doi: 10.1016/j.foodhyd.2013.05.016

39. Hu W, Ye X, Chantapakul T, Chen S, Zheng J. Manosonication extraction of Rg-I pectic polysaccharides from citrus waste: Optimization and kinetics analysis. *Carbohydr Polym.* (2020) 235:115982. doi: 10.1016/j.carbpol.2020.115982

40. Cho E-H, Jung H-T, Lee B-H, Kim H-S, Rhee J-K, Yoo S-H. Green process development for apple-peel pectin production by organic acid extraction. *Carbohydr Polym.* (2019) 204:97–103. doi: 10.1016/j.carbpol.2018.09.086

41. Rodsamran P, Sothornvit R. Microwave heating extraction of pectin from lime peel: Characterization and properties compared with the conventional heating method. *Food Chem.* (2019) 278:364–72. doi: 10.1016/j.foodchem.2018.11.067

42. Cui J, Ren W, Zhao C, Gao W, Tian G, Bao Y, et al. The structure–property relationships of acid- and alkali-extracted grapefruit peel pectins. *Carbohydr Polym.* (2020) 229:115524. doi: 10.1016/j.carbpol.2019.115524

43. Deng Z, Pan Y, Chen W, Chen W, Yun Y, Zhong Q, et al. Effects of cultivar and growth region on the structural, emulsifying and rheological characteristic of mango peel pectin. *Food Hydrocoll.* (2020) 103:105707. doi: 10.1016/j.foodhyd.2020.105707

44. Sousa AG, Nielsen HL, Armagan I, Larsen J, Sørensen SO. The impact of rhamnogalacturonan-I side chain monosaccharides on the rheological properties of citrus pectin. *Food Hydrocoll.* (2015) 47:130–9. doi: 10.1016/j.foodhyd.2015.01.013

frontiers | Frontiers in Nutrition

TYPE Original Research
PUBLISHED 11 August 2022
DOI 10.3389/fnut.2022.982695

Check for updates

OPEN ACCESS

EDITED BY
Xiaolong Ji,
Zhengzhou University of Light Industry, China

REVIEWED BY
Du Meihong,
Beijing Academy of Science and Technology (Beijing Center for Physical and Chemical Analysis), China
Lihui Zhang,
Jiangsu University, China
Yin Wang,
Northwest University, China

*CORRESPONDENCE
Zihan Song
songzihan@caas.cn

SPECIALTY SECTION
This article was submitted to Food Chemistry, a section of the journal Frontiers in Nutrition

RECEIVED 30 June 2022
ACCEPTED 26 July 2022
PUBLISHED 11 August 2022

CITATION
Ti Y, Zhang Y, Ban Y, Wang X, Hou Y and Song Z (2022) Polysaccharide from *Hemerocallis citrina* Borani by subcritical water with different temperatures and investigation of its physicochemical properties and antioxidant activity. *Front. Nutr.* 9:982695. doi: 10.3389/fnut.2022.982695

COPYRIGHT
© 2022 Ti, Zhang, Ban, Wang, Hou and Song. This is an open-access article distributed under the terms of the Creative Commons Attribution License (CC BY). The use, distribution or reproduction in other forums is permitted, provided the original author(s) and the copyright owner(s) are credited and that the original publication in this journal is cited, in accordance with accepted academic practice. No use, distribution or reproduction is permitted which does not comply with these terms.

Polysaccharide from *Hemerocallis citrina* Borani by subcritical water with different temperatures and investigation of its physicochemical properties and antioxidant activity

Yongrui Ti, Yanli Zhang, Yüqian Ban, Xiaoxiao Wang, Yüqing Hou and Zihan Song*

Institute of Vegetables and Flowers, Chinese Academy of Agricultural Sciences, Beijing, China

Hemerocallis citrina Borani as a low-cost vegetable, has various health benefits. However, the industry of *H. citrina* Borani is in the state of primary processing, with poor economic benefits. This study aimed to investigate the physicochemical properties, and the antioxidant activity of *H. citrina* Borani polysaccharide (HCBP) using subcritical water extraction (SWE) at different temperatures, to expand the value of *H. citrina* Borani. HCBP mainly composed of nine monosaccharides (glucose, galactose, rhamnose, fucose, mannose, arabinose, xylose, galacturonic acid, and glucuronic acid), among which the content of neutral sugar was higher and uronic acid was lower. HCBP contained glycosidic bond of β-configurations and trace quantities protein. The molecular weight of HCBP decreased with increasing temperature. Shear thinning occurred in HCBP with the increase of shear rate (0.01–1 s^{-1}), and the apparent viscosity of HCBP decreased at higher temperature (150–160°C) with the increase continuously of shear rate (1–10 s^{-1}), but almost remained constant at lower temperature (130–140°C). Scanning electron microscope showed that HCBP had rough surface, loose structure, obvious particle gap, and irregular shape. In addition, HCBP extracted at 160°C had strong FRAP activity, and HCBP extracted at 130 and 140°C had better ABTS radical scavenging activity. This study suggests that HCBP extracted by SWE could provide a cheap raw material as food thickening agent and natural antioxidants.

KEYWORDS

***Hemerocallis citrina* Borani, subcritical water extraction, polysaccharide, physicochemical properties, antioxidant activity**

Introduction

Hemerocallis citrina Borani is perennial herbs in the Liliaceae family, commonly known as daylily, and its flower buds are one of the most commonly consumed vegetables in Asian countries including China, Japan, and Korea (1). *Hemerocallis citrina* Borani is rich in nutrition, which is a typical health vegetable with rich in protein, vitamins, and minerals. *H. citrina* Borani has been demonstrated multiple functions including antioxidant (2), antidepressant (3, 4), lactation improving (5), and sleep promoting (6), as documented in the medicinal book "Compendium of Materia Medica" (7). The industry of *H. citrina* Borani is so far in the state of primary processing, with poor economic benefits and low value-added. At present, the studies on the deep processing of *H. citrina* Borani mainly focusing on the functional components including flavonoids and alkaloids (8–10). However, few studies are reported on *H. citrina* Borani polysaccharide (HCBP). Moreover, the preparation process is the crucial point for industrial utilization of HCBP.

Many methods have been applied to extract polysaccharide, such as hot-water extraction (11), acid/base extraction (12), microwaving-assisted extraction (13), and ultrasound-assisted extraction (14). These traditional techniques have the shortcomings of higher extraction time, high-energy consumption, low extracting efficiency and yield, as well as limited polysaccharide purity. Water that remains liquid state at high temperature (100–374°C) and under high pressure is called subcritical water (SW), also known as superheated water and pressurized hot water. SW has lower dielectric constant, lower viscosity, and higher diffusivity, which makes SW an effective solvent for both polar and non-polar compounds with acid-base catalytic characteristics (15). Subcritical water extraction (SWE) is a promising green extraction technology that uses SW as the only extraction solvent. Obviously, during the polysaccharide extraction, no other chemical reagents are added except water, avoiding the environmental pollution problem (16). Remarkably, SWE has the advantages of short extraction time, high extraction efficiency, strong specificity, simple operation, good cost effectiveness, and environmental friendliness, which has been widely used in the extraction of natural products (17).

At present, the research on the extraction of polysaccharide by SWE is mainly in the aspects of structure analysis and biological activity evaluation. However, there are few studies on the effects of SWE temperature on polysaccharide. In addition, the extraction temperature is closely related to the structure properties of polysaccharide, which significantly affect the functional properties of polysaccharide. For example, SWE temperature significantly affects the physicochemical properties and biological activity of polysaccharide, such as monosaccharide composition (18), molecular weight (19), and antioxidant activity (20). Therefore, the extraction temperature of SW possessed crucial effects on the properties of polysaccharide, the appropriate extraction temperature should be selected according to the characteristics of polysaccharide in actual production.

In this study, four HCBP samples were prepared by subcritical water with different extraction temperatures (130, 140, 150, and 160°C). The composition, structure, and antioxidant activity of the four HCBP samples were firstly systematically analyzed. In addition, the study also determined the physicochemical properties of the four HCBP samples by gel filtration chromatography, high performance liquid chromatography, ultraviolet–visible spectroscopy, infrared spectroscopy, scanning electron microscope, and hybrid rheometer. The present study could provide theoretical and data support for the further utilization of HCBP in the fields including medicine, food and cosmetics, as well as expand the value of *H. citrina* Borani.

Materials and methods

Sample preparation and chemicals

Hemerocallis citrina Borani was obtained from Qingyang, Gansu, China. Standards of glucose, mannose, fucose, rhamnose, xylose, galactose, arabinose, glucuronic acid, ribose, and galacturonic acid were purchased from Shanghai Yuanye Biotechnology (Shanghai, China). Absolute ethanol was purchased from Fuyu Fine Chemical (Tianjin, China). Trifluoroacetic acid, methanol, sodium hydroxide, hydrochloric acid, carbazole, 1-phenyl-3-methyl-5-pyrazolone, 3,5-dinitrosalicylic acid, sulfuric acid, Coomash bright blue, chloroform, potassium bromide, sodium azide, sodium acetate, anthranone, and other reagents were purchased from Solarbio Biotechnology (Beijing, China). ABTS and FRAP assay kits were purchased from Suzhou Keming Biotechnology (Suzhou, China). Distilled water was used in these experiments.

Subcritical-water extraction

Laboratory-scale SWE had performed using high temperature and pressure reactor. Briefly, *Hemerocallis citrina* Borani powder sample (5 g) and a certain proportion of distilled water (1:10, 1:15, 1:20, 1:25) were placed in a 1 L subcritical reactor at certain temperature (130, 140, 150, and 160°C) and reaction time (5, 10, 15, and 20 min). The *H. citrina* Borani aqueous solution in the reaction kettle was collected and centrifuged at 6,000 rpm for 10 min. Anhydrous ethanol was added to the solution and subsequently precipitated at 4°C for 12 h. The *H. citrina* Borani ethanol solution was centrifuged in a centrifuge at 6,000 rpm for 10 min, the precipitation was collected, and the polysaccharide was cleaned with anhydrous ethanol for three times to obtain the *H. citrina* polysaccharide.

Chemical composition analysis

The neutral sugar content was determined with anthrone-sulfuric acid method with minor modifications, with using glucose as standard (21). Uronic acid was estimated in a modified carbazole method using D- galacturonic acid as standard (22). Reducing sugar analysis was conducted using the 3,5-dinitrosalicylic acid (DNS) method (16). Protein content was measured using the Bradford method (23). Ash content was determined by high temperature combustion in muffle furnace.

Gel permeation chromatography

The molecular weight of HCBP was determined by gel permeation chromatography (24), HCBP was dissolved by sodium azide and sodium acetate and loaded into the chromatography system (40 μL), the column was maintained at 30°C and the flow rate of 1 mL/min. The molecular weight of HCBP was calculated by using calibration curves obtained from standard dextran of different molecular weights.

Monosaccharide composition

The monosaccharide composition of polysaccharide was analyzed by high performance liquid chromatography (HPLC) according to previous research with slight modified (25). Polysaccharide samples (10.0 mg) dissolved in 3 M trifluoroacetic acid (4.0 mL) in a 10 mL ampoule. The ampoule was sealed with an alcohol blowtorch and hydrolyzed for 2 h in an electric oven at 121°C. Then sodium hydroxide solution, PMP methanol solution and lactose internal standard solution were added into polysaccharides hydrolysate and monosaccharides standard for PMP derivatization, and the remaining aqueous phase was filtered by 0.22-μm membrane and analyzed by HPLC. Chromatographic conditions included Agilent ZORBAX Eclipse Plus (C18, 2.1 × 100 mm,1.8 μm, Agilent, USA) capillary column, diode array detector (250 nm detection wavelength), sodium acetate acetonitrile solution (mobile phase A) and acetonitrile (mobile phase B), 0.6 mL/min flow rate and column at 35°C. The monosaccharide standards including fucose, mannose, rhamnose, glucose, galactose, xylose, arabinose, ribose, glucuronic acid, and galacturonic acid were PMP-labeled and determined by HPLC in the same way.

Spectrum analysis

Ultraviolet–visible (UV) spectrometric analysis

The UV spectrum of HCBP samples were determined with ultraviolet–visible spectroscopy (Shimadzu UV-2600, Japan). Briefly, HCBP samples were prepared with distilled water at a concentration of 0.5 mg/ mL, and UV spectrum from 200 to 900 nm were recorded (26).

Fourier transform infrared (FT-IR) spectrometric analysis

Fourier transform infrared spectrophotometer (Thermo Nicolet NEXUS870, Massachusetts, USA) was used to determine the infrared spectrum characteristics of HCBP different temperature samples at a wavelength range of 4,000–400 cm^{-1} (27). The specific use of KBr Tablet pressing method, and then performed for infrared spectrometric determination.

Scanning electron microscope (SEM) analysis

The HCBP samples were fixed on the carrier platform and sprayed with gold powder. The Morphology of HCBP extracted at different extraction temperature was observed by SEM (Hitachi S-4800, Tokyo, Japan) under an acceleration voltage of 10 kV with different magnifications (5-, 10-, 50-, and 100-μm) (28).

Rheological analysis

Rheological properties of HCBP samples (2 g/100 mL) were evaluated using a Hybrid Rheometer (MCR302, Anton Paar, Austria) equipped with a parallel plate geometry (29). The diameters, gap, angular frequency, strain, and temperature of the parallel plate were 40 mm, 1 mm, 10 rad/s, 1%, and 25°C, respectively. The apparent viscosity curves were measured under an increasing shear rate region from 1 to 100 s^{-1}.

Antioxidant activity

ABTS radical scavenging activity

The antioxidant activity of HCBP was estimated by the scavenging activities of ABTS according to the pervious method with slight modifications (30). All HCBP samples with different concentrations (0.5–6.0 mg/mL) were mixed with ABTS reaction solution, and the absorbance was measured at 734 nm after 6 min reaction at room temperature under dark conditions. The ABTS radical scavenging activities (%) was calculated using the following equation:

$$\text{Scavenging activity} = [1 - \frac{(A - A_i)}{A_0}] \times 100\%$$

where A is the absorbance of the sample, A_i is the absorbance of control group, A_0 is the absorbance of blank group.

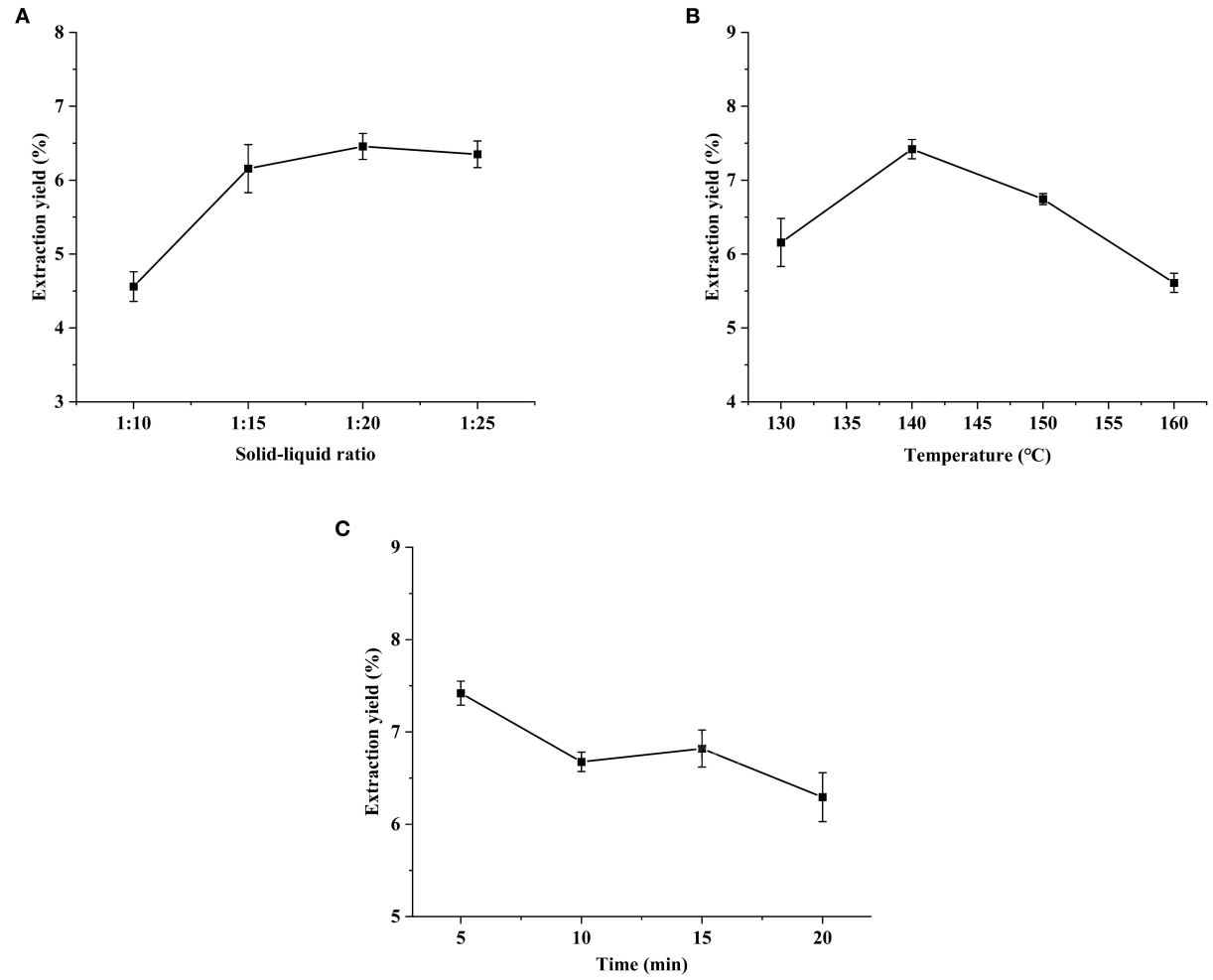

FIGURE 1
Effects of solid-liquid ratio **(A)**, extraction temperature **(B)** and extraction time **(C)** on extraction yield of HCBP.

Ferric reducing assay power (FRAP)

Ferric reducing antioxidant power was determined as described by previous research with minor modifications (31). This method is based on antioxidants reduce a ferric complex (Fe^{3+}-TPTZ) to the bule ferrous form (Fe^{2+}-TPTZ) under acidic conditions. All HCBP samples with different temperature and concentrations were prepared and analyzed. The FRAP of HCBP samples was calculated by calibration curves, and the calibration equation was using Trolox as standard $y = 0.0032x-0.0122$ ($R^2 = 0.9996$), where y was the absorbance, x was the concentration of Trolox. Analyses were performed in triplicate, and the results of FRAP in HCBP were expressed in Trolox /mL.

Statistical analysis

All data were presented as mean ± standard, and statistical significance ($p < 0.05$) was calculated by one-way analysis of variance (ANOVA) using SPSS22.0. Origin (version 2022) was used to plot the pictures.

Results and discussion

Yield of HCBP

In the preparation of HCBP, yield is an important parameter to evaluate the extraction efficiency. In the present study, HCBP yield ranged from 4.56 to 7.42%, which indicated the conditions, including solid-liquid ratio, SWE extraction temperature and extraction time, had significant influence on the HCBP yield.

The optimal solid-liquid ratio in the process of the preparation of HCBP was investigated. The yield of HCBP reached the optimum when the solid-liquid ratio was 1:15, the yield did not increase significantly with the increase of the solid-liquid ratio (Figure 1A). Therefore, 1:15 was selected for subsequent experiments.

The temperature was studied from 130 to 160°C. In the Figure 1B, the yield of HCBP increased and then decreased with increasing extraction temperature, and the maximum yield was achieved at 140°C. We speculated that the extraction ability of subcritical water on HCBP was relatively weak at lower extraction temperature (<140°C), while the extraction ability of subcritical water on HCBP was effectively enhanced with the increase of extraction temperature. The extraction yield of 140°C was the highest, which may be due to the balance between the relative strong extraction ability and mild degradation level of HCBP extracted by SWE. However, when the extraction temperature was higher than 140°C, the degradation of HCBP by subcritical water was stronger than that by extraction, resulting in a sharp decrease in HCBP yield with increasing extraction temperature (19). Therefore, 140°C was selected for subsequent experiments.

The extraction time was studied from 5 to 20 min. As shown in Figure 1C, the yield of HCBP decreased with the increasing extraction time, and the maximum yield of HCBP was achieved at 5 min. This may be due to the strong degradation of HCBP by subcritical water at extraction time longer than 5 min. A sharp decrease in the yield of HCBP was observed beyond this threshold.

Based on the results about the yield of HCBP, the optimal extraction conditions of subcritical water are as follows: solid-liquid ratio 1:15, extraction temperature 140°C and extraction time 5 min. These results indicate SWE can be used as a rapid and efficient method for polysaccharide extraction.

Chemical composition of HCBP with different extraction temperatures

Neutral glucose

Neutral sugar of HCBP was determined with anthrone-sulfuric acid method. The neutral sugar content was calculated using calibration curves, and the calibration equation was using glucose as standard y= 0.0032x-0.0122, where y was the absorbance, x was the concentration of glucose, and the correlation coefficient (R^2) was 0.9988. HCBP extracted by different extraction temperatures were a heteropolysaccharide, the content range of neutral sugar was from 58.17 to 68.27% (Figure 2A). The neutral sugar of HCBP was the highest at 150°C and the lowest at 140°C, and all HCBP samples mainly composed of neutral sugar.

Uronic acid

Uronic acid of HCBP was estimated in carbazole method. The content of uronic acid in HCBP was calculated using the standard curve y= 0.0062x +0.0062 with a correlation coefficient of 0.9994, where y was the absorbance, x was the concentration of D-galacturonic acid. Figure 2B showed that the content of uronic acid in HCBP extracted at different extraction temperatures ranged from 11.05% to 15.31%, and the lowest content at 140°C and the highest content at 150°C.

Reducing sugar

Reducing sugar of HCBP was conducted using the 3,5-dinitrosalicylic acid (DNS) method. The reducing sugar content of HCBP was calculated using calibration curves, and the calibration equation was using glucose as standard y= 0.0012x-0.028, where y was the absorbance, x was the concentration of glucose, and the correlation coefficient was 0.9989. In the Figure 2C, the content of reducing sugar is the highest at 160°C and the lowest at 140°C, and the reducing sugar content of HCBP extracted at different extraction temperatures ranged from 6.94 to 11.86%.

Protein

Protein content of HCBP was measured using the Bradford method. The protein content was calculated using calibration curves, and the calibration equation was using bovine serum albumin as standard y = 0.0039x+0.0107 with a correlation coefficient of 0.9995, where y was the absorbance, x was the concentration of bovine serum albumin. The protein content of HCBP is shown in Figure 2D, all HCBP samples extracted at different extraction temperatures were found trace quantities protein, indicating SWE had a high extraction selectivity for polysaccharide, resulting in a high purity of polysaccharide products (19).

Ash

As shown in Figure 2E, the content of ash in HCBP extracted at different extraction temperatures ranged from 4.45 to 6.77%. The ash content of HCBP increased first and then decreased with the increase of extraction temperature, and its change trend was consistent with the change of extraction yield. The ash in HCBP mainly came from inorganic salts that were bound with polysaccharide molecules through ionic bonds, such as magnesium, potassium, calcium, and sodium salts. Therefore, with the increase of HCBP extraction yield, the ash content would also increase. At 140°C, content of ash was the highest, which was in agreement with the maximum HCBP yield.

According to the results above, 140°C was the temperature at which the yield of polysaccharide extracted by subcritical water was the highest. However, 140°C was the temperature at which the contents of neutral sugar, uronic acid and reducing

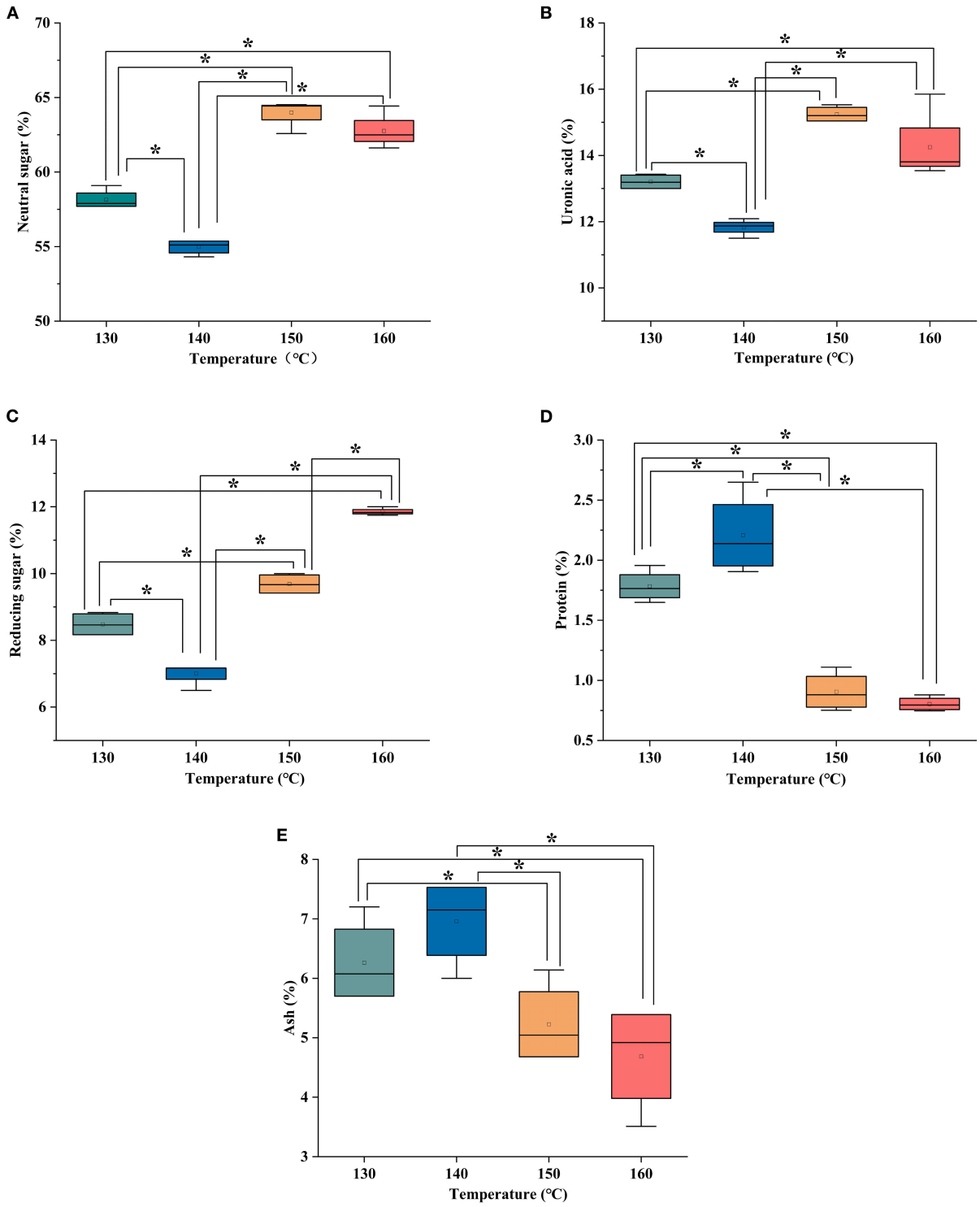

FIGURE 2
The content of neutral sugar **(A)**, uronic acid **(B)**, reducing sugar **(C)**, protein **(D)**, and ash **(E)** of HCBP by subcritical water at different temperatures, $^*p < 0.05$.

sugar were the lowest, and the contents of protein and ash were the highest. Therefore, it could be seen that under the extraction condition with the highest yield, the polysaccharide content was not necessarily the highest. Hence, the production conditions should be selected according to specific requirements in industrial production.

TABLE 1 The molecular weight and monosaccharide content of HCBP samples.

H. citrina Borani polysaccharide	Molecular weight (kDa)	Monosaccharide content (mg/g)								
		Mannose	Rhamnose	Glucuronic acid	Galacturonic acid	Glucose	Galactose	Xylose	Arabinose	Fucose
130°C	159.21	1.77 ± 0.19	3.60 ± 0.44	0.15 ± 0.02	0.24 ± 0.02	31.01 ± 3.92	8.62 ± 1.32	0.79 ± 0.22	1.19 ± 0.23	2.54 ± 0.56
140°C	134.87	1.69 ± 0.28	3.66 ± 0.16	0.17 ± 0.01	0.26 ± 0.00	28.53 ± 0.70	10.60 ± 0.87	0.94 ± 0.27	0.95 ± 0.02	2.89 ± 0.34
150°C	134.06	0.61 ± 0.09	3.35 ± 0.57	0.44 ± 0.08	0.20 ± 0.03	21.25 ± 2.68	7.76 ± 1.24	0.59 ± 0.12	0.61 ± 0.12	1.83 ± 0.26
160°C	58.92	0.59 ± 0.08	3.24 ± 0.04	0.32 ± 0.13	0.19 ± 0.04	18.76 ± 0.89	7.83 ± 0.50	0.40 ± 0.04	0.28 ± 0.03	1.77 ± 0.24

Molecular weight of HCBP with different extraction temperatures

Molecular weight is an important parameter of polysaccharide, which not only reflects the length of molecular chain, but also closely related to the biological activity of polysaccharide (32, 33). The molecular weight of HCBP extracted by different extraction temperatures was determined by GPC. As shown in Table 1, when the extraction temperature increased from 130 to 150°C, the molecular weight of HCBP decreased slightly. Moreover, if the extraction temperature increased to 160°C, the molecular weight of HCBP decreased dramatically. This might be because with the increase of subcritical extraction temperature, especially after the temperature rose to 150°C, the strong thermal degradation of glycosidic bonds increased, leading to the decomposition of polysaccharide molecules into smaller parts (18).

Monosaccharide composition of HCBP with different extraction temperatures

The monosaccharide composition plays an important role in the structural characterization and bioactive studies of polysaccharide (34). Monosaccharide analysis revealed HCBP consisted of heteropolysaccharide (Figure 3), nine monosaccharides (glucose, galactose, rhamnose, fucose, mannose, arabinose, xylose, galacturonic acid and glucuronic acid) were found in all HCBP samples with different contents. Furthermore, the monosaccharide content of HCBP at different extraction temperatures is shown in Table 1, where the mannose was 0.59–1.77 mg/g, rhamnose was 3.24–3.66 mg/g, glucuronic acid was 0.15–0.44 mg/g, galacturonic acid was 0.19–0.26 mg/g, glucose was 18.76–31.01 mg/g, galactose was 7.76–10.60 mg/g, xylose was 0.40–0.94 mg/g, arabinose was 0.28–1.19 mg/g, and fucose was 1.77–2.89 mg/g. Among them, the content of neutral sugars including glucose and galactose were the major components of HCBP samples, and the content of uronic acid including glucuronic acid and galacturonic acid were lower in HCBP samples. The results indicate that the HCBP samples are mainly neutral sugars, which is in agreement with the results of section neutral glucose.

Spectrum analysis of HCBP with different extraction temperatures

Ultraviolet—visible spectrum

As shown in Figure 4A, a similar absorption ultraviolet–visible spectra of 200–900 nm were found in HCBP samples extracted at different temperatures. A weak absorption peak at 280 nm was found in all HCBP samples, which indicated the presence of a small amount of protein. In addition, no other absorption peaks indicated high purity of HCBP samples and low content of non-polysaccharide components, which was in accordance with chemical composition analysis results. However, UV spectrum showed that HCBP extracted at 160°C had the largest absorption peak, while the content of HCBP protein extracted at 140°C was the highest by Bradford's method. This difference may be caused by unknown components in HCBP extracted at different temperatures.

Fourier transform infrared spectrum

The IR spectrum of HCBP is shown in Figure 4B. A high level of similarity of the FT-IR absorption pattern was found between HCBP samples prepared at different temperatures. A peak at 3,417 cm^{-1} belonged to the stretching vibration of O–H, and the strong and broad peak shape was typical of carbohydrates, which indicated the presence of inter-molecular or intra-molecular hydrogen bonds (35). Moreover, the characteristic absorption at 2,931 and 1,244 cm^{-1} was ascribed to C–H stretching and bending vibrations of CH_2 group in the sugar ring (36). The characteristic absorption at around 1,738 cm^{-1} corresponded to the vibration of esterified carboxyl (COO–CH3), and 1,621 cm^{-1} was derived from free carboxyl (COO–) groups, confirming the presence of uronic acid (37). This result was in accordance with the results of section uronic acid. Notably, the peak

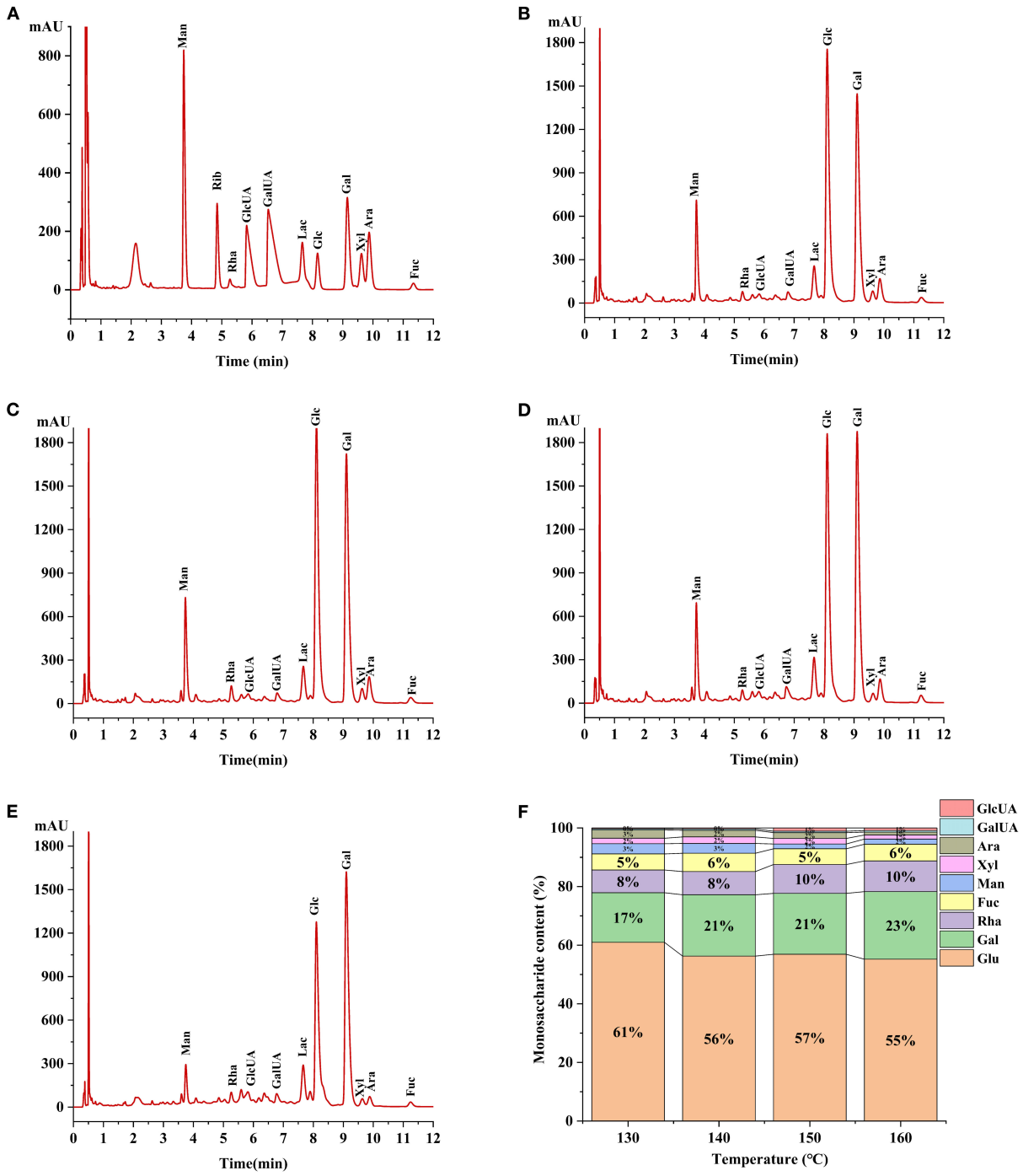

FIGURE 3
(A) Chromatograms of PMP derivatives of monosaccharide standard samples. **(B)** 130°C HCBP sample hydrolysate. **(C)**140°C HCBP sample hydrolysate. **(D)** 150°C HCBP sample hydrolysate. **(E)** 160°C HCBP sample hydrolysate. **(F)** The ratio of monosaccharides of HCBP at different extraction temperatures.

at 1,300–800 cm^{-1} represented the fingerprint region of polysaccharide (19). In addition, the weak bands near 895 cm^{-1} indicated the glucosyl residues in β-configurations existed in HCBP samples.

Scanning electron microscopy analysis

Scanning electron microscopy (SEM) is a technique for observing the morphological characterization including size,

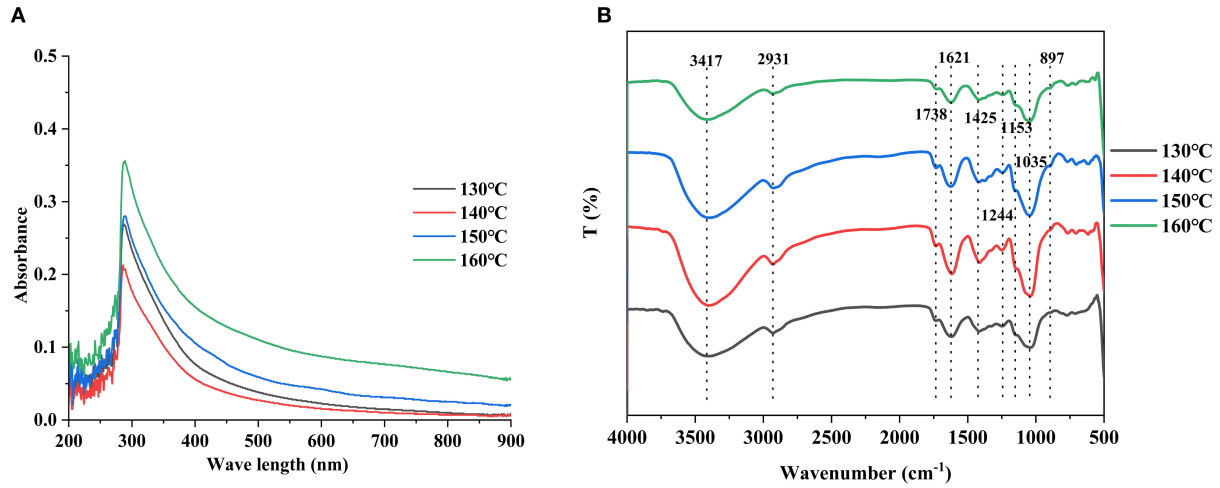

FIGURE 4
UV spectrum **(A)** and FT-IR spectra **(B)** of HCBP samples.

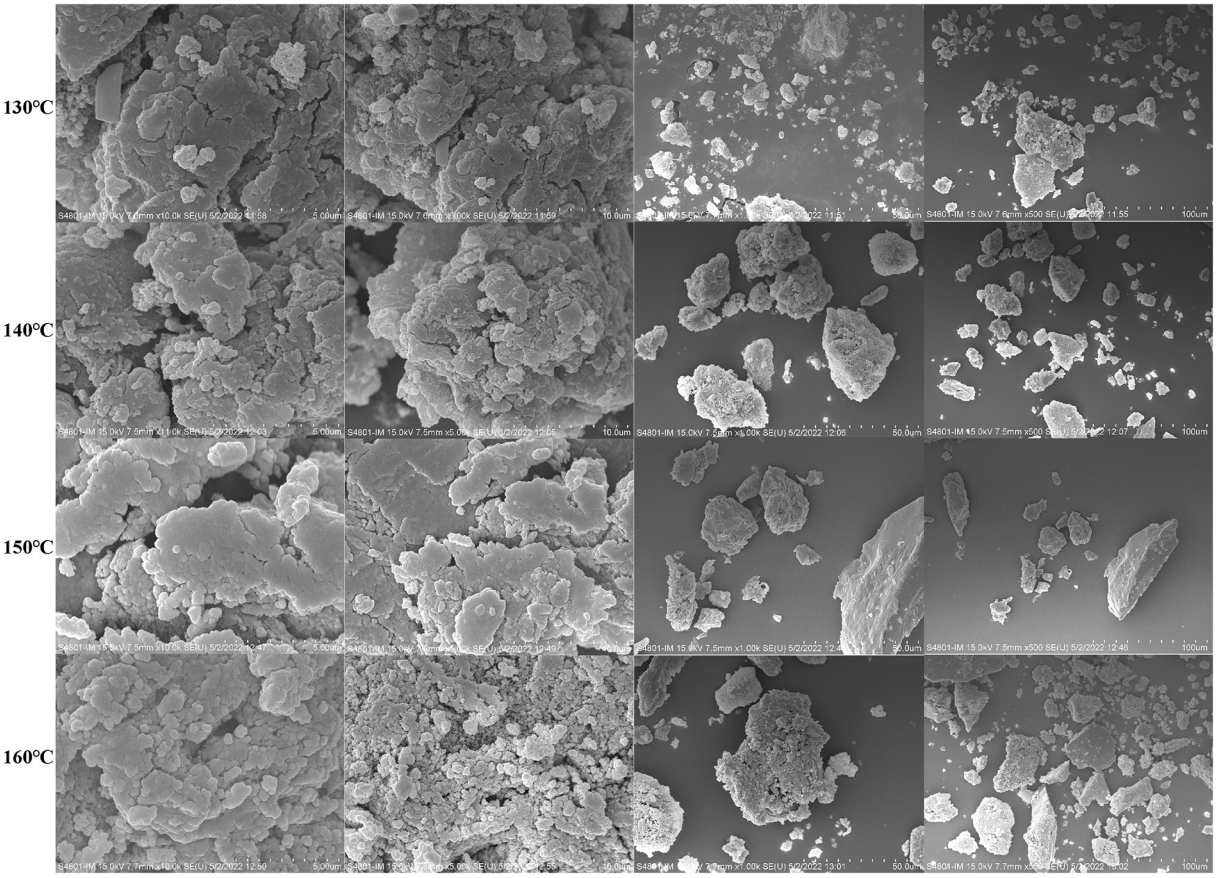

FIGURE 5
SEM images of HCBP extracted by different temperatures at 5-, 10-, 50-, and 100-μm.

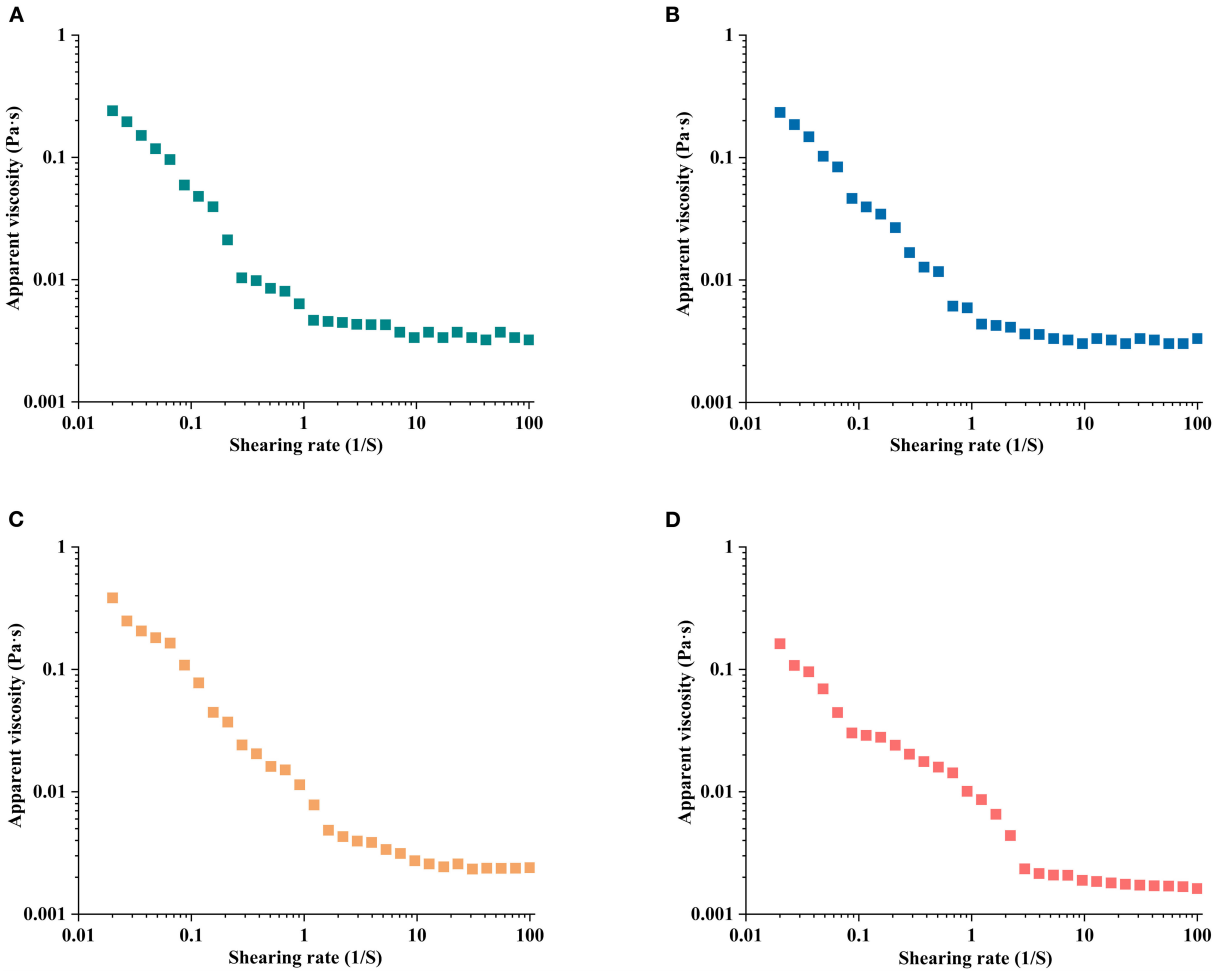

FIGURE 6
The flow behavior of HCBP by subcritical water at 130°C **(A)**, 140°C **(B)**, 150°C **(C)**, and 160°C **(D)**.

shape and porosity of polysaccharide surface (38). The SEM images of HCBP samples at 5-, 10-, 50-, and 100-μm are displayed in Figure 5, and similar SEM images of the HCBP samples with different extraction temperatures were found. All HCBP samples were characterized by rough surface, obvious particle gap, loose structure, and irregular shape. This may be due to the fact that all HCBP samples were mainly composed of neutral sugar, and had less—COOH in the glycosyl, leading to less opportunities for the formation of compact high-level structure between molecules, and resulting in obvious sample gap and loose structure.

Rheological properties of HCBP

The steady shear flow curves of HCBP solutions extracted by 130, 140, 150, and 160°C are described in Figure 6. All HCBP samples displayed a similar and typical shear flow behavior. The apparent viscosity of all HCBP solutions were related to the shear rate, and it decreased obviously with the increase of shear rate. The polymer chain of HCBP flowed directionally in the flow field, resulting in shear thinning. This phenomenon of shear thinning behavior described as pseudoplastic fluid or non-Newtonian fluid (39). With the increase of shear rate, the randomly placed molecules were more aligned in the flow direction, resulting in the decrease of the interaction between adjacent molecules and gradually disentangled of polysaccharide (40). Significantly, the apparent viscosity of HCBP decreased rapidly at low shear rate (0.001–1 s^{-1}) and lower temperature (130–140°C), and the apparent viscosity of HCBP remained almost constant with the increase of shear rate. However, the apparent viscosity of HCBP at higher temperature (150–160°C) still decreased at higher shear rate (1–10 s^{-1}) with the increase of shear rate. Rheological behaviors of samples were strongly related to physiochemical properties of polysaccharide including molecular weight and chain stiffness

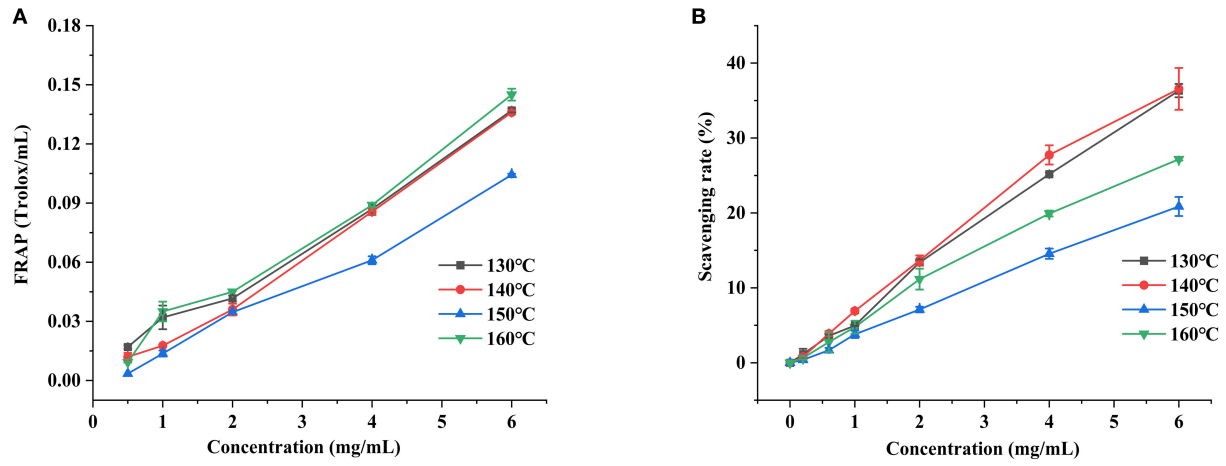

FIGURE 7
Ferric reducing assay power **(A)** and ABTS radical scavenging activity **(B)** of HCBP by subcritical water at different temperatures.

(41). The changes of apparent viscosity and molecular weight of HCBP samples showed a similar downward trend with the increase of temperature. HCBP with different rheological properties could be prepared by regulating SWE conditions. The results showed that HCBP extracted by SWE could be used as a thickening agent in the food industry.

Antioxidant activity

Ferric reducing assay power

FRAP is a method used to determine the total antioxidant capacity of natural substances (42). As shown in Figure 7A, an obvious concentration-dependent at the range of 0.5–6 mg/ml for the total antioxidant capacity of FRAP in the HCBP samples was found. Remarkably, the extraction temperature also had a great influence on the FRAP of HCBP samples, especially for the samples obtained at 160°C, which performed best total antioxidant capacity of FRAP during the test. The polysaccharide extracted at 160°C had lower molecular weight, and the polysaccharide with lower molecular weight often had better antioxidant activity (43). In addition, the reducing sugar content was the highest at 160°C, which might be the reason for the optimal total antioxidant capacity of FRAP.

ABTS radical scavenging activity

ABTS is a non-physiological free radical used to evaluate the antioxidant power of natural products, the ABTS radical scavenging capacity of HCBP is shown in Figure 7B. The scavenging capacity of HCBP to ABTS radical increased with the increase of concentration, showing an obvious dose-dependent at the range of 0.2–6 mg/ml. Moreover, it was also clearly that the extraction temperature played a more important role at improving ABTS radical scavenging capacity, but different from total antioxidant capacity of FRAP (160°C was best total antioxidant capacity of FRAP), the polysaccharide extracted at 130 and 140°C had the higher ABTS scavenging rate. In addition, polysaccharide-protein conjugates containing hydrophobic pores and cracks enhance antioxidant activity (44). Therefore, the polysaccharide-protein conjugate might help the radical scavenging ability of HCBP. The protein content of polysaccharide extracted at 130 and 140 °C was the higher, which might be the reason for its best ABTS radical scavenging capacities.

Conclusion

In this work, SWE was employed to extract polysaccharide from *H. citrina* Borani. The highest yield of HCBP was achieved under the following conditions: a solid–liquid ratio 1:15, extraction temperature of 140°C, and extraction time of 5 min. Then, the physicochemical properties of HCBP extracted by subcritical water at different temperatures were evaluated. The results showed that HCBP extracted at 140°C possessed the lowest contents of neutral sugar, uronic acid and reducing sugar, and the highest contents of protein and ash. HCBP extracted at 150°C had the highest contents of neutral sugar, uronic acid. HPLC revealed all HCBP samples were mainly composed nine monosaccharides with different proportions. GPC showed that the molecular weight of HCBP samples decreased with increasing temperature. UV confirmed that HCBP samples contained a small amount of protein, and FT-IR revealed that the glycosidic bond of HCBP samples were β-configuration. The apparent viscosity of HCBP at higher temperature (150–160°C) decreased with the increase of shear rate (1–10 s^{-1}), but

nearly constant at lower temperature (130–140°C). The HCBP samples had the characteristics of rough surface, obvious particle gap, loose structure and irregular shape observed by SEM. HCBP had good antioxidant effect, among which, the FRAP activity of HCBP extracted at 160°C was the strongest, and the ABTS radical scavenging activity of HCBP extracted at 130 and 140°C was better. In conclusion, our study indicates that the extraction condition of the highest yield may not the optimum condition of polysaccharide content and antioxidant activity. Hence, the production conditions should be selected according to specific requirements. In addition, this study suggests that HCBP extracted by SWE could provide an inexpensive raw material for the development of food thickening agent and natural antioxidants, increase the value of *H. citrina* Borani products and promote its industrial development.

Data availability statement

The raw data supporting the conclusions of this article will be made available by the authors, without undue reservation.

Author contributions

YT: investigation, conceptualization, formal analysis, data curation, writing—original draft, and writing—review and editing. YZ: investigation, formal analysis, and data curation. YB: investigation and data curation. XW: investigation, visualization, and software. YH and XW: investigation. ZS: investigation, methodology, formal analysis, funding acquisition, supervision, and writing—review and editing. All authors contributed to the article and approved the submitted version.

Acknowledgments

The authors thank the National Natural Science Foundation of China (32102043) and Central Public-interest Scientific Institution Basal Research Fund (No. Y2022XK30).

Conflict of interest

The authors declare that the research was conducted in the absence of any commercial or financial relationships that could be construed as a potential conflict of interest.

Publisher's note

All claims expressed in this article are solely those of the authors and do not necessarily represent those of their affiliated organizations, or those of the publisher, the editors and the reviewers. Any product that may be evaluated in this article, or claim that may be made by its manufacturer, is not guaranteed or endorsed by the publisher.

References

1. Qing ZX, Liu JH, Yi XX, Liu XB, Hu GA, Lao J, et al. The chromosome-level *Hemerocallis citrina* Borani genome provides new insights into the rutin biosynthesis and the lack of colchicine. *Hortic Res Engl.* (2021) 8:89. doi: 10.1038/s41438-021-00539-6

2. Lin YL, Lu CK, Huang YJ Chen HJ. Antioxidative caffeoylquinic acids and flavonoids from *Hemerocallis fulva* flowers. *J Agric Food Chem.* (2011) 59:8789–95. doi: 10.1021/jf201166b

3. Yi LT, Li J, Li HC, Zhou Y, Su BF, Yang KF, et al. Ethanol extracts from *Hemerocallis citrina* attenuate the decreases of brain-derived neurotrophic factor, TrkB levels in rat induced by corticosterone administration. *J Ethnopharmacol.* (2012) 144:328–34. doi: 10.1016/j.jep.2012.09.016

4. Gu L, Liu YJ, Wang YB, Yi LT. Role for monoaminergic systems in the antidepressant-like effect of ethanol extracts from *Hemerocallis citrina*. *J Ethnopharmacol.* (2012) 139:780–7. doi: 10.1016/j.jep.2011.11.059

5. Zhong J, Liang Y, Chen Y, Zhang J, Zou X, Deng J, et al. Study and experimental validation of the functional components and mechanisms of *Hemerocallis citrina* Baroni in the treatment of lactation deficiency. *Foods.* (2021) 10:1863. doi: 10.3390/foods10081863

6. Liang Y, Huang R, Chen Y, Zhong J, Deng J, Wang Z, et al. Study on the sleep-improvement effects of *Hemerocallis citrina* Baroni in *Drosophila melanogaster* and targeted screening to identify its active components and mechanism. *Foods.* (2021) 10:883. doi: 10.3390/foods10040883

7. Liu J, Zhong X, Jiang Y, Yu L, Huang X, Dong Z, et al. Systematic identification metabolites of *Hemerocallis citrina* Borani by high-performance liquid chromatography/quadrupole-time-of-flight mass spectrometry combined with a screening method. *J Pharm Biomed Anal.* (2020) 186:113314. doi: 10.1016/j.jpba.2020.113314

8. Lin SH, Chang HC, Chen PJ, Hsieh CL, Su KP, Sheen LY. The antidepressant-like effect of ethanol extract of daylily flowers (Jin Zhen Hua) in rats. *J Tradit Complement Med.* (2013) 3:53–61. doi: 10.4103/2225-4110.106548

9. Tian H, Yang FF, Liu CY, Liu XM, Pan RL, Chang Q, et al. Effects of phenolic constituents of daylily flowers on corticosterone- and glutamate-treated PC12 cells. *BMC Complement Altern Med.* (2017) 17:69. doi: 10.1186/s12906-017-1582-x

10. Wu WT, Mong MC, Yang YC, Wang ZH Yin MC. Aqueous and ethanol extracts of daylily flower (*Hemerocallis fulva* L.) protect HUVE cells against high glucose. *J Food Sci.* (2018) 83:1463–9. doi: 10.1111/1750-3841.14137

11. Yun L, Li D, Yang L Zhang M. Hot water extraction and artificial simulated gastrointestinal digestion of wheat germ polysaccharide. *Int J Biol Macromol.* (2019) 123:174–81. doi: 10.1016/j.ijbiomac.2018.11.111

12. Yi Y, Xu W, Wang HX, Huang F Wang LM. Natural polysaccharides experience physiochemical and functional changes during preparation: a review. *Carbohydr Polym.* (2020) 234:115896. doi: 10.1016/j.carbpol.2020.115896

13. Zeng WC, Zhang Z, Gao H, Jia LR, Chen WY. Characterization of antioxidant polysaccharides from Auricularia auricular using microwave-assisted extraction. *Carbohyd Polym.* (2012) 89:694–700. doi: 10.1016/j.carbpol.2012.03.078

14. Zhang WN, Zhang HL, Lu CQ, Luo JP, Zha XQ. A new kinetic model of ultrasound-assisted extraction of polysaccharides from Chinese chive. *Food Chem.* (2016) 212:274–81. doi: 10.1016/j.foodchem.2016.05.144

15. Cheigh CI, Yoo SY, Ko MJ, Chang PS, Chung MS. Extraction characteristics of subcritical water depending on the number of hydroxyl group in flavonols. *Food Chem.* (2015) 168:21–6. doi: 10.1016/j.foodchem.2014.07.047

16. Meillisa A, Woo HC, Chun BS. Production of monosaccharides and bio-active compounds derived from marine polysaccharides using subcritical

water hydrolysis. *Food Chem.* (2015) 171:70–7. doi: 10.1016/j.foodchem.2014.08.097

17. Chen HM, Fu X, Luo ZG. Properties and extraction of pectin-enriched materials from sugar beet pulp by ultrasonic-assisted treatment combined with subcritical water. *Food Chem.* (2015) 168:302–10. doi: 10.1016/j.foodchem.2014.07.078

18. Zhang J, Wen C, Gu J, Ji C, Duan Y, Zhang H. Effects of subcritical water extraction microenvironment on the structure and biological activities of polysaccharides from *Lentinus edodes*. *Int J Biol Macromol.* (2019) 123:1002–11. doi: 10.1016/j.ijbiomac.2018.11.194

19. Zhang F, Zhang L, Chen J, Du X, Lu Z, Wang X, et al. Systematic evaluation of a series of pectic polysaccharides extracted from apple pomace by regulation of subcritical water conditions. *Food Chem.* (2022) 368:130833. doi: 10.1016/j.foodchem.2021.130833

20. Getachew AT, Chun BS. Molecular modification of native coffee polysaccharide using subcritical water treatment: structural characterization, antioxidant, and DNA protecting activities. *Int J Biol Macromol.* (2017) 99:555–62. doi: 10.1016/j.ijbiomac.2017.03.034

21. Dubois M, Gilles K, Hamilton JK, Rebers PA Smith F. A colorimetric method for the determination of sugars. *Nature.* (1951) 168:167. doi: 10.1038/168167a0

22. Bitter T, Muir HM. A modified uronic acid carbazole reaction. *Anal Biochem.* (1962) 4:330–4. doi: 10.1016/0003-2697(62)90095-7

23. Bradford MM. A rapid and sensitive method for the quantitation of microgram quantities of protein utilizing the principle of protein-dye binding. *Anal Biochem.* (1976) 72:248–54. doi: 10.1016/0003-2697(76)90527-3

24. Jia DD, Zhang YJ, Lan R, Yang HL, Sun Y. A simple preparative method for isolation and purification of polysaccharides from mulberry (*Morus alba* L.) leaves. *Int J Food Sci Tech.* (2013) 48:1275–81. doi: 10.1111/ijfs.12087

25. Dai J, Wu Y, Chen SW, Zhu S, Yin HP, Wang M, et al. Sugar compositional determination of polysaccharides from *Dunaliella salina* by modified RP-HPLC method of precolumn derivatization with 1-phenyl-3-methyl-5-pyrazolone. *Carbohyd Polym.* (2010) 82:629–35. doi: 10.1016/j.carbpol.2010.05.029

26. Ti Y, Wang W, Zhang Y, Ban Y, Wang X, Wang P, et al. Polysaccharide from *Hemerocallis citrina* Borani by subcritical water: bioactivity, purification, characterization, and anti-diabetic effects in T2DM rats. *Int J Biol Macromol.* (2022) 215:169–83. doi: 10.1016/j.ijbiomac.2022.06.101

27. Li F, Wei Y, Liang L, Huang L, Yu G, Li Q. A novel low-molecular-mass pumpkin polysaccharide: Structural characterization, antioxidant activity, and hypoglycemic potential. *Carbohydr Polym.* (2021) 251:117090. doi: 10.1016/j.carbpol.2020.117090

28. Ji X, Yan Y, Hou C, Shi M, Liu Y. Structural characterization of a galacturonic acid-rich polysaccharide from *Ziziphus Jujuba cv. Muzao*. *Int J Biol Macromol.* (2020) 147:844–52. doi: 10.1016/j.ijbiomac.2019.09.244

29. Yang H, Bai J, Ma C, Wang L, Li X, Zhang Y, et al. Degradation models, structure, rheological properties and protective effects on erythrocyte hemolysis of the polysaccharides from *Ribes nigrum* L. *Int J Biol Macromol.* (2020) 165:738–46. doi: 10.1016/j.ijbiomac.2020.09.093

30. Jeddou KB, Chaari F, Maktouf S, Nouri-Ellouz O, Helbert CB, Ghorbel RE. Structural, functional, and antioxidant properties of water-soluble polysaccharides from potatoes peels. *Food Chem.* (2016) 205:97–105. doi: 10.1016/j.foodchem.2016.02.108

31. Pinto D, Vieira EF, Peixoto AF, Freire C, Freitas V, Costa P, et al. Optimizing the extraction of phenolic antioxidants from chestnut shells by subcritical water extraction using response surface methodology. *Food Chem.* (2021) 334:127521. doi: 10.1016/j.foodchem.2020.127521

32. Ji XL, Cheng YQ, Tian JY, Zhang SQ, Jing YS, Shi MM. Structural characterization of polysaccharide from jujube (*Ziziphus jujuba* Mill.) fruit. *Chem Biol Technol Agric.* (2021) 8:54. doi: 10.1186/s40538-021-00255-2

33. Ferreira SS, Passos CP, Madureira P, Vilanova M, Coimbra MA. Structure-function relationships of immunostimulatory polysaccharides: a review (vol 132, pg 378, 2015). *Carbohyd Polym.* (2016) 147:557–8. doi: 10.1016/j.carbpol.2016.04.011

34. Ji XL, Hou CY, Yan YZ, Shi MM, Liu YQ. Comparison of structural characterization and antioxidant activity of polysaccharides from jujube (*Ziziphus jujuba* Mill.) fruit. *Int J Biol Macromol.* (2020) 149:1008–18. doi: 10.1016/j.ijbiomac.2020.02.018

35. Xu YQ, Cai F, Yu ZY, Zhang L, Li XG, Yang Y, et al. Optimisation of pressurised water extraction of polysaccharides from blackcurrant and its antioxidant activity. *Food Chem.* (2016) 194:650–8. doi: 10.1016/j.foodchem.2015.08.061

36. Wang SN, Zhao LL, Li QH, Liu C, Han JL, Zhu LJ, et al. Rheological properties and chain conformation of soy hull water-soluble polysaccharide fractions obtained by gradient alcohol precipitation. *Food Hydrocolloid.* (2019) 91:34–9. doi: 10.1016/j.foodhyd.2019.01.055

37. Kost'alova Z, Hromadkova Z Ebringerova A. Structural diversity of pectins isolated from the Styrian oil-pumpkin (*Cucurbita pepo* var. *styriaca*) fruit. *Carbohyd Polym.* (2013) 93:163–71. doi: 10.1016/j.carbpol.2012.05.017

38. Ktari N, Bkhairia I, Nasri M, Ben Salah R. Structure and biological activities of polysaccharide purified from Senegrain seed. *Int J Biol Macromol.* (2020) 144:190–7. doi: 10.1016/j.ijbiomac.2019.12.087

39. Li WJ, Fan ZG, Wu YY, Jiang ZG, Shi RC. Eco-friendly extraction and physicochemical properties of pectin from jackfruit peel waste with subcritical water. *J Sci Food Agric.* (2019) 99:5283–92. doi: 10.1002/jsfa.9729

40. Qiao L, Li Y, Chi Y, Ji Y, Gao Y, Hwang H, et al. Rheological properties, gelling behavior and texture characteristics of polysaccharide from *Enteromorpha prolifera*. *Carbohydr Polym.* (2016) 136:1307–14. doi: 10.1016/j.carbpol.2015.10.030

41. Naji-Tabasi S, Razavi SM. New studies on basil (*Ocimum bacilicum* L.) seed gum: part II-Emulsifying and foaming characterization. *Carbohydr Polym.* (2016) 149:140–50. doi: 10.1016/j.carbpol.2016.04.088

42. Ji X, Guo J, Pan F, Kuang F, Chen H, Guo X, et al. Structural elucidation and antioxidant activities of a neutral polysaccharide from arecanut (*Areca catechu* L.). *Front Nutr.* (2022) 9:853115. doi: 10.3389/fnut.2022.853115

43. Su Y, Li L. Structural characterization and antioxidant activity of polysaccharide from four auriculariales. *Carbohyd Polym.* (2020) 229:115407. doi: 10.1016/j.carbpol.2019.115407

44. Lee AL, Yu YP, Hsieh JF, Kuo MI, Ma YS, Lu CP. Effect of germination on composition profiling and antioxidant activity of the polysaccharide-protein conjugate in black soybean [*Glycine max* (L.) Merr.]. *Int J Biol Macromol.* (2018) 113:601–6. doi: 10.1016/j.ijbiomac.2018.02.145

frontiers | Frontiers in Nutrition

TYPE Original Research
PUBLISHED 22 August 2022
DOI 10.3389/fnut.2022.969512

Check for updates

OPEN ACCESS

EDITED BY
Xiaolong Ji,
Zhengzhou University of Light Industry, China

REVIEWED BY
Yun peng Fan,
Northwest A&F University, China
Xiaona Zhao,
Shandong Agricultural University, China
Mingchao Liu,
Hebei Agricultural University, China

*CORRESPONDENCE
Hongbin Si
shb2009@gxu.edu.cn
Wenjing Sun
wenjingsun@gxu.edu.cn

†These authors have contributed equally to this work

SPECIALTY SECTION
This article was submitted to Food Chemistry, a section of the journal Frontiers in Nutrition

RECEIVED 15 June 2022
ACCEPTED 25 July 2022
PUBLISHED 22 August 2022

CITATION
Qu D, Lian S, Hu H, Sun W and Si H (2022) Characterization and macrophages immunomodulatory activity of two water-soluble polysaccharides from *Abrus cantoniensis*. *Front. Nutr.* 9:969512. doi: 10.3389/fnut.2022.969512

COPYRIGHT
© 2022 Qu, Lian, Hu, Sun and Si. This is an open-access article distributed under the terms of the Creative Commons Attribution License (CC BY). The use, distribution or reproduction in other forums is permitted, provided the original author(s) and the copyright owner(s) are credited and that the original publication in this journal is cited, in accordance with accepted academic practice. No use, distribution or reproduction is permitted which does not comply with these terms.

Characterization and macrophages immunomodulatory activity of two water-soluble polysaccharides from *Abrus cantoniensis*

Dongshuai Qu[1,2†], Shuaitao Lian[1†], Hongjie Hu[1], Wenjing Sun[3*] and Hongbin Si[1*]

[1]State Key Laboratory for Conservation and Utilization of Subtropical Agro-Bioresources, College of Animal Science and Technology, Guangxi University, Nanning, China, [2]DanAg Agritech Consulting Co. Ltd., Zhengzhou, China, [3]Guangxi Key Laboratory of Agricultural Resources Chemistry and Biotechnology, College of Biology & Pharmacy, Yulin Normal University, Yulin, China

The study aims to elucidate the physicochemical properties and immunomodulatory activity of two polysaccharides (ACP_{t0} and ACP_{t2}) from *Abrus cantoniensis*. Results revealed that ACP_{t0} with a molecular weight of 26.0 kDa, was mainly composed of glucose (83.1%) and galactose (6.1%), and that ACP_{t2} with a molecular weight of 145.6/8.9 kDa, consisted of galactose (25.6%), galacturonic acid (22.2%), arabinos (16.6%) and galactose (11.0%) respectively. AFM and Congo red experiments suggested that ACP_{t0} and ACP_{t2} might be spherical particles with triple-helix conformation in aqueous solution. ACP_{t0} and ACP_{t2} exhibited immunomodulatory activity by promoting the proliferation, augmenting pinocytic and phagocytic capacities, releasing immunoactive molecules such as ROS, NO, iNOS, TNF-α, IL-6 and IL-1β, upregulation of the mRNA levels of corresponding cytokines in macrophages. Moreover, ACP_{t0} and ACP_{t2} were recognized by toll-like receptor 4 (TLR4) and exerted immunomodulatory effects via activating Myeloid differentiation factor 88 (MyD88), mitogen-activated protein kinases (MAPKs) and serine/threonine kinase (Akt) signaling pathways in macrophages. Notably, ACP_{t2} had higher immunomodulatory activity than ACP_{t0}. Based on the present findings, ACP_{t0} and ACP_{t2} could be explored as an active component of immunomodulators in the food and pharmaceutical fields.

KEYWORDS

Abrus cantoniensis **polysaccharide, purification, physicochemical properties, immunoregulation, structure**

Introduction

In recent decades, extensive studies have found that natural active polysaccharides isolated from various plants, especially herbal medicine, possessed rich biological activities, such as immunoregulation, anti-tumor, anti-oxidation, anti-virus, hypolipidemic, hypoglycemic and bacteriostatic activities (1–7). With the continuous research on function, increasing attention has been focused on the immunomodulatory activities of plant polysaccharides, which have become a research hotspot (8, 9).

Both innate and adaptive immunity constitute the immune system of mammals, which is closely related to body health (10). Macrophages play crucial roles in innate immunity, and can exert immune function by engulfing and destroying pathogenic substances directly, including tumor cells or infectious microbes (11). Meanwhile, macrophages can also aid in fighting against infection and inflammation indirectly by releasing bioactive molecules such as nitric oxide (NO), reactive oxygen species (ROS), tumor necrosis factor (TNF)-α, interleukin (IL)-1β, IL-6, IL-8, and IL-10 (12, 13). Therefore, the activation of macrophages is a promising approach for enhancing host immune abilities. In addition, it is reported that macrophages were activated by recognizing and binding to specific receptors. Toll-like receptor (TLR) is a key pattern recognition receptor, and some polysaccharides exert biological effects by acting on TLR2 or TLR4. *Isaria cicadae Miquel* polysaccharide can recognize TLR4 and trigger several intracellular signaling pathways (14). The effect of CPE-II on RAW264.7 is related to TLR4 and TLR2 (15). Thus, macrophages are usually used as ideal cell models to evaluate the immunomodulatory properties of polysaccharides (16).

Abrus cantoniensis, traditional Chinese herbal medicine, belongs to the Abrus genus in the Leguminosae family, and is widely cultivated in Guangdong, Guangxi and Hunan in Southern China. *Abrus cantoniensis* has been widely used as a folk medicine for centuries and is an important ingredient in the "Jigucao capsules." In Guangdong areas, people use this medicinal and edible plant to make herbal teas, beverages and healthy food, such as the red-canned tea "Wong Lo Kat." Total flavonoid extracts from *Abrus cantoniensis*, have potential anti-inflammatory effects against xylene-induced ear swelling and cotton ball granuloma in mice (17). *Abrus cantoniensis* flavonoid could improve ethanol-induced gastric ulcers and CCl_4-induced hepatitis in mice (18, 19). The saponins of *Abrus cantoniensis* exerted potent inhibitory effects on hepatitis B virus replication *in vivo* and *in vitro* (20).

Until now, studies on *Abrus cantoniensis* polysaccharides (ACP) have mainly focused on extraction and isolation, and information on the immunomodulatory activities is not available, especially their structural features. Therefore, the purification, characterization and immunomodulatory activity of ACP *in vitro* were studied. In this study, two fractions named ACP_{t0} and ACP_{t2} were isolated and purified from *Abrus cantoniensis*. Their physicochemical properties include molecular weight, monosaccharide composition, absorption characteristic of infrared, spatial structure and AFM. Moreover, their immunomodulatory activities were investigated *in vitro* by using the macrophage model. This study will enhance our understanding of the characterization and bioactivities of ACP, which can be applied as a potential bioactive ingredient for immunomodulators in the food and pharmaceutical fields.

Materials and methods

Materials and reagents

Abrus cantoniensis were provided by the Guangxi Dahong Pharmaceutical Co., Ltd. (Hechi, Guangxi, China). After being crushed and sun-dried, the material was stored at 4°C.

Dimethyl sulfoxide (DMSO), DEAE cellulose-52, lipopolysaccharide (LPS), ROS assay Kit, RPMI 1640 medium and neutral red were acquired from Solarbio Biotechnology Co., Ltd. (Beijing, China). Monosaccharide standards (glucose, mannose, arabinose, galactose, fucose, rhamnose, glucuronic acid, galacturonic acid, glucosamine, Galactosamine, xylose), trifluoroacetic acid (TFA), 1-phenyl-3-methyl-5-pyrazolone (PMP) were purchased from Sigma (St. Louis, MO, United States). The Vybrant phagocytosis assay kit (V-6694) was obtained from Thermo Fisher Scientific (Waltham, United States). The ELISA kits for mouse tumor necrosis factor (TNF-α), interferon (IFN-γ), interleukin (IL-6, IL-1β) were provided by Jiangsu Jingmei Biotechnology Co., Ltd (Jiangsu, China). The NO and Inducible nitric oxide synthase (iNOS) detecting kit were acquired from Nanjing Jiancheng Institute of Biotechnology (Nanjing, China). Trizol reagent, RealStar Green Fast Mixture and First-strand cDNA Synthesis Mix were bought from GenStar Co., Ltd. (Beijing, China).

Extraction and purification of polysaccharides

The water-ethanol extraction method was used to isolate the crude *Abrus cantoniensis* polysaccharides (21). To remove small molecules, the powder of *Abrus cantoniensis* was first processed with 95% ethanol, and then Savage deproteinization and resin decolorization. DEAE-52 anion exchange chromatography (2.6 × 50 cm) was used to further purify the crude polysaccharides, which was eluted with ultra-pure water and 0.2M NaCl into 2 peaks, the eluents were concentrated and dialyzed (cut-off Mw3500 Da) against distilled water for 36 h and vacuum-dried under freezing to obtain the refined ACP_{t0}, ACP_{t2}, respectively. The process of separation was shown in **Figure 1A**.

10.3389/fnut.2022.969512

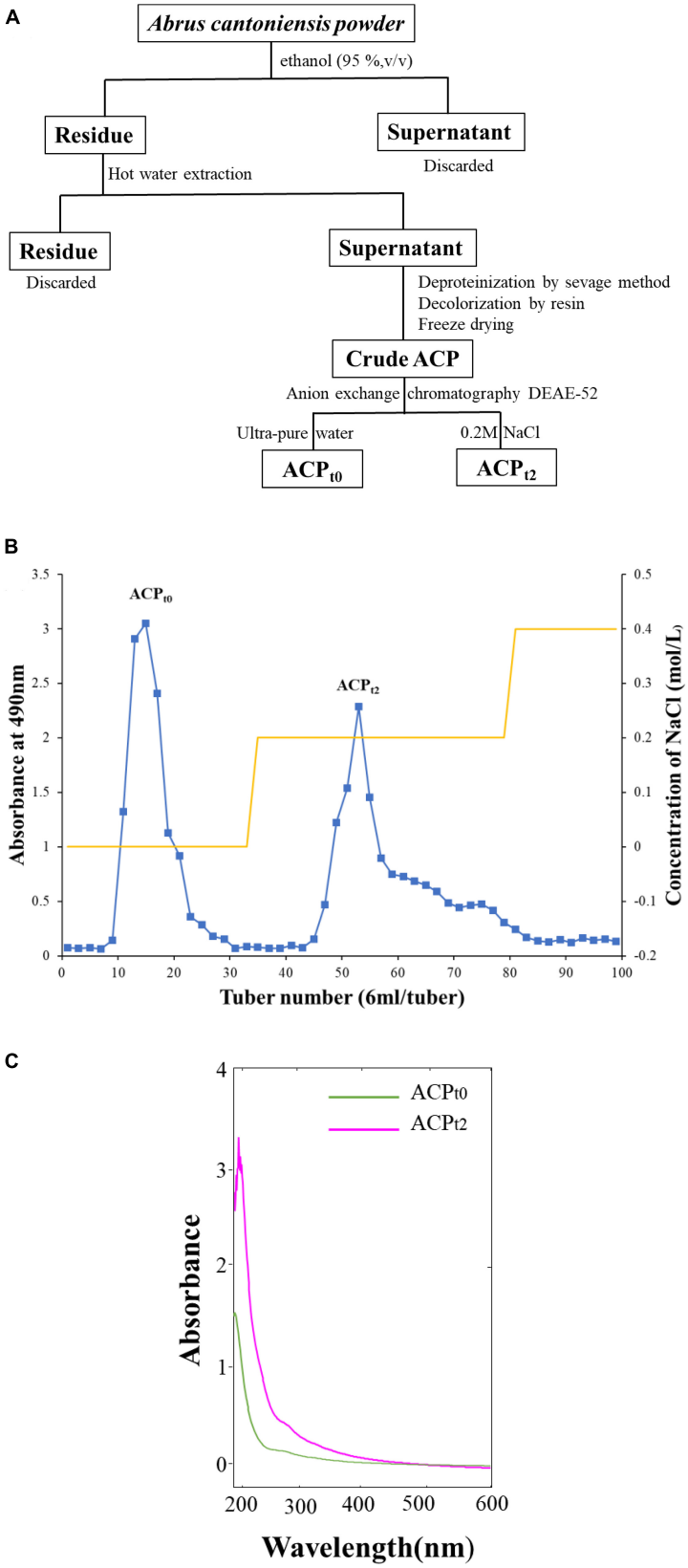

FIGURE 1
(A) The process of separation and purification of ACP. **(B)** Chromatography of crude ACP by DEAE-52 cellulose chromatography column. **(C)** UV spectrum of ACP_{t0} and ACP_{t2}.

Structural characterization of *Abrus cantoniensis* polysaccharides

Determination of contents of total sugar, protein and uronic acid

The total carbohydrate content was determined by the phenol-H_2SO_4 method (22). Using glucuronic acid as a standard, the total uronic acid content was determined by the carbazole sulfate method (23). The coomassie brilliant blue method, which uses bovine serum albumin as a reference, was used to determine the protein content. Visible absorbance was recorded with a UV–Vis spectrophotometer (Model SP-752, China).

Ultraviolet spectrum and Fourier transform infrared spectroscopy analysis

The purified ACP_{t0} and ACP_{t2} (2 mg each) were ground with KBr powder for FT-IR analysis and recorded between 4000 and 400 cm^{-1} on a Thermo Nicolet iS5 FT-IR (ThermoFisher, United States). The ultraviolet absorbance of the ACP_{t0} and ACP_{t2} aqueous solution (1 mg/mL) were scanned in the range of 200–600 nm by a U-6000PC spectrophotometer (Yuanxi, Shanghai, China).

Molecular weight and monosaccharide compositions analysis

The average molecular weight (MW) of ACP_{t0} and ACP_{t2} were analyzed by high-performance gel permeation chromatography (HPGPC) using an Agilent 1260 system (Agilent, United States) equipped with a refractive index detector (RID) and a TSK-GEL GMPWXL column (7.8 mm × 300 mm, 10μm) (Tosoh, Tokyo, Japan). For each run, polysaccharides samples (20 μL, 5.0 mg/mL) were injected at 40°C. Data were analyzed by GPC software and the molecular weight of ACP_{t0} and ACP_{t2} were determined using the standard curve obtained from dextran standards.

The monosaccharide compositions of ACP_{t0} and ACP_{t2} were analyzed by PMP pre-column derived method according to the previous report (24). In brief, the polysaccharides samples were hydrolyzed with 2 M trifluoroacetic acid (TFA) in an ampoule bottle at 120°C for 2 h. Then methanol was added into the hydrolyzate and dried with a nitrogen-blowing apparatus. The process was repeated three times to remove TFA. Next, the resulting residue was dissolved in distilled water and then the samples or monosaccharide standard mixture were mixed with 0.6 M NaOH and 0.5 M methanol solution of PMP. The reaction mixture was cooled to room temperature after incubating at 70°C for 1 h. added 0.3 M HCl to stop the derivative reaction and extracted by $CHCl_3$ thrice. The PMP-labeled sugars were analyzed using an Agilent 1260 HPLC system with C18 column (4.6 mm × 250 mm, 5 μm Thermo, United States), and the chromatography conditions were as follows: temperature, 30°C; the mobile phase consisted of 87% 0.1 M phosphate solution (PH = 6.7) and 13% acetonitrile; detector, 245 nm. The monosaccharide compositions and content of ACP_{t0} and ACP_{t2} were identified according to the retention times and the calibration curve (peak area-concentration) of each monosaccharide standard, respectively.

Determination of a triple-helix structure

The spatial structure of ACP_{t0} and ACP_{t2} were analyzed by the Congo-red method with minor modifications (25). Polysaccharides samples (2 mg each) were dissolved in 1 mL of deionized water and mixed with 2 mL of Congo-red solution (100 μM). Then, 0.1 M phosphate buffer was dropped into the mixtures (PH = 8). The maximum absorption wavelength (λmax) of the complex were recorded using a UV-6000PC spectrophotometer (Yuanxi, Shanghai, China) in the wavelength range of 400–650 nm, which can determine the transition of maximum absorption wavelength of the mixtures.

Atomic force microscopy analysis

The polysaccharide samples (ACP_{t0} and ACP_{t2}) were dissolved in ultrapure water (10 μg/mL). Sample solutions (5 μL each) were dropped onto clean mica sheets and dried at room temperature for 2 h. The surface molecular morphology of ACP_{t0} and ACP_{t2} were scanned by AFM (Bruker, United States).

Determination of immunomodulatory activity

Isolation and culture of peritoneal macrophages

Specific-pathogen-free (SPF) mice (20 ± 2 g) were purchased from Changsha Tianqin Biotechnology Co., Ltd [certificate number: SCXK(Xiang)2019–0014, Hunan, China]. The entire experimental procedures were approved and supervised by the Animal Care and Welfare Committee of Guangxi University (Gxu-2021-116).

Peritoneal macrophages were extracted from mice's abdominal cavity according to the reported methods (26). Briefly, the mice were intraperitoneally injected 1 mL of 0.5% starch broth medium. After two days, the mice were sacrificed and soaked in 75% alcohol for 5 min, then 6 mL of inactivated PBS was injected into the abdominal cavity and the abdomen was gently massaged for 2 min. Next, the peritoneal fluid was retracted, 2000 r/min, 5 min, then the cells were washed and stained with Trypan blue to confirm that the survival rate was above 95%. The concentration was adjusted to 1×10^6 cells/mL with RPMI-1640 supplemented with 10% (v/v) fetal bovine serum (FBS). The cells were added to the cell culture plate and cultured in 37°C, 5% CO_2 incubator.

Cytotoxicity of *Abrus cantoniensis* polysaccharides on macrophages

ACP_{t0} and ACP_{t2} were diluted to 11 concentrations in RMI1640 medium with a range of 1000∼0.98 μg/mL. 100 μL macrophages suspension were plated into 96-well plates with a density of 1×10^6 cells per well, and cultured in 37°C, 5% CO_2 incubator. After 4 h, macrophages were washed with PBS twice to remove the unadherent cells. Then 100 μL of various concentrations of samples were added, and cells cultured alone in RPMI1640 medium were used as control. After culturing for 44 h, 20 μL MTT solution (5 mg/mL) was added to each well for 4 h at 37°C. The supernatant was removed carefully and then 150 μL DMSO solution was added to each well. The plates were shaken for 10 min to completely dissolve the formazan crystals. The absorbance was recorded by a Microplate Reader at 570 nm (Thermo fisher, United States).

Measurement of reactive oxygen species generated by macrophages

The macrophages were plated in 96-well plates and cultured in 37°C, 5% CO_2 incubator for 4 h. After removing the supernatant carefully, RMI1640 medium and various concentrations of ACP_{t0} and ACP_{t2} (3.91∼62.5 μg/mL) and LPS (10 μg/mL) were added to each well, respectively. After 44 h of incubation, all supernatants were carefully removed and 100 μL of DCFH-DA (10 μM) solution was added to each well, followed by incubation at 37°C for 20 min. After that, the supernatant was carefully removed and the cells were washed three times with PBS. The fluorescence intensity of each well was measured at 488 nm excitation and 525 nm emissions on a microplate reader.

Determination of the pinocytic activity of macrophages

The effect of ACP_{t0} and ACP_{t2} on the pinocytic activity of macrophages was determined by neutral red assay. The macrophages were seeded on 96-well plates and treated with different concentrations of ACP_{t0} and ACP_{t2}, RMI1640 medium, and LPS, respectively. After 44 h of culture, the supernatant was removed. Each well was then filled with 100 μL of 0.1% neutral red solution, which was then incubated for 2 h at 37°C. Next, the supernatant was discarded and the cells in the 96-well plates were washed with PBS three times. Subsequently, cell lysate (100 μL per well) was added into each well for 2 h at room temperature. The optical density (OD) was recorded using a Microplate Reader at 540 nm.

Phagocytosis assay of fluorescein isothiocyanate-labeled Escherichia coli

Vybrant phagocytosis assay kit was used to determine the phagocytic effect of two polysaccharide fractions on the phagocytosis fluorescein isothiocyanate (FITC)-labeled *Escherichia coli* at the concentration range of 3.91∼62.5 μg/mL.

TABLE 1 Sequence of primers.

Genes		Primer sequence (5′ to 3′)
β-actin	Forward	GAGGGAAATCGTGCGTGAC
	Reverse	GCTGGAAGGTGGACAGTGAG
TNF-α	Forward	CTCATTCCTGCTTGTGGC
	Reverse	CACTTGGTGGTTTGCTACG
IL-6	Forward	TTCCATCCAGTTGCCTTC
	Reverse	GTAATTAAGCCTCCGACT
IL-1β	Forward	GTTCCCATTAGACAACTGC
	Reverse	AGATTCTTTCCTTTGAGGC
TLR2	Forward	ACCCGCCCTTTAAGCTGTGT
	Reverse	TCGTACTTGCACCACTCGCT
TLR4	Forward	TCTGGGGAGGCACATCTTCT
	Reverse	AGGTCCAAGTTGCCGTTTCT
MyD88	Forward	TCATGTTCTCCATACCCTTGGT
	Reverse	AAACTGCGAGTGGGGTCAG
MAPK	Forward	TGACCCTTATGACCAGTCCTTT
	Reverse	GTCAGGCTCTTCCACTCATCTAT
AKT	Forward	TGAAGCTACTGGGCAAGGG
	Reverse	AAAGCAGAGGCGGTCGTG

Macrophages were seeded on 24-well plates and treated with ACP_{t0}, ACP_{t2}, RMI1640 medium and LPS, respectively (described above). After that, 100 μL of the prepared fluorescent bioparticle suspension (1.0 mg/mL) was added to all the experimental wells and the plate was standed for 2 h at 37°C. Then the bioparticle loading suspension was removed from all of the wells carefully and the cells which phagocytize the fluorescent particles was washed three times with cold PBS. The trypan blue staining was to anchor the cells and then photographed under an inverted fluorescence microscope (EVOS M5000, Invitrogen, America).

Quantitative analysis of nitric oxide, iNOS and cytokines

The peritoneal macrophage was propagated in RMI1640 and stimulated with different concentrations of polysaccharide samples (3.91∼62.5 μg/mL) or LPS (10 μg/mL). 44 h of incubation later, the supernatants of the cells were obtained. Then, the levels of NO, iNOS, TNF-α, IL-6 and IL-1β were determined by the Griess reagent and ELISA kits, respectively.

RNA extraction and quantitative real-time polymerase chain reaction analysis

Macrophages were treated with different concentrations of polysaccharide samples or LPS for 24 h, respectively, according to the above method. The cells were collected for total RNA extraction using Trizol reagent. Then total RNA was reversed into cDNA by the StarScript II First-strand cDNA Synthesis Mix. Complementary DNA generated by reverse transcriptase encoding TNF-α, IL-1β and IL-6 genes was amplified by

quantitative real-time polymerase chain reaction (qPCR). The β-actin was utilized as the internal reference to normalize the gene expression. The $2^{-\Delta\ \Delta\ Ct}$ method was used to calculate the expression levels of mRNA. The blank control was treated with RMI1640 medium alone and the positive control group was treated with LPS (10 μg/mL). Gene amplification was performed by Real Star Green Fast Mixture on the Light Cycler 96 System (Roche). The primer sequences used in this study (Sangon Biotech Co., Ltd, China) are shown in **Table 1**.

Result and discussion

Extraction and purification of polysaccharides

As shown in **Figure 1B**, the crude ACP was further purified by DEAE-52 Cellulose anion-exchange chromatography, and two mainly independent elution peaks were obtained. The content of carbohydrate of ACP_{t0} and ACP_{t2} were 99.6% and 98.8%, respectively. The UV spectrum of two polysaccharides showed no absorption peaks at 260 and 280 nm, indicating that the absence of protein and nucleic acid in ACP_{t0} and ACP_{t2} (**Figure 1C**). The uronic acid contents of ACP_{t0} and ACP_{t2} were 15.9% and 27.9% (**Table 2**). From the subsequent FT-IR analysis and monosaccharide composition analysis, the uronic acid can also be obviously detected, but the proportion is not consistent. Monosaccharide composition tests showed that ACP_{t0} contained a large amount of glucose. Therefore, it is speculated that the high content of uronic acid may be caused by the oxidation of glucose in the polysaccharide to glucuronic acid in ACP_{t0} using sulfuric acid-carbazole method.

Structural characterization of *Abrus cantoniensis* polysaccharides

Molecular weight and monosaccharide composition

ACP_{t0} exhibited one main elution peak with an estimated molecular weight of 26.0 kDa. While, the molecular weight of ACP_{t2} with two peaks was calculated at 145.6 kDa and 8.9 kDa. The monosaccharide composition of ACP_{t0} and ACP_{t2} were analyzed by PMP pre-column derived method. As shown in **Figure 2A**, results indicated ACP_{t0} was mainly composed of glucose (83.1%), galactose (6.1%), and a small amount of galactose uronic acid, glucuronic acid, arabinose and mannose, signifying that glucose was probably the backbone of ACP_{t0}. In contrast, ACP_{t2} contains mainly galactose (25.6%), galactose uronic acid (22.2%), arabinose (16.6%), glucose (11.0%), and a small amount of mannose, xylose, glucuronic acid, rhamnose (**Table 2**).

Infrared spectroscopic Fourier transform infrared spectroscopy analysis

Due to each group's distinctive absorption, IR spectrum analysis is a useful tool for understanding polysaccharide structure. FT-IR spectra of ACP_{t0} and ACP_{t2} were shown in **Figures 2B,C**, respectively. The results showed the broad peak at 3402.16 cm^{-1} for ACP_{t0} and 3402.06 cm^{-1} for ACP_{t2} corresponded to the -OH stretching vibration, and 2928.49 cm^{-1} for ACP_{t0} and 2932.01 cm^{-1} for ACP_{t2} attributed to the stretching vibration of -C-H, which indicated the presence of intermolecular hydrogen bonds in the molecular structure (27). 1646.43 cm^{-1} and 1368.73 cm^{-1} for ACP_{t0} and 1615.51 cm^{-1} and 1418.14 cm^{-1} for ACP_{t2} probably caused by carbonyl or aldehyde or carboxyl (28, 29). Assigned to the C = O stretching vibration of acetyl or carboxylic acid ester, the peaks at 1752.64 cm^{-1} in ACP_{t2} indicated that some carboxyl groups were esterified (30). The O = S = O deformation vibration is indicated by the band at 1238.24 cm^{-1}, which may be an indication of the presence of sulfates in the ACP_{t2} (31). The absorption peaks at 1025.49 cm^{-1} and 1154.09 cm^{-1} for ACP_{t0}, 1076.98 cm^{-1} for ACP_{t2} are supposed to the characteristic peaks of pyran-glycosides (32). The IR spectrum of ACP_{t0} at 1500–500 cm^{-1} was different from those of ACP_{t2}, which may be attributed to the difference in their monosaccharide compositions.

Chain conformation

Congo red is an acidic dye, which can form a complex with triple-helix polysaccharides. In a suitable alkaline condition, the λmax of the complex is red-shifted compared with Congo red. Therefore, Congo red experiment can corroborate the existence of triple helix structure in polysaccharides (33). As shown in **Figure 3A**, the bathochromic shift of λmax value of ACP_{t0} or ACP_{t2}-Congo red complex are 15 nm and 18 nm, respectively compared with Congo red. The results indicated that ACP_{t0} and ACP_{t2} could form a complex with Congo red, indicating the existence of triple helix conformation in ACP_{t0} and ACP_{t2}.

Spectroscopy molecular surface morphology

The AFM is a powerful technique of structure characterization analysis, which can be used to observe the morphology and size of macromolecular chains in samples under room temperature and pressure. AFM has gradually become a vital approach to explore the structures of biological macromolecules, such as polysaccharides and DNA (34). As is shown in **Figures 3B,C**, spherical shell morphology was clearly observed (upper panels). The diameters of ACP_{t0} and ACP_{t2} were estimated to be 11.20–48.60 nm, 60.30–280 nm, respectively, which indicated that ACP_{t0} and ACP_{t2} have the potential of application in the drug carrier field. ACP_{t0} aggregated into dispersed spherical particles significantly smaller than ACP_{t2} in aqueous solution. The 3D figures revealed the island structure of two polysaccharides. Many island-like

10.3389/fnut.2022.969512

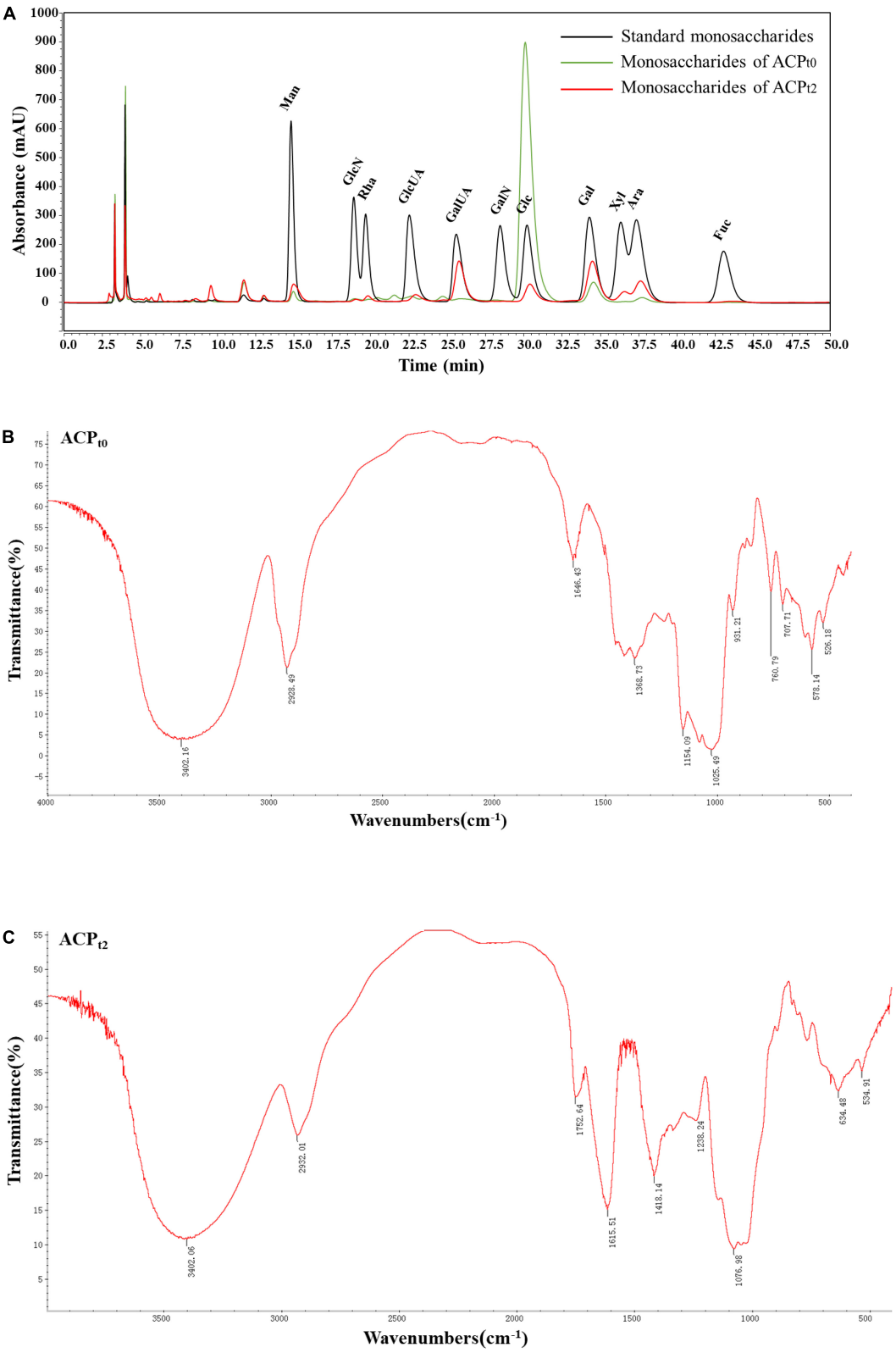

FIGURE 2
(A) Ion chromatogram data of monosaccharide composition of ACP_{t0} and ACP_{t2}, Fourier-transform infrared (FT-IR) spectra of ACP_{t0} **(B)**, and ACP_{t2} **(C)** in the range of 4000–400 cm^{-1}.

TABLE 2 The total sugar, uronic acid, and protein contents, and monosaccharide compositions molecular weight of the ACP_{t0} and ACP_{t2}.

Fraction	Total carbohydrate (%)	Uronic acid (%)	Protein (%)	MW (kDa)	Monosaccharide composition (%)							
					Man (%)	Rha (%)	GlcUA (%)	GalUA (%)	Glc (%)	Gal (%)	Xyl (%)	Ara (%)
ACP_{t0}	98.8	15.9	0.09	26.0	1.4	–	1.6	1.6	83.1	6.1	–	1.6
ACP_{t2}	99.6	27.9	0.11	145.6 /8.9	8.8	1.7	3.9	22.2	11.0	25.6	6.3	16.6

– Not detected.

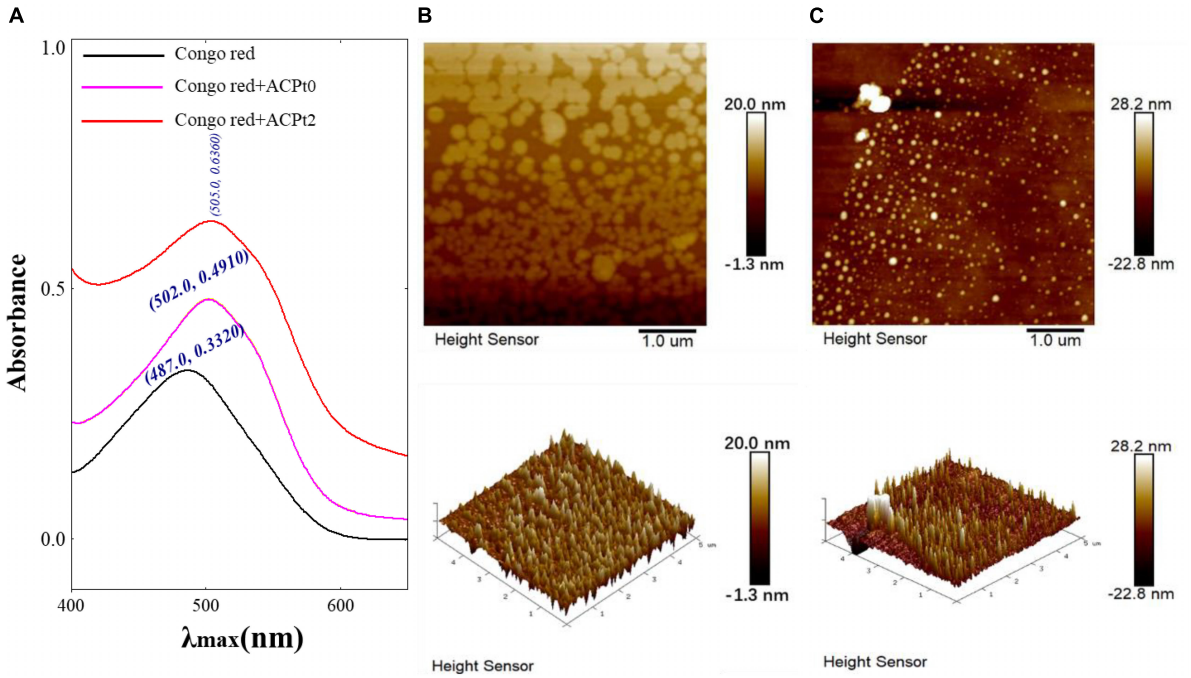

FIGURE 3
(A) Maximum absorption wavelength of Congo red + ACP_{t0} or ACP_{t2} complex and Congo red; AFM spectra of ACP_{t0} **(B)** and ACP_{t2} **(C)**, planar image (upper panels, scan size: 5 μm), cubic image (lower panel, scan size: 5 μm).

protrusions with heights between -22.80 and 28.20 nm were discovered on the surface of ACP_{t0} and ACP_{t2}. The surface height of ACP_{t0} is slightly greater than ACP_{t2}. It indicated that the biological activity of polysaccharides was related to the diameter and surface height of spherical particles focused in aqueous solution.

Determination of immunomodulatory activity

Cytotoxicity of *Abrus cantoniensis* polysaccharides on macrophages

The effects of ACP_{t0} and ACP_{t2} on the proliferation of peritoneal macrophages were investigated at concentrations of 1000~0.98 μg/mL. As shown in Figure 4, ACP_{t0} and ACP_{t2} within a given concentration range had no inhibitory effects on the proliferation of macrophages. Compared with normal control, the growth of macrophages was inhibited notably when the concentration of ACP_{t0} was greater than 62.5 μg/mL ($P < 0.05$), and when concentration exceeded 125 μg/mL, ACP_{t2} could significantly suppress the proliferation of macrophages ($P < 0.05$). In the subsequent experiments, the concentration range of the two polysaccharides was set as 3.91~62.5 μg/mL to facilitate comparison at the same level.

Measurement of reactive oxygen species generated by macrophages

In this study, fluorescence probe DCFH-DA method was used to measure the changes of ROS secretion of

10.3389/fnut.2022.969512

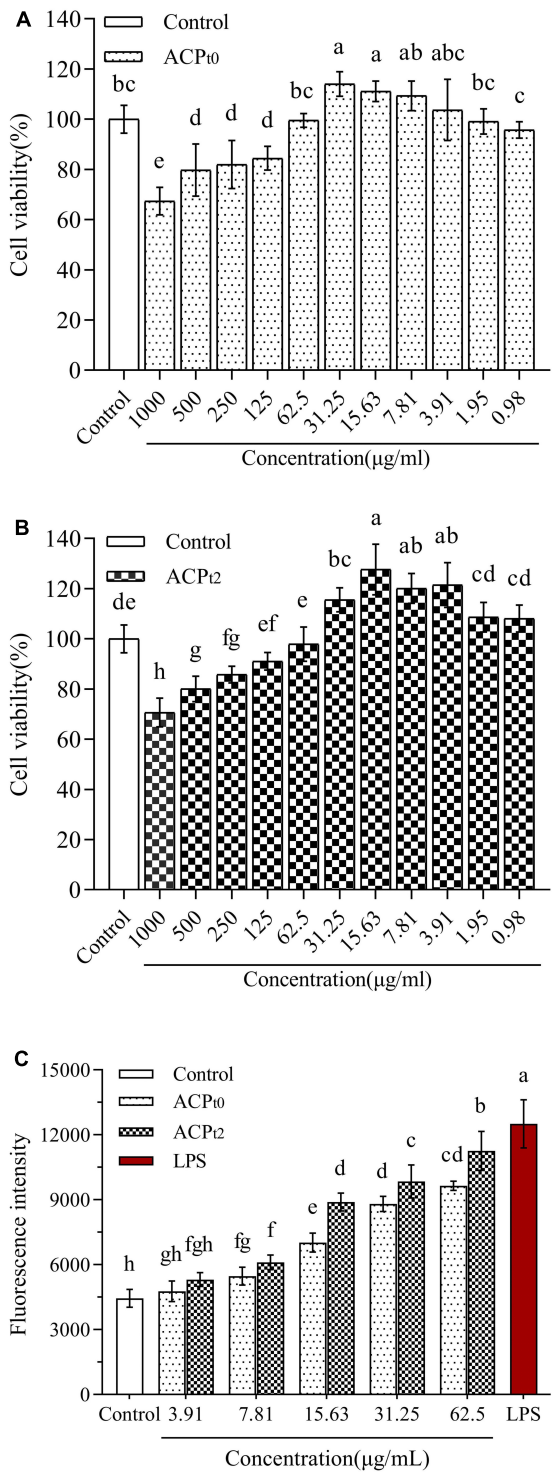

FIGURE 4
The effects of ACP_{t0} **(A)** and ACP_{t2} **(B)** treatment on the viability of macrophages. Effect of different concentrations of ACP_{t0} and ACP_{t2} treatment on ROS generation of macrophages **(C)**. The different letters in the column indicate statistically significant differences ($P < 0.05$).

macrophages after treatment with different concentrations of ACP_{t0} and ACP_{t2} (3.91∼62.5 μg/mL) for 24 h. These probes can easily infiltrate cell membranes and enter cells, and then be hydrolyzed by intracellular esterase to produce 2',7'-dichlorodihydrofluorescein (DCFH) without fluorescence. The DCFH was subsequently oxidized by intracellular ROS to 2',7'-dichlorodihydrofluorescein (DCF) with green fluorescence (35). Therefore, fluorescence intensity is positively correlated with intracellular ROS levels. As shown in **Figure 4C**, the mean fluorescence intensity (ROS levels) of blank control group was 4446.75 ± 415.06, while treatment with LPS (10 μg/mL) and two samples increased ROS production. However, low concentration of ACP_{t0} and ACP_{t2} (3.91 μg/mL) did not significantly increase ROS secretion ($P > 0.05$). With the increase in the concentrations of ACP_{t0} and ACP_{t2}, ROS levels increases in a dose-dependent manner. When the concentration of ACP_{t0} and ACP_{t2} reached 62.5 μg/mL, the ROS secretion levels were 9642.25 ± 209.48 and 11257.50 ± 896.39, respectively, increased by 116.84% and 153.16% compared with blank control group ($P < 0.01$), still significantly lower than that of LPS group (181.23%) ($P < 0.05$). These results suggest that treatment with ACP_{t0} and ACP_{t2} could modulate the immune activity of macrophages moderately.

Effects of *Abrus cantoniensis* polysaccharides on the pinocytic and phagocytic activities of macrophages

As shown in **Figure 5**, except for ACP_{t0} at 3.91 μg/mL, the phagocytosis of neutral red by macrophages was significantly enhanced after 48 h stimulation with different concentrations of ACP_{t0} and ACP_{t2} (3.91∼62.5 μg/mL) ($P < 0.05$). The absorbance value (OD_{540}) of cells pretreated by ACP_{t0} and ACP_{t2} reached the maximum (OD_{540} = 0.268, 0.276) at 31.25, 62.5 μg/mL, which was 106.2%, 112.3% greater ($P < 0.05$) than that of blank control group (OD_{540} = 0.130), respectively. The absorbance value (OD_{540}) of cells treated by LPS reached 0.266, which was significantly higher than that in the normal control ($P < 0.05$). The results showed that ACP_{t0} and ACP_{t2} could promote the uptake of neutral red, and significantly enhance the phagocytosis of macrophages. Especially, the induction effect of ACP_{t2} on macrophages was stronger than ACP_{t0}.

Additionally, the effects of ACP_{t0} and ACP_{t2} on the phagocytic uptake of *E. coli* (FITC-labeled) in macrophages were visualized under inverted fluorescence microscope. The image of the control group showed the darkest fluorescence, indicating little phagocytosis of *E. coli* by the untreated cells. When the concentrations of ACP_{t0} and ACP_{t2} increased, the clear increase in fluorescence was observed. The fluorescence intensity of ACP_{t2}-treated cells was higher than that of ACP_{t0} at the same concentration.

10.3389/fnut.2022.969512

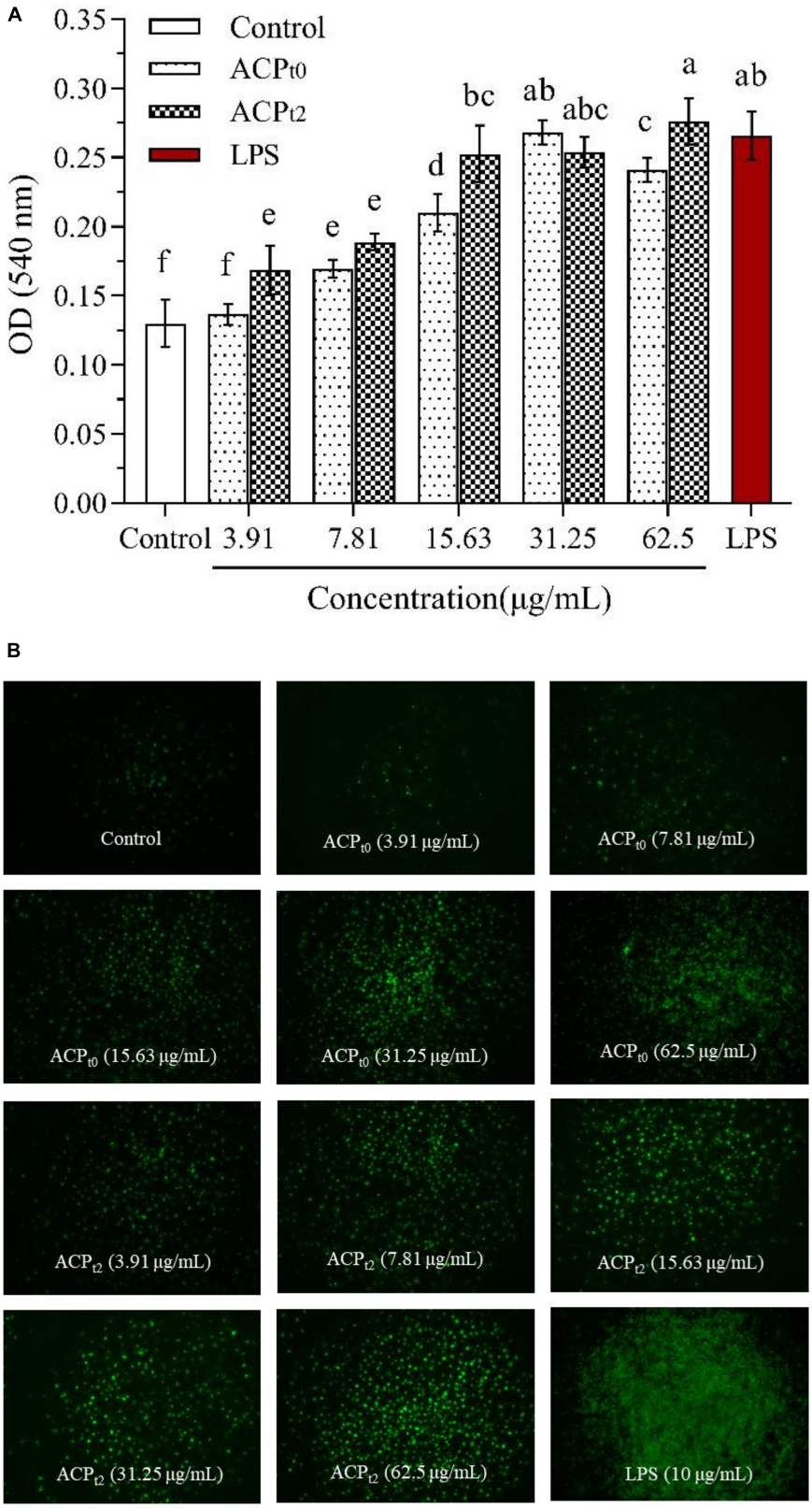

FIGURE 5
Pinocytiosis rate of ACP_{t0} and ACP_{t2} on taking neutral red of macrophages **(A)**. Fluorescence microscopic images of macrophages phagocytosing FITC-labeled *E. coli* **(B)**. The different letters in the column indicate statistically significant differences ($P < 0.05$).

While a significant difference was observed in the brightness and density of macrophages treated with LPS, which was markedly greater than that in the ACP_{t0} and ACP_{t2} treatment groups. These results indicate that ACP_{t0} and ACP_{t2} can regulate immune activity and do not over-activate macrophages. The effect of ACP_{t2} is superior to ACP_{t0}, which is consistent with the result of neutral red experiment.

Quantitative analysis of nitric oxide, iNOS

Compared with the blank control, NO levels were significantly higher ($P < 0.05$) in concentration-dependent after activation of macrophages by different doses of ACP_{t0} and ACP_{t2} (3.91∼62.5 μg/mL) (Figure 6A). When the concentration of polysaccharides increased from 3.91 to 62.5 μg/mL, the level of NO induced by ACP_{t0} gradually increased from 15.46 ± 1.32 to 33.26 ± 1.93 μmol/L. While the levels of NO induced by ACP_{t2} gradually increased from 15.85 ± 1.93 μmol/L to 38.29 ± 1.93 μmol/L. The results revealed ACP_{t2} on NO production from macrophages was stronger than that of ACP_{t0} under high concentrations. However, the levels of NO at all concentrations of ACP_{t0} and ACP_{t2} were markedly lower than those stimulated by LPS ($P < 0.05$).

As shown in Figure 6B, the activity of iNOS was 10.04 ± 0.59 U/mL in the blank control, and the activity of iNOS induced by LPS reached 26.12 ± 0.44 U/mL, which was significantly higher than that in the blank control ($P < 0.05$). ACP_{t0} and ACP_{t2} at all concentrations significantly enhanced the activity of iNOS in macrophages compared with the blank control ($P < 0.05$). The activity of iNOS induced by ACP_{t0} increased in a dose-dependent manner, and reached the highest levels of 17.22 ± 0.68 U/mL at 62.5 μg/mL. Whereas there was no significant difference in the activity of iNOS induced by ACP_{t2} at each concentration. However, it was worth noting that the activity of iNOS induced by ACP_{t2} at the concentrations of 3.91, 7.81, 15.63, 31.25 μg/mL was stronger than the activity of iNOS stimulated by ACP_{t0} ($P < 0.05$).

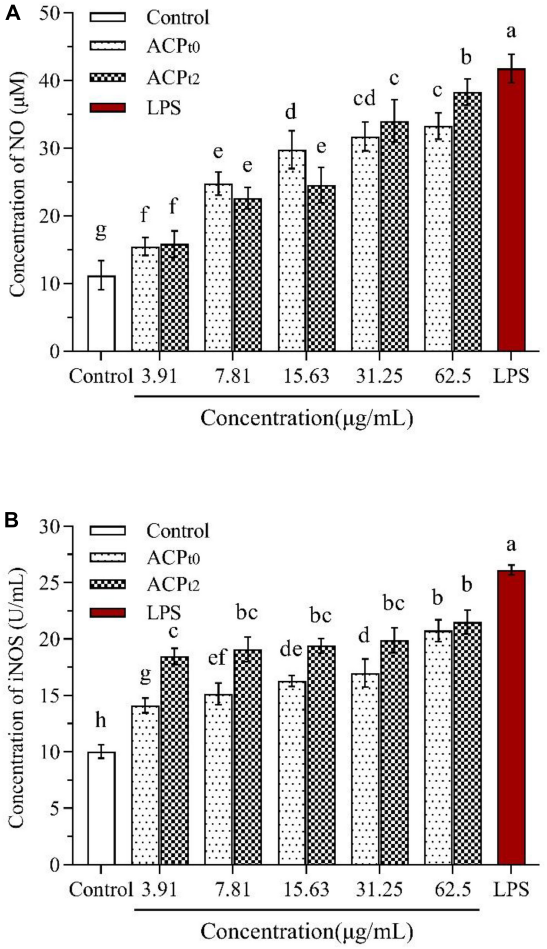

FIGURE 6
Effects of ACP_{t0} and ACP_{t2} on NO secretion **(A)**, the activity of iNOS **(B)** in macrophages. The different letters in the column indicate statistically significant differences ($P < 0.05$).

Quantitative analysis of cytokines and their mRNA expression in macrophages

The effects of ACP_{t0} and ACP_{t2} on the levels of TNF-α, IL-6 and IL-1β in macrophages were detected by ELISA. As shown in Figure 7, ACP_{t0} and ACP_{t2} at concentrations of 3.91∼62.5 μg/mL markedly promoted the secretion of TNF-α, IL-6 and IL-1β in macrophages compared with the normal control ($P < 0.05$). The secretion of TNF-α and IL-6 in macrophages stimulated by ACP_{t2} increased with significant dosage effects, while there was no obvious difference in the ACP_{t0} group at the concentrations ranging from 15.63 to 62.5 μg/mL. With the increase of samples concentrations, IL-1β secretions stimulated by ACP_{t0} and ACP_{t2} gradually increased and reached the highest level, and at 62.5 μg/mL, and ACP_{t0} and ACP_{t2} were 88.302 ± 1.34 pg/mL and 106.267 ± 4.38 pg/mL, respectively. However, except for the effect of ACP_{t2} on IL-1β secretion by macrophages at 62.5 μg/mL, the productions of TNF-α, IL-6 and IL-1β from macrophages activated by ACP were lower than in the LPS-treated group ($P < 0.05$). Notably, overproduction and excessive cytokines are considered to induce inflammation, which is harmful to the organisms. Results indicated that both ACP_{t0} and ACP_{t2} can activate the immune system by stimulating macrophages to secrete TNF-α, IL-6 and IL-1β .

To further verify whether ACP_{t0} and ACP_{t2} modulate the release of cytokines by upregulating gene expression, the mRNA expression levels of TNF-α, IL-6 and IL-1β in macrophages were detected by qRT-PCR and the results were calculated using $2^{-\Delta\Delta Ct}$ method. Since the results showed a better treatment effect at 62.5 μg/mL, the concentration of the samples was selected 62.5 μg/mL for further study. The results are shown in Figures 7D–F, compared to the blank control group, ACP_{t0} and

10.3389/fnut.2022.969512

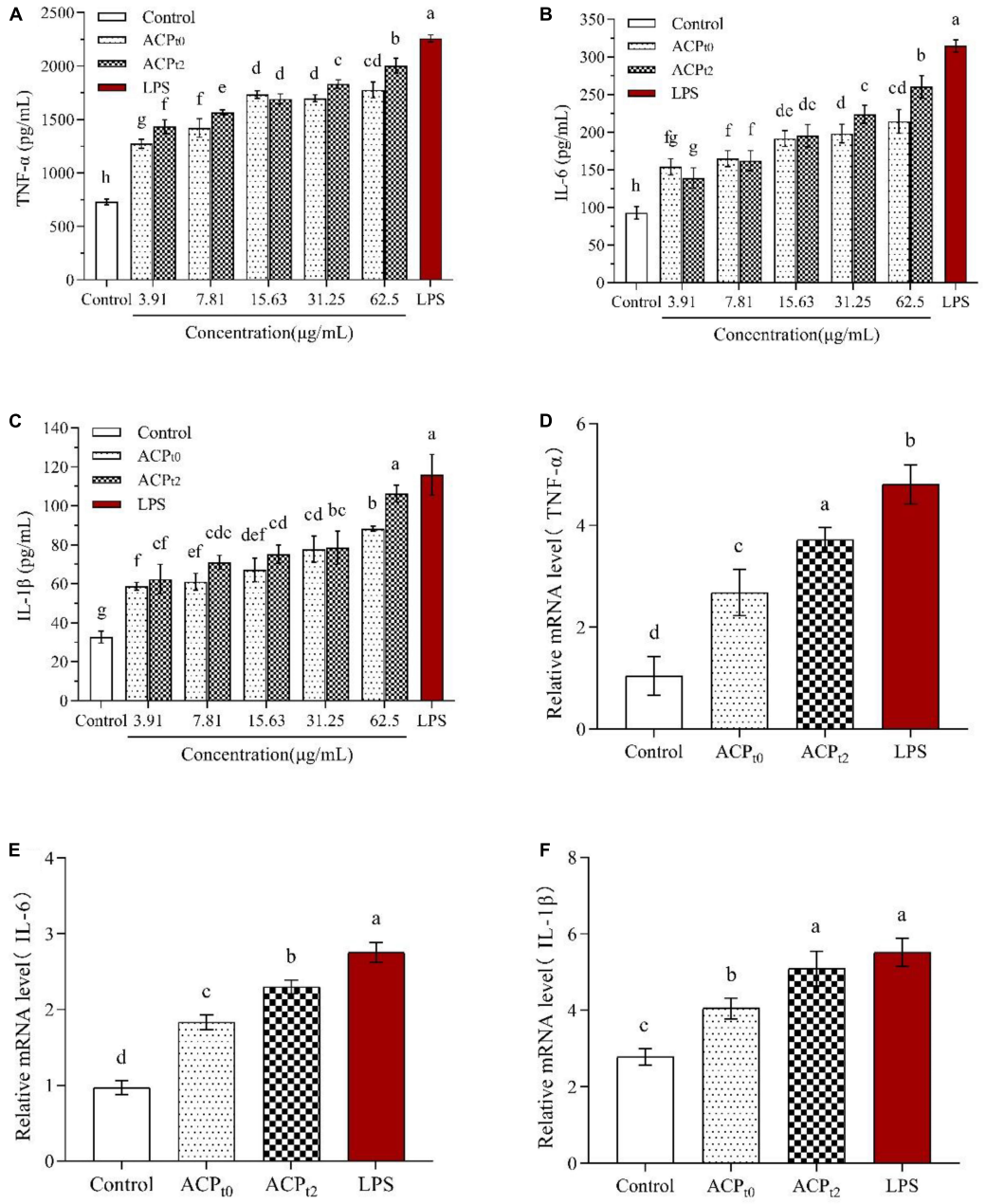

FIGURE 7
Effects of ACP_{t0} and ACP_{t2} on secretion of TNF-α **(A)**, IL-6 **(B)**, and IL-1β **(C)**, relative mRNA expression levels of TNF-α **(D)**, IL-6 **(E)**, and IL-1β **(F)** in macrophages. The different letters in the column indicate statistically significant differences ($P < 0.05$).

ACP_{t2} distinctly enhanced the expression levels of TNF-α, IL-6 and IL-1β at 62.5 μg/mL ($P < 0.05$). Except for the mRNA level of IL-1β in the ACP_{t2} group, the LPS group was significantly higher than that in ACP_{t0} and ACP_{t2} groups ($P < 0.05$). The results indicated that cytokine production was positively correlated with the expression of related genes, and ACP_{t0} and ACP_{t2} could upregulate cytokine secretion and related mRNA expression in macrophages.

Abrus cantoniensis polysaccharides activated signaling pathway of macrophages

The expression of TLR2, TLR4, MyD88, MAPK, and AKT in macrophages was detected by qRT-PCR to determine the regulatory role of ACP_{t0} and ACP_{t2} on macrophage-related genes. As shown in Figure 8, ACP_{t0}, ACP_{t2} and LPS groups remarkably upregulated the levels of TLR4 compared to the blank control group ($P < 0.05$), while there was no effect

10.3389/fnut.2022.969512

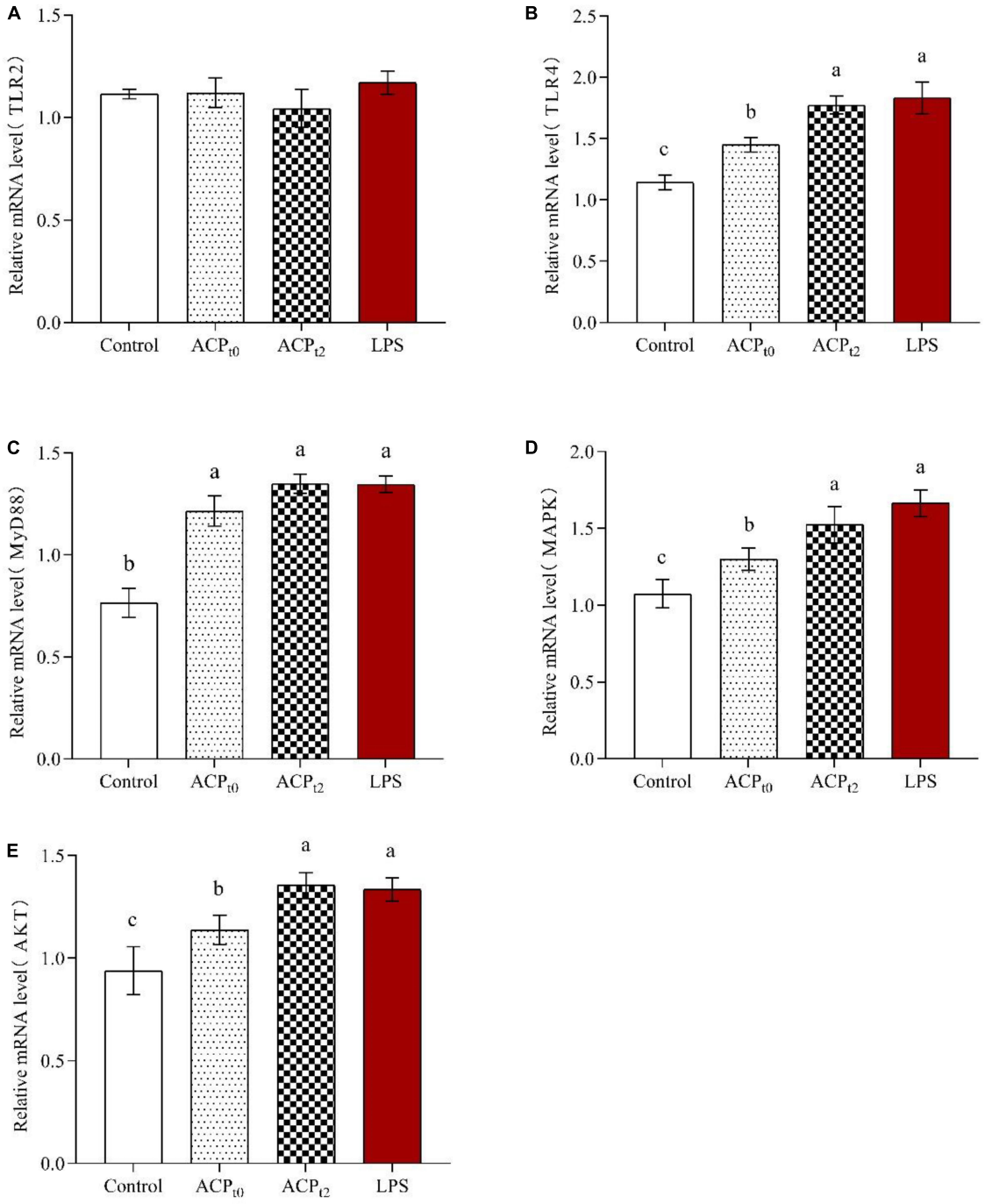

FIGURE 8
Effects of ACP_{t0} and ACP_{t2} on relative mRNA expression levels of TLR2 **(A)**, TLR4 **(B)**, MyD88 **(C)**, MAPK **(D)**, and AKT **(E)** in macrophages. The different letters in the column indicate statistically significant differences ($P < 0.05$).

on the expression of TLR2, suggesting that TLR4 were the major pattern recognition receptors of ACP in macrophages. Meanwhile, the stimulation of LPS, ACP_{t0} and ACP_{t2} resulted in a significant increase in the expression levels of MyD88, MAPK and AKT ($P < 0.05$). These results showed that ACP_{t0} and ACP_{t2} can activate macrophages by recognizing TLR4 to regulate key genes on the MyD88/Akt/MAPKs pathway, thereby enhancing the immune response of mouse macrophages.

Discussion

In this study, the physicochemical properties and immunomodulatory activities of two novel polysaccharides (ACP_{t0} and ACP_{t2}) from *Abrus cantoniensis* were determined. The results showed that ACP_{t0} and ACP_{t2} possessed excellent immunomodulatory activities.

Reactive oxygen species (ROS) are directly or indirectly transformed by oxygen radicals and their derivatives. As the second messenger in many signaling pathways, ROS, especially endogenous ROS, could regulate major molecular signaling pathways, such as MAPK pathway and mitochondria-mediated casepase apoptosis pathway, thus affecting the body's differentiation, metabolism, cell proliferation, cell death and other important cellular activities (36). When inflammation occurs, macrophages and neutrophils are immediately activated, leading to the strengthening of respiration in the body, increasing oxygen consumption and producing ROS, which can participate in the synthesis of a series of inflammatory factors and enhance the phagocytosis ability of macrophages to kill bacteria and other foreign substances (37). Therefore, ROS can be used as a valid biomarker to reflect the immunomodulatory effect of ACP on macrophages. In this study, different concentrations of ACP_{t0} and ACP_{t2} can significantly increase the level of ROS in macrophages, which indicated that ACP could modestly modulated the immune activity of macrophages. Huo reported that polysaccharides (HSP-3) extracted from *Huangshui* can also remarkably stimulate ROS secretion in THP-1 cells (38).

Pinocytic and phagocytic capacities, as the fundamental defense mechanisms of macrophages, act an extremely key role in the defense response to pathogens and in maintaining homeostasis in the body. Therefore, pinocytic and phagocytic capacities can directly reflect the activity of macrophages and is a significant index to evaluate the immune function of the body (39). To investigate the effects of ACP_{t0} and ACP_{t2} on macrophages, pinocytic activity was quantitatively determined by the uptake of neutral red test, and the phagocytosis was visualized by FITC-labeled *E. coli* in fluorescence microscopy. In the present study we found that ACP_{t0} and ACP_{t2} could enhance the pinocytic and phagocytic capacities of macrophages. Besides, other plant polysaccharides, such as *Pueraria lobata Ohwi* polysaccharides (Ge-1) (12) and *Paeonia suffruticosa Andr* polysaccharides (PSAP) (40), can also significantly promote the phagocytosis of neutral red and FITC-labeled *E. coli* by macrophages.

Activated macrophages are able to secrete a range of chemokines and cytokines. NO as a signaling molecule of physiological changes, plays a vital role in cytotoxicity, immune regulation and intracellular bactericidal function of macrophages (41). iNOS can catalyze the conversion of L-arginine to NO in activated macrophages. Many studies show that plant polysaccharides can activate macrophages and enhance the NO level and iNOS activity of macrophages. The polysaccharide isolated from *Huangshui* could increase the level of NO and an acidic polysaccharide from *Citrus grandis* could promote iNOS expression in macrophages (38, 42). In this study, after treatment with ACP_{t0} and ACP_{t2}, the NO secretion and iNOS activity of macrophages enhance markedly.

Cytokines are produced by immune cells stimulated by antigens or mitogens (43). TNF-α, as an immunomodulatory factor, can not only activate immune regulation and mediate inflammatory reactions, but also induce expressions of chemokines on macrophages and neutrophils, enhance cell trafficking. Moreover, TNF-α can enhance phagocytic effects of macrophages to kill exogenous pathogens or inhibit tumor cells (44). IL-6 is a pleiotropic cytokine, which can transmit messages between immune cells and participate in the body's immune defense. IL-1β is involved in a variety of autoimmune inflammatory and immune responses and can stimulate the secretion of IL-6 (45). The rise expression of TNF-α, IL-6 and IL-1β in ACP_{t0} and ACP_{t2} groups was observed in our study, which means the macrophages got activated. Meanwhile, there was a similar trend in the mRNA expression of cytokines. The results indicated that ACP_{t0} and ACP_{t2} can promote the secretion of TNF-α, IL-6 and IL-1β by regulating the mRNA expression of cytokines.

Polysaccharides as macromolecules cannot cross the cell membrane directly. Studies have shown that polysaccharides can first recognize Toll-like receptors (TLRs) on the surface of macrophages, activating various intracellular signaling pathways, causing a series of signal cascade reactions and regulating the expression of related genes (46, 47). Previous studies have shown that TLR4, a classical endotoxin receptor, recognizes a variety of natural polysaccharides (48–50). Pu et al. found that *Solanum nigrum Linne* polysaccharide (SNLP) upregulated gene expression at important nodes in the TLR4-MyD88 signaling pathway, leading to changes of cytokines (TNF-α and IL-6), exerting immune effect (51). There are key genes in the intracellular signaling pathway, such as MyD88, Akt and MAPKs. MyD88 is an important bridging protein in the signaling pathway of TLRs and mainly mediates the expression and secretion of inflammatory cytokines in immune cells. The Akt signaling pathway can be involved in regulating cell proliferation and apoptosis processes. In addition, MAPKs signaling pathway is able to phosphorylate related cytoplasmic proteins, which can activate a variety of related transcription factors in the nucleus and phosphorylate them to promote cell proliferation (52). The expression of TLR4, MyD88, MAPK and AKT of macrophages in ACP_{t0} and ACP_{t2} groups increased, suggesting that ACP can activate macrophages by recognizing TLR4 on the macrophage surface, which in turn regulates key genes in the MyD88/Akt/MAPKs signaling pathway, thereby enhancing the immune response of mouse macrophages.

Conclusion

Two polysaccharide fractions (ACP_{t0} and ACP_{t2}) with average molecular weight of 26.0 kDa and 145.6/8.9 kDa were purified from *Abrus cantoniensis*. Then the physicochemical properties and immunomodulatory activities of ACP_{t0} and ACP_{t2} were investigated and compared. ACP_{t0} and ACP_{t2} possessed significant immunomodulatory activity *in vitro* in terms of elevating the proliferation, enhancing the pinocytic and phagocytic capacity and increasing the secretion of ROS, NO and iNOS in macrophage. Meanwhile, two polysaccharides promoted the secretion of cytokines (TNF-α, IL-6 and IL-1β) by activating the corresponding mRNA expression in macrophage. Besides, TLR4 was identified as the main membrane receptors, and the immunomodulatory activity of ACP on macrophage was mainly through MyD88/AKT/MAPKs signaling pathways. In addition, immunomodulatory activities of ACP_{t2} were stronger than that of ACP_{t0}. These findings suggested ACP_{t0} and ACP_{t2} can be a potential immunostimulator for application in functional foods and pharmaceutical fields.

Data availability statement

The raw data supporting the conclusions of this article will be made available by the authors, without undue reservation.

Author contributions

HS initiated the project and supervised and conducted the experimental work. DQ and WS were responsible for designing experimental ideas, data analysis, protocol designing, and draft editing. SL and HH conducted the experimental work and processed the data. All authors contributed to the article and approved the submitted version.

Funding

This project was funded by the Research Initiation Project for High-level Talents of Yulin Normal University (G2022ZK05), TCM Industrial Pioneers (GuiNongKeMeng202211), the Key Research and Development Plan of Guangxi (AB19245037), and the National Natural Science Foundation of China (31760746).

Acknowledgments

We are grateful to all other staff in the Laboratory of Traditional Chinese Veterinary Medicine of Guangxi University for their assistance in the experiments.

Conflict of interest

DQ was employed by the DanAg Agritech Consulting (Zhengzhou) Co.

The remaining authors declare that the research was conducted in the absence of any commercial or financial relationships that could be construed as a potential conflict of interest.

Publisher's note

All claims expressed in this article are solely those of the authors and do not necessarily represent those of their affiliated organizations, or those of the publisher, the editors and the reviewers. Any product that may be evaluated in this article, or claim that may be made by its manufacturer, is not guaranteed or endorsed by the publisher.

References

1. Zhao Y, Yan Y, Zhou W, Chen D, Huang K, Yu S, et al. Effects of polysaccharides from bee collected pollen of Chinese wolfberry on immune response and gut microbiota composition in cyclophosphamide-treated mice. *J Funct Foods.* (2020) 72:104057. doi: 10.1016/j.jff.2020.104057

2. Zhu B, Qian C, Zhou F, Guo J, Chen N, Gao C, et al. Antipyretic and antitumor effects of a purified polysaccharide from aerial parts of *Tetrastigma hemsleyanum*. *J Ethnopharmacol.* (2020) 253:112663. doi: 10.1016/j.jep.2020.112663

3. Zhou W, Zhao Y, Yan Y, Mi J, Lu L, Luo Q, et al. Antioxidant and immunomodulatory activities in vitro of polysaccharides from bee collected pollen of Chinese wolfberry. *Int J Biol Macromol.* (2020) 163:190–9. doi: 10.1016/j.ijbiomac.2020.06.244

4. Cao P, Wu S, Wu T, Deng Y, Zhang Q, Wang K, et al. The important role of polysaccharides from a traditional Chinese medicine-lung cleansing and detoxifying decoction against the COVID-19 pandemic. *Carbohydr Polym.* (2020) 240:116346. doi: 10.1016/j.carbpol.2020.116346

5. Guo WL, Chen M, Pan WL, Zhang Q, Xu JX, Lin YC, et al. Hypoglycemic and hypolipidemic mechanism of organic chromium derived from chelation of *Grifola frondosa* polysaccharide-chromium (III) and its modulation of intestinal microflora in high fat-diet and STZ-induced diabetic mice. *Int J Biol Macromol.* (2020) 145:1208–18. doi: 10.1016/j.ijbiomac.2019.09.206

6. Ji X, Hou C, Shi M, Yan Y, Liu Y. An insight into the research concerning *Panax ginseng* C. A. Meyer polysaccharides: a review. *Food Rev Int.* (2022) 38:1149–65. doi: 10.1080/87559129.2020.1771363

7. Hou C, Yin M, Lan P, Wang H, Nie H, Ji X. Recent progress in the research of *Angelica sinensis* (Oliv.) Diels polysaccharides: extraction, purification, structure and bioactivities. *Chem Biol Technol Agric.* (2021) 8:13. doi: 10.1186/s40538-021-00214-x

8. Wan X, Yin Y, Zhou C, Hou L, Cui Q, Zhang X, et al. Polysaccharides derived from Chinese medicinal herbs: a promising choice of vaccine adjuvants. *Carbohydr Polym.* (2022) 276:118739. doi: 10.1016/j.carbpol.2021.118739

9. Ji X, Peng B, Ding H, Cui B, Nie H, Yan Y. Purification, structure and biological activity of pumpkin polysaccharides: a review. *Food Rev Int.* (2021). doi: 10.1080/87559129.2021.1904973 [Epub ahead of print].

10. Erturk-Hasdemir D, Oh SF, Okan NA, Stefanetti G, Gazzaniga FS, Seeberger PH, et al. Symbionts exploit complex signaling to educate the immune system. *Proc Natl Acad Sci U.S.A.* (2019) 116:26157–66. doi: 10.1073/pnas.1915978116

11. Zhao Y, Zou W, Du J, Zhao Y. The origins and homeostasis of monocytes and tissue-resident macrophages in physiological situation. *J Cell Physiol.* (2018) 233:6425–39. doi: 10.1002/jcp.26461

12. Dong Z, Zhang M, Li H, Zhan Q, Lai F, Wu H. Structural characterization and immunomodulatory activity of a novel polysaccharide from *Pueraria lobata* (Willd.) Ohwi root. *Int J Biol Macromol.* (2020) 154:1556–64. doi: 10.1016/j.ijbiomac.2019.11.040

13. Cheng X, Wu Q, Zhao J, Su T, Lu Y, Zhang W, et al. Immunomodulatory effect of a polysaccharide fraction on RAW 264.7 macrophages extracted from the wild *Lactarius deliciosus*. *Int J Biol Macromol.* (2019) 128:732–9. doi: 10.1016/j.ijbiomac.2019.01.201

14. Xu Z, Lin R, Hou X, Wu J, Zhao W, Ma H, et al. Immunomodulatory mechanism of a purified polysaccharide isolated from *Isaria cicadae* Miquel on RAW264.7 cells via activating TLR4-MAPK-NF-κB signaling pathway. *Int J Biol Macromol.* (2020) 164:4329–38. doi: 10.1016/j.ijbiomac.2020.09.035

15. Shin M, Park SB, Shin K. Molecular mechanisms of immunomodulatory activity by polysaccharide isolated from the peels of *Citrus unshiu*. *Int J Biol Macromol.* (2018) 112:576–83. doi: 10.1016/j.ijbiomac.2018.02.006

16. Yang D, Lin F, Huang Y, Ye J, Xiao M. Separation, purification, structural analysis and immune-enhancing activity of sulfated polysaccharide isolated from sea cucumber viscera. *Int J Biol Macromol.* (2020) 155:1003–18. doi: 10.1016/j.ijbiomac.2019.11.064

17. Wu E, Sun W, Wang Y, Zhang G, Xu B, Chen X, et al. Optimization of ultrasonic-assisted extraction of total flavonoids from *Abrus cantoniensis* (Abriherba) by response surface methodology and evaluation of its anti-inflammatory effect. *Molecules.* (2022) 27:2036. doi: 10.3390/molecules27072036

18. Li H, Song ZJ, Dai YP, Zhang SL, He X, Guo CR, et al. Antioxidative activity of flavonoids from *Abrus cantoniensis* against ethanol-induced gastric ulcer in mice. *Planta Med.* (2015) 81:784–90. doi: 10.1055/s-0035-1546080

19. Chen M, Wang T, Jiang ZZ, Shan C, Wang H, Wu MJ, et al. Anti-inflammatory and hepatoprotective effects of total flavonoid C-glycosides from *Abrus mollis* extracts. *Chin J Nat Med.* (2014) 12:590–8. doi: 10.1016/S1875-5364(14)60090-X

20. Yao X, Li Z, Gong X, Fu X, Xiao X, He M, et al. Total saponins extracted from *Abrus cantoniensis* hance suppress hepatitis B virus replication in vitro and in rAAV8-1.3HBV transfected mice. *J Ethnopharmacol.* (2020) 249:112366. doi: 10.1016/j.jep.2019.112366

21. Qu D, Hu H, Lian S, Sun W, Si H. The protective effects of three polysaccharides from abrus cantoniensis against cyclophosphamide-induced immunosuppression and oxidative damage. *Front Vet Sci.* (2022) 9:870042. doi: 10.3389/fvets.2022.870042

22. Dubois M, Gilles K, Hamilton JK, Rebert PA, Smith F. A colorimetric method for the determination of sugars. *Nature.* (1951) 168:167.

23. Li J, Kisara K, Danielsson S, Lindström ME, Gellerstedt G. An improved methodology for the quantification of uronic acid units in xylans and other polysaccharides. *Carbohydr Res.* (2007) 342:1442–9. doi: 10.1016/j.carres.2007.03.031

24. Honda S, Akao E, Suzuki S, Okuda M, Kakehi K, Nakamura J. High-performance liquid chromatography of reducing carbohydrates as strongly ultraviolet-absorbing and electrochemically sensitive 1-phenyl-3-methyl-5-pyrazolone derivatives. *Anal Biochem.* (1989) 180:351–7. doi: 10.1016/0003-2697(89)90444-2

25. Ren Y, Zheng G, You L, Wen L, Li C, Fu X, et al. Structural characterization and macrophage immunomodulatory activity of a polysaccharide isolated from *Gracilaria lemaneiformis*. *J Funct Foods.* (2017) 33:286–96. doi: 10.1016/j.jff.2017.03.062

26. Guo M, Meng M, Zhao J, Wang X, Wang C. Immunomodulatory effects of the polysaccharide from *Craterellus cornucopioides* via activating the TLR4-NFκB signaling pathway in peritoneal macrophages of BALB/c mice. *Int J Biol Macromol.* (2020) 160:871–9. doi: 10.1016/j.ijbiomac.2020.05.270

27. Huang Z, Zeng Y, Chen X, Luo S, Pu L, Li F, et al. A novel polysaccharide from the roots of *Millettia speciosa* champ: preparation, structural characterization and immunomodulatory activity. *Int J Mol Sci.* (2020) 145:547–57. doi: 10.1016/j.ijbiomac.2019.12.166

28. Kumar CG, Mongolla P, Pombala S. Lasiosan, a new exopolysaccharide from *Lasiodiplodia* sp strain B2 (MTCC 6000): structural characterization and biological evaluation. *Process Biochem.* (2018) 72:162–9. doi: 10.1016/j.procbio.2018.06.014

29. Yang J, Tu J, Liu H, Wen L, Jiang Y, Yang B. Identification of an immunostimulatory polysaccharide in banana. *Food Chem.* (2019) 277:46–53. doi: 10.1016/j.foodchem.2018.10.043

30. Zhang B, Li Y, Zhang F, Linhardt RJ, Zeng G, Zhang A. Extraction, structure and bioactivities of the polysaccharides from *Pleurotus eryngii*: a review. *Int J Biol Macromol.* (2020) 150:1342–7. doi: 10.1016/j.ijbiomac.2019.10.144

31. Yuan Q, Zhang X, Ma M, Long T, Xiao C, Zhang J, et al. Immunoenhancing glucuronoxylomannan from *Tremella aurantialba* Bandoni et Zang and its low-molecular-weight fractions by radical depolymerization: properties, structures and effects on macrophages. *Carbohydr Polym.* (2020) 238:116184. doi: 10.1016/j.carbpol.2020.116184

32. Gao X, Qi J, Ho C, Li B, Mu J, Zhang Y, et al. Structural characterization and immunomodulatory activity of a water-soluble polysaccharide from *Ganoderma leucocontextum* fruiting bodies. *Carbohyd Polym.* (2020) 249:116874. doi: 10.1016/j.carbpol.2020.116874

33. Wu F, Huang H. Surface morphology and protective effect of *Hericium erinaceus* polysaccharide on cyclophosphamide-induced immunosuppression in mice. *Carbohydr Polym.* (2021) 251:116930. doi: 10.1016/j.carbpol.2020.116930

34. Wu S, Fu X, Brennan M, Brennan C, Chun C. The effects of different purifying methods on the chemical properties, in vitro anti-tumor and immunomodulatory activities of *Abrus cantoniensis* polysaccharide fractions. *Int J Mol Sci.* (2016) 17:511. doi: 10.3390/ijms17040511

35. Liao W, Luo Z, Liu D, Ning Z, Yang J, Ren J. Structure characterization of a novel polysaccharide from *Dictyophora indusiata* and its macrophage immunomodulatory activities. *J Agric Food Chem.* (2015) 63:535–44. doi: 10.1021/jf504677r

36. Ren D, Lin D, Alim A, Zheng Q, Yang X. Chemical characterization of a novel polysaccharide ASKP-1 from *Artemisia sphaerocephala* Krasch seed and its macrophage activation via MAPK, PI3k/Akt and NF-κB signaling pathways in RAW264.7 cells. *Food Funct.* (2017) 8:1299–312. doi: 10.1039/c6fo01699e

37. Cai H, Yang X, Cai Q, Ren B, Qiu H, Yao Z. *Lycium barbarum* L. polysaccharide (LBP) reduces glucose uptake via down-regulation of SGLT-1 in Caco2 cell. *Molecules.* (2017) 22:341. doi: 10.3390/molecules22020341

38. Huo J, Wu J, Zhao M, Sun W, Sun J, Li H, et al. Immunomodulatory activity of a novel polysaccharide extracted from Huangshui on THP-1 cells through NO production and increased IL-6 and TNF-α expression. *Food Chem.* (2020) 330:127257. doi: 10.1016/j.foodchem.2020.127257

39. Yin M, Zhang Y, Li H. Advances in research on immunoregulation of macrophages by plant polysaccharides. *Front Immunol.* (2019) 10:145. doi: 10.3389/fimmu.2019.00145

40. Ma L, Jiao K, Luo L, Xiang J, Fan J, Zhang X, et al. Characterization and macrophage immunomodulatory activity of two polysaccharides from the flowers of *Paeonia suffruticosa* Andr. *Int J Biol Macromol.* (2019) 124:955–62. doi: 10.1016/j.ijbiomac.2018.12.035

41. Zeng F, Chen W, He P, Zhan Q, Wang Q, Wu H, et al. Structural characterization of polysaccharides with potential antioxidant and immunomodulatory activities from Chinese water chestnut peels. *Carbohydr Polym.* (2020) 246:116551. doi: 10.1016/j.carbpol.2020.116551

42. Fan R, Zhu C, Qiu D, Mao G, Zeng J. Activation of RAW264.7 macrophages by an acidic polysaccharide derived from *Citrus grandis* 'tomentosa'. *Int J Biol Macromol.* (2020) 156:1323–9. doi: 10.1016/j.ijbiomac.2019.11.172

43. Li C, Dong Z, Zhang B, Huang Q, Liu G, Fu X. Structural characterization and immune enhancement activity of a novel polysaccharide from *Moringa oleifera* leaves. *Carbohydr Polym.* (2020) 234:115897. doi: 10.1016/j.carbpol.2020.115897

44. Cordeiro Caillot AR, Bezerra IDL, Gusmao Ferreira Palhares LC, Santana-Filho AP, Chavante SF, Sassaki GL. Structural characterization of blackberry wine

polysaccharides and immunomodulatory effects on LPS-activated RAW 264.7 macrophages. *Food Chem.* (2018) 257:143–9. doi: 10.1016/j.foodchem.2018.02.122

45. Sun Q, Li Y, Cui Y, Jiang S, Dong C, Du J. Structural characterization of three polysaccharides from the roots of *Codonopsis pilosula* and their immunomodulatory effects on RAW264.7 macrophages. *Int J Biol Macromol.* (2019) 130:556–63. doi: 10.1016/j.ijbiomac.2019.02.165

46. Yang Y, Zhao X, Li J, Jiang H, Shan X, Wang Y, et al. A beta-glucan from *Durvillaea antarctica* has immunomodulatory effects on RAW264.7 macrophages via toll-like receptor 4. *Carbohydr Polym.* (2018) 191:255–65. doi: 10.1016/j.carbpol.2018.03.019

47. Wu Y, Wang K, Zhao Z, Zhang P, Liu H, Zhou G, et al. A novel polysaccharide from *Dendrobium devonianum* serves as a TLR4 agonist for activating macrophages. *Int J Biol Macromol.* (2019) 133:564–74. doi: 10.1016/j.ijbiomac.2019.04.125

48. Li Q, Chen Z, Xu Z, Ha S, Hao H, Wu J, et al. Binding of the polysaccharide from *Acanthopanax giraldii* Harms to toll-like receptor 4 activates macrophages. *J Ethnopharmacol.* (2019) 241:112011. doi: 10.1016/j.jep.2019.112011

49. Zhao L, Li M, Sun K, Su S, Geng T, Sun H. Hippophae rhamnoides polysaccharides protect IPEC-J2 cells from LPS-induced inflammation, apoptosis and barrier dysfunction in vitro via inhibiting TLR4/NF-kappa B signaling pathway. *Int J Biol Macromol.* (2020) 155:1202–15. doi: 10.1016/j.ijbiomac.2019.11.088

50. Zhou L, Liu Z, Wang Z, Yu S, Long T, Zhou X, et al. *Astragalus* polysaccharides exerts immunomodulatory effects via TLR4-mediated MyD88-dependent signaling pathway in vitro and in vivo. *Sci Rep.* (2017) 7:44822. doi: 10.1038/srep44822

51. Pu Y, Liu Z, Zhong C, Zhang X, Bao Y. Immunomodulatory effects of a polysaccharide from *Solanum nigrum* linne through TLR4-MyD88 signaling pathway. *Int Immunopharmacol.* (2020) 88:106973. doi: 10.1016/j.intimp.2020.106973

52. Zhao X, Hou P, Xin H, Zhang Y, Zhou A, Lai C, et al. A glucogalactomanan polysaccharide isolated from *Agaricus bisporus* causes an inflammatory response via the ERK/MAPK and I kappa B/NF kappa B pathways in macrophages. *Int J Biol Macromol.* (2020) 151:1067–73. doi: 10.1016/j.ijbiomac.2019.10.148

frontiers | Frontiers in Nutrition

TYPE Original Research
PUBLISHED 31 August 2022
DOI 10.3389/fnut.2022.976552

Check for updates

OPEN ACCESS

EDITED BY
Xiaolong Ji,
Zhengzhou University of Light Industry, China

REVIEWED BY
Wenyi Kang,
Henan University, China
Cuina Wang,
Jilin University, China

*CORRESPONDENCE
Tingting Liu
liutingting@jlau.edu.cn

SPECIALTY SECTION
This article was submitted to Food Chemistry, a section of the journal Frontiers in Nutrition

RECEIVED 23 June 2022
ACCEPTED 25 July 2022
PUBLISHED 31 August 2022

CITATION
Zhang X, Liu T, Wang X, Zhou L, Qi J and An S (2022) Structural characterization, antioxidant activity and anti-inflammatory of the phosphorylated polysaccharide from *Pholiota nameko*. *Front. Nutr.* 9:976552. doi: 10.3389/fnut.2022.976552

COPYRIGHT
© 2022 Zhang, Liu, Wang, Zhou, Qi and An. This is an open-access article distributed under the terms of the Creative Commons Attribution License (CC BY). The use, distribution or reproduction in other forums is permitted, provided the original author(s) and the copyright owner(s) are credited and that the original publication in this journal is cited, in accordance with accepted academic practice. No use, distribution or reproduction is permitted which does not comply with these terms.

Structural characterization, antioxidant activity and anti-inflammatory of the phosphorylated polysaccharide from *Pholiota nameko*

Xu Zhang[1,2], Tingting Liu[1]*, Xi Wang[1], Lanying Zhou[2], Ji Qi[2] and Siyu An[2]

[1]College of Food Science and Engineering, Jilin Agricultural University, Changchun, China, [2]Jilin Province Product Quality Supervision and Inspection Institute, Changchun, China

In this study, a novel polysaccharide (SPN) was extracted by high-temperature pressure method and purified by a DEAE-52 column and a Sephadx G-100 gel column. PPN was obtained after phosphorylation of SPN. The differences of structural features, antioxidant activity, and anti-inflammatory effect of the two polysaccharides were investigated by chemical methods and RAW 264.7 cell model. SPN (Mw = 15.8 kDa) and PPN (Mw = 27.7 kDa) are an acidic polysaccharide with β-pyranose configuration, mainly containing rhamnose, mannose, glucose, arabinose, and galacose. FI-IR, NMR, and SEM spectra showed phosphorylation of SPN changed its structure. In methylation analysis, the major chains of SPN and PPN were 1,4-linked Glc*p*, 1,6-linked Gal*p*, 1,2-linked Rha*p*, and 1.6-linked Man*p* with terminals of t-linked Glc*p*, t-linked Ara*f*. The side chain of SPN was 1,4,6-linked Gal*p*, 1,2,5-linked Ara*f*, while the side chain of PPN was 1,4,6-linked Gal*p*, 1,2,4-linked Glc*p*. In antioxidant activity experiments, the free radical scavenging rate of PPN was stronger than that of SPN. Also, PPN always has better anti-inflammatory on RAW 264.7 cells induced by LPS than that of SPN in same concentration, and it plays an anti-inflammatory role by inhibiting PI3K/AKT/mTOR pathway. The results indicated polysaccharide could significantly improve its antioxidant and anti-inflammatory function after phosphorylation. This study provides a potentially antioxidant and anti-inflammatory health food and drug.

KEYWORDS

Pholiota nameko **polysaccharide, high-temperature pressurized extraction, structural characterization, anti-inflammatory, antioxidant**

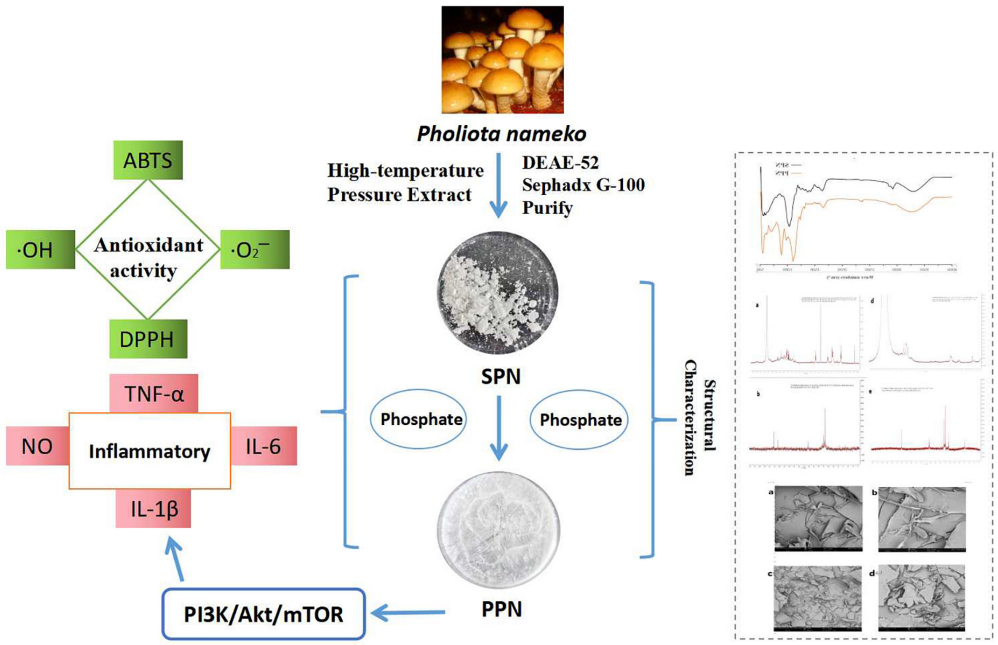

GRAPHICAL ABSTRACT
Structure and bioactivity of phosphorylated *pholiota nameko* polysaccharide.

Introduction

Inflammation is a normal immune defense mechanism of the body, but it is a double-edged sword. The short-term clearance of inflammatory by the defense system can promote the recovery of the body. However, the long-term inflammatory defense could lead to tissue organs damage, causing anaphylactic reactions, or even disease (1). When immune response is stimulated by pathogens, the macrophages secret proinflammatory cytokine (2). Excessive production of inflammatory cytokines could lead to fever, asthma, arthritis, and even cancer (3). Free radicals widely exist in the human body and are important factors in regulating cellular signaling pathways and maintaining body balance (4). Oxidative stress is caused by excessive free radicals, leading to cardiovascular disease (5), inflammatory (6), immunomodulatory (7), hypertension, and even tumor (8).

Edible fungi are mushrooms with edible fruit body and have a long research history in China (9). *Pholiota nameko,* one kind of edible fungi, belongs to genius *Lepidoptera* (Cortinariaceae). It originated in Japan and has distributed in many provinces of China (10). This kind of mushroom can be easily cultivated and is regarded as a healthy food with higher carbohydrate and lower fat. Polysaccharides extracted from edible fungi are normally biological compounds which have functions of anticancer (11), anti-inflammatory (12), antioxidant (13), hypoglycemic (14), intestinal regulation (15), and immunization (16, 17). The chemical composition, structural characteristics, and biological activity of polysaccharides are affected by different extraction methods (18). High-temperature pressure method is a green extraction method with few solvents and low energy consumption. It uses high temperature and high pressure to increase the solubility of target compounds and solvent diffusion rate. Studies have shown that the extraction rate of polysaccharide by high-temperature pressure method was higher than that by microwave, ultrasonic, and hot water extraction methods (19, 20). Lee et al. (21) have shown that polysaccharide with higher molecular weight have better anti-cancer effects. Therefore, the high temperature and pressure method is an effective green extraction method to improve the extraction rate and biological activity of polysaccharide. Moreover, in order to enhance biological function of natural polysaccharides, some methods are used to modify their structure (22). There exist several ways for structure modification, such as chemical methods, physical methods, and biological methods. Among these methods, chemical methods are the most widely adoption (23). Chemical modification can improve or change biological functions of polysaccharides mainly through changing molecular weight and type, position and number of substituents in structure of polysaccharides (24). The principal methods of chemical modification are complexation with metal ions, sulfation, sulfonylation, acetylation, alkylation, selenization, carboxymethylation, phosphorylation, and benzoylation. Phosphorylation of polysaccharides is modified by introducing phosphate ester bonds into structure of polysaccharide (25).

Since phosphate has three negative charges, it can affect certain activities of polysaccharides, like antioxidant activity, anticancer activity by enhancing their electronegativity (26, 27). However, few researches have investigated structures and functions of polysaccharides from fruit body of *P. nameko* and phosphorylated modification of these polysaccharides.

In this study, a novel polysaccharide was extracted from dried body of *P. nameko* and purified by a DEAE-52 column and a Sephadx G-100 gel column. Its structure features, antioxidant activity, and anti-inflammatory effects were determined by chemical methods and RAW267.4 cells. Also, structural and functional comparison between this novel polysaccharide and its phosphorylated polysaccharide were investigated. This study could provide theoretical bases in further researches about a potential anti-inflammatory and antioxidant activity from phosphorylated mushroom polysaccharide.

Materials and methods

Materials and reagents

Pholiota nameko was cultivated in Panshi City, Jilin Province, China, and purchased from the Zhongdong Market in Changchun City, Jilin Province, China. DEAE-52 cellulose was bought from Solarbio Science and Technology Co., Ltd. (Beijing, China) and Sephadex G-100 was purchased from Shanghai Yuanye Biotechnology Co., (Shanghai, China). LPS and standard monosaccharides (rhamnose, mannose, glucose, xylose, galactose, and arabinose) were acquired from Sigma Chemical Co. All other chemical reagents were analytical grade from Beijing Chemical Works.

Polysaccharides preparation

Extraction of crude polysaccharide

According to High-temperature pressurized extraction (28), 100 g dried mushroom mixed with 900-mL distilled water for 12 h at room temperature (25°C). An autoclave (U1000, Xinyi CO., Shanghai, China) was used for extraction of crude polysaccharide (CPN) from the mixture at 110°C, 1.2 MPa for 30 min. After centrifugation, concentration, and deproteinization (Savge method), solution of CPN was obtained. Adding four times ethanol into the solution to stand for 10 h at 4°C then centrifugating at 4,500 rpm for 10 min and lyophilizating for 24 h, crude polysaccharide was obtained.

Isolation and purification of novel polysaccharide

The method was determined by Zhou et al. (29) with slight modification. A DEAE-52 column (2.6 × 40 cm) and a Sephadx G-100 gel column (1.6 × 40 cm) were used for separation and purification (30). Briefly, 1 g CPN was dissolved in deionized water (1:20, *w/v*), centrifuged at 4,500 rpm for 10 min. Then, the supernatant was loaded in a DEAE-52 column, flowed with different concentrations of NaCl solution at 1.0 mL/min. The effluents were collected and measured by phenol sulfuric acid method. The main fractions are showed in **Figure 1A**. For purification, each fraction was subsequently injected in a Sephadx G-100 gel column, eluted by deionized water at 0.5 mL/min. The fraction of the most symmetrical eluting peak was collected (**Figure 1B**). After concentration, dialyzation, and lyophillation, the purified polysaccharide (SPN) was obtained for further study.

Phosphorylation and degree of substitution of phosphorylated polysaccharide

Phosphorylation of SPN was based on method of Xiong et al. (31). Three gram sodium triphosphate and 1 g sodium trimetaphosphate were dissolved in 100-mL distilled water. Then, 500 mg SPN and 2.5 g sodium sulfate was added into this solution. After adjusting pH to 8.5 by NaOH (5 mol/L), the solution was placed at a water bath (80°C) and then dialyzed for 48 h in a dialysis bag (MwCO 8,000–14,000 Da). Adding four times ethanol into this solution for 12 h at 4°C then centrifugating at 4,500 rpm for 10 min and lyophilizating for 24 h, phosphorylated polysaccharide (PPN) was obtained. The degree of substitution is calculated by following formula (32):

$$DS = \frac{5.23P}{100 - 3.32P} \quad (1)$$

P, percentage of phosphorus element; DS, degree of phosphate substitution.

Chemical analysis

The total sugar content of SPN and PPN were measured by phenol-sulfuric acid method (33). The Bradford method was used to measure the protein content of SPN and PPN (34). The uronic acid content of SPN and PPN was determined by the sulfuric acidcarbazole method (35).

The functional groups of SPN and PPN powders in KBr pellets were analyzed by a RESTIGE-21 IR spectrometer (Shimadzu, Japan) at range of 4,000–400 cm^{-1}.

The homogeneity and molecular weights of SPN and PPN were determined by Ultrahydrogel 2000 (12 μm, 7.8 mm × 300 mm) series Ultrahydrogel 500 (10 μm, 7.8 mm × 300 mm), using an alliance 2,695 gel permeation chromatography (Waters, Singapore).

Monosaccharide composition of SPN and PNP was investigated using a UltiMate 3000 high-performance liquid chromatography equipped with photo-diode-array-detector (Thermo, Germany) according to Yang et al. (36).

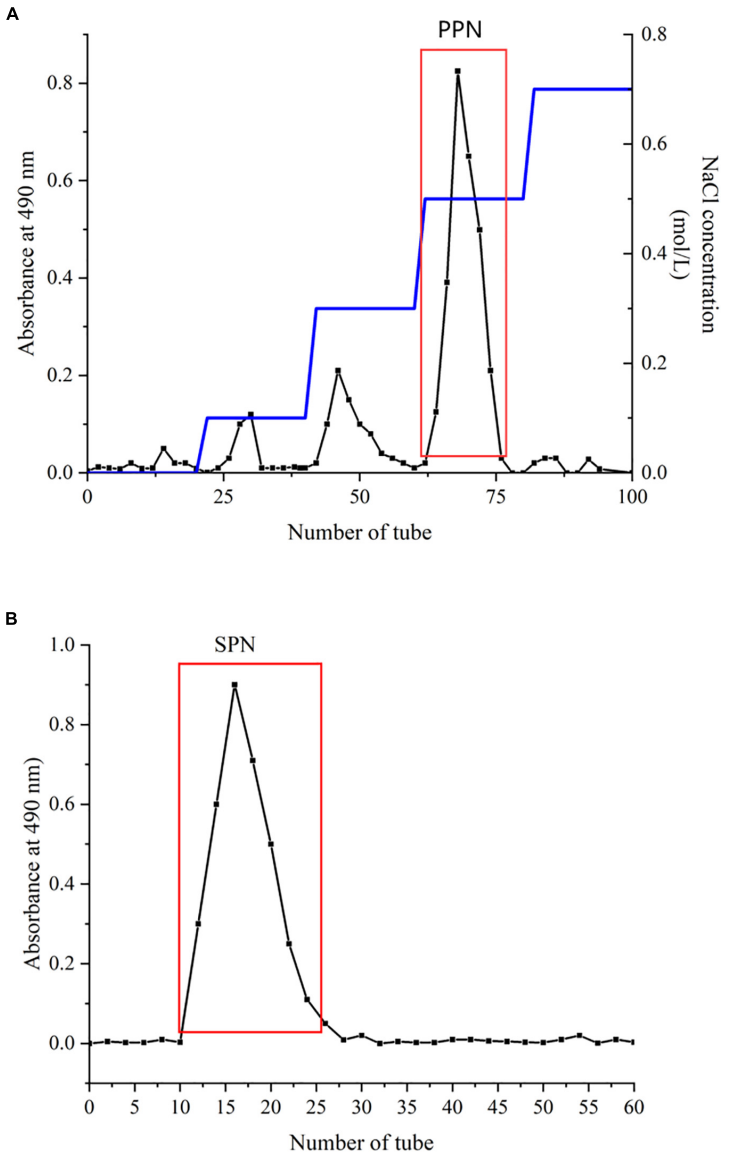

FIGURE 1
Chromatography of SPN on DEAE-52 **(A)** and Sephadex G-100 **(B)**.

Methylation analysis

A method reported by Ji et al. (37) was used for methylation analysis of SPN and PPN with modification. In brief, 5 mg of sample was dissolved in 1-mL distilled water, then the solution was added 200 μL of 0.2 mol/L MES [2-(4-Morpholino) ethanesulfonic] solution and 400 μL of 0.5 mg/L carbodiimide solution. After reaction for 3 h at 25–30°C, 1 mL of 4 mol/L imidazole-HCL solution and 600 μL of 70 μg/L $NaBD_4$ was added into the solution for overnight reaction at 4°C. Afterward, 500 μL ethylic acid was used to stop the reaction. Then, the reduced sample was obtained after dialysis (MWCO 3,500 Da) and lyophilization.

After reduction, 5 mg sample dissolved in 0.5 ml of NaOH/DMSO and methylated with 1 mL CH_3I. After two times of methylation, the OH absorption band around 3,400 cm^{-1} was disappeared determined the methylation was completed. The methylated sample was added with 1 mL trifluoroacetics acid (2 mol/L) at 120°C for 3 h. After removing the trifluoroacetic acid by absolute ethanol, methylated sample was reduced by sodium borohydride (30 μg/L) at room temperature for 12 h. Later, this sample was acetylated by pyridine and acetic anhydride and dissolved in dichloromethane for GC-MS analysis. The methylation result was determined by GC-MS (7890B-5977 Agilent, United States) equipped with a column of Agilent DB-35 ms (30 m × 0.25 mm × 0.25 μm) and an ion trap

MS detector. Its temperature program was as follows: 140°C for 1 min; raised to 170°C at a rate of 10°C/min, maintained 2 min; raised to 180°C at a rate of 2°C/min, maintained 3 min; raised to 220°C at a rate of 4°C /min, maintained 1 min; raised to 280°C at a rate of 20°C /min, maintained 5 min. Helium (0.8 mL/min) was used as the carrier gas.

Nuclear magnetic resonance spectroscopy

^{1}H, ^{31}P, and ^{13}C NMR spectra of the SPN and PPN were recorded on an Avance-600 NMR spectrometer (Bruker, United States).

Scanning electron microscope analysis

SPN and PPN were gold-plated and observed by a SEE-550 SEM (Shimadzu, Japan) with accelerating voltage of 5 kV and amplification of 1,000× and 5,000×.

Assay of antioxidant activity

Assay of DPPH radical scavenging

DPPH (1,1-diphenyl-2-picrylhydrazyl) radical scavenging of SPN and PPN was based on method of Ji et al. (38). The reaction solution composed of 0.5 mL sample solution with different concentrations and 2.0 mL of 0.2 mol/L DPPH solution. The mixture reacted in a dark room at 30°C for 30 min and the absorbance was surveyed at 517 nm. Vitamin C (Vc) was used as a positive control. The equation for calculating radical removal activity was as following:

$$\text{DPPH scavenging rates (\%)} = \frac{\text{Do} - \text{Di}}{\text{Do}} \times 100\% \quad (2)$$

where Do was the blank solution absorbance (distilled water instead of the sample), Di was the sample solution absorbance.

Assay of ABTS radical scavenging

ABTS [2,2′-Azinobis-(3-ethylbenzthiazoline-6-sulphonate)] radical removal rate was determined as previously reported methods with minor modifications (39). The ABTS premix prepared from 10 mL of 2.4 mmol/L ABTS and 10 mL of 7 mmol/L potassium persulfate was kept in dark room for 12 h. The ABTS reaction solution was prepared by diluting the premixed solution with water to the absorbance of 0.700 ± 0.02 at 734 nm. 3 mL sample solution and 3 mL ABTS reaction solution were mixed and retained in a dark room for 10 min. The absorbance was analyzed at 517 nm. Vc was used as a positive control. The equation for calculating radical removal activity was as following:

$$\text{ABTS scavenging rates (\%)} = \frac{\text{Ao} - \text{Ai}}{\text{Ao}} \times 100\% \quad (3)$$

where Ao was the blank solution absorbance (distilled water instead of the sample), Ai was the sample solution absorbance.

Assay of hydroxyl radical scavenging

For hydroxyl radical scavenging assay, 1 mg of sample solution added with 1 mL of 9 mol/L $FeSO_4$, 1 mL of 9 mmol/L salicylic acid, and 1 mL of 6 mmol/L H_2O_2, and reacted at 37°C for 30 min. The absorbance of the sample solution was determined at 510 nm. Vc was used as a positive control. The equation for calculating radical removal activity was as following:

$$\text{Hydroxyl scavenging rates (\%)} = \frac{\text{Ao} - \text{As}}{\text{Ao}} \times 100\% \quad (4)$$

where Ao was the blank solution absorbance (distilled water instead of the sample), As was the sample solution absorbance.

Assay of superoxide anion radical scavenging

For superoxide anion radical scavenging assay, the 0.5 mL sample solution added to 2.5 mL of 50 mmol/L Tris-HCl buffer (pH 8.2) and incubated at 30°C for 30 min. After 0.5 mL of 5 mmol/L pyrogallol was added to the incubated solution, the mixture was shaken quickly, and the absorbance of the reaction solution was determined at 325 nm. Vc was used as a positive control. The equation for calculating radical removal activity was as following:

$$\text{Superoxide anion scavenging rates (\%)} = \frac{\text{Uo} - \text{Uc}}{\text{Uo}} \times 100\% \quad (5)$$

where Uo was the blank solution absorbance (Tris-HCl buffer instead of the sample), Uc was the sample solution absorbance.

Assay for inflammatory effect on RAW 264.7 cells

Cell culture

The RAW 264.7 cells from mice were purchased by ATCC. The cells were cultured in a H-DMEM medium (Hyclone, United States) with 10% FBS (Biological Industries, Israel) and 1% penicillin-streptomycin at an 37℃ incubator with humidified atmosphere of 5% CO_2. RAW 264.7 cells of 3–15 passages were used in this study.

Cell viability analysis

A method reported by Zhuang et al. (40) was used for cell viability analysis with modification. Cell Counting Kit-8

(CCK-8, Bioss Co., Beijing, China) was used to evaluate the cell viability. Briefly, RAW 264.7 cells were cultured in 96-well plates with a density of 5×10^3 cells/mL at a 37°C incubator with humidified 5% CO_2 atmosphere for 4 h. Then, the cells were treated with different concentrations of SPN (50, 100, 200, 300 μg/mL) and PPN (50, 100, 200, 300 μg/mL) for 24 h. After that, 10 μL of CCK-8 solution was added and these cells were incubated at the same conditions for 2 h. The cell viability was determined by a multifunctional enzyme marker (Thermo Fisher, United States) at a wavelength of 450 nm and was expressed as a relative percentage to the blank control group.

NO concentration analysis

The 1.5×10^5 cells/mL of RAW 264.7 cells were cultured in a 96-well plate at 37°C and 5% CO_2 incubator for 24 h, then treated with 100 μL of 1 μg/mL LPS or 100 μL of different concentrations of SPN (100, 200, 300 μg/mL) + LPS and PPN (100, 200, 300 μg/mL) + LPS for 24 h. NO concentration was measured by Griess Reagent method. 100 μL supernate of every well was added with 50 μL sulfanilamide solution (100 g/L) and 50 μL amines-phosphoric acid solution (0.1 g amines dissolved in 10 mL 5% phosphoric acid solution). The absorbance was measured by a multifunctional microplate (Thermo Fisher, United States) reader at wavelength of 540 nm. 1 μg/mL LPS was used as positive control.

Assay of TNF-α, IL-1β, and IL-6 levels

RAW 264.7 cells (1.5×10^5 cells/mL) were incubated in 96-well plate for 24 h. Afterwards, the cells were treated with 1 μg/mL LPS or different concentrations of SPN (100, 200, 300 μg/mL) + LPS and PPN (100, 200, 300 μg/mL) + LPS for 24 h. The TNF-α, IL-1β, and IL-6 levels were measured by related ELISA kits (MultiSciences Co., China). 1 μg/mL LPS was used for positive control.

Assay of mRNA expression levels

The mRNA expression levels were determined by quantitative RT-PCR according to the method of Sun et al. (41). Briefly, RAW 264.7 cells were treated were treated with 1 μg/mL LPS or different concentrations of PPN (100, 200, 300 μg/mL) + LPS for 24 h. And the treated cells were collected for total RNA extraction. cDNA was synthesized by transcription kit (TaKaRa Co., China). The expression levels of PI3K, Akt, and mTOR were analyzed by a quantitative real-time PCR instrument (Roche, Swiss). The mRNA expression levels were calculated by $2^{-\Delta\Delta CT}$ method with β-actin as internal reference gene. The primer design sequences of real-time PCR are shown in **Table 1**.

Assay of protein expression levels

The RAW 264.7 cells were collected after treatment by polysaccharides. The cells were lysed by RIPA and the whole protein lysate was collected. And the protein concentration was determined using the BCA Protein Detection Kit (Solarbio Co., China). The loaded amount of the protein was 10 μg in each experiment. The protein was separated by SDS-PAGE and transferred to PVDF membrane. Then, PVDF membrane was blocked with TBST blocking solution for 1 h. The diluted primary antibody was incubated for 12h at 4°C. The diluted secondary antibody was incubated at room temperature for 1h. The protein expression levels of the p-PI3K, p-Akt, and p-mTOR were detected by gel Imager (Tianneng, China).

Data analysis

All the test data of this study were expressed as means ± SD (no fewer than triplicate determinations) and analyzed with variance (ANOVA) followed multiple tests. SPSS V22.0 was used to all statistical analysis and $p < 0.05$ was considered to be significant.

Results and discussion

Extraction and purification

SPN was extracted from dried mushrooms by high-temperature pressurized method and purified by a DEAE-52 column (2.6 × 40 cm) at mobile phase of 0.5 NaCl solution and a Sephadx G-100 gel column (1.6 × 40 cm) with ultrapure water. The yield of CPN was 41.2% relative to dried mushroom and the yield of SPN was 35.3% relative to CPN.

After phosphorylation of SPN, phosphorylated polysaccharide (PPN) was obtained. The DS of PPN was 0.52 which is similar with other phosphorylated polysaccharides as previous research reported (42).

Chemical analysis

From the phenol-sulfuric acid measurement, the sugar content of SPN and PPN were, respectively, 96.5 and 83.4%. The uronic acid of SPN was 21.3%, while the uronic acid of PPN was 24.7%. Also, their protein contents were separately 1.02 and 0.87%. After phosphorylation, the sugar content decreased, probably resulting from the loss during phosphorylation, which was similar to the results reported by previous researches (43).

In the FI-IR spectrum (**Figure 2**), the wide and big absorption peak around 3,400 cm^{-1} was the characteristic absorption peak of O-H which determined SPN and PPN were polysaccharides (44). Compared to SPN, after substitution of phosphate group, O-H absorption peak of PPN was weaker which indicated that intermolecular hydrogen bonding action

TABLE 1 The primer sequence of real-time PCR.

Primers	Forward	Reverse
β-actin	5′-CGTAGCTAGCTAGCTAGCTC-3′	5′-ACTAGCTAGCTAGTCGATCGTACG-3′
PI3K	5′-ATCGATCGATCGTAGCTAGCTCGA-3	5′-CGTACGTAGCTAGCTAGCTAGCTG-3′
Akt	5′-GTAGCTACTAGCTATCAGTCATCGT-3′	5′-CGTAGCTAGCTAGCTAGCTGATCGC-3′
mTOR	5′-AGTCGATCGTACGTAGCTGATGCT-3′	5′-CGTACTACGTACGATCGTGTACGA-3′

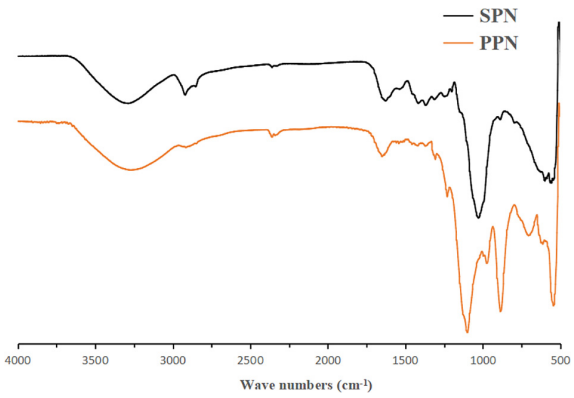

FIGURE 2
FT-IR spectra of SPN and PPN.

of PPN was weaker than that of SPN. The absorption peak between 1,400 and 1,200 cm^{-1} was variable angle vibration of C-H. However, in PPN spectrum, this absorption peak shifted from 1,361 to 1,305 cm^{-1} because of phosphorylation. The absorption peaks of SNP at 895, 1,025 cm^{-1}, and PPN at 895 cm, 1,023 cm^{-1} indicate that they are pyranose containing β configuration. The absorption peaks of SPN at 1,639, 1,423 cm^{-1} and PPN at 1,647, 1,417 cm^{-1} indicated that they were acidic polysaccharides, which was consistent with the determination of uronic acid (45). Also, the new absorption peak of 1,241 cm^{-1} was the asymmetrically stretching vibration of P = O (46) and the new peaks around 727 cm^{-1} attributed to C-O-P symmetrically stretching vibration compared to spectrum of SPN (47), but all peaks were not obvious because the lower degree substitution of phosphate group. FI-IR spectra showed phosphorylation of SPN changed its structure and probably would have effect on its biological function.

According to the standard dextran of different molecular weight (logMw = -0.3991RT + 17.78, R^2 = 0.9968), the average molecular weight of SPN was 15.8 kDa with the retention time of 34.03 min and the average molecular weight of PPN was 27.7 kDa with the retention time of 33.42 min. In addition, both elution peaks were single and symmetric in the GPC spectra, indicating they were both homogeneous fractions (48).

HPLC analysis shown in **Table 2** determines the monosaccharide composition of SPN and PPN. They both mainly contained rhamnose, glucose, arabinose, galacose, and mannose. However, the contents of each monosaccharide in the two polysaccharides were different as previous research reported (49). SPN contained 7.4% rhamnose, 6.4% mannose, 38.6% glucose, 20.5% arabinose, and 27.1% galacose, while PPN contained 8.5% rhamnose, 7.3% mannose, 44.9% glucose, 15.7% arabinose, and 23.6% galacose by area ratio. The results showed that phosphorylation increased the ratio of glucose and arabinose, while decreased the ratio of galactose.

Methylation analysis

In order to analyze the glycosyl linkages of polysaccharides, methylation method with GC-MS was used. After two times of methylation, the characteristic absorption peak of O-H around 3,400 cm^{-1} was almost disappeared in the FI-IR

TABLE 2 Monosaccharide analysis data.

Compositions	SPN content (%, area)	PPN Content (%, area)
Mannose	6.4	7.3
Glucose	38.6	44.9
Galacose	27.1	23.6
Arabinose	20.5	15.7
Rhamnose	7.4	8.5

10.3389/fnut.2022.976552

spectra of methylated samples, indicating the methylation of samples were completed.

Form Table 3, the mainly methylated sugars of SPN contained 2,3,4,6-Me_4-Glc*p*(8.4%), 2,3,6-Me_3-Glc*p*(34.5%), 2,3,4-Me_3-Gal*p*(16.7%), 2,3-Me_2-Gal*p*(7.9%), 2,3,5-Me_3-Ara*f*(6.6%), 3-Me-Ara*f*(5.5%), 2,3-Me_2-Ara*f*(10.9%), 3,5-Me_2-Rha*p*(5.0%) and 2,3,4-Me_3-Man*p*(4.5%), PPN contained 2,3,4,6-Me_4-Glc*p*(12.7%), 2,3,6-Me_3-Glc*p*(21.2%), 2,3,4-Me_3-Gal*p*(13.5%), 2,3-Me_2-Gal*p*(9.5%), 3,6-Me_2-Glc*p*(13.5%), 2,4,6-Me_3-Gal*p*(4.1%), 2,3,5-Me_3-Ara*f*(11.4%), 3,5-Me_2-Rha*p*(6.2%), and 2,3,4-Me_3-Man*p*(7.9%). The relative proportions of terminal residues and branching residues were almost equal, indicating that the polysaccharides were completely methylated (50). In addition, the proportion of glycosyls in methylation analysis was consistent with that in monosaccharide composition. However, the disappeare of 1,2,5-linked Ara*f*, 1,5-linked Ara*f* and the generation of 1,2,4-linked Glc*p*, 1,3-linked Gal*p* in PPN indicated that they were located in the branched chain. The man chains of the SPN and PPN were composed of 1,4-linked Glc*p*, 1,6-linked Gal*p*, 1,2-linked Rha*p*, 1.6-linked Man*p* and the terminals of t-linked Glc*p*, t-linked Ara*f*. This result suggested that phosphorylation did not change the main chain structure of the polysaccharide. The side chain of SPN is 1,4,6-linked Gal*p*, 1,2,5-linked Ara*f*, while PPN is 1,4,6-linked Gal*p*, 1,2,4-linked Glc*p*. It is shown that the phosphorylation changes the branching structure of the polysaccharide. This might be due to the different effects of phosphorylation on the hydrolysis of different glycosidic bonds. For example, the branched chains are easier hydrolyzed than the backbone, and furanose is more hydrolyzed than pyranose (51).

TABLE 3 Methylation analysis data.

Methylated sugars	Linkage patterns	SPN relative amount (%, area)	PPN relative amount (%, area)
2,3,4,6-Me_4-Glc*p*	1-linked Glc*p*	8.4	12.7
2,3,6-Me_3-Glc*p*	1,4-linked Glc*p*	34.5	21.2
3,6-Me_2-Glc*p*	1,2,4-linked Glc*p*	–	13.5
2,3,4-Me_3-Gal*p*	1,6-linked Gal*p*	16.7	13.5
2,3-Me_2-Gal*p*	1,4,6-linked Gal*p*	7.9	9.5
2,4,6-Me_3-Gal*p*	1,3-linked Gal*p*	–	4.1
2,3,5-Me_3-Ara*f*	1-linked Ara*f*	6.6	11.4
3-Me-Ara*f*	1,2,5-linked Ara*f*	5.5	–
2,3-Me_2-Ara*f*	1,5-linked Ara*f*	10.9	–
3,5-Me_2-Rha*p*	1,2-linked Rha*p*	5.0	6.2
2,3,4-Me_3-Man*p*	1.6-linked Man*p*	4.5	7.9

NMR analysis

The NMR spectrum of SNP and PPN are shown in Figure 3. In ^{1}H NMR, the chemical shift range of heterocephalic hydrogen signal from SNP and PPN was less than 5 ppm, which indicated that they contained β configurations (52). At the same time, this conclusion was proved by 102–112 ppm chemical shift peaks of the polysaccharides in ^{13}C NMR (53). The absence of signal peak at 5.40 ppm indicated that PPN and SPN were pyranose, which was consistent with the results of the FI-IR. ^{13}C NMR signals of PPN and SPN were mainly at 170–20 ppm. The signals of PPN at 103.51, 75.70, 73.33, 72.02, 69.55, and 62.49 ppm and SPN at 102.07, 75.73, 73.02, 69.21, 68.47, and 66.16 ppm were attributed to C1–C6 carbon atoms. The shift of chemical from 62.49 to 67 ppm indicated that substitution might take

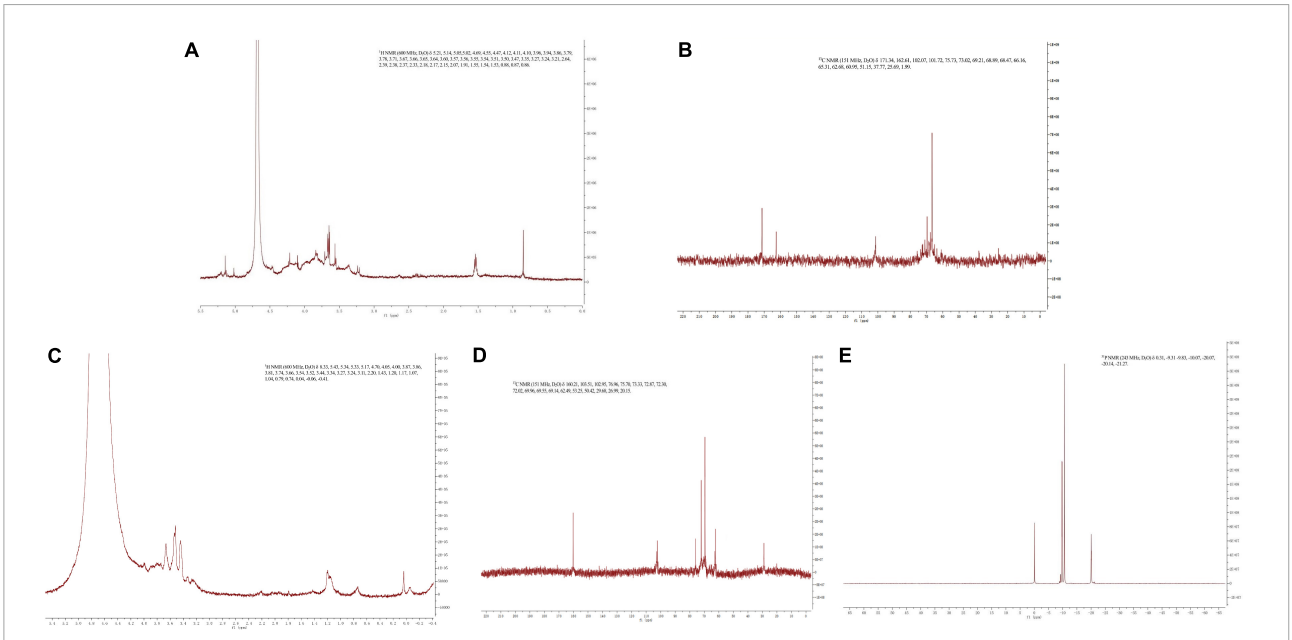

FIGURE 3
^{1}H NMR spectra of SPN **(A)** and PPN **(C)**, ^{13}C NMR spectra of SPN **(B)** and PPN **(D)**, and ^{31}P NMR spectra of PPN **(E)**.

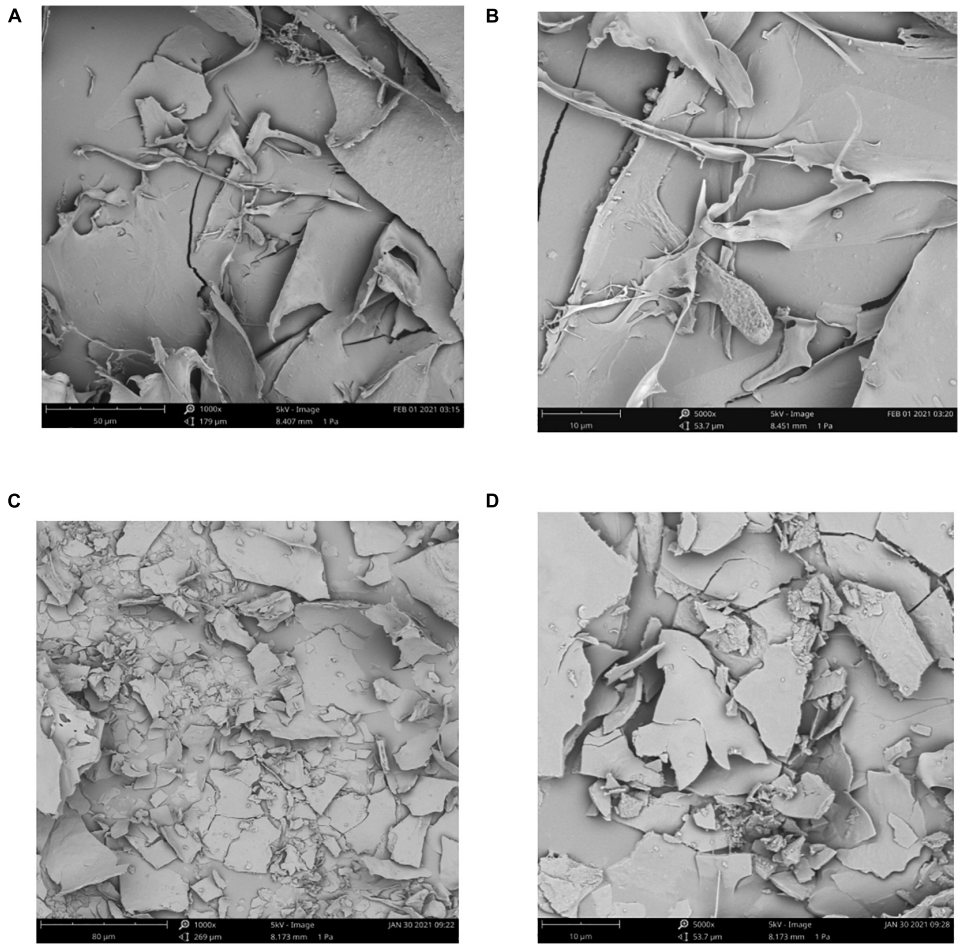

FIGURE 4
SEM spectra of SPN (1000×) **(A)**, SPN (5000×) **(B)**, PPN (1000×) **(C)**, and PPN (5000×) **(D)**.

place at C-6 (54). In addition, the signal peak at 167 ppm was a chemical shift peak caused by phosphate substitution. Due to the insufficient solubility of PPN in D_2O, the carbon spectrum needs to be further studied. The significant absorption peaks at 0.31, −9.83, −10.07, and −20.07 ppm of PPN were shown in the ^{31}P NMR, which indicated phosphorylation substitution reactions occurred at multiple positions from the sugar ring (55). This is consistent with previously published results by Liu and Huang (56).

SEM analysis

In SEM spectra (**Figures 4A,B**), it showed smoothly large chunks of debris with a network on surface of SPN, which indicated that the structure of SPN is tight. However, in SEM spectra of PPN (**Figures 4C,D**), there were many cracks and small debris on the surface of PPN which meant the structure of PPN is loosen and multi-level, probably due to the phosphorylation increased the distance between molecules of PPN. The structure of PPN is more conducive to the entry of water, which increases the solubility and affects the biological activity (57).

Antioxidant activity analysis

DPPH radical scavenging activity

DPPH is a stable-free radical with three benzene rings, DPPH radical scavenging method has the characteristics of easy operation and fast reaction. **Figure 5A** shows the effect of SPN and PPN on DPPH radical scavenging activity at 0–3 mg/mL. With the increase of concentration, the DPPH radical scavenging rate of SPN and PPN increased, presenting a certain dose-dependence. At the concentration of 3 mg/mL, the radical scavenging rates of SPN and PPN were 37.8 and 65.9%, respectively, indicating that phosphorylated polysaccharides

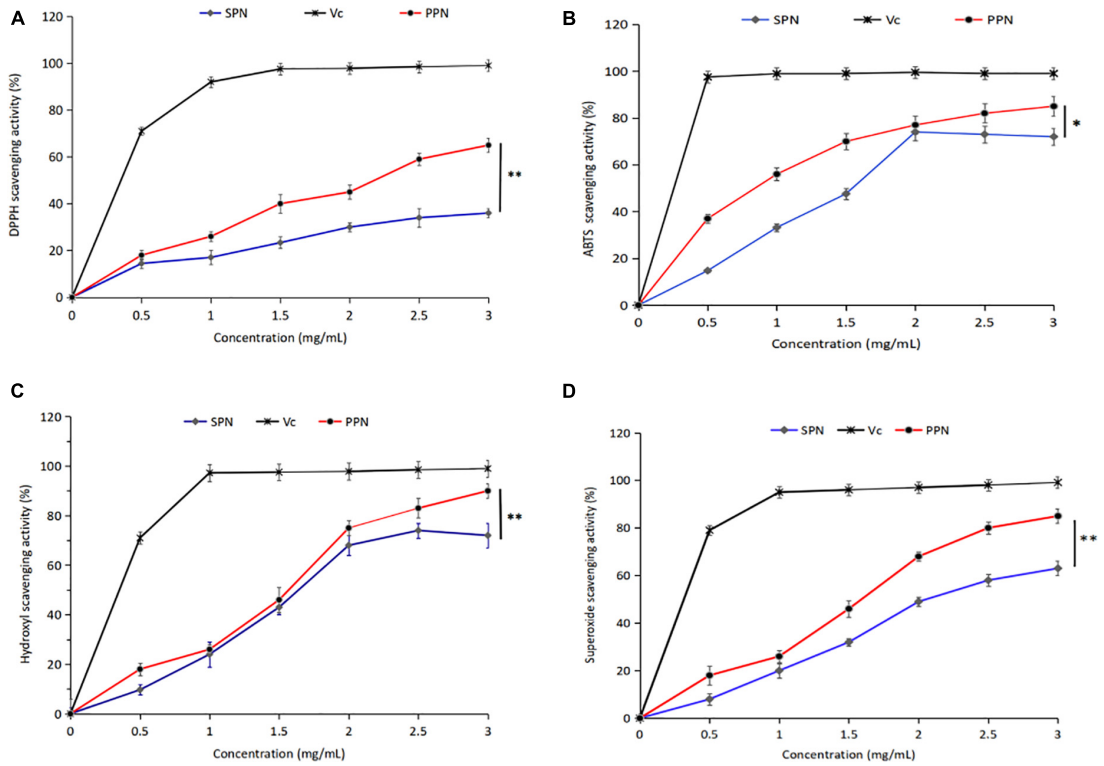

FIGURE 5
DPPH radical scavenging activity **(A)**, ABTS radical scavenging activity **(B)**, Hydroxyl scavenging activity **(C)**, and Superoxide scavenging activity **(D)** of PPN and SPN. *Indicates $P < 0.05$, **indicates $P < 0.01$.

had significantly better DPPH antioxidant activity than natural polysaccharides ($p < 0.01$), but weaker than Vc.

ABTS radical scavenging activity

ABTS radical scavenging method is a common method for the determination of antioxidant activity, which has the advantage of substrate color without interference. From Figure 5B, the ABTS radical scavenging rate escalated with the increase of PPN concentration at 0–3 mg/mL. However the scavenging activity decreased, when the concentration of SPN exceeded 2 mg/mL. The ABTS radical scavenging rate of SPN and PPN were 67.1 and 86.4% at polysaccharide concentration of 3 mg/mL, the difference was significant ($p < 0.05$). The ABTS radical scavenging activity of PPN was higher than SPN and close to Vc.

Hydroxyl radical scavenging activity

Hydroxyl-free radical is a kind of reactive oxygen species, which can react to cellular components, resulting in harm to the body. From Figure 5C, the hydroxyl radical scavenging rate of SPN and PPN ascended with the increase of PPN concentration at 0–3 mg/mL. At polysaccharide concentration of 3 mg/mL, the ABTS radical scavenging rate of SPN and PPN were 78.3 and 93.6%, respectively. PPN has significantly stronger scavenging activity than SPN ($p < 0.01$), and slightly weaker than Vc. Chen and Huang (43) reported that the phosphorylated pumpkin polysaccharide had better free radical scavenging activity than natural polysaccharide.

Superoxide radical scavenging activity

Superoxide-free radical is a kind of reactive oxygen species produced in human body, which can cause lipid peroxidation and accelerate the aging process of the body. From Figure 5D, SPN and PPN had superoxide radical scavenging activity, and their radical scavenging rate were 63.5 and 86.7%, respectively, at concentration of 3 mg/mL, indicating phosphorylation significantly enhanced antioxidant activity ($p < 0.01$). This conclusion is recognized by Chen and Huang (46).

Inflammatory effect on RAW 264.7 cells

Cell viability of RAW 264.7 cells

The cell viability of RAW 264.7 cells treated by different concentrations of SPN and PPN was evaluated by CCK-8 commercial kit. In Figure 6A, SPN and PPN of 50 μg/mL had no significant influence on viability of RAW 264.7 cells compared to control group, while SPN and PPN above 50 μg/mL

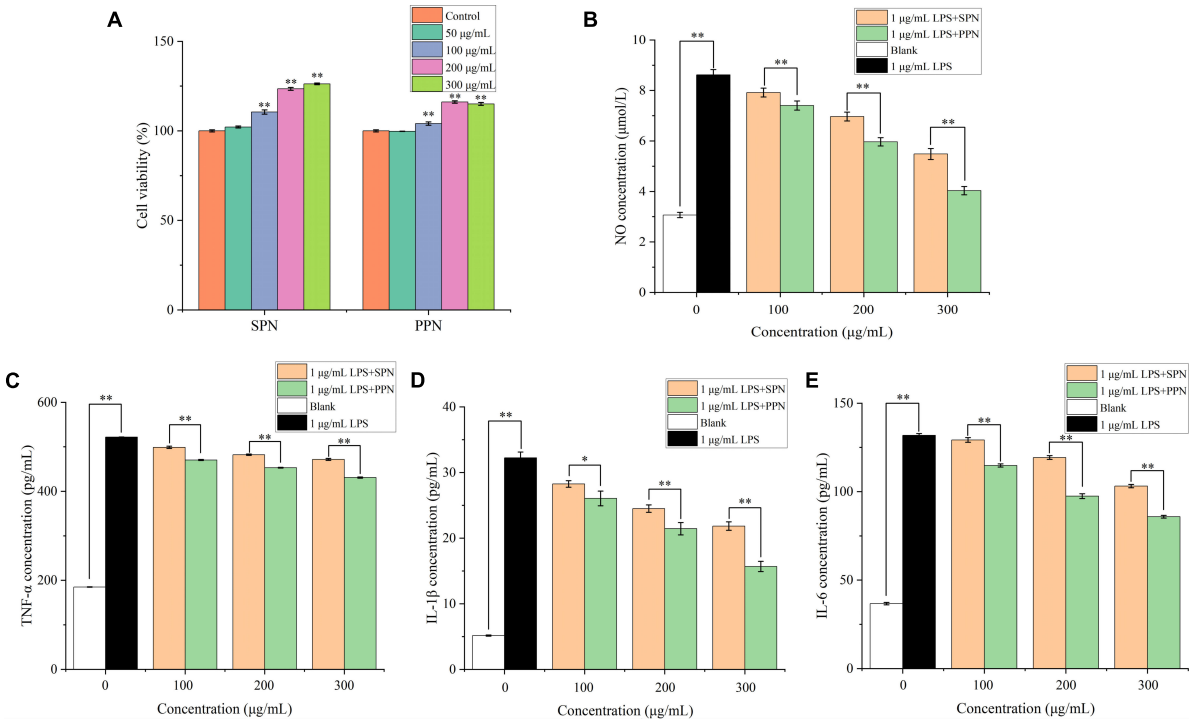

FIGURE 6
Cell viability **(A)**, NO concentration **(B)**, TNF-α concentration **(C)**, IL-1β concentration **(D)** and IL-6 concentration **(E)** of RAW 264.7 cells. *Indicates $P < 0.05$, **indicates $P < 0.01$.

can significantly increase viability of RAW 264.7 cells which indicated both polysaccharides above 50 μg/mL can promote RAW 264.7 cells proliferation. SPN and PPN are non-toxic to macrophages. Therefore, the other three concentrations (100, 200, and 300 μg/mL) were selected for following experiments.

NO concentration analysis

NO is a key cytokine that mediates inflammatory responses and is widely involved in a variety of physiological processes *in vivo*. Previous research proved that NO concentration is an important index to evaluate macrophage activation (58). In **Figure 6B**, the NO concentration in blank control group was 3.1 μmol/L, while RAW 264.7 cells released great amount of NO after 1 μg/mL LPS treatment for 24 h (8.6 μmol/L). Compared with blank control group, the NO concentration of LPS treatment group extremely increased ($p < 0.01$). However, with different concentrations of polysaccharides and LPS treatments for 24 h, the NO levels significantly reduced ($p < 0.01$), and the reducing effects were more significant in higher concentration polysaccharides treatments, compared with LPS treatment group. Besides, the reducing effect of NO concentration by PPN was better than that by SPN in same concentration. This is consistent with previously published results by Yang et al. (59).

TNF-α, IL-1β, and IL-6 levels analysis

TNF-α, mainly produced by monocytes, macrophages, has functions of inflammatory regulation, participation in fever and inflammation occurrence (60). In **Figure 6C**, after 24 h treatment with 1 μg/mL LPS, TNF-α level significantly raised from 184.9 to 521.8 pg/mL ($p < 0.01$), compared with blank control group. Similar with NO concentration results, TNF-α level significantly decreased with polysaccharides concentration increasing ($p < 0.01$), and the effect of SPN was always weaker than that of PPN in same concentration. This result was also identified by Tian et al. (61).

IL-1β, mainly released by activated macrophages, can play a role in inflammatory regulation (62). In **Figure 6D**, the IL-1β level of LPS model group extremely increased from 5.2 to 32.2 pg/mL compared to blank control group ($p < 0.01$). Also, the IL-1β level of polysaccharides treatment groups gradually decreased as concentration of polysaccharides increased. Moreover, the decreasing effect on IL-1β concentration of PPN was always better than that of SPN.

IL-6 is one of the most common pro-inflammatory cytokines secreted mainly by activated macrophages, lymphocytes, and epithelial cells, and has multiple inflammatory functions, which can participate in vivo inflammatory response as an important inflammatory medium (63). From **Figure 6E**,

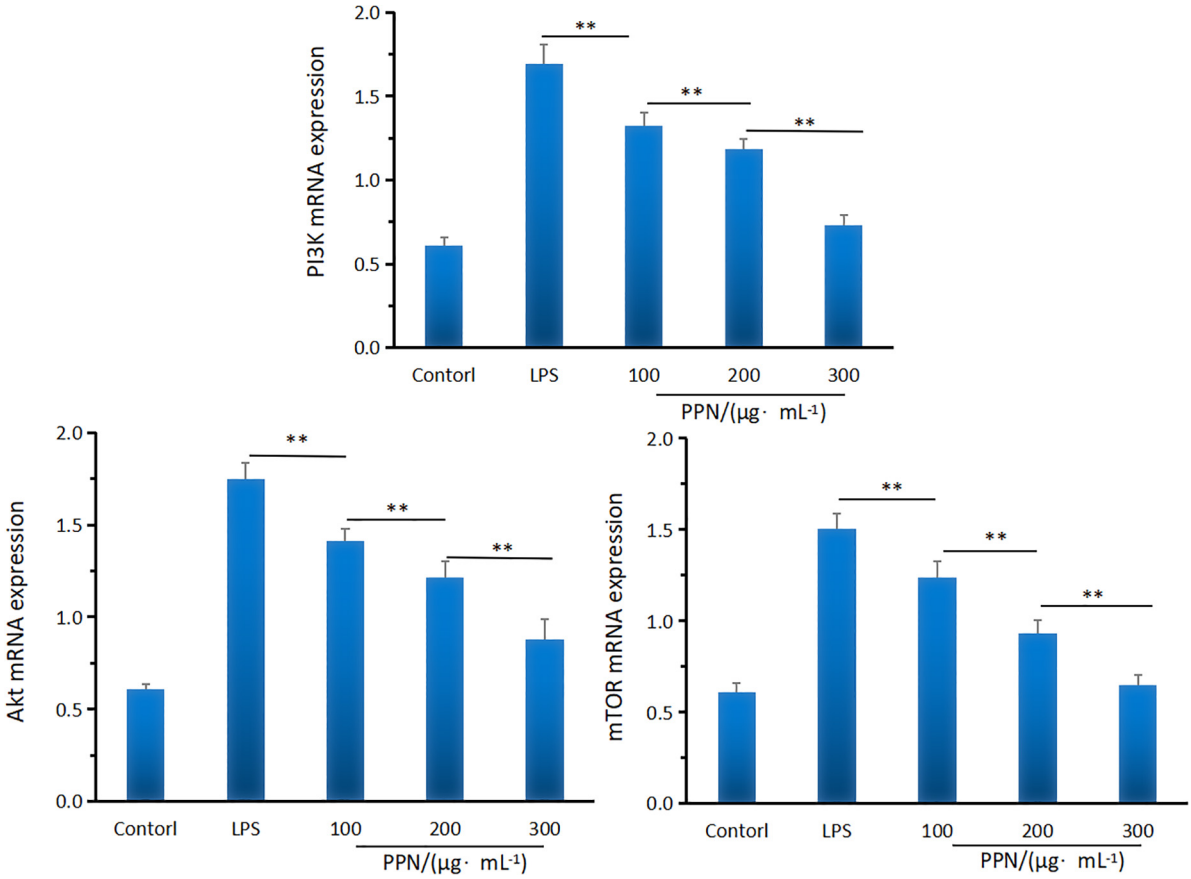

FIGURE 7
The PI3KAktmTOR mRNA expression of SPN and PPN. **Indicates $p < 0.01$.

1 μg/mL LPS treatment for 24 h can significantly enhance the IL-6 level from 36.7 to 131.8 pg/mL compared with blank control group ($p < 0.01$). With the increase of polysaccharides concentration, IL-6 level decreased gradually. In addition, the ability of inhabiting IL-6 release of PPN was always better than that of SPN in every concentration.

mRNA expression levels analysis

Quantitative RT-PCR was used to investigate the effect of PPN on the mRNA expression of PI3K, Akt, and mTOR. From **Figure 7**, 1 μg/mL LPS treatment for 24 h can significantly promote the mRNA expression of PI3K, Akt, and mTOR. Compared with the LPS model group, PPN significantly inhibited the mRNA expression of PI3K, Akt, and mTOR ($p < 0.01$). The mRNA expression level of higher concentration polysaccharide group was significantly higher than that of other concentration group ($p < 0.01$). The level of mRNA expression in cells was dose-dependent with the PPN concentration. The results showed that PPN played an anti-inflammatory role by down regulating the mRNA expression of PI3K, Akt, and mTOR. More data could see the **Supplementary material**.

Protein expression levels analysis

Western blot was used to analyze the effect of PPN on key protein expression of PI3K/Akt/mTOR pathway. From **Figure 8**, compared with LPS model group, PPN groups significantly inhibited the protein expression of p-pI3k, p-Akt and p-mTOR ($p < 0.01$). The protein expression level of high-dose polysaccharide group was significantly lower than that in low-dose group ($p < 0.01$). And the protein expression level was dose-dependent with PPN concentration. PPN could down-regulate p-PI3K expression level, blocking PI3K/AKT signal, decreasing phosphorylation AKT protein level, leading to the decrease expression level of p-mTOR. Thereby the secretion of TNF-α, IL-1β, IL-6 were down regulated which reduced the inflammatory reaction. In conclusion, PPN can regulate inflammatory cytokines through PI3K/Akt/mTOR pathway. From structural analysis of SPN and PPN, it is obvious that phosphorylation has changed the structure of SPN. Apparently, due to the structure changed, the biological function of SPN

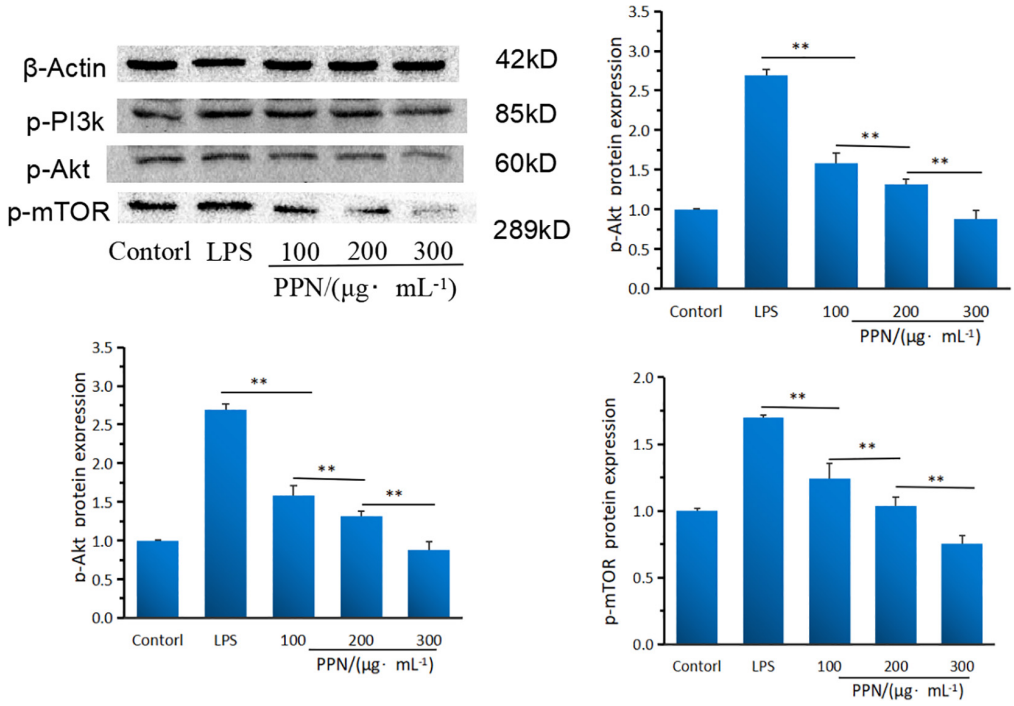

FIGURE 8
The PI3KAktmTOR protein expression of SPN and PPN. **Indicates $p < 0.01$.

and PPN are different. In antioxidant activity experiments, the free radical scavenging rate of PPN was significantly stronger than that of SPN ($p < 0.05$). In cell model experiments, PPN always has significantly better anti-inflammatory effect on RAW 264.7 cells induced by LPS than SPN ($p < 0.01$), especially at same concentration. After substitution of phosphate group, phosphate group replaced some hydroxy groups on original chain of SPN, resulting in changes on its structure which made more hydroxy groups expose (64, 65). In addition, the changes of molecular weight, monosaccharide ratio, and molecular configuration of PPN might affect its biological activity (66). Thus, the biological function of phosphorylated polysaccharide improved.

PI3K/Akt/mTOR pathway is one of the important signaling pathways of the inflammatory response, which can regulate the activation of signal kinase and the expression of downstream gene and proteins to inhibit the inflammatory response of cells (67, 68). In this study, the potential anti-inflammatory mechanism of PPN was analyzed by the gene and protein expression levels of PI3K, Akt and mTOR. PI3K is an inositol kinase and act as a Biomarker to regulate cell differentiation, proliferation and apoptosis. PPN significantly down-regulated the PI3K gene and protein expression levels ($p < 0.01$). Akt is an important downstream factor of PI3K, and lower p-PI3K protein level could lead to Akt phosphorylation level drop. This indicated that PPN blocked PI3K/Akt pathway signals and reduced the protein expression level of p-Akt at threonine 308 site of Akt, which lead to the blocking of p-Akt downstream signal. mTOR (mammalian target of rapamycin) is a downstream target of Akt. The protein expression of p-Akt was blocked, resulting in the inhibition of mTOR activity. Collectively, PPN can down-regulate the secretion level of TNF-α, IL-1β and IL-6 *via* PI3K/Akt/mTOR pathway. However, the structure-function relationship of phosphorylated polysaccharide and the anti-inflammatory interaction of other pathways are still unclear, which need further research.

Conclusion

In this study, we analyzed the structural, antioxidant activity, and anti-inflammatory effect differences of SPN and PPN. SPN and PPN were β-pyranose configuration and mainly contained glucose, galacose, and arabinose. Phosphorylation increased the molecular weight of polysaccharide from 15.8 to 27.7 kDa. FI-IR, NMR, and SEM spectra showed phosphorylation of SPN changed its structure and confirmed that the chemical modification was successful. Besides the phosphorylation did not change the main chain structure but changed the branched chain structure by methylation. Moreover, PPN always has better antioxidant activity and anti-inflammatory than SPN. PPN can inhibit inflammatory by PI3K/AKT/mTOR signal pathway. These findings are helpful to study the structural characterization, antioxidant activity and anti-inflammatory effect of phosphorylated *pholiota nameko* polysaccharide by high-temperature pressurized extraction.

Data availability statement

The original contributions presented in this study are included in the article/**Supplementary material**, further inquiries can be directed to the corresponding author.

Author contributions

XZ: conceptualization, methodology, and writing—original draft. LZ: investigation and resources. JQ: formal analysis and visualization. XW: resources and formal analysis. SA: conceptualization and methodology. TL: resources, data curation, and supervision. All authors contributed to the article and approved the submitted version.

Funding

This research was financially supported by the Jilin Province Science and Technology Development Plan Project of China (grant no. 20210202058NC).

Conflict of interest

The authors declare that the research was conducted in the absence of any commercial or financial relationships that could be construed as a potential conflict of interest.

Publisher's note

All claims expressed in this article are solely those of the authors and do not necessarily represent those of their affiliated organizations, or those of the publisher, the editors and the reviewers. Any product that may be evaluated in this article, or claim that may be made by its manufacturer, is not guaranteed or endorsed by the publisher.

Supplementary material

The Supplementary Material for this article can be found online at: https://www.frontiersin.org/articles/10.3389/fnut.2022.976552/full#supplementary-material

References

1. Takeuchi O, Akira S. Pattern recognition receptors and inflammation. *Cell.* (2010) 140:805–20. doi: 10.1016/j.cell.2010.01.022

2. Divate RD, Chung YC. In vitro and in vivo assessment of anti-inflammatory and anti-inflammatory activities of Xylaria nigripes mycelium. *Funct Foods.* (2017) 35:81–9. doi: 10.1016/j.jff.2017.05.027

3. Ahmed A, Attia F, Liu ZH, Li CQ, Wei JF, Kang WY. Antioxidant activity and total phenolic content of essential oils and extracts of sweet basil (*Ocimum basilicum* L.) plants. *Food Sci Hum Wellness.* (2019) 8:299–305. doi: 10.1016/j.fshw.2019.07.004

4. Qian L, Liu H, Li T, Liu YH, Zhang ZJ, Zhang YN, et al. Purification, characterization and in vitro antioxidant activity of a polysaccharide AAP–3–1 from *Auricularia auricula*. *Int J Med Mushrooms.* (2020) 162:1453–64. doi: 10.1016/j.ijbiomac.2020.07.314

5. Xiang H, Sun-Waterhouse DX, Cui C. Hypoglycemic polysaccharides from *Auricularia auricula* and *Auricularia polytricha* inhibit oxidative stress, NF-kB signaling and proinflammatory cytokine production in streptozotocin-induced diabetic mice. *Food Sci Hum Wellness.* (2021) 10:87–93. doi: 10.1016/j.fshw.2020.06.001

6. Lyhatskyy PH, Fira LS. Free radicals and inflammation in rats of different age in cases of sodium nitrites and tobacco smoke poisoning. *J Int Med Res.* (2017) 1:84–8. doi: 10.11603/ijmmr.2413-6077.2017.1.7923

7. Yin ZH, Liang ZH, Li CQ, Wang JM, Ma CY, Kang WY. Immunomodulatory effects of polysaccharides from edible fungus: a review. *Food Sci Hum Wellness.* (2021) 10:393–400. doi: 10.1016/j.fshw.2020.04.001

8. You L, Gao Q, Feng M, Yang B, Ren J, Gu L, et al. Structural characterisation of polysaccharides from *Tricholoma matsutake* and their antioxidant and antitumour activities. *Food Chem.* (2013) 138:2242–9. doi: 10.1016/j.foodchem.2012.11.140

9. Barzee TJ, Cao L, Pan ZL, Zhang RH. Fungi for future foods. *J Funct Foods.* (2021) 1:25–37. doi: 10.1016/j.jfutfo.2021.09.002

10. Wu JN, Chen XT, Qiao K, Su YC, Liu ZY. Purification, structural elucidation, and in vitro antitumor effects of novel polysaccharides from *Bangia fuscopurpurea*. *Food Sci Hum Wellness.* (2021) 10:63–71. doi: 10.1016/j.fshw.2020.05.003

11. Ji XL, Hou C, Gao Y, Xue Y, Yan Y, Guo X. Metagenomic analysis of gut microbiota modulatory effects of jujube (*Ziziphus jujuba* Mill.) polysaccharides in a colorectal cancer mouse model. *Food Funct.* (2020) 11:163–73. doi: 10.1039/c9fo02171j

12. Hou C, Chen L, Yang L, Ji XL. An insight into anti-inflammatory effects of natural polysaccharides. *Int J Biol Macromol.* (2021) 153:248–55. doi: 10.1016/j.ijbiomac.2020.02.315

13. Liu HC, Fan HX, Zhang J, Zhang S, Zhao W, Liu T, et al. Isolation, purification, structural characteristic and antioxidative property of polysaccharides from *A.cepa* L.var. agrogatum Don. *Food Sci Hum Wellness.* (2020) 9:71–9. doi: 10.1016/j.fshw.2019.12.006

14. Zhang YR, Wang DW, Chen YT, Liu TT, Fan HX, Liu HC, et al. Healthy function and high valued utilization of edible fungi. *Food Sci Hum Wellness.* (2021) 10:408–20. doi: 10.1016/j.fshw.2021.04.003

15. Wu DT, An LY, Liu W, Hu YC, Wang SP, Zou L. In vitro fecal fermentation properties of polysaccharides from *Tremella fuciformis* and related modulation effects on gut microbiota. *Food Res Int.* (2022) 156:111185. doi: 10.1016/j.foodres.2022.111185

16. Lin XM, Li W, Yuen H, Yuen M, Peng Q. Immunomodulatory effect of intracellular polysaccharide from mycelia of *Agaricus bitorquis* (QuéL.) Sacc. Chaidam by TLR4-mediated MyD88 dependent signaling pathway. *Int J Biol Macromol.* (2020) 183:79–89. doi: 10.1016/j.ijbiomac.2021.04.120

17. Sun Y, Zhou XY. Purification, initial characterization and immune activities of polysaccharides from the fungus, *Polyporus umbellatus*. *Food Sci Hum Wellness.* (2014) 3:73–8. doi: 10.1016/j.fshw.2014.06.002

18. Yin ZH, Sun DX, Wang JM, Ma CY, Geoffrey IN, Kang WY. Polysaccharides from edible fungi *Pleurotus* spp.: advances and perspectives. *J Funct Foods.* (2021) 2:128–40. doi: 10.1016/j.jfutfo.2022.01.002

19. Dias IP, Brabieri SF, López Fetzer DE, Corazza ML, Silveira J. Effects of pressurized hot water extraction on the yield and chemical characterization of pectins from *Campomanesia xanthocarpa* Berg fruits. *Int J Biol Macromol.* (2020) 146:431–43. doi: 10.1016/j.ijbiomac.2019.12.261

20. He JL, Guo H, Wei SY, Zhou J, Xiang PY, Zhao L, et al. Effects of different extraction methods on the structural properties and bioactivities of polysaccharides extracted from Qingke (Tibetan hulless barley). *J Cereal Sci.* (2020) 92:102906. doi: 10.1016/j.jcs.2020.102906

21. Lee YS, Kim HJ, Yang DH, Chun HJ. Preparation and anticancer activity evaluation of self-assembled paclitaxel conjugated MPEG-PCL micelles on 4T1 cells. *J Ind Eng Chem.* (2019) 71:369–77. doi: 10.1016/j.jiec.2018.11.048

22. Feng H, Fan J, Yang S, Zhao X, Yi X. Antiviral activity of phosphorylated radix *Cyathulae officinalis* polysaccharide against *Canine parvovirus* in vitro. *Int J Biol Macromol.* (2017) 99:511–7. doi: 10.1016/j.ijbiomac.2017.02.085

23. Liu Y, Sun Y, Huang G. Preparation and antioxidant activities of important traditional plant polysaccharides. *Int J Biol Macromol.* (2018) 111:780–6. doi: 10.1016/j.ijbiomac.2018.01.086

24. Wang J, Wang Y, Xu L, Wu Q, Wang Q, Kong W, et al. Synthesis and structural features of phosphorylated *Artemisia sphaerocephala* polysaccharide. *Carbohydr Polym.* (2018) 181:19–26. doi: 10.1016/j.carbpol.2017.10.049

25. Deng C, Fu H, Xu JJ, Shang JY, Cheng YM. Physiochemical and biological properties of phosphorylated polysaccharides from *Dictyophora indusiata*. *Int J Biol Macromol.* (2015) 72:894–9. doi: 10.1016/j.ijbiomac.2014.09.053

26. Coleman RJ, Lawrie G, Lamber LK, Whittaker M, Jack KS, Grøndahl L. Phosphorylation of alginate: synthesis, characterization, and evaluation of in vitro mineralization capacity. *Biomacromolecules.* (2011) 12:89–97. doi: 10.1021/bm1011773

27. Ming K, Chen Y, Yao F, Shi J, Yang J, Du H, et al. The inhibitory effect of phosphorylated *Codonopsis pilosula* polysaccharide could inhibit the virulence of duck hepatitis A virus compared with *Codonopsis pilosula* polysaccharide. *Int J Biol Macromol.* (2017) 94:28–35. doi: 10.1016/j.psj.2019.11.060

28. Yan Y, Li X, Wan M, Chen J, Li S, Cao M, et al. Effect of extraction methods on property and bioactivity of water-soluble polysaccharides from *Amomum villosum*. *Carbohydr Polym.* (2015) 117:632–5. doi: 10.1016/j.carbpol.2014.09.070

29. Zhou CS, Yu XJ, Zhang YZ, He RH, Ma HL. Ultrasonic degradation, purification and analysis of structure and antioxidant activity of polysaccharide from *Porphyra yezoensis* Udea. *Carbohydr Poly.* (2011) 87:2046–51. doi: 10.1016/j.carbpol.2011.10.026

30. Ji XL, Zhang F, Zhang R, Liu F, Peng Q, Wang M. An acidic polysaccharide from *Ziziphus jujuba* cv. Muzao: purification and structural characterization. *Food Chem.* (2019) 274:494–9. doi: 10.1016/j.foodchem.2018.09.037

31. Xiong W, Chen Y, Wang Y, Liu JG. Roles of the antioxidant properties of icariin and its phosphorylated derivative in the protection against duck virus hepatitis. *BMC Vet Res.* (2014) 10:226. doi: 10.1186/s12917-014-0226-3

32. Chen F, Huang G, Huang H. Preparation, analysis, antioxidant activities in vivo of phosphorylated polysaccharide from *Momordica charantia*. *Carbohydr Polym.* (2021) 252:117–79. doi: 10.1016/j.carbpol.2020.117179

33. Dubois M, Gilles K, Hamilton J, Rebers P, Smith F. Colorimetric method for determination of sugars and related substances. *Anal Chem.* (1956) 28:350–6. doi: 10.1021/AC60111A017

34. Bradford M. A rapid and sensitive method for the quantitation of microgram quantities of protein utilizing the principle of protein binding. *Anal Biochem.* (1976) 72:248–54. doi: 10.1006/abio.1976.9999

35. Zheng L, Ma T, Zhang Y, Meng Q, Yang J, Wang B, et al. Increased antioxidant activity and improved structural characterization of sulfuric acid-treated stepwise degraded polysaccharides from *Pholiota nameko* PN-01. *Int J Biol Macromol.* (2021) 166:1220–9. doi: 10.1016/j.ijbiomac.2020.11.004

36. Yang X, Lin P, Wang J, Liu N, Yin F, Shen N, et al. Purification, characterization and anti-atherosclerotic effects of the polysaccharides from the fruiting body of *Cordyceps militaris*. *Int J Biol Macromol.* (2021) 181:890–904. doi: 10.1016/j.ijbiomac.2021.04.083

37. Ji XL, Cheng YQ, Tian JY, Zhang SQ, Jing YS, Shi MM. Structural characterization of polysaccharide from jujube (*Ziziphus jujuba* Mill.) fruit. *Chem Biol Technol Agric.* (2021) 8:54–62. doi: 10.1186/s40538-021-00255-2

38. Ji XL, Guo JH, Ding DQ, Gao J, Hao L, Guo XD, et al. Structural characterization and antioxidant activity of a novel high-molecular-weight polysaccharide from *Ziziphus jujuba* cv. Muzao. *J Food Meas Charact.* (2022) 16:2191–200. doi: 10.1007/s11694-022-01288-3

39. Zhang X, Liu JX, Wang X, Hu HW, Zhang YR, Liu TT, et al. Structure characterization and antioxidant activity of carboxymethylated polysaccharide from *Pholiota nameko*. *J Food Biochem.* (2022) 46:e14121. doi: 10.1111/jfbc.14121

40. Zhuang S, Ming K, Ma N, Sun JR, Wang DH, Ding XX, et al. *Portulaca oleracea* L. polysaccharide ameliorates lipopolysaccharide-induced inflammatory responses and barrier dysfunction in porcine intestinal epithelial monolayers. *J Funct Food.* (2022) 91:104997. doi: 10.1016/j.jff.2022.104997

41. Sun Y, Zhong S, Yu J, Zhu J, Ji D, Hu G, et al. The aqueous extract of *Phellinus igniarius* (SH) ameliorates dextran sodium sulfate-induced colitis in C57BL/6 mice. *PLoS One.* (2018) 13:e0205007. doi: 10.1371/journal.pone.0205007

42. Cao Y, Ji X, Liao A, Huang J, Thakur K, Li X, et al. Effects of sulfated, phosphorylated and carboxymethylated modifications on the antioxidant activities in-vitro of polysaccharides sequentially extracted from *Amana edulis*. *Int J Biol Macromol.* (2020) 146:887–96. doi: 10.1016/j.ijbiomac.2019.09.211

43. Chen L, Huang G. Antioxidant activities of phosphorylated pumpkin polysaccharide. *Int J Biol Macromols.* (2019) 125:256–61. doi: 10.1016/j.ijbiomac.2018.12.069

44. Wu Y, Ye M, Du Z, Jing L, Suihio M, Yang L. Carboxymethylation of an exopolysaccharide from *Lachnum* and effect of its derivativess on experimental chronic renal failure. *Carbohydr Polym.* (2014) 114:190–5. doi: 10.1016/j.carbpol.2014.07.075

45. Cheng H, Huang G, Huang H. The antioxidant activities of garlic polysaccharide and its derivatives. *Int J Biol Macromol.* (2020) 145:819–26. doi: 10.1016/j.ijbiomac.2019.09.232

46. Chen L, Huang G. The antioxidant activity of derivatized cushaw polysaccharides. *Int J Biol Macromol.* (2019) 128:1–4. doi: 10.1016/j.ijbiomac.2019.01.091

47. Duan Z, Zhang Y, Zhu C, Wu Y, Du B, Ji H. Structural characterization of phosphorylated *Pleurotus ostreatus* polysaccharide and its hepatoprotective effect on carbon tetrachloride-induced liver injury in mice. *Int J Biol Macromol.* (2020) 162:533–47. doi: 10.1016/j.biortech.2008.09.004

48. Ji XL, Guo JH, Pan FB, Kuang FJ, Chen HM, Guo XD, et al. Structural elucidation and antioxidant activities of a neutral polysaccharide from Arecanut (*Areca catechu* L.). *Front Nutr.* (2022) 9:853115. doi: 10.3389/fnut.2022:853115

49. Shang X, Liu C, Dong H, Peng H, Zhu Z. Extraction, purification, structural characterization, and antioxidant activity of polysaccharides from Wheat Bran. *J Mol Struct.* (2021) 1233:130096. doi: 10.1016/j.molstruc.2021.130096

50. Li YX, Sheng Y, Lu XC, Guo X, Xu GY, Han X, et al. Isolation and purification of acidic polysaccharides from *Agaricus blazei* Murill and evaluation of their lipid-lowering mechanism. *Int J Biol Macromol.* (2020) 157:276–87. doi: 10.1016/j.ijbiomac.2020.04.190

51. Redgwell R, Curti D, Fischer M, Nicolas P, Fay B. Coffee bean arabinogalactans: acidic polymers covalently linked to protein. *Carbohydr Res.* (2020) 337:239–53. doi: 10.1016/S0008-6215(01)00316-0

52. Li H, Feng Y, Sun W, Kong Y, Jia L. Antioxidation, anti-inflammation and anti-fibrosis effect of phosphorylated polysaccharides from *Pleurotus djamor* mycelia on adenine-induced chronic renal failure mice. *Int J Biol Macromol.* (2021) 170:652–63. doi: 10.1016/j.ijbiomac.2020.12.159

53. Omarsdottir S, Petersen BO, Barsett H, SmestadPaulsen B, Duus J, Olafsdottir ES. Structural characterisation of a highly branched galactomannan from the lichen *Peltigera canina* by methylation analysis and NMR-spectroscopy. *Carbohydr Poly.* (2016) 63:54–60. doi: 10.1016/j.carbpol.2005.07.023

54. Rout D, Mondal S, Chakraborty I, Pramanik M, Islam SS. Chemical analysis of a new (1?3)-(1?6)- branched glucan from an edible mushroom *Pleurotus florida*. *Carbohydr Res.* (2005) 340:2533–9. doi: 10.1016/j.carres.2005.08.006

55. Xiong X, Huang G, Huang H. The antioxidant activities of phosphorylated polysaccharide from native ginseng. *Int J Biol Macromol.* (2019) 126:842–5. doi: 10.1016/j.ijbiomac.2018.12.266

56. Liu Y, Huang G. Extraction and derivatisation of active polysaccharides. *J Enzyme Inhib Med Chem.* (2019) 34:1690–6. doi: 10.1080/14756366.2019.1660654

57. Xie LM, Shen MY, Wen PE, Hong YZ, Liu X, Xie JH. Preparation, characterization, antioxidant activity and protective effect against cellular oxidative stress of phosphorylated polysaccharide from *Cyclocarya paliurus*. *Food Chem Toxicol.* (2020) 145:111754. doi: 10.1016/j.fct.2020.111754

58. Shen M, Chen X, Huang L, Yu Q, Chen Y, Xie J. Sulfated *Mesona chinensis* benth polysaccharide enhance the anti-inflammatory activities of cyclophosphamide-treated mice. *J Funct Foods.* (2021) 76:104321. doi: 10.1016/j.ijbiomac.2019.06.199

59. Yang YX, Chen JL, Lei L, Li FH, Tang Y, Yuan Y, et al. Acetylation of polysaccharide from *Morchella angusticeps* peck enhances its immune activation and anti-inflammatory activities in macrophage RAW 264.7?cells. *Food Chem Toxicol.* (2019) 125:38–45. doi: 10.1016/j.fct.2018.12.036

60. Zhang M, Tian X, Wang Y, Wang D, Li W, Chen L, et al. Immunomodulating activity of the polysaccharide TLH-3 from Tricholomalobayense in RAW 264.7 macrophages. *Int J Biol Macromol.* (2018) 107:2679–85. doi: 10.1016/j.ijbiomac.2017.10.165

61. Tian H, Liu H, Song W, Zhu L, Zhang T, Li R, et al. Structure, antioxidant and immunostimulatory activities of the polysaccharides from *Sargassum carpophyllum*. *Algal Res.* (2020) 49:101853. doi: 10.1016/j.ijbiomac.2020.06.150

62. Chen L, Lin X, Xiao J, Tian Y, Zheng B, Teng H. *Sonchus oleraceus* Linn protects against LPS-induced sepsis and inhibits inflammatory responses in RAW 264.7 cells. *J Ethnopharmac.* (2019) 236:63–9. doi: 10.1016/j.jep.2019.02.039

63. Liang QX, Zhao QC, Hao XT, Wang JM, Ma CY, Xi XF, et al. The effect of flammulina velutipes polysaccharide on immunization analyzed by intestinal flora and proteomics. *Front Nutr.* (2022) 9:841230. doi: 10.3389/fnut.2022.841230

64. Meng QL, Du XZ, Wang HL, Gu HM, Zhan JP, Zhou ZP. Astragalus polysaccharides inhibits cell growth and pro-inflammatory response in IL-1β-stimulated fibroblast-like synoviocytes by enhancement of autophagy via PI3K/AKT/mTOR inhibition. *Apoptosis.* (2017) 22:1138–46. doi: 10.1007/s10495-017-1387-x

65. Liu XX, Wan ZJ, Shi L, Lu XX. Preparation and antiherpetic activities of chemically modified polysaccharides from *Polygonatum cyrtonema* Hua. *Carbohydr Polym.* (2011) 83:737–42. doi: 10.1016/j.carbpol.2010.08.044

66. Chen JF, Huang GL. The antioxidant activities of carboxymethylated garlic polysaccharide and its derivatives. *Int J Biol Macromol.* (2019) 125:432–5. doi: 10.1016/j.ijbiomac.2019.08.204

67. Chang Y, Kong R. Ganoderic acid A alleviates hypoxia-induced apoptosis, autophagy, and inflammation in rat neural stem cells through the PI3K/AKT/mTOR pathways. *Phytother Res.* (2019) 33:1448–56. doi: 10.1002/ptr.6336

68. Li L, Sun W, Wu T, Lu R, Shi B. Caffeic acid phenethyl ester attenuates lipopolysaccharide-stimulated proinflammatory responses in human gingival fibroblasts via NF-κB and PI3K/Akt signaling pathway. *Eur J Pharmacol.* (2017) 794:61–8. doi: 10.1016/j.ejphar.2016.11.0034

frontiers | Frontiers in Nutrition

TYPE Original Research
PUBLISHED 05 September 2022
DOI 10.3389/fnut.2022.969465

Check for updates

OPEN ACCESS

EDITED BY
Qiu Li,
Qingdao Agricultural University, China

REVIEWED BY
Limin Ning,
Nanjing University of Chinese Medicine, China
Xiang Li,
Nanjing University of Chinese Medicine, China
Feier Cheng,
Shanxi Agricultural University, China

*CORRESPONDENCE
Qiang Peng
pengqiang@nwsuaf.edu.cn

†These authors have contributed equally to this work and share first authorship

SPECIALTY SECTION
This article was submitted to Food Chemistry, a section of the journal Frontiers in Nutrition

RECEIVED 15 June 2022
ACCEPTED 12 July 2022
PUBLISHED 05 September 2022

CITATION
Zhu Y, Liu K, Yuen M, Yuen T, Yuen H and Peng Q (2022) Extraction and characterization of a pectin from sea buckthorn peel.
Front. Nutr. 9:969465.
doi: 10.3389/fnut.2022.969465

COPYRIGHT
© 2022 Zhu, Liu, Yuen, Yuen, Yuen and Peng. This is an open-access article distributed under the terms of the Creative Commons Attribution License (CC BY). The use, distribution or reproduction in other forums is permitted, provided the original author(s) and the copyright owner(s) are credited and that the original publication in this journal is cited, in accordance with accepted academic practice. No use, distribution or reproduction is permitted which does not comply with these terms.

Extraction and characterization of a pectin from sea buckthorn peel

Yulian Zhu[1†], Keshan Liu[1†], Michael Yuen[2], Tina Yuen[2], Hywel Yuen[2] and Qiang Peng[1,3*]

[1]College of Food Science and Engineering, Northwest A&F University, Yanling, China, [2]Puredia Limited, Xining, China, [3]Beijing Engineering and Technology Research Center of Food Additives, Beijing Technology and Business University, Beijing, China

Sea buckthorn peel is the by-product of the sea buckthorn processing, which contains many bioactive compounds. In this paper, sea buckthorn high methoxyl pectin (SBHMP) was obtained, with a yield of 8% and a light-colored. The SBHMP was a high methoxyl with a degree of esterification of 57.75% and uronic acid content of 65.35%. The structural and morphological characterization of SBHMP were analyzed by high-performance liquid chromatography, Fourier-transform infrared spectroscopy, and scanning electron microscopy. Results showed that SBHMP presented a sheet and layered stacked morphological, and was mainly composed of galacturonic acid, arabinose, galactose, rhamnose, and mannose, which indicated that SBHMP mainly consisted of homogalacturonan (HG) and rhamnogalacturonan-I (RG-I) type pectin polysaccharides. In addition, SBHMP also presented significant gel, thickening, and emulsifying properties. The results exhibited that SBHMP could form jelly-like gels under acid and high sucrose conditions, presenting a shear-thinning behavior and increasing apparent viscosity with the enhancement of pectin and sucrose contents. Besides, SBHMP could form oil-in-water emulsions with pectin concentrations of 1.0–3.0%. When the SBHMP concentrations were 2.0 and 3.0%, the emulsions were stable during 7 days of storage. Findings in this paper demonstrated the potential of SBHMP to be a food thickener and emulsifier and support the in-depth utilization of sea buckthorn by-products.

KEYWORDS

sea buckthorn peel, pectin, gelation property, characterization, emulsifying property

Introduction

As a natural biomolecule, pectin is an essential regulator of biological modifiers and is widely used in biochemistry, food, and pharmaceutical industries (1, 2). Due to their high safety, bioactivities, and biodegradability, natural pectin has recently been extensively studied (3). Numerous studies have shown that plant pectin has various biological activities such as antioxidant (4), antitumor (5), and regulation of intestinal microorganisms (6). Pectin is also widely used as a functional food additive due to its unique emulsification and gelation properties (7). According to its DE values, pectin is classified as high methoxyl pectin (HMP DE > 50%) and low methoxyl pectin (LMP DE < 50%). Compared to LMP, HMP can form a gel network with high sugar and acid environment, and the gelation is insensitive to Ca^{2+}. The existence of H^{+} inhibits the dissociation of carboxyl, and the abundance of sugar help to reduce the hydration radius of pectin, resulting in the interaction force between molecules weaker and chains closer. Besides, the hydrophobicity of methyl can also promote the interaction between chains (3). The unique gel-forming mechanism and solution environment allow HMP to be used as a food thickener in a wider range of applications.

Sea buckthorn (*Hippophae rhamnoides*) belongs to the Elaeagnaceae family, and is widely cultivated in China, India, Mongolia, and Europe because of its drought, cold, and salt resistance (8). As a medicinal and edible homologous plant, sea buckthorn has many related pharmacological effects recorded in writings as early as the Tang and Ming dynasties (9). In recent years, relevant studies have shown that extracts of sea buckthorn berries, leaves, and seeds contained a lot of biological activities (10, 11). With the development of the sea buckthorn industry, pomace, peel, seed meal, and other processing by-products have also accumulated, but they have not been fully utilized, resulting in wasted resources.

In recent years, the extraction of pectin from plant by-products has attracted interest due to its low toxicity and biological activity. According to relevant studies, a large amount of pectin is contained in the peel of fruits and vegetables, and the composition and application characteristics of pectin from different sources are quite different (12, 13). Currently, the study on sea buckthorn pectin was limited, and the application characterization of sea buckthorn pectin was unclear. In addition, the bioactive components in sea buckthorn vary in different growth habitats, among which the content and function of bioactive components in sea buckthorn grown in plateau tend to be better than those in plain (14). Therefore, the study of plateau sea buckthorn peel as an important source of pectin and the characterization of its functional properties are of great significance for the development of natural food additives.

This study aims to extract pectin from sea buckthorn peel, effectively improve its color and make it more in line with the market requirements. The gel properties, rheological properties, and emulsifying properties were also studied to develop Sea buckthorn peel pectin as a new natural food additive.

Materials and methods

Materials

Sea buckthorn peel was obtained from Puredia Limited (Xining, Qinghai, China). The sea buckthorn peel was the by-product of the production of sea buckthorn juice. The sea buckthorn fruits were squeezed to get the juice, then the residue was washed and dried, and the sea buckthorn peel was sorted out. The standard monosaccharides were bought from Solaribio Life Sciences Co., Ltd., (Beijing, China). The uronic acid (D-galacturonic acid) was obtained from Aladdin Biochemical Technology Co., Ltd., (Shanghai, China). The ethylene diamine tetraacetic acid (EDTA), citric acid, and sodium ascorbate were all edible grade and purchased from Man Pong Industry Company Limited (Henan, China). All the other chemicals and solvents used in this study were analytical grade.

Preparation of sea buckthorn pectin

According to the previous method (15), sea buckthorn peel was mixed with distilled water at a 1:10 *m/V* liquid-material ratio, 0.5‰ citric acid, 0.5‰ sodium ascorbate, and 0.2‰ EDTA. The pH of the mixture was then adjusted to 2.0 with HCl (1 mol/L) and incubated at 80°C for 1 h. After the incubation, the mixture was collected by centrifugated at 6,500 rpm for 15 min to collect the supernatant and further enrich it with filtration. Then the supernatant was concentrated by rotary evaporation and added 0.0004‰ volume of sodium metabisulfite to decolorize it slightly. Subsequently, the solution was mixed with 1.5 volumes of ethanol and stored for 4 h. SBHMP was obtained after dialyzed and lyophilization.

Chemical characterization

Determination of uronic acid content

According to the previous method (16), the uronic acid content of SBHMP was determined using the carbazole-sulfuric acid method with galacturonic acid as a standard. And the absorbance of the solution was measured at 528 nm with a spectrophotometer (model UV7, METTLER TOLEDO, Zürich, Switzerland).

Degree of esterification

The degree of esterification (SBHMP) of SBHMP was determined by the method of Ma et al. (17). The DE was calculated using the following Equation:

$$DE(\%) = \frac{V_2}{V_1 + V_2} \times 100$$

Where:

V_1 and V_2 demoted the volume of NaOH consumed for the first and second titrations.

Determination of monosaccharide composition

Referring to the method by Mzoughi et al. (18), the monosaccharide composition of SBHMP was determined by pre-column 1-phenyl-3-methyl-5-pyrazolone-derived high-performance liquid chromatography (PMP-HPLC) with Agilent 1100 system (Zorbax Eclipse Plus-C18 column, 4.6 mm×250 mm, 5 μm, Agilent, United States). The mobile phases were phosphate buffer (pH 6.6) and acetonitrile with a flow rate of 1.0 mL/min, and the column temperature was 30°C.

Structural characterization

Fourier-transform infrared spectroscopy analysis

SBHMP and KBr were mixed at the ratio of 1:100 to prepare the disk and detected at the wavelength from 400 to 4,000 cm^{-1} with an FTIR instrument (Vetex70, Bruker Co., Ettlingen, Germany).

Scanning electron microscopy

The surface morphology of SBHMP was obtained from an S-3400N scanning electron microscope (Hitachi, Tokyo, Japan). The freeze-dried SBHMP was attached to a sample stage and plated with gold by a sputter coater. Images of SBHMP were collected at 100×, 500×, and 2,000× .

Thermal analysis

According to the previous by Lin et al. (19) with slight modifications, the thermal property of SBHMP was detected by a differential scanning calorimetry (Q2000, Waters, Milford, MA, United States). The SBHMP sample (3 g) was loaded into an aluminum crucible and sealed immediately. Meanwhile, an empty aluminum crucible was used as a reference. The detection was carried out under the N_2 environment at the flow rate of 50 mL/min, the temperature was raised at the speed of 30°C/min, and the scanning range of temperature was 30–300°/min.

Gel properties

Gel preparation

The gel of SBHMP and sucrose was prepared according to a previous method (20). SBHMP was dissolved with distilled water at 70°C and adjusted the pH to 2.5, the solutions with different concentrations of sucrose (40–60% *m/m*) were prepared and stored at room temperature overnight. In addition, another group of solutions with different pH (2.0–3.5) was also prepared.

Line spread test

Referring to the previous study of Ke et al. (21) with some modifications, the gelation of SBHMP was evaluated by line spread teat on an acrylic plate. The plated was covered with several concentric circles with a spacing of 0.4 cm, and the diameter of the middle circle was 2.8 cm. Subsequently, the sample was positioned in the center of the plate and allowed to flow at room temperature for 2 min. The spread values of each sample were recorded rapidly after flow.

Frequency scanning of sea buckthorn high methoxyl pectin gel

According to the previous study by Rafe and Razavi (22), the rheological characterization of SBHMP gel was carried on a rheometer (DHR-1, Waters, United States) with a 40 mm plate and a 0.1 mm gap. The gel was prepared according to the results of the line spread test and performed as follows: (1) A strain scan (0.02–20%) at an angular frequency of 1 rad/s was first performed to determine the linear viscoelastic zone. (2) A frequency sweep of 0.1–100 rad/s was performed in the linear viscoelastic region (1%) and recorded the storage modulus (G′) and loss modulus (G″). The G′ and G″ of frequency sweep were calculated as the following Equations:

$$G' = K' \times \omega^a$$

$$G'' = K'' \times \omega^b$$

Where k′ (k″) and a (b) refer to the constant and frequency constant, and ω is the angular velocity.

Rheological measurements

The effect of SBHMP concentration (1.0–4.0% m/V), sucrose concentration (10–40% m/V), $CaCl_2$ (0.05–0.3% m/V), and pH (3.0–7.0) on the rheological characteristic of pectin solution were measured according to a relative study (23). All solutions were prepared and stored at room temperature overnight. The rheological properties were measured by a rheometer (DHR-1, Waters, United States) in a 40 mm parallel

plate with a gap of 1 mm. The analyses were carried out at 25°C for 120 s with a shear rate from 0.01 to 100 s^{-1}.

Emulsifying properties

Preparation of emulsion

The SBHMP emulsion was prepared according to the previous method with some modifications (24). Different concentrations (1.0, 1.5, 2.0, and 3.0% m/V) of SBHMP were prepared and mixed with corn germ oil at an equal volume. The mixtures were fully homogenized by a high-speed homogenizer (T18, IKA, Germany) at 10,000 rpm for 2 min to obtain the emulsion. Another group of emulsions with different concentrations (10, 20, 30, and 40% m/V) of corn germ oil and 2.0% SBHMP were also prepared to investigate the effect of oil fraction on the emulsifying properties.

Evaluation of emulsion properties

The emulsions were prepared and stored at room temperature for 7 days. The morphology of emulsions was observed using a fluorescent inverted microscope (LX71, Olympus, Japan) on the first day. Besides, the heights of the mixture and emulsion phase were recorded during the storage, and the creaming index (CI) was calculated as the following Equation (25):

$$CI = \frac{H_t}{H_e} \times 100\%$$

Where the Ht was the height of the total mixture and the He was the height of the emulsion phase.

Particle size evaluation

The particle size of the emulsion was determined using a laser particle size analyzer (LS3320, Beckman Coulter, United States) on the first and last day. The particle size distribution and average particle size of the emulsion were recorded during the measurement.

Statistical analysis

A one-way fixed-effects analysis of variance (ANOVA) test was performed using statistical software (SPSS 18.0, SPSS Inc., Chicago, IL, United States). All trials in this study were done in triplicate, and the statistical means and standard deviations were calculated and shown.

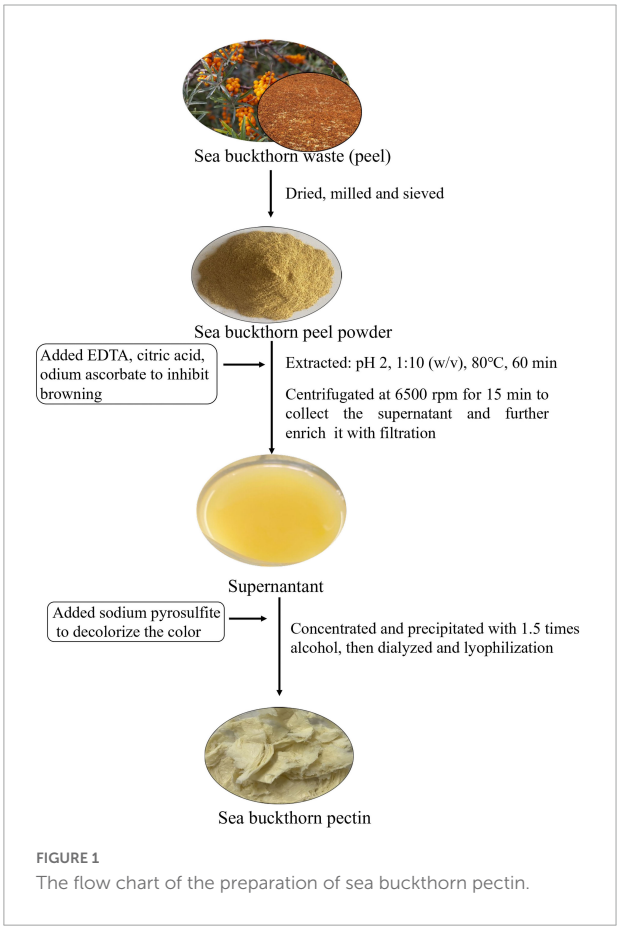

FIGURE 1
The flow chart of the preparation of sea buckthorn pectin.

Results and discussion

Preparation of sea buckthorn pectin polysaccharide

The flow chart of sea buckthorn pectin polysaccharide (SBHMP) was shown in **Figure 1**. Pectin is a group of water-soluble polysaccharides, which exists in the network formed by cellulose and hemicellulose in the plant cell wall (26). Heat solution treatment could disrupt the interaction between plant cell wall, dissolve the pectin polysaccharide into solution, and then add ethanol or metal salt to precipitate it (27). In this study, SBHMP was also prepared with acid and alcohol. Sea buckthorn peel is the by-product of the process of sea buckthorn juice, and therefore, impurities like metal ions may be mixed in during the process, making SBHMP a deepening color (28). Besides, acidic and heat conditions during the extraction of SBHMP may promote the phenomena of Maillard and Caramelization, thus influencing the product's color. Metal chelators could effectively bind metal ions associated with the browning of polysaccharides during extraction (29, 30). The addition of sodium ascorbate in the preparation process can prevent the oxidation of the extract. Relevant studies have shown that combing a small number of multiple browning inhibitors can effectively reduce the color of plant material (31–33). Therefore, citric acid, sodium ascorbate, and EDTA were added as browning inhibitions in the extraction of SBHMP. The final yield of SBHMP was 8%, with a light color and great market acceptability.

Chemical characterization of sea buckthorn pectin

Degree of esterification

The degree of esterification (DE) is one of the most important characteristics of pectin and is closely related to its functional properties such as solubility and gelation. The size and type of DE are influenced by the source and preparation of pectin (34). The DE of SBHMP was 57.75%, indicating that SBHMP was high methoxyl pectin (HMP), indicating that SBHMP could form a stable gel under high sugar and acidic environment (35).

Content of uronic acid

This study determined the uronic acid content of SBHMP by the carbazole-sulfuric acid method. This method dehydrated the uronic acid produced by the hydrolysis of SBHMP in H_2SO_4 to form a furfural derivative, which could be condensed with carbazole to form a purplish red substance with maximum absorbance at 528 nm. Besides, there was a linear relationship between the absorbance of the reaction system and uronic acid content (16). As shown in **Table 1**, the uronic acid content of SBHMP was 65.35%, indicating that SBHMP was a typical pectin polysaccharide, while the specific monosaccharide components required further study.

Structural analysis

Monosaccharide composition

As shown in **Table 1** and **Figure 2**, SBHMP was mainly composed of 9 monosaccharides, galacturonic acid, arabinose, galactose, rhamnose, mannose, glucose, fucose, xylose, and glucuronic acid, and the molar ratio was 66.49: 15.35: 5.73: 4.50: 3.18: 2.31: 1.07: 0.73: 0.64. From the results of monosaccharide composition, SBHMP may be classified as a complex consisting of homogalacturonan (HG) and arabinogalactan (RG-I) type pectin polysaccharides. The high content of galacturonic acid indicted the existence of homogalacturonan, which is mainly composed of GalA in the main chain and classified as an acid polysaccharide (3). Besides, the richness of arabinose and galactose suggested that SBHMP contained them in the branched chains of RG-I and free arabinogalactan as the neutral polysaccharide (36).

TABLE 1 Chemical composition of SBHMP.

Physicochemical features	SBHMP
Uronic acid (%)	65.35
DE (%)	57.75
Monosaccharides (%)	
Mannose (Man)	3.18
Rhamnose (Rha)	4.50
Glucuronic acid (Glc A)	0.64
Galacturonic acid (Gal A)	66.49
Glucose (Glc)	2.31
Galactose (Gal)	5.73
Xylose (Xyl)	0.73
Arabinose (Ara)	15.35
Fucose (Fuc)	1.07

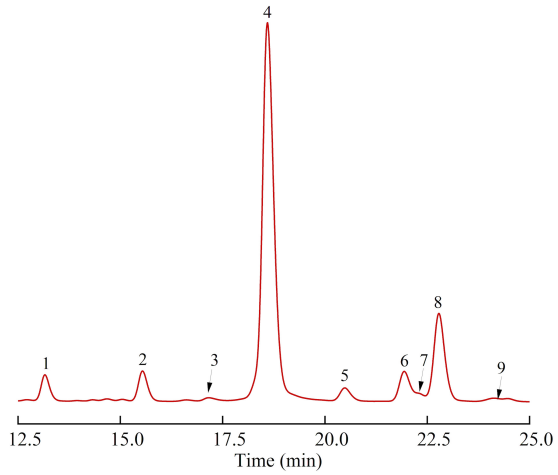

FIGURE 2
The monosaccharide composition of SBHMP (1 Mannose, 2 Rhamnose, 3 Glucuronic acid, 4 Galacturonic acid, 5 Glucose, 6 Galactose, 7 Xylose, 8 Arabinose, and 9 Fucose).

Fourier-transform infrared spectroscopy analysis

FTIR is one of the common methods used for the structural characterization of carbohydrates, the FTIR spectrum of SBHMP is shown in **Figure 3**. The results showed that SBHMP was a typical macromolecular compound linked by hydroxyl-rich monosaccharides through glycosidic bonds (37), thus, there was a strong and broad absorption peak in 2,406 cm^{-1}. Due to the large number of -CH_2 in the sugar ring, the obvious peak at 2,922 cm^{-1} was the stretching vibration of -CH (27). The peak intensity around 1,745 cm^{-1} was related to the vibration of the asymmetric tension of carbonyl methyl ester. The peak near 1,635 cm^{-1} belonged to the vibration of the symmetric tension of carboxylate ions. Besides, the peak area at 1,745 and 1,635 cm^{-1} could reflect the DE of pectin. According to **Figure 3**, the peak at 1,745 cm^{-1} was stronger than 1,635 cm^{-1}, indicating that SBHMP was high in methoxy pectin (4), the same as the results of the DE measurement. The peaks at 1,103 and 1,020 cm^{-1} were probably due to the stretching vibrations of C-OH in the branched chains and C-O-C in the glycosidic bonds (15). Other peaks from 500 to 1,000 cm^{-1} were the characteristic adsorption of the pyran rings in SBHMP (27).

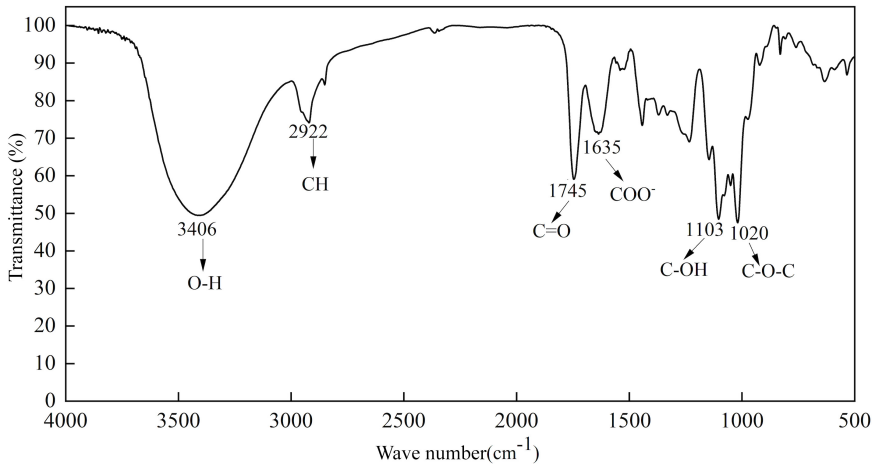

FIGURE 3
FTIR spectra of SBHMP.

Scanning electron micrograph analysis

The morphological property of SBHMP was detected by SEM, and the results were shown in **Figure 4**. It could be concluded that SBHMP presented a sheet and layered stacked structure with a smooth and dense surface. Such a particular structure provided SBHMP with a larger surface and higher solubility for SBHMP. In addition, the lamellar structure of SBHMP made it easier to combine with other substances, which might provide some specific properties (15). These findings were familiar with the pectin polysaccharide extracted from jujube pomace, which also exhibited a smooth surface and a lamellar shape (19).

Thermal analysis results

To further study the thermodynamic properties of SBHMP, its thermal stability was evaluated by differential scanning calorimetry, and the result was shown in **Figure 5**. The DSC diagram has two main peaks: the heat absorption peak and the heat release peak. The heat absorption peak is the melting temperature and the area of the peak is the enthalpy change of melting. The exothermic peak is the degradation temperature, and the area of the peak is the enthalpy change of degradation (38). The melting temperature of SBHMP was 133.48°C, corresponding to the enthalpy of melting of 189.5 J/g, and the enthalpy of degradation was 269.03°C, corresponding to the enthalpy of degradation of 95.97 J/g. The results indicated that SBHMP started to melt at 133.48°C and decompose at 269°C. As the temperature increased, the water molecules within the sample began to disperse, and oxidation and aggregation reactions occurred. With further heating, the galacturonic acid chains within the pectin started to break and degrade, the glycosidic bonds were broken, the carboxylic acid groups underwent decarboxylation reactions, and the structure was drastically altered (39). The higher enthalpy change of melting and stability of SBHMP may be related to the higher degree of esterification and uronic acid content. The higher heat absorption peak indicates that SBHMP had superior water retention and a higher content of hydrophilic groups (19). This was consistent with the results shown by SEM, where the larger surface area and lamellar stacked structure of SBHMP may allow for higher adsorption property.

Gel property analysis

Line spread test

Gelation is one of the most important properties of pectin, and the gelation mechanism of SBHMP as an HMP is closely related to its structure and formation conditions. The high sugar content and low pH facilitate the reduction of intermolecular distances between pectin, and the formation of hydrogen bonds, making pectin molecules form a network structure. The hydrated sucrose molecules can also adsorb in the gaps of the network structure through hydrogen bonding and intermolecular forces, forming a stable gel structure (40). Thus, in this study, the effects of different sucrose contents and pH values on the gelation of SBHMP were studied. As shown in **Figure 6A**, with the increase in sucrose content, the fluidity of the mixture decreased. Under the condition of 1% SBHMP, 55% sucrose, and pH 2.5, a honey-like gel could be developed (with a diameter of 3.1 cm). When the sucrose content increased to 60%, a jelly gel with a certain elasticity could be formed (with a diameter less than 2.8 cm). While with the decrease of sucrose content below 50%, the fluidity of the mixture increased, and gel could not be formed (with a diameter of more than 4.0 cm). And when the sucrose content was reduced to 40%,

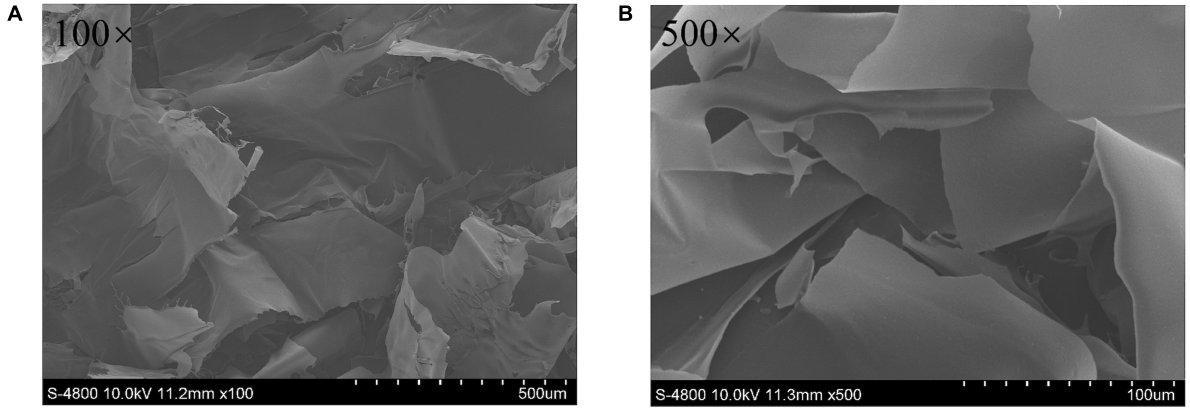

FIGURE 4
SEM images of SBHMP with the magnification of **(A)** 100×, and **(B)** 500×.

the fluidity further enhanced the viscosity of the mixture system and promoted the formation of a stable network structure. The gel formation of HMP is also related to the pH in the mixture. Pectin generally has a negative charge in the solution, and when the pH is below 3.5, the charge in the system can be neutralized. Then with the addition of a binding substance, the highly hydrated pectin dehydrated to form a network structure (41). Therefore, the different gelation states formed at a fixed 1% SBHMP, 60% sucrose, and a pH of 2.0–3.5 were investigated in this study. The results in **Figure 6B** showed that the gelation of SBHMP improved as the pH decreased, with reduced fluidity and increased stability. When the pH is at 2.5 and 2.0 stable gels could be formed (with a diameter less than 2.8 cm). Due to the decrease in pH, the electrostatic interactions between pectin molecular chains and the groups inner the chains increased, resulting in an improvement in the gels' hardness, viscosity, and stability (42). The conclusion could be obtained that a stable gel of SBHMP could be formed at the condition of 1% SBHMP, 60% sucrose, and the pH at 2.0 or 2.5. While the specific rheological properties of the gels need further study.

Rheological property

Based on the results of the line spread test, three groups of SBHMP gels with great gelation were prepared as follows: fixed the content of SBHMP at 1%, added 60% sucrose at pH 2.5 (group A), added 60% sucrose at pH 2.0 (group B) and added 55% sucrose at pH 2.5 (group C), respectively. The rheological properties of A, B, and C can be summarized according to **Figure 7**. The storage modulus (G′) is related to the energy lost in elastic deformation, which reflects the elasticity of the gel. The loss modulus (G″) is related to the energy lost in irreversible deformation, which reflects the viscosity of the gel. The relative magnitudes of G′ and G″ represent the viscoelastic characteristics of the sample (43). As shown in **Figure 7A**, G′ values were always higher than G″ in groups A and B, indicating a solid-state. Group C's G′ and G″ values were lower than groups A and B. With the increase of ω, the curves of G′ and G″ dominated, and the sample changed from a biased solid-state to liquid, with a significant difference between a and b values and poor frequency stability. The unstable gelation might be due to the decreased sucrose content of group C, which increased the water activity of the mixture, reduced the viscosity, and enhanced the fluidity (41, 44). From **Figure 7B**, the complex viscosity η* of three groups decreased with increasing share rate, indicating that they were typical non-Newtonian fluids that exhibited share thinning properties. Compared to group A, B exhibited smaller viscosity values at low shear rates, which was consistent with the state of the gel in **Figure 7B**. However, as the shear rate increased, the viscosity change tended gradually to the same, indicating that they exhibited similar rheological properties at a high shear rate. It could infer that changes in

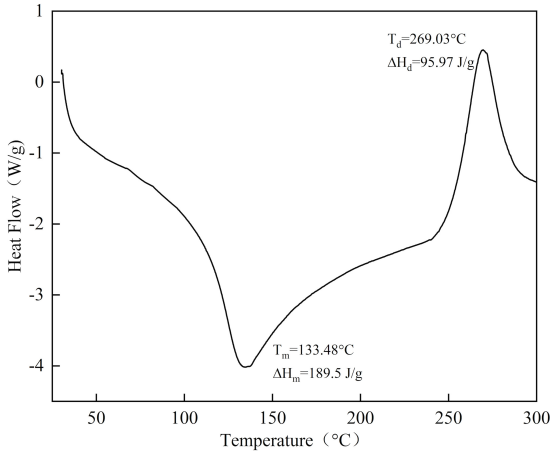

FIGURE 5
DSC thermogram images of SBHMP.

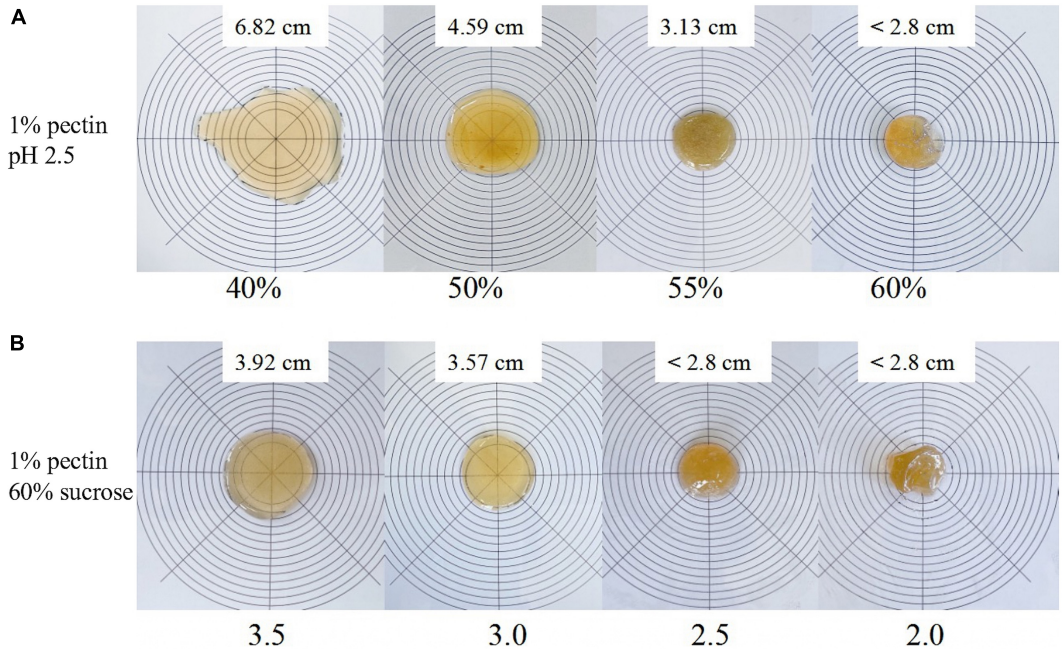

FIGURE 6
The visual aspect of SBHMP gel in line spread tests with various concentrations of sucrose, and under different pH values: **(A)** effects of various concentrations of sucrose on gel morphology **(B)** effect of different pH values on gel morphology.

pH have no significant effect on the gel properties of SBHMP in processing, which may facilitate its usage in the food industry. The viscosity decreased significantly with decreasing sucrose concentration in group C compared to group A, which was familiar with the results in Figure 5. This indicated that the effects of sucrose content change on the mixture's viscosity were more obvious than that of pH change within the range of conditions in this study.

Rheological measurement of sea buckthorn high methoxyl pectin

In recent years, attention has been paid to the research on the rheological properties of food colloids, which are closely related to their functional properties. Compared to other colloidal solutions, the flow characteristics of pectin solutions at low concentrations approximate Newtonian fluid, while exhibiting the properties of the pseudoplastic fluid at high concentrations (21). The viscosity of pectin solutions is not only related to its structural properties but is also influenced by the concentration of pectin in solution, pH, and ion concentration (43).

Influence of sea buckthorn high methoxyl pectin concentration on rheological properties

As shown in Figure 8A, with increasing shear rate, the apparent viscosity of all solutions decreased and showed shear thinning behavior, indicating that the SBHMP solution was a typical non-Newtonian fluid. Besides, as the pectin concentrations increased, the viscosity of solutions increased, and the shear thinning resistance behavior was enhanced. The apparent viscosity of 1, 2, 3, and 4% SBHMP solutions were 0.07, 0.11, 0.17, and 0.27 Pa at the shear rate of 1 s^{-1}, respectively. This might be due to the increase in SBHMP concentration, the number of pectin molecules increased, and the intermolecular force increased, resulting in more viscoelastic chain structures. The viscosity of SBHMP was higher than that of gabiroba pectin (with the apparent viscosity of 0.02 and 0.13 Pa at concentrations of 1 and 3%) and sweet lemon peel pectin (with the apparent viscosity below 0.01 and 0.1 Pa at the concentrations of 1 and 2%) at the same shear rate (45, 46). This showed that SBHMP had better rheological properties, which expanded its potential as a stabilizer and thickener in the food industry.

Influence of sucrose concentration on rheological properties

Figure 8B exhibited that the apparent viscosity of SBHMP solution was enhanced with the increasing sucrose concentration. This might be caused by the sucrose-containing many hydrophilic groups, which would compete with SBHMP for water molecules in solution, reducing the activity of water molecules and leading to a decrease in the solubilization of pectin molecular chains and an enhancement of interaction (46). In this study, when the sucrose concentration reached

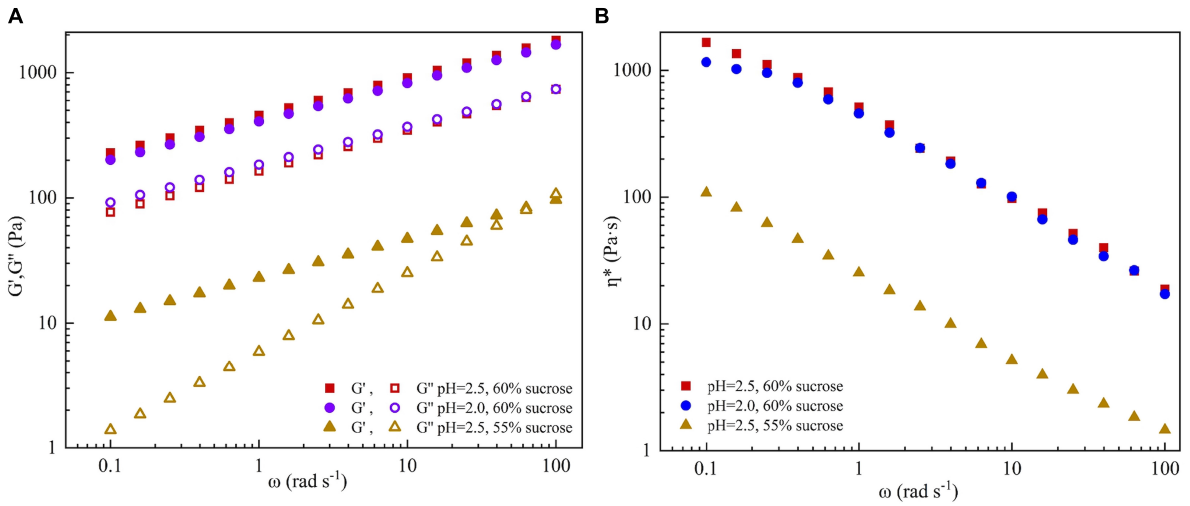

FIGURE 7
The effect of different concentrations of sucrose and pH values on **(A)** storage modulus (G′), loss modulus (G″), and **(B)** complex viscosity (η*, c) of SBHMP gels.

40%, it could significantly enhance the shear-thinning resistance of SBHMP solution, indicating that SBHMP could play a better thickening role in high sugar foods.

Influence of $CaCl_2$ concentration on rheological properties

It could be seen from **Figure 8C** that the addition of low concentrations of Ca^{2+} (0.05 and 0.1%) could increase the apparent viscosity of the SBHMP solution. This may be because Ca^{2+} formed calcium bridges between carboxyl groups of pectin molecules to enhance the network structure and the aggregation state, thus increasing the apparent viscosity. However, due to the higher DE of SBHMP, the effect of Ca^{2+} concentration on its viscosity was limited. When the Ca^{2+} concentration further increased to 0.2% and above, the viscosity of the SBHMP solution did not change significantly. This might be related to the high Ca^{2+} concentration reducing the repulsive force between molecules in solution, resulting in the agglomeration of pectin molecules (47).

Influence of pH on rheological properties

It could be summarized from **Figure 8D**, the apparent viscosity of SBHMP solutions varied with the increasing pH. The viscosity was highest in the pH range at 3–4, and slightly decreased at the same shear rate at pH 5. While the apparent viscosity decreased significantly when the pH reached 6 and 7, and the shear thinning behavior increased. It indicated that SBHMP was more stable when the pH was below 5 and was suitable as a thickener for low-acid products. This might be because the strongly acid condition allowed the carboxyl groups in the SBHMP structure to dissociate into carboxylate ions and the intermolecular repulsion (48). With the increase of pH, the carboxyl group dissociation in the SBHMP molecules was inhibited in the weakly acidic environment, the intermolecular hydrogen bonding force was enhanced, and the solution viscosity was larger. When the pH increased further, the number of H^+ decreased and the number of -OH increased in the solution. The -OH groups interacted with pectin molecules, causing the SBHMP structure to curl and intermolecular forces to weaken, ultimately leading to a decrease in solution viscosity (49).

Emulsifying properties

Carbohydrates such as pectin can form a hydration layer in aqueous oil solutions to prevent oil droplets from collecting. The greater the thickness of the hydration layer formed, the better the emulsion stability (50). The emulsification capacity and emulsion stability of pectin make it a valuable tool for the food industry. The emulsification properties of pectin are closely related to its hydrophobic group content, structural characteristics, and molecular weight (51).

Creaming index evaluation

The mixture of SBHMP and corn oil was stirred at high speed to form a stable and homogeneous emulsion, with no breakage or phase separation within a short time after preparation. After 7 days of storage, phase separation occurred in varying degrees in the individual blends. When the oil phase volume was fixed, the emulsion separation decreased as the concentration of SBHMP increased from 1.0 to 3.0%. Emulsification diminished when the SBHMP concentration was fixed as the oil phase concentration increased (10–40%).

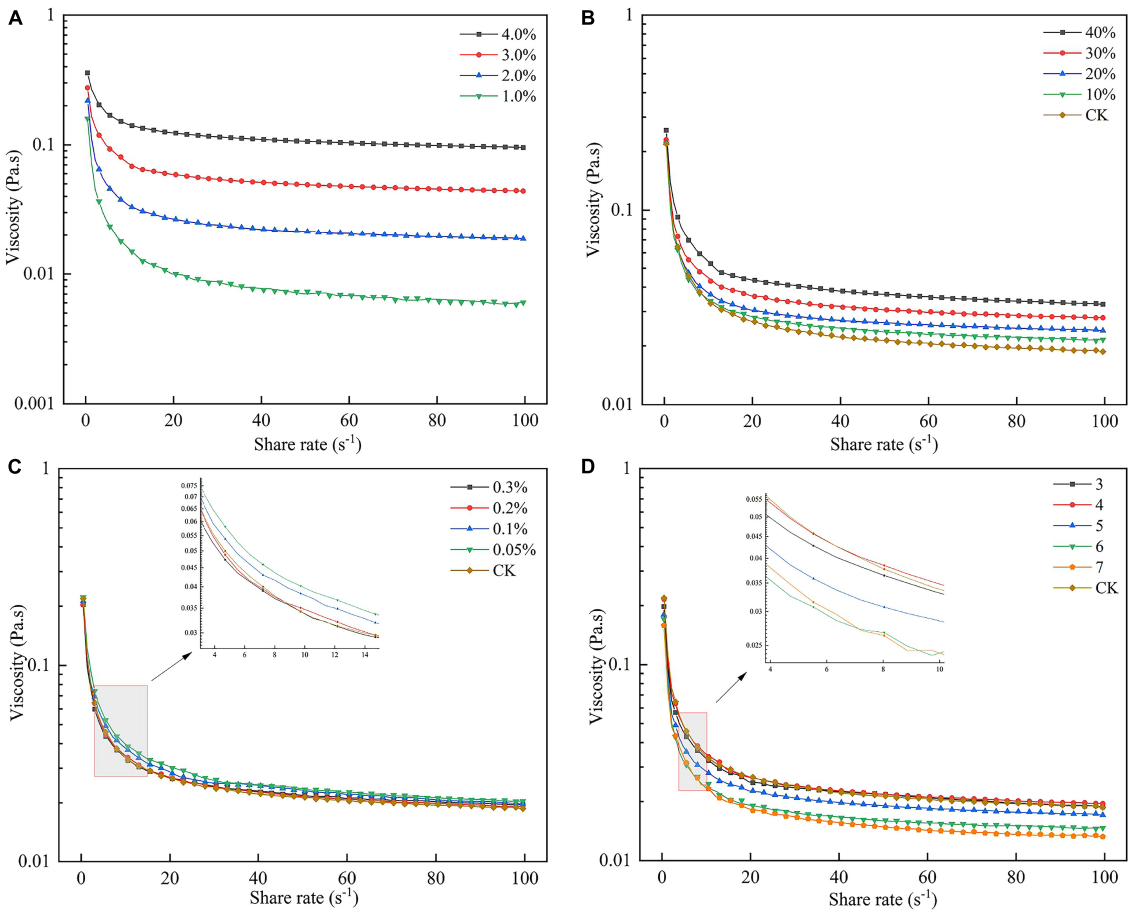

FIGURE 8
Effect of **(A)** various SBHMP concentrations, **(B)** various sucrose concentrations, **(C)** various $CaCl_2$ concentrations, and **(D)** different pH values on the pectin rheological properties.

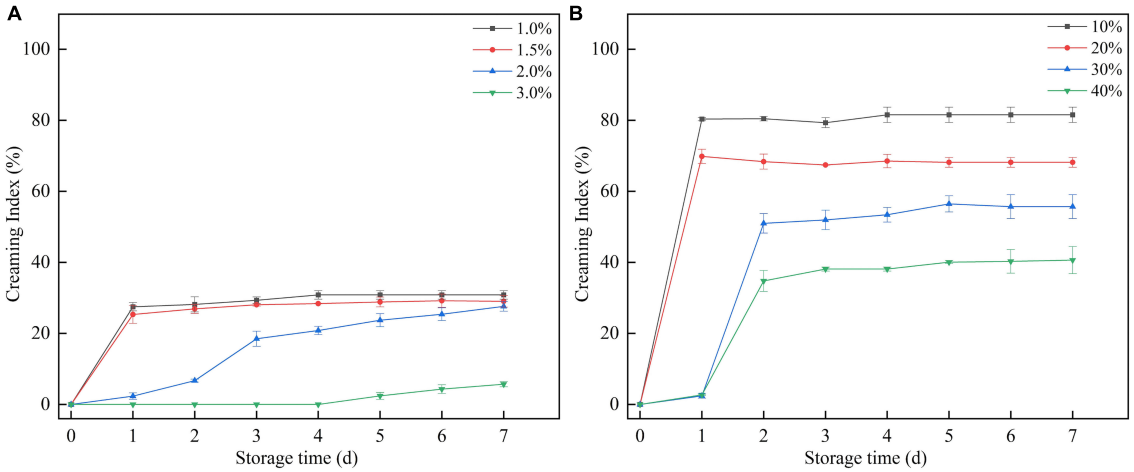

FIGURE 9
The creaming index of the mixtures during storage: **(A)** effect of various SBHMP concentrations on the CI values, **(B)** effect of various sucrose concentrations on the CI values.

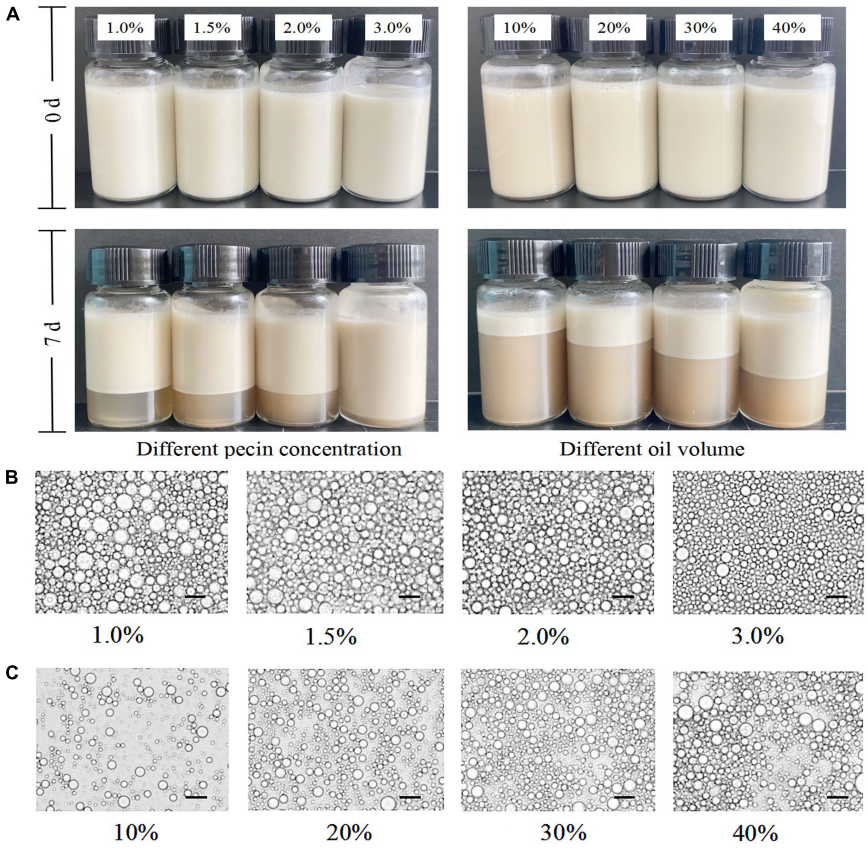

FIGURE 10
(A) Digital photos of oil-in-water emulsions stabilized by different concentrations of pectin and different volumes of oil. Optical micrographs of the emulsions stabilized by various contents of **(B)** SBHMP, and **(C)** oil.

The creaming index of each sample during storage can be seen in Figure 9. The emulsions in the 3.0% group did not emulsify during the storage period of days 1–4. The emulsion index increased slowly from day 4–7 days to 5.69% on day 7, which was lower than that of the other concentrations. This indicated that the emulsification property of pectin is closely related to its concentration. As the concentration of SBHMP increased, the interfacial tension decreased, promoting the formation of emulsified particles. Moreover, the cross-linking of the pectin chain structure of SBHMP in the mixed system is enhanced, forming a greater spatial site resistance, thus preventing the aggregation of oil droplets (52). While, when the SBHMP concentration was fixed, the emulsion index increased significantly after 1 day of storage when the corn oil content increased from 10 to 20%, indicating that rapid and obvious phase separation occurred. The emulsion index increased significantly after 2 days of storage when the corn oil content was 30 and 40%, and the phase separation was completed.

Observation of droplet

The state of the emulsion droplets formed in different conditions could be observed in Figure 10. It could be seen that the emulsion system was an oil-in-water, in which the diameter of the emulsion droplets decreased with the increase of SBHMP concentrations and the distribution was more uniform, indicating that SBHMP played a good emulsification role in the mixed system. It was probably due to the increase of SBHMP concentrations, the viscosity of the emulsion system increased, and the stability of the emulsion enhanced. While as the oil content increased, the oil droplet aggregated, the emulsion particles were larger, and the emulsion stability decreased (53).

Droplet size distribution

The droplet size distribution and the D_{43} of emulsion with different concentrations of SBHMP and oil were shown in Figure 11. As the SBHMP concentrations increased, the main peak of the droplet size distribution plot shifted to the left, with D_{43} gradually decreasing from 26.57 μm (with 0.1% SBHMP) to 10.82 μm (with 0.3% SBHMP), indicating the formation of more small droplets, which is consistent with the microscopic observations. At the concentration of SBHMP of 1.0%, a small number of droplets over 100 μm were produced, whereas at 2.0% of SBHMP, the droplets were all less than 40 μm, indicating that SBHMP played a stronger emulsifying role in the emulsion

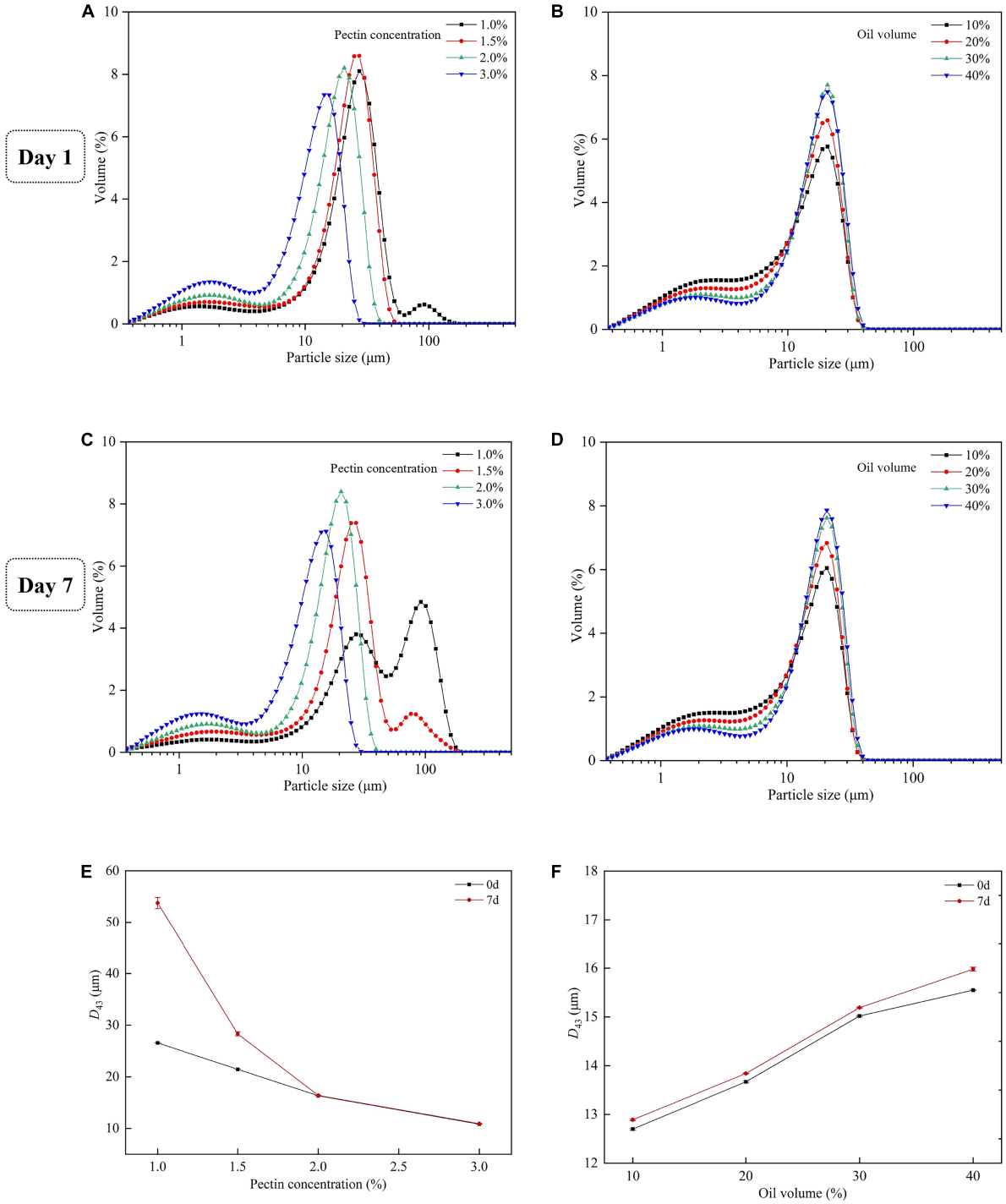

FIGURE 11
Droplet size distributions of emulsions on the first day **(A)** with various concentrations of SBHMP, and **(B)** with different volumes of oil. Droplet size distributions of emulsions after 7 days of storage **(C)** with various concentrations of SBHMP, and **(D)** with different volumes of oil. The D_{43} values of the emulsions during the storage **(E)** with various concentrations of SBHMP, and **(F)** with different volumes of oil.

system as the concentration increased. After 7 days of storage, the particle size distribution of the group with the addition of 1.0 and 1.5% SBHMP changed significantly, with new peaks appearing and a significant increase in D_{43}. The position of the main peak in the addition of 1.0% SBHMP also changed, indicating that emulsion breakage might have occurred in

the mixture. The changes in droplet size distribution again indicated that the emulsification of SBHMP was concentration-dependent. In the emulsification, pectin not only covered the oil droplets but also influenced the emulsification process through its viscosity effect (54). Therefore, the potential of SBHMP as a good rheology modifier needs to be further investigated. Although the change in oil phrase volume did not effectively affect the position of the main peak of the particle size distribution, the area of the peak increased slightly with increasing oil phase volume, with the droplets particle size (D_{43}) increased from 12.70 μm (with 10% oil) to 15.55 μm (with 40% oil). This indicated that the size of the droplet was positively correlated with the oil phase content. As the oil phase content increased, the water-oil interfacial tension decreased, droplet aggregation occurred, and the homogeneous stability of the emulsion decreased (15). It also suggested that the spatial barrier formed by SBHMP at different oil phase contents can inhibit emulsion breakage and maintain emulsion stability in a short period.

Conclusion

In summary, SBHMP was extracted and decolorized from sea buckthorn peel at a yield of 8%. The structural analysis exhibited that SBHMP was a high methoxyl pectin with a smooth and layered morphology. SBHMP was a typical pectin with a DE of 57.75% and a high uronic acid content of 65.35%. Besides, SBHMP was mainly composed of galacturonic acid, arabinose, galactose, rhamnose, and mannose, which could be classified as a complex consisting of HG and RG-I type pectin polysaccharides. The gel properties evaluation exhibited that SBHMP could form a jelly-like gel with an acid and high sucrose condition, exhibiting a shear thinning behavior. The apparent viscosity changed according to the pH values, pectin content, and sucrose concentration. The emulsifying properties measurement showed that SBHMP could form oil-in-water emulsions with different concentrations of SBHMP, and when SBHMP concentration reached 2.0% the emulsions were stable during the storage with the D_{43} values not changing more than 0.5 μm. This study supported that SBHMP could be a natural food additive, and further research should be devoted to exploring its specific functions.

Data availability statement

The original contributions presented in this study are included in the article/supplementary material, further inquiries can be directed to the corresponding author.

Author contributions

YZ: formal analysis, investigation, data curation, and writing— original draft preparation. KL: methodology, validation, visualization and funding acquisition, and writing— review and editing. QP: conceptualization, funding acquisition, and project administration. All authors contributed to the article and approved the submitted version.

Funding

This research was financially supported by the Science and Technology Project of Xining (No. 2021-Y-15), the Beijing Engineering and Technology Research Center of Food Additives, the Beijing Technology and Business University (BTBU), and the Yulin City Science and Technology Plan Project (No. CXY-2020-074).

Acknowledgments

We would like to thank the instrument shared platform of college of food science and engineering of NWAFU, for the assistance in the HPLC analysis (Yuan Zhou) and particle size analysis (Cuicui Ma).

Conflict of interest

MY, TY, and HY were employed by Puredia Limited.

The remaining authors declare that the research was conducted in the absence of any commercial or financial relationships that could be construed as a potential conflict of interest.

Publisher's note

All claims expressed in this article are solely those of the authors and do not necessarily represent those of their affiliated organizations, or those of the publisher, the editors and the reviewers. Any product that may be evaluated in this article, or claim that may be made by its manufacturer, is not guaranteed or endorsed by the publisher.

References

1. Dranca F, Oroian M. Extraction, purification and characterization of pectin from alternative sources with potential technological applications. *Food Res Int.* (2018) 113:327–50.

2. Jin L, Zuo F, Gao Y, Sui S, Zhang D. Purification of pectin by ultrafiltration in combination with sodium citrate. *J Food Eng.* (2022):111158.

3. Li D, Li J, Dong H, Li X, Zhang J, Ramaswamy S, et al. Pectin in biomedical and drug delivery applications: a review. *Int J Biol Macromol.* (2021) 185:49–65.

4. Liu N, Yang W, Li X, Zhao P, Liu Y, Guo L, et al. Comparison of characterization and antioxidant activity of different citrus peel pectins. *Food Chem.* (2022) 386:132683. doi: 10.1016/j.foodchem.2022.132683

5. Tamiello C, Adami E, De Oliveira N, Acco A, Iacomini M, Cordeiro L. Structural features of polysaccharides from edible jambo (*Syzygium jambos*) fruits and antitumor activity of extracted pectins. *Int J Biol Macromol.* (2018) 118:1414–21. doi: 10.1016/j.ijbiomac.2018.06.164

6. Yu J, Ye M, Li K, Wang F, Shi X, Pan C, et al. Fragments of a pectin from *Arctium lappa* L: molecular properties and intestinal regulation activity. *J Funct Foods.* (2022) 88:104900.

7. Li L, Gao X, Liu J, Chitrakar B, Wang B, Wang Y. Hawthorn pectin: extraction, function and utilization. *Curr Res Food Sci.* (2021) 4:429–35. doi: 10.1016/j.crfs.2021.06.002

8. Ciesarova Z, Murkovic M, Cejpek K, Kreps F, Tobolkova B, Koplik R, et al. Why is sea buckthorn (*Hippophae rhamnoides* L.) so exceptional? A review. *Food Res Int.* (2020) 133:109170. doi: 10.1016/j.foodres.2020.109170

9. Pundir S, Garg P, Dviwedi A, Ali A, Kapoor V, Kapoor D, et al. Ethnomedicinal uses, phytochemistry and dermatological effects of *Hippophae rhamnoides* L.: a review. *J Ethnopharmacol.* (2021) 266:113434. doi: 10.1016/j.jep.2020.113434

10. Lee H, Lee C, Choi S, Kim Y, Hur J. Inhibitory effect of sea buckthorn extracts on advanced glycation endproduct formation. *Food Chem.* (2022) 373:131364. doi: 10.1016/j.foodchem.2021.131364

11. Marciniak B, Kontek R, Zuchowski J, Stochmal A. Novel bioactive properties of low-polarity fractions from sea-buckthorn extracts (*Elaeagnus rhamnoides* (*L.*) *A. Nelson*) - (in vitro). *Biomed Pharmacother.* (2021) 135:111141. doi: 10.1016/j.biopha.2020.111141

12. Zhou M, Bi J, Li C, Chen J. Enhancive effect of instant controlled pressure drop (DIC) pre-treatment on pectin extractability from peach pomace. *Food Hydro.* (2022) 130:107696.

13. Karwacka M, Ciurzyńska A, Galus S, Janowicz M. Freeze-dried snacks obtained from frozen vegetable by-products and apple pomace–Selected properties, energy consumption and carbon footprint. *Innov Food Sci Emerg.* (2022) 77:102949.

14. Guo R, Guo X, Li T, Fu X, Liu R. Comparative assessment of phytochemical profiles, antioxidant and antiproliferative activities of Sea buckthorn (*Hippophae rhamnoides* L.) berries. *Food Chem.* (2017) 221:997–1003. doi: 10.1016/j.foodchem.2016.11.063

15. Jiang Y, Xu Y, Li F, Li D, Huang Q. Pectin extracted from persimmon peel: a physicochemical characterization and emulsifying properties evaluation. *Food Hydro.* (2020) 101:105561.

16. Yu M, Xia Y, Zhou M, Guo Y, Zheng J, Zhang Y. Effects of different extraction methods on structural and physicochemical properties of pectins from finger citron pomace. *Carbohydr Polym.* (2021) 258:117662. doi: 10.1016/j.carbpol.2021.117662

17. Ma J, Tong P, Chen Y, Wang Y, Ren H, Gao Z, et al. The inhibition of pectin oligosaccharides on degranulation of RBL-2H3 cells from apple pectin with high hydrostatic pressure assisted enzyme treatment. *Food Chem.* (2022) 371:131097. doi: 10.1016/j.foodchem.2021.131097

18. Mzoughi Z, Abdelhamid A, Rihouey C, Cerf D, Bouraoui A, Majdoub H. Optimized extraction of pectin-like polysaccharide from Suaeda fruticosa leaves: characterization, antioxidant, anti-inflammatory and analgesic activities. *Carbohydr Polym.* (2018) 185:127–37. doi: 10.1016/j.carbpol.2018.01.022

19. Lin X, Liu K, Yin S, Qin Y, Shen P, Peng Q. A novel pectic polysaccharide of jujube pomace: structural analysis and intracellular antioxidant activities. *Antioxidants.* (2020) 9:127. doi: 10.3390/antiox9020127

20. Zheng J, Zeng R, Kan J, Zhang F. Effects of ultrasonic treatment on gel rheological properties and gel formation of high-methoxyl pectin. *J Food Eng.* (2018) 231:83–90.

21. Ke J, Jiang G, Shen G, Wu H, Liu Y, Zhang Z. Optimization, characterization and rheological behavior study of pectin extracted from chayote (*Sechium edule*) using ultrasound assisted method. *Int J Biol Macromol.* (2020) 147:688–98. doi: 10.1016/j.ijbiomac.2020.01.055

22. Rafe A, Razavi S. Scaling law, fractal analysis and rheological characteristics of physical gels cross-linked with sodium trimetaphosphate. *Food Hydro.* (2017) 62:58–65.

23. Barbieri S, Petkowicz C, Godoy R, Azeredo H, Franco C, Silveira J. Pulp and jam of gabiroba (*Campomanesia xanthocarpa* Berg): characterization and rheological properties. *Food Chem.* (2018) 263:292–9. doi: 10.1016/j.foodchem.2018.05.004

24. Schmidt U, Schütz L, Schuchmann H. Interfacial and emulsifying properties of citrus pectin: interaction of pH, ionic strength and degree of esterification. *Food Hydro.* (2017) 62:288–98.

25. Ahsan H, Zhang X, Li Y, Li B, Liu S. Surface modification of microcrystalline cellulose: physicochemical characterization and applications in the Stabilization of Pickering emulsions. *Int J Biol Macromol.* (2019) 132:1176–84. doi: 10.1016/j.ijbiomac.2019.04.051

26. Liu J, Bi J, Mcclements D, Liu X, Yi J, Lyu J, et al. Impacts of thermal and non-thermal processing on structure and functionality of pectin in fruit- and vegetable- based products: a review. *Carbohydr Polym.* (2020) 250:116890. doi: 10.1016/j.carbpol.2020.116890

27. Zhu Y, He Z, Bao X, Wang M, Yin S, Song L, et al. Purification, in-depth structure analysis and antioxidant stress activity of a novel pectin-type polysaccharide from Ziziphus Jujuba cv. Muzaoresidue. *J Funct Foods.* (2021) 80:104439.

28. Shao L, Sun Y, Liang J, Li M, Li X. Decolorization affects the structural characteristics and antioxidant activity of polysaccharides from *Thesium chinense* Turcz: comparison of activated carbon and hydrogen peroxide decolorization. *Int J Biol Macromol.* (2020) 155:1084–91. doi: 10.1016/j.ijbiomac.2019.11.074

29. Li Q, Li X, Ren Z, Wang R, Zhang Y, Li J, et al. Physicochemical properties and antioxidant activity of Maillard reaction products derived from *Dioscorea opposita* polysaccharides. *LWT.* (2021) 149:111833.

30. Benhura M, Mbuya N, Machirori E. Facile formation of caramel colours using the polysaccharide material that is extracted from the fruit of *Azanza garckeana*. *Food Chem.* (1999) 65:303–7.

31. Barbagallo R, Chisari M, Caputa G. Effects of calcium citrate and ascorbate as inhibitors of browning and softening in minimally processed 'Birgah' eggplants. *Postharvest Biol Tec.* (2012) 73:107–14.

32. Rico D, Martín-Diana A, Frías J, Barat J, Henehan G, Barry-Ryan C. Improvement in texture using calcium lactate and heat-shock treatments for stored ready-to-eat carrots. *J Food Eng.* (2007) 79:1196–206.

33. Saftner R, Bai J, Abbott J, Lee Y. Sanitary dips with calcium propionate, calcium chloride, or a calcium amino acid chelate maintain quality and shelf stability of fresh-cut honeydew chunks. *Postharvest Biol Tec.* (2003) 29:257–69.

34. Cai R, Pan S, Li R, Xu X, Pan S, Liu F. Curcumin loading and colon release of pectin gel beads: effect of different de-esterification method. *Food Chem.* (2022) 389:133130. doi: 10.1016/j.foodchem.2022.133130

35. Wan L, Yang Z, Cai R, Pan S, Liu F, Pan S. Calcium-induced-gel properties for low methoxyl pectin in the presence of different sugar alcohols. *Food Hydro.* (2021):112.

36. Huang W, Zhao M, Wang X, Tian Y, Wang C, Sun J, et al. Revisiting the structure of arabinogalactan from *Lycium barbarum* and the impact of its side chain on anti-ageing activity. *Carbohydr Polym.* (2022) 286:119282. doi: 10.1016/j.carbpol.2022.119282

37. Munoz-Almagro N, Vendrell-Calatayud M, Mendez-Albinana P, Moreno R, Cano M, Villamiel M. Extraction optimization and structural characterization of pectin from persimmon fruit (*Diospyros kaki* Thunb. var. Rojo brillante). *Carbohydr Polym.* (2021) 272:118411. doi: 10.1016/j.carbpol.2021.118411

38. Einhorn-Stoll U, Kastner H, Drusch S. Thermally induced degradation of citrus pectins during storage – Alterations in molecular structure, color and thermal analysis. *Food Hydro.* (2014) 35:565–75.

39. Liu H, Dai T, Chen J, Liu W, Liu C, Deng L, et al. Extraction, characterization and spontaneous gelation mechanism of pectin from *Nicandra physaloides* (Linn.) Gaertn seeds. *Int J Biol Macromol.* (2022) 195:523–9. doi: 10.1016/j.ijbiomac.2021.12.032

40. Lin Y, An F, He H, Geng F, Song H, Huang Q. Structural and rheological characterization of pectin from passion fruit (*Passiflora edulis f. flavicarpa*) peel extracted by high-speed shearing. *Food Hydro.* (2021) 114:106555.

41. Li X, Dong Y, Guo Y, Zhang Z, Jia L, Gao H, et al. Okra polysaccharides reduced the gelling-required sucrose content in its synergistic gel with high-methoxyl pectin by microphase separation effect. *Food Hydro.* (2019) 95:506–16.

42. Chen R, Ratcliffe I, Williams P, Luo S, Chen J, Liu C. The influence of pH and monovalent ions on the gelation of pectin from the fruit seeds of the creeping fig plant. *Food Hydro.* (2021) 111:106219.

43. Roque A, Montinola D, Geonzon L, Matsukawa S, Lobarbio C, Taboada E, et al. Rheological elucidation of the viscoelastic properties and network interaction of mixed high-methoxyl pectin and kappa-carrageenan gels. *Food Hydro.* (2022) 129:107647.

44. Abitbol T, Mijlkovic A, Malafronte L, Stevanic J, Larsson P, Lopez-Sanchez P. Cellulose nanocrystal/low methoxyl pectin gels produced by internal ionotropic gelation. *Carbohydr Polym.* (2021) 260:117345. doi: 10.1016/j.carbpol.2020.117345

45. Barbieri S, Amaral S, Ruthes A, Petkowicz C, Kerkhoven N, Silva E, et al. Pectins from the pulp of gabiroba (*Campomanesia xanthocarpa* Berg): structural characterization and rheological behavior. *Carbohydr Polym.* (2019) 214:250–8. doi: 10.1016/j.carbpol.2019.03.045

46. Rahmani Z, Khodaiyan F, Kazemi M, Sharifan A. Optimization of microwave-assisted extraction and structural characterization of pectin from sweet lemon peel. *Int J Biol Macromol.* (2020) 147:1107–15. doi: 10.1016/j.ijbiomac.2019.10.079

47. Yapo B, Koffi K. Extraction and characterization of highly gelling low methoxy pectin from cashew apple pomace. *Foods.* (2013) 3:1–12. doi: 10.3390/foods3010001

48. Yan J, Wang C, Qiu W, Chen T, Yang Y, Wang W, et al. Ultrasonic treatment at different pH values affects the macromolecular, structural, and rheological characteristics of citrus pectin. *Food Chem.* (2021) 341:128216. doi: 10.1016/j.foodchem.2020.128216

49. Einhorn-Stoll U, Kastner H, Urbisch A, Kroh L, Drusch S. Thermal degradation of citrus pectin in low-moisture environment - Influence of acidic and alkaline pre-treatment. *Food Hydro.* (2019) 86:104–15.

50. Jiang W, Qi J, Huang Y, Zhang Y, Yang X. Emulsifying properties of high methoxyl pectins in binary systems of water-ethanol. *Carbohydr Polym.* (2020) 229:115420. doi: 10.1016/j.carbpol.2019.115420

51. Liu H, Deng L, Dai T, Chen J, Liu W, Liu C, et al. Emulsifying and emulsion stabilization mechanism of pectin from *Nicandra physaloides* (Linn.) *Gaertn* seeds: comparison with apple and citrus pectin. *Food Hydro.* (2022) 130:107674.

52. Ngouémazong E, Christiaens S, Shpigelman A, Loey A, Hendrickx M. The Emulsifying and Emulsion-Stabilizing Properties of Pectin: a Review. *Compr Rev Food Sci and F.* (2015) 14:705–18.

53. Cai X, Li C, Tang Q, Zhen B, Xie X, Zhu W, et al. Assembling kaolinite nanotube at water/oil interface for enhancing pickering emulsion stability. *Appl Clay Sci.* (2019) 172:115–22.

54. Qamar S, Bhandari B, Prakash S. Effect of different homogenisation methods and UHT processing on the stability of pea protein emulsion. *Food Res Int.* (2019) 116:1374–85. doi: 10.1016/j.foodres.2018.10.028

frontiers | Frontiers in Nutrition

TYPE Review
PUBLISHED 09 September 2022
DOI 10.3389/fnut.2022.1005181

Check for updates

OPEN ACCESS

EDITED BY
Xin Wang,
Northwest A&F University, China

REVIEWED BY
Honglei Tian,
Shaanxi Normal University, China
Xin Zhang,
Ningbo University, China
Jinhu Tian,
Zhejiang University, China

*CORRESPONDENCE
Jiaqi Tan
tanjq0909@hbu.edu.cn

†These authors have contributed equally to this work

SPECIALTY SECTION
This article was submitted to Food Chemistry, a section of the journal Frontiers in Nutrition

RECEIVED 28 July 2022
ACCEPTED 25 August 2022
PUBLISHED 09 September 2022

CITATION
Xue H, Li P, Bian J, Gao Y, Sang Y and Tan J (2022) Extraction, purification, structure, modification, and biological activity of traditional Chinese medicine polysaccharides: A review. *Front. Nutr.* 9:1005181. doi: 10.3389/fnut.2022.1005181

COPYRIGHT
© 2022 Xue, Li, Bian, Gao, Sang and Tan. This is an open-access article distributed under the terms of the Creative Commons Attribution License (CC BY). The use, distribution or reproduction in other forums is permitted, provided the original author(s) and the copyright owner(s) are credited and that the original publication in this journal is cited, in accordance with accepted academic practice. No use, distribution or reproduction is permitted which does not comply with these terms.

Extraction, purification, structure, modification, and biological activity of traditional Chinese medicine polysaccharides: A review

Hongkun Xue[1†], Pengcheng Li[2†], Jiayue Bian[3], Yuchao Gao[1], Yumei Sang[1] and Jiaqi Tan[1,4*]

[1]College of Traditional Chinese Medicine, Hebei University, Baoding, China, [2]College of Food Science and Technology, Jilin Agricultural University, Changchun, China, [3]School of Basic Medical Sciences, Hebei University, Baoding, China, [4]Medical Comprehensive Experimental Center, Hebei University, Baoding, China

Traditional Chinese medicines (TCM), as the unique natural resource, are rich in polysaccharides, polyphenols, proteins, amino acid, fats, vitamins, and other components. Hence, TCM have high medical and nutritional values. Polysaccharides are one of the most important active components in TCM. Growing reports have indicated that TCM polysaccharides (TCMPs) have various biological activities, such as antioxidant, anti-aging, immunomodulatory, hypoglycemic, hypolipidemic, anti-tumor, anti-inflammatory, and other activities. Hence, the research progresses and future prospects of TCMPs must be systematically reviewed to promote their better understanding. The aim of this review is to provide comprehensive and systematic recombinant information on the extraction, purification, structure, chemical modification, biological activities, and potential mechanism of TCMPs to support their therapeutic effects and health functions. The findings provide new valuable insights and theoretical basis for future research and development of TCMPs.

KEYWORDS

traditional Chinese medicines, polysaccharides, extraction and purification, structure, biological activities

Introduction

Traditional Chinese medicine (TCM) is one of the most important parts of Chinese culture and medical practice. In recent decades, increasing researches have confirmed that the leaves, stems, flowers, fruits, and tubers of TCM contain a variety of bioactive compounds such as polysaccharides, polyphenols, proteins, amino acid, fats, vitamins, and other components (1, 2). TCM polysaccharides (TCMPs), as a kind of biological macromolecules, are composed of 10 or more monosaccharides (3), and TCMPs with different biological activities have become the latest research hotspot. Each monosaccharide molecule is connected by glycosidic bonds and can be represented

by the general formula $(C_6H_{10}O_5)n$ (4). According to statistics, at least 30 kinds of TCMPs have been investigated in standard clinical trials. Growing studies have indicated that TCMPs show various biological activities, such as antioxidant, anti-aging, immunomodulatory, hypoglycemic, hypolipidemic, anti-tumor, anti-inflammatory, and other activities (5, 6). In addition, chemical modifications can improve or change the biological activities of TCMPs and have attracted extensive attention (7). Furthermore, TCMPs show little toxic and side effects. Thus, TCMPs, as a natural active components, have been extensively used in cosmetic, food, and health product industries.

At present, the researches on TCMPs mainly focus on theirs extraction, purification, structural characterization and modification, and biological activities (6). Nowadays, there are various extraction methods of TCMPs, which often affect the types, physicochemical properties, and biological activities of the final polysaccharides extraction products (8). Currently, hot water extraction (HWE) is the main method of polysaccharides extraction because it has the advantages of convenient extraction, no special equipment, and low cost (9). However, some polysaccharides are insoluble in hot water, and this technology can not realize the effective extraction of polysaccharides. Hence, some new extraction methods and techniques have been proposed for the extraction of polysaccharides with different properties (Figure 1). Nevertheless, the purity of polysaccharide is still low due to the limitation of extraction technology. Hence, the purification and structural identification of TCMPs are particularly important. As we all know, the purification of TCMPs is very complex, and it is difficult to obtain high-purity homogeneous polysaccharides fractions (10). Increasing studies have confirmed that the extraction and purification methods have an important impact on the modification and biological activities of polysaccharides (11–13). Consequently, the extraction and purification of TCMPs are an important prerequisite for the analysis of their biological activities and chemical modification. TCMPs can be used as natural candidate drugs for the prevention and treatment of different diseases based on the existing literature. Thus, the research progress and future prospects of TCMPs must be systematically reviewed to better understand TCMPs. In this review, the studies on the extraction and purification methods, structure, chemical modification, and biological activities of TCMPs in recent years were summarized (Figure 1), and the research progress and future development trend were described in detail. This review provides an important scientific basis for further in-depth development and utilization of TCMPs.

Extraction and purification of TCMPs

With the progress of science and technology, the extraction and purification technologies of polysaccharides have been fully developed. The nutritional and medicinal values of TCMPs have attracted extensive attention. The various traditional and novel extraction methods have already been established and proposed (6). Table 1 summarizes the different extraction, purification methods, and the corresponding TCMPs yield. According to the distribution and cell localization of TCMPs, and TCMPs are mainly divided into intracellular and extracellular polysaccharides (54). It is worth noting that the crude extracellular polysaccharides can be directly extracted by ethanol precipitation method (55). As for intracellular TCMPs, they are mainly extracted from the leaves, stems, flowers, fruits, and tubers of TCM by using different extraction methods (56–58). Before extracting intracellular TCMPs, the raw materials need to undergo a series of pretreatment, including washing, drying, crushing, and degreasing. Currently, hot water extraction (HWE) is the most commonly used and convenient extraction method, which is usually used to extract polysaccharides from natural resources in laboratory and industrial applications (59–61). Additionally, dilute alkali/acid methods, as another traditional extraction method, can improve the extraction efficiency and reduce the separation time of TCMPs to a certain extent (62). Nevertheless, the acidic and alkaline conditions must be strictly controlled to avoid the structure destruction of TCMPs. All in all, the traditional extraction methods have some advantages. However, they have significant disadvantages, such as low efficiency, long extraction time, large solvent consumption, and high extraction temperature (6). Hence, these methods are not suitable for large-scale extraction of polysaccharides in industry.

To solve the limitations of traditional extraction methods, some novel and effective extraction methods were proposed according to the principle of enhancing cell wall decomposition without destroying the structure of TCMPs. Notably, ultrasound assisted extraction (UAE), microwave assisted extraction (MAE), enzyme assisted extraction (EAE), and ultra-high pressure assisted extraction (UHPAE) methods have been widely used in the TCMPs extraction to improve theirs yield. Furthermore, the extraction conditions also affect the TCMPs yield to some extent. Thus, to improve the TCMPs yield, some optimization methods, including orthogonal experiments, response surface methodology (RSM), genetic algorithm (GA), and genetic algorithm coupled neural network (GA-NN) are used to optimize the extraction process of TCMPs. Wang et al. prepared polysaccharides from black mulberry by using HWE and optimized extraction process *via* RSM, and then purified crude polysaccharides by DEAE-52 cellulose and Sephadex G-100. The results show that the optimal extraction conditions were extraction time of 3 h, extraction temperature of 87 °C, and liquid-to-solid ratio of 39 mL/g. The yield of polysaccharides from black mulberry was 11.86% ± 0.21%. In addition, two purified fractions of BMP-1-1 with molecular weight of 615 kDa and BMP-2-1 with molecular weight of 405 kDa were obtained (14). Zhu et al. extracted the crude polysaccharides

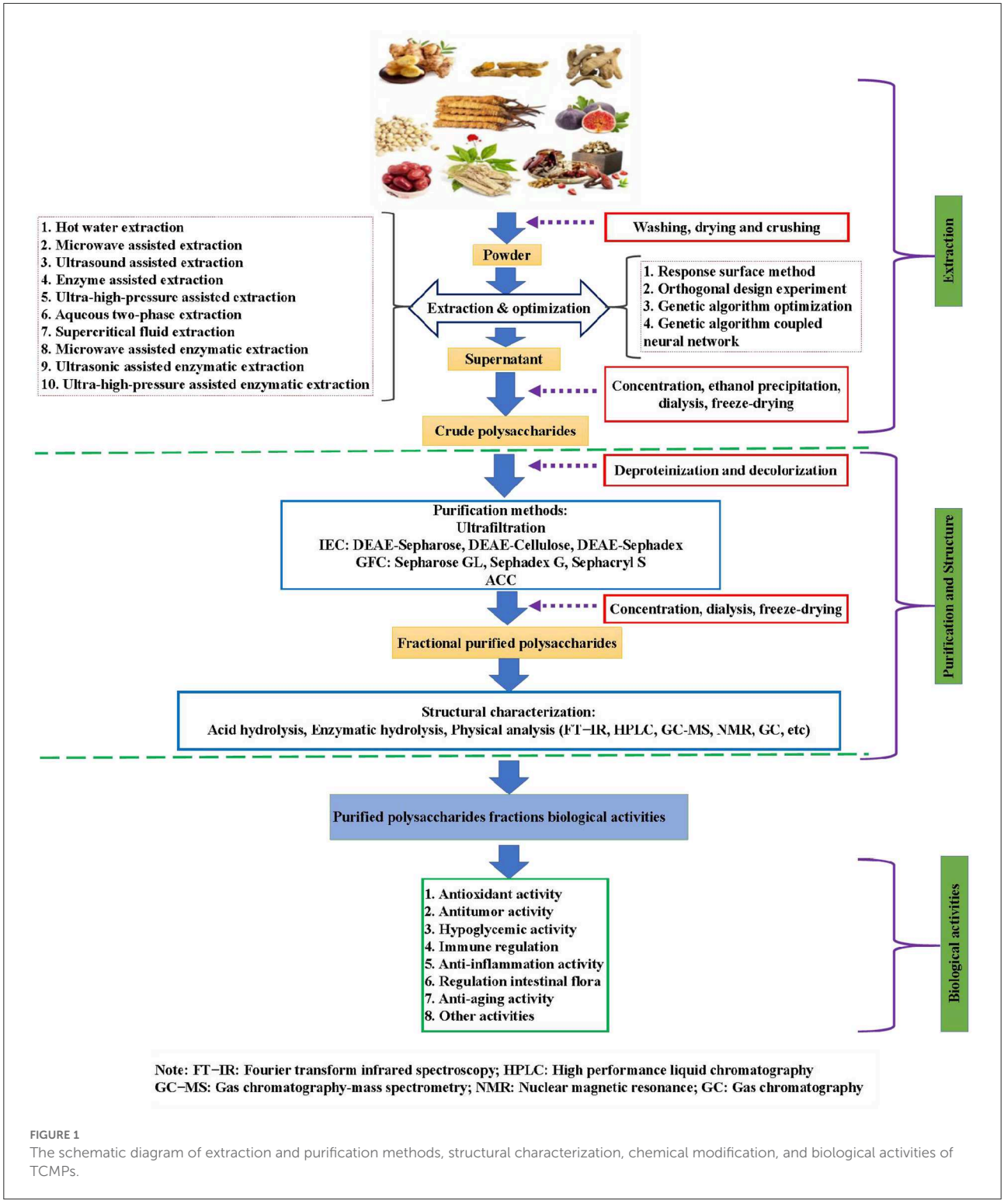

FIGURE 1
The schematic diagram of extraction and purification methods, structural characterization, chemical modification, and biological activities of TCMPs.

from turmeric (TPs) by HWE, optimized extraction conditions, and purified crude TPs by anion-exchange chromatography to obtain the four polysaccharides fractions, namely, TPs-0, TPs-1, TPs-2, and TPs-3, and then evaluated theirs antioxidant activity. The results show that the optimal extraction conditions are as follows: Extraction temperature of 100 °C, extraction time of 2.5 h, liquid-to-material ratio of 20 mL/g, and number of extractions of 2 times, and TPs yield was 2.23 g/100 g. TPs-0 and

TABLE 1 Extraction, purification, structural characterization, biological activities of polysaccharides from traditional Chinese medicines.

Sources	Extraction methods	Yield	Purification methods	Compound name	M_W/kD	Monosaccharide composition(mol% or mole ratio)	Analysis technique	Structure	Biological activities	References
Black mulberry fruit	HWE	11.86% ± 0.21%	DEAE-52, Sephadex G-100	BMP-1-1	615	Man, Rha, GlcA, Gal, Ara	FT–IR, HPGPC	NO	Antioxidant	(14)
				BMP-2-1	405	Rha, GlcA, GalA, Gal, Ara				
Turmeric	HWE	2.23 g/100 g	Anion-exchange chromatography	TPs-0	ND	Rha, Glu, Gal, Ara, Xyl, galacturonic acid, and glucuronic acid	GC, GC-MS, NMR	α-Araf- (1→ 4) -α-Glcp- (1→ 3) -α-Arap- (1→ 3) -β-Galp- (1→ 3,6) -α-Galp- (1→ 5) -α-Araf- (1→ 3) -β-Galp- (1→ R	Antioxidant	(15)
				TPs-1						
				TPs-2						
				TPs-3						
Laminaria japonica	HWE	13.31% ± 0.08%	DEAE glucan gel A-25	LGPs	17.12	Rha, Fuc, Xyl, Man Glu, Gal = 4.51:20.27:12.43: 12.81:10.29: 39.69	UV, FT–IR, GC, HPGPC, NMR	NO	Antioxidant	(16)
Ganoderma lucidum	HWE	ND	Sephadex G-50	ASP	80	GlcA:Glc:Ara:Gal = 1.00:1.70:1.85:5.02	UV, FT–IR, HPGPC	NO	Anti-tumor	(17)
Longan fruit Pericarp	HWE	ND	Sephadex G-100	PLFP	420	Ara:Glc:Gal:GalA = 32.8:17.6:33.7:15	HPGPC, GC, GC–MS, FT–IR, NMR, Methylation	→ 5)-l-Araf-(1→ , → 6)-d-Glcp-(1→		(18)
Longan pulp	HWE	ND	IEC, GFC	LPIIa	44.7	ND	HPGPC, GC, GC–MS, FT–IR, NMR, Methylation	→ 6)-Glc-(1→ , → 5)-Ara-(1→ , → 4)-Man-(1→ and → 6)-Gal-(1→ .	Immunomodulatory	(19)
Schisandra chinensis	HWE	ND	Anion-exchange chromatography	SSP, SCP	ND	Ara, Glc, Gal	HPGPC, FT–IR	ND	Antioxidant, Immunomodulatory	(20)
Mulberry	UAE	3.13%	Anion-exchange chromatography	MFP	ND	ND	FT-IR	ND	Antioxidant, hyperglycemic	(21)

(Continued)

10.3389/fnut.2022.1005181

TABLE 1 (Continued)

Sources	Extraction methods	Yield	Purification methods	Compound name	M_W/kD	Monosaccharide composition(mol% or mole ratio)	Analysis technique	Structure	Biological activities	References
Longan fruit pericarp	UAE	15.41%	ND	PLFP	ND	ND	ND	ND	ND	(22)
Glycyrrhiza	UAE	3.53%	ND	GP	ND	ND	ND	ND	Antioxidant	(23)
Taraxacum officinale	UAE	6.46% ± 0.19%	DEAE-52, Sephadex G-100	Neutral polysaccharide	1.7	ND	FT–IR, HPGPC, Methylation analysis, NMR	(1→ 4)-β-D-Glcp with branching at O-2 of (1→ 2,4)-β-D-Glcp	Antioxidant, anti-tumor	(24)
Radix polygonati officinalis	UAE	ND	DEAE-52, Sephadex G-100	LLPS-1	350.5	Glc:Man = 1:2	FT–IR, HPGPC	NO	Immunomodulatory	(25)
				LLPS-2	403.3	Glc:Man = 1:1				
				LLPS-3	146.2	Ara:Gal:Glc:Man = 2:2:2:1				
Chrysanthemum morifolium cv.	UAE	8.29% ± 0.18%	ND	ND	ND	ND	FT–IR	NO	Antioxidant, α-glucosidase activities	(26)
Tangerine peels	MAE	19.9% ± 0.2%	AEC, GFC	TPPs-2-1	17.8	GalA, Ara, Gal, Rha, Glc, Man	FT–IR, HPGPC, GC–MS	NO	Antioxidant	(27)
Eucommia ulmoides Oliver leaf	MAE	12.31%	Anion exchange chromatography	EULP	38.83	Rha, Ara, Gal, Glu, Xyl, Man, glucuronic acid, and galacturonic acid = 7:4:6:14:1:2:3:1	GC–MS, GC, FT–IR, HPGPC	NO	Antioxidant	(28)
Salvia miltiorrhiza Bunge	MAE	14.11%	DEAE-52, Sephadex G-100	SMP1	6.087	Glu (1%), Gal (1.67%), and Fru (1.12%)	FT–IR, HPGPC, NMR	NO	Antioxidant	(29)
Fructus Meliae Toosendan	MAE	15.75%	Anion exchange chromatography	FMTP	1.288	NO	UV, FT–IR, HPGPC	NO	Antioxidant	(30)
Mulberry	EAA	ND	Anion exchange chromatography	MOS-1a	0.987	NO	UV, FT–IR, GC–MS, GPC	NO	NO	(31)
Cornus officinalis	EAE	9.29% ± 0.31%	Anion exchange chromatography	COP	NO	NO	NO	NO	NO	(32)

(Continued)

10.3389/fnut.2022.1005181

TABLE 1 (Continued)

Sources	Extraction methods	Yield	Purification methods	Compound name	M_W/kD	Monosaccharide composition(mol% or mole ratio)	Analysis technique	Structure	Biological activities	References
Astragalus membranaceus	EAE	29.96% ± 0.14%	ND	ND	ND	ND	ND	NO	Antioxidant	(33)
Korean ginseng	EAE	ND	Anion exchange chromatography	FGWP		Rha, Ara, Gal galacturonic acid, Glu = 1.8:10.1:9.2:17.8:60.6	UV, FT–IR, GC–MS, HPGPC	ND	Immunomodulatory	(34)
Alfalfa	EAE	5.05% ± 0.02%	ND	ND	ND	ND	ND	ND	Antioxidant	(35)
Phellinus linteus	ATPE	63.58% ± 1.12%	Anion exchange chromatography	C-PLPS	15.2	Ara, Xyl, Man, Glc, and Gal with the molar ratios of 1.0:1.5:3.4:25.2:1.1,	UV, FT–IR, HPGPC	ND	Antioxidant, antitumor	(36)
Lycium barbarum L	ATPE	24.79 mg/g	DEAE-52, Sephadex G-100	PTP-1 PTP-2 PTP-3	ND	ND	FT–IR, UV	NO	Antioxidant	(37)
Grifola frondosa	ATPE	90.21%	Anion exchange chromatography	CGFP	2,954	Glu	FT–IR, AFM, HPGPC	NO	Antioxidant	(38)
Schisandra chinensis	ATPE	0.95 mg/g	NO	NO	NO	NO	NO	NO	NO	(39)
Cornus officinalis fruit	UATPE	7.85% ± 0.09%	DEAE-52 and Sephadex G-100	COPs-4-SG	33.64	Galacturonic acid, Ara, Man, Glu, and Gala in a molar ratio of 34.82:14.19:6.75:13.48:12.26.	FT–IR, AFM, CD, HPGPC	NO	NO	(40)
Ziziphus Jujuba cv.	UATPE	8.18%	Anion exchange chromatography	ZMP	NO	Rha, Ara, Xyl, Ma, Glu, Gal, and galacturonic acid with at the ratios of 1.46:2.47:2.27:1.12:1.00:1.57:5.40	HPGPC, UV, FT–IR	NO	Antioxidant	(41)
Lilium davidiivar. unicolor salisb	UATPE	36.58%	DEAE-52, Sephadex G-100	LPS	NO	NO	UV, FT–IR	NO	Antiglycation activity	(42)
Lilium lancifolium thunb	UATPE	15.17% ± 0.21%	DEAE-52, Sephadex G-100	LLPs-2-SG	421.41	Man, Glu, and Gal in a molar ratio of 10.52:23.06:7.19	UV, FT–IR, HPGPC, AFM, SEM	NO	NO	(43)

(Continued)

10.3389/fnut.2022.1005181

TABLE 1 (Continued)

Sources	Extraction methods	Yield	Purification methods	Compound name	M_W/kD	Monosaccharide composition(mol% or mole ratio)	Analysis technique	Structure	Biological activities	References
Lonicerae japonica leaves	UAEE	14.76%	DEAE-52, Sephadex G-100	LJLP	NO	Gal (32.3%), Glu (20.9%), and Rib (15.2%)	UV–vis, FT–IR, HPGPC	NO	Antioxidant	(44)
Momordica charabtia L.	UAEE	29.75% ± 0.48%	Anion exchange chromatography	MCP	NO	NO	NO	NO	NO	(45)
Cucurbita moschata	UAEE	4.33% ± 0.15%	Anion exchange chromatography	CMCP	NO	NO	NO	NO	Antioxidant	(46)
Corn silk	UAEE	4.56%	Anion exchange chromatography	CSPS	105.2	Rha, Ara, Xyl, Man, Gal = 4.17:17.33:5.59:18.65:19.11	UV, FT–IR, HPGPC	NO	Antioxidant and anticancer activities	(47)
Armillaria mellea	UAEE	40.56%	NO	NO	NO	NO	NO	NO	NO	(48)
Hylocereus undatus	UAEE	16.64%	NO	NO	NO	NO	NO	NO	NO	(49)
Ocimum album seed	HWE	7.1%	DEAE-52 and Sephadex G-200	OAP-1A	593	Man (35.7%), Glu (33.32%), Gal (19.6%), and Rha (11.38%)	GC–MS, NMR, FT–IR, HPGPC	→ 3)-β-D-Manp-(1→ , → 3,4)-β-D-Manp-(1→ , → 3,6)-β-D-Manp-(1→ , → 3)-α-D-Glcp-(1→ α-D-Glcp-(1→	Antioxidant	(50)
Glycyrrhiza inflata residue	HWE	NO	DEAE-52 and Sephadex G-150	AGP	2.89	Rha: Ara:Xyl: Man: Glu: Gal with a molar ratio of 1:2.33:2.85:0.69:3.05:1.54	GC–MS, periodate oxidation, Smith degradation, FT–IR, methylation, NMR	→ 6)-β-d-Glcp-(→ backbone	α-glucosidase inhibition activity	(51)

(Continued)

10.3389/fnut.2022.1005181

TABLE 1 (Continued)

Sources	Extraction methods	Yield	Purification methods	Compound name	M_W/kD	Monosaccharide composition(mol% or mole ratio)	Analysis technique	Structure	Biological activities	References
Laminaria japonica	HWE	NO	diethylaminoethyl-cellulose and Sephacryl S-500 chromatography	LJP12	2.31	Ara:Xyl:Man:Glc:Gal = 1:0.17:1.54:2.64:0.18	HPGPC, FT-IR, NMR	1,4-linked and 1,3,6-linked	NO	(52)
Laminaria japonica	HWE	NO	DEAE-A25	WPS-2-1	80	Man:Rha:Fuc = 1.0:2.3:1.2	HPGPC, UV, FT-IR, NMR, Smith degradation	A backbone of array by (1→ 4)-glycosidic linkages	NO	(53)

HWE, Hot water extraction; UAE, Ultrasound assisted extraction; MAE, Microwave assisted extraction; EAE, Enzyme assisted extraction; UHPAE, Ultra-high pressure assisted extraction; ATPE, Aqueous two-phase extraction; UATPE, Ultrasound assisted aqueous two-phase extraction; UAEE, Ultrasound assisted enzyme extraction.

TPs-1 were mainly consisted of glucose (Glu), galactose (Gal), and arabinose (Ara), whereas TPs-2 and TPs-3 were composed of rhamnose (Rha), Glu, Gal, Ara, xylose (Xyl), galacturonic acid, and glucuronic acid. Moreover, TPs showed antioxidant effects on DPPH, $ABTS^+$, and OH radicals, and the antioxidant effect of TPS-2 was the strongest, suggesting that TPs, as a natural antioxidant, are used in the development of functional foods and health products (15). Lu et al. prepared *Laminaria* japonica polysaccharides (LJP) with antioxidant capacity by using HWE and optimized extraction process *via* GA. The results show that the optimal process parameters were pH of 2.0, extraction temperature of 120°C, and extraction time of 3 h. The yield of LJP was 13.31% ± 0.08%. In addition, LJP showed good antioxidant activity including ORAC, $ABTS^+$ radicals scavenging activity and reducing power, suggesting that LJP can be used as a natural antioxidant (16). Furthermore, HWE method is widely used to extract natural polysaccharides from *Ganoderma lucidum*, *Longan*, *Longan* pulp, and *Schisandra chinensis* (17–20). To sum up, HWE method shows some advantages. Nevertheless, the extraction efficiency of this method is low and TCMPs are easy to degrade due to the high extraction temperature. Thus, this method needs to be combined with other technologies to improve the extraction efficiency and expand its the application range.

UAE uses the "cavitation effect" and "mechanical shear effect" produced by ultrasound in the extraction process to destroy the plant cell wall, which can dramatically shorten extraction time, reduce energy and solvent consumption, and quickly achieve the purpose of extracting active ingredients (63). Thus, UAE has been widely used in the extraction polysaccharides from TCM. According to the full review of previous literature reports, TCMPs could usually be extracted by UAE under the following conditions: Extraction temperature of 57–80°C, liquid-to-solid ratio of 15–41 mL/g, ultrasound power of 120–600 W, and extraction time of 12 min−2 h (Table 1) (21–26). By analyzing the above literature reports, it was found that the yield of polysaccharides obtained by UAE was higher than that traditional HWE. A large number of studies have confirmed that higher ultrasonic frequency (above 100 kHz) could destroy the glycosidic bond and lead to the polysaccharides depolymerization, whereas the extraction efficiency of polysaccharides was not significant at low ultrasound frequency (20–50 kHz) (64, 65). Therefore, it is necessary to optimize the conditions of UAE.

MAE uses electromagnetic waves with the frequency of 300 MHz−300 GHz to selectively heat materials. The principle is to use microwave radiation to directly penetrate plant cells. Polar molecules absorb microwave energy, and the temperature in the cell rises rapidly, and then the solvent evaporates to produce cell pressure (66). The synergistic effect of concentration and pressure gradients promotes the diffusion of target components from the inside to the outside of the cell. In addition, the generated pressure can destroy the plant cell wall to

enhance the extraction efficiency of active ingredients (67). Chen et al. extracted tangerines peel polysaccharides (TPPs) by using MAE and optimized the extraction process *via* RSM based on single factor experimental results. The results show that the optimal combination of process parameters was as follows: Microwave power of 704 W, extraction temperature of 52.2°C, and extraction time of 41.8 min, and the yield of polysaccharides was 19.9% ± 0.2% under the optimal extraction conditions (27). Xu et al. prepared *Eucommia ulmoides* Oliver leaf polysaccharides by MAE, optimized the extraction condition through RSM, purified the crude polysaccharides by different purification methods to obtain the homogeneous fraction (EULP) with the molecular weight of 38.83 kDa, and evaluated its antioxidant activity. It was found that the optimal process was obtained as follows: Microwave extraction of 74 °C, solid-to-liquid ratio of 1:29 g/mL, and extraction time of 15 min. The yield of polysaccharides was 12.31% under above extraction conditions. Additionally, the antioxidant activity of EULP was significantly better than the crude polysaccharides (28). Meng et al. extracted polysaccharides from *Salvia miltiorrhiza* Bunge (SMPs) *via* MAE, optimized the extraction process by RSM, purified the crude SMPs by using DEAE-52 and Sephadex G-100 chromatography to obtain a novel the homogeneous fraction (SMP1). The results show that the optimal process parameters are as follows: Microwave power of 1,200 W, liquid-to-solid ratio of 38 mL/g, extraction time of 12 min, and ethanol concentration of 86%. The yield of polysaccharides was 14.11% under above extraction conditions. SMP1 with an average molecular weight of 6.087 kDa was consisted of Glu (1%), Gal (1.67%), and Fru (1.12%). Pharmacological researches display that SMP1 protected from OGD/R-induced ferroptosis by activating Nrf2/HO-1 pathway in PC12 cells, suggesting that SMPs can inhibit iron sagging and reduce oxidative stress damage (29). Xu et al. prepared the polysaccharides from *Fructus Meliae Toosendan* (FMTP) by using MAE, optimized the extraction process *via* RSM based on single factor experimental results, purified the crude polysaccharides to obtain high-purity FMTP polysaccharide fraction with the molecular weight of 1.288 kDa. It was found that the optimum extraction conditions for FMTP: Solvent-to-liquid ratio of 30 mL/mg, extraction time of 20 min, extraction times of 2, and microwave power of 700 W, and the extraction rate of FMTP was 15.75% under the optimum extraction conditions. Furthermore, FMTP could effectively scavenge free radicals (DPPH, OH, and O^{2-}), indicating that FMTP can be used as a potential antioxidant in functional foods and drugs. To sum up, MAE has the advantages of high extraction efficiency, energy conservation, and environmental protection. Nevertheless, microwave causes local high temperature in the extraction solution, resulting in polysaccharides degradation (30). Thus, this method needs to be combined with other extraction methods to expand the application range of microwave in the extraction field.

EAE uses biological enzymes as a biocatalyst to destroy the structure of plant cell wall, improves the permeability of cell membrane and cell wall, reduces the mass transfer resistance of active ingredients, and accelerates the dissolution of active components in cells, which can improve the yield of effective components (68). EAE has the advantages of mild reaction conditions, short extraction time, simple process, high efficiency, low investment cost and energy consumption. Moreover, the biological activities of target components have not been significantly reduced, and less chemical reagents are used in EAE, which is conducive to resource utilization and environmental improvement. Thus, EAE method has been used to extract natural polysaccharides from traditional Chinese medicines, such as mulberry, *Cornus officinalis*, *Astragalus membranaceus*, *Korean ginseng*, and *Schizochytrium limacinum* (31–35) (Table 1). However, the high price and strict extraction conditions of enzyme are difficult to control. Thus, the large-scale industrial application of this technology in the field of food and medical treatment is still very difficult.

Aqueous two-phase extraction (ATPE) refers to mixing two polymers or one polymer with an aqueous solution of a salt to form a two-phase aqueous system for the extraction active components (69). Its principle is to use the different partition coefficients of target components in two phases to extract and separate. This technology has mild conditions and wide biological adaptability. Therefore, it can be used in biological extraction, natural product separation and so on. Wu et al. prepared and separated the *Phellinus linteus* polysaccharides (PLPS) by using ATPE and evaluated its antioxidant activity. It was found that the optimal extraction conditions are as follows: Extraction time of 30 min, extraction temperature of 21.2°C, and 68.9% K_2HPO_4-20%[Chol]Cl, and the extraction ratio of 68.53% ± 0.29% under the above conditions. PLPS with the weight of 15.2 kDa was consisted of Ara (1.0%), Xyl (1.5%), Man (3.4%), Glc (25.2%), and Gal (1.1%). Moreover, PLPS could effectively scavenge free radicals and show good antioxidant activity (36). Hu et al. extracted *Lycium barbarum* L. fruits polysaccharides (LBPs) by using ATPE and optimized the extraction process. The results show that optimal extraction conditions are as follows: Solid-to-liquid ratio of 1:30 g/mL, extraction time of 4 min, and tissue-smashing power of 8,000 rpm, and the yield of LBPs was 24.79 mg/g under the above extraction conditions. In addition, compared with HWE and UAE, the extraction rate of ATPE was the highest (37). Mao et al. extracted and separated polysaccharide from *Grifola frondosa* by using ATPE and anion exchange chromatography, respectively. It was found that the optimized extraction conditions were as follows: pH of 3.22, ethanol volume fraction of 27.9%, and ammonium sulfate mass fraction of 17%. A homogeneous polysaccharide fraction (CGFP) with the weight of 2,954 kDa was obtained, and it was mainly consisted of Glu, and CGFP was a rod-shaped network structure with smooth surface. Moreover, CGFP could improve the levels of SOD, CAT,

GSH-Px, and reduce the levels of MDA, LDH, and ROS, suggesting that CGFP can be used as a natural antioxidant with broad development and application prospects (38). Li et al. prepared polysaccharide from *Schisandra chinensis via* ATPE and optimized the extraction conditions based on BBD-RSM. It was found that the optimal parameters were as follows: K_2HPO_4 addition amount of 1.0 g, PEG6000 addition amount of 1.8 g, centrifugation time of 9 min, and solvent volume of 5 mL, and the yield of polysaccharide was 0.95 mg/g under the above extraction conditions. Through the above reports, it is found that the yield of polysaccharides obtained by ATPE is significantly better than that of traditional HWE (39). However, how to quickly find the optimal ATPS still needs further research.

With the advancement of extraction technology, some combined extraction methods, namely, ultrasound assisted aqueous two-phase extraction (UATPE) and ultrasound assisted enzyme extraction (UAEE), have become promising substitutes for the traditional extraction methods of TCMPs. UATPE method has the advantages of environmentally friendly, high extraction efficiency, low solvent and energy consumption (70). Thus, UATPE method is widely used to extract polysaccharides from *Cornus officinalis fruit, Ziziphus Jujuba cv.*, *Lilium davidiivar. unicolor salisb*, and *Lilium lancifolium* thunb (40–43) (Table 1). UAEE, as a combination of UAE and EAE extraction methods, can be a good method to solve the disadvantages of traditional extraction methods. UAEE has the some merits, such as mild reaction conditions, lower investment costs and energy requirements, simplified manipulation, and environmental protection. Currently, UAEE method is used to extract polysaccharides from *Lonicerae japonica* leaves, *Momordica charabtia* L, *Cucurbita moschata*, corn silk, *Armillaria mellea*, and *Hylocereus undatus* to achieve the maximum yield of polysaccharides (44–49). The combined extraction method can improve the yield of polysaccharides, shorten extraction time, and reduce extraction temperature. However, there are still many problems in the combined extraction method, such as difficult to control the extraction process and complex influencing factors. The further research on extraction methods is needed to efficiently extract polysaccharides from TCM and maintain their biological activities, and establishing a database containing different types of polysaccharides extraction schemes of specific TCM is the key to ensure the utilization of polysaccharides to a large extent.

Isolation and purification of TCMPs

Due to the limitations of extraction methods, the crude polysaccharides contain various impurities, such as proteins, fat, polypeptides, oligosaccharides, and ash (71). These substances will affect the biological activities, stability, and final product quality of polysaccharides. Moreover, the various impurities make it difficult to evaluate the structure-activity relationship of polysaccharides. Therefore, it is necessary to further isolate and purify the crude TCMPs. Figure 1 displays the different TCMPs purification methods. Currently, trichloroacetic acid (TCA) and Sevage methods are mainly used to remove proteins in crude TCMPs. Sevage method is based on the principle that proteins can be denatured in some organic solvents. This method has many advantages, such as mild conditions, simple operation, high purification efficiency reducing the impact on the structure and activity of TCMPs (72). However, this method has disadvantages of high purification cost and long time-consuming (73). TCA method is based on denaturation of proteins by TCA solution. Denatured proteins can be removed by centrifugation, but this method easily leads to the TCMPs degradation (74). Notably, column chromatography, ion exchange chromatography, and gel filtration chromatography are widely used in the purification of polysaccharides. Zhu et al. purified the crude turmeric polysaccharides (TPs) by anion-exchange chromatography to obtain four polysaccharide fractions (TPs-0, TPs-1, TPs-2, and TPs-3). It was found that TPs-0 and TPs-1 were composed of Glu, Gal, and Ara, whereas TPs-2 and TPs-3 were primarily consisted of Rha, Glu, Gal, Ara, Xyl, galacturonic acid, and glucuronic acid. Additionally, compared with TPs-0, TPs-1, TPs-3, and TPs, TPs-2 showed the strongest antioxidant activity (15). Chen et al. isolated and purified the polysaccharides from *Taraxacum officinale* by DEAE-52 and Sephadex G-100 to get high purified polysaccharides fraction (TOP) with the weight of 1.7 kDa. The results show that TOP had a backbone composed of (1→ 4)-β-D-Glcp with branching at O-2 of (1→ 2,4)-β-D-Glcp. Moreover, TOP could effectively scavenge DPPH radicals and inhibit the HepG2 cells proliferation, suggesting that TOP can be used as a new natural antioxidant and anti-tumor drug for disease prevention and treatment (24). Xu et al. purified the crude *Eucommia ulmoides Oliver* leaf. polysaccharides (EUOLPs) by anion exchange chromatography. It was found that a high molecular weight and polydispersity polysaccharides was obtained, and purified polysaccharides belonged to β-type acidic heteropolysaccharide structure with glucan group and high degree of branching (28). Tan et al. isolated and purified the crude *Cornus officinalis* polysaccharides (COPs) by using DEAE-52 and Sephadex G-100 chromatography. The results display that a homogenous fraction (COPs-4-SG) with the weight of 33.64 kDa was obtained and consisted of galacturonic acid, Ara, Man, Glu, and Gal with the molar ratio of 34.82:14.19:6.75:13.48:12.26 (40). Wu, Huang, and Xiang purified the polysaccharides from *Lonicerae japonica* leaves (LJLP) *via* DEAE-52 and Sephadex G-100 and evaluated its antioxidant activity. It was found that LJLP was mainly comprised of Gal (32.3%), Glu (20.9%), and Rib (15.2%). In addition, LJLP could improve SOD, GSH-Px, CAT activities, whereas LJLP could decrease the levels of MDA in both serum and liver (44). Arab et al. used the DEAE-52 cellulose column to purify the crude polysaccharides from *Ocimum album* L.

seed for separating various acidic polysaccharides and neutral polysaccharides. The results show that two fractions, namely, OAP-1A was obtained and its average molecular weight was 593 kDa. In addition, OAP-1A showed strong scavenging activity against DPPH radical (50). Analysis of the above literature found that the purified polysaccharides fractions need to be dialysis and freeze-drying. Finally, the contents of polysaccharides and proteins in the purified fractions are determined by the phenol-sulfuric method and Bradford's method, respectively. Table 1 shows the different extraction and purification methods of TCMPs.

Structure characteristics of TCMPs

The research shows that the structure of TCMPs is complex and diverse. It is necessary to analyze theirs structural characteristics in detail to better understand TCMPs. Currently, the structural analysis of TCMPs has mainly focused on the determination of molecular weight (M_W), monosaccharide composition (MC), glycosidic bond type, glycosidic bond position, monosaccharide sequence, and spatial conformation. Furthermore, the analytical methods for the chemical characterization of TCMPs mainly include gas chromatography (GC), high performance liquid chromatography (HPLC), nuclear magnetic resonance (NMR), methylation analysis, Fourier transform infrared spectroscopy (FT–IR), gas chromatography-mass spectrometry (GC–MS), and Smith degradation analysis (75). Table 1 summarizes the existing information on the basic structural characteristics of TCMPs.

Monosaccharide composition

Notably, polysaccharides are composed of various monosaccharides connected by glycosidic bonds. Firstly, the monosaccharide composition of TCMPs is determined by acid hydrolysis to decompose their glycosidic bonds. After hydrolysis, some polysaccharides need to be neutralized, filtered, derivatized, and then passed through some analytical chemical instruments, including GC, HPLC, PC, TLC, and HPCE, etc. Nowadays, the most common monosaccharide components of TCMPs are glucose (Glu), fructose (Fru), fucose (Fuc), mannose (Man), arabinose (Ara), rhamnose (Rha), galactose (Gal), and xylose (Xyl) (76). Lu et al. prepared the polysaccharide from *Laminaria japonica* (LJPA) by using citric acid extraction. The results show that LJPA with the weight of 17.12 kDa was consisted of Rha (4.51%), Fuc (20.27%), Xyl (12.43%), Man (12.81%), Glu (10.29%), and Gal (39.69%). Moreover, LJPA showed high antioxidant capacities including ORAC, $ABTS^+$ radical scavenging activity and reducing power (16). Xu et al. prepared polysaccharides from *Eucommia ulmoides* oliver leaf and purified crude polysaccharides by anion exchange chromatography. The results show that a homogeneous fraction (EULP) was obtained and composed of Rha (7%), Ara (4%), Gal (6%), Glu (14%), Xyl (1%), Man (2%), Glucuronic acid (3%), and Galacturonic acid (1%) (28). Meng et al. prepared the crude polysaccharides from *Salvia miltiorrhiza* (SMPs) and then purified SMPs by DEAE Sepharose Fast Flow and Sephadex G-100 chromatography. It was found that a novel polysaccharide termed SMP1 was obtained and comprised of Glu, Gal, and Fru in a molar ratio of 1:1.67:1.12, and the molecular weight of SMP1 was 6.087 kDa (29). Tan et al. prepared polysaccharides from *Cornus officinalis* fruit (COPs) by UATPE and purified the crude COPs by DEAE-52 and Sephadex G-100 chromatography in turn. It was observed that COPs-4-SG with molecular weight of 33.64 kDa was obtained and composed of Gal acid (34.82%), Ara (14.19%), Man (6.75%), Glu (13.48%), and Gal (12.26%) (40).

Molecular weight

The average M_W of TCMPs is the critical parameter to determine its chemical properties, and theirs biological activities are closely related to the average M_W of TCMPs. Currently, the M_W of TCMPs is usually determined by HPLC, HPLC–ELSD, high performance gel permeation chromatography (HPGPC), light scattering, gel permeation chromatography (GPC), size exclusion chromatography, and viscosity methods (77). In particular, HPGPC, as a combination of GPC and HPLC, is usually used for polysaccharides analysis and provides molar mass distribution of polysaccharides. Compared with GPC, HPGPC has the merits of accuracy, good reproducibility, high sensitivity, short analysis time, simple operation, and reliable results. However, this method has high requirements for instruments. Mao et al. extracted polysaccharide from *Grifola frondosa* by HWE and then purified the crude polysaccharide *via* DEAE-52 and Sephadex G-100 to produce the purified polysaccharide (CGFP). The results show that CGFP was mainly consisted of Glu, and the M_W of CGFP was 2,954 kDa (38). Zhang et al. prepared the homogenous polysaccharides fraction (AGP) from *Glycyrrhiza* inflata by different purification methods and evaluated its α-glucosidase inhibitory activity. It was found that AGP with molecular weight of 2.89 kDa was composed of Rha (1%), Ara (2.33%), Xyl (2.85%), Man (0.69%), Glc (3.05%), and Gal (1.54%). Moreover, AGP showed significant inhibition α-glucosidase activity (51). Chen et al. extracted and purified the corn silk polysaccharides (CSPS) by UAEE and anion exchange chromatography, respectively. It was found that CSPS with the weight of 105.2 kDa was comprised of Rha, Ara, Xyl, Man, Gal, and Glu with molecular ratios of 4.17:17.33:5.59:18.65:19.11:35.14 (47). Mutaillifu et al. separated and purified the *Glycyrrhiza* glabra polysaccharides (GPN)

by using DEAE-cellulose 52 column and Sephadex G-100 column. The results show that the molecular weight of GPN was 38.7 kDa, and GPN was composed of Glc, Man, Ara, and Gal (78). Lu et al. and Kong, Yao, & Zhang, extracted and purified the polysaccharides from *Laminaria japonicaby* and *Ganoderma lucidum*, respectively. It was found that the molecular weights of LGPS and ASP were 17.12 and 80.00 kDa, respectively (16, 17). It is worth noting that the great difference in molecular weight may be largely due to different materials and experimental conditions.

Chemical structure

The biological activities of TCMPs are closely related to theirs structure. Increasing researchers began to investigate the position and configuration of glycosidic bond, the type of ring structure, the position and proportion. However, the literature on the chemical structure of TCMPs is still relatively insufficient due to the limitations of identification methods. Table 1 shows the structural information of TCMPs reported in the current literature. At present, the main methods (NMR, GC–MS, FT–IR, and Smith degradation) are determined the structural characteristics of TCMPs. Chen et al. extracted polysaccharides from *Taraxacum officinale* by using UAE and purified the crude polysaccharide to produce a novel neutral polysaccharide (TOP), and then identified its structure *via* methylation and NMR analysis. It was found that the molecular weight of TOP was 1.7 kDa, and TOP had a backbone composed of (1→ 4)-β-D-Glcp with branching at O-2 of (1→ 2,4)-β-D-Glcp. Moreover, TOP showed good antioxidant and antitumor activities (24). Yi et al. prepared polysaccharide from longan pulp by HWE, purified the crude polysaccharide *via* ion-exchange chromatography and gel filtration chromatography, and then identified its structure by using NMR analysis. The results show that a homogeneous polysaccharide fraction (LPIIa) with molecular weight of 44.7 kDa was obtained and mainly composed of (→ 6)-Glc-(1→ ,→ 5)-Ara-(1→ ,→ 4)-Man-(1→ and → 6)-Gal-(1→). Additionally, LPIIa showed immunomodulatory activity by stimulating macrophages (19). Bao et al. extracted the crude polysaccharides from longan fruit pericarp by HWE, isolated the crude polysaccharides through Sephadex G-100 gel filtration column to get a homogeneous polysaccharides fraction (PLFP), and then determined its structure *via* methylation analysis, GC–MS, and NMR. It was found that PLFP with molecular weight of 420 kDa was mainly consisted of Ara (32.8%), Glu (17.6%), Gal (33.7%), and galacturonic acid (15.9%), and the backbone consisted of (→ 5)-l-Araf-(1→ , → 6)-d-Glcp-(1→ , → 3)-d-Galp-(1→ , → 3)-d-GalpA-(1→ and → 6)-d-Galp (1→). Moreover, PLFP showed good ability to inhibit glycosylation reaction *in vitro* (18). Zhu et al. extracted and purified polysaccharide from by HWE and anion-exchange chromatography, respectively. The results show that four polysaccharide fractions (TPs-0, TPs-1, TPs-2, and TPs-3) with different molecular weights were obtained. TPs-0 was further studied by methylation, GC-MS, and NMR. The results find that TPs-0 contained a main chain of α-Araf- (1→ 4)-α-Glcp-(1→ 3)-α-Arap-(1→ 3)-β-Galp-(1→ 3,6)-α-Galp-(1→ 5)-α-Araf-(1→ 3)-β-Galp-(1→ R) (15). Furthermore, Peng et al. and Peng et al. purified the crude polysaccharides from *Laminaria japonica* to obtain the two homogenous fractions (LJP12 and WPS-2-1) and identified their structures. It was found that LJP12 with molecular weight of 2.31 kDa was composed of Ara (1.0%), Xyl (0.17%), Man (1.54%), Glc (2.64%), and Gal (0.18%). LJP12 was suggested to be 1,4-linked and 1,3,6-linked while glucose was linked by 1,6-glycosidic bond. Additionally, WPS-2-1 with molecular weight of 80 kDa was composed of Man, Rha, and Fuc in a molar ratio of 1.0:2.3:1.2, and WPS-2-1 had a backbone of array by (1→ 4)-glycosidic linkages (52, 53). Notably, the chemical structures of TCMPs products differ greatly depending on various raw materials and preparation methods. Table 1 summarizes the existing literature on the chemical structures of TCMPs.

Chemical modification of TCMPs

Chemical modification is to modify the polysaccharides structure by chemical, physical, and biological methods. Structural modification can change the molecular structure, molecular weight, viscosity, type, position and number of polysaccharides substituents to enhance biological activities and even obtain new bioactive polysaccharides derivatives (79). Currently, the chemical modification methods include sulfation, carboxymethylation, acetylation, selenidation, and phosphorylation. Chemical modification will replace the hydroxyl group of the original polysaccharides with target groups such as sulfuric acid group, carboxymethyl group, acetyl group, selenium ester group or phosphoric acid group, and the monosaccharide composition, molecular weight, and morphological characteristics change by the above chemical modification methods.

Sulfation modification

The principle of sulfation modification is to dissolve the polysaccharides and corresponding sulfation reagent in a certain solvent and react with each other under certain conditions to introduce the sulfate group into some hydroxyl groups on the residues of the original polysaccharides (80). Sulfation modification is one of the most commonly used method to modify the chemical structure of polysaccharides. This method can change the water solubility and biological activities of polysaccharides (79). Figure 2A describes the sulfation

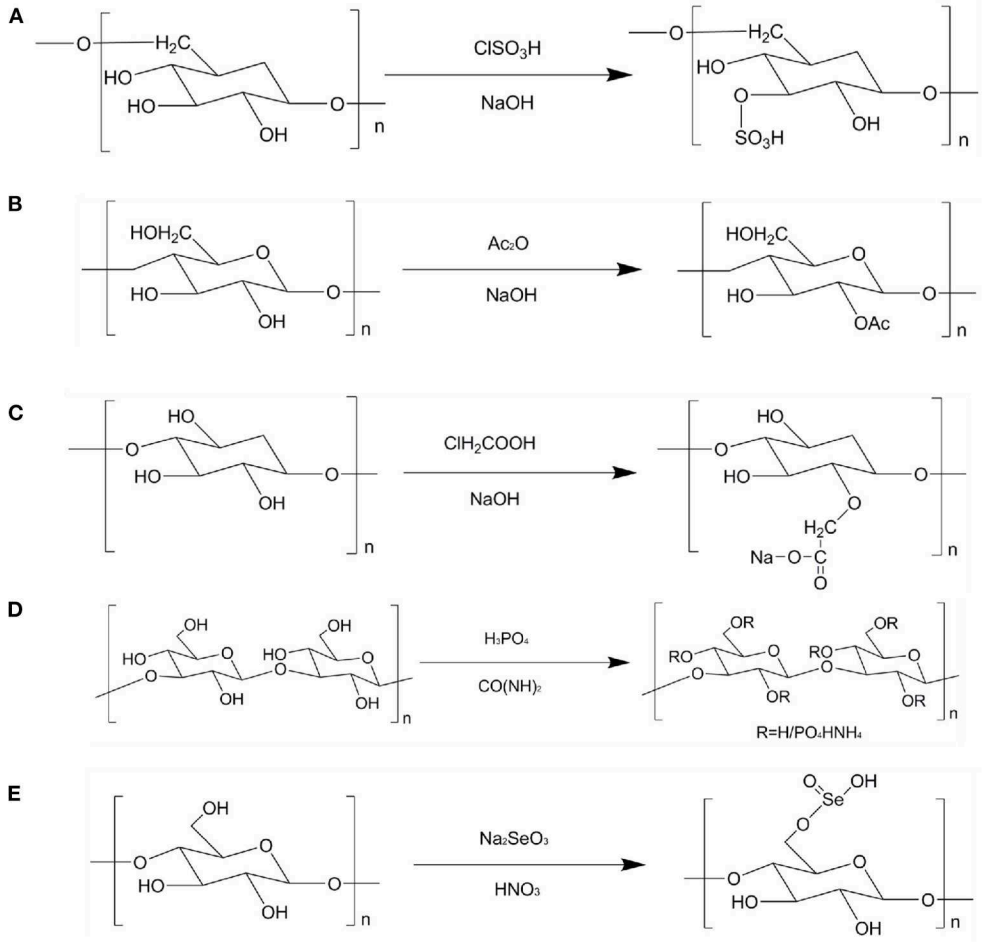

FIGURE 2
Schematic diagram of different modification of TCMPs. **(A)** Sulfation modification; **(B)** acetylation modification; **(C)** carboxymethylation modification; **(D)** phosphorylation modification; **(E)** selenium modification.

modification of polysaccharides. The common modification methods are chlorosulfonic acid pyridine, concentrated sulfuric acid, and sulfur trioxide pyridine methods. Among them, chlorosulfonic acid pyridine method has the advantages of high yield, high degree of substitution, and convenient recovery. Thus, it is the most common method to prepare sulfated polysaccharides. Geng et al. prepared the sulfated polysaccharide (SPPM60-D) by using chlorosulfonic acid pyridine method and evaluated its immunologic activity. The results show that SPPM60-D showed stronger immunologic activity than unmodified polysaccharides. In addition, SPPM60-D could activate TLR4-PI3K-IP3K signal pathway to regulate immune activity (81). Wang et al. investigated three sulfated ginger polysaccharides, namely, SGP, SGP1, and SGP2, and evaluated theirs anticoagulant bioactivity. It was found that SGP and SGP1 have triple helical structure, whereas SGP2 existed random coils. SGP, SGP1, and SGP2 displayed rough surfaces with a large number of small holes. Moreover, GP2, SGP2, and SGP could inhibit the intrinsic pathway of coagulation. Therefore, ginger polysaccharides can be used as an anticoagulant and therapeutic agent for thrombosis (82). Huang et al. prepared a sulfated polysaccharides from Chinese yam (S-CYP) by chlorosulfonic acid pyridine method and evaluated its immunological activity. It was found that S-CYP showed stronger immunological activity than CYP (unmodified polysaccharide). Additionally, S-CYP could up-regulate the levels of IgG and IgM secretion in serum, down-regulate the CD^{4+}/CD^{8+} ratio, indicating that sulfated polysaccharides can improve immunomodulatory activity to some extent (83). Furthermore, the origin polysaccharides from *Laminaria japonica* and *Laminaria angustata* sulfated ginger polysaccharides were sulfated to obtain corresponding sulfated polysaccharides and found that the biological activities of sulfated polysaccharide were

significantly higher than those of original polysaccharides (84, 85).

Acetylation modification

Acetylation modification has become one of the commonly used molecular modification methods in the chemical structure modification of polysaccharides because of its fast reaction speed, mild reaction, and high product conversion rate. Acetylation modification changes the physical and chemical properties of polysaccharides by changing the orientation and horizontal order of polysaccharides. Acetylated polysaccharides will lead to changes in the extension of molecular structure, exposing the hydroxyl groups in their molecular structure, increasing the solubility of polysaccharides, thus affecting the biological activities of polysaccharides (86). Figure 2B shows the acetylation modification of polysaccharides. The acetic anhydride pyridine method uses formamide, methanol, and dimethyl sulfoxide as reaction solvents. Acetic anhydride and acetic acid are acetylating reagents. N-bromosuccinimide (NBS), 4-dimethylaminopyridine (DMAP), and pyridine are used as catalysts. Gu et al. prepared the acetylated polysaccharides derivative from *Ophiopogon japonicus* (ROH05) and evaluated its anti-pancreatic cancer activity. It was found that the molecular weight of ROH05 was 16.7 kDa, and it was composed of 1, 4-linked β-D-Gal and 1, 4, 6-linked β-D-Gal. Furthermore, ROH05A could inhibit BxPC-3 and PANC-1 cells growth in a dose-dependent manner (87). Liu et al. modified polysaccharides from *Polygonatum cyrtonema* Hua by different chemical modification methods (sulfated, acetylated, and phosphorylated). The sulfated derivative (S-PD), phorphorylated derivative (P-PD), and acetylated derivative (Ac-PD) showed good antiherpetic activity. The results suggest that the types of functional groups are very important for the anti-herpetic activity of polysaccharides. Song et al. prepared the acetylated *Pleurotus geesteranus* polysaccharides (AcPPS) and evaluated its anti-inflammatory, antioxidant, and lung protection. AcPPS could decrease the levels of lung index, TNF-α, IL-1β, IL-6, p-IκBα, ROS, MDA, TC, TG, LDL-C, HDL-C, and VLDL-C, whereas AcPPS could increase the levels of SOD, GSH-Px, CAT, and T-AOC. These results imply that the acetylated polysaccharides may be suitable as a natural food to prevent or alleviate liver injury (88). Chen and Huang prepared bitter gourd polysaccharide (P) by HWE and modified its structure *via* carboxymethylated and acetylated modifications to obtain two fractions, namely, CM-P and AcP, and evaluated theirs antioxidant activity. The results display that compared with the original polysaccharides, CM-P and AcP showed stronger free radicals scavenging ability and anti-lipid peroxidation capacity, indicating that different chemical modifications can enhance the antioxidant activity of polysaccharides from bitter gourd (89).

Carboxymethylation modification

Carboxymethylation modification has the advantages of easy availability of reagents, low cost, and low toxicity or non-toxic substances generated by the reaction. Thus, carboxymethylation modification has become one of the commonly used methods for the chemical structure modification of polysaccharides (79, 89). Relevant studies have shown that some polysaccharides have good antitumor activity (90). However, the wide application of polysaccharides is limited due to its high molecular weight and poor solubility. Carboxymethylation modification of polysaccharides structure can effectively improve the water solubility of polysaccharides and play an important role in the biological activities of polysaccharidse. The principle of carboxymethylation modification is to react polysaccharides with monochloroacetic acid under alkaline conditions, which makes carboxymethyl introduced to some hydroxyl groups on the residues of the original polysaccharides (91). Figure 2C shows the carboxymethylation modification of polysaccharides. Ren et al. extracted the crude polysaccharides from *Cordyceps militaris* and then modified the crude polysaccharides to obtain carboxymethylated derivatives (CM-CPS) and acetylated derivatives (AC-CPS). The results imply that the carboxymethylation substitution of polysaccharide might be C-6, C-2, and the acetylation modification might be C-3, C-6 inferred from NMR analysis. In addition, CM-CPS and AC-CPS exhibited good α-glucosidase inhibitory activity. Hence, the change structures of polysaccharides have a certain impact on the biological activities. The degree of substitution and the position of substituent are the factors that affect the biological activities of polysaccharides (92). Zhao et al. prepared carboxymethylated *Schisandra* polysaccharides (CSP), purified CSP by using DEAE-52 column to obtain the main fraction (CSPP), and then investigated its structural feature and biological availability. It was found that CSPP with the molecular weight of 1.698×10^4 g/mol was comprised of Man, Glu, and Gal at ratio of 1: 44.8: 3.7. The water solubility of CSPP was significantly higher than that of unmodified polysaccharides. Additionally, CSPP showed higher immunomodulating activity than unmodified polysaccharide, indicating that CSPP can be used as an effective regulatory immunosuppressant (93). Liu et al. extracted and isolated *Craterellus cornucopioides* polysaccharides and then then modified polysaccharides by carboxymethylation modification to produce two fractions (CCPs-1 and CCPs-2). The results show that CCPs-1 and CCPs-2 were consisted of Rha, Fuc, Ara, Xyl, Man, Glu, and Gal with different molar ratios. CCPs-1 and CCPs-2 were primarily connected by Man with (1→ 3)-linked. In addition, CCPs-1 and CCPs-2 showed good antioxidant activity (94). Wang, Zhang, and Zhao prepared a water-insoluble crude polysaccharides from *Tremella fuciformis* (ATP) and modified ATP structure. It was found that the degree of substitution (DS) of the four carboxymethylated derivatives varied with

the molar number of chloroacetic acid. With the increase of DS content, their water solubility and biological activities increased, suggesting that carboxymethylation modification can effectively improve the potential biological properties of polysaccharides (95).

Phosphorylation modification

Phosphorylation modification is one of the common methods of modifying the chemical structure of polysaccharides. Like other chemical modifications, it is also a covalent modification of molecular branches. After phosphorylation modification, the biological activities of polysaccharides significantly improved. Therefore, phosphorylation modification has attracted the attention of relevant fields. The principle of phosphorylation modification is that the polysaccharides react with the phosphorylation reagent to introduce the phosphate group to some hydroxyl groups on the polysaccharides residues (96). Figure 2D shows the phosphorylation modification of polysaccharides. Deng et al. obtained the water-soluble phosphorylated polysaccharides (P-DIP) by using phosphorylation modification and investigated it's the physiochemical and biological properties. It was found that the water solubility of P-DIP was significantly higher than that of DIP. P-DIP could significantly inhibit the growth of MCF-7 and B16 tumor cells in a dose-dependent manner. Moreover, P-DIP could effectively remove DPPH and OH radicals, implying that phosphorylation modification can help to improve the water solubility of natural DIP and enhance its antioxidant and antitumor activities (97). Ming et al. phosphorylation modified polysaccharides from *Chrysanthemum indicum* to obtain a single fraction (pCIPS). The results show that pCIPS was observed the polysaccharides surface features. Additionally, the anti-DHAV activity of pCIPS enhanced after phosphorylation modification (98). Feng et al. prepared the nine phosphorylated *Radix Cyathulae officinalis* Kuan polysaccharides (pRCPS) and evaluated its antiviral activity. The results observe that the pRCPS1-4, pRCPS7, and pRCPS9 showed significant anti-viral activity. In addition, phosphorylation modification could be used as a method to improve the antiviral activity of polysaccharides (99).

Selenide modification

Selenium is an essential element of human life activities, which can enhance the antioxidant capacity of the body and play an important role in anti-cancer. Relevant experiments have confirmed that selenium polysaccharides formed by organically combining selenium and polysaccharides have a variety of biological activities, which can antagonize heavy metal poisoning and reactive oxygen species damage by improving the activity of related enzymes, blocking the DNA synthesis of cancer cells and inhibiting the growth of cancer cells (100). Selenium polysaccharides take into account the activities of selenium and polysaccharides, and selenium polysaccharides are more easily absorbed and utilized by the body. Due to its low toxicity, low side effects and easy absorption, it has attracted the attention of scientific and technological researchers. Figure 2E shows the selenium modification of polysaccharides. Sun et al. obtained the Se-containing polysaccharide-protein complex (Se-PPC) and evaluated its anti-tumor activity. It was found that Se-PPC could prominently inhibit the growth of cancer cells though induction of apoptosis, and increase the population of apoptotic sub-G1 phase cells, up-regulate the expression of anti-apoptotic (Bcl-2 and Bcl-XL), indicating that Se-PPC is a promising new organic selenium compound, which has the potential to treat human cancer (101). Lian et al. prepared polysaccharides from *Glycyrrhiza uralensis* (GUP) and modified GUP structure *via* selenide modification to produce the selenized GUP (SeGUP) and evaluated its antioxidant activity. The thermal stability and particle size of SeGUP were significantly different from those of GUP. Moreover, SeGUP showed greater antioxidant activities *in vitro* and *in vivo* when compared to GUP. These results show that selenide modification can significantly enhance the antioxidant activity of SeGUP, and SeGUP has the potential to be developed as a natural antioxidant (102). Furthermore, the biological activities of polysaccharides from *Codonopsis pilosula* and *Ganoderma lucidum* mycelia could be significantly improved by selenium modification (103, 104).

The research on the structural modification of polysaccharides has made great achievements. At present, a variety of polysaccharides modification methods have been mastered. However, various modification methods still have different shortcomings. Although the chemical modification method is highly targeted, it can change the structural form and state of a certain part to obtain a certain biological activities of the target polysaccharides. Nevertheless, it is difficult to treat the organic reagent, which is easy to cause environmental pollution. In addition, the reaction process is not easy to control, which is easy to introduce impurities and cause side effects of polysaccharides. The physical modification method is easy to operate and is not easy to damage the structure of polysaccharides. However, this method has no effect on the inherent biological activities. Therefore, under the guidance of science and technology, we should try to combine various methods to modify the structure of polysaccharides in the future. In addition, we should strengthen the research on the structure-activity relationship of modified polysaccharides, and clarify the correlation between structural characterization and biological activities.

Biological activities of TCMPs

Growing studies have indicated that polysaccharides, as one of the key bioactive components of TCM, have various biological activities, such as antioxidant, anti-aging, immunomodulatory, hypoglycemic, hypolipidemic, anti-tumor, anti-inflammatory, and other activities. Currently, increasing TCMPs are used to treat various chronic diseases or developed into special health products to meet the needs of specific populations. Figure 1 summarizes the biological activities of TCMPs.

Antioxidant and anti-aging activities

Oxidative stress will lead to the damage of lipids, proteins, DNA, and lipid membranes in the body, and eventually induce aging (105). Growing studies have shown that TCMPs have strong antioxidant and anti-aging effects (8, 106). TCMPs mainly show their antioxidant effect *in vitro* by scavenging free radicals. In addition, TCMPs can play an anti-aging role by activating various antioxidant enzymes, regulating the expression of anti-aging gene klotho and p53/p12 signaling pathway. TCMPs can improve theirs antioxidant activities *in vitro* by scavenging OH, O^{2-}, DPPH, and $ABTS^{+}$ radicals, and the scavenging effect of TCMPs is basically equivalent to that of V_C (9, 107). The mechanism of TCMPs scavenging free radicals might be that the OH group in TCMPs can provide hydrogen and combine with OH radical to promote the scavenging radical. Moreover, there may be electrophilic groups (aldehydes or ketones) in TCMPs, which will release hydrogen atoms and scavenge O^{2-} radical. The scavenging of DPPH and $ABTS^{+}$ radicals may be related to the monosaccharide composition, glycosidic bond and configuration of TCMPs (3, 108, 109). TCMPs could significantly increase the activities of various enzymes such as SOD, CAT, and GSH-Px in the body by up regulating the expression levels of related antioxidant genes. Moreover, TCMPs could significantly reduce the levels of MDA, TC, and TG, thereby reducing the number of intracellular free radicals, improving the ability of the body to resist oxidative stress, reducing oxidative damage, and delaying aging (110, 111). Furthermore, TCMPs could up regulate the expression of anti-aging klotho gene in liver and kidney to delay aging in mice. The klotho protein started the intracellular signal transduction process by binding to specific receptors on the surface of cell membrane. This signal transmission could inhibit the phosphorylation process of specific target enzymes (PI3K and PKB), resulting in the dephosphorylation of Akt, and Akt dephosphorylation could inhibit the phosphorylation of forkhead transcription factors FOXO family (FOXO1, FOXO3a, FOXO4, etc.), and then directly regulate and promote the expression of SOD2 to eliminate intracellular reactive oxygen species, reduce oxidative stress, and delay the aging of the body (112). Additionally, p53/p12 signaling pathway plays an important role in the regulation of cell aging induced by oxidative stress. p53 and p12 proteins are the key proteins in the regulation pathway of cell aging. When oxidative stress occurred, p53 protein was activated and its expression levels increased, which activated p21 protein and significantly increased its expression levels, eventually leading to the occurrence of aging (113). The mRNA expression levels of p16 and p21 in aging rats induced by D-galactose decreased after gavage *Astragalus* polysaccharides. Western blot analysis shows that *Astragalus* polysaccharides could significantly down regulate the proteins expression levels of p53 and p21 in rat liver and brain, thereby down regulating the expression levels of aging genes (114). Therefore, it is inferred that the main antioxidant and anti-aging mechanisms of TCMPs is shown in Figure 3.

Immunomodulatory activity

Immunomodulatory activity is considered to be an important ability to improve the physical defense mechanism of the elderly and cancer patients. A large number of studies have shown that TCMPs have the effect of immune regulation (115, 116). Hao and Zhao prepared the water-soluble yam polysaccharides (WYPs) by HWE and evaluated its immunomodulatory activity. It was found that WYPs (500 mg/kg) could increase spleen and thymus indices by 22–42%, enhance macrophages' phagocytosis and NK cell activity. Moreover, WYPs (500 mg/kg) could elevate the levels of IL-2 and IFN-γ in the splenocytes, and IL-1β, IL-6, TNF-α, and iNOS in the splenocytes. Furthermore, WYPs could increase the levels of IgM, IgA, and IgG in serum, suggesting that WYPs can be developed into potential immunosuppressants (117). Carboxymethyl *Poria cocos* polysaccharides activated macrophage centered innate immunity and increased the expression levels of activation mmacrophage membrane receptors (CD^{3+}, CD^{4+}, CD^{8+}, and p38 kinases) in RAW264.7 macrophages (118). Additionally, *Poria cocos* polysaccharides could restore $CD4^{+}/CD^{8+}$ in immune injured mice, activate T cells, release a large amount of tumor necrosis factor (TNF-α and IL-1β), stimulate the production of IgG and IgM in serum, activate the immune system and enhance immune regulation function (119). NF-κB is a transcription factor that regulates various genes related to immune and inflammatory responses. In the cytoplasm of unstimulated cells, NF-κB binds to NF-κB inhibitor (IκB) and becomes an inactive complex form. IκB kinase (IKK) complex was activated when cells were stimulated. IKK family catalyzed IκB-α phosphorylation and dissociation from NF-κB. IκB-α degraded and induced nuclear heterotopia of NF-κB, transforming NF-κB into an activated form (120). Increasing studies have shown that TCMPs could activate RAW 264.7 macrophages by activating NF-κB signaling pathway, release a large amount of NO, promote the expression levels of IL-6 and TNF-α, which ultimately played its role in immune

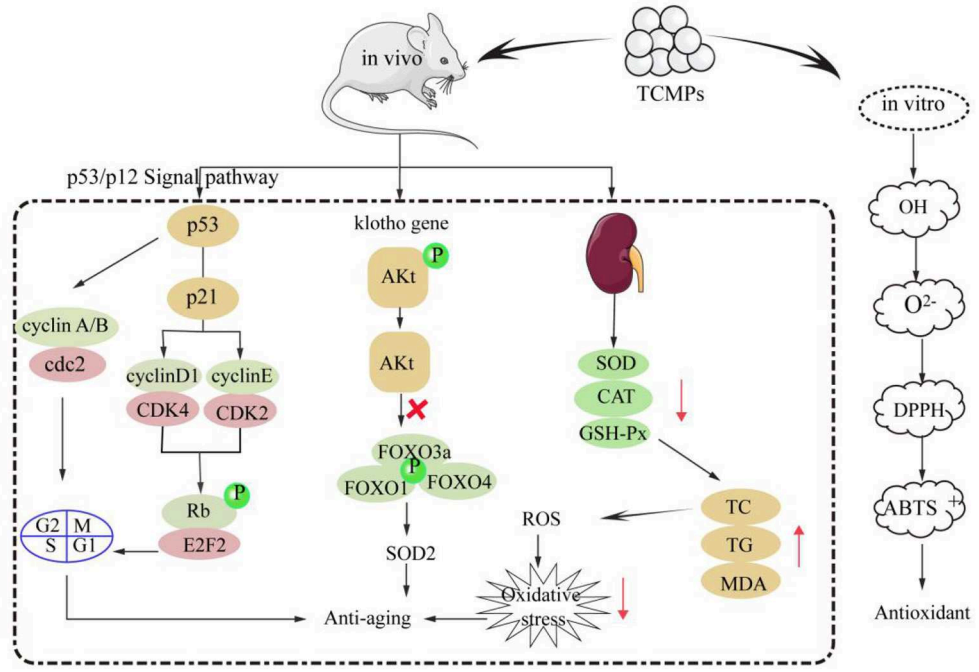

FIGURE 3
The main antioxidant and anti-aging mechanisms of TCMPs.

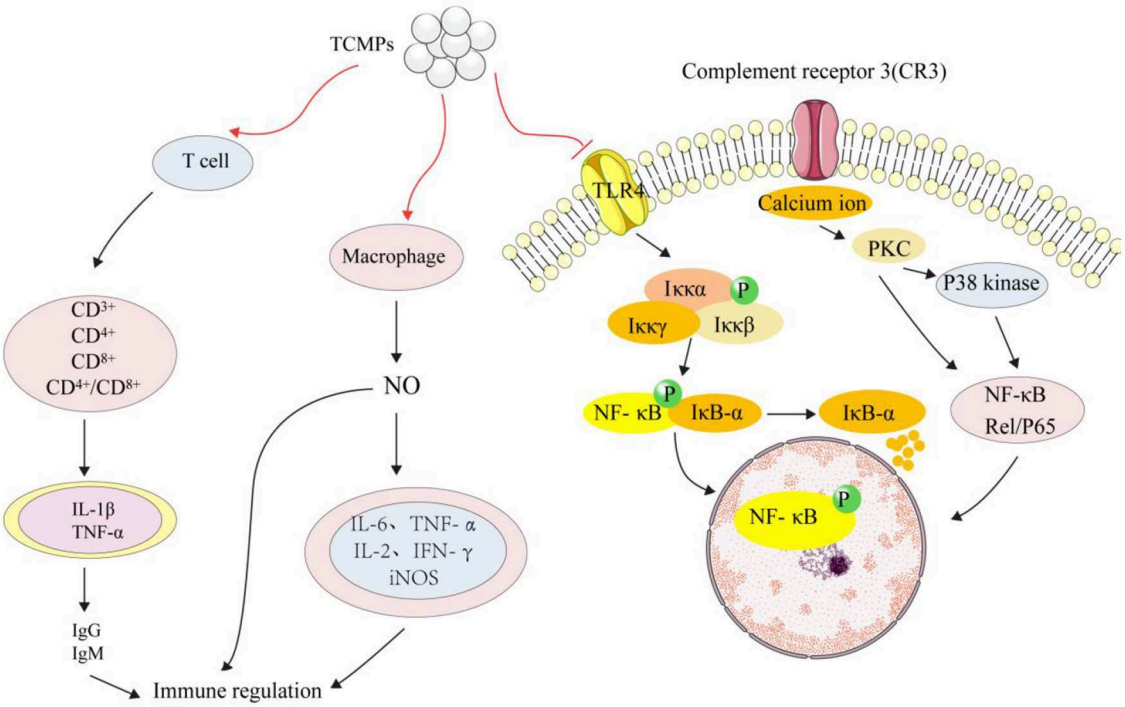

FIGURE 4
The main immunomodulatory mechanism of TCMPs.

regulation. Figure 4 shows the main mechanism of TCMPs in immune regulation.

Hypoglycemic and hypolipidemic activities

At present, the number of "three highs" in China is gradually increasing. In addition, the "three highs" have an obvious trend of being younger, younger, and grassroots (121). Diabetes is a chronic endocrine metabolic disease characterized by long-term hyperglycemia, which is one of the three major diseases in the world (122). Hyperlipidemia is a common and frequently occurring disease in clinic, which is characterized by high levels of cholesterol (TC), triglycerides (TG), low-density lipoprotein cholesterol (LDL-C) and low levels of high-density lipoprotein cholesterol (HDL-C) (123). Currently, some drugs used to treat hypoglycemia and hypolipidemia in clinic have certain side effects. Therefore, it is very important to find green and natural drugs to reduce blood glucose and blood lipids. Qian et al. extracted the *Trichosanthes* peel polysaccharide (TPP), and then purified TPP by using Sephadex G-100 column to produce the homogeneous component (TPP-1), and evaluated its hypoglycemic activity. It was found that TPP-1 was consisted of Ara, Man, Glc, and Gal with a molar ratio of 1.00:3.27:4.26:6.01. Moreover, TPP-1 could reduce the blood glucose levels in hyperglycemia mice. TPP-1 could increase significantly the contents of insulin and total superoxide dismutase of the hyperglycemia mice, whereas TPP-1 could decrease the levels of biochemical indexes, including MDA, creatinine, triglyceride, LDL-C, and blood urea nitrogen (124). Cao et al. isolated and purified polysaccharide from *Sargassum pallidum* to obtain the homogeneous component (PSP-1) with the molecular weight of 1,036 kDa, and determine its antioxidant and hypoglycemic activities. The results show that PSP-1 was comprised of Fuc (18.45%), Ara (2.15%), Gal (19.06%), Glu (1.89%), Xyl (16.07%), Man (1.00%), Galacturonic acid (5.74%), and Glucuronic acid (20.09%). PSP-1 showed good DPPH and OH radicals scavenging activities. Additionally, PSP-1 could remarkably inhibit α-amylase and α-glucosidase activities, improve glucose consumption, glycogen synthesis and the activities of pyruvate kinase and hexokinase in insulin-resistance HepG2 cells, suggesting that PSP-1 can be used as a potential antioxidant and hypoglycemic agent for disease prevention and treatment (125). Lee et al. studied whether yam polysaccharides (YPs) have an effect on insulin resistance. The results show that YPs played an important role in inhibiting insulin resistance induced by TNF-α or ROS. The potential hypoglycemic mechanism of YPs was that YPs could inhibit the Tyr phosphorylation of IRS, increase the levels of IR and phosphorylated serine/p-Akt, thus increasing the activity of Akt/PKB, inhibiting the increase of glucose in mice, and reducing the levels of blood lipids in mice (126). Furthermore, yam polysaccharides could reduce the levels of LDL-C and total TC, inhibit the production of SFAs, reduce the levels of IL-1β and TNF-α in serum, and down regulate the expression levels of MMP-3 protein in visceral adipose tissue to improve insulin resistance and reduce blood lipids (127). Figure 5 shows possible hypoglycemic and hypolipidemic mechanisms of TCMPs.

Anti-tumor activity

Although great progress has been made in the diagnosis and treatment of human malignant tumors, the long-term prognosis is still deal. At present, the treatment of cancer mostly depends on chemical drugs. However, long-term use of chemical drugs will lead to the decline of body immunity. Therefore, it is of great significance to find natural anti-tumor drugs with high efficiency, low toxicity, and low side effects. TCMPs, as natural active ingredients, are used to inhibit the growth of tumor cells through different signal pathways. Zhao et al. extracted *Lentinus edodes* polysaccharides (LEPs) using EAE, and then purified the crude LEPs to obtain two homogeneous polysaccharides fractions (LEPs-1 and LEPs-2). These results observed that LEPs-1 and LEPs-2 could markedly inhibit the proliferation of HCT-116 and HeLa cells, indicating that LEPs can be used as a potential natural anti-tumor candidate (128). Ma et al. isolated two homogeneous polysaccharides fractions (CPPS-1 and CPPS-2) *via* ultrafiltration method and determined their cytotoxicity and antioxidant activity. These results found that the antioxidant activity of CPPS-1 was significantly better than that of CPPS-2. Moreover, CPPS-1 could down-regulate the expression of Bcl-2 and up-regulate the expression of p53 and Bax, suggesting that the anti-tumor activity of CPPS-1 is closely related to its induction of apoptosis by activating the mitochondrial apoptosis pathway. It is noteworthy that the abnormal activation of JAK/STAT and ERK1/2 pathways were closely related to the proliferation, differentiation, invasion, and apoptosis of cancer cells. Reducing cancer toxicity is also one of the anti-tumor mechanisms of TCMPs. TCMPs could inhibit tumor recurrence and metastasis, and reduce organ damage caused by chemotherapy, radiotherapy and drugs in the process of cancer treatment (129). TCMPs could interfere with TGF signaling pathway and reduce the relative expression levels of TGF-βRI (transforming growth factor-beta receptor I) and metastatic proteins in gastric cancer transplanted mice. Additionally, TCMPs could reduce the phosphorylation of FAK and AKT, and significantly inhibit the metastasis and invasion of lung cancer CL1-5 cells (130). TCMPs could reduce the expression levels of MMP-9 and VEGFA proteins in HeLa cells and inhibit the formation of neovascularization, which was not conducive to the migration, invasion, and metastasis of tumor cells (131). The literature review found that TCMPs have significant antitumor activity. However, molecular mechanisms

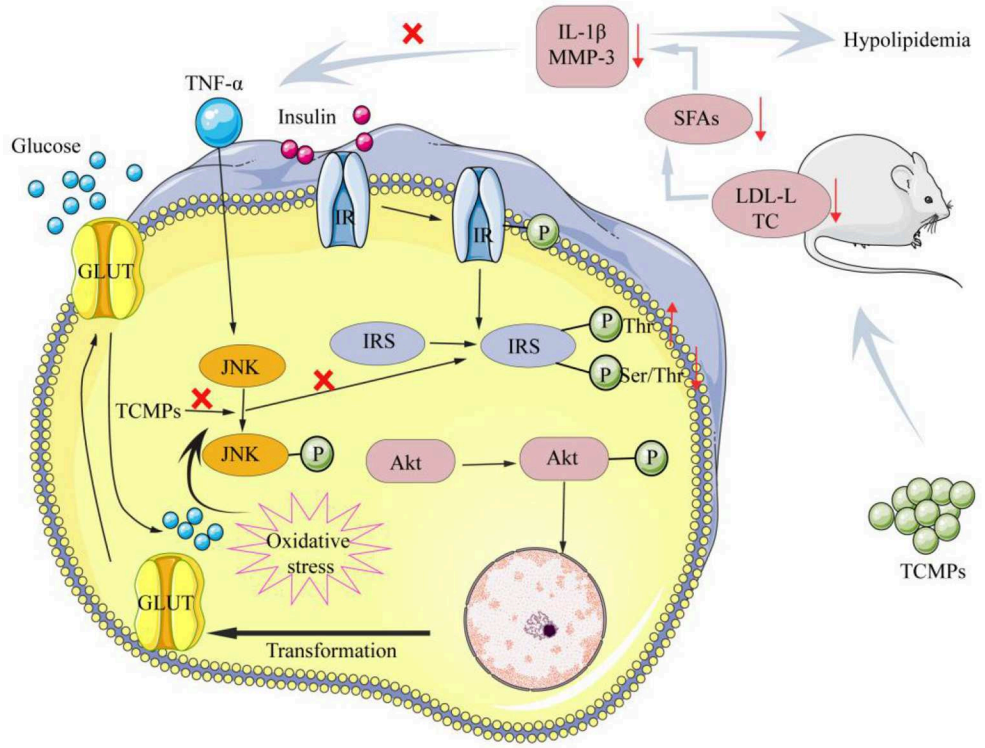

FIGURE 5
The main hypoglycemic and hypolipidemic mechanisms of TCMPs.

of their antitumor activity are still unclear. Hence, the following research still needs to continue to explore the molecular mechanism of TCMPs anti-tumor.

Anti-inflammatory activity

The body can secrete immune factors to improve the immune function when pathogens invade the body. However, excessive immune response such as inflammatory response will cause damage to the body (8, 105). Inflammation is the key factor in the development of various pathological processes such as cancer and depression (132). Jujube polysaccharides have antioxidant capacity to scavenge DPPH, $ABTS^{+}$, and OH radicals. The evaluation results of anti-inflammatory activity *in vitro* show that the jujube polysaccharides still had strong anti-inflammatory ability. It was further inferred that jujube polysaccharides could regulate the activity of intracellular antioxidant enzymes by scavenging excess free radicals to interfere with the relevant targets in the inflammatory reaction and further enhance its anti-inflammatory effect (133). Cytokines are mediators of interaction between cells and play an important role in the occurrence and maintenance of inflammation. The anti-inflammatory cytokines of TCMPs are mainly tumor necrosis factor, including IL-6, IL-1β, and IL-10. Macrophages play an important role in the development of inflammation. Liu et al. found that carboxymethyl *Poria cocos* polysaccharide acted on trinitrobenzene sulphonic acid (TNBS) induced colitis in mice, and myeloperoxidase (MPO) activity and MDA content in colon tissue decreased and protected colitis in mice by regulating potential targeted proteome and key protein metabolism. Carboxymethyl *Poria cocos* polysaccharides could interfere with the down regulation signaling pathways of NF-κB, myosin light chain kinase (MLCK), and phosphorylated myosin light chain (p-MLC) in TNF-α injured Caco-2 cells. In addition, polysaccharides could enhance the expression levels of intestinal tight junction protein and effectively prevent colitis (134). The above mechanisms could inhibit the production of pro-inflammatory factors, increase the levels of anti-inflammatory factors, reduce oxidative stress and intestinal barrier damage, and achieve the anti-colitis effect (135). In conclusion, it is a common method to observe the regulatory effects of TCMPs on inflammatory response by measuring the levels of cytokines. It is of great significance to study the changes of cytokines in inflammation and explore the anti-inflammatory mechanism at the molecular level. However, the structure-activity relationship and specific signal pathways of TCMPs still need to be further revealed and summarized.

Other activities

Furthermore, TCMPs have liver protection, radiation protection, anticoagulation, and other activities. Liu, Liu, and Qian found that *Cynanchum auriculatum* flower polysaccharides have a significant protective effect on ethanol induced liver injury in mice by increasing the activity of liver antioxidant enzymes, reducing the ability of MDA lipid peroxidation and the expression of inflammatory factors (TNF-α, IL-6, IL-1β, and IL-10) (135). *Poria cocos* polysaccharides showed many biological activities, such as anti-oxidation, anti-aging, anti-fatigue, lowering blood sugar and lipid, regulating urinary system, and bacteriostasis (136). Li et al. found that *Sophora japonica* polysaccharide could significantly down regulate the expression levels of JNK phosphorylation and p38 MAPK protein phosphorylation in HaCaT cells exposed to outdoor ultraviolet (UVB) through MAPK pathway, which could effectively protect HaCaT keratinocytes from skin damage caused by UVB, and significantly inhibit UVB induced cytotoxicity (137). Overall, the findings indicate that TCMPs could be used as natural anti-radiation drug candidates.

Conclusions and future prospects

Many diseases, such as malignant tumor, low immunity, gastroenteritis, alcoholic liver, fatty liver, depression, hyperglycemia, etc. induced by poor diet, work, environment and other factors, have aroused widespread concern about traditional Chinese medicines. In recent years, the various active functions of traditional Chinese medicines have been deeply explored, which has great potential in the development of food, drugs and health products. TCMPs combined with Chinese herbal medicines, anticancer drugs, and vaccines will be the research hotspot. The synergistic effect and structure-activity mechanism of TCMPs and other active ingredients deserve further exploration. Different edible parts, sources, storage, and processing methods of traditional Chinese medicines lead to certain differences in the content, structure, and biological activities of TCMPs. Strengthening the quality control of traditional Chinese medicine is the key to keep the chemical structure and biological activities of TCMPs reliable and consistent in food and pharmaceutical applications.

TCMPs have poor water solubility, low yield, difficult separation and purification, and low biological activities. The water-soluble TCMPs produced by modification can enhance the original biological activities or produce new biological activities. Hence, the structural modification of TCMPs is the main research direction of scholars at home and abroad. Currently, carboxymethyl TCMPs are used to develop adjuvant drugs for cancer treatment and put into the market. Great breakthroughs have been made in the market development of TCMPs. However, the study on the relationship between the structure and bioactivity mechanisms of TCMPs is relatively limited due to the limitations of spatial structure testing technology, which limits its development and application. Hence, the quality of TCMPs derivatives can be controlled by further standardizing the quality of TCMPs, deeply studying the various biological activities of TCMPs, and clarifying the fine structure and structure-activity relationship of TCMPs. Especially, the chemical modification degree and reliable pharmacokinetic study of TCMPs derivatives can promote the development of new polysaccharides or health food.

Author contributions

HX and PL: formal analysis (supporting), investigation (equal), and writing-original draft (equal). JB, YG, and YS: formal analysis (supporting) and investigation (equal). JT: funding acquisition (equal), project administration (equal), and writing-review and editing (equal). All authors contributed to the article and approved the submitted version.

Acknowledgments

The authors gratefully thank the financial support provided by Hebei University high-level talent scientific research start-up project (521100221072).

Conflict of interest

The authors declare that the research was conducted in the absence of any commercial or financial relationships that could be construed as a potential conflict of interest.

Publisher's note

All claims expressed in this article are solely those of the authors and do not necessarily represent those of their affiliated organizations, or those of the publisher, the editors and the reviewers. Any product that may be evaluated in this article, or claim that may be made by its manufacturer, is not guaranteed or endorsed by the publisher.

References

1. Ji X, Hou C, Shi M, Yan Y, Liu Y. An insight into the research concerning *Panax ginseng* C. A. Meyer polysaccharides: a review. *Food Rev Int.* (2020) 38:1149–65. doi: 10.1080/87559129.2020.1771363

2. Liang B, Zhu YC, Lu J, Gu N. Effects of traditional Chinese medication-based bioactive compounds on cellular and molecular mechanisms of oxidative stress. *Oxid Med Cell Longev.* (2021) 2021:3617498. doi: 10.1155/2021/3617498

3. Zeng P, Li J, Chen Y, Zhang L. The structures and biological functions of polysaccharides from traditional Chinese herbs. *Prog Mol Biol Transl.* (2019) 163:423–44. doi: 10.1016/bs.pmbts.2019.03.003

4. Xie M, Tao W, Wu F, Wu K, Huang X, Ling G, et al. Anti-hypertensive and cardioprotective activities of traditional Chinese medicine-derived polysaccharides: a review. *Int J Biol Macromol.* (2021) 185:917–34. doi: 10.1016/j.ijbiomac.2021.07.008

5. Hou C, Yin M, Lan P, Wang H, Nie H, Ji X. Recent progress in the research of *Angelica sinensis (Oliv.)* Diels polysaccharides: extraction, purification, structure and bioactivities. *Chem Biol Technol Ag.* (2021) 8:13. doi: 10.1186/s40538-021-00214-x

6. Chen Y, Yao F, Ming K, Wang D, Hu Y, Liu J. Polysaccharides from traditional Chinese medicines: extraction, purification, modification, and biological activity. *Molecules.* (2016) 21:1705. doi: 10.3390/molecules21121705

7. Ji X, Cheng Y, Tian J, Zhang S, Jing Y, Shi M. Structural characterization of polysaccharide from jujube (*Ziziphus jujuba* Mill.) fruit. *Chem Biol Technol Ag.* (2021) 8:54. doi: 10.1186/s40538-021-00255-2

8. Nai J, Zhang C, Shao H, Li B, Li H, Gao L, et al. Extraction, structure, pharmacological activities and drug carrier applications of *Angelica sinensis* polysaccharide. *Int J Biol Macromol.* (2021) 183:2337–53. doi: 10.1016/j.ijbiomac.2021.05.213

9. Wang B, Niu J, Mai B, Shi F, Li M, Chen L, et al. Effects of extraction methods on antioxidant and immunomodulatory activities of polysaccharides from superfine powder *Gynostemma pentaphyllum* Makino. *Glycoconjugate J.* (2020) 37:777–89. doi: 10.1007/s10719-020-09949-5

10. Luan F, Ji Y, Peng L, Liu Q, Cao H, Yang Y, et al. Extraction, purification, structural characteristics and biological properties of the polysaccharides from *Codonopsis pilosula*: a review. *Carbohyd Polym.* (2021) 261:117863. doi: 10.1016/j.carbpol.2021.117863

11. Zhang R, Zhang X, Tang Y, Mao J. Composition, isolation, purification and biological activities of *Sargassum fusiforme* polysaccharides: a review. *Carbohyd Polym.* (2020) 228:115381. doi: 10.1016/j.carbpol.2019.115381

12. Liu L, Xu FR, Wang YZ. Traditional uses, chemical diversity and biological activities of *Panax* L. (*Araliaceae*): a review. *J Ethnopharmacol.* (2020) 263:112792. doi: 10.1016/j.jep.2020.112792

13. Chen J, Li L, Zhou X, Li B, Zhang X, Hui R. Structural characterization and α-glucosidase inhibitory activity of polysaccharides extracted from Chinese traditional medicine Huidouba. *Int J Biol Macromol.* (2018) 117:815–19. doi: 10.1016/j.ijbiomac.2018.05.192

14. Wang W, Li X, Bao X, Gao L, Tao Y. Extraction of polysaccharides from black mulberry fruit and their effect on enhancing antioxidant activity. *Int J Biol Macromol.* (2018) 120:1420–29. doi: 10.1016/j.ijbiomac.2018.09.132

15. Zhu Z, Chen J, Chen Y, Ma Y, Yang Q, Fan Y, et al. Extraction, structural characterization and antioxidant activity of turmeric polysaccharides. *LWTtraction, structur.* (2022) 154:112805. doi: 10.1016/j.lwt.2021.112805

16. Lu J, You L, Lin Z, Zhao M, Cui C. The antioxidant capacity of polysaccharide from *Laminaria japonicaby* citric acid extraction. *Int J Food Sci Tech.* (2013) 48:1352–8. doi: 10.1111/ijfs.12072

17. Kong M, Yao Y, Zhang H. Antitumor activity of enzymatically hydrolyzed *Ganoderma lucidum* polysaccharide on U14 cervical carcinoma-bearing mice. *Int J Immunopath Pharmacol.* (2019) 33:20587. doi: 10.1177/2058738419869489

18. Bao Y, Jiang Y, Zhao M, Feng C, Wang R, Chen Y, et al. Structural characterisation of polysaccharides purified from longan (*Dimocarpus longan* Lour.) fruit pericarp. *Food Chem.* (2009) 115:609–14. doi: 10.1016/j.foodchem.2008.12.082

19. Yi Y, Wang H, Zhang R, Min T, Huang F, Liu L, et al. Characterization of polysaccharide from longan pulp as the macrophage stimulator. *RSC Adv.* (2015) 5:97163–70. doi: 10.1039/C5RA16044H

20. Chen X, Tang R, Liu T, Dai W, Liu Q, Gong G, et al. Physicochemical properties, antioxidant activity and immunological effects *in vitro* of polysaccharides from *Schisandra sphenanthera* and *Schisandra chinensis*. *Int J Biol Macromol.* (2019) 131:744–51. doi: 10.1016/j.ijbiomac.2019.03.129

21. Chen C, You LJ, Abbasi AM, Fu X, Liu RH. Optimization for ultrasound extraction of polysaccharides from mulberry fruits with antioxidant and hyperglycemic activity *in vitro*. *Carbohyd Polym.* (2015) 130:122–32. doi: 10.1016/j.carbpol.2015.05.003

22. Yang B, Zhao M, Jiang Y. Optimization of tyrosinase inhibition activity of ultrasonic-extracted polysaccharides from longan fruit pericarp. *Food Chem.* (2008) 110:294–300. doi: 10.1016/j.foodchem.2008.01.067

23. Wang Y, Zhang X, Ma X, Zhang K, Li S, Wang X, et al. Study on the kinetic model, thermodynamic and physicochemical properties of *Glycyrrhiza* polysaccharide by ultrasonic assisted extraction. *Ultrason Sonochem.* (2018) 51:249–57. doi: 10.1016/j.ultsonch.2018.10.012

24. Chen X, Ji H, Zhang C, Liu A. Optimization of extraction process from *Taraxacum officinale* polysaccharide and its purification, structural characterization, antioxidant and anti-tumor activity. *J Food Meas Char.* (2020) 14:194–206. doi: 10.1007/s11694-019-00281-7

25. Chen Y, Yin L, Zhang X, Wang Y, Chen Q, Jin C, et al. Optimization of alkaline extraction and bioactivities of polysaccharides from rhizome of polygonatumodoratum. *BioMed Res Int.* (2014) 2014:504896. doi: 10.1155/2014/504896

26. Hou X, Huang X, Li J, Jiang G, Shen G, Li S, et al. Extraction optimization and evaluation of the antioxidant and α-glucosidase inhibitory activity of polysaccharides from *Chrysanthemum morifolium* cv. Hangju. *Antioxidants.* (2020) 9:59. doi: 10.3390/antiox9010059

27. Chen R, Jin C, Tong Z, Lu J, Tan L, Tian L, et al. Optimization extraction, characterization and antioxidant activities of pectic polysaccharide from tangerine peels. *Carbohyd Polym.* (2016) 136:187–97. doi: 10.1016/j.carbpol.2015.09.036

28. Xu J, Hou H, Hu J, Liu B. Optimized microwave extraction, characterization and antioxidant capacity of biological polysaccharides from *Eucommia* ulmoides Oliver leaf. *Sci Rep.* (2018) 8:6561. doi: 10.1038/s41598-018-24957-0

29. Meng H, Wu J, Shen L, Chen G, Jin L, Yan M, et al. Microwave assisted extraction, characterization of a polysaccharide from Salvia miltiorrhiza Bunge and its antioxidant effects *via* ferroptosis-mediated activation of the Nrf2/HO-1 pathway. *Int J Biol Macromol.* (2022) 215:398–412. doi: 10.1016/j.ijbiomac.2022.06.064

30. Xu L, Yu JQ, Wang XY, Xu N, Liu JL. Microwave extraction optimization using the response surface methodology of *Fructus Meliae Toosendan* polysaccharides and its antioxidant activity. *Int J Biol Macromol.* (2018) 118:1501–10. doi: 10.1016/j.ijbiomac.2018.06.172

31. Li E, Yang S, Zou Y, Cheng W, Li B, Hu T, et al. Purification, characterization, prebiotic preparations and antioxidant activity of oligosaccharides from mulberries. *Molecules.* (2019) 24:2329. doi: 10.3390/molecules24122329

32. You Q, Yin X, Zhao Y. Enzyme assisted extraction of polysaccharides from the fruit of *Cornus officinalis*. *Carbohyd Polym.* (2013) 98:607–10. doi: 10.1016/j.carbpol.2013.06.036

33. Chen H, Zhou X, Zhang J. Optimization of enzyme assisted extraction of polysaccharides from *Astragalus* membranaceus. *Carbohyd Polym.* (2014) 111:567–75. doi: 10.1016/j.carbpol.2014.05.033

34. Song YR, Sung SK, Jang M, Lim TG, Cho CW, Han CJ, et al. Enzyme-assisted extraction, chemical characteristics, and immunostimulatory activity of polysaccharides from Korean ginseng (*Panax ginseng* Meyer). *Int J Biol Macromol.* (2018) 116:1089–97. doi: 10.1016/j.ijbiomac.2018.05.132

35. Chen W, Jia Z, Huang G, Hong Y. Global optimization for simultaneous extraction of oil and polysaccharides from *Schizochytrium limacinum* by enzyme assisted three phase partitioning. *J Food Process Pres.* (2020) 44:e14824. doi: 10.1111/jfpp.14824

36. Wu Y, Liu H, Li Z, Huang D, Nong L, Ning Z, et al. Purification of polysaccharides from *Phellinus linteus* by using an aqueous two-phase system and evaluation of the physicochemical and antioxidant properties of polysaccharides *in vitro*. *Prep Biochem Biotech.* (2022) 52:89–98. doi: 10.1080/10826068.2021.1911815

37. Hu J, Liu J, Huang X, Di D, Pei D. Efficient extraction of polysaccharides from *Lycium barbarum* L. by aqueous two-phase system combined with tissue-smashing extraction. *Ind Crop Prod.* (2022) 184:115036. doi: 10.1016/j.indcrop.2022.115036

38. Mao G, Yu P, Zhao T, Chen Y, Feng W, Zhang Q, et al. Aqueous two-phase simultaneous extraction and purification of a polysaccharide from *Grifola frondosa*: process optimization, structural characteristics and antioxidant activity. *Ind Crop Prod.* (2022) 184:114962. doi: 10.1016/j.indcrop.2022.114962

39. Li H, Ke HX, Li FJ, Dong HJ, He JX, Zhang JD, et al. Optimization of aqueous two-phase extraction of polysaccharide from *Schisandra* chinensis using

response surface methodology with Box-Behnken design. *J Chin Med Mater.* (2016) 39:593–7. doi: 10.13863/j.issn1001-4454.2016.03.032

40. Tan J, Cui P, Ge S, Cai X, Li Q, Xue H. Ultrasound assisted aqueous two-phase extraction of polysaccharides from *Cornus officinalis* fruit: modeling, optimization, purification, and characterization. *Ultrason Sonochem.* (2022) 84:105966. doi: 10.1016/j.ultsonch.2022.105966

41. Ji X, Peng Q, Yuan Y, Liu F, Wang M. Extraction and physicochemical properties of polysaccharides from *Ziziphus Jujuba* cv. Muzao by ultrasound-assisted aqueous two-phase extraction. *Int J Biol Macromol.* (2018) 108:541–9. doi: 10.1016/j.ijbiomac.2017.12.042

42. Zhang X, Teng G, Zhang J. Ethanol/salt aqueous two-phase system based ultrasonically assisted extraction of polysaccharides from *Lilium davidiivar*. unicolor salisb: physicochemical characterization and antiglycation properties. *J Mol Liq.* (2018) 256:497–506. doi: 10.1016/j.molliq.2018.02.059

43. Xue H, Xu J, Zhang J, Wei Y, Cai X, Tan J. Modeling, optimization, purification, and characterization of polysaccharides from *Lilium lancifolium* thunb. *LWT Food Sci Technol.* (2022) 162:113491. doi: 10.1016/j.lwt.2022.113491

44. Wu W, Huang T, Xiang F. Polyethylene glycol-based ultrasonic-assisted enzymatic extraction, characterization, and antioxidant activity *in vitro* and *in vivo* of polysaccharides from *Lonicerae japonica* leaves. *Food Sci Nutr.* (2019) 7:3452–62. doi: 10.1002/fsn3.1186

45. Fan T, Hu J, Fu L, Zhang L. Optimization of enzymolysis-ultrasonic assisted extraction of polysaccharides from *Momordica charabtia* L. by response surface methodology. *Carbohyd Polym.* (2015) 115:701–6. doi: 10.1016/j.carbpol.2014.09.009

46. Wu H, Zhu J, Diao W, Wang C. Ultrasound-assisted enzymatic extraction and antioxidant activity of polysaccharides from pumpkin (*Cucurbita moschata*). *Carbohyd Polym.* (2014) 113:314–24. doi: 10.1016/j.carbpol.2014.07.025

47. Chen S, Chen H, Tian J, Wang J, Wang Y, Xing L. Enzymolysis-ultrasonic assisted extraction, chemical characteristics and bioactivities of polysaccharides from corn silk. *Carbohyd Polym.* (2014) 101:332–41. doi: 10.1016/j.carbpol.2013.09.046

48. Chen C, Yue CH, Wang YF, Zang XD, Liu P, Yu GP. Ultrasonic assisted enzymatic method extraction of polysaccharide from *Armillaria mellea*. *Sci Tech Food Ind.* (2017) 38:222–6. doi: 10.13386/j.issn1002-0306.2017.08.035

49. Xiong JW, Xu JR, Zhang JY, Wei JF, Cai JY. Study on enzymatic-assisted ultrasonic extraction and antibacterial activity of polysaccharide from *Hylocereus undatus*. *Sci Tech Food Ind.* (2015) 36:229–33. doi: 10.13386/j.issn1002-0306.2015.17.038

50. Arab K, Ghanbarzadeh B, Ayaseh A, Jahanbin K. Extraction, purification, physicochemical properties and antioxidant activity of a new polysaccharide from *Ocimum album* L. seed. *Int J Biol Macromol.* (2021) 180:643–53. doi: 10.1016/j.ijbiomac.2021.03.088

51. Zhang X, Kong X, Hao Y, Zhang X, Zhu Z. Chemical structure and inhibition on α-glucosidase of polysaccharide with alkaline-extracted from *Glycyrrhiza inflata* residue. *Int J Biol Macromol.* (2020) 147:1125–35. doi: 10.1016/j.ijbiomac.2019.10.081

52. Peng FH, Zha XQ, Cui SH, Asghar MN, Pan LH, Wang JH, et al. Purification, structure features and anti-atherosclerosis activity of a *Laminaria japonica* polysaccharide. *Int J Biol Macromol.* (2015) 81:926–35. doi: 10.1016/j.ijbiomac.2015.09.027

53. Peng Z, Liu M, Fang Z, Wu J, Zhang Q. Composition and cytotoxicity of a novel polysaccharide from brown alga (*Laminaria japonica*). *Carbohydr Polym.* (2012) 89:1022–6. doi: 10.1016/j.carbpol.2012.03.043

54. Zhang G, Zeng X, Li C, Li J, Huang Y, Han L, et al. Inhibition of urinary bladder carcinogenesis by aqueous extract of sclerotia of polyporus umbellatus fries and polyporus polysaccharide. *Am J Chin Med.* (2012) 39:135–44. doi: 10.1142/S0192415X11008701

55. Miao J, Regenstein JM, Qiu J, Zhang J, Zhang X, Li H, et al. Isolation, structural characterization and bioactivities of polysaccharides and its derivatives from *Auricularia*—a review. *Int J Biol Macromol.* (2020) 150:102–13. doi: 10.1016/j.ijbiomac.2020.02.054

56. Moradi Z, Kalanpour N. Kefiran, a branched polysaccharide: preparation, properties and applications: a review. *Carbohyd Polym.* (2019) 223:115100. doi: 10.1016/j.carbpol.2019.115100

57. Yan JK, Wang WQ, Wu JY. Recent advances in *Cordyceps sinensis*polysaccharides: mycelial fermentation, isolation, structure, and bioactivities: a review. *J Funct Foods.* (2014) 6:33–47. doi: 10.1016/j.jff.2013.11.024

58. Sharma SK, Gautam N, Atri NS. Optimized extraction, composition, antioxidant and antimicrobial activities of exo and intracellular polysaccharides from submerged culture of *Cordyceps cicadae*. *BMC Complem Altern Med.* (2015) 15:446. doi: 10.1186/s12906-015-0967-y

59. Kakar MU, Naveed M, Saeed M, Zhao S, Rasheed M, Firdoos S, et al. A review on structure, extraction, and biological activities of polysaccharides isolated from *Cyclocarya paliurus* (Batalin) Iljinskaja. *Int J Biol Macromol.* (2020) 156:420–29. doi: 10.1016/j.ijbiomac.2020.04.022

60. Wang XY, Zhang DD, Yin JY, Nie SP, Xie MY. Recent developments in *Hericium erinaceus* polysaccharides: extraction, purification, structural characteristics and biological activities. *Crit Rev Food Sci.* (2019) 59:S96–115. doi: 10.1080/10408398.2018.1521370

61. Xu J, Zhang J, Sang Y, Wei Y, Chen X, Wang Y, et al. Polysaccharides from medicine and food homology materials: a review on their extraction, purification, structure, and biological activities. *Molecules.* (2022) 27:3215. doi: 10.3390/molecules27103215

62. Teng C, Qin P, Shi Z, Zhang W, Ren G. Structural characterization and antioxidant activity of alkali-extracted polysaccharides from quinoa. *Food Hydrocolloid.* (2020) 113:106392. doi: 10.1016/j.foodhyd.2020.106392

63. Liu M, Liu W, Zhang W, Yao J, Mo X. Ultrasound-assisted extraction of boulardii yeast cell wall polysaccharides: characterization and its biological functions on early-weaned lambs. *Food Sci Nutr.* (2021) 9:3617–30. doi: 10.1002/fsn3.2318

64. Liu ZH, Niu FJ, Xie YX, Xie SM, Liu YN, Yang YY, et al. A review: natural polysaccharides from medicinal plants and microorganisms and their anti-herpetic mechanism. *Biomed Pharmacother.* (2020) 129:110469. doi: 10.1016/j.biopha.2020.110469

65. Ren Y, Bai Y, Zhang Z, Cai W, Del Rio Flores A. The preparation and structure analysis methods of natural polysaccharides of plants and fungi: a review of recent development. *Molecules.* (2019) 24:3122. doi: 10.3390/molecules24173122

66. Qiao YM, Chen WQ, Deng BW, Peng H, Xie XC, Zhang H, et al. Microwave-assisted extraction of polysaccharides from *Polyporus umbellatus* optimized by Box-Behnken design-response surface methodology. *J Food Sci Biotechnol.* (2015) 34:986–93. doi: 10.19540/j.cnki.cjcmm.20210311.301

67. Rosello-Soto E, Parniakov O, Deng Q, Patras A, Koubaa M, Grimi N, et al. Application of non-conventional extraction methods: toward a sustainable and green production of valuable compounds from mushrooms. *Food Eng Rev.* (2016) 8:214–34. doi: 10.1007/s12393-015-9131-1

68. Song YR, Han AR, Park SG, Cho CW, Rhee YK, Hong HD. Effect of enzyme-assisted extraction on the physicochemical properties and bioactive potential of lotus leaf polysaccharides. *Int J Biol Macromol.* (2020) 153:169–79. doi: 10.1016/j.ijbiomac.2020.02.252

69. Gang L, Ma X, Jiang Y, Li W, Wang Y, Liu L, et al. Aqueous two-phase extraction of polysaccharides from *Selaginella doederleinii* and their bioactivity study. *Process Biochem.* (2022) 118:274–82. doi: 10.1016/j.procbio.2022.04.024

70. Zhou HY, Liu CZ. Microwave-assisted extraction of solanesol from tobacco leaves. *J Chromatogr A.* (2006) 1129:135–9. doi: 10.1016/j.chroma.2006.07.083

71. Shi L. Bioactivities, isolation and purification methods of polysaccharides from natural products: a review. *Int J Biol Macromol.* (2016) 92:37–48. doi: 10.1016/j.ijbiomac.2016.06.100

72. Peat S, Turvey JR, Rees DA. Carbohydrates of the red alga, *Porphyra umbilicalis*. *J Chem Soc Pakistan.* (2016) 1961:1590–95. doi: 10.1039/jr9610001590

73. Guo YD, Shan B, Li MY. Study on the removal of protein from polysaccharides of *Momordica charantia* L. *J Anhui Agri Sci.* (2009) 37:3225–7. doi: 10.13989/j.cnki.0517-6611.2009.07.028

74. Chen Y, Song ZK, Zhang H. Study on optimization of response surface for the re-movement of protein from polysaccharide of *Solanum nigrum* fruit by chloroacetic acid method. *Food Ferm Ind.* (2020) 46:198–203. doi: 10.13995/j.cnki.11-1802/ts.024854

75. Ji X, Guo J, Ding D, Gao J, Hao L, Guo X, et al. Structural characterization and antioxidant activity of a novel high-molecular-weight polysaccharide from *Ziziphus Jujuba cv*. Muzao. *J Food Meas Char.* (2022) 16:2191–200. doi: 10.1007/s11694-022-01288-3

76. Gong T, Liu S, Wang H, Zhang M. Supercritical CO_2 fluid extraction, physicochemical properties, antioxidant activities and hypoglycemic activity of polysaccharides derived from fallen ginkgo leaves. *Food Biosci.* (2021) 42:101153. doi: 10.1016/j.fbio.2021.101153

77. Xie MY, Nie SP. Structure and bioactivities of polysaccharides from natural products. *Food Biosci.* (2016) 40:100875. doi: 10.16429/j.1009-7848.2010.02.035

78. Mutaillifu P, Bobakulov K, Abuduwaili A, Huojiaaihemaiti H, Nuerxiati R, Aisa HA, et al. Structural characterization and antioxidant activities of a watersoluble polysaccharide isolated from *Glycyrrhiza glabra*. *Int J Biol Macromol.* (2020) 144:751–9. doi: 10.1016/j.ijbiomac.2019.11.245

79. Xiao Y, Huang Q, Zheng Z, Guan H, Liu S. Construction of a *Cordyceps sinensis* exopolysaccharide-conjugated selenium nanoparticles and

enhancement of their antioxidant activities. *Int J Biol Macromol.* (2017) 99:483–91. doi: 10.1016/j.ijbiomac.2017.03.016

80. Wang Z, Xie J, Shen M, Nie S, Xie M. Sulfated modification of polysaccharides: synthesis, characterization and bioactivities. *Trends Food Sci Technol.* (2018) 74:147–57. doi: 10.1016/j.tifs.2018.02.010

81. Geng Y, Xing L, Sun M, Su F. Immunomodulatory effects of sulfated polysaccharides of pine pollen on mouse macrophages. *Int J Biol Macromol.* (2016) 91:846–55. doi: 10.1016/j.ijbiomac.2016.06.021

82. Wang C, He Y, Tang X, Li N. Sulfation, structural analysis, and anticoagulant bioactivity of ginger polysaccharides. *J Food Sci.* (2020) 85:2427–34. doi: 10.1111/1750-3841.15338

83. Huang R, Xie J, Liu X, Shen M. Sulfated modification enhances the modulatory effect of yam polysaccharide on gut microbiota in cyclophosphamide-treated mice. *Food Res Int.* (2021) 145:110393. doi: 10.1016/j.foodres.2021.110393

84. Zhao X, Xue CH, Li BF. Study of antioxidant activities of sulfated polysaccharides from *Laminaria japonica*. *J Appl Phycol.* (2007) 20:431–6. doi: 10.1007/s10811-007-9282-4

85. Saha S, Navid MH, Bandyopadhyay SS, Schnitzler P, Ray B. Sulfated polysaccharides from *Laminaria angustata*: structural features and *in vitro* antiviral activities. *Carbohydr Polym.* (2012) 87:123–30. doi: 10.1016/j.carbpol.2011.07.026

86. Xie L, Shen M, Hong Y, Ye H, Huang L, Xie J. Chemical modifications of polysaccharides and their anti-tumor activities. *Carbohydr Polym.* (2020) 229:115436. doi: 10.1016/j.carbpol.2019.115436

87. Gu D, Huang L, Chen X, Wu Q, Ding K. Structural characterization of a galactan from *Ophiopogon japonicus* and anti-pancreatic cancer activity of its acetylated derivative. *Int J Biol Macromol.* (2018) 113:907–15. doi: 10.1016/j.ijbiomac.2018.03.019

88. Liu XX, Wan ZJ, Lin S, Lu XX. Preparation and antiherpetic activities of chemically modified polysaccharides from *Polygonatum cyrtonema* hua. *Carbohydr Polym.* (2011) 83:737–42. doi: 10.1016/j.carbpol.2010.08.044

89. Chen F, Huang G. Extraction, derivatization and antioxidant activity of bitter gourd polysaccharide. *Int J Biol Macromol.* (2019) 141:14–20. doi: 10.1016/j.ijbiomac.2019.08.239

90. Liu Y, You Y, Li Y, Zhang L, Tang T, Duan X. Characterization of carboxymethylated polysaccharides from *Catathelasma ventricosum* and their antioxidant and antibacterial activities. *J Funct Foods.* (2017) 38:355–62. doi: 10.1016/j.jff.2017.09.050

91. Yan YY, Yuan S, Ma HH, Zhang XF. Structural modification and biological activities of carboxymethyl *Pachymaran*. *Food Sci Nutr.* (2021) 9:4335–48. doi: 10.1002/fsn3.2404

92. Ren YY, Sun PP, Ji YP, Wang XT, Dai SH, Zhu ZY. Carboxymethylation and acetylation of the polysaccharide from *Cordyceps militaris* and their α-glucosidase inhibitory activities. *Nat Prod Res.* (2020) 34:369–77. doi: 10.1080/14786419.2018.1533830

93. Zhao T, Guo Y, Yan S, Li N, Ji H, Hu Q, et al. Preparation, structure characterization of carboxymethylated schisandra polysaccharides and their intervention in immunotoxicity to polychlorinated biphenyls. *Int J Biol Macromol.* (2022) 115:30–41. doi: 10.1016/j.procbio.2022.02.005

94. Liu Y, Duan X, Zhang M, Li C, Zhang Z, Hu B, et al. Extraction, structure characterization, carboxymethylation and antioxidant activity of acidic polysaccharides from *Craterellus cornucopioides*. *Ind Crops Prod.* (2021) 159:113079. doi: 10.1016/j.indcrop.2020.113079

95. Wang X, Zhang Z, Zhao M. Carboxymethylation of polysaccharides from *Tremella fuciformis* for antioxidant and moisture-preserving activities. *Int J Biol Macromol.* (2015) 72:526–30. doi: 10.1016/j.ijbiomac.2014.08.045

96. Nuerxiati R, Mutailipu P, Abuduwaili A, Dou J, Aisa HA, Yili A. Effects of different chemical modifications on the structure and biological activities of polysaccharides from *Orchis chusua* D. Don. *J Food Sci.* (2021) 86:2434–2444. doi: 10.1111/1750-3841.15734

97. Deng C, Fu H, Xu J, Shang J, Cheng Y. Physiochemical and biological properties of phosphorylated polysaccharides from *Dictyophora indusiata*. *Int J Biol Macromol.* (2015) 72:894–9. doi: 10.1016/j.ijbiomac.2014.09.053

98. Ming K, Chen Y, Shi J, Yang J, Yao F, Du H, et al. Effects of *Chrysanthemum indicum* polysaccharide and its phosphate on anti-duck hepatitis a virus and alleviating hepatic injury. *Int J Biol Macromol.* (2017) 102:813–21. doi: 10.1016/j.ijbiomac.2017.04.093

99. Feng H, Fan J, Yang S, Zhao X, Yi X. Antiviral activity of phosphorylated *Radix Cyathulae officinalis* polysaccharide against *Canine Parvovirus in vitro*. *Int J Biol Macromol.* (2017) 99:511–18. doi: 10.1016/j.ijbiomac.2017.02.085

100. Shi XD, Tian YQ, Wu JL, Wang SY. Synthesis, characterization, and biological activity of selenium nanoparticles conjugated with polysaccharides. *Crit Rev Food Sci Nutr.* (2021) 61:2225–36. doi: 10.1080/10408398.2020.1774497

101. Sun X, Zhong Y, Luo H, Yang Y. Selenium-containing polysaccharide-protein complex in se-enriched ulva fasciata induces mitochondria-mediated apoptosis in A549 human lung cancer cells. *Mar Drugs.* (2017) 15:215. doi: 10.3390/md15070215

102. Lian KX, Zhu XQ, Chen J, Liu G, Gu XL. Selenylation modification: enhancement of the antioxidant activity of a *Glycyrrhiza uralensis* polysaccharide. *Glycoconjugate J.* (2018) 35:243–53. doi: 10.1007/s10719-018-9817-8

103. Qin T, Ren Z, Liu X, Luo Y, Long Y, Peng S, et al. Study of the selenizing *Codonopsis pilosula* polysaccharides protects RAW264.7cells from hydrogen peroxide-induced injury. *Int J Biol Macromol.* (2019) 125:534–43. doi: 10.1016/j.ijbiomac.2018.12.025

104. Dong Z, Dong G, Lai F, Wu H, Zhan Q. Purification and comparative study of bioactivities of a natural selenized polysaccharide from *Ganoderma Lucidum* mycelia. *Int J Biol Macromol.* (2021) 190:101–12. doi: 10.1016/j.ijbiomac.2021.08.189

105. Yang S, Sun J, Gu D, Li P, Yao L, Shi D, et al. Antioxidant activities of sulfated Codonopsis polysaccharides in acute oxidative stress. *J Food Biochem.* (2021) 45:e13974. doi: 10.1111/jfbc.13974

106. Zhu Y, Yu X, Ge Q, Li J, Wang D, Wei Y, et al. Antioxidant and anti-aging activities of polysaccharides from *Cordyceps cicadae*. *Int J Biol Macromol.* (2020) 157:394–400. doi: 10.1016/j.ijbiomac.2020.04.163

107. Zhan Y, An X, Wang S, Sun M, Zhou H. Basil polysaccharides: a review on extraction, bioactivities and pharmacological applications. *Bioorg Med Chem.* (2020) 28:115179. doi: 10.1016/j.bmc.2019.115179

108. Zoete V, Vezin H, Bailly F, Vergoten G, Catteau JP, Bernier JL. 4-Mercaptoimidazoles derived from the naturally occurring antioxidant ovothiols 2. Computational and experimental approach of the radical scavenging mechanism. *Free Radical Res*. (2000) 32:525–33. doi: 10.1080/10715760000300531

109. Huang SQ, Ding S, Fan L. Antioxidant activities of five polysaccharides from *Inonotus obliquus*. *Int J Biol Macromol.* (2012) 50:1183–7. doi: 10.1016/j.ijbiomac.2012.03.019

110. Petrosyan A, Gonçalves OF, Hsieh IH, Saberi K. Improved functional abilities of the life-extended Drosophila mutant Methuselah are reversed at old age to below control levels. *Age*. (2014) 36:213–21. doi: 10.1007/s11357-013-9568-1

111. Su J, Sun J, Jian T, Zhang G, Ling J. Immunomodulatory and antioxidant effects of polysaccharides from the parasitic fungus *Cordyceps kyushuensis*. *BioMed Res Int.* (2020) 2020:8257847. doi: 10.1155/2020/8257847

112. Guo Y, Hu D, Chen J, Peng D, Li Y. Research progress of aging related gene Klotho. *Chin J Gerontol.* (2017) 37:759–61. doi: 10.13241/j.cnki.pmb.2017.26.046

113. Oda T, Sekimoto T, Kurashima K, Fujimoto M, Nakai A, Yamashita T. Acute HSF1 depletion induces cellular senescence through the MDM2-p53-p21 pathway in human diploid fibroblasts. *J Cell Sci.* (2018) 131:210724. doi: 10.1242/jcs.210724

114. Liu P, Zhao H, Luo Y. Anti-Aging implications of *Astragalus membranaceus* (Huangqi): a well-known Chinese tonic. *Aging Dis.* (2017) 8:868–86. doi: 10.14336/AD.2017.0816

115. Hu Y, He Y, Niu Z, Shen T, Zhang J, Wang X, et al. A review of the immunomodulatory activities of polysaccharides isolated from *Panax* species. *J Ginseng Res.* (2022) 46:23–32. doi: 10.1016/j.jgr.2021.06.003

116. Ren L, Zhang J, Zhang T. Immunomodulatory activities of polysaccharides from *Ganoderma* on immune effector cells. *Food Chem.* (2021) 340:127933. doi: 10.1016/j.foodchem.2020.127933

117. Hao LX, Zhao XH. Immunomodulatory potentials of the water-soluble yam (*Dioscorea opposita* thunb) polysaccharides for the normal and cyclophosphamide suppressed mice. *Food Agric Immunol.* (2016) 27:667–77. doi: 10.1080/09540105.2016.1148666

118. Liao H, Deng X, Luo X, Zhou Y, Zhou L. Effects of carboxymethylpachymaran on polarization of macrophages. *Chin J Exp Tradit Med Formulae*. (2016) 22:122–6. doi: 10.13422/j.cnki.syfjx.2016130122

119. Lee KY, You HJ, Jeong HG, Kang JS, Kim HM, Rhee SD, et al. Polysaccharide isolated from Poria cocos sclerotium induces NF-KappaB/Rel activation and iNOS expression through the activation of p38 kinase in murine macrophages. *Int Immunopharmacol.* (2004) 4:1029–38. doi: 10.1016/j.intimp.2004.03.014

120. Hasegawa M, Fujimoto Y, Lucas PC, Nakano H, Fukase K, Núñez G, et al. A critical role of RICK/RIP2 polyubiquitination in Nod-induced NF-kappaB activation. *EMBO J.* (2008) 27:373–83. doi: 10.1038/sj.emboj.7601962

121. Liu Q, Xin R, Zhao Y, Yu M, Jin C, Shou S, et al. Dynamic changes of emergency visits: a retrospective observational study. *BMC Emerg Med.* (2022) 22:105. doi: 10.1186/s12873-022-00654-0

122. Yaribeygi H, Sathyapalan T, Atkin SL, Sahebkar A. Molecular mechanisms linking oxidative stress and diabetes mellitus. *Oxid Med Cell Longev*. (2020) 2020:8609213. doi: 10.1155/2020/8609213

123. Yao YS, Li TD, Zeng ZH. Mechanisms underlying direct actions of hyperlipidemia on myocardium: an updated review. *Lipids Health Dis*. (2020) 19:23. doi: 10.1186/s12944-019-1171-8

124. Qian K, Tan T, Ouyang H, Yang SL, Zhu WF, Liu RH, et al. Structural characterization of a homopolysaccharide with hypoglycemic activity from the roots of *Pueraria lobata*. *Food Funct*. (2020) 11:7104–14. doi: 10.1039/D0FO01234C

125. Cao C, Li C, Chen Q, Huang Q, Pérez M, Fu X. Physicochemical characterization, potential antioxidant and hypoglycemic activity of polysaccharide from *Sargassum pallidum*. *Int J Biol Macromol*. (2019) 139:1009–17. doi: 10.1016/j.ijbiomac.2019.08.069

126. Lee BH, Hsu WH, Pan TM. Inhibitory effects of dioscorea polysaccharide on TNF-α induced insulin resistance in mouse FL83B cells. *J Agr Food Chem*. (2011) 59:5279–85. doi: 10.1021/jf200651c

127. Cheng Z, Hu M, Tao J, Yang H, Yan P, Wang H. The protective effects of Chinese yam polysaccharide against obesity-induced insulin resistance. *J Funct Foods*. (2019) 55:238–47. doi: 10.1016/j.jff.2019.02.023

128. Zhao YM, Wang J, Wu ZG, Yang JM, Li W, Shen LX. Extraction, purification and anti-proliferative activities of polysaccharides from *Lentinus edodes*. *Int J Biol Macromol*. (2016) 93:136–44. doi: 10.1016/j.ijbiomac.2016.05.100

129. Ma G, Yang W, Fang Y, Ma N, Pei F, Zhao L, et al. Antioxidant and cytotoxicites of *Pleurotus eryngii* residue polysaccharides obtained by ultrafiltration. *LWT Food Sci Technol*. (2016) 73:108–16. doi: 10.1016/j.lwt.2016.05.049

130. Lin TY, Lu MK, Chang CC. Structural identification of a fucose-containing 1,3-β-mannoglucan from Poria cocos and its anti-lung cancer CL1-5 cells migration *via* inhibition of TGFβR-mediated signaling. *Int J Biol Macromol*. (2020) 157:311–18. doi: 10.1016/j.ijbiomac.2020.04.014

131. Xu J, Tan ZC, Shen ZY, Shen XJ, Tang SM. *Cordyceps cicadae* polysaccharides inhibit human cervical cancer hela cells proliferation *via* apoptosis and cell cycle arrest. *Food Chem Toxicol*. (2021) 148:111971. doi: 10.1016/j.fct.2021.111971

132. Shi Q, Lang W, Wang S, Li G, Bai X, Yan X, et al. Echinacea polysaccharide attenuates lipopolysaccharide-induced acute kidney injury *via* inhibiting inflammation, oxidative stress and the MAPK signaling pathway. *Int J Mol Med*. (2021) 47:243–55. doi: 10.3892/ijmm.2020.4769

133. Jiao R, Liu Y, Gao H, Xiao J, So KF. The anti-oxidant and antitumor properties of plant polysaccharides. *Am J Chin Med*. (2016) 44:463–88. doi: 10.1142/S0192415X16500269

134. Liu X, Yu X, Xu X, Zhang X, Zhang X. The protective effects of *Poria cocos*-derived polysaccharide CMP33 against IBD in mice and its molecular mechanism. *Food Funct*. (2018) 9:5936–49. doi: 10.1039/C8FO01604F

135. Liu ZX, Liu C, Qian H. Protective effect of *Cynanchum auriculatum* flower polysaccharide on alcoholic liver injury in mice. *Food Res Dev*. (2020) 41:72–9. doi: 10.12161/j.issn.1005-6521.2020.13.012

136. Tang J, Nie J, Li D, Zhu W, Zhang S, Ma F, et al. Characterization and antioxidant activities of degraded polysaccharides from *Poria cocos* sclerotium. *Carbohydr Polym*. (2014) 105:121–6. doi: 10.1016/j.carbpol.2014.01.049

137. Li L, Huang T, Lan C, Ding H, Yan C, Dou Y. Protective effect of polysaccharide from *Sophora japonica* L. flower buds against UVB radiation in a human keratinocyte cell line (HaCaT cells). *J Photochem Photobiol B*. (2019) 191:135–42. doi: 10.1016/j.jphotobiol.2018.12.001

frontiers | Frontiers in Nutrition

TYPE Original Research
PUBLISHED 15 September 2022
DOI 10.3389/fnut.2022.1001334

Check for updates

OPEN ACCESS

EDITED BY
Qiu Li,
Qingdao Agricultural University, China

REVIEWED BY
Xiangyu Cao,
Liaoning University, China
Xiaofeng Ren,
Jiangsu University, China

*CORRESPONDENCE
Rentang Zhang
rentangzhang@163.com

†These authors have contributed equally to this work and share first authorship

SPECIALTY SECTION
This article was submitted to Food Chemistry, a section of the journal Frontiers in Nutrition

RECEIVED 23 July 2022
ACCEPTED 26 August 2022
PUBLISHED 15 September 2022

CITATION
Zhang G, Liu C and Zhang R (2022) A novel acidic polysaccharide from blackened jujube: Structural features and antitumor activity *in vitro*. *Front. Nutr.* 9:1001334. doi: 10.3389/fnut.2022.1001334

COPYRIGHT
© 2022 Zhang, Liu and Zhang. This is an open-access article distributed under the terms of the Creative Commons Attribution License (CC BY). The use, distribution or reproduction in other forums is permitted, provided the original author(s) and the copyright owner(s) are credited and that the original publication in this journal is cited, in accordance with accepted academic practice. No use, distribution or reproduction is permitted which does not comply with these terms.

A novel acidic polysaccharide from blackened jujube: Structural features and antitumor activity *in vitro*

Guifeng Zhang†, Chuang Liu† and Rentang Zhang*

Key Laboratory of Food Processing Technology and Quality Control of Shandong Higher Education Institutes, College of Food Science and Engineering, Shandong Agricultural University, Tai'an, Shandong, China

Liver cancer is one of the most common cancers, with increasing trends in incidence and mortality. A novel acidic polysaccharide (BJP-2) obtained from blackened jujube was extracted by hot water followed by chromatographic purification employing DEAE-cellulose 52 and Sephadex G-100 column. And then BJP-2 was identified by SEC-MALLS-RI, GC-MS, methylation and NMR for the following characteristics: molecular weight of 6.42 × 10^4 Da, monosaccharide composition of glucuronic acid (GalA), arabinose (Ara), galactose (Gal), rhamnose (Rha), xylose (Xyl), glucuronic acid (GlcA), glucose (Glc), fucose (Fuc) and mannose (Man) with the percentage of 39.78, 31.93, 16.86, 6.43, 1.86, 1.28, 1.02, 0.61, and 0.23%, as well as the main chain of →5)-α-L-Ara*f*(1→4)-β-D-Gal(1→, T-α-L-Ara*f*(1→4)-β-D-Gal(1→, and →4)-α-L-6MeGalA*p*(1→. The effect of BJP-2 on the apoptosis of HepG2 cells and its anti-tumor mechanism were further explored. The analysis by MTT and flow cytometry showed that BJP-2 suppressed cell proliferation by inducing apoptosis in a concentration-dependent manner. Cell scratching and Transwell revealed that BJP-2 was able to block the invasion and metastasis of tumor cells. Western blot results demonstrated that BJP-2 exhibited antitumor activity through a mitochondria-dependent pathway, as evidenced by overexpression of Bax, Cleaved Caspase-3/Caspase-3 and Cleaved Caspase-9/Caspase-9 and downregulation of Bcl-2. Therefore, BJP-2 has broad research prospects as a tumor preventive or therapeutic agent.

KEYWORDS

blackened jujube, polysaccharides, structural features, antitumor activity, mechanism

Introduction

At present, malignant tumors are one of the most serious diseases that threaten human health and life, and are classified into liver cancer, lung cancer, breast cancer, colorectal cancer and so on, according to their sites of development (1–3). Of these, liver cancer has a high incidence in China, accounting for more than 50% of new liver cancer patients worldwide each year, and its danger should not be underestimated (4). With the advancement of medical technology, surgery, radiotherapy and chemotherapy

are three key and effective means of cancer treatment (5). However, many of the side effects can lead to a decrease in the immune function of the patient's organism, while the drug relieves symptoms and extends the patient's life (6). Therefore, the investigation and discovery of novel antitumor drugs with low cost, low toxicity and high efficiency are of vital importance.

Plant polysaccharides, a polymeric sugar polymer carbohydrate consisting of more than 10 monosaccharides extracted from plants, has various pharmacological effects such as antitumor, anti-inflammatory, antioxidant, immunomodulatory and hypoglycemic (7–9). Among them, the antitumor activity of plant polysaccharides has been widely studied and recognized, and the mechanisms include prevention of tumorigenesis, activation of immune response, direct inhibition and killing of tumor cells, enhancement of the body's anti-free radical effect and inhibition of angiogenesis in tumor tissues (10).

Jujube (*Ziziphus jujuba* Mill.) contains abundant active ingredients such as polysaccharides, flavonoids, polyphenols and saponins, and thus has versatile health and medicinal values (11, 12). The cell experiments showed that a polysaccharide fraction (HJP3) obtained from *Zizyphus jujuba cv. Muzao* significantly suppressed the proliferation of HepG2 cells, but was not cytotoxic to non-tumor cell lines, and the analysis might be that HJP3 exerted anti-tumor activity directly and induced apoptosis of tumor cells (13). *Zizyphus jujuba cv.Ruoqiangzao* seed polysaccharides, obtained by ultrasound-assisted-hot water extraction, exhibited concentration-dependent inhibition of proliferation of HeLa cells, probably through induction of apoptosis (14). A *Zizyphus jujuba cv. Goutouzao* polysaccharide with antioxidant activity that prevented LoVo cells growth, which was mediated by inducing apoptosis and enhancing intracellular reactive oxygen species secretion (15). Blackened jujube, a new kind of jujube processing product, is made by fermenting dried jujube in a high temperature and high humidity environment (16–18). Blackened jujube polysaccharides purified from *Z. jujuba cv. Hamidazao* have previously been reported to exert excellent antioxidant capacity *in vitro* compared to dried jujube, including free radical scavenging and total reducing capacity (19). *Z. jujuba cv. Huizao* polysaccharides have been shown to have immunomodulatory effects by improving serum hemolysin formation and increasing the phagocytic capacity of macrophages (20). Taking into account the close relationship between antitumor ability and immunomodulatory activity, we speculated that black jujube polysaccharide had good anti-tumor activity. To the best of our knowledge, the anti-tumor activity of polysaccharides from blackened jujube has never been investigated. This greatly limited their application in the field of pharmaceuticals and functional foods. Therefore, it is quite necessary to evaluate the structural characteristics and anti-tumor activity of polysaccharides from blackened jujube (made from *Z. jujuba cv. Huizao*).

The highest mass yield of BJP-2 (25.8%) was obtained by using the earlier described technique which employed hot water extraction followed by a DEAE-cellulose 52 and Sephadex G-100 column (21). In this study, the structure of BJP-2 was systematically presented by multi-angle laser light scattering combined with SEC and differential refractive index detector (SEC-MALLS-RI), gas chromatography-mass spectrometry (GC-MS), methylation, and nuclear magnetic resonance (NMR, 1D and 2D). Furthermore, human hepatocellular carcinoma cells (HepG2) were used as a model to investigate its anti-tumor ability and mechanism.

Materials and methods

Materials

Z. jujuba cv. Huizao fruits were provided by Guorentang Food Technology Co., Ltd. (Shandong, China). HepG2 cells were obtained from Shandong Analysis and Testing Center (Jinan, China). High glucose Dulbecco's modified eagle medium (DMEM), fetal bovine serum (FBS), penicillin and streptomycin were provided from Gibco Biotechnology Co., Ltd. (Grand Island, New York, USA). Monosaccharide standards (Fuc, Rha, Ara, Gal, Glc, Xyl, Man, Fru, Rib, GalA, GulA, GlcA and ManA), 3-(4,5-dimethylthiazol-2-yl)-2,5-diphenyltetrazolium bromide (MTT), trifluoroacetic acid (TFA), Mitomycin C and $NaBH_4$ were bought from Sigma-Aldrich (St. Louis, MO, USA).Bicinchoninic Acid (BCA) protein kit and protein extraction kit were purchased from Beyotime Biotechnology Co., Ltd. (Shanghai, China). The Annexin V-Fluorescein Isothiocyanate/Propidium Iodide (FITC/PI) Apoptotic Cell Detection Kit and antibodies (Bcl-2, Bax, Caspase-3, Cleaved Caspase-3, Caspase-9 and Cleaved Caspase-9) were obtained from Wanlei Biotechnology Co., Ltd. (Shenyang, China). All other chemicals and reagents were of analytical reagent grade.

Structural features of BJP-2

Chemical analysis

The chemical composition of BJP-2 was determined based on the previous method (22, 23). To determine total sugar content, the phenol-sulfuric acid method was used, with glucose as the standard. Using bovine serum albumin as the reference, the Bradford method was adopted to assay the protein content. For the determination of total phenol content, the Folin-Ciocalteu colorimetric method was applied. The total flavonoid content was estimated with sodium nitrite-aluminum nitrite method, using rutin as the standard.

Molecular weight distribution

As described by previous studies (24), briefly, the solution of BJP-2 (1 mg/ml) was configured with 1 M $NaNO_3$ as a solvent and passed through a filter (0.45 μm). A DAWN HELEOS-II laser photometer (Wyatt Technology Co., Santa Barbara, CA, USA) equipped with three tandem columns (300 × 8 mm, Shodex OH-pak SB-805, 804 and 803; Showa Denko K.K., Tokyo, Japan) was used for the determination under the following conditions: column temperature of 45°C, flow rate of 0.4 ml/min, injection volume of 100 μl, and mobile phase A of 0.1 M $NaNO_3$. Data were acquired and processed using ASTRA6.1 (Wyatt Technologies Inc., USA).

Monosaccharide composition

5.00 mg of BJP-2 powder was transferred to a chromatographic sample bottle and then hydrolyzed by TFA (2 M, 1 ml) for 2 h at 121°C, after which it was repeatedly washed three times with methanol and blow-dried with nitrogen. The residue was re-dissolved in deionized water and purified through a 0.22 μm microporous filter before determination on an HPAEC-PAD (Thermo Fisher ICS-5000+, USA) equipped with a Dionex™ CarboPac™ PA-20 chromatography column (Dionex, 3 × 150 mm). Conditions: flow rate, 0.5 ml/min; injection volume, 5 μl; solvent system, B: (0.1 M NaOH, 0.2 M NaAc); gradient program, 95:5 V/V at 0 min, 80:20 V/V at 30 min, 60:40 V/V at 30.1 min, 60:40 V/V at 45 min, 95:5 V/V at 45.1 min, 95:5 V/V at 60 min (25). The different monosaccharides were identified and quantified based on the retention time and peak area of the monosaccharide standards.

Methylation analysis

As previously reported data (19), the BJP-2 solution (10 mg/ml, 1 ml) was added to carbodiimide (100 mg/ml, 1 ml) for 2 h and then reacted with imidazole and $NaBD_4$ (10 mg/ml, 1 ml) for 3 h, respectively. The mixture was terminated by acetic acid (10 μl), followed by dialysis and freeze-drying. Next, the sample was dissolved by DMSO (500 μl) and then treated by methylation with NaOH (50 μl) and methyl iodide solutions for 30 min and 1 h, respectively. The target, obtained by dichloromethane extraction followed by nitrogen flow drying, was hydrolyzed by TFA (2 M, 100 μl) at 121°C for 1.5 h and then treated by ammonia (2 M, 50 μl) and $NaBD_4$ (1 M, 50 μl) at room temperature for 2.5 h. After termination by acetic acid (20 μl)and blowing dry under nitrogen, the resulting sample was acetylated for 2.5 h at 100°C using acetic anhydride (250 μl) and finally extracted with dichloromethane (500 μl). A gas chromatograph-mass spectrometer (GC-MS, Agilent 7890A-5977B, Agilent, Santa Clara, CA, USA) equipped with a BPX70 GC column (30 cm × 0.25 mm × 0.25 μm) was employed. GC parameters: injection volume of 1 μl, splitting ratio of 10:1, carrier gas of high-purity helium, initial temperature of 140°C held for 2.0 min, program of 3°C/min, 230°C held for 3 min. MS parameters: a mode of full scan and a mass scan range setting of 30–600 m/z.

NMR spectroscopy analysis

1D NMR spectra (^1H and ^{13}C) and 2D NMR spectra [correlation spectroscopy (COSY), heteronuclear single quantum coherence (HSQC), heteronuclear multiple bond coherence (HMBC) and nuclear overhauser effect spectroscopy (NOESY)] were performed by high-resolution AVANCE III 600 NMR spectrometer (Bruker, Germany). After dissolving 30 mg of BJP-2 in D_2O, it was added to the NMR tube, and then the spectra were recorded at 25°C.

Antitumor activity of BJP-2 *in vitro*

Cell culture and viability

DMEM medium containing penicillin (100 U/ml) with 10% FBS, 1% penicillin and 1% streptomycin was used to incubate HepG2 cells at 37°C with 5% CO_2. The effects of BJP-2 on the viability of HepG2 cells were assayed by MTT assay (26). HepG2 cells (5×10^3 cells/well) were stimulated for 48 h with different concentrations of BJP-2 (0, 50, 100, 200, 400, 800 μg/ml) after cells were cultured overnight in 96-well plates. Reaching time, the medium was removed and 20 μl MTT was added to each well, and then placed in an incubator at 37°C and 5% CO_2 for 4 h. After that, the cell supernatant was aspirated and 150 μl of Formanzan was added, and the optical density (OD) of the reaction solution at 570 nm was recorded on an microplate reader (ELX-800, Biotek, USA). Cell viability was computed as follows:

$$\textbf{Cell viability} = \frac{\textbf{ODsample}}{\textbf{ODblank}} \times \textbf{100\%} \quad (1)$$

Apoptosis detection by flow cytometry

Cells were cultured in 6-well plates at a quantity of 5×10^5, referring to Section Cell culture and viability. After centrifugation (150 g, 5 min) and aspiration of the supernatant, apoptosis was examined using Annexin V-FITC/PI Apoptosis Detection Kit based on the instructions. The flow cytometer (NovoCyte, ACEA, USA) was utilized for the following analysis.

Scratch assay

Cells were scratched using a sterile pipette (200 μl), and then the cell surface was washed once with serum-free medium and observed and photographed under a microscope (100 ×, IX53,

Olympus, Japan). Replaced with serum-free medium, cells were kept in an incubator for 24 h under 37°C and 5% CO_2 and then photographed and recorded. Mitomycin C (1 mg/ml) was employed to exclude the interference caused by proliferation on migration (27). The cell migration rate was calculated according to the following equation:

$$\textbf{Cell migration rate} = 1 - \frac{\textbf{scratch width of 48 h}}{\textbf{scratch width of 0 h}} \times \textbf{100\%} \quad (2)$$

Transwell assay

The Transwell chambers (LABSELECT, Anhui, China) were placed in 24-well plates and coated with Matrigel gel (Corning, New York, USA) after overnight thawing at 4°C, and then incubated for 2 h at 37°C (28). Cell cultures from each group were discarded, washing twice with PBS, after which cells were digested by adding trypsin. Resuspension of cells in serum-free medium and adjustment of cell numbers. The Transwell inserts containing Matrigel gel were placed in a 24-well plate, with 800 μl of culture medium containing 10% FBS in the lower chamber and 200 μl of cell suspension in the upper chamber, respectively, and adjusted the cell concentration to 6×10^4 cells/well and placed in the incubator at 37°C. Transwell inserts were washed twice with PBS and fixed in 4% paraformaldehyde (Aladdin, Shanghai, China) at room temperature for 20 min. After that, they were stained with 0.5% crystalline violet (Amresco, USA) staining solution for 5 min, rinsed with distilled water, and observed under an inverted microscope (200 ×).

Western blot

Western blot analysis based on the method of literature (29). Briefly, proteins were isolated and quantified using protein extraction and BCA protein assay kits, respectively. Various concentrations of polyacrylamide gels (5–14%) were prepared and subjected to protein electrophoresis, after which the proteins were transferred to polyvinylidene difluoride (PVDF) film. PVDF films were removed and immersed in Tris-buffered saline with Tween 20 (TBST) with shaking for 5 min, then the membrane were immersed in 5% (m/v) skim milk powder solution with shaking for 1 h. Conditions of the primary antibody incubation were Bcl-2 (1:500), Bax (1:1,000), Caspase-3/Cleaved Caspase-3 (1:500), Caspase-9/Cleaved Caspase-9 (1:1,000) and β-actin (1:400), overnight at 4°C. After that, the films were removed from the hybridization bag and soaked in TBST for four washes, and then the goat anti-rabbit IgG HRP secondary antibodies were incubated at a dilution ratio of 1:5,000 for 45 min at 37°C. After six times washing, the membranes were added ECL reagent, and were photographed by WD-9413B imaging system (Beijing LIUYI Biotechnology Co., Ltd., Beijing, China).

Statistical analysis

Results are denoted as mean ± standard deviation (SD). The significance of differences was evaluated using the one-way analysis of variance (ANOVA) followed by Tukey's test by SPSS software at $p < 0.05$.

Results and discussion

Basic chemical composition and molecular weight

The total sugar and total flavonoids of BJP-2 were 92 ± 0.05% and 0.81 ± 0.01%, respectively. Its total phenols and protein content were 1.68 ± 0.01% and 0.52 ± 0.01%. The average molecular weight of BJP-2 was 6.42×10^4 Da and the polydispersity index was 3.797. The BJP-2 was principally comprised of GalA (39.78%), Ara (31.93%), Gal (16.86%) and Rha (6.43%), and contained a small amount of Xyl (1.86%), GlcA (1.28%), Glc (1.02%), Fuc (0.61%) and Man (0.23%), showing that BJP-2 was a acidic polysaccharide (Figures 1A,B). Compared to the *Z. jujuba cv. Huizao* polysaccharide (HP-2), they both consisted mainly of GalA, Ara, and Gal, but possessed different percentages, and the molecular weight of BJP-2 (64.2 kDa) was smaller than that of HP-2 (111 kDa) (20). This phenomenon was explained as being caused by blackened jujube during processing, but the specific changes still depend on subsequent systematic research.

Methylation analysis of BJP-2

The linkage types and ratios of glycosidic bonds are usually determined by methylation analysis. As summarized in Table 1, the BJP-2 were identified as containing seventeen derivatives. Among them, (1→4)-linked-Gal*p*A was the most dominant linkage pattern (46.11%), followed by Ara*f* (1→ (12.94%), →4) Gal*p* (1→ (11.60%) and →5) Ara*f* (1→ (8.31%), together accounting for 78.96% of the total methylated sugars. Meanwhile, some of the discrepancies between the above results and the analysis of monosaccharide composition were explained by the fact that the dialysis step of acidic sugars when undergoing pre-treatment could have an effect on the results. However, the qualitative and quantitative analyses of the monosaccharide composition of BJP-2 were reliable, and the qualitative results of the methylation results on the type of glycosidic bonds and the mode of attachment were also correct (30). The structure of BJP-2 was further confirmed by NMR spectra.

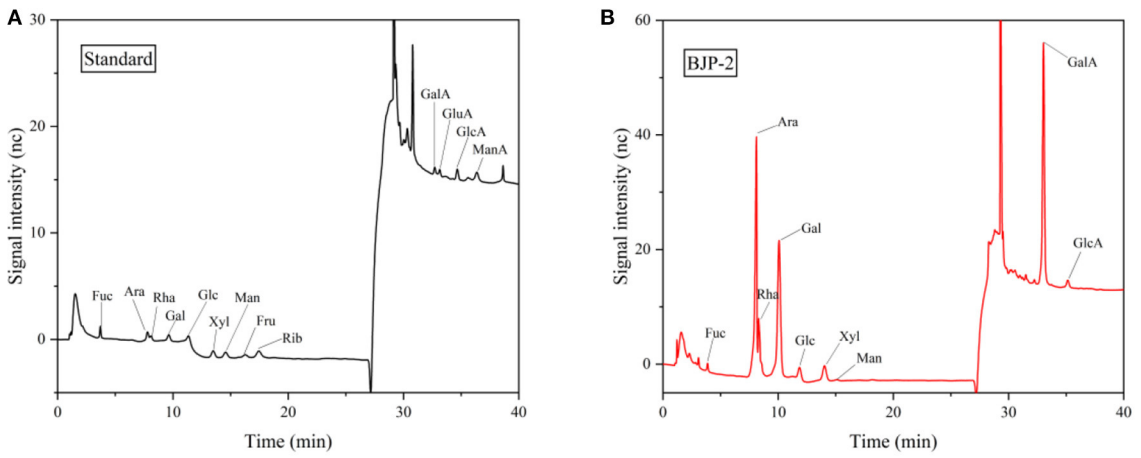

FIGURE 1
GC-MS analysis of the standard monosaccharides **(A)** and BJP-2 **(B)**.

TABLE 1 Results of methylation analysis of BJP-2.

Retention time (min)	Linkage types	Methylated sugars	Molar ratio (%)
5.459	t-Rha*p*	1,5-di-O-acetyl-6-deoxy-2,3,4-tri-O-methyl rhamnitol	0.725
5.72	t-Ara*f*	1,4-di-O-acetyl-2,3,5-tri-O-methyl arabinitol	12.943
6.988	t-Ara*p*	1,5-di-O-acetyl-2,3,4-tri-O-methyl arabinitol	1.010
8.452	2-Rha*p*	1,2,5-tri-O-acetyl-6-deoxy-3,4-di-O-methyl rhamnitol	1.565
9.575	t-Gal*p*	1,5-di-O-acetyl-2,3,4,6-tetra-O-methyl galactitol	3.539
9.575	t-Gal*p*A	1,5-di-O-acetyl-2,3,4,6-tetra-O-methyl galactitol	3.517
10.214	5-Ara*f*	1,4,5-tri-O-acetyl-2,3-di-O-methyl arabinitol	8.306
12.016	2,4-Rha*p*	1,2,4,5-tetra-O-acetyl-6-deoxy-3-O-methyl rhamnitol	3.900
12.46	3-Gal*p*	1,3,5-tri-O-acetyl-2,4,6-tri-O-methyl galactitol	0.959
13.365	4-Gal*p*	1,4,5-tri-O-acetyl-2,3,6-tri-O-methyl galactitol	11.592
13.365	4-Gal*p*A	1,4,5-tri-O-acetyl-2,3,6-tri-O-methyl galactitol	46.105
13.666	4-Glc*p*	1,4,5-tri-O-acetyl-2,3,6-tri-O-methyl glucitol	0.448
13.666	4-Glc*p*A	1,4,5-tri-O-acetyl-2,3,6-tri-O-methyl glucitol	0.297
15.055	6-Gal*p*	1,5,6-tri-O-acetyl-2,3,4-tri-O-methyl galactitol	1.199
15.328	3,4-Gal*p*	1,3,4,5-tetra-O-acetyl-2,6-di-O-methyl galactitol	0.894
15.328	3,4-Gal*p*A	1,3,4,5-tetra-O-acetyl-2,6-di-O-methyl galactitol	0.889
18.472	3,6-Gal*p*	1,3,5,6-tetra-O-acetyl-2,4-di-O-methyl galactitol	2.112

NMR spectral analysis of BJP-2

As shown in Figure 2A, BJP-2 exhibited five major anomeric proton signals (δ 5.10, 5.16, 5.07, 4.97, and 4.65) in the ^{1}H NMR spectrum, which were labeled as A, B, C, D, and E, respectively. Meanwhile, the chemical shifts of the protons from C-2 to C-6 of the residues were mainly distributed in the range of δ 4.75–3.40 ppm. Referring to the HSQC spectrum, there were five heterocephalic signals at δ 107.48, 107.05, 98.92, 100.39, and 104.33 ppm at the ^{13}C NMR spectrum (Figure 2B). Based on the reported literature, these ^{1}H and ^{13}C signals were assigned to the ^{1}H-^{1}H COSY (Figure 2C) and HSQC (Figure 2D) spectra (31–34). Table 2 provided information on the signal assignments of the protons and carbons for the five major residues in BJP-2. The anomeric proton and carbon of residue A produced the chemical shifts at δ_C 107.48/δ_H 5.10 ppm (C-1), δ_C 80.88/δ_H 4.14 ppm (C-2), δ_C 76.53/δ_H 3.95 ppm (C-3), δ_C 83.82/δ_H 4.04 ppm (C-4) and δ_C 67.91/δ_H

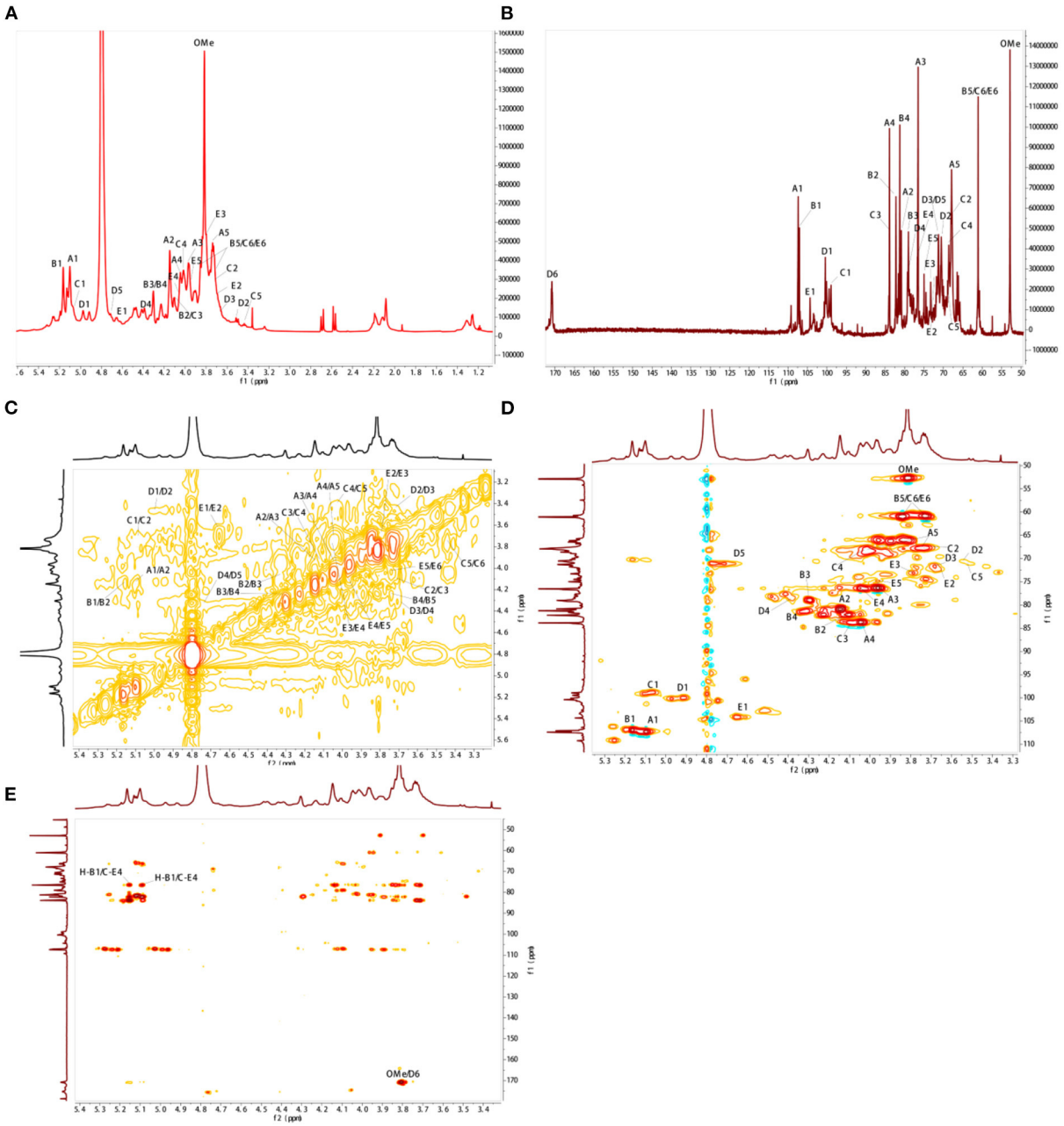

FIGURE 2
NMR spectral analysis of BJP-2. **(A)** ^{1}H-NMR; **(B)** ^{13}C-NMR; **(C)** ^{1}H-^{1}H COSY; **(D)** HSQC; **(E)** HMBC.

(3.75/4.02 ppm) (C-5), respectively. Summarizing these NMR data, it was inferred that it belongs to →5)-α-L-Ara*f*(1→ (31). Furthermore, B–E were designated as T-α-L-Ara*f*(1→, T-β-D-Gal*p*(1→, →4)-α-L-GalA*p*(1→, →4)-β-D-Gal (1→ (32, 33). Additionally, signals of OMe were also observed as δ_H 3.81/δ_C 52.91. Taking the results of methylation analysis into consideration, it was supposed that the presence of terminal signal suggested as T-α-L-Ara*f*(1→ and T-β-D-Gal*p*(1→ in BJP-2 (19). In the HMBC spectrum, some inter-residual cross peaks were found: A H-1 to E C-4, B H-1 to E C-4; OMe to δ_C 170.81 (Figure 2E). In summary, the main chains of BJP-2 were →5)-α-L-Ara*f*(1→4)-β-D-Gal(1→, T-α-L-Ara*f*(1→4)-β-D-Gal(1→, and →4)-α-L-6MeGalA*p*(1→, with two different terminal residues of T-α-L-Ara*f*(1→ and T-β-D-Gal*p*(1→.

TABLE 2 Assignments of ^{1}H and ^{13}C NMR spectra for BJP-2.

			1	2	3	4	5	6
A	→5)-α-L-Ara*f*(1→	C	107.48	80.88	76.53	83.82	67.91	
		H	5.10	4.14	3.95	4.04	3.75/4.02	
B	T-α-L-Ara*f*(1→	C	107.05	82.20	79.08	81.23	61.05	
		H	5.16	4.09	4.28	4.30	3.84/3.75	
C	T-β-D-Gal*p*(1→	C	98.92	67.73	83.87	68.61	70.69	61.05
		H	5.07	3.70	4.09	3.99	3.53	3.84/3.75
D	→4)-α-L-Gal*p*A(1→	C	100.39	70.55	71.32	79.00	71.24	170.81
		H	4.97	3.50	3.68	4.38	4.66	
E	→4)-β-D-Gal (1→	C	104.33	71.78	73.27	76.69	74.98	61.05
		H	4.65	3.68	3.78	4.05	3.94	3.84/3.75
OMe	52.91/3.81							

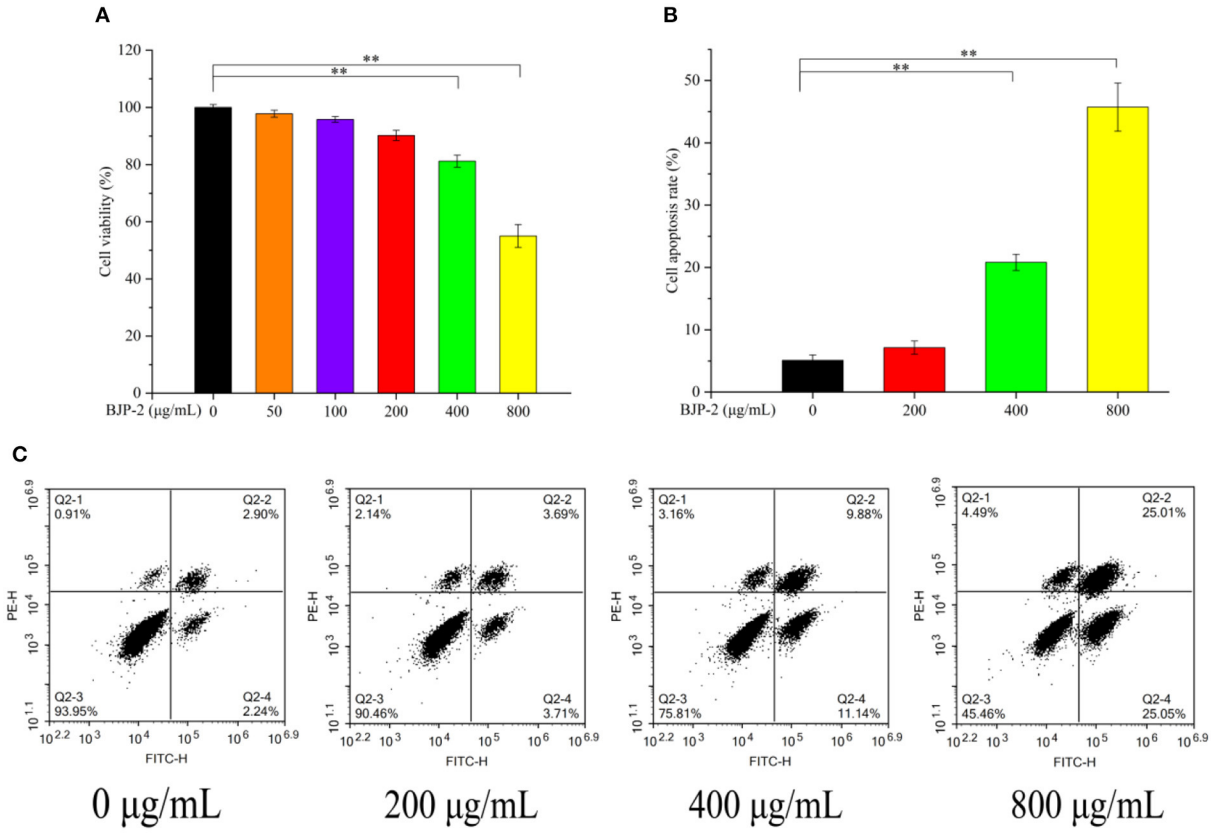

FIGURE 3
(A) Changes of HepG2 cell viability after 48 h incubation with different concentrations of BJP-2. **(B)** Column bar graph of apoptotic HepG2 cells. **(C)** The apoptosis of HepG2 cells treated with BJP-2 at different concentrations for 48 h and were detected by flow cytometry. Values are expressed as mean ± SD. *$p < 0.05$; **$p < 0.01$.

Antitumor effects *in vitro*

Cell viability of BJP-2

Evaluation of the impact of BJP-2 on the cell viability of HepG2 cells stimulated for 48 h by MTT assay. As seen in Figure 3A, BJP-2 exhibited significant toxicity at concentrations of 400 and 800 μg/ml, with cell viability of 81.2 ± 2.1% and 55.0 ± 4.0%, respectively ($p < 0.01$). Results showed that BJP-2 inhibited the growth of HepG2 cells within a certain range, and the effect was gradually enhanced with increasing concentration. All together, three optimal concentrations of BJP-2 (200, 400, 800 μg/ml) were selected for subsequent experiments.

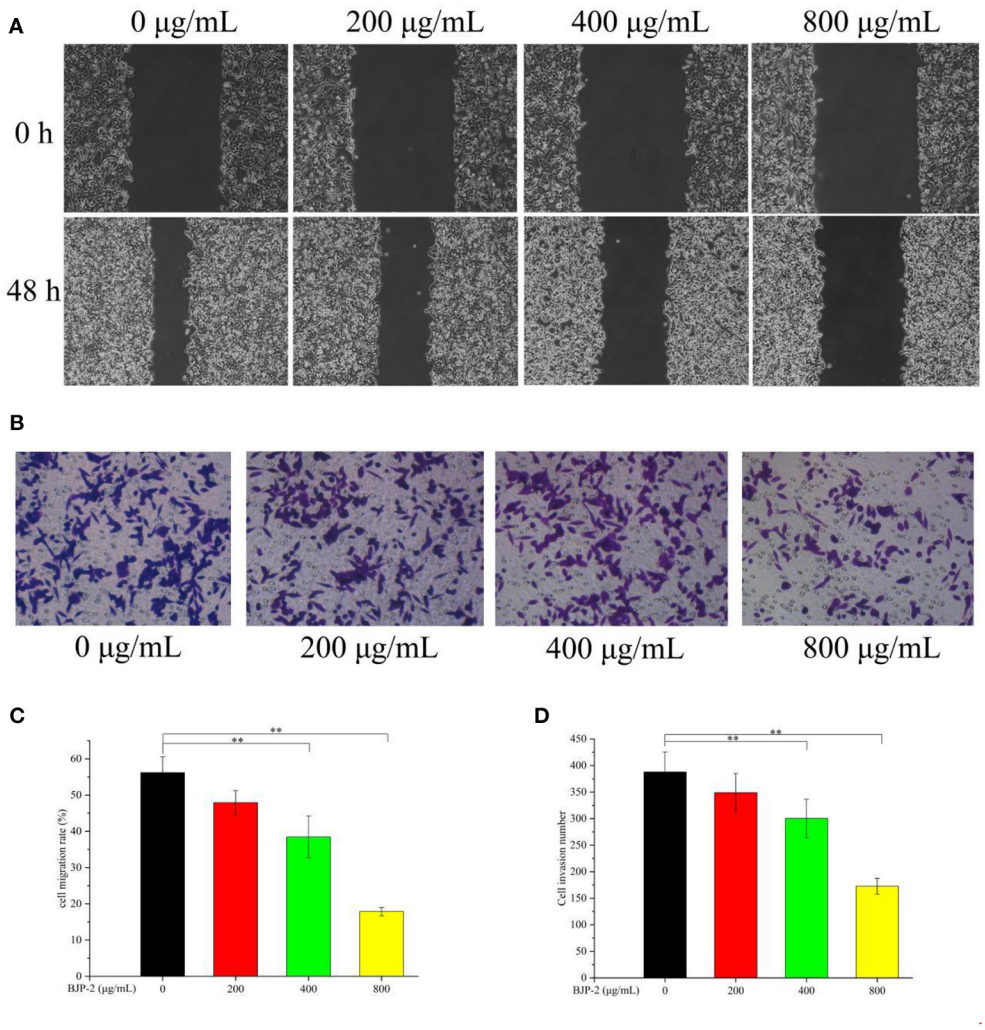

FIGURE 4
(A) The changes of BJP-2 on the migration of HepG2 cells were observed by a inverted phase contrast microscope (100 ×). **(B)** The effects of invasion on HepG2 cells after BJP-2 stimulation were observed by a inverted phase contrast microscope (200 ×). **(C)** Column bar graph of migration rate of HepG2 cells. **(D)** Bar graph summarizes the number of invasion.

BJP-2 inhibited tumor cell growth in a similar trend to other polysaccharides. For example, the *Polygonum multiflorum* polysaccharides at 400 μg/ml inhibited the growth of HepG-2 cells by 53.35%; and the mango pomace polysaccharide was active against HepG-2 cells in a quantitatively dependent manner (35, 36).

The effect of BJP-2 on apoptosis

Triggering tumor decline by enhancing apoptosis of cancer cells is one of the roles of antitumor drugs (37). Therefore, we detected the apoptosis of HepG-2 cells at different concentrations of BJP-2 using flow cytometry. As presented in Figure 3B, in comparison with the blank control group (5.11 ± 0.86%), the apoptosis rates increased to 20.81 ± 1.3% and 45.72 ± 3.8% by 400 and 800 μg/ml BJP-2 action on HepG-2 cells for 48 h ($p < 0.01$). No significant effect of low doses of BJP-2 (200 μg/ml) was observed, which is consistent with the results of cell viability. After stimulation of HepG2 cells with BJP-2 of 800 μg/ml, the early (Annexin V-FITC+/PI–) and late (Annexin V-FITC+/PI+) apoptosis rates were 25.05 and 25.01 %, respectively, which were significantly higher than that of the control group at 2.24 and 2.90% (Figure 3C). In summary, BJP-2 (800 μg/ml) could cause more than 40% of HepG-2 cells to enter an apoptotic state, suggesting that the induced apoptosis might be one of the mechanisms of action.

BJP-2 suppressed HepG-2 cell migration

One of the key issues in treating cancer is to prevent tumor cells from invading and metastasizing (38). The scratch assay and Transwell assay were applied to detect the effect of BJP-2

10.3389/fnut.2022.1001334

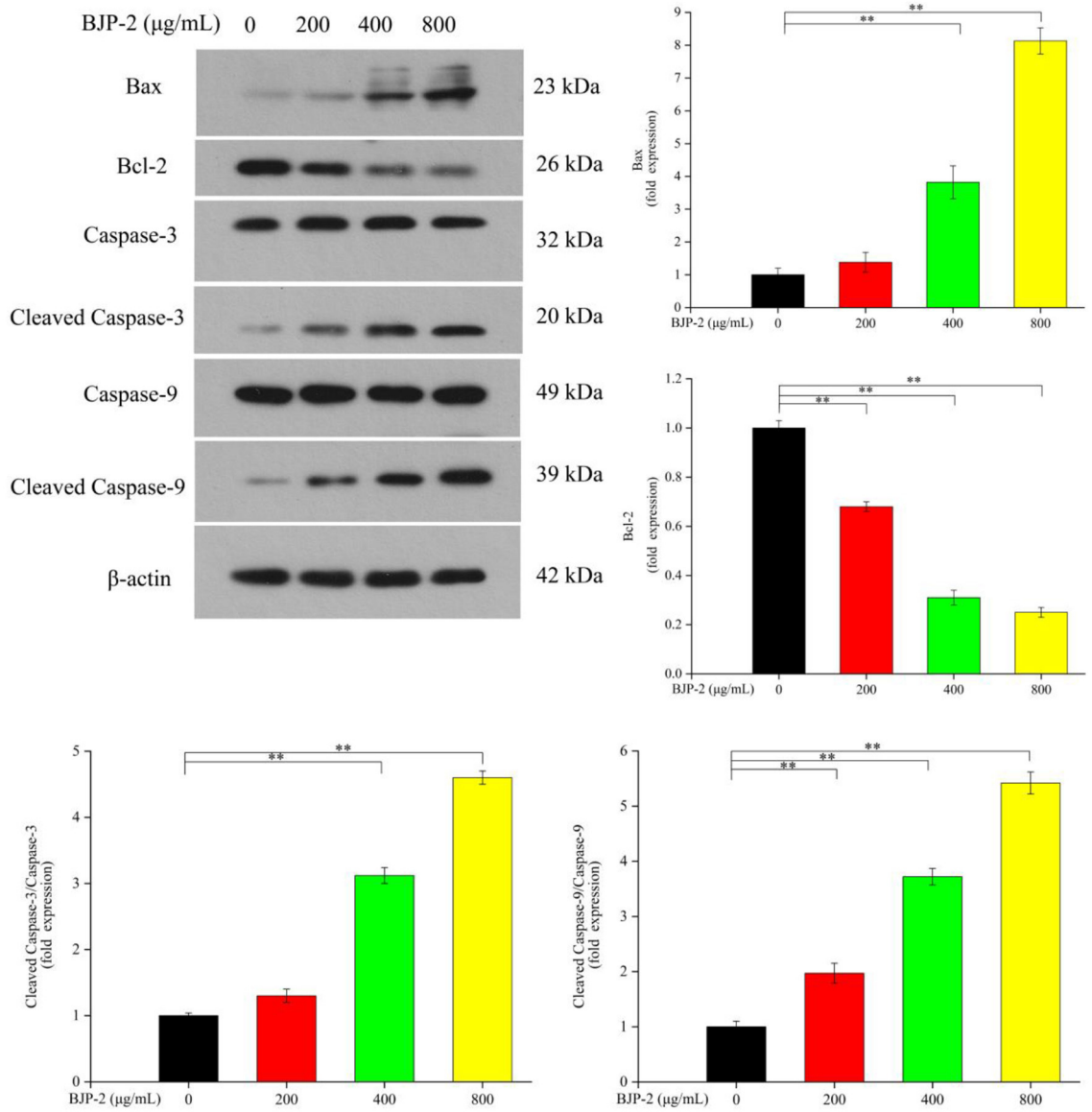

FIGURE 5
The protein levels of Bax, Bcl-2, Caspase-3, Cleaved Caspase-3, Caspase-9, Cleaved Caspase-9, β-actin by different concentrations of BJP-2 for 48 h. Values are expressed as mean ± SD. *$p < 0.05$; **$p < 0.01$.

on the migration of HepG-2 cells. As shown in Figures 4A,B, supplementation of BJP-2 inhibited the ability of HepG2 cells to heal wounds and cross over to the lower chamber, in contrast to the blank control. Figure 4C showed that the cell migration rate in the control group was 56.20 ± 4.4%, which were significantly decreased to 38.45 ± 5.7% ($p < 0.01$) and 17.86 ± 2.1% ($p < 0.01$) due to the treatment with high doses of BJP-2 (400 and 800 μg/ml). The numbers of cell invasion were 300 ± 35 and 172 ± 14 for BJP-2 at 400 and 800 μg/ml concentrations, respectively, which was significantly lower than that of 387 ± 38 for the control group ($p < 0.01$) (Figure 4D). It was demonstrated that BJP-2 possessed the ability to block the migration and invasion of HepG-2 cells, which inferred that the mechanism might be related to the inhibition of epithelial-mesenchymal transition (EMT). EMT in cancers allows cells to detach from the original tumor tissue and may cause an invasion-metastasis cascade (39). Various polysaccharides have demonstrated anti-tumor mechanisms by inhibiting EMT, such as Ganoderma lucidum polysaccharides, Huaier polysaccharides and Se-lentinan (40–42).

BJP-2 modulated gene expression

Promoting apoptosis, a key mechanism by which plant polysaccharides exert their antitumor effects, its critical pathways includes the mitochondrial pathway (43). As known, the pro-apoptotic factor Bax and the anti-apoptotic factor Bcl-2 are antagonistic to each other, where Bax promotes tumor cell apoptosis by promoting the release of cytochrome C, while Bcl-2 does the opposite. Furthermore, the activated Caspase-9 convenes and activates Caspase-3, which is a major executor of apoptosis, thereby triggering a Caspase cascade response to induce apoptosis in tumor cells (44). By Western blot method, the changes of apoptosis-related protein expression in HepG-2 cells after stimulation with different concentrations of BJP-2 were investigated. From Figure 5, as compared with the control group, there were dose-dependent increases in Bax, Cleaved Caspase-3/Caspase-3, Cleaved Caspase-9/Caspase-9 levels on HepG-2 cells after BJP-2 treatment, especially in the high dose group (800 μg/ml) by 2.54-fold, 7.6-fold and 33.52-fold, respectively ($p < 0.01$). By contrast, the expression of Bcl-2 was significantly reduced ($p < 0.01$). Other polysaccharides with similar mode of antitumor effects were also found, such as those derived from Grifola frondosa, *Boletus edulis* and Ganoderma applanatum (45–47).

Conclusion

In summary, BJP-2 is an acidic polysaccharide with a molecular weight of 6.42×10^4 Da, mainly composed of GalA, Ara, Gal and Rha, which was extracted and isolated from blackened jujube. And its main chain consisted of →5)-α-L-Ara*f*(1→4)-β-D-Gal(1→, T-α-L-Ara*f*(1→4)-β-D-Gal(1→, and →4)-α-L-6MeGalA*p*(1→. Furthermore, the present study demonstrated for the first time that blackened jujube polysaccharides could inhibit the proliferation of tumor cells causing apoptosis through the mitochondrial pathway with a certain degree of dose-dependence. The western blotting analysis indicated that BJP-2 could regulate the expression of apoptosis-related proteins such as Bax, Cleaved Caspase-3, Caspase-3, Cleaved Caspase-9, Caspase-9 and Bcl-2. In addition, BJP-2 initially expressed the ability to suppress the migration and invasion of HepG-2 cells, of which further validation by subsequent experiments was required. It is well know that the biological activities of polysaccharides are closely related to their molecular weight, monosaccharide composition, glycosidic bond type and other chemical properties. On the one hand, high molecular weight plays an important role in enhancing the immune and antitumor activity of polysaccharides. On the other hand, the higher the Glc content, the stronger the anttumor activity. Besides, studies have shown that the activity of the α configuration was poor, while the activity of the β configuration polysaccharide was good. All of these results demonstrated the anti-tumor activity of BJP-2 and presented a theoretical support for further study on the structure-activity relationship. Therefore, there is potential value for BJP-2 to be developed as a new antitumor agent drug against hepatocellular carcinoma. Meanwhile, other anti-tumor mechanisms of blackened jujube polysaccharides are still to be studied and revealed in depth and systematically.

Data availability statement

The raw data supporting the conclusions of this article will be made available by the authors, without undue reservation.

Author contributions

GZ and CL: conceptualization, data curation, writing—original draft, software, resources, and investigation. RZ: writing—reviewing and editing and supervision. All authors contributed to the article and approved the submitted version.

Funding

This work was supported by the Central Guidance on Local Science and Technology Development Program (YDZX2021071), Shandong Province Key Research and Development Program (Rural revitalization of science and technology innovation boosting action) (2021TZXD011); Dezhou Health Food Industry Innovation and Entrepreneurship Community, and Shandong Land and Rural Revitalization Group Co., Ltd., Project Key Technology Integration and Industrialization Demonstration of the Whole Industry Chain for Efficient Green Production and High Value Utilization of Jujube.

Conflict of interest

The authors declare that the research was conducted in the absence of any commercial or financial relationships that could be construed as a potential conflict of interest.

Publisher's note

All claims expressed in this article are solely those of the authors and do not necessarily represent those of their affiliated organizations, or those of the publisher, the editors and the reviewers. Any product that may be evaluated in this article, or claim that may be made by its manufacturer, is not guaranteed or endorsed by the publisher.

References

1. Sung H, Ferlay J, Siegel RL, Laversanne M, Soerjomataram I, Jemal A, et al. Global cancer statistics 2020: GLOBOCAN estimates of incidence and mortality worldwide for 36 cancers in 185 countries. *CA Cancer J Clin.* (2021) 71:209–49. doi: 10.3322/caac.21660

2. Jiang D, Zhang L, Liu W, Ding Y, Yin J, Ren R, et al. Trends in cancer mortality in China from 2004 to 2018: a nationwide longitudinal study. *Cancer Commun.* (2021) 41:1024–36. doi: 10.1002/cac2.12195

3. Siegel RL, Miller KD, Goding Sauer A, Fedewa SA, Butterly LF, Anderson JC, et al. Colorectal cancer statistics, 2020. *CA Cancer J Clin.* (2020) 70:145–64. doi: 10.3322/caac.21601

4. Wang YQ Li HZ, Gong WW, Chen YY, Zhu C, Wang L, et al. Cancer incidence and mortality in Zhejiang Province, Southeast China, 2016: a population-based study. *Chin Med J.* (2021) 134:1959–66. doi: 10.1097/CM9.0000000000001666

5. Trifanescu OG, Gales LN, Serbanescu GL, Zgura AF, Iliescu L, Mehedintu C, et al. Long-term oncological outcome in patients with cervical cancer after 3 trimodality treatment (radiotherapy, platinum-based chemotherapy, and robotic surgery). *Medicine.* (2021) 100:e25271. doi: 10.1097/MD.0000000000025271

6. Islam MR, Islam F, Nafady MH, Akter M, Mitra S, Das R, et al. Natural small molecules in breast cancer treatment: understandings from a therapeutic viewpoint. *Molecules.* (2022) 27:2165. doi: 10.3390/molecules27072165

7. Yarley OPN, Kojo AB, Zhou C, Yu X, Gideon A, Kwadwo HH, et al. Reviews on mechanisms of *in vitro* antioxidant, antibacterial and anticancer activities of water-soluble plant polysaccharides. *Int J Biol Macromol.* (2021) 183:2262–71. doi: 10.1016/j.ijbiomac.2021.05.181

8. Yang W, Zhao P, Li X, Guo L, Gao W. The potential roles of natural plant polysaccharides in inflammatory bowel disease: a review. *Carbohydr Polym.* (2022) 277:118821. doi: 10.1016/j.carbpol.2021.118821

9. Mirzadeh M, Lelekami AK, Khedmat L. Plant/algal polysaccharides extracted by microwave: a review on hypoglycemic, hypolipidemic, prebiotic, and immune-stimulatory effect. *Carbohydr Polym.* (2021) 266:118134. doi: 10.1016/j.carbpol.2021.118134

10. Xie L, Shen M, Hong Y, Ye H, Huang L, Xie J. Chemical modifications of polysaccharides and their anti-tumor activities. *Carbohydr Polym.* (2020) 229:115436. doi: 10.1016/j.carbpol.2019.115436

11. Li J, Huang G. Extraction, purification, separation, structure, derivatization and activities of polysaccharide from Chinese date. *Process Biochem.* (2021) 110:231–42. doi: 10.1016/j.procbio.2021.08.018

12. Lu Y, Bao T, Mo J, Ni J, Chen W. Research advances in bioactive components and health benefits of jujube (Ziziphus jujuba Mill) fruit. *J Zhejiang Univ-SCI B.* (2021) 22:431–49. doi: 10.1631/jzus.B2000594

13. Wang Y, Liu X, Zhang J, Liu G, Liu Y, Wang K, et al. Structural characterization and *in vitro* antitumor activity of polysaccharides from *Zizyphus jujuba cv. Muzao. RSC Adv.* (2015) 5:7860–7. doi: 10.1039/C4RA13350A

14. Wu Z, Li H, Wang Y, Yang D, Tan H, Zhan Y, et al. Optimization extraction, structural features and antitumor activity of polysaccharides from *Z. jujuba cv Ruoqiangzao seeds. Int J Biol Macromol.* (2019) 135:1151–61. doi: 10.1016/j.ijbiomac.2019.06.020

15. Liang Q, Wang X, Yang S, Yu L, Gao Q, Yang X, et al. Characterization of the antioxidative polysaccharides from *Ziziphus jujube cv.* Goutouzao and its tumor-inhibitory effects on human colorectal carcinoma LoVo cells via immunocyte activation. *J Food Biochem.* (2020) 44:e13462. doi: 10.1111/jfbc.13462

16. Sun X, Gu D, Fu Q, Gao L, Shi C, Zhang R, et al. Content variations in compositions and volatile component in jujube fruits during the blacking process. *Food Sci Nutr.* (2019) 7:1387–95. doi: 10.1002/fsn3.973

17. Wang F, Song Y, Vidyarthi SK, Zhang R. Physicochemical properties, and volatile compounds of blackened jujube vinegar as prepared by optimized fermentation process. *Int J Food Prop.* (2022) 25:288–304. doi: 10.1080/10942912.2022.2032735

18. Song Y, Chen C, Wang F, Zhang Y, Pan Z, Zhang R. Physicochemical properties and antioxidant activities of jujubes (*Ziziphus jujuba* Mill): effect of blackening process on different cultivars. *Int J Food Prop.* (2022) 25:1576–90. doi: 10.1080/10942912.2022.2093361

19. Yuan L, Qiu Z, Yang Y, Liu C, Zhang R. Preparation, structural characterization and antioxidant activity of water-soluble polysaccharides and purified fractions from blackened jujube by an activity-oriented approach. *Food Chem.* (2022) 385:132637. doi: 10.1016/j.foodchem.2022.132637

20. Zou M, Chen Y, Sun-Waterhouse D, Zhang Y, Li F. Immunomodulatory acidic polysaccharides from *Zizyphus jujuba cv.* Huizao: Insights into their chemical characteristics and modes of action. *Food Chem.* (2018) 258:35–42. doi: 10.1016/j.foodchem.2018.03.052

21. Yang Y, Qiu Z, Li L, Vidyarthi SK, Zheng Z, Zhang R. Structural characterization and antioxidant activities of one neutral polysaccharide and three acid polysaccharides from *Ziziphus jujuba cv. Hamidazao:* a comparison. *Carbohydr Polym.* (2021) 261:117879. doi: 10.1016/j.carbpol.2021.117879

22. Gu J, Zhang H, Zhang J, Wen C, Zhou J, Yao H, et al. Optimization, characterization, rheological study and immune activities of polysaccharide from *Sagittaria sagittifolia* L. *Carbohydr Polym.* (2020) 246:116595. doi: 10.1016/j.carbpol.2020.116595

23. Liu Y, Ye Y, Hu X, Wang J. Structural characterization and anti-inflammatory activity of a polysaccharide from the lignified okra. *Carbohydr Polym.* (2021) 265:118081. doi: 10.1016/j.carbpol.2021.118081

24. Zheng Z, Huang Q, Ling C. Water-soluble yeast β-glucan fractions with different molecular weights: extraction and separation by acidolysis assisted-size exclusion chromatography and their association with proliferative activity. *Int J Biol Macromol.* (2019) 123:269–79. doi: 10.1016/j.ijbiomac.2018.11.020

25. Wang L, Zhang B, Xiao J, Huang Q, Li C, Fu X. Physicochemical, functional, and biological properties of water-soluble polysaccharides from Rosa roxburghii Tratt fruit. *Food Chem.* (2018) 249:127–35. doi: 10.1016/j.foodchem.2018.01.011

26. Wei X, Yao J, Wang F, Wu D, Zhang R. Extraction, isolation, structural characterization and antioxidant activity of polysaccharides from elderberry fruit. *Front Nut.* (2022) 9:947706. doi: 10.3389/fnut.2022.947706

27. Xiang A, Ling C, Zhang W, Chen H. Effects of rhizopus nigricans exopolysaccharide on proliferation, apoptosis, and migration of breast cancer MCF-7 cells and AKT signaling pathway. *Int J Polym Sci.* (2021) 2021:5621984. doi: 10.1155/2021/5621984

28. Wu CL, Xu LL, Peng J, Zhang DH. Al-MPS obstructs EMT in breast cancer by inhibiting lipid metabolism *via* miR-215-5p/SREBP1. *Endocrinology.* (2022) 163:bqac040. doi: 10.1210/endocr/bqac040

29. Sun Y, Huo J, Zhong S, Zhu J, Li Y, Li X. Chemical structure and anti-inflammatory activity of a branched polysaccharide isolated from *Phellinus baumii. Carbohydr Polym.* (2021) 268:118214. doi: 10.1016/j.carbpol.2021.118214

30. Pettolino FA, Walsh C, Fincher GB, Bacic A. Determining the polysaccharide composition of plant cell walls. *Nat Protoc.* (2012) 7:1590–607. doi: 10.1038/nprot.2012.081

31. Ji X, Guo JH, Ding DQ, Gao J, Hao LR, Guo XD, et al. Structural characterization and antioxidant activity of a novel high-molecular-weight polysaccharide from *Ziziphus Jujuba cv. Muzao. J Food Meas Charact.* (2022) 16:2191–200. doi: 10.1007/s11694-022-01288-3

32. Ji X, Cheng YQ, Tian JY, Zhang SQ, Jing YS, Shi MM. Structural characterization of polysaccharide from jujube (*Ziziphus jujuba* Mill) fruit. *Chem Biol Technol Agric.* (2021) 8:54. doi: 10.1186/s40538-021-00255-2

33. Ji X, Guo JH, Pan FB, Kuang FJ, Chen HM, Guo XD, et al. Structural elucidation and antioxidant activities of a neutral polysaccharide from Arecanut (*Areca catechu* L). *Front Nut.* (2022) 9:853115. doi: 10.3389/fnut.2022.853115

34. Liu XX, Liu HM, Yan YY, Fan LY, Yang JN, Wang XD, et al. Structural characterization and antioxidant activity of polysaccharides extracted from jujube using subcritical water. *LWT.* (2020) 117:108645. doi: 10.1016/j.lwt.2019.108645

35. Zhu W, Xue X, Zhang Z. Ultrasonic-assisted extraction, structure and antitumor activity of polysaccharide from *Polygonum multiflorum. Int J Biol Macromol.* (2016) 91:132–42. doi: 10.1016/j.ijbiomac.2016.05.061

36. Hu H, Zhao Q, Pang Z, Xie J, Lin L, Yao Q. Optimization extraction, characterization and anticancer activities of polysaccharides from mango pomace. *Int J Biol Macromol.* (2018) 117:1314–25. doi: 10.1016/j.ijbiomac.2018.05.225

37. Barati N, Momtazi-Borojeni AA, Majeed M, Sahebkar A. Potential therapeutic effects of curcumin in gastric cancer. *J Cell Physiol.* (2019) 234:2317–28. doi: 10.1002/jcp.27229

38. Aust G, Zheng L, Quaas M. To detach, migrate, adhere, and metastasize: CD97/ADGRE5 in cancer. *Cells.* (2022) 11:1538. doi: 10.3390/cells11091538

39. Pan G, Liu Y, Shang L, Zhou F, Yang S. EMT-associated microRNAs and their roles in cancer stemness and drug resistance. *Cancer Commun.* (2021) 41:199–217. doi: 10.1002/cac2.12138

40. de Camargo MR, Frazon TF, Inacio KK, Smiderle FR, Amôr NG, Dionísio TJ, et al. Ganoderma lucidum polysaccharides inhibit *in vitro* tumorigenesis, cancer stem cell properties and epithelial-mesenchymal transition in oral squamous cell carcinoma. *J Ethnopharmacol.* (2022) 286:114891. doi: 10.1016/j.jep.2021.114891

41. Tian Y, Wu J, Zeng L, Zhou L, Hu Y, Pan Q, et al. Huaier polysaccharides suppress triple-negative breast cancer metastasis and epithelial-mesenchymal transition by inducing autophagic degradation of Snail. *Cell Biosci.* (2021) 11:1–15. doi: 10.1186/s13578-021-00682-6

42. Liu YR, Sun B, Zhu GH, Li WW, Tian YX, Wang LM, et al. Selenium–lentinan inhibits tumor progression by regulating epithelial–mesenchymal transition. *Toxicol Appl Pharmacol.* (2018) 360:1–8. doi: 10.1016/j.taap.2018.09.019

43. Niu J, Wang S, Wang B, Chen L, Zhao G, Liu S, et al. Structure and anti-tumor activity of a polysaccharide from *Bletilla ochracea* Schltr. *Int J Biol Macromol.* (2020) 154:1548–55. doi: 10.1016/j.ijbiomac.2019.11.039

44. Yin F, Zhou H, Fang Y, Li C, He Y, Yu L, et al. Astragaloside IV alleviates ischemia reperfusion-induced apoptosis by inhibiting the activation of key factors in death receptor pathway and mitochondrial pathway. *J Ethnopharmacol.* (2020) 248:112319. doi: 10.1016/j.jep.2019.112319

45. Chen P, Liu HP, Ji HH, Sun NX, Feng YY. A cold-water soluble polysaccharide isolated from *Grifola frondosa* induces the apoptosis of HepG2 cells through mitochondrial passway. *Int J Biol Macromol.* (2019) 125:1232–41. doi: 10.1016/j.ijbiomac.2018.09.098

46. Meng T, Yu SS, Ji HY, Xu XM, Liu AJ. A novel acid polysaccharide from Boletus edulis: extraction, characteristics and antitumor activities *in vitro*. *Glycoconj J.* (2021) 38:13–24. doi: 10.1007/s10719-021-09972-0

47. Zhen D, Su L, Miao Y, Zhao F, Ren G, Mahfuz S, et al. Purification, partial characterization and inducing tumor cell apoptosis activity of a polysaccharide from Ganoderma applanatum. *Int J Biol Macromol.* (2018) 115:10–7. doi: 10.1016/j.ijbiomac.2018.03.062

frontiers | Frontiers in Nutrition

TYPE Original Research
PUBLISHED 16 September 2022
DOI 10.3389/fnut.2022.966705

Check for updates

OPEN ACCESS

EDITED BY
Xiaolong Ji,
Zhengzhou University of Light Industry, China

REVIEWED BY
Lili Wang,
Institute of Food Science and Technology (CAAS), China
Dianzhi Hou,
Beijing Technology and Business University, China
Xijuan Yang,
Qinghai University, China

*CORRESPONDENCE
Qiang Ma
maqiang@cqtgmc.edu.cn
Yang Yao
yaoyang@caas.cn

SPECIALTY SECTION
This article was submitted to Food Chemistry, a section of the journal Frontiers in Nutrition

RECEIVED 11 June 2022
ACCEPTED 15 July 2022
PUBLISHED 16 September 2022

CITATION
Shi Z, Li S, Wei Z, Wang Y, Zhou N, Ma Q and Yao Y (2022) Immunomodulatory activity of glycoproteins isolated from chickpea (*Cicer arietinum* L.). *Front. Nutr.* 9:966705. doi: 10.3389/fnut.2022.966705

COPYRIGHT
© 2022 Shi, Li, Wei, Wang, Zhou, Ma and Yao. This is an open-access article distributed under the terms of the Creative Commons Attribution License (CC BY). The use, distribution or reproduction in other forums is permitted, provided the original author(s) and the copyright owner(s) are credited and that the original publication in this journal is cited, in accordance with accepted academic practice. No use, distribution or reproduction is permitted which does not comply with these terms.

Immunomodulatory activity of glycoproteins isolated from chickpea (*Cicer arietinum* L.)

Zhenxing Shi[1,2,3], Shiyu Li[1], Zuchen Wei[1,4], Yuanji Wang[1], Nong Zhou[4], Qiang Ma[2]* and Yang Yao[1]*

[1]Institute of Crop Science, Chinese Academy of Agricultural Sciences, Beijing, China, [2]Department of Basic Medicine, Chongqing Three Gorges Medical College, Chongqing, China, [3]School of Food Science and Technology, Henan University of Technology, Zhengzhou, China, [4]Laboratory for Green Cultivation and Deep Processing of Three Gorges Reservoir Area's Medicinal Herbs, College of Life Science and Engineering, Chongqing Three Gorges University, Chongqing, China

Chickpea (*Cicer arietinum* L.) is a well-known legume widely used as traditional medicine. This study aimed to characterize the structure and evaluate the immunomodulatory activity of one glycoprotein [crude chickpea glycoprotein-1 (CAG-1)] isolated from chickpea. CAG-1 was extracted with hot alkaline water and purified with DEAE-Sepharose Fast Flow and Superdex-200 column chromatography. CAG-1, with a molecular weight of 8,106 Da, contained 57.12% polysaccharide and 35.41% protein. The polysaccharide part was mainly composed of glucose (Glc). The protein part was connected mainly by aspartic (Asp) and glutamic (Glu). The results of nuclear magnetic resonance (NMR) analysis indicated the presence of α-d-Glc*p*-(1 → 4)-α-d-Glc*p*-(1 → 4)-α-d-Glc*p*-(1 → . In addition, the sugar chains of the glycoprotein were not hydrolyzed under alkaline conditions, suggesting that the glycoprotein was N-glycosidic; thus, the sugar chain was linked to the protein chain by Asp. An immunological study showed that CAG-1 stimulated the production of nitric oxide (NO), interleukin-6 (IL-6), tumor necrosis factor-α (TNF-α), and monocyte chemotactic protein 1 (MCP-1) in RAW 264.7 macrophages in a dose-dependent manner.

KEYWORDS

glycoprotein, structural characterization, immunomodulatory, RAW 264.7 murine macrophage cell, chickpea

Introduction

An innate immune system is the body's first line of defense against harmful foreign substances, such as bacteria, viruses, and fungi (1). Macrophages are important effector cells of the immune system. Activation of macrophages to release molecules with immunomodulatory activity, such as nitric oxide (NO), interleukin-1β (IL-1β), and tumor necrosis factor-α (TNF-α), has been reported to play a key role in the resistance to external pathogens (2). In recent years, various natural products from plants were demonstrated to exhibit immunomodulatory activity through the stimulation of the release of proinflammatory cytokines, with low toxicity and side effects (3, 4).

Glycoprotein is composed of two parts of sugar and protein connected by covalent bonds. Plant-derived glycoprotein performs various pharmacological activities in the body, such as anti-inflammatory (5), antihyperglycemia (6), antiproliferation (7), antioxidant (8), antiallergy (9), and immunomodulatory. Among them, immunomodulatory activity was the most widely reported. Niu et al. (10) demonstrated the immunomodulatory activity of Chinese yam glycoprotein by evaluating its effect on the production of TNF-α, interleukin-6 (IL-6), and NO in peritoneal macrophages. Nowadays, studies on the relationship between the chemical structure and bioactivity of glycoproteins have attracted great attention. In a previous study, the hypoglycemic activity of glycoproteins isolated from pea was found to be related to molecular weight (6).

As one of the most consumed legumes worldwide, chickpea (*Cicer arietinum* L.) represents nearly 20% of global legume production (11). Chickpea has a long history of planting and application in China due to its pharmacology activities, especially in Uygur traditional Chinese medicine (12). Accumulated studies showed that chickpea is rich in functional phytochemicals, such as isoflavones and peptides, which have physiological effects such as antidiabetic (9) and antiproliferative activities (13). The water-extracted polysaccharide in chickpea was claimed to have many biological activities, such as antioxidant activity (14) and angiotensin I converting enzyme (ACE-I) inhibitory activity (15). In addition, three polysaccharides were obtained under neutral conditions and performed a strong immunomodulatory activity in immunodeficient mice (16). However, to the best of our knowledge, there is a rare study that focuses on the chemical structure and immunomodulatory activity of chickpea glycoprotein. Therefore, in this study, a glycoprotein fraction was isolated from chickpea [crude chickpea glycoprotein-1 (CAG-1)] and purified with ion-exchange chromatography and gel-filtration chromatography, and the chemical structure was characterized by multiple methods. Then, the *in vitro* immunomodulatory activity was evaluated.

Materials and methods

Materials and reagents

Chickpea seeds (Xinying No. 3) were obtained from the Xinjiang Academy of Agricultural Sciences. DEAE-Sepharose Fast Flow and Superdex-200 were obtained from GE Healthcare Bio-Sciences Co. (Piscataway, NJ, USA). Griess reagent, arabinose (Ara), rhamnose (Rha), xylose (Xyl), galacturonic acid (GalA), galactose (Gal), glucose (Glc), glucuronic acid (GlcA), amino acid standard solution (AAS18), and 3-(4,5-dimethylthiazol-2-yl)-2,5-diphenyltetrazolium bromide (MTT) were purchased from Sigma-Aldrich (St. Louis, Miss., USA). RPMI-1640 media, Dulbecco's modified Eagle's medium (DMEM), lipopolysaccharide (LPS), phosphate-buffered saline (PBS), and fetal bovine serum (FBS) were obtained from Gibco BRL Life Technologies (Grand Island, NY, USA). The RAW 264.7 murine macrophage cell line was purchased from the Cell Resources Centre of the Chinese Academy of Sciences (Shanghai, China). OptEIA enzyme-linked immunosorbent assay (ELISA) kits for detecting tumor necrosis factor-α (TNF-α), monocyte chemotactic protein 1 (MCP-1), and IL-6 were purchased from BD Biosciences (San Diego, CA, USA). All other chemicals and solvents used were of analytical grade unless otherwise specified.

Extraction of CAG

The CAG was extracted according to our previous method (3) with some modifications. Chickpea seed powder was extracted with 95% ethanol (1:10 w/v) for 24 h and then with alkaline water (1:20 w/v, pH 9.0) two times for 4 h (50°C). Non-extractable solid was removed by centrifugation (4,000 g, 15 min). The supernatant was precipitated with 95% ice-cold ethanol (1:4, v/v) overnight. The precipitate was collected and redissolved in distilled water. The Sevage method was used to remove free protein. The supernatant was collected and precipitated with 95% ice-cold ethanol (1:4, v/v) overnight, again, to obtain the CAG.

Purification of glycoproteins

The CAG was dissolved in distilled water with centrifugation (10,000 g, 10 min), and then, the supernatant was loaded onto an ÄKTA explorer 100 purification system with a DEAE-Sepharose Fast Flow column (2.6 cm^2 × 100 cm), which was first washed with distilled water and the bound polysaccharides were eluted with a 0–2.0 M NaCl gradient at a flow rate of 4 ml/min. Two elution peaks were obtained in the profile, and only the first fraction was studied due to its high yield. After that, the first fractions were dialyzed, lyophilized, and further purified with a Superdex-200 column. A high-performance liquid chromatography system (LC-20AT, Shimadzu, Japan) with a Shimadzu RID-10A refractive index detector (Kyoto, Japan) was used to monitor the elution. One glycoprotein, named CAG-1, was collected, dialyzed, and lyophilized. Polysaccharide content and protein content were determined, respectively, by the Kjeldah method and the phenol–sulfuric acid reaction method.

Determination of molecular weight

The molecular weight of CAG-1 was measured using a high performance size exclusion chromatography system coupled with a multi-angle laser light scattering and refractive index

(HPSEC-MALLS-RID) detector, which consisted of a pump (LC-20AD, Shimadzu, Kyoto, Japan), an HPSEC column (SB-805HQ, Shodex, Kyoto, Japan), a MALLS detector (DAWN HELEOS-II, Wyatt Technology, Santa Barbara, CA, USA), and an RI detector (Optilab Rex, Wyatt Technology, Santa Barbara, CA, USA). Samples were filtered through a 0.45-μm pore membrane before injection (200 μl) and eluted with 0.1 M NaCl (0.5 ml/min). The column temperature was maintained at 40°C.

Determination of monosaccharide composition

The method of determining the composition of monosaccharides was carried out in a previous study (17). Approximately 2 mg of CAG-1 was mixed with 1 ml of trifluoroacetic acid (TFA) (2 M) to hydrolyze (120°C, 90 min) and evaporated to dryness on a rotary evaporator. Approximately 2 ml of double-distilled water and 100 mg of sodium borohydride were added to reduce the residue, and glacial acetic acid to neutralize it, and then, it was evaporated by rotary steam and oven dried at 110°C. Approximately 1 ml of acetic anhydride was added and heated at 100°C for 1 h and 3 ml of toluene was added and evaporated to dryness after cooling, repeated four to five times to remove excess acetic anhydride. The acetylated product was dissolved in 3 ml of chloroform and transferred to a separatory funnel. After adding distilled water and shaking completely, the upper aqueous solution was removed for five times. The chloroform layer was dried with an appropriate amount of anhydrous sodium sulfate to a constant volume of 10 ml. The gas chromatography-mass spectrometer (GC-MS) (Shimadzu, GCMS-QP 2010, Kyoto, Japan) was used for sample analysis of the acetylation product.

Determination of amino acid composition

Gas chromatography-mass spectrometry was used to determine the amino acid composition of samples (18). Briefly, the sample was mixed with 6 M HCl in a hydrolysis tube and hydrolyzed at 100°C for 12 h. The solvent was removed from HCl by rotary evaporation, n-butanol was added, incubated at 100°C for 1 h, and then rotated to dryness. Acetylate trifluoroacetic anhydride was mixed with the sample at 50°C for 10 min. The standards used the same derivation method. The reaction was stopped with water and extracted with dichloromethane (CH_2Cl_2). In addition, the conditions of GC-MS were listed as follows: the chromatographic column was 30 m × 0.25 mm × 0.25 μm (RXI-5 SIL MS, Shimadzu, Tokyo, Japan); the temperature program conditions were an initial temperature of 60°C, heating at 4°C/min up to 280°C/min and maintained for 5 min, the inlet temperature was 250°C, the detector temperature was 250°C/min, the carrier gas was helium, and the flow rate was 1 ml/min.

Analysis of Fourier transform infrared spectroscopy spectra

Functional groups of CAG-1 were analyzed by Fourier transform infrared (FT-IR) spectroscopy (Bruker, Rheinstetten, Germany). Approximately 2 mg of the sample was mixed with 200 mg of KBr and completely ground. The KBr powder was considered blank. They were placed in the pellets for scanning and recording in the range of 4,000–400 cm^{-1}.

Methylation analysis

Methylation analysis was carried out according to a previously described method (19). Briefly, 10 mg of CAG-1 was added with 100 μl of dimethyl sulfoxide and 2 mg of NaOH, sealed and ultrasonically dissolved. Approximately 1 ml of methyl iodide (CH_3I) was added and reacted at 30°C for 60 min. Finally, 2 ml of ultrapure water was added to the above mixture to terminate the methylation reaction.

The methylated sample was mixed with 1 ml of 2 M TFA and hydrolyzed for 90 min and subsequently evaporated by a rotary evaporator. The residue was reduced by adding 2 ml of double-distilled water and 60 mg of sodium borohydride for 8 h, followed by adding glacial acetic acid for neutralization and rotary steaming at 101°C. Approximately 1 ml of acetic anhydride was added into the solution and reacted at 100°C for 1 h and cooled. Then, 3 ml of toluene was added to remove excess acetic anhydride for five times. The acetylated sample was dissolved with 3 ml of CH_2Cl_2 and transferred to a separatory funnel. After adding a small amount of distilled water and shaking sufficiently, the upper aqueous solution was removed four times. The CH_2Cl_2 layer was dried with an appropriate amount of anhydrous sodium sulfate, fixed to a volume of 10 ml, and placed in a liquid phase vial. The Shimadzu GCMS-QP 201 GC-MS was used to determine the acetylated product samples.

^{1}H and ^{13}C nuclear magnetic resonance analysis

The purified CAG-1 sample (20 mg) was dissolved in a D_2O solution at 20°C. Bruker Avance 600 and Bruker Avance 500 nuclear magnetic resonance (NMR) spectrometers (Bruker, Ettlingen Germany) were used (operating frequencies of ^{1}H: 600.1 and 499.8 MHz, operating frequencies of ^{13}C: 150.9 and 125.7 MHz). ^{1}H and ^{13}C spectra, Dept135, HSQC, HHCOSY, and HMBC spectra, and CWP and CWP-0.2 spectra were

recorded at 30 MHz with an MBC spectrometer (Bruker, Rheinstetten, Germany).

Immunostimulatory activity analysis

The evaluation of the immunostimulatory activity was performed by the previous method in the laboratory (3). RAW 264.7 cells in the logarithmic growth phase were washed two times with PBS, digested with trypsin, and then centrifuged (4°C, 1,000 rpm, 4 min). After resuspending the cell, the cell density was adjusted to 2.5×10^6 cells/ml in RPMI-1640 complete medium. Then, 100 μl of cells were added to a 96-well plate, placed in a CO_2 incubator (5% CO_2, 37°C, saturated humidity), cultured for 24 h, and the medium was subsequently discarded. Approximately 100 μl of cells and 100 μl of samples (20, 40, 60, 80, and 100 μg/ml) were added in a 96-well plate, and the LPS solution was used as a control group with the concentration of 1 μg/ml. Roughly 100 μl of culture medium was considered as a blank group. Among them, they were placed in a CO_2 incubator (5% CO_2, 37°C, saturated humidity) for 24 h, and 50 μl of each of the supernatants of each group was taken after 24 h adding 50 μl of Griess reagent, then reacted at room temperature for 15 min. After removing the bubbles, the absorbance at 540 nm was measured, and the amount of immune mediator (NO) in the supernatant was calculated. The production of TNF-α, MCP-1, and IL-6 cytokines was measured by ELISA kits according to the instructions (Becton, Dickinson and Company, NJ, USA).

Cytoxiocity of CAG-1 on RAW 264.7 cell was evaluated according to the previous method with some modifications (20). Cells in the logarithmic growth phase were washed two times with PBS, digested with trypsin, and then centrifuged (4°C, 1,000 rpm, 4 min). After resuspending the cell, the cell density was adjusted to 2.5×10^6 cells/ml in RPMI-1640 complete medium. Then, 100 μl of cells were added to a 96-well plate, placed in a CO_2 incubator (5% CO_2, 37°C, saturated humidity), and cultured for 24 h, and the medium was subsequently discarded. Approximately 100 μl of RPMI-1640 complete medium contained in samples (20, 40, 60, 80, and 100 μg /ml) was added in each well after washing two times with PBS cultured for 24 h. Approximately 10 μl of MTT reagent (5 mg/ml) was added and placed in a CO_2 incubator and was continued to culture for 4 h. Dimethyl sulfoxide was added to each well after washing two times with PBS and incubated for 1 h. The absorbance of each well solution was measured at a wavelength of 570 nm, and the cell viability was calculated based on the absorbance.

$$Cell\ survival\ rate\ (\%) = (absorbance\ of\ sample / absorbance\ of\ control\ group) \times 100 \quad (1)$$

Statistical analysis

Data were presented as mean ± standard deviation (SD). Statistical analysis was performed by GraphPad Prism 8.0.2 (GraphPad Software, San Diego, CA, USA) Statistical significance of differences was considered statistically significant at a $p < 0.05$ and assessed by a one-way analysis of variance (ANOVA) test.

Results and discussion

Purification of CAG

Chickpea seed powder was extracted under alkali conditions to obtain alkali-extracted crude chickpea glycoprotein. CAG was further purified with a DEAE-Sepharose column with a yield of 2.15% (Figure 1A). Then, it was filtered again through a Superdex-200 column, and one glycoprotein (CAG-1) was obtained (Figure 1B) with a yield of 16.8%. The polysaccharide content and protein content of CAG-1 were determined as 57.12 and 35.41% (Table 1), respectively. Glycoproteins contain more proteins than polysaccharides, and Qin et al. (6) reported that glycoproteins isolated from legumes (peas) with hot water contained 55.98–85.93% protein and 12.0–41.94% of polysaccharide. However, the extraction condition significantly influences the composition of the extracted products. Chen et al. (21) found that alkali-soluble polysaccharide/protein conjugates contained more neutral sugar and uronic acid than protein. In previous studies, the molecular weight of plant-derived glycoproteins was reported to be 14.4–897.4 kDa (6, 22). In the present study, the molecular weight of CAG-1 was determined to be 8,106 Da (Table 1), which is lower than the previous results. The slight differences with our results could also be due to differences in extraction methods.

FT-IR spectra analysis

Fourier transform infrared spectroscopy spectra indicated chemical functional groups in the samples. As seen in Figure 2, the results of CAG-1 indicated that the absorption peak at 3,415 and 2,925 cm^{-1} were the O-H stretching vibration and the C-H stretching vibration, whose absorption peak at 3,415 was the characteristic peak of sugars (23). Meanwhile, the absorption peak at 1,656 cm^{-1} was induced by C=O asymmetric stretching vibration (6, 24). In the range from 1,420 to 1,200 cm^{-1}, the absorption peaks were caused by the variable-angle vibration of C-H (6). The main absorption peaks in this region were 1,413 and 1,243 cm^{-1}. In addition, the absorption peak at 1,200–1,000 cm^{-1} was a wide peak, which was mainly caused by C-O stretching vibrations, namely C-O-H and C-O-C (6).

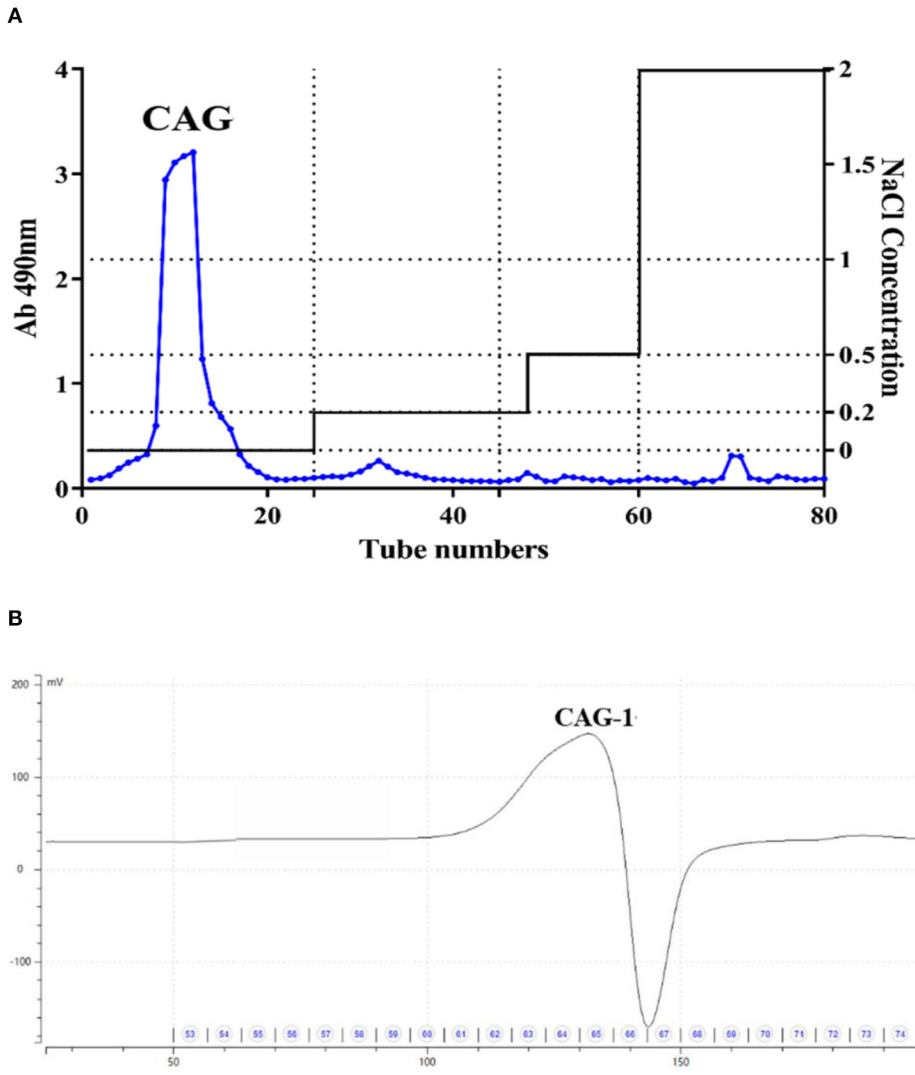

FIGURE 1
Purification of chickpea glycoproteins. **(A)** Crude chickpea glycoprotein (CAG) was passed from the DEAE-Sepharose column; **(B)** A purified fraction from the Superdex-200 column.

The asymmetric ring stretching vibration was performed at absorption peaks of 919 cm^{-1}.

Monosaccharide composition and glycosidic linkage analysis

Seven monosaccharides were used as a standard to measure the monosaccharide composition of CAG-1 by GC-MS analysis. As seen in Figure 3, only Glc was found. A previous study showed that arabinan (Ara) was rich in chickpea hull (25); however, Ara was not detected in CAG-1, which may be in part because CAG-1 originated from chickpea seeds rather than chickpea hulls. On the contrary, the alkali solution was beneficial for the dissolution of Glc. Through methylation analysis, it has been found that CAG-1 has five kinds of glycosidic bonds. Among them, → 4)-Glc*p*-(1 → and → 4,6)-Glc*p*-(1 → were the main glycosidic bonds detected (Table 2).

TABLE 1 The polysaccharide content, protein content, and molecular weight of crude chickpea glycoprotein-1 (CAG-1).

Sample ID	Polysaccharide content (%)	Protein content (%)	Mw (Da)
CAG-1	57.1 ± 2.3	35.4 ± 3.2	8,106

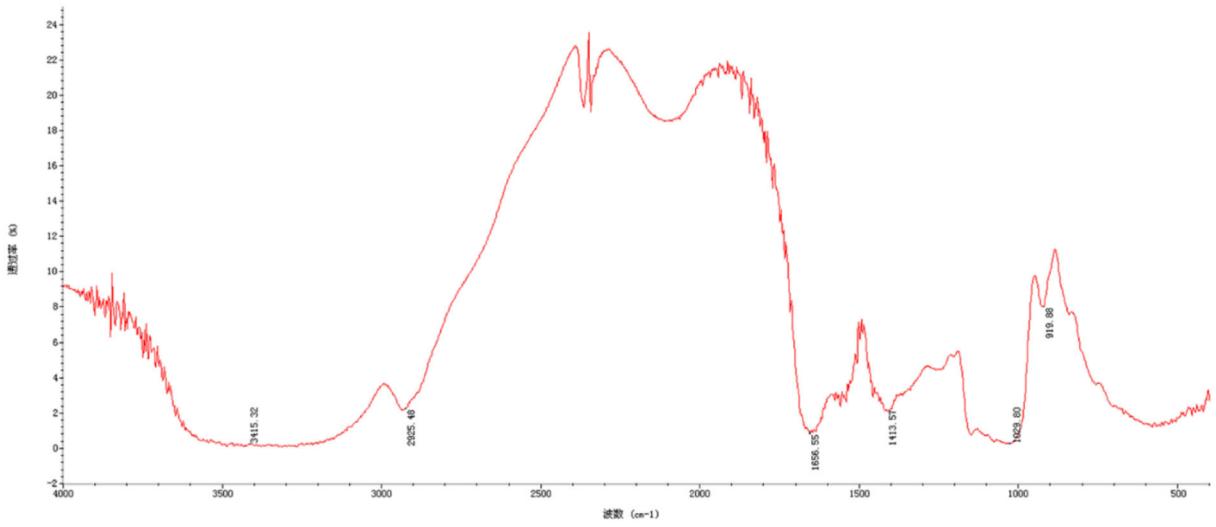

FIGURE 2
Fourier-transform infrared (FT-IR) spectrum of CAG-1.

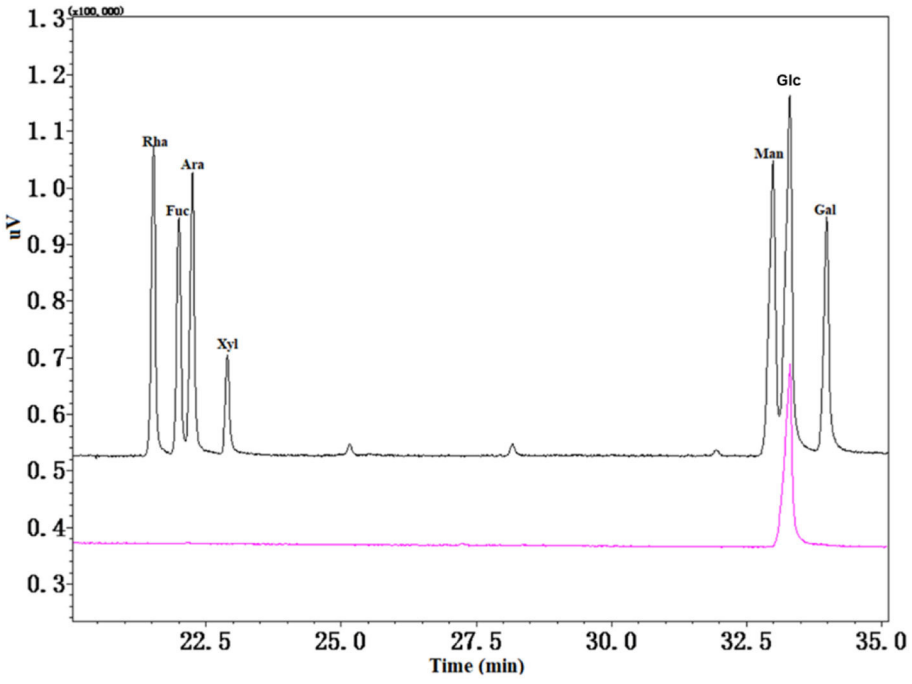

FIGURE 3
Gas chromatography-mass spectrometer (GC-MS) spectra of monosaccharide composition in CAG-1.

Amino acid composition analysis

A total of eight amino acids, which included alanine (Ala), threonine (Thr), serine (Ser), leucine (Leu), proline (Pro), aspartic (Asp), phenylalanine (Phe), and glutamic (Glu), were found in CAG-1 (Figure 4). Based on the peak area, the relative amino acid content was calculated. As seen in Table 3, the content of Glu and Asp was higher than that of others. The bulky side chains of Glu affected the activity of acetylcholinesterase, which was important in the treatment of Alzheimer's disease (26). In addition, Ala, Thr, and Ser existed in CAG-1. More information was obtained by analytical NMR.

TABLE 2 Glycosidic bonds and types of linkage in CAG-1.

RT (min)	Glycosidic bonds	Mass fragments (m/z)	Molar ratios	Type of linkage
16.239	2,3,4,6-Me_4-Glc*p*	43,71,87,101,117,129,145,161,205	0.14	Glc*p*-(1 →
21.378	2,3,6-Me_3-Glc*p*	43,87,99,101,113,117,129,131,161,173,233	0.53	→ 4)-Glc*p*-(1 →
24.723	2,6-Me_2-Glc*p*	43,87,97,117,159,185	0.10	→ 3,4)-Glc*p*-(1 →
27.242	2,3-Me_2-Glc*p*	43,71,85,87,99,101,117,127,159,161,201	0.20	→ 4,6)-Glc*p*-(1 →
30.09	2-Me_1-Glc*p*	43,58,87,97,117,139	0.03	→ 3,4,6)-Glc*p*-(1 →

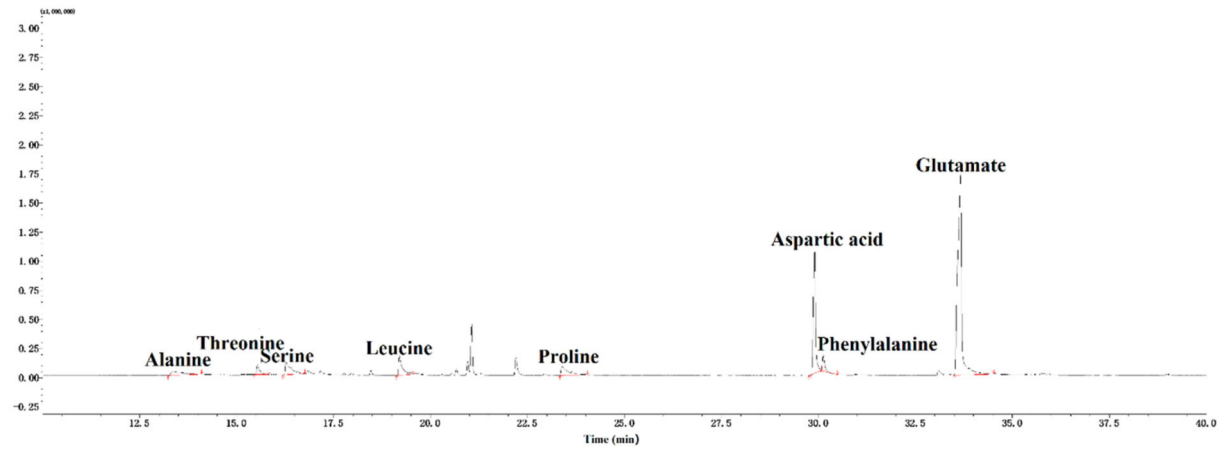

FIGURE 4
GC-MS spectra of amino acids in CAG-1.

TABLE 3 Amino acids in CAG-1.

RT (min)	Type	Content (g/100 g)
13.348	Ala	1.1
15.537	Thr	0.7
16.27	Ser	1.8
19.195	Leu	1.8
23.385	Pro	1.6
29.901	Asp	7.1
30.124	Phe	0.8
33.664	Glu	20.4

NMR spectroscopy analysis

The ^{1}H NMR spectrum, ^{13}C NMR spectrum, DEPT135 one-dimensional spectrum, and two-dimensional spectrum were measured with an NMR instrument, and the results of CAG-1 are illustrated in Figure 5. These signal peaks were distributed mainly in the 1–8 ppm area according to the ^{1}H NMR spectrum (Figure 5A). In addition, the 0–3.2, 3.2–5.2, and 6.5–8 ppm regions were mainly attributed to aliphatic alkane hydrogen signal peaks, polysaccharide hydrogen signal peaks, and the aromatic hydrogen signal peaks, respectively (Figure 5A). According to the ^{13}C NMR spectrum, 130.1 and 130.5 ppm were attributed to the aromatic benzene ring peaks and 158.1 and 162.2 ppm to the amide bond carbon. Moreover, 174.2, 174.9, 179.1, and 182.7 ppm were the amino acid carboxyl group, and 97.1 and 101.1 ppm were the dextran anomeric hydrogen signal peaks (Figure 5B). According to the ^{13}C NMR and DEPT135 spectra, methylene signal peaks were mainly 23.50, 25.92, 27.75, 29.01, 32.54, 34.92, 35.04, 39.96, 40.66, 41.98, 43.98, 49.37, 61.73, 62.56, and 63.02 ppm, of which 61.73, 62.56, and 63.02 ppm were the sugar C_6 signal peaks (Figure 5C). Others were the methylene signal peaks in the polypeptide, while 14.51, 19.93, and 21.61 ppm were methyl signals. The results of methylation demonstrated that the glycosidic bond of the polysaccharide part of the glycoprotein was mainly composed of Glc*p*-(1 → 4)-Glc*p*-(1 → , so the polysaccharide part of the glycoprotein was mainly 1,4-linked dextran sugar.

According to the HSQC spectrum, δ101.23 was observed, which was the anomeric carbon signal, and the corresponding anomeric hydrogen signal in the HSQC spectrum was δ5.29 (Figure 5D). The HH-COSY, used to mark the signal of H_{1-2}, H_{2-3-}, and H_{3-4}, indicated that H_1, H_2, H_3, and H_4 were δ5.29, δ3.5, δ3.89, and δ3.57, respectively (Figure 5E). The corresponding chemical shifts of C_1–C_4 were δ101.23, δ72.75,

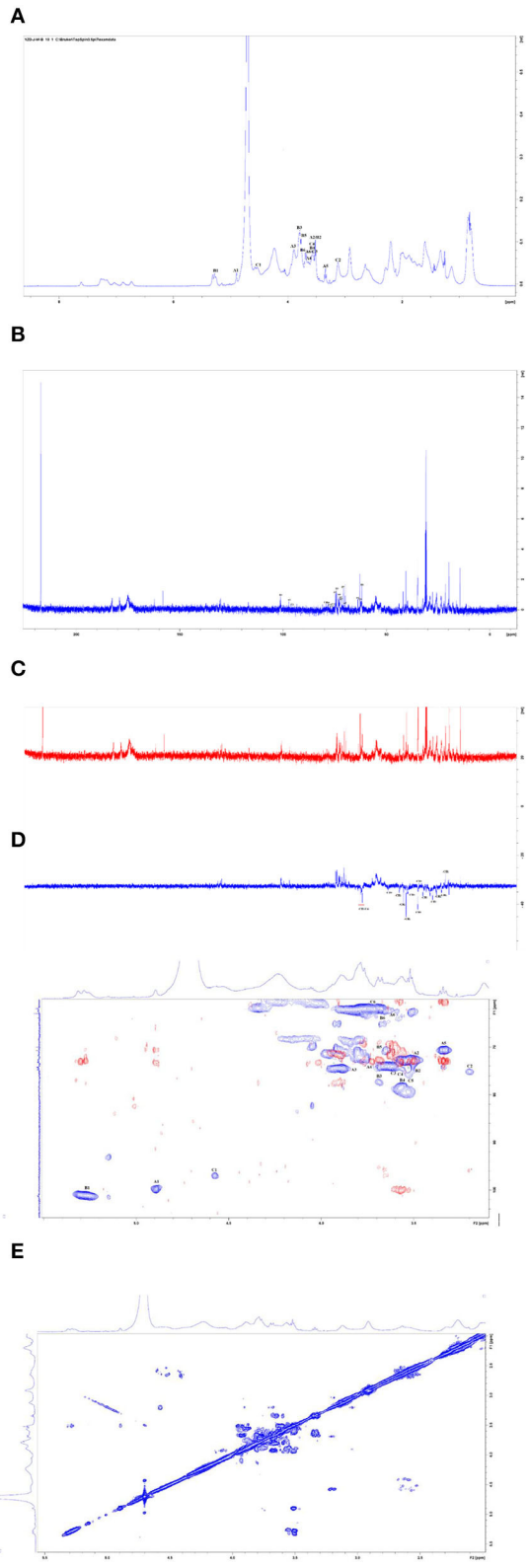

FIGURE 5
Nuclear magnetic resonance (NMR) spectra of CAG-1 in D_2O. **(A)** ^{1}H spectra; **(B)** ^{13}C spectra; **(C)** $DEPT_{135}$; **(D)** HSQC (in blue) + HMBC spectra (in red); and **(E)** COSY spectra.

TABLE 4 ^{1}H and ^{13}C nuclear magnetic resonance (NMR) chemical shifts in CAG-1 (ppm).

Glycosyl residues	H1a,b	H2	H3	H4	H5	H6a	H6b
	C1	C2	C3	C4	C5	C6	
Residue A	4.89	3.5	3.92	3.66	3.35	3.68	
α-d-Glc*p*-(1 →	99.71	73.052	74.88	73.88	70.5	63.02	
Residue B	5.29	3.5	3.89	3.57	3.76	3.73	3.76
→ 4)-α-d-Glc*p*-(1 →	101.23	72.75	74.66	78.6	72.45	61.73	
Residue C	4.57	3.2	3.68	3.58	3.53	3.77	
→ 4)-β-d-Glc*p*	97.2	75.07	77.58	78.75	75.9	61.99	

δ74.66, and δ78.6. The corresponding C_5 was δ 72.45, and its chemical shift of C_6 was δ61.73. Therefore, the signal attributed to the glycosidic bond → 4)-α-Glc*p*-(1 → . It was observed that the anomeric carbon signal was δ99.71, and the corresponding anomeric hydrogen signal in the HSQC spectrum was δ4.89 (Figure 5D). When the HH-COSY appeared, the signal of H_{1-2} was 4.89/3.50, and the signal of H_{2-3} was 3.50/3.92. Meanwhile, the signal of H_{3-4} was 3.92/3.66 (Figure 5E). It was deduced that H_1, H_2, H_3, and H_4 were δ4.89, δ3.5, δ3.92, and δ3.66, respectively. The corresponding chemical shifts from C_1-C_4 were δ99.71, δ73.052, δ74.88, and δ73.88. The corresponding C_5 was 70.50, and the chemical shift of C_6 was δ63.02. Therefore, the signal should be attributed to the glycosidic bond α-Glc*p*-(1 → , and the correlation peaks are presented in Table 4.

HMBC analysis showed that the anomeric hydrogen of the polysaccharide has a correlation peak with its own C_4, indicating the existence of → 4)-α-d-Glc*p*-(1 → 4)-α-d-Glc*p*-(1 → glycosidic bond. The anomeric carbon of α-d-Glc*p*-(1 → and its → 4)-α-d-Glc*p*-(1 → H4) have correlation peaks, indicating the presence of α-d-Glc*p*-(1 → 4)-α-d-Glc*p*-(1 → 4)-α-d-Glc*p*-(1 → . In addition, the protein component of the glycoprotein was mainly connected by Asp acid and Glu acid and contains some Ala, Thr, Ser, Leu, Pro, and Phe. As the sample was extracted with alkaline water, similar to the β-elimination reaction, the sugar chains in the glycoprotein were not hydrolyzed under alkaline conditions, indicating that the polysaccharide had an N-glycosidic bond. The sugar chain was linked to the protein chain by Asp acid.

Immunomodulatory activity

With an increase in sample concentration, the survival rate of RAW264.7 macrophages did not change significantly ($p < 0.05$) (data not shown). Immune activity was evaluated by cell viability, cellular NO release, TNF-α, MCP-1, and IL-6 (Figure 6). As an important signaling molecule, NO regulates a diverse range of physiological processes in many tissues. LPS caused cells to swell by increasing NO release, so the LPS group

10.3389/fnut.2022.966705

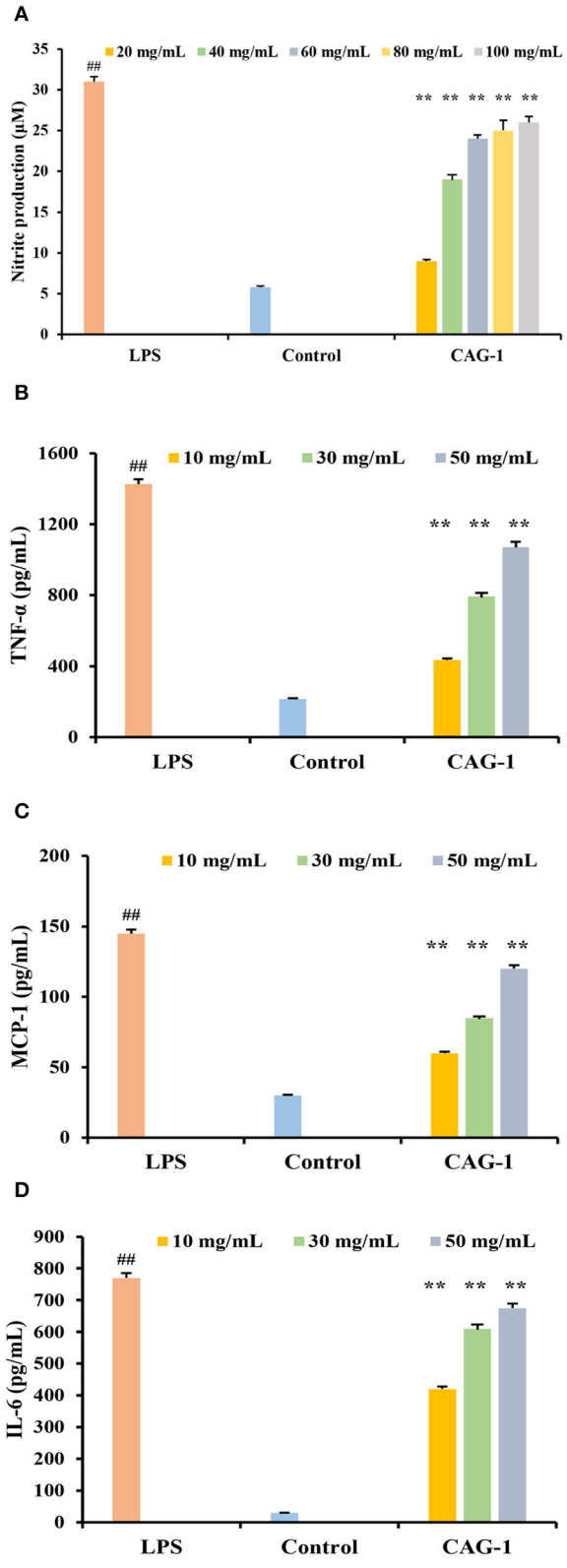

FIGURE 6
Effects of CAG-1 on the production of nitric oxide (NO), tumor necrosis factor-α (TNF-α), monocyte chemotactic protein 1 (MCP-1), and interleukin-6 (IL-6) in macrophages RAW 264.7 cells. **(A)** NO; **(B)** TNF-α; **(C)** MCP-1; and **(D)** IL-6. Values are mean ± standard deviation (SD) ($n = 3$). $^{\#\#}p < 0.01$ compared to control and $^{**}p < 0.01$ compared to lipopolysaccharide (LPS).

was considered a positive control (10). NO production in the control and LPS groups was 5.02 and 32.07 μM, respectively. At the experimental concentration (20–100 μg/ml), the production of NO was associated with the concentration of CAG-1. The production of NO in CAG-1 was 8.07 μM at 20 μg/ml, while it increased to 24.53 μM at 100 μg/ml, indicating its strong effect on macrophage activation. Associated with proinflammatory properties, TNF-α plays a key role in innate and adaptive immunity, especially in host defense mechanisms that terminate intracellular bacteria (27). Accumulating studies uncovered that TNF-α also plays important immunoregulatory roles and is directly associated with the maintenance of immune homeostasis (28). This indicates that the net effect of TNF-α is balanced between its immunosuppressive and proinflammatory functions and is decided by the cellular microenvironment and differs (29). In this study, TNF-α, MCP-1, and IL-6 were also significantly increased in the LPS group as the inflammation was caused by LPS (30, 31). In this study, the release of cytokines (TNF-α, MCP-1, and IL6) was significantly increased by 232.61, 162.09, and 86.52% compared to CAG-1 at 10 μg/ml, respectively. It indicated that CAG-1 moderated inflammation by LPS, which was also observed in glycoproteins isolated from *Cudrania tricuspidata* Bureau (32). In CAG-1 at 10 μg/ml, the TNF-α, MCP-1, and IL-6 levels were detected to be 428.30, 55.85, and 413.11 pg/ml, respectively.

Conclusion

One alkali-soluble glycoprotein (CAG-1), with a molecular weight of 8,106 Da, was purified from chickpea seeds. Glc was found to be the main component of the polysaccharide part of CAG-1, and → 4)-Glc*p*-(1 → and → 4,6)-Glc*p*-(1 → were the main glycosidic bonds detected in CAG-1. A total of eight amino acids were detected in CAG-1; among them, Asp and Glu were the two most important amino acids. The results of NMR analysis indicated the presence of α-d-Glc*p*-(1 → 4)-α-d-Glc*p*-(1 → 4)-α-d-Glc*p*-(1 → . Moreover, the sugar chains in glycoproteins were not hydrolyzed under alkaline conditions, suggesting that the polysaccharide had an N-glycosidic bond, by which the sugar chain was linked to the protein chain by Asp acid. An immunological study showed that CAG-1 stimulated the production of NO, IL-6, TNF-α, and MCP-1 in RAW 264.7 macrophages in a dose-dependent manner. These results suggest that alkali-extracted glycoprotein

of chickpea had immunomodulatory activities and could be beneficial for health.

Data availability statement

The original contributions presented in the study are included in the article/supplementary material, further inquiries can be directed to the corresponding authors.

Author contributions

ZS, SL, and ZW contributed to conception and design of the study. YW organized the database. NZ performed the statistical analysis. ZS wrote the first draft of the manuscript. SL, ZW, YW, and NZ wrote sections of the manuscript. All authors contributed to manuscript revision, read, and approved the submitted version.

Funding

This work was supported by the National Key R&D Program of China (2021YFD1600100), the earmarked fund for the China Agriculture Research System (CARS-08-G21), the Key Laboratory of Grain Crop Genetic Resources Evaluation and Utilization, and the Science and Technology Research Projects of Chongqing Education Commission (KJQN202102705).

Conflict of interest

The authors declare that the research was conducted in the absence of any commercial or financial relationships that could be construed as a potential conflict of interest.

Publisher's note

All claims expressed in this article are solely those of the authors and do not necessarily represent those of their affiliated organizations, or those of the publisher, the editors and the reviewers. Any product that may be evaluated in this article, or claim that may be made by its manufacturer, is not guaranteed or endorsed by the publisher.

References

1. Chavez-Sanchez L, Espinosa-Luna JE, Chavez-Rueda K, Legorreta-Haquet MV, Montoya-Diaz E, Blanco-Favela F. Innate immune system cells in atherosclerosis. *Arch Med Res.* (2014) 45:1–14. doi: 10.1016/j.arcmed.2013.11.007

2. Franken L, Schiwon M, Kurts C. Macrophages: sentinels and regulators of the immune system. *Cell Microbiol.* (2016) 18:475–87. doi: 10.1111/cmi.12580

3. Yao Y, Zhu YY, Ren GX. Antioxidant and immunoregulatory activity of alkali-extractable polysaccharides from mung bean. *Int J Biol Macromol.* (2016) 84:289–94. doi: 10.1016/j.ijbiomac.2015.12.045

4. Yu X, Yang X, Cui B, Wang L, Ren G. Antioxidant and immunoregulatory activity of alkali-extractable polysaccharides from North American ginseng. *Int J Biol Macromol.* (2014) 65:357–61. doi: 10.1016/j.ijbiomac.2014.01.046

5. Sheng XT, Yan JM, Meng Y, Kang YY, Han Z, Tai GH, et al. Immunomodulatory effects of Hericium erinaceus derived polysaccharides are mediated by intestinal immunology. *Food Funct.* (2017) 8:1020–7. doi: 10.1039/C7FO00071E

6. Qin GYX, Xu W, Liu JP, Zhao LY, Chen GT. Purification, characterization and hypoglycemic activity of glycoproteins obtained from pea (*Pisum sativum* L.). *Food Sci Hum Wellness.* (2021) 10:297–307. doi: 10.1016/j.fshw.2021.02.021

7. Tsai PF, Ma CY, Wu JSB. A novel glycoprotein from mushroom Hypsizygus marmoreus (Peck) Bigelow with growth inhibitory effect against human leukaemic U937 cells. *Food Chem.* (2013) 141:1252–8. doi: 10.1016/j.foodchem.2013.04.024

8. Oh PS, Lim KT. Antioxidant activity of Dioscorea batatas Decne glycoprotein. *Eur Food Res Technol.* (2008) 226:507–15. doi: 10.1007/s00217-007-0563-6

9. Oh PS, Lim KT. Glycoprotein isolated from Dioscorea batatas Decne modulates expressions of IL-4 and IL-10 in primary-cultured mouse lymphocytes. *Cell Biochem Funct.* (2009) 27:316–22. doi: 10.1002/cbf.1577

10. Niu X, He Z, Li W, Wang X, Zhi W, Liu F, et al. Immunomodulatory activity of the glycoprotein isolated from the Chinese Yam (*Dioscorea opposita* Thunb). *Phytother Res.* (2017) 31:1557–63. doi: 10.1002/ptr.5896

11. Martinez KAA, Mejia EG. Comparison of five chickpea varieties, optimization of hydrolysates production and evaluation of biomarkers for type 2 diabetes. *Food Res Int.* (2021) 147:110572. doi: 10.1016/j.foodres.2021.110572

12. Ma HR, Wang J, Qi HX, Gao YH, Pang LJ, Yang Y, et al. Assessment of the estrogenic activities of chickpea (*Cicer arietinum* L) sprout isoflavone extract in ovariectomized rats. *Acta Pharmacol Sin.* (2013) 34:380–6. doi: 10.1038/aps.2012.160

13. Giron-Calle J, Alaiz M, Vioque J. Effect of chickpea protein hydrolysates on cell proliferation and in vitro bioavailability. *Food Res Int.* (2010) 43:1365–70. doi: 10.1016/j.foodres.2010.03.020

14. Ye ZP, Wang W, Yuan QX, Ye H, Sun Y, Zhang HC, et al. Box-Behnken design for extraction optimization, characterization and *in vitro* antioxidant activity of *Cicer arietinum* L. hull polysaccharides. *Carbohydr polym.* (2016) 147:354–64. doi: 10.1016/j.carbpol.2016.03.092

15. Ghribi AM, Sila A, Gafsi IM, Blecker C, Danthine S, Attia H, et al. Structural, functional, and ACE inhibitory properties of water-soluble polysaccharides from chickpea flours. *Int J Biol Macromol.* (2015) 75:276–82. doi: 10.1016/j.ijbiomac.2015.01.037

16. Akhtar HMS, Ye ZP, Abdin M, Hamed YS, Chen GJ, Zeng XX. Immunomodulatory activity in vitro and *in vivo* of polysaccharides from Kabuli Chickpea (*Cicer arietinum* L.) Hull. *Food Technol Biotechnol.* (2020) 58:370–80. doi: 10.17113/ftb.58.04.20.6634

17. Ji X, Guo J, Pan F, Kuang F, Chen H, Guo X, et al. Structural elucidation and antioxidant activities of a neutral polysaccharide from Arecanut (*Areca catechu* L.). *Front Nutr.* (2022) 9:853115. doi: 10.3389/fnut.2022.853115

18. Li ZR, Wang B, Chi CF, Gong YD, Tang JJ, Luo HY. Purification and characterization of an antioxidant glycoprotein from the hydrolysate of Mustelus griseus. *Int J Biol Macromol.* (2013) 52:267–74. doi: 10.1016/j.ijbiomac.2012.10.025

19. Ji X, Cheng Y, Tian J, Zhang S, Shi M. Structural characterization of polysaccharide from jujube (*Ziziphus jujuba* Mill.) fruit. *Chem Biol Technol Agric.* (2021) 8:54. doi: 10.1186/s40538-021-00255-2

20. Rusanov AL, Luzgina NG, Lisitsa AV. Sodium dodecyl sulfate cytotoxicity towards HaCaT keratinocytes: comparative analysis of methods for evaluation of cell viability. *Bull Exp Biol Med.* (2017) 163:284–8. doi: 10.1007/s10517-017-3785-z

21. Chen X, Lin Z, Ye Y, Zhang R, Yin J, Jiang Y, et al. Suppression of diabetes in non-obese diabetic (NOD) mice by oral administration of water-soluble and alkali-soluble polysaccharide conjugates prepared from green tea. *Carbohydr Polym.* (2010) 82:28–33. doi: 10.1016/j.carbpol.2010.04.017

22. Zhou Y, Ma Y, Li L, Yang X. Purification, characterization, and functional properties of a novel glycoprotein from tartary buckwheat (*Fagopyrum tartaricum*) seed. *Food Chem.* (2020) 309:125671. doi: 10.1016/j.foodchem.2019.125671

23. Kacurakova M, CAGek P, Sasinkova V, Wellner N, Ebringerova A. FT-IR study of plant cell wall model compounds: pectic polysaccharides and hemicelluloses. *Carbohydr Polym.* (2000) 43:19. doi: 10.1016/S0144-8617(00)00151-X

24. Cui FJ, Li YH, Zan XY, Yang Y, Sun WJ, Qian JY, et al. Purification and partial characterization of a novel hemagglutinating glycoprotein from the cultured mycelia of *Hericium erinaceus*. *Process Biochem.* (2014) 49:1362–9. doi: 10.1016/j.procbio.2014.04.008

25. Sathyanarayana S, Prashanth KVH. Malting process has minimal influence on the structure of arabinan-rich rhamnogalacturonan pectic polysaccharides from chickpea (*Cicer arietinum* L.) hull. *J Food Sci Technol.* (2019) 56:1732–43. doi: 10.1007/s13197-019-03600-4

26. Tsai CH, Yen YH, Yang JPW. Finding of polysaccharide-peptide complexes in Cordyceps militaris and evaluation of its acetylcholinesterase inhibition activity. *J Food Drug Anal.* (2015) 23:63–70. doi: 10.1016/j.jfda.2014.05.006

27. Pfeffer K. Biological functions of tumor necrosis factor cytokines and their receptors. *Cytokine Growth Factor Rev.* (2003) 14:185–91. doi: 10.1016/S1359-6101(03)00022-4

28. De Bandt M, Sibilia J, Le Loet X, Prouzeau S, Fautrel B, Marcelli C, et al. Systemic lupus erythematosus induced by anti-tumour necrosis factor alpha therapy: a French national survey. *Arthritis Res Ther.* (2005) 7:R545–51. doi: 10.1186/ar1715

29. Ernandez T, Mayadas TN. Immunoregulatory role of TNF alpha in inflammatory kidney diseases. *Kidney Int.* (2009) 76:262–76. doi: 10.1038/ki.2009.142

30. Kim HL, Ha AW, Kim WK. Effect of saccharin on inflammation in 3T3-L1 adipocytes and the related mechanism. *Nutr Res Pract.* (2020) 14:109–16. doi: 10.4162/nrp.2020.14.2.109

31. Scheller J, Chalaris A, Schmidt-Arras D, Rose-John S. The pro- and anti-inflammatory properties of the cytokine interleukin-6. *Biochim Biophys Acta Mol Cell Res.* (2011) 1813:878–88. doi: 10.1016/j.bbamcr.2011.01.034

32. Joo HY, Lim KT. Glycoprotein isolated from *Cudrania tricuspidata* bureau inhibits iNO and COX-2 expression through modulation of NF-kappa B in LPS-stimulated RAW 264.7 cells. *Environ Toxicol Pharmacol.* (2009) 27:247–52. doi: 10.1016/j.etap.2008.10.014

frontiers | Frontiers in Nutrition

TYPE Original Research
PUBLISHED 20 September 2022
DOI 10.3389/fnut.2022.992102

Check for updates

OPEN ACCESS

EDITED BY
Xiaolong Ji,
Zhengzhou University of Light Industry, China

REVIEWED BY
Zhaojun Wei,
Hefei University of Technology, China
Min Zhao,
Northeast Forestry University, China

*CORRESPONDENCE
Yuan-Feng Zou
yuanfengzou@sicau.edu.cn

†These authors have contributed equally to this work

SPECIALTY SECTION
This article was submitted to Food Chemistry, a section of the journal Frontiers in Nutrition

RECEIVED 12 July 2022
ACCEPTED 30 August 2022
PUBLISHED 20 September 2022

CITATION
Li L-X, Feng X, Tao M-T, Paulsen BS, Huang C, Feng B, Liu W, Yin Z-Q, Song X, Zhao X, Liang X-X, Yin L-Z, Tang H-Q and Zou Y-F (2022) Benefits of neutral polysaccharide from rhizomes of *Polygonatum sibiricum* to intestinal function of aged mice. *Front. Nutr.* 9:992102. doi: 10.3389/fnut.2022.992102

COPYRIGHT
© 2022 Li, Feng, Tao, Paulsen, Huang, Feng, Liu, Yin, Song, Zhao, Liang, Yin, Tang and Zou. This is an open-access article distributed under the terms of the Creative Commons Attribution License (CC BY). The use, distribution or reproduction in other forums is permitted, provided the original author(s) and the copyright owner(s) are credited and that the original publication in this journal is cited, in accordance with accepted academic practice. No use, distribution or reproduction is permitted which does not comply with these terms.

Benefits of neutral polysaccharide from rhizomes of *Polygonatum sibiricum* to intestinal function of aged mice

Li-Xia Li[1†], Xin Feng[1†], Meng-Ting Tao[1†], Berit Smestad Paulsen[2], Chao Huang[3], Bin Feng[4], Wei Liu[5], Zhong-Qiong Yin[1], Xu Song[1], Xinghong Zhao[1], Xiao-Xia Liang[1], Li-Zi Yin[1], Hua-Qiao Tang[6] and Yuan-Feng Zou[1*]

[1]Natural Medicine Research Center, College of Veterinary Medicine, Sichuan Agricultural University, Chengdu, China, [2]Department of Pharmacy, Section Pharmaceutical Chemistry, Area Pharmacognosy, University of Oslo, Oslo, Norway, [3]Laboratory of Experimental Animal Disease Model, College of Veterinary Medicine, Sichuan Agricultural University, Chengdu, China, [4]Animal Nutrition Institute, Sichuan Agricultural University, Chengdu, China, [5]Key Laboratory of the Ministry of Education for the Standardization of Traditional Chinese Medicine, Pharmacy College, Chengdu University of Traditional Chinese Medicine, Chengdu, China, [6]Key Laboratory of Animal Disease and Human Health of Sichuan Province, College of Veterinary Medicine, Sichuan Agricultural University, Chengdu, China

One purified neutral polysaccharide fraction was obtained from the rhizome of *Polygonatum sibiricum* by DEAE ion exchange and gel chromatography. Structure elucidation was performed by methanolysis, methylation, FT-IR, and NMR. The results indicated that PSP-NP was composed of 1,4-β-D-Gal,1, 4, 6-β-D-Gal, T-α-D-Man,1, 4-α-D-Glc, and T-α-D-Glc with a molecular weight of 43.0 kDa. We supplied this polysaccharide to aged mice and found it is of benefits to intestinal functions, as indicated by better tissue integrity and motility, improved oxidative stress and inflammation, reduced intestinal permeability and serum LPS level, as well as balanced gut microbial composition and short-chain fatty acids production. These results display a novel *Polygonatum sibiricum* polysaccharide to improve the intestinal function of aged mice, which provides pieces of evidence for its further development and utilization.

KEYWORDS

heteropolysaccharide, *Polygonatum sibiricum*, anti-aging, jejunum, colon

Introduction

Aging is a process that accumulates detrimental changes to cellular components and thus affects tissue homeostasis, resulting in disease or increased risk of morbidity and mortality (1). Previously work revealed tightly integration between aging and chronic inflammation, and multiple aging-related factors are implicated, such as redox imbalance, mitochondrial damages, senescence of the immune/endocrine system (2), etc. The gastrointestinal tract is an important organ of body immunity, the mucosal immune system of which provides the first defense-line against environmental insults and pathogens (3). The gastrointestinal tract, especially the intestine, couples signals from gut microbiota, metabolites, stress, and immune response and is implicated in controlling immune defense not just itself but also elsewhere in the body (4, 5). As aging compromises the intestinal immune response that affects innate and adaptive immunity and subsequently leads to detrimental systemic effects on the entire organism, improvements to intestinal function could bring about benefits to aging-related defects.

Polygonati Rhizoma, the rhizome from the Liliaceae Polygonatum plant that is widely distributed throughout China with more than 30 species (2, 6). *Polygonati Rhizoma* has been used as food and medicine in China for more than 2000 years, and the beneficial effects of which are very accurate in Chinese clinical practice (7, 8). Three of *Polygonati Rhizoma* are now listed in Chinese Pharmacopeia as Traditional Chinese Medicine, including the rhizome of *Polygonatum sibiricum*, *P. kingianum* Coll. et Hemsl and *P. cyrtonema* Hua. *Polygonati Rhizoma* has a wide range of pharmacological effects of anti-diabetes, anti-fatigue, Antioxidant, antimicrobial as well as anti-aging and immune improvement (9–11). While a variety of bioactive compositions like steroidal saponins, triterpenes, flavones, phytosterols and volatile oils have been isolated from *Polygonati Rhizoma*, polysaccharides are thought to be one of the most important bioactive-compounds from it (12). Multiple polysaccharides have been isolated from these three species of *Polygonati Rhizoma* with different methods, but most of them lack systematic research on isolation, purification and their bio-activity, and the comparative studies on neutral polysaccharide components in different species have also not been reported (7, 13). Most importantly, the function of *Polygonati Rhizoma* polysaccharides in the intestine, where polysaccharides are degraded and display their bioactivities, is not well understood.

Here in this study, we aim to isolate and purify the polysaccharides from the rhizome of *Polygonatum sibiricum*, *P. kingianum* Coll. et Hemsl and *P. cyrtonema* Hua. *Polygonati Rhizoma* by DEAE ion exchange chromatography and gel filtration, screen polysaccharides with high bioactivities *in vitro*, and then structurally characterize them and study their benefits to the intestine of aged mice.

Materials and methods

Materials

Polygonatum sibiricum was collected from Baiyun Mountain, Luoyang City, Henan Province, China. *P. kingianum* was collected from Mile Mountain, Mile City, Yunnan Province, China. *P. cyrtonema* was collected from Longcanggou, Yingjing County, Yaan City, Sichuan Province, China. It was identified as *Polygonatum sibiricum* by Dr. Lixia Li, College of Veterinary Medicine, Sichuan Agricultural University. The rhizomes of all materials were washed, sliced, steamed for 60 mins, and then dried at 50°C.

Standard acetic acid, propionic acid, and butyric acid were purchased from Sigma-Aldrich. EMB medium, MRS medium, and BS medium were obtained from Hope Bio Biotechnology Co., Ltd. (Qingdao, China). H&E and AB-PAS stain kits were purchased from Solarbio (Beijing, China). RevertAid First Strand cDNA was purchased from Thermo Fisher Scientific. SYBR Green Supermix was purchased from Bio-Rad.

The standards of D-Mannose (Man); L-Rhamnose (Rha); D-Glucuronic acid (GlcA); D-Galactose (Gal); D-Glucose (Glc); D-Galacturonic acid (GalA); D-Fucose (Fuc); D-Xylose (Xyl); L-Arabinose (Ara); and D-Fructose (Fru) were purchased from Solarbio (Beijing, China). All other chemicals, such as phenol, sulfuric acid, trichloromethane, isopropyl alcohol, ethanal, etc., were all of analytical grade and obtained from the Kelong Chemical factory (Chengdu, China).

Extraction of polysaccharides from *Polygonatum sibiricum*

Processed rhizomes from *P. sibiricum*, *P. kingianum*, and *P. cyrtonema* were extracted by 95% and 50% ethanol separately to remove low-molecular-weight and different-polarity lipophilic compounds. Then dried residuals were extracted twice with boiling water to obtain crude extracts. Those extracts were concentrated (RE-3000, Yarong Bio-chemical Instruments Factory, Shanghai, China) and precipitated by absolute ethanol. After lyophilized, the crude polysaccharide was obtained and named PSP, PKP, and PCP.

Purification of polysaccharides from *Polygonatum sibiricum*

The crude polysaccharide (400 mg) was dissolved in distilled water (20 mL), and applied to a DEAE Sepharose (Fast Flow, FF) column (50 mm × 40 cm, Beijing Rui Da Heng Hui Science Technology Development Co., Ltd., Beijing, China) after having been filtered through a 0.45 μm filter. The neutral fraction was eluted with a 3-fold column volume (approximately 2 L) of

distilled water at a speed of 2 mL/min. Afterward, the acidic fraction was further eluted with linear gradient NaCl solution (0∼1.5 M) with a flow rate 2 mL/min. The related fractions were pooled together based on the phenol-sulfuric acid assay, dialyzed at a cut-off of 3500 Da against distilled water to remove NaCl, and lyophilized. Then, it was dissolved in 10 mM NaCl buffer and purified by gel filtration on a Sepharose 6FF column (2.5 cm × 100 cm, Beijing Rui Da Heng Hui Science Technology Development Co., Ltd., Beijing, China) after filtration through a 0.45 μm filter, and eluted with 10 mM NaCl at 1.0 mL/min. Both neutral and acid fractions were pooled based on the phenol-sulfuric acid assay, dialyzed, and lyophilized, and the neutral fractions were named PSP-NP, PKP-NP, and PCP-NP, while the acidic fractions were named PSP-AP, PKP-AP, and PCP-AP.

Cell culture, cell viability assay, and quantitative real-time PCR

The porcine epithelial (IPEC-J2) cells were cultured in DMEM (Gibco) medium containing 10% FBS (Gibco) in an incubator with the atmosphere of 5% CO_2 at 37°C. Cells were plated in 6-well cell plates (1×10^6 cells per well), and the CCK-8 solution (10 μL per well) was added co-culturing for 1 h after adding polysaccharide (at the final concentration of 5 and 10 μg/mL) at the plates for 12 h. The absorbance of each well was finally read at 450 nm using a microplate reader for the cell viability assay. In the meantime, after the polysaccharide was supplied, the cells were collected to extract the total RNA by lysing with Trizol Regent according to the manufacturer's instructions. The concentration was measured with a spectrophotometer (NanoDrop 2000, Thermo Fisher Scientific, Shanghai, China) and the quality of RNA was assessed by agarose gel. Then the cDNA was obtained by reverse transcription with reverse transcriptase, according to the manufacturer's instructions (Thermo Fisher Scientific, United States). Quantitative real-time PCR was performed by the Bio-Rad CFX96 system, using GAPDH as an internal reference. Primer sequences are as follow: SOD1: Fr 5′-GCAGGGCACCATCTACTTCG-3′, Rv 5′-CTGCACTGGTACAGCCTTGT-3′.

Characterization of polysaccharide fraction with high antioxidant activity

Chemical compositions and linkage determination

According to previous study (14), the methanolysis of the fraction was performed with 3 M hydrochloric acid in anhydrous methanol for 24 h at 80°C, and Mannitol was used as an internal standard. The methylglycosides obtained were converted into their corresponding derivatives — trimethylsilylated (TMS), and then analyzed by gas and then analyzed by gas chromatography (GCThermo Scientific, Milan, Italy). Glycosidic linkage elucidation was performed by methylation studies. Polysaccharide samples were methylated, hydrolyzed, reduced, and acetylated (15). Finally, the derivatives were analyzed by GC-MS using a GCMS-QP2010 (Shimadzu, Kyoto, Japan) attached to a Restek Rxi-5MS column (30 m; 0.25 mm, i.d.; 0.25 μm film). The injector temperature was 280°C; the ion source temperature was 200°C; and the interface temperature was 300°C. The column temperature was 80°C when the sample was injected and then increased 10°C/min to 140°C, followed by 4°C/min to 210°C, and then 20°C/min to 300°C, using helium as the carrier gas (pressure control: 80 kPa). The compound at each peak was characterized by an interpretation of the retention times and the characteristic mass spectra. The relative amount of each type of linkage was determined based on the area of each compound and related to the total amount of each monosaccharide type as determined by methanolysis (16).

Molecular weight determination

Determination of homogeneity and molecular weight of polysaccharide was performed by size exclusion chromatography on a HiloadTM 16/60 SuperdexTM 200 prep grade column (GE Healthcare, Uppsala, Sweden) combined with the Äkta system (FPLC, Pharmacia Äkta, Amersham Pharmacia Biotech, Uppsala, Sweden). Dextran polymers (Pharmacia, NJ, United States) of 10, 40, 70, 500, and 2,000 kDa were used as calibration standards (17).

FT-IR and NMR spectroscopy

The FT-IR studies were done on a sample after grinding and pressing a mixture of a 1 mg polysaccharides sample with dried KBr into a 1 mm thick disk by a Table Press Machine (Daxiang Electronic Machinery, Guangzhou, China). The spectrum was then recorded in a PerkinElmer FT-IR spectrophotometer (PerkinElmer, Waltham, MA, United States) in the wavelength range of 4000–400 cm^{-1} (18).

The 1H-NMR and 13C-NMR spectra of polysaccharides were recorded in D2O solution on an AV600 spectrometer (600 MHz, Bruker, Rheinstetten, Germany) after a three-time deuterium exchange with D2O by freeze-drying.

Protective activities of polysaccharide *in vivo*

Animal experimental design

All animal studies were performed in accordance with the Guidelines for the Care and Use of Laboratory Animals of Sichuan Province, China (The People's Government of Sichuan Province, China, 2019) and the Regulations for the Administration of Affairs concerning Experimental Animals

(The State Science and Technology Commission of China, Rev 2017-1), and they were reviewed and approved by the Animal Care and Use Committee of Sichuan Agricultural University, with the permit No. DYXY141142115. Sixty-four SPF C57BL/6Cnc mice (10 months old, 28−32 g, male) were purchased from Beijing Vital River Laboratory Animal Technology Co., Ltd. (Beijing, China). The mice were housed in a standard polypropylene cage, given ad libitum access to diet and tap water in a controlled environment with a temperature of 21 ± 1°C, relative humidity of 50–60%, and a 12 h light/12 h dark cycle. After 7 days of acclimatization with free access to food and water, they were randomly divided into 4 groups, (16 mice in each group), one normal control group and three polysaccharide administration groups. The normal control group (Ctr) received intragastric administration with saline. The other three groups received different doses of purified polysaccharides (50, 100, and 200 mg/kg/day), named as low, medium, and high groups, respectively. All mice were successively administered with the above concoctions for 6 weeks. The 24 h after the last drug administration, blood samples were collected. The intestines were rapidly excised and were separated as jejunum and colon. All the samples were dissected into two portions. One portion was frozen in liquid nitrogen and subsequently stored at −80°C for gene expression analysis. And the other one was stored in 4% paraformaldehyde for histopathological evaluation.

Histological evaluation and goblet cells analysis

To estimate the pathological changes in the intestinal tissue, H&E staining was conducted for paraffin embedded sections. The jejunum was dehydrated, embedded in paraffin wax, cut into slices with a thickness of 5 μm, and then deparaffinized, rehydrated, and stained with hematoxylin and eosin. The degree of microscopic injury was evaluated on the basis of a previously published scoring system (1; Table 1). The length of the villi and the depth of crypt were then measured by Image-Pro Plus, and ratios were compared. The goblet cells were counted after AB-PAS staining according to the manufacturer's instructions. After rehydration, tissues were stained with alcian blue, oxidant, Schiff reagent, and hematoxylin. Gene expression of Mucin 2 was measured by qRT-PCR.

TABLE 1 Intestinal mucosal injury score.

Grade	Standards
0	Normal mucosal villi
1	Development of subepithelial Gruenhagen's space at the apex of the villus with capillary congestion
2	Extension of the subepithelial space with moderate lifting of epithelial layer from the lamina propria
3	Massive epithelial lifting down the sides of villi and a few tips may be denuded
4	Dull villi with lamina propria and dilated capillaries exposed and increased inflammatory infiltration of the lamina propria
5	Digestion and disintegration of lamina propria; hemorrhage and ulceration.

Determination of the motility function of the intestinal

Total RNA in jejunum and colon was obtained by a Trizol reagent, and cDNA was collected by a reverse transcription with a reverse transcriptase. Quantitative real-time PCR was performed to analyze relative gene expressions of vasoactive intestinal peptide (VIP) in the jejunum and colon using β-actin as an internal reference. Primer sequences are shown in Table 2.

Determination of the intestinal mucosal barrier

ELISA assay was conducted to measure the LPS concentration in serum; the gene expressions of mucin; and the tight junction proteins, including ZO-1 and Occludin,

TABLE 2 Primer sequences for quantitative real-time PCR.

Prime	5′→3′
β-actin	Fr 5′-GGCTGTATTCCCCTCCATCG-3′
	Rv 5′-CCAGTTGGTAACAATGCCATGT-3′
VIP	Fr 5′-AGTGTGCTGTTCTCTCAGTCG-3′
	Rv 5′ -GCCATTTTCTGCTAAGGGATTCT-3′
Mucin 2	Fr 5′-ATGCCCACCTCCTCAAAGAC-3′
	Rv 5′ -GTAGTTTCCGTTGGAACAGTGAA-3′
ZO-1	Fr 5′- ACCACCAACCCGAGAAGAC-3′
	Rv 5′ - CAGGAGTCATGGACGCACA-3′
Occludin	Fr 5′-TTGAAAGTCCACCTCCTTACAGA-3′
	Rv 5′ -CCGGATAAAAAGAGTACGCTGG-3′
IL-1β	Fr 5′-GAAATGCCACCTTTTGACAGTG -3′
	Rv 5′-TGGATGCTCTCATCAGGACAG-3′
IL-4	Fr 5′- GGTCTCAACCCCCAGCTAGT-3′
	Rv 5′ -GCCGATGATCTCTCTCAAGTGAT-3′
IL-6	Fr 5′-TAGTCCTTCCTACCCCAATTTCC-3′
	Rv 5′ -TTGGTCCTTAGCCACTCCTTC-3′
IL-10	Fr 5′- GCTCTTACTGACTGGCATGAG-3′
	Rv 5′ -CGCAGCTCTAGGAGCATGTG-3′
IL-12A	Fr 5′-CTGTGCCTTGGTAGCATCTATG-3′
	Rv 5′ -GCAGAGTCTCGCCATTATGATTC-3′
IL-12B	Fr 5′-TGGTTTGCCATCGTTTTGCTG-3′
	Rv 5′ -ACAGGTGAGGTTCACTGTTTCT-3′
IL-17	Fr 5′- TTTAACTCCCTTGGCGCAAAA-3′
	Rv 5′ -CTTTCCCTCCGCATTGACAC-3′
IL-23	Fr 5′-ATGCTGGATTGCAGAGCAGTA-3′
	Rv 5′ -ACGGGGCACATTATTTTTAGTCT-3′
TNF-α	Fr 5′-CTGAACTTCGGGGTGATCGG-3′
	Rv 5′-GGCTTGTCACTCGAATTTTGAGA-3′
TGF-β	Fr 5′- CTCCCGTGGCTTCTAGTGC-3′
	Rv 5′- GCCTTAGTTTGGACAGGATCTG-3′

10.3389/fnut.2022.992102

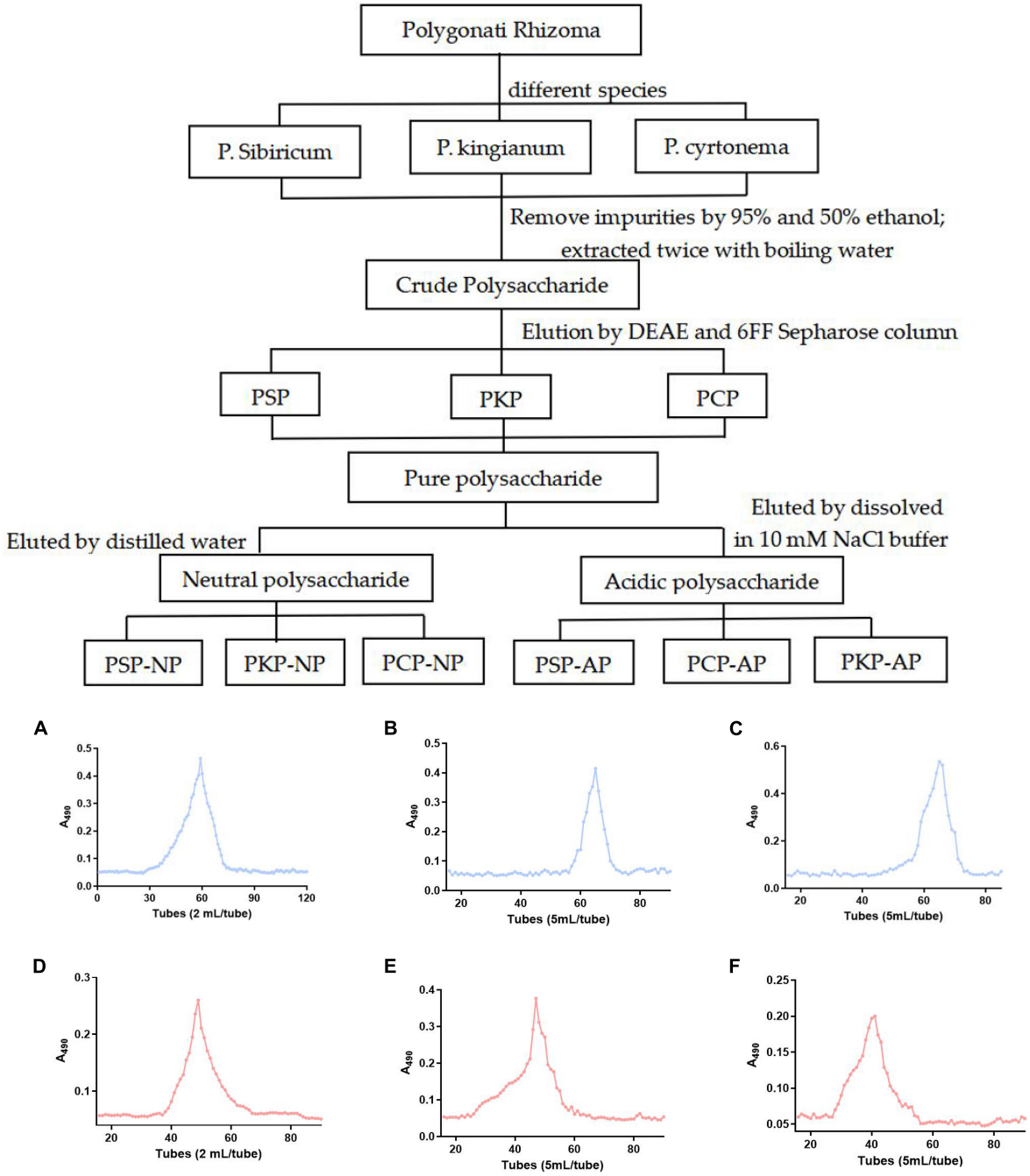

FIGURE 1
Technical roadmap for extraction and purification of Polygonatum Polysaccharide from different varieties and elution profiles of polysaccharides in gel column. **(A)** PSP-NP, **(B)** PCP-NP, **(C)** PKP-NP, **(D)** PSP- AP, **(E)** PCP-AP, **(F)** PKP-AP.

TABLE 3 The yield of crude polysaccharides and purified fractions from different species of *Polygonati Rhizoma*.

Crude polysaccharides	Yield (mg/g)	Neutral polysaccharide	Yield (mg/g)	Acidic polysaccharide	Yield (mg/g)
PSP	37.0	PSP-NP	17.2	PSP-AP	7.2
PKP	30.8	PKP-NP	8.1	PKP-AP	2.2
PCP	10.3	PCP-NP	1.6	PCP-AP	14.7

were studied by qRT-PCR. Primer sequences are shown in Table 2.

Determination of the intestinal immune function

Jejunum and colon were ground by liquid nitrogen in sterile mortars, and then homogenized in 10-fold volumes (g/mL) of PBS. The supernatants were obtained for the sIgA and carbonylated proteins assay using an ELISA kit after centrifuging at 3000 g/min for 10 min.

Determination of inflammatory factors in the intestinal

Detected genes of interleukins were *IL-1*β, *IL-2*, *IL-4*, *IL-6*, *IL-10*, *IL-12*, *IL-17*, *IL-23*, *TNF*-α, and *TGF*-β. β-*actin* was used as an internal reference. Primer sequences are shown in Table 2.

Influence on gut microbiome

Differential cultivation of cecum contents

The fluence of polysaccharides on gut microbiome was evaluated by bacterial counts and short-chain fatty acids (SCFA) in contents of the gut. The contents in cecum were obtained on the last day of this research. They were weighted and homogenized in saline and diluted with 10-fold dilutions from 102 to 107. Each dilutes was added to a culture medium in triplicate for bacterial differential cultivation. Bifidobacterium and Lactobacillus were respectively cultured in MRS and BS agar mediums in an anaerobic incubator with 85% N_2, 10% H_2, 5% CO_2 (Thermo Fisher Scientific 1029, Waltham, MA, United States) at 37°C. *Escherichia coli* were incubated in an EMB agar medium in an aerobic incubator (DHP-9082, Jiecheng Experimental Apparatus Co., Ltd., Shanghai, China). The bacteria count was expressed as log10 CFU (colony-forming unit)/g of cecum content.

Determination of short-chain fatty acids

In order to determine the concentration of SCFA in cecum contents, they were weighted and homogenized in 0.15 mL ddH_2O. They were centrifuged at 10,000 rpm for 10 min to obtain the supernatant, after being placed in room temperature for 30 min. Then, 20 μL 25% metaphosphoric acid and 1.52 μL 210 mmol/L crotonic acid were added to 100 μL of the supernatant and placed at 4°C for 30 min. After centrifuging at 12,000 rpm for 10 min, 100 μL of ethanol was added to100 μL of supernatant then filtered through a 0.22 μm filter membrane for gas chromatography (GC) determination (X). SCFA concentration (M, mmol/L) of sample was calculated as below:

$$M = X \times 2 \times 1.2125$$

The standards of different concentrations were prepared as acetic acid (3.575, 3.660, 2.745, 1.830, and 0.915 mmol/L), propionic acid (4.256, 3.405, 2.554, 1.703, and 0.851 mmol/L), and butyric acid (1.385, 1.108, 0.831, 0.554, and 0.277 mmol/L) with the same concentration of internal standard crotonic acid (1.13125 mmol/L) (19). Then a standard curve was established.

The samples were analyzed using a Varian CP-3800 gas chromatograph (Palo Alto, CA, United States) equipped with an HP-FFAP column (30 m × 0.535 mm × 1 μm) and a flame ionization detector (FID). 1 μL sample was injected at 250°C with a detector temperature of 300°C and nitrogen as the carrier gas at a speed of 35 mL/min and a split ratio of 50:1. The column temperature increased from 100 to 190°C with 20°C/min and then maintained for 1 min (20).

Statistical analysis

All data were analyzed by SPSS (version 20, SPSS Inc., CO, United States) with the one-way analysis of variance (ANOVA) by LSD test, and expressed as mean ± standard error of mean (SEM). The difference was considered statistically significant at $P < 0.05$.

Results and discussions

Comparison of polysaccharide fractions from different species of *Polygonati Rhizoma*

To obtain the polysaccharide with better biological activity, boiling water extraction was applied to obtain crude polysaccharide from a different resource of *Polygonati Rhizoma*. As shown in Figure 1 and Table 3, the yield of crude polysaccharides varied from 10.3 mg/g to 37.0 mg/g under the same extraction conditions, and the crude polysaccharides from *P. sibiricum* exhibited the highest yield than other two species. The yield of polysaccharide in the present study was slightly higher than the yield of 2.5% thrice refluxed with 95% ethanol, distilled water at 90°C then precipitated with EtOH [1:4 (v/v)], but it was a bit lower than the yield of 10% seen in other research (21, 22). The main reason might be different extraction methods, especially when 50% ethanol was used.

As shown in Table 3, after purification by ion-exchange chromatography and gel filtration, the yield of neutral polysaccharide and acidic polysaccharide fractions became different. As it is shown in Table 3, the highest yield of neutral polysaccharide fraction is PSP-NP, while the highest yield of acidic polysaccharide fraction comes from PCP-AP. The yields of PKP-NP and PKP-AP are very low compared to other two species. Therefore, those two fractions are not subjected to the biological test due to their low yield.

In previous studies, polysaccharide from Polygonati Rhizoma exhibited potential antioxidant activity *in vitro* (23). Polysaccharides cannot be directly absorbed, but can

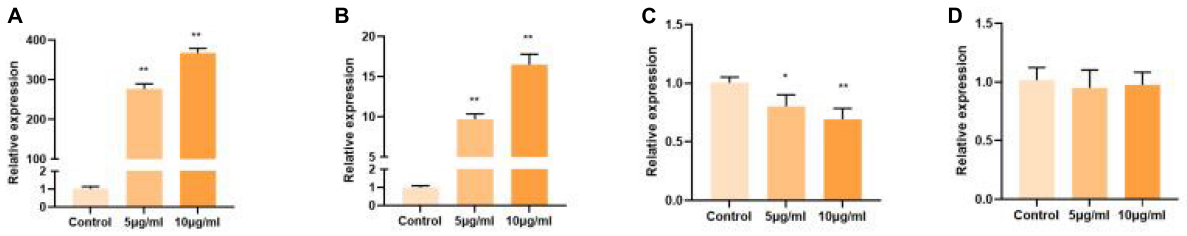

FIGURE 2
Comparison of polysaccharide fractions from different species of Polygonati Rhizoma. Influence of purified polysaccharides on cell gene expression of SOD1 *in vitro*. **(A)** PSP-NP; **(B)** PSP-AP; **(C)** PCP-AP; **(D)** PCP-NP. *Indicated significant difference compared with a control group, $P < 0.05$; ** indicated significantly.

be degraded by intestinal microorganisms, so the intestine is considered to be the target of polysaccharide activity. Therefore, in the present study, to select the polysaccharide fraction with the highest antioxidant activity for further study, the IPEC-J2 were used as *in vitro* study model. As shown in Figure 2, the polysaccharide fraction PSP-NP exhibited the highest antioxidant activity by promoting the expression of SOD1 *in vitro* compared to other fractions. Thus, the fraction PSP-NP was subjected to structure elucidation and *in vivo* study.

Structure elucidation of PSP-NP

Chemical composition and molecular weight of PSP-NP

The monosaccharide composition of PSP-NP was analyzed by methanolysis and GC analysis. PSP-NP was composed of Gal, Man, and Glc in a ratio of 68.7:24.3:7.0. The results suggested that PSP-NP was mainly composed of Gal and Man, which account for more than 90% of total sugar. From the literatures related the polysaccharide from *P. sibiricum*, they also report the presence of a small amount of Ara except the presence of Man, Glc, and Gal (24–26), while the Ara was not detected in the present study. In another study, the polysaccharide from *P. sibiricum* was composed of Gal and Rha with trace amounts of Man, Glc, and Xyl (27). Additionally, a previous report on the characterization of the other two PSP indicated that one of them only consisted of Gal and another fraction was composed of Gal and Man in a ratio of 88.8:11.2 (28). Collectively, the monosaccharide compositions of PSP-NP are similar with some reports, however, with different ratios and/or compositions.

According to the results of size exclusion chromatography, the standard curve was y $-0.0354x+5.5247, R^2$ 0.9989, the average molecular weight of PSP-NP was calculated as 43.0 kDa, which was different from those of polysaccharides as 1.4 kDa (29), 8.9 kDa (30), and 76.0 kDa (26) obtained in another research. Five polysaccharides from *P. cyrtonema* were obtained in another study by ethanol precipitation after extraction with hot water and different concentrations of NaOH solutions, and the molecular weights were found to be 2.1, 24.1, 34.3, 38.6, and 42.6 kDa (31), respectively. But the structure of the polysaccharide extracted by water was different from those extracted by NaOH. The molecular weights of polysaccharides obtained from *P. kingianum* were identified to be 8.1, 134.7, 160, and 178.6 kDa (32–34). It suggested that the molecular weights of polysaccharides from different origins of Polygonati Rhizoma varied. The polysaccharide extracted by water with the molecular weight of 43.0 kDa was not found in other studies.

Chemical composition and molecular weight of PSP-NP

Linkage analysis showed that 4 methylation-derived glycosyl ion fragments were detected from hydrolyzed fragments of PSP-NP. These are T-Man, 1,4-Gal, 1,4-Glc, and 1,4,6-Gal, being quite different from other studies. Polysaccharide from *P. sibiricum* was found to be composed of 1→6 and 1→2,6-Gal and T-Man (26). T-Man was the common composition in the two studies, but there was also a significant difference in glycosidic linkages of Gal. Research also showed that the main chain of polysaccharides from *P. sibiricum* was composed of 1→4Man and 1→4Glc (25). Besides, T-Gal (35) and 1→3Glc (36) were also detected in other studies. The large differences in the structure of PSP might be due to different extraction conditions or gel column purification.

FT-IR and NMR analysis

The FT-IR chromatogram of fraction PSP-NP showed characteristic absorptions of polysaccharides (Figure 3A). The absorption at 3349.82 cm^{-1} indicated the presence of O-H stretching (37). The band at 2936.89 cm^{-1} contributed to C-H stretching and bending vibrations of C-H, CH2, and CH3 (38). The stretching peak at 1024.38 cm^{-1} was due to the presence of C-O glycosidic bonds, suggesting the presence of a pyranoid ring (39).

1D NMR spectroscopy was carried out to further study the structure of PSP-NP. The chemical shift values were analyzed by referring to published literature (28, 29, 40). The 1H spectrum (Figure 3B) showed five-strong signals in the chiral carbon

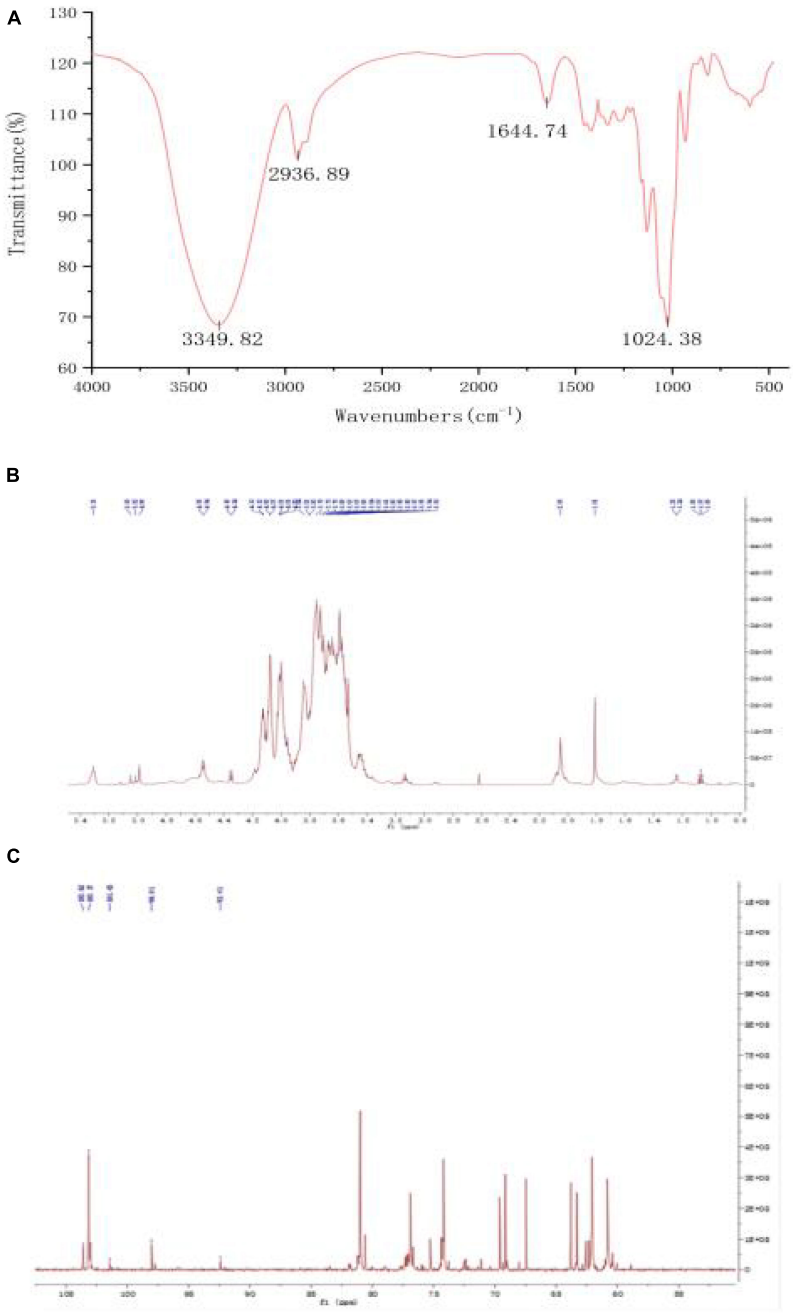

FIGURE 3
Structure elucidation of PSP-NP. **(A)** FT-IR spectrum. **(B)** 1H NMR spectrum. **(C)** 13C NMR spectrum.

region, namely δ 5.35 ppm, δ 5.05 ppm, δ 5.02 ppm, δ 4.99 ppm, and δ 3.55 ppm. It indicated that both α− and β−glycosidic bonds in PSP-NP. δ 5.35 ppm were anomeric protons of the 1,4-α-D-Glc residue, and δ 5.05 ppm was an anomeric proton of the T-α-D-Man residue, while δ 5.02 ppm belonged to T-α-D-Glc. δ 4.99 ppm and δ 3.55 ppm belonged to the anomeric proton with 1,4-β-D-Gal and 1,4,6-β-D-Gal residues, respectively. The rest of the signals belonged to H2∼H6.

In the 13C spectrum (Figure 3C), there were 103.62 ppm, 103.17 ppm, 101.73 ppm, 98.01 ppm, and 92.41 ppm in the chiral carbon region, belonging to 1,4-β-D-Gal, 1,4,6-β-D-Gal, T-α-D-Man, 1,4-α-D-Glc, and T-α-D-Glc, respectively. The rest of the signals belonged to C2∼C6.

The results of the structural analysis showed that PSP-NP was a neutral heteropolysaccharide composed of 1,4-β-D-Gal, 1,4,6-β-D-Gal, T-α-D-Man, 1,4-α-D-Glc, and T-α -D-Glc.

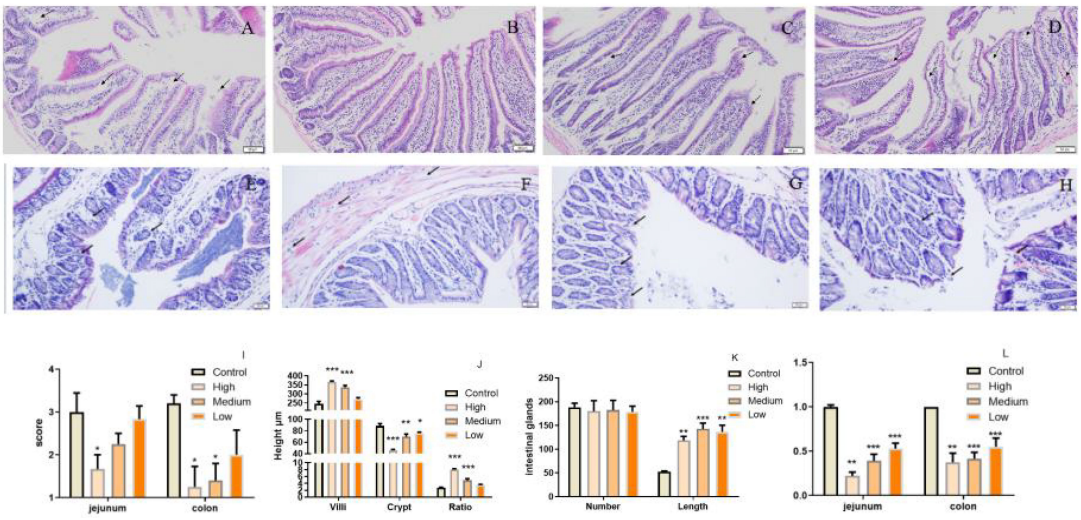

FIGURE 4
PSP-NP improves intestinal integrity of aged mice. **(A–D)** HE stain of jejunum in the control, high, medium and low dose groups, respectively. Arrows indicated the gaps between villi and epithelial cells. It showed that severe shedding of intestinal villi epithelium and gaps at the top of the villi were improved after drug administration. Bar: 200 μm; **(E–H)** HE stain of colon in the control, high, medium and low dose groups, respectively. Arrows indicated the epithelium and intestinal glands. It showed that epithelium dysplastic and intestinal glands were improved after drug administration. Bar: 200 μm; **(I)** The degree of microscopic injury was evaluated by mucosal and inflammatory conditions from a previously published and wildly used scoring system. The jejunum and colon scores decreased as the concentrations of PSP-NP increased and showed remarkable changes in the high group. **(J)** The length of villi and the depth of crypt in HE stain slice were analyzed by Image-Pro Plus, and the ratios were compared. PSP-NP increased the villi length and suppressed the crypt depth, thus heightening the ratio of villus length/crypt depth in jejunum. **(K)** The number and the length of Colonic glands in HE stain slice were analyzed by Image-ProPlus. PSP-NP increased the length of intestinal glands in colon. There was no significant effect on the number of intestinal glands. **(L)** Gene expression of VIP measured by qRT-PCR in jejunum and colon was significantly reduced in all three doses of PSP-NP. Control indicated control group administrated with saline; and High, Medium and Low indicated high, medium and low dose groups administrated with 200/100/50 mg/kg PSP-NP, respectively. Error bars indicated SEM. $N = 8$. All data were analyzed by SPSS with the one-way analysis of variance (ANOVA) by LSD test, $^{*}P < 0.05$, $^{**}P < 0.01$, $^{***}P < 0.001$, compared with the control group.

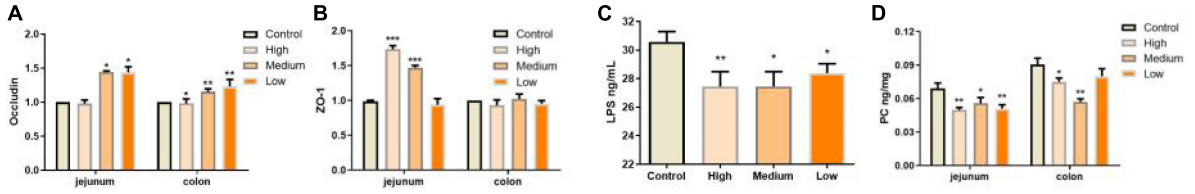

FIGURE 5
PSP-NP improves intestinal integrity of aged mice. **(A)** Gene expressions of tight junction protein Occludin in jejunum were up-regulated in jejunum but down-regulated in colon. $N = 8$. **(B)** Gene expressions of ZO-1 in jejunum and colon, which were both up-regulated. $N = 8$. **(C)** The LPS contents in serum (ng/mL) were analyzed by ELISA, and it was remarkably decreased after administration of PSP-NP, $N = 16$. **(D)** The content of carbonylated proteins (ng/mg) in jejunum and colon was determined by ELISA, and it was statistically reduced by PSP-NP in all the three groups of PSP-NP. Control indicated the control group administrated with saline, and High, Medium and Low indicated the high, medium and low dose groups administrated with 200/100/50 mg/kg PSP-NP, respectively. Error bars indicated SEM. $N = 16$. All data were analyzed by SPSS with the one-way analysis of variance (ANOVA) by LSD test, $^{*}P < 0.05$, $^{**}P < 0.01$, $^{***}P < 0.001$, compared with the control group.

PSP-NP improves intestinal integrity of aged mice

Polygonati Rhizoma was reported to be efficacy in promoting immune response and protecting against aging. The intestine is critical for body immunity and sensitivity to aging progress (41, 42). To determine whether neutral polysaccharides from Polygonati Rhizoma play a role in these processes, we supplied PSP-NP to aged male mice (1-year-old) with different doses and evaluated its effects on intestinal immune function. No statistical difference of bodyweight was found after PSP-NP supplement (Data not shown), and the jejunum of small intestine and colon of large intestine were selected to study the benefits of PSP-NP to intestine. We first focus on the morphology integrity of intestine, which is fundamental for intestinal function and immunity (43, 44). Histologically, while observed defects in

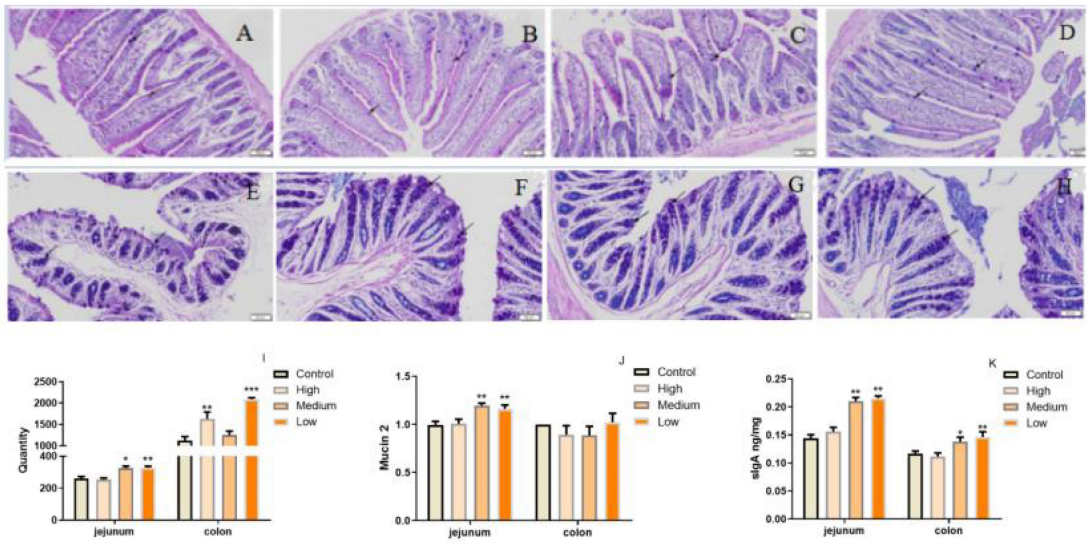

FIGURE 6
PSP-NP enhances the intestinal immunity of aged mice. **(A–D)** AB-PAS stain of jejunum in the control, high, medium and low dose groups, respectively. Arrows indicated the goblet cells. It showed the goblet cells in jejunum treated with different doses of PSP-NP. Bar: 200 μm. **(E–H)** AB-PAS stain of colon in the control, high, medium and low dose groups, respectively. Arrows indicated the goblet cells. It showed the goblet cells in colon treated with different doses of PSP-NP. Bar: 200 μm. **(I)** The goblet cell count of jejunum and colon in the control, high, medium and low dose groups, respectively, it showed the goblet cells increased as the concentrations of PSP-NP increased and showed remarkable changes in the high group. $N = 4$. **(J)** The Gene expression of Mucin 2 in jejunum and colon was measured by qRT-PCR. The quantification showed that PSP-NP up-regulated gene expression of Mucin 2 in jejunum, there is no significant effect in the colon. $N = 4$. **(K)** The content of sIgA in jejunum and colon was analyzed by ELISA. PSP-NP improved the content of sIgA (μg/mg) in the jejunum and colon in the medium and high dose groups. $N = 8$. Error bars indicated SEM. All data were analyzed by SPSS with the one-way analysis of variance (ANOVA) by LSD test, $^{*}P < 0.05$, $^{**}P < 0.01$, $^{***}P < 0.001$, compared with a control group.

intestinal integrity like jejunal villi fracture/fall-off and colonic glands deficiency could be found in aged mice, PSP-NP supplement remarkably improves these phenotypes in a dose-dependent manner (**Figures 4A–H**). These improvements were also revealed by increased "intestinal mucosal injury score" in PSP-NP supplied mice (**Figure 4I**). In addition to this, we quantified the height of jejunal villi and depth of crypt, finding increased villi height and decreased crypt depth, as well as increased ratio of villus length/crypt depth in PSP-NP supplied mice (**Figure 4J**), which suggest enhanced functions like secretion, villi epithelial cells regeneration, digestion and absorption of jejunum (45, 46). Meanwhile, PSP-NP enhanced the length of colonic glands (**Figure 4K**). Congruent with this, in jejunum and colon, we found PSP-NP suppressed the expression of critical neuropeptide—VIP (47) that has the effects on vasodilation and smooth muscle relaxation, also suggesting improvement of intestinal function (**Figure 4L**).

Except for morphology integrity, the intestinal barrier integrity exhibited by epithelial cells performs pivotal roles against external factors and is an important part of intestinal immunity (43). Intestinal epithelial cells-expressed tight junction proteins, including occludin, claudins, zonula occludens (ZOs), etc., are crucial for maintaining epithelial barrier integrity (48). In our study, we found that, especially in the jejunum, PSP-NP could promote the expressions of occludin and ZO-1 in aged mice, suggesting improved barrier function (**Figures 5A,B**). Consistently, in PSP-NP supplied mice, we detected much less concentration of serum LPS, which could be a result of increased intestinal permeability that is affected by aging progress (49; **Figure 5C**). Oxidative stress and damages are thought to be one of the most important pathological characteristics affecting intestinal permeability in aging progress (3, 50, 51). We observed decreased level of intestinal protein carbonyl, an irreversible and oxidatively modified protein product (52), in jejunum and colon of PSP-NP supplied mice (**Figure 5D**), indicating PSP-NP functions with benefits to intestine by mitigating aging-induced oxidative stress. Collectively, these data reveal that PSP-NP could improve defects in morphology, barrier integrity and function of intestine of aged mice.

PSP-NP enhances the intestinal immunity of aged mice

Considering PSP-NP enhances intestinal integrity and function, it is predicted that PSP-NP may have good benefits to the intestinal immunity of aged mice. To address this issue, AB-PAS staining was first performed to quantify the goblet cells is important for intestinal immunity at mucosal surfaces

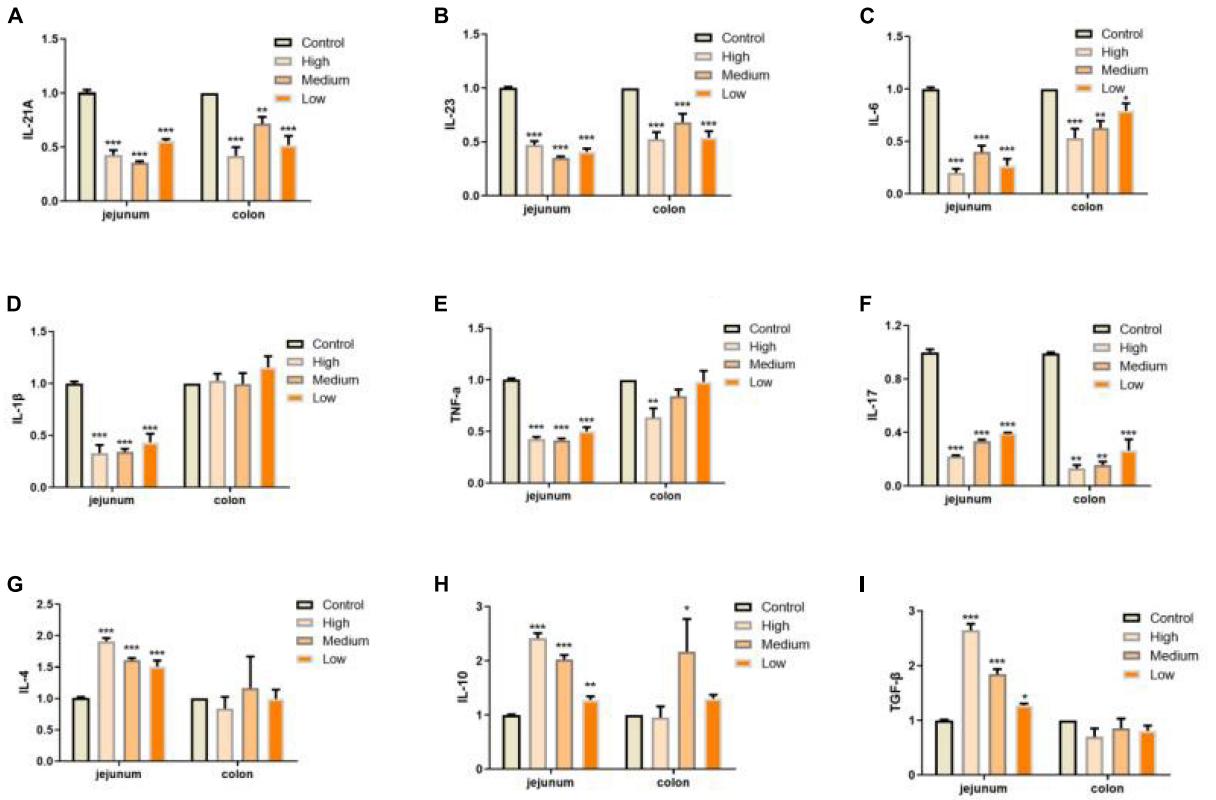

FIGURE 7
PSP-NP enhances the intestinal immunity of aged mice. **(A–I)** Gene expressions of IL-12A, IL-23, IL-6, IL-1β, TNF-α, IL-17, IL-4, IL-10, and TGF-β measured by qRT-PCR in jejunum and colon, respectively. PSP-NP significantly down-regulated the gene expressions of pro-inflammatory factors including IL-12A, IL-23, IL-6, IL-1β (No significant effect in colon), TNF-α and IL-17, and up-regulated anti-inflammatory factors involving IL-4, IL-10, and TGF-β. Control indicated the control group administrated with saline, and High, Medium and Low indicated high, medium and low dose groups administrated with 200/100/50 mg/kg PSP-NP, respectively. Error bars indicated SEM. $N = 8$. All data were analyzed by SPSS with the one-way analysis of variance (ANOVA) by LSD test, $^{*}P < 0.05$, $^{**}P < 0.01$, $^{***}P < 0.001$, compared with a control group.

(53), and the expression of Mucin that is a critical secreted protein from goblet cells that forms a hydrophobic mucus layer on the mucosal surface (54), was then detected. We found that PSP-NP increased the goblet cells' number in jejunum and colon (**Figures 6A–I**), and promoted the expression of Mucin in jejunum (**Figure 6J**). Besides, another secretory immunoglobulin—sIgA was also increased in jejunum and colon of PSP-NP supplied mice (**Figure 6K**). These results reveal the effects of PSP-NP on improving intestinal mucosal immune response.

In addition to defects in intestinal integrity, permeability, inflammation is another phenotype in intestine along with aging progress (55). In our study, we evaluated the expressions of several pro-inflammation cytokines (IL-12A, IL-23, IL-6, IL-1β, TNF-α, and IL-17) and anti-inflammation cytokines (IL-4, IL-10, and TGF-β; 55–57) in jejunum and colon of mice from different groups. We found that PSP-NP could significantly suppress the expressions of inflammation factors and promote the expressions of anti-inflammation factors, suggesting the anti-inflammation bioactivity of PSP-NP in intestine (**Figures 7A–I**). During inflammatory progress, the initial CD4+ T lymphocytes were stimulated by antigen signals, and then differentiated into different T lymphocytes under different conditions, including traditional Th1 and Th2 type effector cells, helper T-cells17 (Th17), and regulatory T-cell (Tregs) (58). The balance of Th1/Th2 cells and Th17/Treg cells are important for intestinal function and immunity. They affect each other, restrict each other, and form a network to maintain a dynamic balance through secreted cytokines (58). IL-12 stimulates the proliferation of activated T cells and promotes the differentiation of Th0 cells to Th1 cells, while Th1 cells secrete IL-6 and further strengthen Th1 cell differentiation (59–61). Th2 cells secrete IL-4 and IL-10, and lymphocytes are mainly differentiated into Th2 cells when IL-4 is highly expressed (60). In this study, IL-12 and IL-6 decreased, while IL-4 and IL-10increased under the treatment of PSP-NP, indicating that the balance of Th1/Th2 trended toward Th2. The presence of Th17 cells can promote inflammation in tissue, while Treg Cells inhibit autoimmunity and inflammation in inflammatory diseases (62, 63). Therefore, the balance between Th17 and

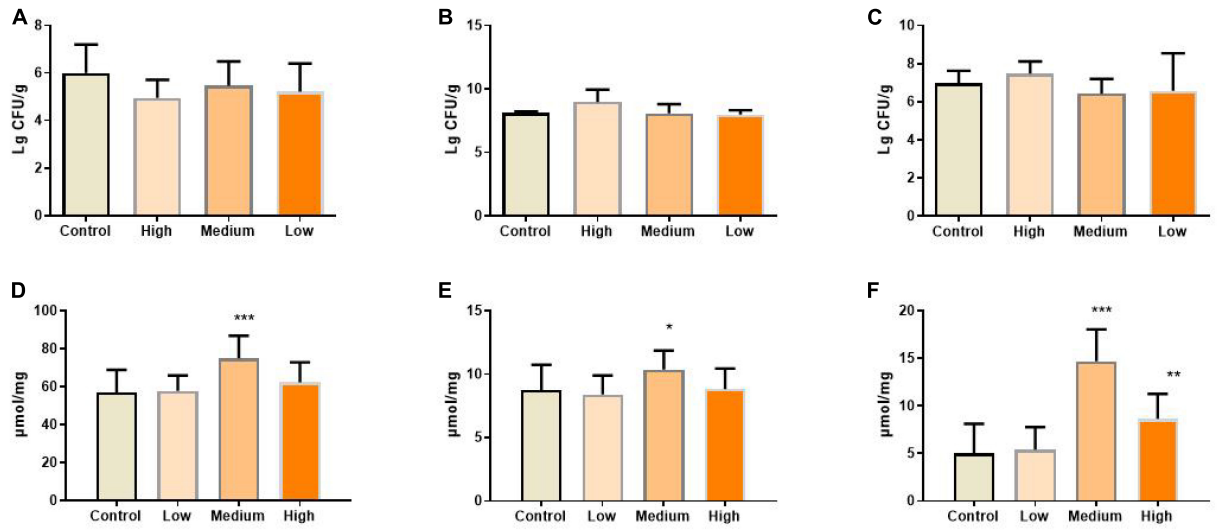

FIGURE 8
(A) The amount of *Escherichia coli* in the content of the intestine was calculated after diluted with 10-fold dilutions of saline from 102 to 107 and cultured in EMB agar medium. It was expressed as. It was reduced by PSP-NP, but showed no significance. **(B)** Bifidobacteria in the content of intestine was cultured in MRS and the amount of Bifidobacteria was calculated and expressed the same as panel **(A)**. It was significantly increased in the high dose group of PSP-NP. **(C)** Lactobacillus in the content of intestine was cultured in BS and the amount of Lactobacillus was calculated and expressed the same as panel **(A)**. The results showed that PSP-NP improved the amount of Lactobacillus. **(D–F)** The contents of acetic acid, propionic acid and butyric acid, respectively, were analyzed by GC. They were all remarkably increased, and the middle dose group showed the best activities. Control indicated the control group administrated with saline, and High, Medium, and Low indicated the high, medium and low dose groups administrated with 200/100/50 mg/kg PSP-NP, respectively. Error bars indicated SEM. $N = 16$. All data were analyzed by SPSS with the one-way analysis of variance (ANOVA) by LSD test, $^{*}P < 0.05$, $^{**}P < 0.01$, $^{***}P < 0.001$, compared with the control group.

Treg cells is crucial. High expression of TGF-β initiates Treg differentiation, which will induce Th17 to highly express both TGF-β and IL-6, and the IL-23 secreted by Th17 maintains the stability and maturity of Th17 in later stages of differentiation (64). In this study, PSP-NP suppressed the expression of interleukins related to Th17, including IL-23, IL-6, IL-1β, TNF-α, and IL-17, while the gene expression of IL-4, IL-10, and the TGF-β expression secreted by Treg cells was increased under PSP-NP treatment. These results suggest that the balance of Th17/Treg cells was also implicated in intestinal inflammatory progress affected by PSP-NP supplement in aged mice.

PSP-NP improves the compositions of gut microbe and short chain fatty acid

Gut bacteria are crucial for maintaining immune and metabolic homeostasis and protecting against pathogens (65), and multiple polysaccharides were reported to be involved in regulating gut microbe homeostasis (62, 66). Aging progress was reported to affect the intestinal microbial diversity shrinks, reducing the number of beneficial bacteria and increasing facultative anaerobic bacteria (67). For example, higher amounts of Enterobacteriaceae and Coccus were found in aged subjects, while the amounts of Bifidobacterium and Lactobacillus reduced significantly (68, 69). Also, the gut microbiome implicates in age-related inflammation and intestinal permeability defects (55). To determine whether the benefits of PSP-NP to intestinal function and immunity are due to its effects on regulating the composition of gut bacteria, the level of Bifidobacterium, Lactobacillus, and *Escherichia coli* in the gut contents were quantified. Results showed that the population of Bifidobacterium and Lactobacillus increased, while *Escherichia coli* decreased in PSP-NP-supplied mice (**Figures 8A–C**). Congruent with improvements in gut microbe homeostasis, the levels of three kinds of short-chain fatty acids (SCFAs), which is produced by gut microbes and important immune signal molecules, are increased in gut of aged mice supplied with PSP-NP (**Figures 8D–F**). This result is consistent with the findings showing polysaccharides from *P. kingianum* also increase the amount of Lactobacillus in gut (32, 70). As Bifidobacterium and Lactobacillus were reported to promote the secretion of sIgA, we think that the increased level of sIgA in PSP-NP supplied mice would be due to enrichment of Bifidobacterium and Lactobacillus populations (71, 72). In addition, Bifidobacterium and Lactobacilli are also implicated in mediating Treg/Th17 balance toward Treg, which affects the balance of cytokines (73). Therefore, improvements in microbe homeostasis defects could be the fundamental mechanism regulating intestinal function and immunity by PSP-NP.

Conclusion

In this study, one neutral polysaccharide with a high yield was obtained from rhizomes of *P. sibiricum*. PSP-NP was characterized as a neutral heteropolysaccharide composed of 1,4-β-D-Gal,1,4, 6-β-D-Gal, T-α-D-Man, 1, 4-α-D-Glc, and T-α-D-Glc with a molecular weight of 43.0 kDa. Experiments on aged mice *in vivo* showed that PSP-NP could regulate the composition of intestinal microbiome, and promote short chain fatty acids generation to increase intestinal morphology integrity and barrier function, enhance immune function, inhibit inflammation in the intestine of aged mice, which will be valuable for its further applications on the treatments of aging-related intestinal diseases.

Data availability statement

The original contributions presented in this study are included in the article/supplementary material, further inquiries can be directed to the corresponding author.

Ethics statement

This animal study was reviewed and approved by the Animal Care and Use Committee of Sichuan Agricultural University.

Author contributions

MT-T carried out the data curation. XF carried out the formal analysis. L-XL carried out the funding acquisition. BF and WL investigated the data. CH, XZ, and L-ZY performed the methodology. Y-FZ carried out the project administration. BP carried out the resources. X-XL and H-QT carried out the software. Z-QY supervised the data. BF and XS validated the data. L-XL and XF wrote the original draft of the manuscript. M-TT and CH wrote, reviewed, and edited the manuscript. All authors read and agreed to the published version of the manuscript.

Funding

This work was supported in part by the Youth Science Fund Project of National Natural Science Foundation of China (82004041). We acknowledge the support by the Natural Medicine Research Center, College of Veterinary Medicine of Sichuan Agricultural University for providing the experimental site and relevant experimental instruments.

Conflict of interest

The authors declare that the research was conducted in the absence of any commercial or financial relationships that could be construed as a potential conflict of interest.

Publisher's note

All claims expressed in this article are solely those of the authors and do not necessarily represent those of their affiliated organizations, or those of the publisher, the editors and the reviewers. Any product that may be evaluated in this article, or claim that may be made by its manufacturer, is not guaranteed or endorsed by the publisher.

References

1. Singh T, Newman AB. Inflammatory markers in population studies of aging. *Ageing Res Rev.* (2011) 10:319–29. doi: 10.1016/j.arr.2010.11.002

2. Xie Y, Mu C, Kazybay B, Sun Q, Kutzhanova A, Nazarbek G, et al. Network pharmacology and experimental investigation of *Rhizoma polygonati* extract targeted kinase with herbzyme activity for potent drug delivery. *Drug Deliv.* (2021) 28:2187–97. doi: 10.1080/10717544.2021.1977422

3. Drozdowski L, Thomson AB. Aging and the intestine. *World J Gastroenterol.* (2006) 12:7578–84. doi: 10.3748/wjg.v12.i47.7578

4. Mowat AM, Agace WW. Regional specialization within the intestinal immune system. *Nat Rev Immunol.* (2014) 14:667–85. doi: 10.1038/nri3738

5. Funk MC, Zhou J, Boutros M. Ageing, metabolism and the intestine. *EMBO Rep.* (2020) 21:e50047. doi: 10.15252/embr.202050047

6. Jiao J, Jia X, Liu P, Zhang Q, Liu F, Ma C, et al. Species identification of polygonati rhizoma in China by both morphological and molecular marker methods. *C R Biol.* (2018) 341:102–10. doi: 10.1016/j.crvi.2017.10.004

7. Hong-Min R, Ya-Ling D, Jin-Lian Z, Xian-Wen YE, Lan-Ting X, Min-Min L, et al. [Research progress on processing history evolution, chemical components and pharmacological effects of Polygonati Rhizoma]. *Zhongguo Zhong Yao Za Zhi.* (2020) 45:4163–82. doi: 10.19540/j.cnki.cjcmm.20200522.601

8. Li XL, Ma RH, Zhang F, Ni ZJ, Thakur K, Wang S, et al. Evolutionary research trend of Polygonatum species: a comprehensive account of their transformation from traditional medicines to functional foods. *Crit Rev Food Sci Nutr.* (2021) [Online ahead of print]. doi: 10.1080/10408398.2021.1993783.

9. Zhao P, Zhao C, Li X, Gao Q, Huang L, Xiao P, et al. The genus Polygonatum: a review of ethnopharmacology, phytochemistry and pharmacology. *J Ethnopharmacol.* (2018) 214:274–91. doi: 10.1016/j.jep.2017.12.006

10. Li L, Thakur K, Cao YY, Liao BY, Zhang JG, Wei ZJ. Anticancerous potential of polysaccharides sequentially extracted from *Polygonatum cyrtonema* Hua in Human cervical cancer Hela cells. *Int J Biol Macromol.* (2020) 148:843–50. doi: 10.1016/j.ijbiomac.2020.01.223

11. Li L, Thakur K, Liao BY, Zhang JG, Wei ZJ. Antioxidant and antimicrobial potential of polysaccharides sequentially extracted from *Polygonatum cyrtonema* Hua. *Int J Biol Macromol.* (2018) 114:317–23. doi: 10.1016/j.ijbiomac.2018.03.121

12. Li L, Liao BY, Thakur K, Zhang JG, Wei ZJ. The rheological behavior of polysaccharides sequential extracted from *Polygonatum cyrtonema* Hua. *Int J Biol Macromol.* (2018) 109:761–71. doi: 10.1016/j.ijbiomac.2017.11.063

13. Chen H, Feng R, Guo Y, Sun L, Jiang J. Hypoglycemic effects of aqueous extract of *Rhizoma Polygonati Odorati* in mice and rats. *J Ethnopharmacol.* (2001) 74:225–9. doi: 10.1016/s0378-8741(00)00359-7

14. Austarheim I, Christensen BE, Hegna IK, Petersen BO, Duus JO, Bye R, et al. Chemical and biological characterization of pectin-like polysaccharides from the bark of the Malian medicinal tree *Cola cordifolia*. *Carbohyd Polym.* (2012) 89:259–68. doi: 10.1016/j.carbpol.2012.03.005

15. Ciucanu I, Kerek F. A simple and rapid method for the permethylation of carbohydrates. *Carbohyd Res.* (1984) 131:209–17. doi: 10.1016/0008-6215(84)85242-8

16. Sweet DP, Shapiro RH, Albersheim P. Quantitative analysis by various g.l.c. response-factor theories for partially methylated and partially ethylated alditol acetates. *Carbohyd Res.* (1975) 40:217–25. doi: 10.1016/S0008-6215(00)82604-X

17. Zhu ZY, Liu RQ, Si CL, Fang Z, Zhang YM. Structural analysis and anti-tumor activity comparison of polysaccharides from Astragalus. *Carbohyd Polym.* (2011) 85:895–902. doi: 10.1016/j.carbpol.2011.04.020

18. Yan JK, Lin L, Wang ZM, Wu JY. Structural elucidation of an exopolysaccharide from mycelial fermentation of a *Tolypocladium* sp. fungus isolated from wild *Cordyceps sinensis*. *Carbohyd Polym.* (2010) 79:125–30. doi: 10.1016/j.carbpol.2009.07.047

19. Zhou P, Zhao Y, Pan Z, Li Y, Gui T, Wang J, et al. Microbial mechanistic insight into the role of inulin in improving maternal health in a pregnant sow model. *Front Microbiol.* (2017) 8:2242. doi: 10.3389/fmicb.2017.02242

20. Bradford MM. A rapid and sensitive method for the quantitation of microgram quantities of proteins utilizing the principle of protein-dye-binding. *Anal Biochem.* (1976) 72:248–54. doi: 10.1006/abio.1976.9999

21. Fang, HU, Zhou JJ, Chen AJ. The optimum methods of polygonatum polysaccharide by microwave-assisted extraction. *Res Pract Chin Med.* (2015) 29:52–54. doi: 10.13728/j.1673-6427.2015.04.017

22. Fu S, Qian J, Chen L, Liu L. Extracting of polygonatum polysaccharides and effecting on the immunological activity in immunosuppressed mice. *J Chin Institute Food Sci Technol.* (2013) 13:68–72.

23. Zai QQ, Qin Z, Ye L. Effect of rhizoma polygonati on the function of endothelial progenitor cells and telomerase activity in nature senescent rats. *Chin J Integr Tradit West Med.* (2016) 36:1480–85.

24. Cui X, Wang S, Cao H, Guo H, Li Y, Xu F, et al. A review. The bioactivities and pharmacological applications of *Polygonatum sibiricum* polysaccharides. *Molecules.* (2018) 23:1170. doi: 10.3390/molecules23051170

25. Yelithao K, Surayot U, Lee JH, You S. RAW264.7 cell activating glucomannans extracted from rhizome of *Polygonatum sibiricum*. *Prev Nutr Food Sci.* (2016) 21:245–54. doi: 10.3746/pnf.2016.21.3.245

26. Zhang H, Cao Y, Chen L, Wang J, Tian Q, Wang N, et al. A polysaccharide from *Polygonatum sibiricum* attenuates amyloid-β-induced neurotoxicity in PC12 cells. *Carbohyd Polym.* (2015) 117:879–86. doi: 10.1016/j.carbpol.2014.10.034

27. Liu N, Dong Z, Zhu X, Xu H, Zhao Z. Characterization and protective effect of *Polygonatum sibiricum* polysaccharide against cyclophosphamide-induced immunosuppression in Balb/c mice. *Int J Biol Macromol.* (2018) 107:796–802. doi: 10.1016/j.ijbiomac.2017.09.051

28. Liu L, Dong Q, Dong XT, Fang JN, Ding K. Structural investigation of two neutral polysaccharides isolated from rhizome of *Polygonatum sibiricum*. *Carbohyd Polym.* (2007) 70:304–9. doi: 10.1016/j.carbpol.2007.04.012

29. Li, Tian LN, Ren ZX, Long ZJ. Structural analysis and functional activity research progress of *Polygonatum sibiricum* polysaccharides. *Chin J Exp Tradit Med Formul.* (2015) 362:430–40. doi: 10.1016/j.jmb.2006.07.007

30. Zhang TT, Wei HU, Wang HF, Ran YX, Zheng CY. Separation, purification and chemical characterization of a polysaccharide fraction from *Polygonatum cyrtonema* Hua in Jiuhua mountain. *Food Sci.* (2011) 32:48–51. doi: 10.1007/s11518-011-5154-1

31. Wang K, Yue YD, Tang F, Hang X, Sun J, Wang J. Sequential extraction and structural analysis of polysaccharides from *Polygonatum cyrtonema* Hua. *Nat Prod Res Dev.* (2014) 26:364–9.

32. Gu W, Wang Y, Zeng L, Dong J, Bi Q, Yang X, et al. Polysaccharides from *Polygonatum kingianum* improve glucose and lipid metabolism in rats fed a high fat diet. *Biomed Pharmacother.* (2020) 125:109910. doi: 10.1016/j.biopha.2020.109910

33. Wang Y, Liu N, Xia X, Li Q, Sun D, Zhao Z. Purification, structural characterization and in vivo immunoregulatory activity of a novel polysaccharide from *Polygonatum sibiricum*. *Int J Biol Macromol.* (2020) 160:688–94. doi: 10.1016/j.ijbiomac.2020.05.245

34. Wu QR, Hu S, Yang GZ, Mei ZN. Separation, purification and structural studies of polysaccharides from *Polygonatum kingianum*. *Chem Indus For Prod.* (2005) 25:80–2.

35. Shu-Jie LI, Lin HZ, Shi SY, Lin JM. Separation, purification, and structual analysis of PSP-1-A of *Polygonatum sibiricmu* polysaccharides. *Henan Tradit Chin Med.* (2015) 5:253–7. doi: 10.16367/j.issn.1003-5028.2015.06.0604

36. Wei B, Min XU, Lei YU, Yang Y. Isolation, purification and characterization of oligosaccharide from Polygonati Rhizoma. *Chin Tradit Patent Med.* (2012) 34:694–7.

37. Han L, Suo Y, Yang Y, Meng J, Hu N. Optimization, characterization, and biological activity of polysaccharides from *Berberis dasystachya* Maxim. *Int J Biol Macromol.* (2016) 85:655–66. doi: 10.1016/j.ijbiomac.2015.10.038

38. Wang Y, Liu X, Zhang J, Liu G, Liu Y, Wang K, et al. Structural characterization and in vitro antitumor activity of polysaccharides from *Zizyphus jujuba* cv. Muzao. *RSC Adv.* (2015) 5:7860–7.

39. Chai Y, Zhao M. Purification, characterization and anti-proliferation activities of polysaccharides extracted from *Viscum coloratum* (Kom.) Nakai. *Carbohydr Polym.* (2016) 149:121–30. doi: 10.1016/j.carbpol.2016.04.090

40. Zhao P, Zhou H, Zhao C, Li X, Wang Y, Wang Y, et al. Purification, characterization and immunomodulatory activity of fructans from *Polygonatum odoratum* and *P. cyrtonema*. *Carbohydr Polym.* (2019) 214:44–52. doi: 10.1016/j.carbpol.2019.03.014

41. Wang Q, Qi Y, Shen W, Xu J, Wang L, Chen S, et al. The aged intestine: performance and rejuvenation. *Aging Dis.* (2021) 12:1693–712. doi: 10.14336/ad.2021.0202

42. Mabbott NA, Kobayashi A, Sehgal A, Bradford BM, Pattison M, Donaldson DS. Aging and the mucosal immune system in the intestine. *Biogerontology.* (2015) 16:133–45. doi: 10.1007/s10522-014-9498-z

43. Chelakkot C, Ghim J, Ryu SH. Mechanisms regulating intestinal barrier integrity and its pathological implications. *Exp Mol Med.* (2018) 50:1–9. doi: 10.1038/s12276-018-0126-x

44. Zhang K, Hornef MW, Dupont A. The intestinal epithelium as guardian of gut barrier integrity. *Cell Microbiol.* (2015) 17:1561–9. doi: 10.1111/cmi.12501

45. Tang X, Liu H, Yang S, Li Z, Zhong J, Fang R. Epidermal growth factor and intestinal barrier function. *Mediat Inflamm.* (2016) 2016:1927348. doi: 10.1155/2016/1927348

46. O'Brien DP, Nelson LA, Huang FS, Warner BW. Intestinal adaptation: structure, function, and regulation. *Semin Pediatr Surg.* (2001) 10:56–64. doi: 10.1053/spsu.2001.22383

47. Talbot J, Hahn P, Kroehling L, Nguyen H, Li D, Littman DR. Feeding-dependent VIP neuron-ILC3 circuit regulates the intestinal barrier. *Nature.* (2020) 579:575–80. doi: 10.1038/s41586-020-2039-9

48. Günzel D, Yu AS. Claudins and the modulation of tight junction permeability. *Physiol Rev.* (2013) 93:525–69. doi: 10.1152/physrev.00019.2012

49. Ma TY, Hollander D, Dadufalza V, Krugliak P. Effect of aging and caloric restriction on intestinal permeability. *Exp Gerontol.* (1992) 27:321–33. doi: 10.1016/0531-5565(92)90059-9

50. Liguori I, Russo G, Curcio F, Bulli G, Aran L, Della-Morte D, et al. Oxidative stress, aging, and diseases. *Clin Interv Aging.* (2018) 13:757–72. doi: 10.2147/cia.S158513

51. Hagen TM. Oxidative stress, redox imbalance, and the aging process. *Antioxid Redox Signal.* (2003) 5:503–6. doi: 10.1089/152308603770310149

52. Sohal RS, Orr WC. The redox stress hypothesis of aging. *Free Radic Biol Med.* (2012) 52:539–55. doi: 10.1016/j.freeradbiomed.2011.10.445

53. Knoop KA, Newberry RD. Goblet cells: multifaceted players in immunity at mucosal surfaces. *Mucosal Immunol.* (2018) 11:1551–7. doi: 10.1038/s41385-018-0039-y

54. Ma J, Rubin BK, Voynow JA. Mucins, mucus, and goblet cells. *Chest.* (2018) 154:169–76. doi: 10.1016/j.chest.2017.11.008

55. Thevaranjan N, Puchta A, Schulz C, Naidoo A, Szamosi JC, Verschoor CP, et al. Age-associated microbial dysbiosis promotes intestinal permeability, systemic inflammation, and macrophage dysfunction. *Cell Host Microbe.* (2017) 21:455–466.e4. doi: 10.1016/j.chom.2017.03.002

56. Murphy CA, Langrish CL, Chen Y, Blumenschein W, McClanahan T, Kastelein RA, et al. Divergent pro- and antiinflammatory roles for IL-23 and IL-12 in joint autoimmune inflammation. *J Exp Med.* (2003) 198:1951–7. doi: 10.1084/jem.20030896

57. Deng Y, Chang C, Lu Q. The inflammatory response in psoriasis: a comprehensive review. *Clin Rev Allergy Immunol.* (2016) 50:377–89. doi: 10.1007/s12016-016-8535-x

58. Bettelli E, Carrier Y, Gao W, Korn T, Strom TB, Oukka M, et al. Reciprocal developmental pathways for the generation of pathogenic effector TH17 and regulatory T cells. *Nature.* (2006) 441:235–8. doi: 10.1038/nature 04753

59. Bystrom J, Clanchy FI, Taher TE, Mangat P, Jawad AS, Williams RO, et al. TNFα in the regulation of Treg and Th17 cells in rheumatoid arthritis and other autoimmune inflammatory diseases. *Cytokine.* (2018) 101:4–13. doi: 10.1016/j.cyto. 2016.09.001

60. McGuirk P, Mills KH. Pathogen-specific regulatory T cells provoke a shift in the Th1/Th2 paradigm in immunity to infectious diseases. *Trends Immunol.* (2002) 23:450–5. doi: 10.1016/s1471-4906(02)02288-3

61. Moser M, Murphy KM. Dendritic cell regulation of TH1-TH2 development. *Nat Immunol.* (2000) 1:199–205. doi: 10.1038/79734

62. Lee JY, Hall JA, Kroehling L, Wu L, Najar T, Nguyen HH, et al. Serum amyloid a proteins induce pathogenic Th17 cells and promote inflammatory disease. *Cell.* (2020) 180:79–91.e16. doi: 10.1016/j.cell.2019.11.026

63. Lee GR. The balance of Th17 versus treg cells in autoimmunity. *Int J Mol Sci.* (2018) 19:730. doi: 10.3390/ijms19030730

64. Li S, Bi Y, Wang Q, Xu M, Ma Z, Yang Y, et al. Transplanted mouse liver stem cells at different stages of differentiation ameliorate concanavalin A-induced acute liver injury by modulating Tregs and Th17 cells in mice. *Am J Transl Res.* (2019) 11:7324–37.

65. Thursby E, Juge N. Introduction to the human gut microbiota. *Biochem J.* (2017) 474:1823–36. doi: 10.1042/bcj20160510

66. Holscher HD. Dietary fiber and prebiotics and the gastrointestinal microbiota. *Gut Microbes.* (2017) 8:172–84. doi: 10.1080/19490976.2017.1290756

67. Odamaki T, Kato K, Sugahara H, Hashikura N, Takahashi S, Xiao JZ, et al. Age-related changes in gut microbiota composition from newborn to centenarian: a cross-sectional study. *BMC Microbiol.* (2016) 16:90. doi: 10.1186/s12866-016-0708-5

68. Amara AA, Shibl A. Role of Probiotics in health improvement, infection control and disease treatment and management. *Saudi Pharm J.* (2015) 23:107–14. doi: 10.1016/j.jsps.2013.07.001

69. Agans R, Rigsbee L, Kenche H, Michail S, Khamis HJ, Paliy O. Distal gut microbiota of adolescent children is different from that of adults. *FEMS Microbiol Ecol.* (2011) 77:404–12. doi: 10.1111/j.1574-6941.2011.01120.x

70. Yan H, Lu J, Wang Y, Gu W, Yang X, Yu J. Intake of total saponins and polysaccharides from *Polygonatum kingianum* affects the gut microbiota in diabetic rats. *Phytomedicine.* (2017) 26:45–54. doi: 10.1016/j.phymed.2017.01.007

71. Camilleri M, Madsen K, Spiller R, Greenwood-Van Meerveld B, Verne GN. Intestinal barrier function in health and gastrointestinal disease. *Neurogastroenterol Motil.* (2012) 24:503–12. doi: 10.1111/j.1365-2982.2012.01921.x

72. Macpherson AJ, Uhr T. Induction of protective IgA by intestinal dendritic cells carrying commensal bacteria. *Science.* (2004) 303:1662–5. doi: 10.1126/ science.1091334

73. de Toro-Martín J, Arsenault BJ, Després JP, Vohl MC. Precision nutrition: a review of personalized nutritional approaches for the prevention and management of metabolic syndrome. *Nutrients.* (2017) 9:913. doi: 10.3390/nu9080913

frontiers | Frontiers in Nutrition

TYPE Original Research
PUBLISHED 20 September 2022
DOI 10.3389/fnut.2022.998942

Check for updates

OPEN ACCESS

EDITED BY
Xin Wang,
Northwest A&F University, China

REVIEWED BY
Fernando Amaury Ferreira,
Universidad de la República, Uruguay
Chaofan Guo,
Kunming University of Science and Technology, China
Yajing Qi,
Jiangsu University, China

*CORRESPONDENCE
Jun Ming
mingjun@caas.cn
Panpan Yang
yangpanpan@caas.cn

†These authors share first authorship

SPECIALTY SECTION
This article was submitted to Food Chemistry, a section of the journal Frontiers in Nutrition

RECEIVED 20 July 2022
ACCEPTED 29 August 2022
PUBLISHED 20 September 2022

CITATION
Song Z, Zhang Y, Luo Y, Ti Y, Wang W, Ban Y, Tang Y, Hou Y, Xu L, Ming J and Yang P (2022) Systematic evaluation on the physicochemical characteristics of a series polysaccharides extracted from different edible lilies by ultrasound and subcritical water. *Front. Nutr.* 9:998942. doi: 10.3389/fnut.2022.998942

COPYRIGHT
© 2022 Song, Zhang, Luo, Ti, Wang, Ban, Tang, Hou, Xu, Ming and Yang. This is an open-access article distributed under the terms of the Creative Commons Attribution License (CC BY). The use, distribution or reproduction in other forums is permitted, provided the original author(s) and the copyright owner(s) are credited and that the original publication in this journal is cited, in accordance with accepted academic practice. No use, distribution or reproduction is permitted which does not comply with these terms.

Systematic evaluation on the physicochemical characteristics of a series polysaccharides extracted from different edible lilies by ultrasound and subcritical water

Zihan Song[1†], Yanli Zhang[1†], Yulin Luo[2†], Yongrui Ti[1], Weizhen Wang[3], Yuqian Ban[1], Yuchao Tang[1], Yuqing Hou[1], Leifeng Xu[1], Jun Ming[1*] and Panpan Yang[1*]

[1]Institute of Vegetables and Flowers, Chinese Academy of Agricultural Sciences, Beijing, China, [2]College of Horticulture, Shanxi Agricultural University, Taigu, China, [3]School of Agriculture, Yunnan University, Kunming, China

A series polysaccharide samples extracted from three edible lilies (*Lilium davidii* var. *willmottiae*, *Lilium brownii* var. *viridulum*, and *Lilium lancifolium*) by subcritical water and ultrasound-assisted extraction were systematically compared. The results showed that extraction method was a more important factor than lily species. Subcritical water extracted lily polysaccharides (S-LP) with higher yield, molecular weight, neutral glucose and uronic acid content as well as apparent viscosity. Ultrasound-assisted extracted lily polysaccharides (U-LP) with higher reducing sugars and protein content. Moreover, due to the degradation of glycosidic bonds, ultrasonic extraction was easier to obtain lower molecular weight polysaccharides. In addition, the extraction method significantly affected the monosaccharide proportion of polysaccharides, but had no effect on type. Glucose was the main component in S-LP, and glucose and mannose were the main components in U-LP. The micromorphology of different polysaccharide samples was similar, and the scanning electron microscope (SEM) images showed regular/irregular particle clusters with different particle sizes. Overall, the relationships between extraction methods, lily species and polysaccharide properties were preliminarily elucidated, providing a reference for the targeted extraction of specific lily polysaccharides (LP).

KEYWORDS

lily, polysaccharides, subcritical water, ultrasonic-assisted extraction, physicochemical properties

Abbreviations: LP, Lily polysaccharides; S-LP, Subcritical water extracted lily polysaccharides; U-LP, Ultrasound-assisted extracted lily polysaccharides; LDWP, *Lilium davidii* var. *willmottiae* polysaccharides; LBVP, *Lilium brownii* var. *viridulum* polysaccharides; LLAP, *Lilium lancifolium* polysaccharides.

Introduction

Lily belongs to the genus *Lilium* of the family Liliaceae. It is not only ornamental, but also has edible and medicinal value. In China, *Lilium davidii* var. *willmottiae*, *Lilium brownii* var. *viridulum* and *Lilium lancifolium* are the largest planting species and known as the "three edible lilies." Bulb, as the important edible part of lily, is not only a good source of nutrient substances including starch, protein and dietary fiber, but also contains a variety of bioactive substances, such as polysaccharides, saponin, and alkaloids (1, 2). Lily polysaccharides (LP) show various biological capacities including such as anti-tumor (3), anti-oxidation (4) and immunomodulatory effects (5). At present, the studies on Lily polysaccharides mainly focus on functional and structural analysis (6–8). There are few studies on the chemical composition, monosaccharide composition and rheology of different lily species on polysaccharides.

There are numerous extraction methods which have been explored for the preparation of polysaccharides, and different methods have their own advantages and disadvantages (9). Ultrasonic-assisted extraction (UAE) is a common method to extract lily polysaccharides (10). The technique extracts polysaccharides through cavity effect, thermal effect and mechanical effect produced by ultrasound. However, temperature rise during extraction is difficult to monitor, which may lead to low reproducibility of results (10). In addition, ultrasound treatment is easy to generate polysaccharides with low molecular weight (Mw) and can degrade part of the polysaccharides (11, 12).

Subcritical water (SW) is increasingly used for the extraction of polysaccharides and other bioactive substances in recent years due to its advantages of energy saving, environmental protection and high extraction efficiency (13). However, no systematic evaluation on lily polysaccharides extracted by subcritical water has been reported. Subcritical water is a liquid hot water with a temperature above the boiling point (100°C) and below the critical point (374°C) (14). In the subcritical state, the dielectric constant, polarity and viscosity of water decrease and the ionization constant increases, which can improve the heat transfer process and increase the extraction efficiency of polysaccharides (15–17). However, subcritical water is not suitable for industrial production due to its cumbersome operation.

To the best of our knowledge, there has not been systematic evaluation for the relationship between the extraction methods and different lily species on physicochemical properties of polysaccharides. In this study, we collected the bulbs of *Lilium davidii* var. *willmottiae*, *Lilium brownii* var. *Viridulu*m, and *Lilium lancifolium* as raw materials to prepare polysaccharides. And systematically compared the polysaccharide samples obtained by subcritical water and ultrasonic-assisted extraction for the first time. By comparing the yield, physicochemical, spectral and rheological properties, the regularity of LP prepared by two extraction methods was clarified, and the differences of physicochemical indexes of different lily species were observed. This study will provide some references for the extraction method and variety selection of lily polysaccharides based on different research purposes.

Materials and methods

Materials and reagents

Fresh bulbs from three edible lily species, *Lilium davidii* var. *willmottiae*, *Lilium brownii* var. *viridulum*, and *Lilium lancifolium*. were collected from Lanzhou City, Gansu Province, Longhui County, Hunan Province, and Longshan County, Hunan Province, China, respectively. Monosaccharides (fucose, rhamnose, arabinose, galactose, glucose, xylose, mannose, fructose, ribose, galacturonic acid, glucuronic acid, mannuronic acid, and guluronic acid) were purchased from Sigma Company (St. Louis, MO, USA). A series of polyethylene glycol standards were purchased from PSS Polymer Standards Service GmbH. Other commonly used reagents were analytically pure and purchased from local suppliers.

The polysaccharide extraction

Subcritical water extraction

Briefly, subcritical water extraction was carried out in a reactor equipped with a heating system and a control system. The dry powder of lily bulb and distilled water were added in a 1 L reaction kettle with a ratio of 1:15, and extracted for 10 min when the temperature raised to 150°C. After the reaction, the mixture was centrifuged at 6,000 rpm for 10 min to obtain the supernatant. The supernatant was added with anhydrous ethanol (>99.5%) and precipitated at 4°C for 12 h. The precipitates were collected by centrifugation again and freeze-dried to obtain three kinds of lily polysaccharides (9, 18).

Ultrasonic-assisted extraction

Ultrasonic processor was used for ultrasonic-assisted extraction. The ratio of material to liquid was 1:20 and the reaction condition was 65°C for 20 min. The three kinds of lily polysaccharides were obtained by the same process of alcohol precipitation, centrifugation and freeze-dried described above. The lily polysaccharides yield (%) was calculated as follows:

$$\text{Lily polysaccharides Yield (wt\%)} = W_2/W_1 \times 100 \quad (1)$$

Where: W_1 was the residue dried (g) weight of lily bulb, W_2 was the weight of the extracted lily polysaccharides (g) (19).

Physiochemical properties of lily polysaccharides

Chemical composition

The content of neutral sugar and uronic acid were determined by phenol-sulfuric acid method and carbazole method, respectively, using glucose and D-galacturonic acid as standard (20, 21). The content of reducing sugar was determined using the 3,5-dinitrosalicylic acid (DNS) method (22). Protein content was determined by Bradford method with bovine serum albumin as standard (23).

Molecular weight

The Molecular weight (Mw) of LP samples were detected by gel permeation chromatography (GPC) (Agilent1260, California, USA) (9). 40 μl LP solution (1 mg/ml) was dissolved in sodium azide and sodium acetate was added into the chromatographic system. Waters Ultrahydrogel TM120 TM250 TM500 water-soluble gel column (7.8 × 300 mm triple column series) was used for the determination. Forty microliters LP solution (1 mg/ml) was dissolved in sodium azide and sodium acetate was added into the chromatographic system. The analyzed at 30°C at a flow rate of 1 ml/min. Polyethylene glycol standards with different molecular weights (1,960; 4,290; 7,130; 12,600; 20,600; 25,300; 44,000; 78,300; 152,000; 326,000) were administered for calibration.

Monosaccharide composition

The monosaccharide composition of lily polysaccharides was determined by high performance anion exchange chromatography (HPAEC) (24). Five milligrams crude LP samples were hydrolyzed in sealed ampoule with trifluoroacetic acid (2 M) at 121°C for 2 h. Then the samples were dried by nitrogen and washed by methanol, and the procedure was repeated three times. The residue was re-dissolved in deionized water and filtered by 0.22 μm microporous membrane for measurement. The chromatographic system was a Thermo ICS5000 ion chromatography system (ICS5000, Thermo Fisher Scientific, MA, USA). Chromatographic conditions included a CarboPac PA-20 Ionic Exchange column (3 × 150 mm) and a pulsed Amperometric detector (PAD; Dionex ICS 5000 system; Shanghai, China). The loading volume was 5 μl, and the flow rate was 0.5 ml/min. The solvent system included solvent system A: (ddH_2O), solvent system B: (0.1 M NaOH), solvent system C: (0.1 M NaOH, 0.2 M NaAc); The gradient program was shown in **Table 1**. In addition, the 11 monosaccharide standards needed in this experiment were purchased from Sigma Company (St. Louis, MO, USA), and the information of standard products is shown in **Table 2**.

TABLE 1 Gradient program for high performance anion exchange chromatography (HPAEC).

Time (min)	A (%)	B (%)	C (%)
0	95	5	0
26	85	5	10
42	85	5	10
42.1	60	0	40
52	60	40	0
52.1	95	5	0
60	95	5	0

Spectrometric analysis of lily polysaccharides

Ultraviolet–visible spectrum

The ultraviolet–visible (UV) spectrum of LP samples were determined with ultraviolet–visible spectroscopy (Shimadzu UV-2600, Tokyo, Japan). LP samples were prepared as 0.5 mg/ml polysaccharides solution with distilled water, and the UV absorption curves of the solution were recorded in the wavelength range of 200–900 nm (25).

Fourier transform infrared spectrum

The infrared spectrum characteristics of LP samples were determined by Fourier infrared spectrophotometer (Thermo Nicolet NEXUS870, Massachusetts, USA) within the wavenumber range of 4,000–500 cm^{-1}. And the samples were prepared by KBr Tablet pressing method (18, 26).

Scanning electron microscope analysis of lily polysaccharides

Field emission scanning electron microscopy (Hitachi S-4800, Tokyo, Japan) was used to observe the apparent morphology of LP obtained by different extraction methods. The polysaccharide samples were fixed on the carrier platform and sprayed with gold powder. The magnification used includes 25, 50, 250, and 500× (27).

Rheological analysis

Hybrid Rheometer (MCR302, Anton Paar, Austria) was used to measure the static shear rheology properties of LP fractions (0.02 g/ml). Flow curves were measured under an increasing shear rate region (0.1–100 s^{-1}) with a 40 mm parallel plate geometry with a gap size of 1.0 mm, and the angular frequency of 10 rad/s and the strain of 1% at 25°C were used (28).

TABLE 2 Information on monosaccharide standards.

Name	Abbreviation	CAS number	Molecular formula
Fucose	Fuc	2438-80-4	$C_6H_{12}O_5$
Rhamnose	Rha	10030-85-0	$C_6H_{14}O_6$
Arabinose	Ara	5328-37-0	$C_5H_{10}O_5$
Galactose	Gal	26566-61-0	$C_6H_{12}O_6$
Glucose	Glc	50-99-7	$C_6H_{12}O_6$
Xylose	Xyl	58-86-6	$C_5H_{10}O_5$
Mannose	Man	3458-28-4	$C_6H_{14}O_6$
Fructose	Fru	57-48-7	$C_6H_{12}O_6$
Ribose	Rib	50-69-1	$C_5H_{10}O_5$
Galacturonic acid	Gal-UA	14982-50-4	$C_6H_{10}O_7$
Glucuronic acid	Glc-UA	6556-12-3	$C_6H_{10}O_7$
Mannuronic acid	Man-UA	6814-36-4	$C_6H_{10}O_7$
Guluronic acid	Gul-UA	15769-56-9	$C_6H_{10}O_7$

Statistical analysis

All data reported were averages of three replicates. And ANOVA and Duncan's multiple range test were used to analyze the differences between data ($P < 0.05$). Finally, Origin software (2021 version) was used to draw the resulting image.

Results and discussion

The yield of lily polysaccharides

The yield is a crucial parameter to evaluate the extraction efficiency of subcritical and ultrasound-assisted extraction methods. In this study, the yield of LP extracted by SW was higher than 34.73% and ranged from 34.73 to 54.91%, while the yield of polysaccharides extracted by UAE was lower, ranging from 3.69 to 7.69% (Table 3). The yield of ultrasound-assisted extracted lily polysaccharides (U-LP) was less than 10%, which is similar to that reported by Xie et al. They used ultrasound-assisted different enzymes to extract polysaccharides of *Lilium davidii* var. *willmottiae* (6).

Obviously subcritical water method is a more suitable method to extract the high yield of LP. This may be attributed to the following two aspects: on the one hand, decreasing polarity of subcritical water dissolved polysaccharides contained in lily more easily and quickly. Also, the low density and viscosity of subcritical water contributed to the solubilization of polysaccharides (29–32). On the other hand, in the subcritical state, the ionization degree of aqueous solvent increased, and the high concentration of hydrogen and hydroxide ions could be used as acid-base catalysts to improve the yield of acidic polysaccharides (15, 33).

TABLE 3 The yield and molecular weight of lily polysaccharides.

Extraction method	Polysaccharide type	Yield (%)	Molecular weight (kDa)
S-LP	LDWP	34.73 ± 0.87^{Cc}	322
	LBVP	54.91 ± 0.63^{Aa}	333
	LLAP	49.32 ± 2.87^{Bb}	389
U-LP	LDWP	7.69 ± 1.82^{Dd}	3
	LBVP	3.69 ± 0.69^{Ee}	53
	LLAP	4.53 ± 0.23^{Ee}	26

The differences between the data can be represented by uppercase ($P < 0.01$) and/or lowercase letters ($P < 0.05$).

As shown in Table 2, the yield of LP was significantly different among different species ($p < 0.05$). Under the subcritical water extraction, the yield of *Lilium brownii* var. *viridulum* polysaccharides (LBVP) was the highest. Concerning the ultrasound-assisted extraction, the yield of *Lilium davidii* var. *willmottiae* polysaccharides (LDWP) was the highest, while the yields of LBVP and *Lilium lancifolium* polysaccharides (LLAP) were similar. The results indicate that subcritical water extraction had great potential in increasing the yield of lily polysaccharides. Moreover, *Lilium brownii* var. *viridulum* was a better species for the preparation of lily polysaccharides.

Chemical composition of lily polysaccharides

The effects of two extraction methods on the chemical composition of lily polysaccharides were studied by anthrone-sulfuric acid method, carbazole method, DNS method, and Bradford method. The specific chemical compositions of crude lily polysaccharides were shown in Figure 1. The results showed that the extraction method had a significant effect on the chemical composition of LP. In addition, the proportions of neutral sugar, acid sugar, reducing sugar, and protein in different LP were different.

Neutral sugar

Neutral sugar content in crude polysaccharides of lily was shown in orange in Figure 1. Compared with ultrasound-assisted extraction, subcritical water extraction increased neutral sugar content by 3.35–19.70%. In addition, with the same extraction method, the neutral sugar content in lily polysaccharides of different species was also different. The neutral sugar content of LLAP was the highest in subcritical water extraction, while the LDWP was the highest in ultrasound-assisted extraction. Huang et al. also reported the difference of neutral sugar content in different LP (*Lilium lancifolium*, *Lilium davidii* var. *Unicolor*, and *Lilium brownii* var. *viridulum* Baker) with hot water extraction (32). The results

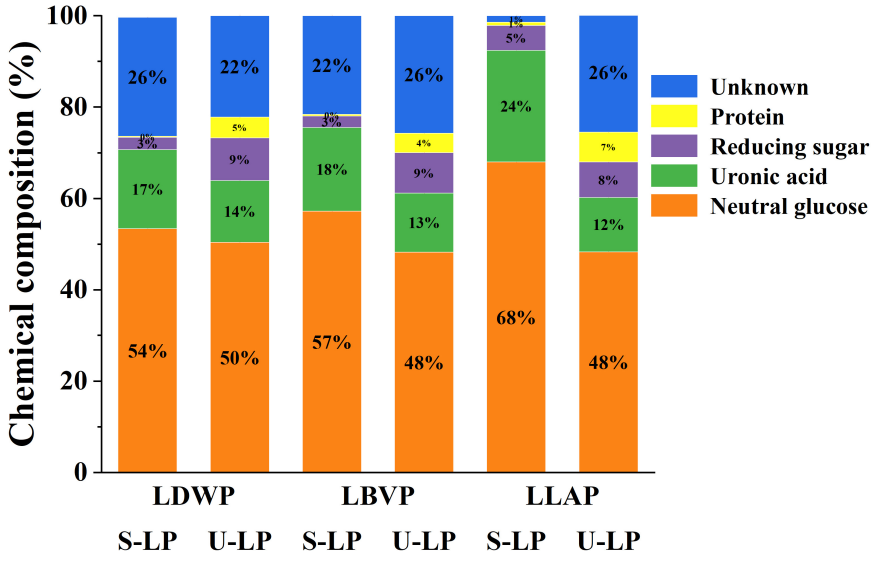

FIGURE 1
The chemical composition (%) of three lily polysaccharides extracted by different extraction methods.

showed that subcritical water extraction and *Lilium lancifolium* were better choices for obtaining high neutral sugar content.

Uronic acid

Uronic acids are considered to have enormous potential in the cosmetic, pharmaceutical and food industries (34). The content of uronic acid in crude LP showed the same trend as neutral sugar content (The green part of Figure 1). In other words, the content of uronic acid in crude LP obtained by subcritical water treatment was higher, ranged from 17.32 to 26.24%. And the proportion of uronic acid in LP obtained by ultrasonic-assisted extraction was less than 14%. Under the condition of subcritical water, the high concentration of hydronium ion promoted the hydrolysis of pectin in lily bulb to uronic acid. It has been reported that the highest yield of uronic acid can reach 79.7 g kg^{-1} with subcritical water hydrolysis of pectin rich biomass (31).

In addition, the content of uronic acid was also affected by lily species. This may be due to the difference in pectin content in lily bulbs of different species (35). In conclusion, the subcritical water extraction combined with the species of *Lilium lancifolium* Thunb was the best choice for obtaining high uronic acid content.

Reducing sugar

The reducing sugar content was shown in purple in Figure 1. The reducing sugar content of crude polysaccharides extracted from subcritical water ranged from 2.53 to 5.00%, while that of ultrasonic assisted extraction ranged from 7.08 to 9.36%. Obviously, compared with the differences of lily species, the extraction method was a more important reason for the changes in reducing sugar content. Reducing sugars were known to come from the breakdown of complex carbohydrates. Ismadji et al. reported that high temperature (120–160°C) and long reaction time (3–5 h) contribute to the breakdown of carbohydrates (36). Although the SW method in this study was carried out at high temperature, the reaction time was short (15 min) and only a small amount of carbohydrates could be decomposed. Therefore, the reducing sugar proportion of crude polysaccharides extracted from subcritical water was relatively low.

Protein

The protein content of crude polysaccharides was shown in yellow in Figure 1. The protein content of crude polysaccharides extracted by subcritical water extraction was less than 1%, and the protein content of S-LDWP was the lowest, as low as 0.29%. The protein content of crude polysaccharides obtained by ultrasonically assisted extraction ranged from 4.26 to 6.55%. The lower protein content indicated that the two extraction methods were able to extract polysaccharides from different lily species with higher purity, and subcritical water had higher extraction selectivity for polysaccharides.

In addition, with the exception of neutral sugars, acidic sugars, reducing sugars, and proteins, all samples also include some unknown composition, which may be composed of ash, pigments, and total phenols. Overall, the unknown components remained at a low level, further indicating that both the subcritical water method and the ultrasonic assisted extraction method have a high extraction selectivity for lily polysaccharides.

Molecular weight of lily polysaccharides

It is well-known that the molecular weight of polysaccharides not only reflects the length of molecular chain, but also closely related to the physicochemical properties and biological activities of polysaccharides (37, 38). Therefore, the molecular weight of LP was determined by GPC technology in this paper (Table 2), and the results showed that there were multiple differences between the molecular weight of lily polysaccharides obtained by two extraction methods. The molecular weights of LP obtained by SW treatment ranged from 322 to 389 kDa. The molecular weight of LP extracted by UAE ranged from 3 to 53 kDa. The results showed that ultrasonic degradation of glycosidic bonds was stronger than that of subcritical water, resulting in the rupture of polysaccharides

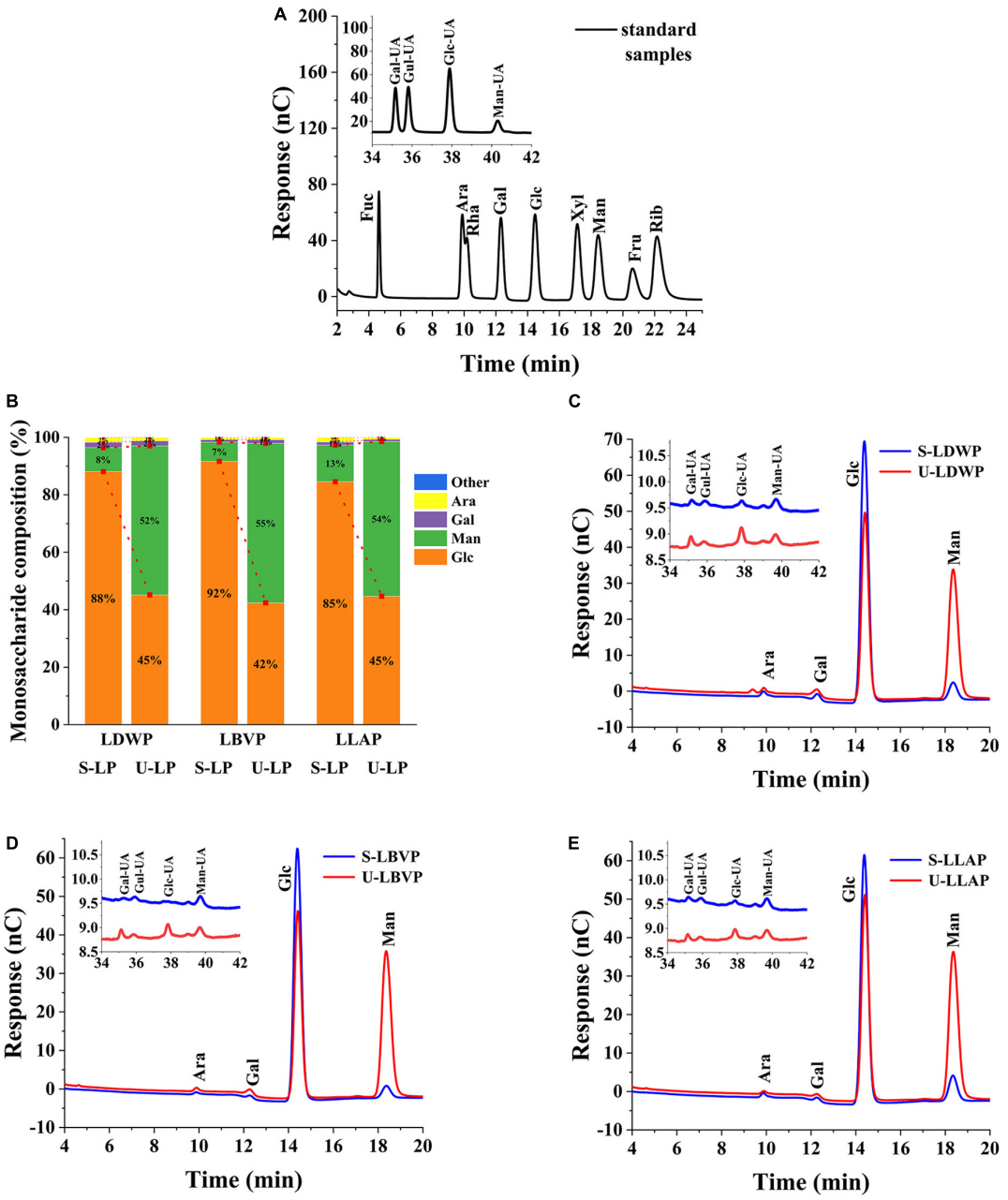

FIGURE 2
Diagram of HPAEC results. **(A)** Standard sample. **(B)** Monosaccharide ratio of all samples. **(C)** *Lilium davidii* var. *willmottiae* polysaccharides (LDWP) sample. **(D)** *Lilium brownii* var. *viridulum* polysaccharides (LBVP) sample. **(E)** *Lilium lancifolium* polysaccharides (LLAP) sample.

into smaller parts. In addition, for subcritical water extraction, the largest molecular weight was LLAP, whereas for ultrasonic extraction, the largest molecular weight was LBVP. The molecular weight of LDWP obtained by the two extraction methods was the lowest. In a word, molecular weight is closely related to the lily species and extraction method. Therefore, the appropriate species and extraction methods should be selected according to the actual production purposes.

Monosaccharide composition

Polysaccharides consist of one or more monosaccharides linked by glycosidic bonds. According to the monosaccharide formation of polysaccharides, it can be divided into homopolysaccharides and heteropolysaccharides (39). As shown in the **Figure 2**, LP were heteropolysaccharides, which were mainly composed of glucose (Glc), mannose (Man), galactose (Gal), and arabinose (Ara) and contained a small amount of galacturonic Acid (Gal-UA), glucuronic Acid (Glc-UA), mannose Acid (Man-UA), and Guluronic Acid (Gul-UA). Specifically, compared with lily species, extraction methods had a greater effect on monosaccharide composition, as can be seen from the percentage of monosaccharides in all LP samples (**Figure 2B**). The Glc content in LP extracted from subcritical water was the highest. And the proportions of Glc in S-LDWP, S-LBVP and S-LLAP were 88.09, 91.67, and 84.57%, respectively. However, for UAE extracted LP, Glc and Man were the main components, the percentage of Glc in U-LP ranged from 42.41 to 45.16%, and the proportion of Man in U-LP ranged from 51.85 to 55.50%. The proportion of other monosaccharides in U-LP except Glc and Man is between 1 and 3%.

These results showed that different extraction methods had no significant effect on the monosaccharide types, but significantly affected the percentage and molar ratio of monosaccharide. Monosaccharide composition has been reported to affect the biological activity of polysaccharides to some extent (40, 41). Therefore, the extraction method and species can be selected according to the purpose of preparing the polysaccharides.

Spectroscopic characterization of lily polysaccharides

Ultraviolet–visible spectrum

UV absorption spectra of the series lily polysaccharides obtained by different extraction methods were shown in **Figures 3A–C**. All the LP samples showed weak absorption peaks only at 280 nm, which indicated that the content of non-polysaccharides with UV absorption in crude LP samples were

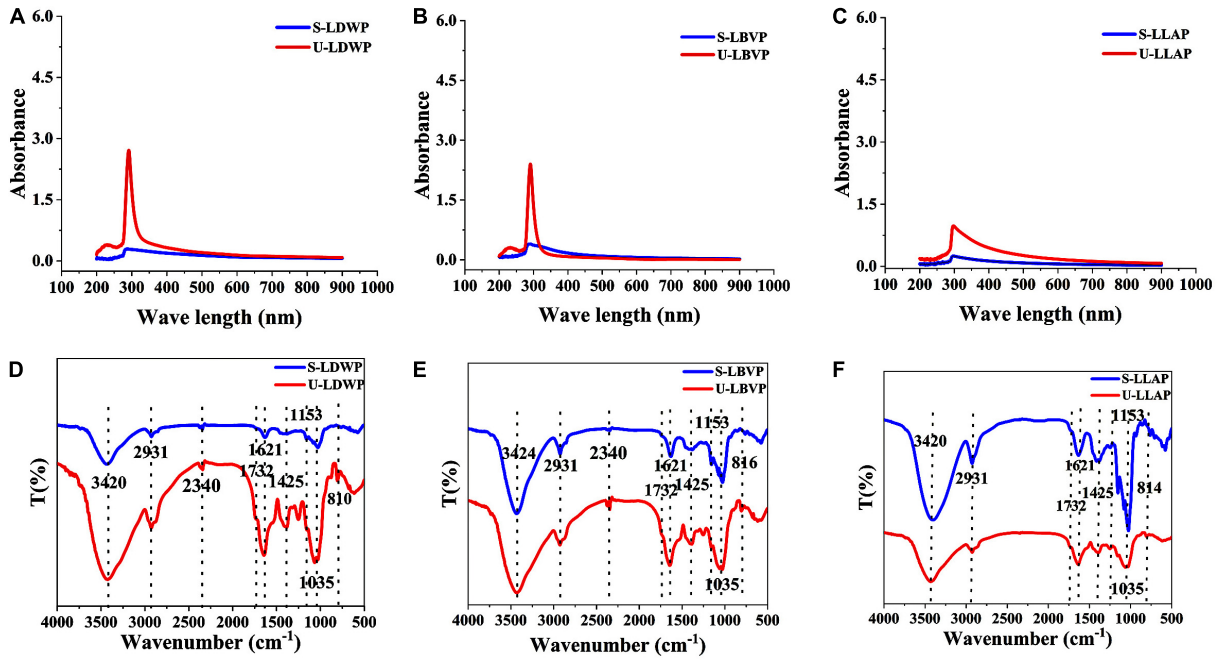

FIGURE 3
Spectrum properties of three lily polysaccharides extracted by different extraction methods. **(A–C)** The ultraviolet–visible (UV) analysis. **(D–F)** Fourier transform infrared (FT-IR) analysis.

low except protein. Moreover, it was obvious that the absorption peak of subcritical water extracted lily polysaccharides (S-LP) at 280 nm was much lower than that of U-LP, which is consistent with the previous results of protein content measured by coomassie brilliant blue. The results showed that subcritical water method could obtain polysaccharides with lower protein content.

Fourier transform infrared spectrum

Regardless of the extraction method and species, the absorption peaks of LP samples showed high similarity (**Figures 3D–F**). The broad peak at 3,420–3,424 cm^{-1} was attributed to the stretching vibration of O-H and the strong and broad peak shape was a typical band for carbohydrates, which indicated the presence of inter-molecular or intra-molecular hydrogen bonds (42). The peak at 2,931 cm^{-1} was caused by C-H stretching vibration of LP (43). Except for LLAP, LDWP, and LBVP had characteristic absorption peaks at 2,340 cm^{-1}, indicating that amide groups exist in LDWP and LBVP. Moreover, the absorption peaks at 1,621 and 1,732 cm^{-1} were caused by the free carboxyl (COO^-) groups and esterified carboxyl group ($COO\text{-}CH_3$) in all polysaccharides (9). In addition, the peak at 1,425 cm^{-1} was also caused by CH_2 vibration. 1,153 and 1,035 cm^{-1} correspond to the absorption vibrations of pyranose and Glc, respectively (44). In addition, the weak bands near 816 cm^{-1} may be compatible with the presence of α-D-mannose in LP samples (9).

Scanning electron microscopy analysis of lily polysaccharides

Different micromorphology characteristics is one of the key factors leading to the complexity of polysaccharides (45).

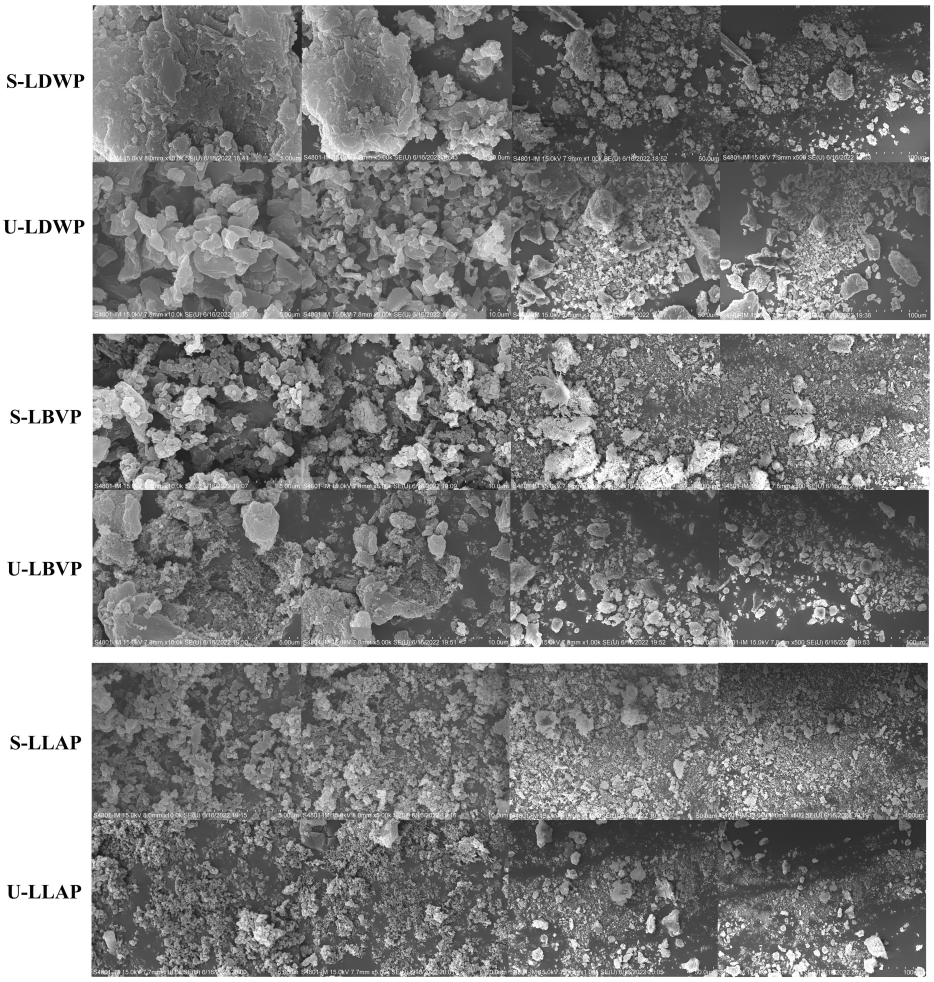

FIGURE 4
Scanning electron microscope (SEM) images of three lily polysaccharides extracted by different extraction methods at 5, 10, 50, and 100 μm.

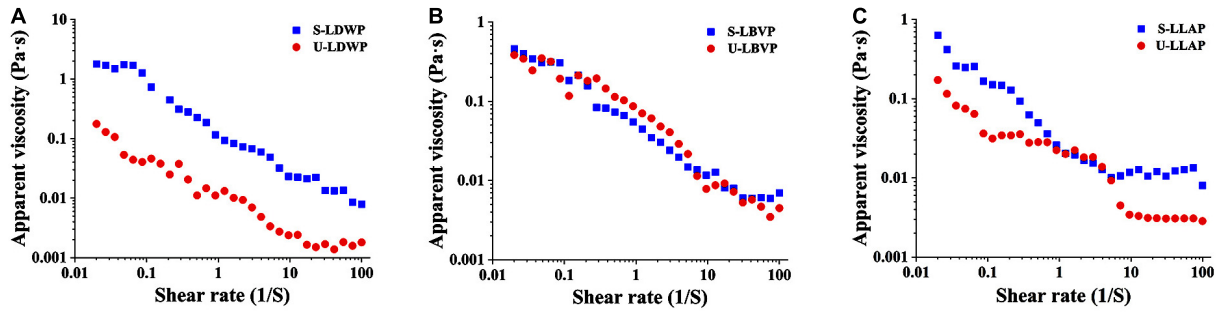

FIGURE 5
The flow behavior of three lily polysaccharides extracted by different extraction methods. **(A)** *Lilium davidii* var. *willmottiae* polysaccharides (LDWP), **(B)** *Lilium brownii* var. *viridulum* polysaccharides (LBVP), **(C)** *Lilium lancifolium* polysaccharides (LLAP).

As shown in Figure 4, the surface morphology and structure of LP were affected by different extraction methods. Duan et al. obtained the same conclusion in the extraction of Lentinan (42). Although all polysaccharide samples showed agglomeration phenomenon, there were some differences in the micromorphology of LP between different species. In detail, LDWP samples had smooth surfaces and irregular properties. Moreover, both LBVP and LLAP samples showed dense clusters of quasi-spherical honeycomb particles, and LLAP samples had smaller particle sizes. Ji et al. speculated that the structural aggregation of polysaccharide molecules may be closely related to the presence of carboxyl and hydroxyl groups (37).

Rheological characterization

Some natural polysaccharides have been widely used in the preparation of gels, thickeners and emulsifiers due to their excellent viscosity (46). As shown in Figure 5, with the increase of shear rate, the apparent viscosity of LP samples decreased significantly, and which showed typical shear-thinning behavior of Newtonian fluid or pseudoplastic fluid (33). The shear thinning behavior of polysaccharides may be related to the unwinding of molecular chains in solution (47). Interestingly, independent of species, both initial and final viscosity of S-LP samples were higher than those of U-LP at high shear rates. Polysaccharide samples extracted by subcritical water with high apparent viscosity are suitable for development as gels or thickeners.

Conclusion

In conclusion, compared with lily species, the extraction method has a greater impact on the properties of LP. Subcritical water extraction could increase the polysaccharides yield by 4.52–14.88 times than ultrasound-assisted extraction. S-LP samples have high contents of neutral glucose and uronic acid. Ultrasound-assisted extraction was easier to obtain polysaccharides with higher reducing sugar content and lower molecular weight. Moreover, the extraction method also had a significant effect on the monosaccharide composition of polysaccharides. Glc was the key component in S-LP, while Glc and Man were the key components in U-LP. In addition, the rheological behavior of polysaccharides indicated that LDWP extracted from subcritical water had the largest apparent viscosity. Interestingly, S-LDWP samples had low solubility, making them suitable for development as gels, thickeners, and emulsifiers. Hence, the extraction method and lily species had a great influence on the physicochemical properties of lily polysaccharides, and the most suitable method and species should be selected according to the research purpose in practical production applications.

Data availability statement

The original contributions presented in this study are included in the article/supplementary material, further inquiries can be directed to the corresponding authors.

Author contributions

ZS: investigation, conceptualization, formal analysis, writing—original draft, and writing—review and editing. YZ: formal analysis, data curation, and writing—original draft. YL: investigation and visualization. YRT: investigation, methodology, and data curation. WW, YB,

YCT, YH, and LX: investigation. JM: funding acquisition, supervision, and writing—review and editing. PY: investigation, funding acquisition, supervision, and writing—review and editing. All authors contributed to the article and approved the submitted version.

Funding

This work was financially supported by the National Natural Science Foundation of China (Nos. 31902043 and 32172612), the National Key R&D Program of China (No. 2019YFD1001002), the National Natural Science Foundation of China (No. 32102043), and the Central Public-interest Scientific Institution Basal Research Fund (No. Y2022XK30).

Conflict of interest

The authors declare that the research was conducted in the absence of any commercial or financial relationships that could be construed as a potential conflict of interest.

Publisher's note

All claims expressed in this article are solely those of the authors and do not necessarily represent those of their affiliated organizations, or those of the publisher, the editors and the reviewers. Any product that may be evaluated in this article, or claim that may be made by its manufacturer, is not guaranteed or endorsed by the publisher.

References

1. You X, Xie C, Liu K, Gu Z. Isolation of non-starch polysaccharides from bulb of tiger lily (*Lilium lancifolium* Thunb.) with fermentation of Saccharomyces cerevisiae. *Carbohydr Polym.* (2010) 81:35–40. doi: 10.1016/j.carbpol.2010.01.051

2. Huang H, Ge Z, Limwachiranon J, Li L, Li W, Luo Z. UV-C treatment affects browning and starch metabolism of minimally processed lily bulb. *Postharvest Biol Technol.* (2017) 128:105–11. doi: 10.1016/j.postharvbio.2017.02.010

3. Zhao Q, Xie B, Yan J, Zhao F, Xiao J, Yao L, et al. In vitro antioxidant and antitumor activities of polysaccharides extracted from Asparagus officinalis. *Carbohydr Polym.* (2012) 87:392–6. doi: 10.1016/j.carbpol.2011.07.068

4. Gao J, Zhang T, Jin Z-Y, Xu X-M, Wang J-H, Zha X-Q, et al. Structural characterisation, physicochemical properties and antioxidant activity of polysaccharide from *Lilium lancifolium* Thunb. *Food Chem.* (2015) 169:430–8. doi: 10.1016/j.foodchem.2014.08.016

5. Fan Y, Ma X, Ma L, Zhang J, Zhang W, Song X. Antioxidative and immunological activities of ophiopogon polysaccharide liposome from the root of *Ophiopogon japonicus*. *Carbohydr Polym.* (2016) 135:110–20. doi: 10.1016/j.carbpol.2015.08.089

6. Li WM, Wang YJ, Wei HL, Zhang YB, Guo ZH, Qiu Y, et al. Structural characterization of Lanzhou lily (*Lilium davidiivar*.unicolor) polysaccharides and determination of their associated antioxidant activity. *J Sci Food Agric.* (2020) 100:5603–16. doi: 10.1002/jsfa.10613

7. Wang PY, Li J, Attia FAK, Kang WY, Wei JF, Liu ZH, et al. A critical review on chemical constituents and pharmacological effects of *Lilium*. *Food Sci Hum Wellness.* (2019) 8:330–6. doi: 10.1016/j.fshw.2019.09.001

8. Xue HK, Xu JQ, Zhang JL, Wei YN, Cai X, Tan JQ. Modeling, optimization, purification, and characterization of polysaccharides from *Lilium lancifolium* Thunb. *Lwt Food Sci Technol.* (2022) 162:113491. doi: 10.1016/j.lwt.2022.113491

9. Zhang F, Zhang L, Chen J, Du X, Lu Z, Wang X, et al. Systematic evaluation of a series of pectic polysaccharides extracted from apple pomace by regulation of subcritical water conditions. *Food Chem.* (2022) 368:130833. doi: 10.1016/j.foodchem.2021.130833

10. Leong YK, Yang FC, Chang JS. Extraction of polysaccharides from edible mushrooms: Emerging technologies and recent advances. *Carbohydr Polym.* (2021) 251:117006. doi: 10.1016/j.carbpol.2020.117006

11. Li X, Wang L. Effect of extraction method on structure and antioxidant activity of *Hohenbuehelia serotina* polysaccharides. *Int J Biol Macromol.* (2016) 83:270–6. doi: 10.1016/j.ijbiomac.2015.11.060

12. Yan J-K, Wang Y-Y, Ma H-L, Wang Z-B. Ultrasonic effects on the degradation kinetics, preliminary characterization and antioxidant activities of polysaccharides from *Phellinus linteus* mycelia. *Ultrason Sonochem.* (2016) 29:251–7. doi: 10.1016/j.ultsonch.2015.10.005

13. Chen H-m, Fu X, Luo Z-g. Properties and extraction of pectin-enriched materials from sugar beet pulp by ultrasonic-assisted treatment combined with subcritical water. *Food Chem.* (2015) 168:302–10. doi: 10.1016/j.foodchem.2014.07.078

14. Yoo H-U, Ko M-J, Chung M-S. Hydrolysis of beta-glucan in oat flour during subcritical-water extraction. *Food Chem.* (2020) 308:125670. doi: 10.1016/j.foodchem.2019.125670

15. Getachew AT, Chun BS. Influence of pretreatment and modifiers on subcritical water liquefaction of spent coffee grounds: A green waste valorization approach. *J Clean Prod.* (2017) 142:3719–27. doi: 10.1016/j.jclepro.2016.10.096

16. Zhang J, Wen C, Zhang H, Zandile M, Luo X, Duan Y, et al. Structure of the zein protein as treated with subcritical water. *Int J Food Propert.* (2018) 21:143–53. doi: 10.1080/10942912.2017.1414839

17. Lang QY, Wai CM. Supercritical fluid extraction in herbal and natural product studies – a practical review. *Talanta.* (2001) 53:771–82. doi: 10.1016/s0039-9140(00)00557-9

18. Ti Y, Wang W, Zhang Y, Ban Y, Wang X, Wang P, et al. Polysaccharide from *Hemerocallis citrina* Borani by subcritical water: Bioactivity, purification, characterization, and anti-diabetic effects in T2DM rats. *Int J Biol Macromol.* (2022) 215:169–83. doi: 10.1016/j.ijbiomac.2022.06.101

19. Zhao BT, Zhang J, Guo X, Wang JL. Microwave-assisted extraction, chemical characterization of polysaccharides from *Lilium davidii* var.unicolor Salisb and its antioxidant activities evaluation. *Food Hydrocoll.* (2013) 31:346–56. doi: 10.1016/j.foodhyd.2012.11.021

20. Dubois M, Gilles K, Hamilton JK, Rebers PA, Smith F. A colorimetric method for the determination of sugars. *Nature.* (1951) 168:167–167. doi: 10.1038/168167a0

21. Bitter T, Muir HM. A modified uronic acid carbazole reaction. *Anal Biochem.* (1962) 4:330–4. doi: 10.1016/0003-2697(62)90095-7

22. Meillisa A, Woo H-C, Chun B-S. Production of monosaccharides and bioactive compounds derived from marine polysaccharides using subcritical water hydrolysis. *Food Chem.* (2015) 171:70–7. doi: 10.1016/j.foodchem.2014.08.097

23. Bradford MM. Rapid and sensitive method for quantitation of microgram quantities of protein utilizing principle of protein-dye binging. *Anal Biochem.* (1976) 72:248–54. doi: 10.1016/0003-2697(76)90527-3

24. Wang L, Zhang B, Xiao J, Huang Q, Li C, Fu X. Physicochemical, functional, and biological properties of water-soluble polysaccharides from Rosa roxburghii Tratt fruit. *Food Chem.* (2018) 249:127–35. doi: 10.1016/j.foodchem.2018.01.011

25. Wang W, Ma X, Jiang P, Hu L, Zhi Z, Chen J, et al. Characterization of pectin from grapefruit peel: A comparison of ultrasound-assisted and conventional heating extractions. *Food Hydrocoll.* (2016) 61:730–9. doi: 10.1016/j.foodhyd.2016.06.019

26. Ji X, Guo J, Ding D, Gao J, Hao L, Guo X, et al. Structural characterization and antioxidant activity of a novel high-molecular-weight polysaccharide from *Ziziphus Jujuba* cv. Muzao. *J Food Meas Charact.* (2022) 16:2191–200. doi: 10.1007/s11694-022-01288-3

27. Ji X, Yan Y, Hou C, Shi M, Liu Y. Structural characterization of a galacturonic acid-rich polysaccharide from *Ziziphus jujuba* cv. Muzao. *Int J Biol Macromol.* (2020) 147:844–52. doi: 10.1016/j.ijbiomac.2019.09.244

28. Morales-Contreras BE, Rosas-Flores W, Contreras-Esquivel JC, Wicker L, Morales-Castro J. Pectin from husk tomato (*Physalis ixocarpa* Brot.): Rheological behavior at different extraction conditions. *Carbohydr Polym.* (2018) 179:282–9. doi: 10.1016/j.carbpol.2017.09.097

29. Aida TM, Shiraishi N, Kubo M, Watanabe M, Smith RL. Reaction kinetics of D-xylose in sub- and supercritical water. *J Supercrit Fluids.* (2010) 55:208–16. doi: 10.1016/j.supflu.2010.08.013

30. Moller M, Nilges P, Harnisch F, Schroder U. Subcritical water as reaction environment: Fundamentals of hydrothermal biomass transformation. *Chemsuschem.* (2011) 4:566–79. doi: 10.1002/cssc.201000341

31. Pinkowska H, Krzywonos M, Wolak P, Zlocinska A. Production of uronic acids by hydrothermolysis of pectin as a model substance for plant biomass waste. *Green Process Synth.* (2019) 8:683–90. doi: 10.1515/gps-2019-0039

32. Huang JH, Zhou RR, He D, Chen L, Yang YY, Xie HL, et al. Rapid identification of *Lilium* species and polysaccharide contents based on near infrared spectroscopy and weighted partial least square method. *Int J Biol Macromol.* (2020) 154:182–7. doi: 10.1016/j.ijbiomac.2020.03.109

33. Zhang JX, Wen CT, Gu JY, Ji CC, Duan YQ, Zhang HH. Effects of subcritical water extraction microenvironment on the structure and biological activities of polysaccharides from Lentinus edodes. *Int J Biol Macromol.* (2019) 123:1002–11. doi: 10.1016/j.ijbiomac.2018.11.194

34. Tomaszewska J, Bielinski D, Binczarski M, Berlowska J, Dziugan P, Piotrowski J, et al. Products of sugar beet processing as raw materials for chemicals and biodegradable polymers. *Rsc Adv.* (2018) 8:3161–77. doi: 10.1039/c7ra12782k

35. Lang L, Dou X, Ying K, Huan W, Jinrong B. . Analysis of nutrient components of lily bulbs from different origins. *Sci Technol Food Industry.* (2022) 43:339–50.

36. Purnomo A, Yudiantoro YAW, Putro JN, Nugraha AT, Irawaty W, Ismadji S. Subcritical water hydrolysis of durian seeds waste for bioethanol production. *Int J Ind Chem.* (2016) 7:29–37. doi: 10.1007/s40090-015-0059-3

37. Ji X, Cheng Y, Tian J, Zhang S, Jing Y, Shi M. Structural characterization of polysaccharide from jujube (*Ziziphus jujuba* Mill.) fruit. *Chem Biol Technol Agric.* (2021) 8:54. doi: 10.1186/s40538-021-00255-2

38. Ferreira SS, Passos CP, Madureira P, Vilanova M, Coimbra MA. Structure-function relationships of immunostimulatory polysaccharides: A review *Carbohydr Polym.* (2016) 147:557–8. doi: 10.1016/j.carbpol.2016.04.011

39. Wang Q, Wang F, Xu Z, Ding Z. Bioactive mushroom polysaccharides: A review on monosaccharide composition, biosynthesis and regulation. *Molecules.* (2017) 22:955. doi: 10.3390/molecules22060955

40. Liu M, Jing H, Zhang J, Che G, Zhou M, Gao Z, et al. Optimization of mycelia selenium polysaccharide extraction from agrocybe cylindracea SL-02 and assessment of their antioxidant and anti-ageing activities. *PLoS One.* (2016) 11:e0160799. doi: 10.1371/journal.pone.0160799

41. Chou C-H, Sung T-J, Hu Y-N, Lu H-Y, Yang L-C, Cheng K-C, et al. Chemical analysis, moisture-preserving, and antioxidant activities of polysaccharides from *Pholiota nameko* by fractional precipitation. *Int J Biol Macromol.* (2019) 131:1021–31. doi: 10.1016/j.ijbiomac.2019.03.154

42. Zhang J, Wen C, Qin W, Qin P, Zhang H, Duan Y. Ultrasonic-enhanced subcritical water extraction of polysaccharides by two steps and its characterization from *Lentinus edodes*. *Int J Biol Macromol.* (2018) 118:2269–77. doi: 10.1016/j.ijbiomac.2018.07.098

43. Chen C, Zhang B, Fu X, You L-J, Abbasi AM, Liu RH. The digestibility of mulberry fruit polysaccharides and its impact on lipolysis under simulated saliva, gastric and intestinal conditions. *Food Hydrocoll.* (2016) 58:171–8. doi: 10.1016/j.foodhyd.2016.02.033

44. Zhang C, Zhu X, Zhang F, Yang X, Ni L, Zhang W, et al. Improving viscosity and gelling properties of leaf pectin by comparing five pectin extraction methods using green tea leaf as a model material. *Food Hydrocoll.* (2020) 98:105246. doi: 10.1016/j.foodhyd.2019.105246

45. Xu Y, Liu G, Yu Z, Song X, Li X, Yang Y, et al. Purification, characterization and antiglycation activity of a novel polysaccharide from black currant. *Food Chem.* (2016) 199:694–701. doi: 10.1016/j.foodchem.2015.12.078

46. Yuan Y, Li C, Zheng Q, Wu J, Zhu K, Shen X, et al. Effect of simulated gastrointestinal digestion in vitro on the antioxidant activity, molecular weight and microstructure of polysaccharides from a tropical sea cucumber (*Holothuria leucospilota*). *Food Hydrocoll.* (2019) 89:735–41. doi: 10.1016/j.foodhyd.2018.11.040

47. Jin Q, Cai Z, Li X, Yadav MP, Zhang H. Comparative viscoelasticity studies: Corn fiber gum versus commercial polysaccharide emulsifiers in bulk and at air/liquid interfaces. *Food Hydrocoll.* (2017) 64:85–98. doi: 10.1016/j.foodhyd.2016.11.002

frontiers | Frontiers in Nutrition

TYPE Original Research
PUBLISHED 20 September 2022
DOI 10.3389/fnut.2022.998462

Check for updates

OPEN ACCESS

EDITED BY
Xiaolong Ji,
Zhengzhou University of Light Industry, China

REVIEWED BY
Di Wang,
Jilin Agricultural University, China
Zhuo Alex Wang,
Institute of Process Engineering (CAS), China
Tao Zhang,
Affiliated Hospital of Zunyi Medical College, China
Zhibo Jiang,
North Minzu University, China
Xiao Bin Zeng,
Jinan University, China

*CORRESPONDENCE
Hongxing Xiao
xiaohx771@nenu.edu.cn
Lin Sun
sunl925@nenu.edu.cn

†These authors have contributed equally to this work

SPECIALTY SECTION
This article was submitted to Food Chemistry, a section of the journal Frontiers in Nutrition

RECEIVED 20 July 2022
ACCEPTED 22 August 2022
PUBLISHED 20 September 2022

CITATION
Qi X, Yu Y, Wang X, Xu J, Wang X, Feng Z, Zhou Y, Xiao H and Sun L (2022) Structural characterization and anti-oxidation activity evaluation of pectin from *Lonicera japonica* Thunb.
Front. Nutr. 9:998462.
doi: 10.3389/fnut.2022.998462

COPYRIGHT
© 2022 Qi, Yu, Wang, Xu, Wang, Feng, Zhou, Xiao and Sun. This is an open-access article distributed under the terms of the Creative Commons Attribution License (CC BY). The use, distribution or reproduction in other forums is permitted, provided the original author(s) and the copyright owner(s) are credited and that the original publication in this journal is cited, in accordance with accepted academic practice. No use, distribution or reproduction is permitted which does not comply with these terms.

Structural characterization and anti-oxidation activity evaluation of pectin from *Lonicera japonica* Thunb.

Xiaodan Qi[1,2†], Yang Yu[1†], Xinyi Wang[1], Jialei Xu[1], Xiang Wang[1], Zhangkai Feng[1], Yifa Zhou[1], Hongxing Xiao[1*] and Lin Sun[1*]

[1]School of Life Sciences, Northeast Normal University, Changchun, China, [2]Department of Clinical Biochemistry, Qiqihar Medical University, Qiqihar, China

Pectins are nutrient components of plants and are widely used in the food industry. In this study, one major pectin fraction (WLJP-A0.2b) with Mw of 40.6 kDa was purified from *Lonicera japonica* Thunb. The structural feature and antioxidant activity of it was investigated. Monosaccharide composition, Fourier transform infrared (FT-IR) spectra, enzymatic hydrolysis, and nuclear magnetic resonance (NMR) spectra analysis indicated that WLJP-A0.2b consisted of rhamnogalacturonan I (RG-I), rhamnogalacturonan II (RG-II), and homogalacturonan (HG) domains, with mass ratio of 0.4:1.0:2.1. The RG-I domain contained highly branched α-L-1,5-arabinan, β-D-1,4-galactan and type II arabinogalactan (AG-II) side chains. The HG domain was released in the form of un-esterified and partly methyl-esterified and/or acetyl-esterified oligogalacturonides with degree of polymerization 1–8 after degradation by endo-polygalacturonase. Radical scavenging assays indicated that WLJP-A0.2b exhibited antioxidant activity through the synergistic effects of different pectin domains. Oligogalacturonides, especially de-esterified oligogalacturonides, showed better antioxidant activities than RG-II and RG-I domains. Moreover, de-esterified oligogalacturonides remarkably reduced H_2O_2-induced reactive oxygen species production in HEK-293T cells. These results provide useful information for screening of natural antioxidants from *Lonicera japonica* Thunb. and application of pectin in functional food field.

KEYWORDS

***Lonicera japonica* Thunb., pectin, endo-polygalacturonase, structural characterization, antioxidant activity**

Introduction

Lonicera japonica Thunb. (family: Caprifoliaceae) is native to East Asian countries and recognized as edible and medicinal food in daily life (1, 2). The edible flowers and buds are usually used in healthy beverage to improve physical performance and prevent disease in the form of tea, liquor, beverages, acidophilous milk, and oral liquids (3, 4). In the past decades, most of the studies focused on chlorogenic acid, essential oils, and iridoids in *Lonicera japonica* Thunb. In recent years, polysaccharides from *Lonicera japonica* Thunb. have attracted considerable attention due to their diverse biological activities such as anti-tumor, immunomodulation, anti-inflammatory, anti-oxidant, and other biological activities (5–10). Pectin is a family of galacturonic acid-rich polysaccharides found in the primary cell wall of plants (11). It is basically composed of linear homogalacturonan (HG) domain having no side chains, and rhamnogalacturonan I and II (RG-I and RG-II) domains with diverse side chains (12). Some pectin fractions have been purified from *Lonicera japonica* Thunb. Lin et al. isolated a homogenous pectin fraction termed LJ-02-1 from *Lonicera japonica* Thunb. by DEAE-cellulose and Sephacryl S-200HR column. Further analysis revealed that LJ-02-1 had an average molecular weight of 54 kDa and was mainly composed of rhamnose, galacturonic acid, galactose, and arabinose in the molar ratio of 10.77:7.88:15.45:65.89 (5). Liu et al. isolated a pectic polysaccharide (LFA03-a) from *Lonicera japonica* Thunb. Structural analysis revealed that it possessed a RG-I backbone and substituted at O-4 of L-rhamnose with β-D-1,4-Galp, β-D-1,3-Galp, β-D-1,3,6-Galp, and α-L-1,5-Araf side chains (6). In addition, Zhang et al. purified one neutral fraction (LJP-N) and four acidic fractions (LJP-A-1 ∼ LJP-A-4) from *Lonicera japonica* Thunb. Among these fractions, LJP-A-3 was defined as HG-type pectin with a trace of RG-I domain which exhibited antioxidant activity (9). Although the chemical structures of a few pectin fractions from *Lonicera japonica* Thunb. have been analyzed, their detailed structures remain unknown, and their structure-activity relationships need to be further investigated.

Oxidative stress or an elevated level of reactive oxygen species (ROS) can induce oxidative damage, and consequently cause the occurrence and development of diseases like diabetes mellitus (13), cancer (14), cardiovascular (15), Alzheimer's disease (16), inflammatory diseases (17), aging (18), etc. Therefore, finding suitable antioxidants to neutralize free radicals is of great importance to protect cells from excessive oxidative stress. In recent years, pectic polysaccharides have been widely reported to exhibit antioxidant activities. Pectin can be viewed as a carrier of hydrogen which could bind with free radicals to terminate free radical chain reaction. Pectin derived from edible and medicinal plants is safe and healthy, therefore, it is a new type of natural antioxidant. The antioxidant activities of pectins from different sources depend on their structural characteristics, however, the structure-antioxidant activity relationship of pectin remain unclear.

In the present study, pectin polysaccharides were extracted from *Lonicera japonica* Thunb., systematically fractionated and structurally characterized. Moreover, pectin domains were prepared by enzymatic hydrolysis and the structure and antioxidant activities of different domains were intensively studied. These findings provide new information on structure-antioxidant activity relationships of pectins from *Lonicera japonica* Thunb., and facilitate their utilization in the field of functional food.

Materials and methods

Materials and reagents

Lonicera japonica Thunb. was purchased from Henan Province, China. DEAE-Cellulose was acquired from Shanghai Chemical Reagent Research Institute (Shanghai, China). Sepharose CL-6B and Sephadex G-75 were obtained from GE Healthcare (Pittsburgh, PA, United States). Endo-polygalacturonase (Endo-PG) was purchased from Megazyme (Bray, Ireland). All other chemicals were of analytical or HPLC grade made in China.

General methods

Total carbohydrate and uronic acid contents were measured by phenol-sulfuric acid and meta-hydroxydiphenyl methods, using the mixture of major monosaccharides and galacturonic acid (GalA) as standards independently (19, 20). Starch-like polysaccharide was determined by using the I_2–KI method. Kdo and Dha are the component of RG-II, which was qualitatively detected by using the modified thiobarbituric acid (TBA) method (21). Protein content was determined by using the Bradford assay with bovine serum albumin (BSA) as standard (22). Homogeneity and molecular weight (Mw) were determined by using high performance gel-permeation chromatography (HPGPC) with a TSK-gel G-3000 PWXL column (7.8 × 300 mm, TOSOH, Japan) coupled to a Shimadzu high performance liquid chromatography (HPLC) system (Tokyo, Japan) (23). Monosaccharide composition was analyzed by using HPLC and PMP pre-column derivatization method as previously described (24). Fourier transform infrared (FT-IR) spectra was recorded over a range of 4000 and 500 cm^{-1} using a PerkinElmer Spectrum Two FT-IR spectrometer (Perkin Elmer, United States).

Extraction of polysaccharides from *Lonicerae japonicae* Thunb.

Lonicerae Japonicae Thunb. (1 kg) was washed to remove the dust and immersed in 16 L distilled water overnight, and then extracted at 100°C for 3 h. After filtration, the residues were extracted twice again under the same conditions. The filtrates were combined, concentrated, and then centrifuged (4500 rpm × 15 min). The supernatant was precipitated overnight by the addition of 95% ethanol (three volumes). The precipitates were obtained by centrifugation (4500 rpm × 15 min) and washed with 95% ethanol and anhydrous ethanol, and then dried at room temperature. The water-soluble *Lonicerae Japonicae* Thunb. polysaccharides was obtained and named WLJP.

Purification of pectin from WLJP

WLJP (60 g) was dissolved in distilled water (50 mg/ml) and applied to a DEAE-Cellulose column. It was eluted with distilled water to give the un-bound fraction WLJP-N and then with 0.5 M NaCl to give the bound fraction WLJP-A. WLJP-A (20 g) was then applied to DEAE-Cellulose column, and eluted stepwise with distilled water, 0.2, 0.3, and 0.5 M NaCl to produce four fractions WLJP-AH, WLJP-A0.2, WLJP-A0.3, and WLJP-A0.5. The major fraction WLJP-A0.2 was further purified by using a Sepharose CL-6B column (3.0 × 90 cm), and two sub-fractions WLJP-A0.2a and WLJP-A0.2b were obtained, with the latter as the major pectic fraction.

Enzymatic hydrolysis and de-esterification

WLJP-A0.2b was dissolved in HAc-NaAc buffer solution (50 mM, pH 4.5) and incubated with Endo-PG at 40°C for 24 h. The enzyme was inactivated by heating at 100°C for 10 min and removed by centrifugation (12000 rpm × 5 min). The hydrolysate was fractionated on a Sephadex G-75 (3.0 × 90 cm) column and eluted with 0.15 M NaCl at 0.4 ml/min. The eluates (8 ml per tube) were collected and assayed for distribution of total carbohydrate and uronic acid contents. The appropriate fractions were combined, desalted (1 kDa cutoff dialysis tubes or a Sephadex G-10 column) and freeze-dried to give three sub-fractions WLJP-A0.2b-E1∼E3.

The de-esterification was performed according to the previous method (25). WLJP-A0.2b-E3 was saponified by 0.1 M NaOH and held at 4°C for 4 h with mild stirring. The reaction solutions were neutralized with 10% glacial acetic acid, and de-esterified pectin fractions were obtained and called D-WLJP-A0.2b-E3.

Nuclear magnetic resonance spectroscopy

^{13}C, Heteronuclear Single Quantum Coherence (HSQC), and Heteronuclear Multiple Bond Correlation (HMBC) NMR spectra were recorded at 25°C on a Bruker Avance 600 MHz spectrometer (Bruker, Karlsruhe, Germany) with a Bruker 5 mm broadband probe. Samples (20 mg) were dissolved in D_2O (99.8%, 0.5 ml) and centrifuged to remove undissolved components. Chemical shifts were given in ppm, with acetone as an internal chemical shift reference. Data were analyzed using standard Bruker software.

ESI-MS analysis

Oligosaccharide fraction (1 mg/ml in 50% (v/v) acetonitrile) was analyzed by electrospray ionization-mass spectrometry (ESI-MS) using an Amazon ETD Ion Trap Mass Spectrometer (Bruker Inc., Germany). The sample was delivered to electrospray source using a syringe pump at a flow rate of 5 μL/min. ESI-MS detection was performed in negative mode with capillary voltage 3500 V, capillary temperature 200°C and dry gas 2 ml/min. The mass scan range was m/z 100 to 2000. Data were processed using Trap-control software.

In vitro antioxidant activity

ABTS radical scavenging activity

The scavenging capacity for 2,2′-Azinobis-(3-ethylbenzthiazoline-6-sulphonate) (ABTS) free radical was measured following previous research (26), with some modifications. Solutions of ABTS (7 mM) and potassium persulfate (2.45 mM) were mixed and incubated in the dark at room temperature for 12–16 h to prepare ABTS radical. In the moment of use, the ABTS radical solution was diluted with phosphate-buffered saline (0.1 M PBS, pH 7.4) to obtain an absorbance of 0.70 (±0.05) at 734 nm. 50 μL of pectin samples solution at five concentrations (0.5, 1.0, 2.0, 5.0, and 10.0 mg/ml) and 500 μL of the diluted ABTS radical solution were mixed evenly and incubated at 37°C for 30 min. The absorbance was measured at 734 nm. Distilled water was used as blank control, and ascorbic acid (V_C) was used as positive control. Each group was tested for three times in parallel. ABTS radical scavenging activity was calculated according to the following equation:

$$\text{Scavengingactivity}(\%) = [1 - (A_x - A_{x0})/A_0] \times 100\%$$

A_0: The absorbance value of blank control;

A_x: The absorbance value of sample solution;

A_{x0}: The absorbance value of the sample background (PBS instead of ABTS radical solution).

Hydroxyl radical scavenging activity

The hydroxyl radical scavenging activity was determined as previously reported (27), with some modifications. 50 μL of pectin samples solution at five concentrations (0.5, 1.0, 2.0, 5.0, and 10.0 mg/ml), 100 μL of 9 mM $FeSO_4$, 100 μL of 9 mM anhydrous ethanol-salicylic acid and 100 μL of 8.8 mM H_2O_2 were mixed evenly and incubated at 25°C for 30 min. Then the mixture was centrifuged (12000 rpm × 5 min), and the absorbance of supernatant was measured at 510 nm. Distilled water was used as blank control, and V_C was used as positive control. Each group was tested for three times in parallel. The hydroxyl radical scavenging activity was calculated according to the formula:

$$\text{Scavengingactivity}(\%) = [1 - (A_x - A_{x0})/A_0] \times 100\%$$

A_0: The absorbance value of blank control;

A_x: The absorbance value of sample solution;

A_{x0}: The absorbance value of the sample background (distilled water instead of H_2O_2 solution).

DPPH radical scavenging activity

The 1,1-Dihpenyl-2-picrylhydrazyl (DPPH) radical scavenging ability was assessed according to the reported method (28), with some modifications. 50 μL of pectin samples solution at five concentrations (0.5, 1.0, 2.0, 5.0, and 10.0 mg/ml) and 200 μL of 0.004% anhydrous methanol-DPPH solution were mixed evenly and incubated at 25°C for 30 min in the dark. Then the mixture was centrifuged (12000 rpm × 5 min), the absorbance of supernatant was measured at 517 nm. Distilled water was used as blank control, and V_C was used as positive control. Each group was tested for three times in parallel. The DPPH radical scavenging activity was calculated according to the formula:

$$\text{Scavengingactivity}(\%) = [1 - (A_x - A_{x0})/A_0] \times 100\%$$

A_0: The absorbance value of blank control;

A_x: The absorbance value of sample solution;

A_{x0}: The absorbance value of the sample background (anhydrous methanol instead of DPPH solution).

Antioxidant activity against H_2O_2 induced oxidative stress in HEK-293T cells

Cell culture and treatment

HEK-293T cells were provided by Cell Resource Center, Institute of Basic Medical Sciences, Chinese Academy of Medical Sciences (Beijing, China). The cells were cultured in DMEM medium supplemented with 10% fetal bovine serum (Clark), 100 U/ml penicillin and 100 μg/ml streptomycin at 37°C in 5% CO_2. The cells were plated in 6-well plates at a density of 1×10^5 cells per well before experimentation. Adherent cells were pretreated with indicated concentrations (10, 50, and 100 μg/ml) of de-esterified pectin samples (D-WLJP-A0.2b-E3) for 24 h, respectively, and then treated with H_2O_2 (200 μm) for 6 h.

Reactive oxygen species measurement

The reagent 2, 7-dichlorodihydrofluorescein diacetate (DCFH-DA) was used to determine the intracellular levels of ROS. After pretreatment, the cells were harvested and washed with phosphate-buffered saline (PBS). Then the cells were incubated with 10 mM DCFH-DA (Sigma-Aldrich, Saint Louis, MO, United States) for 30 min at 37°C in dark. After DCFH-DA was removed, the cells were washed twice with PBS and re-suspended for detection with flow cytometer (BD Biosciences, United States) (29).

Statistical analysis

All experiments were performed in triplicate, and the data were shown as the mean ± standard deviation (SD). Student's *t*-test was used for single comparison. A value of $p < 0.05$ was considered statistically significant. IC_{50} values were calculated using SPSS 19.0 software.

Results and discussion

Preparation of pectin from *Lonicerae japonicae* Thunb.

Water-soluble *Lonicerae Japonicae* Thunb. polysaccharide (WLJP) was obtained following hot water extraction and ethanol precipitation, with the yield of 7.6%. Monosaccharide composition analysis (**Table 1**) showed that WLJP mainly consisted of GalA (30.9%), Ara (30.9%), Gal (15.9%), and Glc (14.2%), with minor Rha (4.5%), Man (1.9%), Xyl (1.2%), and GlcA (0.5%). The I2-KI assay indicated that it contained small amounts of starch-like polysaccharide.

WLJP was fractionated by using anion-exchange and size-exclusion chromatographies (**Figure 1A**). First, WLJP was separated by anion exchange chromatography into neutral polysaccharide fraction WLJP-N and acidic polysaccharide fraction WLJP-A. WLJP-N contained little GalA, and thus was not further discussed in this paper. WLJP-A is mainly composed of GalA (50.4%), typical for pectin. The charge distribution of WLJP-A was not homogeneous (**Figure 1B**). Therefore, WLJP-A was further separated by using anion exchange chromatography, and four fractions WLJP-AH (yield 1.2%), WLJP-A0.2 (yield 71.8%), WLJP-A0.3 (yield 9.7%), and WLJP-A0.5 (yield 2.5%) were obtained. The main fraction WLJP-A0.2 was further purified by size exclusion chromatography (**Figure 1C**), and the

10.3389/fnut.2022.998462

TABLE 1 Yields, Mws, and monosaccharide compositions of polysaccharide fractions from *Lonicerae japonicae* Thunb.

Fraction	Yield (w%)	Mw (kDa)	TBA	Monosaccharide composition (mol%)							
				GalA	Rha	Gal	Ara	Glc	GlcA	Xyl	Man
WLJP				30.9	4.5	15.9	30.9	14.2	0.5	1.2	1.9
WLJP-N	34.2[a]			2.9	4.9	25.3	33.7	22.9	2.8	2.0	5.5
WLJP-A	31.6[a]			50.4	7.0	10.8	26.2	4.0	–	1.6	–
WLJP-A0.2b	11.1[a]	40.6		72.2	2.8	5.8	15.9	2.0	0.5	0.6	0.2
WLJP-A0.2b-E1	7.6[b]	90.0	-	10.3	7.5	27.8	50.7	3.7	–	–	–
WLJP-A0.2b-E2	20.8[b]	14.1	+	70.8	9.4	4.6	10.7	2.2	1.4	–	0.9
WLJP-A0.2b-E3	43.0[b]	4.7	-	90.5	6.6	1.1	1.0	0.8	–	–	–

[a]Yield in relation to WLJP.
[b]Yield in relation to WLJP-A0.2b.

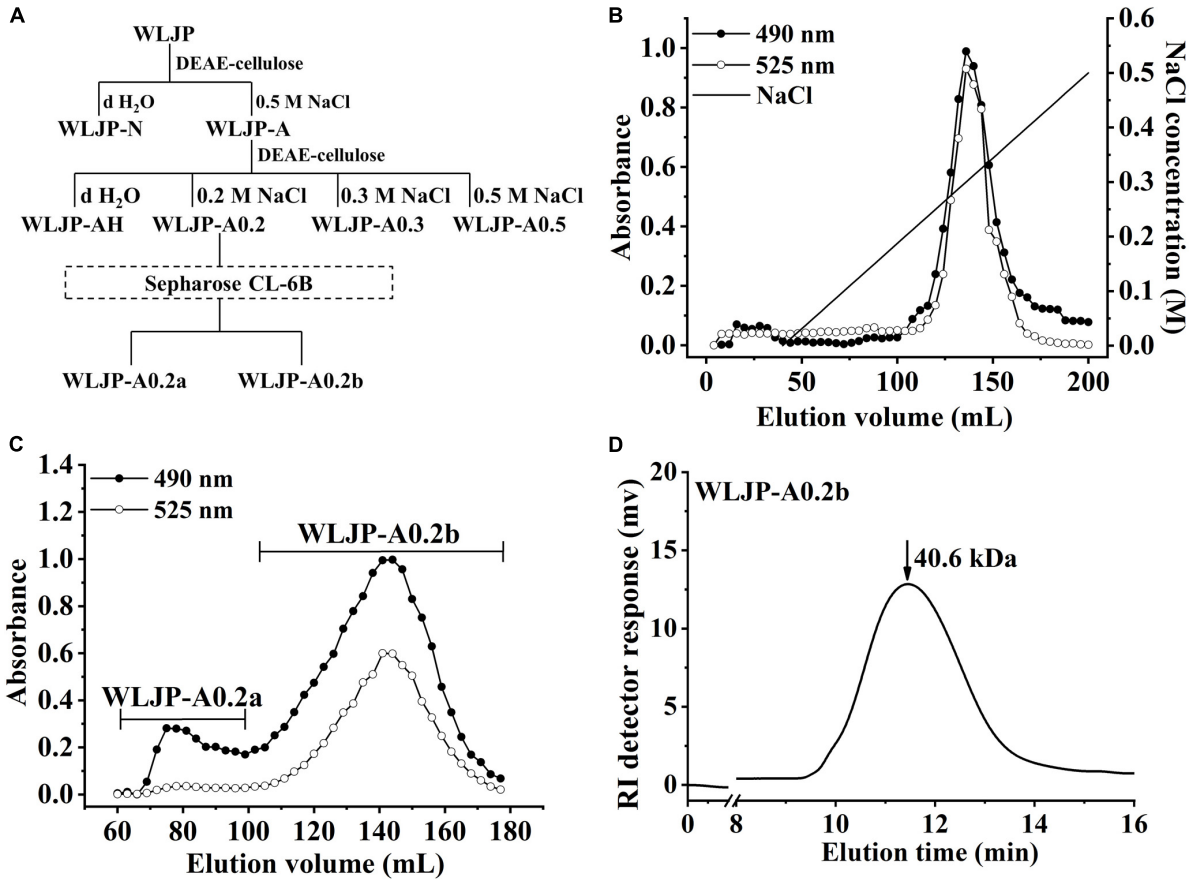

FIGURE 1
Preparation of pectin from *Lonicerae japonicae* Thunb. **(A)** Fractionation scheme of WLJP by anion-exchange and size-exclusion chromatographies. **(B)** Linear gradient elution profile of WLJP-A on DEAE-cellulose column. **(C)** Elution profile of WLJP-A0.2 on Sepharose CL-6B column. (-●- total carbohydrate; -○- uronic acid). **(D)** Molecular weight distribution of WLJP-A0.2b by high performance gel-permeation chromatography (HPGPC) analysis.

major pectic fraction WLJP-A0.2b was obtained. WLJP-A0.2b showed single symmetrical peak on HPGPC (Figure 1D) with molecular weight of 40.6 kDa. It was mainly composed of GalA (72.2%), with minor Ara (15.9%), Gal (5.8%), and Rha (2.8%) (Table 1). The structure of WLJP-A0.2b will be analyzed in detail in this study.

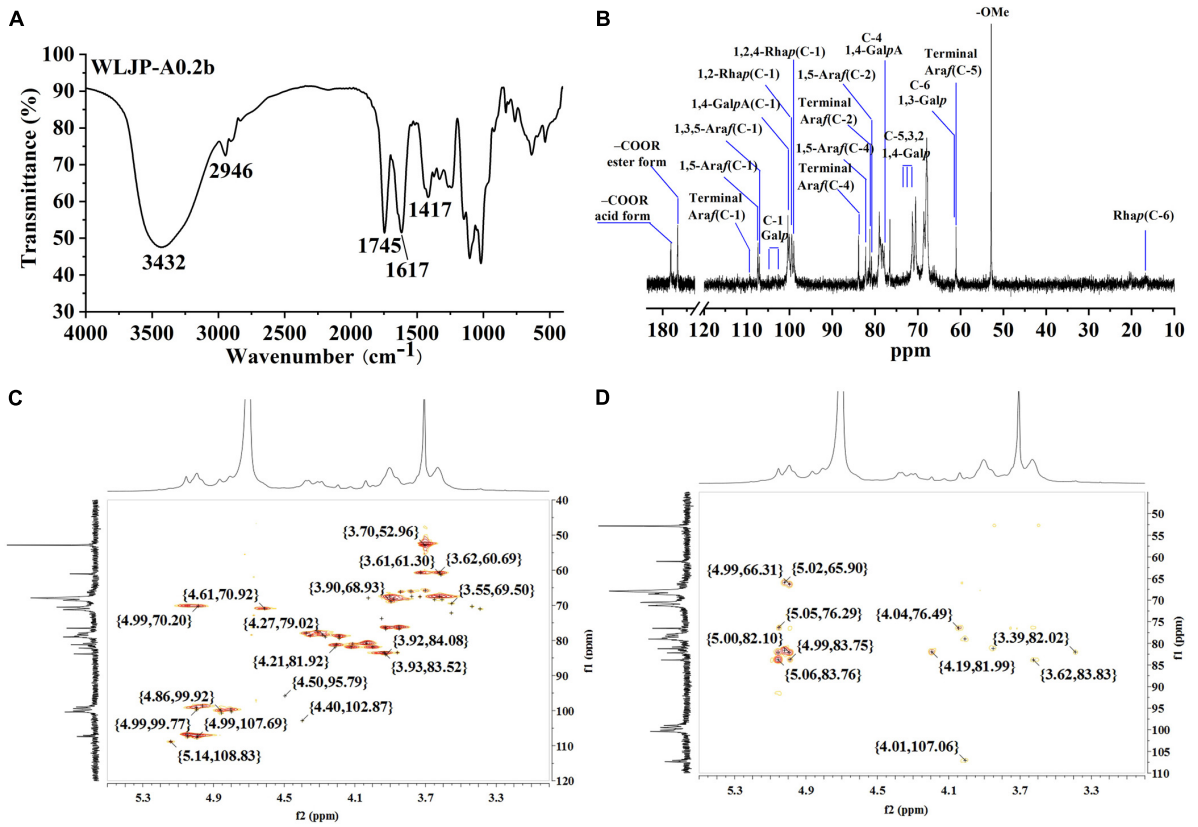

FIGURE 2
Structural analysis of WLJP-A0.2b. **(A)** Fourier transform infrared (FT-IR) spectrum. **(B)** ^{13}C nuclear magnetic resonance (NMR) spectrum. **(C)** HSQC spectrum. **(D)** HMBC spectrum.

Structural analysis of WLJP-A0.2b

Fourier transform infrared analysis of WLJP-A0.2b

The FT-IR spectra of WLJP-A0.2b was presented in Figure 2A. The typical broad peak near 3432 cm^{-1} was assigned to the stretching vibration of O-H, and the adsorption around 2946 cm^{-1} was attributed to C–H stretching of CH_2 groups (30). The bands around 1745, 1617, and 1417 cm^{-1} confirmed the presence of uronic acid. The peaks at around 1745 and 1617 cm^{-1} represent methyl-esterified carbonyl stretching (COOR) and ionic carboxyl band (COO-), respectively (31). The degree of methyl-esterification (DM) was calculated by the area of the band at 1745 cm^{-1} to the sum of the areas of the bands at 1745 and 1617 cm^{-1} (32). The result showed that the DM of WLJP-A0.2b was 32.9%, which was low esterification pectin. The stretching bands between 1010 and 1150 cm^{-1} (e.g., 1018, 1103, and 1145 cm^{-1}) corresponded to the absorption of C-O and C-C glycosidic bonds and the pyranose rings (33). In addition, the peaks around 858 and 896 cm^{-1} suggested the presence of α-linked and β-linked glycosyl residues, respectively (28).

Nuclear magnetic resonance analysis of WLJP-A0.2b

Structural feature of WLJP-A0.2b was characterized by ^{13}C NMR spectrum (Figure 2B). The chemical shifts were assigned predominantly according to ^{1}H and ^{13}C correlations in the HSQC (Figure 2C) and HMBC spectra (Figure 2D).

The typical resonance signals at 100.05/4.80, 68.59/3.60, 70.46/3.90, 77.87/4.31, 70.63/4.61, and 174.91 ppm were assigned to C-1/H-1 to C-5/H-5 and C-6 of unesterified 1,4-α-D-Gal*p*A, respectively, suggesting the presence of HG-type pectin. The signal at 170.68 and 52.77 ppm were attributed to C-6 of methyl-esterified 1,4-α-D-Gal*p*A and methyl groups, respectively. The weak signal at 20.03/2.07 ppm was attributed to acetyl group attached to α-D-Gal*p*A. The resonance signals at 16.81/1.21 and 16.22/1.16 ppm were assigned to C-6/H-6 of 1,2,4-α-L-Rha*p* and 1,2-α-L-Rha*p*, respectively, indicating the presence of RG-I type pectin. The anomeric signals at 108.98/5.14, 107.38/4.99, and 107.06/5.04 ppm corresponded to C-1/H-1 of terminal α-L-Ara*f*, 1,5-α-L-Ara*f*, and 1,3,5-α-L-Ara*f*, respectively. Signals at 104.05/4.40, 103.35/4.37, 103.35/4.37, 103.18/4.35, and 102.31/4.28 ppm were attributed to C-1/H-1

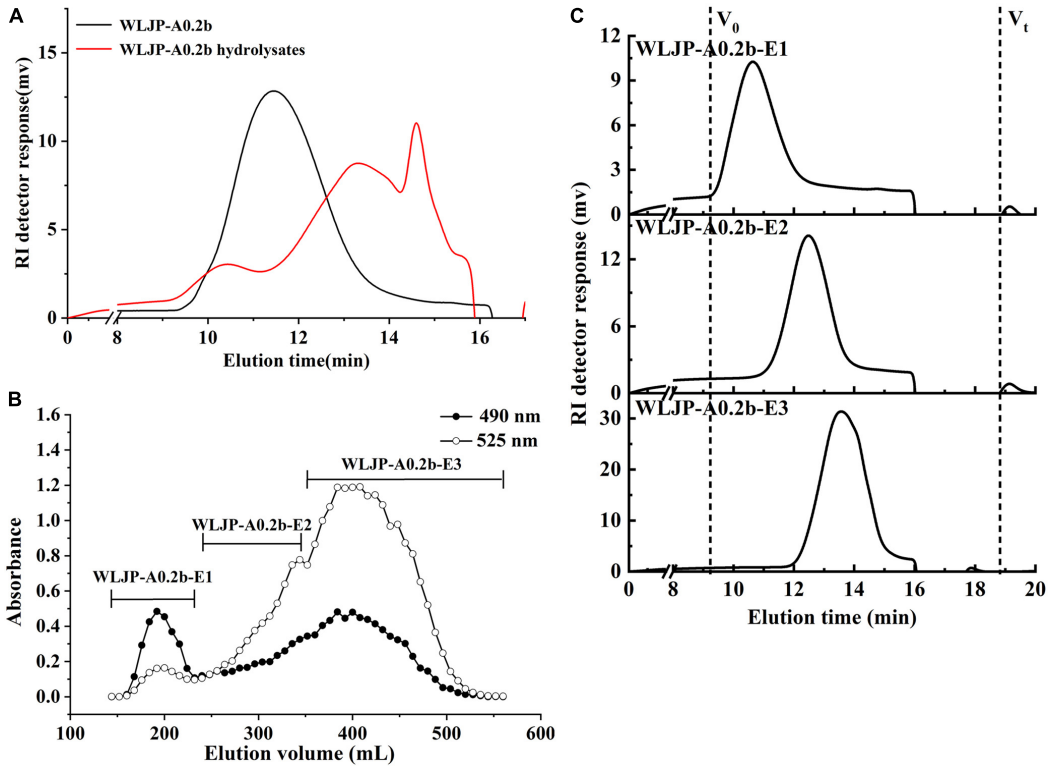

FIGURE 3
(A) The molecular weight distributions of WLJP-A0.2b before and after endo-polygalacturonanase (Endo-PG) hydrolysis. **(B)** The elution profile of enzymatic hydrolysis product of WLJP-A0.2b on Sephadex G-75 (-●- total carbohydrate; -○- uronic acid). **(C)** High performance gel-permeation chromatography (HPGPC) elution profiles of three sub-fractions of WLJP-A0.2b.

of 1,4-β-D-Gal*p*, 1,3,6-β-D-Gal*p*, terminal β-D-Gal*p*, 1,6-β-D-Gal*p*, and 1,3-β-D-Gal*p*, respectively. The complex and overlapped signals at 60 ppm-85 ppm were assigned to C-2 to C-5 of different linkages of Rha, Ara and GalA, and C-2 to C-6 of β-D-Gal*p*. These chemical shift assignments were listed in **Supplementary Table 1**. Additionally, some characteristic signals representing for RG-II type pectin were also found. Signals at 107.36/4.98, 103.38/4.40, and 96.53/4.50 ppm were attributed to C-1/H-1 of α-Ara*f*, α-Ara*p*, and 2-O-Me-α-Xyl*p*, respectively. Signals at 95.11 and 91.87 ppm were assigned to C-2 of α-Kdo*p* and α-Ace*f*A (34, 35). NMR analysis showed that WLJP-A0.2b was composed of HG, RG-I, and RG-II domains. Further analysis of HSQC and HMBC spectra revealed that WLJP-A0.2b contained terminal α-L-Ara*f*, α-L-1,5-Ara*f*, α-L1,3,5-Ara*f*, and β-D-1,3,6-Gal*p* glycosyl linkages, which might form α-L-1,5-arabinan and AG-II side chains in RG-I.

Enzymatic analysis of WLJP-A0.2b

Enzymatic degradation is an efficient tool for elucidating the structure of pectin. To further analyze the structure of WLJP-A0.2b, it was degraded by Endo-PG which could hydrolyze at least four continuous un-esterified α-(1-4)-GalA in HG to release different pectin domains (36, 37). After degradation of WLJP-A0.2b by Endo-PG, the product was detected by HPGPC (**Figure 3A**). As can be seen, the molecular weight distribution of WLJP-A0.2b changed significantly after enzymatic hydrolysis. After separation by size-exclusion chromatography, three sub-fractions (WLJP-A0.2b-E1, WLJP-A0.2b-E2, and WLJP-A0.2b-E3) were obtained, with yield of 7.6, 20.8, and 43.0%, respectively (**Figure 3B**).

WLJP-A0.2b-E1 contained Gal, Ara, Rha, and GalA as major monosaccharides (**Table 1**), and the molar ratio of Rha/GalA was 0.7, typical for RG-I type pectin (38). WLJP-A0.2b-E1 showed single symmetrical peaks on HPGPC with a TSK-gel G-3000 PW_{XL} column, and the molecular weight of it was estimated to be 90.0 kDa (**Figure 3C**). WLJP-A0.2b-E2 was mainly composed of GalA (70.8%), and the molecular weight of it was 14.1 kDa. TBA assay showed positive result, indicating WLJP-A0.2b-E2 was RG-II type pectin. WLJP-A0.2b-E3 contained more than 90% GalA, with molecular weight of 4.7 kDa, indicating that it was oligogalacturonide produced by Endo-PG hydrolyzing of HG domains.

Based on these results, we concluded that WLJP-A0.2b was composed of RG-I, RG-II, and HG domains with mass ratio of 0.4:1.0:2.1, and HG was the dominant domain in WLJP-A0.2b. Different domains were covalently linked and

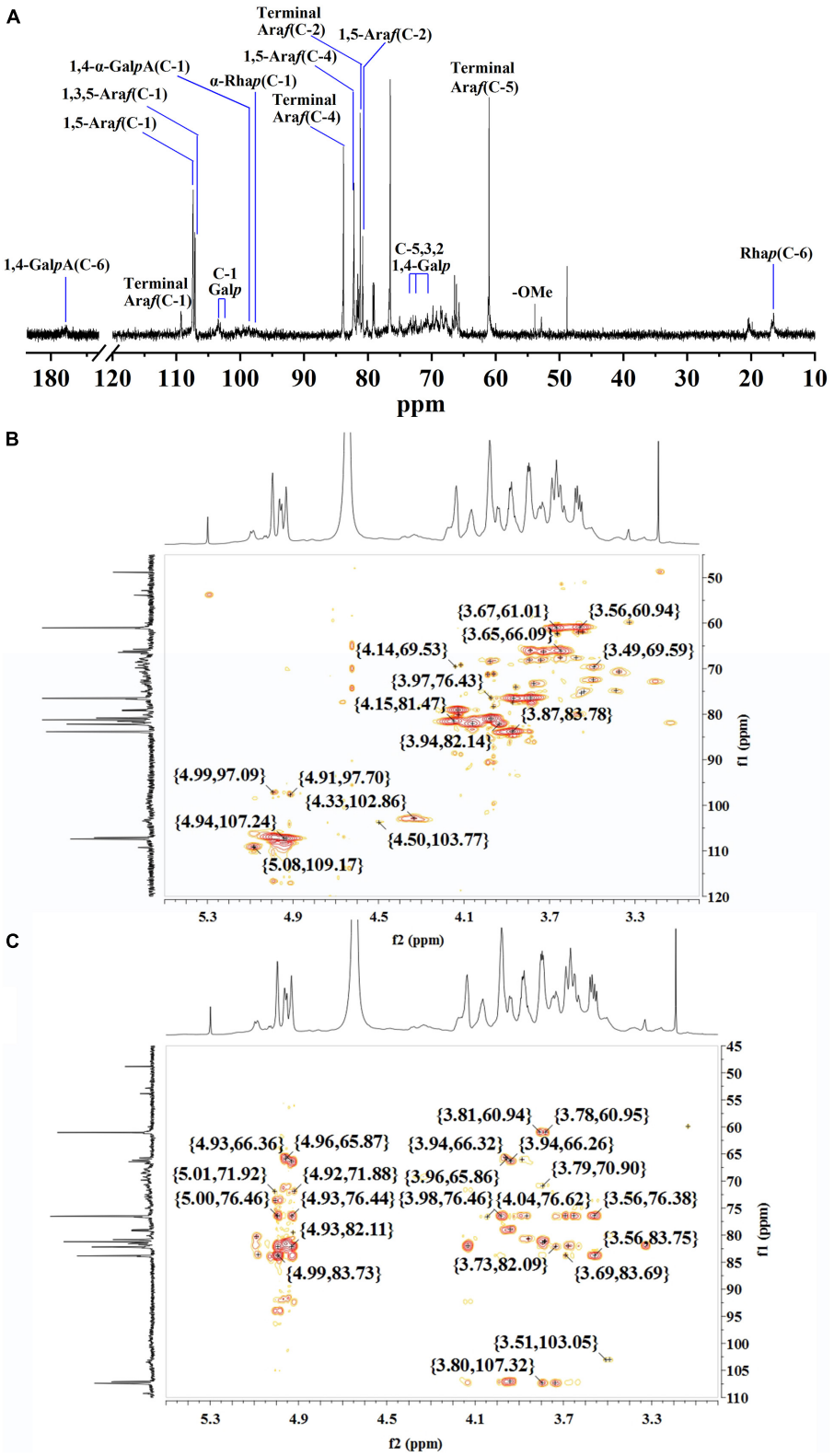

FIGURE 4
Nuclear magnetic resonance (NMR) spectra of WLJP-A0.2b-E1. **(A)** ^{13}C NMR spectrum. **(B)** HSQC spectrum. **(C)** HMBC spectrum.

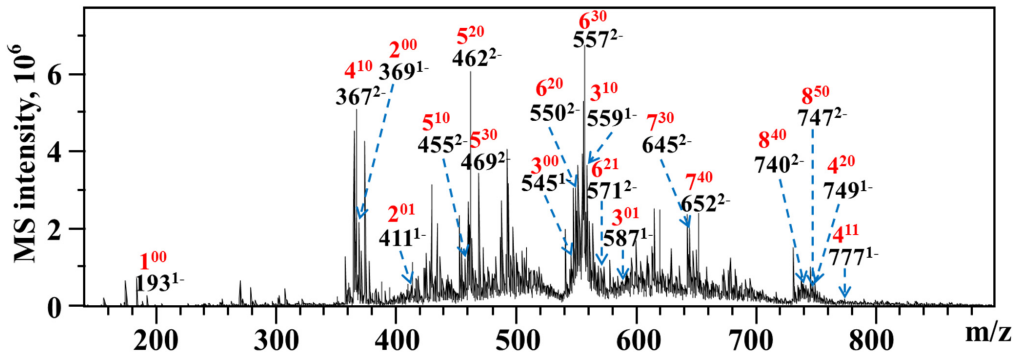

FIGURE 5
ESI-MS analysis of WLJP-A0.2b-E3. Peak annotation: 4^{20}, DP 4, 2 *O*-methyl-ester group, 0 *O*-acetyl group.

released after Endo-PG degradation (27). As RG-II is a type of structurally conserved pectin, it was not further analyzed in this study. We continued to investigate the structures of RG-I and oligogalacturonides.

Structural analysis of pectin domains from WLJP-A0.2b

Nuclear magnetic resonance analysis of rhamnogalacturonan I domain

The structure of WLJP-A0.2b-E1 was analyzed by ^{13}C NMR spectrum (**Figure 4A**). ^{1}H and ^{13}C signals were assigned by using HSQC (**Figure 4B**) and HMBC spectra (**Figure 4C**). The assignments of the major chemical shifts were listed in **Supplementary Table 2**. The signals at 173.64 and 98.60 ppm were attributed to C-6 and C-1 of 1,4-α-D-Gal*p*A, respectively. The resonance signals at 16.46/1.08 and 16.78/1.15 ppm were assigned to C-6/H-6 of 1,2-α-L-Rha*p* and 1,2,4-α-L-Rha*p*, with their corresponding anomeric resonances at 97.47/5.00 ppm. These signals indicated WLJP-A0.2b-E1 contained RG-I backbone. The anomeric signals at 109.26/5.08, 107.38/4.93, and 107.06/4.94 ppm were attributed to C-1/H-1 of terminal α-L-Ara*f*, 1,5-α-L-Ara*f*, and 1,3,5-α-L-Ara*f*, respectively. The anomeric signal at 102.64/4.33 ppm and the corresponding C-6/H-6 signal at 59.75/3.56 ppm were attributed to terminal β-D-Gal*p*. The C-1/H-1 signals at 103.38/4.50, 103.10/4.49, 102.64/4.33, and 102.60/4.32 ppm, and the corresponding C-6/H-6 signals at 59.96/3.55, 69.23/4.11, 69.23/4.11, and 61.18/3.67 ppm were assigned to 1,4-β-D-Gal*p*, 1,3,6-β-D-Gal*p*, 1,6-β-D-Gal*p*, and 1,3-β-D-Gal*p*, respectively. The typical signal at 76.68/3.87 ppm was assigned to C-4/H-4 of 1,4-β-D-Gal*p*. NMR analysis result indicated that WLJP-A0.2b-E1 possessed α-L-1,5-arabinan, β-D-1,4-galactan and AG-II side chains in RG-I domain. As signals corresponding to 1,3,4-β-D-Gal*p* or 1,4,6-β-D-Gal*p* were not clearly observed, AG-I side chains might be not present in WLJP-A0.2b-E1 (39).

ESI-MS analysis of oligogalacturonides

As WLJP-A0.2b-E3 was oligogalacturonide, the structure of it was further analyzed by ESI-MS (**Figure 5**). An overview of *m*/*z* values and speculated structures were shown in **Supplementary Table 3**.

ESI-MS result indicated that WLJP-A0.2b-E3 was composed of un-esterified and partly methyl-esterified and/or acetylated oligogalacturonides with degree of polymerization (DP) from 1 to 8. The monomer (1^{00}), dimer (2^{00}), and trimer (3^{00}) were un-esterified, while other oligogalacturonides were methyl-esterified and/or acetylated. It was possible that the presence of esterification in HG domain caused the resistance of Endo-PG, which acts on four continuous un-esterified α-(1,4)-GalA linkages (40). In WLJP-A0.2b-E3, GalA dimers, trimers, and tetramers containing one to two methyl-esters and/or one acetyl group were detected (2^{01}, 3^{01}, 4^{10}, 4^{11}, and 4^{20}). GalA oligomers with DP 5–6 carrying one to three methyl-ester groups and/or one acetyl group (5^{10}, 5^{20}, 5^{30}, 6^{20}, 6^{21}, and 6^{30}) were found. Oligosaccharide fragments with higher DP containing methyl-ester substitutions, e.g., GalA oligomers with DP 7–8 carrying three to five methyl ester groups (7^{30}, 7^{40}, 8^{40}, and 8^{50}) were also found.

In vitro antioxidant activity assays

The antioxidant activities of WLJP-A0.2b and its different domains including RG-I (WLJP-A0.2b-E1), RG-II (WLJP-A0.2b-E2), and oligogalacturonides (WLJP-A0.2b-E3) were determined by using ABTS, hydroxyl and DPPH radical scavenging assays. As shown in **Figure 6**, WLJP-A0.2b exhibited effective antioxidant activities in the three scavenging assays. After degradation by Endo-PG, the pectin domains isolated from WLJP-A0.2b displayed different antioxidant activities. Compared with RG-I and RG-II domains, oligogalacturonides (WLJP-A0.2b-E3) exhibited the highest antioxidant activities.

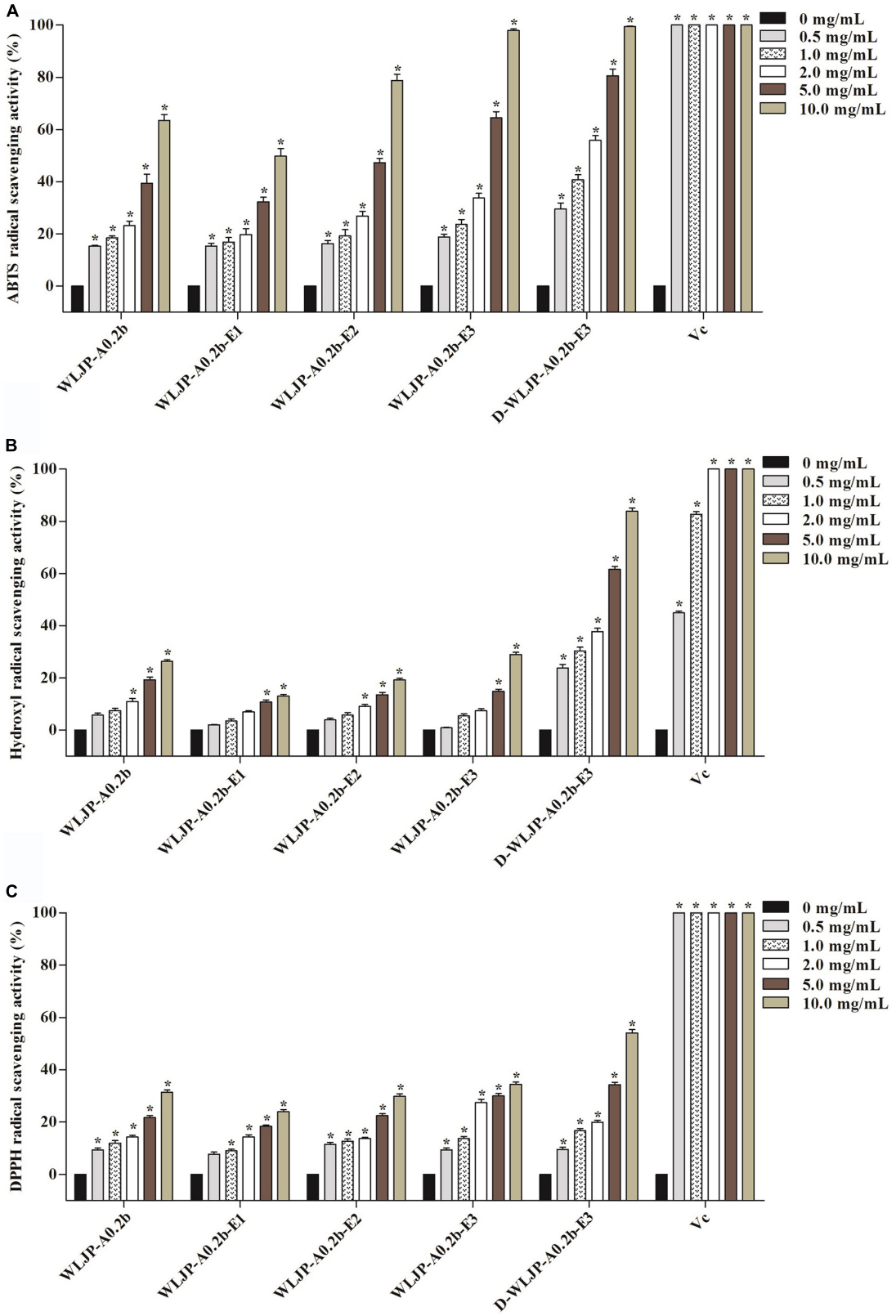

FIGURE 6
Scavenging abilities of pectin from *Lonicera japonica* Thunb. on **(A)** ABTS radical, **(B)** hydroxyl radical, **(C)** DPPH radical. Vc was used as the positive control. Each value represented the mean ± SD ($n = 3$, $^*p < 0.05$). All experiments were performed in triplicate.

Meanwhile, the antioxidant activity of oligogalacturonides was also higher than that of WLJP-A0.2b. The radical scavenging abilities of oligogalacturonides were dose-dependent with the increase of the concentration from 0.5 to 10 mg/ml, but weaker than that of ascorbic acid (Vc). The IC_{50} values (**Table 2**) further indicated that the antioxidant activity of oligogalacturonides was better than RG-II and followed by RG-I domains. Similar results have been reported that SPS-3 and SPS-2 from fruit of Actinidia arguta were HG-rich pectin, which displayed higher antioxidant activities than RG-rich pectin (41).

The higher antioxidant activities of oligogalacturonides might be related to its lower molecular weight and higher GalA content (42, 43). As shown in **Supplementary Figure 1**, the IC_{50} of WLJP-A0.2b-E1 to E3 decreased gradually along with the decrease of their molecular weights, while their IC_{50} values decreased with the increase of galacturonic acid content. The possible reason might be that oligogalacturonides with lower molecular weight would have more reductive hydroxyl group terminals (on per unit mass basis) to accept and eliminate the free radicals (44, 45). Moreover, higher amounts of GalA units present more electrophilic groups, which facilitates the liberation of hydrogen from O-H bond, and thus have good hydrogen supply capacity to scavenge the radical (45, 46).

TABLE 2 IC_{50} values of different pectins from *Lonicera japonica* Thunb. toward the scavenging of ABTS, hydroxyl, and DPPH radical.

Fractions	IC_{50} values (mg/ml)		
	ABTS	·OH⁻	DPPH
WLJP-A0.2b	6.76 ± 0.11	51.69 ± 0.52	53.71 ± 0.58
WLJP-A0.2b-E1	13.63 ± 0.51	182.15 ± 0.87	125.27 ± 0.91
WLJP-A0.2b-E2	4.14 ± 0.13	121.19 ± 0.91	86.81 ± 0.41
WLJP-A0.2b-E3	2.40 ± 0.03	25.14 ± 0.80	27.06 ± 0.53
D-WLJP-A0.2b-E3	1.29 ± 0.08	2.51 ± 0.27	9.41 ± 0.12

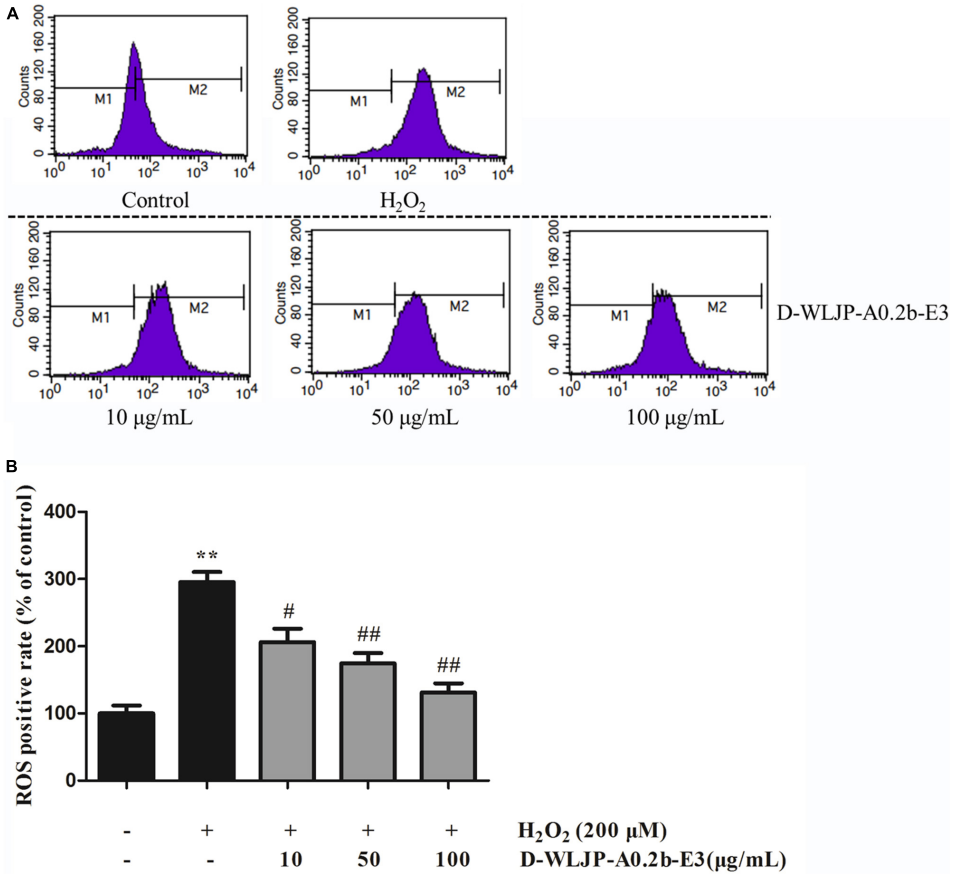

FIGURE 7
Effects of D-WLJP-A0.2b-E3 treatment at different concentrations on H_2O_2-induced intracellular accumulation of reactive oxygen species (ROS) in HEK-293T cells. **(A)** The intracellular levels of ROS analyzed by flow cytometry. **(B)** Histogram analysis of intracellular accumulation of ROS. Data are presented as means ± SD from three independent experiments. $^{**}p < 0.01$ vs. the control group, $^{\#}p < 0.05$ vs. H_2O_2 model group, and $^{\#\#}p < 0.01$ vs. H_2O_2 model group.

In addition, the degree of methyl-esterification (DM) might be also related to the antioxidant activity of oligogalacturonides (45, 47). ESI-MS result indicated that WLJP-A0.2b-E3 contained mostly methyl-esterified oligogalacturonides. To investigate the relationship between DM and antioxidant activities, WLJP-A0.2b-E3 was saponified by alkali to remove methyl-ester groups which was confirmed by FT-IR spectrum (**Supplementary Figure 2**). The de-esterified oligogalacturonides named D-WLJP-A0.2b-E3 was then obtained. The molecular weight distributions of D-WLJP-A0.2b-E3 was the same as WLJP-A0.2b-E3 on HPGPC (**Supplementary Figure 3**). As shown in **Figure 6**, D-WLJP-A0.2b-E3 showed stronger antioxidant capacity than WLJP-A0.2b-E3. The radical scavenging abilities of it increased dose-dependently with the increase of concentration from 0.5 to 10 mg/ml, but still weaker than Vc. It was supposed that more carboxylic groups and electrophilic groups were exposed after de-esterification which were benefit for antioxidant activity. The result was consistent with previous findings (48).

Based on above analysis, we speculated that the antioxidant activity of WLJP-A0.2b was due to the synergistic effects of different pectin domains. Among different domains, oligogalacturonides derived from HG domain displayed the best antioxidant activities, followed by RG-II domain and then RG-I domain. The structural differences including molecular weight, the content of galacturonic acid and the degree of methyl-esterification in different domains appear to explain their varied activities. The de-esterified oligogalacturonide which contained the highest content of galacturonic acid, the lowest molecular weight and the lowest degree of methyl-esterification might be the reason for its strongest antioxidant activity.

Oligogalacturonides reduced intracellular reactive oxygen species generation

Oxidative stress with the excessive production of ROS is considered as the key factor to damage important cellular components including protein, lipid, and DNA, thus resulting in cytotoxicity (49), even leading to cell apoptosis (50, 51). Hence, scavenging the increased ROS to decrease the oxidative stress level and maintain the balance of cellular redox has become urgent. *In vitro* antioxidant activity assays, we have found that de-esterified oligogalacturonides (D-WLJP-A0.2b-E3) displayed the strongest antioxidant activities. To further assess its antioxidant activities, the level of intracellular ROS production after treatment by the oligogalacturonides was tested by flow cytometry. As shown in **Figure 7**, ROS levels increased significantly after being injured with H_2O_2 (248.49 ± 17.37) in contrast to the control group (117.74 ± 13.63) in HEK-293T cells. However, pretreatment with oligogalacturonides significantly reduced the levels of H_2O_2-induced ROS formation with a dose-dependent manner. When the concentration of oligogalacturonides was 100 μg/ml, the ROS level was reduced to 138.60 ± 15.86. These results indicated that oligogalacturonides could protect HEK-293T cells from H_2O_2-induced oxidative stress injury by inhibiting ROS generation, and further confirmed the antioxidant activity of oligogalacturonides.

Conclusion

In the present work, one major pectin fraction WLJP-A0.2b was purified from *Lonicera japonica* Thunb. Structural analysis indicated that it was dominated by HG domains, covalently linked with RG-I and RG-II domains. The mass ratio of RG-I, RG-II, and HG domains in WLJP-A0.2b was 0.4:1.0:2.1. After Endo-PG hydrolysis, HG domain was degraded into oligogalacturonides with DP 1–8 carrying less than 5 methyl-ester groups. RG-I domain from WLJP-A0.2b contained α-L-1,5-arabinan, β-D-1,4-galactan, and AG-II side chains. Radical scavenging assays and intracellular ROS production assay indicated. oligogalacturonides showed the best antioxidant activities compared with RG-II and RG-I domains, and the antioxidant activity of WLJP-A0.2b was due to the synergistic effects of different pectin domains. Therefore, pectic polysaccharides especially oligogalacturonides from *Lonicera japonica* Thunb. could be potential candidates as natural antioxidants and applied in functional food.

Data availability statement

The original contributions presented in this study are included in the article/**Supplementary material**, further inquiries can be directed to the corresponding authors.

Author contributions

XQ and YY: investigation and writing – original draft. XYW, JX, and XW: investigation. ZF: formal analysis. YZ: modifying the manuscript. HX and LS: writing – review and editing. All authors contributed to the article and approved the submitted version.

Funding

This work was supported by the National Natural Science Foundation of China (No. 31870796), the Scientific and Technologic Foundation of Jilin Province (No. 20200201004JC), Innovation Platform Project of Qinghai Province (2021-ZJ-T02), and the Foundation of Qiqihar Science and Technology Bureau (LSFGG-2022053).

Conflict of interest

The authors declare that the research was conducted in the absence of any commercial or financial relationships that could be construed as a potential conflict of interest.

Publisher's note

All claims expressed in this article are solely those of the authors and do not necessarily represent those of their affiliated organizations, or those of the publisher, the editors and the reviewers. Any product that may be evaluated in this article, or claim that may be made by its manufacturer, is not guaranteed or endorsed by the publisher.

Supplementary material

The Supplementary Material for this article can be found online at: https://www.frontiersin.org/articles/10.3389/fnut.2022.998462/full#supplementary-material

References

1. Xiao Z, Wang X, Peng Z, Huang S, Yang P, Li Q, et al. Molecular docking, kinetics study, and structure-activity relationship analysis of quercetin and its analogous as *Helicobacter pylori* urease inhibitors. *J Agric Food Chem.* (2012) 60:10572–7. doi: 10.1021/jf303393n

2. Shang X, Pan H, Li M, Miao X, Ding H. *Lonicera japonica* Thunb.: ethnopharmacology, phytochemistry and pharmacology of an important traditional Chinese medicine. *J Ethnopharmacol.* (2011) 138:1–21. doi: 10.1016/j.jep.2011.08.016

3. Liu N, Liu W, Wang D, Zhou Y, Lin X, Wang X, et al. Purification and partial characterization of polyphenol oxidase from the flower buds of *Lonicera japonica* Thunb. *Food Chem.* (2013) 138:478–83. doi: 10.1016/j.foodchem.2012.10.103

4. Liu Z, Liu C, Liu Q, Ren J, Li L, Huang X, et al. Iridoid glycosides from the flower buds of *Lonicera japonica* and their nitric oxide production and α-glucosidase inhibitory activities. *J Funct Foods.* (2015) 18:512–9. doi: 10.1016/j.jff.2015.08.017

5. Lin L, Wang P, Du Z, Wang W, Cong Q, Zheng C, et al. Structural elucidation of a pectin from flowers of *Lonicera japonica* and its antipancreatic cancer activity. *Int J Biol Macromol.* (2016) 88:130–7. doi: 10.1016/j.ijbiomac.2016.03.025

6. Liu P, Shen H, Zhang Q, Zhou L, Bai X, Zhang T. Inhibition of reinstatement of alcohol-induced conditioned place preference in mice by *Lonicera japonica* polysaccharide. *Food Funct.* (2022) 13:8643–51. doi: 10.1039/d2fo01719a

7. Fang Q, Wang J, Zha X, Cui S, Cao L, Luo J. Immunomodulatory activity on macrophage of a purified polysaccharide extracted from *Laminaria japonica*. *Carbohydr Polym.* (2015) 134:66–73. doi: 10.1016/j.carbpol.2015.07.070

8. Bai X, Chai Y, Shi W, Li Y, Zhang T, Liu P. *Lonicera japonica* polysaccharides attenuate ovalbumin-induced allergic rhinitis by regulation of Th17 cells in BALB/c mice. *J Funct Foods.* (2020) 65:103758. doi: 10.1016/j.jff.2019.103758

9. Zhang T, Liu H, Bai X, Liu P, Yang Y, Huang J, et al. Fractionation and antioxidant activities of the water-soluble polysaccharides from *Lonicera japonica* Thunb. *Int J Biol Macromol.* (2020) 151:1058–66. doi: 10.1016/j.ijbiomac.2019.10.147

10. Liu P, Bai X, Zhang T, Zhou L, Li J, Zhang L. The protective effect of *Lonicera japonica* polysaccharide on mice with depression by inhibiting NLRP3 inflammasome. *Ann Transl Med.* (2019) 7:811. doi: 10.21037/atm.2019.12.64

11. Willats WGT, McCartney L, Mackie W, Knox JP. Pectin: cell biology and prospects for functional analysis. *Plant Mol Biol.* (2001) 47:9–27. doi: 10.1023/A:1010662911148

12. Ridley BL, O'Neill MA, Mohnen DA. Pectins: structure, biosynthesis, and oligogalacturonide-related signaling. *Phytochemistry.* (2001) 57:929–67. doi: 10.1016/S0031-9422(01)00113-3

13. Grankvist N, Amable L, Honkanen RE, Sjoholm A, Ortsater H. Serine/threonine protein phosphatase 5 regulates glucose homeostasis in vivo and apoptosis signalling in mouse pancreatic islets and clonal MIN6 cells. *Diabetologia.* (2012) 55:2005–15. doi: 10.1007/s00125-012-2541-1

14. Li H, Su L, Chen S, Zhao L, Wang H, Ding F, et al. Physicochemical characterization and functional analysis of the polysaccharide from the edible microalga Nostoc sphaeroides. *Molecules.* (2018) 23:508. doi: 10.3390/molecules23020508

15. Zacharski LR, Shamayeva G, Chow BK. Iron reduction response and demographic differences between diabetics and non-diabetics with cardiovascular disease entered into a controlled clinical trial. *Metallomics.* (2018) 10:264–77. doi: 10.1039/c7mt00282c

16. Bronzuoli MR, Facchinetti R, Steardo L, Scuderi C. Astrocyte: an innovative approach for Alzheimer's disease therapy. *Curr Pharm Des.* (2017) 23:4979–89. doi: 10.2174/1381612823666170710163411

17. Chu Q, Zhang S, Yu L, Li Y, Liu Y, Ye X, et al. *Apios americana* medikus tuber polysaccharide exerts anti-inflammatory effects by activating autophagy. *Int J Biol Macromol.* (2019) 130:892–902. doi: 10.1016/j.ijbiomac.2019.03.012

18. Feng S, Cheng H, Xu Z, Shen S, Yuan M, Liu J, et al. Thermal stress resistance and aging effects of *Panax notoginseng* polysaccharides on *Caenorhabditis elegans*. *Int J Biol Macromol.* (2015) 81:188–94. doi: 10.1016/j.ijbiomac.2015.07.057

19. Dubois M, Gilles KA, Hamilton JK, Rebers PA, Smith F. Colorimetric method for determination of sugars and related substances. *Anal Chem.* (1956) 28:350–6. doi: 10.1021/ac60111a017

20. Blumenkrantz N, Asboe-Hansen G. New method for quantitative determination of uronic acids. *Anal Biochem.* (1973) 54:484–9. doi: 10.1016/0003-2697(73)90377-1

21. York WS, Darvill AG, McNeil M, Albersheim P. 3-deoxy-d-manno-2-octulosonic acid (KDO) is a component of rhamnogalacturonan II, a pectic polysaccharide in the primary cell walls of plants. *Carbohydr Res.* (1985) 138:109–26. doi: 10.1016/0008-6215(85)85228-9

22. Sedmak JJ, Grossberg SE. Rapid, sensitive, and versatile assay for protein using Coomassie brilliant blue G250. *Anal Biochem.* (1977) 79:544–52. doi: 10.1016/0003-2697(77)90428-6

23. Zhang X, Yu L, Bi H, Li X, Ni W, Han H, et al. Total fractionation and characterization of the water-soluble polysaccharides isolated from *Panax ginseng* C. A. Meyer. *Carbohydr Polym.* (2009) 77:544–52. doi: 10.1016/j.carbpol.2009.01.034

24. Yu L, Zhang X, Li S, Liu X, Sun L, Liu H, et al. Rhamnogalacturonan I domains from ginseng pectin. *Carbohydr Polym.* (2010) 79:811–7. doi: 10.1016/j.carbpol.2009.08.028

25. Thibault JF, Renard CMGC, Axelos MAV, Roger P, Crépeau MJ. Studies of the length of homogalacturonic regions in pectins by acid hydrolysis. *Carbohydr Res.* (1993) 238:271–86. doi: 10.1016/0008-6215(93)87019-O

26. Chen S, Shang H, Yang J, Li R, Wu H. Effects of different extraction techniques on physicochemical properties and activities of polysaccharides from comfrey (*Symphytum officinale* L.) root. *Ind Crop Prod.* (2018) 121:18–25. doi: 10.1016/j.indcrop.2018.04.063

27. Ning X, Liu Y, Jia M, Wang Q, Sun Z, Ji L, et al. Pectic polysaccharides from Radix Sophorae Tonkinensis exhibit significant antioxidant effects. *Carbohydr Polym.* (2021) 262:117925. doi: 10.1016/j.carbpol.2021.117925

28. Yan J, Zhu L, Qu Y, Qu X, Mu M, Zhang M, et al. Analyses of active antioxidant polysaccharides from four edible mushrooms. *Int J Biol Macromol.* (2019) 123:945–56. doi: 10.1016/j.ijbiomac.2018.11.079

29. Yu Q, Nie S, Wang J, Huang D, Li W, Xie M. Toll-like receptor 4 mediates the antitumor host response induced by ganoderma atrum polysaccharide. *J Agric Food Chem.* (2015) 63:517–25. doi: 10.1021/jf5041096

30. Zhang H, Chen J, Li J, Yan L, Li S, Ye X, et al. Extraction and characterization of RG-I enriched pectic polysaccharides from mandarin citrus peel. *Food Hydrocoll.* (2018) 79:579–86. doi: 10.1016/j.foodhyd.2017.12.002

31. Ogutu FO, Mu TH. Ultrasonic degradation of sweet potato pectin and its antioxidant activity. *Ultrason Sonochem.* (2017) 38:726–34. doi: 10.1016/j.ultsonch.2016.08.014

32. Amamou S, Lazreg H, Hafsa J, Majdoub H, Rihouey C, Le Cerf D, et al. Effect of extraction condition on the antioxidant, antiglycation and alpha-amylase inhibitory activities of Opuntia macrorhiza fruit peels polysaccharides. *LWT Food Sci Technol.* (2020) 127:109411. doi: 10.1016/j.lwt.2020.109411

33. Li J, Li S, Zheng Y, Zhang H, Chen J, Yan L, et al. Fast preparation of rhamnogalacturonan I enriched low molecular weight pectic polysaccharide by ultrasonically accelerated metal-free Fenton reaction. *Food Hydrocoll.* (2019) 95:551–61. doi: 10.1016/j.foodhyd.2018.05.025

34. Cui L, Wang J, Huang R, Tan Y, Zhang F, Zhou Y, et al. Analysis of pectin from *Panax ginseng* flower buds and their binding activities to galectin-3. *Int J Biol Macromol.* (2019) 128:459–67. doi: 10.1016/j.ijbiomac.2019.01.129

35. Wu D, Cui L, Yang G, Ning X, Sun L, Zhou Y. Preparing rhamnogalacturonan II domains from seven plant pectins using *Penicillium oxalicum* degradation and their structural comparison. *Carbohydr Polym.* (2018) 180:209–15. doi: 10.1016/j.carbpol.2017.10.037

36. Sun L, Ropartz D, Cui L, Shi H, Ralet MC, Zhou Y. Structural characterization of rhamnogalacturonan domains from *Panax ginseng* C. A. Meyer. *Carbohydr Polym.* (2019) 203:119–27. doi: 10.1016/j.carbpol.2018.09.045

37. Sharma N, Rathore M, Sharma M. Microbial pectinase: sources, characterization and applications. *Rev Environ Sci Biotechnol.* (2013) 12:45–60. doi: 10.1007/s11157-012-9276-9

38. Sun L, Wu D, Ning X, Yang G, Lin Z, Tian M, et al. α-Amylase-assisted extraction of polysaccharides from *Panax ginseng*. *Int J Biol Macromol.* (2015) 75:152–7. doi: 10.1016/j.ijbiomac.2015.01.025

39. Leivas CL, Iacomini M, Cordeiro LMC. Structural characterization of a rhamnogalacturonan I-arabinan-type I arabinogalactan macromolecule from starfruit (*Averrhoa carambola* L.). *Carbohydr Polym.* (2015) 121:224–30. doi: 10.1016/j.carbpol.2014.12.034

40. Ognyanov M, Remoroza C, Schols HA, Georgiev YN, Petkova NT, Krystyjan M. Structural, rheological and functional properties of galactose-rich pectic polysaccharide fraction from leek. *Carbohydr Polym.* (2020) 229:115549. doi: 10.1016/j.carbpol.2019.115549

41. Zhu R, Zhang X, Wang Y, Zhang L, Zhao J, Chen G, et al. Characterization of polysaccharide fractions from fruit of *Actinidia arguta* and assessment of their antioxidant and antiglycated activities. *Carbohydr Polym.* (2019) 210:73–84. doi: 10.1016/j.carbpol.2019.01.037

42. Mateos-Aparicio I, Mateos-Peinado C, Jimenez-Escrig A, Ruperez P. Multifunctional antioxidant activity of polysaccharide fractions from the soybean byproduct okara. *Carbohydr Polym.* (2010) 82:245–50. doi: 10.1016/j.carbpol.2010.04.020

43. Ji X, Cheng Y, Tian J, Zhang S, Jing Y, Shi M. Structural characterization of polysaccharide from jujube (*Ziziphus jujuba* Mill.) fruit. *Chem Biol Technol Agric.* (2021) 8:54. doi: 10.1186/s40538-021-00255-2

44. Fan L, Li J, Deng K, Ai L. Effects of drying methods on the antioxidant activities of polysaccharides extracted from *Ganoderma lucidum*. *Carbohydr Polym.* (2012) 87:1849–54. doi: 10.1016/j.carbpol.2011.10.018

45. Wang J, Hu S, Nie S, Yu Q, Xie M. Reviews on mechanisms of in vitro antioxidant activity of polysaccharides. *Oxid Med Cell Longev.* (2016) 2016:5692852. doi: 10.1155/2016/5692852

46. Chen R, Li S, Liu C, Yang S, Li X. Ultrasound complex enzymes assisted extraction and biochemical activities of polysaccharides from Epimedium leaves. *Process Biochem.* (2012) 47:2040–50. doi: 10.1016/j.procbio.2012.07.022

47. Zou YF, Zhang YY, Paulsen BS, Rise F, Chen ZL, Jia RY, et al. Structural features of pectic polysaccharides from stems of two species of Radix Codonopsis and their antioxidant activities. *Int J Biol Macromol.* (2020) 159:704–13. doi: 10.1016/j.ijbiomac.2020.05.083

48. Chen R, Luo S, Wang C, Bai H, Lu J, Li T, et al. Effects of ultra-high pressure enzyme extraction on characteristics and functional properties of red pitaya (*Hylocereus polyrhizus*) peel pectic polysaccharides. *Food Hydrocoll.* (2021) 121:107016. doi: 10.1016/j.foodhyd.2021.107016

49. Ji X, Guo J, Ding D, Gao J, Hao L, Guo X, et al. Structural characterization and antioxidant activity of a novel high-molecular-weight polysaccharide from *Ziziphus jujuba* cv. Muzao. *J Food Meas Charact.* (2022) 16:2191–200. doi: 10.1007/s11694-022-01288-3

50. Chun F, Zhang B, Lin H, Gao C, Min WD-. Fagomine attenuates high glucose-induced endothelial cell oxidative damage by upregulating the expression of PGC-1 alpha. *J Agric Food Chem.* (2018) 66:2758–64. doi: 10.1021/acs.jafc.7b05942

51. Zhai X, Yuan S, Yang X, Zou P, Li L, Li G, et al. Chitosan oligosaccharides induce apoptosis in human renal carcinoma via reactive-oxygen-species-dependent endoplasmic reticulum stress. *J Agric Food Chem.* (2019) 67:1691–701. doi: 10.1021/acs.jafc.8b06941

frontiers | Frontiers in Nutrition

TYPE Original Research
PUBLISHED 29 September 2022
DOI 10.3389/fnut.2022.1016961

Check for updates

OPEN ACCESS

EDITED BY
Xiaolong Ji,
Zhengzhou University of Light Industry, China

REVIEWED BY
Bin Du,
Hebei Normal University of Science and Technology, China
Zhen Ma,
Shaanxi Normal University, China
Ding-Tao Wu,
Chengdu University, China

*CORRESPONDENCE
Qingbin Guo
guoqingbin008322@tust.edu.cn
Shaoping Nie
spnie@ncu.edu.cn

SPECIALTY SECTION
This article was submitted to Food Chemistry, a section of the journal Frontiers in Nutrition

RECEIVED 11 August 2022
ACCEPTED 16 September 2022
PUBLISHED 29 September 2022

CITATION
Guo X, Yang M, Wang C, Nie S, Cui SW and Guo Q (2022) Acetyl-glucomannan from *Dendrobium officinale*: Structural modification and immunomodulatory activities.
Front. Nutr. 9:1016961.
doi: 10.3389/fnut.2022.1016961

COPYRIGHT
© 2022 Guo, Yang, Wang, Nie, Cui and Guo. This is an open-access article distributed under the terms of the Creative Commons Attribution License (CC BY). The use, distribution or reproduction in other forums is permitted, provided the original author(s) and the copyright owner(s) are credited and that the original publication in this journal is cited, in accordance with accepted academic practice. No use, distribution or reproduction is permitted which does not comply with these terms.

Acetyl-glucomannan from *Dendrobium officinale*: Structural modification and immunomodulatory activities

Xiaoyu Guo[1], Mingguan Yang[2], Changlu Wang[1], Shaoping Nie[3]*, Steve W. Cui[4] and Qingbin Guo[1]*

[1]State Key Laboratory of Food Nutrition and Safety, College of Food Science and Technology, Tianjin University of Science and Technology, Tianjin, China, [2]College of Food Science and Engineering, Qilu University of Technology (Shandong Academy of Sciences), Jinan, China, [3]State Key Laboratory of Food Science and Technology, China-Canada Joint Laboratory of Food Science and Technology (Nanchang), Nanchang University, Nanchang, China, [4]Guelph Research and Development Centre, Agriculture and Agri-Food Canada, Guelph, ON, Canada

To understand the mechanisms of immunomodulatory effect, *Dendrobium Officinale* polysaccharides (DOP) were treated by ultrasound and mild base separately to generate fractions of various weight-average molecular weight (Mw) and degrees of acetylation (DA). The structural features, conformational properties, functional properties and immunomodulatory activities of original and modified DOPs were investigated. Ultrasonic treatment decreased the Mw and apparent viscosity and improved the water solubility of DOP. Mild base treatment remarkably reduced the DA and the water solubility, while the overall apparent viscosity was increased. Conformational analysis by triple-detector high performance size-exclusion chromatography showed that the molecular chain of DOP turned more compact coil conformation with decreased DA. Results from the macrophages RAW 264.7 analysis showed that samples sonicated for 200 min (Mw 34.2 kDa) showed the highest immune-regulation effects. However, the immunomodulatory effects of the samples after de-acetylation were all compromised compared to the original DOP. This study inspires further research to establish the structural-immunomodulatory relationships, which promote the application of DOP in both the food and medicine fields.

KEYWORDS

***Dendrobium officinale* polysaccharide, O-acetylation, immunomodulatory, structural modification, glucomannan**

Introduction

Dendrobium officinale polysaccharides (DOP) have been successfully discovered and widely used in healthy food and medicine due to the broad spectrum of their biological properties. Many *in vitro* and *in vivo* studies indicated that DOP had immunomodulatory, antitumor, maintenance of colonic health, gastro-protective, hypoglycemic, antiinflammatory, antioxidative, antimutagenic, hepatoprotective, and vasodilating effects (1–3). These effects are closely related to various structural characteristics of DOP, e.g., molecular weight, higher-order structure (i.e., conformation), functional groups, and degree of branching (4, 5). DOP is a linear glucomannan consisting of D-mannose and D-glucose linked by β-1,4 glycosidic bonds at varied ratios. Acetyl groups in DOP have been identified to attach to O-2 and O-3 of mannan in the majority of mono-substituted and small amounts of di-substituted forms (6, 7). The M_W of DOP has been reported to be varied from 8.5 to 399 kDa (4).

A variety of biological activities, such as immunomodulating and immuno-pharmacological activities, are observed with DOP. DOP plays a vital role in regulating the immune system by strengthening one or several nonspecific immune responses, cellular-mediated immune responses, and humoral immune responses (4). Results of recent *in vitro* experiments on different kinds of murine or human cells (dendritic cells, spleen cells, macrophage cells, and THP-1 cells) demonstrated that DOP could promote cell viability, NO production, and cytokine secretion (TNF-α, IL-1β). Some *in vivo* studies have shown that DOP could stimulate the proliferation of splenocytes, balance the ratio of spleen lymphocyte subsets and the secretion of serum cytokines, up-regulate the serum IgM, IgG, and haemolysin formation, and accelerate the phagocytotic function of peritoneal macrophage (8–10). The immune response exerted by DOP was reported to be mediated through the TLR-4 signaling pathway (8). However, detailed information regarding the relationship between the molecular structure of DOP and its immunomodulatory effects remains scant.

To bridge the gap between the molecular structure and immunomodulatory effects of DOP, structural modification is not neglectable. Different molecular degradation and derivatization methods have been used, including alkylation, carboxymethylation, sulfation, selenylation, phosphorylation, ultrasonic disruption, and the degradation of polysaccharides, which are generally classified as chemical, physical, and biological modifications (11). However, finding a suitable modification method is difficult. For example, decreasing the Mw of polysaccharides without affecting the other structural features, e.g., degree of branching or monosaccharide composition, is challenging. Recently, our team have tried trifluoroacetic acid (TFA) hydrolysis, xylanase treatment, and ultrasonication treatment to degrade arabinoxylan from wheat bran. Results indicated that TFA favored the removal of the arabinose side chain; xylanase treatment results in two fractions with different Mw; only ultrasonication treatment could decrease the Mw without affecting the overall degree of branching and solubility of arabinoxylan (12). Similarly, to understand the effects of DA on the bioactive properties of DOP, either acetylation or de-acetylation needs to be conducted to obtain samples of varied DA. However, the acetylation reaction can not control the reaction sites, given that the acetyl groups of naturally occurring DOP locate only on O-2 and/or O-3 positions of mannose residues (7). For de-acetylation reaction, strong bases such as NaOH solution excludes most acetyl groups altogether, even under a small concentration and short time duration. The produced DOPs by NaOH treatment contains only trace amount of acetyl groups, leading to poor water solubility (13). Therefore, mild bases, e.g., Na_2CO_3, were gradually used to remove the acetyl group to get DOP fractions with varied DA values (14).

In this study, DOP was degraded and de-acetylated using the ultrasonic and Na_2CO_3 treatments separately. The structural features, conformational properties, functional properties, and immunomodulatory activities of native and modified DOPs were investigated, aiming to understand their structure-bioactivity relationships and facilitate applications in health and functional food areas.

Materials and methods

Materials

The RAW 264.7 macrophages were obtained from the key laboratory of food nutrition and safety, Tianjin University of Science and Technology, Tianjin, China. The monosaccharide standards (D-Glucose, D-Xylose, L-Rhamnose, D-Mannose, L-Arabinose, and D-Galactose) were purchased from Sigma Chemical Co. (St. Louis, MO, USA). The ELISA kits were purchased from Multisciences (Lianke) Biotech Co. Ltd. (Hangzhou, China). All other chemical reagents and solvents purchased were all analytical grade unless otherwise stated.

Extraction and purification of *Dendrobium Officinale* polysaccharides

The extraction and purification of DOP were conducted according to Wang et al. with slight modifications (15). Briefly, dry powder of the *D. officinale* herbal (250 g) was suspended in 95% ethanol (250 ml) in a beaker with constant stirring for 24 h. The suspension was subjected to two more cycles of 24-h soaking and subsequent centrifugation at 10,000 *g* and 25°C for 20 min. Then, the residue was extracted with water (1:20 w/v) stirred at 70°C for 4 h followed by centrifugation

at 10,000 *g* and 25°C for 20 min. The obtained supernatants were concentrated (to 1/4 of the original volume) using a rotary evaporator, and then ethanol precipitated (1:3 ratio, v/v) at room temperature to accumulate the crude polysaccharide. Subsequently, thermostable α-amylase (3,000 units/ml) was added to 1% polysaccharide solution, stirred at 70°C for 2 h, and then cooled to room temperature. The small molecular weight contaminants produced by the hydrolysis were removed by dialysis against deionized water (with 3,500 Da cut-off) for 72 h. The solution was further freeze-dried to obtain a dry sample of purified polysaccharide (DOP).

Chemical composition analysis

The total sugar content was determined by the phenol-sulfuric acid method with glucose as the standard (16). The soluble protein was determined using the Ninhydrin colorimetry method (Amino acid detection kit, Solarbio) (15).

Molecular modification of *Dendrobium Officinale* polysaccharides

The ultrasonic treatment of DOP was performed according to Striegel et al. with slight modifications (17). About 30 ml DOP solution (10 mg/ml) was prepared at room temperature under constant stirring. Ultrasonic treatment was then performed by an ultrasonic homogenizer (JY92-IIN, Ningbo Scientz Biotechnology Corporation, China) under controlled conditions (500 W, 40°C, on for 2 s, off for 1 s) for 60, 200, and 720 min, respectively. The samples were then ethanol precipitated (1:3 ratio, v/v) to obtain the modified DOPs, which were termed as US-60, US-200, and US-720, respectively.

De-acetylation of DOP was carried out according to Tamaki with slight modifications (18). Briefly, DOP (50 mg) was completely dissolved in distilled water (20 ml). After adding an equal volume of 0.2 M Na_2CO_3 solution, the suspension was then reacted at 25°C for 3, 5, and 25 min separately with continuous mixing. The mixture was quickly adjusted to pH 4.5 with 1 M HCl, dialyzed against distilled water, and then freeze-dried. These samples obtained were depicted as DA-3, DA-5, and DA-25, respectively.

Structural characterization

Degree of acetylation

The degree of acetylation (DA)of modified DOPs was determined by the titration method according to Huang et al. with slight modifications (19). Twenty milligram of grounded sample was added to the aqueous solution of sodium hydroxide (0.01 M, 10 ml) and kept in the water bath (50°C) for 2 h. The excess alkali was titrated with 0.01 M hydrochloride acid using phenolaphtalen as the indicator. The degree of de-acetylation (DD) was calculated according to the equation as follows (20).

$$DA\,(\%) = [(V_0C_0 - V_1C_1) \times 0.043 \times 100]\,/M \quad (1)$$

Where V_0 is the volume of NaOH in ml, C_0 is the concentration of NaOH in mol/L, V_1 is the volume of HCl in ml, C_1 is the concentration of HCl in mol/L, M is the weight of the sample (dry) in g.

$$DD\,(\%) = \frac{A_1 - A_0}{A_1} \times 100 \quad (2)$$

A_1 is the acetyl group content of DOP in %, A_0 is the acetyl group content of de-acetylated DOP in %.

Methylation analysis

The methylation analysis was performed as described previously (21). Firstly, 3 mg of sample was fully dissolved in dimethyl sulfoxide (0.5 ml) and then dried NaOH powder (20 mg) was added to the solution with stirring for 2 h at room temperature. Methyl iodide (0.6 ml) was then added to fully convert all the free hydroxyl groups into methoxy groups and evaporated by a stream of nitrogen. The dried methylated polysaccharides were hydrolyzed by TFA (4 M), reduced using sodium borodeuteride (4 mg) and acetylated with acetic anhydride (50 μl) to produce the partially methylated alditol acetates (PMAA). PMAAs were then analyzed using GC-MS (Agilent 7890, USA) equipped with an HP-5 column programmed from 160 to 210°C at 2°C/min, and then 210 to 240°C at 5°C/min.

FT-IR analysis

FT-IR spectra of samples were obtained according to the KBr disk method. Briefly, 1 mg polysaccharide was ground with 150 mg KBr into a fine powder and then pressed into a pellet, which is measured using the FT-IR spectrometer (Nicolet IS50, USA) in the frequency range of 4,000–400 cm^{-1} with 32 scans at a resolution of 4 cm^{-1}.

Water solubility test

The water solubility was evaluated according to Zhu et al. with slight modifications (22). Briefly, samples (0.5%, w/v) were dispersed in distilled water followed by incubation at 25°C for 90 min and mixing for 5 s every 30 min. The mixture was centrifuged (10,000 *g* and 25°C for 5 min) to collect the insoluble sediment, followed by freeze-drying. The solubility was calculated based on the following equation as follows:

$$\text{Solubility}(\%) = \frac{w_i - w_p}{w_i} \times 100 \quad (3)$$

Where w_i is the initial weight of the complete sample in g, and w_p is the weight of the dried sediment in g.

High performance size-exclusion chromatography analysis

The chain conformation of samples was analyzed using an high performance size-exclusion chromatography (HPSEC) equipped with multi-detectors (multi-angle laser light scattering, refractive index, ultraviolet detector, and online viscometer). Samples were eluted at a flow speed of 0.6 ml/min within Shodex TM OHpak SB-803 HQ (8.0 × 300 mm, 6 μm) and SB-805 HQ (8.0 × 300 mm, 13 μm) columns (Showa Denko K.K., Tokyo, Japan) in series. The columns and detectors were maintained at 40°C. Data was analyzed using the ASTRA 7.1.3 software. A refractive index increment (dn/dc) of 0.146 ml/g was used in the calculation.

Immunomodulatory assays

Cell culture

RAW264.7 macrophages were cultured in RPMI-1640 medium (Gibco, USA) supplemented with 10% fetal bovine serum (Gemini, USA) and 1% penicillin-streptomycin (Hyclone, USA) and incubated at 37°C with a 5% CO_2 humidified atmosphere in a carbon dioxide cell incubator (Thermo, USA). The cells were stimulated with the control group (without polysaccharides), positive control group (LPS: 2 μg/mL) and various concentrations of DOP and modified DOPs (50, 100, 200, 400, and 800 μg/mL) (23).

The proliferation and phagocytosis activity assays

Cells were adjusted to a concentration of 5×10^4 cells/ml, loaded onto the 96-well plates (100 μl/well), and continuously incubated for 12 h. Then, the cells were stimulated with the blank control group (without polysaccharides), LPS and polysaccharide samples (50, 100, 200, 400, and 800 μg/ml). After incubation for 24 h, the proliferation activity was determined using the CCK-8 method (24). Each concentration was repeated six times in the well. RAW264.7 cells (5×10^4 cells/ml) were seeded into a 96-well flat-bottom plate and cultured for 12 h. Then, samples (100 μg/ml: the optimal concentration screened from proliferation activity) were added, followed by another 24 h incubation. After that, the phagocytosis activity was determined by the neutral red staining method (25). Each concentration was repeated six times in the well.

Quantitative analysis of NO and cytokines

RAW264.7 cells (1×10^5 cells/ml) were seeded into a 24-well flat-bottom plate and cultured for 12 h. Then, control, LPS, and polysaccharide samples (100 μg/ml) were added to cells. After incubation for another 24 h, the cultured supernatants were collected (26). The quantifications of cytokines TNF-α, IL-6, and IL-10 were measured using commercial ELISA kits. The total NO content were measured using the Nitric Oxide Assay Kit according to the manufacturer's instructions (Nanjing Jiancheng Institute of Biotechnology, China).

RT-qPCR analysis

RAW264.7 cells (1×10^6 cells/ml) were seeded into a six-well flat-bottom plate and cultured for 12 h. Then, control (blank), LPS, and polysaccharide samples (100 μg/ml) were added to cells. After incubation for another 24 h, the total RNA of the cultured cells was isolated using kit (OMEGA, USA), and then cDNA was immediately synthesized using a reverse transcription kit (Thermo, USA). The specific primers (**Supplementary Table 1**) for RT-qPCR were designed to amplify a portion (nucleotides about 150-bp) of the 3′ end of the target genes to analyze the mRNA-expression levels of IL-6, IL-10, and TNF-α in RAW264.7 cells (23). The amplification conditions were PCR initial activation step (95°C for 30 s), and 40 cycles of denaturation (95°C for 5 s), annealing (60°C for 30 s), and extension (72°C for 60 s) using the Stratagene Mx3000P thermocycler (Applied Technologies, USA). Expression of gene was measured in triplicate, and was analyzed via $2^{-\Delta\Delta CT}$ method (8).

Statistical analysis

The results were presented as mean ± SD (standard deviation). In addition, Duncan's test and one-way analysis of variance (ANOVA) were used for multiple comparisons by the SPSS 20.0 software package.

Results and discussion

Structural characterization

Degree of de-acetylation (DD) by the hydrolysis method

The contents of neutral sugar and protein in DOP were determined to be 89.21 wt% and 3.12 wt% in dry base, respectively, indicating DOP has a good purity. In addition, DOP contained 6.84 wt% acetyl groups, which has been reported to be vital for the good water solubility of glucomannan (27). In our study, Na_2CO_3 treatment significantly decreased the DA of DOP. The DD value was increased from 39.33 to 86.84% when the Na_2CO_3 treatment duration was elevated from 3 to 25 min (**Table 1**). The addition of alkali plays an efficient role in facilitating the de-acetylation of the molecular chain. Similarly, Li et al. (28) reported that alkali concentration and treating time were both positively related to the DD of the konjac glucomannan. In contrast to Na_2CO_3 treatment, ultrasonic treatment only slightly decreased the DA of DOP.

TABLE 1 The structural characterization of native and modified DOPs.

	DOP	US-60	US-200	US-720	DA-3	DA-5	DA-25
DA (%)	6.84 ± 0.06^{a}	6.01 ± 0.01^{b}	5.02 ± 0.03^{c}	4.12 ± 0.11^{d}	4.15 ± 0.21^{d}	2.54 ± 0.06^{e}	0.90 ± 0.14^{f}
DD (%)	0^{a}	12.13 ± 0.21^{b}	26.61 ± 0.41^{c}	39.69 ± 1.55^{d}	39.33 ± 3.10^{d}	62.87 ± 0.83^{e}	86.84 ± 2.07^{f}
Solubility (%)	57.5 ± 2.2^{a}	63.6 ± 1.8^{b}	68.9 ± 2.7^{c}	78.2 ± 2.1^{d}	28.7 ± 1.1^{e}	21.1 ± 1.9^{f}	3.2 ± 0.6^{g}
Molecular parameters							
Mn (kDa)	47.3	43.7	27.7	23.7	56.5	58.5	19.9
Mp (kDa)	60.2	48.6	32.4	28.7	67.5	70.3	16.5
Mw (kDa)	85.4	58.0	34.2	30.2	95.9	106.7	56.2
PDI = (Mw/Mn)	1.8	1.3	1.2	1.3	1.7	1.8	2.8
Linkage patterns (mol%)							
→4)-Man*p*-(1→	91.4	91.6	91.5	91.4	92.7	91.6	92.8
→4)-Glc*p*-(1→	8.6	8.4	8.5	8.6	7.3	8.4	6.2

Data are mean± SD of three replicates.
Data in the same row with different letters indicated significant differences at $p < 0.05$.

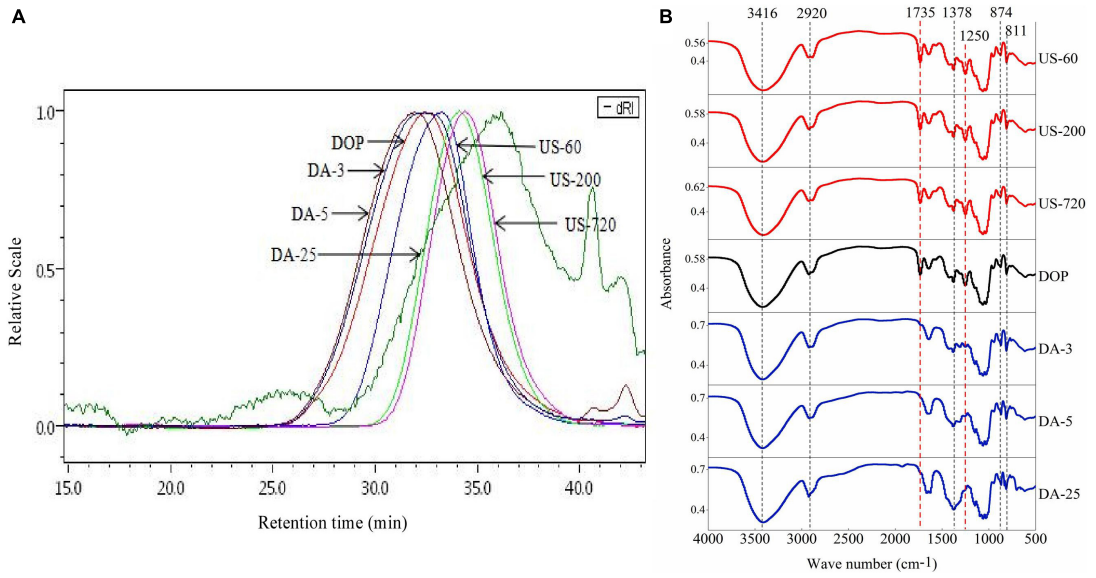

FIGURE 1
HPSEC elution profiles **(A)** and Infrared spectra **(B)** of the native and modified DOPs.

The DD value followed the sequence of US-60 (12.13%) < US-200 (26.61%) < US-720 (39.69%), suggesting that ultrasound favored chain degradation over the cleavage of the acetyl groups.

Mw analysis

The molecular weights of DOP before and after modification were obtained from multi-detector HPSEC analysis. As shown in Table 1 and Figure 1A, except for DA-25, all the other modified DOPs showed a relatively low Mw distribution after treatment as indicated by the low polydispersity index (PDI = Mw/Mn) value. Samples derived from the ultrasonic treatment decreased in the Mw order of DOP (85.4 kDa) > US-60 (58.0 kDa) > US-200 (34.2 kDa) > US-720 (30.2 kDa). The Mw of DOP reduced by 32.1, 60.0, and 64.6% after treatment for 60, 200, and 720 min, respectively. The results indicated that ultrasonic treatment could effectively degrade DOP, and higher treating time led to the lower Mw until a plateau was reached. Similar results have also been reported for schizophyllan (29), dextran (30), apple pectin (31), and polysaccharides from the seeds of *Plantago asiatica* L. (32). The influence of ultrasound on the degradation of the polysaccharides ascribes to the cavitation action, which involves two mechanisms: mechanical degradation of the polysaccharide from collapsed cavitation bubble and chemical degradation because of the chemical reaction between the polysaccharide and high-energy molecules, e.g., the hydroxyl radicals produced during cavitation (33). In our study, the Mw of Na_2CO_3 treated samples increased slightly compared to the natural DOP, which was likely caused by the

conformational change induced by de-acetylation treatment as well as the formation of aggregation. This was consistent with the Mw data reported by Salah et al. (34).

Glycosidic linkage patterns

The linkage patterns of DOP before and after modification, derived from the methylation analysis, are compared in **Table 1**. According to the methylation analysis result of DOP, there were two main glycosidic linkage patterns, (1→4)-D-Man*p* and (1→4)-D-Glc*p* with a molar ratio of nearly 10.6:1.0. Ultrasonic and mild base treatments did not change the overall monosaccharide composition and linkage patterns. This finding indicated that ultrasonic and de-acetylation treatments had no major impact on the monosaccharide composition and linkage patterns of polysaccharides, which confirmed the previous findings by Dou et al. (35) and Wang et al. (36).

FT-IR analysis

The structural changes of DOP before and after modification are compared using FT-IR (**Figure 1B**). The intensified and broad absorbance bands at around 3,416, 2,920, 1,378 cm^{-1} were attributed to O–H hydroxyl stretching vibration, C–H stretching vibration of the methyl group, the symmetric C–H bending vibration of the methyl group, respectively (6). The band at approximately 1,735 cm^{-1} was assigned to the valence vibration of C=O (37), and the strong peak at 1,250 cm^{-1} indicates the presence of C–O vibration of O-acetyl groups, confirming the presence of acetyl groups (4). The two specific bands at 811 and 874 cm^{-1} confirmed the existence of mannan in DOP, as expected (38). For the modified samples, these characteristic peaks were preserved after ultrasonic treatment, suggesting ultrasound treatment had no clear alteration in the functional group of DOP. However, Na_2CO_3 treatment weakened the two absorption bands at 1,735 and 1,250 cm^{-1}. The disappearance of the signal peak at 1,735 cm^{-1} in the de-acetylated polysaccharide samples (DA-3, DA-5, DA-25) indicated the mild base treatment disrupted the C=O double bond of the acetyl group. Meanwhile, the relative peak intensity of 1,250 cm^{-1} (C–O vibration of O-acetyl groups) signal decreased with increasing DD, double confirming this deduction.

It can be herein concluded ultrasonic treatment significantly decreased the Mw of DOP while mildly affecting DA. The DA of DOP reduced significantly after mild base treatment for 3 (DA: 4.15%, DD: 39.33%), 5 (DA: 2.54%, DD: 62.87%), and 25 min (DA: 0.90%, DD: 86.84%). Both treatments did not affect the overall monosaccharide composition and glycosidic linkages of DOP.

Water solubility

Using the centrifugation method, the water solubility of native DOP at room temperature was 57.5% (**Table 1**), which respectively increased to 63.6, 68.9, and 78.2% under 60, 200, and 720 min of ultrasonic treatment. This result was in accordance with our previous study on arabinoxylan (12), which implied that the decrease in molecular size due to the breakage of glycosidic bonds and chain scission during ultrasound treatment improved the water solubility of polysaccharide molecules (33).

In contrast, increasing Na_2CO_3 treating times in de-acetylation reaction conferred a negative effect on the water solubility. As shown in **Table 1**, upon Na_2CO_3 concentration of 0.2 M and hydrolysis time of 25 min, the insoluble fractions significantly increased, resulting in the solubility of the DA-25 being only 3.2%. The decrease in solubility could be due to the loss of acetyl groups, which decreased the intermolecular steric hindrance, thereby increasing the intermolecular interaction through hydrogen bonding and decreasing the solubility (27). Our results are well matched with the report from Chokboribal et al. (39) who found that de-acetylation of acemannan from *Aloe vera* decreased water solubility. They articulated that de-acetylation reduced the steric hindrance of molecular chain and increased crystalline structure which had lower solubility.

Conformational characterization

The conformation of polysaccharide molecules dictates their three-dimensional shape in solid-state or in solutions, such as spherical, random coil, double-helix, triple-helix, worm-like, rod-like. In this study, the chain conformation of native and modified DOPs was studied to understand the influences of structural modifications on their conformational properties. The parameters Rhz (z-average hydrodynamic radius), Rgz (z-average radius of gyration), and $[\eta]_w$ (weight-average intrinsic viscosity) obtained from multi-detector HPSEC are presented in **Table 2**. The values of Rhz, Rgz and $[\eta]_w$ for DOP were determined to be 21.4 nm, 32.4 nm, and 264.2 mL/g, respectively. However, these molecular parameters decreased after ultrasonic treatment, implying that ultrasonication disrupted the polymer aggregates and cleaved the polymer chains in solution (40). For the mild base treatment, their parameters Rhz, Rgz, and $[\eta]_w$ were increased, which were likely attributed to the removal of the acetyl group.

The characteristic parameter ρ (Rg/Rh) has been previously used to reflect the conformational properties of polysaccharides (**Table 2**). The different ρ values reflect various molecular conformations, $\rho \geq 2.00$ for rigid chains (cylinders), 1.50–1.80 for random coils in a good solvent while 1.30 in a θ solvent, 1.00–1.11 for loosely hyper-branched chains and 0.78 for compact spheres (41). Our study calculated the characteristic parameter ρ of DOP as 1.514, indicating that DOP was a random coil conformation. After ultrasonic treatment, the ρ value was in the range of 1.5–1.8, which can be assigned to flexible coil conformations. In addition, an increasing chain rigidity was noticed for ultrasonication treated samples with increasing

TABLE 2 Conformational characterizations of native and modified DOPs.

	DOP	US-60	US-200	US-720	DA-3	DA-5	DA-25
$[\eta]_w$(ml/g)	264.2	199.5	127.5	115.6	287.8	299.7	101.0
Rhz (nm)	21.4	13.8	10	9.2	22.1	28	13.2
Rgz (nm)	32.4	24	17.7	16.8	33.0	32.8	27.9
$\rho(= Rg_z/Rh_z)$	1.51	1.74	1.77	1.83	1.49	1.17	2.11
Mark-Houwink-Sakurada equation: $[\eta] = K_\eta M^\alpha$							
α	0.64	0.86	0.86	0.90	0.80; 0.35	0.80; 0.26	–
logKη	−0.70	−1.77	−1.79	−1.97	−1.50; 0.93	−1.44; 1.38	–
Conformational power-law equation: $Rg = K_g M^\nu$							
ν	0.57	0.63	0.65	0.69	0.52; −0.10	0.51; −0.12	–
logKg	−1.45	−1.70	−1.75	−1.92	−1.16; 2.27	−1.10; 2.32	–

duration (DOP < US-60 < US-200 < US-720), showing the lower the Mw of fractions, the more rigid the molecular chain for DOP. For mild base treatment (de-acetylation treatment), the ρ value gradually decreased with decreasing DA, implying that the chain conformation turned more compact from DA-3 to DA-5.

Furthermore, the relationships of Mw with cumulative weight fraction, [η] (**Supplementary Figure 1**), and Rg (**Supplementary Figure 2**) were established. The double logarithmic plot of the [η]-Mw and Rg-Mw have been well described using the Mark-Houwink ($[\eta] = k_\eta M^\alpha$), conformational power-law equation ($Rg = k_g M^\nu$), respectively (40, 42). For the native DOP, a good linear regression (R^2 = 0.9818) was found between [η] and Mw in the log Mw range of 4.4–6.3, the slope α was obtained as 0.6389 (**Figure 2A**), indicating that DOP was flexible random coil conformation. As expected, the chain conformation became gradually rigid while increasing ultrasound time and decreasing molecular weight or molecular size (**Figure 2B**). In terms of the mild base (de-acetylation) treatment, it is worth noting the curves in **Figure 2B** were not completely linear, i.e., a decreased slope was observed in DA-3 or DA-5 with increasing Mw. Hence, two linear regressions were used to fit the curve. The slope (α) had no clear change in the log Mw range of 4.4–5.3, suggesting the destruction of acetyl groups may not mainly occur on low molecular weight polysaccharides. However, in the high logMw range of 5.3–6.0, with the decrease of DA value, α value gradually decreases, indicating that DA-3 (0.3463) / DA-5 (0.2630) exhibited more compact chain conformation in the high Mw range, likely as the result of the reduction in steric effects from the acetyl groups. Among the α values of these modified samples, DA-25 did not show a good linear regression due to the poor solubility.

The value of ν for DOP was 0.5686 in the logMw range of 4.4–5.8, confirming that the native DOP had a random coil conformation in an aqueous solution. After ultrasound treatment (**Figure 2C**), the chain conformations for US-60 (0.6306), US-200 (0.6454), US-720 (0.6859) became more rigid with increased treating time, in accordance with the results of Mark-Houwink equation. After de-acetylation treatment (**Figure 2D**), the changes of ν values showed a similar trend to that of α, which double confirmed the previous deduction.

Based on the above conformational analysis, native DOP demonstrated a typical flexible random coil chain conformation in solution. The coil conformation became rigid when decreasing the Mw, while with the decrease of DA value, the molecular chain turned more compact coil conformation, especially for high Mw fractions.

Immunomodulatory activities

The proliferation and phagocytosis activities

Macrophages, the primary effector cells of innate immune, play a critical role in immediate response against pathogens. In this study, RAW264.7 macrophages were applied to investigate the direct effect of molecular modification on immunomodulatory activities.

Cell viability was first examined to ensure that the sample dosages used were not toxic to cells, and the results are presented in **Figure 3A**. Compared to the control, samples showed positive effects on proliferation activity in 50–400 μg/ml, but the cell viability was suppressed at 800 μg/ml. In addition, the cell viability of polysaccharide samples reached the highest at 100 μg/ml compared to other concentrations. Therefore, 100 μg/ml was selected as the optimum dosage for other immunological tests.

The cell proliferation rate and phagocytosis activities of native and modified DOPs are presented in **Figures 3B,C**. Under polysaccharide stimulation, proliferation and phagocytosis activities were significantly increased in RAW264.7 macrophages. US-200 demonstrated significantly higher proliferation and phagocytosis activities than DOP, US-60, and US-720, indicating DOP with a specific molecular size (weight) range can exert better activity. However, the immunomodulatory effect of glucomannan was compromised when the Mw was too low. In terms of the mild base treated

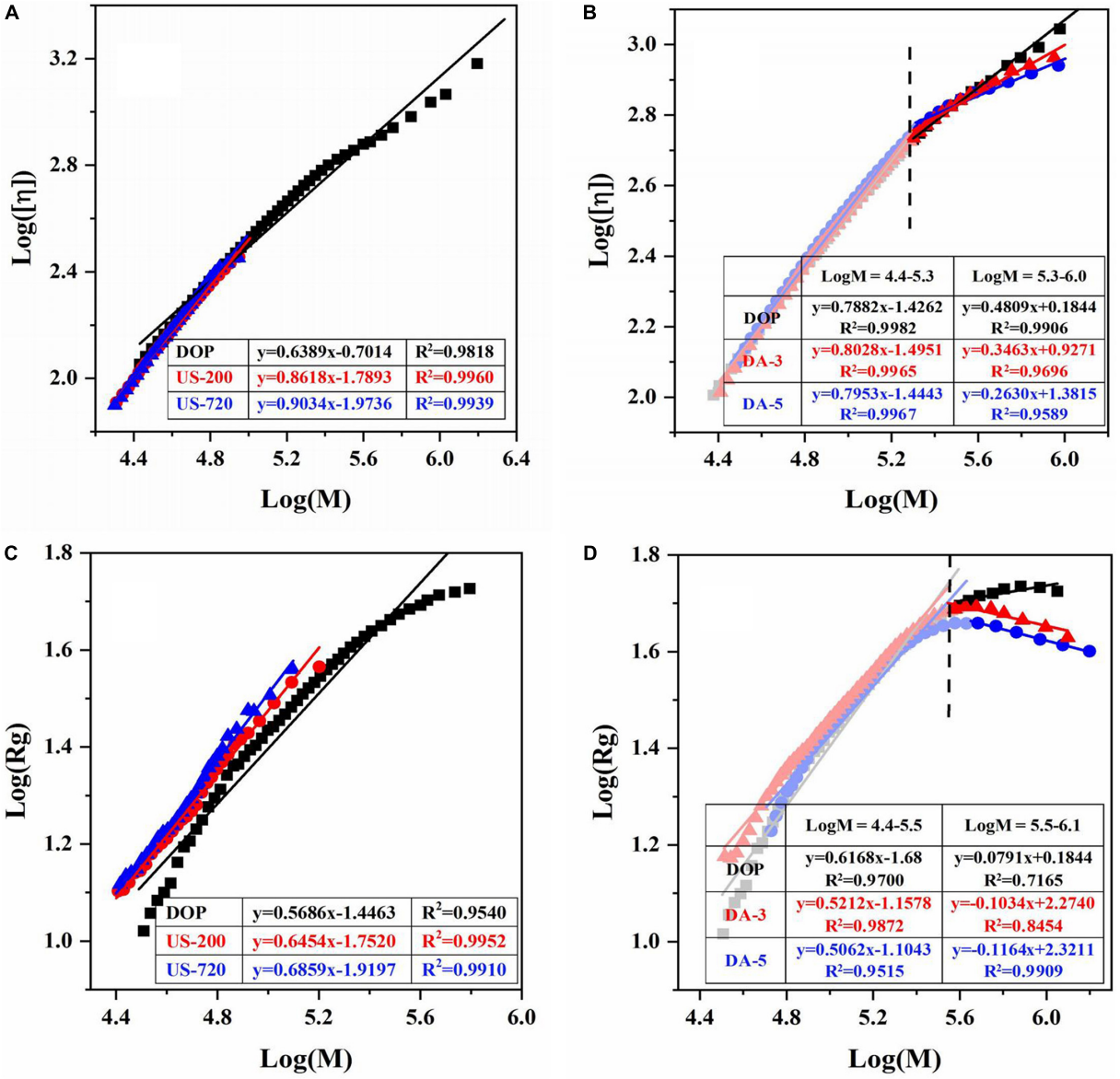

FIGURE 2
Logarithmic plot of the molecular weight vs intrinsic viscosity, radius of gyration of native and modified DOPs in aqueous solution. The Mark-Houwink plots of ultrasound **(A)** and de-acetylated **(B)** samples. The Rg power-law plots of ultrasonic **(C)** and de-acetylated **(D)** samples.

samples (de-acetylation), the proliferation and phagocytosis activities were significantly decreased compared with the native DOP. It was concluded that DOP with a DA of 6.84% exerted better activity, indicating the acetyl group is one of the key factors in the cell activities. Simões et al. demonstrated that acemannan with a higher degree of acetylation had better biological activity, and this activity decreased with decrease degree of acetylation (43). Moreover, Chokboribal et al. (39) indicated that the bioactivity of acemannan was reduced after de-acetylation. These data well matched with our finding that glucomannan with a higher degree of acetylation had increased biological activity.

Effects on cytokine production

Macrophage activation by immunomodulators induces several signaling pathways to produce various immune factors, triggering related immune responses. The effects of native and modified DOPs on macrophage NO, TNF-α, IL-6, and IL-10 production were analyzed in this study. As shown in Figure 4, compared to the blank control, incubating RAW264.7 cells with LPS and various DOP fractions significantly increased the secretions of TNF-α, IL-6, IL-10, and NO.

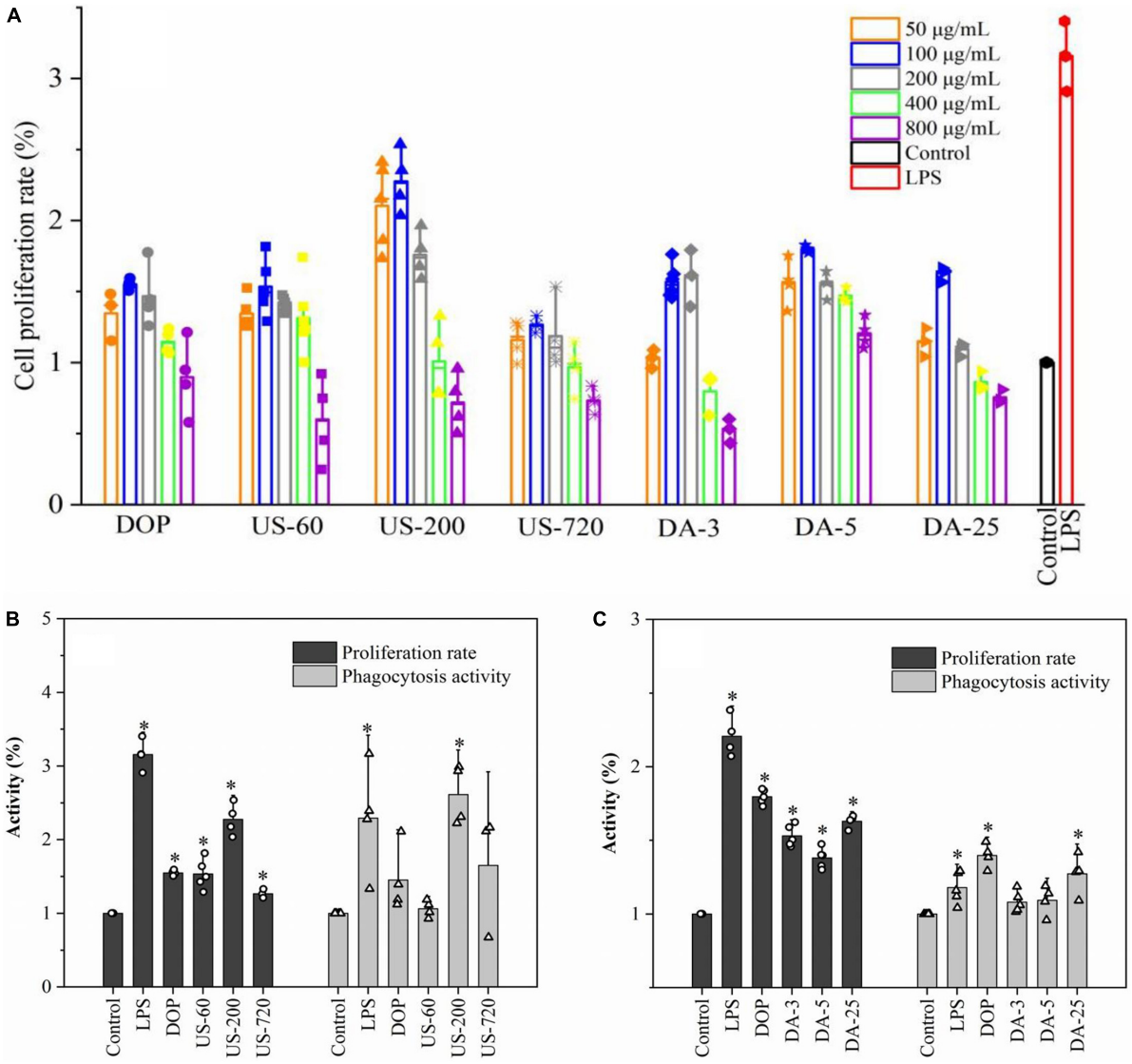

FIGURE 3
Polysaccharide induced proliferation and phagocytosis of macrophages. **(A)** Determination of optimal concentration (50, 100, 200, 400, 800 μg/ml). The proliferation and phagocytosis activities of ultrasonic **(B)** and de-acetylated **(C)** samples (100 μg/ml). All data are representative of at least three independent experiments. *$p < 0.05$ vs. control.

For the ultrasonication treated DOP, US-200 showed the highest NO concentration (16.59 μmol/ml), which was increased by 30% compared to DOP (Figure 4A). Similarly, US-200 showed the highest positive effects on IL-6 (Figure 4B), IL-10 (Figure 4C), and TNF-α (Figure 4D) production, possibly attributed to the appropriate molecular size and DA value. ELISA analysis showed that the cellular release of NO (Figure 4E), IL-6 (Figure 4F), IL-10 (Figure 4G), and TNF-α (Figure 4H) were reduced after mild base treatment, indicating the loss of acetyl group compromised the related immune effects. Therefore, the presence of acetyl groups in DOP could directly affect and regulate their bioactive properties. Similar results have also been reported for acemannan from *Aloe vera* (34).

Effects on mRNA expression

Stimulation of immunomodulators leads to the initiation of intracellular signaling pathways and eventually induces transcriptional activation and expression of cytokines. The expression of cytokines, including TNF-α, IL-10, and IL-6 is essential for host survival from infection. In addition, they are recognized as important host defense molecules that affect tumor cells. To determine whether the increases in IL-10, and IL-6, and TNF-α secretion are attributable to the facilitated gene expression of IL-10, and IL-6, and TNF-α. Cells were treated

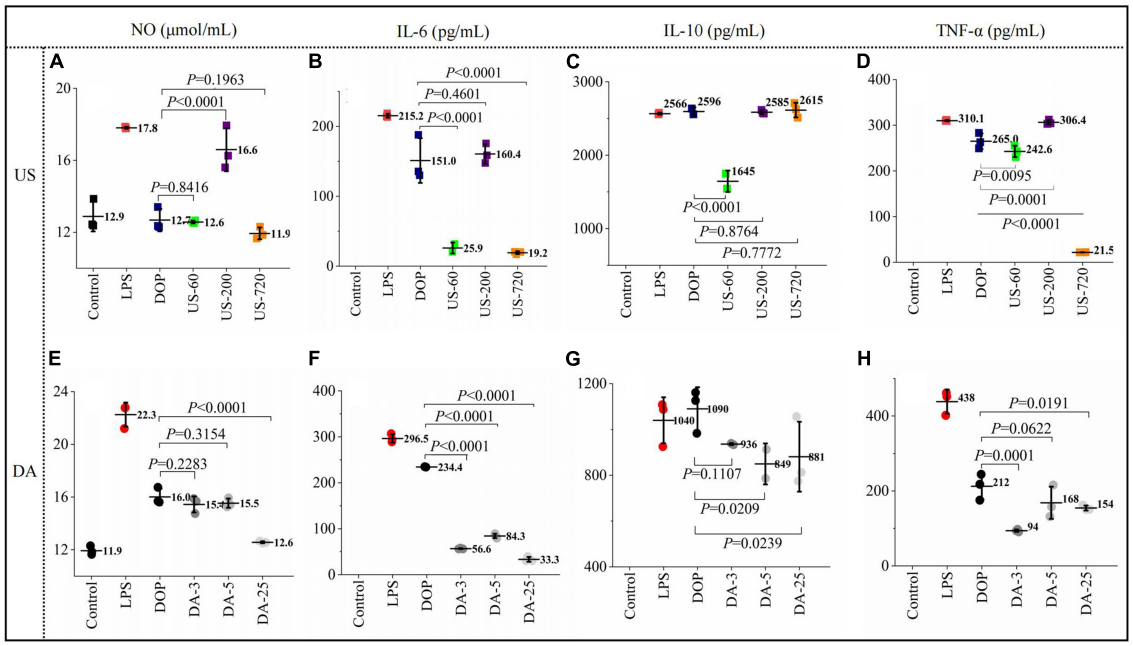

FIGURE 4
Polysaccharides induced production of immune factors NO **(A,E)**, IL-6 **(B,F)**, IL-10 **(C,G)**, TNF-α **(D,H)** productions (24 h) by macrophages RAW264.7 exposed to ultrasonic and de-acetylated samples (100 μg/ml) were assessed by ELISA. All data are representative of at least triplicate culture.

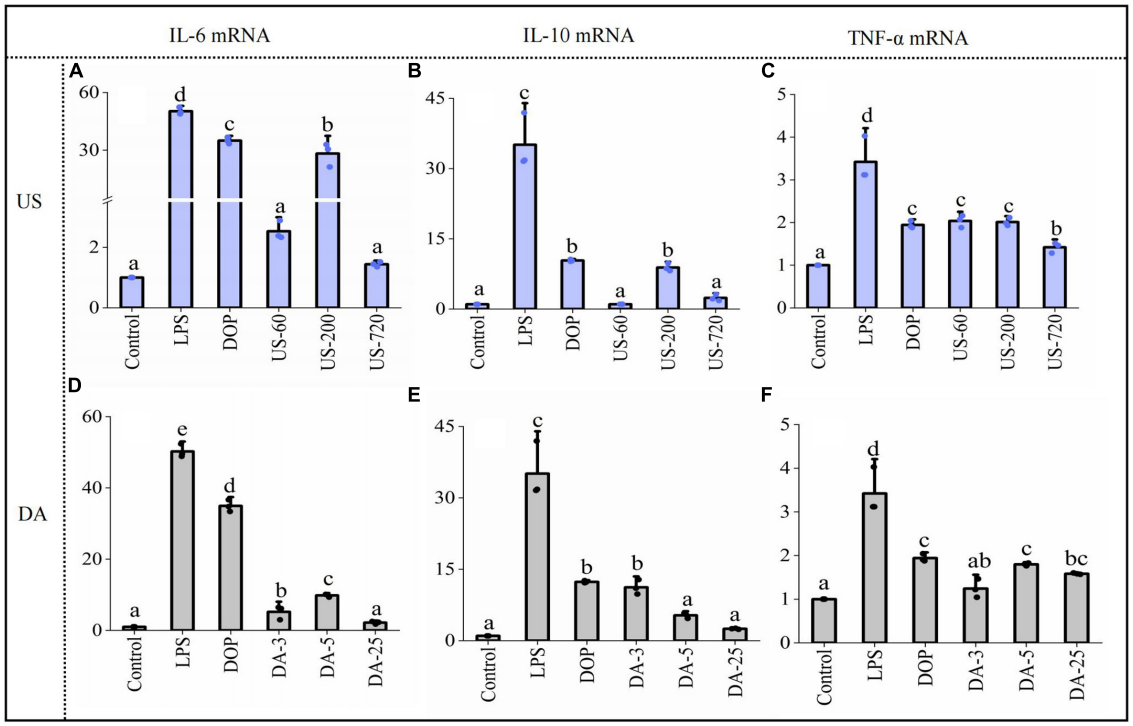

FIGURE 5
Polysaccharides induced gene expression of cytokine IL-6 **(A,D)**, IL-10 **(B,E)**, TNF-α **(C,F)** productions (24 h) by macrophages RAW264.7 exposed to ultrasonic and de-acetylated samples (100 μg/ml) were assessed by RT-qPCR. Data are expressed as means plus SD of triplicate culture (different letters indicated significant differences at $p < 0.05$).

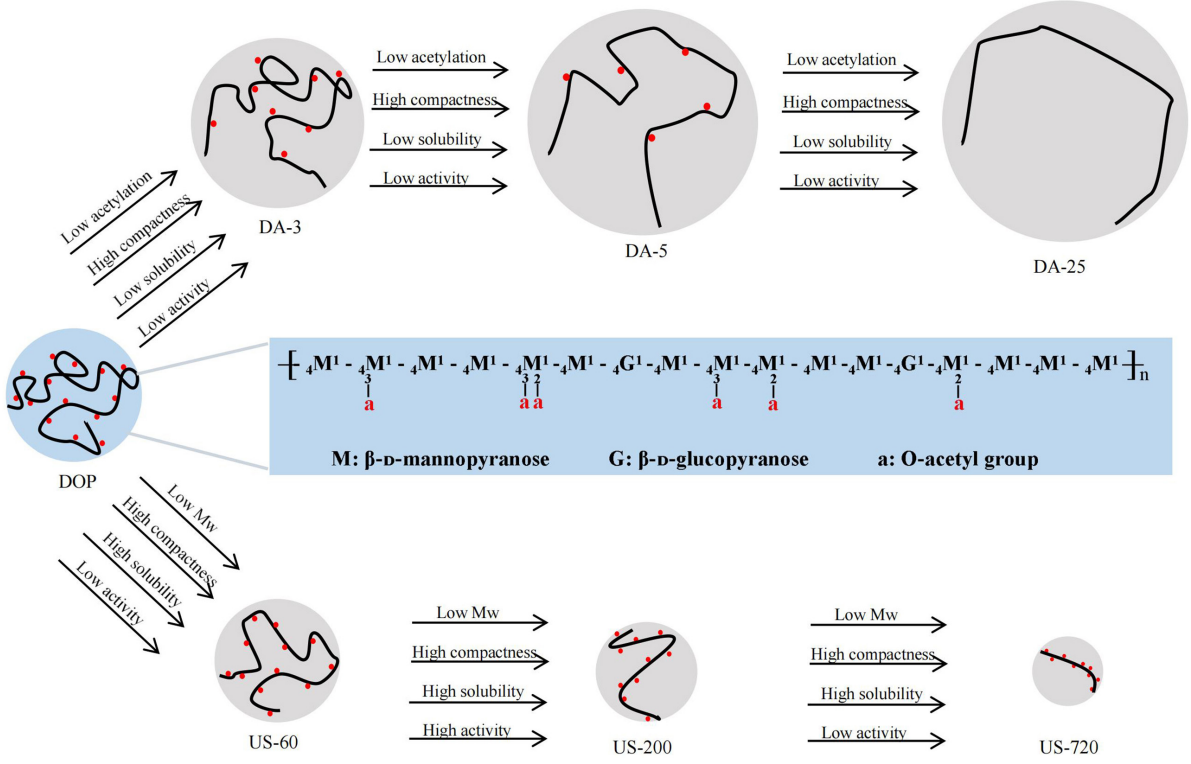

FIGURE 6
Schematic diagram of structural-conformational-immunomodulatory relationships of DOP The major structure of DOP adapted from Xing et al. (7).

with 100 μg/ml samples for 24 h, then cytokine mRNA levels were measured by RT-qPCR. The results showed that cytokines mRNAs were barely detectable in unstimulated RAW cells. After co-cultured with native and modified DOPs, the mRNA levels for all these immune factors increased significantly. Moreover, the expression of IL-6 (**Figure 5A**), IL-10 (**Figure 5B**), and TNF-α (**Figure 5C**) treated by US-200 was highest among all samples. By contrast, the de-acetylated fractions (DA-3, DA-5, and DA-25) significantly reduced the mRNA expression of cytokines, confirming the O-acetylation level is one of the critical determinants of immunomodulatory (**Figures 5D–F**).

It was well known that TNF-α and IL-6 are pro-inflammatory cytokines and IL-10 was an anti-inflammatory cytokine. Therefore, the present data indicated that DOP exhibited both pro-inflammatory and anti-inflammatory activity. This dual-direction regulation was reported for other polysaccharides (44, 45), which indicated that the immunomodulatory activity of polysaccharides was a complicated process and needed to be further studied.

We confirmed the acetyl group was one of the critical determinants of immunomodulatory to modulate the immune system. As demonstrated by Scully et al. (46), O-acetylation is necessary to induce effective opsonophagocytic killing responses. Similarly, Kumar et al. (47) reported that the activation effect of native or over-acetylated or de-acetylated acemannan on macrophages, the results showed that removal of O-acetyl groups resulted in a lower immunomodulatory, while the over-acetylated polysaccharide has stronger effects on immunomodulation. It has also been demonstrated that ultrasound decreased the Mw and improved the immunomodulatory activity of DOP. Many studies also proved that ultrasonic degradation is an effective way to improve various bioactivities of natural polysaccharides (32, 33, 35). However, the immunomodulatory effect of glucomannan was compromised when the Mw was too low, suggesting the immune cells can only be activated if the Mw or molecular size of DOP was large enough. It is worth pointing out that low degree of acetylation and low Mw can confer good solubility property and induce compact coil conformation of glucomannan. Some specific physicochemical parameters, such as degree of acetylation of glucomannan, proper ranges of Mw, water solubility and molecular conformation, all shed lights on the immunomodulatory effects (**Figure 6**). The effects may be correlated with a receptor-ligand binding in macrophages, given that glucomannan has been reported to trigger the activation of immune cell through the interactions with TLR4 receptor (8), TLR2 receptor (48), TLR22 receptor (49), or mannose receptor (50, 51).

Conclusion

Based on our study results, ultrasound is conducive to chain degradation rather than acetyl cracking, and the acetylation level of sonicated samples only changed slightly. Na_2CO_3 treatment is conducive to de-acetylation rather than chain degradation, the Mw of Na_2CO_3 treated samples changed slightly. Thus, samples with different molecular weights and degrees of acetylation were obtained by ultrasound and alkali treatments to establish the structural-immunomodulatory relationships. As a result, DOP with a higher degree of acetylation had increased biological activity, and this activity reduced with decreasing DA, indicating the O-acetylation level was one of the critical determinants of immunomodulatory to modulate the immune system. In addition, slightly reduced the Mw of DOP (US-200, Mw of 34.2 kDa) significantly increased immune-regulation effects of DOP. However, the results also showed that the immunomodulatory effect of glucomannan was compromised when the Mw was too low. Acetyls and low Mw confer the solubility property and compact coil conformation of glucomannan. The specific physicochemical parameters, such as degree of acetylation of glucomannan, proper ranges of Mw, water solubility and molecular conformation, all make contribution to their immunomodulatory effects.

Data availability statement

The original contributions presented in this study are included in the article/**Supplementary material**, further inquiries can be directed to the corresponding authors.

Author contributions

XG and QG conceived and designed the research, and wrote the manuscript. XG and MY conducted the experiments. CW, SN, and SC supervised and revised the manuscript. All authors contributed to the article and approved the submitted version.

Funding

This work was financially supported by the National Natural Science Foundation of China (32072173), the Open Project Program of State Key Laboratory of Food Nutrition and Safety, Tianjin University of Science & Technology (No. SKLFNS-KF-201913), and Tianjin Science and Technology Planning Project (21ZYQCSY00050).

Conflict of interest

The authors declare that the research was conducted in the absence of any commercial or financial relationships that could be construed as a potential conflict of interest.

Publisher's note

All claims expressed in this article are solely those of the authors and do not necessarily represent those of their affiliated organizations, or those of the publisher, the editors and the reviewers. Any product that may be evaluated in this article, or claim that may be made by its manufacturer, is not guaranteed or endorsed by the publisher.

Supplementary material

The Supplementary Material for this article can be found online at: https://www.frontiersin.org/articles/10.3389/fnut.2022.1016961/full#supplementary-material

References

1. He Y, Li L, Chang H, Cai B, Gao HJ, Chen GY, et al. Research progress on extraction, purification, structure and biological activity of *Dendrobium officinale* polysaccharides. *Front Nutr.* (2022) 9:965073. doi: 10.3389/fnut.2022.965073

2. Tao SC, Ren ZY, Yang ZR, Duan SN, Wan ZX, Huang JH, et al. Effects of different molecular weight polysaccharides from *Dendrobium officinale* Kimura & Migo on human colorectal cancer and transcriptome analysis of differentially expressed genes. *Front Pharmacol.* (2021) 12:704486. doi: 10.3389/fphar.2021.704486

3. Chen WH, Wu JJ, Li XF, Lu JM, Wu W, Sun YQ, et al. Isolation, structural properties, bioactivities of polysaccharides from *Dendrobium officinale* Kimura et. Migo: a review. *Int J Biol Macromol.* (2021) 184:1000–13. doi: 10.1016/j.ijbiomac.2021.06.156

4. Shi XD, Yin JY, Cui SW, Wang Q, Wang SY, Nie SP. Plant-derived glucomannans: sources preparation methods structural features and biological properties. *Trends Food Sci Technol.* (2020) 99:101–16. doi: 10.1016/j.tifs.2020.02.016

5. Zhang GY, Nie SP, Huang XJ, Hu JL, Cui SW, Xie MY, et al. Study on *Dendrobium officinale* O-Acetyl-glucomannan (Dendronan). 7. Improving effects on colonic health of mice. *J Agric Food Chem.* (2016) 64:2485–91. doi: 10.1021/acs.jafc.5b03117

6. Xing X, Cui SW, Nie S, Phillips GO, Goff HD, Wang Q. Study on *Dendrobium officinale* O-acetyl-glucomannan (Dendronan§): part I. Extraction purification and partial structural characterization. *Bioact Carbohydr Diet Fibre.* (2014) 4:74–83. doi: 10.1016/j.bcdf.2014.06.004

7. Xing XH, Cui SW, Nie S, Phillips GO, Goff HD, Wang Q. Study on *Dendrobium officinale* O-acetyl-glucomannan (Dendronan (R)) Part II. Fine structures of O-acetylated residues. *Carbohydr Polym.* (2015) 117:422–33. doi: 10.1016/j.carbpol.2014.08.121

8. Huang YP, He TB, Cuan XD, Wang XJ, Hu JM, Sheng J. 14-beta-D-glucomannan from *Dendrobium officinale* activates NF-kappa B via TLR4 to regulate the immune response. *Molecules.* (2018) 23:2658. doi: 10.3390/molecules23102658

9. Liu JJ, Yu LY, Wang C, Zhang YF, Xi HX, Si JP, et al. Preparation structural features and in vitro immunostimulatory activity of a glucomannan from fresh *Dendrobium catenatum* stems. *Front Nutr.* (2022) 8:823803. doi: 10.3389/fnut.2021.823803

10. Guo QB, Huang XJ, Kang J, Ding HH, Liu Y, Wang NF, et al. Immunomodulatory and antivirus activities of bioactive polysaccharides and structure-function relationship. *Bioact Carbohydr Diet Fibre.* (2022) 27:100301. doi: 10.1016/j.bcdf.2021.100301

11. Li SJ, Xiong QP, Lai XP, Li X, Wan M, Zhang JN, et al. Molecular modification of polysaccharides and resulting bioactivities. *Compr Rev Food Sci Food Saf.* (2016) 15:237–50. doi: 10.1111/1541-4337.12161

12. Liu Y, Wang SW, Kang J, Wang NF, Xiao M, Li ZJ, et al. Arabinoxylan from wheat bran: molecular degradation and functional investigation. *Food Hydrocoll.* (2020) 107:105914. doi: 10.1016/j.foodhyd.2020.105914

13. Tahtat D, Boutrig HH, Khodja AN, Benamer S, Hammache Y, Mahlous M. The synergistic effect of gamma irradiation and alkaline soaking at low temperature on the pre-deacetylation of α-chitin: optimization by design of experiment. *Carbohydr Polym.* (2019) 215:39–46. doi: 10.1016/j.carbpol.2019.03.063

14. Williams MAK, Foster TJ, Martin DR, Norton IT, Yoshimura M, Nishinari KA. Molecular description of the gelation mechanism of konjac mannan. *Biomacromolecules.* (2000) 1:440–50. doi: 10.1021/bm005525y

15. Wang NF, Zhang XJ, Wang SW, Guo QB, Li ZJ, Liu HH, et al. Structural characterisation and immunomodulatory activity of polysaccharides from *white asparagus skin*. *Carbohydr Polym.* (2020) 227:115314. doi: 10.1016/j.carbpol.2019.115314

16. Dubios M, Gilles K, Hamilton JK, Rebers PA, Smith F. Colorimetric method for determination of sugar and related substances. *Anal Biochem.* (1956) 28:250–6. doi: 10.1021/ac60111a017

17. Striegel AM. Influence of anomeric configuration on mechanochemical degradation of polysaccharides: cellulose versus amylose. *Biomacromolecules.* (2007) 8:3944–9. doi: 10.1021/bm700959a

18. Tamaki Y, Konishi T, Fukuta M, Tako M. Isolation and structural characterisation of pectin from endocarp of *Citrus depressa*. *Food Chem.* (2008) 107:352–61. doi: 10.1016/j.foodchem.2007.08.027

19. Huang DF, Nie SP, Jiang LM, Xie MY. Preparation and immunoregulatory activity of acetylated polysaccharide from the seeds of *Plantago asiatica L. J Comp Zool.* (2013) 252:289–98.

20. Tong W, Yu Q, Li H, Cui SW, Nie SP. Chemical modification and immunoregulatory activity of polysaccharides from *Dendrobium officinale*. *Food Sci.* (2017) 38:155–60.

21. Xu YX, Dong Q, Qiu H, Cong RH, Ding K. Structural characterization of an arabinogalactan from *Platycodon grandiflorum* roots and antiangiogenic activity of its sulfated derivative. *Biomacromolecules.* (2010) 11:2558–66. doi: 10.1021/bm100402n

22. Zhu DY, Ma YL, Wang CH, Wang H, Ren YF, Zhang JG, et al. Insights into physicochemical and functional properties of polysaccharides sequentially extracted from onion *(Allium cepa L.). Int J Biol Macromol.* (2017) 105:1192–201. doi: 10.1016/j.ijbiomac.2017.07.164

23. Wang NF, Wu Y, Jia GG, Wang CL, Xiao DG, Goff HD, et al. Structural characterization and immunomodulatory activity of mycelium polysaccharide from liquid fermentation of *Monascus purpureus* (Hong Qu). *Carbohydr Polym.* (2021) 262:117945. doi: 10.1016/j.carbpol.2021.117945

24. Hou GH, Chen X, Li JL, Ye ZY, Zong S, Ye M. Physicochemical properties immunostimulatory activity of the *Lachnum* polysaccharide and polysaccharide-dipeptide conjugates. *Carbohydr Polym.* (2019) 206:446–54. doi: 10.1016/j.carbpol.2018.09.067

25. Wu FF, Zhou CH, Zhou DD, Ou SY, Liu ZJ, Huang HH. Immune-enhancing activities of chondroitin sulfate in murine macrophage RAW 264.7 cells. *Carbohydr Polym.* (2018) 198:611–9. doi: 10.1016/j.carbpol.2018.06.071

26. Wu DT, Zhao YX, Yuan Q, Wang SP, Gan RY, Hu YC, et al. Influence of ultrasound assisted metal-free Fenton reaction on the structural characteristic and immunostimulatory activity of a β-D-glucan isolated from *Dictyophora indusiata*. *Int J Biol Macromol.* (2022) 220:97–108. doi: 10.1016/j.ijbiomac.2022.08.058

27. Wardhani DH, Puspitosari D, Ashidiq MA, Aryanti N, Prasetyaningrum A. "Effect of deacetylation on functional properties of glucomannan,"in *Proceedings of the Green Process Material and Energy: A Sustainable Solution for Climate Change*. (New York, NY: AIP Publishing) (2017) 1855 p doi: 10.1063/1.4985490

28. Li J, Ye T, Wu X, Chen J, Wang S, Lin L, et al. Preparation and characterization of heterogeneous deacetylated konjac glucomannan. *Food Hydrocoll.* (2014) 40:9–15. doi: 10.1016/j.foodhyd.2014.02.001

29. Zhong K, Zhang Q, Tong LT, Liu LY, Zhou XR, Zhou SM. Molecular weight degradation and rheological properties of schizophyllan under ultrasonic treatment. *Ultraso. Sonochem.* (2015) 23:75–80. doi: 10.1016/j.ultsonch.2014.09.008

30. Pu YY, Zou QS, Hou DZ, Zhang YP, Chen S. Molecular weight kinetics and chain scission models for dextran polymers during ultrasonic degradation. *Carbohydr Polym.* (2017) 156:71–6. doi: 10.1016/j.carbpol.2016.09.017

31. Zhang LF, Ye XQ, Ding T, Sun XY, Xu YT, Liu DH. Ultrasound effects on the degradation kinetics structure and rheological properties of apple pectin. *Ultrason Sonochem.* (2013) 20:222–31. doi: 10.1016/j.ultsonch.2012.07.021

32. Hu JL, Nie SP, Li C, Wang S, Xie MY. Ultrasonic irradiation induces degradation and improves prebiotic properties of polysaccharide from seeds of *Plantago asiatica L.* during in vitro fermentation by human fecal microbiota. *Food Hydrocoll.* (2018) 76:60–6. doi: 10.1016/j.foodhyd.2017.06.009

33. Qiu JQ, Zhang H, Wang ZY. Ultrasonic degradation of Polysaccharides from *Auricularia auricula* and the antioxidant activity of their degradation products. *Lwt Food Sci Technol.* (2019) 113:108266. doi: 10.1016/j.lwt.2019.108266

34. Salah F, El Ghoul Y, Mandhi A, Majdoub H, Jarroux N, Sakli F. Effect of the deacetylation degree on the antibacterial and antibiofilm activity of acemannan from *Aloe vera*. *Ind Crops Prod.* (2017) 103:13–8. doi: 10.1016/j.indcrop.2017.03.031

35. Dou ZM, Chen C, Fu X. The effect of ultrasound irradiation on the physicochemical properties and alpha-glucosidase inhibitory effect of blackberry fruit polysaccharide. *Food Hydrocoll.* (2019) 96:568–76. doi: 10.1016/j.foodhyd.2019.06.002

36. Wang HS, Chen JR, Ren PF, Zhang YW, Onayango SO. Ultrasound irradiation alters the spatial structure and improves the antioxidant activity of the yellow tea polysaccharide. *Ultrason Sonochem.* (2021) 70:105355. doi: 10.1016/j.ultsonch.2020.105355

37. Wu DT, An LY, Liu W, Hu YC, Wang SP, Zou L. In vitro fecal fermentation properties of polysaccharides from *Tremella fuciformis* and related modulation effects on gut microbiota. *Food Res Int.* (2022) 156:111185. doi: 10.1016/j.foodres.2022.111185

38. Chen L, Huang GL. The antioxidant activity of derivatized cushaw polysaccharides. *Int J Biol Macromol.* (2019) 128:1–4. doi: 10.1016/j.ijbiomac.2019.01.091

39. Chokboribal J, Tachaboonyakiat W, Sangvanich P, Ruangpornvisuti V, Jettanacheawchankit S, Thunyakitpisal P. Deacetylation affects the physical properties and bioactivity of acemannan an extracted polysaccharide from *Aloe vera*. *Carbohydr Polym.* (2015) 133:556–66. doi: 10.1016/j.carbpol.2015.07.039

40. Liu Y, Xiao M, Zhao J, Zhang XM, Hu XZ, Goff HD, et al. Fluorescent labeling affected the structural/conformational properties of arabinoxylans. *Carbohydr Polym.* (2021) 265:118064. doi: 10.1016/j.carbpol.2021.118064

41. Guo R, Tian S, Li XJ, Wu XJ, Liu X, Li DS, et al. Pectic polysaccharides from purple passion fruit peel: a comprehensive study in macromolecular and conformational characterizations. *Carbohydr Polym.* (2020) 229:115406. doi: 10.1016/j.carbpol.2019.115406

42. Zhang Y, Wang HX, Guo QB, Wang JQ, Cui SW. Structural characterization and conformational properties of a polysaccharide isolated from *Dendrobium nobile Lindl*. *Food Hydrocoll.* (2020) 98:104904. doi: 10.1016/j.foodhyd.2019.01.044

43. Simoes J, Nunes FM, Domingues P, Coimbra MA, Domingues MR. Mass spectrometry characterization of an *Aloe vera* mannan presenting immunostimulatory activity. *Carbohydr Polym.* (2012) 90:229–36. doi: 10.1016/j.carbpol.2012.05.029

44. Sun HX, Zhang J, Chen FY, Chen XF, Zhou ZH, Wang H. Activation of RAW264.7 macrophages by the polysaccharide from the roots of *Actinidia eriantha* and its molecular mechanisms. *Carbohydr Polym.* (2015) 121:388–402. doi: 10.1016/j.carbpol.2014.12.023

45. Li JK, Wang Y, Ji JJ, Cao LY, Bai YN, Gao JP. Structural characterization and immunomodulatory activity of a glucan from *Radix Codonopsis*. *J Funct Foods.* (2021) 83:104537. doi: 10.1016/j.jff.2021.104537

46. Scully IL, Pavliak V, Timofeyeva Y, Liu YD, Singer C, Anderson AS. O-Acetylation is essential for functional antibody generation against *Staphylococcus aureus capsular* polysaccharide. *Hum Vaccin Immunother.* (2018) 14:81–4. doi: 10.1080/21645515.2017.1386360

47. Kumar S, Kumar R. Role of acemannan O-acetyl group in murine radioprotection. *Carbohydr Polym.* (2019) 207:460–70. doi: 10.1016/j.carbpol.2018.12.003

48. Feng YX, Mu RY, Wang ZZ, Xing PF, Zhang JF, Dong L, et al. A toll-like receptor agonist mimicking microbial signal to generate tumor-suppressive macrophages. *Nat Commun.* (2019) 10:2272. doi: 10.1038/s41467-019-10354-2

49. Chen MR, Wang HJ, Yan QP, Zheng QR, Yang M, Lv ZZ, et al. Effects of dietary oxidized konjac glucomannan sulfates (OKGMS) and acidolysis-oxidized konjac glucomannan (A-OKGM) on the immunity and expression of immune-related genes of *Schizothorax prenanti*. *Fish Shellfish Immunol.* (2016) 56:96–105. doi: 10.1016/j.fsi.2016.07.003

50. Gan JJ, Dou YY, Li YR, Wang ZZ, Wang LT, Liu S, et al. Producing anti-inflammatory macrophages by nanoparticle-triggered clustering of mannose receptors. *Biomaterials.* (2018) 178:95–108. doi: 10.1016/j.biomaterials.2018.06.015

51. Shahbuddin M, Shahbuddin D, Bullock AJ, Ibrahim H, Rimmer S, MacNeil S. High molecular weight plant heteropolysaccharides stimulate fibroblasts but inhibit keratinocytes. *Carbohydr Res.* (2013) 375:90–9. doi: 10.1016/j.carres.2013.04.006

frontiers | Frontiers in Nutrition

TYPE Original Research
PUBLISHED 29 September 2022
DOI 10.3389/fnut.2022.1028727

Check for updates

OPEN ACCESS

EDITED BY
Xin Wang,
Northwest A&F University, China

REVIEWED BY
Huihuang Ding,
University of Guelph, Canada
Hui Zhang,
University of Shanghai for Science and Technology, China
Yan Wu,
Shanghai Jiao Tong University, China

*CORRESPONDENCE
Jingsong Zhang
syja16@saas.sh.cn

SPECIALTY SECTION
This article was submitted to Food Chemistry, a section of the journal Frontiers in Nutrition

RECEIVED 26 August 2022
ACCEPTED 14 September 2022
PUBLISHED 29 September 2022

CITATION
Liu Y, Tang Q, Feng J, Liu J, Tang C, Yan M, Zhou S, Liu L, Zhou J and Zhang J (2022) Effects of molecular weight on intestinal anti-inflammatory activities of β-D-glucan from *Ganoderma lucidum*. *Front. Nutr.* 9:1028727. doi: 10.3389/fnut.2022.1028727

COPYRIGHT
© 2022 Liu, Tang, Feng, Liu, Tang, Yan, Zhou, Liu, Zhou and Zhang. This is an open-access article distributed under the terms of the Creative Commons Attribution License (CC BY). The use, distribution or reproduction in other forums is permitted, provided the original author(s) and the copyright owner(s) are credited and that the original publication in this journal is cited, in accordance with accepted academic practice. No use, distribution or reproduction is permitted which does not comply with these terms.

Effects of molecular weight on intestinal anti-inflammatory activities of β-D-glucan from *Ganoderma lucidum*

Yanfang Liu[1,2,3], Qingjiu Tang[1,2,3], Jie Feng[1,2,3], Jing Liu[1,2,3], Chuanhong Tang[1,2,3], Mengqiu Yan[1,2,3], Shuai Zhou[1,2,3], Liping Liu[1,2,3], Jing Zhou[1,2,3,4] and Jingsong Zhang[1,2,3]*

[1]Institute of Edible Fungi, Shanghai Academy of Agricultural Sciences, Ministry of Agriculture, Shanghai, China, [2]Key Laboratory of Edible Fungi Resources and Utilization (South), Ministry of Agriculture, Shanghai, China, [3]National Engineering Research Center of Edible Fungi, Shanghai, China, [4]Shanghai Baixin Bio-Tech Co., Ltd., Shanghai, China

To investigate the influence of molecular weight (M_w) on the anti-inflammatory activity of β-D-glucan from *Ganoderma lucidum*, ultrasonic irradiation was applied to treat the β-D-glucan (GLP, 2.42×10^6 g/mol) solution to obtain two degraded fractions with molecular weight of 6.53×10^5 g/mol (GLPC) and 3.49×10^4 g/mol (GLPN). Structural analysis proved that the degraded fractions possessed similar repeated units with the original β-D-glucan. The *in vitro* anti-inflammatory activity studies showed that all fractions could significantly inhibit LPS-induced expression of cytokines including TNF-α, IL-8, MIF and MCP-1 in Caco-2 cells at certain concentrations. Moreover, GLPC and GLPN exhibited better anti-inflammatory activity than GLPC. The intestinal anti-inflammatory activity evaluated by dextran sulfate sodium (DSS)—induced colitis mice model showed that intragastric administration of GLPN (lower M_w fraction) could significantly recover inflamed tissues of mice. Compared with GLP and GLPC, GLPN exhibited stronger ability to inhibit the secretion of pro-inflammatory cytokines (TNF-α, IL-1β, and IL-6). The results revealed that M_w of β-D-glucan influenced its anti-inflammatory activity and decreasing of M_w would improve the activity, which provided evidence for the potential use of β-D-glucan from *G. lucidum* as anti-colitis ingredients.

KEYWORDS

***Ganoderma lucidum*, β-(1→ 3,1→ 6)-D-glucan, molecular weight, inflamed Caco-2 cells, DSS-induced colitis, inflammatory cytokines**

Introduction

In recent years, inflammatory bowel disease (IBD) has gradually become a common disease in the world with the increase in the consumption of high-fat and high-sugar diets (1). IBD, including Crohn's disease (CD) and ulcerative colitis (UC), is characterized by chronic inflammatory disorders of the gastrointestinal tract without clearly defined causes (2). IBD disease had a significant impact on quality of life due to some ongoing symptoms including reduced ability to work, social stigma, management

of toilet access issues and difficulty with physical intimacy. Although the exact pathogenesis of IBD is not clear, it is generally accepted that the uncontrolled immune responses lead to intestinal inflammation, which is associated with the increase of pro-inflammatory cytokines including tumor necrosis factor-α (TNF-α) and interleukins such as Interleukin-1β (IL-1β), Interleukin-6 (IL-6), and Interleukin-8 (IL-8) in the intestine (3, 4). Hence, the priority for the therapy is to regulate the immune disorders by suppressing the levels of inflammatory mediators to control the progression of IBD. In recent years, interest on the development of efficient new drugs or supplements derived from natural sources for the treatment of IBD is growing due to their efficacy and safety (5).

The polysaccharides obtained from natural resources including plants, animals and microorganisms have been found to exhibit the advantages of safety and high therapeutic efficacy, especially for regulating the immune system (6). Some researchers have discovered that several kinds of polysaccharides, such as pectin, chitosan and polysaccharides from microorganisms, could effectively cure UC inflammatory diseases (7–9). These polysaccharides showed effective influence on the treatment of UC *via* the regulation of inflammatory cytokines, intestinal flora and immune system (6), which provided some alternatives for the treatment of inflammatory bowel disease.

β-glucans, the main active polysaccharides from natural resources, especially those from fungi, have exhibited several bioactivities including anti-cancer, immune-modulating and anti-inflammatory properties (1, 10). These β-glucans normally had β-(1→ 3)-linked D-glucose as the backbone with various β-(1→ 6)-D-glucopyranosyl branching units. The difference in sources and preparation methods can affect the physicochemical features of polysaccharides, such as the solubility, degree of branching, molecular weights and conformational structures, which might significantly influence their activities (11–14). Recently, several studies demonstrated that oral administration of β-glucans from yeast or mushrooms exhibited anti-inflammatory effects on dextran sulfate sodium (DSS)-induced colitis in mice (7, 9, 15), which indicated that β-glucans from yeast or mushrooms might be effective drugs or healthcare products to prevent and treat UC in clinical application. Previous studies revealed that the molecular weight (M_w) of polysaccharides was associated with their physiological characteristics and biological activities (16, 17). It was reported that molecular weight showed obvious influence on the antitumor and immunological activities of polysaccharides (18–20).

Ganoderma lucidum (*G. lucidum*), a famous medicinal mushroom used as traditional Chinese medicine for centuries in China, has been reported to contain many kinds of bioactive compounds which could stimulate the immune system and promote health and longevity. As one of the main polysaccharides, β-D-glucan has been extracted and purified from *G. lucidum* and exhibited many pharmacological activities, especially for immunoregulation (21–23). Our previous research also indicated that the molecular weight of β-(1→ 3)-D-glucan with β-(1→ 6) branches from *G. lucidum* had impacts on the immune-enhancing activity, and the fractions with high M_w ($>1.8 \times 10^6$ g/mol) exhibited better activity (21). However, the influence of M_w on anti-inflammatory activity of β-D-glucan was not investigated well. Moreover, the comprehension of the relationship between M_w and anti-inflammatory activities of β-D-glucan from *G. lucidum* is necessary for their further application. It has been reported that ultrasonic degradation was a useful physical method for producing polymers with lower M_w, and the chemical structure of the polymer could be maintained during the degradation process (24, 25). In order to investigate the association of M_w and anti-inflammatory activities of β-D-glucan from *G. lucidum*, ultrasonic treatment was performed to obtain two β-D-glucan fractions with lower M_w, and the anti-inflammatory effects of β-D-glucans with different M_w were compared. Furthermore, the anti-inflammatory activities of β-D-glucans were evaluated through a DSS-induced colitis mice model, which could be useful for further study and application of β-D-glucan from *G. lucidum*.

Abbreviations: DSS, Dextran sulfate sodium; IBD, Inflammatory bowel disease; HPSEC, High-performance size exclusion chromatography; MALLS, Multiple (eight) angle laser light scattering detector; RI, Refractive index detector; VS, Viscosity detector; M_w, Weight average molecular weight; M_n, Number-average molecular weight; *PDI*, Polydispersity index; R_g, Radius of gyration; R_h, Hydrodynamic radius; TFA, Trifluoroacetic acid; PMAA, Partially methylated alditol acetates; GC-MS, Gas chromatography-mass spectrometry; D_2O, Deuterium oxide; Me_2SO-*d6*, Dimethyl sulfoxide-d6; qPCR, Quantitative real-time polymerase chain reaction; ANOVA, Analysis of variance; TNF-α, Tumor necrosis factor-α; IL-1β, Interleukin-1β; IL-6, Interleukin-6; IL-8, Interleukin-8; MIF, Macrophage migration inhibitory factor; MCP, Monocyte chemoattractant protein; DAI, Disease activity index; ELISA, Enzyme-linked immunosorbent assay.

Materials and methods

Materials

Ganoderma lucidum fruit bodies (cultivar longzhi No. 2) were cultivated and collected from Zhejiang province in China. Human epithelial colorectal adenocarcinoma (Caco-2) cells line was purchased from the cell bank at the Chinese Academy of Sciences. Minimum essential medium (MEM) and fetal bovine serum (FBS) were from Invitrogen-Gibco (New York, USA). Human cytokine ELISA kits including TNF-α, IL-8, MIF, and MCP-1were from Beijing 4A Biotech Co., Ltd (Beijing, China). Mouse cytokine ELISA kits including TNF-α, IL-1β, and IL-6 were purchased from Shanghai Jiake Bio. Tech. Co.,

Ltd (Shanghai, China). Dextran sulfate sodium (DSS, M_w: 36,000–50,000 g/mol) was purchased from MP Biomedicals LLC (California, USA). Dextran (M_w, 80,000 g/mol) was from Sigma-Aldrich (Missouri, USA). All other reagents except otherwise specified were analytical grade and from Chinese sources.

Animals

C57BL/6 mice (4 weeks of age, male) were from Shanghai SLAC Laboratory Animal Co., Ltd. Animal quality certificate number: SCXK (Hu) 2017-0005. The animals were housed in plastic cages under normal feeding conditions. Every experimental protocol involving the animals was performed according to the line of legislation and ethical guidelines of the People's Republic of China, and was approved by the Ethics Committee of Experimental Animal Care at Shanghai University of Traditional Chinese Medicine (Permit No. PZSHUTCM210926015).

Preparation of β-D-glucan with different molecular weights

β-D-glucan (GLP) was isolated and purified from hot water extracts of *Ganoderma lucidum* fruit bodies by 20% (v/v) ethanol precipitation according to the previous article (21). The total sugar content was determined to be 96.1% based on the phenol-sulfuric acid method. GLP was suspended in distilled water and stirred under 80°C for several hours to obtain the solution with a concentration of 2 mg/mL. Then GLP solution was treated with 20 kHz ultrasonic irradiation at 900 W using an ultrasonic reactor (JY-99 II, Ningbo Xin Zhi Biotechnology Co., Ltd., China) for 2 h under a controlled temperature lower than 50°C. After being centrifuged at 8,000 × *g* for 15 min, the supernatant was collected and freeze-dried to obtain the degraded fraction GLPC. GLPC solution (2 mg/mL) was continually treated with ultrasonic irradiation at 1,200 W for 2 h under a controlled temperature lower than 50°C. After being centrifuged at 8,000 × *g* for 15 min, the supernatant was collected and freeze-dried to obtain the degraded fraction GLPN. The M_w and characteristics of three fractions were analyzed below.

Molecular weight distribution and characteristics analysis

2–5 mg samples (GLP, GLPC, and GLPN) were weighed in tube and dissolved in 1 mL mobile solution containing 0.15 mol/L $NaNO_3$, 0.05 mol/L NaH_2PO_4, and 0.02% NaN_3 (pH 7.0), and the supernatant was collected for analysis after centrifugation. High-performance size exclusion chromatography (HPSEC) was applied to perform the molecular weight determination and conformational character evaluation. Among all the detectors, the eight-angle laser light scattering detector (MALLS, Wyatt Technology Corp, USA) was used for determining the absolute molar mass and size of polymers. The refractive index detector (RI, Waters Corporation, USA) was to assess the concentration of the solution. The online viscosity detector (VS, Wyatt Technology Corp, USA) was used for viscosity determination of the solution. Several SEC columns from TSK gel series (Japan) including a guard column, G6000 PW_{XL}, G4000 PW_{XL}, and G2500 PW_{XL} with different separation ranges of molecular weight distribution were connected to analyze the samples. The *dn/dc* value was set to 0.151 mL/g for polysaccharide polymers (21).

Methylation and NMR analysis

In order to investigate the structure character and confirm that the original β-glucan and the degraded fractions possessed similar repeat units, the methylation analysis and 1D NMR spectra were performed in the study. Methylation analysis of three samples was performed based on the previous method (11), and the partially methylated alditol acetates (PMAA) were analyzed by a GC-MS system according to the reported procedures (12). GLP, GLPC and GLPN were dissolved in the mixture of Me_2SO-*d6* and D_2O (6:1, v/v) to a concentration of 30 mg/mL, respectively. 1D ^1H and ^{13}C NMR spectra were recorded at 70°C by using a NMR spectrometer (Bruker VNMRS 600, Germany).

Inflamed Caco-2 cells model induced by LPS

Caco-2 cells were cultured in MEM containing 20% fetal bovine serum (FBS), penicillin (100 IU/mL) and streptomycin (100 μg/mL) in 5% CO_2 at 37°C. The medium was renewed twice a week. The effect of samples on the viability of Caco-2 cells was evaluated by alamar blue assay. Briefly, cells were seeded at 1×10^5 cells/well in a 96-well plate. After incubation for 24 h, the cells were treated with different concentrations of samples for 24 h. Then, 30 μL 0.01% alamar blue solutions were added and the cells were cultured for an additional 4–6 h. The cell viability was determined according to the instruction of the alamar blue assay.

To investigate the inhibition effect of samples on the pro-inflammatory cytokine expression levels in inflamed Caco-2 cells induced by LPS, 1 mL cells suspension (5×10^5 cells/mL) was seeded in each well of 24-well plate, and 50 μL sample solutions (final concentrations of 10, 50, and 200 μg/mL) were added into each well. After being cultured for 2 h, the inflammation was induced by addition of 50 μL LPS (final concentration of 2 μg/mL). After being co-cultured for 24 h, the cells in each

well were collected and homogenized in RIPA lysis buffer with protease inhibitor cocktail after 24 h (Thermo, USA). Then the homogenate was centrifuged at 3,000 × *g* for 10 min at 4°C, and the supernatant was diluted to the same final concentrations of protein based on the BCA assay (Thermo, USA) analysis. The pro-inflammatory cytokine TNF-α, IL-8, and macrophage migration inhibitory factor (MIF), monocyte chemoattractant protein-1 (MCP-1) levels in cells homogenate were analyzed by the corresponding ELISA quantitative kits according to the manufacturer's protocols.

Dextran sulfate sodium induced colitis in animal experiments

C57BL/6 mice were housed on a 12 h light-dark cycle with free access to water and normal diets. After 1 week of adaptive feeding, they were randomly divided into 11 groups ($n = 10$). The animal experiments were performed as described in the published article (12) with some modifications. The detailed design was shown in Figure 1. The whole experimental period was divided into two periods including pre-treatment with polysaccharides for 7 days (days 1–7) and treatment for another 9 days (days 8–16) with administration of 4% (w/v) DSS solution. During the pre-treatment period, all mice were freely given common drinking water and nine polysaccharide treated groups of mice were administrated by gavage with three different dosages (10 mg, 50 mg, and 200 mg per kg of body weight) of GLP, GLPC, and GLPN, respectively. During treatment period, 4% (w/v) DSS was added into common drinking water for model group and all polysaccharide treated groups of mice, while the manner of polysaccharides gavage remained the same. All groups were named as follows: control group, model group, GLP-L group (10 mg/kg GLP), GLP-M group (50 mg/kg GLP), GLP-H group (200 mg/kg GLP), GLPC-L group (10 mg/kg GLPC), GLPC-M group (50 mg/kg GLPC), GLPC-H group (200 mg/kg GLPC); GLPN-L group (10 mg/kg GLPN); GLPN-M group (50 mg/kg GLPN); GLPN-H group (200 mg/kg GLPN). Body weights of all groups of mice were recorded daily. Finally, the mice were euthanized by cervical dislocation and tissues were collected.

Assessment of disease activity index

The disease activity index (DAI) was evaluated by scoring the changes of body weight loss, diarrheal condition and fecal bleeding, which is the average score of the three parameters. The scores of each parameter were assigned based on the reported method (26), respectively. Loss of body weight was scored as 0 (no weight loss) and 1–4 (weight loss of 1–5, 5–10, 10–20, and more than 20% from baseline). Diarrhea score were divided into different grades including 0: normal stool; 1: mildly soft stool; 2: soft stool; 3: very soft stool; 4: watery stool; 5: completely watery stool (27). The fecal bleeding score was also divided into 0–5 grades to refer to normal colored stool, brown stool, reddish stool, mildly bloody stool, bloody stool and very bloody stool, respectively (28).

Evaluation of colonic histopathological score

The colons collected from different groups of mice were gently washed with ice-cold PBS, and fixed in 4% paraformaldehyde for overnight, then embedded in paraffin. After slicing, the colon tissue sections were stained with hematoxylin and eosin (H&E) and examined under the light microscope. The histopathological score was assessed according to the previously reported methods (29).

RNA isolation and real-time PCR

Total RNA was extracted and isolated from colon tissues using TRIzol lysis (TAKARA Biotechnology Company, Liaoning, China) and used to synthesize cDNA with PrimeScript^{TM} RT Master Mix (Perfect Real Time) Reagent Kit (TAKARA Biotechnology Company, Liaoning, China) according to the manufacturer's instructions. Then mRNA expression levels of GAPDH, TNF-α, IL-1β, and IL-6 were analyzed with quantitative real-time polymerase chain reaction (qPCR) assays using SYBR$^{®}$ Premix Ex TaqTM II (TAKARA Biotechnology Company, Liaoning, China) in the ViiA^{TM} 7 Real-time fluorescence PCR system (Applied Biosystems, USA). The primers of forward and reverse sequences from 5′-3′ used in this experiment were listed in Supplementary Table 1. Data were calibrated to the endogenous reference (*GAPDH* gene) and calculated according to the $2^{-\Delta\Delta Ct}$ method.

Measurement of pro-inflammatory cytokine levels in colonic tissues

Frozen colonic tissue was homogenized in T-PER^{TM} tissue protein extraction reagent with protease inhibitor cocktail from Thermo at pH 7.6 and extracted for 15 min on ice to obtain tissue protein solutions. Then the extracted solutions were centrifuged, and the supernatant was diluted to the same final concentrations of protein based on the BCA assay (Thermo, USA) analysis. The concentration levels of IL-1β, IL-6, and TNF-α were measured by the corresponding ELISA quantitative kits according to the manufacturer's protocols.

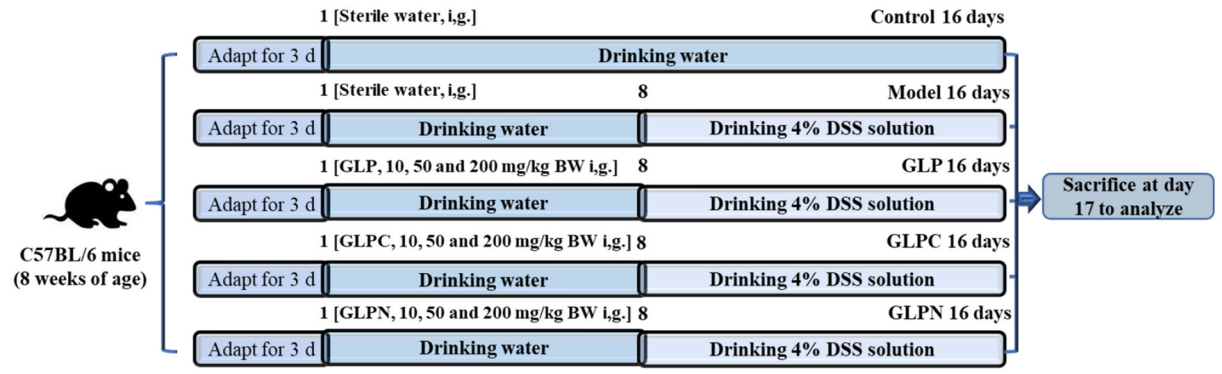

FIGURE 1
Animal experimental design.

Statistical analysis

The data were drawn by GraphPad Prism version 5.01 (San Diego, CA, USA) and the results were presented as the mean ± SD. Duncan's multiple-range test and one-way analysis of variance (ANOVA) used to analyze the difference between data from different groups and statistical differences were considered significant and extremely significant at the P value < 0.05 and < 0.01, respectively.

Results and discussion

Molecular characteristics of β-D-glucan and the degraded fractions

HPSEC eluted differential refractive index (RI) and light scattering (LS) profiles, as well as the molar mass distributions for the original β-D-glucan (GLP) and the ultrasonic degraded fractions (GLPC and GLPN) are shown in Figure 2. The single symmetrical peak occurred in the RI profiles for all fractions, illustrating that ultrasonic degradation could yield homogeneous polysaccharide with the decrease of molecular weight. One single peak detected by LS detector in GLP and GLPC was in agreement with their RI profiles (Figures 2A,B), respectively, indicating no obvious aggregation occurred in GLP and GLPC. Although one single RI peak was detected in GLPN, two peaks detected by LS detector were found in GLPN, indicating some aggregates might be in GLPN solution because the LS signal was more sensitive to large size aggregates than to the concentration of samples (17).

The molecular parameters for all samples including molecular weight (M_w), polydispersity index (M_w/M_n), radius of gyration (R_g), hydrodynamic radius (R_h), and the ρ-values (R_g/R_h) were listed in Table 1. The relative low polydispersity index for three fractions (1.32–1.68) revealed that polysaccharide molecules were well-dispersed in the solution. The original β-D-glucan GLP (M_w, 2.42×10^6 g/mol) from *G. lucidum* and the sonicated fraction GLPC (M_w, 6.53×10^5 g/mol) both exhibited rigid chain conformation with ρ (R_g/R_h) values higher than 2, which have been proved to exhibit triple helix conformation in aqueous solution (30). For further ultrasonic degraded fraction GLPN, the weight-average molecular weight decreased sharply. The molecular weight distribution analysis of GLPN based on column G2500 PW_{XL} showed that GLPN exhibited a symmetric peak with relatively narrow distribution (Figure 2C) and its M_w was determined to be 3.49×10^4 g/mol. The R_g value of GLPN could not be obtained based on HPSEC-MALLS-RI-VS analysis system due to its low M_w, and the R_h value was calculated to be 5.7 nm, which was much smaller than those of GLP and GLPC. According to some researches, the polysaccharide fractions with M_w lower than 1×10^5 g/mol could not form triple helix conformation in aqueous solution (31, 32). Therefore, GLPN exhibited different conformational characteristics with GLP and GLPC.

Methylation and NMR analysis for polysaccharide fractions

In order to elucidate the primary repeat unit of the ultrasonic degraded fractions and confirm if they were similar with that of polysaccharide GLP, the methylation analysis was performed to analyze their linkage types of sugar residues and the corresponding ratios. Total ion chromatograms of the methylated products for GLP and the ultrasonic degraded fractions (Figure 3A) showed that GLPC and GLPN exhibited three obvious peaks, which were the same as GLP and identified as terminal-linked Glc*p*, (1→ 3)-linked Glc*p* and (1→ 3,6)-linked Glc*p*, respectively. The percent molar ratios (Table 2) of three main residues in all fractions seemed similar and were

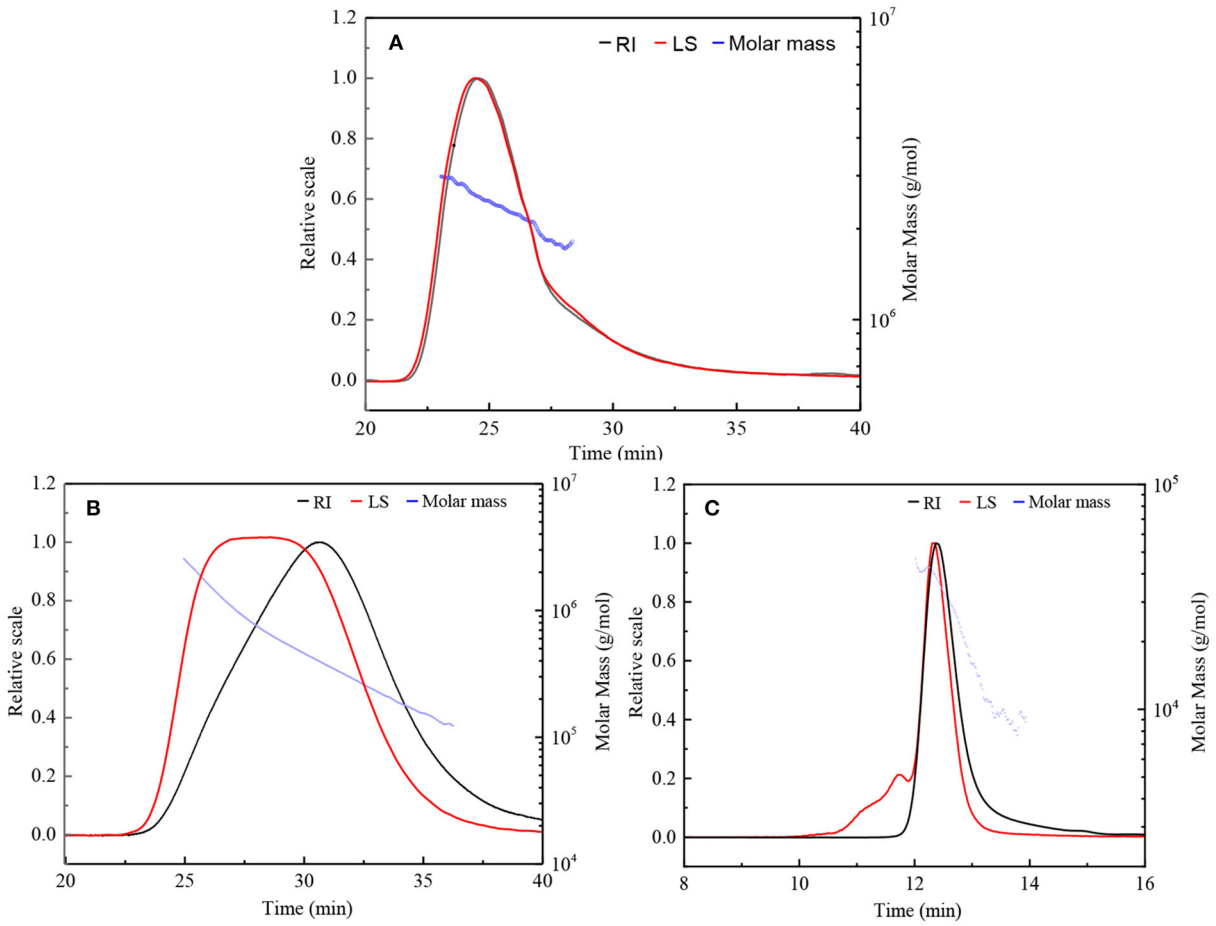

FIGURE 2
HPSEC elution profiles and molar mass distributions of three fractions. **(A,B)** Represents HPSEC elution profile and molar mass of GLP and GLPC based on columns G6000 PW_{XL} and G4000 PW_{XL} in series connection system, respectively. **(C)** Represent HPSEC elution profile and molar mass of GLPN based on column G2500 PW_{XL} system. RI, differential refractive index; LS, light scattering.

TABLE 1 Experimental results from HPSEC-MALLS-RI-VS system for β-D-glucan (GLP) and the ultrasonic degraded fractions (GLPC and GLPN) in PBS buffer.

Samples	M_w (g/mol)	Polydispersity (M_w/M_n)	R_g (nm)	R_h (nm)	ρ (R_g/R_h)
GLP[a]	2.42×10^6	1.32	166.2	78.5	2.12
GLPC[a]	6.53×10^5	1.68	69.3	33.1	2.09
GLPN	3.49×10^4	1.37	/	5.7	/

[a]Data of GLP and GLPC were from reference (30).

calculated to be about 1:2:1 for terminal-linked Glc*p*, (1→ 3)-linked Glc*p* and (1→ 3,6)-linked Glc*p*, indicating that GLPC and GLPN might possess similar repeat unit with the GLP. The structure features of GLPC and GLPN were further confirmed by ^{1}H and ^{13}C NMR spectra analysis (Figures 3B,C). Both of the two fractions showed similar peaks as those detected in GLP, suggesting the primary structures for the degraded fractions were not changed. The assignments of protons and carbons were labeled according to the chemical shifts of reported β-D-glucan GLP (21). All three fractions possessed similar repeat unit with different molecular weights and elucidated as β-(1→ 3)-linked D-glucan with a (1→ 6)-D-glucopyranosyl side-branching unit on every third residue (Figure 3D). It has been reported that ultrasonic degradation could produce homologous series of polymers with lower M_w (24) and the structure of polymers could be kept during the degradation process (25). In

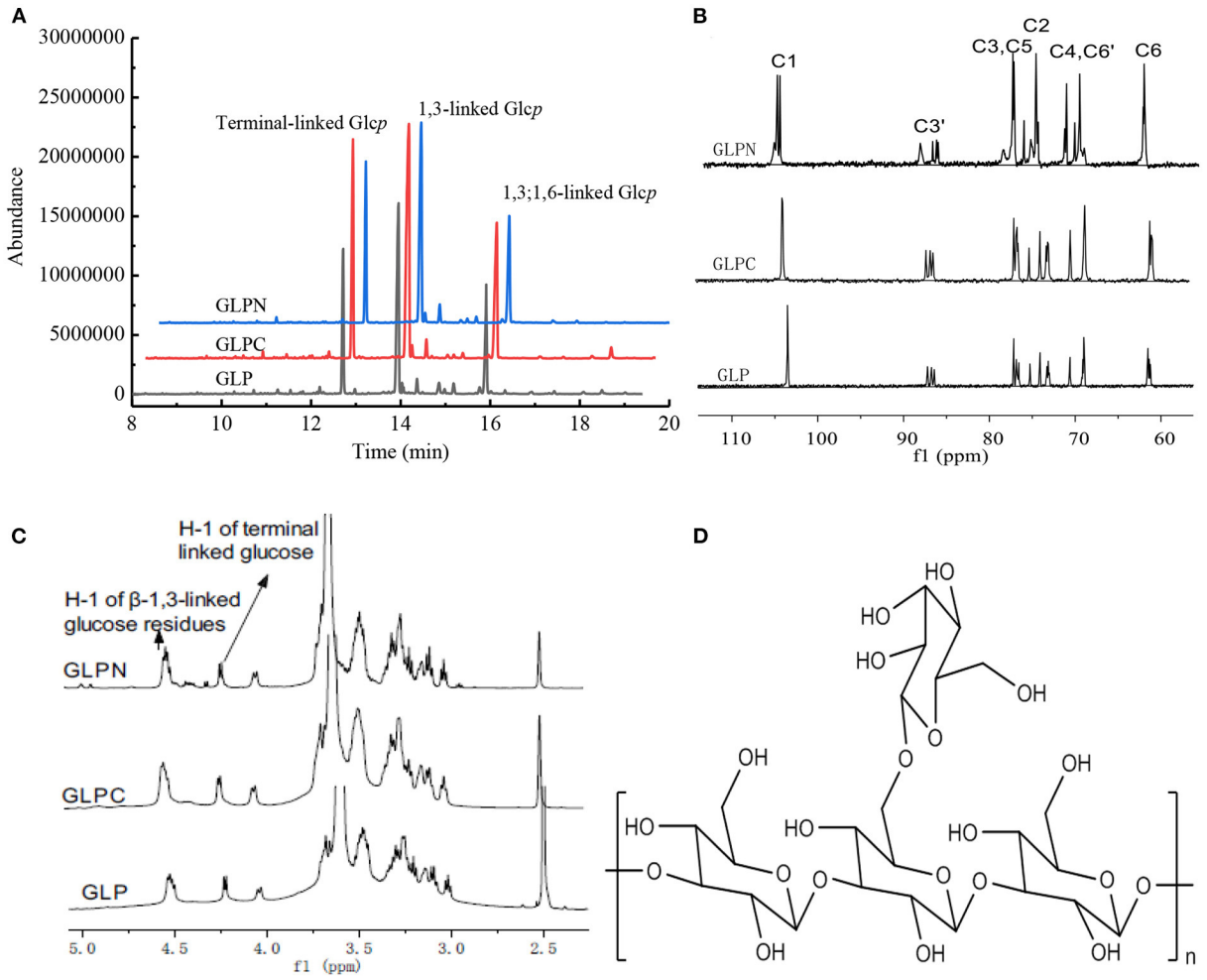

FIGURE 3
Structure analysis of GLP, GLPC, and GLPN. **(A)** Total ion chromatogram of the methylated products of GLP, GLPC, and GLPN. **(B)** ^{13}C NMR spectra of GLP, GLPC, and GLPN. **(C)** ^{1}H NMR spectra of GLP, GLPC, and GLPN. **(D)** Primary repeat unit for GLP, GLPC, and GLPN.

our study, it was also proved that the two degraded fractions both exhibited similar primary structures with GLP, which could be used to investigate the effects of M_w on the bioactivities of β-D-glucan.

β-D-glucans inhibited the expression levels of inflammatory cytokines in inflamed Caco-2 cells

To investigate the effect of β-D-glucans with different M_w on the growth of Caco-2 cells, the cell viability was detected using alamar blue assay after being treated with GLP, GLPC and GLPN for 48 h. Results (Figure 4) showed that the survival rate of cells treated with each fraction (50–500 μg/mL) ranged from 96.21 to 102.34%, indicating that three β-D-glucan fractions had no obvious cytotoxicity on the growth of Caco-2 cells in the tested concentration. So the effects of fractions on the expression levels of inflammatory cytokines in LPS-induced inflamed Caco-2 model could be performed in this range.

It was reported that intestinal inflammatory response was concerted by several cytokines released from epithelial cells (33), which played an important role in the initiation and perpetuation of the inflammatory reaction in IBD. So the selection of inhibitors for cytokines could be an effective therapeutic target in IBD (34). TNF-α is a critical cytokine in the inflammatory process of IBD pathogenesis, and several anti-TNF-α therapies have been proved to effectively reduce pathology in IBD patients (35). Recently, it was found that the macrophage migration inhibitory factor (MIF) also played an important role in the inflammatory

TABLE 2 Methylation analysis of polysaccharide fractions.

Methylated sugar (as alditol acetate)	Linkage types	Percent molar ratios (%)			Major mass fragments (*m*/*z*)
		GLP	GLPC	GLPN	
2,3,4,6-Me_4-Glc*p*	1-linked-Glc*p*	25.6	27.0	26.2	43, 45, 87, 102, 118, 129, 161, 162, 205
2,4,6-Me_3-Glc*p*	1→ 3-linked Glc*p*	50.4	48.6	48.9	43, 45, 71, 87, 101, 118, 129, 161, 217, 234, 277
2,4-Me_2-Glc*p*	1→ 3,6-linked Glc*p*	24.0	24.4	24.9	43, 87, 102, 118, 129, 189, 234, 305

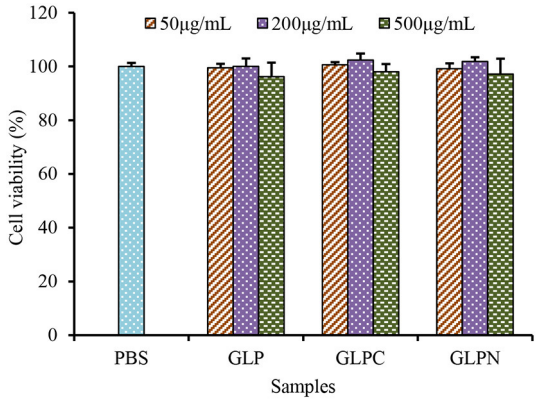

FIGURE 4
Effects of GLP and the degraded fractions (GLPC and GLPN) on cell viability of Caco-2 cells.

process (36). Furthermore, the accumulation of TNF-α and MIF appeared to be pivotal activators of the epithelium to produce pro-inflammatory cytokines such as interleukin (IL)-8 and monocyte chemoattractant protein (MCP)-1 (37). Therefore, TNF-α, MIF, IL-8, and MCP-1 could be thought as inflammatory biomarkers for IBD, and the anti-inflammatory activities can be evaluated by measuring these biomarkers in Caco-2 cells. Our results (Figure 5) showed that the addition of LPS (2 μg/mL) resulted in a remarked increase in TNF-α, MIF, IL-8, and MCP-1 expression levels in Caco-2 cells, while GLP and the corresponding degraded fractions all exhibited significant inhibition on LPS-induced cytokine expression at certain concentrations, indicating that β-D-glucans with different M_w possessed anti-inflammatory potential in LPS-inflamed Caco-2 cells. Among three fractions, the degraded β-D-glucan GLPC (6.53×10^5 g/mol) and GLPN (3.49×10^4 g/mol) exhibited better inhibitory activity compared with the original GLP (2.42×10^6 g/mol), demonstrating that the relatively low molecular β-D-glucans might possess better anti-inflammatory activity in colitis. It was reported that β-glucan from oat with lower molecular weight exhibited stronger activity on reduction of inflammatory markers levels, which might be due to the abundant exposure of glucans in per molar substance to cell receptors in contrast with the fraction with higher molecular weight (38).

β-D-glucans with different M_w ameliorated clinical symptoms in DSS-induced colitis model

To confirm the potential therapeutic interventions, DSS-induced colitis animal model is commonly established to study the UC pathogenesis (29). In this study, DSS-induced colitis animal model was applied to compare the anti-inflammatory activity of β-D-glucans with different M_w. DSS is a commonly reagent for UC modeling, which can cause symptoms like weight loss and diarrhea. Mice in the model group (DSS-treated group) exhibited significant weight loss than those in the control group from day 13 to 17, whereas oral administration of β-D-glucans could significantly reduce the loss of body weight induced by DSS, especially for GLPN at the dosage of 50 mg/kg (GLPN-M group; Figure 6A). The DAI scores, are usually used to estimate the severity of clinical symptoms in mice with DSS-induced colitis (27). As shown in Figure 6B, the mice treated with β-D-glucans obtained a lower DAI values than those in the model group from day 14 to 17. High dosage of GLPN (200 mg/kg) exhibited extremely significantly lower DAI scores than those of the DSS group, indicating the better anti-inflammatory property on DSS-induced colitis mice.

Additionally, the colon length of mice shortened in DSS-induced model of colitis, which was attenuated by GLPN administration in dose dependence (Figures 6C,D), and high dosage of GLPN (200 mg/kg) exhibited significantly attenuation activity. However, high dosage of GLPC (200 mg/kg) and middle dosage of GLP (50 mg/kg) only presented trends for preventing colon length shortening, indicating that low M_w fraction GLPN (3.49×10^4 g/mol) exhibited better anti-inflammatory effects on DSS-induced colitis in mice.

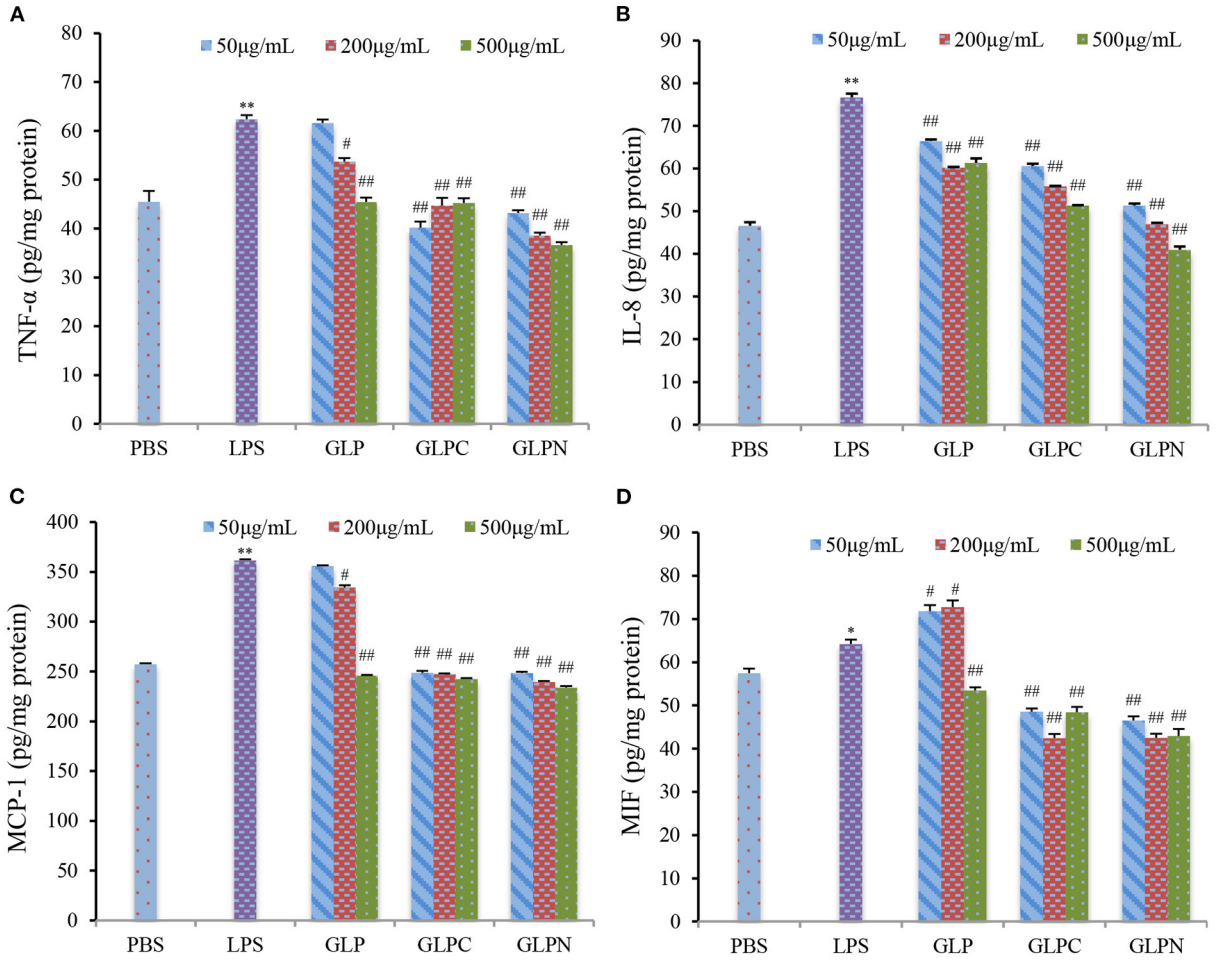

FIGURE 5
Effects of GLP and the degraded fractions (GLPC and GLPN) on expression levels in Caco-2 cells induced by LPS (2 μg/mL). TNF-α **(A)**, IL-8 **(B)**, MCP-1 **(C)**, and MIF **(D)** expression levels in cells were measured by ELISA. Data are presented as means ± SD ($n = 3$). Significant differences with PBS group were designated as: $^{*}P < 0.05$; $^{**}P < 0.01$. Significant differences with LPS-induced group were designated as: $^{\#}P < 0.05$; $^{\#\#}P < 0.01$.

It has been reported that among three exopolysaccharides with high (1.44×10^6 g/mol), medium (9.36×10^5 g/mol) and low (1.97×10^5 g/mol) M_w from *Schizophyllum commune*, oral administration of high M_w fraction could inhibit the shortening of the colon in DSS-induced colitis (39). This was not consistent with the present results and might be due to the different M_w ranges of β-D-glucans for testing.

H&E staining of colon tissues was performed to further analyze the anti-inflammatory of β-D-glucans with different M_w. As depicted in Figure 6E, DSS-induced model group displayed severe colonic tissue damage such as inflammatory cell infiltration, lesion formation and crypt destruction compared with control group, while the group treated with β-D-glucans exhibited lightening of colonic damage. The histological score evaluation (Figure 6F) revealed that the lower M_w fraction GLPN significantly reduced the colonic tissue damage and exhibited a pronounced reduction in the inflammatory response and histological scores, indicating that GLPN significantly relieved the symptoms of colonic inflammation. Some researchers reported that oral administration of *Schizophyllum commune* exopolysaccharides with high (1.44×10^6 g/mol) and medium M_w (9.36×10^5 g/mol) possessed intestinal anti-inflammatory activity by recovering inflammation severity. In our results, low M_w fraction GLPN (3.49×10^4 g/mol) was further confirmed to decrease histological score in DSS-induced colitis and exhibited better activity than the other two fractions. The source of β-D-glucans and different M_w ranges of tested samples might lead to different results for investigating the influence of M_w on anti-inflammatory activities of β-D-glucan.

10.3389/fnut.2022.1028727

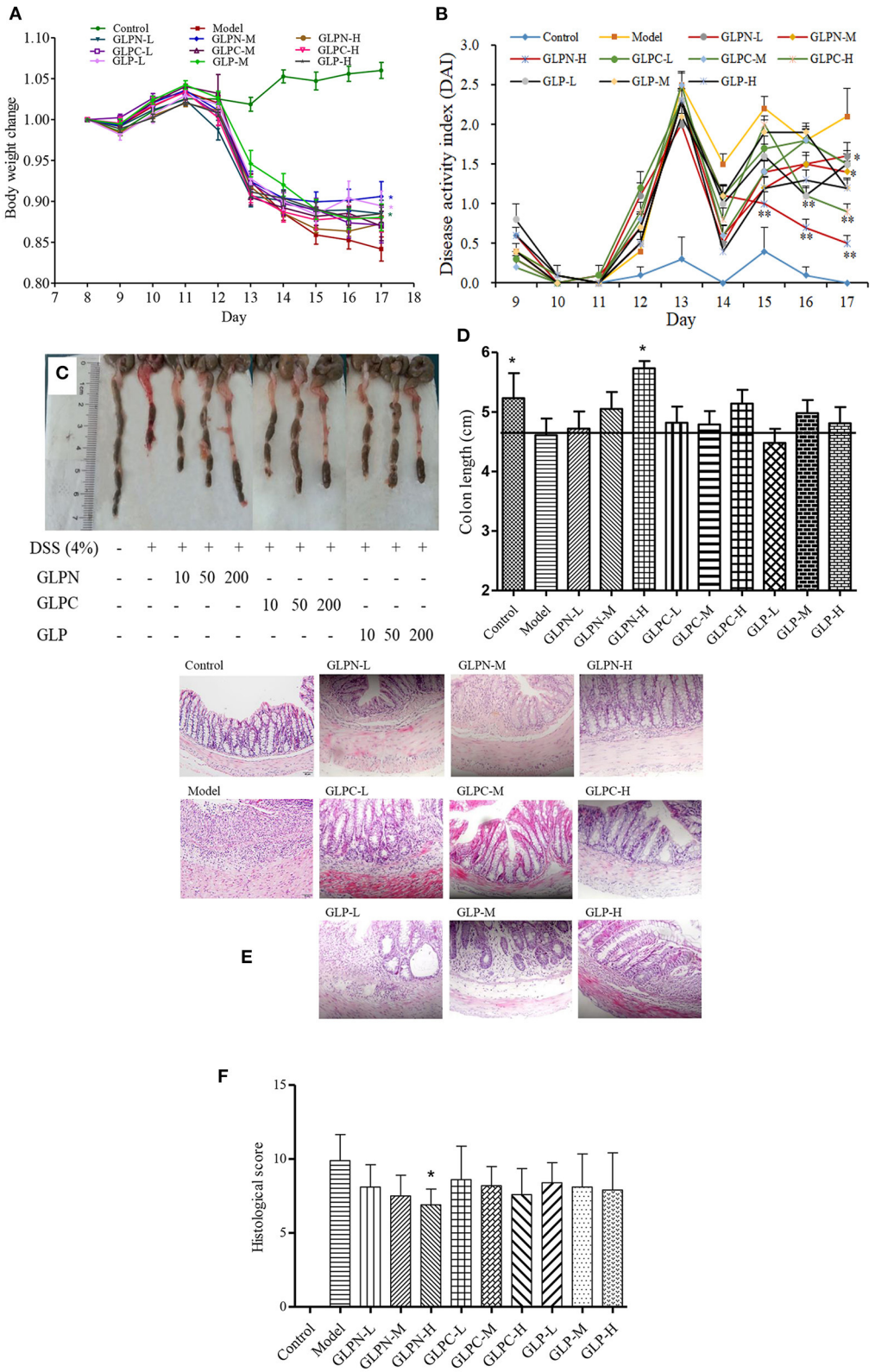

FIGURE 6
Effect of GLP and the degraded fractions (GLPC and GLPN) on body weight change, disease activity index, and pathological indicators. **(A)** Body weight change; **(B)** Disease activity index; **(C)** The picture of colons in different groups; **(D)** The measured length of colons; **(E)** Representative picture of the colon sections stained with hematoxylin and eosin (H&E); **(F)** Histological score. Data are expressed as mean ± SD, $n = 10$ ($^{*}P < 0.05$, $^{**}P < 0.01$ vs. DSS model group).

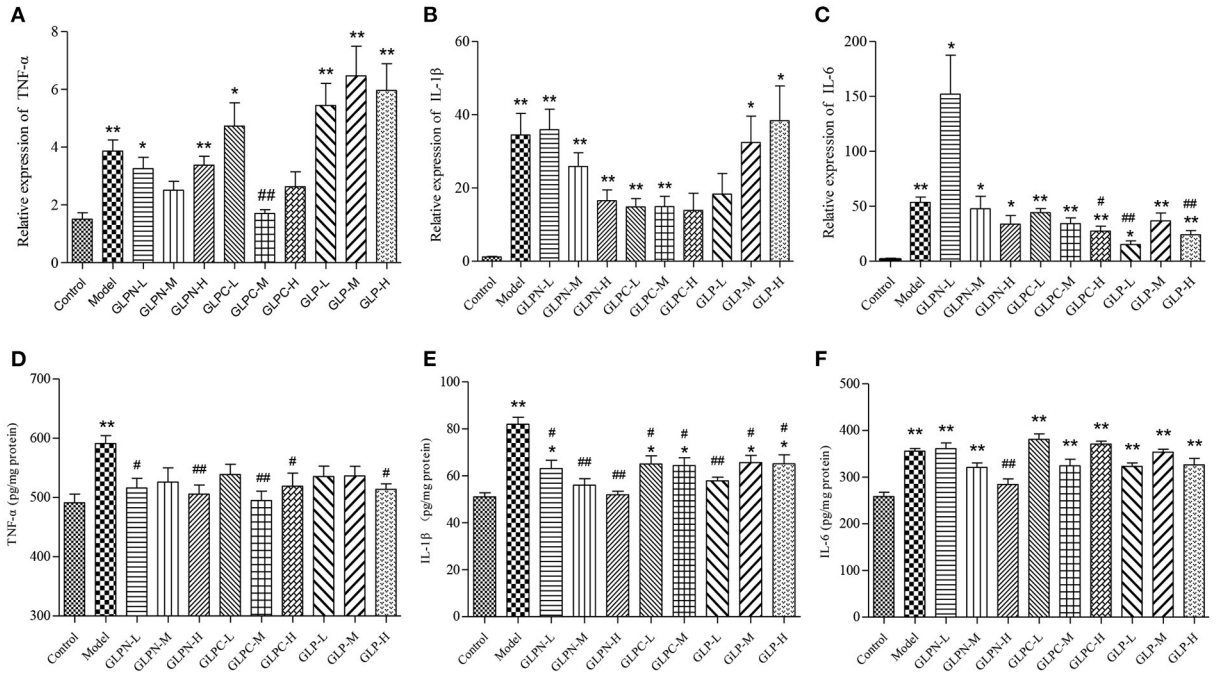

FIGURE 7
Effects of GLP and the degraded fractions (GLPC and GLPN) on mRNA and protein expression levels of pro-inflammatory cytokines in the colon tissues of different groups of mice. **(A–C)** Represent mRNA expression levels of TNF-α, IL-1β, and IL-6 determined by RT-PCR, respectively. **(D–F)** Represent the expression levels of TNF-α, IL-1β, and IL-6 in colon tissues determined by ELISA, respectively. Data are expressed as mean ± SD, $n = 10$ (*$P < 0.05$, **$P < 0.01$ vs. normal control group; $^{\#}P < 0.05$, $^{\#\#}P < 0.01$ vs. DSS model group).

Effect of β-D-glucans with different M_w on suppressing the inflammatory cytokine levels

Normally the intestinal mucosa with inflammation contains a complex array of inflammatory mediators that can reflect the degree of inflammation. It was reported that these pro-inflammatory mediators played a key role in the pathophysiology of IBD (40). The cytokines (TNF-α, IL-6, and IL-1β) have been implicated as important inflammatory mediators in patients with intestinal inflammation (41, 42). Previous studies have revealed that blockade of these pro-inflammatory cytokines signal in chronic intestinal inflammation caused significant inhibition of colitis (43–45). In the present study, the colon tissues of DSS-induced colitis treated by β-D-glucans with different M_w were performed to test the mRNA and protein expression levels of the inflammatory cytokines (Figure 7). Compared with the normal control group, the mRNA expression levels of inflammatory cytokines in model group were all significantly up-regulated (Figures 7A–C). GLP did not inhibit the up-regulation of mRNA expression levels of TNF-α and IL-1β in the tested dosage, however, it showed obvious inhibition on mRNA expression of IL-6. The degraded fractions GLPC and GLPN could inhibit the mRNA expression levels of TNF-α, IL-6, and IL-1β at a certain dose, indicating the degraded β-D-glucan possessed better anti-inflammatory activity on intestinal inflammation. The expression in protein levels of pro-inflammatory cytokines (Figures 7D–F) also showed that the lower M_w fraction GLPN exhibited extremely significant inhibition on three kinds of pro-inflammatory cytokines at high dosage with 200 mg/kg, which was better than those of GLP and GLPC. The result was consistent with those in inflamed Caco-2 cells model *in vitro*, indicating that GLPN could effectively lessen DSS-induced colitis. These results further confirmed that low M_w β-D-glucan fraction possessed better anti-inflammatory effects.

Some studies showed that the change of M_w could influence the anti-inflammatory activity of polysaccharides. Chang et al. (46) investigated the anti-inflammatory activity of chitosan with different molecular weights *in vitro*, and the result showed that the larger chitosans (M_w, 1.56×10^5 g/mol and 7.2×10^4 g/mol) significantly inhibited TNF-α and IL-6 production, whereas the smaller chitosan (M_w, 7.1×10^3 g/mol) significantly induced their production (10). Du et al. reported that the triple helical structure of exopolysaccharide from *Schizophyllum commune* would change into random coiled structure by ultrasonic treatment (39). The medium (9.36×10^5 g/mol) and high M_w (1.44×10^6 g/mol) fractions with the conformation of triple

helix and single helix showed obvious anti-inflammatory activity in DSS-induced colitis than the low M_w (1.97×10^5 g/mol) fraction with random coiled conformation (39). The study on the effects of oat β-glucan with different M_w in colitis revealed that higher M_w β-glucan showed stronger effects on the reverse in lymphocyte percentage, while lower M_w fraction exhibited stronger suppress effects of the inflammatory markers secretion (38). It was also assumed that high M_w β-glucan might form a protective layer on the internal intestinal wall based on its physical properties, which can reduce inflammatory damages, and low M_w β-glucan was more effective on reducing cytokines through regulating the signal pathways due to its specific molecular structure (38). In our study, the lower M_w fraction (3.49×10^4 g/mol) of β-D-glucan from *G. lucidum* also exhibited significant anti-inflammatory activity than the high (2.42×10^6 g/mol) and middle M_w (6.53×10^5 g/mol) fractions with triple helical conformation structures, especially for reduction on pro-inflammatory cytokines, indicating that decreasing of M_w would improve the anti-inflammatory activity of β-D-glucan from *G. lucidum*. The relationship between M_w and the anti-colitis activity showed difference on polysaccharides with different structures, which might be due to the structural characteristics of these polymers. More fractions with different M_w should be prepared for further investigating the effects of M_w on activities and the deep mechanisms. Our results provided evidence for the potential use of β-D-glucan from *G. lucidum* as a preventive measure for IBD patients.

Conclusion

In this study, the influence of molecular weight on the intestinal anti-inflammatory of β-D-glucan from *G. lucidum* was investigated. The ultrasonicated fraction GLPC (M_w, 6.53×10^5 g/mol) had a similar primary structure and triple helix conformation with the original β-(1→ 3,1→ 6)-D-glucan (GLP, M_w 2.42×10^6 g/mol) from *G. lucidum*, and GLPN (M_w, 3.49×10^4 g/mol) also possessed the similar repeat unit as GLP but different conformation characteristics due to its lower M_w. The molecular weight showed significant impacts on the anti-inflammatory activity in LPS-induced inflamed Caco-2 cells and DSS-induced colitis model. The degraded fraction (GLPC and GLPN) exhibited better anti-inflammatory activities by inhibiting LPS-induced expression of TNF-α, IL-8, MIF, and MCP-1. Moreover, GLPN with lower M_w fraction exhibited anti-inflammatory activity through preventing colon length shortening and inhibiting the production of pro-inflammatory cytokines including TNF-α, IL-1β, and IL-6 in DSS-induced colitis mice. The results proved that degradation of β-D-glucan could improve its anti-inflammatory activity and contribute to the potential use of β-D-glucan from *G. lucidum* as anti-colitis ingredients.

Data availability statement

The raw data supporting the conclusions of this article will be made available by the authors, without undue reservation.

Ethics statement

The animal study was reviewed and approved by the Ethics Committee of Experimental Animal Care at Shanghai University of Traditional Chinese Medicine (Permit No. PZSHUTCM210926015). Written informed consent was obtained from the owners for the participation of their animals in this study.

Author contributions

YL: conceptualization, funding acquisition, and writing-review and editing. QT: methodology, data curation, investigation, and analysis. JF: methodology, visualization, and investigation. JL: methodology and formal analysis. CT, MY, and JZho: investigation and analysis. SZ: formal analysis, methodology, and investigation. LL: methodology and analysis. JZha: conceptualization, validation, and funding acquisition. All authors contributed to the article and approved the submitted version.

Funding

This work was supported financially by Shanghai Agriculture Applied Technology Development Program, China (Grant No. X2021-02-08-00-12-F00797), Natural Science Foundation of Shanghai, China (Grant No. 20ZR1418700), Leading Talents Fund in Minhang District of Shanghai, China (Grant No. 201844), and the Project for Excellent Research Team of Shanghai Academy of Agricultural Sciences (Grant No. G2022003).

Conflict of interest

Author JZho was employed by Shanghai Baixin Bio-Tech Co., Ltd.

The remaining authors declare that the research was conducted in the absence of any commercial or financial relationships that could be construed as a potential conflict of interest.

Publisher's note

All claims expressed in this article are solely those of the authors and do not necessarily represent those

of their affiliated organizations, or those of the publisher, the editors and the reviewers. Any product that may be evaluated in this article, or claim that may be made by its manufacturer, is not guaranteed or endorsed by the publisher.

Supplementary material

The Supplementary Material for this article can be found online at: https://www.frontiersin.org/articles/10.3389/fnut.2022.1028727/full#supplementary-material

References

1. Progatzky F, Sangha NJ, Yoshida N, Mcbrien M, Cheung J, Shia A, et al. Dietary cholesterol directly induces acute inflammasome-dependent intestinal inflammation. *Nat Commun*. (2014) 5:5864. doi: 10.1038/ncomms6864

2. Xavier RJ, Podolsky DK. Unravelling the pathogenesis of inflammatory bowel disease. *Nature*. (2007) 448:427–34. doi: 10.1038/nature06005

3. Biesiada G, Czepiel J, Ptak-Belowska A, Targosz A, Krzysiek-Maczka G, Strzalka M, et al. Expression and release of leptin and proinflammatory cytokines in patients with ulcerative colitis and infectious diarrhea. *J Physiol Pharmacol.* (2012) 63:471–81. doi:_10.1002/cphy.c110065

4. Gordon JN, Pickard KM, Sabatino AD, Prothero JD, Pender SLF, Goggin PM, et al. Matrix metalloproteinase-3 production by gut IgG plasma cells in chronic inflammatory bowel disease. *Inflamm Bowel Dis.* (2010) 14:195–203. doi: 10.1002/ibd.20302

5. Joo YE. Natural product-derived drugs for the treatment of inflammatory bowel diseases. *Intest Rese.* (2014) 12:103–9. doi: 10.5217/ir.2014.12.2.103

6. Du B, Lin C, Bian ZX, Xu B. An insight into anti-inflammatory effects of fungal beta-glucans. *Trends Food Sci Tech.* (2015) 41:49–59. doi: 10.1016/j.tifs.2014.09.002

7. Liu Y, Zhao J, Zhao Y, Zong S, Tian Y, Chen S, et al. Therapeutic effects of lentinan on inflammatory bowel disease and colitis-associated cancer. *J Cell Mol Med.* (2019) 23:750–60. doi: 10.1111/jcmm.13897

8. Smiderle FR, Baggio CH, Borato DG, Santana-Filho AP, Sassaki GL, Iacomini M, et al. Anti-inflammatory properties of the medicinal mushroom *Cordyceps militaris* might be related to its linear (1→ 3)-β-D-glucan. *PLoS ONE*. (2014) 9:e110266. doi: 10.1371/journal.pone.0110266

9. Sun Y, Shi X, Zheng X, Nie S, Xu X. Inhibition of dextran sodium sulfate-induced colitis in mice by baker's yeast polysaccharides. *Carbohyd Polym.* (2018) 207:371–81. doi: 10.1016/j.carbpol.2018.11.087

10. Chen J, Seviour R. Medicinal importance of fungal β-(1→ 3), (1→ 6)-glucans. *Mycol Res.* (2007) 111:635–52. doi: 10.1016/j.mycres.2007.02.011

11. Bae IY, Kim HW, Yoo HJ, Kim ES, Lee S, Park DY, et al. Correlation of branching structure of mushroom β-glucan with its physiological activities. *Food Res Int.* (2013) 51:195–200. doi: 10.1016/j.foodres.2012.12.008

12. Ken-Ichi I, Miura NN, Yoshiyuki A, Naohito O, Toshiro Y. Relationship between solubility of grifolan, a fungal 1, 3-β-D-glucan, and production of tumor necrosis factor by macrophages *in vitro*. *Biosci Biotech Bioch.* (2001) 65:1993–2000. doi: 10.1271/bbb.65.1993

13. Xu X, Pan C, Zhang L, Ashida H. Chain structures of glucans from Lentinus edodes and their effects on NO production from RAW 2647 macrophages. *Carbohy Polym.* (2012) 87:1855–62. doi: 10.1016/j.carbpol.2011.10.015

14. Zhang Y, Kong H, Fang Y, Nishinari K, Phillips GO. Schizophyllan: a review on its structure, properties, bioactivities and recent developments. *Bioact Carbohy Diet Fibre.* (2013) 1:53–71. doi: 10.1016/j.bcdf.2013.01.002

15. Sigrid EMH, David LW, Olaf W, Sybren LM, Siamon G, Wouter JJ. Orally delivered β-glucans aggravate dextran sulfate sodium (DSS)-induced intestinal inflammation. *Nutr Res.* (2015) 35:1106–12. doi: 10.1016/j.nutres.2015.09.017

16. Ken-Ichi I, Miura NN, Yoshiyuki A, Hiroshi T, Shigenori T, Naohito O. The solubilization and biological activities of *Aspergillus* β-(1 → 3)-D-glucan. *Fems Immunol Med Mic.* (2004) 42:155–66. doi: 10.1016/j.femsim.2004.04.004

17. Sun XY, Zhang H, Liu J, Ouyang JM. Repair activity and crystal adhesion inhibition of polysaccharides with different molecular weights from red algae *Porphyra yezoensis* against oxalate-induced oxidative damage in renal epithelial cells. *Food Funct.* (2019) 10:3851–67. doi: 10.1039/C8FO02556H

18. Falch BH, Espevik T, Ryan L, Stokke BT. The cytokine stimulating activity of (1→ 3)-beta-D-glucans is dependent on the triple helix conformation. *Carbohy Res.* (2000) 329:587–96. doi: 10.1016/S0008-6215(00)00222-6

19. Jiang Y, Qi X, Gao K, Liu W, Li N, Cheng N, et al. Relationship between molecular weight, monosaccharide composition and immunobiologic activity of *Astragalus* polysaccharides. *Glycoconjugate J.* (2016) 33:755–61. doi: 10.1007/s10719-016-9669-z

20. Jin W, Zhang W, Liu G, Yao J, Shan T, Sun C, et al. The structure-activity relationship between polysaccharides from *Sargassum thunbergii* and anti-tumor activity. *Int J Biol Macromol.* (2017) 105:686–92. doi: 10.1016/j.ijbiomac.2017.07.089

21. Liu YF, Zhang JS, Tang QJ, Yang Y, Guo Q, Wang Q, et al. Physicochemical characterization of a high molecular weight bioactive β-D-glucan from the fruiting bodies of *Ganoderma lucidum*. *Carbohy Polym.* (2014) 101:968–74. doi: 10.1016/j.carbpol.2013.10.024

22. Ren L, Zhang J, Zhang T. Immunomodulatory activities of polysaccharides from *Ganoderma* on immune effector cells. *Food Chem.* (2021) 340:127933. doi: 10.1016/j.foodchem.2020.127933

23. Wang J, Yuan Y, Yue T. Immunostimulatory activities of β-d-glucan from *Ganoderma lucidum*. *Carbohy Polym.* (2014) 102:47–54. doi: 10.1016/j.carbpol.2013.10.087

24. Schittenhelm N, Kulicke WM. Producing homologous series of molar masses for establishing structure-property relationships with the aid of ultrasonic degradation. *Macromol Chem Phys.* (2000) 201:1976–84. doi: 10.1002/1521-3935(20001001)201:15<1976::AID-MACP1976>3.0.CO;2-0

25. Zhong K, Zhang Q, Tong L, Liu L, Zhou X, Zhou S. Molecular weight degradation and rheological properties of schizophyllan under ultrasonic treatment. *Ultrason Sonochem.* (2015) 23:75–80. doi: 10.1016/j.ultsonch.2014.09.008

26. Han F, Fan H, Yao M, Yang S, Han J. Oral administration of yeast beta-glucan ameliorates inflammation and intestinal barrier in dextran sodium sulfate-induced acute colitis. *J Funct Foods.* (2017) 35:115–26. doi: 10.1016/j.jff.2017.05.036

27. Mu HX, Liu J, Fatima S, Lin CY, Shi XK, Du B, et al.. Anti-inflammatory actions of (+)-3′α-angeloxy-4′-keto-3′,4′-dihydroseselin (Pd-Ib) against dextran sulfate sodium-induced colitis in C57BL/6 mice. *J Nat Prod*. (2016) 79:1056–62. doi: 10.1021/acs.jnatprod.5b01071

28. Shin HS, Satsu H, Bae MJ, Zhao Z, Ogiwara H, Totsuka M, et al. Anti-inflammatory effect of chlorogenic acid on the IL-8 production in Caco-2 cells and the dextran sulphate sodium-induced colitis symptoms in C57BL/6 mice. *Food Chem.* (2015) 168:167–75. doi: 10.1016/j.foodchem.2014.06.100

29. Xiao HT, Peng J, Hu DD, Lin CY, Du B, Tsang SW, et al. Qing-dai powder promotes recovery of colitis by inhibiting inflammatory responses of colonic macrophages in dextran sulfate sodium-treated mice. *Chin Med.* (2015) 10:29 doi: 10.1186/s13020-015-0061-x

30. Liu YF, Tang QJ, Zhang JS, Xia Y, Yang Y, Wu D, et al. Triple helix conformation of β-D-glucan from *Ganoderma lucidum* and effect of molecular weight on its immunological activity. *Int J Biol Macromol*. (2018) 114:1064–70. doi: 10.1016/j.ijbiomac.2018.03.054

31. Rao Z, Dong Y, Zheng X, Tang K, Liu J. Extraction, purification, bioactivities and prospect of lentinan: a review. *Biocatal Agr Biotech.* (2021) 37:102163. doi: 10.1016/j.bcab.2021.102163

32. Saitô H, Yoshioka Y, Uehara N, Aketagawa J, Tanaka S, Shibata Y. Relationship between conformation and biological response for (1→ 3)-β-d-glucans in the activation of coagulation Factor G from limulus amebocyte lysate and host-mediated antitumor activity. Demonstration of single-helix conformation as a stimulant. *Carbohy Res.* (1991) 217:181–90. doi: 10.1016/0008-6215(91)84128-2

33. Baumgart DC, Carding SR. Inflammatory bowel disease: cause and immunobiology. *Lancet*. (2007) 369:1627–40. doi: 10.1016/S0140-6736(07)60750-8

34. Atreya R, Neurath MF. Chemokines in inflammatory bowel diseases. *Digest Dis*. (2010) 28:386–94. doi: 10.1159/000320392

35. Magro F, Portela F. Management of inflammatory bowel disease within fliximab and other anti-tumor necrosis factor alpha therapies. *Biodrugs*. (2010) 24:3–14. doi: 10.2165/11586290-000000000-00000

36. Alam A, Haldar S, Thulasiram HV, Kumar R, Goyal M, Iqbal MS, et al. Novel anti-inflammatory activity of epoxyazadiradione against macrophage migration inhibitory factor. *J Biolo Chem*. (2012) 287:24844–61. doi: 10.1074/jbc.M112.341321

37. Tu J, Xu Y, Xu J, Ling Y, Cai Y. Chitosan nanoparticles reduce LPS-induced inflammatory reaction via inhibition of NF-κB pathway in Caco-2 cells. *Int J Biol Macromol*. (2016) 86:848–56. doi: 10.1016/j.ijbiomac.2016.02.015

38. Zyla E, Dziendzikowska K, Gajewska M, Wilczak J, Harasym J, Gromadzka-Ostrowska J. Beneficial effects of oat beta-glucan dietary supplementation in colitis depend on its molecular weight. *Molecules*. (2019) 24:3591. doi: 10.3390/molecules24193591

39. Du B, Yang Y, Bian Z, Xu B. Molecular weight and helix conformation determine intestinal anti-inflammatory effects of exopolysaccharide from *Schizophyllum commune*. *Carbohy Polym*. (2017) 172:68–77. doi: 10.1016/j.carbpol.2017.05.032

40. Soufli I, Toumi R, Rafa H, Touil-Boukoffa C. Overview of cytokines and nitric oxide involvement in immuno-pathogenesis of inflammatory bowel diseases. *World J Gastrointest Pharmacol Therapeut*. (2016) 7:353–60. doi: 10.4292/wjgpt.v7.i3.353

41. Gong Z, Zhao S, Zhou J, Yan J, Wang L, Du X, et al. Curcumin alleviates DSS-induced colitis via inhibiting NLRP3 inflammsome activation and IL-1β production. *Mol Immunol*. (2018) 104:11–9. doi: 10.1016/j.molimm.2018.09.004

42. Xiao YT, Yan WH, Cao Y, Yan JK, Cai W. Neutralization of IL-6 and TNF-α ameliorates intestinal permeability in DSS-induced colitis. *Cytokine*. (2016) 83:189–92. doi: 10.1016/j.cyto.2016.04.012

43. Popivanova BK, Kitamura K, Wu Y, Kondo T, Kagaya T, Kaneko S, et al. Blocking TNF-α in mice reduces colorectal carcinogenesis associated with chronic colitis. *J Clin Invest*. (2008) 118:560. doi: 10.1172/JCI32453

44. Noguchi D, Wakita D, Tajima M, Ashino S, Iwakura Y, Zhang Y, et al. Blocking of IL-6 signaling pathway prevents $CD4^+$ T cell-mediated colitis in a Th17-independent manner. *Int Immunol*. (2007) 19:1431–40. doi: 10.1093/intimm/dxm114

45. Yin Q, Pi X, Jiang Y, Ren G, Liu Z, Liu H, et al. An immuno-blocking agent targeting IL-1β and IL-17A reduces the lesion of DSS-induced ulcerative colitis in mice. *Inflammation*. (2021) 44:1724–36. doi: 10.1007/s10753-021-01449-4

46. Chang SH, Lin YY, Wu GJ, Huang CH, Tsai GJ. Effect of chitosan molecular weight on anti-inflammatory activity in the RAW 2647 macrophage model. *Int J Biol Macromol*. (2019) 131:167–75. doi: 10.1016/j.ijbiomac.2019.02.066

frontiers | Frontiers in Nutrition

TYPE Review
PUBLISHED 05 October 2022
DOI 10.3389/fnut.2022.1021448

Check for updates

OPEN ACCESS

EDITED BY
Xin Wang,
Northwest A&F University, China

REVIEWED BY
Yue Gao,
University of Maryland, College Park, United States
Lei Luo,
Hubei University of Chinese Medicine, China

*CORRESPONDENCE
Li Wang
wangli08zb@126.com
Xudan Guo
guoxudan123@126.com
Xiangzhen Zhu
zhuxiangzhen318@163.com

SPECIALTY SECTION
This article was submitted to Food Chemistry, a section of the journal Frontiers in Nutrition

RECEIVED 17 August 2022
ACCEPTED 16 September 2022
PUBLISHED 05 October 2022

CITATION
Zhu Y, Feng X, Guo J, Wang L, Guo X and Zhu X (2022) A review of extraction, purification, structural properties and biological activities of legumes polysaccharides. *Front. Nutr.* 9:1021448. doi: 10.3389/fnut.2022.1021448

COPYRIGHT
© 2022 Zhu, Feng, Guo, Wang, Guo and Zhu. This is an open-access article distributed under the terms of the Creative Commons Attribution License (CC BY). The use, distribution or reproduction in other forums is permitted, provided the original author(s) and the copyright owner(s) are credited and that the original publication in this journal is cited, in accordance with accepted academic practice. No use, distribution or reproduction is permitted which does not comply with these terms.

A review of extraction, purification, structural properties and biological activities of legumes polysaccharides

Yingying Zhu[1], Xuewei Feng[1], Jianhang Guo[1], Li Wang[2]*, Xudan Guo[3]* and Xiangzhen Zhu[2]*

[1]Henan Key Laboratory of Cold Chain Food Quality and Safety Control, College of Food and Bioengineering, Henan Collaborative Innovation Center for Food Production and Safety, Zhengzhou University of Light Industry, Zhengzhou, China, [2]State Key Laboratory of Cotton Biology, Institute of Cotton Research, Chinese Academy of Agricultural Sciences, Anyang, China, [3]Basic Medical College, Hebei Higher Education Institute Applied Technology Research Center on TCM Formula Preparation, Hebei TCM Formula Preparation Technology Innovation Center, Hebei University of Chinese Medicine, Shijiazhuang, China

In recent years, polysaccharides derived from legumes polysaccharides have aroused worldwide interests. Phytochemical and pharmacological studies have studied the physicochemical properties (emulsification, stability and foaming) and demonstrated the biological activities (immune regulation, anti-oxidation, anti-tumor, hypoglycemic, hypolipidemic and intestinal flora regulation) of legumes polysaccharides. Besides, it is reported that the extraction methods will affect the structural features of polysaccharides, thus further changing their physicochemical properties and biological activities. This review appraised the available literatures described the extraction, purification, structural characterization, biological activity and functional properties of legumes polysaccharides in recent years. It can provide useful research underpinnings and updated information for the development and application of related polysaccharides in functional food and medicinal field.

KEYWORDS

legumes, polysaccharides, extraction methods, structural characterization, biological activity

Introduction

Legumes are a large group with pods as a common feature. They are the third largest family of angiosperms, with about 690 genera and more than 17,600 species, widely distributed all over the world. Legumes mainly include soybeans, black beans, adzuki beans, mung beans, lentils, cowpeas, kidney beans, peas, chickpeas, etc. Modern chemical and pharmacological studies have shown a positive correlation between the consumption of legumes and a reduced risk of Chronic metabolic diseases, such as cardiovascular disease, diabetes, obesity and cancer (1, 2). This is related to the fact that legumes are rich in polysaccharides, protein, vitamins, minerals, unsaturated fatty acids, phenolic compounds and other beneficial nutritional factors (3).

In recent years, the research on legumes has mainly focused on protein, but with the rapid development of glycochemistry and glycobiology technology, legumes polysaccharide has gradually become a research hotspot of scholars worldwide (4, 5). Legumes polysaccharides obtained by different extraction and purification methods have different physicochemical properties and biological activities, including immune regulation, anti-oxidation, anti-tumor, hypoglycemic, gastrointestinal protection and so on (6–10). Additionally, legumes polysaccharides have physical and chemical properties such as emulsifying and stability, which can improve the quality and appearance of dairy products (11, 12).

However, throughout the available literatures, there has been no systematic review of legumes polysaccharides, neither on the extraction and purification methods nor on the structural characterization and biological activities. Moreover, legumes polysaccharides are widely used and can be used in milk beverages, flour products, functional foods and health care products. Therefore, this paper systematically reviews the extraction, isolation, purification, structural characteristics, biological activities and functional properties of legume polysaccharides, which lays a foundation for promoting the research of legumes polysaccharides in the food industry and biomedicine.

Extraction, isolation and purification methods

Legumes polysaccharides are structural components of the plant cell wall, so extraction methods are usually based on the deconstruction of the cell wall. The extraction method is to dissolve the polysaccharide from the cell wall under moderate extraction conditions without changing their structure of the legume's polysaccharides (7, 13, 14). The extraction and purification of legumes polysaccharides are shown in Figure 1 and Table 1. First, the legumes were dried, crushed, and passed through a 50-mesh sieve; then, the powder was soaked in 95% ethanol for 3 h to remove pigments, lipids, oligosaccharides and other small molecular substances (23); next, the dry legumes powder was extracted with hot water at 60–95°C, centrifuged (3,000–5,000 rpm), the supernatant was collected, concentrated, and four times the volume of absolute ethanol was added, overnight at 4°C to precipitate the legumes polysaccharide; finally, the crude legumes polysaccharides were redissolved, deproteinized, decolorized, dialyzed, and freeze-dried to obtain the legumes polysaccharide (18, 24). At present, the extraction methods of legumes polysaccharides are mainly divided into hot water extraction, acid-base extraction, enzymatic extraction, ultrasonic-assisted extraction, microwave-assisted extraction, hot-compressed water extraction and subcritical extraction (12, 22, 25, 26).

Hot-water extraction is most commonly used for laboratory extraction of polysaccharides and is also widely used in industrial extraction processes. Liu et al. (15) used response surface methodology to optimize the extraction conditions of black soybean polysaccharides: extraction temperature 92°C; extraction time 6.4 h; ratio of water to material of 20 ml/g. Under these conditions, the extraction yield of three rounds was 2.56%. Yao et al. (17) first used hot water extraction and then alkali extraction, increasing the extraction temperature of polysaccharides, and the polysaccharide yield increased to 9.59%. In order to improve the yield of polysaccharides, methods such as microwave and ultrasound are also used to assist extraction (7, 20, 27). Maryanne et al. (28) optimized ultrasonic-assisted extraction of pea polysaccharide using response surface methodology. The optimal extraction conditions were: ultrasonic power 135.34 W, extraction time 48.61 mins, extraction temperature 68.25°C and ratio of water to raw material of 33.6:1, here conditions, the polysaccharide extraction was 7.37%. Han et al. (7) compared the extraction of soybean hull polysaccharides by hot water extraction, microwave-assisted ammonium oxalate extraction and microwave-assisted sodium citrate extraction. Among them, the microwave-assisted ammonium oxalate extraction method had the highest yield (9.3%), the microwave-assisted sodium citrate method had the second highest yield (3.6%), and the hot water extraction method had the lowest yield (1.2%). Ultrasound and microwave can damage the cell wall, cause the outflow of intracellular substances, and improve the extraction efficiency of polysaccharides, but long-term use can lead to structural damage of polysaccharide (29). In addition to physical extraction, enzymatic extraction of legumes polysaccharides is also used. Enzymes can change the permeability of the cell wall and dissolve the cell contents, thereby increasing the extraction efficiency (30). Jiang et al. (21) used cellulase to assist the extraction of mung bean skin polysaccharide, and the extraction rate was 1.61%, which was much higher than that of hot water extraction.

To sum up, the hot water extraction method is simple and convenient, but the extraction rate is low; both ultrasonic-assisted and microwave-assisted extraction methods can improve the extraction efficiency, but long-term ultrasonic or microwave irradiation will change the polysaccharide structure; enzyme-assisted extraction method has the advantages of mild reaction and high extraction efficiency, but the production cost is high.

It is reported that soybean polysaccharide is a heteropolysaccharide containing different components. In order to determine the composition and structure of legumes polysaccharide, it is necessary to further purify the crude polysaccharide. At present, polysaccharide purification methods mainly include fractional alcohol precipitation, ultrafiltration and column chromatography (31, 32). Among them, the fractional alcohol precipitation and ultrafiltration are the preliminary separation, and then the column chromatography is used for further purification. Column chromatography

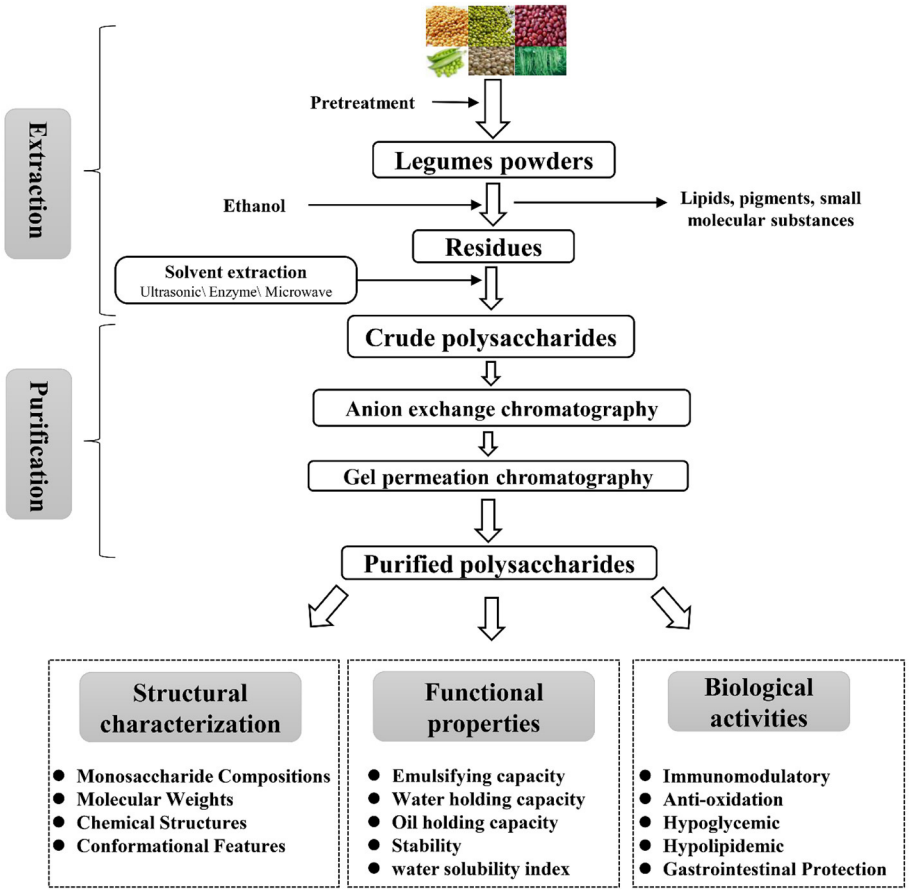

FIGURE 1
Schematic representation of the extraction, purification, and bioactivity of polysaccharides from legumes.

can be divided into anion exchange chromatography and gel permeation chromatography. Anion chromatography columns (DEAE-Cellulose and DEAE-Sepharose Fast Flow) separate acidic and medium polysaccharides based on polysaccharide polarity. Gel permeation chromatography (Sephadex-G series and Sephacryl-S series) separates polysaccharides based on molecular weight differences (27, 31, 33). For example, Wang et al. (6) used different concentrations of NaCl to separate three different polysaccharides (F1, F2, F3) by DEAE Sepharose Fast Flow. Hu et al. (34) used DEAE-Cellulose to separate neutral polysaccharides (SSPS-N) and acidic polysaccharides (SSPS-A) from Okara. Ye et al. (35) used DEAE Fast Flow and Sephadex G-100 to separate and purify CHPS-1, CHPS-2 and CHPS-3 with molecular weights of 3.1×10^6, 1.5×10^6 and 7.8×10^5 Da from chickpea hull polysaccharides, respectively. Zhang et al. (36) isolated two fractions, W-DE-GPP and N-DE-GPP, from pea, using DEAE Fast Flow and Sephadex G-100 to separate and purify two main components.

Physiochemical and structural features

The structure of plant polysaccharides is diverse and complex, and the biological activities of polysaccharides with different structures are also different. Generally, the structural characteristics of plant polysaccharides mainly include monosaccharide composition, molecular weight, chemical structure, and spatial conformation (27). The homogeneous legumes polysaccharides obtained by separation and purification can be obtained by acid hydrolysis, methylation analysis, periodate oxidation, Smith degradation, infrared spectroscopy (IR), gas chromatography-mass spectrometry (GC-MS), nuclear magnetic resonance (NMR), high performance liquid chromatography (HPLC), gas chromatography (GC), scanning electron microscope (SEM), atomic force microscope (AFM), X-ray diffraction (XRD) and other instrumental analysis methods are used to determine the basic chemical structure (5, 30, 31, 37). The structural characteristics of legumes polysaccharides such

TABLE 1 A summary of the extraction of legumes polysaccharides.

Types	Time (h)	Solid-liquid ratio	Temperature (°C)	Solvent	Other conditions	Yield (%)	References
BSPS	6.4	1:20	92	Water	3 times	2.56	(15)
SHP	2	1:10	65	Water	1–3 times	9.2	(6)
BSCP	2.22	1:22.3	100	Water	1 time	10.56	(16)
A-SSCP	0.33	1:20	85	0.6% (w/v) ammonium oxalate	Microwave power 480 W	9.3	(7)
AAP	4	1:20	90	Alkali solution	0.3% (w/w) $NaBH_4$ 2 times	3.28	(17)
MWP	4		90	Water	Ultrasonic power 700 W 2 times	3.25	(18)
MEMP	0.019	1:17		Water	Microwave power 700 W	6.003	(19)
MSP	0.5	1:20	25	Water	Ultrasonic power 150 W 2 times	7.6	(20)
MBP-1	3	1:20	55	Water	(2%, w/w) cellulase	1.61	(21)
sCW	0.5	1:12	120	0.2% aqueous citric acid	Subcritical water extraction pressure 50 bra	11.8	(22)

as monosaccharide composition, molecular weight, chemical structure and biological activity are summarized in Table 2.

Monosaccharide compositions

Monosaccharide composition is the most basic and core of the study of plant polysaccharide structure. In most cases, the glycosidic bonds in polysaccharides are completely destroyed by acid hydrolysis, followed by derivatization, and the derivatives are qualitatively and quantitatively analyzed by GC, GC-MS, HPLC (5, 13, 41). Due to the different varieties, sources and extraction and purification processes of legumes, the monosaccharide components extracted from legumes polysaccharides are different, but the polysaccharides are composed of glucose (Glu), galactose (Gal), arabinose (Ara), mannose (Man), xylose (Xyl) and different uronic acids in different molar ratios, and the composition and molar ratio of different monosaccharides were related to the sources and extraction methods of legumes polysaccharides (3). According to Table 2, black soybean polysaccharides were mainly composed of glucose and galactose; soybean polysaccharides were mainly composed of glucose, galactose and arabinose; adzuki bean polysaccharides were mainly composed of galactose and mannose; mung bean polysaccharides were mainly composed of glucose and galactose. For example, Liu et al. (15) used DEAE-52 and Sepharose CL-4B to separate and purify three component polysaccharides (BSPS-1, BSPS-2, BSPS-3) from black soybean. Chemical analysis indicated that BSPS-1 was composed of arabinose, rhamnose (Rha), galactose, glucose and mannose in the molar ratio of 1.79:1.00:2.59:26.54:1.01; BSPS-2 was composed of arabinose, rhamnose, xylose, galactose and mannose in the molar ratio of 8.10:4.80:9.15:13.38:1.00; BSPS-3 was composed of arabinose, rhamnose, galactose and mannose in the molar ratio of 16.80: 3.60:33.66:1.00. Meanwhile, Yao et al. (17) compared the effects of different extraction methods on the monosaccharide composition of adzuki bean, and found that the monosaccharide composition of the water extraction component was mainly composed of rhamnose, arabinose, mannose, galactose and glucose; the alkaline extraction components are mainly composed of rhamnose, arabinose, mannose, galactose and galacturonic acid.

Molecular weights

At present, the measurement methods of molecular weight mainly include osmotic pressure method, viscosity method, sedimentation method and HPLC, especially high-performance gel permeation chromatography (HPGPC) is the most widely used method for molecular weight measurement (29, 42). The study found that the molecular weight of legumes polysaccharides is generally between 10^3 and 10^6 Da, and polysaccharides with higher molecular weights tend to have stronger physicochemical properties. Meanwhile, different extraction methods have a great impact on the molecular weight of soy polysaccharides, such as long-term ultrasonic or microwave treatment will destroy the polysaccharide molecular chain, resulting in the fragmentation of the polysaccharide main chain and reducing the molecular weight of the polysaccharide (43). Two polysaccharide fractions with immunomodulatory activity (MWP-1, MWP-2) were isolated from mung bean and their molecular weights were 68.4 and 52.4 kDa (18). In addition, two kinds of polysaccharides with molecular weights of 139 and 208 kDa were extracted from mung bean husk by enzyme extraction method and hot water extraction method, respectively. It was found that the polysaccharide with larger molecular weight was more stable in structure and stronger in activity (21). Nomura et al. (44) compared the effect of different pH on lentil polysaccharides, and the molecular weight of polysaccharides under acidic conditions (830 kg/mol) was lower than that under neutral conditions (1,130 kg/mol).

TABLE 2 Legumes polysaccharide: source, chemical structure, biological activity.

No.	Compound name	Source	Mw (Da)	Monosaccharide composition	Structures	Biological activities	References
1	BSPS-1	Black soybeans	1.95×10^5	Ara, Rha, Gal, Glu, and Man in the molar ratio of 1.79:1.00:2.59:26.54:1.01.	Backbone consisting of α-(1→6)-D-Glc*p* residues		(38)
2	BSPS-3	Black soybeans	1.88×10^5	Ara, Rha, Gal, and Man in the molar ratio of 16.80:3.60:33.66:1.00	Backbone consisting of β-(1→3)-D-Gal*p* residues, branch consisting of α-(1→5)-L-Ara*f*, α-(1→2)-L-Rha*p* and *O*-Me-β-(1→4)-D-GlcA*p* residues		(38)
3	BSCP-1	Black soybean	7.55×10^5	Gal, Man, Rha in the ratio of 6.01:3.56:1.00.		Anti-cancer	(16)
4	SSPS-N-b	Okara	8.6×10^3	Glu, Gal, Man in the ratio of 36.6:34.6:26.6	Backbone consisting of β-(1→4)-D-Man and β-(1→4)-D-Glu residues	Antioxidant	(34)
5	PMP	Soybean curd residue	3.07×10^6	Rha, Ara, Xyl, Man, Glu, and Gal in the ratio of 0.08:0.25:0.16:0.07:0.28:1.00		Antioxidant	(8)
6	P_A-150	Soy hulls		Ara, Gal, Glu, Xyl, Man in the ratio of 39.2:25.9:30.7:2.1:2.1	Backbone consisting of α-L-Arabinofuranosyl, 4-*O*-Me-α-D-Glc*p*A and α-D-Gal		(26)
7	SHP-1	Soy hull	4.85×10^5	Gal*p*A, Gal, Rha Ara in the ratio of 46.5:17.95:14.77:13.97	Backbone consisting of α-(1→4)-D-Gal*p*A, α-(1→2)-L-Rha*p*, β-(1→4)-D-Gal, α-(1→2)-L-Ara residues		(39)
8	AWP-2	Adzuki beans	2.96×10^4	Ara, Man, Gal, Glu in the ratio of 0.4:2.6:5.3:0.7.		Antioxidant, Immunoregulation	(17)
9	MBP-2	Mung bean	2.08×10^5	Rha, Ara, Gal, Glc, Xyl, Man, GalA in the ratio of 0.15:0.67:0.29:3.64:0.22:0.12:1.11		Antioxidant, antibacterial	(21)
10	WPUCP	Chickpeas	7.68×10^5	Gal, Ara, Rha, GalpA	Backbone consisting of β-(1→4)-D-Gal*p*, α-(1→5)-L-Ara*f* residues	Antioxidant	(40)

Chemical structures

In addition to the study of monosaccharide composition and molecular weight of legumes polysaccharide, the chemical structure of polysaccharide is also the focus of research (Table 2). The chemical structures of polysaccharides were obtained by methylation analysis, Smith degradation, IR, NMR and other methods (23). So far, chemical structures of legumes polysaccharides have been reported (Figure 2). Liu et al. (38) analyzed the structures of the two purified polysaccharide components (BSPS-1 and BSPS-2). According to the methylation analysis and NMR results, the possible structural units of the polysaccharides were speculated as shown in Figure 2A. They found that BSPS-1 is produced by 1,6-α-D-glucopyranosyl residues, which is a linear (1→6)-α-D-glucan; whereas BSPS-3 is mainly composed of a 1,3-β-D-galactopyranosyl residue backbone with side chains substituted at the *O*-6 position consisting which is a type II arabinogalactan.

Yang et al. (39) used microwave-assisted ammonium oxalate to extract a novel acidic polysaccharide (SHP-1) with a molecular weight of 4.81×10^5 g/mol from soybean. It is speculated

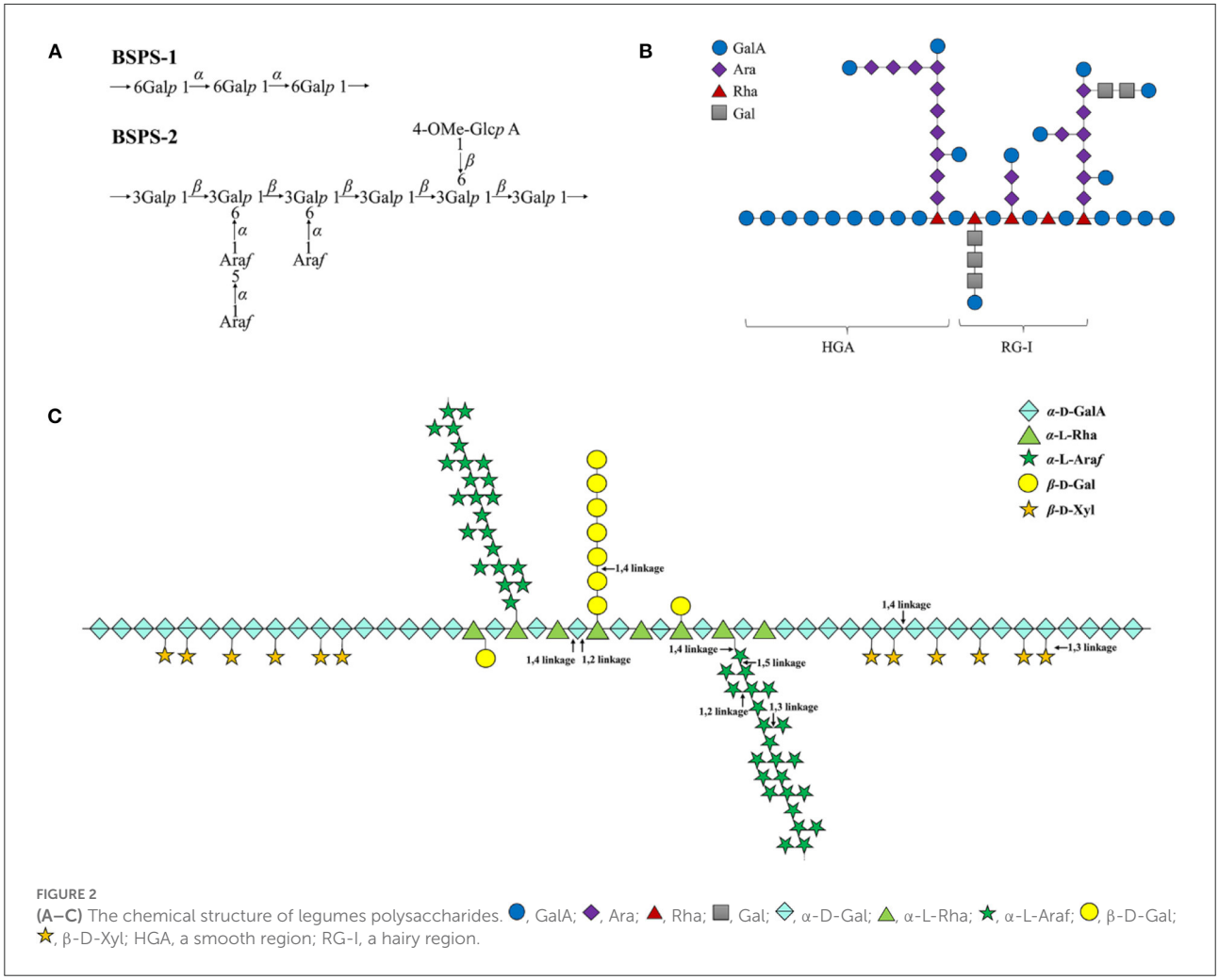

FIGURE 2
(A–C) The chemical structure of legumes polysaccharides. ●, GalA; ◆, Ara; ▲, Rha; ■, Gal; ◇, α-D-Gal; △, α-L-Rha; ★, α-L-Araf; ○, β-D-Gal; ★, β-D-Xyl; HGA, a smooth region; RG-I, a hairy region.

that its chemical structure is that type I pectin is composed of 2/3HG and 1/3RG-I as shown in Figure 2B. It is divided into a smooth region (HGA) and a hairy region (RG-I), and the smooth region consists of α-D-galacturonic acid residue through a 1→4 glycosidic bond in linear homogalacturonans; the hairy region was highly branched, and replaced by galactan, arabinan or arabinogalactan.

Noguchi et al. (45) used pectinase and biochemical methods to analyze the structure of pea pectin polysaccharide, and deduced the structure of pea pectin polysaccharide as shown in Figure 2C. Pea pectin polysaccharide contains 50% arabinose, and the neutral sugar side chain is attached to the rhamnose residue of rhamnogalacturonan-I (RG-I). The RG-I backbone was calculated to contain multiple repeats of [→2)-α-L-Rha-(1→4)-α-D-GalA-(1→]. Galactose and galactooligosaccharides were attached to ∼35% of the rhamnose residues in RG-I. Long β-(1→4)-galactan was also present as the side chains. Considering the influence of neutral sugars in the main chain, the molar ratio of RG-I, XGA and HG was 7:1:2.

Goff et al. (46) isolated a polysaccharide component composed of galacturonic acid and xylose from pea, and the methylation results showed that the polysaccharide backbone was composed of α-(1→4) galacturonan, the side chain consists of (1→2) xylosyl residues.

Conformational features

So far, there have been a lot of studies on the primary structure of legumes polysaccharides, but few reports on the chain conformation (43). At present, the advanced structure characterization of polysaccharide mainly includes SEM, AFM, XRD, Congo red (5, 14). For example, the polysaccharide (PMP) extracted from legumes dregs has a smooth surface under SEM and AFM, showing an irregular loose sheet-like structure. In the Congo red experiment, the polysaccharide and Congo red formed a complex, and there was an obvious red shift phenomenon, indicating that PMP has a triple helix structure (8). Guo et al. (47) extracted leguminous polysaccharide (CHPS)

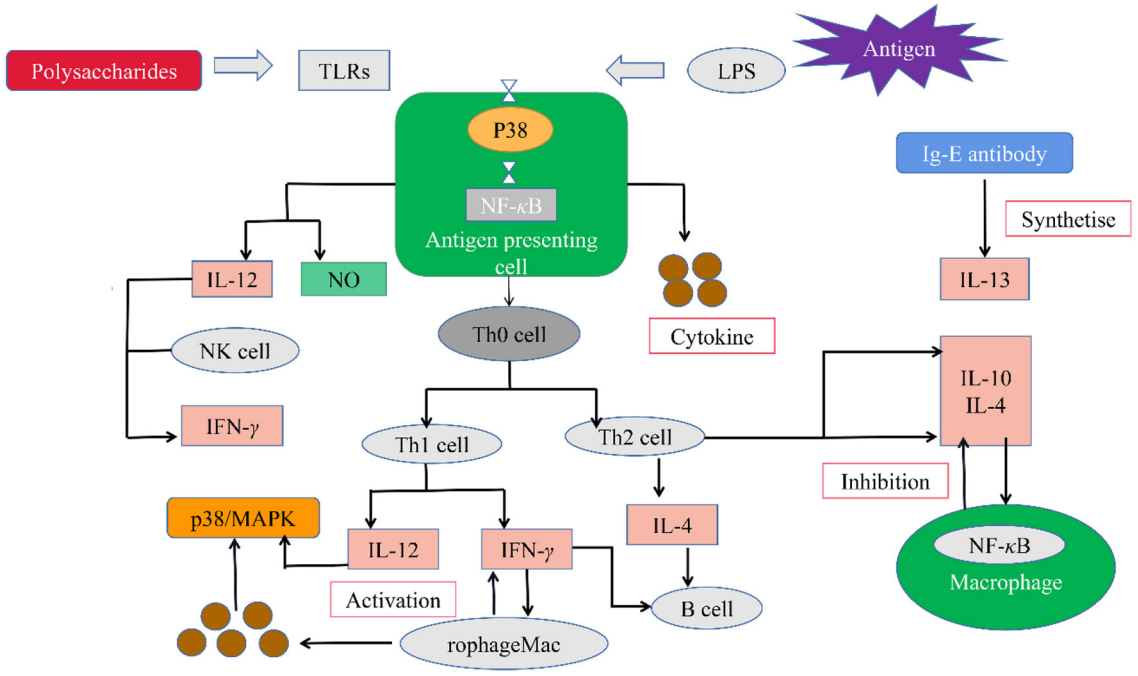

FIGURE 3
The potential immunomodulatory mechanisms of legumes polysaccharides.

from chickpea shells by hot water extraction. The surface of CHPS was loose and porous under SEM, and there was a dispersion peak under XRD, thus confirming that CHPS is semi-crystalline in nature.

Biological activities

In recent years, with the in-depth research on legumes polysaccharides, it has been found that has good biological activities. For example, it can prevent hypertension, diabetes, and heart disease. In addition, it also has certain effects in antioxidant, immune regulation, gastrointestinal protection, anti-tumor, and antibacterial (2, 3). A large number of experiments have shown that polysaccharides are important biologically active components in legumes, and the biological activity is closely related to the structure of polysaccharides (43).

Immunomodulatory

Immunomodulation is the most important biological activity of plant polysaccharides and an important defense strategy against infection, inflammation and cancer (32). Polysaccharides play an immune role mainly by enhancing the functions of natural killer cells, lymphocytes, T-cells, B-cells, macrophages and other immune cells (48). The schematic diagram of the immunomodulatory mechanism of polysaccharides is shown in Figure 3. Polysaccharides combine with TLRs to promote antigenic cells to release cytokines such as interleukin-2 (IL-2), interleukin-6 (IL-6), interferon-γ (IFN-γ), tumor necrosis factor-α (TNF-α), nitric oxide (NO) (42).

Wang et al. (6) investigated the immune activity of soybean chitin polysaccharide (SHP) on macrophages. The study found that SHP can promote the proliferation of RAW 264.7 cells, produce NO, IL-6, TNF-α, which was specifically recognized by Toll-like receptor 2, and then up-regulate the expression levels of mitogen-activated protein kinase and nuclear factor κB pathway downstream proteins.

In one case, three novel polysaccharides (AWP-1, AWP-2, AAP-1) were isolated from adzuki bean, all of which stimulated macrophages to produce NO in a dose-dependent manner, but AWP-2 had the strongest activation effect on macrophages. At the same time, AWP-2 can promote the production of TNF-α and IL-6 in RAW 264.7 macrophages, and enhance the anti-inflammatory and anti-tumor activities (17). Similarly, two polysaccharides (MWP-1, MWP-2) with molecular weights of 68.4 kDa and 52.4 kDa were isolated from mung bean, which could stimulate mouse macrophages to secrete NO, TNF-α and IL-6 in a concentration-dependent manner (18).

Studies have found that polysaccharide structure such as molecular weight, chemical structure, and monosaccharide

composition can have a huge impact on the immunomodulatory activity of polysaccharides (43). For example, Ketha et al. (49) studied the immune activity of mung bean non-starch polysaccharides and found that molecular weight, uronic acid, arabinose, galactose and type II arabinogalactan content appeared to play a key role in macrophage activation.

Anti-oxidation

Oxidative stress and imbalance of free radicals in the body are the main factors leading to the occurrence of diseases such as aging, inflammation, and cancer (32). The antioxidant capacity of legumes polysaccharides is usually evaluated by various free radical tests, such as *in vitro* DPPH free radical, OH free radical, $ABTS^{+}$ free radical, O^{2-} radical scavenging ability.

For example, Hu et al. (34) isolated different components of polysaccharides (SSPS, SSPS-N, SSPS-A) from bean dregs, and found that their ability to scavenge DPPH radicals, OH radicals, and O^{2-} radicals was concentration-dependent. Both SSPS and SSPS-A could scavenge DPPH radicals, OH radicals and O^{2-} radicals, and the most significant concentration was 10 mg/ml, while SSPS-N could only scavenge DPPH radicals and O^{2-} radicals. Wang et al. (19) isolated two polysaccharides from mung bean skin by microwave-assisted hot water extraction. MEMP-1 is mainly composed by mannose and galactose, while MEMP-2 is mainly composed of rhamnose and galactose. Antioxidant results showed that both polysaccharides had strong hydroxyl radical and DPPH radical scavenging activities, among which MEMP-2 had the highest antioxidant activity. This may be due to the differences in the composition and molecular weight of monosaccharides, which lead to different functions of polysaccharides. Meanwhile, Jalili Safaryan et al. (28) used ultrasound-assisted hot water to extract pea polysaccharide (GPPP), and its *in vitro* antioxidant activity was concentration-dependent. At the concentration of 0.9 mg/ml, GPPP had better DPPH radical scavenging ability (91.03%), reducing ability (0.63), and iron ion reducing ability (0.34 mmol/l).

Hypoglycemic and hypolipidemic

Studies have reported that soy polysaccharides can lower blood sugar and blood lipids, and reduce the risk of diabetes (3). In the study of the effects of soybean polysaccharides on postprandial blood glucose in non-insulin-dependent diabetes mellitus, it was found that soybean polysaccharides could significantly reduce postprandial blood glucose and triglyceride levels (50). Similarly, feeding high-fat diet rats with soybean oligosaccharides at different doses showed that soybean oligosaccharides significantly reduced abnormal blood sugar and blood lipid levels in animal models at all doses (51). Soybean oligosaccharides can reduce the oxidative stress induced by high-fat diet, improve the level of dyslipidemia, and reduce the occurrence of cardiovascular and cerebrovascular diseases.

Gastrointestinal protection

A large number of studies have proved that plant polysaccharides have activities such as protecting the gastrointestinal tract, regulating intestinal flora, and preventing colorectal cancer (52). Xie et al. (10) investigated the effect of mung bean peel polysaccharide (MBP-2) on the intestinal flora and short-chain fatty acids (SCFAs) in mice. The study found that MBP-2 can increase the colon length and the production of SCFAs in mice, and improve the intestinal microenvironment and promote the growth of beneficial bacteria through SCFAs. Besides, Akhtar et al. fermented chickpea chitin polysaccharides (CHPS) by mimicking human gut flora (53). Studies have shown that CHPS can significantly increase the beneficial gut microbiota and elevate SCFAs.

Other

Except as mentioned above biological activities, other biological activities of legumes polysaccharides were also evaluated. Hu et al. (16) isolated a novel galactomannan (BSCP-1) with a molecular weight of 7.55×10^{5} Da from the seed coat of black bean, and found that it had an inhibitory effect on human gastric cancer cells. Moreover, Jiang et al. compared the effects of different extraction methods on the antibacterial activity of mung bean skin polysaccharides (21). The study found that the enzyme-extracted polysaccharide (MBP-1) and the hot-water extracted polysaccharide (MBP-2) showed good antibacterial activity against both Gram-positive bacteria (G^{+}) and Gram-negative bacteria (G^{-}).

Functional properties

Legumes polysaccharides also have excellent stability and emulsifying properties, and are mainly used in food and medicine products to improve product stability and emulsifying properties of oil droplets, and significantly improve their quality (3).

For example, two components HMF and LMF with different molecular weights were isolated from soybean polysaccharide. Studies have shown that HMF exhibited high ability to emulsify oil droplets and stabilize α-casein dispersions in acidic environments, and LMF has higher anti-emulsifying lipid oxidation activity (11). Moreover, the functional properties of polysaccharides depend on the ability of the polymer to absorb oil and the interaction between water and polysaccharides (12). It was found that the mung bean water-soluble polysaccharide

(MBP-1) had good hydration properties and oil holding capacity (24). Similarly, polysaccharides (CHPS) extracted from chickpea shells have good fat-binding, foaming and emulsifying properties (47).

Conclusions and perspectives

Like proteins and nucleic acids, polysaccharides also play important roles in living organisms. Bean polysaccharide is the main active ingredient in beans, and is widely used in biology, medicine and functional food due to its excellent functional property and biological activity. In this paper, the extraction, separation and purification, structural properties, biological activities and functional properties of soy polysaccharides are reviewed. Although the research on legumes polysaccharides has made significant progress, there are still many problems to be solved in terms of the current research results. First of all, the extraction and purification method of soybean polysaccharide is inefficient, and there is currently a lack of industrialized and large-scale preparation methods. Second, the structure-activity relationship of soy polysaccharides has not been fully elucidated. Third, regarding the potential risks or toxicity of soy polysaccharides and their derivatives, comprehensive *in vitro* and *in vivo* toxicological studies or risk assessments are required.

Author contributions

YZ, XF, JG, and XZ contributed to conception and design of the study. YZ wrote the first draft of the manuscript. LW and XG wrote sections of the manuscript. LW, XG, and XZ contributed to funding of the study and writing-review and editing. All authors contributed to the article and approved the submitted version.

Funding

This work was supported by the National Key R&D Program of China (2021YFD1600100), the earmarked fund for China Agriculture Research System (CARS-08-G21), the National Natural Science Foundation of China (82204668), the Science and Technology Research Project of Higher Education in Hebei Province (QN2020233), and the Agricultural Science and Technology Innovation Program of Chinese Academy of Agricultural Sciences.

Conflict of interest

The authors declare that the research was conducted in the absence of any commercial or financial relationships that could be construed as a potential conflict of interest.

Publisher's note

All claims expressed in this article are solely those of the authors and do not necessarily represent those of their affiliated organizations, or those of the publisher, the editors and the reviewers. Any product that may be evaluated in this article, or claim that may be made by its manufacturer, is not guaranteed or endorsed by the publisher.

References

1. Kan L, Nie S, Hu J, Wang S, Cui SW, Li Y, et al. Nutrients, phytochemicals and antioxidant activities of 26 kidney bean cultivars. *Food Chem Toxicol.* (2017) 108:467–77. doi: 10.1016/j.fct.2016.09.007

2. Li H, Zou L, Li XY, Wu DT, Liu HY, Li HB, et al. Adzuki bean (Vigna angularis): Chemical compositions, physicochemical properties, health benefits, and food applications. *Compr Rev Food Sci F.* (2022) 21:2335–62. doi: 10.1111/1541-4337.12945

3. Jia X, Chen M, Wan JB, Su H, He C. Review on the extraction, characterization and application of soybean polysaccharide. *RSC Adv.* (2015) 5:73525–34. doi: 10.1039/C5RA12421B

4. Qiu SM, Aweya JJ, Liu X, Liu Y, Tang S, Zhang W, et al. Bioactive polysaccharides from red seaweed as potent food supplements: a systematic review of their extraction, purification, and biological activities. *Carbohyd Polym.* (2022) 275:118696. doi: 10.1016/j.carbpol.2021.118696

5. Ji X, Peng Q, Yuan Y, Shen J, Xie X, Wang M. Isolation, structures and bioactivities of the polysaccharides from jujube fruit (Ziziphus jujuba Mill): a review. *Food Chem.* (2017) 227:349–57. doi: 10.1016/j.foodchem.2017.01.074

6. Wang M, Fu C, Zhang M, Zhang Y, Cao L. Immunostimulatory activity of soybean hull polysaccharide on macrophages. *Exp Ther Med.* (2022) 23:389. doi: 10.3892/etm.2022.11316

7. Han L, Song H, Fu L, Li J, Yang L, Liu H. Effect of extraction method on the chemical profiles and bioactivities of soybean hull polysaccharides. *Food Sci Nutr.* (2021) 9:5928–38. doi: 10.1002/fsn3.2483

8. Li S, Tang D, Wei R, Zhao S, Mu W, Qiang S, et al. Polysaccharides production from soybean curd residue via morchella esculenta. *J Food Biochem.* (2019) 43:e12791. doi: 10.1111/jfbc.12791

9. Ursekar BM, Soni PS, Date AA, Nagarsenker MS. Characterization of soy polysaccharide and its in vitro and in vivo evaluation for application in colon drug delivery. *AAPS PharmSciTech.* (2012) 13:934–43. doi: 10.1208/s12249-012-9810-7

10. Xie J, Song Q, Yu Q, Chen Y, Hong Y, Shen M. Dietary polysaccharide from mung bean [Vigna radiate (Linn) Wilczek] skin modulates gut microbiota and short-chain fatty acids in mice. *Int J Food Sci Tech.* (2021) 57:2581–9. doi: 10.1111/ijfs.15030

11. Li J, Matsumoto S, Nakamura A, Maeda H, Matsumura Y. Characterization and functional properties of sub-fractions of soluble soybean polysaccharides. *Biosci Biotech Bioch.* (2009) 73:2568–75. doi: 10.1271/bbb.70799

12. Cheng M, Qi JR, Feng JL, Cao J, Wang JM, Yang XQ. Pea soluble polysaccharides obtained from two enzyme-assisted extraction methods and their application as acidified milk drinks stabilizers. *Food Res Int.* (2018) 109:544–51. doi: 10.1016/j.foodres.2018.04.056

13. Ji X, Shen Y, Guo X. Isolation, structures, and bioactivities of the polysaccharides from gynostemma pentaphyllum (thunb) Makino: a review. *Biomed Res Int.* (2018) 2018:6285134. doi: 10.1155/2018/6285134

14. Ji X, Yin M, Nie H, Liu Y. A review of isolation, chemical properties, and bioactivities of polysaccharides from bletilla striata. *Biomed Res Int.* (2020) 2020:5391379. doi: 10.1155/2020/5391379

15. Liu J, Wen XY, Zhang XQ, Pu HM, Kan J, Jin CH. Extraction, characterization and in vitro antioxidant activity of polysaccharides from black soybean. *Int J Biol Macromol.* (2015) 72:1182–90. doi: 10.1016/j.ijbiomac.2014.08.058

16. Hu BY, Deng JC, Yang CQ, Hu Y, Zhang J, Yang WY, et al. Extraction optimization, purification and characterization of polysaccharides from the seed coat of black soybean. *PLoS ONE.* (2017) 12:e0190202. doi: 10.1371/journal.pone.0190202

17. Yao Y, Xue P, Zhu Y, Gao Y, Ren G. Antioxidant and immunoregulatory activity of polysaccharides from adzuki beans (Vigna angularis). *Food Res Int.* (2015) 77:251–6. doi: 10.1016/j.foodres.2015.05.029

18. Yao Y, Zhu Y, Ren G. Immunoregulatory activities of polysaccharides from Mung bean. *Carbohyd Polym.* (2016) 139:61–6. doi: 10.1016/j.carbpol.2015.12.001

19. Zhong K, Lin W, Wang Q, Zhou S. Extraction and radicals scavenging activity of polysaccharides with microwave extraction from mung bean hulls. *Int J Biol Macromol.* (2012) 51:612–7. doi: 10.1016/j.ijbiomac.2012.06.032

20. Lai F, Wen Q, Li L, Wu H, Li X. Antioxidant activities of water-soluble polysaccharide extracted from mung bean (Vigna radiata L) hull with ultrasonic assisted treatment. *Carbohyd Polym.* (2010) 81:323–9. doi: 10.1016/j.carbpol.2010.02.011

21. Jiang L, Wang W, Wen P, Shen M, Li H, Ren Y, et al. Two water-soluble polysaccharides from mung bean skin: physicochemical characterization, antioxidant and antibacterial activities. *Food Hydrocolloid.* (2020) 100:105412. doi: 10.1016/j.foodhyd.2019.105412

22. Ramirez CSV, Temelli F, Saldaña MDA. Production of pea hull soluble fiber-derived oligosaccharides using subcritical water with carboxylic acids. *J Supercrit Fluids.* (2021) 178:105349. doi: 10.1016/j.supflu.2021.105349

23. Ji X, Han L, Liu F, Yin S, Peng Q, Wang M, et al. mini-review of isolation, chemical properties and bioactivities of polysaccharides from buckwheat (Fagopyrum Mill). *Int J Biol Macromol.* (2019) 127:204–9. doi: 10.1016/j.ijbiomac.2019.01.043

24. Song Q, Jiang L, Yang X, Huang L, Yu Y, Yu Q, et al. Physicochemical and functional properties of a water-soluble polysaccharide extracted from Mung bean (Vigna radiate L) and its antioxidant activity. *Int J Biol Macromol.* (2019) 138:874–80. doi: 10.1016/j.ijbiomac.2019.07.167

25. Yao Y, Zhu Y, Ren G. Antioxidant and immunoregulatory activity of alkali-extractable polysaccharides from mung bean. *Int J Biol Macromol.* (2016) 84:289–94. doi: 10.1016/j.ijbiomac.2015.12.045

26. Liu HM, Wang FY, Liu YL. Hot-compressed water extraction of polysaccharides from soy hulls. *Food Chem.* (2016) 202:104–9. doi: 10.1016/j.foodchem.2016.01.129

27. Ji X, Hou C, Guo X. Physicochemical properties, structures, bioactivities and future prospective for polysaccharides from Plantago L. (Plantaginaceae): a review. *Int J Biol Macromol.* (2019) 135:637–46. doi: 10.1016/j.ijbiomac.2019.05.211

28. Jalili Safaryan M, Ganjloo A, Bimakr M, Zarringhalami S. Optimization of ultrasound-assisted extraction, preliminary characterization and *in vitro* antioxidant activity of polysaccharides from green pea pods. *Foods.* (2016) 5:78. doi: 10.3390/foods5040078

29. Ji X, Peng B, Ding H, Cui B, Nie H, Yan Y. Purification, structure and biological activity of pumpkin polysaccharides: a review. *Food Rev Int.* (2021) 1—13. doi: 10.1080/87559129.2021.1904973

30. Ji X, Hou C, Guo X. The fruit malus prunifolia (Malus micromalus mak): a minireview of current knowledge of fruit composition and health benefits. *J Chem.* (2020) 2020:1–8. doi: 10.1155/2020/2418626

31. Ji X, Hou C, Shi M, Yan Y, Liu Y. An insight into the research concerning panax ginseng c. A meyer polysaccharides: a review. *Food Rev Int.* (2020) 38:1149–65. doi: 10.1080/87559129.2020.1771363

32. Liu J, Wang Y, Wu J, Georgiev MI, Xu B, Wong KH, et al. Isolation, structural properties, and bioactivities of polysaccharides from mushrooms termitomyces: a review. *J Agr Food Chem.* (2022) 70:21–33. doi: 10.1021/acs.jafc.1c06443

33. Hou C, Yin M, Lan P, Wang H, Nie H, Ji X. Recent progress in the research of Angelica sinensis (Oliv.) Diels polysaccharides: extraction, purification, structure and bioactivities. *Chem Biol Technol Ag.* (2021) 8. doi: 10.1186/s40538-021-00214-x

34. Hu Y, Wang S, Shi Z, Zhai L, Fu J, Zhao J. Purification, characterization, and antioxidant activity of polysaccharides from Okara. *J Food Process Pres.* (2022) 46:1–13. doi: 10.1111/jfpp.16411

35. Ye Z, Wang W, Yuan Q, Ye H, Sun Y, Zhang H, et al. Box-Behnken design for extraction optimization, characterization and *in vitro* antioxidant activity of Cicer arietinum L. hull polysaccharides. *Carbohyd Polym.* (2016) 147:354–64. doi: 10.1016/j.carbpol.2016.03.092

36. Zhang SJ, Hu TT, Chen YY, Wang S, Kang YF. Analysis of the polysaccharide fractions isolated from pea (Pisum sativum L) at different levels of purification. *J Food Biochem.* (2020) 44:e13248. doi: 10.1111/jfbc.13248

37. Xu J, Zhang J, Sang Y, Wei Y, Chen X, Wang Y, et al. Polysaccharides from medicine and food homology materials: a review on their extraction, purification, structure, and biological activities. *Molecules.* (2022) 27:3215. doi: 10.3390/molecules27103215

38. Liu J, Wen XY, Kan J. Jin CH. Structural characterization of two water-soluble polysaccharides from black soybean (glycine max (l) Merr). *J Agr Food Chem.* (2015) 63:225–34. doi: 10.1021/jf505172m

39. Yang L, Zhang H, Zhao Y, Huang J, Zhu D, Wang S, et al. Chemical structure, chain conformation and rheological properties of pectic polysaccharides from soy hulls. *Int J Biol Macromol.* (2020) 148:41–8. doi: 10.1016/j.ijbiomac.2020.01.047

40. Bai YP, Zhou HM, Zhu KR, Li Q. Impact of thermally induced wall breakage on the structural properties of water-soluble polysaccharides in chickpeas. *Int J Biol Macromol.* (2022) 208:869–82. doi: 10.1016/j.ijbiomac.2022.03.186

41. Sheng K, Wang C, Chen B, Kang M, Wang M, Liu K, et al. Recent advances in polysaccharides from Lentinus edodes (Berk): isolation, structures and bioactivities. *Food Chem.* (2021) 358:129883. doi: 10.1016/j.foodchem.2021.129883

42. Zhang J, Wen C, Zhang H, Duan Y. Review of isolation, structural properties, chain conformation, and bioactivities of psyllium polysaccharides. *Int J Biol Macromol.* (2019) 139:409–20. doi: 10.1016/j.ijbiomac.2019.08.014

43. Liu H, Xu J, Xu X, Yuan Z, Song H, Yang L, et al. Structure/function relationships of bean polysaccharides: a review. *Crit Rev Food Sci.* (2021) 1—15. doi: 10.1080/10408398.2021.1946480

44. Nomura K, Sakai M, Ohboshi H, Nakamura A. Extraction of a water-soluble polysaccharide fraction from lentils and its potential application in acidified protein dispersions. *Food Hydrocoll.* (2021) 117:106740. doi: 10.1016/j.foodhyd.2021.106740

45. Noguchi M, Hasegawa Y, Suzuki S, Nakazawa M, Ueda M, Sakamoto T. Determination of chemical structure of pea pectin by using pectinolytic enzymes. *Carbohyd Polym.* (2020) 231:115738. doi: 10.1016/j.carbpol.2019.115738

46. Goff AL, Renard C, Bonnin E, Thibault JF. Extraction, purification and chemical characterisation of xylogalacturonans from pea hulls. *Carbohyd Polym.* (2001) 45:325–34. doi: 10.1016/S0144-8617(00)00271-X

47. Akhtar HMS, Abdin M, Hamed YS, Wang W, Chen G, Chen D, et al. Physicochemical, functional, structural, thermal characterization and α-amylase inhibition of polysaccharides from chickpea (Cicer arietinum L.) hulls. *LWT.* (2019) 113:108265. doi: 10.1016/j.lwt.2019.108265

48. Xu SY, Huang X, Cheong KL. Recent advances in marine algae polysaccharides: Isolation, structure, and activities. *Mar Drugs.* (2017) 15:388. doi: 10.3390/md15120388

49. Ketha K, Gudipati M. Immunomodulatory activity of non starch polysaccharides isolated from green gram (Vigna radiata). *Food Res Int.* (2018) 113:269–76. doi: 10.1016/j.foodres.2018.07.010

50. Tsai AC, Vinik AI, Lasichak A, Lo GS. Effects of soy polysaccharide on postprandial plasma glucose, insulin, glucagon, pancreatic polypeptide, somatostatin, and triglyceride in obese diabetic patients. *Am J Clin Nutr.* (1987) 45:596–601. doi: 10.1093/ajcn/45.3.596

51. Chen H. Liu LJ, Zhu JJ, Xu B, Li R. Effect of soybean oligosaccharides on blood lipid, glucose levels and antioxidant enzymes activity in high fat rats. *Food Chem.* (2010) 119:1633–6. doi: 10.1016/j.foodchem.2009.09.056

52. Ji X, Peng Q, Wang M. Anti-colon-cancer effects of polysaccharides: a mini-review of the mechanisms. *Int J Biol Macromol.* (2018) 114:1127–33. doi: 10.1016/j.ijbiomac.2018.03.186

53. Akhtar HMS, Abdin M, Ahmed S, Aslam F. Digestion by saliva, simulated gastric and small intestinal juices and in vitro fermentation by human gut microbiota of polysaccharides from cicer arietinum L. hulls. *J Microb Biotec Food.* (2021) 11:e3966. doi: 10.15414/jmbfs.3966

frontiers | Frontiers in Nutrition

TYPE Original Research
PUBLISHED 19 October 2022
DOI 10.3389/fnut.2022.970540

Check for updates

OPEN ACCESS

EDITED BY
Xiaolong Ji,
Zhengzhou University of Light Industry, China

REVIEWED BY
Zhu Bitong,
Huaqiao University, China
Yiping Zhang,
Third Institute of Oceanography, Ministry of Natural Resources, China

*CORRESPONDENCE
Guangya Zhang
zhgyghh@hqu.edu.cn

SPECIALTY SECTION
This article was submitted to Food Chemistry, a section of the journal Frontiers in Nutrition

RECEIVED 16 June 2022
ACCEPTED 22 July 2022
PUBLISHED 19 October 2022

CITATION
Cai L, Zheng Y, Chu Y, Lin Y, Liu L and Zhang G (2022) The synergism of lytic polysaccharide monooxygenases with lichenase and their co-immobilization on silica nanospheres for green conversion of lichen biomass. *Front. Nutr.* 9:970540. doi: 10.3389/fnut.2022.970540

COPYRIGHT
© 2022 Cai, Zheng, Chu, Lin, Liu and Zhang. This is an open-access article distributed under the terms of the Creative Commons Attribution License (CC BY). The use, distribution or reproduction in other forums is permitted, provided the original author(s) and the copyright owner(s) are credited and that the original publication in this journal is cited, in accordance with accepted academic practice. No use, distribution or reproduction is permitted which does not comply with these terms.

The synergism of lytic polysaccharide monooxygenases with lichenase and their co-immobilization on silica nanospheres for green conversion of lichen biomass

Lixi Cai[1,2,3], Ying Zheng[4], Yunmeng Chu[2], Yuanqing Lin[2], Lixing Liu[1,3] and Guangya Zhang[2]*

[1]College of Basic Medicine, Putian University, Putian, China, [2]Department of Bioengineering and Biotechnology, Huaqiao University, Xiamen, China, [3]Key Laboratory of Translational Tumor Medicine in Fujian Province, Putian University, Putian, China, [4]College of Pharmaceutical and Medical Technology, Putian University, Putian, China

Enzyme-assisted valorization of lichenan represents a green and sustainable alternative to the conventional chemical industry. The recently discovered lytic polysaccharide monooxygenases (LPMOs) are essential components of state-of-the-art enzyme cocktails for lichenin bioconversion. The LPMOs named SpyTag fused LPMOs (AST) from *Chaetomium globosum* was functionally expressed in *E. coli* and exhibited 1.25-fold synergism with lichenase, whereas AST alone produced no detectable reducing sugars. HPLC results further confirm that AST does not alter the endogenous hydrolysis mode of lichenase but rather enhances its hydrolysis efficiency by disrupting the long chain of lichenan and releasing more reducing ends. To the best of our knowledge, this was the first report on the synergistic effect of LPMOs and lichenase, which may have great synergistic potential in the conversion of lichen biomass. Furthermore, a novel strategy for the covalently immobilizing AST and lichenase on silica nanoparticles (SNPs) from the cell lysate in a single step was proposed, which exhibited high activity recovery (82.9%) and high immobilization yield (94.8%). After 12 independent runs, about 67.4 % of the initial activity of the immobilized enzymes was retained. The resulted biocatalyst systems exhibited the green and sustainable strategy in the bioconversion of lichen biomass as well as other diverse polysaccharides.

KEYWORDS

lytic polysaccharide monooxygenase, synergistic effect, lichenase, silica nanoparticles, multi-enzyme immobilization

Introduction

Lichens, the symbionts of fungi and algae, have attracted wide attention due to their abundant sources, huge reserves, and low production costs. Lichenan (β-1,3-1,4-glucan) is a linear polysaccharide derived from lichen, accounting for approximately 62% of the total carbohydrates in lichen, but the high viscosity of lichens in water results in low utilization (1). Lichenase (EC 3.2.1.73) could cleave linear lichenan consisting of β-1,3 and β-1,4 bonds with strict specificity for the β-1,4 glycosidic bond adjacent to the 3-O-glucopyranose residue (2–4), which can reduce viscosity for processing into biofuels (i.e., ethanol) or high value-added products (5, 6). Lichenase plays a promising role in the green conversion of lichen biomass (7, 8). However, lichenase suffers from some drawbacks that may impede its industrial application, such as time-consuming purification processes, thermal instability, and poor reusability. Thus, combining existing lichenase with co-proteins to reduce the enzyme load or adopting enzyme immobilization technology may effectively solve these deficiencies (9).

Lytic polysaccharide monooxygenases (LPMOs) are novel copper ion-dependent biomass-degrading enzymes (10), with copper ions bonded to the characteristic histidine scaffold and endowing LPMOs with a significant oxidative capacity (11–13). LPMOs can oxidatively cleave glycosidic bonds in polysaccharides that cannot be inaccessibly cleaved by glycosidic hydrolases, such as cellobiohydrolases or endoglucanases. By increasing the accessibility of substrates and generating more reducing ends, LPMOs enhance the overall efficiency of glycosidases in degrading insoluble polysaccharides (14). Thus, LPMOs are novel biomass-degrading enzyme that enriches and changes the paradigm of biomass conversion (15, 16). Dimarogona found that in the presence of a reductant, the loading of LPMOs from *Sporotrichum Thermophile* resulted in a 20% increase in oligosaccharide recovery from pretreated spruce (16). Meanwhile, by loading LPMOs to Novozymes' cellulase system in Denmark, the production cost of cellulosic ethanol has approached that of starch ethanol or gasoline, down to about $2/gallon. LPMOs have been found to significantly boost the efficiency of the enzymatic digestion of cellulase, 1,4-xylanase, amylase, and chitosanase, making them an ideal synergistic enzyme for the degradation of polysaccharides (17–19). However, there are no studies on the synergistic effect of lichenase by LPMOs. Besides, the studies on the synergistic degradation of biomass by LPMOs are all based on free enzymes. Therefore, exploring more glycoside hydrolases that can synergize with LPMOs and establishing a reliable multi-enzyme immobilization strategy for large-scale use of LPMOs in biorefineries may become an essential field for biomass processing in the future.

In recent years, the idea of biomimetic mineralization has been gradually introduced into the design and preparation of immobilized carriers (20). Among them, silica carriers obtained by biomimetic silicification have attracted much attention due to their mild and efficient preparation conditions, well-ordered structure, and high thermal stability (21, 22). Recently, our team found that cationic elastin-like polypeptides (ELPs) have the ability to rapidly prepare biomimetic silica nanoparticles (SNPs). ELPs are temperature-responsive and can be obtained with high purity by the simple multiple reversible phase transition cycling (ITC) method (23, 24). Thus, ELPs are endowed with dual functions of biomimetic silicification and purification tags, and allow biomimetic mineralization to prepare inexpensive carriers that simplify the immobilization process. However, two or more enzymes are often required for synergistic hydrolysis in the hydrolysis of lichenan. Multi-enzyme immobilization can thoroughly combine the catalytic properties of different enzymes and improve the overall reaction efficiency. The enzymes in traditional immobilization methods are non-specifically bound to the carrier with multiple sites, resulting in different degrees of enzyme activity. Fusion expression, separation, and purification of multi-enzymes and molecular adhesives, and then immobilization on biomimetic siliconized carriers is an effective way to solve this problem. It can also shorten the distance between enzymes, generate substrate channels, and improve the overall catalysis performance.

Herein, the LPMOs derived from the fungus *Chaetomium globosum* was successfully expressed in *E. coli* and explored its synergistic effects with lichenase, that is, the first report on the synergistic effect of lichenase and LPMOs to our best knowledge. Then we introduced lysine into acidic ELPs to design basic ELPs with biomimetic ability (K5V4F) and then fused them with the molecular binder SpyCatcher (K5SC). The temperature-responsive of ELPs was used to isolate, and purify the fusion proteins and combine the biomimetic ability of ELPs to generate silica nanocarriers (K5SC@SiO_2). Meanwhile, SpyTag fused lichenase (BST) and SpyTag fused LPMOs (AST) were designed and synthesized, since SpyTag rapidly forms a spontaneous intermolecular isopeptide bond to its partner SpyCatcher (25, 26). As a result, K5SC@SiO_2 can intelligently capture the target dual-enzyme (BST and AST) containing SpyTag, enabling self-immobilization of the dual-enzyme. This green strategy allows for the purification and self-immobilization of multi-enzyme from cell lysates in one step, which may have great potential in the bioconversion of lichen biomass as well as other diverse polysaccharides.

Materials and methods

Plasmid construction and protein expression

AST and BST: the genes encoding for molecular binder SpyTag were synthesized by Genscript and then fused to the

N-terminus of the LPMOs (No. MN190001) and lichenase (BglS, No. 937470) respectively, resulting in pET-22bST-A (AST), and pET-22bST-B (BST) respectively. BglsE: the genes encoding for lichenase (BglS, No. 937470) were synthesized by Sangon Biotech and then ligated into the pET-22b-ELPs [KV8F-40] at the N-terminus of the ELPs, resulting in pET-22bBglS-ELP (BglsE). K5SC: the genes encoding for molecular binder SpyCatcher were synthesized by Sangon Biotech and then ligated into the pET-22b-ELPs [K5V4F-40] at the N-terminus of the ELPs, resulting in pET-22bSC-K5 (K5SC, No. MN136291).

The resulting plasmids were transformed into BL21 (DE3) cells for expression in *E. coli*, and incubated in a fresh TB medium containing 100 mg/mL ampicillin for 4 h at 37°C to make the OD600 reached 0.4, and then loaded with 0.5 mmol/L IPTG. Cells were collected by centrifugation at 4,000 × *g* for 20 min and sonicated on ice. The sonicated cell suspension was centrifuged at 12,000 × *g* for 20 min to remove insoluble cell debris, and the supernatant contains cell lysates of AST, BST, and K5SC. Then the cell lysate of AST was purified by using a Ni-affinity column (Smart-Lifesciences, China) with elution buffer (50 mmol/L Tris–HCl buffer, 80 mmol/L imidazole, and 500 mmol/L NaCl, respectively).

The recombinant protein of K5SC and BglsE were purified by the modified ITC cycle. Briefly, a final concentration of 2.5 mol/L NaCl was loaded to the cell lysate to trigger the phase transition aggregation of K5SC at 37°C (27). The resulting aggregates were collected from the cell lysate by simple centrifugation at 4°C (13,400 × *g*, 10 min). Subsequently, the aggregates of K5SC and BglsE were resuspended in ice PBS buffer for 60 min and centrifuged at 4°C (13,400 × *g*, 20 min) to remove the impurities. The ITC process was repeated twice, as mentioned above, to obtain high-purity recombinant protein of K5SC and BglsE.

Synergistic effects of lytic polysaccharide monooxygenases on lichenase

Different molar ratios of AST and BglsE (0:1, 1.6:1, 2.6:1, 3.2:1, 4:1, 6.4:1, 16:1, and 32:1; the amount of BglsE was fixed at 2.4 mg/g) were added to citrate phosphate buffer (CPB, 20 mmol/L, pH 6.6). To terminate the enzymatic reaction, 3,5-dinitrosalicylic acid (DNS) was added to the reaction mixture and heated at 100°C for 5 min, then centrifugated at 12,000 × *g* for 8 min to remove the precipitate. Temperature (25–60°C) and pH (4.0–8.0) changes were measured at 540 nm using D-glucose as the reducing sugar standard. The time profile was measured by 2.4 mg/g lichenase along with 4.64 mg/g AST at 50°C for 36 h to measure the reducing sugar yield at each time period (Kim et al. (28). The degree of synergy (DS) was determined as follows.

$$\mathrm{Ds} = \frac{M_{AB}}{M_B}$$

Where M_{AB} was the yield of reducing sugars produced by AST and BglsE, and M_B was the yield of reducing sugars produced by BglsE alone.

The relative enzyme activities were calculated by measuring the activities of BglsE and AST before and after immobilization with EDTA and metal cations (Mn^{2+}, Zn^{2+}, K^{+}, Mg^{2+}, Cu^{2+}, Ba^{2+}, Ni^{2+}, Co^{2+}, Ca^{2+}) at a final concentration of 10 mmol/L respectively.

High-performance liquid chromatography

To characterize the composition of enzymatic digestion products from lichenan *via* the synergistic effect of lichenase and LPMOs, the high-performance liquid chromatography (HPLC, Agilent 1260) equipped with an oscillometric refractive index detector and Waters Sugar-Par^{TM} column (USA, 5 μm, 6.5 mm × 300 mm) were used. Elute the sample solution with ultrapure water at a flow rate of 0.5 mL/min at a column temperature of 75°C and a detector temperature of 40°C (29).

Biomimetic silicification and carrier characterization

The SiO_2 carriers were synthesized by biomimetic mineralization using K5SC as the catalyst and TMOS as the silica source. Briefly, K5SC protein (300 μmol/L) and TMOS (1 mol/L) were mixed thoroughly in a volume ratio of 9:1 at room temperature for 5 min. The auto-formed K5SC@SiO_2 carriers were separated from the reaction system by centrifugation at 5,000 × *g* for 3 min. The size and surface morphology of K5SC@SiO_2 were studied by FESEM.

Purification and immobilization of lichenase and lytic polysaccharide monooxygenases

The recombinant enzyme of AST and BST were covalently purified and immobilized onto the K5SC@SiO_2 NPs by the modified SpyCather/SpyTag reaction (30). Briefly, the above-prepared K5SC@SiO_2 were loaded into the cell lysate AST and BST, mixed thoroughly, and reacted for 1 h at 30°C in a constant temperature vortex mixer. After centrifugation at 5,000 × *g* for 3 min at 4°C, the precipitate was collected and suspended in an equal volume of Tris–HCl buffer (pH 7.0) to form the immobilized enzyme solution. To make the electrophoresis results after immobilization clearer, we added some pure AST into the cell lysate for K5-C@SiO_2 capture.

However, pure AST was not added in other experiments. The method described by Sheldon uses three indicators were used to analyze the immobilization effect of enzymes: immobilization yield, immobilization efficiency, and activity recovery (31).

$$\text{Immobilizationyield}(\%) = \frac{\text{At}}{\text{Ao}} \times 100\%$$

$$\text{Activityrecovery}(\%) = \frac{\text{As}}{\text{Ao}} \times 100\%$$

$$\text{Immobilizationefficiency}(\%) = \frac{\text{As}}{\text{At}} \times 100\%$$

where:

Ao: Starting activity of free enzyme; As: Observed activity; At: Immobilized activity.

Reusability of the immobilized enzyme

The reusability of immobilized AST and BST were measured at optimum conditions for 10 min, the immobilized biocatalyst was immediately centrifuged at 4°C (1 min 12,000 rpm), and the supernatant was collected for determination of enzyme activity at each cycle. The recycled precipitate was washed with buffer to remove residual sugar before adding the new lichenan substrate for the next cycle of experiments. The activity of the first cycle was defined as 100%, and a total of 12 rounds were repeated.

Results and discussion

Expression and purification of the recombinant proteins

The purified proteins of BglsE and AST were verified by SDS-PAGE with the clear band around each of the molecular weights at 39 kDa (**Supplementary Figure 1A**, lane 1) and 25 kDa (**Supplementary Figure 1B**, lane 1), which were in general agreement with their theoretical values. The final yields of BglsE and AST were 7.46 ± 0.39 mg and 0.68 ± 0.08 mg per 200 mL of fermentation culture tested by the BCA kit. The preparation process of BglsE protein only requires simple centrifugation technology and cheap reagents such as NaCl, indicating that the expensive and cumbersome chromatographic purification process can be avoided, and the large-scale production of lichenase can be easily prepared with only two rounds of ITC.

Synergistic or stabilizing effect of lytic polysaccharide monooxygenases

When purified AST was incubated with insoluble lichenan for 2 h, no detectable yield of reducing sugars could be detected (**Figure 1A**). However, the yield of reducing sugars produced by co-incubation of BglsE and AST for 2 h was significantly higher than that of BglsE alone, with a synergistic effect of 1.25-fold, indicating that AST does not directly hydrolyze lichenan but enhances the hydrolytic efficiency of lichenase. AST, a typical metalloprotease is often activated by the reduction of Cu^{2+} in coordination with the catalytic center of the LPMOs (32, 33). To exclude the effect of Cu^{2+} on the enzymatic activity of lichenase, 10 mmol/L Cu^{2+} were loaded in the BglsE alone or BglsE/AST, which found that Cu^{2+} had a strong inhibitory effect on the activity of both BglsE (44.48%) or BglsE/AST (25.99%). Furthermore, to verify whether the effect of AST on BglsE was based on stabilizing or synergistic effect, bovine serum albumin (BSA) was chosen as the additional control protein because it is widely applied in the stabilization of enzymes (28). Comparing the effects of AST and BSA on the hydrolysis rate of lichenan, the improvement of AST on the relative reducing sugar yield was significantly greater (e.g., 1.25-fold, $p < 0.01$) than that of BSA with the same molar mass (e.g., 1.08-fold, $p < 0.05$), indicating that AST can act on C1, C4, or C1, C6 on lichenan, and it has a synergistic rather than a stabilizing effect with lichenase. To the best of our knowledge, it is the first report on the synergistic hydrolysis of lichenase by LMPOs.

To characterize the hydrolysis pattern of the synergistic action of BglsE and AST, the product profiles of the enzymatic reactions of lichenan with BglsE in the presence or absence of AST were analyzed by HPLC. The endo-hydrolysis of lichenan by BglsE produced various oligosaccharides with different degrees of polymerization (**Figure 1B**), and the sugar profiles obtained by the hydrolysis of AST and BglsE were similar to those obtained by the action of BglsE alone, but the addition of AST resulted in a higher overall abundance of lichenan (**Figure 1C**). For example, the peak area obtained by BglsE alone at 4.747 min was 278539 nC*min, while the combination of BglsE and AST was 473991 nC*min, with a synergistic effect value as high as 1.7 (**Supplementary Table 1**). These results also suggest that AST does not alter the endogenous hydrolysis pattern of the BglsE; instead, AST may assist BglsE to efficiently catalyze the substrate by attacking the most refractory part of the substrate, thereby generating more reducing ends to assist the BglsE in efficient catalysis of the substrate. In previous studies, similar results were observed for the synergistic effect of AST on the hydrolysis of 1,4-xylan, cellulase, and 1,3-xylan (28, 34). Where the distribution of sugars was also unaltered and indicated that AST has multiple substrate specificities.

Effect of ratios and electron donors on AST/BglsE synergy

When determining the feasibility of synergistic proteins for industrial applications, the degree of synergy, especially the amount of synergistic protein loading, is the key determinant

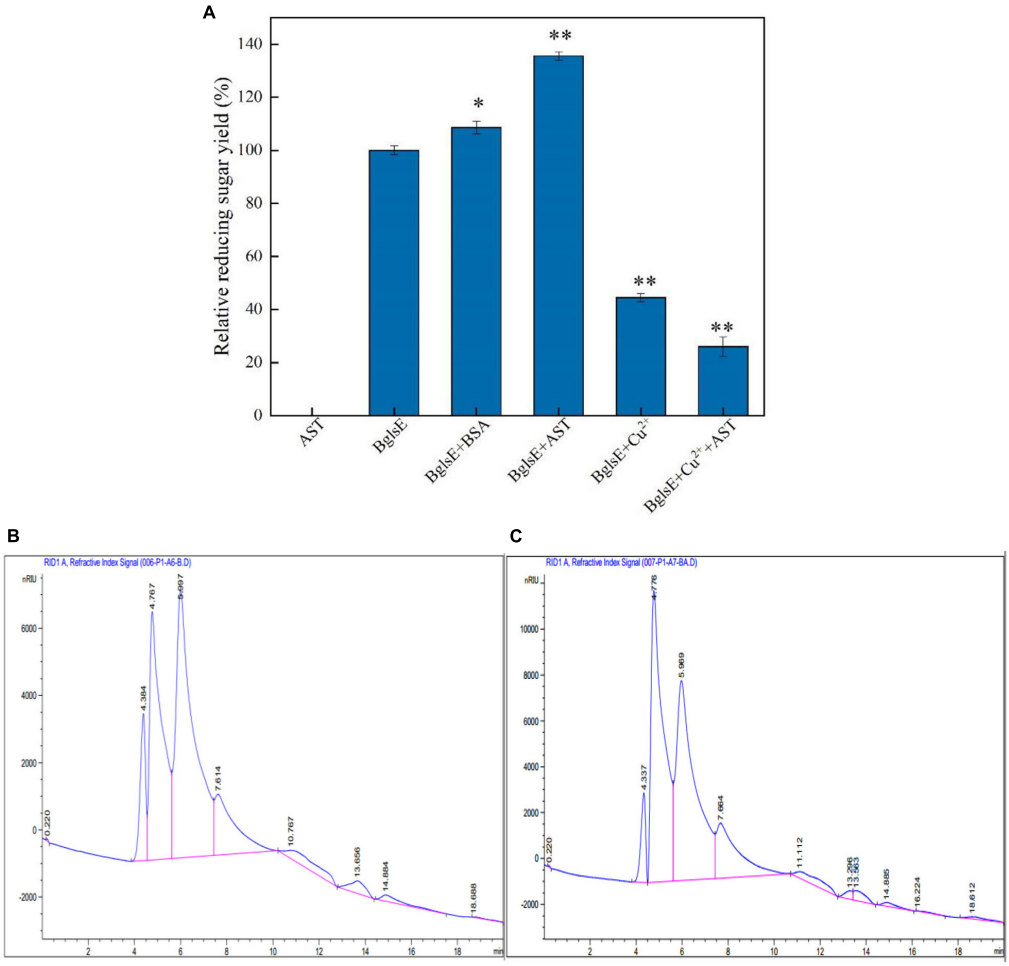

FIGURE 1
(A) Effects of LPMOs, Cu^{2+}, and BSA on lichenase activity. **(B)** Product profiles of the hydrolysis reactions of BglsE analyzing by HPLC. **(C)** Product profiles of the hydrolysis reactions of BglsE and AST analyzing by HPLC. *Significant difference from the control ($p < 0.05$); **very significant difference from the control ($p < 0.01$).

(32, 35). Therefore, the effects of the mass ratio of AST and lichenase (0, 1.6, 2.6, 3.2, 4, 6.4, 16, to 32, BglsE was fixed at 2.4 mg/g lichenan) on synergism in lichenan hydrolysis were analyzed (**Figure 2A**). With the increasing ratio of AST/BglsE, the DS value firstly increased and then decreased. When the molar ratio of AST/BglsE was 3.2:1, the yield of reducing sugar reached the highest value, and the DS value was 1.31. However, a sharp downward trend was found when the ratio of AST/BglsE increased from 3.2 to 32, indicating that the synergistic effect became saturated as the increasing mole ratio, and the activity of BglsE might be inhibited by the enrichment of the intermediate products such as peroxides produced by AST (36, 37).

Lytic polysaccharide monooxygenases rely on the electron donors to activate molecular oxygen and then oxidatively cleave the glycosidic bonds of the polysaccharide chain (38, 39). Seven different types of electron donors, such as nicotinamide, lactic acid, ethanol, sodium acetate, sodium lactate, riboflavin, and ascorbic acid were loaded into the reaction system to analyze the synergistic degradation enzymatic activity (40). All donors, except lactic acid, enhanced the synergistic activity of AST/BglsE, with relative reducing sugar yields increased by 2.18 to 43.41% compared without donors (**Figure 2B**). When 2 mmol/L ascorbic acid was used as a reductant, the relative reducing sugar yield was increased by 43.41%. Therefore, 2 mmol/L ascorbic acid was used as the electron donor for all subsequent hydrolysis reactions.

Effect of temperature and pH on AST/BglsE synergy

To characterize the optimum temperature of BglsE and BglsE/AST with or without 2 mmol/L ascorbic acids, the

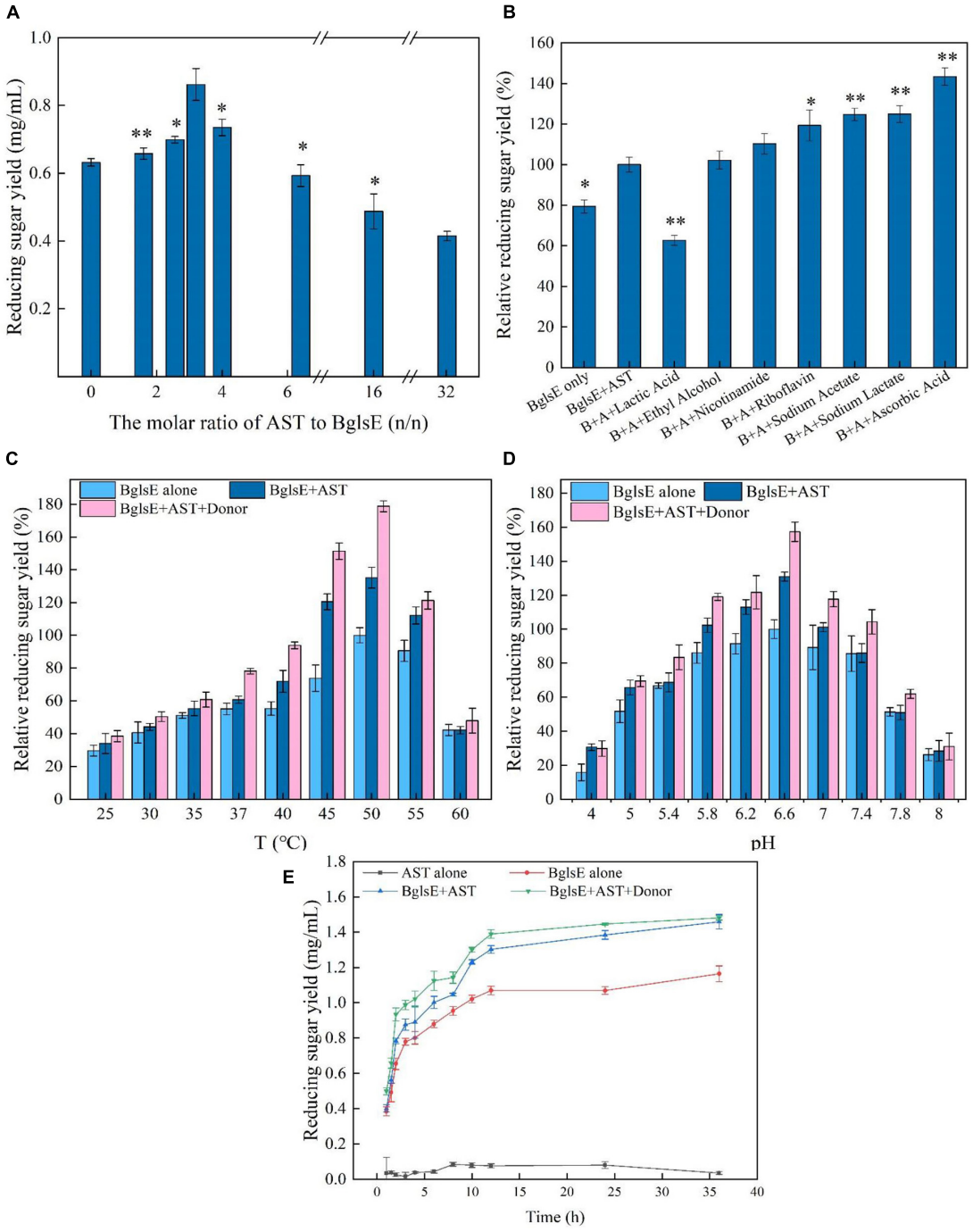

FIGURE 2
(A) Influences of AST/BglsE ratio on synergism in the hydrolysis of lichenin. **(B)** Influences of electron donors on synergism in the hydrolysis of lichenin. **(C)** Effect of temperature on the synergism of AST and BglsE in the hydrolysis of lichenin. **(D)** Effect of pH on the synergism of AST and BglsE in the hydrolysis of lichenin. **(E)** Time course of the synergistic effect of AST with BglsE in the hydrolysis of lichenin. *Significant difference from the control ($p < 0.05$); **very significant difference from the control ($p < 0.01$).

hydrolytic activities were measured at different temperatures from 25 to 60°C (Figure 2C). Interestingly, the greatest yields of reducing sugars were all observed at 50°C for both BglsE or AST/BglsE with and without electron donors, indicating that loading of AST and electron donors did not alter the optimal reaction properties of lichenase.

The optimal pH was measured by incubating BglsE and BglsE/AST with or without 2 mmol/L ascorbic acid for 2 h

at pH 4.0–8.0 (Figure 2D). The optimum pH of both BglsE and BglsE/AST were 6.6, further indicating that the addition of AST and electron donor did not change the optimum reaction properties of lichenase.

Time course of AST/BglsE synergy in lichenan hydrolysis

By incubating BglsE, AST, or BglsE/AST with lichenan for 0–36 h and comparing the yield of reducing sugars released at each enzymatic reaction (Figure 2E). AST alone did not produce detectable yields of reducing sugars from lichenan. The yield of reducing sugars produced by BglsE/AST was significantly higher at all reaction times than in the presence of BglsE alone. In particular, a 1.3-fold synergistic effect was observed at 24 h, indicating that AST did not directly hydrolyze lichenan, but increased the hydrolysis efficiency of lichenase. The substrate may need to be structurally modified by AST to improve the accessibility of the substrate with lichenase, which has difficulty in fully reaching insoluble lichenan. Furthermore, the yield of reducing sugars was 1.43 times greater than that of BglsE/AST after 2 h incubation. After 36 h, the same yield of reducing sugars was produced in the samples with and without electron donors, which may be due to those soluble small-molecule oligosaccharides produced by enzymatic degradation were already available as electron donors for AST, and the donor no longer affects the enzymatic hydrolysis process.

Synthesis and characterization of silica nanoparticles

Cationic ELPs, which capable of biomimetic silicification was, fused with SpyCatcher to generate the bifunctional ELPs-SpyCatcher chimera (K5SC). The K5SC chimera was self-purified from cell lysates by two simple ITC cycles, and the SDS-PAGE yielded one band of 32 kDa (Supplementary Figure 2). Meanwhile, the K5SC@SiO_2 NPs were synthesized *via* simple ELP-silicification within seconds at room temperature, which was analyzed by SEM with a diameter ranging from 500 to 800 nm (Figure 3A).

Purification and immobilization of BST and AST in one-step

To date, most enzyme immobilization strategies need pre-purification of the target enzyme, which is a notoriously time-consuming and expensive process (21, 41). Therefore, a green and novel strategy to simultaneously purify and immobilize multi-enzymes was proposed. Briefly, 40 mg of K5SC@SiO_2 carriers were loaded to the cell lysates containing BST and AST, respectively. After incubating at 37°C for 1 h, the silicon nanocomposites, including BST and AST *via* the SpyCather/SpyTag reaction, were collected by simple centrifugation, and the target bands of BST (28 kDa, lane 2, Figure 3B) and AST (25 kDa, lane 2, Figure 3C) in the supernatant significantly reduced, while the locations and amounts of other impurities remained unchanged. Meanwhile, the control experiment was performed with SiO_2 carriers mediated by the ELPs without SpyCather (K5@SiO_2). The proteins in the cell lysates of BST (lane 3, Figure 3B) and AST (lane 3, Figure 3C) did not change before and after immobilization, especially the target enzymes of BST and AST. Furthermore, the immobilized K5@silica carriers were not detected to be capable of purifying and immobilizing and have any enzyme activity. Accordingly, non-specific adsorption and immobilization of the enzyme by the silica carriers were excluded. These results demonstrate that K5SC@SiO_2 are unique carriers that are capable of purifying and immobilizing multi-enzymes from cell lysates in one step. AST and BST have been specifically immobilized on suitably sized silica NPs carriers modified with SpyCatcher. Finally, the effectiveness of the dual-enzyme isolation and purification with integrated immobilization was characterized by four metrics. The protein loading of K5SC@SiO_2 carriers for AST and BST were 429.54 and 487.91 μg/mg, respectively, and the immobilization yield, activity recovery, and immobilization efficiency of the captured AST/BST dual-enzyme reached 94.8, 82.9, and 87.4%, respectively. It is further proved that this is a cost-effective and environmentally friendly strategy for multi-enzyme immobilization.

Temperature and pH on the free or immobilized dual-enzyme

To modulate the microenvironment of the immobilized AST/BST on K5SC@SiO_2, the effect of temperature on the enzymatic activities was analyzed ranging from 25 to 60°C (Figure 4A). The optimum temperature of AST/BST before and after immobilization were the same, both at 50°C, indicating that the oriented and mild immobilization process would not change the optimum reaction properties of the enzymes. Furthermore, the hydrolytic activities of free and immobilized BST/AST were assayed at pH 4.0∼8.0 for 2 h (Figure 4B). Both free and immobilized BST/AST had the same influence trend of enzyme activity, and the maximum relative activities were all observed at pH 7.0, which may be due to that the dual-enzyme were immobilized on the surface of the carrier through covalent bonding, and their mild process did not significantly change the pH values of BST and AST.

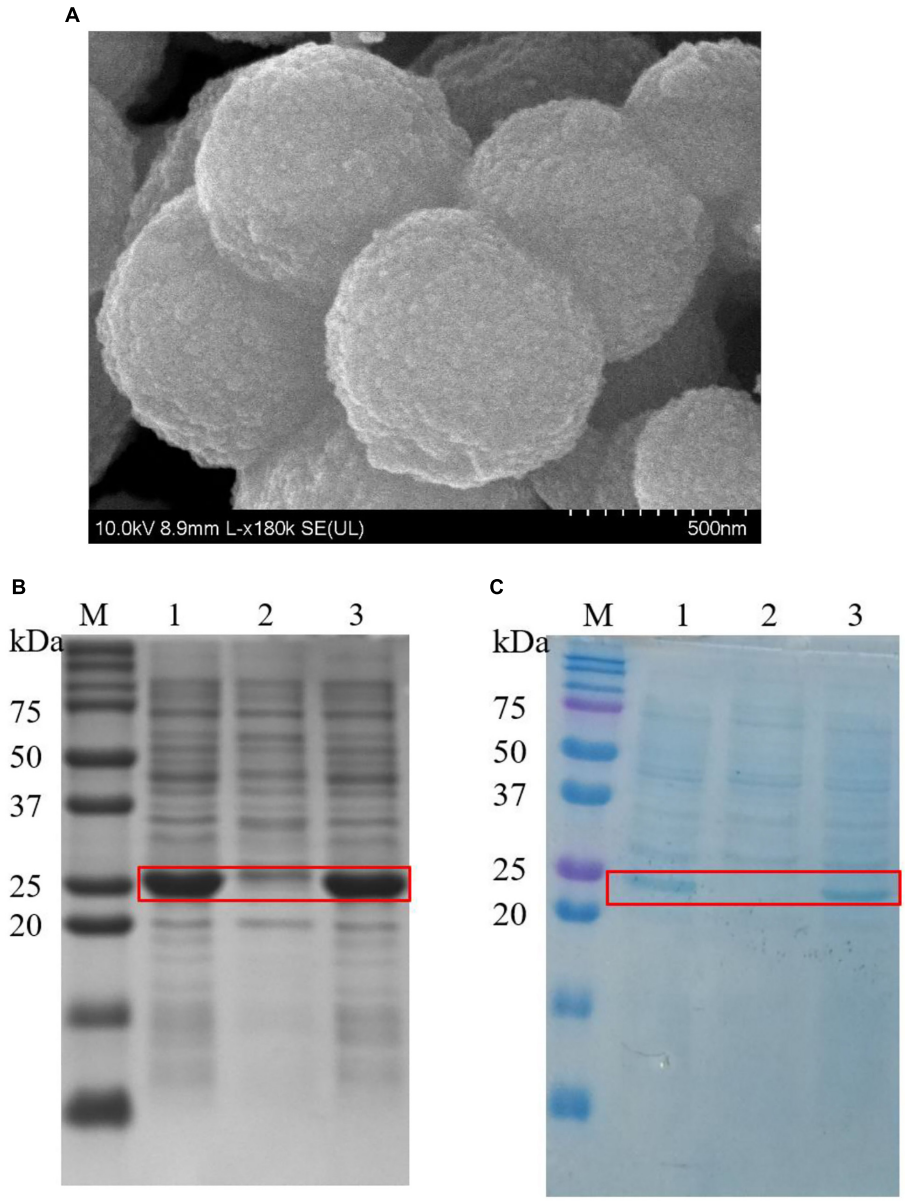

FIGURE 3
(A) SEM micrograph of K5-C@silica (scale bar is 0.5 μm); **(B)** The SDS-PAGE of expression, purification, and immobilization of lichenase, Red box indicates the position of the bands corresponding to BST; Lane M: marker; 1: cell lysate of BST; 2: cell lysate of BST after immobilization employing K5SC@SiO_2; 3: cell lysate of BST after immobilization employing K5@SiO_2; **(C)** The SDS-PAGE of expression, purification, and immobilization of AST, Red box indicates the positions of the bands corresponding to AST. 1: cell lysate of AST; 2: cell lysate of AST after immobilization employing K5SC@SiO_2; 3: cell lysate of AST after immobilization employing K5@SiO_2.

Time course of the synergistic hydrolysis by free or immobilized dual-enzyme

To investigate the effect of the immobilized procedure on the synergistic hydrolysis, the time course of the hydrolysis of lichenan by BST/AST before and after immobilization was analyzed. As shown in Figure 4C, the yield of reducing sugars for the free BST/AST was always higher than that of the immobilized form. After 36 h, the final reducing sugar yield for the free and immobilized BST/AST was 1.46 and 1.14 mg/mL, respectively. However, the reducing sugar yield of the immobilized BST/AST was 22.1% less than that of the free form. It is a normal loss by the immobilization process or by being immobilized the enzyme on the carriers, which becomes less in contact with the insoluble substrate. However, the immobilized enzyme has incomparable advantages over the free

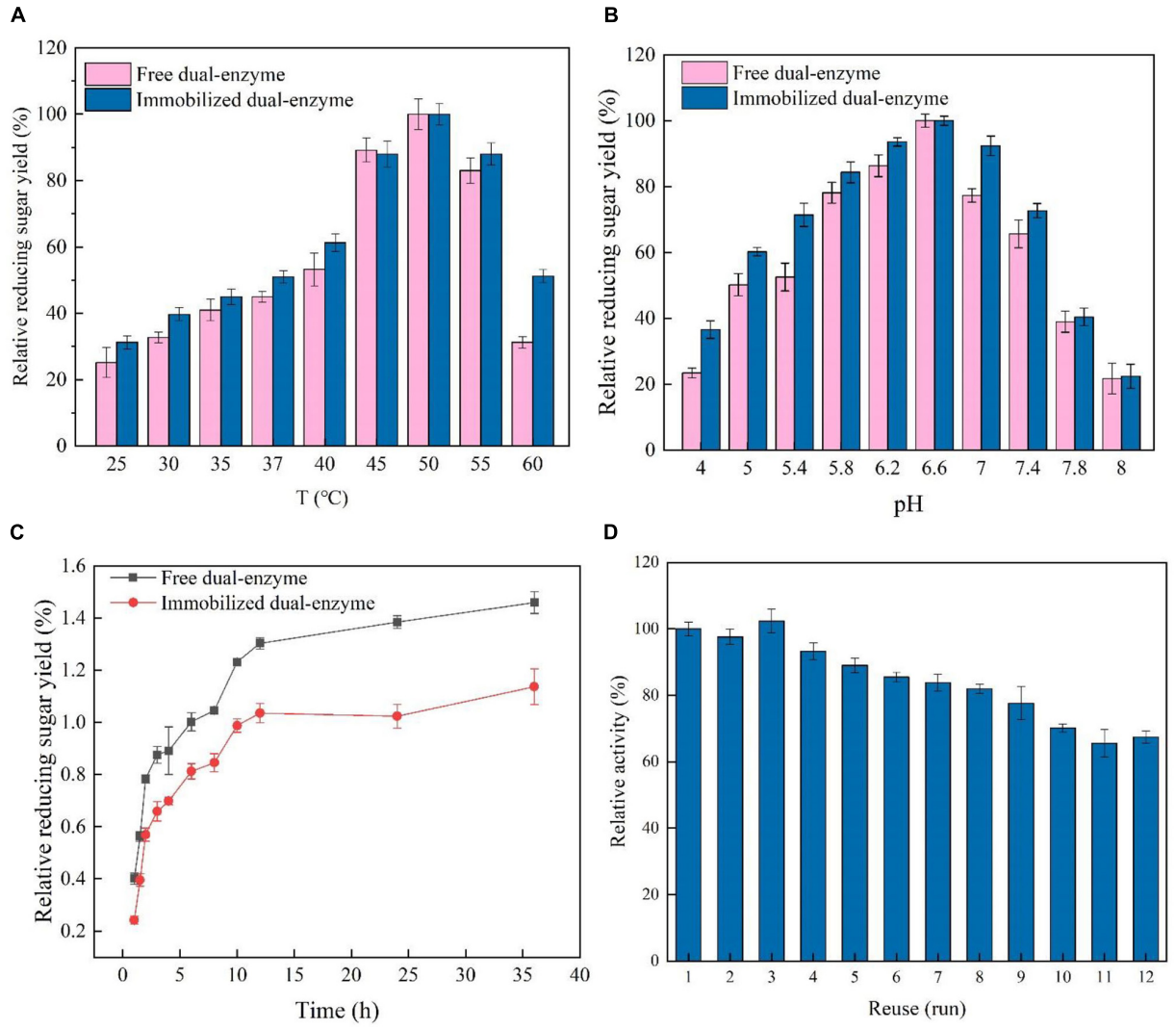

FIGURE 4
(A) Effect of temperature on the synergism of the immobilized and free dual-enzyme in the hydrolysis of lichenin. **(B)** Effect of pH on the synergism of the immobilized and free dual-enzyme in the hydrolysis of lichenin. **(C)** Time course of the synergism of the free or immobilized dual-enzyme in the hydrolysis of lichenin. **(D)** Reusability of the immobilized dual-enzyme.

enzyme, such as relative stability and recyclability. Therefore, the immobilized enzyme is a kind of nano-biocatalysts with great potential in the bioconversion of lichen.

Effect of metal ions on the free or immobilized dual-enzyme

The effects of 10 mmol/L metal ions and EDTA on the synergistic activity of free and immobilized AST/BST were investigated (Table 1). Ca^{2+}, Ni^{2+}, Ba^{2+}, and Mg^{2+} promoted the synergistic activity of AST/BST before and after immobilization by 9.2–27.4%, confirming that some divalent metal ions can promote the activity of dissolved polysaccharide monooxygenase. But, Cu^{2+} showed the strongest inhibition effect. Overall, dual-enzyme are more sensitive to metal ions.

Reusability of immobilized dual-enzyme

The industrial application of expensive enzymes always needs, in many instances, its reuse and recovery to make the process economical and feasible (9, 42). Covalent immobilization on the carrier is one of the most stable strategies for enzyme immobilization, which effectively reduces

TABLE 1 The influences of metal ions and chemicals on the activity of the free or immobilized Bgls and AST.

Metal ion (10 mM)	RA (%) free BC	RA (%) immobilized BC	Metal ion (10 mM)	RA (%) free BC	RA (%) immobilized BC
Control	100.00	100.00			
Zn^{2+}	61.58 ± 3.62	59.36 ± 1.47	Mn^{2+}	59.42 ± 3.90	68.31 ± 1.08
Ca^{2+}	113.12 ± 5.53	118.66 ± 0.92	Mg^{2+}	113.16 ± 1.65	109.24 ± 0.87
Ni^{2+}	127.21 ± 2.16	127.38 ± 0.67	K^{+}	88.37 ± 2.61	97.26 ± 2.31
Co^{2+}	87.48 ± 2.05	96.43 ± 3.38	Ba^{2+}	117.99 ± 2.39	119.54 ± 2.47
EDTA	79.12 ± 3.68	84.31 ± 2.34	Cu^{2+}	25.99 ± 3.67	41.21 ± 4.62

RA, relative activity; BC, Bgls+AST.

the chance that the enzyme falls off the carrier and thus generally achieves good reproducibility (43, 44). To analyze the reusability of immobilized AST/BST, 12 reaction cycles were performed using lichenan as substrates (**Figure 4D**). The immobilized AST/BST retained approximately 93.2% of the initial activity in the 4th cycle and 67.4% in the 12th cycle. Meanwhile, the immobilized BST retained approximately 91.7% of the initial activity in the 4th cycle and 66.8% in the 12th cycle, conforming that the synergistic effect of AST and immobilized AST/BST on silica NPs show excellent durability and reusability.

Adsorption, entrapment, and cross-linking are three commonly used enzyme immobilization technologies. The adsorption method has relatively weak bonding, which causes the loss of the enzyme and the detachment of the carriers during the operation; the encapsulation method is not suitable for macromolecular substrates. In contrast, cross-linking generally provides stronger bonding, less enzyme loss, and thus better reusability (45). For example, Kheirkhah reported that lipase was entrapped in the ZIF-8 carriers, retaining only 25% of original protein loading after 10 cycles (46). Cui et al. reported that the catalase adsorbed on the Fe^{3+}-TA carriers retained only 20% of the initial activity (47). By drawing on these results, the cross-linked dual-enzyme on the carriers can be reused for at least 12 cycles without a big loss of initial activity, and the slight decrease in activity may be due to the loss of carriers during the process of centrifugation. In short, by combining ELP-based silicification and SpyCatcher/SpyTag-based covalent bioconjugation, we developed a novel all-in-one strategy to fabricate nanomaterials capable of target-specific covalent multi-enzyme immobilization from cell lysate without pre-purification, which have great potentials for polysaccharides bioconversion.

Conclusion

The LPMOs named AST from *Chaetomium globosum* was verified to have 1.25-fold synergism with lichenase. HPLC results further confirmed that AST did not alter the endogenous hydrolysis mode of lichenase, but improved the hydrolysis efficiency of lichenase by breaking the long chain at the reducing end of polysaccharides. To the best of our knowledge, it is the first report of the synergistic effect of LPMOs with lichenase, which may have great synergistic potential in the hydrolysis of lichen biomass. Meanwhile, a green and novel strategy for the covalent immobilization of dual-enzyme (LMPOs and lichenase) on SNPs directly from the cell lysate was proposed. The immobilized dual-enzyme showed excellent immobilization efficiency (87.4%) and good reusability. Further confirms the practicality of the immobilization strategy, which has obvious advantages in the bioconversion of lichen biomass.

Data availability statement

The original contributions presented in this study are included in the article/**Supplementary material**, further inquiries can be directed to the corresponding author.

Author contributions

LC designed and performed the experiment and wrote the original draft. YZ performed enzyme experiments. YC did statistic analysis. YL performed enzyme characterization. LL investigated and validated the experiments. GZ reviewed and edited the manuscript. All authors read and approved the submitted manuscript.

Funding

This work was funded by the Natural Science Foundation of Fujian Province of China (2021J011110), Open Project of Putian University Key Laboratory of Translational Tumor Medicine in Fujian Province (2018KF001), the Foundation of Fujian Educational Committee for Young and Middle-aged Teachers (JAT200496), and the Scientific Research Start-up Project of Putian University (2021071).

Conflict of interest

The authors declare that the research was conducted in the absence of any commercial or financial relationships that could be construed as a potential conflict of interest.

Publisher's note

All claims expressed in this article are solely those of the authors and do not necessarily represent those of their affiliated organizations, or those of the publisher, the editors and the reviewers. Any product that may be evaluated in this article, or claim that may be made by its manufacturer, is not guaranteed or endorsed by the publisher.

Supplementary material

The Supplementary Material for this article can be found online at: https://www.frontiersin.org/articles/10.3389/fnut.2022.970540/full#supplementary-material

References

1. Podterob P. Chemical composition of lichens and their medical applications. *Pharm Chem J.* (2008) 42:582–8. doi: 10.1007/s11094-009-0183-5

2. Chaari F, Chaabouni SE. Fungal β-1,3-1,4-glucanases: production, proprieties and biotechnological applications. *J Sci Food Agric.* (2019) 99:2657–64. doi: 10.1002/jsfa.9491

3. Lin YQ, Jin WH, Wang JD, Cai ZW, Wu SY, Zhang GY. A novel method for simultaneous purification and immobilization of a xylanase-lichenase chimera via SpyTag/SpyCatcher spontaneous reaction. *Enzyme Microb Technol.* (2018) 115:29–36. doi: 10.1016/j.enzmictec.2018.04.007

4. Tyurin AA, Suhorukova AV, Deineko IV, Pavlenko OS, Goldenkova-Pavlova IV. A high throughput assay of lichenase activity with Congo red dye in plants. *Plant Methods.* (2021) 1:102. doi: 10.21203/rs.3.rs-689823/v1

5. Ji X, Cheng Y, Tian J, Zhang S, Jing Y, Shi M. Structural characterization of polysaccharide from jujube (*Ziziphus jujuba* Mill.) fruit. *Chem Biol Technol Agric.* (2021) 8:54. doi: 10.1186/s40538-021-00255-2

6. Li F, Pak S, Zhao J, Wei Y, Zhang Y, Li Q. Structural characterization of a neutral polysaccharide from cucurbia moschata and its uptake behaviors in Caco-2 cells. *Foods.* (2021) 10:2357. doi: 10.3390/foods10102357

7. Goldenkova-Pavlova IV, Tyurin AA, Mustafaev ON. The features that distinguish lichenases from other polysaccharide-hydrolyzing enzymes and the relevance of lichenases for biotechnological applications. *Appl Microbiol Biotechnol.* (2018) 9:3951–65. doi: 10.1007/s00253-018-8904-x

8. Contato AG, de Oliveira TB, Aranha GM, de Freitas EN, Vici AC, Nogueira KMV, et al. Prospection of fungal lignocellulolytic enzymes produced from jatoba (*Hymenaea courbaril*) and tamarind (*Tamarindus indica*) seeds: scaling for bioreactor and saccharification profile ofsugarcane bagasse. *Microorganisms.* (2021) 9:533. doi: 10.3390/microorganisms9030533

9. Cai LX, Liu X, Qiu Y, Liu M, Zhang GY. Enzymatic degradation of algal 1,3-xylan: from synergism of lytic polysaccharide monooxygenases with β-1,3-xylanases to their intelligent immobilization on biomimetic silica nanoparticles. *Appl Microbiol Biotechnol.* (2020) 104:5347–60. doi: 10.1007/s00253-020-10624-w

10. Quinlan RJ, Sweeney MD, Lo Leggio L, Otten H, Poulsen JCN, Johansen KS, et al. Insights into the oxidative degradation of cellulose by a copper metalloenzyme that exploits biomass components. *Proc Natl Acad Sci U.S.A.* (2011) 37:15079–84. doi: 10.1073/pnas.1105776108

11. Aachmann FL, Sorlie M, Skjak-Braek G, Eijsink VGH, Vaaje-Kolstad G. NMR structure of a lytic polysaccharide monooxygenase provides insight into copper binding, protein dynamics, and substrate interactions. *Proc Natl Acad Sci U.S.A.* (2012) 46:18779–84. doi: 10.1073/pnas.1208822109

12. Ciano L, Davies GJ, Tolman WB, Walton PH. Bracing copper for the catalytic oxidation of C–H bonds. *Nat Catal.* (2018) 8:571–7. doi: 10.1038/s41929-018-0110-9

13. Hemsworth GR, Taylor EJ, Kim RQ, Gregory RC, Lewis SJ, Turkenburg JP, et al. The copper active site of CBM33 polysaccharide oxygenases. *J Am Chem Soc.* (2013) 16:6069–77. doi: 10.1021/ja402106e

14. Forsberg Z, Mackenzie AK, Srlie M, Rhr AK, Eijsink VGH. Structural and functional characterization of a conserved pair of bacterial cellulose-oxidizing lytic polysaccharide monooxygenases. *Proc Natl Acad Sci U.S.A.* (2014) 23:8446–51. doi: 10.1073/pnas.1402771111

15. Cannella D, Hsieh CWC, Felby C, Jorgensen H. Production and effect of aldonic acids during enzymatic hydrolysis of lignocellulose at high dry matter content. *Biotechnol Biofuels.* (2012) 5:1–10. doi: 10.1186/1754-6834-5-26

16. Dimarogona M, Topakas E, Olsson L, Christakopoulos P. Lignin boosts the cellulase performance of a GH-61 enzyme from *Sporotrichum thermophile*. *Bioresour Technol.* (2012) 110:480–7. doi: 10.1016/j.biortech.2012.01.116

17. Jia L, Goncalves GAL, Takasugi Y, Mori Y, Noda S, Tanaka T, et al. Effect of pretreatment methods on the synergism of cellulase and xylanase during the hydrolysis of bagasse. *Bioresour Technol.* (2015) 185:158–64. doi: 10.1016/j.biortech.2015.02.041

18. Hu J, Chandra R, Arantes V, Gourlay K, van Susan DJ, Saddler JN. The addition of accessory enzymes enhances the hydrolytic performance of cellulase enzymes at high solid loadings. *Bioresour Technol.* (2015) 186:149–53. doi: 10.1016/j.biortech.2015.03.055

19. Hu J, Arantes V, Pribowo A, Gourlay K, Saddler JN. Substrate factors that influence the synergistic interaction of AA9 and cellulases during the enzymatic hydrolysis of biomass. *Energy Environ Sci.* (2014) 7:2308–15.

20. Cai LX, Chu YM, Liu LX, Qiu Y, Zhang GY. A novel all-in-one strategy for purification and immobilization of beta-1,3-xylanase directly from cell lysate as active and recyclable nanobiocatalyst. *Microb Cell Fact.* (2021) 1:37. doi: 10.1186/s12934-021-01530-5

21. Lin YQ, Jin WH, Cai LX, Liu X, Qiu Y, Zhang GY. Green preparation of covalently co-immobilized multienzymes on silica nanoparticles for clean production of reducing sugar from lignocellulosic biomass. *J Clean Prod.* (2021) 314:127994. doi: 10.1016/j.jclepro.2021.127994

22. Lin YQ, Jin WH, Qiu Y, Zhang GY. Programmable stimuli-responsive polypeptides for biomimetic synthesis of silica nanocomposites and enzyme self-immobilization. *Int J Biol Macromol.* (2019) 134:1156–69. doi: 10.1016/j.ijbiomac.2019.05.159

23. Fletcher EE, Yan D, Kosiba AA, Zhou Y, Shi H. Biotechnological applications of elastin-like polypeptides and the inverse transition cycle in the pharmaceutical industry. *Protein Expr Purif.* (2019) 153:114–20. doi: 10.1016/j.pep.2018.09.006

24. Yeboah A, Cohen RI, Rabolli C, Yarmush ML, Berthiaume F. Elastin-like polypeptides: a strategic fusion partner for biologics. *Biotechnol Bioeng.* (2016) 113:1617–27. doi: 10.1002/bit.25998

25. Wang JD, Wang YL, Wang XZ, Zhang DD, Wu SY, Zhang GY. Enhanced thermal stability of lichenase from Bacillus subtilis 168 by SpyTag/SpyCatcher-mediated spontaneous cyclization. *Biotechnol Biofuels.* (2016) 9:1–9. doi: 10.1186/s13068-016-0490-5

26. Fierle JK, Abram-Saliba J, Brioschi M, Detiani M, Coukos G, Dunn SM. Integrating SpyCatcher/SpyTag covalent fusion technology into phage display workflows for rapid antibody discovery. *Sci Rep.* (2019) 1:12815. doi: 10.1038/s41598-019-49233-7

27. Ge ZQ, Xiong Z, Zhang D, Li X, Zhang GY. Unique phase transition of exogenous fusion elastinlike polypeptides in the solution containing polyethylene glycol. *Int J Mol Sci.* (2019) 20:3560. doi: 10.3390/ijms20143560

28. Kim IJ, Nam KH, Yun EJ, Kim S, Youn HJ, Lee HJ, et al. Optimization of synergism of a recombinant auxiliary activity 9 from *Chaetomium globosum*

with cellulase in cellulose hydrolysis. *Appl Microbiol Biotechnol.* (2015) 20:8537–47. doi: 10.1007/s00253-015-6592-3

29. Ji XL, Guo JH, Pan FB, Kuang F, Chen HM, Guo XD, et al. Structural elucidation and antioxidant activities of a neutral polysaccharide from arecanut (*Areca catechu* L.). *Front Nutr.* (2022) 9:853115. doi: 10.3389/fnut.2022.853115

30. Khairil Anuar INA, Banerjee A, Keeble AH, Carella A, Nikov GI, Howarth M. Spy&Go purification of SpyTagproteins using pseudo-SpyCatcher to access an oligomerization toolbox. *Nat Commun.* (2019) 1:1734. doi: 10.1038/s41467-019-09678-w

31. Sheldon RA, van PS. Enzyme immobilisation in biocatalysis: why, what and how. *Chem Soc Rev.* (2013) 42:6223–35. doi: 10.1039/c3cs60075k

32. Keller MB, Felby C, Labate CA, Pellegrini VOA, Blossom BM. A simple enzymatic assay for the quantification of C1-specific cellulose oxidation by lytic polysaccharide monooxygenases. *Biotechnol Lett.* (2020) 1:93–102. doi: 10.1007/s10529-019-02760-9

33. Courtade G, Ciano L, Paradisi A, Lindley PJ, Aachmann FL. Mechanistic basis of substrate-O2 coupling in review within a chitin-active lytic polysaccharide monooxygenase: an integrated NMR/EPR study. *Proc Natl Acad Sci U.S.A.* (2020) 32:19178–89. doi: 10.1073/pnas.2004277117

34. Kim IJ, Youn HJ, Kim KH. Synergism of an auxiliary activity 9 (AA9) from *Chaetomium globosum* with xylanase on the hydrolysis of xylan and lignocellulose. *Process Biochem.* (2016) 10:1445–51. doi: 10.1016/j.procbio.2016.06.017

35. Rudolf A, Baudel H, Zacchi G, Hahn-Hgerdal B, Lidén G. Simultaneous saccharification and fermentation of steam-pretreated bagasse using *Saccharomyces cerevisiae* TMB3400 and *Pichia stipitis* CBS6054. *Biotechnol Bioeng.* (2010) 99:783–90. doi: 10.1002/bit.21636

36. Singh RK, Oort BV, Mollers B, Russo DA, Bjerrum MJ. Detection. and characterization of a novel copper-dependent intermediate in a lytic polysaccharide monooxygenase. *bioRxiv* [Preprint]. doi: 10.1101/610865

37. Kont R, Pihlajaniemi V, Borisova AS, Aro N, Vljame P. The liquid fraction from hydrothermal pretreatment of wheat straw provides lytic polysaccharide monooxygenases with both electrons and H2O2 co-substrate. *Biotechnol Biofuels.* (2019) 12:235. doi: 10.1186/s13068-019-1578-5

38. Vaaje-Kolstad G, Westereng B, Horn SJ, Liu Z, Zhai H, Sørlie M, et al. An oxidative enzyme boosting the enzymatic conversion of recalcitrant polysaccharides. *Science.* (2010) 330:219–22. doi: 10.1126/science.1192231

39. Stepnov AA, Forsberg Z, Sorlie M, Nguyen GS, Wentzel A, Rhr SK, et al. Unraveling the roles of the reductant and free copper ions in LPMO kinetics. *Biotechnol Biofuels.* (2021) 14:28. doi: 10.1186/s13068-021-01879-0

40. Ji XL, Guo JH, Ding D, Gao J, Hao L, Guo XD, et al. Structural characterization and antioxidant activity of a novel high-molecular-weight polysaccharide from *Ziziphus jujuba* cv. Muzao. *J Food Meas Charact.* (2022) 3:2191–200. doi: 10.1007/s11694-022-01288-3

41. Ngo TP, Li A, Tiew KW, Li Z. Efficient transformation of grease to biodiesel using highly active and easily recyclable magnetic nanobiocatalyst aggregates. *Bioresour Technol.* (2013) 145:233–9. doi: 10.1016/j.biortech.2012.12.053

42. Woodley JM, Sheldon RA. Role of biocatalysis in sustainable chemistry. *Chem Rev.* (2018) 2:801–38. doi: 10.1021/acs.chemrev.7b00203

43. Silva T, Keijok WJ, Guimaraes MCC, Cassini STA, Oliveira JPD. Impact of immobilization strategies on the activity and recyclability of lipases in nanomagnetic supports. *Sci Rep.* (2022) 1:6815. doi: 10.1038/s41598-022-10721-y

44. Sotelo LD, Sotelo DC, Ornelas-Soto N, Cruz JC, Osma JF. Comparison of acetaminophen degradation by laccases immobilized by two different methods via a continuous flow microreactor process scheme. *Membranes Basel.* (2022) 12:298. doi: 10.3390/membranes12030298

45. Mahmoodi NM, Saffar-Dastgerdi MH. Clean laccase immobilized nanobiocatalysts (graphene oxide-zeolite nanocomposites): from production to detailed biocatalytic degradation of organic pollutant. *Appl Catal B Environ.* (2020) 268:118443. doi: 10.1016/j.apcatb.2019.118443

46. Kheirkhah R, Badoei-dalfard A, Karami Z. Encapsulation and biochemical characterization of lipase on a silica-coated@ZIF-8@/graphene oxide (GSLZIF) and its application on the biodiesel production. *J Iran Chem Soc.* (2021) 1:71–83. doi: 10.1007/s13738-021-02284-y

47. Cui J, Ren S, Lin T, Feng Y, Jia S. Shielding effects of Fe3+-tannic acid nanocoatings for immobilized enzyme on magnetic Fe3O4@silica core shell nanosphere. *Chem Eng J.* (2018) 343:629–37. doi: 10.1016/j.cej.2018.03.002

frontiers | Frontiers in Nutrition

TYPE Original Research
PUBLISHED 20 October 2022
DOI 10.3389/fnut.2022.1025897

Check for updates

OPEN ACCESS

EDITED BY
Xiaolong Ji,
Zhengzhou University of Light Industry, China

REVIEWED BY
Junyi Yin,
Nanchang University, China
Qingbin Guo,
Tianjin University of Science and Technology, China

*CORRESPONDENCE
Ding-Tao Wu
wudingtao@cdu.edu.cn
Liang Zou
zouliang@cdu.edu.cn

†These authors have contributed equally to this work

SPECIALTY SECTION
This article was submitted to Food Chemistry, a section of the journal Frontiers in Nutrition

RECEIVED 23 August 2022
ACCEPTED 06 October 2022
PUBLISHED 20 October 2022

CITATION
Li W, Li J, Wang J, He Y, Hu Y-C, Wu D-T and Zou L (2022) Effects of various degrees of esterification on antioxidant and immunostimulatory activities of okra pectic-polysaccharides. *Front. Nutr.* 9:1025897. doi: 10.3389/fnut.2022.1025897

COPYRIGHT
© 2022 Li, Li, Wang, He, Hu, Wu and Zou. This is an open-access article distributed under the terms of the Creative Commons Attribution License (CC BY). The use, distribution or reproduction in other forums is permitted, provided the original author(s) and the copyright owner(s) are credited and that the original publication in this journal is cited, in accordance with accepted academic practice. No use, distribution or reproduction is permitted which does not comply with these terms.

Effects of various degrees of esterification on antioxidant and immunostimulatory activities of okra pectic-polysaccharides

Wei Li[1,2†], Jie Li[1†], Jin Wang[1], Yuan He[3], Yi-Chen Hu[1], Ding-Tao Wu[1*] and Liang Zou[1*]

[1]Key Laboratory of Coarse Cereal Processing (Ministry of Agriculture and Rural Affairs), Sichuan Engineering and Technology Research Center of Coarse Cereal Industrialization, School of Food and Biological Engineering, Chengdu University, Chengdu, Sichuan, China, [2]School of Preclinical Medicine, Chengdu University, Chengdu, Sichuan, China, [3]Sichuan Institute of Food Inspection, Chengdu, Sichuan, China

Pectic-polysaccharides are considered as one of the most abundant bioactive components in okra, which possess various promising health-promoting effects. However, the knowledge regarding the structure-bioactivity relationship of okra pectic-polysaccharides (OPP) is still limited. In this study, effects of various degrees of esterification (DEs) on *in vitro* antioxidant and immunostimulatory activities of OPP were analyzed. Results displayed that OPP with high (42.13%), middle (25.88%), and low (4.77%) DE values were successfully prepared by mild alkaline de-esterification, and their primary chemical structures (compositional monosaccharide and glycosidic linkage) and molecular characteristics (molecular weight distribution, particle size, and rheological property) were overall stable. Additionally, results showed that the notable decrease of DE value did not significantly affect antioxidant activities [2,2'-azino-bis (3-ethylbenzthiazoline-6-sulphonic acid) (ABTS) and nitric oxide (NO) radical scavenging abilities as well as ferric reducing antioxidant power (FRAP)] of OPP, suggesting that the DE was not closely related to its antioxidant activity. In fact, the slight decrease of antioxidant activity of OPP after the alkaline de-esterification might be attributed to the slight decrease of uronic acid content. Nevertheless, the immunostimulatory effect of OPP was closely related to its DE, and a suitable degree of acetylation was beneficial to its *in vitro* immunostimulatory effect. Besides, the complete de-acetylation resulted in a remarkable reduction of immune response. The findings are beneficial to better understanding the effect of DE value on antioxidant and immunomodulatory activities of OPP, which also provide theoretical foundations for developing OPP as functional foods or health products.

KEYWORDS

***Abelmoschus esculentus*, pectic-polysaccharides, structure-activity relationship, degree of esterification, immunostimulatory effect**

Introduction

Pectic-polysaccharides are complex heteropolysaccharides existed in the primary cell walls of vegetables and fruits, which are predominantly composed of homogalacturonan (HG), rhamnogalacturonan I (RG-I), and rhamnogalacturonan II (RG-II) domains (1). Recently, pectic-polysaccharides extracted from vegetables and fruits have attracted increasing attention to be developed into functional food ingredients owing to their various health-promoting properties, such as antioxidant, anti-inflammatory, immunomodulatory, anti-tumor, anti-hyperlipidemic, anti-hyperglycemic, anti-obesity, and prebiotic properties (1–3). A great number of studies have demonstrated that the ratio of HG/RG-I, molecular mass, branched chain length, degree of esterification (DE), glycosidic linkage, and compositional monosaccharide of pectic-polysaccharides are critical chemical structures for their health beneficial effects (1–3). Nevertheless, the knowledge regarding the precise structure-biological activity relationships of pectic-polysaccharides is still limited because of a lack of pure samples and fine structure analysis. Therefore, it is important to uncover the relationship between the precise structures of pectic-polysaccharides and their biological activities, which is beneficial to better promoting the application of pectic-polysaccharides in the functional food industry.

Abelmoschus esculentus L. Moench, known as okra or lady's finger, is a vital edible and medicinal plant in China. It is native to the Africa but can now be found throughout tropical and subtropical areas of the world (4). Okra is not only consumed as a delicious vegetable, but also utilized as a folk medicine for the treatment of various diseases (5). Due to its promising health benefits, such as antioxidant, immunomodulatory, anti-diabetic, anti-cancer, anti-hypertensive, and anti-microbial effects, okra has attracted increasing attention to be developed and utilized as functional foods in recent years (4). Lots of studies have demonstrated that pectic-polysaccharides, proteins, flavonoids, and phenolic acids exist as the major bioactive components in okra, which contribute to its various beneficial properties (4, 6). Especially, pectic-polysaccharides are considered as one of the most abundant bioactive components in okra, which play a critical role in its biological activities (6). Indeed, the backbone of okra pectic-polysaccharides (OPP) is identified as →4)-α-D-GalA*p*-(1→2,4)-α-L-Rha*p*-(1→, confirming that the RG I segment is rich in okra (7–9). Besides, the HG segment is also found in okra (6). Indeed, OPP also have a low degree of methyl esterification and a high degree of acetylation (10, 11). Generally, pectic-polysaccharides are complex biomacromolecules, their physicochemical or structural features can directly impact the biological functions. Several studies have indicated that the molecular mass of OPP significantly affect their antioxidant, prebiotic, and anti-inflammatory activities (12, 13), as well as immune stimulating activity (14). Besides, a recent study has shown that biological activities of OPP can be improved through the degradation by ultrasound assisted H_2O_2/Vc reaction, and the *in vitro* antioxidant and immunostimulatory effects of OPP are related to its molecular mass, branched chain length, and DE (9). Furthermore, the DE value has gained much attention in the investigation of pectic-polysaccharides, because the DE value can obviously affect biological activities and functional properties of pectic-polysaccharides, such as inhibitory effect on α-amylase, modulation of gut microbial composition, immunoregulatory effect, gel property, and emulsifying ability (15–18). Indeed, the mild alkaline de-esterification has been considered as one of the most important methods to reduce the esterification of pectic-polysaccharides (15, 19). However, the potential relationships between DE value and biological activity of OPPare still unclear, which require to be systematically investigated.

Therefore, in order to further clarify the potential structure-bioactivity relationship of OPP, effects of various degrees of esterification on *in vitro* antioxidant capacities and immunostimulatory activities of OPP were investigated in the present study.

Materials and methods

Materials and chemicals

Okra fruits of *Abelmoschus esculentus* cv. Wufu used in this study were harvested from Chengdu, Sichuan Province, China. Monosaccharide standards, 2,2′-azino-bis (3-ethylbenzthiazoline-6-sulphonic acid) (ABTS), sodium nitroprusside (SNP), vitamin C (Vc), griess reagent, lipopolysaccharide (LPS), and 3-(4,5-dimethylthiazol-2-yl)-2,5-diphenyl tetrazolium bromide (MTT) were purchased from Sigma-Aldrich (St. Louis, MO, USA).

Preparation of okra pectic-polysaccharides with various degrees of esterification

The preparation of purified OPP was performed as previously reported (20). Briefly, the crude water-soluble polysaccharides from okra fruit powders were extracted by ultrasound assisted-extraction (650 W, 24 kHz, Scientz, Ningbo, China) as previously reported (20). Afterward, the supernatants were sequentially precipitated (three volumes of 95% ethanol), redissolved, dialyzed (molecular mass cutoff, 3.5 kDa), and separated by a DEAE anion exchange column (5 × 50 cm) to prepare purified OPP. Moreover, the modification of OPP was carried out to improve its *in vitro* biological activities as previously reported (9). Briefly, 50.0 mL of OPP solutions (10.0 mg/mL) were mixed with ascorbic acid and H_2O_2 at the

final concentrations of 20.0 and 40.0 mM, respectively, and then degraded by ultrasound (650 W, 24 kHz, Scientz, Ningbo, China) at the power of 520 W for 0.5 h (9). Finally, the degraded product of okra pectic-polysaccharides (DOPP) with promoted biological functions was obtained.

Furthermore, the preparation of DOPP with various DE values was carried out according to a previous study with a few modifications (19). In brief, the mild alkaline de-esterification was carried out by stirring 0.5% (*w/v*) of DOPP in NaOH solution at basic pH values of 11.0 and 13.0 for 0.5 h under 4°C, respectively. At the end of reaction, the sample solution was acidified to pH = 6.0 by adding HCl (1 M). Then, after dialysis (molecular mass cutoff, 3.5 kDa) and freeze-drying in turn, okra pectic-polysaccharides with a middle DE value (DOPP-MDE) and a low DE value (DOPP-LDE) were obtained. Indeed, the yields of DOPP-MDE and DOPP-LDE were measured to be 95.73 and 90.82%, respectively. Correspondingly, the original DOPP was named DOPP-HDE, which possessed a relatively high DE value.

Structural characterization of okra pectic-polysaccharides with various degrees of esterification

Total polysaccharides, uronic acids, and proteins of OPP with various DE values were detected by colorimetric methods as previously reported (21). Molecular weight (M_w), molecular weight distribution (M_w/M_n), and radius of gyration (R_g) as well as rheological property of DOPP-HDE, DOPP-MDE, and DOPP-LDE were also measured as previously reported (9, 22). In brief, a TSKgel GMPWXL column (300 × 7.8 mm, i.d.) was utilized for the separation of DOPP-HDE, DOPP-MDE, and DOPP-LDE, respectively. Both multi-angle laser light scattering detection and refractive index detection (Wyatt Technology Co., Santa Barbara, CA, USA) were applied for the analysis of DOPP-HDE, DOPP-MDE, and DOPP-LDE, respectively. The apparent viscosities of DOPP-HDE, DOPP-MDE, and DOPP-LDE were measured by a Discovery Hybrid Rheometer-1 (DHR-1, TA Instruments, New Castle, DE, USA). For the investigation of primary chemical structures, the monosaccharide compositions, FT-IR spectra, and ^{1}H NMR spectra of OPP with various DE values were analyzed. In brief, monosaccharide compositions of DOPP-HDE, DOPP-MDE, and DOPP-LDE were analyzed by HPLC (Thermo Fisher Scientific, Waltham, MA, USA) as previously reported (23). A C18 column (150 × 4.6 mm, 5 μm, Thermo Fisher Scientific, Waltham, MA, USA) was carried out for the separation of monosaccharides, and the signals were recorded at 245 nm. Additionally, ^{1}H NMR spectra of DOPP-HDE, DOPP-MDE, and DOPP-LDE were also recorded on a Bruker Ascend 600 MHz spectrometer (Bruker, Rheinstetten, Germany) as previously reported (24, 25). Furthermore, the FT-IR spectra of DOPP-HDE, DOPP-MDE, and DOPP-LDE were also analyzed according to a previous reported method (26, 27). Indeed, the DE value was estimated based on the FT-IR spectra at 1,700–1,750 cm^{-1} (about 1,730 cm^{-1}) and 1,600–1,640 cm^{-1} (about 1,635 cm^{-1}), which was estimated based on the following equation:

$$\mathrm{DE}(\%) = \left(\frac{\mathrm{A1730}}{\mathrm{A1730} + \mathrm{A1635}}\right) \times 100$$

TABLE 1 Chemical composition, molecular weight (M_w), polydispersity (M_w/M_n), radius of gyration (R_g), and constituent monosaccharide of okra pectic-polysaccharides (OPP) with various degrees of esterification.

	DOPP-HDE	DOPP-MDE	DOPP-LDE
Total polysaccharides (%)	92.59 ± 2.31^a	92.26 ± 3.16^a	93.21 ± 2.00^a
Total uronic acids (%)	33.51 ± 1.64^a	32.91 ± 1.93^a	27.51 ± 1.77^b
Total proteins (%)	1.25 ± 0.27^a	1.00 ± 0.04^a	0.81 ± 0.32^a
Esterification degree (%)	42.13 ± 0.14^a	25.88 ± 0.47^b	4.77 ± 0.34^c
$M_w \times 10^5$ (Da)	1.897 (±0.928%)^a	1.865 (±0.693%)^a	1.753 (±1.036%)^a
M_w/M_n	1.786 (±1.381%)	1.736 (±1.049%)	1.773 (±1.658%)
R_g	30.3 (±2.9%)^a	30.0 (±3.6%)^a	29.6 (±2.4%)^a
Monosaccharide compositions and molar ratios			
Rhamnose	1	1	1
Galactose	2.14	2.11	2.08
Galacturonic acid	1.10	1.09	1.07
Mannose	0.48	0.37	0.34
Arabinose	0.19	0.17	0.16
Glucuronic acid	Trace	Trace	Trace

DOPP-HDE, DOPP-MDE, and DOPP-LDE indicate okra pectic-polysaccharides with high, middle, and low degrees of esterification, respectively; total polysaccharides (%, *w/w*), uronic acids (%, *w/w*), and proteins (%, *w/w*) indicate the total content of neutral and acidic polysaccharides, the total content of uronic acids, and the total content of proteins in okra pectic-polysaccharides; esterification degree (%) indicates the esterification degree of total uronic acids; different superscript lowercase letters indicated significance ($p < 0.05$) in each row.

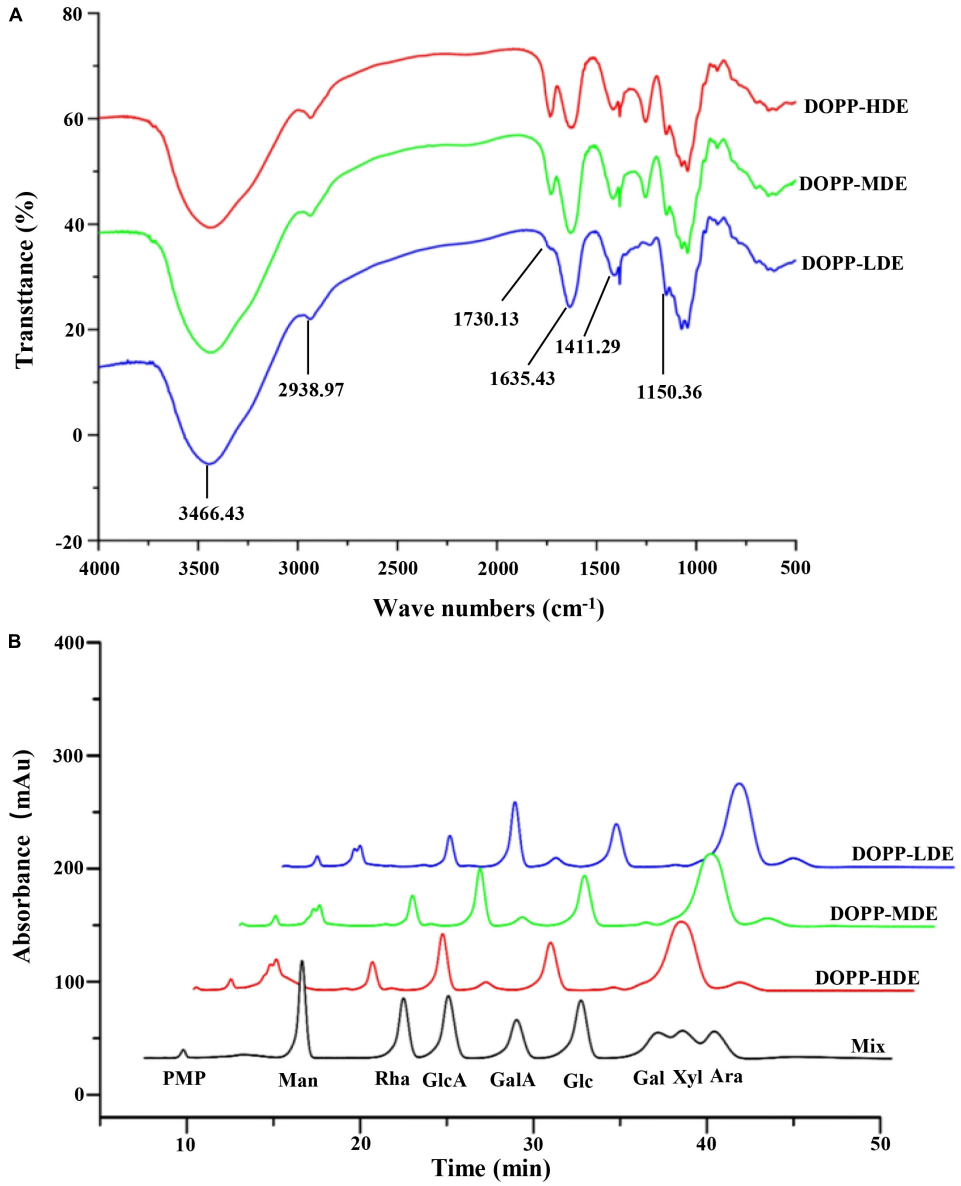

FIGURE 1
FT-IR spectra **(A)** and high-performance liquid chromatograms of compositional monosaccharides **(B)** of okra pectic-polysaccharides (OPP) with various degrees of esterification. DOPP-HDE, DOPP-MDE, and DOPP-LDE indicate OPP with high, middle, and low degrees of esterification, respectively; Mix indicates the monosaccharide standards, which was analyzed by HPLC under the same conditions of samples. PMP, 1-phenyl-3-methyl-5-pyrazolone; Man, mannose; Rha, rhamnose; GlcA, glucuronic acid; GalA, galacturonic acid; Glc, glucose; Gal, galactose; Xyl, xylose; Ara, arabinose.

Evaluation of *in vitro* antioxidant activities of okra pectic-polysaccharides with various degrees of esterification

The ferric reducing antioxidant power (FRAP), ABTS radical scavenging ability, and nitric oxide (NO) radical scavenging ability of OPP with various DE values were evaluated according to previously reported methods (26). In brief, for the determination of ABTS radical scavenging ability, the ABTS radical cation working solution (200 μL) was mixed with 20 μL of each sample (2.0–10.0 mg/mL) in a 96-well microplate to react at 30°C for 20 min; for the determination of NO radical scavenging ability, each sample (450 μL, 2.0–10.0 mg/mL) was mixed with 50 μL of SNP (10 mM) to react at 25°C for 3 h, and then 250 μL of Griess reagent was added. Besides, the IC_{50} values (mg/mL) of DOPP-HDE, DOPP-MDE, and DOPP-LDE for scavenging free radicals could be determined

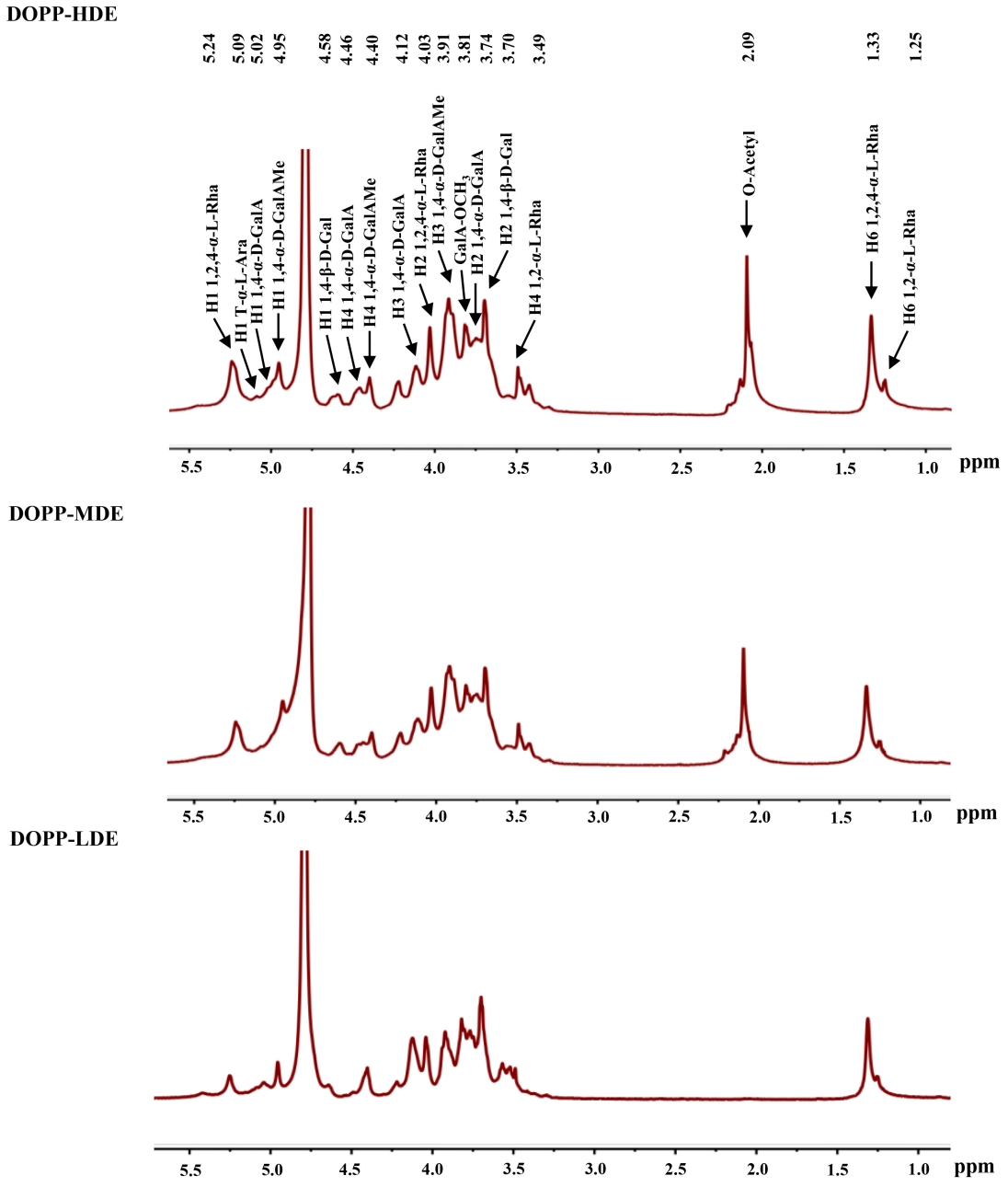

FIGURE 2
^{1}H NMR spectra of okra pectic-polysaccharides (OPP) with various degrees of esterification. The sample codes were the same in **Figure 1**.

on the basis of a logarithmic regression curve. Additionally, for the determination of FRAP, 100 μL of each sample (2.0–10.0 mg/mL) was mixed with 100 μL of potassium ferricyanide (1%, *w/w*) at 50°C for 20 min, and then 100 μL of trichloroacetic acid (10%, *w/v*) was added and centrifugated. Finally, both distilled water (100 μL) and ferric chloride (20 μL) were added into the supernatant (100 μL). The absorbance of the mixture was recorded at 593 nm. Vc was used as a positive control in each experiment.

Evaluation of immunostimulatory activities of okra pectic-polysaccharides with various degrees of esterification

Immunostimulatory activities of OPP with various DE values were evaluated by using an *in vitro* model of RAW 264.7 macrophages according to a previously reported method (9). In brief, effects of OPP with various DEs at the

concentrations ranged from 5 to 320 μg/mL on the proliferation of RAW 264.7 macrophages were determined by the MTT colorimetric method. Additionally, the production of NO and release of cytokines [interleukin-6 (IL-6) and tumor necrosis factor-α (TNF-α)] from RAW 264.7 macrophages were also detected as previously reported (9). After the RAW 264.7 macrophage was stimulated with DOPP-HDE, DOPP-MDE, and DOPP-LDE at the concentrations ranged from 5 to 320 μg/mL, the NO production was measured by Griess reagent. Besides, the release of IL-6 and TNF-α from RAW 264.7 macrophages were measured by ELISA kits according to the manufacturer's procedures (eBioscience, San Diego, CA, USA).

Statistical analysis

Each experiment was carried out in triplicate. Data are presented as mean ± standard deviation. Statistical analysis was performed by using a two-tailed Student's *t*-test and one-way analysis of variance followed by a Duncan's test, respectively.

Results and discussion

Structural features of okra pectic-polysaccharides with various degrees of esterification

Chemical structures of okra pectic-polysaccharides with various degrees of esterification

The chemical compositions of OPP with different DE values are summarized in **Table 1**. Total polysaccharides in DOPP-HDE, DOPP-MDE, and DOPP-LDE were detected to be 92.59, 92.26, and 93.21%, respectively, indicating that the contents of total polysaccharides were not affected by mild alkaline de-esterification. However, total uronic acids in DOPP-HDE, DOPP-MDE, and DOPP-LDE slightly decreased from 33.51 to 27.51% by mild alkaline de-esterification, which might be due to the fact that the elimination reaction could induce the hydrolysis of pectic-polysaccharides by splitting their backbone (15, 28). Additionally, minor proteins were found in DOPP-HDE, DOPP-MDE, and DOPP-LDE, which were similar with a previous study (9).

Furthermore, in order to confirm the primary chemical structures of OPP with different DE values, the monosaccharide compositions, FT-IR spectra, and ^{1}H NMR spectra were systematically analyzed. As shown in **Figure 1A**, similar FT-IR spectra were found in DOPP-HDE, DOPP-MDE, and DOPP-LDE, indicating that the major chemical groups of OPP were stable after the treatment of mild alkaline de-esterification. The typical absorption bands of pectic-polysaccharides, including 3466.43, 2938.97, 1730.13, 1635.43, 1411.29, and 1150.36 cm^{-1}, were found in all tested samples (28, 29). However, as shown in **Figure 1A**, the peak areas of absorption band at around 1730.13 cm^{-1} related to esterified functional groups remarkably changed after the treatment of mild alkaline de-esterification (28). Indeed, the DE values of DOPP-HDE, DOPP-MDE, and DOPP-LDE were estimated to be 42.13, 25.88, and 4.77% based on the peak areas of absorption bands at around 1730.13 and 1635.43 cm^{-1} (**Table 1**), respectively, indicating that OPP with various DE values were successfully prepared. Additionally, as shown in **Figure 1B**, the same types of monosaccharides were found in DOPP-HDE, DOPP-MDE, and DOPP-LDE, and galacturonic acid, rhamnose, and galactose were determined as the major monosaccharides as previously reported (9). Indeed, similar molar ratios of constituent monosaccharides were also found in all samples (**Table 1**), suggesting that the primary chemical structures of OPP, except the DE, were relatively stable after the treatment of mild alkaline de-esterification. Furthermore, ^{1}H NMR spectra of OPP with various DE values were also analyzed for the confirmation of their chemical structures (**Figure 2**). More specifically, the signal at around 2.09 ppm in DOPP-HDE was assigned to acetyl groups (10, 11), which might locate on *O*-2 or *O*-3 of galacturonosyl residues and *O*-3 of rhamnosyl residues (11). The intensity of this signal obviously decreased in DOPP-MDE or even disappeared in DOPP-LDE, indicating that the degree of acetylation of galacturonosyl or rhamnosyl residues in OPP could be decreased by mild alkaline de-esterification. Additionally, the signal at around 3.81 ppm in DOPP-HDE was assigned to methoxyl groups (10, 11). This signal could be also found in DOPP-MDE and DOPP-LDE, suggesting that methoxyl groups bonded to carboxyl groups of galacturonic acid could still exist in OPP under the mild alkaline de-esterification conditions. Similar phenomena were also found in previous studies that the methoxyl group from the esterified units of galacturonic acids could not be completely removed under the mild alkaline conditions (15, 28). Collectively, these results indicated that the decrease of DE value in DOPP-MDE and DOPP-LDE compared to DOPP-HDE might be mainly attributed to the complete de-acetylation and the partial de-methylation.

Moreover, the typical signals, including 1,4-α-D-GalA*p* (H-1, 5.02 ppm), 1,4-α-D-GalAMe*p* (H-1, 4.95 ppm), 1,2-α-L-Rha*p* (H-6, 1.25 ppm), 1,2,4-α-L-Rha*p* (H-1/H-6, 5.24/1.33 ppm), 1,4-β-D-Gal*p* (H-1, 4.58 ppm), could be found in DOPP-HDE, DOPP-MDE, and DOPP-LDE. These results suggested that the RG-I backbone with galactan side chains existed as the main pectic-polysaccharides in DOPP-HDE, DOPP-MDE, and DOPP-LDE (7, 9, 10, 28), and the primary chemical structures of OPP, except the DE, were overall stable after the treatment of mild alkaline de-esterification.

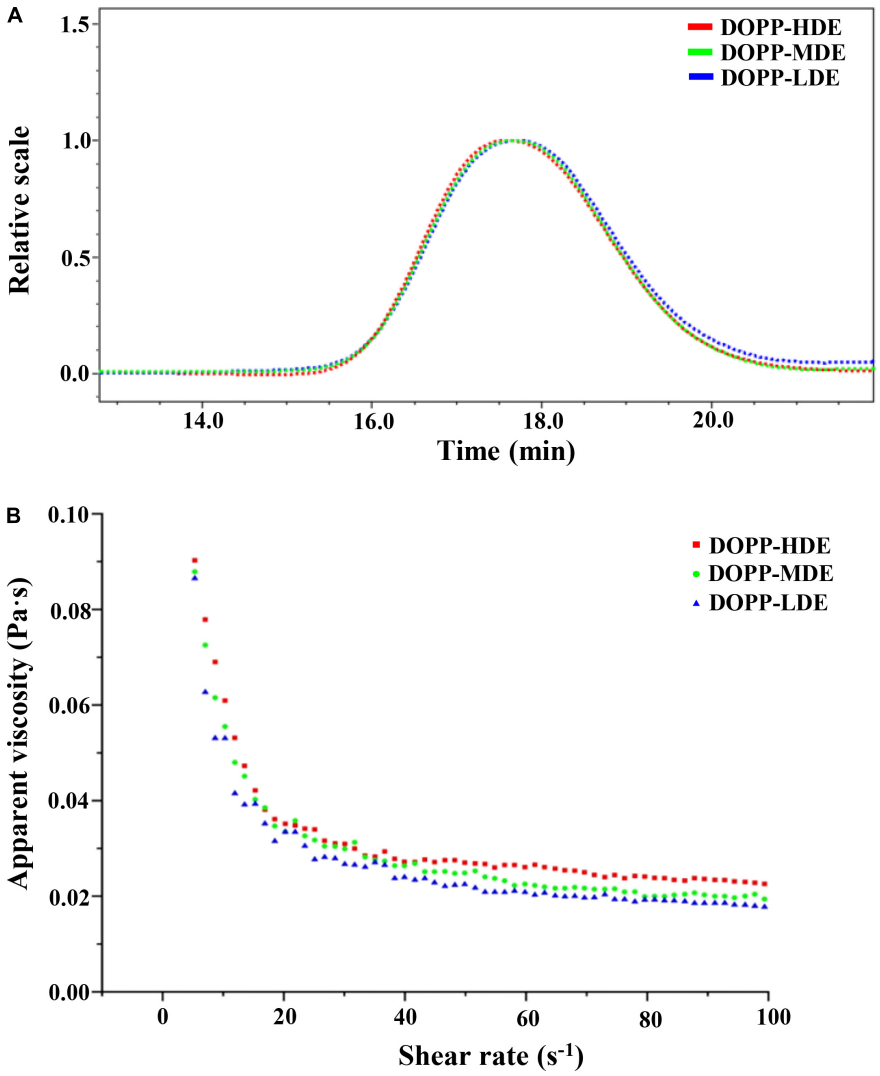

FIGURE 3
Size exclusion chromatograms **(A)** and dependences of apparent viscosity on the shear rate **(B)** of okra pectic-polysaccharides (OPP) with various degrees of esterification. The sample codes were the same in **Figure 1**.

Molecular mass and particle size of okra pectic-polysaccharides with various degrees of esterification

Macromolecular characteristics of pectic-polysaccharides, such as molecular mass, molecular mass distribution, and particle size, have significant impacts on their biological properties and applications in the functional food industry (9, 30, 31). Consequently, macromolecular characteristics of OPP with various DE values were measured and compared. As shown in **Figure 3A**, similar size exclusion chromatography (SEC) profiles were found in OPP with various DE values, which exhibited a single symmetrical peak. Results showed that the retention time of DOPP-HDE, DOPP-MDE, and DOPP-LDE were almost the same, suggesting that the molecular mass and molecular mass distribution of OPP were overall stable after the treatment of mild alkaline de-esterification. Indeed, as shown in **Table 1**, the molecular masses of DOPP-HDE, DOPP-MDE, and DOPP-LDE were detected to be 1.897×10^5, 1.865×10^5, and 1.753×10^5 Da, respectively, suggesting that the mild alkaline de-esterification could slightly (no significant difference) degrade the molecular weight of OPP. This phenomenon was similar with previous studies that β-elimination reaction could cause the degradation of molecular mass (15, 28). Besides, the molecular mass distributions of OPP with different DE values were similar, which ranged from 1,736 to 1,786. Additionally, corresponding with the changes in molecular mass, the particle size of DOPP-HDE also slightly (no significant difference) decreased from 30.3 to 29.6 nm after the treatment of mild alkaline de-esterification.

10.3389/fnut.2022.1025897

Rheological properties of okra pectic-polysaccharides with various degrees of esterification

Rheological property is considered as one of the most important factors that affect the biological functions and food applications of pectic-polysaccharides (28, 32). **Figure 3B** displays the dependences of apparent viscosity on shear rate of OPP (40 mg/mL) with different DE values. As expected, the apparent viscosities of DOPP-HDE, DOPP-MDE, and DOPP-LDE affected by the shear rate. More specifically, the apparent viscosities of each sample declined with the increase of the shear rate ranged from 0.01 to 50 s^{-1}, indicating that each sample solution exhibited non-Newtonian shear thinning fluid behavior (32). In addition, the apparent viscosities of each sample declined slightly with the increase of the shear rate ranged from 50 to 100 s^{-1}, exhibiting Newtonian flow fluid behavior (9, 21). This rheological character of OPP might be due to the fact that the chains of pectin were arranged in an orderly manner along the fluid direction with the increase of the shear rate, and the interactions between the adjacent chains and the viscosity decreased (33). Furthermore, compared with DOPP-HDE, the apparent viscosities of DOPP-MDE and DOPP-LDE slightly reduced, indicating that the obvious decrease of DE value did not cause a sharp decrease of apparent viscosity. This result is different from a previous study that the pectin with a lower degree of esterification is often accompanied by a decrease of viscosity (34). In this study, DOPP-LDE with a lower degree of esterification also exhibited a higher apparent viscosity which might be attributed to the fact that the viscosity of the sample was affected by several factors, such as molecular mass, chain conformation, monosaccharide composition (9, 21, 32). Collectively, although the DE value of OPP was significantly decreased, its apparent viscosity was relatively stable after the treatment of mild alkaline de-esterification.

Effects of various degrees of esterification on *in vitro* antioxidant activities of okra pectic-polysaccharides

The antioxidant activity has been demonstrated as one of the most important biological functions of okra (4), and OPP have remarkable *in vitro* antioxidant capacities against different free radicals (9, 21, 26, 35). Several studies have shown that the antioxidant activities of crude OPP may be related to their molecular mass, chain conformation, uronic acid, and DE as well as conjugated polyphenols (21, 26, 35, 36). A recent study also showed that the antioxidant activity of a purified okra pectic-polysaccharide might be closely related to the combination effect of molecular

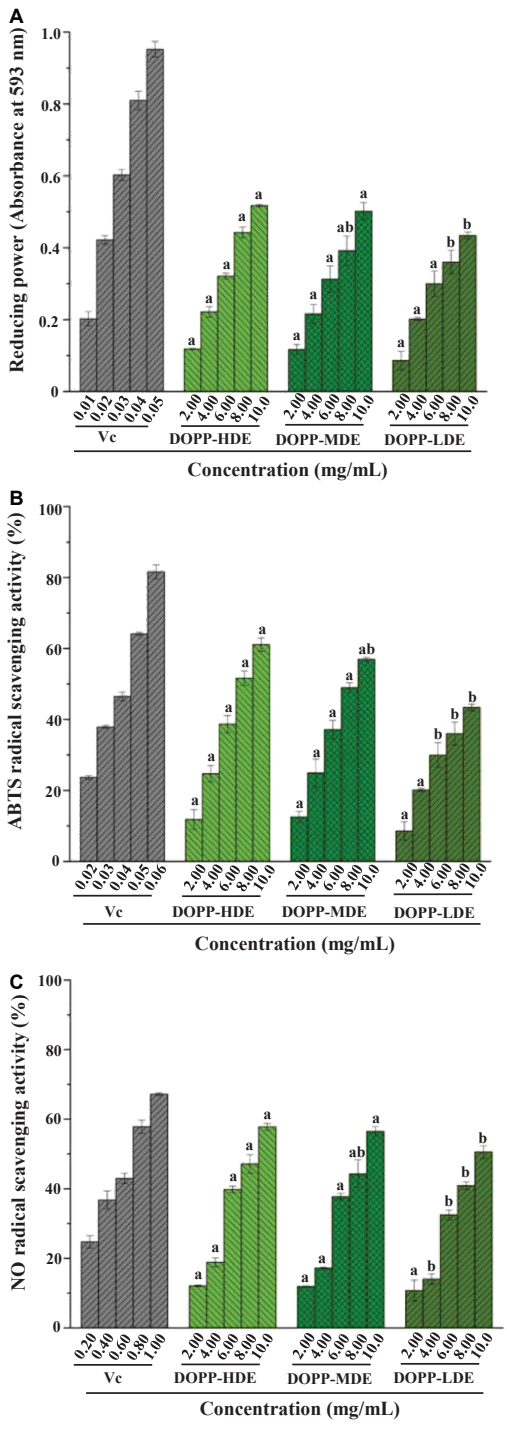

FIGURE 4
Ferric reducing antioxidant power (FRAP) **(A)**, 2,2′-azino-bis (3-ethylbenzthiazoline-6-sulphonic acid) (ABTS) radical scavenging activity **(B)**, and nitric oxide (NO) radical scavenging activity **(C)** of okra pectic-polysaccharides (OPP) with various degrees of esterification. The sample codes were the same in **Figure 1**; the error bars are standard deviations; significant ($p < 0.05$) differences among OPP with various degrees of esterification are shown by data bearing different letters (a-b); statistical significances were carried out by ANOVA and Ducan's test.

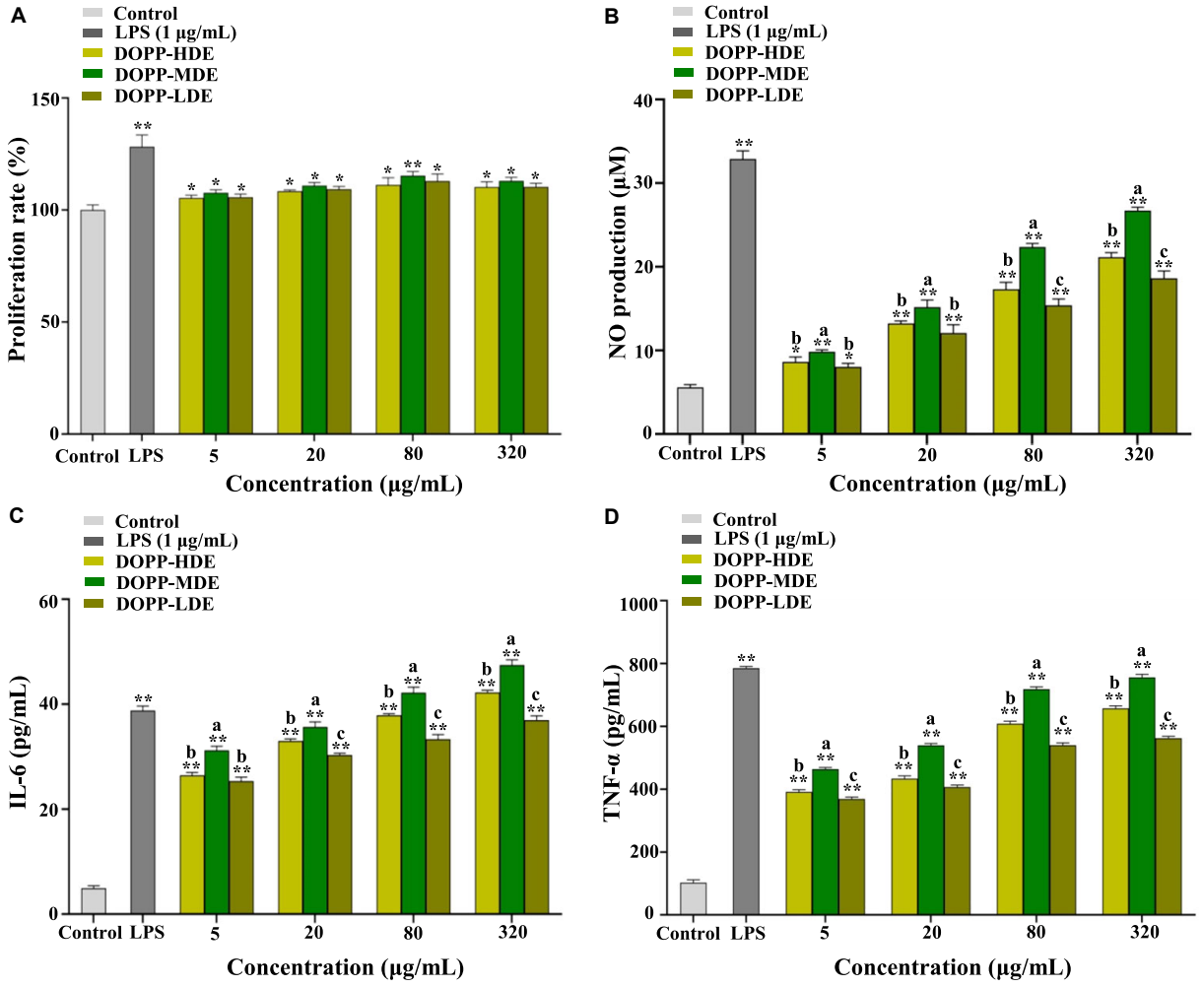

FIGURE 5
Effects of okra pectic-polysaccharides (OPP) with various degrees of esterification on proliferation **(A)**, nitric oxide (NO) production **(B)**, interleukin-6 (IL-6) production **(C)**, and tumor necrosis factor-α (TNF-α) production **(D)** of RAW 264.7 macrophages. The sample codes were the same in **Figure 1**; the error bars are standard deviations; significant differences of cell proliferation and release of NO, IL-6, and TNF-α in LPS, DOPP-HDE, DOPP-MDE, and DOPP-LDE vs. control are shown by $*p < 0.05$, $**p < 0.01$. Significant differences ($p < 0.05$) of release of NO, IL-6, and TNF-α among DOPP-HDE, DOPP-MDE, and DOPP-LDE are shown by data bearing different letters (a–c).

mass and DE (9). However, whether the DE can directly affect the antioxidant activity of OPP is still not clear. Therefore, in the present study, in order to evaluate the precise degree of esterification on *in vitro* antioxidant activity of OPP, three OPP with high, middle, and low degrees of esterification were prepared and their antioxidant activities were evaluated.

Figure 4 displays the FRAPs and ABTS radical scavenging capacities as well as NO radical scavenging capacities of OPP with high, middle, and low DE values. Results showed that OPP with various DE values exhibited remarkable antioxidant activities with a dose-dependent manner. For the FRAP, the absorbance values of DOPP-HDE, DOPP-MDE, and DOPP-LDE at 593 nm were detected to be 0.52 ± 0.01, 0.50 ± 0.02, and 0.43 ± 0.01 at the concentration of 10 mg/mL, respectively, which were lower than that of Vc (0.95 ± 0.02). Additionally, in terms of ABTS radical scavenging activity, the IC_{50} values of DOPP-HDE, DOPP-MDE, and DOPP-LDE were detected to be 7.76 ± 0.31, 8.40 ± 0.32, and 10.24 ± 0.72 mg/mL, respectively, which were higher than that of Vc (0.04 mg/mL). Furthermore, in terms of NO radical scavenging activity, the IC_{50} values of DOPP-HDE, DOPP-MDE, and DOPP-LDE were detected to be 8.43 ± 0.21, 9.02 ± 0.49, and 10.64 ± 0.38 mg/mL, respectively, which were also higher than that of Vc (0.62 ± 0.02 mg/mL). Surprisingly, results showed that DOPP-LDE with the lowest DE value (4.77%) among three samples exhibited the lowest antioxidant activities in the present study. Besides, although the DE value of DOPP-MDE (25.88%) was significantly lower than that of DOPP-HDE (42.13%), the *in vitro* antioxidant activities of

DOPP-HDE and DOPP-MDE were similar. Therefore, these results indicated that the remarkable decrease of DE value (mainly degree of acetylation) of OPP by mild alkaline de-esterification did not obviously affect their antioxidant activity, suggesting that the DE was not closely correlated to the antioxidant activity of OPP. This phenomenon is quite different from previous studies that the lower DE of pectic-polysaccharides is closely related to their higher antioxidant activity (37, 38). In fact, the antioxidant activity of pectic-polysaccharides is assigned to their hydrogen-donating abilities, and several studies have shown that the presence of free uronic acids in the pectic-polysaccharides can activate the hydrogen atom of the anomeric carbon (39, 40). However, in this study, the decrease of DE value was mainly attributed to the de-acetylation of galacturonosyl residues in OPP (**Figure 2**), which might not obviously affect the rate of unmethylated uronic acids. Besides, the antioxidant capacity of pectic-polysaccharides is often closely related to their molecular mass and uronic acids (12, 15, 36, 41). Therefore, in this study, according to the structural differences measured as abovementioned, the slight decrease of antioxidant activity of DOPP-LDE compared to DOPP-HDE might be due to the slight decrease of uronic acid content (**Table 1**).

Effects of various degrees of esterification on *in vitro* immunostimulatory activities of okra pectic-polysaccharides

Immunity refers to the protection effects of biological organisms against foreign bacteria, viruses, and other harmful substances. A large number of studies have demonstrated that dietary polysaccharides from edible and medicinal plants can maintain the human health by regulating the immune system (42, 43). Generally, the immunostimulatory effects of dietary polysaccharides are associated with their molecular mass, branched chain length, uronic acid, chain conformation, and glycosidic linkage (44, 45). In fact, several studies have shown that pectic-polysaccharides isolated from different parts of okra possess remarkable *in vitro* and *in vivo* immunostimulatory effects (14, 46–48). A previous study also showed that the immunostimulatory effect of a purified okra pectic-polysaccharide was closely related to the combination effect of molecular mass, branched chain length, and DE (9). However, whether the DE can directly affect the immunostimulatory effect of OPP remains unclear.

Therefore, the RAW 264.7 macrophage was applied as a cell model for the determination of immunostimulatory effects of OPP with various DE values. **Figure 5** displays the immunostimulatory effects of DOPP-HDE, DOPP-MDE, and DOPP-LDE. As shown in **Figure 5A**, all tested samples could slightly promote the proliferation of RAW 264.7 macrophages at the concentrations ranged from 5 to 320 μg/mL, indicating that DOPP-HDE, DOPP-MDE, and DOPP-LDE had no toxicity effects. Furthermore, macrophages can exert their functions by secreting NO and various cytokines, such as IL-6 and TNF-α (49). NO is a biologically active cell messenger that plays a critical role in killing pathogenic microorganisms and tumor cells; TNF-α is active in regulating inflammation and autoimmunity; IL is involved in the immune response in the host that plays a key role in maintaining homeostasis. As shown in **Figures 5B–D**, OPP with different DE values could remarkably promote the release of NO, IL-6, and TNF-α from RAW 264.7 macrophages in a dose-dependent manner, respectively. Interestingly, OPP with various DE values exhibited notably different effects on the release of NO, IL-6, and TNF-α from RAW 264.7 macrophages. More specifically, the higher productions of NO, IL-6, and TNF-α from RAW 264.7 macrophages were found in DOPP-MDE compared to DOPP-HDE, while the lower productions of NO, IL-6, and TNF-α were found in DOPP-LDE compared to DOPP-HDE. Collectively, according to the structural differences among DOPP-HDE, DOPP-MDE, and DOPP-LDE, these results indicated that the immunostimulatory effect of OPP was closely related to its DE. A previous study also showed that the DE played a key role in the immunostimulatory effect of pectic-polysaccharides from *Asparagus officinalis* L., and a relatively high DE value was associated with the relatively high immunostimulatory effect (50). Indeed, the acetyl groups of a purified polysaccharide from *Polygonatum cyrtonema* might also benefit its immunostimulatory effect (51). In addition, several studies have demonstrated that the acetylation modification of natural polysaccharides can enhance their immunostimulatory effects (52, 53), while removing the acetyl groups resulted in the remarkable decrease of immunostimulatory functions (54, 55). Therefore, the findings in the present study indicate that OPP with a DE value of 25.88% possess remarkable *in vitro* immunostimulatory effect, and the complete de-acetylation in DOPP-LDE results in a remarkable reduction of immune response. Nevertheless, the precise structure-immunostimulatory activity relationship of OPP and related mechanism of action are required to be deeply uncovered in the future.

Conclusion

Pectic-polysaccharides are regarded as one of the most abundant bioactive components in okra. However, the

knowledge about the precise structure-bioactivity relationships of OPP is still limited. Therefore, in order to further clarify the potential structure-bioactivity relationship of okra pectic-polysaccharides, effects of various degrees of esterification on *in vitro* antioxidant capacities and immunostimulatory activities of OPP were investigated. Results showed that the decrease of DE was mainly attributed to the de-acetylation of OPP according to the ^{1}H NMR spectra analysis. In addition, results showed that the DE value was not related to the antioxidant activity of OPP. However, the immunostimulatory effect of OPP was closely related to its DE value, and a suitable DE value is beneficial to its *in vitro* immunostimulatory effect. Collectively, the findings are beneficial to revealing the effect of esterification degree on antioxidant activity and immunomodulatory activity of OPP. However, due to the limitations of *in vitro* models, it is necessary to evaluate the bioactivities of okra pectic-polysaccharide and its structure dependent relationships in animal models in the future.

Data availability statement

The original contributions presented in this study are included in the article/supplementary material, further inquiries can be directed to the corresponding authors.

Author contributions

WL and JL: investigation, formal analysis, resources, software, and writing – original draft. JW: investigation, formal analysis, and validation. YH: investigation and validation. Y-CH: resources and software. D-TW: data curation, methodology, formal analysis, funding acquisition, and writing – review and editing. LZ: methodology, formal analysis, supervision, resources, and writing – review and editing. All authors contributed to the article and approved the submitted version.

Funding

This work was supported by the Open Research Project Programme of the State Key Laboratory of Quality Research in Chinese Medicine, University of Macau (No. SKL-QRCM-OP21001) and the Scientific Research Foundation of Chengdu University (2081921047).

Conflict of interest

The authors declare that the research was conducted in the absence of any commercial or financial relationships that could be construed as a potential conflict of interest.

Publisher's note

All claims expressed in this article are solely those of the authors and do not necessarily represent those of their affiliated organizations, or those of the publisher, the editors and the reviewers. Any product that may be evaluated in this article, or claim that may be made by its manufacturer, is not guaranteed or endorsed by the publisher.

References

1. Zhang, S, Waterhouse GIN, Xu F, He Z, Du Y, Lian Y, et al. Recent advances in utilization of pectins in biomedical applications: a review focusing on molecular structure-directing health-promoting properties. *Crit Rev Food Sci Nutr.* (2021) 1–34. doi: 10.1080/10408398.2021.1988897

2. Jin M-Y, Li M-Y, Huang R-M, Wu X-Y, Sun Y-M, Xu Z-L. Structural features and anti-inflammatory properties of pectic polysaccharides: a review. *Trends Food Sci Technol.* (2021) 107:284–98. doi: 10.1016/j.tifs.2020.10.042

3. Yu CX, Wu DM, Zhu K, Hou L, Xiao H, Ding T, et al. Challenges of pectic polysaccharides as a prebiotic from the perspective of fermentation characteristics and anti-colitis activity. *Carbohydr Polym.* (2021) 270:118377. doi: 10.1016/j.carbpol.2021.118377

4. Agregán R, Pateiro M, Bohrer BM, Shariati MA, Nawaz A, Gohari G, et al. Biological activity and development of functional foods fortified with okra (*Abelmoschus esculentus*). *Crit Rev Food Sci Nutr.* (2022) 1–16. doi: 10.1080/10408398.2022.2026874

5. Dantas TL, Alonso Buriti FC, Florentino ER. Okra (*Abelmoschus esculentus* L.) as a potential functional food source of mucilage and bioactive compounds with technological applications and health benefits. *Plants.* (2021) 10:1683. doi: 10.3390/plants10081683

6. Zhu X-M, Xu R, Wang H, Chen J-Y, Tu Z-C. Structural properties, bioactivities, and applications of polysaccharides from okra [*Abelmoschus esculentus* (L.) Moench]: a review. *J Agric Food Chem.* (2020) 68:14091–103. doi: 10.1021/acs.jafc.0c04475

7. Liu J, Zhao Y, Wu Q, John A, Jiang Y, Yang J, et al. Structure characterisation of polysaccharides in vegetable "okra" and evaluation of hypoglycemic activity. *Food Chem.* (2018) 242:211–6. doi: 10.1016/j.foodchem.2017.09.051

8. Zhang T, Xiang J, Zheng G, Yan R, Min X. Preliminary characterization and anti-hyperglycemic activity of a pectic polysaccharide from okra (*Abelmoschus esculentus* (L.) Moench). *J Funct Foods.* (2018) 41:19–24. doi: 10.1016/j.jff.2017.12.028

9. Wu D-T, He Y, Fu M-X, Gan R-Y, Hu Y-C, Peng L-X, et al. Structural characteristics and biological activities of a pectic-polysaccharide from okra affected by ultrasound assisted metal-free Fenton reaction. *Food Hydrocoll.* (2022) 122:107085. doi: 10.1016/j.foodhyd.2021.107085

10. Kpodo FM, Agbenorhevi JK, Alba K, Bingham RJ, Oduro IN, Morris GA, et al. Pectin isolation and characterization from six okra genotypes. *Food Hydrocoll.* (2017) 72:323–30. doi: 10.1016/j.foodhyd.2017.06.014

11. Alba K, Laws AP, Kontogiorgos V. Isolation and characterization of acetylated LM-pectins extracted from okra pods. *Food Hydrocoll.* (2015) 43:726–35. doi: 10.1016/j.foodhyd.2014.08.003

12. Yeung YK, Kang Y-R, So BR, Jung SK, Chang YH. Structural, antioxidant, prebiotic and anti-inflammatory properties of pectic oligosaccharides hydrolyzed

from okra pectin by Fenton reaction. *Food Hydrocoll.* (2021) 118:106779. doi: 10.1016/j.foodhyd.2021.106779

13. Wu D-T, He Y, Yuan Q, Wang S, Gan R-Y, Hu Y-C, et al. Effects of molecular weight and degree of branching on microbial fermentation characteristics of okra pectic-polysaccharide and its selective impact on gut microbial composition. *Food Hydrocoll.* (2022) 132:107897. doi: 10.1016/j.foodhyd.2022.107897

14. Trakoolpolpruek T, Moonmangmee S, Chanput W. Structure-dependent immune modulating activity of okra polysaccharide on THP-1 macrophages. *Bioact Carbohydr Diet Fibre.* (2019) 17:100173. doi: 10.1016/j.bcdf.2018.10.002

15. Liang W-L, Liao J-S, Qi J-R, Jiang W-X, Yang X-Q. Physicochemical characteristics and functional properties of high methoxyl pectin with different degree of esterification. *Food Chem.* (2022) 375:131806. doi: 10.1016/j.foodchem.2021.131806

16. Wu Q, Fan L, Tan H, Zhang Y, Fang Q, Yang J, et al. Impact of pectin with various esterification degrees on the profiles of gut microbiota and serum metabolites. *Appl Microbiol Biotechnol.* (2022) 106:3707–20. doi: 10.1007/s00253-022-11926-x

17. Bai Y, Atluri S, Zhang Z, Gidley MJ, Li E, Gilbert RG. Structural reasons for inhibitory effects of pectin on α-amylase enzyme activity and in-vitro digestibility of starch. *Food Hydrocoll.* (2021) 114:106581. doi: 10.1016/j.foodhyd.2020.106581

18. Beukema M, Jermendi É, Oerlemans MMP, Logtenberg MJ, Akkerman R, An R, et al. The level and distribution of methyl-esters influence the impact of pectin on intestinal T cells, microbiota, and Ahr activation. *Carbohydr Polym.* (2022) 286:119280. doi: 10.1016/j.carbpol.2022.119280

19. Hua X, Yang H, Din P, Chi K, Yang R. Rheological properties of deesterified pectin with different methoxylation degree. *Food Biosci.* (2018) 23:91–9. doi: 10.1016/j.fbio.2018.03.011

20. Nie XR, Fu Y, Wu DT, Huang TT, Jiang Q, Zhao L, et al. Ultrasonic-assisted extraction, structural characterization, chain conformation, and biological activities of a pectic-polysaccharide from okra (*Abelmoschus esculentus*). *Molecules.* (2020) 25:1155. doi: 10.3390/molecules25051155

21. Nie X-R, Li H-Y, Du G, Lin S, Hu R, Li H-Y, et al. Structural characteristics, rheological properties, and biological activities of polysaccharides from different cultivars of okra (*Abelmoschus esculentus*) collected in China. *Int J Biol Macromol.* (2019) 139:459–67. doi: 10.1016/j.ijbiomac.2019.08.016

22. Wu D-T, An L-Y, Liu W, Hu Y-C, Wang S-P, Zou L. *In vitro* fecal fermentation properties of polysaccharides from *Tremella fuciformis* and related modulation effects on gut microbiota. *Food Res Int.* (2022) 156:111185. doi: 10.1016/j.foodres.2022.111185

23. Ji X, Guo J, Pan F, Kuang F, Chen H, Guo X, et al. Structural elucidation and antioxidant activities of a neutral polysaccharide from arecanut (*Areca catechu* L.). *Front Nutr.* (2022) 9:853115. doi: 10.3389/fnut.2022.853115

24. Wu DT, Feng KL, Huang L, Gan RY, Hu YC, Zou L. Deep eutectic solvent-assisted extraction, partially structural characterization, and bioactivities of acidic polysaccharides from lotus leaves. *Foods.* (2021) 10:2330. doi: 10.3390/foods10102330

25. Ji X, Guo J, Ding D, Gao J, Hao L, Guo X, et al. Structural characterization and antioxidant activity of a novel high-molecular-weight polysaccharide from *Ziziphus Jujuba* cv. *Muzao*. *J Food Meas Charact.* (2022) 16:2191–200. doi: 10.1007/s11694-022-01288-3

26. Yuan Q, Lin S, Fu Y, Nie X-R, Liu W, Su Y, et al. Effects of extraction methods on the physicochemical characteristics and biological activities of polysaccharides from okra (*Abelmoschus esculentus*). *Int J Biol Macromol.* (2019) 127:178–86. doi: 10.1016/j.ijbiomac.2019.01.042

27. Wu D-T, Liu W, Yuan Q, Gan R-Y, Hu Y-C, Wang S-P, et al. Dynamic variations in physicochemical characteristics of oolong tea polysaccharides during simulated digestion and fecal fermentation *in vitro*. *Food Chem X.* (2022) 14:100288. doi: 10.1016/j.fochx.2022.100288

28. Bai L, Zhu P, Wang W, Wang M. The influence of extraction pH on the chemical compositions, macromolecular characteristics, and rheological properties of polysaccharide: the case of okra polysaccharide. *Food Hydrocoll.* (2020) 102:105586. doi: 10.1016/j.foodhyd.2019.105586

29. Ji X, Cheng Y, Tian J, Zhang S, Jing Y, Shi M. Structural characterization of polysaccharide from jujube (*Ziziphus jujuba* Mill.) fruit. *Chem Biol Technol Agric.* (2021) 8:54. doi: 10.1186/s40538-021-00255-2

30. Yin L, Fu S, Wu R, Wei S, Yi J, Zhang L-M, et al. Chain conformation of an acidic polysaccharide from green tea and related mechanism of α-amylase inhibitory activity. *Int J Biol Macromol.* (2020) 164:1124–32. doi: 10.1016/j.ijbiomac.2020.07.125

31. Guo R, Tian S, Li X, Wu X, Liu X, Li D, et al. Pectic polysaccharides from purple passion fruit peel: a comprehensive study in macromolecular and conformational characterizations. *Carbohydr Polym.* (2020) 229:115406. doi: 10.1016/j.carbpol.2019.115406

32. Hou Z, Chen S, Ye X. High pressure processing accelarated the release of RG-I pectic polysaccharides from citrus peel. *Carbohydr Polym.* (2021) 263:118005. doi: 10.1016/j.carbpol.2021.118005

33. Yan J-K, Wang C, Qiu W-Y, Chen T-T, Yang Y, Wang W-H, et al. Ultrasonic treatment at different pH values affects the macromolecular, structural, and rheological characteristics of citrus pectin. *Food Chem.* (2021) 341:128216. doi: 10.1016/j.foodchem.2020.128216

34. Hu W, Ye X, Chantapakul T, Chen S, Zheng J. Manosonication extraction of RG-I pectic polysaccharides from citrus waste: optimization and kinetics analysis. *Carbohydr Polym.* (2020) 235:115982. doi: 10.1016/j.carbpol.2020.115982

35. Chen Z-L, Wang C, Ma H, Ma Y, Yan J-K. Physicochemical and functional characteristics of polysaccharides from okra extracted by using ultrasound at different frequencies. *Food Chem.* (2021) 361:130138. doi: 10.1016/j.foodchem.2021.130138

36. Wang C, Yu Y-B, Chen T-T, Wang Z-W, Yan J-K. Innovative preparation, physicochemical characteristics and functional properties of bioactive polysaccharides from fresh okra (*Abelmoschus esculentus* (L.) Moench). *Food Chem.* (2020) 320:126647. doi: 10.1016/j.foodchem.2020.126647

37. Chen R, Luo S, Wang C, Bai H, Lu J, Tian L, et al. Effects of ultra-high pressure enzyme extraction on characteristics and functional properties of red pitaya (*Hylocereus polyrhizus*) peel pectic polysaccharides. *Food Hydrocoll.* (2021) 121:107016. doi: 10.1016/j.foodhyd.2021.107016

38. Naqash F, Masoodi FA, Gani A, Nazir S, Jhan F. Pectin recovery from apple pomace: physico-chemical and functional variation based on methyl-esterification. *Int J Food Sci Tech.* (2021) 56:4669–79. doi: 10.1111/ijfs.15129

39. Wang Z-B, Pei J-J, Ma H-L, Cai P-F, Yan J-K. Effect of extraction media on preliminary characterizations and antioxidant activities of *Phellinus linteus* polysaccharides. *Carbohydr Polym.* (2014) 109:49–55. doi: 10.1016/j.carbpol.2014.03.057

40. Wang J, Hu S, Nie S, Yu Q, Xie M. Reviews on mechanisms of *in vitro* antioxidant activity of polysaccharides. *Oxid Med Cell Longev.* (2016) 2016:5692852. doi: 10.1155/2016/5692852

41. Wu D-T, Fu M-X, Guo H, Hu Y-C, Zheng X-Q, Gan R-Y, et al. Microwave-assisted deep eutectic solvent extraction, structural characteristics, and biological functions of polysaccharides from sweet tea (*Lithocarpus litseifolius*) leaves. *Antioxidants.* (2022) 11:1578. doi: 10.3390/antiox11081578

42. Yin M, Zhang Y, Li H. Advances in research on immunoregulation of macrophages by plant polysaccharides. *Front Immunol.* (2019) 10:145. doi: 10.3389/fimmu.2019.00145

43. Mohan K, Muralisankar T, Uthayakumar V, Chandirasekar R, Revathi N, Ramu Ganesan A, et al. Trends in the extraction, purification, characterisation and biological activities of polysaccharides from tropical and sub-tropical fruits – A comprehensive review. *Carbohydr Polym.* (2020) 238:116185. doi: 10.1016/j.carbpol.2020.116185

44. Mzoughi Z, Majdoub H. Pectic polysaccharides from edible halophytes: insight on extraction processes, structural characterizations and immunomodulatory potentials. *Int J Biol Macromol.* (2021) 173:554–79. doi: 10.1016/j.ijbiomac.2021.01.144

45. Ferreira SS, Passos CP, Madureira P, Vilanova M, Coimbra MA. Structure–function relationships of immunostimulatory polysaccharides: a review. *Carbohydr Polym.* (2015) 132:378–96. doi: 10.1016/j.carbpol.2015.05.079

46. Chen H, Jiao H, Cheng Y, Xu K, Jia X, Shi Q, et al. *In vitro* and *in vivo* immunomodulatory activity of okra (*Abelmoschus esculentus* L.) polysaccharides. *J Med Food.* (2016) 19:253–65. doi: 10.1089/jmf.2015.3513

47. Chen Y, Zhou R, He L, Wang F, Yang X, Teng L, et al. Okra polysaccharide-2 plays a vital role on the activation of RAW264.7 cells by TLR2/4-mediated signal transduction pathways. *Int Immunopharm.* (2020) 86:106708. doi: 10.1016/j.intimp.2020.106708

48. Zheng W, Zhao T, Feng W, Wang W, Zou Y, Zheng D, et al. Purification, characterization and immunomodulating activity of a polysaccharide from flowers of *Abelmoschus esculentus*. *Carbohydr Polym.* (2014) 106:335–42. doi: 10.1016/j.carbpol.2014.02.079

49. Huang LX, Shen MY, Morris GA, Xie JH. Sulfated polysaccharides: immunomodulation and signaling mechanisms. *Trends Food Sci. Technol.* (2019) 92:1–11. doi: 10.1016/j.tifs.2019.08.008

50. Wang NF, Jia GG, Wang XF, Liu Y, Li ZJ, Bao HH, et al. Fractionation, structural characteristics and immunomodulatory activity of polysaccharide fractions from asparagus (*Asparagus officinalis* L.) skin. *Carbohydr Polym.* (2021) 256:117514. doi: 10.1016/j.carbpol.2020.117514

51. Zhao P, Zhou H, Zhao C, Li X, Wang Y, Wang Y, et al. Purification, characterization and immunomodulatory activity of fructans from *Polygonatum odoratum* and *P. cyrtonema*. *Carbohydr Polym.* (2019) 214:44–52. doi: 10.1016/j.carbpol.2019.03.014

52. Yang Y, Chen J, Lei L, Li F, Tang Y, Yuan Y, et al. Acetylation of polysaccharide from *Morchella angusticeps* peck enhances its immune activation and anti-inflammatory activities in macrophage RAW264.7 cells. *Food Chem Toxicol.* (2019) 125:38–45. doi: 10.1016/j.fct.2018.12.036

53. Liu X, Xie J, Jia S, Huang L, Wang Z, Li C, et al. Immunomodulatory effects of an acetylated *Cyclocarya paliurus* polysaccharide on murine macrophages RAW264.7. *Int J Biol Macromol.* (2017) 98:576–81. doi: 10.1016/j.ijbiomac.2017.02.028

54. Martins VMR, Simões J, Ferreira I, Cruz MT, Domingues MR, Coimbra MA. *In vitro* macrophage nitric oxide production by *Pterospartum tridentatum* (L.) Willk. inflorescence polysaccharides. *Carbohydr Polym.* (2017) 157:176–84. doi: 10.1016/j.carbpol.2016.09.079

55. Hsieh YSY, Chien C, Liao SKS, Liao S-F, Hung W-T, Yang W-B, et al. Structure and bioactivity of the polysaccharides in medicinal plant *Dendrobium huoshanense*. *Bioorg Med Chem.* (2008) 16:6054–68. doi: 10.1016/j.bmc.2008.04.042

frontiers | Frontiers in Nutrition

TYPE Original Research
PUBLISHED 01 November 2022
DOI 10.3389/fnut.2022.1035760

Check for updates

OPEN ACCESS

EDITED BY
Xiaolong Ji,
Zhengzhou University of Light Industry, China

REVIEWED BY
Zhu Rugang,
Liaoning University, China
Hanqing Chen,
Hefei University of Technology, China

*CORRESPONDENCE
Rina Wu
wrn6956@163.com

†These authors have contributed equally to this work

SPECIALTY SECTION
This article was submitted to Food Chemistry, a section of the journal Frontiers in Nutrition

RECEIVED 03 September 2022
ACCEPTED 12 October 2022
PUBLISHED 01 November 2022

CITATION
An F, Ren G, Wu J, Cao K, Li M, Liu Y, Liu Y, Hu X, Song M and Wu R (2022) Extraction, purification, structural characterization, and antioxidant activity of a novel polysaccharide from *Lonicera japonica* Thunb. *Front. Nutr.* 9:1035760. doi: 10.3389/fnut.2022.1035760

COPYRIGHT
© 2022 An, Ren, Wu, Cao, Li, Liu, Liu, Hu, Song and Wu. This is an open-access article distributed under the terms of the Creative Commons Attribution License (CC BY). The use, distribution or reproduction in other forums is permitted, provided the original author(s) and the copyright owner(s) are credited and that the original publication in this journal is cited, in accordance with accepted academic practice. No use, distribution or reproduction is permitted which does not comply with these terms.

Extraction, purification, structural characterization, and antioxidant activity of a novel polysaccharide from *Lonicera japonica* Thunb.

Feiyu An[1†], Guangyu Ren[1†], Junrui Wu[1,2], Kaixin Cao[1], Mo Li[1], Yumeng Liu[1], Yanfeng Liu[1], Xinyu Hu[1], Meijun Song[1] and Rina Wu[1,3*]

[1]College of Food Science, Shenyang Agricultural University, Shenyang, China, [2]Key Laboratory of Microbial Fermentation Technology Innovation, Shenyang, China, [3]Engineering Research Center of Food Fermentation Technology, Liaoning, China

A novel water-soluble polysaccharide (HEP-4) with a molecular weight of 1.98×10^5 Da was extracted from honeysuckle. Structural characterization was performed using high-performance liquid chromatography (HPLC), gas chromatography, Fourier transform-infrared (FT-IR) spectrum, nucleus magnetic resonance (NMR) spectra, and scanning electron microscopy. The results showed that HEP-4 is primarily composed of mannose, rhamnose, galacturonic acid, glucose, galactose, and arabinose with a mole ratio of 6.74:1.56:1.04:14.21:4.31:5.4, and the major types of the glycosidic bond types of HEP-4 were 1-α-D-Glc*p*, 1,4-β-D-Glc*p*, 1-β-D-Ara*p*, 1,3,4-β-D-Ara*p*, and 1,3,6-β-D-Man*p*. The results of bioactivity experiments revealed that HEP-4 had antioxidant *in vitro*. In addition, HEP-4 inhibited H_2O_2-induced oxidative damage and increased the activity of HepG2 cells by reducing MDA levels and inhibiting ROS production. Meanwhile, HEP-4 significantly enhanced the activities of GSH-Px and CAT, indicating that HEP-4 exerts a protective effect on H_2O_2-induced oxidative stress. These results indicate that HEP-4 could be a potential natural antioxidant.

KEYWORDS

honeysuckle, polysaccharide, antioxidant activity, oxidative stress, structural characterization

Introduction

Honeysuckle (*Lonicera japonica* Thunb.) belongs to the *Caprifoliaceae* family of medicinal plants (1). It is widely distributed in the Yellow River and Yangtze River basins of China and is largely planted in Hunan, Henan, Shandong, and other provinces. Several studies have reported that Honeysuckle has anti-cancer, anti-inflammatory,

anti-allergic, antipyretic, and other effects (2–5), which could be related to the various bioactive components present in Honeysuckle, such as polysaccharides, saponins, tannins, and flavonoids, etc., (6, 7).

Of the numerous functional components in honeysuckle, polysaccharides are especially important as a pleiotropic biological response modifier, and their pharmacological activities largely include antioxidant (5), anti-allergy (6), immune regulation (8), and neuroprotection (9), etc. Among these, the antioxidant capacity has received extensive attention recently, and several researchers have studied the antioxidant activities of other natural plant polysaccharides such as areca nut (10), jujube (11), Tossa jute leaves (12), and wheat bran (13). Relevant research results demonstrate that plant polysaccharides exert a strong antioxidant activity and low side effects, and can be used as an important source of antioxidants to prevent the risk of free radical injury and the production of several related diseases (14).

Several researchers believe that the monosaccharide composition, molecular weight, functional groups, glycosidic bond composition, branching, and conformation of polysaccharides are closely related to their antioxidants and other biological activities (15). For instance, Zhang et al. reported that pinecone polysaccharides with a high content of L-rhamnose and L-arabinose had better antioxidant activity (16). Zhi et al. found that water-soluble polysaccharides with antioxidant activity isolated from roots of *Dioscorea opposita* Thunb. may be related to its low molecular weight (17). Therefore, to reveal and explore the structural-biological activity relationship of polysaccharides, we need to conduct structure-biological activity studies on various polysaccharides from different sources and conduct comparative analysis.

At present, the major antioxidant active polysaccharide components in the total sugar of honeysuckle are not known, hindering the in-depth study of the structure and antioxidant activity of honeysuckle polysaccharides. In this study, we extracted a novel polysaccharide (HEP-4) from honeysuckle and characterized its structural features. In addition, the antioxidant activity of HEP-4 was evaluated, and the protective effect of HEP-4 on H_2O_2-induced oxidative stress was studied in combination with cell experiments. The research results provide a basis for the comprehensive development and utilization of honeysuckle polysaccharides.

Materials and methods

Materials

The honeysuckle was purchased from the Shenyang of Liaoning province, China. DEAE-52 cellulose, Sephadex G-75, Vitamin-C, and monosaccharide standards were purchased from Yuanye Bio-Technology Co., Ltd. (Shanghai China). DMEM cell culture, fetal bovine serum (FBS), and penicillin were purchased from HyClone (Logan, Utah, USA). HepG2 cell line was purchased from Stem Cell Bank, Chinese Academy of Sciences.

Extraction, isolation, and purification of polysaccharides

The peel of honeysuckle was removed and it was lyophilized to constant weight and ground. The powder was immersed in 95% ethanol to remove the lipids/pigments and filtered (18). The prepared honeysuckle powder (100 g) was extracted with distilled water (1,000 ml) at 80°C for 3 h. All extraction solutions were collected and concentrated using the vacuum rotary evaporator (60°C), to which 95% ethanol was added and left to stand for 24 h; the solution was centrifuged (10,000 rpm, 10 min) and the precipitate was dissolved in ultrapure water (19).

Proteins were removed using the Sevag method as described previously (20). Next, the crude polysaccharide sample obtained after elution was equipped with a DEAE-52 cellulose column (2.6 cm × 30 cm), which was stepwise eluted with distilled water and 0.1, 0.2, 0.3, 0.4, and 0.5 M gradients of NaCl solutions sequentially at a flow rate of 1.5 ml/min. All tubes were quantified by phenol–sulfuric acid method. Next, the Sephadex G-75 gel chromatography column (2.6 cm × 100 cm) was used for further purification. Thus, five fine polysaccharide components HEPs were obtained. After comprehensive comparison of the antioxidant activities of the scavenging effects of $ABTS^{\cdot+}$, DPPH·, superoxide, and hydroxyl, HEP-4 was selected and freeze-dried to obtain purified polysaccharide powder for further use.

Evaluation of structure characteristics of HEP-4

Chemical analysis

The phenol-sulfuric acid method, Coomassie brilliant blue method, and m-hydroxy biphenyl method were used to evaluate the content of the overall sugar, proteins, and uronic acid in the polysaccharide fraction.

Determination of molecular weight distribution

The mean molecular weight of the sample was determined by high-performance gel permeation chromatography (21). The column was eluted with 0.2 M Na_2SO_4 solution at a flow rate of 0.6 ml/min. The column temperature was maintained at 35 ± 0.1°C. The injection volume was 20 μL and the average molecular weight of HEP-4 was calculated by the standard curve, which was established using the T-series dextran.

Monosaccharide composition analysis

The monosaccharide composition of HEP-4 was analyzed according to a previously described method with certain modifications (22) and the detailed method is presented in **Supplementary method 1**.

Methylation analysis

Methylation analysis of polysaccharides was performed as described previously with minor modifications (23), and the specific experimental method is presented in **Supplementary method 2**.

Periodate oxidation and Smith degradation reaction

Periodate oxidation and Smith degradation of HEP-4 were conducted according to the method described by Meng et al. (24). The standard curve equation of sodium periodate solution was obtained as follows Y = 2.222X + 3.6491, R2 = 0.9991.

Fourier transform-infrared spectroscopy analysis

The infrared spectrum of HEP-4 was determined using an FT-IR spectrometer (Nicolet 6,700, Thermo Fisher Scientific, Waltham, MA, USA). The dried HEP (2 mg) was ground with KBr (200 mg) and pressed into pellets for FT-IR measurement in the frequency range of 4,000–400 cm^{-1} at a resolution of 4 cm^{-1} (25).

Nucleus magnetic resonance analysis

HEP-4 (60 mg/ml) was dissolved and deutero-exchanged with D_2O and afterward re-dissolved in 0.5 ml of D_2O. The ^1H NMR and ^{13}C NMR of the polysaccharides were recorded with a VNMRS600 NMR spectrometer (Agilent, CA, USA) at 60°C. The MestReNova software was used to process the NMR data, and chemical shifts (δ) are expressed in ppm (26).

Scanning electron microscopy analysis

The morphology of HEP-4 was evaluated by scanning electron microscopy. An appropriate amount of HEP-4 sample was fixed and coated with a layer of conductive gold film and afterward examined using an SEM system (SU1510, Hitachi, Tokyo, Japan) (27).

Antioxidant activity

The DPPH·scavenging activity of HEP-4 was assessed according to the reported method with minor modifications (28), and the specific experimental methods were presented in **Supplementary method 3**. The superoxide anion scavenging activities were determined using the method described by Liang et al. (29) and the specific experimental method is presented in **Supplementary method 4**. The detailed method of the $ABTS^{\cdot+}$ radical scavenging assay is presented in **Supplementary method 5**. The hydroxyl radical scavenging activity of HEP-4 was determined as described previously in the literature (30) and the detailed method is presented in **Supplementary method 6**.

Inducing HepG2 cells with H_2O_2

Cell culture and treatments

HepG2 cells were cultured in DMEM with FBS (10% v/v) and penicillin (1% v/v) in 95% air and 5% CO_2 humidified atmosphere at 37°C. After passaging thrice, the cells were used to seed 6-well culture plates.

HepG2 cells were treated with different concentrations of HEP-4 (200, 400, and 800 μg/mL) for 4 h and washed with warm PBS thrice. In addition, 800 μg/mL Vc was used as the control group. Except for the blank group, the cells of other groups were added to 6 mmol/L H_2O_2 for 1.5 h and washed with PBS. Next, 200 μL of the cracking solution was added to each well and placed in a refrigerator at 4°C for 15 min. Afterward, it was sucked out and collected in 1.5 mL centrifuge tubes.

Hoechst 33342 fluorescence staining

HepG2 cells were grown in five glass-bottom cell culture dishes for 24 h and treated with 6 mmol/L H_2O_2 and different concentrations (200, 400, and 800 μg/mL) of HEP-4. The cells were washed twice with PBS. Next, the cells were stained with 500 μL of the medium and mixed with 5 μL of Hoechst 33342 for 10–20 min at 25°C. Finally, the washed cells were observed using a laser confocal microscope (31).

Analysis of cell reactive oxygen species

To visualize and quantify intracellular reactive oxygen species (ROS) production, the generation of ROS was monitored using a fluorometric intracellular ROS kit (Nanjing Jiancheng Bio Co., Ltd., Nanjing, Jiangsu, China).

Analysis of glutathione peroxidase catalase, malondialdehyde, and catalase

To study the influence of HEP-4 samples on the oxidative stress status of H_2O_2-induced HepG2 cells, the content of protein was measured using a bicinchoninic acid kit (Beyotime, China). The activities of glutathione peroxidase catalase (GSH-Px) (Nanjing Jiancheng, China) and catalase (CAT) (Solarbio, Beijing, Hebei, China), and the content of malondialdehyde (MDA) (Nanjing Jiancheng, China) were determined according to the manufacturer's instructions.

Statistical analysis

The experiments were repeated thrice. All data are expressed as mean ± standard deviation (SD). Statistical significance was

calculated by one-way analysis of variance (ANOVA), and the difference was considered significant at $P < 0.05$.

Results and discussion

Purification of HEP-4 and determination of molecular weight

In this study, *Honeysuckle* as raw material, crude polysaccharides were extracted by hot water extraction method, and the protein was removed by the Sevag method. The polysaccharide content in crude HEP was 2.09 ± 0.21%. Five fractions (HEP-1, HEP-2, HEP-3, HEP-4, and HEP-5) were separated on the DEAE-52 column, among which HEP-4 had the highest elution peak (**Figure 1A**) and had the highest resistance to oxidative activity (data not shown). Therefore, we further purified HEP-4 crude fractions using gel filtration chromatography (**Figure 1B**), and afterward collected and lyophilized them to obtain HEP-4. The basic chemical composition analysis of the lyophilized fraction revealed that the contents of total sugar, proteins, and uronic acid in HEP-4 were 88.62 ± 2.04%, 1.71 ± 0.58%, and 2.20 ± 0.09%, respectively. In addition, the average molecular weight of HEP-4 was estimated to be 1.98×10^5 Da. Zhang et al. reported that the average molecular weights of four honeysuckle water-soluble polysaccharides ranged from 1.9×10^4 to 3.84×10^5 Da, among which the average molecular weights of antioxidant polysaccharides were relatively high and similar to HEP-4 (5). Sheng et al. proposed that polysaccharides from the fern *Polydonta* had strong hydroxyl radical scavenging ability at low molecular weight, whereas a strong reducing ability and DPPH· radical scavenging ability at the high molecular weight (32). Therefore, we believe that the effect of molecular weight of polysaccharides on their antioxidant activity is not absolute, and the joint effects of other structural factors need to be studied.

Monosaccharide composition of HEP-4

As shown in **Supplementary figure 1**. HEP-4 is primarily composed of mannose, rhamnose, galacturonic acid, glucose, galactose, and arabinose in a ratio of 6.74:1.56:1.04:14.21:4.31:5.4. Compared with the results of a previous study on honeysuckle polysaccharides (5, 9), we found differences in the monosaccharide composition, which could be attributed to the differences in separation and purification methods and raw materials, which will also lead to differences in their active functions.

It has been demonstrated that monosaccharide composition is intricately related to the antioxidant activity of polysaccharides. For example, Mehmood et al. reported that *Tricholoma lobayense* heteroglycan with high glucose and galactose content showed a strong antioxidant activity (33). In addition, the *T. lobayense* heteroglycan contains a certain amount of rhamnose, which was the reason for its high antioxidant activity. In this study, HEP-4 showed a high content of glucose and mannose, and rhamnose, indicating its high potential for antioxidant activity.

Structural characterization of HEP-4

Methylation analysis of HEP-4

In addition to the composition of monosaccharides, the activity of polysaccharides is intricately related to the changes

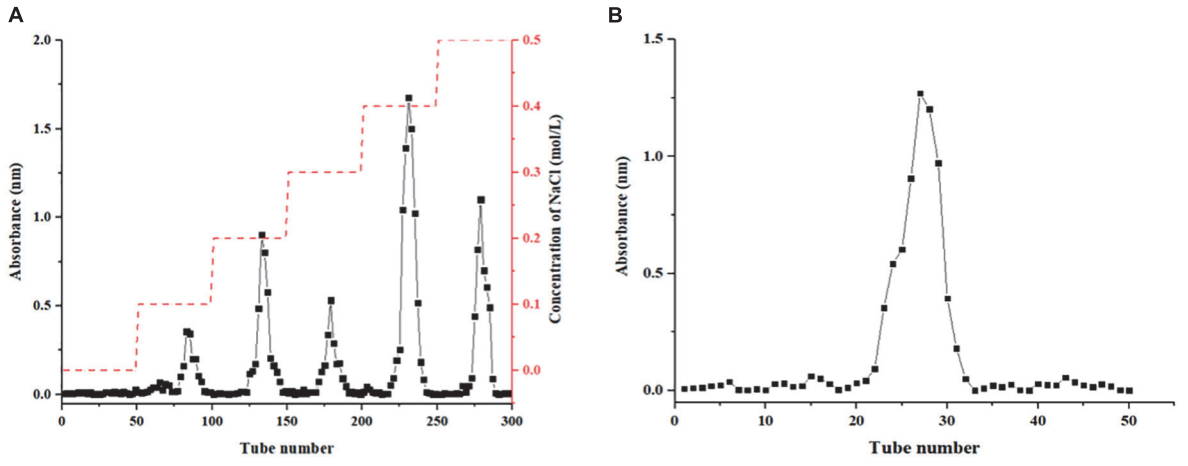

FIGURE 1
Results column chromatography results of honeysuckle polysaccharide. **(A)** DEAE-52 column chromatography of honeysuckle polysaccharide. **(B)** Sephadex G-75 column chromatography of HEP-4.

in chemical structures such as spatial conformation and the type of glycoside linkage (10). Methylation analysis is widely used to identify the linkage types between glucosyl residues. The analysis result is summarized in Table 1. Three types of Glc residues are mainly composed of 2,3,6-Me_3-Glc*p*, 2,3,4,6-Me_4-Glc*p*, and 2,4,6-Me_3-Glc*p* with a molar ratio of 50.8:24.5:16.59. In addition, two types of Ara and one type of Man were detected, which were characterized as 2,3,5-Me_3-Ara*f*, 2,3,-Me_2-Ara*f*, and 2,4-Me_2-Man*p*. The results showed that HEP-4 was primarily induced by 1-linked-Glc, 1,4-linked-Glc, 1,3-linked-Glc, 1-linked-Ara, 1,3,4-linked-Ara, and 1,3,6-linked-Man, and the highest content of 1,4-linked-Glc was probably contained in the main chain. The results of the analysis were consistent with those of monosaccharide composition analysis.

Sodium periodate oxidation and Smith degradation reaction

The sodium periodate oxidation results showed that 1 M glycosyl consumed 0.7491 mol of NaIO4 and liberated 0.007 mol of formic acid. The consumption of NaIO4 was more than double that of HCOOH, indicating the possible existence of 1→2, 1→2,6, 1→4, or 1→4,6, as well as 1→ or 1→6 linked glycosidic bonds (34). Furthermore, the GC analysis of the products of Smith degradation showed that it contained glycerin, further indicating that monosaccharides of HEP-4 could be connected largely by 1→2 or 1→2,6, and 1→ or 1→6 linked glycosidic bonds (34). Additionally, the presence of galactose was indicative of HEP-4 with the existence of 1→3, 1→3,4, and 1→3,6, linkages that cannot be oxidized (24).

Fourier transform-infrared analysis

Supplementary figure 2 shows the results of infrared spectrum analysis of honeysuckle polysaccharide. We obtained a broad and strong absorption peak of O-H stretching vibration peak between 3,600 and 3,400 cm^{-1}, which was the characteristic absorption peak of polysaccharides (35). The absorption peak at 2,925.71 cm^{-1} is the C-H stretching vibration peak (36). The absorption band generated at 1,608.44 cm^{-1} could be the C-O stretching vibration peak in the sample. The absorption peak observed at 1,385.08 cm^{-1} could be attributed to the variable-angle vibration of C-H (37). The two strong peaks observed at 1,272.83 cm^{-1} and 1,049.98 cm^{-1} indicated that the polysaccharide sample contained a pyran polysaccharide (38).

Nucleus magnetic resonance spectroscopy analysis of HEP-4

The NMR spectroscopy can be used to confirm monosaccharides, identify alpha or beta-anomeric configurations, and elucidate glycosidic bonds (39). In ^1H NMR, the chemical shift δ is greater than 5.0 ppm, indicating the α configuration of the heterotopic hydrogen of the polysaccharide molecule, whereas a chemical shift δ of less than 5.0 ppm indicates the β configuration of the heterotopic hydrogen of the polysaccharide molecule. The ^1H NMR spectrum of typical polysaccharides was mostly in the range of 3–5 ppm. The chemical shifts from 4.48 to 3.4 ppm in the 1H NMR spectrum were sugars H-2 to H-6 signal, and 1.20 ppm was assigned to the methyl group in the rhamnose residue. In addition, 3.2–4.0 ppm was the sugar ring proton signal (40). In ^{13}C NMR, the C2-C6 resonance signals were located at the region of 80.99 of 59.86 ppm. The chemical shifts of 109.9 of 96.4 ppm corresponded to the signal of the terminal sugar. In addition, 96.4–96.6 ppm corresponded to the terminal carbon signal of glucose (41).

As shown in Supplementary figure 3A. The ^1H NMR proton spectrum signals of HEP-4 were largely concentrated between 3.40 and 5.15 ppm. There was no proton signal at 5.40 ppm, indicating that HEP-4 was composed of glucopyranose. Furthermore, we observed only a weak signal at 5.14 ppm, which was presumed to be α-glucose signal. The chemical shifts of HEP-4 from 4.70 to 3.41 ppm in the ^1H NMR spectrum corresponded to sugars H-2 to H-6 signals. In addition, the band at 1.175 ppm indicated that the structure of polysaccharides could contain methyl groups of rhamnose residues. As shown in Supplementary figure 3B, HEP-4 showed several anomeric carbon signals from 95.0 to 110.0 ppm and multiple anomeric carbon signals in a broad region from 84.0 to 60.9 ppm. The resonances at 68.46, 71.86, 72.44, 62.45, and 66.36 ppm were assigned to C-2, C-3, C-4, C-5, and C-6, respectively. In addition, the NMR analysis data were consistent with the other structural characterization results described above.

TABLE 1 GC-MS results of methylation analysis of HEP-4.

Peaks	T_R (min.)	Methylated sugar	Molar ratio (%)	Linkage type	Major mass fragment (m/z)
1	10.017	2,3,5-Me_3-Ara*f*	3.77	Ara*f*-(1→	43,71,87,101,117,129,145,161
2	16.421	2,4-Me_2-Man*p*	5.22	→3,6)-Man*p*-(1→	43,71,87,99,101,117,129,159,161,189
3	16.815	2,3,-Me_2-Ara*f*	11.92	→3,4)-Ara*f*-(1→	43,71,85,99,101,117,127,159,161
4	20.460	2,3,4,6-Me_4-Glc*p*	24.5	Glc*p*-(1→	43,71,87,101,117,129,145,161,205
5	22.757	2,3,6-Me_3-Glc*p*	30.8	→4)-Glc*p*-(1→	43,71,87,99,101,113,117,129,131,161,173
6	26.533	2,4,6-Me_3-Glc*p*	16.59	→3)-Glc*p*-(1→	43,45,71,87,101,117,129,159,161,234

In summary, the backbone of HEP-4 was 1,4-β-D-Glc*p*, 1-α-D-Glc*p*, and other rhamnose residues branched at 1-β-D-Ara*p*, 1,3,4-β-D-Ara*p*, or 1,3,6-β-D-Man*p*. Compared with the previous studies on honeysuckle polysaccharides, the structural characteristics of the isolated polysaccharide in this study are different, and it is a novel polysaccharide that has not been reported.

Scanning electron microscopy analysis of HEP-4

The surface morphology of HEP-4 was analyzed by SEM. As shown in **Figure 2**, HEP-4 exhibited a mixture of irregular structures at a magnification of 2,000× and 5,000×. The majority of them were flaky, and the others were heterogeneous granule shapes with no surface pores, similar to the microstructure of the blue honeysuckle polysaccharides studied by Ma et al. (42).

Antioxidant activity of HEP-4

DPPH· free radical scavenging assay is widely used to evaluate the antioxidant activity *in vitro* (43). As shown in **Figure 3A**, the polysaccharide samples showed DPPH· scavenging activity. With an increase in the concentrations of polysaccharides from 0 to 0.6 mg/mL, the DPPH· radical scavenging activity increased, showing a positive linear correlation. At a concentration of 1.0 mg/mL, the scavenging rate of HEP-4 on DPPH· free radical reached 69.73%, and the scavenging rate of Vc on DPPH· free radical reached 97.01%. Therefore, we speculated that polysaccharides of honeysuckle had a certain role in scavenging DPPH· free radical activity.

As shown in **Figure 3B**, with an increase in the HEP-4 concentration, the scavenging rate of superoxide free radical increased. The scavenging rate of HEP-4 on superoxide free radical reached 40.62%, and that of Vc reached 59.43%. Therefore, HEP-4 exerts a certain scavenging effect on superoxide free radicals; however, its scavenging ability is lower than that of Vc at the same concentration.

The ABTS·$^+$ free radical scavenging assay is used to evaluate the total antioxidant capacity of natural products. The relevant test results showed that the positive control (Vc) presented a strong dose-dependent scavenging activity, and HEP-4 also established a good scavenging effect on ABTS·$^+$ free radicals (**Figure 3C**). Within the range of mass concentration of 0–1.0 mg/mL, the scavenging ability of HEP-4 on ABTS·$^+$ free radical was gradually enhanced. At a concentration of 1.0 mg/ml, the scavenging rate of HEP-4 on ABTS·$^+$ free radical was 92.47%, and that of Vc on ABTS·$^+$ free radical was 99.12%. These results indicated that honeysuckle polysaccharides should be explored as potential antioxidants.

Among the reactive oxygen species, hydroxyl radical is considered the most harmful free radical, which can stimulate the peroxidation of biomacromolecules in cells (44). As shown in **Figure 3D**, the scavenging rate of polysaccharides increased with an increase in their concentrations, followed by a flat trend. When the concentration was 1.0 mg/mL, the scavenging rate reached 39.78%, and the scavenging rate of Vc was up to 80.99%.

The above-mentioned four antioxidant capacity detection methods were used to systematically evaluate the antioxidant activity of honeysuckle polysaccharides (HEP-4) from different perspectives. These methods avoided the one-sidedness and inadequacy of evaluating the antioxidant activity of a single antioxidant method. In summary, antioxidant activity test results and comparison with previous research results of honeysuckle water-soluble polysaccharides (5) exhibited that HEP-4 has a strong scavenging activity against DPPH·, superoxide, ABTS·$^+$, and hydroxyl radicals. The antioxidant

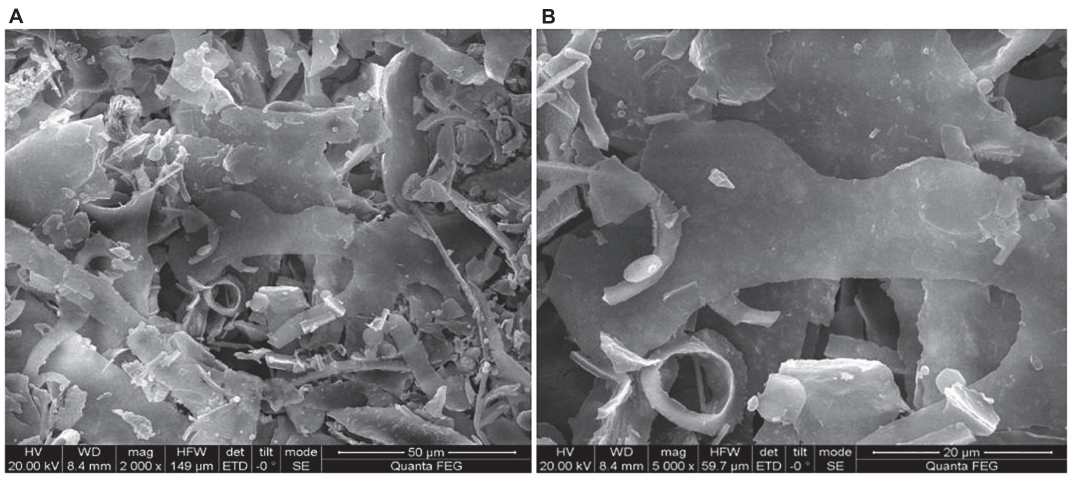

FIGURE 2
Scanning electron microscopy (SEM) images of HEP-4. **(A)** Magnification 2000× and **(B)** Magnification 5000×.

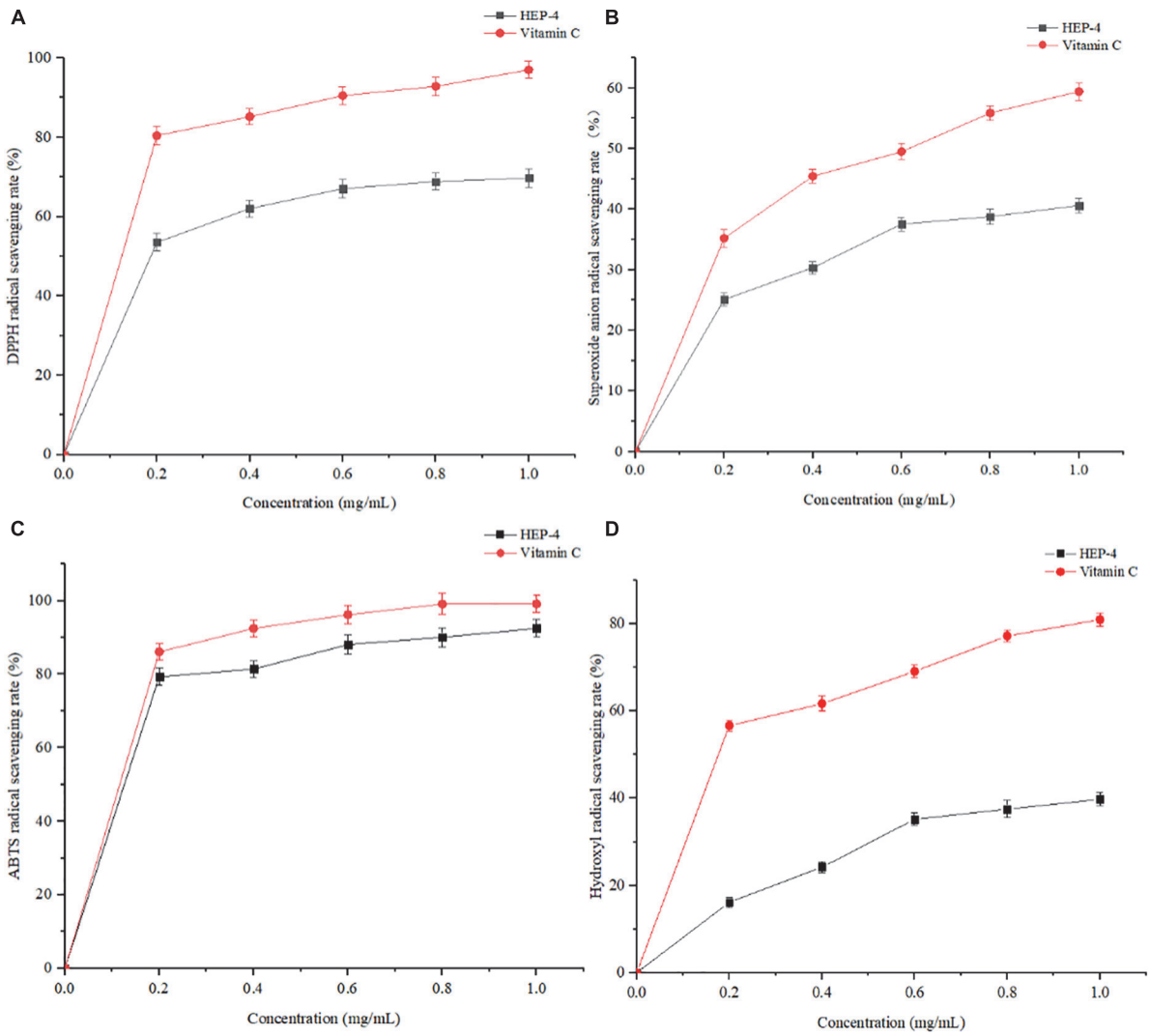

FIGURE 3
Antioxidant activity results of HEP-4. **(A)** DPPH· radical scavenging assay, **(B)** Superoxide radical scavenging assay, **(C)** ABTS radical scavenging assay, **(D)** and hydroxyl radical scavenging assay.

activities of HEP-4 in different reaction systems vary, which could be related to certain structural features of polysaccharides. The results could lay the foundation for the research and comprehensive development and utilization of honeysuckle polysaccharides in natural antioxidants.

Hoechst 33342 fluorescent staining analysis

Hoechst 33342 is a cell-permeable blue fluorescent dye (45) that stains nuclei with blue fluorescence. As shown in Figure 4, the effect of different concentrations of HEP-4 on H_2O_2-stimulated HepG2 cells was observed. In the control group, HepG2 cells have a uniform nuclear size with clear edges. After treatment with H_2O_2 alone, certain cells displayed apoptotic morphological changes such as blurred edges and increased internuclear spacing. In contrast, HEP-4-treated cells significantly reduced the degree of apoptosis in a concentration-dependent manner. The results showed that HEP-4 significantly inhibited the formation of apoptotic and relieved nuclear shrinkage induced by oxidative stress on HepG2 cells.

Effects of HEP-4 on intracellular reactive oxygen species levels of HepG2 cells

It is well known that ROS is a by-product of aerobic metabolism and is involved in different signaling pathways and

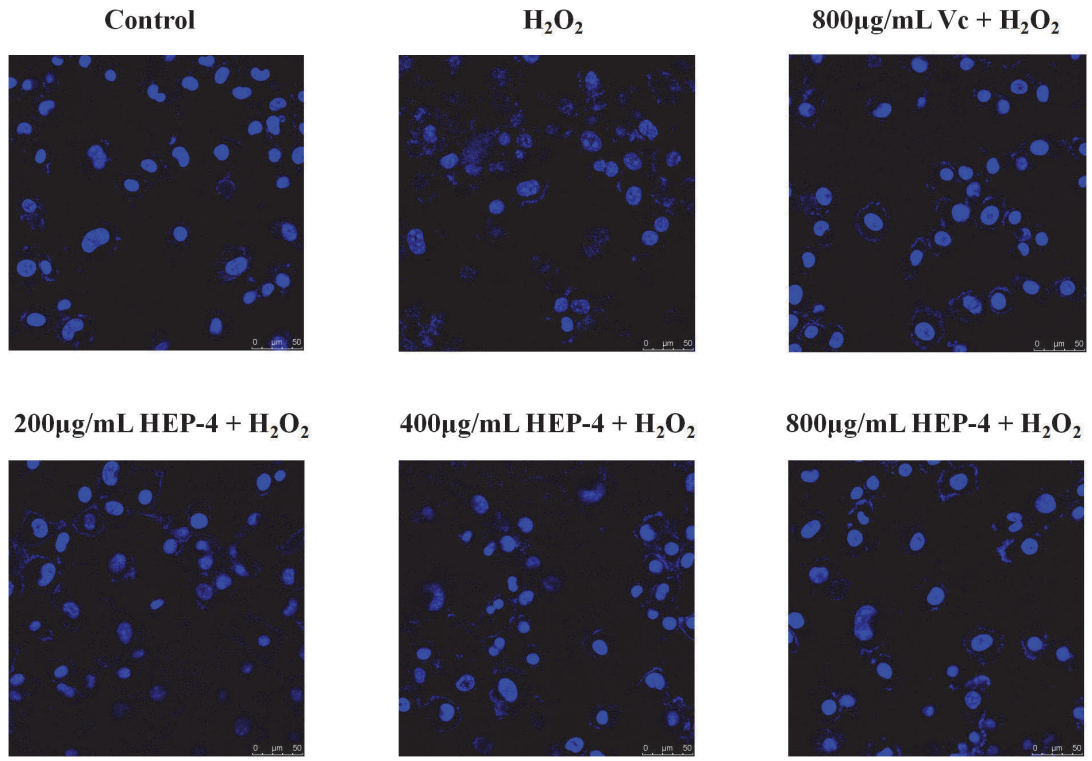

FIGURE 4
Nuclear condition after Hoechst 33258 staining.

cell homeostasis. However, excessive ROS can induce apoptosis by damaging the DNA and other biomacromolecules (46). As shown in **Figure 5**, compared with the control group and the pre-treatment group, cells treated with H_2O_2 showed various changes, and the HEP-4 pre-treatment group showed significant inhibition of the production of ROS (**Figure 5A**). In addition, the protection of HepG2 cells by HEP-4 was found to be dose-dependent in the tested concentration range.

Effects of HEP-4 on the activities of glutathione peroxidase catalase and catalase in H_2O_2-treated HepG2 cells

Glutathione peroxidase catalase and catalase are major antioxidant enzymes and play a crucial role in interception (47). Previous studies have demonstrated that plant polysaccharides can reduce cell apoptosis by increasing the activities of CAT and GSH-Px, thereby reducing H_2O_2-induced oxidative damage to hepatocytes (48). As expected, the results of this study showed that the activity of GSH-Px in H_2O_2-induced HepG2 cells was significantly increased after pre-treatment of HepG2 cells with different concentrations of HEP-4 (**Figure 5B**). Similarly, the CAT activity of HepG2 cells treated with H_2O_2 demonstrated a downward trend (**Figure 5C**), whereas, at a concentration of 800 μg/mL, the CAT activity of HepG2 cells pre-treated with HEP-4 was significantly increased, indicating that HEP-4 improved the inhibition of H_2O_2 on cell activity.

Effects of HEP-4 on the content of malondialdehyde in H_2O_2-treated HepG2 cells

Following the H_2O_2-induced oxidative stress in HepG2 cells, the MDA levels modified significantly. For example, You et al. reported that polysaccharides from Panax notoginseng root extract inhibited H_2O_2-oxidative stress and reduced cell damage by decreasing ROS and MDA content (49). Consistent with this report, HEP-4 protected the cells from oxidative stress by eliminating ROS and reducing MDA levels. As shown in **Figure 5D**, the effect of HEP-4 on the MDA levels of HepG2 cells showed that the MDA levels of HepG2 cells were significantly increased after H_2O_2 treatment, whereas the MDA levels of HEP-4 group were lower than those of the H_2O_2 group ($P < 0.05$). When HEP-4 concentration was 800 μg/mL HEP-4, the MDA level of HepG2 cells decreased most significantly.

In summary, an oxidative damage cell model was established by H_2O_2 induction, and the cellular antioxidant capacity of honeysuckle polysaccharide HEP-4 was studied. The

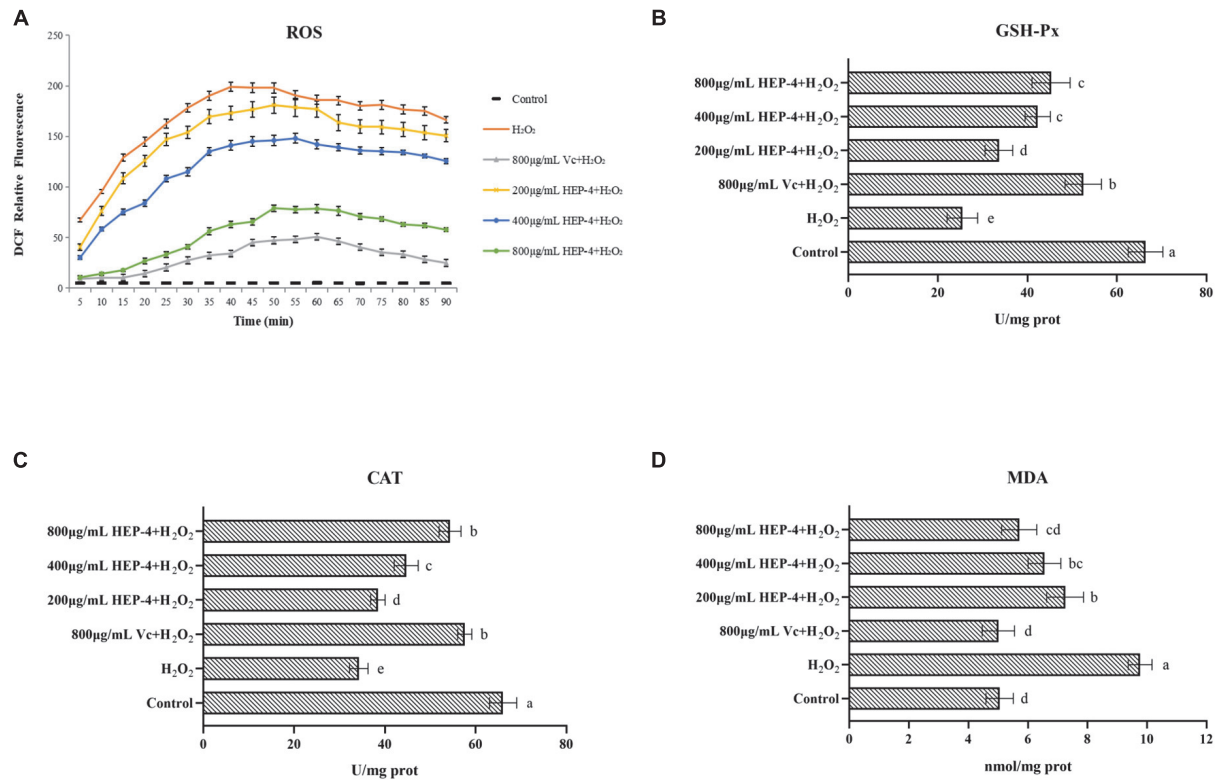

FIGURE 5
HEP-4 alleviates H_2O_2-induced oxidative stress. **(A)** Effect of HEP-4 on H_2O_2-induced ROS generation in HepG2 cells. **(B)** Effect of HEP-4 on glutathione peroxidase (GSH-Px). **(C)** Effect of HEP-4 on catalase (CAT). **(D)** Effect of HEP-4 on malondialdehyde (MDA) level. Values bearing different letters are significantly different ($P < 0.05$).

results showed that HEP-4 significantly reduced the levels of intracellular ROS and the degree of oxidative damage, whereas significantly increased the activities of antioxidant enzymes such as CAT and GSH-Px, and reduced the content of harmful substances such as MDA. Furthermore, a comprehensive analysis of structural characterization and *in vitro* antioxidant research results indicated that honeysuckle polysaccharide HEP-4 could be used as a novel natural antioxidant with potential application values in the food and pharmaceutical industries.

Conclusion

In conclusion, a polysaccharide from honeysuckle was extracted by hot water, and the primary fraction HEP-4 was obtained by DEAE-52 and Sephadex G-75 columns, and its molecular weight was 1.98×10^5 Da. The monosaccharide composition analysis results showed that HEP-4 was primarily composed of monosaccharides such as glucose, mannose, and galactose. In addition, a combination of periodate oxidation, Smith degradation, FI-IR, and NMR revealed that 1,4-β-D-Glc accounted for the majority of glycosidic bond types in polysaccharide components. HEP-4 exerts a strong antioxidant ability by scavenging $ABTS^{\cdot+}$ and DPPH· free radicals. Furthermore, the results of the research showed that HEP-4 exerted a certain protective effect on HepG2 cells and protected them from oxidative stress damage. These results provide a basis for further understanding the polysaccharides obtained from honeysuckle and their applications in functional foods and pharmacology. However, the antioxidant effect and the structure–activity relationship of HEP-4 still require further comprehensive investigation to comprehensively elucidate the underlying mechanism. In addition, studies have reported that the application of modern chemical techniques, such as methylation, to chemically modify the structure of natural polysaccharides can improve their biological activity and even endow them with new biological activities, which is also the direction of our future work.

Data availability statement

The original contributions presented in this study are included in the article/**Supplementary material**, further inquiries can be directed to the corresponding author.

Author contributions

FA and GR: investigation, data curation, methodology, formal analysis, writing – original draft, and software. KC, ML, YML, and YFL: methodology, formal analysis, and writing – review and editing. XH and MS: data curation, validation, software, investigation, data curation, software, investigation. JW: supervision, funding acquisition, and project administration. RW: conceptualization, supervision, project administration, and writing – review and editing. All authors contributed to the article and approved the submitted version.

Funding

This work was supported by the National Natural Science Foundation of China (Grant No. 31972047), National Natural Science Regional Innovation Joint Development Fund (U20A20400), Shenyang City Youth Science and Technology Innovation Leading Talent Project (RC200495), and Shenyang Science and Technology Innovation Platform Project (21-103-0-14 and 21-104-0-28).

Conflict of interest

The authors declare that the research was conducted in the absence of any commercial or financial relationships that could be construed as a potential conflict of interest.

Publisher's note

All claims expressed in this article are solely those of the authors and do not necessarily represent those of their affiliated organizations, or those of the publisher, the editors and the reviewers. Any product that may be evaluated in this article, or claim that may be made by its manufacturer, is not guaranteed or endorsed by the publisher.

Supplementary material

The Supplementary Material for this article can be found online at: https://www.frontiersin.org/articles/10.3389/fnut.2022.1035760/full#supplementary-material

References

1. Guo SF, Yu SF, Huang XH. Effect of La (III) on some physiological index and ultrastructure of honeysuckle (*Lonicera japonica* Thunb.). *AMR*. (2013) 864-867:295–8.

2. Bai X, Chai Y, Shi W, Li Y, Zhang T, Liu P. *Lonicera japonica* polysaccharides attenuate ovalbumin-induced allergic rhinitis by regulation of Th17 cells in BALB/c mice. *J Funct Foods*. (2020) 65:103758. doi: 10.1016/j.jff.2019.103758

3. Dong X-D, Feng Y-Y, Liu Y-N, Ji H-Y, Yu S-S, Liu A, et al. A novel polysaccharide from *Castanea mollissima* Blume: preparation, characteristics and antitumor activities in vitro and in vivo. *Carbohydr Polym*. (2020) 240:116323. doi: 10.1016/j.carbpol.2020.116323

4. Lin L, Wang P, Du Z, Wang W, Cong Q, Zheng C, et al. Structural elucidation of a pectin from flowers of *Lonicera japonica* and its antipancreatic cancer activity. *Int J Biol Macromol*. (2016) 88:130–7. doi: 10.1016/j.ijbiomac.2016.03.025

5. Zhang T, Liu H, Bai X, Liu P, Yang Y, Huang J, et al. Fractionation and antioxidant activities of the water-soluble polysaccharides from *Lonicera japonica* Thunb. *Int J Biol Macromol*. (2020) 151:1058–66. doi: 10.1016/j.ijbiomac.2019.10.147

6. Tian J, Che H, Ha D, Wei Y, Zheng S. Characterization and anti-allergic effect of a polysaccharide from the flower buds of *Lonicera japonica*. *Carbohydr Polym*. (2012) 90:1642–7. doi: 10.1016/j.carbpol.2012.07.044

7. Kumar N, Singh B, Bhandari P, Gupta AP, Uniyal SK, Kaul VK. Biflavonoids from *Lonicera japonica*. *Phytochemistry*. (2005) 66:2740–4. doi: 10.1016/j.phytochem.2005.10.002

8. Zhou X, Dong Q, Kan X, Peng L, Xu X, Fang Y, et al. Immunomodulatory activity of a novel polysaccharide from *Lonicera japonica* in immunosuppressed mice induced by cyclophosphamide. *PLoS One*. (2018) 13:e0204152. doi: 10.1371/journal.pone.0204152

9. Wang P, Liao W, Fang J, Liu Q, Yao J, Hu M, et al. A glucan isolated from flowers of *Lonicera japonica* Thunb. inhibits aggregation and neurotoxicity of Aβ42. *Carbohydr Polym*. (2014) 110:142–7. doi: 10.1016/j.carbpol.2014.03.060

10. Ji X, Guo J, Ding D, Gao J, Hao L, Guo X, et al. Structural characterization and antioxidant activity of a novel high-molecular-weight polysaccharide from *Ziziphus Jujuba cv. Muzao*. *Food Measure*. (2022) 16:2191–200. doi: 10.1007/s11694-022-01288-3

11. Ji X, Guo J, Pan F, Kuang F, Chen H, Guo X, et al. Structural elucidation and antioxidant activities of a neutral polysaccharide from arecanut (*Areca catechu* L.). *Front Nutr*. (2022) 9:853115. doi: 10.3389/fnut.2022.853115

12. Ben Yakoub AR, Abdehedi O, Jridi M, Elfalleh W, Bkhairia I, Nasri M, et al. Bioactive polysaccharides and their soluble fraction from Tossa jute (*Corchorus olitorius* L.) leaves. *Food Biosci*. (2020) 37:100741. doi: 10.1016/j.fbio.2020.100741

13. Shang X-L, Liu C-Y, Dong H-Y, Peng H-H, Zhu Z-Y. Extraction, purification, structural characterization, and antioxidant activity of polysaccharides from Wheat Bran. *J Mol Struct*. (2021) 1233:130096. doi: 10.1016/j.molstruc.2021.130096

14. Andrade D, Gil C, Breitenfeld L, Domingues F, Duarte AP. Bioactive extracts from *Cistus ladanifer* and *Arbutus unedo* L. *Indust Crops Products*. (2009) 30:165–7. doi: 10.1016/j.indcrop.2009.01.009

15. Liu Y, Tang T, Duan S, Li C, Lin Q, Wu H, et al. The purification, structural characterization and antidiabetic activity of a polysaccharide from *Anoectochilus roxburghii*. *Food Funct*. (2020) 11:3730–40. doi: 10.1039/C9FO00860H

16. Zhang H, Zou P, Zhao H, Qiu J, Regenstein JM, Yang X. Isolation, purification, structure and antioxidant activity of polysaccharide from pinecones of *Pinus koraiensis*. *Carbohydr Polym*. (2021) 251:117078. doi: 10.1016/j.carbpol.2020.117078

17. Zhi F, Yang T-L, Wang Q, Jiang B, Wang Z-P, Zhang J, et al. Isolation, structure and activity of a novel water-soluble polysaccharide from *Dioscorea opposita* Thunb. *Int J Biol Macromol*. (2019) 133:1201–9. doi: 10.1016/j.ijbiomac.2019.04.087

18. Wang X, Zhang S, Li Z, Wang M, Sun R. Comparison on structure, chain conformation, and antioxidant activity of polysaccharides extracted from *Liriopes radix* with hot water and ultrasound. *J Carbohydr Chem*. (2020) 39:145–62. doi: 10.1080/07328303.2020.1746329

19. Chen Z, Zhao Y, Zhang M, Yang X, Yue P, Tang D, et al. Structural characterization and antioxidant activity of a new polysaccharide from *Bletilla striata* fibrous roots. *Carbohydr Polym*. (2020) 227:115362. doi: 10.1016/j.carbpol.2019.115362

20. Hu H-B, Liang H-P, Li H-M, Yuan R-N, Sun J, Zhang L-L, et al. Isolation, purification, characterization and antioxidant activity of polysaccharides from the

stem barks of *Acanthopanax leucorrhizus*. *Carbohydr Polym*. (2018) 196:359–67. doi: 10.1016/j.carbpol.2018.05.028

21. Ji X, Cheng Y, Tian J, Zhang S, Jing Y, Shi M. Structural characterization of polysaccharide from jujube (*Ziziphus jujuba* Mill.) fruit. *Chem Biol Technol Agric*. (2021) 8:54. doi: 10.1186/s40538-021-00255-2

22. Yang X, Zhou S, Li H, An J, Li C, Zhou R, et al. Structural characterization of *Alpiniae oxyphyllae* fructus polysaccharide 2 and its activation effects on RAW264.7 macrophages. *Int Immunopharmacol*. (2021) 97:107708. doi: 10.1016/j.intimp.2021.107708

23. Li G, Chen P, Zhao Y, Zeng Q, Ou S, Zhang Y, et al. Isolation, structural characterization and anti-oxidant activity of a novel polysaccharide from garlic bolt. *Carbohydr Polym*. (2021) 267:118194. doi: 10.1016/j.carbpol.2021.118194

24. Meng M, Cheng D, Han L, Chen Y, Wang C. Isolation, purification, structural analysis and immunostimulatory activity of water-soluble polysaccharides from *Grifola Frondosa* fruiting body. *Carbohydr Polym*. (2017) 157:1134–43. doi: 10.1016/j.carbpol.2016.10.082

25. Zhang Y, Zeng Y, Cui Y, Liu H, Dong C, Sun Y. Structural characterization, antioxidant and immunomodulatory activities of a neutral polysaccharide from *Cordyceps militaris* cultivated on hull-less barley. *Carbohydr Polym*. (2020) 235:115969. doi: 10.1016/j.carbpol.2020.115969

26. Zhou Y, Qian C, Yang D, Tang C, Xu X, Liu E-H, et al. Purification, structural characterization and immunomodulatory effects of polysaccharides from *Amomumvillosum Lour*. on RAW 264.7 macrophages. *Molecules*. (2021) 26:2672. doi: 10.3390/molecules26092672

27. Hu L, Liu R, Wu T, Sui W, Zhang M. Structural properties of homogeneous polysaccharide fraction released from wheat germ by hydrothermal treatment. *Carbohydr Polym*. (2020) 240:116238. doi: 10.1016/j.carbpol.2020.116238

28. Chen F, Huang G. Antioxidant activity of polysaccharides from different sources of ginseng. *Int J Biol Macromol*. (2019) 125:906–8. doi: 10.1016/j.ijbiomac.2018.12.134

29. Liang X-X, Gao Y-Y, Pan Y, Zou Y-F, He M, He C-L, et al. Purification, chemical characterization and antioxidant activities of polysaccharides isolated from *Mycena dendrobii*. *Carbohydr Polym*. (2019) 203:45–51. doi: 10.1016/j.carbpol.2018.09.046

30. Liu D, Sun Q, Xu J, Li N, Lin J, Chen S, et al. Purification, characterization, and bioactivities of a polysaccharide from mycelial fermentation of *Bjerkandera fumosa*. *Carbohydr Polym*. (2017) 167:115–22. doi: 10.1016/j.carbpol.2017.03.029

31. Wu Q, Luo M, Yao X, Yu L. Purification, structural characterization, and antioxidant activity of the COP-W1 polysaccharide from *Codonopsis tangshen* Oliv. *Carbohydr Polym*. (2020) 236:116020. doi: 10.1016/j.carbpol.2020.116020

32. Sheng J, Sun Y. Antioxidant properties of different molecular weight polysaccharides from *Athyrium multidentatum* (Doll.) Ching. *Carbohydr Polym*. (2014) 108:41–5. doi: 10.1016/j.carbpol.2014.03.011

33. Mehmood S, Zhou L-Y, Wang X-F, Cheng X-D, Meng F-J, Wang Y, et al. Structural elucidation and antioxidant activity of a novel heteroglycan from Tricholoma Lobayense. *J Carbohydr Chem*. (2019) 38:192–211.

34. Abuduwaili A, Mutailifu P, Nuerxiati R, Gao Y, Aisa HA, Yili A. Structure and biological activity of polysaccharides from *Nitraria sibirica* pall fruit. *Food Biosci*. (2021) 40:100903. doi: 10.1016/j.fbio.2021.100903

35. Bai L, Zhu P, Wang W, Wang M. The influence of extraction pH on the chemical compositions, macromolecular characteristics, and rheological properties of polysaccharide: the case of okra polysaccharide. *Food Hydrocolloids*. (2020) 102:105586. doi: 10.1016/j.foodhyd.2019.105586

36. Yuris A, Goh KK, Hardacre AK, Matia-Merino L. The effect of gel structure on the in vitro digestibility of wheat starch-Mesona chinensis polysaccharide gels. *Food Funct*. (2019) 10:250–8. doi: 10.1039/C8FO01501E

37. Chen Y, Jiang X, Xie H, Li X, Shi L. Structural characterization and antitumor activity of a polysaccharide from ramulus mori. *Carbohydr Polym*. (2018) 190:232–9. doi: 10.1016/j.carbpol.2018.02.036

38. Wu F, Zhou C, Zhou D, Ou S, Zhang X, Huang H. Structure characterization of a novel polysaccharide from *Hericium erinaceus* fruiting bodies and its immunomodulatory activities. *Food Funct*. (2018) 9:294–306. doi: 10.1039/C7FO01389B

39. Shi Y, Ye Y-F, Zhang B-W, Liu Y, Wang J-H. Purification, structural characterization and immunostimulatory activity of polysaccharides from *Umbilicaria esculenta*. *Int J Biol Macromol*. (2021) 181:743–51. doi: 10.1016/j.ijbiomac.2021.03.176

40. Gao J, Zhang T, Jin Z-Y, Xu X-M, Wang J-H, Zha X-Q, et al. Structural characterisation, physicochemical properties and antioxidant activity of polysaccharide from *Lilium lancifolium* Thunb. *Food Chem*. (2015) 169:430–8. doi: 10.1016/j.foodchem.2014.08.016

41. Wang Y-Q, Huang J-X, Zhou W-W. Isolation, characterization and cytoprotective effects against UV radiation of exopolysaccharide produced from *Paenibacillus polymyxa* PYQ1. *J Biosci Bioeng*. (2020) 130:283–9. doi: 10.1016/j.jbiosc.2020.05.001

42. Ma C, Bai J, Shao C, Liu J, Zhang Y, Li X, et al. Degradation of blue honeysuckle polysaccharides, structural characteristics and antiglycation and hypoglycemic activities of degraded products. *Food Res Int*. (2021) 143:110281. doi: 10.1016/j.foodres.2021.110281

43. Zhu R, Zhang X, Wang Y, Zhang L, Zhao J, Chen G, et al. Characterization of polysaccharide fractions from fruit of *Actinidia arguta* and assessment of their antioxidant and antiglycated activities. *Carbohydr Polym*. (2019) 210:73–84. doi: 10.1016/j.carbpol.2019.01.037

44. Yu G, Zhao J, Wei Y, Huang L, Li F, Zhang Y, et al. Physicochemical properties and antioxidant activity of pumpkin polysaccharide (*Cucurbita moschata* Duchesne ex Poiret) modified by subcritical water. *Foods*. (2021) 10:197. doi: 10.3390/foods10010197

45. Kim Y-S, Lee S-J, Hwang J-W, Kim E-K, Kim S-E, Kim E-H, et al. In vitro protective effects of *Thymus quinquecostatus* Celak extracts on t-BHP-induced cell damage through antioxidant activity. *Food Chem Toxicol*. (2012) 50:4191–8. doi: 10.1016/j.fct.2012.08.015

46. Yuan L, Duan X, Zhang R, Zhang Y, Qu M. Aloe polysaccharide protects skin cells from UVB irradiation through Keap1/Nrf2/ARE signal pathway. *J Dermatolog Treat*. (2020) 31:300–8. doi: 10.1080/09546634.2019.1591579

47. Qin T, Ren Z, Liu X, Luo Y, Long Y, Peng S, et al. Study of the selenizing *Codonopsis pilosula* polysaccharides protects RAW264.7 cells from hydrogen peroxide-induced injury. *Int J Biol Macromol*. (2019) 125:534–43. doi: 10.1016/j.ijbiomac.2018.12.025

48. Yue C, Chen J, Hou R, Tian W, Liu K, Wang D, et al. The antioxidant action and mechanism of selenizing *Schisandra chinensis* polysaccharide in chicken embryo hepatocyte. *Int J Biol Macromol*. (2017) 98:506–14. doi: 10.1016/j.ijbiomac.2017.02.015

49. You S, Shi X, Yu D, Zhao D, An Q, Wang D, et al. Fermentation of *Panax notoginseng* root extract polysaccharides attenuates oxidative stress and promotes type I procollagen synthesis in human dermal fibroblast cells. *BMC Complement Med Ther*. (2021) 21:34. doi: 10.1186/s12906-020-03197-8

Frontiers in Nutrition

Explores what and how we eat in the context of health, sustainability and 21st century food science

A multidisciplinary journal that integrates research on dietary behavior, agronomy and 21st century food science with a focus on human health.

Discover the latest Research Topics

See more →

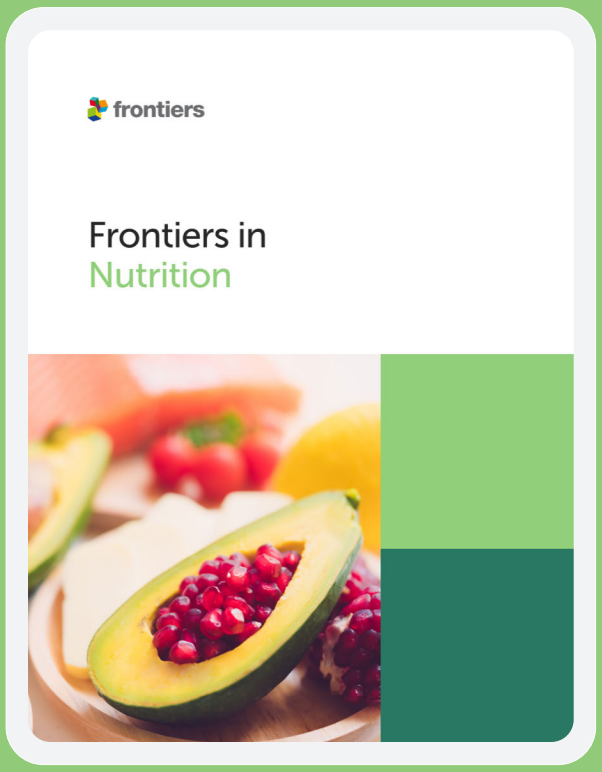

Frontiers

Avenue du Tribunal-Fédéral 34
1005 Lausanne, Switzerland
frontiersin.org

Contact us

+41 (0)21 510 17 00
frontiersin.org/about/contact